

ADRIAN M.K. THOMAS
ARPAN K. BANERJEE
UWE BUSCH
EDITORS

*Classic Papers in
Modern Diagnostic
Radiology*

A.M.K. Thomas, A.K. Banerjee, U. Busch

Classic Papers in Modern Diagnostic Radiology

Adrian M.K. Thomas
Arpan K. Banerjee
Uwe Busch
EDITORS

Classic Papers in Modern Diagnostic Radiology

Foreword by Willi A. Kalender, Erlangen

Dr. Adrian M.K. Thomas
Consultant Radiologist
Royal Princess Hospital Dept. of Nuclear Medicine
Orpington, Kent BR6 8ND, UK

Dr. Arpan K. Banerjee, MBBS, FRCP, FRCR
Consultant Radiologist
Birmingham Heartlands and
Solihull Hospitals NHS Trust
Birmingham B9 5SS, UK

Dr. Uwe Busch
Medical Physicist
Deutsches Röntgen-Museum
Schwelmer Straße 41
42897 Remscheid, Germany

ISBN 3-540-21927-7 Springer Berlin Heidelberg New York

Library of Congress Control Number: 2004110773

This work is subject to copyright. All rights are reserved, whether the whole or part of the material is concerned, specifically the rights of translation, reprinting, reuse of illustrations, recitation, broadcasting, reproduction on microfilm or in any other way, and storage in data banks. Duplication of this publication or parts thereof is permitted only under the provision of the German Copyright Law of September 9, 1965, in its current version, and permission for use must always be obtained from Springer-Verlag. Violations are liable to prosecution under the German Copyright Law.

Springer is a part of Springer Science+Business Media
springeronline.com

© Springer-Verlag Berlin Heidelberg 2005
Printed in Germany

The use of designations, trademarks, etc. in this publication does not imply, even in the absence of a specific statement, that such names are exempt from the relevant protective laws and regulations and therefore free for general use.

Product liability: The publisher can not guarantee the accuracy of any information about dosage and application contained in this book. In every individual case the user must check such information by consulting the relevant literature.

Editor: Dr. U. Heilmann, Heidelberg, Germany
Desk editor: W. McHugh, Heidelberg, Germany
Production: PRO EDIT GmbH, Heidelberg, Germany
Cover-Design: Frido Stein-Broo, Pau, Spain
Typesetting and Reproduction: AM-productions GmbH, Wiesloch, Germany

Printed on acid-free paper 21/3150Di - 5 4 3 2 1 0

Dedications

For my father Professor P. K. Thomas

Adrian M.K. Thomas

For my daughters Shonali and Shiuli

Arpan K. Banerjee

For my family Ulrike, Bjoern, Florian and Alina

Uwe Busch

Foreword

I am very pleased to have been asked to write the foreword to this book. The technical advances in diagnostic radiology in the last few decades have transformed clinical practice and have been nothing short of astonishing.

The subject of diagnostic radiology is now very large and radiology departments are involved in all areas of modern patient care. The defining event in modern radiology, and arguably the most significant development in radiology since Wilhelm Röntgen discovered X-rays, was the invention of the CT scanner in the 1970s. The CT scanner introduced modern cross-sectional imaging and also digital imaging. We now have MRI and ultrasound and these techniques are replacing many traditional X-ray procedures. The developments in radiology have been the result of a fruitful interaction between the basic sciences, clinical medicine and the manufacturers. This can be seen by looking at the various sources of these publications. Change is produced by the interactions between the various disciplines.

The editors have had a very difficult task in selecting the key discoveries and descriptions. The radiological literature is very large. Medical imaging continues to develop rapidly and these papers are the foundations of our current practice.

Prof. Dr. Willi A. Kalender
Institute of Medical Physics
Friedrich-Alexander-University, Erlangen-Nürnberg

Preface

In the past few decades the practice of diagnostic radiology has been transformed almost beyond recognition. In traditional radiological practice, diagnostic techniques often showed the pathology indirectly; for example, the presence of a pancreatic pseudocyst could be inferred by the displacement of a barium-filled stomach. Diagnostic tests were often invasive and these would then be followed by conventional surgery. We are now moving to a position where diagnosis is made by a non-invasive imaging procedure and treatment is by minimally invasive surgery. Performing angiography for placental localization and even the traditional oral cholecystogram are now only memories. The patient who needs surgery will have had appropriate imaging so the surgeon can plan the most effective course of action and may also suggest that surgery is not the most appropriate course of action.

It is always interesting to read about the great names who have by their discoveries advanced the practice of clinical medicine. There have been a number of books which have given the original descriptions of the writers, such as the "Classic Descriptions of Disease" by Ralph Major and the "Source Book of Medical History" compiled by Logan Glendenning. The sources of both of these books reach back into antiquity. The history of radiology is considerably younger and is a little more than 100 years old, having started with the discovery of X-rays by Wilhelm Röntgen in 1895. André Bruwer did the radiological community a great service when in 1964 he produced his two volumes of "Classic Descriptions in Diagnostic Roentgenology". In these two books he reproduced the classic accounts of diagnostic radiology from the earliest days and gave an account of the techniques that were then in use. Radiology has transformed beyond all recognition since 1964. We now have ultrasound, CT, MRI and interventional radiology. The traditional contrast media have been replaced by the modern agents and X-ray film is disappearing and is being replaced by an electronic image. However, radiology remains central to modern patient care.

In this book we provide a selection of classic papers of modern radiology. The choice of papers is obviously personal; however, we feel that the papers chosen have stood the test of time. There are many important papers that have not been included. In this book the papers are reproduced in their original form so that the reader is able to read what was originally said. In the introduction to each section the significance of the paper is discussed with some biographical details where appropriate. Nuclear medicine has not been included.

In general there is a bias towards the more technical papers. However, the articles chosen have resulted in many clinical papers. It is when the papers are brought together that the extent of the achievements of clinical radiology becomes apparent.

Adrian M. K. Thomas
Arpan K. Banerjee
Uwe Busch

Acknowledgements

We would like to thank Ute Heilmann and her colleagues at Springer for their encouragement and support for this project. Furthermore, we would like to thank the following people for their help in providing us with information for our book: Torsten Almén, Robert Brasch, Ruediger Brennecke, Brigitte Bukovics, Lawrence Cheung, Jim Culley, Lars Edler, Dave Fellers, Leila Gray, Brian Lentle, Shannon Hamilton, Paul Heintzen, Kazuhiro Hishinima, Hans-Joachim Holländer, Stephen Horii, The late Sir Godfrey Hounsfield, Bernie Huang, Lothar Jeromin, Willi Kalender, Stuart S Kaplan, Hisatoyo Kato, Gerald M. Kolodny, Robert A. Kruger, Paul Lauterbur, José Leborgne, Denny Lee, Heinz U. Lemke, Betty Levine, Sir Peter Mansfield, Charles A. Mistretta, Peter R. Mueller, Sol Nudelman, John A. Parker, Stephen H. Parker, Jean Pringot, John Reid, The late Neil Ridyard, Stephen J. Riederer, John Rowlands, Ulrich Sigwart, Ralph Smathers, Eric vanSonnenberg, László K. Tabár, René van Tiggelen, Peter Vock, Hans-Joachim Weinmann, Nellie Wild, Joseph Woo, and Wei Zhao.

Our special thanks for granting us permission to use the original papers free of charge are extended to:

American Association of Physicists in Medicine
American Physical Society
American Roentgen Ray Society
British Institute of Radiology
Computers in Cardiology
Lippincott Williams & Wilkins
Massachusetts Medical Society
MMW Fortschritte der Medizin
M Pacquet JBR-BTR
Radiological Society of North America
Royal College of Obstetricians and Gynaecologists
Saxon Academy of Science
Sociedad de Cirugia del Uruguay
Taylor & Francis Group
Walter De Gruyter

Contents

1 Computer Tomography

- | | | |
|-----|--|----|
| 1.1 | Über die Bestimmung von Funktionen durch ihre Integralwerte längs gewisser Mannigfaltigkeiten
<i>J. Radon</i> | 5 |
| 1.2 | Representation of a function by its line integrals, with some radiological applications
<i>A.M. Cormack</i> | 23 |
| 1.3 | Computerized transverse axial scanning (tomography). Part I. Description of system
<i>G.N. Hounsfield</i> | 30 |
| 1.4 | Computerized transverse axial scanning (tomography). Part II. Clinical application
<i>J. Ambrose</i> | 38 |
| 1.5 | Spiral volumetric CT with single-breathhold technique, continuous transport, and continuous scanner rotation
<i>W.A. Kalender, W. Seißler, E. Klotz, P. Vock</i> | 64 |

2 Magnetic Resonance Imaging

- | | | |
|-----|--|-----|
| 2.1 | Measurement of nuclear spin by the method of molecular beams
<i>I.I. Rabi, V.W. Cohen</i> | 73 |
| 2.2 | Nuclear Induction
<i>F. Bloch, W.W. Hansen, M.E. Packard</i> | 81 |
| 2.3 | Resonance absorption by nuclear magnetic moments in a solid
<i>E.M. Purcell, H.C. Torrey, R.V. Pound</i> | 84 |
| 2.4 | Tumor detection by nuclear magnetic resonance
<i>R.V. Damadian</i> | 87 |
| 2.5 | Image Foundation by induced local interactions: Example employing nuclear magnetic resonance
<i>P.C. Lauterbur</i> | 93 |
| 2.6 | Planar spin imaging by NMR
<i>P. Mansfield, A.A. Maudsley</i> | 96 |
| 2.7 | Medical Imaging by NMR
<i>P. Mansfield, A.A. Maudsley</i> | 103 |

2.8	Human whole body line scan imaging by NMR	111
	<i>P. Mansfield, I.L. Pykett, P.G. Morris, R.E. Coupland</i>	
2.9	NMR imaging of the brain in multiple sclerosis	114
	<i>I.R. Young, A.S. Hall, C.A. Pallis et al.</i>	
2.10	MRI: Clinical use of the inversion recovery sequence	119
	<i>G.M. Bydder, I.R. Young</i>	

3 Ultrasound

3.1	Über die Möglichkeit, hochfrequente mechanische Schwingungen als diagnostische Mittel zu verwerten	144
	<i>K.T. Dussik</i>	
3.2	The application of echo ranging techniques to the detection of structure of biological tissues	162
	<i>J.J. Wild, J.M. Reid</i>	
3.3	The use of ultrasonic Reflectoscope for the continuous recording of the movements of heart walls	170
	<i>I. Edler, C.H. Hertz</i>	
3.4	The ultrasonic visualization of soft tissue structures in the human body	193
	<i>J.H. Holmes, D.H. Howry, G.J. Posakony, C.R. Cushman,</i>	
3.5	Investigation of Abdominal Masses by Pulsed Ultrasound	213
	<i>I. Donald, J. MacVicar, T.G. Brown</i>	
3.6	Ultrasonic Doppler method for the inspection of cardiac functions	224
	<i>S. Satomura</i>	
3.7	Neue Möglichkeiten der Ultraschalldiagnostik in der Gynäkologie und Geburtshilfe	230
	<i>D. Hofmann, H.-J. Holländer, P. Weiser</i>	
3.8	The prediction of fetal maturity by ultra-sonic measurement of the biparietal diamenter	236
	<i>S. Campbell</i>	
3.9	Development of an ultrasonic system for three-dimensional reconstruction of the fetus	245
	<i>K. Baba, K. Satoh, S. Sakamoto, T. Okai, S. Ishii</i>	

4 Digital Imaging

- | | | |
|-----|---|-----|
| 4.1 | Digital Processing of Videoangiocardigraphic Image Series
<i>R. Brennecke, T.K. Brown, J.H. Bürsch, P.H. Heintzen</i> | 257 |
| 4.2 | Computerized fluoroscopy in real time for noninvasive visualization of the cardiovascular system
<i>R.A. Kruger, C.A. Mistretta, S.J. Riederer, C.G. Shaw et al.</i> | 266 |
| 4.3 | Intravenous angiography using digital video subtraction: X-ray imaging system
<i>T.W. Ovitt, P.C. Christenson, H.D. Fisher 3rd, M.M. Frost, S. Nudelman, H. Roehrig</i> | 278 |
| 4.4 | Computed radiography utilizing scanning laser stimulated luminescence
<i>M. Sonoda, M. Takano, J. Miyahara, H. Kato</i> | 289 |
| 4.5 | Digital radiography of the chest: clinical experience with a prototype unit
<i>R.G. Fraser, E. Breatnach, G.T. Barnes</i> | 298 |
| 4.6 | A new digital detector for projection radiography
<i>D.L. Lee, L.K. Cheung, L.S. Jeromin</i> | 304 |
| 4.7 | X-ray imaging using amorphous selenium: Feasibility of a flat panel self-scanned detector for digital radiology
<i>W. Zhao, J.A. Rowlands</i> | 319 |

5 PACS

- | | | |
|-----|---|-----|
| 5.1 | Applications of Picture Processing, Image Analysis and Computer Graphics Techniques to Cranial CT Scans
<i>H.U. Lemke, H.S. Stiehl, H. Scharnweber, D. Jackél</i> | 334 |
| 5.2 | An All-digital Nuclear Medicine Department
<i>J.A. Parker, H.D. Royal, R.F. Uren, D. Front, J.G. Bliss, M. Rabussi, D. Jansons, M.S. Kolodny, G.M. Kolodny</i> | 349 |
| 5.3 | Digital Radiology at the University of California, Los Angeles: A Feasibility Study
<i>H.K. Huang, Z. Barbaric, N.J. Mankovich, C. Moler</i> | 358 |
| 5.4 | Assessment of the Integration of HIS/RIS with a PACS
<i>B.A. Levine, S.K. Mun, H.R. Benson, S.C. Horii</i> | 367 |
| 5.5 | Environmental Designs for Reading from Imaging Workstations: Ergonomic and Architectural Features
<i>S.C. Horii et al.</i> | 377 |

6 Contrast Agents

- | | | |
|-----|---|-----|
| 6.1 | Contrast agent design. Some aspects on the synthesis of water-soluble contrast agents of low osmolality
<i>T. Almén</i> | 391 |
| 6.2 | Development of nonionic contrast media
<i>T. Almén</i> | 403 |
| 6.3 | Intravenous chelated gadolinium as a contrast agent in NMR imaging of cerebral tumours
<i>D.H. Carr, J. Brown, G.M. Bydder, H.-J. Weinmann, U. Speck, D.J. Thomas, I.R. Young</i> | 412 |
| 6.4 | Characteristics of gadolinium-DTPA complex: a potential NMR contrast agent
<i>H.-J. Weinmann, R.C. Brasch, W.-R. Press, G.E. Wesbey</i> | 416 |
| 6.5 | Contrast-enhanced NMR imaging: animal studies using gadolinium-DTPA complex
<i>R.C. Brasch, H.-J. Weinmann, G.E. Wesbey</i> | 423 |

7 Angiography and Interventional Radiology

- | | | |
|-----|---|-----|
| 7.1 | Catheter replacement of the needle in percutaneous arteriography: A new technique
<i>S.I. Seldinger</i> | 437 |
| 7.2 | Percutaneous trocar (needle) nephrostomy in hydronephrosis
<i>W.E. Goodwin, W.C. Casey, W. Woolf</i> | 447 |
| 7.3 | Cine coronary arteriography
<i>F.M. Sones, E.K. Shirey, W.L. Proudfit, R. Westcott</i> | 452 |
| 7.4 | Mesenteric Arteriography
<i>A.R. Margulis, P. Heinbecker</i> | 455 |
| 7.5 | Transluminal treatment of arteriosclerotic obstruction: description of a new technique and a preliminary report of its application
<i>C.T. Dotter, M.P. Judkins</i> | 467 |
| 7.6 | Selective coronary arteriography
<i>M.P. Judkins</i> | 485 |
| 7.7 | Non-operative retained biliary tract stone extraction. A new roentgenologic technique
<i>H.J. Burhenne</i> | 496 |
| 7.8 | Perkutane Rekanalisation chronischer arterieller Verschlüsse mit einem neuen Dilatationskatheter
<i>A.R. Grüntzig, H. Hopff</i> | 509 |

7.9	Transluminal dilatation of coronary-artery stenosis <i>A.R. Grüntzig</i>	514
7.10	Percutaneous biliary drainage, technical and catheter related problems in 200 procedures <i>P.R. Mueller, E. van Sonnenberg, J.T. Ferrucci</i>	516
7.11	Expandable intrahepatic portacaval shunt stents: early experience in the dog <i>J.C. Palmaz, R.R. Sibbitt, S.R. Reuter et al.</i>	525
7.12	Intravascular stents to prevent occlusion and restenosis after transluminal angioplasty <i>U. Sigwart, J. Puel et al.</i>	531

8 Mammography

8.1	Diagnóstico de los tumores de la mama por la radiografía simple <i>R. Leborgne</i>	545
8.2	La radiographie de la glande mammaire <i>C.M. Gros, R. Sigrist</i>	564
8.3	Experience with mammography in tumor institution: evaluation of 1000 studies <i>R.L. Egan</i>	608
8.4	Evaluation of periodic breast cancer screening with mammography. Methodology and early observations <i>S. Shapiro, L. Venet, P. Strax</i>	616
8.5	Xerography of the breast <i>J.N. Wolfe</i>	626
8.6	Reduction in mortality from breast cancer after mass screening with mammography <i>L. Tabár, C.J.G. Fagerberg, A. Gad, L. Baldetorp, L.H. Holmberg, O. Gröntoft et al.</i>	635
8.7	Mammographic Microcalcifications: Detection with Xerography, Screen-Film, an Digitized Film Display <i>R.L. Smathers et al.</i>	645
8.8	Breast imaging: Dual-energy projection radiography with digital radiography <i>T. Asaga, S. Chiyasu, S. Matsuda, H. Mastuura, H. Kato, M. Ishida, T. Komaki</i>	651
8.9	Stereotactic breast biopsy with a biopsy gun <i>S.H. Parker, J.D. Lovin, W.E. Jobe, J.M. Luethke, K.D. Hopper, W.F. Yakes, B.J. Burke</i>	656
	References	665

Authors Index

- Almén T 392, 403
Ambrose J 39
Asaga T 654
- Baba K 246
Baldetorp L 637
Barbaric Z 360
Barnes GT 299
Benson HR 369
Bliss JG 352
Bloch F 83
Brasch RC 417, 425
Breatnach E 299
Brennecke R 259
Brown BW 646
Brown J 413
Brown TG 217
Brown TK 259
Burhenne HJ 497
Burke BJ 657
Bürsch JH 259
Bush E 646
Bydder GM 115, 120, 413
- Campbell S 236
Carr DH 413
Casey WC 448
Cheung LK 307
Chiyasu S 654
Christenson PC 281
Cohen VW 75
Cormack AM 24
Coupland RE 112
Crummy AB 269
Cushman CR 197
- Damadian RV 89
Donald I 217
Dotter CT 468
Drace J 646
Dussik KT 146
- Edler I 174
Egan RL 609
- Fagerberg CJG 637
Ferrucci JT 518
Fisher HD 3rd 281
- Flemming D 269
Fraser RG 299
Front D 352
Frost MM 281
- Gad A 637
Goodsitt MM 269
Goodwin WE 448
Gröntoft O 637
Gros CM 565
Grüntzig AR 510, 515
- Hall AS 115
Hansen WW 83
Heinbecker P 456
Heintzen PH 259
Hertz CH 174
Hofmann D 231
Holländer H-J 231
Holmberg LH 637
Holmes JH 197
Houk TL 269
Hopff H 510
Hopper KD 657
Horii SC 369, 378
Hounsfield GN 31
Howry DH 197
Huang HK 360
- Ishida M 654
Ishii S 246
- Jackél D 335
Jansons D 352
Jeromin LS 307
Jobe WE 657
Joffre F 532
Judkins MP 468, 486
- Kalender WA 66
Kappenberger L 532
Karras B 646
Kato H 292
Kato H 654
Klotz E 66
Kolodny GM 352
Kolodny MS 352
Komaki T 654
Kruger RA 269

-
- Lancaster JC 269
Lauterbur PC 94
Leborgne R 546
Lee DL 307
Legg NJ 115
Lemke HU 335
Levine BA 369
Ljungquist U 637
Lovin JD 657
Luethke JM 657
Lundström B 637

MacVicar J 217
Mankovich NJ 360
Mansfield P 98, 104, 112
Månson JC 637
Margulis AR 456
Mastuura H 654
Matsuda S 654
Maudsley AA 98, 104
Mirkovitch V 532
Mistretta CA 269
Miyahara J 292
Moler C 360
Morris PG 112
Mueller PR 518
Mun SK 369

Nudelman S 281

Okai T 246
Ovitt TW 281

Packard ME 83
Pallis CA 115
Palmaz JC 526
Parker JA 352
Parker SH 657
Posakony GJ 197
Pound RV 85
Press WR 417
Proudfit WL 453
Puel J 532
Purcell EM 85
Pykett IL 112

Rabi II 75
Rabussi M 352
Radon J 6
Reid JM 166
Reuter SR 526
Riederer SJ 269
Roehrig H 281

Rowe GG 269
Rowlands JA 321
Royal HD 352

Sakamoto S 246
Satoh K 246
Satomura S 225
Scharnweber H 335
Seißler W 66
Seldinger SI 438
Shapiro S 617
Shaw CG 269
Shirey EK 453
Sibbitt RR 526
Sigrist R 565
Sigwart U 532
Smathers RL 646
Sommer FG 646
Sonnenberg E, van 518
Sones FM 453
Sonoda M 292
Speck U 413
Steiner RE 115
Stevens M 646
Stiehl HS 335
Strax P 617

Tabár L 637
Takano M 292
Tio FO 526
Torrey HC 85

Uren RF 352

Venet L 617
Vock P 66

Weinmann HJ 413
Weinmann HJ 413, 417, 425
Weiser P 231
Wesbey GE 417, 425
Westcott R 453
Wild JJ 166
Wolfe JN 626
Woolf W 448

Yakes WF 657
Young IR 115
Young IR 115, 112, 413
Young IR 413

Zhao W 321
Zwiebel W 269

1 Computer Tomography

- | | | |
|------------|---|----|
| 1.1 | Über die Bestimmung von Funktionen durch ihre Integralwerte längs gewisser Mannigfaltigkeiten.
Ber. Sächs. Akad. Wiss 69 (1917): 262–277
<i>J. Radon</i> | 5 |
| 1.2 | Representation of a function by its line integrals, with some radiological applications.
Journal Applied Physics 34 (1964): 2722–2727
<i>A.M. Cormack</i> | 23 |
| 1.3 | Computerized transverse axial scanning (tomography). Part I. Description of system.
British Journal of Radiology 46 (1973): 1016–1022
<i>G.N. Hounsfield</i> | 30 |
| 1.4 | Computerized transverse axial scanning (tomography). Part II. Clinical application.
British Journal of Radiology 46 (1973): 1023–1047
<i>J. Ambrose</i> | 38 |
| 1.5 | Spiral volumetric CT with single-breathhold technique, continuous transport, and continuous scanner rotation.
Radiology 176 (1990): 181–183
<i>W.A. Kalender, W. Seifler, E. Klotz, P. Vock</i> | 64 |

Introduction

The history of the development of computerized axial tomography is complex [1]. James Bull, the pioneer neuroradiologist, reviewed the history of computed tomography and says that seldom in the history of medicine has a new discovery swept the world quite so quickly as computed tomography [2]. Godfrey Hounsfield and Alan Cormack received the Nobel Prize jointly in 1979 “for the development of computer-assisted tomography.”

In the 1960s Godfrey Hounsfield was working at EMI Ltd in Middlesex. He was interested in pattern recognition and also in computers. He had worked on radar with the RAF in the Second World War and had built the first solid-state electronic computer in the UK. Hounsfield was looking at internal structure and considered a closed box with an unknown number of items inside. The box could be looked at from many directions using an X-ray source and a radiation detector. The results of the transmission readings could then be analyzed by the computer and then presented three-dimensionally as a series of slices in a single plane. Hounsfield developed a mathematical approach to determine the nature of the objects in the box in a process of reconstruction.

Hounsfield then looked at practical applications of the technique and approached the Department of Health in London. If a medical use could be found

then this would stimulate the development of the project. Hounsfield met Mr Gregory and Mr Higson, who were scientific advisers. Hounsfield was then introduced to Dr Ewan Lennon, a radiological adviser to the Department of Health. Lennon knew that Dr (later Professor) Frank Doyle from the Hammersmith Hospital was looking at bone density measurements. Frank Doyle gave Hounsfield two lumbar vertebrae of different densities. Hounsfield examined the vertebrae and returned to Doyle with computer printouts of numbers in the coronal plane of the vertebral body. Hounsfield had already worked out a scale of numbers and Doyle was impressed with the result. It was a recurring theme with Hounsfield even after the development of the EMI scanner that he preferred the computer printout of numbers to a pictorial presentation of the data. Lennon also made contact with two other radiologists. These were Dr James Ambrose and Dr Louis Kreel. James Ambrose was a neuroradiologist from Atkinson Morley's Hospital in South London and Louis Kreel was from the Royal Free Hospital, subsequently moving to Northwick Park Hospital in Harrow. It became apparent that EMI would not spend any more money on developing the new technique without the support and a contribution from the Department of Health. Lennon and Higson reported to the Department of Health, who agreed to the necessary support. The three radiologists then worked more closely with EMI. Frank Doyle supplied bone specimens, James Ambrose supplied brain specimens and Louis Kreel supplied abdominal specimens. Work continued on specimen radiography and then on the 14th January 1970 there was a meeting at the Department of Health between the three radiologists and Dr Lennon, Mr Gregory and Mr Higson. The initial results were very promising and it was agreed to produce a prototype machine. Because of the difficulties of abdominal scanning it was agreed that the prototype would be a brain machine. This was to be at Atkinson Morley's Hospital [3]. Atkinson Morley's hospital had several advantages. The hospital was quite close to EMI, the scanner could be placed in a discreet location and patients could be examined without too much advertisement and the department had an innovative approach to radiological practice. James Ambrose developed a close relationship with Godfrey Hounsfield. The prototype scanner was installed in the hospital on the 1 October 1971. The scanning time was 4 min per slice with a slice thickness of a little over 1 cm. There was no computer attached to the machine and the data were taken on magnetic tape to be analyzed by EMI. Ambrose had felt that at least 6 months of work would be needed to build up an appreciation of the normal and abnormal. The first patient was a 41-year-old lady with a possible frontal lobe tumour. The data was acquired and the tapes were sent to EMI. The results were returned after 2 days. The tumour in the frontal lobe was clearly shown, and Ambrose said the result caused Hounsfield and himself to jump up and down like football players who had just scored a winning goal. Radiology was changed forever.

The results were presented at the 32nd Annual Congress of the British Institute of Radiology, which was held at Imperial College in April 1972. The session was held on the afternoon of Thursday 20 April, chaired by George du Boulay, and was entitled 'New Techniques for Diagnostic Radiology.' The paper presented by Ambrose and Hounsfield was entitled "Computerised axial tomography (A new means of demonstrating some of the soft tissue structures of the brain without the use of contrast media)." As might be expected the paper produced a sensation and the first press announcement was in *The Times* on 21 April 1972. The presentation appeared as an abstract in the *British Journal of Radiology* [4] with three papers appearing later that year. The first paper by Hounsfield [5] described the technical background, the second paper was by Ambrose [6] and described the clinical findings, and the third paper by Perry and Bridges [7] looked at radiation doses. EMI then started the production of a brain machine and made five: one for the National Hospital, Queen Square, one for Manchester, one for Glasgow and

two for the United States, one for the Mayo Clinic and the other for the Massachusetts General Hospital. All machines were installed in the summer of 1973. James Bull described the new machine to Dr Fred Plum, a leading American neurologist. Plum said that United States would need at least 170 brain machines to cover the neurology departments and that it would soon become unethical for a neurologist to practice without access to a brain machine since it saved many patients from unnecessary suffering from the currently available techniques. Ambrose also looked at the use of the new scanner in orbital lesions which were previously difficult to image [8].

Whilst the new scanner was obviously effective it was also very expensive. EMI had various problems, which Melvyn Marcus outlined in the *Sunday Telegraph* of 30 July, 1978 in an article entitled 'It's crisis time for scanners.' The difficulties that EMI experienced were from two directions. Firstly, competition from other companies: there were several court cases for patent infringements, including a suit filed by EMI against Ohio-Nuclear in 1976 and Pfizer in 1977. However, more significant was the clampdown on hospital expenditure in the United States under the administration of President Jimmy Carter. America was the largest market for the EMI scanner and hospitals had to meet very rigorous conditions to be able to undertake any major capital expenditure.

However, in spite of the problems experienced by EMI and the EMI scanner, CT has continued to develop.

The award of the Nobel Prize for Medicine and Physiology to Godfrey Hounsfield and Alan Cormack in 1979 emphasised the arrival of the new technique. Alan Cormack had developed the mathematical basis of CT scanning [9] but he had worked independently from Godfrey Hounsfield. Cormack had developed a mathematical approach to looking at the problems of variations in body tissues that are important in radiotherapy. At the time there was no commercial interest and the subject was not pursued. There were a number of workers looking at the same area, for example Oldendorf and David Kuhl [10]. Cormack became aware of the pioneering work of Radon only in the late 1970s [11]. Radon had stated that if the line integrals of a particular property of an object, such as its density, could be known for all lines intersecting a slice of an object and coplanar with the slice then the density can be reconstructed exactly. Cormack then considered how many measurements need be made since only a finite number of measurements can be made with beams of a finite width. It is very salutary to observe the number of disconnected workers considering the same problem but coming from quite different directions.

References

1. Webb S (1990) From the watching of shadows. The origins of radiological tomography. Adam Hilger, Bristol and New York
2. Bull J (1981) History of computed tomography. In: Newton TH, Potts DG (eds) Radiology of the skull and brain: technical aspects of computed tomography. Mosby: St Louis. Pp 3835-3852
3. Ambrose J (1996) You never know what is just around the corner. Rivista di Neuroradiologia 9: 399-404
4. Ambrose J, Hounsfield G (1973) Computerised transverse axial tomography. British Journal of Radiology 46: 148-149
5. Hounsfield GN (1973) Computerized transverse axial scanning (tomography). Part 1. Description of system. British Journal of Radiology 46: 1016-1022
6. Ambrose J (1973) Computerized transverse axial scanning (tomography). Part 2. Clinical application. British Journal of Radiology 46: 1023-1047
7. Perry BJ, Bridges C (1973) Computerized transverse axial scanning (tomography). Part 3. Radiation dose considerations. British Journal of Radiology 46: 1048-1051

8. Ambrose JAE, Lloyd GAS, Wright JE (1974) A preliminary evaluation of fine matrix computerized axial tomography (Emiscan) in the diagnosis of orbital space-occupying lesions. *British Journal of Radiology* 47: 747-751
9. Cormack AM (1964) Representation of a function by its line integrals, with some radiological applications. *Journal Applied Physics* 34: 2722-2727
10. Friedland W, Thurber BD (1996) The birth of CT. *American Journal of Radiology* 167:1365-1370
11. Cormack AM (1978) Sampling the Radon transform with beams of finite width. *Physics in Medicine and Biology*. 23: 1141-1148

Spiral CT

Spiral CT represents a significant advance in the technology of CT scanning and has significantly increased the clinical value of CT. The first clinical cases and performance measurements were presented as work in progress by Willi Kalender, Peter Vock and Wolfgang Seissler at the 75th anniversary meeting of the Radiological Society of North America in 1989 [1, 2]. The technique was then fully described in a paper in *Radiology* in 1990 which is our classic paper [3].

The development of spiral CT was made possible by the advances in computing. Data no longer have to be taken away for analysis but can be reconstructed almost instantaneously. In spiral CT, the X-ray source rotation and the patient table translation are made simultaneously and so the time for acquisition of the raw data is significantly reduced. Compared to conventional CT scanning, spiral CT scanning adds two parameters. These are the helical pitch and the reconstruction interval. The pitch can be defined as the ratio between the table increment and the detector collimation. The reconstruction interval is the longitudinal interval between reconstructed adjacent slices. The principles of spiral CT have been well reviewed by Vannier and Wang [4].

Willi Kalender has recently reviewed the use of spiral CT [5] and describes the amazing results that can be achieved by modern scanners. We now have improved spatial resolution with virtual endoscopy and faster scanning enabling complex dynamic studies. The most dramatic improvement was made because of the provision of higher continuous X-ray power. Kalender finishes his article with the words: "Predictions are particularly difficult when they are concerned with the future." In looking at the development of CT we have to agree with him.

References

1. Vock P, Jung H, Kalender WA (1989) Single-breathhold volumetric CT of the hepatobiliary System. *Radiology* 173(P): 377
2. Kalender WA, Seissler W, Vock P (1989) Single-breath-hold spiral volumetric CT by continuous patient translation and scanner rotation. *Radiology* 173 (P): 414
3. Kalender WA, Seissler W, Klotz E, Vock P (1990) Spiral volumetric CT with single-breath-hold technique, continuous transport, and continuous scanner rotation. *Radiology* 176: 181-18
4. Vannier MW, Wang G (1996) Principles of spiral CT. In: Rémy-Jardin M, Rémy J (eds) *Spiral CT of the Chest*. Springer, Berlin Heidelberg New York, pp1-32
5. Kalender WA (1996) Spiral CT in the year 2000. In: Rémy-Jardin M, Rémy J (eds) *Spiral CT of the Chest*. Springer, Berlin Heidelberg New York, pp322-329

1.1 Über die Bestimmung von Funktionen durch ihre Integralwerte längs gewisser Mannigfaltigkeiten

Johann Radon (1887–1956)

Johann Radon was born on December 16th 1887 in Tetschen, Bohemia (now Decin in the Czech Republic). He attended school in Leitmeritz (now Litomerice) in Bohemia. In 1905 he entered the University of Vienna and studied mathematics and physics. Radon obtained his PhD in 1910 with a dissertation on the calculus of variations.

In 1911 he lived in Goettingen in Germany for one year. Between 1912 and 1919 Radon became assistant professor for mathematics at the Department for Mathematics at the Technische Hochschule Wien (Technical University Vienna, Austria).

In 1919 Radon became assistant professor at the University of Hamburg and in 1922 was appointed full professor of mathematics in Greifswald, Germany. In 1925 he moved to the Friedrich-Alexander University in Erlangen and from 1928 to 1945 he was at the University of Breslau. On 1 October 1946 Radon was appointed full Professor for Mathematics at the University of Vienna. He was appointed dean of the philosophical faculty in 1951 and rector of the University of Vienna in 1956.

Johann Radon applied the calculus of variations to differential geometry, leading to applications in number theory. In 1917 he published his fundamental work on the “Radon transform,” which mathematically transforms two-dimensional images with lines into a domain of possible line parameters, where each line in the image will give a peak positioned at the corresponding line parameters. This idea of reconstructing a function from a set of projections plays a large role in the development of computed tomography.

In honor of the great mathematician, the Austrian Academy of Sciences inaugurated the Johann Radon Institute for Computational and Applied Mathematics (RICAM) on the University Campus of the Johannes Kepler University Linz, Austria.

Johann Radon died after a five-month illness on 25 May 1956.



BERICHTE
ÜBER DIE
VERHANDLUNGEN

DER KÖNIGLICH SÄCHSISCHEN
GESELLSCHAFT DER WISSENSCHAFTEN
ZU LEIPZIG.

MATHEMATISCH-PHYSISCHE KLASSE.
NEUNUNDSECHZIGSTER BAND.

1917.

MIT 86 FIGUREN IM TEXT
UND 1 LICHTDRUCKTAFEL.

LEIPZIG
BEI B. G. TEUBNER.



SITZUNG VOM 30. APRIL 1917.

Über die Bestimmung von Funktionen durch ihre Integralwerte längs gewisser Mannigfaltigkeiten.

Von

JOHANN RADON.

Integriert man eine geeigneten Regularitätsbedingungen unterworfenen Funktion zweier Veränderlichen x, y — eine *Punktfunktion* $f(P)$ in der Ebene — längs einer beliebigen Geraden g , so erhält man in den Integralwerten $F(g)$ eine *Geradenfunktion*. Das in Abschnitt A vorliegender Abhandlung gelöste Problem ist die Umkehrung dieser linearen Funktionaltransformation, d. h. es werden folgende Fragen beantwortet: kann jede, geeigneten Regularitätsbedingungen genügende Geradenfunktion auf diese Weise entstanden gedacht werden? Wenn ja, ist dann f durch F eindeutig bestimmt und wie kann es ermittelt werden?

Im Abschnitte B gelangt das dazu in gewisser Hinsicht duale Problem der Bestimmung einer Geradenfunktion $F(g)$ aus ihren Punktmittelwerten $f(P)$ zur Lösung.

Schließlich werden im Abschnitte C gewisse Verallgemeinerungen kurz besprochen, zu denen insbesondere die Betrachtung nichteuklidischer Mannigfaltigkeiten sowie höherer Räume Anlaß gibt.

Die Behandlung dieser an sich interessanten Probleme gewinnt ein erhöhtes Interesse durch die zahlreichen Beziehungen, die zwischen diesem Gegenstande und der Theorie des logarithmischen und NEWTONSchen Potentials bestehen, auf die an den bezüglichen Stellen zu verweisen sein wird.

A. Bestimmung einer Punktfunktion in der Ebene aus ihren geradlinigen Integralwerten.

1. Es sei $f(x, y)$ eine für alle reellen Punkte $P = [x, y]$ erklärte reelle Funktion, die folgende Regularitätsbedingungen erfülle:

a₁) $f(x, y)$ sei stetig.

b₁) Es konvergiere das über die ganze Ebene zu erstreckende Doppelintegral

$$\iint \frac{|f(x, y)|}{\sqrt{x^2 + y^2}} dx dy.$$

c₁) Wird für einen beliebigen Punkt $P = [x, y]$ und jedes $r \geq 0$

$$\bar{f}_P(r) = \frac{1}{2\pi} \int_0^{2\pi} f(x + r \cos \varphi, y + r \sin \varphi) d\varphi$$

gesetzt, so gelte für jeden Punkt P :

$$\lim_{r \rightarrow \infty} \bar{f}_P(r) = 0.$$

Dann gelten folgende Sätze:

Satz I: Der geradlinige Integralwert von f für die Gerade g mit der Gleichung $x \cos \varphi + y \sin \varphi = p$, der durch

$$(I) \quad F(p, \varphi) = F(-p, \varphi + \pi) = \int_{-\infty}^{+\infty} f(p \cos \varphi - s \sin \varphi, p \sin \varphi + s \cos \varphi) ds$$

gegeben ist, ist „im allgemeinen“ vorhanden; das soll heißen: auf jedem Kreise bilden die Berührungspunkte jener Tangenten, für welche F nicht existiert, eine Menge vom linearen Maße Null:

Satz II: Bildet man den Mittelwert von $F(p, \varphi)$ für die Tangenten des Kreises mit dem Zentrum $P = [x, y]$ und dem Radius q :

$$(II) \quad \bar{F}_P(q) = \frac{1}{2\pi} \int_0^{2\pi} F(x \cos \varphi + y \sin \varphi + q, \varphi) d\varphi,$$

so konvergiert dieses Integral für alle P, q absolut.

Satz III: Der Wert von f ist durch F eindeutig bestimmt und läßt sich folgendermaßen berechnen:

$$(III) \quad f(P) = -\frac{1}{\pi} \int_0^\infty \frac{d\bar{F}_P(q)}{q}.$$

Dabei ist das Integral im STIELTJESSchen Sinne zu verstehen und kann auch durch die Formel:

$$(III') \quad f(P) = \frac{1}{\pi} \lim_{\varepsilon \rightarrow 0} \left(\frac{\bar{F}_P(\varepsilon)}{\varepsilon} - \int_{\varepsilon}^{\infty} \frac{\bar{F}_P(q)}{q^2} dq \right)$$

definiert werden.

Indem wir zum Beweise schreiten, bemerken wir vorweg, daß die Bedingungen $a_1 - c_1$ gegenüber Bewegungen der Ebene invariant sind. Wir können also den Punkt $[0, 0]$ immer als Repräsentanten irgendeines Punktes der Ebene betrachten.

Man erkennt nun das Doppelintegral:

$$(I) \quad \int \int_{x^2 + y^2 > q^2} \frac{f(x, y)}{\sqrt{x^2 + y^2 - q^2}} dx dy$$

als absolut konvergent. Vermöge der Transformation

$$x = q \cos \varphi - s \sin \varphi, \quad y = q \sin \varphi + s \cos \varphi$$

geht dasselbe über in:

$$\begin{aligned} & \int_0^{2\pi} d\varphi \int_0^{\infty} f(q \cos \varphi - s \sin \varphi, q \sin \varphi + s \cos \varphi) ds \\ &= \int_0^{2\pi} d\varphi \int_{-\infty}^0 f(q \cos \varphi - s \sin \varphi, q \sin \varphi + s \cos \varphi) ds, \end{aligned}$$

so daß man seinen Wert auch durch

$$\frac{1}{2} \int_0^{2\pi} d\varphi \int_{-\infty}^{+\infty} f(q \cos \varphi - s \sin \varphi, q \sin \varphi + s \cos \varphi) ds = \frac{1}{2} \int_0^{2\pi} F(q, \varphi) d\varphi$$

ausdrücken kann. Nach bekannten Eigenschaften der absolut konvergenten Doppelintegrale folgen hieraus die Behauptungen der Sätze I und II.

Um auf die Formel (III) zu kommen, kann man folgenden Weg einschlagen: Einführung von Polarkoordinaten in (I) liefert

$$\int_q^{\infty} dr \int_0^{2\pi} \frac{f(r \cos \varphi, r \sin \varphi)}{\sqrt{r^2 - q^2}} d\varphi$$

oder mit Hilfe der Mittelwertsbezeichnung von c_1 :

$$2\pi \int_q^\infty \frac{\bar{f}_0(r) dr}{\sqrt{r^2 - q^2}}.$$

Verglichen mit dem zuletzt erhaltenen Werte von (I) resultiert:

$$(2) \quad \bar{F}_0(q) = 2 \int_q^\infty \frac{\bar{f}_0(r) dr}{\sqrt{r^2 - q^2}}$$

Führt man in dieser Integralgleichung erster Art die Variablen $r^2 = v$, $q^2 = u$ ein, so kann man sie leicht nach Art der bekannten ABELSchen lösen und erhält die Formel (III) für

$$\bar{f}_0(0) = f(0, 0).$$

Bei dieser Ableitung erscheint es aber schwer, ohne weitere Bedingungen für f auszukommen, daher geben wir einer direkten Verifikation den Vorzug.

Zunächst ist, um die Gleichheit der Ausdrücke (III) und (III') zu zeigen, zu beweisen, daß:

$$\lim_{q \rightarrow \infty} \frac{\bar{F}_0(q)}{q} = 0.$$

Vermöge (2) ist

$$\begin{aligned} \left| \frac{\bar{F}_0(q)}{q} \right| &\leq \frac{2}{q} \left| \int_q^{2q} \frac{\bar{f}_0(r) dr}{\sqrt{r^2 - q^2}} \right| + \frac{2}{q} \left| \int_{2q}^\infty \frac{\bar{f}_0(r) r dr}{\sqrt{r^2 - q^2}} \right| \\ &\leq 2\sqrt{3} |\bar{f}_0(t)| + \frac{4}{\sqrt{3}} \int_{2q}^\infty |\bar{f}_0(r)| dr \quad (q < t < 2q) \end{aligned}$$

und dies konvergiert wegen b_1 und c_1 für $q \rightarrow \infty$ gegen Null.

Die rechte Seite von (III') geht nun durch Einführung von (2) über in:

$$\frac{2}{\pi} \lim_{\varepsilon \rightarrow 0} \left[\frac{1}{\varepsilon} \int_\varepsilon^\infty \frac{r \bar{f}_0(r)}{\sqrt{r^2 - \varepsilon^2}} dr - \int_\varepsilon^\infty \frac{dq}{q^2} \int_q^\infty \frac{r \bar{f}_0(r)}{\sqrt{r^2 - q^2}} dr \right]$$

Vertauscht man in dem zweiten Integral die Integrationsfolge, so kann man nach q integrieren, erkennt dabei das Integral als

absolut konvergentes Doppelintegral, was die Vertauschung rechtfertigt, und findet für obigen Ausdruck den Wert

$$\frac{2}{\pi} \lim_{\varepsilon \rightarrow 0} \int_{\varepsilon}^{\infty} \frac{\bar{f}_0(r)}{r \sqrt{r^2 - \varepsilon^2}} dr,$$

was tatsächlich $\bar{f}_0(0) = f(0, 0)$ liefert, wie unschwer zu zeigen ist.

2. Es sei $F(p, \varphi) = F(-p, \varphi + \pi)$ eine Geradenfunktion, die folgende Regularitätsbedingungen erfüllt:

a₂) F und die Ableitungen $F_p, F_{pp}, F_{ppp}, F_\varphi, F_{p\varphi}, F_{pp\varphi}$ seien für alle $[p, \varphi]$ stetig.

b₂) $F, F_\varphi, pF_p, pF_{p\varphi}$ und pF_{pp} konvergieren für $p \rightarrow \infty$ gleichmäßig in φ gegen Null.

c₂) Die Integrale:

$$\int_0^\infty F_{pp} lp dp, \quad \int_0^\infty F_{ppp} p lp dp, \quad \int_0^\infty F_{pp\varphi} p lp dp$$

konvergieren absolut und gleichmäßig in φ .

Dann können wir beweisen:

Satz IV: Bildet man nach (III) bzw. (III') $f(P)$, so erfüllt dieses die Bedingungen a₁, b₁, c₁ und liefert als geradlinige Integralwerte das vorgelegte $F(p, \varphi)$. Infolge Satz III ist es die einzige derartige Funktion.

Führen wir in (III) Polarkoordinaten ein, so ergibt sich:

$$\begin{aligned} f(\varrho \cos \psi, \varrho \sin \psi) &= -\frac{1}{2\pi^2} \int_0^\infty \frac{dp}{p} \int_0^{2\pi} F_p(\varrho \cos \omega + p, \omega + \psi) d\omega \\ &= \frac{1}{2\pi^2} \int_0^\infty lp dp \int_0^{2\pi} F_{pp}(p + \varrho \cos \omega, \omega + \psi) d\omega. \end{aligned}$$

Es ist nämlich:

$$\begin{aligned} \int_0^{2\pi} F_p(\varrho \cos \omega + p, \omega + \psi) d\omega &= \int_0^{2\pi} F_p(\varrho \cos \omega, \omega + \psi) d\omega \\ &\quad + \int_0^{2\pi} d\omega \int_0^p F_{pp}(\varrho \cos \omega + t, \omega + \psi) dt \end{aligned}$$

und der erste Bestandteil ist wegen $F(p, \varphi) = F(-p, \varphi + \pi)$ gleich Null. Deshalb konvergiert das Produkt des Integrals mit lp

für $p \rightarrow 0$ gegen Null. Auf Grund derselben Eigenschaft von F folgt weiter:

$$(3) \quad f(\varrho \cos \psi, \varrho \sin \psi) = \frac{1}{2\pi^2} \int_0^\pi d\omega \int_{-\infty}^{+\infty} F_{pp}(p, \omega + \psi) l |p - \varrho \cos \omega| dp.$$

Es genügt nun, wenn wir zeigen:

$$(4) \quad \int_{-\infty}^{+\infty} f(\varrho, 0) d\varrho = F\left(0, \frac{\pi}{2}\right),$$

da die Bedingungen $a_2 - c_2$ gegenüber Bewegungen invariant sind.

Wir setzen:

$$F(p, \varphi) = F\left(p, \frac{\pi}{2}\right) + \cos \varphi \cdot G(p, \varphi).$$

G genügt leicht angebbaren Regularitätsbedingungen. Es zerfällt nun dieser Zerlegung zufolge $f(\varrho, 0)$ in zwei Bestandteile $f_1(\varrho)$ und $f_2(\varrho)$, die getrennt zu untersuchen sind. Wegen:

$$\int_0^\pi l |p - \varrho \cos \omega| d\omega = \begin{cases} \pi l \frac{|p| + \sqrt{p^2 - \varrho^2}}{2}, & |p| > |\varrho| \\ \pi l \frac{|\varrho|}{2}, & |p| \leq |\varrho| \end{cases}$$

ergibt sich:

$$\begin{aligned} f_1(\varrho) &= \frac{1}{2\pi^2} \int_0^\pi d\omega \int_{-\infty}^{+\infty} F_{pp}\left(p, \frac{\pi}{2}\right) l |p - \varrho \cos \omega| dp \\ &= \frac{1}{2\pi} \int_{|\varrho|}^{\infty} F_{pp}\left(p, \frac{\pi}{2}\right) l \frac{|p| + \sqrt{p^2 - \varrho^2}}{|\varrho|} dp \\ &\quad + \frac{1}{2\pi} \int_{-\infty}^{-|\varrho|} F_{pp}\left(p, \frac{\pi}{2}\right) l \frac{|p| + \sqrt{p^2 - \varrho^2}}{|\varrho|} dp. \end{aligned}$$

Dies ist nun nach ϱ von $-\infty$ bis $+\infty$ absolut integrabel, wie durch Vertauschung der Integrationsfolge ersichtlich wird. Als Wert des Integrales erhält man:

$$\begin{aligned} \int_{-\infty}^{+\infty} f_1(\varrho) d\varrho &= \frac{1}{2\pi} \int_{-\infty}^{+\infty} F_{pp}\left(p, \frac{\pi}{2}\right) \int_{-|p|}^{+|p|} l \frac{|p| + \sqrt{p^2 - \varrho^2}}{|\varrho|} d\varrho dp \\ &= \frac{1}{2} \int_{-\infty}^{+\infty} F_{pp}\left(p, \frac{\pi}{2}\right) |p| dp = F\left(0, \frac{\pi}{2}\right) \end{aligned}$$

Was nun $f_2(q)$ anbelangt, so werden wir zeigen, daß es ebenfalls absolut integabel ist und von $-\infty$ bis $+\infty$ integriert Null ergibt.

Wir können nämlich $f_2(q)$ folgendermaßen schreiben:

$$\begin{aligned} f_2(q) &= \frac{1}{2\pi^2} \int_0^\pi d\omega \int_{-\infty}^{+\infty} G_{pp}(p, \omega) l |p - q \cos \omega| \cdot \cos \omega d\omega \\ &= \frac{1}{2\pi^2} \int_0^\pi d\omega \int_{-\infty}^{+\infty} G_{pp}(p, \omega) \left[l \left| \frac{p - q \cos \omega}{q \cos \omega} \right| \cos \omega + \frac{qp \cos^2 \omega}{1 + q^2 \cos^2 \omega} \right] dp, \end{aligned}$$

da die hinzugefügten Glieder integriert Null ergeben, und in dieser Gestalt führt die Integration nach q auf ein *absolut* konvergentes dreifaches Integral. Es ist nämlich:

$$\begin{aligned} &\int_{-\infty}^{+\infty} \left| \cos \omega l \left| \frac{p - q \cos \omega}{q \cos \omega} \right| + \frac{qp \cos^2 \omega}{1 + q^2 \cos^2 \omega} \right| dq \\ &= |p| \int_{-\infty}^{+\infty} \left| l \left| 1 - \frac{1}{\tau} \right| + \frac{p^2 \tau}{1 + p^2 \tau^2} \right| d\tau = \lambda(p) \end{aligned}$$

mit

$$\lim_{|p| \rightarrow \infty} \frac{\lambda(p)}{|p| l |p|} = 2.$$

Die Integration nach q liefert als Wert des Integrales:

$$\int_{-\infty}^{+\infty} f_2(q) dq = 0,$$

womit (4) bewiesen ist.

Wir haben noch zu zeigen, daß f den Forderungen a_1 — c_1 genügt.

Die Stetigkeit folgt aus der Darstellung (3) wegen der Voraussetzungen a_2 — c_2 . Forderung b_1 ist gleichfalls erfüllt, denn

$$\int_{-\infty}^{+\infty} |f(q \cos \psi, q \sin \psi)| dq$$

ist, wie man leicht sieht, nach ψ integrierbar.

Um noch c_1 nachzuweisen, bilden wir:

$$\begin{aligned}
 \bar{f}_0(\varrho) &= \frac{1}{2\pi} \int_0^{2\pi} f(\varrho \cos \psi, \varrho \sin \psi) d\varphi \\
 &= \frac{1}{4\pi^2} \int_0^\pi d\omega \int_0^{2\pi} d\psi \int_{-\infty}^{+\infty} F_{pp}(p, \psi) l |p - \varrho \cos \omega| dp \\
 &= \frac{1}{4\pi^2} \int_0^{2\pi} d\psi \left[\int_{-\infty}^{-|\varrho|} F_{pp}(p, \psi) l \frac{|p| + \sqrt{p^2 - \varrho^2}}{2} dp \right. \\
 &\quad \left. + \int_{|\varrho|}^{+\infty} F_{pp}(p, \psi) l \frac{|p| + \sqrt{p^2 - \varrho^2}}{2} dp \right. \\
 &\quad \left. + F_p(\varrho, \psi) l \frac{\varrho}{2} - F_p(\varrho, \psi) l \frac{\varrho}{2} \right],
 \end{aligned}$$

woraus man die Richtigkeit von c_1 erkennt. Damit ist Satz IV bewiesen.

B. Bestimmung einer Geradenfunktion aus ihren Punktmittelwerten.

3. $F(p, \varphi) = F(-p, \varphi + \pi)$ sei eine Geradenfunktion, die folgende Regularitätsbedingungen erfülle:

- a₃) F, F_φ, F_p seien stetig, $|F_\varphi| < M$ für alle p, φ .
- b₃) $F_p \cdot l |p|$ konvergiere für $p \rightarrow \infty$ gleichmäßig in φ gegen Null
- c₃) $\int_{-\infty}^{+\infty} |F_p| \cdot l |p| dp$ konvergiere gleichmäßig in φ .

Diese Bedingungen sind wieder gegenüber Bewegungen invariant.

Wir bilden den Punktmittelwert von $F(p, \varphi)$ für $P = [x, y]$:

$$(5) \quad f(x, y) = \frac{1}{\pi} \int_{-\frac{\pi}{2}}^{+\frac{\pi}{2}} F(x \cos \varphi + y \sin \varphi, \varphi) d\varphi.$$

270

JOHANN RADON:

Dann gilt:

Satz V: Durch Angabe von f ist F eindeutig bestimmt und zwar ist:

$$(V) \quad F\left(0, \frac{\pi}{2}\right) = -\frac{1}{2\pi} \int_{-\infty}^{+\infty} \frac{dx}{x} \int_{-\infty}^{+\infty} f_x(x, y) dy,$$

wo das Integral nach x als CAUCHYScher Hauptwert zu deuten ist und der Wert von F für irgendeine andere Gerade aus der angegebenen Formel durch eine entsprechende Bewegung abgeleitet werden kann.

Zum Beweise leiten wir aus (5) zunächst ab:

$$(6) \quad \int_{-A}^B f_x(x, y) dy = \frac{1}{\pi} \int_{-\frac{\pi}{2}}^{+\frac{\pi}{2}} d\varphi \int_{-A}^B F_p(x \cos \varphi + y \sin \varphi, \varphi) \cos \varphi dy,$$

wo A, B zwei positive Konstante sind.

Wir setzen nun, wie schon früher analog geschehen ist:

$$F(p, \varphi) = F(p, 0) + \sin \varphi G(p, \varphi),$$

wobei $G(p, \varphi)$ im Integrationsgebiete beschränkt bleibt und für $p \rightarrow \infty$ den Grenzwert Null erhält. Aus:

$$\begin{aligned} & \int_{-A}^B G_p(x \cos \varphi + y \sin \varphi, \varphi) \cos \varphi \cdot \sin \varphi dy \\ &= [G(x \cos \varphi + B \sin \varphi, \varphi) - G(x \cos \varphi - A \sin \varphi, \varphi)] \cos \varphi \end{aligned}$$

folgt, daß der zweite Bestandteil von (6) für $A \rightarrow \infty, B \rightarrow \infty$ den Grenzwert Null erhält, so daß nur der erste zu untersuchen bleibt. Durch die analoge Integration erkennt man, daß in diesem ersten Bestandteil das Integral nach φ über jedes $\varphi = 0$ nicht enthaltende Intervall für $A \rightarrow \infty, B \rightarrow \infty$ ebenfalls Null wird; es bleibt also zu betrachten:

$$\lim_{\substack{A \rightarrow \infty \\ B \rightarrow \infty}} \frac{1}{\pi} \int_{-\varepsilon}^{+\varepsilon} d\varphi \int_{-A}^B F_p(x \cos \varphi + y \sin \varphi, 0) \cos \varphi dy, \quad 0 < \varepsilon < \frac{\pi}{2}.$$

Man kann dieses Integral schreiben:

$$\frac{1}{\pi} \int_{-\varepsilon}^{+\varepsilon} d\varphi \int_{x \cos \varphi - A \sin \varphi}^{x \cos \varphi + B \sin \varphi} F_p(p, 0) \operatorname{ctg} \varphi dp$$

und erhält daraus, wenn A und B genügend groß angenommen werden, durch Vertauschung der Integrationsfolge nach einiger Rechnung den Wert:

$$\begin{aligned} & \frac{1}{\pi} \int_{x \cos \varepsilon - B \sin \varepsilon}^{x \cos \varepsilon + B \sin \varepsilon} l \frac{(B^2 + x^2) \sin \varepsilon}{|Bp - x \sqrt{B^2 + x^2 - p^2}|} F_p(p, 0) dp \\ & + \frac{1}{\pi} \int_{x \cos \varepsilon - A \sin \varepsilon}^{x \cos \varepsilon + A \sin \varepsilon} l \frac{(A^2 + x^2) \sin \varepsilon}{|Ap - x \sqrt{A^2 + x^2 - p^2}|} F_p(p, 0) dp. \end{aligned}$$

Es genügt, den Grenzwert des zweiten Integrales für $A \rightarrow \infty$ zu ermitteln. Wir schreiben es so:

$$\begin{aligned} & \frac{1}{\pi} l(A \sin \varepsilon) [F(x \cos \varepsilon + A \sin \varepsilon, 0) - F(x \cos \varepsilon - A \sin \varepsilon, 0)] \\ & + \frac{1}{\pi} \int_{x \cos \varepsilon - A \sin \varepsilon}^{x \cos \varepsilon + A \sin \varepsilon} l \frac{1}{|p - x|} F_p(p, 0) dp \\ & + \frac{1}{\pi} \int_{x \cos \varepsilon - A \sin \varepsilon}^{x \cos \varepsilon + A \sin \varepsilon} l \frac{|Ap + x \sqrt{A^2 + x^2 - p^2}|}{A |p + x|} F_p(p, 0) dp. \end{aligned}$$

Da der Logarithmus in dem letzten Integral für $A \rightarrow \infty$ *gleichmäßig* gegen Null geht, so folgt als Grenzwert:

$$- \frac{1}{\pi} \int_{-\infty}^{+\infty} F_p(p, 0) l |p - x| dp,$$

womit der Grenzwert von (6) erhalten wird:

$$\int_{-\infty}^{+\infty} f_x(x, y) dy = - \frac{2}{\pi} \int_{-\infty}^{+\infty} F_p(p, 0) l |p - x| dp.$$

Es mag hier bemerkt werden, daß letzterer Ausdruck die Randwerte des Imaginärteils einer in der oberen Halbebene regulären analytischen Funktion darstellt, für welche die Randwerte des Realteiles den Wert $2F(x, 0)$ haben.

Bilden wir jetzt im Sinne der Formel (V):

$$-\int_{-\infty}^{+\infty} \frac{dx}{x} \int_{-\infty}^{+\infty} f_x(x, y) dy = \frac{2}{\pi} \int_0^{\infty} \frac{dx}{x} \int_{-\infty}^{+\infty} F_p(p, 0) l \left| \frac{p-x}{p+x} \right| dx,$$

so ist dieses Doppelintegral absolut konvergent und führt wegen

$$\int_0^{\infty} l \left| \frac{p-x}{p+x} \right| \frac{dx}{x} = -\frac{\pi^2}{2} \operatorname{sgn} p$$

genau zur Formel (V).

4. Es sei nun f eine Punktfunktion mit folgenden Regularitätseigenschaften:

a₄) f sei mit seinen Ableitungen bis zur zweiten Ordnung einschließlich stetig.

b₄) Die Ausdrücke,

$$f(x, y), \quad \sqrt{x^2 + y^2} l(x^2 + y^2) f_x(x, y), \quad \sqrt{x^2 + y^2} l(x^2 + y^2) f_y(x, y)$$

haben für $x^2 + y^2 \rightarrow \infty$ den Grenzwert Null.

c₄) Die Integrale

$$\int_{-\infty}^{+\infty} \int_{-\infty}^{+\infty} D_1 f \cdot \frac{l(x^2 + y^2)}{\sqrt{x^2 + y^2}} dx dy \quad \text{und} \quad \int_{-\infty}^{+\infty} \int_{-\infty}^{+\infty} D_2 f \cdot l(x^2 + y^2) dx dy,$$

wo $D_1 f$ jede erste, $D_2 f$ jede zweite Ableitung von f bedeutet, konvergieren absolut.

Diese Bedingungen sind wieder gegenüber Bewegungen invariant.

Dann gilt:

Satz VI: Die aus f nach (V) gebildete Geradenfunktion besitzt die Punktmittelwerte $f(x, y)$.

Es genügt, den Beweis für den Nullpunkt zu erbringen. Für eine beliebige Gerade durch diesen ergibt (V) nach einer partiellen Integration:

$$F(0, \varphi) = \frac{1}{2\pi} \int_{-\infty}^{+\infty} \int_{-\infty}^{+\infty} [f_{xx} \cos^2 \varphi + 2f_{xy} \sin \varphi \cos \varphi + f_{yy} \sin^2 \varphi] l |x \cos \varphi + y \sin \varphi| dx dy$$

oder nach Einführung von Polarkoordinaten ϱ, ψ :

$$\begin{aligned} F(0, \varphi) = & \frac{1}{2\pi} \int_0^\infty \varrho d\varrho \int_0^{2\pi} \left[\frac{\partial^2 f}{\partial \varrho^2} \cos^2(\varphi - \psi) \right. \\ & + 2 \frac{\partial^2 f}{\partial \varrho \partial \psi} \frac{\sin(\varphi - \psi) \cos(\varphi - \psi)}{\varrho} + \frac{\partial^2 f}{\partial \psi^2} \frac{\sin^2(\varphi - \psi)}{\varrho^2} \\ & + \frac{\partial f}{\partial \varrho} \frac{\sin^2(\varphi - \psi)}{\varrho} \\ & \left. - 2 \frac{\partial f}{\partial \psi} \frac{\sin(\varphi - \psi) \cos(\varphi - \psi)}{\varrho^2} \right] l | \varrho \cos(\varphi - \psi) | d\psi. \end{aligned}$$

Um den Punktmittelwert für $[0, 0]$ zu bilden, kann man die Integration nach φ unter dem Doppelintegral von 0 bis 2π ausführen und hat dann noch durch 2π zu dividieren. Das Glied mit $\frac{\partial^2 f}{\partial \psi^2}$, das dabei zum Vorschein kommt, fällt vermöge Integration nach ψ weg und es bleibt:

$$\frac{1}{2\pi} \int_0^{2\pi} d\psi \int_0^\infty \left[\frac{1}{4} \left(\varrho \frac{\partial^2 f}{\partial \varrho^2} - \frac{\partial f}{\partial \varrho} \right) + \frac{1}{2} l \frac{\varrho}{2} \frac{\partial}{\partial \varrho} \left(\varrho \frac{\partial f}{\partial \varrho} \right) \right] d\varrho,$$

was sich in der Tat auf $f(0, 0)$ reduziert.

Um die eindeutige Bestimmtheit von F zu zeigen, wären die Bedingungen $a_3 - c_3$ als erfüllt nachzuweisen, was offenbar noch weitere Voraussetzungen über f nötig macht.

5. Es möge hier folgende Bemerkung Platz finden, die ich, wie überhaupt die Problemstellung B , Herrn W. BLASCHKE verdanke: Die beiden hier behandelten Aufgaben stehen in engem Zusammenhang mit der Theorie des NEWTONSchen Potentials. Betrachten wir nämlich den Übergang von einer Punktfunktion f zu ihren geradlinigen Mittelwerten F als eine lineare Funktionaltransformation

$$F = Rf,$$

und ebenso den Übergang von einer Geradenfunktion F zu ihren Punktmittelwerten v :

$$v = BF,$$

so liegt es nahe, die zusammengesetzte, durch

$$v = Hf = B[Rf] = BRf$$

definierte Transformation $H \triangleq BR$ zu betrachten.

Man sieht nun sofort, daß Hf nichts anderes ist, als das NEWTONsche Potential der mit der Massendichte $\frac{1}{\pi}f$ belegten Ebene in den Punkten der Ebene selbst. Daraus kann man nach einer Bemerkung von G. HERGLOTZ die Umkehrung der Transformation H gewinnen; es ergibt sich dabei:

$$f(P) = H^{-1}v = -\frac{1}{2} \int_0^\infty \frac{d\bar{v}_P(r)}{r} = -\frac{1}{4\pi} \int_{-\infty}^{+\infty} \int_{-\infty}^{+\infty} \frac{\Delta v(x'y')}{r_{PP'}} dx' dy',$$

wo \bar{v}_P eine zu den früher eingeführten analoge Mittelwertsbezeichnung ist und Δ den LAPLACESchen Operator bedeutet.

Nun liegt der Gedanke nahe, die in 1.—3. direkt geleitete Umkehrung von R und H durch den Ansatz

$$R^{-1} = H^{-1}B \quad \text{bzw.} \quad B^{-1} = RH^{-1}$$

zu leisten. Tatsächlich habe ich die Umkehrungsformel (IV) zuerst auf diesem Wege gefunden, aber eine strenge Durchführung dieses Gedankens scheint schwieriger zu sein als die direkte Verifikation und versagt auch in den gleich zu besprechenden nichteuklidischen Fällen.

Schließlich sei bemerkt, daß die in A und B zugrunde gelegten Regularitätsbedingungen selbstredend bei weitem nicht die allgemeinsten sind, wie sich an einfachen Beispielen zeigen läßt.

C. Verallgemeinerungen.

6. Eine weitgehende Verallgemeinerung des in A behandelten Problems ließe sich etwa folgendermaßen formulieren: es sei eine Fläche S gegeben, auf der irgendwie ein Bogendifferential ds definiert sei, ferner eine zweifach unendliche Schar von Kurven C auf S . Es soll eine Punktfunktion der Fläche aus ihren Integralwerten $\int f ds$ längs der Kurven C bestimmt werden.

Die nächstliegende Spezialisierung erhält man, wenn man für S eine nichteuklidische Ebene, für ds das zugehörige Bogenelement und für die Kurven C die Geraden nimmt. Im elliptischen Falle kann man die Aufgabe auf die Kugelgeometrie hinüberspielen; indem man in bekannter Weise ein diametrales Punktepaar der Kugel als Punkt der elliptischen Ebene deutet, erhält man die Aufgabe, eine gerade — d. h. in diametralen Punkten gleichwertige — Funktion auf der Kugel aus ihren Großkreisintegralen

zu bestimmen. MINKOWSKI hat diese Aufgabe im Prinzip zuerst behandelt¹⁾ und durch Entwicklung nach Kugelfunktionen gelöst; P. FUNK hat später die MINKOWSKISCHE Lösung durchgeführt und gezeigt, wie man die Lösung mit Hilfe der ABELSCHEN Integralgleichung finden kann²⁾ und dieser Methode verdanke auch ich die Lösung des Problems A. Die FUNKSCHES Lösung ist ganz analog zu (III), nur tritt in den Nenner der Sinus des sphärischen Radius und additiv zu dem Integral der Wert von F im Pole des betreffenden Großkreises dividiert durch π . Aber auch in der hyperbolischen Ebene hat die gestellte Aufgabe die zu (III) analoge Lösung:

$$f(P) = -\frac{1}{\pi} \int_0^{\infty} \frac{d\bar{F}_P(q)}{\sin q}$$

(es ist hier das Krümmungsmaß $= -1$ angenommen), wie sich ganz konform zu der in I. angedeuteten Ableitung von (III) zeigen läßt.

In beiden Fällen kann man auch die zu B. analoge Frage stellen. In der elliptischen Geometrie erhält man vermöge der absoluten Polarität nichts Neues, im hyperbolischen Falle scheint eine zu (V) analoge Lösung nicht zu existieren.

Eine zweite Spezialisierung ergibt sich, wenn man (in der euklidischen oder nichteuklidischen Geometrie) als Kurven C die Kreise mit konstantem Radius nimmt. Hier kann man auf der Kugel die MINKOWSKISCHE Behandlung mit Kugelfunktionen anwenden und die Aufgabe in gewissem Grade lösen. Interessant ist in diesem Falle, daß die Eindeutigkeit der Lösung verloren gehen kann; es gibt nämlich für gewisse, durch die Nullstellen der LEGENDRESCHEN Polynome gerader Ordnung definierte Radien ϱ gerade Funktionen auf der Kugel, die längs jedes Kreises vom sphärischen Radius ϱ integriert, Null ergeben, ohne identisch zu verschwinden. Im euklidischen Falle tritt an Stelle der Kugelfunktionenreihen das Integraltheorem der Besselfunktionen; hier gibt es stets Funktionen, die über alle Kreise von festem Radius integriert, Null geben und doch nicht identisch verschwinden; ist der Radius 1, so sind es (in Polarkoordinaten ϱ, φ) die Funktionen

$$J_n(x_\nu \varrho) \cos n\varphi, \quad J_n(x_\nu \varrho) \sin n\varphi,$$

und ihre Linearkombinationen, wo x_ν eine Nullstelle von J_0 ist. Im hyperbolischen Falle treten an Stelle der Besselfunktionen die

1) Ges. Abb., Bd. II, S. 277 f. 2) Math. Ann., Bd. 74, S. 283—288.

sogenannten Kegelfunktionen, für die das zugehörige Integraltheorem von WEYL¹⁾ bewiesen ist. Die Ergebnisse sind analog zum euklidischen Falle.

7. In anderer Richtung verallgemeinern sich die Ergebnisse von A und B beim Übergang zu höheren Räumen. In einem euklidischen R_n kann man eine Punktfunktion $f(P) = f(x_1, x_2, \dots, x_n)$ aus ihren Integralwerten $F(\alpha_1 \dots \alpha_n, p)$ über alle Hyperebenen $\alpha_1 x_1 + \dots + \alpha_n x_n = p$ ($\alpha_1^2 + \dots + \alpha_n^2 = 1$) zu bestimmen trachten. Analog zu dem in 1. eingehaltenen Vorgang bilden wir den Mittelwert $\bar{F}_0(q)$ von F über die Tangentialebenen der Kugel vom Zentrum $[0, 0 \dots 0]$ und Radius q . Er ist durch das $n - 1$ fache Integral:

$$\bar{F}_0(q) = \frac{1}{\Omega_n} \int F(\alpha, q) d\omega$$

gegeben, wo $d\omega$ das Oberflächenelement, $\Omega_n = \frac{2\pi^{\frac{n}{2}}}{\Gamma(\frac{n}{2})}$ die Oberfläche der n -dimensionalen Kugel $\alpha_1^2 + \dots + \alpha_n^2 = 1$ bedeutet.

Man kann \bar{F}_0 durch ein n -faches Integral über f darstellen und zwar ergibt sich:

$$(7) \quad \bar{F}_0(q) = \frac{\Omega_{n-1}}{\Omega_n} \int \dots \int_{x_1^2 + \dots + x_n^2 > q^2} f(x_1, x_2, \dots, x_n) \frac{(x_1^2 + \dots + x_n^2 - q^2)^{\frac{n-3}{2}}}{(x_1^2 + \dots + x_n^2)^{\frac{n-2}{2}}} dx_1 \dots dx_n$$

oder in einer nun schon oft verwendeten Mittelwertsbezeichnung:

$$F_0(q) = \Omega_{n-1} \int_q^\infty \bar{f}_0(r) (r^2 - q^2)^{\frac{n-3}{2}} r dr.$$

Dies ist die zu (1) analoge Formel, an die sich entsprechende Folgerungen anschließen. Die Substitution $r^2 = v$, $q^2 = u$ führt auf die Integralgleichung:

$$\Phi(u) = \frac{\Omega_{n-1}}{2} \int_u^\infty \varphi(v) (v - u)^{\frac{n-3}{2}} dv.$$

1) Gött. Nachr. 1910, S. 454.

Ist n gerade, so ergibt $\left(\frac{n}{2} - 1\right)$ -maliges Differenzieren nach u dieselbe Gleichung wie (2) und man kann hieraus

$$\varphi(0) = f(0, 0, \dots, 0)$$

finden, wozu also bei gegebenem F die Bildung von F , Differentiationen und eine Integraloperation nötig sind. Bei ungeradem n fällt diese Integraloperation weg, denn jetzt ergibt $\left(\frac{n-1}{2}\right)$ -maliges Differenzieren:

$$\varphi(0) = \frac{2(-1)^{\frac{n-1}{2}}}{\Omega_{n-1} \left(\frac{n-3}{2}\right)!} \Phi^{\left(\frac{n-3}{2}\right)}(0).$$

Besonders einfach gestaltet sich der dreidimensionale Fall; diesen kann man aber auch nach einer Methode behandeln, die zu 5. analog ist und sehr elegante Ergebnisse liefert. Aus (7) geht nämlich für $q = 0$ der Punktmittelwert von F hervor:

$$\bar{F}_0 = \frac{1}{2} \iiint \frac{f(x, y, z)}{\sqrt{x^2 + y^2 + z^2}} dx dy dz,$$

der als das NEWTONSche Potential des mit der Massendichte $\frac{1}{2}f$ belegten Raumes anzusprechen ist. Also folgt:

$$f(x, y, z) = -\frac{1}{2\pi} \Delta F,$$

wo \bar{F} den Punktmittelwert von F bedeutet.

Hier kann man auch die zu B. analoge Aufgabe lösen und findet nach der in 5. angedeuteten Methode für eine Ebenenfunktion F , deren Punktmittelwerte f bekannt sind:

$$F(E) = -\frac{1}{2\pi} \iint \Delta f d\sigma,$$

wo $d\sigma$ das Flächenelement der Ebene E ist. Δ ist der LAPLACEsche Operator für den dreidimensionalen Raum, die Integration über die ganze Ebene E zu erstrecken.

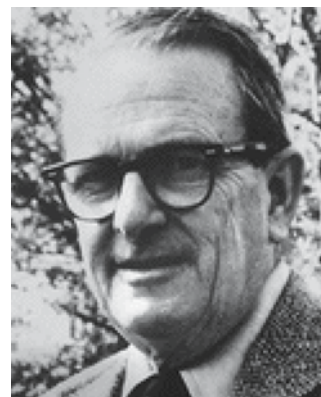
1.2 Representation of a function by its line integrals, with some radiological applications

Allan MacLeod Cormack (1924–1998)

Allan Cormack was born in Johannesburg, South Africa in February 1924. Cormack matriculated from Rondebosch Boys High School in 1941. He graduated in physics from the University of Cape Town in 1944. His master's thesis, which he completed in 1945, was on X-ray crystallography. He then went to St. John's College, Cambridge in the UK as a research student. He worked at the Cavendish Laboratory under Otto Frisch. Cormack then returned to Cape Town to continue his researches into nuclear physics.

In 1956 Cormack worked at Groote Schuur Hospital with the radiotherapist Dr. J. Muir Grieve. He became interested in the absorption of radiation in the body and his interest in the basis of what became computed tomography was kindled. He took a sabbatical from his post in South Africa in 1958 and worked on the Harvard University cyclotron. Cormack was offered a position as assistant professor in the department of physics in Tufts University, Massachusetts, USA, which he accepted. Cormack moved to the USA and became a US citizen in 1966. Cormack continued to work on CT and by 1963 he had developed his ideas which were published in the *Journal of Applied Physics*. The papers are the basis of axial tomography. Cormack had tested his ideas using phantoms. When his papers appeared there was little response. He was chairman of the physics department at Tufts University from 1968 to 1976. He remained interested in nuclear physics and the interaction of subatomic particles.

Allan Cormack retired in 1980. He was a member of the American Academy of Arts and Sciences. He was awarded the Nobel Prize for Physiology or Medicine jointly with Godfrey Hounsfield in 1979. He died in Winchester, Massachusetts on 7 May 1998.



Representation of a Function by Its Line Integrals, with Some Radiological Applications

A. M. CORMACK

Physics Department, Tufts University, Medford, Massachusetts

(Received 28 January 1963; in final form 26 April 1963)

A method is given of finding a real function in a finite region of a plane given its line integrals along all straight lines intersecting the region. The solution found is applicable to three problems of interest for precise radiology and radiotherapy: (1) the determination of a variable x-ray absorption coefficient in two dimensions; (2) the determination of the distribution of positron annihilations when there is an inhomogeneous distribution of the positron emitter in matter; and (3) the determination of a variable density of matter with constant chemical composition, using the energy loss of charged particles in the matter.

I. INTRODUCTION

THE exponential absorption of a parallel beam of x or gamma rays passing through homogeneous materials has been known and used quantitatively for a long time, but the problem of the quantitative determination of the variable absorption coefficient in inhomogeneous media has received little or no attention. To be sure, all radiography depends on the variation of the absorption coefficient of a medium in space, but the correct interpretation of radiographs depends on the art of the radiographer rather than on measurements.

While the problem of determining such variable absorption coefficients is interesting in itself, it also has an important application in any attempt at precise radiotherapy. The object of the radiotherapist is to direct an external beam, or beams, of x rays at a patient in such a way that a particular region of the patient's interior receives a known dose of radiation, while other parts of the patient receive as small a dose as possible. It is clearly necessary to know the absorption coefficients of the patient's various kinds of bone and tissue in order to make a precise estimate of the dosage received at any point of his interior, and it is equally clear that such information may only be obtained from measurements made exterior to the patient.

It is sufficient to consider the problem in two dimensions, since, if a solution can be found for two dimensions, the three-dimensional case may be solved by considering it to be a succession of two-dimensional layers.

The problem may be quantitatively formulated as follows. Let D be a finite, two-dimensional domain in which there is absorbing material characterized by a linear absorption coefficient g which varies from point to point in D and is zero outside D . Although $g \geq 0$, it is convenient to allow it to be negative for purposes of discussion. Suppose a parallel, indefinitely thin beam of monoenergetic gamma rays traverses D along a straight line L , and that the intensity of the beam incident on D is I_0 , and the intensity of the beam emerging from D is I . Then

$$I = I_0 \exp \left[- \int_L g(s) ds \right], \quad (1)$$

where the L under the integral indicates that the integral is to be evaluated along all of L in D , and s is a measure of distance along L . If $f_L = \ln(I_0/I)$, then

$$f_L = \int_L g(s) ds. \quad (2)$$

The problem is to find g , knowing the line integrals f_L for a number of lines L which intersect D .

One might think that a suitable way of finding g (suggested by taking two radiographs in directions at right angles to each other) would be by measuring f_L along two sets of parallel lines at right angles to each other. That this will not do may be seen as follows. Suppose that D is a square, and that this square is subdivided into n^2 equal smaller squares. Suppose also that the directions along which the line integrals are evaluated are parallel to the sides of the square. If in each small square, g assumes its average value in that square, then the line integrals in Eq. (2) may be approximated by the sums of the average values of g in the rows and columns of smaller squares. This procedure yields $2n$ values of f_L , and Eq. (2) reduces to a set of $2n$ equations in the n^2 average values of g in the small squares. Furthermore, the sum of the n values of f_L parallel to a side must be equal to the sum of the n values parallel to a side at right angles, hence, only $2n-1$ of the equations are independent. The problem is thus indeterminate except for the trivial case $n=1$. This indeterminacy is illustrated in the case $n=2$, which yields three independent equations in four unknowns. Consider a square to be subdivided into four equal smaller squares, and suppose $g=-1$ in two diagonally opposite squares, and $g=1$ in the other two. Then the line integrals (in the exact sense) along all lines parallel to the sides are zero, and furthermore, they are unaffected by the interchange of the above values of g , even though $g \neq 0$.

One is naturally led to consider measuring f_L along lines parallel to a larger number of different directions. Here again one can construct examples in which the f_L are zero along all lines parallel to a number of directions even though $g \neq 0$. For example, consider g to be confined to a circle, and let it have the value $A \cos n\theta$ in

the circle, where $n > 0$. Then the line integrals of g are zero along all lines perpendicular to the directions $\theta = (2m+1)\pi/2n$, where $m = 0, 1, 2, \dots, 2n-1$. However, the f_L is not zero along lines other than those specified.

These considerations suggest that if a solution to the problem can be found at all, it must be sought by considering f_L along all lines intersecting D and then seeing whether an approximate solution may be found by considering only a finite number of lines, so that the problem may be tractable in practice. The following problem is thus considered. An unknown, suitably restricted, real function g exists in a finite two-dimensional domain D and is zero outside D , and the line integrals of g along all straight lines intersecting D are known. Is it possible to determine g ? One would think that this problem would be a standard part of the nineteenth century mathematical repertoire, but the author has found no reference to it in standard works.

The same mathematical problem occurs in two other radiological procedures. In the first,¹ to locate tumors in say the head, the patient is given Cu^{64} or some other positron emitter. This tends to concentrate in abnormal tissue in the brain but unfortunately it also tends to concentrate in the muscles of the face and neck. The positrons annihilate and pairs of annihilation photons are emitted in very nearly opposite directions, the very small deviations from colinearity being caused by the momentum distributions of the electrons and positrons which annihilate. The annihilation photons are observed by two counters in coincidence, located on opposite sides of the head. The coincidence rate is determined by the distribution of the rate of annihilation along the line joining the counters, and by the absorption of annihilation radiation along that line. The latter factor can be found by measurements made external to the head. It can be shown that if g is the rate at which annihilations occur along the line L joining the counters, and if f_L is the observed coincidence rate corrected for absorption, f_L and g are related by Eq. (2).

The next application of the solution of Eq. (2) concerns the recent use of the peak in the Bragg curve for the ionization caused by protons, to produce small regions of high ionization in tissue.² The radiotherapist is confronted with the problem of determining the energy of the incident protons necessary to produce the high ionization at just the right place, and this requires knowing the variable specific ionization of the tissue through which the protons must pass. This problem is very complicated, for the rate of energy loss of protons depends on both their energy and the chemical composition of the material in which they are slowing down.

However, the problem is the same as the one considered for x rays, if one can assume that the tissue varies in density but not in chemical composition. In this case, if a fine beam of protons passes along L , and their energies incident on, and emergent from, D are known, the number of g/cm² of material along L can be found from the range-energy relation for the material. This can be represented by f_L , and the relation between f_L and the local density, g , is again given by Eq. (2). The applicability to this case of the results given below seems more difficult than in the above two cases. For one thing, bone and tissue have variable chemical composition so the procedure could be at best approximate, and for another, the difference between the energies of the incident and emergent protons is difficult to measure accurately because of the finite spread in energy of any incident beam and because of straggling.

2. FORMULATION OF THE PROBLEM AS A SET OF INTEGRAL EQUATIONS

It is sufficient to consider the domain of g to be a circle of radius R . For one thing, any finite domain may be contained in a circle, and, as is later seen, the circle has a special significance for the method by which the solution is obtained. For simplicity the circle is taken to have unit radius. The origin of polar coordinates (r, θ) may be taken to be at the center of the circle and we may write $g = g(r, \theta)$. The line L along which g is to be integrated may be defined by the parameters (p, ϕ) , where p is the perpendicular distance from the origin to the line L , and ϕ is the angle which the normal to L makes with the $\theta = 0$ axis, and f_L may be considered to be a function of the polar coordinates (p, ϕ) . The unique property of the circular domain is now apparent: in the (p, ϕ) plane, the domain of f is the same as the domain of g , namely a circle of unit radius. Equation (2) may now be written

$$f(p, \phi) = \int_{L(p, \phi)} g(r, \theta) ds. \quad (3)$$

Equation (3) is an integral equation in two variables, but it may be reduced to a set of integral equations in one variable as follows. Suppose that g is finite, single-valued and continuous, except along a finite number of arcs in the circle, then it may be expanded in a Fourier series:

$$g(r, \theta) = \sum_{n=-\infty}^{+\infty} g_n(r) e^{in\theta}, \quad (4)$$

where

$$g_n(r) = \frac{1}{2\pi} \int_0^{2\pi} g(r, \theta) e^{-in\theta} d\theta. \quad (5)$$

Consider the contribution df to $f(p, \phi)$ from two equal elements of arc ds of the line $L(p, \phi)$. If the elements of arc are on opposite sides of the point (p, ϕ) and

¹ F. W. Wrenn, M. L. Good, and P. Handler, *Science* **113**, 525 (1951); G. L. Brownell and W. H. Sweet, *Nucleonics* **11**, 40 (1953).

² R. R. Wilson, *Radiology* **47**, 487 (1946); B. Larsson, L. Leksell, B. Rexed, P. Saurander, W. Mair, and B. Andersson, *Nature* **182**, 1222 (1958).

are equally spaced from it, then

$$df = \sum_n [g_n(r)e^{in\theta} + g_n(r)e^{i(n+2\phi-\theta)}]ds,$$

since if one element is at the point (r, θ) the other must be at $(r, 2\phi - \theta)$. Thus

$$df = 2 \sum_n g_n(r)e^{in\phi} \cos[n(\theta - \phi)].$$

Then since $s = (r^2 - p^2)^{1/2}$, and $\theta - \phi = \cos^{-1}(p/r)$,

$$f(p, \phi) = \sum_n e^{in\phi} 2 \int_p^1 \frac{g_n(r) \cos[n \cos^{-1}(p/r)] r dr}{(r^2 - p^2)^{1/2}}. \quad (6)$$

Now $f(p, \phi)$ is a function of polar coordinates (p, ϕ) in the unit circle, so it may be expanded in a Fourier series:

$$f(p, \phi) = \sum_{n=-\infty}^{+\infty} f_n(p) e^{in\phi}, \quad (7)$$

where

$$f_n(p) = \frac{1}{2\pi} \int_0^{2\pi} f(p, \phi) e^{-in\phi} d\phi. \quad (8)$$

Comparing Eqs. (6) and (7) it is seen that the problem separates, and its solution depends on the solution of the set of one-dimensional integral equations:

$$f_n(p) = 2 \int_p^1 \frac{g_n(r) \cos[n \cos^{-1}(p/r)] r dr}{(r^2 - p^2)^{1/2}}. \quad (9)$$

$\cos(n \cos^{-1} x)$ is a polynomial of degree n in x known as the Tschelbycheff polynomial of the first kind. It is denoted by $T_n(x)$, and Eq. (9) is written

$$f_n(p) = 2 \int_p^1 \frac{g_n(r) T_n(p/r) r dr}{(r^2 - p^2)^{1/2}}, \quad (10)$$

because in the solution of this equation, $T_n(x)$ is used for $x > 1$ for which the cosine representation is inconvenient.

Some properties of the $T_n(x)$ are given below. A complete account of them can be found in Tricomi.³ (i) $T_n(1) = 1$. (ii) $T_n(x)$ has n distinct zeros, say x_1, x_2, \dots, x_n , which satisfy the inequality $-1 < x_1 < x_2 < \dots < x_n < 1$, where $x_n = \cos(\pi/2n)$. (iii) The $T_n(x)$ are orthogonal in $(-1, 1)$ with weight function $(1-x^2)^{-1/2}$. (iv) $T_n(-x) = (-1)^n T_n(x)$.

3. SOME PROPERTIES OF THE $f_n(p)$

The restrictions placed on $g(r, \theta)$ and hence on the $g_n(r)$, imply restrictions on the behavior of the $f_n(p)$. Some of these are interesting in that they enable one to anticipate the behavior of the $f_n(p)$ in experimental

situations, but others are of greater importance since they bear on the uniqueness of the solution of the problem.

(a) If $g_n(r)$ is bounded and piecewise continuous, $f_n(p)$ is bounded and continuous.

(b) $f_n(p)$ is uniquely determined by $g_n(r)$ through Eq. (10).

Suppose that there were two different functions $g_{n1}(r)$ and $g_{n2}(r)$ which both gave rise to the same $f_n(p)$. Then their difference $G_n(r)$ would satisfy

$$\int_p^1 \frac{G_n(r) T_n(p/r) r dr}{(r^2 - p^2)^{1/2}} = 0. \quad (11)$$

By properties (i) and (ii) above, $T_n(x) \geq 0$ for $x_n \leq x \leq 1$. Consider Eq. (11) for $p \geq x_n$. Then $x_n \leq p \leq (p/r) \leq 1$, so $T_n(p/r) \geq 0$ and the integrand is positive apart from $G_n(r)$. Hence, the only continuous solution of Eq. (11) in $x_n \leq p \leq 1$ is $G_n(r) = 0$. Thus it is only necessary to consider

$$\int_p^{x_n} \frac{G_n(r) T_n(p/r) r dr}{(r^2 - p^2)^{1/2}} = 0. \quad (12)$$

Now let $x_n^2 \leq p \leq x_n$. Then $x_n \leq (p/x_n) \leq (p/r) \leq 1$. Hence again $T_n(p/r) \geq 0$ for $x_n^2 \leq p \leq x_n$, and Eq. (12) only has the solution $G_n(r) = 0$ for $x_n^2 \leq r \leq x_n$. Repetition of this process m times shows that the only solution of Eq. (11) in $x_n^m \leq r \leq 1$ is $G_n(r) = 0$. Let $m \rightarrow \infty$, then $x_n^m \rightarrow 0$ since $x_n < 1$. Hence the only solution of Eq. (11) is $G_n(r) = 0$ in $0 < r \leq 1$, and the $f_n(p)$ are uniquely determined by the $g_n(r)$ except at $p = 0$.

(c) $|f_n(p)| \leq 2M_n(1-p^2)^{1/2}$ for $x_n \leq p \leq 1$, where M_n is some positive constant.

It was proved above that $T_n(p/r) \geq 0$ if $x_n \leq p \leq 1$. It is also decreasing in this range. Then, since $g_n(r)$ is bounded, $|g_n(r)| \leq M_n$ where M_n is some positive constant, so

$$|f_n(p)| \leq 2M_n T_n(1) \int_p^1 \frac{r dr}{(r^2 - p^2)^{1/2}} = 2M_n(1-p^2)^{1/2}.$$

In particular, $f_n(1) = 0$.

(d) $f_{2n+1}(0) = 0$, $f_{2n}(0) = (-1)^n 2 \int_0^1 g_n(r) r dr$.

Consider $f(0, \phi)$ for $g(r, \theta) = g_n(r) \cos n\theta$ or $g_n(r) \sin n\theta$ and the result can be seen from the symmetry of the problem.

(e) $f(0, \phi) = f(0, \phi + \pi)$.

This result must hold since nowhere in the formulation of the problem has a positive direction for the evaluation of the line integral been assigned. The formal demonstration is:

$$f(0, \phi + \pi) = \sum_n f_n(0) (-1)^n e^{in\phi} = \sum_n f_n(0) e^{in\phi} = f(0, \phi),$$

since $f_{2n+1}(0) = 0$.

(f) $f_{2n}(p)$ and $f_{2n+1}(p)$ each change sign at least n times in $0 < p < 1$.

³ F. G. Tricomi, *Vorlesungen Über Orthogonal Reihen* (Springer-Verlag, Berlin, 1955).

REPRESENTATION OF A FUNCTION BY ITS LINE INTEGRALS 2725

Multiply both sides of Eq. (10) by p^k and integrate from $p=0$ to $p=1$:

$$\begin{aligned}\int_0^1 f_n(p) p^k dp &= 2 \int_0^1 p^k dp \int_0^1 \frac{g_n(r) T_n(p/r) r dr}{(r^2 - p^2)^{1/2}} \\ &= 2 \int_0^1 g_n(r) r dr \int_0^1 \frac{p^k T_n(p/r) dp}{(r^2 - p^2)^{1/2}} \\ &= 2 \int_0^1 g_n(r) r^{k+1} dr \int_0^1 \frac{t^k T_n(t) dt}{(1-t^2)^{1/2}}.\end{aligned}$$

If n is even (odd), $T_n(x)$ is orthogonal in $(0,1)$ to any even (odd) polynomial of degree less than n because of the orthogonality of the $T_n(x)$ in $(-1,1)$ and because of their symmetry [property (iv)]. In particular, depending on the evenness or oddness of n and k , $T_n(x)$ is orthogonal to t^k , so for $k < n$

$$\int_0^1 f_{2n}(p) p^{2k} dp = 0, \quad \int_0^1 f_{2n+1}(p) p^{2k+1} dp = 0. \quad (13)$$

With Eq. (13) established, the proof is very like the proof of the number of zeros of orthogonal polynomials. Suppose that $n > 0$, then $\int_0^1 f_{2n}(p) dp = 0$. Hence $f_{2n}(p)$ must change sign at least once in $(0,1)$. Suppose that it changes sign m times, at points $p_1, p_2, p_3, \dots, p_m$, and consider the integral

$$I = \int_0^1 f_{2n}(p) (p^2 - p_1^2)(p^2 - p_2^2) \cdots (p^2 - p_m^2) dp.$$

The integrand is either everywhere positive except at the zeros, or it is everywhere negative except at the zeros, that is $|I| > 0$. But

$$\begin{aligned}I &= a_1 \int_0^1 f_{2n}(p) p^{2m} dp \\ &\quad + a_2 \int_0^1 f_{2n}(p) p^{2m-2} dp + \cdots + a_m \int_0^1 f_{2n}(p) dp,\end{aligned}$$

where a_1, a_2, \dots, a_m are some constants, and from Eq. (13), the integrals are zero if $m < n$. This contradicts the assumption that $|I| > 0$, unless $m \geq n$. Hence, $f_{2n}(p)$ changes sign at least n times in $0 < p < 1$. A similar proof holds for $f_{2n+1}(p)$, since if $\int_0^1 p f_{2n+1}(p) dp = 0$, $f_{2n+1}(p)$ must change sign at least once. Consideration of the integral

$$I = \int_0^1 f_{2n+1}(p) (p^2 - p_1^2)(p^2 - p_2^2) \cdots (p^2 - p_n^2) p dp$$

then yields the desired result.

4. SOLUTION OF THE EQUATIONS

Multiply both sides of Eq. (10) by $T_n(p/z)(z/p) \times (p^2 - z^2)^{-1/2}$, integrate from $p=z$ to $p=1$ and interchange the order of integration on the right hand side:

$$\begin{aligned}\int_z^1 \frac{z T_n(p/z) f_n(p) dp}{p(p^2 - z^2)^{1/2}} \\ = 2 \int_z^1 g_n(r) dr \int_z^r \frac{r z T_n(p/z) T_n(p/r) dp}{p(r^2 - p^2)^{1/2} (p^2 - z^2)^{1/2}}.\end{aligned} \quad (14)$$

If the p integration on the right is denoted by $I_n(r, z)$, where

$$I_n(r, z) = r z \int_z^r \frac{T_n(p/z) T_n(p/r) dp}{(r^2 - p^2)^{1/2} (p^2 - z^2)^{1/2}}, \quad (15)$$

then it can be shown that $I_{n+1} = I_{n-1}$, $I_0 = I_1 = \pi/2$, so

$$I_n(r, z) = \pi/2. \quad (16)$$

Hence, Eq. (14) becomes

$$\pi \int_z^1 g_n(r) dr = z \int_z^1 \frac{f_n(p) T_n(p/z) dp}{(p^2 - z^2)^{1/2}} \quad (17)$$

and, by differentiating with respect to z

$$g_n(r) = -\frac{1}{\pi} \frac{d}{dr} \int_z^1 \frac{r f_n(p) T_n(p/r) dp}{(p^2 - r^2)^{1/2} p}. \quad (18)$$

It has been shown that $g_n(r)$ determines $f_n(p)$ uniquely by Eq. (10), and it should now be shown that the above inversion formulae determine g_n uniquely. Suppose that there are two functions f_{n1} and f_{n2} which yield the same function g_n in Eq. (17), and let $f_{n1} - f_{n2} = F_n$. Then F_n satisfies the equation

$$\int_r^1 \frac{r T_n(p/r) F_n(p) dp}{(p^2 - r^2)^{1/2} p} = 0. \quad (19)$$

In the range $r \leq p \leq 1$, $(p/r) \geq 1$, therefore, $T_n(p/r) \geq 1$. Hence, $T_n(p/r)(p^2 - r^2)^{-1/2} p^{-1} \geq 0$ in the range of integration, and the only continuous solution of Eq. (19) is $F_n(p) = 0$. Thus, Eq. (17) determines $g_n(r)$ uniquely. If Eq. (18) is examined for uniqueness, ignoring its origin in Eq. (17), the proof requires an extra step, caused by the additional operation of differentiation. For if f_{n1}, f_{n2} , and F_n have the same meaning as before, the equation which F_n must satisfy is

$$\int_r^1 \frac{r T_n(p/r) F_n(p) dp}{(p^2 - r^2)^{1/2} p} = c = \text{constant}. \quad (20)$$

Solutions of this exist which are not identically zero. For example, take $n=1$, $F_1 = p(1-p^2)^{-1/2}$, then $c = (\pi/2)$. But this choice of F_1 violates the condition (c) of Sec. 3, which states that $|F_n(p)| \leq 2M_n(1-p^2)^{1/2}$ for $x_n \leq p \leq 1$,

and it can be shown, by letting $r \rightarrow 1$, that if F_n satisfies this condition, c must be zero. Therefore, the above proof applies, $F_n = 0$, and the solution is unique.

5. A GENERALIZATION

From a mathematical point of view, it is interesting to see whether the problem can be formulated and solved if the line integrals of a function are taken along families of curves other than straight lines. A formal solution has been found for a family of circles through the origin.

Let the circles be defined by two parameters (p, ϕ) and let the equation of the circles be

$$r = p \cos(\theta - \phi). \quad (21)$$

Then, if $f(p, \phi)$ is the line integral of $g(r, \theta)$ along the circle defined by (p, ϕ) , one may proceed exactly as before with the Fourier analysis of both f and g and arrive at the set of integral equations

$$f_n(p) = 2p \int_0^p \frac{g_n(r) T_n(r/p) dr}{(p^2 - r^2)^{1/2}} \quad (22)$$

Multiplying the left-hand side by $T_n(z/p)(z^2 - p^2)^{-1/2}$ and integrating from $p=0$ to z , and changing the order of integration on the right, one gets

$$\int_0^z \frac{f_n(p) T_n(z/p) dp}{(z^2 - p^2)^{1/2}} = 2 \int_0^z g_n(r) dr \int_r^z \frac{T_n(z/p) T_n(r/p) p dp}{(z^2 - p^2)^{1/2} (p^2 - r^2)^{1/2}} \quad (23)$$

Making the substitution $t = rz/p$, and using Eq. (16),

$$\int_r^z \frac{T_n(z/p) T_n(r/p) p dp}{(z^2 - p^2)^{1/2} (p^2 - r^2)^{1/2}} = \frac{\pi}{2} \quad (24)$$

Substitution of Eq. (24) into Eq. (23) and differentiating as before yields

$$g_n(r) = -\frac{1}{\pi} \frac{d}{dr} \int_0^r \frac{f_n(p) T_n(r/p) dp}{(r^2 - p^2)^{1/2}} \quad (25)$$

This solution has not been investigated in any detail, but its existence leads one to think that such generalizations may be carried further.

6. AN EXPERIMENTAL TEST

An experiment was carried out in the simplest case where g was a function of r only. The specimen was a disk, 5 cm thick and 20 cm in diameter, made in the following way. A central cylinder of aluminum, 1.13 cm in diameter was surrounded by an aluminum annulus with an inner diameter of 1.13 cm and an outer diameter of 10.0 cm, and this in turn was surrounded with a wooden (oak) annulus with an inner diameter of 10.0

cm and an outer diameter of 20.0 cm. A peculiarity in the results lead to an investigation of the materials used, and it transpired that the central cylinder had been made of pure aluminum while the annulus had been made with an aluminum alloy. A 7-mCi Co^{60} source produced a gamma-ray beam which was collimated by a 15-cm lead shield with a circular hole in it. The gamma rays were detected by a Geiger counter which was well shielded and preceded by a second collimator. The gamma-ray beam had an over-all width of 7 mm. Because of the symmetry of the sample it was only necessary to measure $f(p, \phi)$ at one angle, and it was measured for $p=0$ cm to $p=12.5$ cm at 5-mm intervals. At least 20 000 counts were taken at each setting to reduce statistical counting errors to less than 1%, and the usual corrections for backgrounds and dead-time were made.

For this case, ($n=0$), the solution (18) may be written

$$g_0(r) = -\frac{d}{dr} \left[\frac{r}{\pi} \int_r^1 \frac{f_0(p) dp}{(p^2 - r^2)^{1/2} p} \right] = -\frac{dJ(r)}{dr}. \quad (26)$$

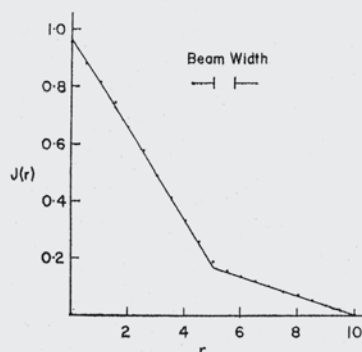


FIG. 1. $J(r)$ vs r in cm. Straight lines represent $J(r)$ calculated from measured values of the absorption coefficients, points give $J(r)$ calculated from Eq. (26).

The expression $J(r)$ was found from the experimentally determined $f_0(p)$ by numerical integration, except that an analytic approximation was used in evaluating the integral near the singularity at $p=r$. The values of $J(r)$ so found are shown as points in Fig. 1. The values of the absorption coefficients of the aluminum alloy and the wood were found to be $0.161 \pm 0.002 \text{ cm}^{-1}$ and $0.0340 \pm 0.0005 \text{ cm}^{-1}$, respectively, and a value⁴ of 0.150 cm^{-1} was assumed for the inner aluminum cylinder. $J(r)$ was calculated using these values and is shown by the straight lines in Fig. 1. The agreement is good. The full width of the gamma-ray beam is also shown in Fig. 1.

This experiment is a test of the method only in the simplest case, but it does indicate that the effects of beam width need not be too serious. More stringent tests

⁴ C. M. Davisson and R. D. Evans, Phys. Rev. **81**, 404 (1951).

with more complicated samples are needed and these are being undertaken.

ACKNOWLEDGMENTS

The author would like to thank Dr. J. M. Grieve of the Radiology Department of Groote Schuur Hospital,

Cape Town, for pointing out the necessity for a solution of the absorption problem, and A. M. Koehler of the Harvard Cyclotron Laboratory for pointing out that the solution could be used in the coincidence problem. The partial support of this work by the United States Atomic Energy Commission is also acknowledged.

Residual Temperatures of Shocked Copper*

JOHN W. TAYLOR

Los Alamos Scientific Laboratory, University of California, Los Alamos, New Mexico

(Received 1 April 1963)

A photoelectric technique is described for measuring the residual temperature of strongly shocked metals. Data for copper shocked to pressures ranging from 0.9 to 1.7 Mbars are in good agreement with published calculations of temperatures.

INTRODUCTION

THE methods which may be used to deduce a complete thermodynamic equation of state from shock-wave data which yield a single (P, V, E) locus have been discussed extensively by Rice, McQueen, and Walsh¹ and by Walsh and Christian². The calculations may be done in more than one way but they are all based on certain assumptions. The most important of these are: the metal is in thermodynamic equilibrium behind a shock wave, the elastic limit at high pressures does not increase by orders of magnitude above its value at zero pressure, and the Mie-Grüneisen equation of state,

$$(P - P_s)V = \gamma(V)(E - E_s), \quad (1)$$

is valid over the entire pressure-volume-energy surface of interest. The subscript s refers to any standard state. Calculations for most materials are made with the additional assumption that gamma is a function of volume only and is given by the Dugdale-MacDonald formula,

$$\gamma(V) = -(V/2)[\partial^2(PV^{\frac{1}{2}})/\partial V^2] - \frac{1}{2}. \quad (2)$$

Gamma also can be shown to be equal at zero pressure to the limit $2S-1$ where, $S = (dU_s/dU_p)_{U_p=0}$. U_s is shock velocity and U_p is shock particle velocity. It is necessary to assume that the yield point does not depend markedly on pressure in order to be able to employ the theory of the isentropic flow of an ideal fluid in a consideration of release waves at the free surface of a shocked metal.

Recent work in which time-resolved measurements were made of the free surface velocity of shocked-annealed copper indicates that the elastic limit remains substantially constant up to 100 kbars (one kbar is 10^9 dyn/cm²) at least and that shocks at pressures in excess of about 50 kbars in copper are propagated essentially as discontinuities.³ Russian work⁴ in which sound speeds were measured in copper at pressures in excess of 1000 kbar indicates that the high-pressure elastic limit is finite but still small and shows good agreement with sound speeds calculated with the Dugdale-MacDonald formula and Hugoniot data.⁵ These results combined with the observation that at zero pressures the "dynamic" gamma $(2S-1)$ agrees very well with the "thermodynamic" gamma $V(\partial P/\partial T)_s/C_v$ lead one to suspect that copper is the metal most likely to conform to all the necessary assumptions and is, therefore, the most logical candidate for an experimental check of the theory.

The way of calculating temperatures chosen by Walsh and Christian was to assume that $\gamma/V = b$ is constant and use the equation,

$$T_H = T_0 \exp\{b(V_0 - V_H)\} + \exp\{-bV_H\} \times \left[\int_{V_0}^{V_H} \frac{f(V) \exp\{bV\}}{C_v} dV \right], \quad (3)$$

where T_0, V_0 are temperature and volume under ambient conditions and T_H, V_H are the same quantities on the Hugoniot, and

$$f(V) = \frac{1}{2}[P_H + (V_0 - V_H)(\partial P/\partial V)_H]. \quad (4)$$

* Work done under the auspices of the U. S. Atomic Energy Commission.

¹ M. H. Rice, R. G. McQueen, and J. M. Walsh in *Solid State Physics*, edited by F. Seitz and D. Turnbull (Academic Press Inc., New York, 1958), Vol. VI.

² J. M. Walsh and R. H. Christian, *Phys. Rev.* **97**, 1544 (1955).

³ J. W. Taylor and M. H. Rice (to be published).

⁴ L. V. Al'tshuler, S. B. Kormer, A. A. Bakanova, and R. F. Trunin, *Zh. Eksperim. i Teor. Fiz.* **38**, 1061 (1960) [English transl.: *Soviet Phys.-JETP* **11**, 766 (1960)].

⁵ R. G. McQueen and S. P. Marsh, *J. Appl. Phys.* **31**, 1253 (1960).

1.3 Computerized transverse axial scanning (tomography). Part I. Description of system.

Sir Godfrey Newbold Hounsfield (1919–2004)

Godfrey Hounsfield was born in Newark in Nottinghamshire in the UK on 28 August 1919. He went to school at the Magnus Grammar School in Newark.

In the Second World War he joined the Royal Air Force as a volunteer reservist. He became interested in radar and radio communications and worked as a radar mechanic instructor. He then went to the Royal College of Science in South Kensington, which was occupied by the RAF, and then to the Cranwell Radar School. He passed the City and Guilds examination in radio communications.

After the war Hounsfield attended the Faraday House Electrical Engineering College in London, and received their diploma. Hounsfield joined EMI in Middlesex in 1951. He worked on guided weapons and on radar. He was also involved with computers, which were only in their infancy, and built the first solid-state computer constructed in Britain, the EMIDEC 1100. By 1972 he was head of the medical systems research department.

Godfrey Hounsfield received many honours. In 1972 he received the MacRobert Award and the referee said that “no comparable discovery has been made in this field since Röntgen discovered X-rays in 1895.” He was elected to the Fellowship of the Royal Society. In 1974, with James Ambrose, Godfrey Hounsfield received the Barclay Prize of the British Institute of Radiology, followed by the honorary membership of the Institute in 1980. In 1979 he received the Nobel Prize in Physiology or Medicine jointly with Allan Cormack. Godfrey Hounsfield was knighted in 1981. Until his death on the 21st August 2004 after a long illness Hounsfield remained interested in the development of CT and in MRI.



1973, *British Journal of Radiology*, 46, 1016-1022

Computerized transverse axial scanning (tomography): Part I. Description of system

G. N. Hounsfield

Central Research Laboratories of EMI Limited, Hayes, Middlesex

(Received February, 1973 and in revised form July, 1973)

ABSTRACT

This article describes a technique in which X-ray transmission readings are taken through the head at a multitude of angles: from these data, absorption values of the material contained within the head are calculated on a computer and presented as a series of pictures of slices of the cranium. The system is approximately 100 times more sensitive than conventional X-ray systems to such an extent that variations in soft tissues of nearly similar density can be displayed.

For many years past, X-ray techniques have been developed along the same lines, namely the recording on photographic film of the shadow of the object to be viewed. Recently, it has been realized that this is not the most efficient method of utilizing all the information that can be obtained from the X-ray beam. Oldendorf (1961) carried out experiments based on principles similar to those described here, but it was not then fully realized that very high efficiencies could be achieved and so, picture reconstruction techniques were not fully developed.

As the exposure of the patient to X rays must be restricted, there is an upper limit to the number of photons that may be passed through the body during the examination, and so to the amount of information that can be obtained. It is, therefore, of great importance that the method of examination ensures that all the information obtained is fully utilized and interpreted with maximum efficiency.

In the conventional film technique a large proportion of the available information is lost in attempting to portray all the information from a three-dimensional body on a two-dimensional photographic plate, the image superimposing all objects from front to rear. In order that any one internal structure may be seen, it must clearly stand out against the variations of the materials in front and behind it.

The technique to be described divides the head into a series of slices, each being irradiated via its edges; the radiation is confined to the slice and for this reason, unlike conventional X-ray techniques, the information derived from any object within the slice is unaffected by variations in the material on either side of the slice. Data are processed and displayed by digital computer methods.

A report on this work was presented at the April 1972 Annual Congress of the British Institute of

Radiology (Ambrose and Hounsfield, 1973). A short account has also appeared in the *New Scientist* (*Technology Review*), 1972.

PRINCIPLES OF THE METHOD

The aim of the system is to produce a series of images by a tomographic method as illustrated in Fig. 1. Each image shown at the bottom of the figure is derived from a particular slice.

In the actual equipment, the patient is scanned by a narrow beam of X rays. The X-ray tube, detectors, and collimators are fixed to a common frame, as shown in Fig. 2, those rays which pass through the head being detected by two collimated sensing devices (scintillation detectors) which always point towards the X-ray source. Both X-ray source and detectors scan across the patient's head linearly taking 160 readings of transmissions through the head as shown in scan 1 on the scanning sequence diagram (Fig. 3). At the end of the scan the scanning system is rotated 1 deg. and the process is repeated, as shown in scans 2 and 3. This continues for 180 deg. when 28,800 (180×160) readings of transmission will have been taken by each detector. These are stored in a disc file for processing by a mini computer. A picture is reconstructed from the data by the following method:

A separate detector measures the intensity of the X-ray source and the readings taken from this can be used to calculate absorption by the material along the X-ray beam path, where

$$\text{Absorption} = \log \frac{\text{Intensity of X rays at source}}{\text{Intensity of X rays at detector}}$$

If the body is divided into a series of small cubes each having a calculable value of absorption, then the sum of the absorption values of the cubes which are contained within the X-ray beam will equal the total absorption of the beam path. Each beam path, therefore, forms one of a series of 28,800 simultaneous equations, in which there are 6,400 variables and, providing that there are more equations than variables, then the values of each cube in the slice can be solved. In short there must be more X-ray readings than picture points.

DECEMBER 1973

Computerized transverse axial scanning (tomography): Part I. Description of system

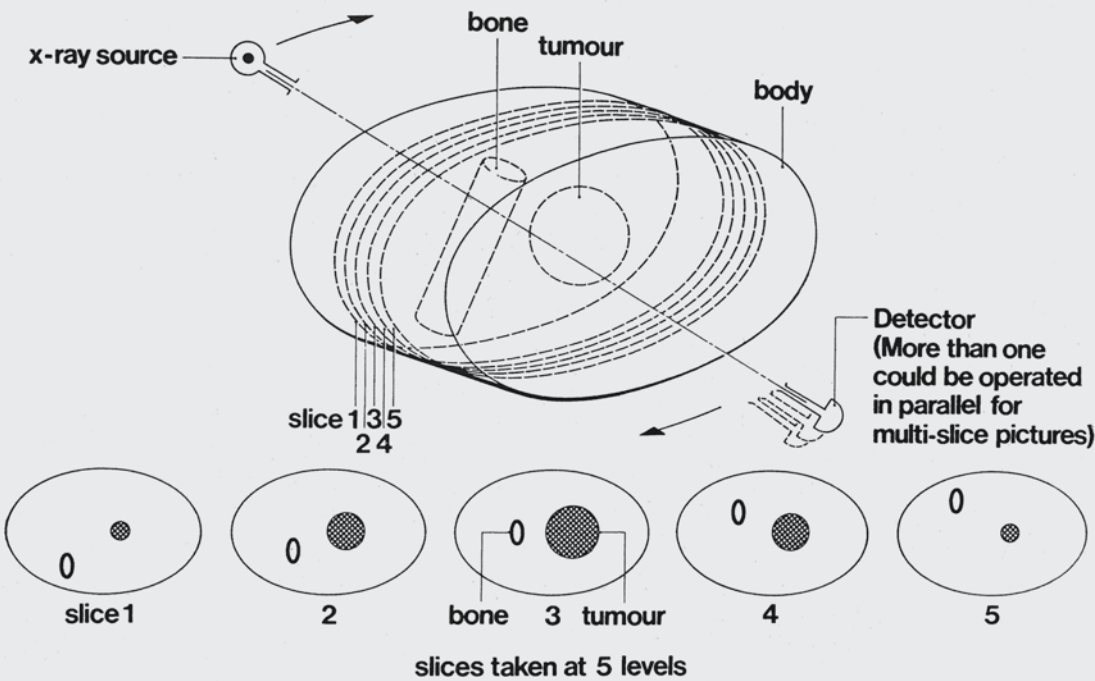


FIG. 1.

Computerized transverse axial techniques on a body containing bone and tumour.

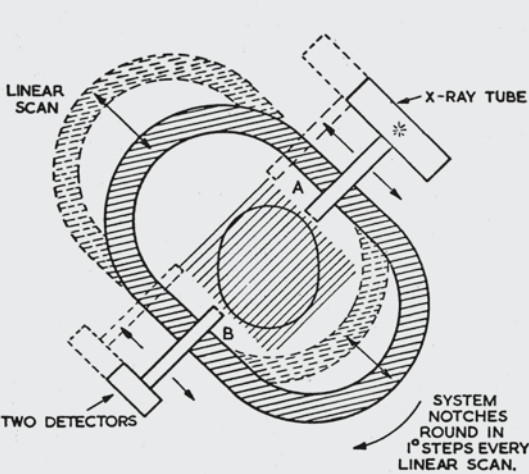


FIG. 2.

Motion of scanning frame and detectors for producing two continuous slices.

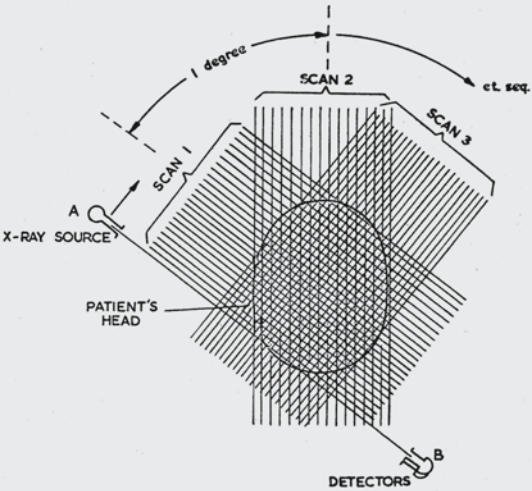


FIG. 3.

Simplified illustration of the scanning sequence.

VOL. 46, No. 552

G. N. Hounsfield

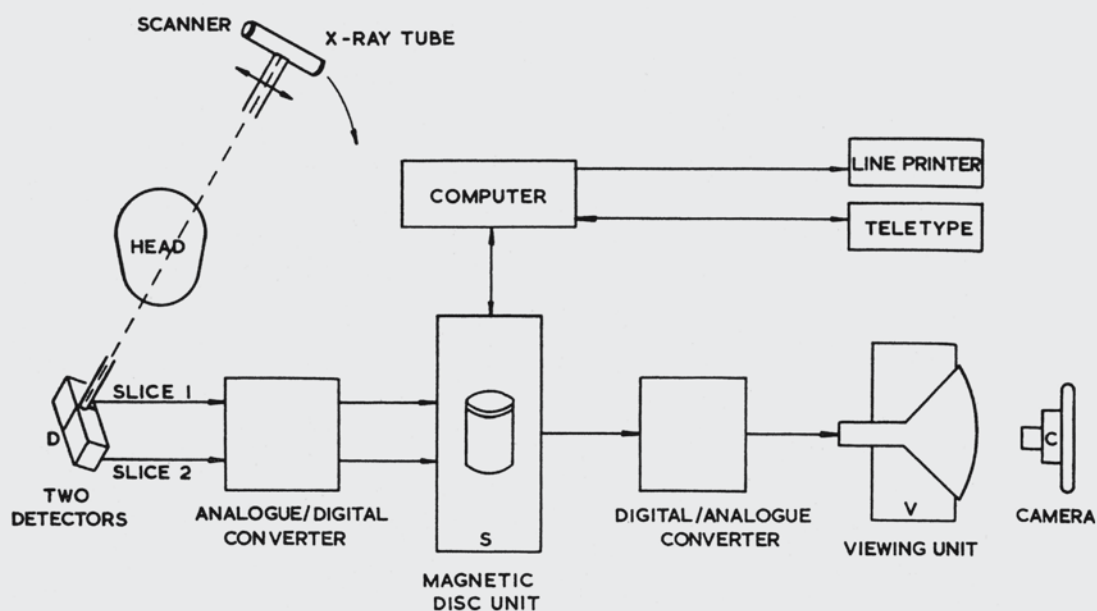


FIG. 4.

Block diagram illustrating how the readings from the two detectors are digitized, stored in a disc unit, processed in the computer and printed out on a line printer. They are also stored in the disc unit as fully processed pictures to be viewed on the viewing unit.

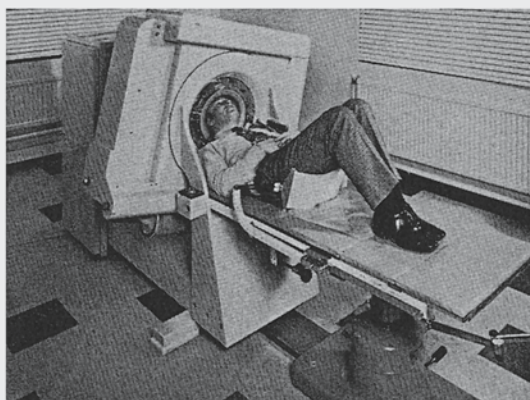


FIG. 5.
Illustration of the patient in position.

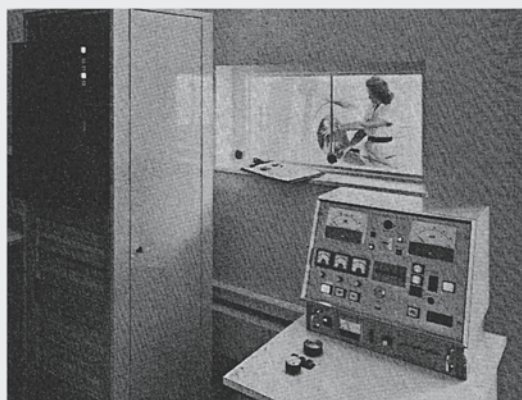


FIG. 6.
X-ray control console.

The picture is built up in the form of an 80×80 matrix of picture points to each of which a numerical value is ascribed. Each of these points indicates the value of the absorption coefficient of the corresponding volume of material in the slice. After appropriate scaling, as explained later in the text, the absolute values of absorption coefficient of various tissues

are calculated to an accuracy of $\frac{1}{2}$ per cent. values are printed out on a line printer or viewed a cathode ray-tube (Fig. 4).

THE SCANNER UNIT

Figure 5 shows part of the system in use at the Atkinson Morley's Hospital, Wimbledon. The

DECEMBER 1973

Computerized transverse axial scanning (tomography): Part I. Description of system

patient's head is placed within a rubber cap in a circular orifice around which the X-ray source and detectors rotate.

The rubber cap forms the front face of a box containing water, and when this is pumped out the rubber cap expands and the patient's head is inserted at the correct angle. The water is then caused to flow back allowing the cap to collapse on the patient's head. Since the sides of the box are parallel, and the air around the head has been replaced by water which is of similar absorption to the head, the variations of transmission through the box during the scan will be considerably less than if the head were to be scanned in air. This reduces the range

of the readings from the machine and so eases the calculations required to be made by the computer, thereby increasing the accuracy of the machine.

The control console for the X-ray tube and the patient scan "start" and "stop" mechanism is shown in Fig. 6, and the computer console in Fig. 7. Readings from the scanning unit for one cut are stored on a removable disc pack and processed (five minutes per picture) during the scanning of the following cut. The processor is time shared with the scanner unit, its speed being such that it is able to keep pace with the flow of patients through the scanner unit. This assumes an average of 35 minutes per patient and six pictures are taken during this period. The removable disc pack can store more than 60 pictures any of which can be selected and viewed on the viewing unit (Fig. 8).

ACCURACY OF PICTURE READINGS

Laboratory measurements (for a tube operated at 120 kV) of water and various body fluids and tissues are shown on the chart (Fig. 9). It can be seen that fat has an absorption coefficient 10 per cent less than water and tissue, on average, a value approximately 3 per cent greater than that of water. Variation of tissue absorption found in the head including the ventricles covers a 4 per cent range. The picture brightness and contrast can be adjusted so that this 4 per cent range, or "window", covers full black to peak white, illustrated in Fig. 9 as "Tone Range". As the absorption coefficient in this range can be measured to an accuracy better than 0.5 per cent, this means that at least eight different levels can be detected within the "window". The height of the "window" can also be adjusted to the level of any



FIG. 7.

Computer console for processing and storing the pictures.

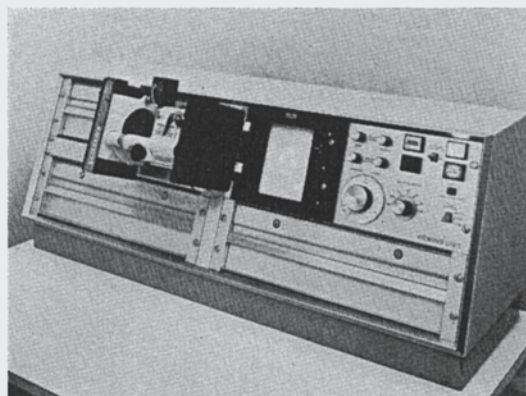


FIG. 8.

Viewing unit and camera.

VOL. 46, No. 552

G. N. Hounsfield

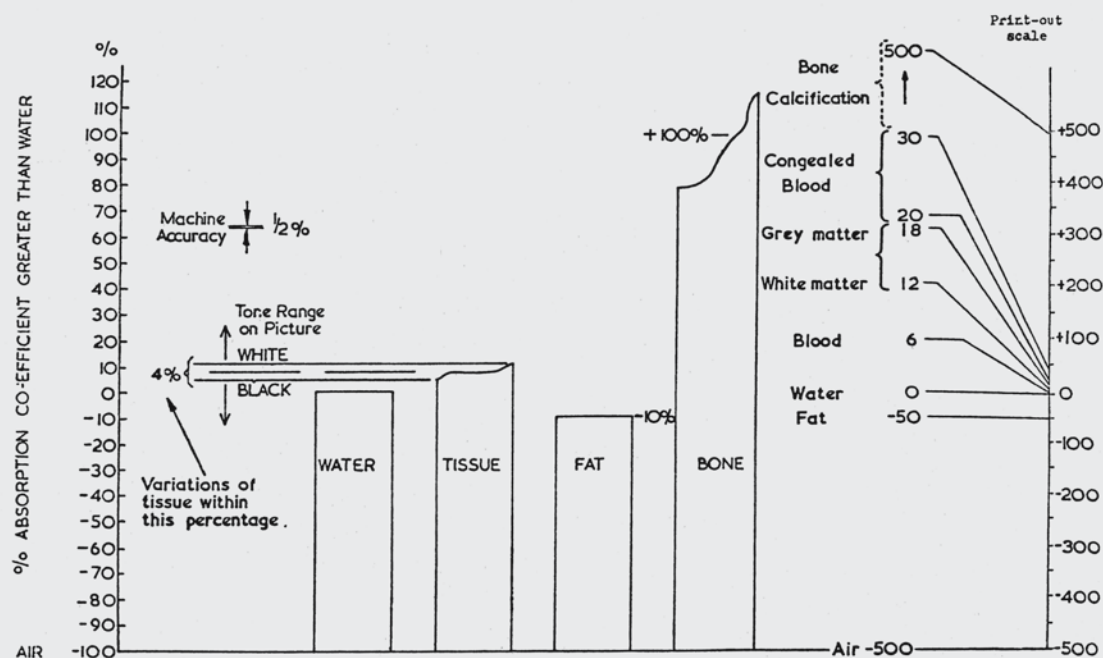


FIG. 9.

Illustration of machine sensitivity. The scale on the right is an arbitrary scale used on the print-out and is related to water = 0, air = 500 units. It can be seen that most materials to be detected fall within 20 units above zero and can be covered by the adjustable 4 per cent "window".

material which is to be viewed. A more convenient scale used on the print-outs (of absorption values) is given on the right where air is shown as -500, water as 0, and bone as approximately +500; this scale is used on the machine.

The pictures shown in Fig. 10 illustrate in practice how the picture changes, similar to a television "contrast" control, when the "window level" control is raised from -20% (-100 units) to +70% (+350 units).

As this scale uses water as a reference (*i.e.* water = 0), to obtain the absorption coefficient of any material for the 120 kV X-ray beam, 500 must be added to the readings and multiplied by a factor of $0.19/500$, the absorption coefficient of water for this beam being 0.19 cm^{-1} .

DETERMINATION OF ATOMIC NUMBER OF MATERIAL

It is possible to use the machine for determining approximately the atomic number of the material within the slice. Two pictures are taken of the same slice, one at 100 kV and the other at 140 kV. If the scale of one picture is adjusted so that the values of normal tissue are the same on both pictures, then

the picture containing material with a high atomic number will have higher values at the corresponding place on the 100 kV picture. One picture can then be subtracted from the other by the computer so that areas containing high atomic numbers can be enhanced. (In practice a contrast medium, sodium iothalamate containing 420 mg of atomic iodine per millilitre (Conray 420) can be readily detected at a concentration of one part in 1,000 by the machine.) For example, tests carried out to date have shown that iodine ($Z=53$) can be readily distinguished from calcium ($Z=20$). The scope of this technique is under further investigation at present.

RADIATION DOSE

The skin area irradiated is confined to a narrow band around the edge of each slice and provided the slices do not overlap the skin dose will not increase with the number of slices taken (although the area irradiated will increase). The exposure at the patient's skin is 1.9 R for an examination which provides six tomographic slices covering the whole of the head. This exposure is approximately equivalent to a conventional skull X-ray examination. Two pic-

DECEMBER 1973

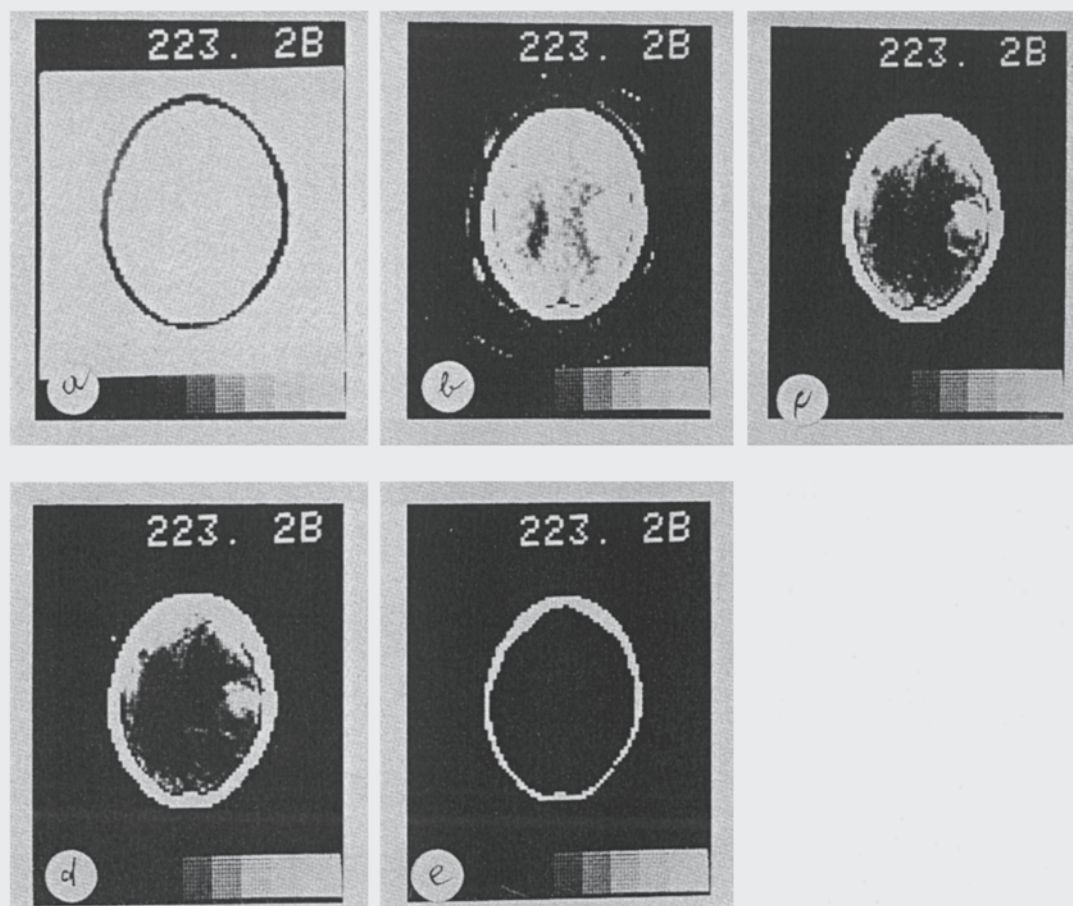
Computerized transverse axial scanning (tomography): Part I. Description of system

FIG. 10.

Illustration of "window level" adjustment.

- (a) (Window level setting—100 units.) The black ring represents the patient's hair and the air trapped in it.
- (b) (Setting 0) shows water in the ventricles.
- (c) (Setting +15 units) shows tumour and haemorrhage.
- (d) (Setting +20 units) shows details in the haemorrhage.
- (e) (Setting +350 units) the white ring represents the bone of the skull.

tures side by side are taken at the same time during each scan of the patient.

DISCUSSION

It is evidently of interest to consider how far the sensitivity of this procedure exceeds that available with established techniques. The material presented in Fig. 9 gives some indication of the detectability of particular tissues; further analysis of the data presented suggests that the system may have a sensitivity two orders of magnitude greater than conventional methods in detecting soft tissue abnormalities.

It is possible that this technique may open up a new chapter in X-ray diagnosis. Previously, various tissues could only be distinguished from one another if they differed appreciably in density. In this procedure absolute values of the absorption coefficient of the tissues are obtained. The increased sensitivity of computerized X-ray section scanning thus enables tissues of similar density to be separated and a picture of the soft tissue structure within the cranium to be built up.

ACKNOWLEDGMENTS

The author wishes to thank the Directors of EMI Ltd., for permission to publish this article.

VOL. 46, No. 552

G. N. Hounsfeld

The author also wishes to thank the research team at EMI, particularly Mr. P. G. Langstone, Mr. S. R. Bates, Mr. R. S. Starkey and Mr. J. D. Coppen and the staff of the Central Research Laboratories Workshop.

REFERENCES

AMBROSE, J., and HOUNSFELD, G., 1973. Computerized

transverse axial tomography. *British Journal of Radiology*, 46, 148 (abstract).

OLDENDORF, W. H., 1961. Isolated flying spot detection of radiodensity discontinuities—displaying the internal structural pattern of a complex object. *I.R.E. Transactions on Bio-medical Electronics*, 8, 68–72.

TECHNOLOGY REVIEW, 1972. X-ray diagnosis peers inside the brain. *New Scientist*, 54, 207.

Book review

Radiation Protection. By J. Shapiro, pp. xx+339, illus., 1972 (Cambridge, Mass., Harvard University Press, and London, Oxford University Press), £7.50 (hardback); £3.50 (paper covers).

This manual on radiation protection has two conflicting objectives. The author claims in the preface that "This manual was written for individuals who wish to become qualified in radiation protection as an adjunct to working with sources of ionizing radiation or using radionuclides in the field of medicine. It provides the radiation user with information needed to protect himself and others and to understand and comply with governmental and institutional regulations regarding the use of radionuclides and radiation machines." The guide to the use of the manual, however, informs the reader that "This manual was written for the training programme in the safe use of radionuclides in research conducted by the Harvard University Health Services." If this second objective had been implied in the title rather than the first, the manual would be a far more useful publication, especially as certain sections now dealt with inadequately would then have been irrelevant and presumably deleted. To meet the first objectives a more rigorous and extensive treatment is necessary on the use of "radiation machines", particularly in view of the contribution diagnostic radiography makes to population exposure; the section on "X-rays" takes up only twenty-nine pages!

The manual is divided into six parts.

Part I—Historical Prologue.

Part II—Principles of Radiation Protection. Referred to as a primer on the principles of radiation protection, contributes approximately a third to the volume of the book. Even at this stage, in its tables and illustrations, the presentation is very much biased towards the use of radionuclides at the expense of "radiation machines".

Part III—Radiation Dose Calculations. This deals exclusively with calculations on topics dealing with radionuclides and provides some very useful data and formulae for the

radionuclide worker. The author elaborates with detailed dose calculations on ^3H , ^{131}I , ^{133}Xe and ^{32}P , chosen for their universal use in nuclear medicine.

Part IV—Radiation Measurements. The "various kinds of radiation detectors, the types of signals they produce and means of analysing these signals, with particular attention to Geiger-Müller counters and scintillation detectors as examples of the constant output and proportional output detectors respectively" are discussed. Included is a short but completely inadequate section on personnel and environmental monitoring. The presentation of radiation measurements from radionuclides and their interpretation are dealt with after an introduction to the statistical methods required for this.

Part V—Practical Aspects of the Use of Radionuclides contains little practical information for the radionuclide user in the United Kingdom. Reference is only made to the various regulations pertaining to radiation control in the U.S.A. Also included are practical safety precautions required when handling radionuclides. This is information which is readily available to the U.K. user in the Codes of Practice for the protection of persons against ionizing radiations.

Part VI—Ionizing Radiation and Public Health provides extensive and up-to-date data on the potential hazards involved in the large scale use of ionizing radiations. The merit of such a detailed account in a manual of this kind is questionable. A condensed version would not have detracted from its usefulness in keeping radiation hazards in perspective.

The manual ends with two appendices, the first on the use of powers of ten in dose calculations, the second contains a set of 25 problems for the reader to tackle, all dealing with radionuclides. A selected bibliography is appended for easy reference to a more rigorous treatment of the text, together with further useful references and an index.

M. H. DAVIES.

1.4 Computerized transverse axial scanning (tomography). Part II.

James Ambrose (born 1923)

James Ambrose was born in Pretoria, South Africa on 5 April 1923. He initially studied science at Johannesburg. During the Second World War he joined the Royal Air Force. After the war he studied medicine at Cape Town and came to the United Kingdom in 1954 to study radiology, initially at the Middlesex Hospital and then at Guy's Hospital.

Ambrose became interested in neuroradiology and in 1959 went to work at Atkinson Morley's Hospital, where he spent his working life. Atkinson Morley's Hospital was in Wimbledon in South London and by 1948 it had become the busiest neurosurgical unit in London. Neurosurgery had been developed by Wylie McKissock. McKissock had visited Stockholm and had been very impressed by the close collaboration between Herbert Olivecrona and the radiologist Eric Lysholm. McKissock disliked the current invasive neuroradiological techniques. James Ambrose shared his concerns, and the department at Atkinson Morley's Hospital actively investigated alternative imaging techniques including cranial ultrasound and nuclear medicine with the support of the physics department at St George's Hospital. Ambrose presented his work on cranial ultrasound in 1969 to the meeting of the British Medical Association in Leicester and although the paper was well received Ambrose would admit that the technique was not generally useful. Ambrose was therefore well prepared to respond positively to Godfrey Hounsfield and to his novel ideas regarding cranial imaging.

In 1974 James Ambrose and Godfrey Hounsfield jointly received the Barclay Prize of the British Institute of Radiology, and James Ambrose received honorary membership in 1993. In retirement Ambrose now lives in Argyll in Scotland and remains modest as ever about his major achievements.



1973, *British Journal of Radiology*, 46, 1023-1047

DECEMBER 1973

Computerized transverse axial scanning (tomography): Part 2. Clinical application*

By James Ambrose

Atkinson Morley's Hospital, London, S.W.20

(Received February, 1973)

ABSTRACT

A new and fundamentally different X-ray method is described. The cranium is scanned in successive layers by a narrow beam of X rays, in such a way that the transmission of the X-ray photons across a particular layer can be measured, and by means of a computer, used to construct a picture of the internal structure.

Employing a suitably designed scanning gantry, a continuously operating X-ray tube, and a narrow collimated X-ray beam, the transmissions of X-ray photons across a slice of tissue may be measured by a system of crystal detectors in such a way that 28,800 readings are obtained. These form the basis of 28,000 simultaneous equations which are solved by a computer. The solutions are transformed into absorption coefficients and by means of a

suitable algorithm related to their correct cells in a matrix of chosen size.

The results are stored, computed, and then made available from a magnetic disc to construct a picture on a CRT. The numerical results are available from a print-out.

The examination is, therefore, qualitative and quantitative. Pictures thus obtained are looked at in much the same way as radiographs. Structures are identified and shape, size, and position defined. Changes in tissue density are then looked for.

Lesions are seen as alterations of normal density and are interpreted in the light of pathological changes which are known to occur. Increased density may be due to blood clot, calcium deposition in tumours, and other lesions. In haemorrhage, once clotting has occurred, the concentrated blood constituents show up as an area of high density. Average tissue density is lowered in tissue necrosis, oedema, cyst formation, and haemorrhage where clotting has not occurred.

Tissue density may be artificially enhanced by the intravenous injection of substances containing large atoms;

*This preliminary communication is a slightly expanded version of a short paper which was presented at the Annual Congress of the British Institute of Radiology on April 19, 1972.

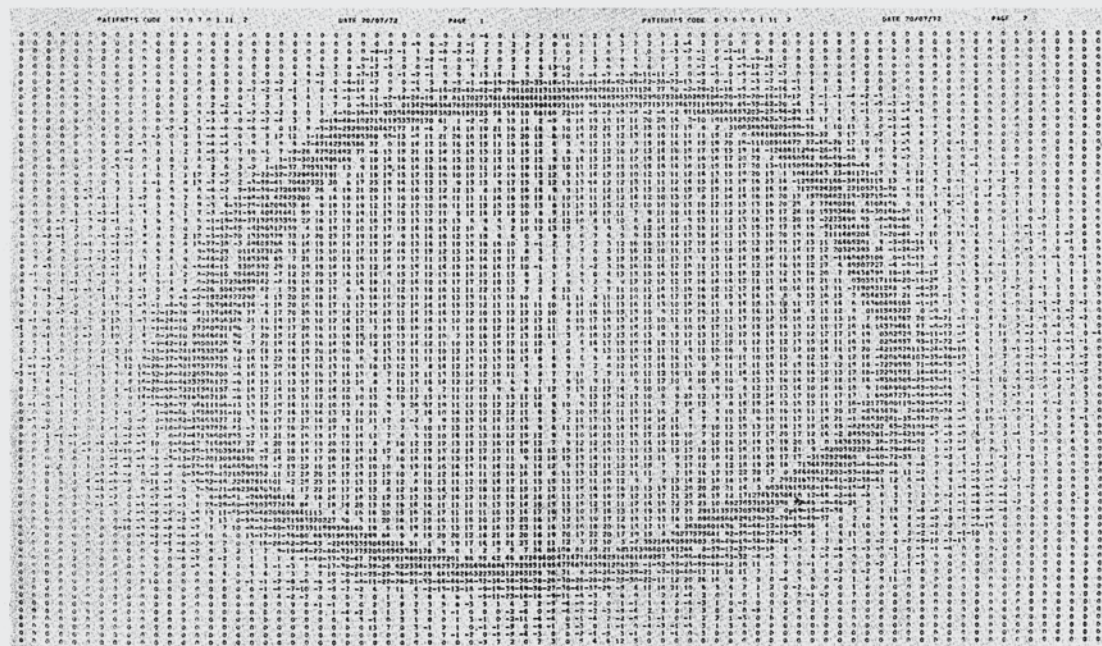


FIG. 1.

Normal scan.

Computer print-out of scan through a section 1.3 cm thick and 3.5 cm above the orbito-meatal line. The matrix size is 80 × 80 and each number is the calculated absorption coefficient of a discrete volume of tissue at that point. *Note:* The highest values are recorded in the surrounding compact bone while the lowest values are found in the fluid filled ventricles.

VOL. 46, No. 552

J. Ambrose

sodium iothalamate has been found to be ideal and the tissue density of a variety of tumours may be enhanced by this means.

Computerized transverse axial scanning is a new method of "imaging" in which the patient is scanned by a narrow beam of X rays. Measurements of the transmission of X-ray photons across a section of a part of the body are taken by an arrangement of crystal detectors, in such a way that a picture can be constructed by a computer and displayed on a cathode-ray tube.

The apparatus used is a prototype which has been designed to examine the cranium and to provide transverse axial tomographic scans, showing the tissue structure of the brain in each successive slice.

Two contiguous slices of the brain, each 1.3 cm thick on either side of a selected plane to which the

X-ray beam has been centred, are examined in each scan.

The results are displayed in three ways:

- (1) A paper record of the computer print-out of the absorption coefficients relating to small previously defined volumes of tissue (Fig. 1).
- (2) A cathode-ray tube display of the processed information from magnetic tape.
- (3) A Polaroid camera picture of the cathode-ray tube display (Fig. 2).

OPERATION

The operation of the apparatus, being geared to the collection of data in numerical form, is different from that of a conventional X-ray machine. Radiographers must become versed in the operation of an apparatus which is simple to use and which requires the carrying out of the following main procedures:

- (1) positioning the patient in an expanded rubber head-cap which is allowed to shrink on to the patient's head by releasing water pressure from behind (Fig. 3).
- (2) using a measuring system to locate the plane of section;
- (3) operating a control console, which starts the reciprocating and rotating movements of the mechanical scanner and records the reading of X-ray transmission taken by the crystal detectors (Fig. 8, Part 1);
- (4) operating a viewer console after the picture has been processed (Fig. 9, Part 1).

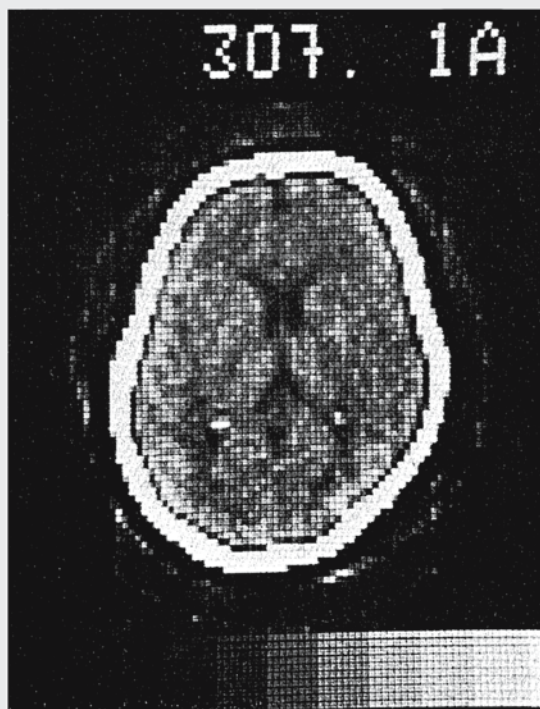


FIG. 2.

Normal scan.

Polaroid picture of computer print out shown in Fig. 1. The tissues exhibiting the highest density are shown as peak white areas, while tissues of lowest density are shown as black areas. The subarachnoid space, the interhemispherical fissure, the difference between the cortex and white matter, the lateral ventricles, septum pellucidum, 3rd ventricle and choroid plexuses are major features which are easily defined.

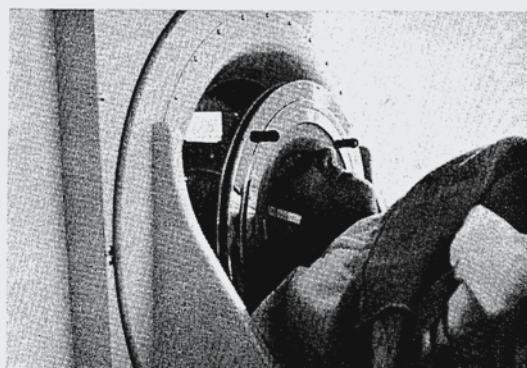


FIG. 3.

The patient's head has been positioned in the expanding rubber head cap which has then been allowed to shrink on to the scalp, reducing the air gap to a minimum. Note the marking tape on the side of the head.

DECEMBER 1973

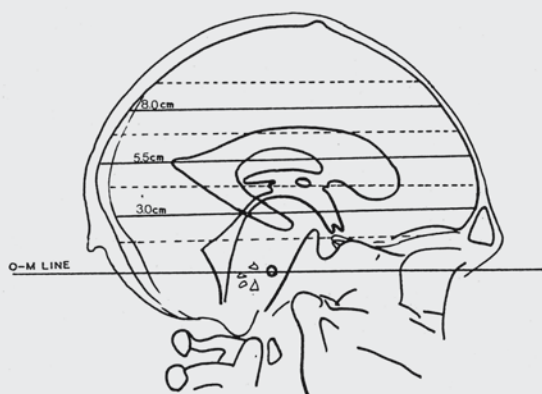
Computerized transverse axial scanning (tomography): Part 2. Clinical application

FIG. 4A.

Line drawing showing the orbito-meatal line.

The continuous lines at 3, 5.5 and 8 cm are the reference planes on which the X-ray beam is centred. The dotted lines on each side of the respective planes indicate the thickness (1.3 cm) of each slice which will be examined. Although the total thickness of tissue examined in each scan is 2.6 cm a more practical measurement of 2.5 cm is made.



FIG. 4B.

Identification of levels to be scanned.

A strip of white tape has been fixed to the head in front of the ear and the orbito-meatal line drawn, using a black grease pencil. The levels to be scanned are marked on the tape.

These systems require to be correctly integrated and a system of interlocking controls and safeguards is provided.

In order to provide a method for measuring the level of each scan which, for purposes of comparison, may also be applied to lateral skull radiographs, brain scans, or contrast studies, a line joining the outer angle of the eye to the external auditory meatus (*i.e.* the orbitomeatal line) is adopted as a base (Figs. 4A and B).

This line is marked on the patient's face with a black grease pencil and the levels of the selected planes to be examined are then marked on a strip of

white tape fixed to the side of the head immediately in front of the right ear (Fig. 4B).

Variations in the shape of the skull in individuals will produce differences in the levels at which specific structures will be seen, but the thickness of each adjacent slice of tissue examined (1.3 cm) provides for considerable overlap. A series of five successive examination planes, *i.e.* ten slices covering 13 cm, should in most cases encompass the calvarium from the base to the vertex.

In practice, so far, we have seldom found it necessary to scan below 3 cm or above 8.5 cm. This means that three scanning "runs" in most cases will be sufficient, *i.e.* six pictures.

The patient is then lifted onto an X-ray couch fitted with a hydraulic lift and the head is gently pushed into the hollow formed by the rubber cap until it is firmly held by a plastic cone behind the cap. The water pressure is then allowed to increase slowly so as to permit the rubber cap to envelope the head from the supra-orbital margins to the vertex, thus excluding any air gap.

Once this operation has been carried out, the marks on the tape are read off against a scale in the water box, and this enables the patient to be accurately positioned with respect to the X-ray beam.

Once a scanning "run" has been started, the patient is required to remain quite still for approximately four minutes, which is the time required for the X-ray tube to rotate through 180 deg. and to make 180 linear scanning motions. Any patient who is able to co-operate sufficiently for a radioisotope brain scan will be able to cope with the requirements for a computerized transverse axial scan.

RESULTS AND INTERPRETATION

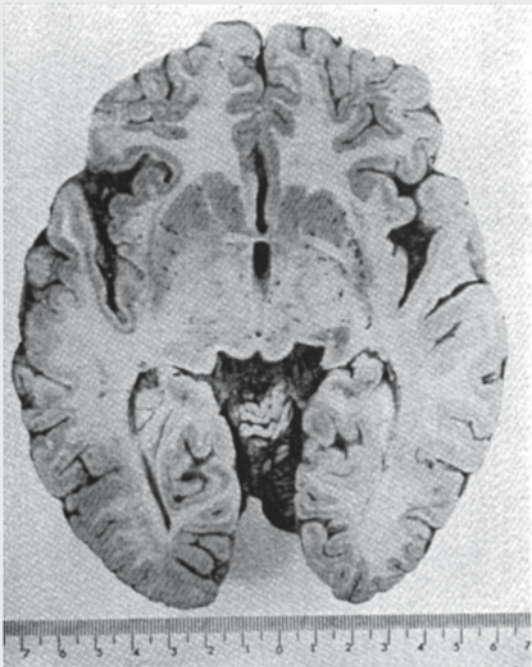
The normal scan

Since each section or slice has been scanned by the X-ray beam in a transverse axial plane, the Polaroid camera pictures taken from the cathode-ray tube display must be viewed as if the cranial contents at a particular level were being looked at from above. With the serial number at the top of the picture the viewer is correctly orientated as to left and right side, front and back.

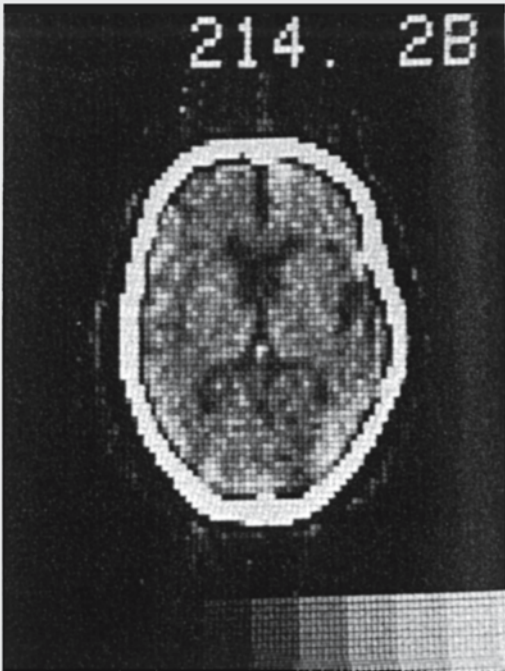
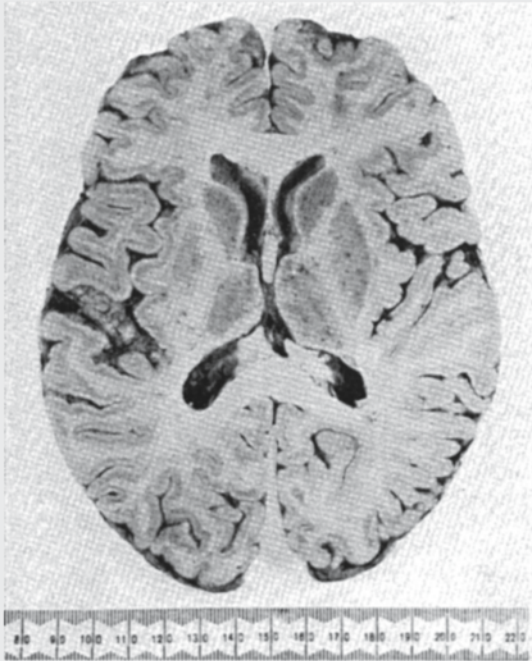
Figures 5A, B and C, show the cut top surfaces of horizontal sections made through a normal brain removed at autopsy. The sections are 1 cm thick and are selected to show some of the major anatomical features which can be seen in computerized transverse axial scans made at similar levels. The features which may be defined include the difference between white and grey matter, the Sylvian fissures, the inter-hemispherical fissure, the lateral ventricles, the

VOL. 46, No. 552

J. Ambrose



A



B

FIG. 5.
1026

DECEMBER 1973

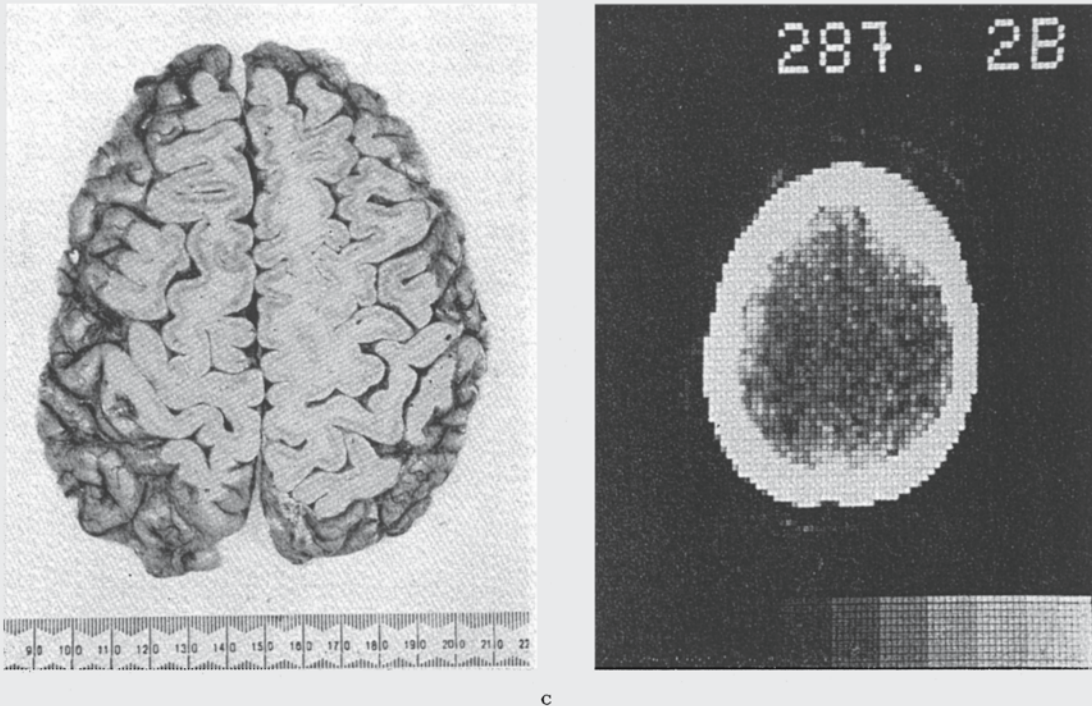
Computerized transverse axial scanning (tomography): Part 2. Clinical application

FIG. 5A, B, C.

Relation of scans to sections through normal brain. The brain sections are each 1 cm thick and were made 3, 4, and 7 cm above the floor of the temporal fossa. Scans made at comparable levels are shown with each section. The major features which can be defined are: the subarchnoid space, the Sylvian fissures, 3rd ventricle, lateral ventricles, interhemispherical fissure, pineal body, choroid plexuses, corpus striatum (the internal capsule can just be discerned in Fig. 5B). The difference between white and grey matter can also be defined. *Note:* The scan in Fig. 5B shows changes due to cerebral atrophy.

3rd ventricle, the calcified pineal body, and choroid plexuses. The thin low density band surrounding the brain in part represents fluid in the subarachnoid space, but some is without doubt due to computer overswing, the system having to drop abruptly from the high density of compact bone down to near zero for cerebrospinal fluid.

The computer "print-out" which accompanies each section is the numerical record of the absorption coefficients of small previously defined volumes of tissue at each picture point. The "print-out" has been shaped to conform broadly with the outline of the cranium at the level selected (Fig. 1).

The values vary according to the density of tissues included in the predetermined volume. Using a matrix made up of 80×80 cells, each 3×3 mm \times the thickness of the tissue slice which can be either 13 or 8 mm.

The values of the absorption coefficients are calculated on a standard scale, adopting zero as the value for water. Cerebrospinal fluid on this scale has

a value of plus one. The range of values is from approximately plus 500 for compact bone to minus 500 for air in the mastoid air cells or paranasal sinuses.

Since the absorption coefficients are measured to an accuracy of 0.5 per cent, the method is able to detect and register small differences in tissue density. The cerebral cortex is appreciably more dense than the deeper white matter. Differences in tissue density are also registered in the deeper structures of the corpus striatum. Spaces filled with cerebrospinal fluid are shown as areas of low density. A fluid filled ventricle would show up as a group of low values approaching zero. (The value for cerebrospinal fluid is actually about +1 due principally to the salt content.) Volumes at the periphery of a fluid filled space may include tissue boundaries and the absorption coefficients will therefore be higher depending on the proportion of tissue and fluid included in each separate small volume.

In the Polaroid camera pictures, with the appropriate window level setting, tissues of higher density

VOL. 46, No. 552

J. Ambrose

than grey or white matter show up as "white" areas. Diminishing tissue density is shown as darker shades of grey or black.

In normal operation the density variation of tissue is confined to values within a 4-6 per cent range above zero. The picture brightness and contrast can be adjusted within this small range from peak white down to full black. In a normal scan the picture brightness can therefore be adjusted so that the cerebral cortex will show as a thin white band, while the deeper white matter will be shown in varying shades of grey. The ventricles and other fluid filled spaces will show up as black areas (Fig. 6).

The values of the suitably scaled absorption coefficients (see Part 1) for the cerebral cortex vary between 19 and 23 and from 13 to 17 for the white matter. Fluid filled spaces vary from zero to values as high as seven or eight, according to how much of the fluid filled space has been included in the cut. The extreme measurements are compact bone +500 and air -500. The values for tissues containing calcium will depend on the amount of calcium present or whether it is aggregated, and can vary from 20 to as high as 200. The pineal body and choroid

plexuses are good examples. The amount of calcium present in these structures may be insufficient to show in skull radiographs, but with the greatly increased sensitivity of the method these structures show up clearly as "white" dense areas (Fig. 5).

The abnormal scan

In neurological practice the common lesions which require to be identified are cerebral neoplasms of all varieties, haematomas, infarctions, and infections. To this list must be added cerebral oedema which often accompanies these lesions and complicates the clinical picture as well as the findings presented by other methods of investigation.

Examination of transverse axial scan pictures is conducted in much the same way as that of any radiograph. Structures are identified and their shape, size, and position defined. The perspective presented may at first be found to be unusual but later, with usage, no real difficulties are encountered. Changes in tissue density are then looked for, and in this respect, symmetry between the two hemispheres is an important factor in enabling an abnormality to be identified. For a lesion to be precisely

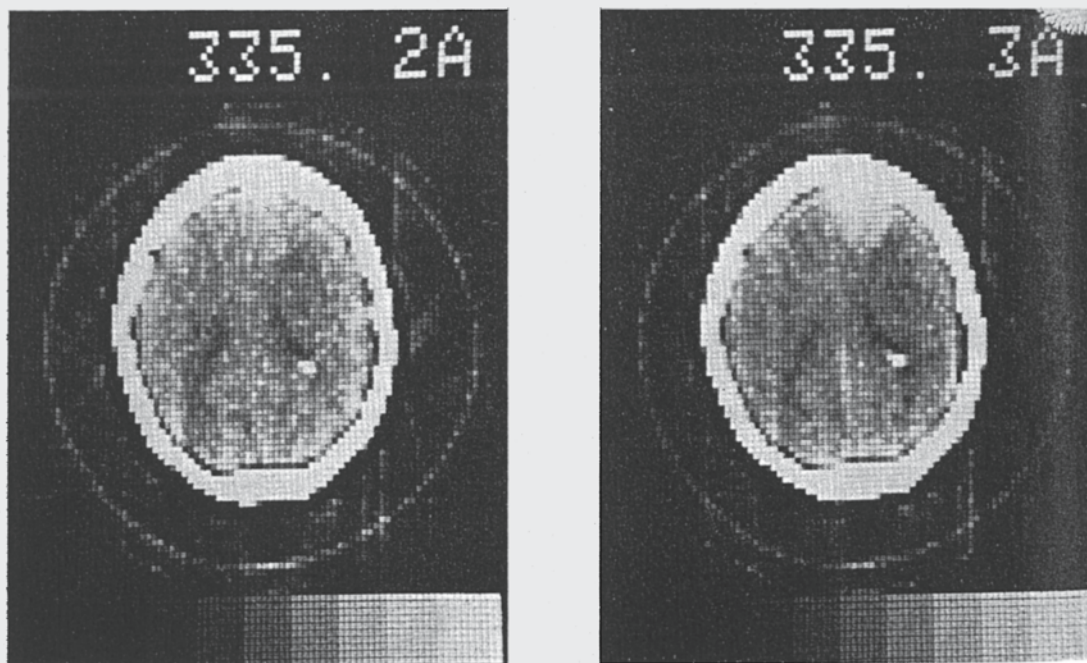


FIG. 6.

Right frontal cortical meningioma.

Scan 2A shows the tumour as slight increase of tissue density. The lesion is much better seen in 3A after tissue density enhancement with sodium iothalamate by intravenous injection.

DECEMBER 1973

Computerized transverse axial scanning (tomography): Part 2. Clinical application

located in the picture, the density of the abnormal tissues must be either higher or lower than that of the surrounding normal tissue. If, however, the average density of the lesion is the same as that of normal surrounding tissue, then it will not ordinarily be detected in the scan. Artificial enhancement of the density of abnormal tissue is discussed in a following section.

Slow-growing neoplasms and a variety of other pathological entities with a closely knit or fibrotic structure would be expected to be more dense than normal tissue.

Calcification in the form of calcospherites or larger aggregates occurring in a variety of different lesions will greatly raise the density of affected tissues. Meningioma, low grade astrocytoma, oligo-

dendroglioma and ependymoma are examples of neoplasms which may show up as "white" areas because of their high tissue density (Figs. 6, 7 and 8). Calcium aggregates in other lesions such as angiomas, the walls of large aneurysms, and some varieties of benign cysts, degenerations and indolent infective diseases would similarly be expected to be shown in scans passing through the affected tissues.

In intracerebral haemorrhage the associated tissue damage will usually result in some surrounding oedema and therefore reduction of tissue density, but once clotting has taken place the high concentration of calcium ions, the haemoglobin in the clot and the squeezing out of serum all combine to produce a great increase in average density, enabling the lesion to be instantly recognized, and the extent

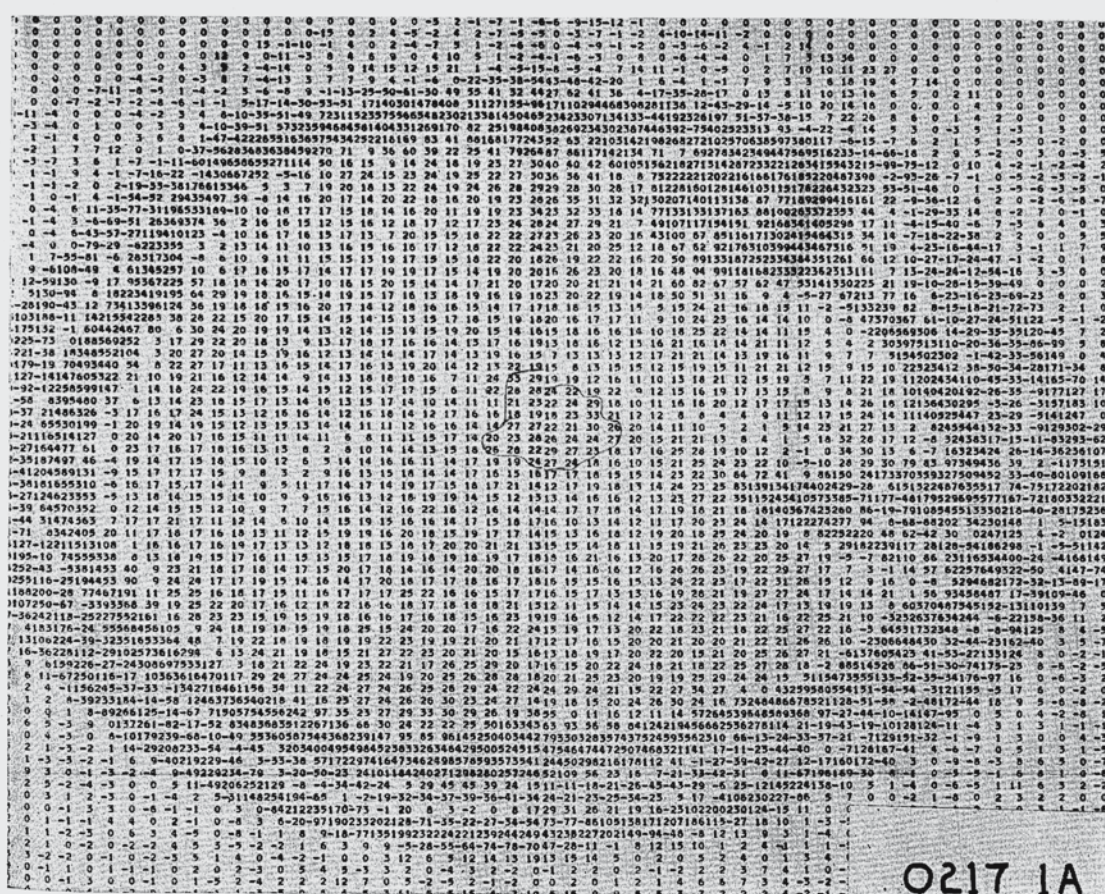


FIG. 7A.

Computer print-out

Third ventricle ependymoma in a young adult female patient. Faint suprasellar calcification was detected in the skull X rays. The small calcium aggregates account for the height average density of the tumour.

VOL. 46, No. 552

J. Ambrose

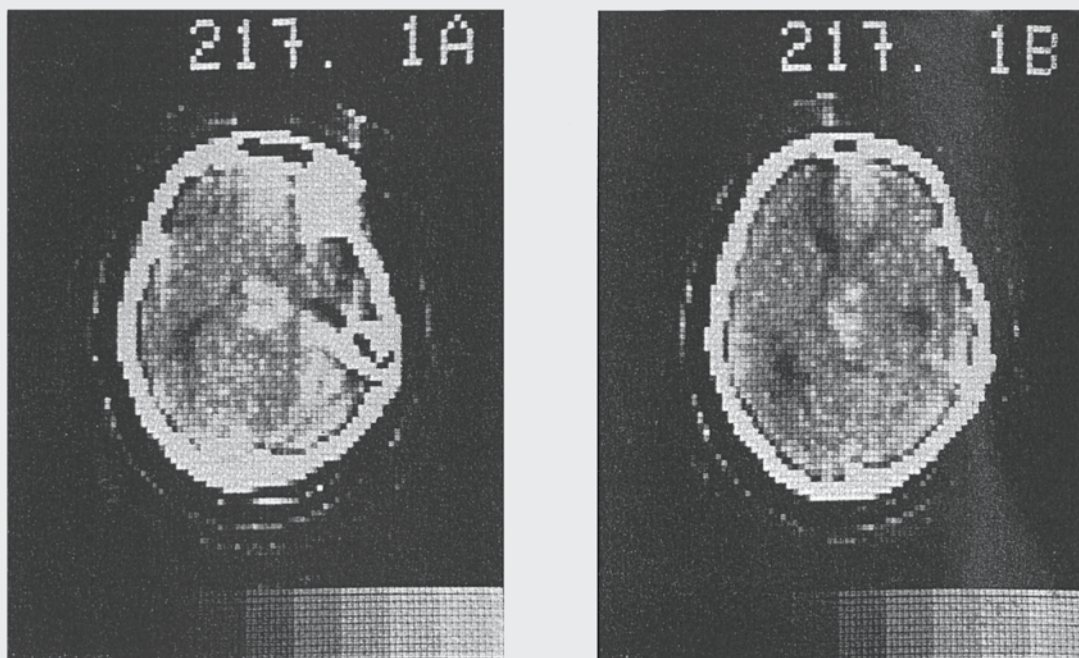


FIG. 7B.

Polaroid picture of 7A.

The scan was made 3 cm above the orbito-meatal line and is slightly oblique. The pictures represent adjacent slices each 1.3 cm thick. The 3rd ventricle is occluded by the tumour. In picture 1B the inferior portions of the anterior horns of the lateral ventricles are seen.

and relation to other structures to be defined (Fig. 9D).

Since the accuracy and sensitivity of the method is of a very high order, artificially raising the density of abnormal tissue or enhancing the density difference at the boundaries of the affected tissue becomes a possibility. The break-down of the blood brain barrier in an abnormal area should enable small amounts of circulating substances to pass into the abnormal tissue and to be retained for relatively long periods of time.

The attraction of being able to inject a compound containing atoms of high atomic number into the circulation, allowing sufficient time for it to concentrate in a tumour or abnormal tissue, and then to demonstrate the lesion by means of a plain radiograph, has in the past, formed the basis of a number of experiments. Unfortunately, the substances which showed most promise were too toxic to be used in sufficient amounts, and for compounds of low toxicity, the conventional X-ray method was not sufficiently sensitive.

We have repeated these experiments using a pre-

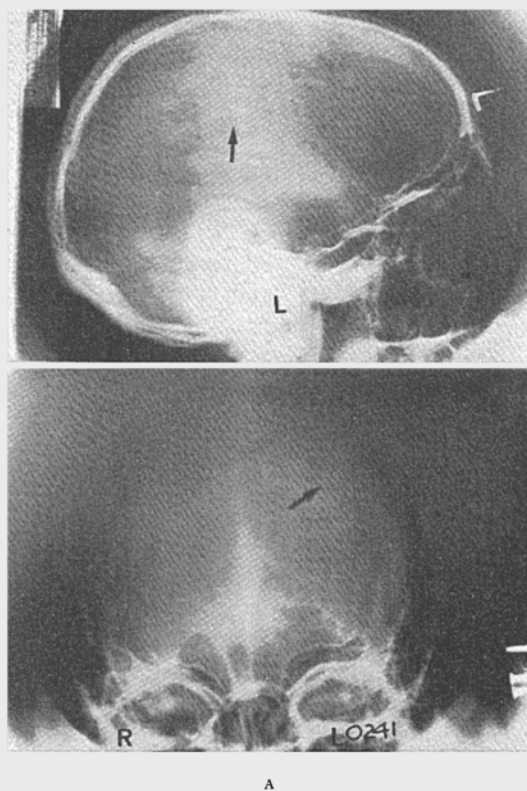
paration of sodium iothalamate which contains 420 mg of iodine per ml. A dose of 20–40 ml. is administered by intravenous injection. Scans taken at 5, 10, 15, and 20 minutes after the injection showed appreciable increases in the density of a variety of tumours (Figs. 10 and 11).

Meningiomas, as would be expected, exhibit a marked increase in density. Some tumours appear to be able to retain the iodine containing molecules of the contrast medium used for arteriography for some hours following injection (Fig. 12).

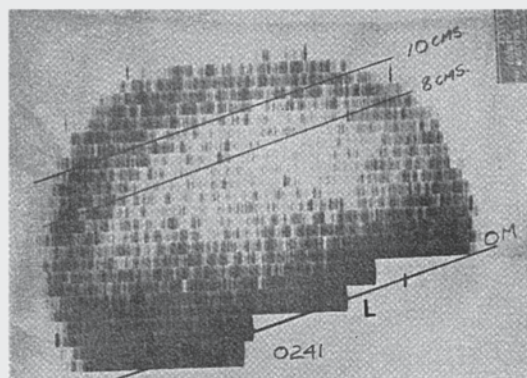
Diminished tissue density on the other hand, may arise out of a larger number of pathological conditions. The break-down of cell structure in infarctions, massive coagulative necrosis in malignant tumours, macroscopic and microscopic cyst formation, degenerative alterations of various kinds and oedema, are some of the main changes which will reduce tissue density and are observed as darker areas in the scan pictures.

While no really distinctive pattern has yet emerged from our study of the numerical absorption coefficient values in low density lesions, it should be

DECEMBER 1973

Computerized transverse axial scanning (tomography): Part 2. Clinical application

A



B

FIG. 8.

Unverified cerebral tumour exhibiting calcification.

- (A) Skull radiographs showing calcification in the left parietal lobe.
 (B) $^{99}\text{Tc}^{\text{m}}$ brain scan of the same patient showing the orbito-meatal line and the levels at which the scans were carried out, i.e. 8 cm and 10 cm.

VOL. 46, No. 552

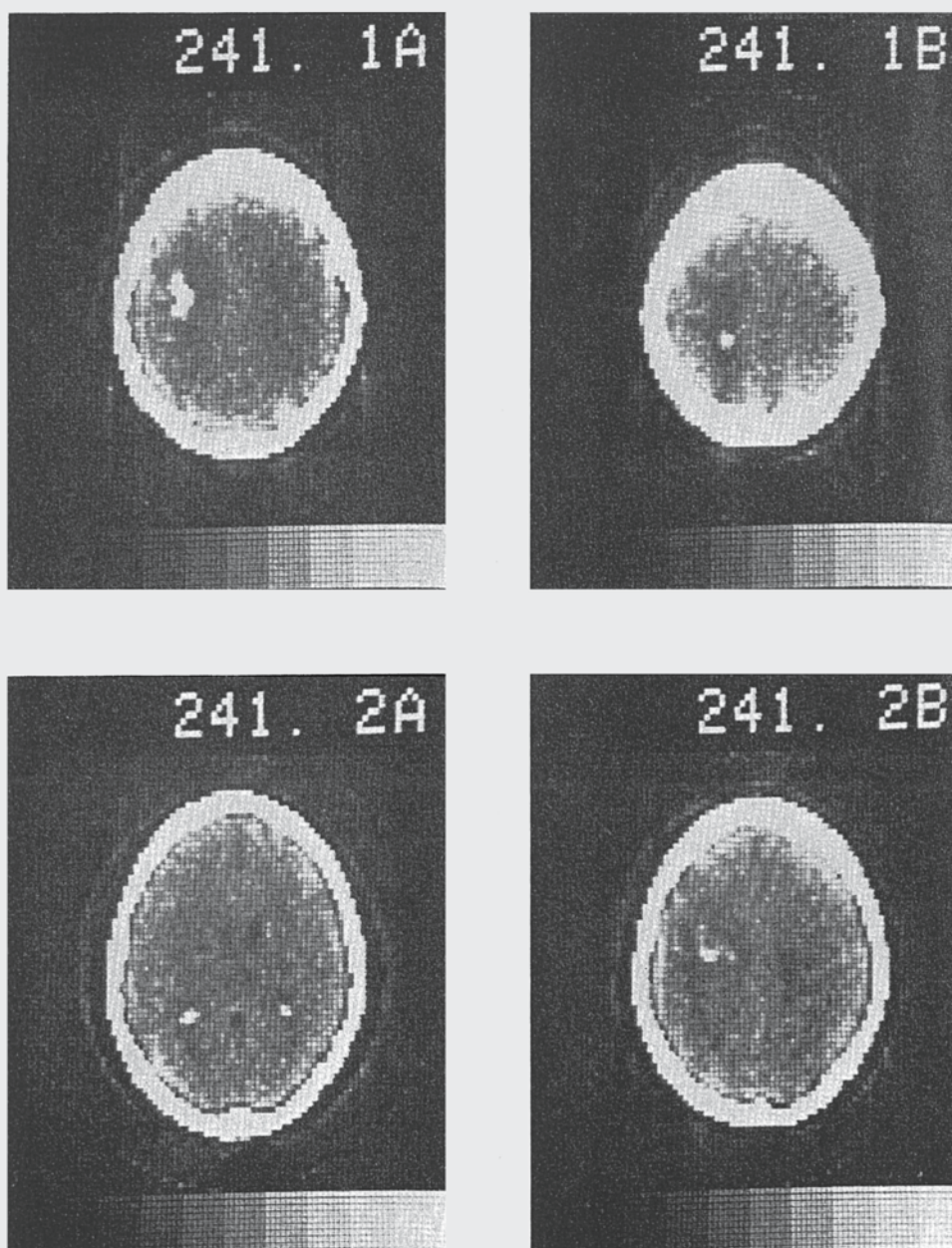
J. Ambrose

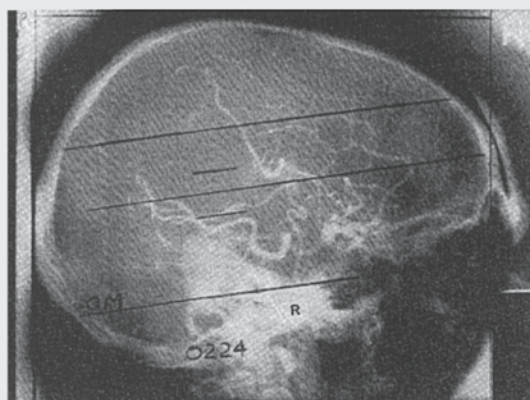
FIG. 8c.

Unverified cerebral tumour exhibiting calcification.

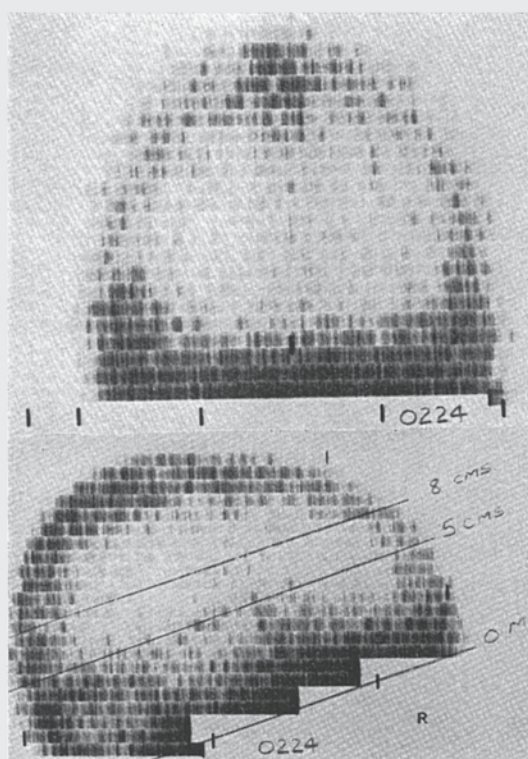
(c) Computerized scans, Polaroid pictures.

Pictures 2A and 2B are the sections below and above the 8 cm line while 1A and 1B are the sections below and above the 10 cm line. The low density area surrounding the calcification represents abnormal tissue, *i.e.* tissue affected oedema or possibly uncalcified tumour of a higher grade of malignancy. *Note:* The calcification has print-out values of over 100.

DECEMBER 1973

Computerized transverse axial scanning (tomography): Part 2. Clinical application

A



B

FIG. 9.

Primary intracerebral haemorrhage.

(A) Right carotid arteriogram showing the displacement and spreading of the branches of the middle cerebral artery. The orbito-meatal line and the levels scanned (5 and 8 cm respectively), are indicated by black lines.

(B) ^{99}Tcm brain scan. The haematoma is not localized. There is a small amount of increased activity in the right mid-temporal area which is probably arising from the Sylvian veins and the inferior anastomotic vein.

VOL. 46, No. 552

J. Ambrose

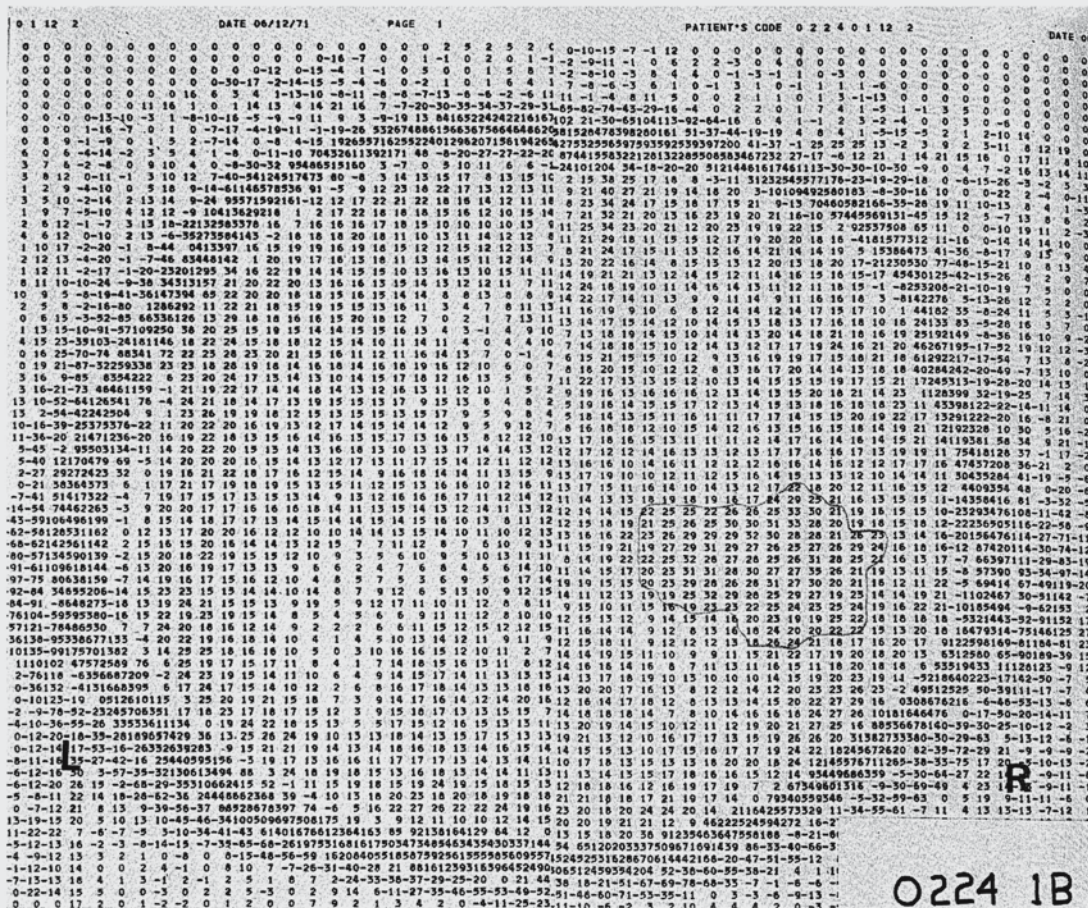


FIG. 9C.

(c) Computerized scan. Print-out. The haematoma is defined by high absorption coefficient values due most probably to calcium ions within the haematoma, and the concentrated clot, most of the serum having been absorbed. The displaced ventricular system is defined by low values arising from the fluid contents.

possible in the majority of cases to differentiate tumours from degenerative and other non-neoplastic lesions. The pattern of tissue involvement, the tendency to necrosis and cyst formation in malignant tumours and the displacement and distortion of identifiable structures such as the ventricular system and pineal body may aid in identifying the nature of an abnormality (Figs. 13 and 14).

In infarctions it may be possible to identify the lesion by the greater involvement of white matter and the absence of features usually seen in association with space occupying lesions (Fig. 15).

Cerebral metastases are identified as such by their multiplicity (Fig. 16).

Some solitary lesions may be seen as well defined tissue abnormalities of either low or increased density. Local oedema which frequently accompanies these lesions may, as in other methods of investigation, mask the true extent of the neoplastic tissue. Cystic degeneration or haemorrhage which also occur in cerebral metastases, are easily identified as such by defined low density areas or irregular areas of high density.

Some benign tumours because of their location

DECEMBER 1973

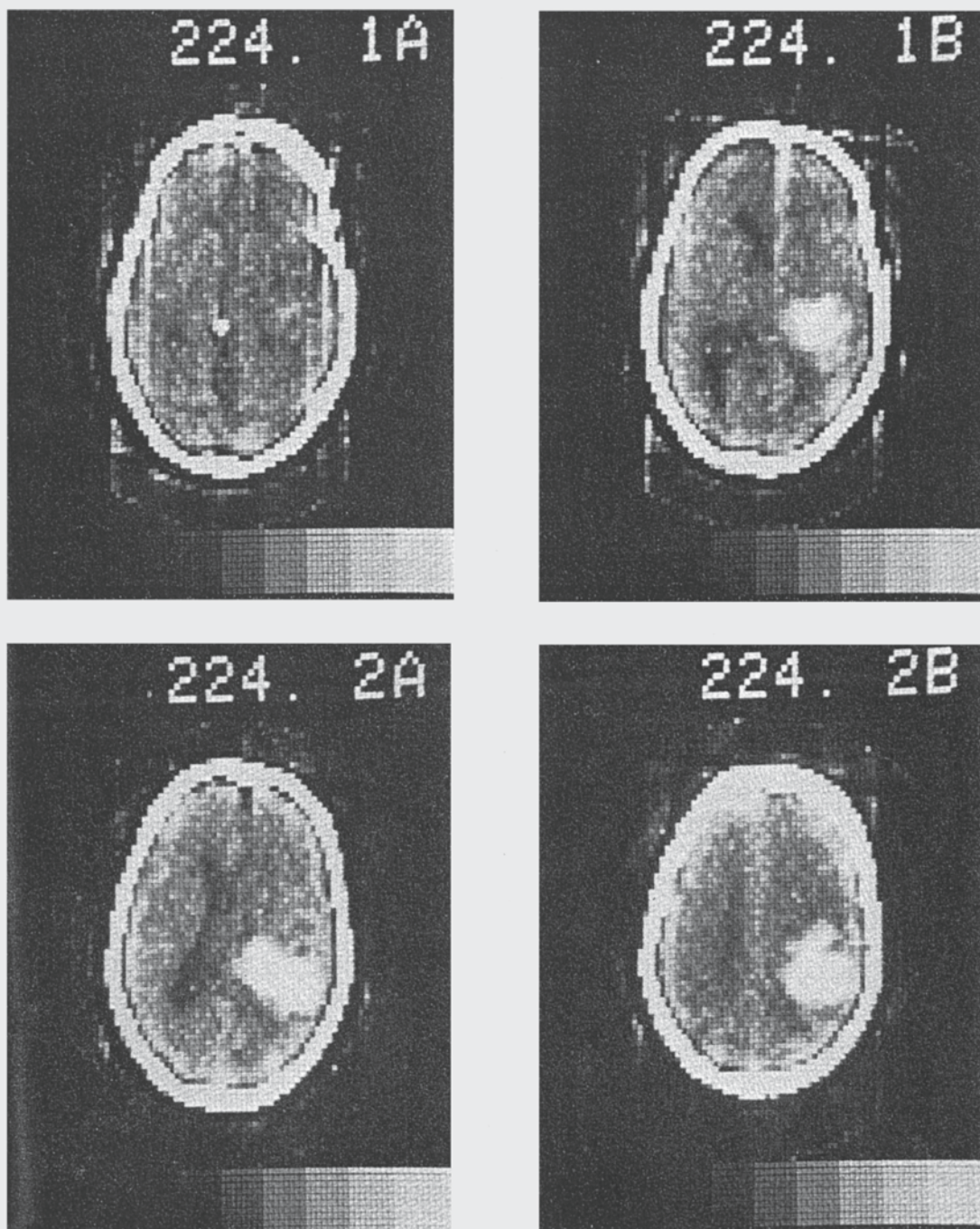
Computerized transverse axial scanning (tomography): Part 2. Clinical application

FIG. 9D.

(D) Polaroid pictures of scans made at 5 and 8 cm respectively. Note the displaced pineal body and the displaced ventricular system. The successive adjoining sections show the haematoma in a new and different perspective. The relationship to deep structures as well as the approach to the surface of the brain, are exhibited.

VOL. 46, No. 552

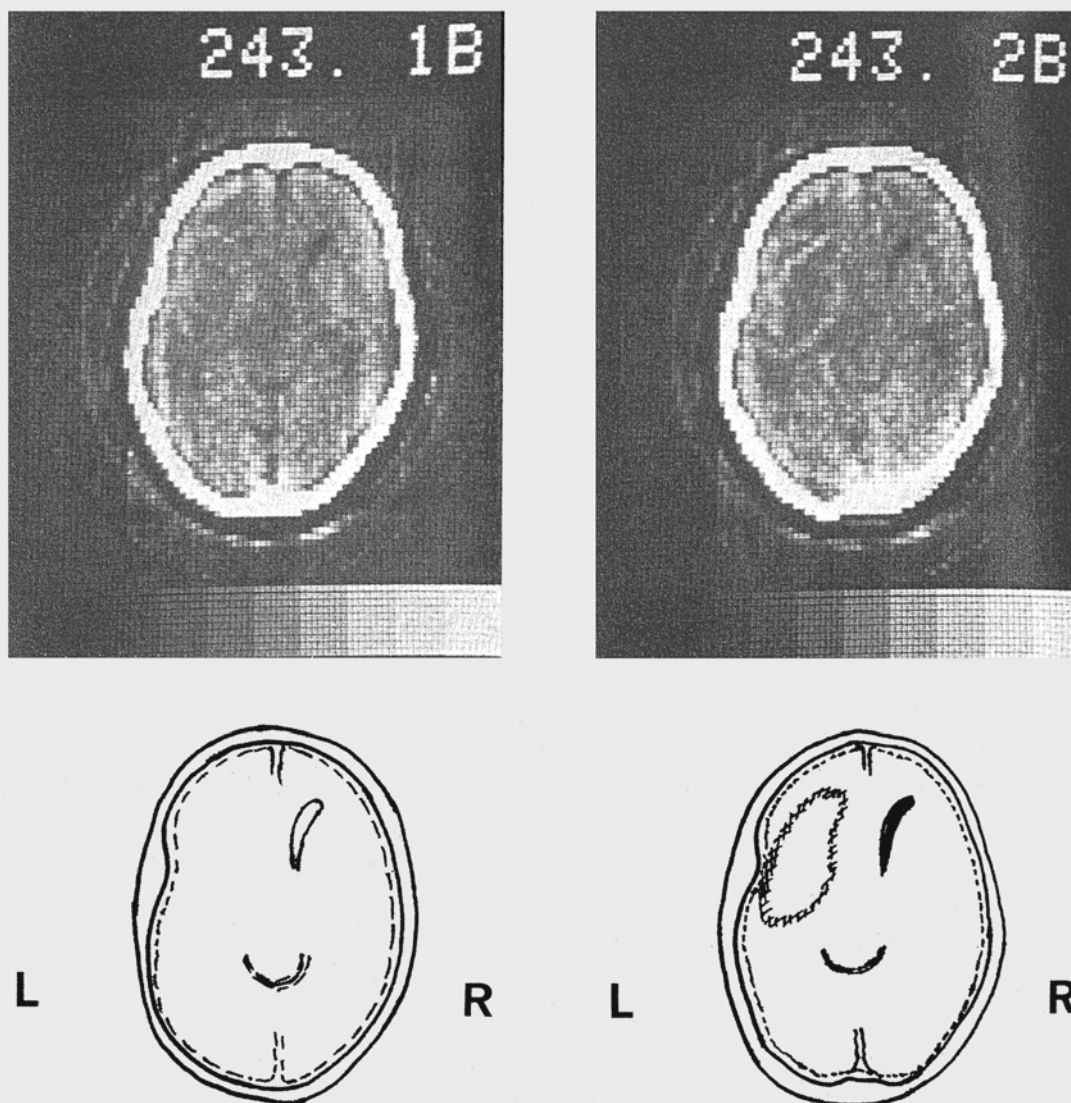
J. Ambrose

FIG. 10.

Left inferior frontal tumour.

Scan 1B shows the displaced ventricular system and a barely discernable change of tissue density in the anterior portion of the left hemisphere. Scan 2B was taken at the same level 20 minutes after the administration of 20 ml. of sodium iothalamate by intravenous injection. A rim of high density tumour tissue is now clearly seen. Astrocytoma Grade III proved by craniotomy and histological examination.

and constitution, may exhibit characteristics enabling a specific identification to be made. Cystic craniopharyngioma, epidermoid cyst, or cholesteatoma are examples of such tumours. The cyst contents being of a fatty nature, will have a density

lower than water and will therefore be represented as negative values on the chosen scale of absorption coefficients. Calcification which may be present in the form of sheets or plaques in the cyst wall or capsule, is easily identified by its high density (Fig. 17).

DECEMBER 1973

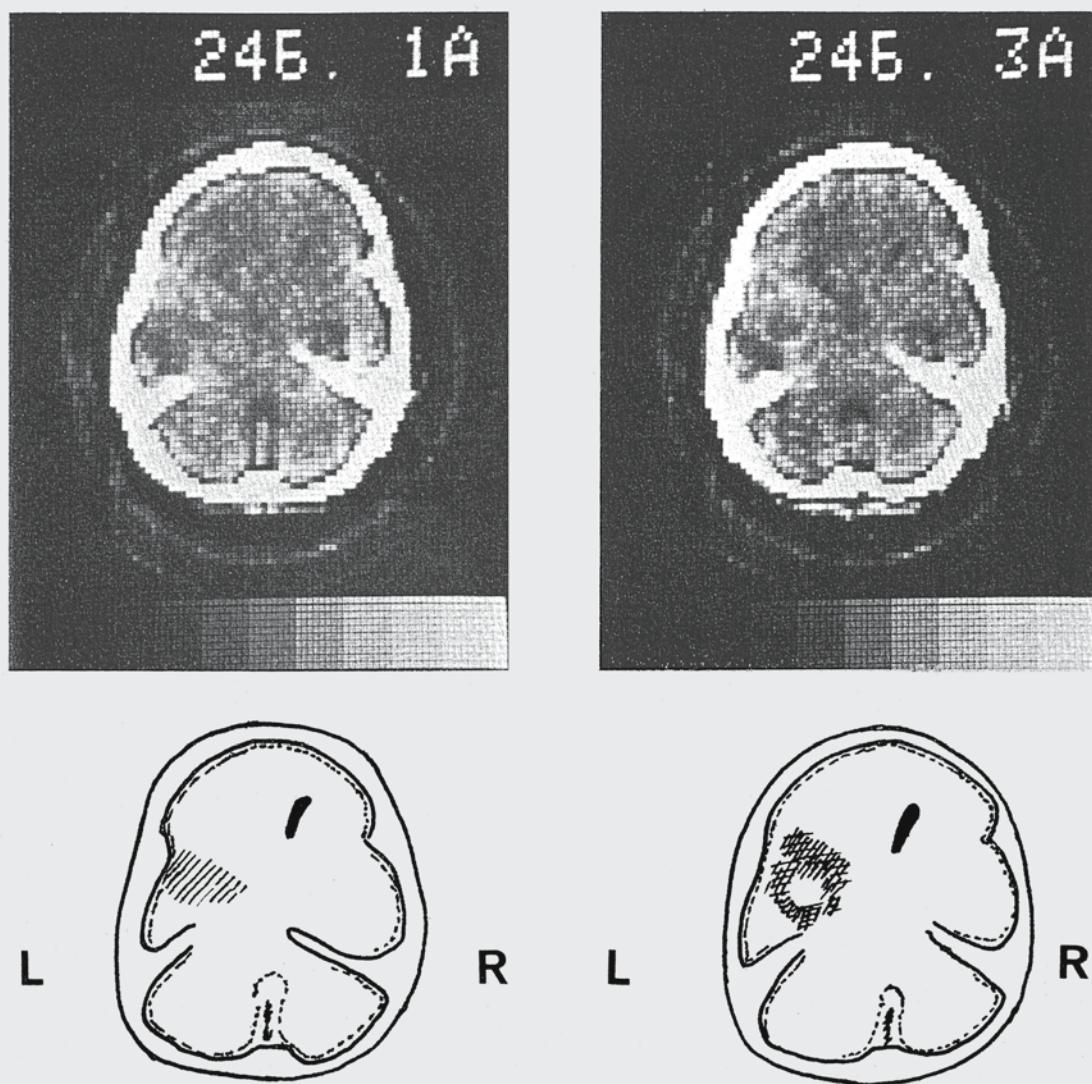
Computerized transverse axial scanning (tomography): Part 2. Clinical application

FIG. 11.

Left temporal tumour.

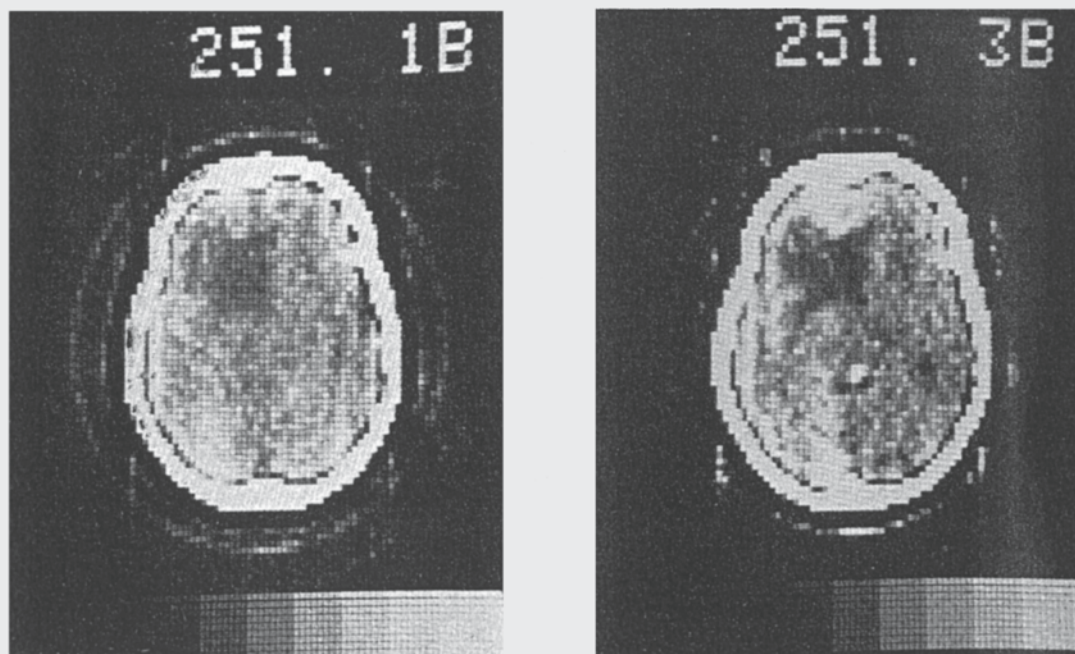
Scan 1A shows a slight difference of density between the two temporal regions. Scan 3A was taken 20 minutes after the injection of 40 ml. of sodium iothalamate (Conray 420) by intravenous injection. The tumour is now clearly seen. Astrocytoma Grade III proved by craniotomy.

We have so far been able to examine only seven patients with chronic subdural haematoma. We had expected to be able to demonstrate the lesion as an extracerebral lens shaped area of either high or low absorption depending on the density of the haematoma fluid. In all the patients examined we have demonstrated the displacement of the ventricular

system or pineal body but in six patients, the expected demonstration of the actual haematoma was not found. This was due to the haematoma fluid having the same average density as the brain. A thin poorly defined low density line marking the boundary between haematoma and brain was all that could be defined (Fig. 18).

VOL. 46, No. 552

J. Ambrose



IG. 12.

Left frontal meningioma.

Scan 1B shows a dense left front tumour immediately behind a local thickening of the left frontal bone. The area of low density behind the tumour is oedematous brain. Scan 3B was taken two hours after carotid arteriography and at a slightly lower level. Note the increased density due to retention of contrast medium by tumour tissue.

In the seventh and last patient however, the haematoma was of a higher average density than the brain tissue and could easily be identified (Fig. 19).

In cranio-cerebral trauma it may be important (and difficult) to distinguish between cerebral contusion, cerebral laceration, or cerebral oedema on the one hand and an intracerebral haemorrhage on the other. In these cases computerized transverse axial scanning is capable of providing specific differentiation. Because of the locally high concentration of calcium ions, a haematoma is seen as an area of high density, while tissues affected by oedema will exhibit low density.

DISCUSSION

Computerized transverse axial tomography is a new and fundamentally different diagnostic X-ray method. Modern electronic and computer technology have been allied to X-ray detection and measurement to analyse the information content of a beam of X-ray photons passing through tissue,

in such a way that remarkable tissue differentiation becomes possible.

It is possible that the method will not immediately reduce the present practice of cerebral arteriography or pneumo-encephalography but, like radio-isotope brain scanning, it will undoubtedly come to occupy an increasingly important position, and in similar fashion will no doubt, supersede contrast radiological procedures in the investigation of many patients.

The hope is, that the majority of patients requiring investigation for a neurological complaint will need to be subjected only to plain skull radiography, a radio-isotope brain scan and a computerized transverse axial scan, either singly or in combination. These investigations should provide sufficient information in respect of location, tissue abnormality structural displacement, and possibly the nature of a lesion for the institution of definitive treatment.

As this communication is intended to be a preliminary description of a new method, it has not

DECEMBER 1973

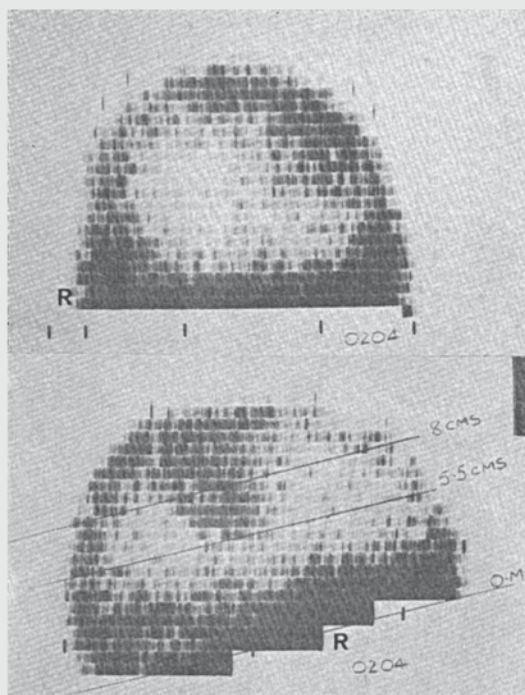
Computerized transverse axial scanning (tomography): Part 2. Clinical application

FIG. 13A.

*Left parietal tumour.*⁹⁹Tc^m brain scan with the scanning levels indicated.

been possible to give more than an indication of the potential for locating and identifying disease processes. Increased use of the method will, however, no doubt result in a greater pool of knowledge and a more accurate definition of its scope, but at the present stage of development some of the limitations require to be stated:

1. Movement limitation

A small amount of movement will introduce aberrations into the readings. This will reduce the quality of the pictures. A considerable amount of patient co-operation is therefore required and, although the introduction of shaped plastic head cones has greatly reduced the amount of small

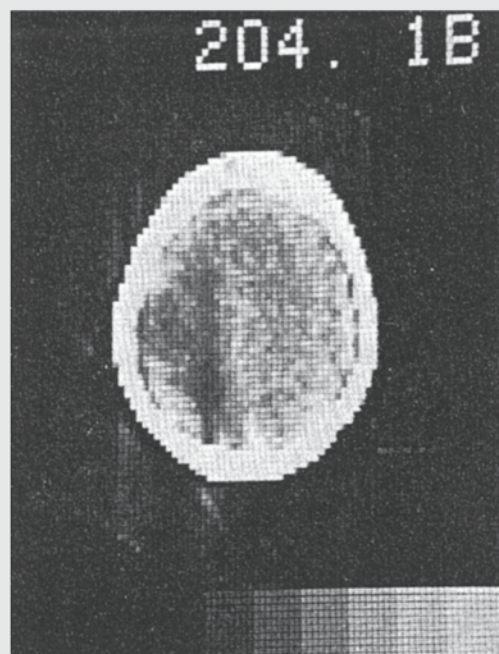
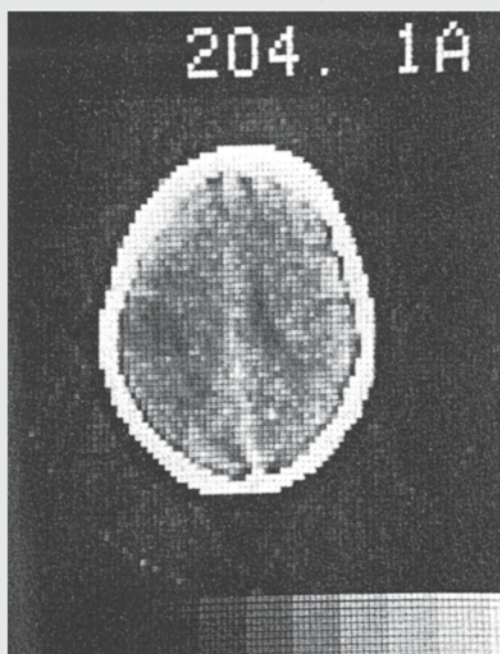


FIG. 13B.

Computerized scan showing the large irregular low density area due to necrotic tumour and oedematous brain tissue. Astrocytoma Grade III proved by craniotomy.

VOL. 46, No. 552

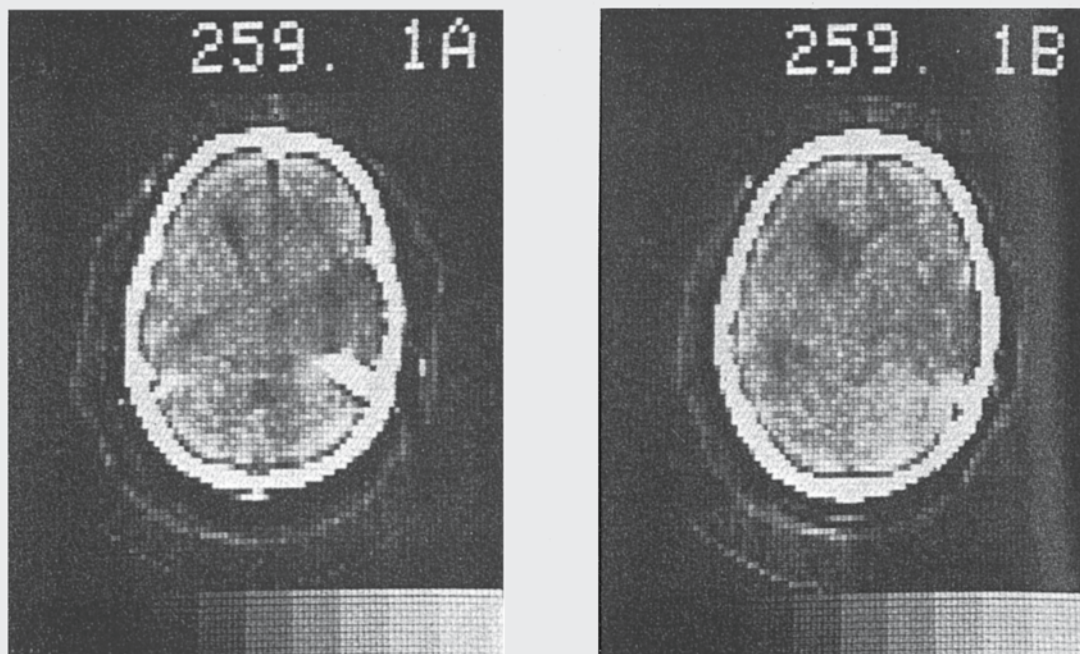
J. Ambrose

FIG. 14.

Right temporal tumour.

Scan made at 4 cm. The large irregular low density area in the right temporal region indicates the tumour. Note the displacement of the ventricular system. Astrocytoma Grade III proved by craniotomy.

inadvertent movement, four minutes is a long time for a patient to remain perfectly still, and some small movements nearly always occur. In scans of the mid-section of the cranium these movements do not seriously affect the quality of the pictures, but lower down near the base, the effect is much more serious. This effect is seen as vertical streaking (Fig. 9D, 1A, 1B). Heavy sedation has been used in restless patients but this is clearly much less satisfactory than conscious co-operation.

2. Examinations involving the skull base, posterior fossa, and high convexity of the cranium

Examinations involving these areas tend to be less satisfactory than those of the broad mid-section of the cranium. The method operates to maximum advantage when there are no large changes in tissue density. In the skull base, the air-filled sinuses and

mastoid air cells give rise to large negative values, while the complex bony structures provide high positive values. Small movements of the head in these conditions will, therefore, affect the accuracy of the readings to a considerable degree.

To examine the posterior fossa, it is necessary to angle the plane of examination with respect to the orbito-meatal line, so that some of the complex bony structures of the floor of the anterior and middle cranial fossae are avoided. In the high convexity of the cranium the bony walls slope increasingly steeply to the sagittal midline, so that the plane of section, although still normal to the long axis of the body, is no longer also normal to the body wall. Some brain tissue will therefore be hidden by the slope of the bone contained in the width of the section (1.3 cm). This difficulty can be partially overcome by using a smaller slit, thus reducing the

DECEMBER 1973

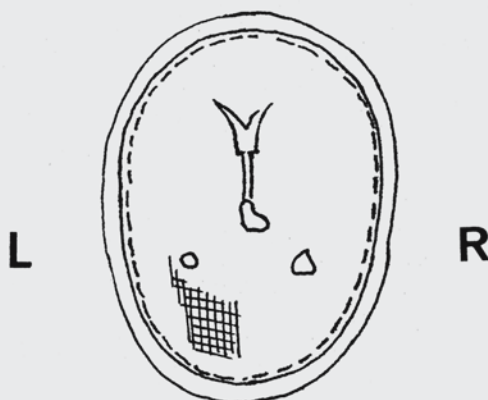
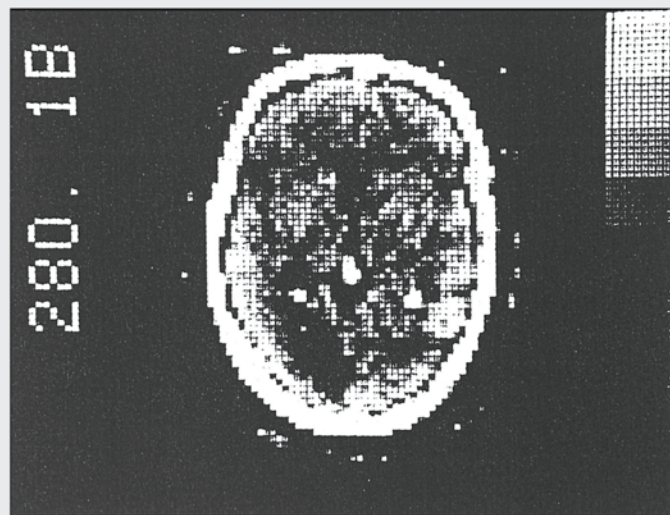
Computerized transverse axial scanning (tomography): Part 2. Clinical application

FIG. 15.

Left occipital infarction.

The scan has been made at 5 cm. The low density area in the left occipital area indicates the extent of infarcted tissue. The ventricular system is normal. Note the midline pineal body and symmetry of the choroid plexuses.

VOL. 46, No. 552

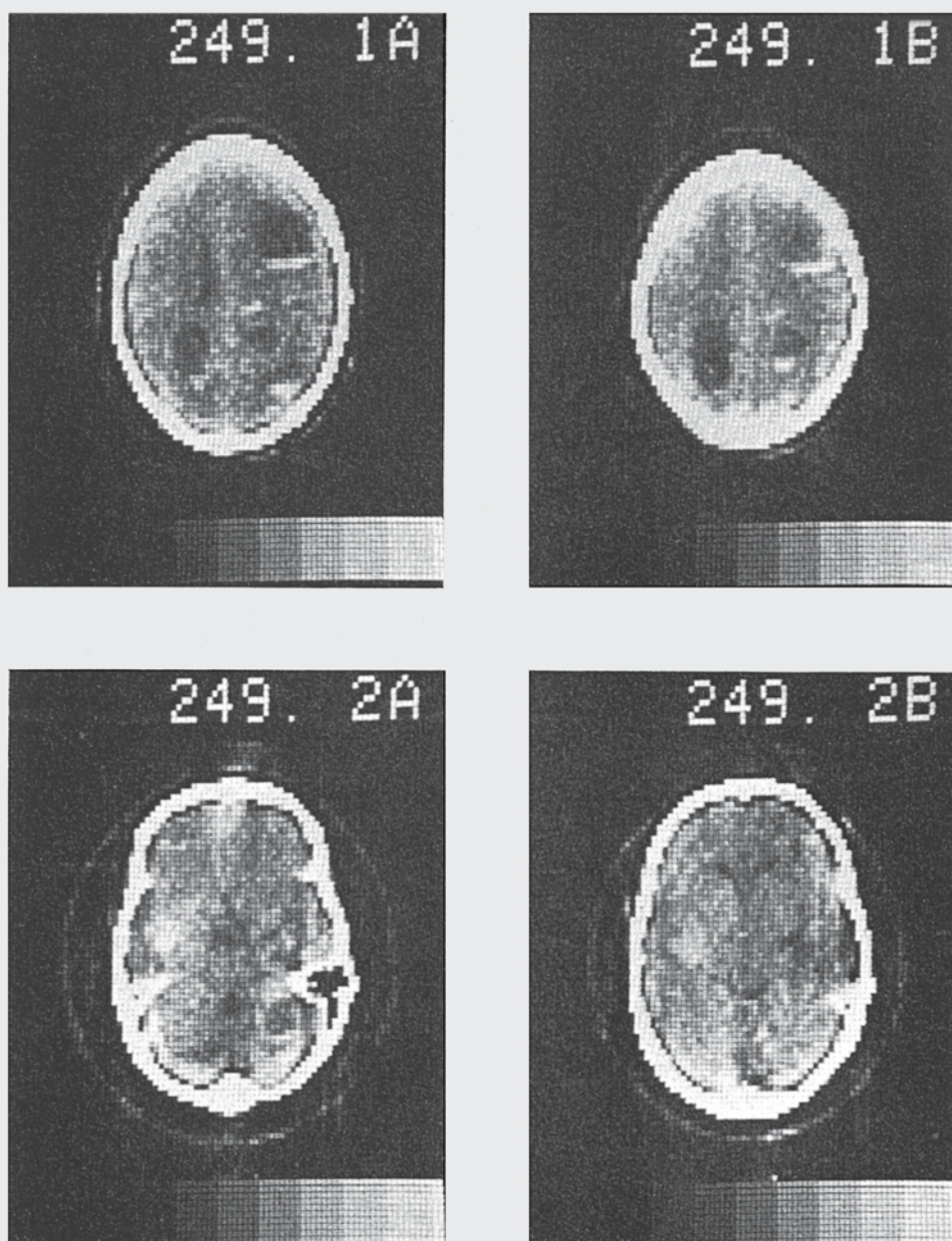
J. Ambrose

FIG. 16.

Cerebral metastases.

The patient had previously undergone resection of the left lung for a squamous cell carcinoma. The scans have been made at 9 cm and 5.5 cm respectively. Note the cystic lesions in the right frontal, parietal and occipital areas and the single large lesion in the left posterior parietal area. A fairly large metastasis is also seen in the right cerebellum (Scan 2A).

DECEMBER 1973

Computerized transverse axial scanning (tomography): Part 2. Clinical application



FIG. 17A.

Scans made at 4.5 and 6 cm. Middle-aged male patient with life-long poor vision, lately becoming blind in the left eye. (A) Computer print-out of the lower scan made at 4.5 cm. The negative values of the absorption coefficients for the cyst contents indicate that they are of a lower density than water and therefore most likely to be cholesterol.

VOL. 46, No. 552

J. Ambrose

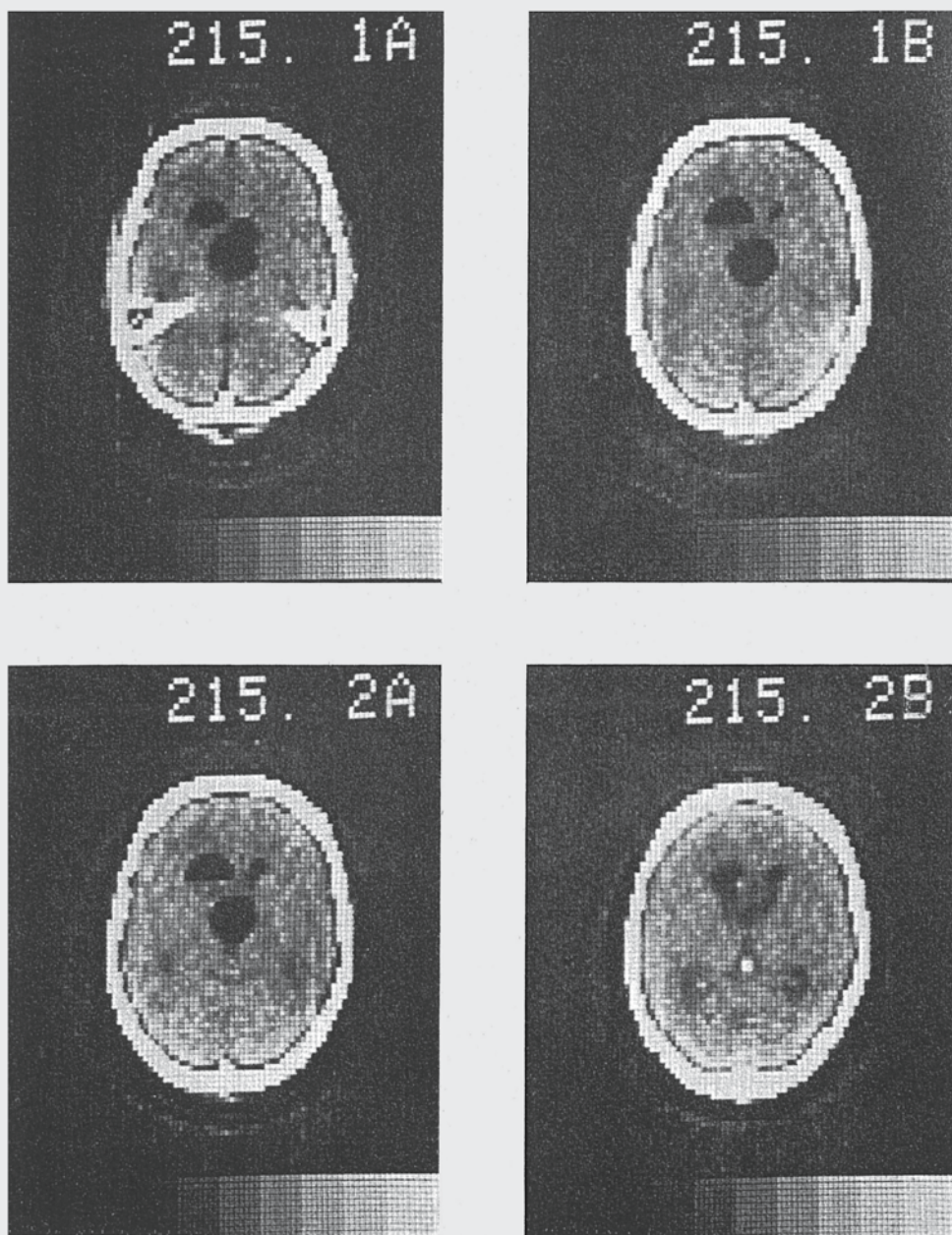


FIG. 17B.

Craniopharyngioma.

(B) Polaroid pictures. Note the central cyst with a locule extending into the left frontal lobe. Specks of calcification are visible in the cyst wall in Scan 2A and 2B. In Scan 2B the top of the cyst protrudes into the floor of the anterior aspects of the lateral ventricles.

DECEMBER 1973

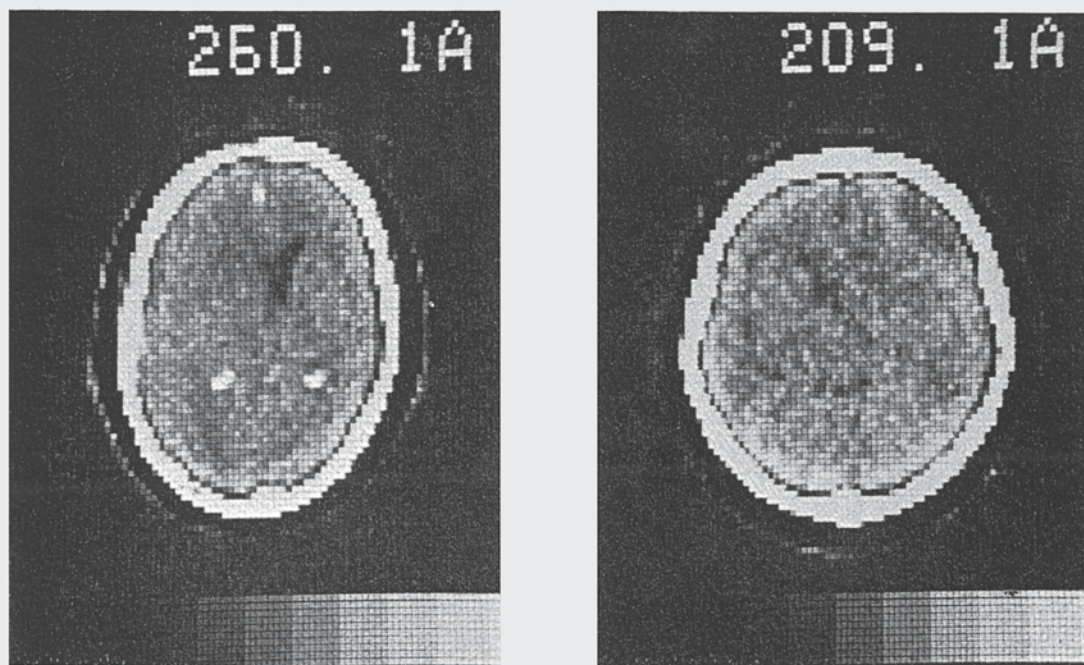
Computerized transverse axial scanning (tomography): Part 2. Clinical application

FIG. 18.

Scan 260 1A. Left chronic subdural haematoma.

The ventricular system is displaced. The choroid plexuses are asymmetrical and the pineal body is displaced. The only other indication of the location of the subdural haematoma is the poorly defined diagonal translucent line in the left parietal area.

Scan 209 1B. Right frontal subdural abscess.

The ventricular system is displaced to the left, but here due to the different nature of the fluid in the subdural space, the lesion is easily located as a lens shaped area of low density.

VOL. 46, No. 552

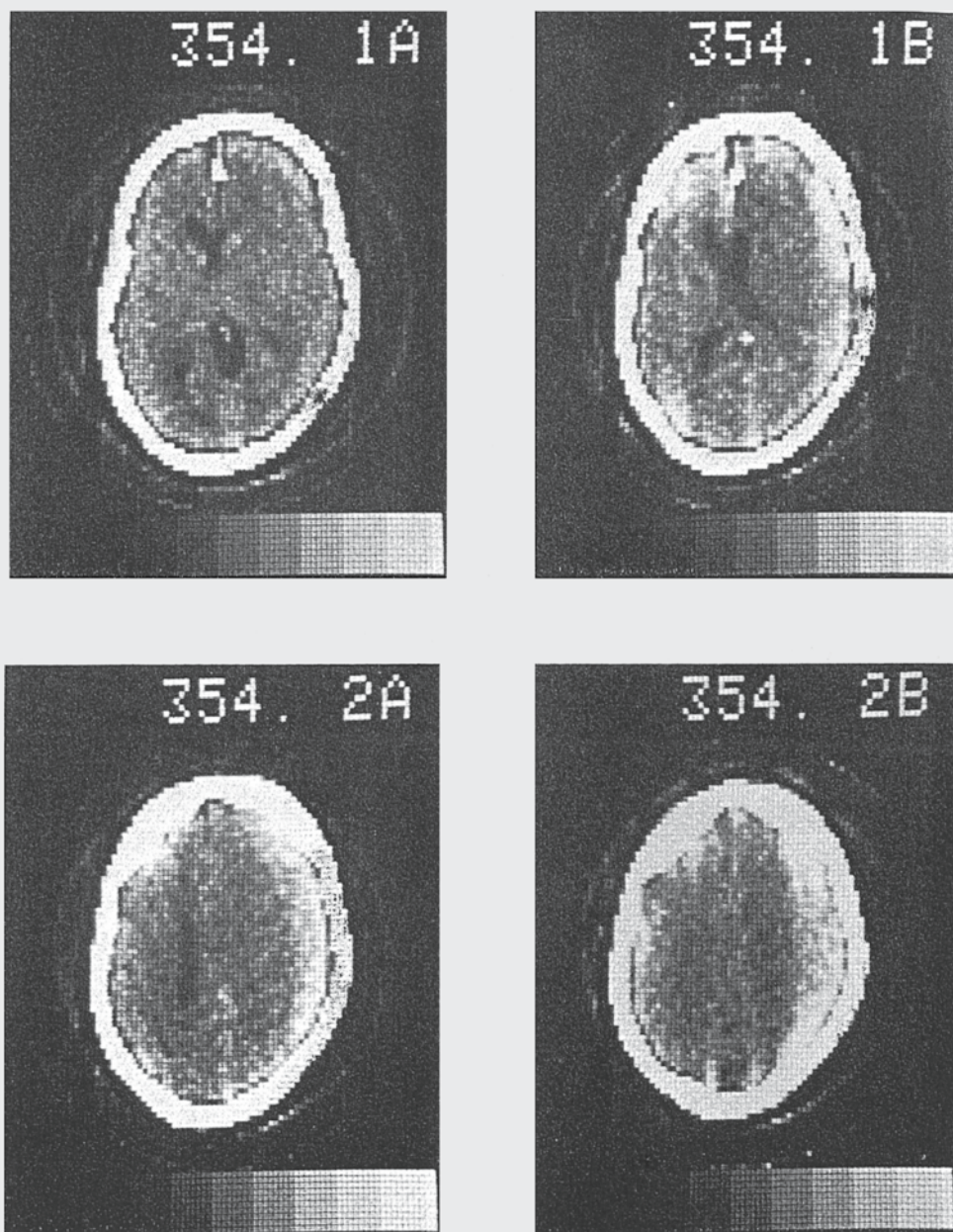
J. Ambrose

FIG. 19.

Chronic subdural haematoma.

In a small series of seven patients with chronic subdural haematoma, this was the only instance where the haematoma could be seen as a typical lens shaped area of increased density (scans 2A and 2B). Note the displacement of the ventricular system to the left.

DECEMBER 1973

Computerized transverse axial scanning (tomography): Part 2. Clinical application

width of the section to 0.8 cm. However, the number of photons is also reduced and the picture quality will therefore suffer to some small extent.

3. Resolution of small detail anatomy

For the present it is unlikely that the method will be able to provide sufficient resolution of small structures. The practical problems presented by aqueduct stenosis, chiasmic and optic nerve compression or small tumour in the cerebello-pontine angles, are a few examples in this respect. At the present time pneumo-encephalography is the main method of investigation with cerebral arteriography used in a complementary role.

Similarly, in the investigation of cerebral haemorrhage, carotid and vertebral angiography remain the only effective methods for displaying the blood vessels and associated abnormalities, *i.e.* aneurysms, angiomas, spasm, atherosclerotic disease, stenosis,

or occlusion. However, in the overall investigation of cerebro-vascular disease, computerized transverse axial scanning will, without doubt, come to be an invaluable means of distinguishing between haemorrhage and infarction.

ACKNOWLEDGMENTS

The author wishes to thank Dr. E. A. Lennon and Mr. C. Gregory for arranging the first meeting with Mr. G. N. Hounsfield on whose original idea and design the EMI-scanner is based, and for their continued support during the development of the project. Grateful acknowledgments are also due to the following for invaluable advice during the initial experimental stage and in the design, development and construction of the prototype scanner: Mr. G. R. Higson, Dr. N. A. Slark, Mr. O. A. McCabe of the Department of Health and Social Security; Mr. Brian Keane of the Royal Sussex Hospital; Dr. Louis Kreel and Dr. Frank Doyle who participated in the original experiments; members of the Design Team at EMI particularly Mr. P. G. Langstone, Mr. J. D. Coppen and Mr. S. Bates, and also Mr. K. R. Hill for help in assembling the material and in preparing this paper; and members of my own Department at Atkinson Morley's Hospital.

Book review

Bone Loss in Normal and Pathological Conditions. By J. Dequeker, pp. xi + 214, 1972 (Kapellán, The Netherlands, Leuven University Press), 177 F.

There are two main aims to the investigations which Dr. Dequeker has carried out; they are first the determination of normal standards of bone loss with age, and second the evaluation of bone loss in pathological conditions with respect to the loss observed in the normal state.

Cortical bone loss is evaluated in terms of geometric properties of the shaft of the second metacarpal; the measurements on radiographs of shaft width and cortical thickness are readily performed by hand, requiring only a pair of calipers. A novel method of removing the influence of skeletal size on the results has been developed which is of considerable value in comparing different individuals, sexes and races. Dr. Dequeker makes the original observation that at the start of adult life both whites and negroes of both sexes have the same amount of bone for a given skeletal size.

Trabecular bone loss is evaluated from iliac crest biopsies and is expressed as a ratio of the volume of bone tissue within the biopsy to the external volume of the biopsy plug. The effects of trabecular bone loss from the spine are assessed in terms of a height/span index and from the biconcavity of the lumbar vertebral bodies. Interesting observations of the site to site variability in the biopsy parameters are made, and it is concluded that iliac crest biopsies do not permit changes in amount of bone to be followed in the individual.

A great deal of valuable data is provided for each of the measured variables, many of which are age-related. Two variables shown to be independent of age are the vertebral biconcavity index and the composition of trabecular bone. In connection with the latter, the collagen solubility is shown to increase with age and is attributed to the increased intermolecular cross-linking. With the age-related norms established, bone remodelling is investigated in patients with symptomatic and disuse osteoporosis, and with endocrine disorders. Endosteal bone loss is shown to be exaggerated in patients with femoral neck fracture, disuse osteoporosis of hemiplegia, rheumatoid arthritis, primary hyperparathyroidism and Turner's syndrome. The diagnostic usefulness of a number of morphometric parameters of the metacarpal are compared in each disease category. Finally the effects of calcium infusion therapy in patients with vertebral collapse are described; in addition to clinical improvement, there was found to be a significant decrease in total hydroxyproline excretion.

This book is concise and to the point, and although the bibliography is somewhat limited, sets the experiments which are described in their proper context. The logical progress of the book from experiment to experiment is highly commendable, and the provision of extensive tables of results makes it an invaluable addition to the library of those concerned with quantitative studies of bone in normal and disease states.

A. HORSEMAN.

1.5 Spiral volumetric CT with single-breathhold technique, continuous transport, and continuous scanner rotation

Willi A Kalender (born 1949)

Willi Kalender was born in Thor, Nordrhein-Westfalen, Germany, in 1949. Kalender received both his master's degree and his PhD in medical physics from the University of Wisconsin, Madison in 1979. In 1988 he completed his post-doctoral lecturing qualifications (habilitation) for medical physics at the University of Tübingen in Germany.

From 1979 to 1995 Kalender worked in the research laboratories of Siemens Medical Systems in Erlangen, Germany. He was the head of the department of medical physics from 1988 to 1995. He became adjunct associate professor of medical physics at the University of Wisconsin in 1991 and from 1993 to 1995 he lectured at the Technical University of Munich in Germany. Kalender was appointed full professor and director of the newly established Institute of Medical Physics at the Friedrich-Alexander-University Erlangen-Nürnberg, Germany in 1995.

His main research interests are in the area of diagnostic imaging, and the development and introduction of volumetric spiral CT has been a particular focus. Other fields of research include radiation protection and the development of quantitative diagnostic procedures.

He was nominated as distinguished visiting professor at Stanford University Department of Radiology in 2001, and adjunct full professor of the department of medical physics at the University of Wisconsin. He is also a member of the International Commission on Radiation Units and Measurement (ICRU). He was honorary lecturer of the European Congress of Radiology and the European Association of Radiology in 2002.

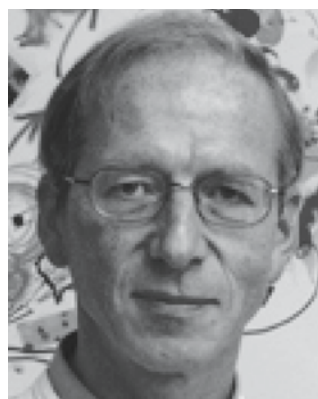


Peter Vock (born 1946)

Peter Vock was born on 12 November 1946 in Aarau, Switzerland. He qualified in medicine at the University of Bern in 1966, obtaining his MD in 1973. He started his residency in radiotherapy at the University Hospital Bern in 1973. He moved to diagnostic radiology at the University Hospital Bern in 1974 and to nuclear medicine in 1976, returning to diagnostic radiology in 1978. Vock took a residency in internal medicine from 1976 to 1978 at the Medical Propedeutic Clinic, Tiefenauhospital Bern.

From 1982 to 1984 Vock was a visiting research associate in thoracic radiology at the department of radiology at Duke University Medical Center, Durham, USA. He was appointed clinical staff member at the department of radiology, University of Bern, Switzerland from 1979 and in 1986 he took his post-doctoral lecturing qualifications (habilitation) at the medical faculty of the University of Bern and was then appointed lecturer. Two years later Peter Vock was appointed chief of MRI and in then 1987 chief of body CT and director of the teaching program at the department of radiology, University of Bern.

Peter Vock is currently professor of radiology and chairman of the Institute of Diagnostic Radiology and chairman of the Department of Radiology, Neuro-radiology and Nuclear Medicine at the University of Bern, Switzerland.



Peter Vock has been on many committees, including the Swiss Radiology Examination Board and the Swiss Society of Medical Radiology, serving periods as chair of the diagnostic section. From 1997 to 1998 he was president of the Société d'Imagerie Thoracique, and since 1988 he has been secretary general of the European Association of Radiology (EAR). He has been treasurer of the European Society of Thoracic Imaging since 1999 and was chest subcommittee chairman of the European Congress of Radiology in 1999 and 2000. Peter Vock was chairman of the Swiss Radiology Congress in 2000.

Peter Vock is on the editorial boards of "*Der Radiologe*", "*Schweiz. Medizinische Wochenschrift*", "*Therapeutische Umschau*" and "*European Radiology*" (chest section).

W. Seißler

E. Klotz

Thoracic Radiology

Willi A. Kalender, PhD • Wolfgang Seissler • Ernst Klotz, DiplPhys • Peter Vock, MD

Spiral Volumetric CT with Single-Breath-Hold Technique, Continuous Transport, and Continuous Scanner Rotation¹

Continuous computed tomographic (CT) scanning of organ volumes during a single breath hold was studied. The authors modified the table feed mechanism of a continuously rotating CT scanner to allow patient transport at low, but accurately controlled, speeds (0.1–11.0 mm/sec) during continuous 1-second scanning. An algorithm was designed to reconstruct artifact-free images for arbitrary table positions from the helical data by interpolating between adjacent scans. Section sensitivity profiles were enlarged; the section width for a 10-mm section and a speed of 10.0 mm/sec was increased by a factor of 1.3, compared with the nominal value. Clinical examples were presented for studies of lung nodules and studies enhanced with contrast medium. Major advantages are the possibility of continuous scanning of extended volumes within a breath-hold period and retrospective, arbitrary selection of anatomic levels.

Index terms: Computed tomography (CT), image quality • Computed tomography (CT), physics • Computed tomography (CT), technology • Lung, CT, 60.1214

Radiology 1990; 176:181–183

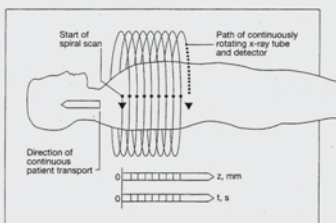


Figure 1. Sketch of the scanning geometry in spiral volumetric CT. t, s = time in seconds, z = section position.

IN whole-body computed tomography (CT), inconsistent levels of inspiration from scan to scan or patient motion may cause omission of some anatomic levels or repeated scanning of others. These factors may jeopardize the success of an examination (eg, the search for and diagnosis of pulmonary nodules) (1–4). These inconsistencies will also disturb image quality in three-dimensional displays and in multiplanar reformations, in which discontinuities due to motion between scans are frequent. Also, respiration between scans prolongs examination times; in particular, contrast material-enhanced studies of extended volumes cannot be completed within the vascular enhancement phase (5–7).

In this study, our aim was to continuously scan complete organ volumes or subvolumes during a single breath hold. This can be achieved with CT scanners that allow continuous data acquisition over multiple rotations if the patient or object is simultaneously transported continuously through the gantry.

MATERIALS AND METHODS

CT Equipment

We used a standard continuously rotating CT scanner (Somatom Plus; Siemens Medical Systems, Erlangen, Federal Re-

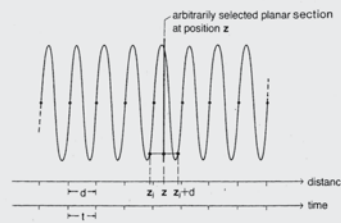


Figure 2. Principle of image reconstruction in spiral volumetric CT. Planar data for arbitrary table positions are calculated from the spiral data by means of linear interpolation.

public of Germany) that produces up to 12 consecutive 1-second scans. Tube currents ranged from 250 mA for 5-second scanning to 170 mA for 12-second scanning; section thicknesses of 1, 2, 5, 8, and 10 mm were available. The x-ray tube has a storage capacity of 3.5 million heat units.

In an experimental modification of the table feed mechanism, we incorporated a stepper motor to allow continuous transport of the patient at low, but accurately controlled, speeds (0.1–11.0 mm/sec) during scanning.

Scanning Geometry and Image Reconstruction

In this type of scanning, the x-ray focus performs a spiral motion on a virtual cylinder surface with a constant radius equal to the distance of focus to the center of rotation (Fig 1). Data that would have been obtained in planar geometry can be estimated for arbitrary table positions from the spiral data by interpolating between adjacent scans (Fig 2). For each angular position θ and section position z , the projection value $P_z(i, \theta)$ for detector element i is calculated as

$$P_z(i, \theta) = (1 - w) \cdot P_j(i, \theta) + w \cdot P_{j+1}(i, \theta),$$

where j is the number of the last scan reaching angle θ before reaching position z , and $P_j(i, \theta)$ is obtained at position z_j . The weight w is calculated as $(z - z_j)/d$, where d is the table feed distance for every 360° scan and $0 \leq w \leq 1$.

¹ From Siemens Medical Systems, Henkestrasse 127, 8520 Erlangen, Federal Republic of Germany (W.A.K., W.S., E.K.) and the Department of Radiology, University of Bern, Switzerland (P.V.). From the 1989 RSNA annual meeting. Received December 22, 1989; revision requested January 26, 1990; revision received February 22; accepted March 12. Address reprint requests to W.A.K.

© RSNA, 1990

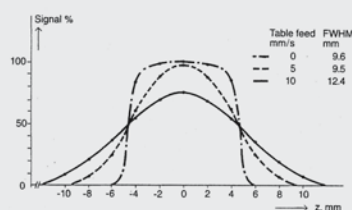


Figure 4. Sensitivity profiles as a function of table speed for a nominal 10-mm section. FWHM = full width at half maximum, z = section position.

These synthesized projection data sets undergo the standard image reconstruction process. The position, spacing, and number of planes can be arbitrarily chosen within the scanned range. All the original spiral data are employed in generating interpolated data; however, at both ends of the spiral—for a range of one table feed distance d —no planar image can be reconstructed with this interpolation method.

Phantom and Clinical Studies

We employed water phantoms of 20 cm in circular diameter and 20 × 30-cm oval shape to assess noise characteristics and uniformity. A standard hole pattern was used to test spatial resolution. To determine section sensitivity profiles, we employed two polyethylene disks with a perforated sheet of polyvinyl chloride, 0.1 mm thick, mounted between them. For standard CT, the phantom was advanced in 0.5-mm increments; for spiral volumetric CT, the phantom was moved continuously, and images were reconstructed afterward in 0.5-mm increments as well. The CT number for a 30-mm-diameter circular region of interest placed in the central perforation was evaluated for both series of images and plotted as a function of table position to represent the section sensitivity profiles. The characteristics of artifacts were assessed in clinical studies of the thorax and abdomen (4,7). All performance measurements were taken at 120 kV, 170 mAs, and 10-mm section thickness; image reconstructions were done with the standard body convolution kernel.

RESULTS

Images reconstructed from spiral geometric data have artifacts that closely resemble the typical motion artifacts often encountered in clinical studies (Fig 3a). However, these effects do not compromise image quality when reconstructions are performed in planar geometry, as described previously (Fig 3b).

Pixel noise values in the corrected images of a 20-cm water phantom were reduced by a factor of about 0.8, from 4.4 HU standard deviation in a

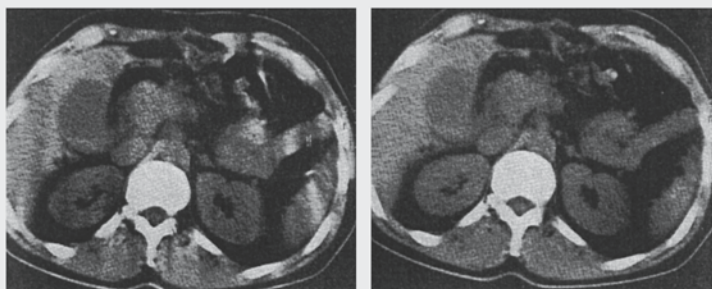


Figure 3. Image quality in spiral volumetric CT scans. (a) Direct reconstruction from the spiral data results in motionlike artifacts. (b) Reconstructions from synthesized planar data are free from such artifacts.

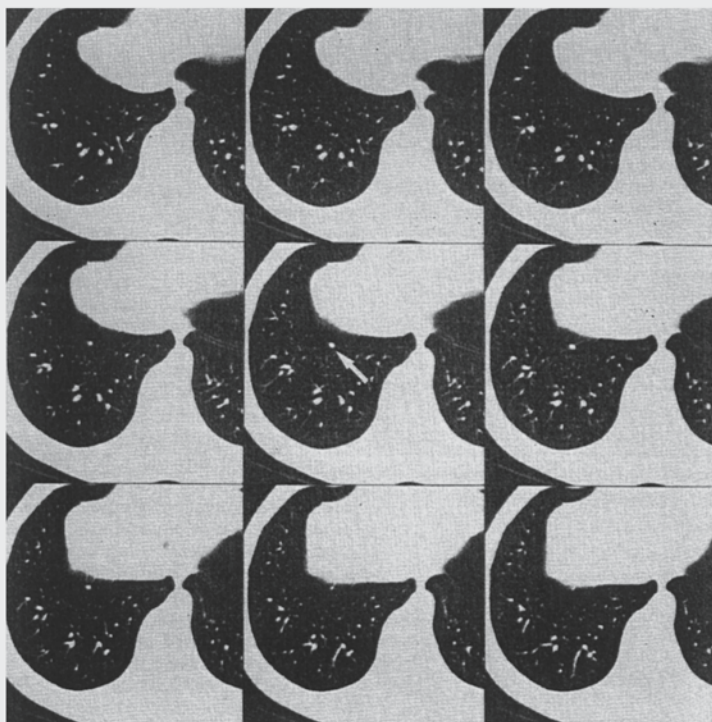


Figure 5. Spiral volumetric CT study of a pulmonary nodule (arrow) (12 1-second scans of a 24-mm subvolume, 2-mm nominal section thickness, 2 mm/sec table feed). Nine consecutive reconstructions, spaced 1 mm apart, are shown.

standard 10-mm section to 3.6 HU in the spiral mode. The reduction factor is independent of the table speed; it is due to the interpolation between adjacent sections, independent of their spacing. The scanning mode did not affect image uniformity. Spatial resolution is also independent of the scanning mode; the measurements yielded resolution of the 0.6-mm holes in standard body mode for

standard CT and for spiral volumetric CT.

Section thicknesses, specified as the full width at half maximum of the section sensitivity profiles, were enlarged, compared with the nominal values; in addition, the shape of the sensitivity profiles deteriorated compared with that of the ideal rectangular profile (Fig 4). Effective section thickness values are included in

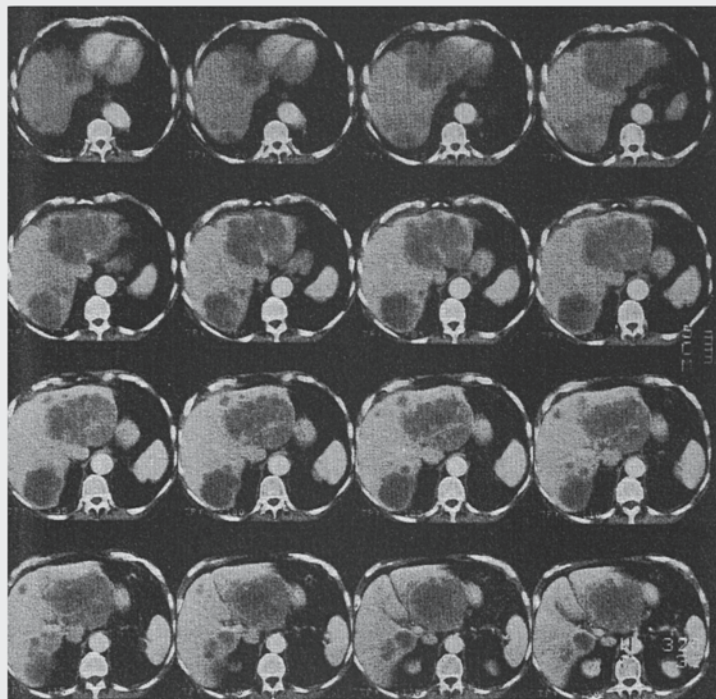


Figure 6. Spiral volumetric CT study, enhanced with contrast material, of multiple metastases in the liver from carcinoma of the colon (12 1-second scans of a 120-mm subvolume, 10-mm nominal section thickness, 10 mm/sec table feed). Sixteen consecutive reconstructions, spaced 5 mm apart, are shown.

Figure 4 for a 10-mm section as a function of the table feed. For a table feed value of 10 mm/sec, the effective section width was enlarged by a factor of 1.3.

In our preliminary investigations in patients with focal lung disease, spiral volumetric CT demonstrated the lesions in a continuous sequence in all 20 cases studied (4). Because images can be reconstructed for arbitrary table positions, the center of the lesion could always be depicted in a manner suitable for size assessment and densitometry (Fig 5). In 20 contrast material-enhanced studies of the liver, we examined volumes of 12×10 mm in extent with spiral volumetric CT performed with a bolus injection technique in a single-breath-hold period of 12 seconds (Fig 6).

DISCUSSION

From principal considerations, truly continuous scanning, independent of breathing or other patient motion, demands continuous data acquisition and patient transport (ie, a helical or spiral scanning geometry). Respective ideas have been promoted only in the patent literature (8); however, to our knowl-

edge, no practical solution has been presented until now. The advent of continuously rotating CT scanners and of electron beam scanners, in principle, provided the necessary technical basis. The adaptation of the table feed mechanism to continuously transport the patient in synchrony with continuous data acquisition, although labeled experimental in this first report, can be considered state of the art.

The physical performance characteristics of spiral volumetric CT conformed to expectations. Noise is slightly reduced because the synthesized planar data are derived by means of interpolation. Section sensitivity profiles are filtered or convolved with a smoothing function and widened due to transport during scanning. All other performance parameters are unchanged; this applies to spatial resolution, uniformity, linearity, and contrast. This had to be expected because sampling parameters, the effective energy of the spectrum, beam hardening effects, and possible scatter contributions remain unchanged. Radiation dose to the patient also remains unchanged if one chooses a table feed distance d per scan equal to the nominal section thickness S . For overlapped spiral scanning, the dose will be increased

according to the ratio S/d .

In spiral volumetric CT, reliable continuity of sections is achieved in clinical studies, and omission of some anatomic levels and repeated scanning of others are prevented. These features are particularly important in searching for pulmonary nodules and in reliably depicting their center for densitometry. Complete organ volumes or subvolumes can be scanned in a single breath hold and, possibly more important, during the early vascular enhancement phase. The numbers of scans and breathing commands that the patient must follow are reduced considerably; these reductions may be considered additional practical advantages.

Presently, spiral volumetric CT is limited primarily by the available x-ray power (ie, the limited milliamperage settings, particularly for extended scanning times). This limitation is reflected in the decrease from 250 mA for 5-second scanning to 170 mA for 12-second and to 130 mA for 24-second scanning. Adequate computing power and data storage capacities can certainly be provided in the future, even for extended volumetric scanning. The limitation of a single-breath-hold period of 12 seconds or less in our studies can be justified for whole-body CT by practical patient-related considerations. However, this limitation above all constitutes a pragmatic decision, a compromise aimed at providing both sufficiently high tube currents and adequately long spiral scanning intervals. The importance of the high-power x-ray tube available to us is evident. Still, the high potential of spiral volumetric CT can only be fully exploited with further improvements in x-ray power. ■

References

1. Zerhouni EA, Spivey JF, Morgan RH, Leo FP, Stitik FP, Siegelman SS. Factors influencing quantitative CT measurements of solitary pulmonary nodules. *J Comput Assist Tomogr* 1982; 6:1075-1087.
2. Siegelman SS, Khouri NF, Leo FP, Fishman EK, Braverman RM, Zerhouni EA. Solitary pulmonary nodules: CT assessment. *Radiology* 1986; 160:307-312.
3. Shaffer K, Pugatch RD. Small pulmonary nodules: dynamic CT with a single-breath technique. *Radiology* 1989; 173:567-568.
4. Vock P, Jung H, Kalender W. Single-breath-hold spiral volumetric CT of the lung (abstr). *Radiology* 1989; 173(P):400.
5. Freeny PC. Hepatic CT: state of the art. *Radiology* 1988; 168:319-323.
6. Zeman RK, Clements LA, Silverman PM, et al. CT of the liver: a survey of prevailing methods for administration of contrast material. *AJR* 1988; 150:107-109.
7. Vock P, Jung H, Kalender W. Single-breath-hold spiral volumetric CT of the hepatobiliary system. *Radiology* 1989; 173(P):377.
8. Slavin PE. X-ray helical scanning means for displaying an image of an object within the body being scanned. U.S. patent no. 3432657; 1969.

2 Magnetic Resonance Imaging

- | | | |
|------|--|-----|
| 2.1 | Measurement of nuclear spin by the method of molecular beams
The nuclear spin of sodium <i>Physical Review</i> 46 (1934): 707–712
<i>I.I. Rabi, V.W. Cohen</i> | 73 |
| 2.2 | Nuclear Induction.
<i>Physical Review</i> 69 (1946): 127
<i>F. Bloch, W.W. Hansen, M.E. Packard</i> | 81 |
| 2.3 | Resonance absorption by nuclear magnetic moments in a solid.
<i>Physical Review</i> 69 (1946): 37–38
<i>E.M. Purcell, H.C. Torrey, R.V. Pound</i> | 84 |
| 2.4 | Tumor detection by nuclear magnetic resonance.
<i>Science</i> 171 (1971): 1151–1153
<i>R.V. Damadian</i> | 87 |
| 2.5 | Image Foundation by induced local interactions: Example employing nuclear magnetic resonance.
<i>Nature</i> 242 (1973): 190–191
<i>P.C. Lauterbur</i> | 93 |
| 2.6 | Planar spin imaging by NMR
<i>J. Phys. C: Solid State Phys.</i> 9 No 15 (1976): L409–L412
<i>P. Mansfield, A.A. Maudsley</i> | 96 |
| 2.7 | Medical Imaging by NMR.
<i>Brit. Jour. Radiol.</i> 50 (1977): 188–194
<i>P. Mansfield, A.A. Maudsley</i> | 103 |
| 2.8 | Human whole body line scan imaging by NMR.
<i>Brit. Jour. Radiol.</i> 51 (1978): 921–922
<i>P. Mansfield, I.L. Pykett, P.G. Morris, R.E. Coupland</i> | 111 |
| 2.9 | NMR imaging of the brain in multiple sclerosis.
<i>Lancet ii</i> (1981): 1063–1066
<i>I.R. Young, A.S. Hall, C.A. Pallis et al.</i> | 114 |
| 2.10 | MRI: Clinical use of the inversion recovery sequence.
<i>J Computer Assisted Tomography</i> 9 (1985): 659–675
<i>G.M. Bydder, I.R. Young</i> | 119 |

Introduction

Magnetic resonance imaging is a relatively new radiological technique. The magnetic properties of nuclei, which form the basis of MRI, were first measured by Isidor Rabi in the 1930s. Felix Bloch and Edward Purcell independently discovered nuclear magnetic resonance in 1946. All these three pioneers went on to receive the Nobel Prize for physics, Rabi in 1944 and Bloch and Purcell in 1952.

In 1973 Paul Lauterbur, who was working at the State University of New York at Stony Brook, discovered that it was possible to make two-dimensional images of a sample by adding a gradient to the magnetic field. The paper was published on 16 March 1973 in *Nature* and was titled 'Image formation by induced local interaction examples employing magnetic resonance'. Lauterbur, professor of chemistry, named this new technique *zeugmatography* (from the Greek *zeugmo*, meaning yoke or a joining together). This experiment enabled the single dimension of NMR spectroscopy to move into the spatial orientation, which is the basis of MRI. Dr Raymond Damadian discovered the basis for using magnetic resonance imaging as a tool for medical diagnosis. He found that different kinds of animal tissue emitted different signals, which varied in length, and that cancerous tissues emitted signals that lasted longer than those from non-cancerous tissues. He filed a patent for this entitled 'An apparatus and method for detecting cancer in tissue', which was granted in 1974 and this was the world's first patent issued in the field of MRI. By 1977 Dr Damadian had completed construction of the first whole-body MRI scanner.

In 1974 *in vivo* NMR spectroscopy was introduced in Oxford under the pioneers George K. Radda and Rex E. Richards. Other members of this research team included Hoult and Gadian, who carried out important early work on MRI spectroscopy.

In 1975 Peter Mansfield and Andrew Maudsley from Nottingham proposed a line technique, which in 1977 led to the first image of *in vivo* human anatomy, a cross section through a finger. The following year Mansfield presented his first image through the abdomen. In 1977 the Nottingham team, including Brian Worthington, succeeded in producing an image of a wrist. This was followed by more human thoracic and abdominal images and by 1978 Hugh Clow and Ian R. Young, working at EMI, reported the first transverse NMR image through the human head. By 1980 William Moore and his colleagues had presented first coronal and sagittal images through the human head. More pioneering research in Britain was conducted at the University of Aberdeen under the group of John Mallard. They developed the spin warp technique. Their team published the first image through the body of a mouse in 1974. Peter Mansfield further developed the use of gradients in the magnetic field. He was a pioneer in the fast imaging techniques such as echo planar imaging. This was introduced in the 1980's. The first commercial cryogenic magnet in Europe was installed in Manchester (Isherwood and Pullan). In the 1980s fast imaging techniques were developed by Jurgen Hennig from the University of Freiburg, who introduced RARE (rapid acquisition and relaxation enhancement) imaging in 1986. This is now better known as fast or turbo spin echo imaging. Gradient echo sequences were introduced by Haase and colleagues from the Max Planck Institute in Göttingen. Roger Ordridge from Mansfield's group in Nottingham presented the first movie in 1981. In 1984 Dennis H. Carr from the Hammersmith Hospital MRI group and Wolfgang Schorner from Berlin published the first images using the intravenous MRI contrast agent, gadolinium DTPA dimeglumine, in man. Magnetic resonance imaging has resulted in the award of two Nobel Prizes in chemistry. In 1991 Richard Ernst from Switzerland was awarded the Nobel Prize for his contributions to the development of the use of nuclear magnetic resonance spectroscopy. In 2002 Kurt Wüthrich

from Switzerland also was awarded the Nobel Prize for the development of NMR spectroscopy for determination of three-dimensional structure of biological macromolecules. In 2003 Dr Lauterbur and Dr Mansfield were awarded the Nobel Prize in medicine for their pioneering researches. Clinical studies using this new technique proliferated throughout the 1980s and now MRI is used in the investigation of neurological, and musculo-skeletal disorders as well in cancer. New sequences continued to be discovered, including the inversion recovery sequences described by Bydder and Young. Today MRI has progressed such that functional imaging is possible, allowing both anatomical and physiological information to be obtained in patients. The technique of diffusion-weighted imaging today allows more accurate assessment of patients with strokes, as do techniques involving perfusion imaging. Technological innovations in magnet design include open magnets which enable interventional procedures to be conducted under MRI imaging guidance

References

- Rabi I, Cohen VW (1933) The nuclear spin of sodium *Physical Review* 43: 582
- Rabi I, Cohen VW (1934) Measurement of nuclear spin by the method of molecular beams: The nuclear spin of sodium *Physical Review* 46: 707-712 *The Physical Review*
- Bloch F, Hansen WW, Packard ME (1946) Nuclear Induction. *Physical Review*. 69: 127-129
- Purcell EM, Torrey HC, Pound RV (1946) resonance absorption by nuclear magnetic moments in a solid. *Physical Review* 69: 37-38
- Ernst RR, Anderson WA (1966) Anwendung von Fourier-Transformation Spektroskopie zur Magnetresonanz, *Polwender Sci. Instrum.* 37: 93
- Hutchison JMS, Mallard JR, Goll CC (1974) In vivo imaging of body structures using proton resonance. *Proc 18th Ampere Congress* (Ed. PS Allen, ER Andre and CA Bates) pp 283-284, University of Nottingham.
- This is one of the first descriptions of a relaxation time image showing pathology (using a whole mouse). The colour coded image is illustrated in "In vivo NMR imaging in medicine" Phil. Trans. R. Soc. London 1980 pp 519-533, plate 1.*
- Edelstein WA, Hutchison JMS, Johnson G, Redpath TW (1980) Spin Warp NMR imaging and its application to whole body imaging, *Physics Med. Biol.* 25: pp 751-756
- An important paper addressed by all the major manufacturers.*
- Smith FW, Mallard JR, Hutchison JMS et al. (1981) Clinical application of nuclear magnetic resonance. *Lancet* i: pp 78-79
- One of the earliest clinical papers dealing with body images from the Aberdeen group*
- Young IR, Brui M, Clarke GJ et al. (1981) Magnetic properties of hydrogen: Imaging the posterior fossa. *AJR* 187: pp 895-901
- This paper provides the reasons why MR was considered superior to CT in posterior fossa imaging.*
- Mansfield P, Blamire AM, Coxon R et al. (1990) Snapshot echo-planar imaging methods: current trends and future perspectives *Phil. Trans. R. Soc. Lond. A*, 333: pp 495-506
- Worthington BS, Firth JL, Morris GK et al. (1990) The clinical potential of ultra-high-speed echo-planar imaging *Phil. Trans. R. Soc. Lond. A* 333: pp 507-514
- These two papers are really review papers but provide all the references to Mansfield's work on echo-planar imaging for which in part he was awarded the Nobel prize and Worthington elected FRS*
- Hoult DI, Busby SJW, Gadian DG et al. (1974) Observation of tissue metabolites using 31 p nuclear magnetic resonance. *Nature* 252: pp 285-287
- This paper demonstrated that high resolution spectra, particularly from 31p could be obtained from intact tissue samples.*
- Haase A, Frahm JM, Matthaei D, Haenicke W, Merboldt KD (1986) FLASH imaging. Rapid NMR imaging using low flip angle pulses. *J Magn Resonance* 67: 93-102
- Early description of gradient echo imaging*

Hennig J, Friedburg H, Stroebel B (1986) Rapid non-tomographic approach to MR myelography without contrast agents. JCAT 10: 375-378

Early description of what is now known as turbo-spin echo sequence

Young IR, Hall AS, Pallis CA, Legg NJ, Bydder GM, Steiner RE (1981) Nuclear Magnetic Resonance Imaging of the brain in multiple sclerosis Lancet ii: 1063-6

Early description of mri in the diagnosis of multiple sclerosis

Schenk JF, Jolesz FA, Roemer PB, Cline HE, Lorensen WE, Kikinis R et al. (1995) Superconducting open – configuration MR imaging system for image guided therapy. Radiology 195: 805-814

First description of open superconducting mri system

2.1 Measurement of nuclear spin by the method of molecular beams

Isidor Isaac Rabi (1898–1988)

Isidor Isaac Rabi was born in Raymanov, Austria, on 29 July 1898, the son of David Rabi and Janet Teig. He was brought to the United States by his family, in 1899, and his early education was in New York City (Manhattan and Brooklyn). In 1919 he graduated Bachelor of Chemistry at Cornell University (New York). After three years in non-scientific jobs, he started postgraduate studies in physics at Cornell in 1921, which he later continued at Columbia University. In 1927 he received his PhD degree for work on the magnetic properties of crystals. Aided by fellowships, he spent two years in Europe, working at different times with Sommerfeld, Bohr, Pauli, Stern, and Heisenberg. On his return in 1929 he was appointed lecturer in Theoretical Physics at Columbia University, and after promotion through the various grades became professor in 1937.

In 1940 he was granted leave from Columbia to work as Associate Director of the Radiation Laboratory at the Massachusetts Institute of Technology on the development of radar and the atomic bomb. In 1945 he returned to Columbia as executive officer of the Physics Department. In this capacity he was also concerned with the Brookhaven National Laboratory for Atomic Research, Long Island, an organization devoted to research into the peaceful uses of atomic energy.

His early work was concerned with the magnetic properties of crystals. In 1930 he began studying the magnetic properties of atomic nuclei, developing Stern's molecular beam method to great precision as a tool for measuring these properties. His apparatus was based on the production of ordinary electromagnetic oscillations of the same frequency as that of the Larmor precession of atomic systems in a magnetic field. By an ingenious application of the resonance principle he succeeded in detecting and measuring single states of rotation of atoms and molecules and in determining the mechanical and magnetic moments of the nuclei.

Prof. Rabi published his most important papers in *The Physical Review*, of which he was an Associate Editor for two periods. In 1939 he received the Prize of the American Association for the Advancement of Science and in 1942 the Elliott Cresson Medal of the Franklin Institute. He was awarded the Medal for Merit, the highest civilian award in World War II, in 1948, the King's Medal for Service in the Cause of Freedom the same year, and is an Officer of the Legion of Honour.

He was an honorary DSc of Princeton, Harvard, and Birmingham universities. He was a Fellow of the American Physical Society (its President in 1950) and a member of the National Academy of Sciences, the American Philosophical Society, and the American Academy of Arts and Sciences. In 1944 he was awarded a Nobel Prize in physics.

In 1959 he was appointed a member of the Board of Governors of the Weizmann Institute of Science, Rehovoth, Israel. He held foreign memberships of the Japanese and Brazilian Academies, and was a member of the General Advisory Committee to the Arms Control and Disarmament Agency and of the United States National Commission for UNESCO. At the International Conference on Peaceful Uses of Atomic Energy (Geneva, 1955) he was the United States delegate and Vice-President. He was also a member of the Science Advisory Committee of the International Atomic Energy Agency.



Dr. Rabi married Helen Newmark in 1926. They had two daughters. His recreations were travel, walking, and the theatre. Isidor Isaac Rabi died in 1988.

From Nobel Lectures, Physics 1942–1962, Elsevier Publishing Company, Amsterdam

V.W. Cohen

OCTOBER 15, 1934

PHYSICAL REVIEW

VOLUME 46

Measurement of Nuclear Spin by the Method of Molecular Beams

The Nuclear Spin of Sodium

I. I. RABI AND V. W. COHEN, *Columbia University*

(Received August 24, 1934)

A simple method of velocity selection of arbitrary resolving power for atomic and molecular beams is described. The method consists in spreading the beam into a velocity spectrum, through the action of external fields, and then selecting a portion thereof by means of a movable selector slit. Since all the atoms of the beam of the given velocity interval are utilized, this type of selection has the maximum efficiency. In addition a method of focussing the selected beam to increase intensity and resolution is applied. A

ballistic method of using the surface ionization detector was evolved extending its use to beams of exceedingly low intensity. A selected beam of slow Na atoms, obtained and measured in this fashion, was analyzed in a weak and inhomogeneous magnetic field. Four distinct peaks of equal intensity were obtained which represent the $(2i+1)$ nuclear magnetic levels. The spin of the Na nucleus is accordingly equal to $3/2$, in units of $h/2\pi$.

INTRODUCTION

THE most direct demonstration of the space quantization of angular momentum was the celebrated Stern-Gerlach experiment. The purpose of the experiments to be described is to demonstrate and measure the angular momentum of the nucleus directly by means of its effect on the space quantization of the angular momentum of the extranuclear configuration in a magnetic field.

The influence of a magnetic field on the different magnetic levels of an atom with nuclear spin " i " situated therein has been described in previous papers.^{1,2,3} For the particular case of the alkalis in their normal $^2S_{1/2}$ states, values of the magnetic moments of the various magnetic levels as functions of the magnetic field are shown in Fig. 1 for the nuclear spin $3/2$. The total number of magnetic levels is always $2(2i+1)$.

The schematic arrangement of the experiment is shown in Fig. 2. A narrow beam of sodium atoms, defined by slits S_1 and S_2 is allowed to pass through a magnetic velocity selector consisting essentially of an inhomogeneous magnetic field which spreads the beam into the usual velocity spectrum, the field being of sufficient intensity to cause a rather complete decoupling between electronic and nuclear spins. For sodium a field of 2000 gauss is sufficient. In this case the magnetic moments of the $2i+1$ levels arising from a par-

ticular value of m_i differ very slightly. By means of a movable selector slit S_3 a portion of the beam is selected for further analysis. After passing through S_3 the beam is homogeneous to an extent to be described below and contains atoms in equal numbers in all the magnetic levels arising from the $2i+1$ values of m_i but associated with only one value of m_i , namely, $+1/2$ or $-1/2$, depending on the direction of the field. The beam is then permitted to pass through a second

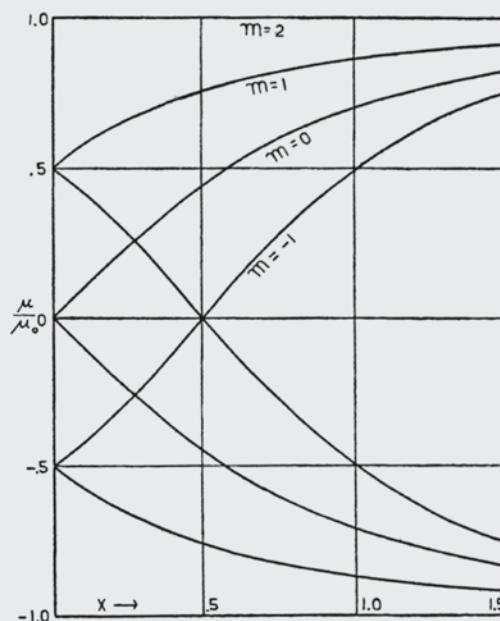


FIG. 1. Variation of the magnetic moments (in Bohr magnetons) of the atoms in the different magnetic levels for $i=3/2$ plotted against $x = (2\mu_0 \cdot hc\Delta\nu)/H$.

¹ Breit and Rabi, *Phys. Rev.* **38**, 2082 (1931).

² Rabi and Cohen, *Phys. Rev.* **43**, 582 (1933).

³ Rabi, Kellogg and Zacharias, *Phys. Rev.* **46**, 157 (1934).

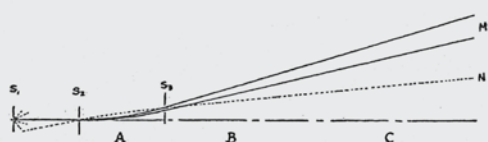


FIG. 2. Schematic arrangement of the slits and field showing the selected and scattered beams.

field of the Stern-Gerlach type. The field is so chosen that there is strong coupling between the nuclear and electronic spins. For sodium this field is of the order of 300 gauss. This brings us into the region of $x=1/2$ in Fig. 1. The atoms are subject to forces which are different for each of the $2i+1$ magnetic levels and the beam is therefore separated into $2i+1$ components, since it is homogeneous in velocity. The spin is evaluated by merely counting the number of peaks in the deflection pattern.

APPARATUS

The apparatus, (Fig. 3) constructed of solder-coated brass tubing, is divided into two sections, an oven chamber and an observation chamber. These are connected by a ground joint cemented with picien wax. Each half of the system is pumped independently, the oven chamber being connected to a fast three stage mercury diffusion pump while the observation chamber is pumped by two umbrella type single stage diffusion pumps. During the runs a "sticking" vacuum as measured by a McLeod gauge is maintained in both parts of the system. Connections for the pumps, gauge and electrical leads are made through ground joints. Mercury and grease vapors are frozen out with liquid air traps.

The oven and oven slit are constructed of nickel and show no signs of corrosion by the alkali metal. The bottom is cut with three radial grooves which rest on three nickel pegs fastened firmly to the floor of the oven chamber. This three point support permits the oven to be removed and replaced accurately to the same position. The narrowness of the pegs and the small area of contact with the oven serve to insulate it from the floor of the chamber which is water-cooled.

The oven is heated by two spirals of 10 mil tungsten wire enclosed in holes drilled in the body

of the oven above and below the slit. This arrangement serves to keep the region near the slit at a temperature slightly higher than the rest of the oven. A copper constantan thermocouple is inserted into the body of the oven for temperature measurement. The oven well is covered with a tapered monel metal plug. This plug is hollowed out to permit the alkali vapor to reach the slit through a canal and at the same time to check the creeping of the liquid metal along the nickel surface to the slit. The jaws forming the oven slit are set 0.013 mm apart.

The collimating slit S_2 , 0.016 mm wide and 9 cm from the oven slit, is set in a disk which can be rotated by means of a screw about the axis of the beam. If the observation chamber and one-half of the collimating slit be removed, the oven slit is observable from the observation side of the collimating slit. The one edge of the slit remaining is then adjusted parallel to the oven slit with the aid of a telemicroscope and a filar micrometer. The two slits must then be adjusted laterally so that the plane of the beam is aimed parallel to the edges of the pole pieces of the magnets. This is determined by sighting at the oven slit through the observation chamber with a telescope and filar micrometer.

THE VELOCITY SELECTOR

A large Dubois magnet (4, Figs. 2 and 3) fitted with pole pieces of the Stern-Gerlach type 6 cm long with a furrow 8 mm wide and a knife edge 4 mm distant furnishes the magnetic field. The selector slit S_3 , 0.035 mm wide, was mounted eccentrically on a ground joint and was movable by rotating the joint. The distance from collimator to the selector was 10 cm and the two were adjusted parallel to each other by rotation of the large ground joint which connects the oven chamber to the detecting chamber.

Since the deflection of an atom in a constant field of force perpendicular to its original direction of motion is given by $s = \text{const.}/v^2$ we have $dv/v = ds/2s$. Under the conditions of this experiment dv/v was of the order of 1/10. The velocity selected is varied simply by changing the magnetic field. The resolution can be varied by changing the position of the selector slit.

Where it is undesirable to make the velocity selection with a magnetic field, the same result

NUCLEAR SPIN OF SODIUM

709

can probably be attained by spreading the beam into a velocity spectrum by means of an inhomogeneous electric field. For heavy atoms or molecules even the gravitational field of the earth is not out of the question. The principal technical difficulty which is always involved when a velocity selection is made is to detect the much enfeebled beam.

THE ANALYZER

The analyzer follows directly after the selector slit and consists of two magnets having pole pieces similar to magnet *A* but the first being 18 cm long and the second 16 cm, with 1.5 cm space between the two. The first magnet *B* supplies the weak analyzing field and is made long in order to obtain sufficient deflection with the small forces available. Magnet *C* has a strong field and serves as a focussing device. The pole pieces of the magnets are so arranged that the furrows of the *B* and *C* magnets are on the same side of the beam as the knife edge of the *A* magnet. This is important for the purpose of resolving the different components. The reason for this can be seen by considering the fact that the selected beam contains a finite velocity range. From any portion of the original beam the faster atoms pass through the selector slit on the side nearer the original beam and the slower atoms on the farther side since the slower atoms suffer the greater deflection. A subsequent deflection in a field similar to the first would therefore broaden the beam still further. Even if the field in the

second magnet is reversed this is still the case because an atom with its magnetic moment oriented parallel to the field will be deflected toward the strong field (and *vice versa* for those opposed to the field). If the second field is reversed in direction the magnetic moment will change in direction to follow the direction of the field since the rate of change is small in the period of the Larmor precession. This is to be expected from the theorem of adiabatic transformability applied to the space quantization with respect to the field. However, by changing the pole pieces about, the stronger field is now in the opposite direction and the forces acting, being opposite to those in the first field cause the beam to become narrower instead of broader.

Magnet *C* has a strong field in which all the components are subject to the same force and the effect is to displace the whole deflection pattern toward the center and thus increase the resolution. Magnet *C* has also another very important rôle due to the fact that in addition to the selected beam some atoms scattered in the oven chamber pass through the collimator in the direction of the selector slit and form an additional beam. This is represented by the broken line in Fig. 2. These atoms have the Maxwellian distribution of velocities and are fast compared to the selected beam. This scattered beam comes nearer the center than the selected beam. Although these atoms form about one-five hundredth the total beam intensity, the velocity selection cuts down the intensity to such an extent that the scattered

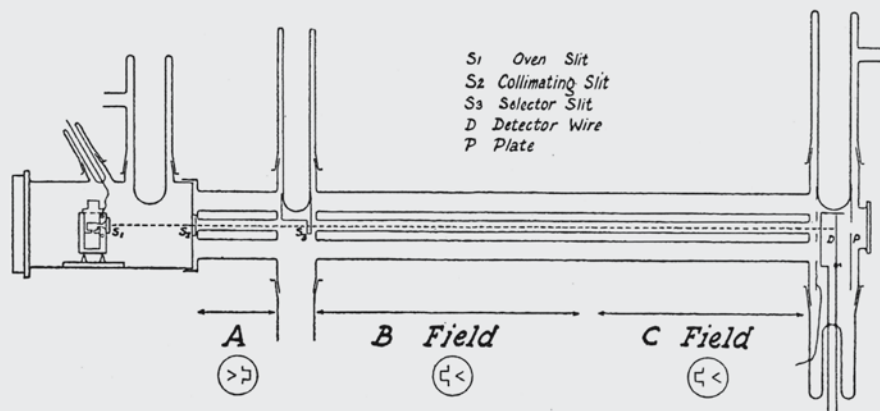


FIG. 3. Diagram of the apparatus.

atoms are as numerous as the selected atoms. The effect of magnet C is to shift the entire deflection pattern away from the region of this scattered peak so as to make the interpretation of the results unambiguous.

THE DETECTOR

Detection was effected by means of the surface ionization detector.⁴ The 2 mil tungsten filament was mounted eccentrically on a ground joint and was moved laterally by turning the joint. The wire was supported by two adjustable arms so that it could be set parallel to the slit system. For the detection of sodium the wire must be provided with an oxide coat to raise its work function. No special method was used to obtain this coating. When a wire is first used it is carefully heated for a short time at about 1800°K until most of the oxide is driven off. After the beam is detected the wire is heated again until the residual positive ion current when the wire is outside the beam is reduced to about 10^{-13} amp. with the filament at a dull red heat. If too much of the oxide has been removed the wire can usually be activated by admitting a small quantity of air into the apparatus with the filament at about 1400°K. With the beam intensities used in this experiment a well sensitized filament will remain so for the entire run. The filament is maintained at a potential of 45 volts above ground. The positive ion current is measured by means of an FP-54 vacuum tube amplifier with a grid leak of 5×10^8 ohms. With the galvanometer used the current sensitivity was 10^{-14} A/mm.

The selected beam is usually too weak to measure directly because of background fluctuations. However, by allowing the sodium atoms to deposit on the cold filament from one to three minutes and then suddenly heating the filament, large ballistic throws were obtained. The multiplication factor over the direct beam readings was 20 per minute of deposition. This method eliminates the effect of background fluctuations. All the points except those of Fig. 3 were taken in this way. The galvanometer readings are almost proportional to the amount of sodium deposited if the background is less than the net

ballistic reading (ballistic throws minus the background).

PROCEDURE

The sodium used was doubly distilled in vacuum. When the oven is to be loaded the still is cracked and the sodium dropped directly into a dish of petroleum ether and is then transferred to the oven. The lid is then pressed in, the oven set in place and the system is evacuated. During the loading process the sodium is in contact with the air for a fraction of a second and with the petroleum ether for the time taken to evacuate the oven through the slit. The oven is heated slowly to about 200°C to help remove the petroleum ether and occluded gas after which the oven is allowed to cool and stand overnight under vacuum.

In preparation for a run the oven is heated at the rate of 3°C per minute until the beam is first detected at about 300°. The heating rate is then slowed down gradually until 360° is reached, at which temperature the beam intensity is sufficiently high for convenient working conditions. The galvanometer deflection in the center of the beam is about 10^3 cm, while the vapor pressure in the oven is about 0.2 mm Hg.

When the beam intensity has become stabilized the A field is turned on and the deflection pattern observed. The initial beam and the A field deflection pattern are shown in Fig. 4.

The A field is then thrown off and the selector slit is turned into the center of the beam. This gives a fiducial position from which slit is turned so that atoms of the required velocity will be selected. The velocities used in this experiment correspond to an energy of about $1/2 kT$. On Fig. 4 this would correspond to atoms which would arrive at about 80 on the scale. The low velocity is necessary in order to obtain sufficient resolution because of the small forces in the analyzing field. The resulting beam is shown in Fig. 5I. The peak at 78 is the selected beam and the one at 71 is the scattered beam. The C field is then turned on and the selected beam is deflected to the other side of the scattered beam as in Fig. 5II. It is to be noted that the scattered beam does not change its position appreciably. The analyzing field is then turned on and the deflection patterns are observed for the different values of the field.

⁴ Taylor, *Zeits. f. Physik* 57, 242 (1929).

NUCLEAR SPIN OF SODIUM

711

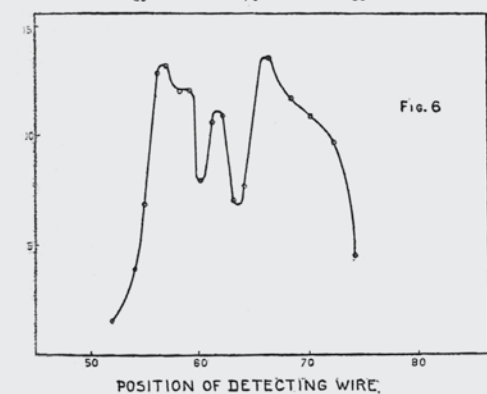
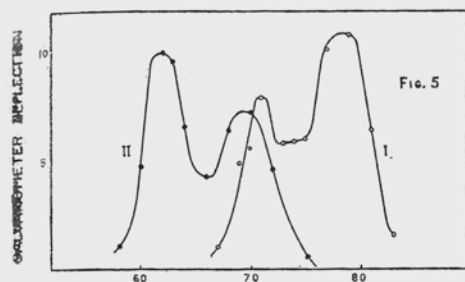
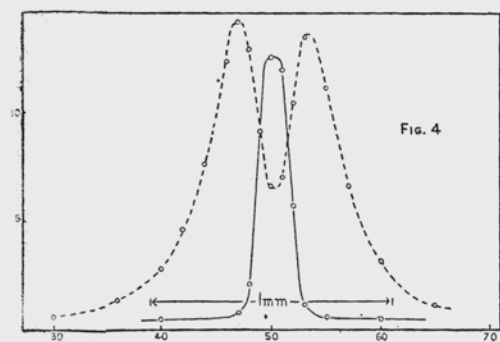


FIG. 4. Experimental curve of the direct beam (full line) and deflection pattern obtained with A field alone (dotted line). The ordinate scale of the dotted curve is 5 times that of the full curve.

FIG. 5. Experimental curve of selected and scattered beams; curve I without C field and curve II with C field. The B field was zero in each case.

FIG. 6. Deflection pattern with 55 m.a. through B magnet, A and C fields as in Fig. 5.

RESULTS

The different deflection patterns obtained with the various values of the current through the analyzing magnet B are shown in Figs. 6–10. In Fig. 6 the resolution is not yet sufficient to resolve all the peaks. Fig. 7, taken at a somewhat higher field shows the pattern shifted toward the left, that is, toward the position of the original

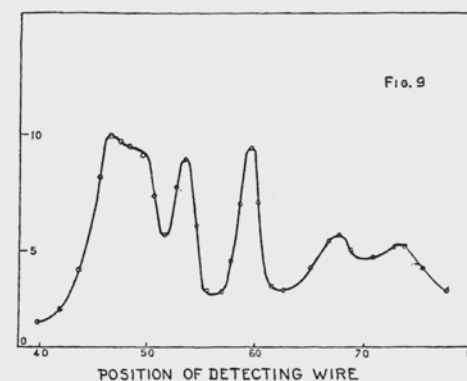
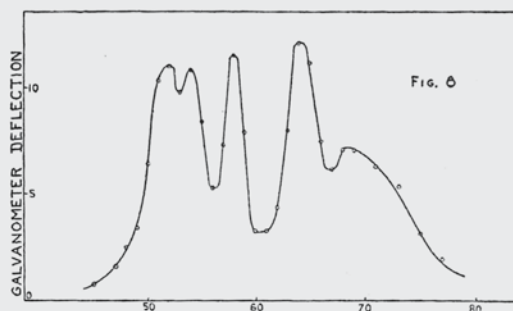
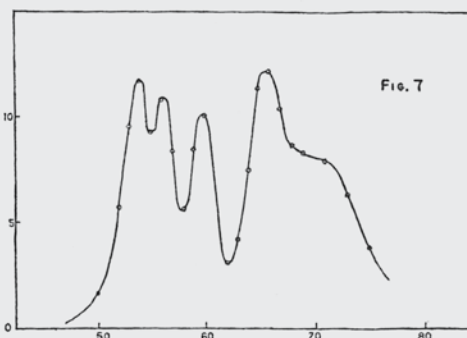


FIG. 7. Same as in Fig. 6 with B magnet current 70 m.a.

FIG. 8. Same as in Fig. 6 with B magnet current 85 m.a.

FIG. 9. Same as in Fig. 6 with B magnet current 110 m.a.

beam and shows four clearly resolved peaks. The shelf on the right is due to the scattered atoms. Fig. 8 shows this still better and the scattered atoms are now almost separated from the pattern of the selected atoms. Fig. 9 shows the scattered atoms in a stronger field being split up into the ordinary Stern-Gerlach pattern, the center of which still remains at the original position of 70 scale divisions, while the deflection pattern of the selected atoms already shows the setting on of the Paschen-Back effect in the failure to resolve

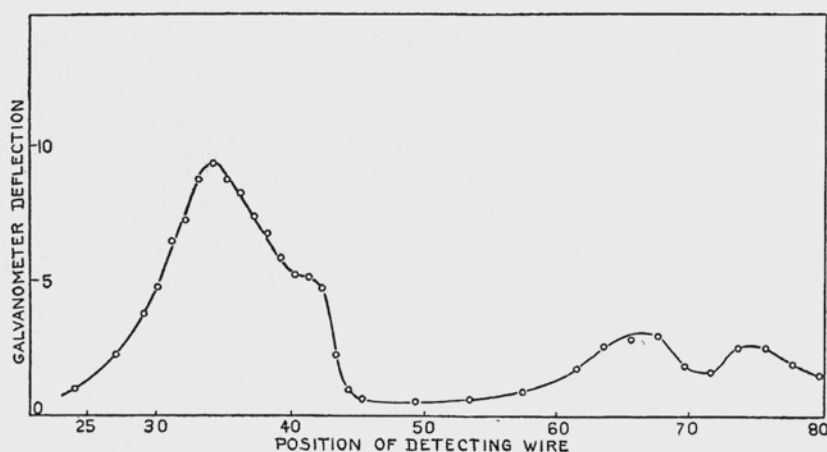


FIG. 10. Same as in Fig. 6 with B magnet current 187 m.a.

the two furthest peaks. Fig. 10, taken at a much higher field where the Paschen-Back effect is well advanced no longer shows the individual peaks. The scattered atoms are still further split in the Stern-Gerlach pattern with the center still at the same position although the selected atoms have been shifted a distance well over a millimeter. It is also of interest to note that one of the peaks in Figs. 6 and 7 are actually to the right of the position of the selected beam showing that these components have magnetic moments in weak fields opposite in sign to the strong field case as is to be expected for values of x less than $1/2$ (Fig. 1).

The four peaks obtained are of practically the same intensity, which is to be expected and have

the width of the original beam. Since the number of peaks is equal to $2i+1$, the spin of the sodium nucleus is $3/2$ in units of $h/2\pi$.*

It should be mentioned that since this result is obtained only by counting the number of peaks, it is independent of any assumption as to the Maxwellian distribution of molecular velocities, or of any measurements of field, gradient or of the temperature of the oven.

* This value of the nuclear spin has been confirmed since our first publication (Phys. Rev. **43**, 582 (1933)) by Joffe from intensities in the band spectrum of the Na_2 molecule (Phys. Rev. **45**, 468 (1934)) by Granath and Van Atta from intensity measurements of the hyperfine structure of the resonance lines (Phys. Rev. **44**, 935 (1933)) and by Heydenburg and Ellett from the polarization of resonance radiation of Na in a weak magnetic field. (Phys. Rev. **44**, 326 (1933)).

2.2 Nuclear Induction

Felix Bloch (1905–1983)

Felix Bloch was born in Zurich, Switzerland, on 23 October 1905, the son of Gustav Bloch and Agnes Bloch (*née* Mayer). From 1912 to 1918 he attended the public primary school and subsequently the “Gymnasium” of the Canton of Zurich, which he left in the fall of 1924 after having passed the “Matura”, i.e. the final examination which entitled him to attend an institution of higher learning.

Planning originally to become an engineer, he entered directly the Federal Institute of Technology (Eidgenössische Technische Hochschule) in Zurich. After one year's study of engineering he decided instead to study physics, and changed therefore to the Division of Mathematics and Physics at the same institution. During the following two years he attended, among others, courses given by Debye, Scherrer and Weyl, as well as Schrödinger, who taught at the same time at the University of Zurich and through whom he became acquainted, toward the end of this period, with the new wave mechanics. Bloch's interests had by that time turned toward theoretical physics. After Schrödinger left Zurich in the fall of 1927 Bloch continued his studies with Heisenberg at the University of Leipzig, where he received his degree of Doctor of Philosophy in the summer of 1928 with a dissertation dealing with the quantum mechanics of electrons in crystals and developing the theory of metallic conduction. Various assistantships and fellowships, held in the following years, gave him the opportunity to work with Pauli, Kramers, Heisenberg, Bohr, and Fermi and led to further theoretical studies of the solid state as well as of the stopping power of charged particles.

Upon Hitler's ascent to power, Bloch left Germany in the spring of 1933, and a year later he accepted a position which was offered to him at Stanford University. The new environment in which he found himself in the United States helped toward the maturing of the wish he had had for some time to undertake also experimental research. Working with a very simple neutron source, it occurred to him that a direct proof for the magnetic moment of the free neutrons could be obtained through the observation of scattering in iron. In 1936, he published a paper in which the details of the phenomenon were worked out and in which it was pointed out that it would lead to the production and observation of polarized neutron beams. The further development of these ideas led him in 1939 to an experiment, carried out in collaboration with L.W. Alvarez at the Berkeley cyclotron, in which the magnetic moment of the neutron was determined with an accuracy of about 1%.

During the war years Dr. Bloch was also engaged in the early stages of the work on atomic energy at Stanford University and Los Alamos and later in counter-measures against radar at Harvard University. Through this latter work he became acquainted with the modern developments of electronics which, toward the end of the war, suggested to him, in conjunction with his earlier work on the magnetic moment of the neutron, a new approach toward the investigation of nuclear moments.

These investigations were begun immediately after his return to Stanford in the fall of 1945 and resulted shortly afterward in collaboration with W.W. Hansen and M.E. Packard in the new method of nuclear induction, a purely electromagnetic procedure for the study of nuclear moments in solids, liquids, or gases. A few



weeks after the first successful experiments he received the news of the same discovery having been made independently and simultaneously by E.M. Purcell and his collaborators at Harvard. Most of Bloch's work in the subsequent years was devoted to investigations with the use of this new method. In particular, he was able, by combining it with the essential elements of his earlier work on the magnetic moment of the neutron, to remeasure this important quantity with great accuracy in collaboration with D. Nicodemus and H.H. Staub (1948). In 1954, Bloch took a leave of absence to serve for one year as the first Director General of CERN in Geneva. After his return to Stanford University he continued his investigations on nuclear magnetism, particularly in regard to the theory of relaxation.

In 1961, he received an endowed Chair by his appointment as Max Stein Professor of Physics at Stanford University. In 1952 he shared the nobel prize in physics with Purcell. Prof. Bloch married in 1940 Dr. Lore Misch, a refugee from Germany and herself a physicist. Felix Bloch died in 1983.

From Nobel Lectures, Physics 1942–1962, Elsevier Publishing Company, Amsterdam

W.W. Hansen

M.E. Packard

electric accelerating fields are to be obtained by replacing the usual "dee" assembly and acceleration chamber by a cavity resonator, similar to types now commonly employed in radar. The use of such a cavity becomes practical only in an iron-less device, because of the limitation imposed by the air-gap in present accelerators.

The maximum orbit radius is to be small. This requires a large guiding magnetic field, but at the same time greatly reduces the volume through which this field must be maintained. It, therefore, appears practicable to immerse the entire accelerator in a liquified gas, such as hydrogen or nitrogen. Cooling the assembly materially reduces ohmic resistance losses in the field windings, and thus simplifies the problem of passing large current pulses. It has also the advantage of increasing the "Q" of the resonator.

Although many of the commoner types of cavity resonators⁷ exhibit electric field configurations adapted to producing resonance acceleration, the type describable as a "sphere (or spheroid) and reentrant cones"⁸ seems particularly suitable. In such a cavity, the electric field lines appear as arcs of circles, terminating on the surfaces of the reentrant cones. Small slots are to be made at points in the conical surfaces, through which the accelerated particles are to pass in their circular orbits. Injection may conveniently be accomplished from a point external to the accelerating fields by placing the injector gun within one of the cones. A target may also be conveniently located within the cones. It will probably be necessary to partially "open-circuit" the cavity walls for low frequency currents generated by the guide field. This can readily be done.

Within a resonator such as described, it should be possible to obtain exceptionally high accelerating potential drops, of the order of several hundred thousand volts. This follows from the fact that a cavity resonator is an extremely efficient device, often exhibiting an electrical "Q" greater than 100,000 and consequently requiring a relatively small energy input to produce large internal fields. The upper limit of attainable electric fields within an evacuated cavity should be very high, and will probably be imposed by field emission effects. In the use of such a resonator, it is convenient to employ the cavity itself as the frequency controlling element of a power oscillator, thus eliminating problems of accurate frequency control.

Some small advantage may also be gained from enclosing the particle orbits within a closed conducting surface, in that this will minimize that part of the radiation losses contributed by low order harmonics. It has been shown,^{5,6} however, that these harmonics contribute only slightly to the total radiative dissipation.

The conditions for "resonant" increase of energy^{1,2} can be satisfied at all times during an acceleration cycle, provided the amplitude of the resonance electric field is increased simultaneously with the rise of the magnetic field. It can be shown that under these conditions the effect of the magnetic component of the cavity field will be negligible throughout the cycle, provided adequate focusing forces are established by the guide field.

To provide the necessary pulses of current through the field windings, three methods could be employed: (a) a "pulse transformer" excited from a d.c. source, (b) a

short-circuited d.c. generator (following Kapitza's technique), or (c) a bank of high capacity storage batteries of the type used in submarines. A large ignitron and delay-line extinguishing circuit would serve as the switching element. The limits on the particle yield of the accelerator will be set by the available power and by the allowable rate of heat dissipation from the field windings.

Some design calculations have been made for a 500-Mev electron accelerator.

The author wishes to express his appreciation for counsel and suggestions given by Mr. H. F. Kaiser, Dr. Ross Gunn, and Mr. D. dePackh of the Naval Research Laboratory.

¹ Veksler, J. Phys. Acad. Sci. USSR 9, 153 (1945).

² E. M. McMillan, Phys. Rev. 68, 143 (1945).

³ Terletzky, J. Phys. Acad. Sci. USSR 9, 159 (1945).

⁴ D. Iwanenko and I. Pomeranchuk, Phys. Rev. 65, 343 (1944).

⁵ Arzimovich and Pomeranchuk, J. Phys. Acad. Sci. USSR 9, 267 (1945).

⁶ E. M. McMillan, Phys. Rev. 68, 144 (1945).

⁷ W. W. Hansen and R. D. Richtmyer, J. App. Phys. 10, 189 (1939).

⁸ Schelkunoff, *Electromagnetic Waves* (D. Van Nostrand Company, New York, 1943), p. 288.

Nuclear Induction

F. BLOCH, W. W. HANSEN, AND MARTIN PACKARD
Stanford University, Stanford University, California
January 29, 1946

THE nuclear magnetic moments of a substance in a constant magnetic field would be expected to give rise to a small paramagnetic polarization, provided thermal equilibrium be established, or at least approached. By superposing on the constant field (z direction) an oscillating magnetic field in the x direction, the polarization, originally parallel to the constant field, will be forced to precess about that field with a latitude which decreases as the frequency of the oscillating field approaches the Larmor frequency. For frequencies near this magnetic resonance frequency one can, therefore, expect an oscillating induced voltage in a pick-up coil with axis parallel to the y direction. Simple calculation shows that with reasonable apparatus dimensions the signal power from the pick-up coil will be substantially larger than the thermal noise power in a practicable frequency band.

We have established this new effect using water at room temperature and observing the signal induced in a coil by the rotation of the proton moments. In some of the experiments paramagnetic catalysts were used to accelerate the establishment of thermal equilibrium.

By use of conventional radio techniques the induced voltage was observed to produce the expected pattern on an oscillograph screen. Measurements at two frequencies ν showed the effect to occur at values H of the z field such that the ratio H/ν had the same value. Within our experimental error this ratio agreed with the g value for protons, as determined by Kellogg, Rabi, Ramsey, and Zacharias.¹

We have thought of various investigations in which this effect can be used fruitfully. A detailed account will be published in the near future.

¹ J. M. B. Kellogg, I. I. Rabi, N. F. Ramsey, and J. R. Zacharias, Phys. Rev. 56, 738 (1939).

2.3 Resonance absorption by nuclear magnetic moments in a solid

Edward M. Purcell (1912–1997)

Edward Mills Purcell was born in Taylorville, Illinois, USA, on 30 August 1912. His parents, Edward A. Purcell and Mary Elizabeth Mills, were both natives of Illinois. He was educated in the public schools in Taylorville and in Mattoon, Illinois, and in 1929 entered Purdue University in Indiana. He graduated from Purdue in electrical engineering in 1933.

His interest had already turned to physics, and through the kindness of Professor K. Lark-Horovitz he was able, while an undergraduate, to take part in experimental research in electron diffraction. As an Exchange Student of the Institute of International Education, he spent one year at the Technische Hochschule, Karlsruhe, Germany, where he studied under Professor W. Weizel. He returned to the United States in 1934 to enter Harvard University, where he received the Ph.D. degree in 1938. After serving two years as instructor in physics at Harvard, he joined the Radiation Laboratory, Massachusetts Institute of Technology, which was organized in 1940 for military research and development of microwave radar. He became Head of the Fundamental Developments Group in the Radiation Laboratory, which was concerned with the exploration of new frequency bands and the development of new microwave techniques. This experience turned out to be very valuable. Perhaps equally influential in his subsequent scientific work was the association at this time with a number of physicists, among them I.I. Rabi, with a continuing interest in the study of molecular and nuclear properties by radio methods.

The discovery of nuclear magnetic resonance absorption was made just after the end of the war, and at about that time Purcell returned to Harvard as Associate Professor of Physics. He became Professor of Physics in 1949 and subsequently Gerhard Gade University Professor. He continued to work in the field of nuclear magnetism, with particular interest in relaxation phenomena, related problems of molecular structure, measurement of atomic constants, and nuclear magnetic behavior at low temperatures. He made some contributions to the subject of radioastronomy.

He was a Fellow of the American Physical Society, a member of the National Academy of Sciences, of the American Academy of Arts and Sciences, and of the President's Science Advisory Committee under President Eisenhower from 1957–1960 and under President Kennedy as from 1960. In 1952 he was awarded the Nobel Prize in physics with Felix Bloch.

In 1937, Purcell married Beth C. Busser. They had two sons, Dennis and Frank.

E. M. Purcell died in 1997.

From Nobel Lectures, Physics 1942–1962, Elsevier Publishing Company, Amsterdam



H.C. Torrey

R.V. Pound

LETTERS TO THE EDITOR

37

The suggestion is also made that CO_2 may be strongly dissociated by the metastable Xe atoms (and H_2O somewhat less strongly), thus producing oxygen atoms which combine to form the O_2 molecules; ($D(\text{CO}_2)=5.5$ v, $D(\text{H}_2\text{O})=5.0$ v). If so, the fact that CO did not yield the bands would indicate that the dissociation energy of CO is greater than the energy of the upper metastable state of Xe, namely 9.4 volts. (Energy of lower metastable state equals 8.3 v.) This appears to be direct evidence in favor of the 9.6-volt value of $D(\text{CO})$ as determined by Hagstrum and Tate¹ from appearance potentials in the mass spectrograph, or for the 11.11 v-value obtained in a recent spectral analysis by Gaydon and Penney,² but against the 9.14-volt value determined from certain predissociation data.³ The higher value appears to be more in accord also with thermochemical data as brought out by Hagstrum and Tate,¹ and also by Asundi and Samuel.⁴

¹ H. D. Hagstrum and J. T. Tate, *Phys. Rev.* **59**, 365 (1941).

² A. G. Gaydon and W. G. Penney, *Proc. Roy. Soc. A* **183**, 374 (June, 1945).

³ For a review see G. Herzberg, *Molecular Spectra and Molecular Structure* (Prentice-Hall, Inc., New York, 1939), Chap. VIII.

⁴ R. K. Asundi and R. Samuel, *Ind. Acad. Sci.* **3A**, 562 (1936).

Resonance Absorption by Nuclear Magnetic Moments in a Solid

E. M. PURCELL, H. C. TORREY, AND R. V. POUND*
Radiation Laboratory, Massachusetts Institute of Technology,
Cambridge, Massachusetts

December 24, 1945

IN the well-known magnetic resonance method for the determination of nuclear magnetic moments by molecular beams,¹ transitions are induced between energy levels which correspond to different orientations of the nuclear spin in a strong, constant, applied magnetic field. We have observed the absorption of radiofrequency energy, due to such transitions, in a *solid* material (paraffin) containing protons. In this case there are two levels, the separation of which corresponds to a frequency, ν , near 30 megacycles/sec., at the magnetic field strength, H , used in our experiment, according to the relation $h\nu=2\mu H$. Although the difference in population of the two levels is very slight at room temperature ($h\nu/kT\sim 10^{-5}$), the number of nuclei taking part is so large that a measurable effect is to be expected providing thermal equilibrium can be established. If one assumes that the only local fields of importance are caused by the moments of neighboring nuclei, one can show that the imaginary part of the magnetic permeability, at resonance, should be of the order $h\nu/kT$. The absence from this expression of the nuclear moment and the internuclear distance is explained by the fact that the influence of these factors upon absorption cross section per nucleus and density of nuclei is just cancelled by their influence on the width of the observed resonance.

A crucial question concerns the time required for the establishment of thermal equilibrium between spins and

lattice. A difference in the populations of the two levels is a prerequisite for the observed absorption, because of the relation between absorption and stimulated emission. Moreover, unless the relaxation time is very short the absorption of energy from the radiofrequency field will equalize the population of the levels, more or less rapidly, depending on the strength of this r-f field. In the expectation of a long relaxation time (several hours), we chose to use so weak an oscillating field that the absorption would persist for hours regardless of the relaxation time, once thermal equilibrium had been established.

A resonant cavity was made in the form of a short section of coaxial line loaded heavily by the capacity of an end plate. It was adjusted to resonate at about 30 mc/sec. Input and output coupling loops were provided. The inductive part of the cavity was filled with 850 cm³ of paraffin, which remained at room temperature throughout the experiment. The resonator was placed in the gap of the large cosmic-ray magnet in the Research Laboratory of Physics, at Harvard. Radiofrequency power was introduced into the cavity at a level of about 10^{-11} watts. The radiofrequency magnetic field in the cavity was everywhere perpendicular to the steady field. The cavity output was balanced in phase and amplitude against another portion of the signal generator output. Any residual signal, after amplification and detection, was indicated by a microammeter.

With the r-f circuit balanced the strong magnetic field was slowly varied. An extremely sharp resonance absorption was observed. At the peak of the absorption the deflection of the output meter was roughly 20 times the magnitude of fluctuations due to noise, frequency, instability, etc. The absorption reduced the cavity output by 0.4 percent, and as the loaded Q of the cavity was 670, the imaginary part of the permeability of paraffin, at resonance, was about $3\cdot 10^{-6}$, as predicted.

Resonance occurred at a field of 7100 oersteds, and a frequency of 29.8 mc/sec., according to our rather rough calibration. We did not attempt a precise calibration of the field and frequency, and the value of the proton magnetic moment inferred from the above numbers, 2.75 nuclear magnetons, agrees satisfactorily with the accepted value, 2.7896, established by the molecular beam method.

The full width of the resonance, at half value, is about 10 oersteds, which may be caused in part by inhomogeneities in the magnetic field which were known to be of this order. The width due to local fields from neighboring nuclei had been estimated at about 4 oersteds.

The relaxation time was apparently shorter than the time (\sim one minute) required to bring the field up to the resonance value. The types of spin-lattice coupling suggested by I. Waller² fail by a factor of several hundred to account for a time so short.

The method can be refined in both sensitivity and precision. In particular, it appears feasible to increase the sensitivity by a factor of several hundred through a change in detection technique. The method seems applicable to the precise measurement of magnetic moments (strictly, gyromagnetic ratios) of most moderately abundant nuclei.

It provides a way to investigate the interesting question of spin-lattice coupling. Incidentally, as the apparatus required is rather simple, the method should be useful for standardization of magnetic fields. An extension of the method in which the r-f field has a rotating component should make possible the determination of the sign of the moment.

The effect here described was sought previously by Gorter and Broer, whose experiments are described in a paper³ which came to our attention during the course of this work. Actually, they looked for dispersion, rather than absorption, in LiCl and KF. Their negative result is perhaps to be attributed to one of the following circumstances: (a) the applied oscillating field may have been so strong, and the relaxation time so long, that thermal equilibrium was destroyed before the effect could be observed—(b) at the low temperatures required to make the change in permeability easily detectable by their procedure, the relaxation time may have been so long that thermal equilibrium was never established.

* Harvard University, Society of Fellows (on leave).

¹ Rabi, Zacharias, Millmann, and Kusch, *Phys. Rev.* **53**, 318 (1938).

² I. Waller, *Zeits. f. Physik* **79**, 370 (1932).

³ Gorter and Broer, *Physica* **9**, 591 (1942).

The γ -Rays of Radium D

TSIEN SAN-TSIANG*

Laboratoire Curie, Institut du Radium, and Laboratoire de Chimie
Nucéaire du Collège de France, Paris, France

December 13, 1945

FOR many years RaD was regarded as a radioactive substance which emits nuclear β -rays of very low energy and monochromatic γ -rays of quantum energy 46.7 kev. Just before the war, however, it was shown by Amaldi and Rasetti,¹ using the method of selective absorption, that the radiation is complex, the well-known 46.7 kev line being accompanied by a much weaker component of energy 43 kev. Following the publication of this result,² a systematic study of the subject was started in Paris with a very strong source of RaD of about 100 mC, extracted previously by Professors Irène Joliot-Curie and F. Joliot. The following is a brief summary of the main experimental results, obtained in the Curie Laboratory and in the Laboratory of Nuclear Chemistry in the difficult conditions which prevailed from 1942–1945. The results deal with the detailed structure of the γ -radiation, the absolute intensity of the different lines, and the nature of γ -rays of quantum energy 46.7 kev.

In the region between 25 and 100 kev, the analysis made by the methods of selective absorption² and crystal diffraction³ leads to the conclusion that RaD emits in this region four γ -lines (*A*, *B*, *C*, *D*) and two lines of x-rays of K-83, the corresponding energy and intensity being given in Table I.

The existence of these six different radiations is confirmed by another series of experiments in which the corresponding quantum energies are determined by measuring the true

range of the photoelectrons which they project in a Wilson chamber.^{4,5} This method also suggested the existence of an additional weak line at about 65 kev (x) and relatively intense radiations below 25 kev.

TABLE I. γ -rays from RaD.

γ -ray line	<i>E</i> (kev)	<i>I</i> (quanta per 100 disintegrations)	Reference
(X)	(65 \pm 5)	(<0.2)	(5) ⁶
<i>A</i>	46.7 \pm 0.1	2.8 \pm 0.6	(1, 2, 3, 5, 8)
<i>B</i>	43 \pm 1	0.2 \pm 0.1	(1, 2, 3, 5)
<i>C</i>	37 \pm 1	0.2 \pm 0.1	(2, 3, 5)
<i>D</i>	32 \pm 1	0.4 \pm 0.2	(2, 3, 5, 6)
<i>E</i>	23.2 \pm 0.6	1.0 \pm 0.5	(5, 6)
<i>F</i>	7.3 \pm 0.7	\sim 10	(6, 7)

In order to study the region below 25 kev, experiments were made with a Wilson chamber operating at suitable low pressure.⁶ It was thus found that in addition to the *L* spectrum of element 83, there is a new γ -ray line (*E*) of 23.2 \pm 0.6 kev. This line has thus almost exactly half the quantum energy of the principle line (*A*) and would be confused in diffraction spectrum experiments with the second-order image of the (*A*) line. Another very intense γ -ray line (*F*) of 7.3 \pm 0.7 kev has been observed in the energy region below the *L* levels of element 83.^{6a} This radiation has been observed previously by Droste⁷ who classified it as one of the components of the *L* spectrum of element 83. From the energy determinations in our present experiments, it seems more reasonable to regard it as a new γ -ray line.

In order to investigate the nature of the principle line (*A*) we have determined the intensity of the conversion electrons of this radiation by the usual methods of magnetic β -ray spectrography and obtained the value 2.9 for the internal conversion coefficient, N_e/N_γ , in the *L*₁ level.^{8,2} The comparison with the theoretical calculation of Fisk⁹ indicates that the 46.7 kev line is most probably a quadrupole radiation. For other γ -rays there is no information available about their conversion electrons¹⁰ to permit similar deduction about their nature to be made.

I should like to thank Professors I. Joliot-Curie and F. Joliot for their continuous interest and help, and Drs. Frilley, Surugue, and Ouang, and Mr. Marty for their important contributions and friendly collaboration in the course of these investigations.

* Now temporarily at H. H. Wills Physics Laboratory, Bristol, England.

¹ E. Amaldi and F. Rasetti, *Ricerca Scient.* **10**, 111 (1939).

² Tsién San-Tsiang, *Comptes rendus* **216**, 765 (1943); **218**, 503 (1944).

³ M. Frilley, *Comptes rendus* **218**, 505 (1944).

⁴ Tsién San-Tsiang, *Ann. d. Physik* **19**, 327 (1944).

⁵ Tsién San-Tsiang and C. Marty, *Comptes rendus*, Seance of 7th May 1945 (in press).

⁶ Tsién San-Tsiang and C. Marty, *Comptes rendus*, Seance of 30th July, 1945 (in press).

^{6a} M. Frilley and Tsién San-Tsiang, *Comptes rendus* (Jan., 1945).

⁷ G. von Droste, *Zeits. f. Physik* **84**, 17 (1933).

⁸ Ouang Te-Tchao, J. Surugue, and Tsién San-Tsiang, *Comptes rendus* **217**, 535 (1943).

⁹ J. S. Fisk, *Proc. Roy. Soc.* **143**, 674 (1934).

¹⁰ H. O. W. Richardson and A. Leigh-Smith, *Proc. Roy. Soc.* **160**, 454 (1937).

2.4 Tumor detection by nuclear magnetic resonance

Raymond V. Damadian (born 1936)

Born in Forest Hills, New York, Damadian attended the Juilliard School of Music for eight years, studying violin. He received his BS in mathematics in 1956 from the University of Wisconsin and an MD degree from the Albert Einstein College of Medicine in New York in 1960. Damadian later served as a fellow in nephrology at Washington University School of Medicine and as a fellow in biophysics at Harvard University, where he completed academic work in physics, physical chemistry, and mathematics. He studied physiological chemistry at the School of Aerospace Medicine in San Antonio, Texas. After serving in the Air Force, Damadian joined the faculty of the State University of New York Downstate Medical Center in 1967. His training in medicine and physics led him to develop a new theory of the living cell, his ion exchanger resin theory. Damadian founded the FONAR Corporation in 1978 and became its president and chairman.

Raymond Damadian invented the magnetic resonance imaging (MRI) scanner, which has revolutionized the field of diagnostic medicine. MRI obtains information through the use of static and dynamic magnetic fields, a method that yields radio signal outputs from the body's tissue that can be either transformed into images or analyzed to provide the chemical composition of the tissue being examined. His MRI produced images of the interior of the body far more detailed than was possible with X-ray devices such as the CAT scanner. Since the device's approval in 1984 by the Food and Drug Administration hundreds have been put to use in medical institutions around the world.

Although the technology used in Damadian's machine – nuclear magnetic resonance (NMR or MR), where harmless magnetic fields and radio waves cause atoms to emit tiny, detectable radio signals – had existed for 25 years, Damadian was the first to successfully apply the physics of NMR to clinical medicine. In 1971, Damadian demonstrated for the first time that the MR signal could overcome one of medicine's longstanding deficiencies – the inability of the X-ray to create the contrast needed to see the body's vital organs. Citing this contrast deficiency in a paper published in *Science*, Damadian proposed that the profound differences between the decay rate of the MR signal of soft tissues and the decay rate of the MR signal of cancerous tissues had the potential to address this long-standing, critical need in medicine. He proposed the creation of a new body scanner based on the MR signal and on his discovery of the critical differences in the MR signals that existed in the body's vital tissues. The images of the interior of the human body that resulted from Damadian's work were far superior in detail to those of existing X-ray devices because the MR could generate the tissue contrast that was missing in X-ray pictures.

As with any groundbreaking invention, Damadian's MR scanner was met with great skepticism. "What I learned in the process of developing the MR scanner was that criticism is an integral part of the process and always has been," comments Damadian. "The bolder the initiative, the harsher the criticism."

Damadian, a violin student who left the Juilliard School of Music to pursue a medical education, first became interested in medicine at the age of ten, after witnessing his grandmother's pain and suffering from cancer. He chose medical research over clinical practice because he believed that carefully executed experi-



ments could result in major medical contributions with the potential to benefit many people. Damadian felt that research would allow him to help many millions of people, rather than the thousands he would be able to beneficially reach in the day-to-day practice of medicine.

Today, Damadian oversees FONAR Corporation, the Melville, NY-based company he formed in 1978 to produce and market his MRI scanner. After twenty-three years in business, FONAR continues to research and develop, manufacture, sell and ship its own MRI scanners.

FONAR's recent MRI innovations include a full-sized MRI operating room that allows unrestricted 360-degree access to the patient and the Stand-Up MRI™ – the only scanner to allow MRI patients to simply walk in and be scanned while standing. The revolutionary design of the Stand-Up MRI™ allows all parts of the body to be scanned in the weight-bearing position.

Reprinted from
19 March 1971, Volume 171, pp. 1151-1153

DOCUMENT 1

SCIENCE

Tumor Detection by Nuclear Magnetic Resonance

Raymond Damadian

Copyright© 1971 by the American Association for the Advancement of Science

Tumor Detection by Nuclear Magnetic Resonance

Abstract. *Spin echo nuclear magnetic resonance measurements may be used as a method for discriminating between malignant tumors and normal tissue. Measurements of spin-lattice (T_1) and spin-spin (T_2) magnetic relaxation times were made in six normal tissues in the rat (muscle, kidney, stomach, intestine, brain, and liver) and in two malignant solid tumors, Walker sarcoma and Novikoff hepatoma. Relaxation times for the two malignant tumors were distinctly outside the range of values for the normal tissues studied, an indication that the malignant tissues were characterized by an increase in the motional freedom of tissue water molecules. The possibility of using magnetic relaxation methods for rapid discrimination between benign and malignant surgical specimens has also been considered. Spin-lattice relaxation times for two benign fibroadenomas were distinct from those for both malignant tissues and were the same as those of muscle.*

At present, early detection of internal neoplasms is hampered by the relatively high permeability of many tumors to x-rays. In principle, nuclear magnetic resonance (NMR) techniques combine many of the desirable features of an external probe for the detection of internal cancer. Magnetic resonance measurements cause no obvious deleterious effects on biologic tissue (1), the incident radiation consisting of common radio frequencies at right angles to a static magnetic field. The detector is external to the sample, and the method permits one to resolve information emitted by the sample to atomic dimensions. Thus the spectroscopist has available for study a wide range of nuclei for evidence of deviant chemical behavior.

The resonance technique selected for this particular application belongs to a group of techniques known as "transient" or induction methods. In this experimental arrangement the sample continues to emit a radio-frequency signal for a brief but measurable period after the incident radiation (pulse) has been removed. This method makes possible the direct measurement of spin-lattice (T_1) and spin-spin (T_2) relaxation times, thus avoiding the uncertainties of estimating them from the line width measurements of steady-state NMR spectra. In addition, it also makes possible the characterization of biologic tissues on the basis of the properties of their emitted radio frequency.

In order to determine whether neo-

plastic tissues could be recognized from their NMR signals, I studied the proton resonance emissions from cell water. Recent NMR work of Copc (2), Hazlewood *et al.* (3), and Bratton *et al.* (4) has provided fresh insight into the physical nature of cell water. These authors have independently concluded that the decreased NMR relaxation times observed for cell water relative to distilled water (Tables 1 and 2) are due to the existence of a highly ordered fraction of cell water in which the protons of the water molecules have correlation times substantially less than the Larmor period. The reduction of the correlation times is presumably due to the adsorption of water molecules at macromolecular interfaces, findings that are consistent with the proposal by Ling (5) that intracellular water (endosolvent) exists as multiple polarized layers adsorbed onto cell proteins.

Two lines of evidence suggested that proton signals from the water in cancerous tissue would be distinct from the radio-frequency emissions of normal tissue. My own experiments with *Escherichia coli* (6) suggested that altered selectivity coefficients of alkali cations in biologic tissue, such as occur in neoplastic tissue (5), can indicate alterations in tissue water structure. In addition, Hazlewood and his co-workers have recently reported evidence from NMR measurements that growth and maturation of skeletal muscle in the newborn rat is accompanied by simultaneous changes in water structure and

Table 1. Spin-lattice (T_1) and spin-spin (T_2) relaxation times (in seconds) of normal tissues.

Rat No.	Weight (g)	Tissue							
		Rectus muscle		Liver		Stomach	Small intestine	Kidney	Brain
		T_1	T_2	T_1	T_2	T_1	T_1	T_1	T_1
1	156	0.493	0.050	0.286	0.050	0.272	0.280	0.444	0.573
2	150	.548	.050	.322	.060	.214	.225	.503	.573
3	495	.541	.050	.241	.050	.260	.316	.423	.596
4	233	.576 (0.600)*	.070	.306 (0.287)*	.048	.247 (0.159)*	.316 (0.280)*	.541 (0.530)*	.620 (0.614)*
5	255	.531		.300		.360	.150	.489	.612
Mean and standard error									
		0.538 ± 0.015	0.055 ± 0.005	0.293 ± 0.010	0.052 ± 0.003	0.270 ± 0.016	0.257 ± 0.030	0.480 ± 0.026	0.595 ± 0.007

* Spin-lattice relaxation time after the specimen stood overnight at room temperature.

in the alkali cation composition of the muscle (7). These results suggest that dedifferentiation and anaplasia, commonly equated with neoplasia, may be associated with profound alterations in endosolvent structure. These data (7) suggest the nature of the alteration in H_2O structure that should be observed for dedifferentiated or neoplastic tissue. Substantially narrower line widths [the result of a decreased ordering of cell water (2, 3)] were observed for immature skeletal muscle than for mature muscle. On this basis undifferentiated neoplastic tissue can be expected to manifest increased relaxation times (narrow line widths).

The experiments were performed with Sprague-Dawley rats previously infected with either Walker sarcoma (solid form) or Novikoff hepatoma. The rats ranged in weight from 150 to 500 g and were selected at random in order to exclude variations in the age of the rat as a material consideration (8). The animals were killed by cervical fracture when tumor size reached approximately 1.5 ml in volume (4 to 5 days after inoculation in the case of animals with Novikoff hepatoma and 10 days in the case of animals with Walker sarcoma). The samples were excised and packed in cellulose nitrate tubes. In all cases the NMR measurements were obtained within 5 minutes after the death of the animal.

The experimental arrangement consisted of an electromagnet (Varian) 12 inches (30.5 cm) in diameter operating at approximately 5610 gauss, a pulse spectrometer (Nuclear Magnetic Resonance Specialties Corporation PS-60 AW), and a probe of cross-coil design operating at 24 Mhz.

Two types of NMR experiments were performed. Spin-lattice relaxation time was measured by the method of Carr and Purcell (9). In this method a sequence of two pulses is used with pulse widths for the two pulses set to produce a 180° nutation followed by a

90° nutation. With this sequence, one observes a free induction decay after the second pulse whose amplitude is given by

$$M(\tau) = M_0(1 - 2e^{-\tau/T_1})$$

where M_0 is the equilibrium value of the pulse amplitude and τ is the interval between pulses. This equation implies that, if T_1 is multiplied by the natural logarithm of 2, the product is equal to the pulse interval that produces no free induction decay after the 90° pulse. In actual practice, once the two pulses were phased and pulse widths set for the proper nutation angle, an oscilloscope (Fairchild 766 H/F, 25 and 50 Mhz) was synchronized to trigger on the second pulse and the pulse interval was adjusted until the null free induction decay was obtained. The interval between the two pulses was obtained from a frequency counter (Com-

puter Measurement Company 200CN) interfaced with the output of the PS-60 spectrometer programmer.

I measured the spin-spin relaxation time by using a 90° to 180° pulse sequence and making use of the Carr-Purcell modification (9) to obtain the echo decay envelope. This method for measuring T_2 is free of diffusion effects and field inhomogeneities (9). Since the envelope height E is given by

$$E(2n\tau) \propto e^{-2n\tau/T_2}$$

where n represents integral multiples of the pulse separation τ , T_2 was estimated from the oscilloscope trace as the time required for the envelope height to decay to $1/e$.

The spin echo resonance measurements are listed in Tables 1 and 2. The contrast between the relaxation rates of malignant Novikoff hepatoma and normal liver illustrates the degree of perturbation of endosolvent structure that can accompany malignant transformation. The considerable increase in relaxation times for the hepatoma (T_1 , 0.826 second; T_2 , 0.118 second) relative to normal liver (T_1 , 0.293 second; T_2 , 0.050 second) suggests a significant decrease in the degree of ordering of intracellular water (2) in malignant tissue. In addition, it is apparent from the prolonged relaxation times of the two malignant tumors reported in Table 2 that NMR techniques would make it possible for one to detect the presence of metastatic infiltrates of the liver from either Walker sarcoma or Novikoff hepatoma.

It was also found that the differences between the relaxation rates of malignant tumors and normal liver could be used to distinguish the two malignancies from all of the normal tissues studied [P values less than .01 (Table 2)]. The values of T_1 in Walker sarcoma (0.736 second) and Novikoff hepatoma (0.826 second) were significantly greater than the values of T_1 in any of the normal tissues (0.293 to 0.595 second). The

Table 2. Spin-lattice (T_1) and spin-spin (T_2) relaxation times (in seconds) in tumors.

Rat No.	Weight (g)	T_1	T_2
<i>Walker sarcoma</i>			
6	156	0.700	0.100
7	150	.750	.100
8	495	.794 (0.794)*	.100
9	233	.688	
10	255	.750	
Mean and S.E.		0.736 ± 0.022	.100
P		< .01†	
<i>Novikoff hepatoma</i>			
11	155	0.798	0.120
12	160	.852	.120
13	231	.827	.115
Mean and S.E.		0.826 ± 0.013	0.118 ±
P		< .01†	0.002
<i>Fibroadenoma (benign)</i>			
14		0.448	
15		.537	
Mean		.492	
<i>Distilled water</i>			
		2.691	
		2.690	
		2.640	
Mean and S.E.		2.677 ± 0.021	

* Spin-lattice relaxation time after the specimen stood overnight at room temperature. † The P values are the probability estimates of the significance of the difference in the means of T_1 for the malignant tumor and for brain.

values of T_2 in the malignant tumors (0.100 and 0.118 second) were about twice the values of T_2 in rectus muscle (0.055 second) and liver (0.052 second). Furthermore, replicate measurements of T_1 in the malignant tissues were found to be highly reproducible (standard error of the mean, $< .02$) and the normal tissues had a standard error of the mean of .03 or less despite deliberate scrambling of the ages and weights of the animals in the experimental colony.

On the whole, these results support the findings of Hazlewood and his co-workers (7) and are in general agreement with Szent-Györgyi's assertion that cancerous tissue has a lower degree of organization and less water structure than normal tissue (10). Furthermore, the data conformed to the results expected on the basis of a knowledge of the cation content of cancerous tissue. Dunham *et al.* have reported that with "few exceptions the potassium content of malignant neoplasms is increased" by comparison with that of normal cells (11). Ling has pointed out that the variations in alkali cation selectivity observed by Dunham *et al.* are readily explained by the association-induction hypothesis (5, p. 523). Nuclear magnetic resonance line width measurements in my laboratory (6) have demonstrated a correlation between narrowing of the line width of the cell water signal and potassium enrichment in bacteria (*E. coli*), which, in turn, is consistent with the aqueous properties of potassium as a "structure-breaking" agent (12). "Structure-breaking" by the alkali cations below Na in the periodic table (K, Rb, Cs), producing decreased ordering of the molecules in bulk water, results in narrowing of the NMR line width (6).

The measurements were also unaffected by any change in the elevation of the sample position in the probe, packing and repacking of the specimen, or the stepwise rotation of the sample tube in the probe through 360°. In fact T_1 proved to be even relatively unchanged after the specimens stood overnight at room temperature (Tables

1 and 2, parenthetical values for rats 4 and 8).

These studies indicate that NMR methods may be used to discriminate between two malignant tumors and a representative series of normal tissues. The results suggest that this technique may prove useful in the detection of malignant tumors.

The possibility that NMR might be used for rapid discrimination between benign and malignant surgical specimens was also considered. Relaxation times for two benign tumors (fibroadenomas) were distinct from those of the malignant tissues and were the same as those of muscle (Tables 1 and 2)

RAYMOND DAMADIAN*

Biophysical Laboratory, Department of Medicine, State University of New York, Brooklyn 11203

References and Notes

1. M. F. Barnothy, Ed., *Biological Effects of Magnetic Fields* (Plenum, New York, 1964), p. 17.
2. F. W. Cope, *Biophys. J.* 9, 303 (1969).
3. C. F. Hazlewood, B. L. Nichols, N. F. Chamberlain, *Nature* 222, 747 (1969).
4. C. B. Bratton, A. L. Hopkins, J. W. Weinberg, *Science* 147, 738 (1965).
5. G. N. Ling, *A Physical Theory of the Living State* (Blaisdell, Waltham, Mass., 1962).
6. R. Damadian, M. Goldsmith, K. S. Zaner, in preparation.
7. C. F. Hazlewood and B. L. Nichols, *Physiologist* 12, 251 (1969); —, B. Brown, personal communication.
8. The rats with Walker sarcoma were prepared by J. Patti and were provided by Dr. B. Gardner's laboratory, Department of Surgery, State University of New York, Brooklyn. The animals with hepatoma came from Dr. A. Novikoff's laboratory, Albert Einstein College of Medicine, New York, and were provided by C. Davis and Dr. M. Beard.
9. H. Y. Carr and E. M. Purcell, *Phys. Rev.* 94, 630 (1954).
10. A. Szent-Györgyi, *Bioenergetics* (Academic Press, New York, 1957).
11. L. Dunham, S. Nichols, A. Brunschwig, *Cancer Res.* 6, 230 (1946).
12. O. Y. Samoilov, *Structure of Aqueous Electrolyte Solutions and the Hydration of Ions* (Consultants Bureau, New York, 1965).
13. I am grateful to P. Yajko, president of Nuclear Magnetic Resonance Specialties Corporation, for providing the Varian electromagnet used in these studies, and to F. Wyant and T. Hill for their assistance with instrumentation. I thank M. Goldsmith, graduate student in biophysics, for contributing the term "endosolvent" for intracellular water. Studies supported by grant 12-1804A from the New York Heart Association and grant 12-6065C from the Health Research Council of the City of New York.

* Career scientist of the Health Research Council of the City of New York.

12 October 1970; revised 18 November 1970

2.5 Image Foundation by induced local interactions: Example employing nuclear magnetic resonance

Paul C. Lauterbur (born 1929)

A native of Sidney, Ohio, Paul C. Lauterbur was born on 6 May 1929. He received the BS degree in chemistry from Case Institute of Technology in 1951. Between 1951 and 1953, he worked as a Research Associate at the Mellon Institute, where he was involved in the studies of organosilicon chemistry, vulcanizing systems and reinforcing fillers of silicone elastomers. He served in the Army Chemical Center Laboratories between 1953 and 1955, where he worked on the biological testing of chemical warfare agents and studies on aerosols. While he was at the Army Chemical Center, he also set up the nuclear magnetic resonance laboratory and began research on NMR spectroscopy. After his military service, he returned to the Mellon Institute and continued his graduate education, receiving the Ph.D. degree in chemistry from the University of Pittsburgh in 1962. From 1963 to 1984, he was on the faculty of the State University of New York at Stony Brook, where he served as a Professor in the Departments of Chemistry and Radiology. During this period, Lauterbur worked on NMR spectroscopy and its applications to the studies of the structures of molecules, solutions and solids. He also extended his NMR studies to applications in biochemistry and biophysics when he discovered nuclear magnetic resonance imaging. In 1984, he was named as University Professor at SUNY Stony Brook until his departure in 1985. Currently, he is a professor at the College of Medicine and in the Department of Chemistry of the University of Illinois at Urbana-Champaign and the Director of Magnetic Resonance Imaging Research at the same institution. He also holds the position of Adjunct University Professor at SUNY Stony Brook.

Lauterbur has published more than 110 scientific articles in various aspects of NMR and its applications. His work at SUNY Stony Brook has laid the foundations for the entire field of nuclear magnetic resonance imaging, which is also known as nuclear magnetic resonance zeugmatography. From his work came a new medical diagnostic instrument and his discovery provided a new field of endeavor for physicists, engineers and clinicians. The discovery of NMR imaging has impacted the medical instrumentation industry positively by opening new horizons.

Recognition of Lauterbur's outstanding achievements includes an honorary PhD from the University of Liege, Belgium and numerous awards including the Gold Medal of the Society of Magnetic Resonance in Medicine, the Michelson-Morley Award, American Physical Society Prize in Biological Physics and Harvey Prize in Science and Technology, the national medal of science (USA) and the gold medal of the Radiological Society of North America in 1987 and the gold medal of the European Congress of Radiology in 1999. He was awarded the IEEE Medal of Honor in 1987, "For the discovery of nuclear magnetic resonance imaging." In 2003 Lauterbur was bestowed with the Nobel Prize in Medicine together with his British colleague Sir Peter Mansfield.



microamorphous, and microaphanitic, and further on a geometric basis into microgranular, microlamellar, and microfibrous. More recently, Kloss¹² reported that, unlike macrocrystalline quartz crystals, microcrystalline quartz crystals generally show no sharp inversion point, and the inversion takes place over an interval of nearly 50° C. Our work suggests that it is best to describe the product of powdering quartz as microcrystalline quartz, which has an X-ray structure corresponding to quartz but is not normally detectable by d.t.a. unless carried out at high heating rates. In addition, this microcrystalline quartz contains chemisorbed H₂O.

We thank Professor R. A. Howie, Moreton Moore, E. Nave, N. Walsh and Miss P. S. Osborn, and the Science Research Council.

G. S. M. MOORE
H. E. ROSE

*Powder Science Laboratory,
Department of Mechanical Engineering,
King's College, Strand,
London WC2*

Received October 10, 1972.

- ¹ Dempster, P. B., and Ritchie, P. D., *J. Appl. Chem.*, **3**, 182 (1953).
- ² Hillebrand, W. F., *J. Amer. Chem. Soc.*, **30**, 1120 (1908).
- ³ Keith, M. L., and Tuttle, O. F., *Amer. J. Sci.*, Bowen vol., 203 (1952).
- ⁴ Ray, R. C., *Proc. Roy. Soc.*, **101**, A, 509 and 640 (1922).
- ⁵ Sosman, R. B., and Merwin, H. E., *J. Wash. Acad. Sci.*, **14**, 117 (1924).
- ⁶ Dale, A. J., *Trans. Brit. Ceram. Soc.*, **23**, 211 (1924).
- ⁷ Clelland, D. W., and Ritchie, P. D., *J. Appl. Chem.*, **2**, 42 (1952).
- ⁸ Dempster, P. B., and Ritchie, P. D., *J. Appl. Chem.*, **3**, 187 (1953).
- ⁹ Sakabe, H., et al., *Bull. Nat. Inst. Indust. Jap.*, **4**, 1 (1960).
- ¹⁰ Soda, R., *J. Chem. Soc. Jap.*, **34**, 1491 (1961).
- ¹¹ Sosman, R. B., *The Phases of Silica*, 218 (Rutgers University Press, 1965).
- ¹² Smykatz-Kloss, W., *Contr. Mineral. Petrol.*, **36**, 1 (1972).

Image Formation by Induced Local Interactions: Examples Employing Nuclear Magnetic Resonance

AN image of an object may be defined as a graphical representation of the spatial distribution of one or more of its properties. Image formation usually requires that the object interact with a matter or radiation field characterized by a wavelength comparable to or smaller than the smallest features to be distinguished, so that the region of interaction may be restricted and a resolved image generated.

This limitation on the wavelength of the field may be removed, and a new class of image generated, by taking advantage of induced local interactions. In the presence of a second field that restricts the interaction of the object with the first field to a limited region, the resolution becomes independent of wavelength, and is instead a function of the ratio of the normal width of the interaction to the shift produced by a gradient in the second field. Because the interaction may be regarded as a coupling of the two fields by the object, I propose that image formation by this technique be known as zeugmatography, from the Greek ζευγμα, "that which is used for joining".

The nature of the technique may be clarified by describing two simple examples. Nuclear magnetic resonance (NMR) zeugmatography was performed with 60 MHz (5 m) radiation and a static magnetic field gradient corresponding, for proton resonance, to about 700 Hz cm⁻¹. The test object consisted of two 1 mm inside diameter thin-walled glass capillaries of H₂O attached to the inside wall of a 4.2 mm inside diameter glass tube of D₂O. In the first experiment, both capillaries contained pure water. The proton resonance line width, in the absence of the transverse field gradient, was about 5 Hz.

Assuming uniform signal strength across the region within the transmitter-receiver coil, the signal in the presence of a field gradient represents a one-dimensional projection of the H₂O content of the object, integrated over planes perpendicular to the gradient direction, as a function of the gradient coordinate (Fig. 1). One method of constructing a two-dimensional projected image of the object, as represented by its H₂O content, is to combine several projections, obtained by rotating the object about an axis perpendicular to the gradient direction (or, as in Fig. 1, rotating the gradient about the object), using one of the available methods for reconstruction of objects from their projections¹⁻⁵. Fig. 2 was generated by an algorithm, similar to that of Gordon and Herman⁴, applied to four projections, spaced as in Fig. 1, so as to construct a 20 × 20 image matrix. The representation shown was produced by shading within contours interpolated between the matrix points, and clearly reveals the locations and dimensions of the two columns of H₂O. In the second experiment, one capillary contained pure H₂O, and the other contained a 0.19 mM solution of MnSO₄ in H₂O. At low radio-frequency power (about 0.2 mgauss) the two capillaries gave nearly identical images in the

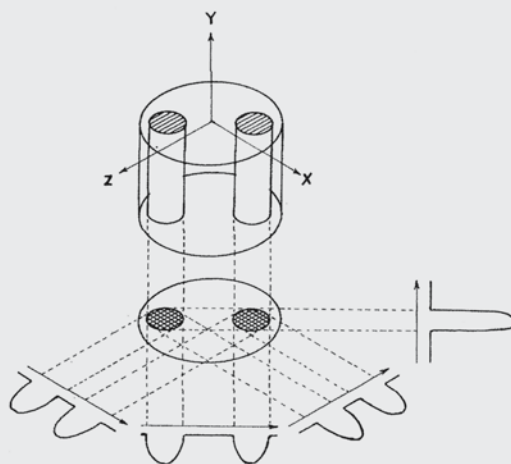


Fig. 1 Relationship between a three-dimensional object, its two-dimensional projection along the Y-axis, and four one-dimensional projections at 45° intervals in the XZ-plane. The arrows indicate the gradient directions.

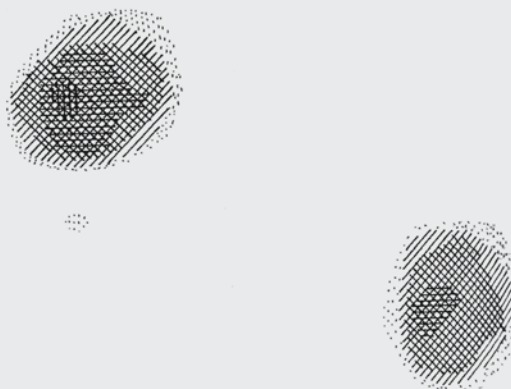


Fig. 2 Proton nuclear magnetic resonance zeugmatogram of the object described in the text, using four relative orientations of object and gradients as diagrammed in Fig. 1.

NATURE VOL. 242 MARCH 16 1973

191

zeugmatogram Fig. 3a). At a higher power level (about 1.6 mW), the pure water sample gave much more saturated signals than the sample whose spin-lattice relaxation time T_1 had been shortened by the addition of the paramagnetic Mn^{2+} ions, and its zeugmatographic image vanished at the contour level used in Fig. 3b. The sample region with long T_1 may be selectively emphasized (Fig. 3c) by constructing a difference zeugmatogram from those taken at different radio-frequency powers.

Applications of this technique to the study of various inhomogeneous objects, not necessarily restricted in size to those commonly studied by magnetic resonance spectroscopy, may be anticipated. The experiments outlined above demonstrate the ability of the technique to generate pictures of the distributions of stable isotopes, such as H and D, within an object. In the second experiment, relative intensities in an image were made to depend upon relative nuclear relaxation times. The variations in water contents and proton relaxation times among biological tissues should permit the generation, with field gradients large compared to internal magnetic inhomogeneities, of useful zeugmatographic images from the rather sharp water resonances of organisms, selectively picturing the various soft structures and tissues. A possible application of considerable interest at this time would be to the *in vivo* study of malignant tumours, which have been shown to give proton nuclear magnetic resonance signals with much longer water spin-lattice relaxation times than those in the corresponding normal tissues⁶.

The basic zeugmatographic principle may be employed in many different ways, using a scanning technique, as described above, or transient methods. Variations on the experiment, to be described later, permit the generation of two- or three-dimensional images displaying chemical compositions, diffusion coefficients and other properties of objects measurable by spectroscopic techniques. Although applications employing nuclear magnetic resonance in liquid or liquid-like systems are simple and attractive because of the ease with which field gradients large enough to shift the narrow resonances by many

line widths may be generated, NMR zeugmatography of solids, electron spin resonance zeugmatography, and analogous experiments in other regions of the spectrum should also be possible. Zeugmatographic techniques should find many useful applications in studies of the internal structures, states, and compositions of microscopic objects.

P. C. LAUTERBUR

Department of Chemistry,
State University of New York at Stony Brook,
Stony Brook, New York 11790

Received October 30, 1972; revised January 8, 1973.

¹ Bracewell, R. N., and Riddle, A. C., *Astrophys. J.*, **150**, 427 (1967).

² Vainshtein, B. K., *Soviet Physics-Crystallography*, **15**, 781 (1971).

³ Ramachandran, G. N., and Lakshminarayanan, A. V., *Proc. US Nat. Acad. Sci.*, **68**, 2236 (1971).

⁴ Gordon, R., and Herman, G. T., *Comm. Assoc. Comput. Mach.*, **14**, 759 (1971).

⁵ Klug, A., and Crowther, R. A., *Nature*, **238**, 435 (1972).

⁶ Weisman, I. D., Bennett, L. H., Maxwell, Sr., L. R., Woods, M. W., and Burk, D., *Science*, **178**, 1288 (1972).

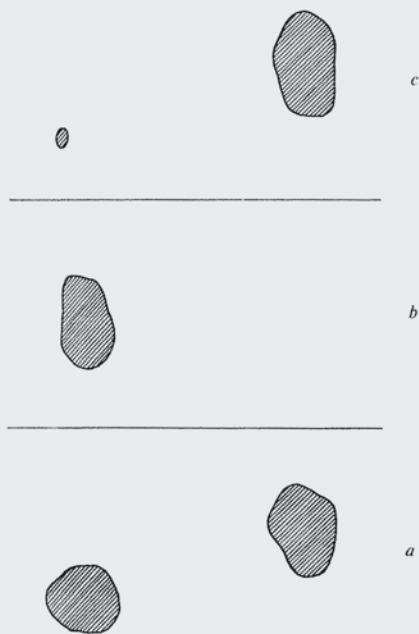
BIOLOGICAL SCIENCES

Island Lizards: the Genetic-Phenetic Variation Correlation

NATURAL populations of many organisms are known to contain much more genetic variation than would have been predicted by all but a minority¹ of geneticists two decades ago. Individuals of several species have up to 22% of their loci heterozygous, and from 0–50% or more of the loci in a population are polymorphic, although the higher estimates may result from sampling error^{2–4}; vertebrates tend to be at the lower end of these ranges. Estimates such as these are based on electrophoretically detectable variation in proteins, so the true levels of genetic variation are probably higher⁵. These generalizations are gaining wide acceptance, but there is still some unease about their accuracy. The fundamental question is whether the loci being sampled are representative of the genome as a whole. We here present evidence that the electrophoretic approach is relatively unbiased.

Two groups of lizards were used: eight species of *Anolis* from the West Indies and thirteen populations of the side-blotched lizards *Uta stansburiana*, *sensu lato*, from California and Mexico, caught in 1971 and 1972. Geographic variation is not a source of heterogeneity, as all specimens from a locality were collected within a few hundred metres of one another. After capture, they were transported alive or on dry ice to the laboratory and stored at -76°C until needed. After skinning, water-soluble proteins were routinely extracted and electrophoresed⁶. Six of the eight *Anolis* species were from Puerto Rico, and two, *A. extremus* and *A. roquet*, were from Barbados and Martinique, respectively.

A single morphological character was used to estimate morphological variation in the *Anolis* species; the number of subdigital scales on the longest toe (second) on the hind foot, starting with the most distal lamella and counting proximally. Variability in this character is correlated with variability in other scale characters, but the other characters were not scored as accurately. Estimates of genetic variation in the *Anolis* species were derived from the starch-gel electrophoresis patterns of enzymes and nonenzymatic proteins, which together appear to represent the gene products of twenty-one or twenty-two loci. The proteins assayed were lactate dehydrogenases, malate dehydrogenases, α -glycerol-phosphate dehydrogenase,



2.6 Planar spin imaging by NMR

Sir Peter Mansfield (born 1933)

Sir Peter Mansfield was born on 9 October 1933 in London, Great Britain. His primary education was spent partly in Devon during the Second World War evacuation of London. His initial secondary school was Peckham Central, but after the 1948 education act, all the boys were transferred from that school to William Penn School, Choumert Road, Peckham. William Penn School was later transferred to the site on Red Post Hill where The Charter School now stands. He was told by a careers teacher that science wasn't for him. He then had to leave school at 15. Before joining the army Mansfield worked in a print shop and then took A-levels at night school. In 1959 he gained a BSc from Queen Mary College, University of London and three years later he attained his PhD in physics from the University of London. Between 1962–64 he became Research Associate at the Department of Physics, University of Illinois and in 1964 Lecturer at the Department of Physics, University of Nottingham. In 1979 Sir Peter Mansfield was appointed Professor of physics at the Department of Physics, University of Nottingham.

Sir Peter Mansfield was awarded the Gold Medal of the Society of Magnetic Resonance in Medicine for pioneering scientific contributions to biology and medicine (1983); Fellow of the Royal Society (1987); the Silvanus Thompson Medal by the British Institute of Radiology (1988); jointly with Paul Lauterbur the International Society of Magnetic Resonance (ISMAR) prize in recognition of "contributions to the fundamentals of NMR and its applications, especially NMR imaging" (1992); the Gold Medal of the European Congress of Radiology and the European Association of Radiology (1995); the Nobel Prize for Medicine together with Paul Lauterbur (2003).

His interests outside physics are languages, flying – he holds a private pilot's licence for both airplanes and helicopters – and reading.



Andrew A. Maudsley (born 1952)

Andrew A. Maudsley was born June 1, 1952 in Nairobi, Kenya. He completed a PhD in physics under the direction of Sir Peter Mansfield in 1976. His PhD work included the very early development of MRI and resulted in the first MR image from the human body, which was of his finger and was published in 1977. Following his PhD work he did a postdoctoral fellowship with Professor Richard Ernst, working in the area of heteronuclear two-dimensional spectroscopy. In 1979, Dr. Maudsley was appointed to a faculty position in the department of radiology at Columbia Presbyterian Medical Center, New York, where he worked on the construction of the first 1.5-T superconducting magnet system located in a clinical setting. Over the next several years Dr. Maudsley and colleagues published several early papers in the area of technique developments for MRI and in vivo spectroscopy, including the development of spectroscopic imaging methods and the first sodium and phosphorus imaging in animals and humans.

In 1987, Dr. Maudsley joined the faculty at the University of California, San Francisco, where he continued development of MR spectroscopy methods for ex-



amination of brain diseases in humans, including the areas of stroke, epilepsy, and traumatic brain injury. This work is now being continued at the University of Miami, where he moved in 2002. In recent years he has concentrated on the development and clinical applications of MR spectroscopic imaging, and is currently directing a project to implement improved data processing methods for MRI.

Dr. Maudsley's publications include 94 papers, 14 book chapters, and 8 patents. He has received several grants and awards from the National Institutes of Health, is a Fellow of the International Society for Magnetic Resonance in Medicine (1999) and is currently serving on the Medical Imaging study section of the National Institutes of Health.

J. Phys. C: Solid State Phys., Vol. 9, 1976. Printed in Great Britain. © 1976

LETTER TO THE EDITOR

Planar spin imaging by NMR

P Mansfield and A A Maudsley

Department of Physics, University of Nottingham, England

Received 24 May 1976

Abstract. A new method of spin-density imaging by NMR is described which allows simultaneous observation and differentiation of signals arising from spins distributed throughout a thin layer or plane within the specimen. The method, which is based on selective RF irradiation of the sample in switched magnetic-field gradients, can produce visual pictures considerably faster than previously described line-scan imaging methods. A simple example of a two-dimensional image obtained by the method is presented.

We wish to describe a new nuclear magnetic resonance (NMR) method for producing cross-sectional images corresponding to the macroscopic spin-density distribution within a specimen. A number of other methods of NMR imaging have recently been described (Garroway *et al* 1974, Hinshaw 1974, 1976, Kumar *et al* 1975, Lauterbur 1973, 1974). In the sensitive point imaging experiments of Hinshaw, the pictures produced were formed point by point. In the line-scan selective excitation method (Mansfield *et al* 1976), the picture data is output line by line. In the new method described here, signals from the spins distributed throughout a whole layer or plane within a three-dimensional object can be simultaneously read-out and differentiated. By this means the process of image formation can be speeded up considerably. This speed is vitally important if we are to see NMR imaging usefully applied for biological and medical imaging in live animals and man. The method relies on selective irradiation of the specimen in switched magnetic-field gradients and is an extension of previous work (Garroway *et al* 1974).

The sample is placed in a strong static magnetic field B_0 which defines the z axis of quantization of the nuclei. For simplicity, we shall restrict the preliminary discussion to two-dimensional imaging only. That is to say, we shall assume that the spin-density distribution to be determined has cylindrical symmetry along the x axis. In practice this specialization to a layer of spins of thickness Δx can be achieved by a selective excitation pulse in a field gradient G_x if thin layers are required, or for thicker layers one may simply rely on the natural spatial selectivity inherent in the receiver-coil geometry.

In this case, the cycle of events may in the simplest arrangement be described in two phases A and B, lasting for times t_a and t_b , respectively. In phase A a magnetic field gradient G_y is switched on and a selective excitation pulse is applied simultaneously to those spins lying in a grid of strips of width Δy and grid spacing b (figure 1). (N.B. Neither the grid nor strip widths need be uniformly spaced but could be selectively tailored to any desired distribution. This pulse tailoring corresponds to shaping the transmitter pulses

L409

L410

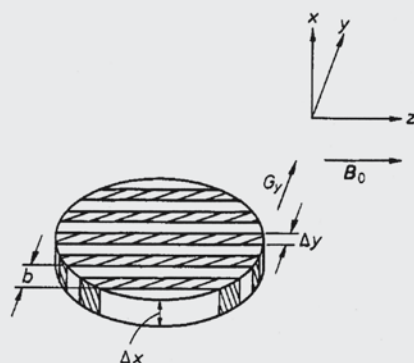
Letter to the Editor

Figure 1. Sketch showing multistrip or grid selection in G_y within one layer of magnetization of thickness Δx . The shading corresponds to the perturbed spin regions.

so that they have the desired spectral distribution profile.) The excitation pulse referred to here could nutate the initially undisturbed spins through any angle θ , but here we shall think of θ as being 90° .

At the end of the A excitation pulse, a second gradient G_z is switched on so that the precessing spins experience the combined effect of both G_y and G_z . The FID from all volume elements $m\Delta x\Delta yz$ spaced at $y = y_0 + mb$ in the plane x_0 is observed and Fourier-transformed to give the spin-density distribution within the solid $\rho(x_0, y, z)$. When the FID has decayed, i.e. in a time $t_b = t_a$, various signal-refocussing arrangements (selective 180° pulses, 90° pulses and various combinations together with field gradient reversals) may be employed to recall the signal for signal-averaging purposes. These arrangements will be described elsewhere.

Application of a magnetic-field gradient to a three-dimensional or even two-dimensional continuous distribution of spins will not ordinarily allow all elements of the distribution to be uniquely assigned magnetically. However, if they could be uniquely assigned, then the 'absorption' lineshape would in a single trace reveal the entire spin-density distribution.

By a process of selective irradiation, a discrete lattice structure can be superimposed on the otherwise continuous spin distribution. That is to say, we can arrange that we observe only those spins lying on a well defined lattice structure, the dimensions of which are controlled by selective excitation etc.

The selection of the spin system in the A phase involves the gradient G_y and RF pulses which nutate some of the spins through 90° . Precisely which spins are affected will depend on the magnitude of the field gradient and the spectral distribution of the perturbing tailored RF pulse.

For simplicity we may represent the combined effects of such a tailored pulse and field gradient by a spatially selective operator \hat{S}_y . If the spin-density distribution is $\rho(x, y, z)$ then $\hat{S}_y\rho(x, y, z)$ represents the distribution of spins which receive a 90° nutation. In a full three-dimensional version of the experiment, the selection of the layer itself in G_x may be represented by the operator \hat{S}_x .

In a generalization of these experiments, we have in mind that the selection processes embodied in the operators \hat{S}_x and \hat{S}_y correspond not to single layers of material, but multiple layers. We shall specialize to equally spaced layers of thickness Δx , strips of width Δy and points of spacing Δz (set by signal sampling) with spatial periodicities a , b and c .

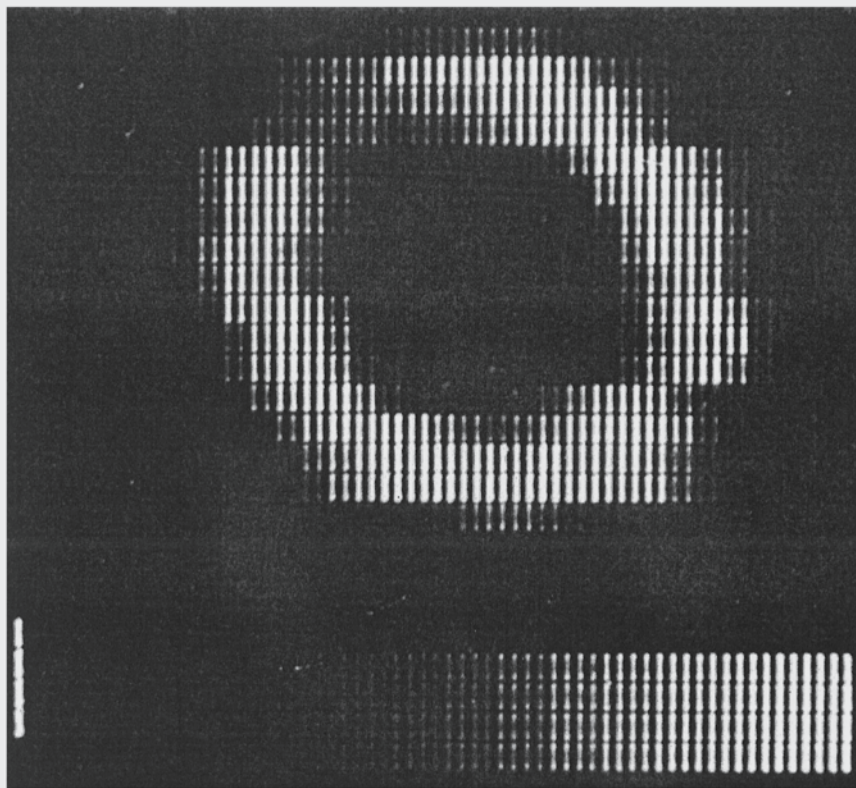


Figure 2. A cross-sectional proton spin-density image of a mineral oil annulus produced by planar spin imaging. An intensity scale corresponding to a linear density wedge is also included across the bottom of the figure.

(facing page L410)

Letter to the Editor

L411

In the limit that the undisturbed spin ranges Δx and Δy approach zero, and for discrete sampling of the distribution along z , we have

$$\hat{S}_x \hat{S}_y \hat{S}_z \rho(x, y, z) \rightarrow \rho(la, mb, nc) = \rho_{lmn} \quad (l, m, n \text{ integer}) \quad (1)$$

where \hat{S}_z is the spatial sampling operator. The effective density, therefore, becomes a discrete distribution ρ_{lmn} corresponding to the lattice points $x = al$, $y = bm$ and $z = cn$. In this limit, the FID signal as a function of time t becomes

$$S = \sum \rho_{lmn} \cos t [l\Delta\omega_x + m\Delta\omega_y + n\Delta\omega_z] \Delta v_{lmn} \quad (2)$$

where Δv_{lmn} is the volume of spins at a lattice point contributing to the signal. The angular frequency increments are given by

$$\Delta\omega_x = \gamma a G_x \quad (3)$$

etc, where γ is the magneto-gyric ratio.

We see from equation (2) that if the gradients and lattice constants are chosen so that

$$N\Delta\omega_z \leq \Delta\omega_y \leq \frac{\Delta\omega_x}{M} \quad (4)$$

where M and N are the largest values of m and n , respectively, all points in the distribution ρ_{lmn} are uniquely defined in the frequency domain. (N.B. Although we are talking here about superimposing a regular lattice by selective irradiation and sampling, the above point is true for a natural orthorhombic lattice).

Fourier transformation of S in equation (2) will thus yield in one calculation the complete three-dimensional density distribution function ρ_{lmn} .

The imaging method has been tried out for protons in a liquid mineral oil sample in the form of a cylindrical annulus. The measured outer sample diameter is 13.7 mm and the inner occlusion is 8.1 mm diameter. The experiments were performed at 15.0 MHz using a computer-controlled spectrometer. The sample was selectively irradiated with a radiation pattern corresponding to five equally spaced equal-intensity narrow rectangular peaks in the RF spectral distribution arranged to span the sample. The transverse response following this selection pulse was Fourier-transformed, yielding directly the planar spin distribution with a fairly coarse grid along the y direction. A finer grid was obtained by an interlacing procedure in which the radiation pattern was shifted up in frequency by $\frac{1}{4}$, $\frac{1}{2}$ and $\frac{3}{4}$ of the frequency spacing between adjacent peaks in the RF spectral distribution. This gives a four-fold finer grid resolution across the specimen and thus allows us to produce a visual image. This is shown in figure 2 and consists of a 20×40 array. The transformed data is used to modulate the spot intensity of an oscilloscope in a television raster display. A linear grey scale of sixteen levels of spot brightness covering the range black to white is used (Baines and Mansfield 1976).

The time to perform these particular planar spin imaging experiments, though five times faster than line-scan imaging, has been limited by the number of points in our discrete Fourier-transfer program as well as the speed of the computer and associated hardware. With a faster computer there seems no obstacle to producing planar images one and possibly two orders of magnitude faster than by line-scanning methods.

A full account of this work is being prepared and will appear elsewhere.

We are grateful to the Science Research Council for an equipment grant.

L412 *Letter to the Editor***References**

- Baines T and Mansfield P 1976 *J. Phys. E: Sci. Instrum.* **9** in press
Garroway A N, Grannell P K and Mansfield P 1974 *J. Phys. C: Solid St. Phys.* **7** L457–62
Hinshaw W S 1974 *Phys. Lett.* **48A** 87–8
—— 1976 *J. Appl. Phys.* in press
Kumar A, Welte D and Ernst R R 1975 *J. Magn. Reson.* **18** 69–83
Lauterbur P C 1973 *Nature* **242** 190–1
—— 1974 *Pure Appl. Chem.* **40** 149–57
Mansfield P, Maudsley A A and Baines T 1976 *J. Phys. E: Sci. Instrum.* **9** 271–8

2.7 Medical Imaging by NMR

Sir Peter Mansfield (born 1933)

see Chapter 2.6 on page 96.

Andrew A. Maudsley (born 1952)

see Chapter 2.6 on page 96.

1977, *British Journal of Radiology*, 50, 188–194

Medical imaging by NMR

By P. Mansfield, B.Sc., Ph.D., and A. A. Maudsley B.Sc., Ph.D.

Department of Physics, University of Nottingham

(Received June, 1976 and in revised form November, 1976)

ABSTRACT

Application of the new nuclear magnetic resonance (NMR) method of fast scan proton imaging is described. Cross sectional proton scans of a human finger *in vivo* are measured and reveal considerable anatomical detail, particularly of the soft tissue regions. Imaging of tumour tissue is also briefly discussed.

During the past few years new techniques have been developed in nuclear magnetic resonance (NMR) which make it possible to form two dimensional cross-sectional images related to the distribution of protons in biological structures (Hinshaw, 1974a&b, 1976; Kumar *et al.*, 1975; Lauterbur, 1973, 1974; Mansfield and Grannell, 1973, 1975a). The methods are non-invasive and of low radiation hazard and could therefore have some clinical value in medical diagnosis. The first crude medical picture of a human finger taken *in vivo* (Mansfield *et al.*, 1974; see also Mansfield and Grannell, 1975b) relied on a slow and inexact imaging method based on reconstruction from a number of projection absorption profiles. Only the gross outline with no internal detail was revealed.

Recently we introduced a new imaging technique which does not depend on reconstruction from projections (Garroway *et al.*, 1974). It relies on selective irradiation of the specimen in switched magnetic field gradients. In the fast scan adaptation of this method (Mansfield *et al.*, 1976) the mobile proton spin density is obtained directly, line by line across the specimen cross-section. Since this work, the apparatus and display have been considerably improved (Baines and Mansfield, 1976) thus enabling us to produce reasonably detailed pictures of a human specimen *in vivo*.

In this paper we wish to report new results obtained with live fingers, particularly with reference to the anatomical information obtained by NMR imaging in normal tissue. Brief reference will be made to imaging of tumour tissue, though we hope to present a more detailed discussion of this aspect of imaging elsewhere.

Principle of operation

The study of structure in materials cannot ordinarily be attempted with conventional NMR techniques. This is because NMR measures frequency differences or magnetic field variations and

each piece of resonant material in a specimen is not uniquely defined magnetically. However, by using a combination of switched linear magnetic field gradients plus selective irradiation of the sample, it is possible to uniquely assign a frequency to a particular point in the specimen. The NMR signal coming from a localized region of the sample is directly related to the mobile proton density at that point. By mobile protons we have in mind those contained in the free or nearly free water, fat or oil distributed throughout the soft tissue regions of the specimen. Bone structures, therefore, which contain relatively few mobile protons, are generally detectable through their lack of signal, while tumours and other soft tissues give strong signals. This behaviour contrasts with that of conventional X-rays which are scattered only rather weakly by protons and so usually give pictures for soft tissue regions with relatively poor definition.

METHOD

The specimen is placed in a large static magnetic field B which polarizes all nuclear spins. (Since biological tissue contains 75–80% by weight of water we are particularly interested in the proton spin

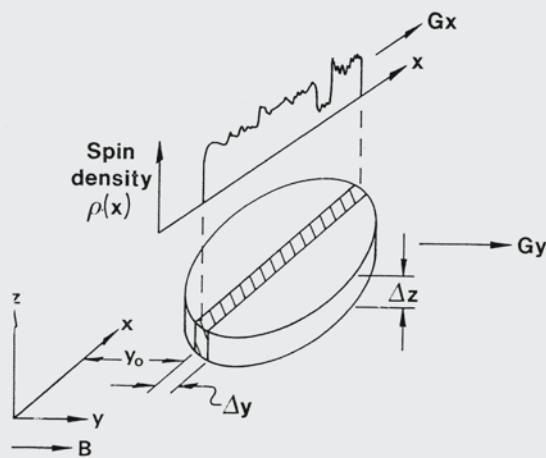


FIG. 1.

Sketch illustrating the principle of line scanning by selectively irradiating a narrow strip within an isolated slice of magnetization.

MARCH 1977

Medical imaging by NMR

magnetization, though one could with less sensitivity observe other nuclei.) In addition to this field, switched linear magnetic field gradients are applied along two (or three) principal coordinate axes. We first consider a thin disc or slice of magnetization of thickness Δz within the specimen. Such a slice is sketched in Fig. 1 and is, of course, part of an extended specimen along the z axis.

The field gradient G_y alone is switched on and the spins within the narrow strip Δy at y_0 are selectively excited by applying a "tailored" r.f. pulse to the specimen. The tailoring of the pulse consists of shaping the r.f. envelope such that its spectral distribution is confined to a narrow band of frequencies. A square unshaped pulse, by contrast, has a sinc function frequency spectrum with a width characterized by the inverse pulse length but with extensive sidebands. The r.f. components of the tailored pulse interact with spins in a narrow strip (shaded strip of Fig. 1). This interaction is brought about because the spins within the disc of material have a range of nuclear Larmor frequencies through the action of the linear magnetic field gradient G_y .

Thus only those spins within the shaded strip, which have the right Larmor resonance frequency, can respond to the selective r.f. pulse.

Immediately following this selective excitation pulse, the field gradient is switched from G_y to G_x and the spin response or free induction decay (FID) signal is recorded and Fourier transformed. For a narrow strip (Δy small) at position y_0 in either a thin slice (Δz small), or for a sample with cylindrical symmetry, this Fourier transformed signal is directly proportional to the proton spin density $\rho(x, y_0)$ along x . The transformed signals for each strip of the specimen are used to modulate the spot intensity of an oscilloscope in a television raster display to form a cross-sectional picture of the object. The display employs a 16-level linear grey scale covering the intensity range black for zero signal to white for high spin density (Baines and Mansfield, 1976).

The initial specialization to a layer or plane can itself be achieved by a selective irradiation procedure in a third field gradient G_z . In these experiments, however, specialization to a layer is achieved simply by relying on the receiver coil geometry. This is a flat coil of 2 cm diameter and our experiments show that most of the received signal comes from a layer approximately 8 mm thick.

A simplified diagram of the imaging apparatus is shown in Fig. 2. The 15 MHz r.f. excitation pulses

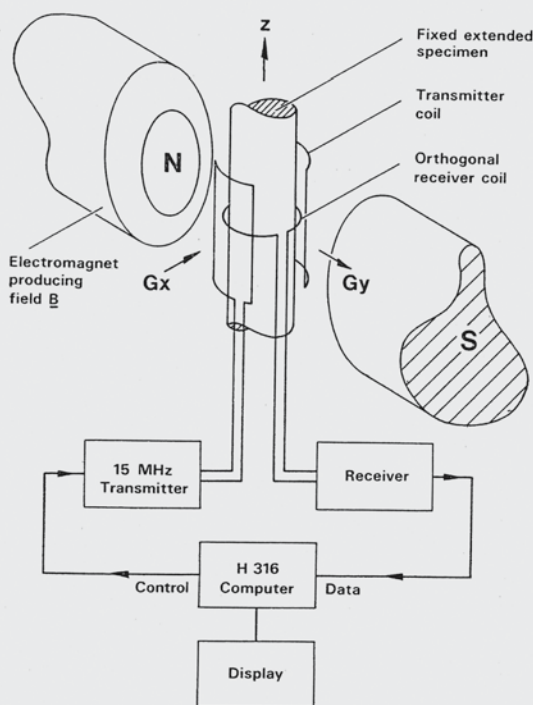


FIG. 2.

Simplified representation of the 15 MHz NMR imaging apparatus. The field gradient coils producing G_x and G_y are not shown.

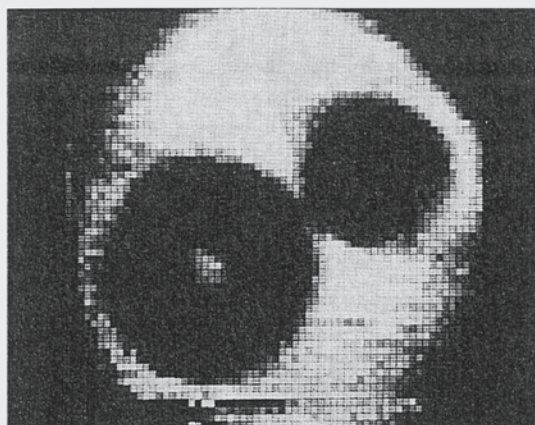


FIG. 3.

Cross-sectional proton scan of a phantom filled with mineral oil (see text for details). The time to produce this picture was 40.5 min. The full picture size slightly exceeds a 64×64 data array, thus squaring off the circular edges. The missing data were not lost but overflowed into the other quadrants of a 128×128 data array. The field gradients were $G_x = 0.69 \text{ G cm}^{-1}$ and $G_y = 0.86 \text{ G cm}^{-1}$. Each line of the picture was averaged 128 times.

VOL. 50, No. 591

P. Mansfield and A. A. Maudsley

are fed from the transmitter to a pair of cylindrical Helmholtz coils (Ginsberg and Melchner, 1970) surrounding the sample as shown. The peak pulse power was 1.0 watt and the pulse duration 7.4 msec. The production and shaping of the pulses, switching of the field gradients, data acquisition, Fourier transformation and data display are all performed on-line with a Honeywell H316 minicomputer. A more detailed description of the apparatus and the method is given by Mansfield *et al.* (1976). Placing the finger in the receiver coil was found to increase the received noise through the antenna action of the body. However, we found that simply holding an earthed sheet with the free hand reduced the pick up. No other special precautions were taken to shield the receiver coil against induced noise.

RESULTS

Phantom test

Figure 3 is a cross-sectional picture of the proton distribution of mineral oil in a phantom object and illustrates the spatial resolution obtainable in the present line-scan imaging experiments. The sample consisted of a thick-walled 1.4 mm bore glass capillary tube and a solid circular glass rod immersed in mineral oil, the whole being contained in a circular cross-section glass test-tube of inside diameter 14.6 mm. This picture and all biological pictures presented in the next sections are made up from 64×64 point arrays.

A linear grey scale wedge is added to later pictures to aid intensity comparisons; however, for precise measurements actual data can be output numerically.

Spin-lattice relaxation effects

We assume here that the local spin magnetization at coordinates x, y in a given plane z is destroyed following one selective excitation pulse, but recovers exponentially, through a single simple spin-lattice relaxation process in a characteristic time $T_1(xy)$. Thus the effective spin density $\rho(xy\tau)$ observed in these images depends on the time delay τ between successive excitation pulses according to the relationship $\rho(xy\tau) = \rho(xy)[1 - e^{-\tau/T_1(xy)}]$. That is to say, it is possible for localized regions of the specimen to give a picture brightness which is less than the localized spin density would suggest; for example, if the ratio $\tau/T_1(xy)$ is small. We refer to this effect as spin-lattice relaxation time discrimination and most of the intensity variations between tissue types seem to be attributable to this effect rather than to real density variations, though if present, these too will aid picture contrast.

The variations in $T_1(xy)$ within a specimen are a reflection of the variations of both the mobility of the free water, fat or oil and the concentration of dissolved minerals, nutrients, etc., characteristic of the various tissues.

Finger images recorded in vivo.

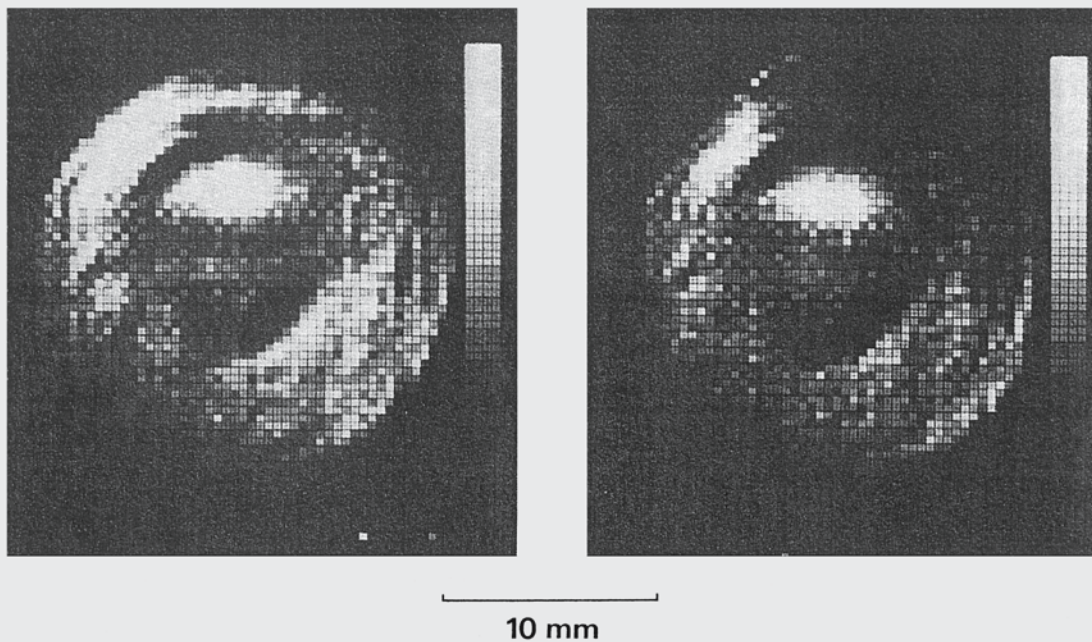
A number of cross-sectional proton scans have been produced at various positions along the right hand third digit of AAM. We have found that quite good discrimination between the various tissues can be obtained using a delay of 0.5 sec. Similar results and discrimination were found with the finger of another subject (PM).

Two scans midway along the mid-phalanx of AAM's third right hand digit are shown in Fig. 4 and correspond to cross-sectional views looking into the end of the digit. The dorsal plane passes through the top and the palmar plane through the bottom of each picture. The delay in Fig. 4A was 0.5 sec. Each line of this picture was averaged 48 times. The final picture took 23 mins to produce. Figure 4B is a proton scan of the same cross-section as 4A, but with the delay τ reduced to 0.3 sec. This picture took 15 min. to produce. The irradiation gradient G_y was 0.41 G cm^{-1} and the read gradient G_x was 0.34 G cm^{-1} for both pictures. Figures 5A and B are colour representations of the data of Figs. 4A and B. The data are presented through a window comprising eight distinguishable colours corresponding to eight out of the original 16 data levels. In order to give easier discrimination the window base level and the colour scales were set in each case to maximize colour contrast between data levels. Figure 6 is a sketch traced off Fig. 4A showing more clearly the anatomical details that we have been able to recognize. (Kaplan, 1965; Landsmeer, 1976). (Inevitably some clarity is lost from these pictures in the photographic reproduction.)

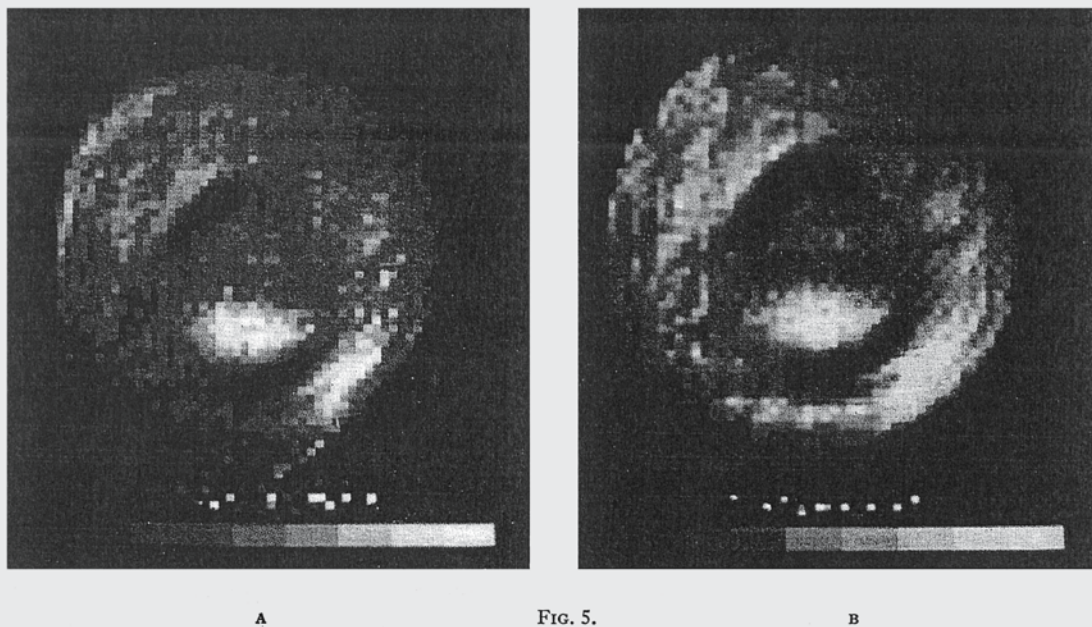
Strong signals are received from the skin and subcutaneous areolar and fibro-fatty tissue giving the general outline of the mid-phalangeal cross-section. The bone tissue shows as a dark ring surrounding the bright zone produced by strong signals from the marrow region. Immediately below the bone is a second dark ring structure of the fibrous flexor tendon sheath. Within this and slightly brighter are the central flexor profundus and the two unresolved components of the flexor sublimis tendons (flexor digitorum superficialis). Above the bone towards the dorsal plane is a dark horizontal line corresponding to the unresolved mid- and lateral bands of the mid-phalanx extensor tendons. Figures 4B and 5B show the same general characteristics as 4A and 5A, but the

MARCH 1977

Medical imaging by NMR



A FIG. 4. B
 Cross-sectional images of a finger obtained *in vivo* by NMR (see text for full details).
 (A) delay $\tau=0.5$ sec. (B) delay $\tau=0.3$ sec.



Colour versions of the finger images shown in Figs. 4A and B.
 (A) The eight colours black through to white correspond to data levels 6-13. The delay time $\tau=0.5$ sec.
 (B) The eight colours black through to white correspond to data levels 2-9.
 In both pictures, data falling outside the window limits are presented as all black or all white as appropriate.

VOL. 50, No. 591

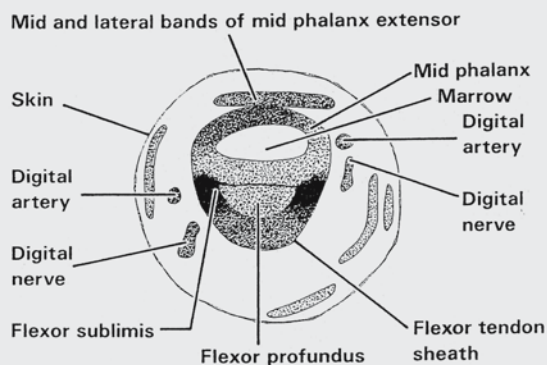
P. Mansfield and A. A. Maudsley

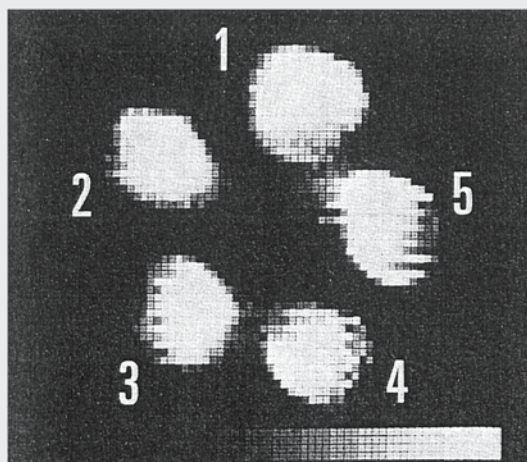
FIG. 6.

A reduced tracing from Fig. 4A showing the recognizable anatomical detail that we have been able to obtain from it.

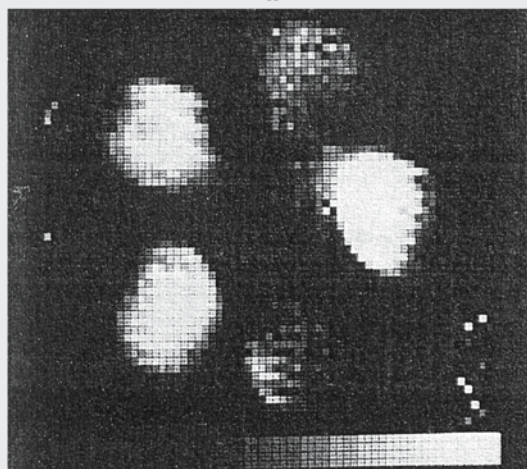
overall brightness and level of discrimination of the black and white image is reduced with the shorter delay. Differentiation of the flexor profundus from the periosteum and chiasma tendinum are less pronounced indicating that the T_1 of the flexor profundus is of the order of 0.3 sec. The marrow region, on the other hand, remains quite bright. This suggests a T_1 much less than 0.3 sec.

The digital arteries and nerves are just resolved in Figs. 4A and 5A and their positions sketched in Fig. 6. The fact that one can distinguish the arteries from the surrounding tissue means that, with higher resolution or with larger blood vessels in other parts of the anatomy, NMR imaging offers the possibility of making direct blood flow measurements. The principle of such measurements depends on the replenishment of spin saturated blood caused by flow of fresh polarized (unsaturated) blood into the sample coil region, thus producing an apparent reduction in the spin-lattice relaxation time of the blood directly related to its flow rate. Slight modifications to the imaging method described would be necessary for such measurements.

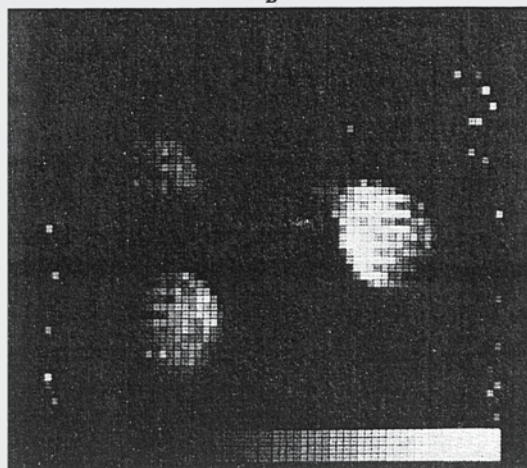
Also apparent in these pictures are darker sliver-like concentric regions or pockets as indicated in the sketch. We ascribe these to discontinuous regions



A



B



C

FIG. 7.

Proton scans showing spin-lattice relaxation time discrimination of images obtained from excised rat specimens of normal and malignant tissue. The tissue was contained in 3 mm glass tubes labelled as follows: 1. hepatoma (D23); 2. normal skin tissue; 3. liver; 4. sarcoma (MC7); 5. water control. The specimens in each picture are the same but the delay time τ was varied: (A) $\tau=1.2$ sec; (B) $\tau=0.67$ sec; (C) $\tau=0.37$ sec.

MARCH 1977

Medical imaging by NMR

within the fibro-fatty layer which could be either variation in fibro-fatty content or branches of digital nerves or blood vessels. Adipose layers are likely to have a shorter T_1 (Hollis *et al.*, 1975) and would thus appear as bright regions. It would seem from Fig. 4B that these regions, as with other parts of the finger, owe their contrast in the NMR image principally to localized T_1 variations rather than to significant spin density variations.

Cross-sectional scans have also been made through the distal phalangeal joint and the mid point and tip of the distal phalanx. In all cases the general features as reported here are reproduced, though the distal flexor and extensor tendons are more diffuse at the joint and the bone somewhat smaller in the distal region as expected.

TISSUE TYPES

From the point of view of the present NMR imaging studies, tissue types can be classified by their mobile proton density (in many cases this is essentially the free water content) and spin lattice relaxation time T_1 (see for example Kiricuta and Simplaceanu, 1975; Hollis *et al.*, 1975). If T_1 is similar between two tissue types, one must rely on more accurate measurement of water concentration to differentiate between them. Our measurements are accurate to only one part in 16 (the display range). Lack of computer core has forced us to discard the original information which had an accuracy of 1 in 10^3 . Nevertheless, through T_1 differences, striking contrast can be achieved.

Figures 7A-C show a series of NMR images for decreasing delay τ obtained from the same set of excised tissue specimens taken from young normal white wistar rats. The samples were contained in four 3 mm i.d. glass tubes, labelled 1-4 in Fig. 7. As a control the fifth tube, number 5, contained doped water with $T_1 \approx 100$ msec. Tubes 1-4 contained respectively hepatoma (D23), a sample of normal skin tissue, normal liver and sarcoma (MC7). Samples 2-4 were taken from the same animal. Both animals were injected with 0.5 ml of the anti-coagulant heparin. The NMR images were produced within 2 hours of sacrifice. The delay in Fig. 7A was 1.2 sec resulting in no noticeable discrimination between the various specimens. In Fig. 7B, the delay was reduced to 0.67 sec and clear differentiation between the normal and malignant tissues results. The numerical data for this picture show a slight discrimination between the two normal specimens, numbers 2 and 3, and between the two malignant specimens, numbers 1 and 4. Further reduction of the delay time in Fig. 7C reduces the tumour images

to almost zero intensity and begins to affect the intensity of the normal tissue images too. According to Damadian (1971) and others (Weissman *et al.*, 1972; Frey *et al.*, 1972), T_1 in malignant tissue is about 1.5 times longer than that of the corresponding normal tissue. In spite of this small factor, strong intensity contrast is possible in our images by adjusting the delay time τ .

CONCLUSION

We have demonstrated that NMR imaging of fingers *in vivo* is able to produce reasonably clear cross-sectional anatomical pictures in times up to 23 min. No special precautions were taken to clamp the subjects' hand so that blood flow and general movement, at one time considered to be a possible limit to spatial resolution, have not been found to be troublesome. By implication, therefore, we do not anticipate problems in producing cross-sectional images of the limbs and head where movement can be made negligible. Involuntary movements in other parts of the anatomy are likely to be troublesome, however, unless the scan time can be considerably reduced below 23 min. The experiments described produced no sensation in the finger and the mean r.f. power levels used were well below any perceptible heating level.

The results on normal and malignant tissue suggest that tumorous regions of a subject will give good image contrast against a background of normal tissue. This should aid the detection and diagnosis of tumours in cases where there are no obvious geometrical distortions, that is to say in the early detection of cancer.

Our magnet system has restricted the maximum specimen size to a diameter of 2.0 cm. However, we are planning shortly to study much larger specimens at operating frequencies in the range 1-2 MHz using a specially designed low field spherical electro-magnet which is under construction.

ACKNOWLEDGMENTS

We wish to thank Dr. M. R. Price for supplying the rat tissue specimens and Dr. H. Clow, Mr. P. Walters and the Directorate of the Central Research Laboratories of EMI for producing the colour pictures of our data.

We are also grateful to Professor R. E. Coupland for his helpful comments on the manuscript.

REFERENCES

- BAINES, T., and MANSFIELD, P., 1977. An improved picture display for NMR imaging. *Journal of Physics E. Scientific Instruments* (in press).
- DAMADIAN, R., 1971. Tumour Detection by Nuclear Magnetic Resonance, *Science N.Y.*, **171**, 1151-1153.
- FREY, H. E., KNISPEN, R. R., KRUUV, J., SHARP, A. R., THOMPSON, R. T., and PINTAR, M. M., 1972. Proton

Vol. 50, No. 591

P. Mansfield and A. A. Maudsley

- spin-lattice relaxation studies of non-malignant tissues of tumorous mice. *Journal of the National Cancer Institute*, 49, 903-906.
- GARROWAY, A. N., GRANNEL, P. K., and MANSFIELD, P., 1974. Image formation in NMR by a selective irradiative process. *Journal of Physics, C. Solid State Physics*, 7, L457-L461.
- GINSBERG, D. M., and MELCHNER, M. J., 1970. Optimum geometry of saddle shaped coils for generating a uniform magnetic field. *The Review of Scientific Instruments*, 41, 122-123.
- HINSHAW, W. S., 1974a. Spin mapping: the application of moving gradients to NMR. *Physics Letters*, 48A, 87-88.
- 1974b. The application of time dependent field gradients to NMR spin mapping. *Proceedings of the 18th Congress Ampere*, 2, 433-434.
1976. Image formation by nuclear magnetic resonance; the sensitive point method. *Journal of Applied Physics*, 47, 3709-3721.
- HOLLIS, P. H., LEON, A. S., EGGLESTON, J. C., and MORRIS, H. P., 1975. Nuclear magnetic resonance studies of cancer. *Journal of The National Cancer Institute*, 54, 1469-1472.
- KAPLAN, E. B., 1965. *A Functional and Surgical Anatomy of the hand* (J. B. Lippincott Co., Philadelphia).
- KIRICUTA, I. C., and SIMPLACEANU, V., 1975. Tissue water content and nuclear magnetic resonance in normal and tumour tissue. *Cancer Research*, 35, 1164-1167.
- KUMAR, A., WELTI, D., and ERNST, R. R., 1975. NMR Fourier zeugmatography. *Journal of Magnetic Resonance*, 18, 69-83.
- LANDSMEER, J. M. F., 1976. *Atlas of Anatomy of the Hand*: (Churchill Livingstone, London).
- LAUTERBUR, P. C., 1973. Image formation by induced local interactions: examples employing nuclear magnetic resonance. *Nature*, 242, 190-191.
1974. Magnetic resonance zeugmatography. *Pure and Applied Chemistry*, 40, 149-157.
- MANSFIELD, P., and GRANNEL, P. K., 1973. NMR diffraction in solids? *Journal of Physics C, Solid State Physics*, 6, L422-L426.
- 1975a. Diffraction and microscopy in solids and liquids by NMR. *Physical Review B*, 12, 3618-3634.
- 1975b. Microscopy *in vivo* by nuclear magnetic resonance. *Physics in Medicine and Biology*, 20, 477-482.
- MANSFIELD, P., GRANNEL, P. K., and MAUDSLEY, A. A., 1974. Diffraction and microscopy in solids and liquids by NMR. *Proceedings of the 18th Congress Ampere*, 2, 431-432.
- MANSFIELD, P., MAUDSLEY, A. A., and BAINES, T., 1976. Fast scan proton density imaging by NMR. *Journal of Physics E, Scientific Instruments*, 9, 271-278.
- WEISSMAN, I. D., BENNETT, L. H., MAXWELL, L. R., WOODS, M. W., and BURK, D., 1972. Recognition of cancer *in vivo* by nuclear magnetic resonance. *Science*, N.Y. 173, 1288-1289.

Book review

Radiosterilization of Medical Products, 1974. Pp.536, 1975 (Vienna, International Atomic Energy Agency), \$33.00.

This volume contains the proceedings of a symposium held under the auspices of the International Atomic Energy Agency at Bombay in December 1974. Of the 42 papers presented in eight sessions, the majority are in English, seven in Russian, three in French and one in Spanish.

Three sessions deal with the conditions required for the control of microbiological contamination and the dosimetric problems involved. The effects of radiation on the materials

being sterilized are considered in two sessions and an interesting final session is devoted to the types of radiation plant being used, or about to be commissioned, in different parts of the world. Also included is a report by a working party of the IAEA in which are set out revised recommendations for the radiosterilization of medical products.

This book will be useful not only for those involved in the production of sterile medical equipment, but for those wishing to obtain some background in this field.

N. E. GILLIES.

2.8 Human whole body line scan imaging by NMR

Sir Peter Mansfield (born 1933)

see Chapter 2.6 on page 96.

I.L. Pykett

P.G. Morris

R.E. Coupland

1978, *British Journal of Radiology*, 51, 921-922

NOVEMBER 1978

Short communications

Human whole body line-scan imaging by NMR

By P. Mansfield, I. L. Pykett, and P. G. Morris

Department of Physics, University of Nottingham

and R. E. Coupland

Department of Human Morphology, School of Medicine, University of Nottingham

(Received July, 1978)

Historically, the first nuclear magnetic resonance (NMR) pictures demonstrating live human anatomy were produced recently (Mansfield and Maudsley, 1976; 1977) using a line-scanning technique. The original specimens studied were limited in object size to cross-sectional views through fingers. A number of other approaches to imaging by NMR are also being developed and are compared, discussed and referred to elsewhere (Brunner and Ernst, 1978; Pykett and Mansfield, 1978).

Recent development and expansion of our imaging apparatus has now allowed us to examine objects of the dimensions of the whole human body. In this paper we wish to report the first NMR line-scan medical image of a thin cross-sectional slice of a live human body.

Our work should be seen in the general context of other medical imaging schemes (Hounsfield, 1973; Hill, 1976; Budinger, 1974), where improvements in techniques and picture quality have recently achieved very high standards. NMR imaging, however, is in its infancy, but nevertheless has merit as a non-invasive and, we believe, non-hazardous technique. There is also the possibility of using NMR imaging in conjunction with other measurable NMR parameters for normal and abnormal tissue characterization and for physiological studies including blood flow measurements.

Our NMR imaging technique, based on selective excitation in switched magnetic field gradients, was first described by Garraway *et al.* (1974). A slightly modified version of the

fast line-scanning adaptation (Mansfield *et al.*, 1976) is the basis of the technique reported in this paper. The thickness of the cross-sectional slice examined was set to approximately four cm in these first experiments. Selected lines of material across the slice are scanned from one edge of the subject to the other and the subsequent data sets for each scanned line are stored in a computer for subsequent display as a picture (Baines and Mansfield, 1976). Large signals which produce the bright zones in the images come in general from high concentrations of mobile protons contained within or near the various tissues and organs. By mobile protons, we have in mind those associated with the free water, fat or oil contained in or distributed throughout the various tissues and organs of the body.

The whole body image shown in Fig. 1 is a transverse section through the abdominal region (of PM) at the level of the third and lower part of the second lumbar vertebrae. Figure 2 is a line tracing of Fig. 1 labelling the recognizable morphological features. The liver is visible as a well-defined mass mainly on the right of the picture and blends with the abdominal wall at the periphery. The vertebrae are identifiable in the mid-line and the kidneys lie in the mid-lateral region with the spleen adjacent on the left. The central circular images probably correspond to the abdominal aorta, with the pancreas lying anterior, inferior vena cava and duodenum. We believe that the variable dense anterior central

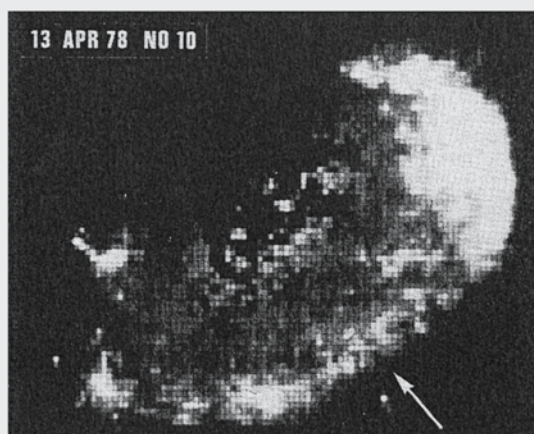


FIG. 1.

Cross-sectional line-scan NMR image through the abdomen at L2-3. Arrow indicates mid-line posterior. Left side lies to the left of the illustration. Bright zones correspond in general to high mobile proton content. See Fig. 2 for labelled details.

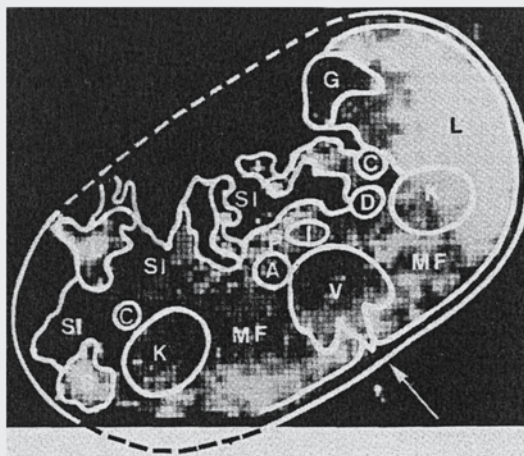


FIG. 2.

Labelled image of Fig. 1. A=aorta, C=colon, D=duodenum, G=gall-bladder, I=inferior vena cava, K=kidneys, L=liver, P=pancreas, S=spleen, SI=stomach and intestines, V=vertebra. Abdominal muscles and retroperitoneal fat (MF) are seen adjacent to the vertebra.

VOL. 51, No. 611

Short communications



FIG. 3.

Cross-sectional line-scan NMR image through a cadaver thigh. The scan time for this picture was approximately 26 min. The profile of the femur is clearly visible (upper left) with central bone marrow.

region shows parts of the stomach and intestines and profiles of colon are anterior to the kidneys. The ovoid outline anteriorly and to the right, associated with the liver image, is probably gall-bladder.

The image of Fig. 1 comprises 75×90 picture elements and took 40 min. to produce. Each line of the picture was averaged 96 times. Some loss of picture quality is ascribed both to involuntary bodily movements, especially respiration, and lack of complete r.f. penetration at 4.0 MHz, the NMR resonance frequency used in these experiments. Some correction for the latter effect and some data enhancement has been applied in Fig. 1. The effect of movement could be minimized by using ultra high-speed planar NMR imaging techniques (Mansfield and Pykett, 1978).

A cadaver thigh section image shown in Fig. 3 reveals the femur, femoral vessels and profunda femoris vessels and other morphological detail using raw data only. The extra clarity reflects the importance of restricting movement.

Magnetic field gradients of approximately 0.04 G cm^{-1} were used and passed through the whole of the torso region. Switching the gradients in $50 \mu\text{sec}$ produced no sensations whatsoever. As an initial precaution live rabbits, rats and guinea pigs were previously subjected to switched gradients and a cat was scanned with no problems a day before the human experiments.

The first whole-body line-scan experiment was performed during the evening of April 13, 1978 and has produced no acute or chronic ill-effects to date.

The electromagnet used for this work was built by Oxford Instruments and comprises four air-cored concentric coils approximating to a spherical magnet design. Dispersed iron used in the construction of the physics research building impairs the static performance of the magnet and causes some non-linearity and degradation of the spatial resolution of our first whole-body pictures.

Our experiments were performed at a repetition frequency of 3 Hz. As a general caveat we suggest that frequencies in the range 30–150 Hz, known to be dangerous in a.c. electric shock, should be avoided in any future experiments. Similar precautions should also be taken to avoid known alpha-wave brain frequencies if head scanning experiments are planned.

ACKNOWLEDGMENTS

We are grateful to the MRC for support of the whole body NMR imaging project, the SRC for some staff support, D. Kerr and R. Ordidge for their assistance in the design and construction of some of the apparatus, and D. Whelpton and R. Potter for use of and assistance with the computing facilities of the Medical Physics Department.

We are especially indebted to T. Baines for the design and construction of the electronic apparatus and V. Bangert for his assistance in the design of the gradient coils.

REFERENCES

- BAINES, T., and MANSFIELD, P., 1976. An improved picture display for NMR imaging. *Journal of Physics*, **E**, *9*, 81–83.
- BRUNNER, P., and ERNST, R. R., 1978. Sensitivity and performance time in NMR imaging. *Journal of Magnetic Resonance* (in press).
- BUDINGER, T. F., 1974. *Recent Advances in Nuclear Medicine*, ch. 2, ed. J. H. Lawrence (Grune and Stratton, New York).
- GARROWAY, A. N., GRANNEL, P. K., and MANSFIELD, P., 1974. Image formation in NMR by a selective irradiative process. *Journal of Physics*, **C**, *7*, L 457–461.
- HILL, C. R., 1976. Ultrasonic imaging. *Journal of Physics*, **E**, *9*, 153–162.
- HOUNSFIELD, G. N., 1973. Computerized transverse axial scanning (tomography). *British Journal of Radiology*, **46**, 1016–1022.
- MANSFIELD, P., and MAUDSLEY, A. A., 1976. Planar and line-scan imaging by NMR. Proc. 19th Congress Ampere, Heidelberg (Gronpeinent Ampere, Heidelberg, Geneva) 247–252.
- 1977. Medical imaging by NMR. *British Journal of Radiology*, **50**, 188–194.
- MANSFIELD, P., MAUDSLEY, A. A., and BAINES, T., 1976. Fast scan proton density imaging by NMR. *Journal of Physics*, **E**, *9*, 271–278.
- MANSFIELD, P., and PYKETT, I. L., 1978. Biological and medical imaging by NMR. *Journal of Magnetic Resonance*, **29**, 355–373.
- PYKETT, I. L., and MANSFIELD, P., 1978. A line scan study of a tumorous rat leg by NMR. *Physics in Medicine and Biology* **23**, 961–967.

2.9 NMR imaging of the brain in multiple sclerosis

Ian Robert Young (born 1932)

Ian Robert Young was born on 11 January 1932. He was educated at Sedbergh School in Yorkshire and proceeded to qualify with a BSc and a PhD from Aberdeen University in Scotland. He is a Fellow of the Institute of Electrical Engineers. From 1976 to 1981 Ian Young worked for EMI Ltd. and from 1981 to 1997 he worked for GEC plc. It was while he was at EMI that his fruitful collaboration with Graeme Bydder started, which led to many important technical and clinical developments in MRI in the UK. From 1986 onwards he was a visiting professor of radiology at the Royal Postgraduate Medical School at the Hammersmith Hospital in London. In 1985 he was awarded an OBE. In 1989 he was elected Fellow of the Royal Society of London. In 1990 he was made an honorary FRCR. In 1992 he was awarded an honorary DSc from Aberdeen University and in 1995 he was made an honorary member of the American Society of Neuroradiologists. In addition to having published over 100 papers on topics related to magnetic resonance imaging, he also is the owner of 50 separate patents.



A.S. Hall

C.A. Pallis

The Lancet • Saturday 14 November 1981

NUCLEAR MAGNETIC RESONANCE IMAGING OF THE BRAIN IN MULTIPLE SCLEROSIS

I. R. YOUNG

A. S. HALL

*Central Research Laboratories, Thorn-EMI Ltd, Hayes, Middlesex*C. A. PALLIS
G. M. BYDDERN. J. LEGG
R. E. STEINER*Departments of Medicine (Neurology) and Radiology,
Royal Postgraduate Medical School, Hammersmith Hospital,
London W12 0HS*

Summary Ten patients with multiple sclerosis (MS) were scanned by means of cranial X-ray computed tomography (CT) with and without intravenous contrast enhancement, and by nuclear magnetic resonance (NMR) using an inversion-recovery sequence. Altogether 19 lesions varying in size between about 7 mm × 5 mm and 13 mm × 8 mm were demonstrated by CT. They were all situated in the periventricular region. Two patients also showed moderate ventricular enlargement. In addition to these abnormalities 112 further lesions were demonstrated on the NMR scans. These lesions varied in size from 4 mm × 3 mm to 12 mm × 7 mm and were particularly well seen in the periventricular region and brainstem. Care is required in the assessment of NMR scans to exclude artefacts, background noise, and mottle as well as normally situated grey matter and partial volume effects from cerebral sulci. NMR nevertheless demonstrates abnormalities in MS on a scale not previously seen except at necropsy.

Introduction

ALTHOUGH the clinical diagnosis of multiple sclerosis (MS) is sometimes straightforward it can also prove a major challenge. In doubtful cases the detection of subclinical lesions with evoked potentials and X-ray computed tomography (CT)^{1,2} may be valuable, and CSF analysis may also be useful.³ Even so, post-mortem studies usually reveal many more lesions than were suspected during life.

In a previous paper we described the striking differentiation between grey and white matter of the brain seen with nuclear magnetic resonance (NMR) imaging, and we suggested that this technique might find application in diseases in which demyelination was a prominent feature.⁴

We now present the results of NMR examination of ten patients' MS and compare them with those obtained with CT.

Patients and Methods

Patients

Ten patients investigated in the Department of Medicine (Neurology) at Hammersmith Hospital were chosen for evaluation. Eight (patients 1 to 8) fulfilled the criteria for a diagnosis of "clinically definite" MS suggested by McDonald and Halliday.⁵ Patient 9 fell into their "progressive probable" category and patient 10 into their "early probable" group.

Age at onset of the disease ranged from 18 to 50 years, and the duration of the disease at the time of scanning varied from 7 months to 25 years. Seven patients had evidence of brainstem lesions such as ataxic nystagmus, internuclear ophthalmoplegia, facial numbness, or facial paresis, and eight had clinical evidence of cerebellar involvement. Seven had pallor of the optic discs or gave a history suggestive of retrobulbar neuritis, and the visual evoked responses were abnormal in each of these cases. The cerebrospinal fluid had been examined at some stage in every case and found to be abnormal. The abnormalities varied in specificity and ranged from a pleocytosis of 5 or more cells/ml to the presence of IgG of oligoclonal origin. The main features are summarised in table 1.

Methods

In each patient cranial CT scans were made with a Siemens Somatom 2 whole-body scanner operating at 125 kVp, with and without intravenous contrast enhancement with 60-100 ml of 76% sodium and meglumine diatrizoate. 10 s 230 mAs scans of the brain, of 8 mm slice width, were made at 10 mm intervals.

10-13 NMR inversion-recovery scans, approximately 9 mm wide, were made on each patient at intervals of 10 mm corresponding in position to the CT scans. The machine and scanning sequence have been described elsewhere.⁴ The NMR scanning procedure conformed to guidelines provided by the National Radiological Protection Board,⁶ and informed consent was obtained before the examination in all patients.

The CT scans were examined for evidence of focal areas of low attenuation, abnormal contrast enhancement, ventricular enlargement, and cortical atrophy, according to generally accepted criteria.^{7,8}

After a preliminary examination of all the NMR scans areas of abnormality were tentatively identified. 10 cranial NMR scans of normal volunteers of mean age 38 years were then examined for evidence of abnormalities similar to those seen on the scans of the MS patients. From these two sets of data diagnostic criteria were

TABLE I—CLINICAL FEATURES OF MULTIPLE-SCLEROSIS PATIENTS

Patient	Sex	Age at onset of MS (yr)	Duration (yr)	Clinical lesions					CSF abnormality
				Visual pathways	Brainstem	Cerebellum	Cortico-spinal tracts	Sensory pathways	
1	F	43	8	0	+	±	±	+	+
2	F	50	12	0	+	+	+	+	+
3	F	29	13	+	+	0	+	+	+
4	F	28	6	0	+	+	+	+	+
5	F	32	3	+	+	0	0	+	+
6	M	25	25	+	0	+	+	—	+
7	F	31	4	+	0	+	+	+	+
8	F	40	11	+	0	+	+	+	+
9	M	38	2	+	+	+	+	+	+
10	F	18	0.6	+	+	+	+	+	+

established which excluded possible suspect areas in normal volunteers. These criteria were then reapplied to the MS patients to provide a basis for diagnosis. These minimum criteria are summarised below:

1. The lesions had to have a longer relaxation time than adjacent white matter, giving a grey appearance on images produced with the present display system.
2. Only areas within white matter were considered, and special care was taken to exclude the basal ganglia, thalamus, red nucleus, and substantia nigra.
3. The lesions had to have well-defined margins.
4. Areas of artefact, noise, or significant background mottle were excluded.
5. When the margins were particularly clearly defined, lesions were accepted down to a size limit of approximately 4 mm × 3 mm on good-quality images. With large abnormal areas care was taken to distinguish a single lesion from multiple confluent ones.
6. Problems in distinguishing lesions from partial volume effects produced by cortical sulci effectively excluded much of the supraventricular region and the peripheral subcortical areas. Care was also taken to exclude partial volume effects from the posterior horns of the lateral ventricles.

It was accepted that the size limit might exclude small lesions which in all other respects had the features of MS. It was also recognised that the deliberate exclusion of the subcortical regions and cerebral grey matter (where many plaques may be seen at necropsy) would result in an underestimate of the number of lesions.

TABLE II—DISTRIBUTION OF CT AND NMR LESIONS

Level of scan	No. of slices	No. of lesions	
		CT scan	NMR scan
Supraventricular	23	3	9
High ventricular	12	2	18
Mid-ventricular	13	10	35
Low ventricular	18	4	31
Mesencephalon	16	0	17
Pons	12	0	15
Medulla	12	0	6
Total	106	19	131

Results

The number and distribution of lesions seen by the two techniques are summarised in table II.

19 lesions were identified by CT. These varied in size between about 7 mm × 5 mm and 13 mm × 8 mm. They were all seen in relation to the lateral ventricles, particularly the posterior horns and superior aspect. Two such lesions are demonstrated in fig. 1A (arrows). None of the lesions displayed contrast enhancement, and abnormal enhancement was not seen in other areas of the patients' brains. Two patients showed ventricular enlargement, and in one of these there was possibly a mild degree of cortical atrophy.

On the NMR scans between 9 and 22 lesions were seen in each patient, and a total of 131 lesions was recorded in the ten patients. The abnormalities were seen in the periventricular region in relation both to the lateral margins of the lateral

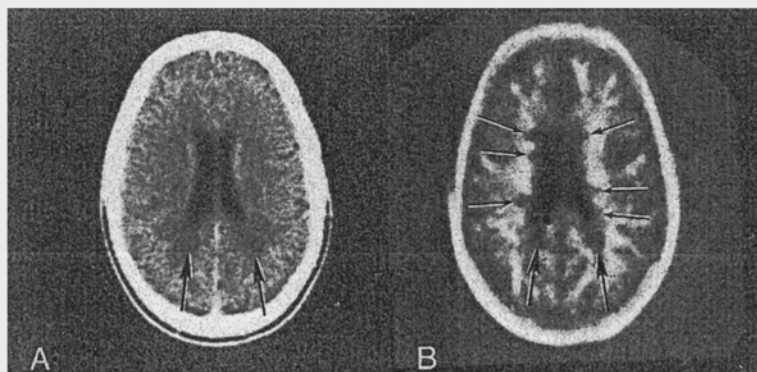


Fig. 1—Comparable CT (A) and NMR (B) scans in patient 10 at mid-ventricular level.

The two posterior periventricular lesions seen on the CT scan are also seen on the NMR scan (large arrows). In addition 6 smaller lesions are seen on the NMR scan at the lateral margin of the lateral ventricles (small arrows). The sharply defined area on the medial margin of the left posterior horn is a circular artefact.

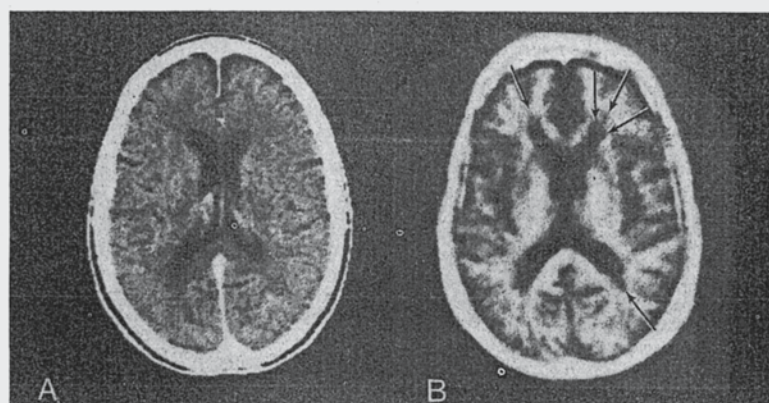


Fig. 2—Comparable CT (A) and NMR (B) scans in patient 6 at low ventricular level.

No abnormality can be identified on the CT scan, but 5 lesions are seen on the NMR scan in relation to the anterior and posterior horns of the lateral ventricles (arrows).

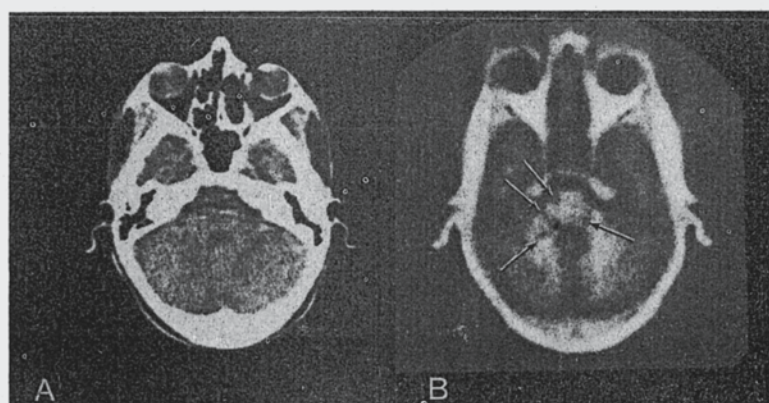


Fig. 3—Comparable CT (A) and NMR (B) scans in patient 10 at pontine level.

No abnormality is seen on the CT scan, but 4 lesions are seen within the pons and middle cerebellar peduncles on the NMR scan. The two small grey areas slightly to the right of the midline within the pons have not been included since their size (2 mm × 2 mm) does not meet the diagnostic criteria used for this study. There is a circular artefact to the left of the midline.

ventricles (fig. 1B) and to the anterior and posterior horns (fig. 2B). Lesions were also frequently seen within the brainstem and cerebellum, where they were not disclosed by CT (fig. 3). The abnormal areas were often irregular. Smaller lesions were usually circular or bar-shaped, and larger tortuous ones were also seen, particularly in the brainstem. Curvilinear defects were seen following the direction of fibre tracts, particularly within the middle cerebellar peduncle. "Scooped out" areas were observed at the margins of the lateral ventricles. Not infrequently the margins of the lateral ventricle were irregular—an appearance which could have been due to the effects of multiple small defects. In the brainstem, lesions were frequently seen at the external surface, as well as extending from the lateral angles of the fourth ventricle. Their size varied from about 4 mm × 3 mm to 12 mm × 7 mm.

The application of the size criteria used in this study is illustrated in fig. 3B, where the arrowed lesions have been included but the smaller (2 mm × 2 mm) grey circular areas just to the right of the midline within the pons have been

excluded. Focal areas with increased relaxation times were also noted in grey matter, particularly the thalamus, but they have also been excluded.

In all cases where a lesion was recognised on CT it was also seen on NMR, usually with a better-defined margin (fig. 1). The difference in the number of lesions seen with CT (19) and NMR (131) was highly significant on a paired *t* test ($p < 0.001$). The number of lesions detected at different levels of the brain is shown in table II. In both cases in which ventricular enlargement was seen on CT it was also evident on the corresponding NMR scan.

All three patients without clinical evidence of brainstem disease showed lesions in the brainstem on NMR scan. No significant correlation was found between the length of history and the number of lesions seen on NMR scan.

Discussion

NMR revealed abnormalities in patients with multiple sclerosis on a scale not previously seen except at necropsy,

although the specificity of these abnormalities is uncertain at present.

The finding of CT lesions in five of our ten patients was more than the 37% of 110 patients⁷ and the 24% of 66 patients⁸ found in larger series. The results in these two series were obtained with early-model CT scanners, but even using a more modern scanner with 5 mm slices examination of two cadaver brains showed the minimum detectable size of a CT lesion to be 7 mm.⁹ In the latter study only 8 of a total of 70 lesions demonstrated at necropsy were detected on initial CT examination, and a further 6 retrospectively. These findings are consistent with the relative insensitivity of CT in detecting MS lesions found in the present study.

There are a number of reasons for regarding the lesions demonstrated by NMR as representing MS plaques. Firstly, the areas of abnormality satisfying the diagnostic criteria for NMR lesions were seen in all ten patients with MS but in none of the ten normal volunteers. Secondly, the 19 lesions seen on CT scans which satisfied the generally accepted CT criteria for the diagnosis of MS plaques were all seen on NMR scans in corresponding positions. Thirdly, the distribution of NMR lesions in the brainstem and periventricular regions, with particular emphasis on the angles of the anterior and posterior horns, corresponds to the distribution of plaques at necropsy.^{10,11} The size and shape of NMR lesions also corresponds to what is seen macroscopically. Lastly, differentiation between grey and white matter by NMR scans in the normal brain depends on the short relaxation time of hydrogen within lipid.¹² Loss of lipid in MS plaques would therefore be associated with increased relaxation time, as seen in the defects we describe.

The potential of NMR in the diagnosis of MS needs little emphasis. NMR scanning promises to be of value both in patients presenting with symptoms and signs referable to the brain and in those in whom disease appears confined to the spinal cord. The technique may also provide a measure of the severity of disease in established cases, and thus be used to monitor the effectiveness of therapeutic regimens.

We thank the Department of Health and Social Security, and in particular Mr Gordon Higson and Mr John Williams, for their continued support and encouragement; and the Director, Central Research Laboratories, Thorn-EMI Ltd., for permission to publish this paper.

Requests for reprints should be addressed to R. E. S., Department of Diagnostic Radiology, Royal Postgraduate Medical School, Ducane Road, London W12 0HS.

REFERENCES

1. Mastaglia FL, Black JL, Collins DWK. Visual and spinal evoked potentials in diagnosis of multiple sclerosis. *Br Med J* 1976; ii: 732.
2. Aita JF, Bennett DR, Anderson RE, Ziter F. Cranial CT appearances of acute multiple sclerosis. *Neurology* 1978; 28: 251-55.
3. Hershey LA, Trotter JL. The use and abuse of the cerebrospinal fluid IgG profile in the adult: a practical evaluation. *Ann Neurol* 1980; 8: 426-34.
4. Doyle FH, Gore JC, Penlock JM, et al. Imaging of the brain by nuclear magnetic resonance. *Lancet* 1981; ii: 53-57.
5. McDonald WI, Halliday AM. Diagnosis and classification of multiple sclerosis. *Br Med Bull* 1977; 33: 4-8.
6. National Radiological Protection Board. Exposure to nuclear magnetic resonance clinical imaging 1980. Available from the Secretary, NRPB, Chilton Didcot, Oxon OX11 0RQ.
7. Gyldensted C. Computer tomography of the brain in multiple sclerosis. *Acta Neurol Scand* 1976; 53: 386-89.
8. Harshey LA, Gado MH, Troller JL. Computerised tomography in the diagnostic evaluation of multiple sclerosis. *Ann Neurol* 1979; 5: 32-39.
9. Houghton VM, Ho KC, Williams AL, Eldevik OP. CT detection of demyelinated plaques in multiple sclerosis. *AJR* 1979; 132: 213-15.
10. Brownell B, Hughes JT. The distribution of plaques in the cerebrum in multiple sclerosis. *J Neurol Neurosurg Psychiatr* 1962; 25: 315-20.
11. Lumsden CE. The neuropathology of multiple sclerosis. In: Vinken PJ, Bruyn GW, eds. *Handbook of clinical neurology*. 1970; vol 9, 217-309.
12. Gore JC, Doyle FH, Penlock JM. Nuclear magnetic resonance (NMR) imaging at Hammersmith Hospital. *Proc SPIE* 1981; 273: 8-10.

DRUG THERAPY FOR PLASMODIUM FALCIPARUM MALARIA RESISTANT TO PYRIMETHAMINE-SULFADOXINE (FANSIDAR)

A Study of Alternate Regimens in Eastern Thailand, 1980

MARK REACHER

JOHN FREEMAN

A. DAVID BRANDLING-BENNETT

CARLOS C. CAMPBELL

E. BRIAN DOBERSTYN

Vector Biology and Control Division, Center for Infectious Diseases, Centers for Disease Control, Public Health Service, Department of Health and Human Services, Atlanta, Georgia, U.S.A.; American Baptist Mission, Thailand; World Health Organisation, Thailand; and the Thai National Malaria Program

Summary A trial of drug regimens for treating *Plasmodium falciparum* malaria was conducted in a refugee camp in eastern Thailand where extensive 'Fansidar' (pyrimethamine-sulfadoxine) resistance had been demonstrated. The efficacy of quinine alone was compared to that of quinine combined with either fansidar or tetracycline. Quinine alone cleared the parasitaemia in 57 of 59 patients but failed to cure approximately one-third of these patients after 7 or 10 days of therapy. The addition of fansidar to quinine therapy did not significantly improve the overall cure rate. Tetracycline given for 10 days in combination with quinine cured all patients, suggesting that tetracycline should be considered in treating patients with falciparum malaria contracted in the area of the Thai-Kampuchean border.

Introduction

THE emergence in 1979 of *Plasmodium falciparum* malaria resistant to 'Fansidar' (tablets containing pyrimethamine 25 mg, sulfadoxine 500 mg) in eastern Thailand¹ has created a serious problem in malaria chemotherapy. Widespread resistance to fansidar was initially recognised in Khmer refugee camps along the Thai-Kampuchean border,² where *P. falciparum* was the predominant species of malaria.³ Chloroquine-resistant falciparum malaria, first documented in Thailand in 1962,⁴ has been prevalent throughout the country since the early 1970s;^{5,6} therefore, in areas that also have fansidar resistance no single-dose or short-course therapy for the cure of falciparum malaria has been available.

Observations in early 1980 suggested that quinine, given alone or in combination with other antimalarials, would be needed to cure multiple-drug-resistant *P. falciparum* infections. Previous reports from Thailand^{7,8} indicated that 6 or 7 days of quinine therapy (1.8 g salt/day) would cure 75-85% of infections. A decade ago tetracycline was shown to be highly effective against chloroquine-resistant *P. falciparum*^{9,10} when given in combination with quinine. Whereas fansidar had limited efficacy when administered alone, it potentially retained a therapeutic effect when combined with a rapid schizontocidal drug such as quinine.¹¹

To determine whether the combination of fansidar or tetracycline with quinine would shorten the course of therapy and produce a higher overall cure rate of fansidar-resistant *P. falciparum*, we evaluated malaria chemotherapy in the Khmer refugee camp with the highest prevalence of malaria during the peak 1980 transmission season. The results of this study identified drug regimens which are effective against fansidar-resistant *P. falciparum* infections in Thailand.

2.10 MRI: Clinical use of the inversion recovery sequence

Graeme M. Bydder (born 1944)

Professor Graeme M Bydder was born on 1 May 1944 in New Zealand. After early education in schools in New Zealand he qualified from the University of Otago Medical School in Dunedin in 1969. After early jobs in Otago Medical School, Graeme Bydder travelled to London, where he worked at the Clinical Research Centre in Northwick Park Hospital as an MRC Research Fellow. In 1981 he moved to the Hammersmith Hospital, where he spent over 20 years, becoming a Professor of Diagnostic Radiology in 1989. In 2003 he moved to the University of California in San Diego as a Professor of Radiology. At the Hammersmith Hospital, in the Robert Steiner MRI Unit, Professor Bydder was instrumental in much of the early pioneering clinical research into this technology. He is the author of many important clinical papers on magnetic resonance imaging and has been the recipient of many honours, including the gold medal of the Society of Magnetic Resonance in Medicine in 1997 and the gold medal of the Royal College of Radiologists UK 2001.



Ian Robert Young (born 1932)

see Chapter 2.9 on page 114.

MR Imaging: Clinical Use of the Inversion Recovery Sequence

G. M. Bydder and I. R. Young

Abstract: The properties of the inversion recovery (IR) sequence are considered and its use in clinical practice is illustrated. The effect of changing repetition time, inversion time (TI), and echo time; the method of data encoding; the type of data collection; and the method of image processing are analysed. Normal appearances and clinical examples in the central nervous system and the remainder of the body are used to illustrate the many options available with this sequence. The short TI IR sequence has advantages in magnetic resonance imaging of the body, and medium TI sequences are of value in localisation in the brain and in demonstrating contrast enhancement. Long TI sequences can be used in pediatrics and for separating tumour and oedema. Suppression or partial suppression of fat and fluid signals are two useful options with IR sequences. **Index Terms:** Inversion recovery—Nuclear magnetic resonance, techniques—Nuclear magnetic resonance.

For some time we have been intrigued by the fact that most groups performing magnetic resonance (MR) imaging use spin echo (SE) sequences almost exclusively and make little or no use of the inversion recovery (IR) sequence. Although we make considerable use of the SE sequence and drew attention to its value in imaging of the brain early in the development of clinical MR (1), we also make extensive use of the IR sequence (2-6) and believe that this sequence is in many ways the most interesting of the three sequences in general use. From an imaging point of view both the SE sequence and the partial saturation (PS) sequence can be regarded as limiting cases of the IR sequence, the scope of which includes all the options available with both of these sequences as well as its own unique features. To draw attention to the value of the IR sequence we describe the sequence in non-mathematical terms, discuss the effect of changing different imaging parameters, and illustrate its use in a variety of clinical situations.

From the Department of Diagnostic Radiology, Royal Postgraduate Medical School, Hammersmith Hospital, London (G. M. Bydder), and Picker International, Hirst Research Centre, Wembley, Middlesex (I. R. Young), England. Address correspondence and reprint requests to Dr. G. M. Bydder at Department of Diagnostic Radiology, Royal Postgraduate Medical School, Hammersmith Hospital, Du Cane Road, London W12 0HS, England.

DESCRIPTION OF THE IR SEQUENCE

The dependence of signal intensity seen with the IR sequence on proton density, T1, and T2 has been described in mathematical terms in previous articles in this journal (4,7,8) but our principal interest in this paper is clinical and we will use a qualitative description of the IR sequence.

The prototype Picker imaging machine used in these studies has been described previously (4) and operates at 0.15 T. We can represent the proton magnetisation induced in the patient by the static magnetic field by a vector M . The component of the magnetisation in the transverse plane at any given time is then represented by M_{xy} , and that in the longitudinal direction at the same time by M_z . The effect of a 90° pulse is to rotate M_z into the transverse plane to become M_{xy} (Fig. 1). Following a 90° pulse, M_z increases exponentially from zero with time constant T1 (Fig. 2a) and M_{xy} decays exponentially with time constant T2 (Fig. 2b). At the following 180° pulse M_z is inverted to become $-M_z$ and recovers with a time constant T1 but at *twice* the rate for the earlier longitudinal recovery after the 90° pulse. At the next 90° pulse M_z is rotated to become M_{xy} . M_{xy} then decays exponentially with time constant T2. Using a field echo or free induction decay data collection, signal is collected at a mean echo time (TE) after the 90° pulse and the cycle is repeated (a field echo uses symmetrical gra-

660

G. M. BYDDER AND I. R. YOUNG

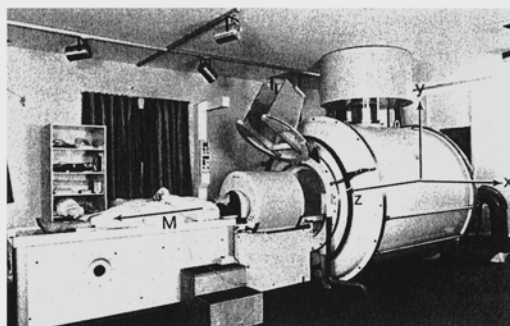


FIG. 1. A magnetic resonance imaging machine. The cryomagnet produces a net magnetisation M in the longitudinal axis of the volunteer; 90° pulses are used to rotate this magnetisation into the transverse plane. The x , y , and z axes are shown.

dient fields to form the echo). We can use a composite diagram following first M_z then M_{xy} after the second 90° pulse to represent the "potential signal intensity" at various stages in the sequence (Fig. 2c) to understand how this may be varied.

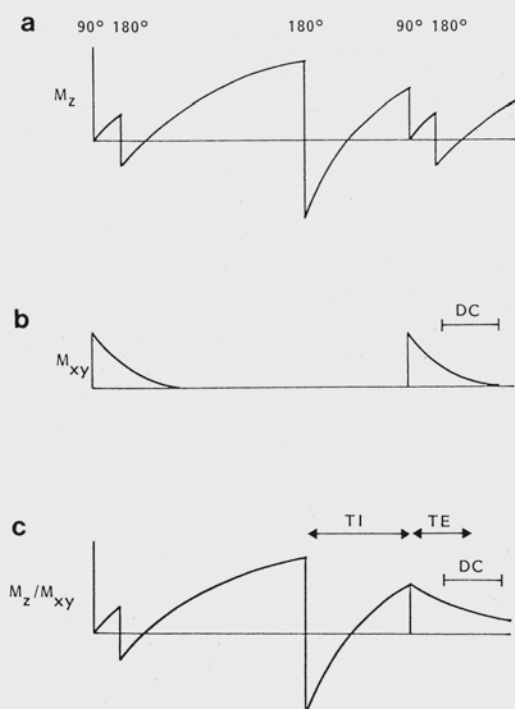


FIG. 3. Changes in M_z (a) and M_{xy} (b) with time in the inversion recovery sequence (medium inversion time, TI) using a spin echo data collection (DC). c: M_z initially and M_{xy} in the last segment. TE, echo time.

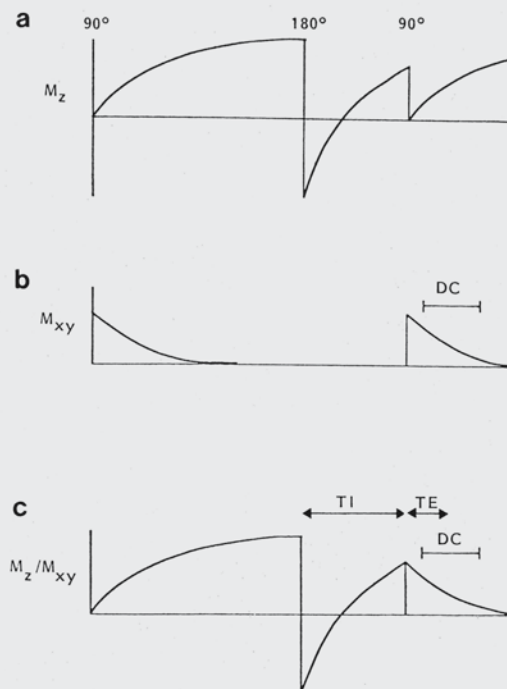


FIG. 2. Changes in M_z (a) and M_{xy} (b) with time in the inversion recovery sequence (medium inversion time, TI) using a field echo data collection (DC). c: M_z in the first two segments and M_{xy} in the last segment. TE, echo time.

In Fig. 3 the corresponding figures are drawn for the situation where an SE pulse is used with an SE data collection in the last stage of the sequence. The figures are similar except that the data collection is delayed compared with the previous case, and the magnetisation is inverted again by the additional 180° pulse (only T2 is considered rather than T2*; additional decay due to field inhomogeneity is reduced as a result of the refocusing 180° pulse). The size of the received signal and ultimately the signal intensity or pixel value in the image is proportional to M_{xy} at the time of the data collection. M_{xy} is also proportional to tissue proton density. The inversion time (TI) and TE as used in the American College of Radiology convention are shown in Figs. 2 and 3. Repetition time (TR) is the duration of each cycle of the sequence, TI is the time between the inverting 180° pulse and the following 90° pulse, and TE is the time from the last 90° pulse to the following echo.

Using Fig. 2c as our model of the IR sequence, we can compare the signal intensities of white matter (a tissue with a relatively short TI), grey matter (a tissue with a longer TI), and cerebrospinal fluid (CSF) (which has a very long TI) in Fig. 4.

MR IMAGING: THE IR SEQUENCE

661

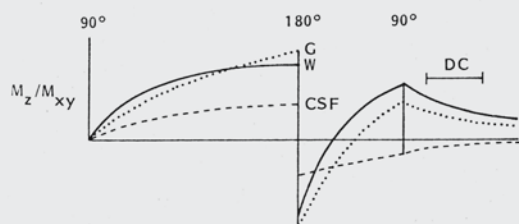


FIG. 4. Changes in M_z/M_{xy} with time in the inversion recovery sequence (medium inversion time) for white matter (W), grey matter (G), and cerebrospinal fluid (CSF) using field echo data collection (DC).

The signal intensity observed is proportional to the height of M_{xy} in Fig. 4, and it can be seen that the shorter T1 of white matter results in a higher signal intensity than for grey matter. The very long T1 of CSF results in a low signal intensity that may be negative as in Fig. 4. Note that the last segment of the decay converges towards zero for both grey and white matter with their positive signal intensities, as well as for CSF with its negative signal intensity. Display of the resultant image after phase corrected processing (see later) gives white for white matter, light grey for grey matter, dark grey for zero signal intensity, and black for CSF. The signal for grey matter is slightly greater than that for white matter at the time of the 180° pulse because of its 10% greater proton density. We next consider the effects of changing TR, T1, TE, the imaging processing technique, and other parameters on the signal intensity at the time of data collection.

Effect of Changes in TR

The general rule is that a time of at least 3T1 should be allowed for recovery of the longitudinal magnetisation between the 90° of the last pulse cycle and the following 180° pulse of the next pulse cycle to allow a high level of recovery of M_z , although, in practice, it is possible to use times less than this. It is important to note: (a) That the rule above applies to all the tissues in a slice and, as many lesions have an increased T1, this sets a lower limit for TR that may be much greater than it would be for normal tissues. (b) It is also important to note that fluids such as CSF, urine, and small bowel contents usually have a very long T1 and do not fully recover with the values of TR in general use. This may be an advantage for some purposes; for example, it may be helpful to have the CSF signal less than brain (see later). (c) Values of T1 at the operating field in this study are listed in Table 1. At higher fields, tissue T1 is increased; for example, at 10 times the static field used here, T1 is approximately doubled for many tissues (9) although fat does not increase this much, and CSF changes relatively little. T2 is essentially unchanged with field.

TABLE 1. Values of T1, T2, and the ratio of T1/T2 at 0.15 T for various tissues

Tissue	T1 (ms)	T2 (ms)	T1/T2
Grey matter	453 ± 77	101 ± 13	4.5
White matter	353 ± 60	92 ± 22	3.8
Cardiac muscle	377 ± 60	57 ± 16	6.6
Liver	206 ± 45	43 ± 14	4.8
Spleen	364 ± 69	62 ± 37	5.9
Kidney	368 ± 99	58 ± 24	6.3
Skeletal muscle	330 ± 59	47 ± 13	7.0
Fat	173 ± 49	84 ± 36	2.1

From ref. 9.

Reducing TR produces a reduction in signal intensity for tissues with a long T1, although there is little effect on tissues with a short T1 where TR is still greater than 3T1. Reducing TR is therefore used to reduce the relative signal intensity of tissues, such as the spleen, which have a long T1, or of fluids, such as CSF, which have a very long T1 (see later). There is little advantage in increasing TR beyond 3T1.

Effect of Changes in T1

It is useful to consider three variants of the IR sequence according to their values of T1: (a) short T1 (T1 approximately 0–250 ms); (b) medium T1 (T1 approximately 250–700 ms); (c) long T1 (T1 approximately 700 ms and longer). These T1 categories are applicable at 0.15 T. The approximate factors by which to multiply T1 and TR to achieve the same effects at higher fields by compensating for the increase in tissue T1 are listed in Table 2 (derived from ref. 9).

Short T1

The values of T1 included here are approximately 0–250 ms. In the limit where T1 equals zero (or, from a practical point of view approximately 1 ms) the 90 and 180° pulses add to give a 270° pulse that

TABLE 2. Ratio of T1 at different fields to that at 0.15 T for various tissues

Tissue	Field strength (T)				
	0.15	0.3	0.5	1	1.5
Grey matter	1	1.24	1.45	1.79	2.03
White matter	1	1.27	1.52	1.93	2.23
Cardiac muscle	1	1.28	1.55	1.99	2.30
Liver	1	1.30	1.58	2.05	2.39
Spleen	1	1.24	1.49	1.88	2.15
Kidney	1	1.19	1.35	1.60	1.77
Skeletal muscle	1	1.34	1.66	2.22	2.63
Fat	1	1.13	1.24	1.39	1.50

From ref. 9.

is equivalent to a -90° pulse. Using magnitude reconstruction (see later), this is equivalent to a 90° pulse and the sequence in Fig. 2c becomes 90° -data collection, or the PS sequence. Thus, the PS sequence can be regarded as a limiting case of the IR sequence with $TI = 0$. The same reasoning applies when an SE data collection is used (Fig. 3c) and the IR sequence (with $TI = 0$) becomes equivalent to an SE sequence. This is the basis for regarding both the SE and the PS sequences as limiting cases of the IR sequence. Using magnitude reconstruction with TI in the range of 0 to approximately 250 ms, an IR image of the brain appears like an SE one although with greater grey-white matter contrast. The magnetisation curves can be represented as shown in Fig. 5. Note that following the final 90° pulse the $T1$ contrast and the $T2$ contrast are *additive*, i.e., increasing the $T1$ of a tissue increases the relative signal intensity of the tissue and so does increasing its $T2$. (This is *not* the case in Fig. 2c or Fig. 3c, which illustrate medium values of TI .) The short TI IR (STIR) sequence is sensitive to changes in $T1$ and $T2$ and can be used as a screening sequence in the brain in a similar way to SE sequences with long TE and long TR such as $SE_{1,500/80}$. To reduce the signal intensity of CSF to less than that of white matter, TR can be shortened, as suggested in the previous section, to 1,000 ms with a sequence such as $IR_{1,000/100/44}$.

Since many pathological lesions produce an increase in both $T1$ and $T2$, the addition of these two types of contrast with the STIR sequence produces high net tissue contrast. This type of sequence also enables some $T1$ dependent decay to be substituted for the $T2$ dependent decay in the equivalent SE sequence. This is of particular value where the $T1$ and $T2$ decays of the tissues differ and explains why the grey-white matter contrast of this sequence is greater than the equivalent SE sequence. In the body there is another reason for making this substitution when an SE data collection is used, as it allows a reduced value of TE for equivalent soft tissue contrast thus reducing the vulnerability of the sequence to motion.

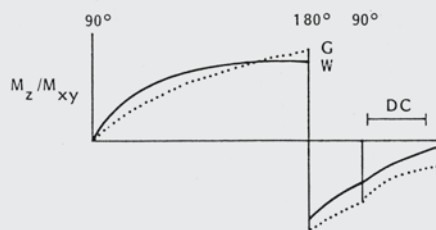


FIG. 5. Changes in M_z/M_{xy} time for a short inversion time inversion recovery sequence. The magnitude of the signal from grey matter (G) is greater than that for white matter (W) using field echo data collection (DC).

It is also possible to choose particular values of TI so that the signal intensity of a particular tissue is zero at the time of the 90° pulse (Fig. 6). (This occurs at a value of TI typically between 0.56 and $0.69 T1$ for $TR > 3T1$.) Values of approximately 100 ms are suitable to eliminate the fat signal, and 255 ms is adequate for white matter. In this situation the tissue signal is said to be "suppressed." Suppression or partial suppression of the fat signal is of particular value in the orbit, breast, and abdomen. In the abdomen respiratory artefact frequently arises from subcutaneous fat and reduction of the fat signal minimises this. In addition, SE sequences with long TE and TR produce a relatively high signal intensity from soft tissue lesions that have an increased $T2$, but since fat also has a long $T2$ these lesions may be indistinguishable from fat. Suppression or partial suppression of the fat signal avoids this problem. Other uses of these sequences include suppression of the high signal from fat adjacent to a surface coil and the suppression of the signal from liver to highlight lesions.

Medium TI

The working rule to obtain an image with good contrast between two tissues of different $T1$ values is to choose a value of TI intermediate between the two tissues of interest (neglecting the effects of proton density and $T2$), so that satisfactory contrast between white matter ($T1 = 350$ ms) and grey matter ($T1 = 450$ ms) is achieved with a TI of approximately 400 ms. Note that the signal intensity is not maximal at this point so the image appears noisier than that obtained with, for example, $TI = 500$ ms where the signal is higher (although the grey-white matter contrast is less). In theory maximum contrast is obtained when TI is approximately 0.65 times the average of the $T1$ for the two tissues, but the signal levels in this case are close to zero, and

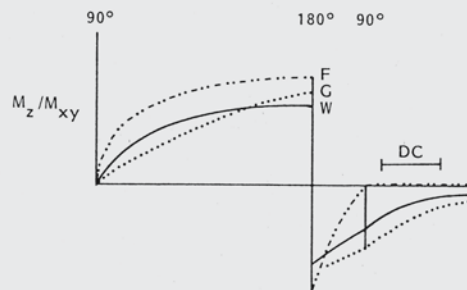


FIG. 6. Changes in M_z/M_{xy} with time for fat (F), white matter (W), and grey matter (G) using a fat-suppressed short inversion time inversion recovery sequence. The signal from G is greater than that for W and F gives no signal using field echo data collection (DC).

MR IMAGING: THE IR SEQUENCE

663

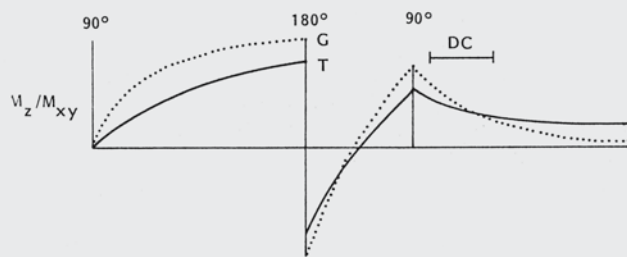


FIG. 7. Changes in M_z/M_{xy} with time for grey matter (G) and a tumour (T) using a medium inversion time inversion recovery sequence. There is a relative reduction in the signal from T during the first two segments of the sequence (T1 dependent section) but a relative increase in the last section (T2 dependent section) using field echo data collection (DC).

maximise the appearance of the noise in the image. Note that the TI for optimum contrast between grey and white matter will not be optimal for that between grey matter and a tumour that has an increased T1 (Fig. 7).

There are two additional modifying factors. The increased mobile proton density of grey matter relative to white matter results in slightly less tissue contrast. More important is the fact that the T2 dependent period following the 90° pulse and prior to data collection may produce a *reduction* in tissue contrast. This is particularly so for lesions that follow the common pattern in which T1 and T2 are both increased. The T2 dependent decay, in the last component of the sequence, reduces the T1 contrast developed earlier in the sequence.

The method of image reconstruction and the type of data collection affect TE. Echo time is generally shorter with projection-reconstruction than with two-dimensional Fourier transformation (2DFT) since a single vector encoding gradient is used, without the need for a previous phase encoding period as with 2DFT. A field echo data collection can be completed earlier than an SE collection with the same band width, although the former is more vulnerable to B_0 field inhomogeneities.

With the brain (T2 approximately 100 ms), the T2 dependence of the IR sequence is not such a big problem as it is in the body where values of T2 are typically half those in the brain (45–60 ms) making the same IR sequence much more T2 dependent than when it is used in the brain. The use of short

values of TE to control this problem becomes important. The alternative is to use short values of TI so that the T1 and T2 contrast after the 90° pulse is additive as outlined in the previous section.

Long TI

For reasons outlined above these sequences may be useful in separating tumour from oedema (where both have increased values of T1). Sequences designed for this purpose require an increase in the value of TR. They are also useful in pediatrics where the T1 of normal brain may be increased 3–400% when compared with adults (5). Another use is suppression of long T1 fluids such as CSF, urine, and bowel contents where values of T1 of 800–1200 ms can be used. It is also possible to use a “double” IR (DIR) with the first TI (e.g., $T_{I1} = 1,200$ ms) used to suppress a fluid and the second TI ($T_{I2} = 100$ ms) used to suppress fat (e.g., $DIR_{3,000/1,200/100/44}$) (Fig. 8) although this type of sequence is slow and may show some reduction in lesion contrast. The value of TI required to suppress small bowel contents is less than that for purer fluids such as CSF.

Effect of Changes in TE

Increasing TE increases the T2 dependence of the IR sequence. This is useful for short TI sequences, generally not useful for medium TI sequences, and of limited value for long TI sequences.

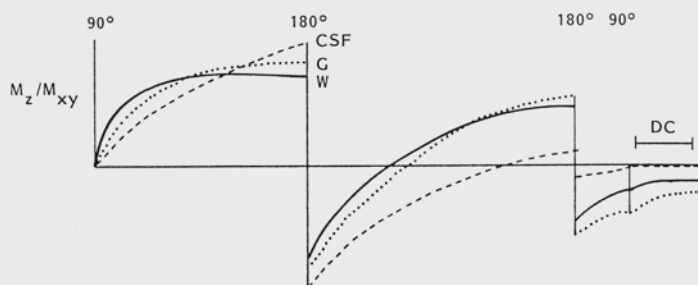


FIG. 8. Changes in M_z/M_{xy} with time for CSF, white matter (W), and grey matter (G) for the double inversion recovery sequence. The signal from G is greater than that for W and cerebrospinal fluid (CSF) gives no signal using field echo data collection (DC).

Short TI

The rule for maximum contrast for SE sequences is to use TE halfway between the T2 values of the two tissues of interest (neglecting proton density and T1 effects). It is most useful to increase TE when imaging tissues with a long T2 such as spleen or kidney (and of course brain). The rule for STIR sequences is to use TE rather less than this value because of the additional T1 dependent contrast. Additional echoes can be usefully added to this type of sequence.

Medium TI

In general TE should be reduced to a minimum. Projection-reconstruction with a field echo data collection may be used for this purpose.

Long TI

Echo time can be increased with this type of sequence to increase the relative T2 dependence although the contrast may be ambiguous unless TI is quite long (as for the DIR sequence).

Effects of Methods of Processing

There are two types of image reconstruction available—*phase corrected* where positive values of signal intensity are shown positive and negative values appear negative, and *magnitude* reconstruction where the magnitude of the signal is used irrespective of its sign. For STIR sequences using phase corrected processing white matter is white and grey matter is grey but the reverse is so with magnitude processing (10). For medium TI sequences the CSF appears dark with phase corrected processing but may show a “rebound” with a lighter central area with magnitude processing. The signal intensities follow directly from considering Figs. 4 and 5.

Effects of Multislice or Single Slice Imaging

The 90° pulse in the IR sequence is always slice selected, although for single slice scans the 180° pulse(s) need not be. However, when the IR sequence is used to obtain an interleaved set of slices, 180° pulse(s) must be slice selected. When the 180° pulse is slice selected, it is possible for flowing blood to experience only part of the IR sequence depending on where it is at the times of the inversion pulses. For example, blood flowing into a slice may only experience a 90° pulse and behave as though it is being imaged with a PS sequence producing a high signal intensity rather than the usual low signal intensity.

CLINICAL ILLUSTRATIONS OF THE USE OF THE IR SEQUENCE

Many of the applications of the IR sequence follow directly from considerations in the previous section. Typical sequences and their applications in the central nervous system (CNS) and in the body are listed in Table 3 and some of these are illustrated below.

Applications in the CNS

The STIR sequences can be used for disease detection (Fig. 9). Both TR and TI can be adjusted so that one version of the sequence generates images with the signal intensity of CSF slightly less than that of white matter in order that periventricular lesions can be recognised without confusion from partial volume effects, and the other version generates images with the CSF signal greater than that of brain (Fig. 10).

Separation of tumour from oedema may also be accomplished (Fig. 11), and additional lesions may also be seen in vascular disease (Fig. 12). Medium TI IR scans provide localisation of disease, assessment of mass effects, and developmental information in older infants. Contrast enhancement is usually maximal with this sequence (11) (Fig. 13). The sequence also provides a better technique for computing T1 maps than that using two SE sequences.

“Short T1 short T2” tumours including some meningiomas and some acoustic neuromas are well demonstrated with medium TI IR sequences (Fig. 14) as are subacute hemorrhage and usually multiple sclerosis (MS) lesions in the brain stem. Long TI IR sequences may help in distinguishing tumour from oedema as well as in pediatric applications (Fig. 15). The DIR sequence can be used to suppress CSF (Fig. 16) as well as to suppress bile ducts and urine. Some cord lesions are better defined with the IR sequence (Fig. 17).

Applications in the Body

Mediastinal and chest wall lesions can be well displayed with the STIR sequences. This avoids confusion of fat with long TE sequences and the confusion of lung with tumour using medium TI IR sequences although fat can also be a valuable marker of tissue planes.

The STIR sequences are of value in imaging the abdomen and pelvis. In Fig. 18 a contrast enhanced CT scan is compared with an IR_{1,500/100/44} sequence. The extent of the tumour in the left lobe of the liver is better shown on the IR scan. Dilated bile ducts are also highlighted. Using a DIR sequence in a patient with metastases to the liver, an additional metastasis is seen in the right adrenal gland (Fig.

MR IMAGING: THE IR SEQUENCE

665

TABLE 3. Typical inversion recovery sequences (at 0.15 T)

Purpose	TR (ms)	TI (ms)	TE (ms)	Field/spin echo (F/S)	Reconstruction (PR/2DFT)	Processing Phase corrected (PC) or magnitude (M)	Resolution	Comment
Brain and spinal cord								
Disease detection [cerebrospinal fluid (CSF) signal less than white matter]	1,500	80	44	S	2DFT	M	256 × 256	
Disease detection (CSF signal greater than white matter)	1,000	100	44	S	2DFT	M	256 × 256	
Disease detection (CSF signal greater than white matter)	1,500	100	44	S	2DFT	M	256 × 256	
Adult anatomy and localisation	2,000	100	80	S	2DFT	M	256 × 256	
	1,200	200	8	F	PR	M	115 × 115	Older sequence
	1,500	500	44	S	2DFT	PC	256 × 256	
	1,400	400	5	F	PR	PC	115 × 115	Older sequence
Pediatric development and localisation	3,000	1,000	44	S	2DFT	PC	256 × 256	Premature infant
	2,400	800	44	S	2DFT	PC	256 × 256	0–3 months
	1,800	600	44	S	2DFT	PC	256 × 256	3 months–2 years
Contrast enhancement	1,500	500	44	S	2DFT	PC	256 × 256	
	1,400	400	13	F	PR	PC	115 × 115	Less T2 dependent than sequence above
CSF suppression (DIR)	3,000	1,200						
		100	44	S	2DFT	M	256 × 256	
Orbital fat suppression	1,500	100	44	S	2DFT	M	256 × 256	
Body								
Mediastinal mass	1,500	100	44	S	2DFT		256 × 256	Cardiac gated and ROPE
Myocardium	Double beat	600	13	F	2DFT	M	128 × 192	Cardiac gated and ROPE
Liver and pancreas	1,500	100	30	S	2DFT	M	256 × 256	With ROPE
	1,500	100	44	S	2DFT	M	256 × 256	With ROPE
	1,000	100	44	S	2DFT	M	256 × 256	With ROPE
	1,400	400	13	F	2DFT	PC	128 × 192	With ROPE
Contrast enhancement	1,400	400	13	F	2DFT	PC	128 × 192	(positive enhancement)
Spleen and kidney	1,500	100	60	S	2DFT	M		
	1,500	100	80	S	2DFT	M		
Pelvis DIR	3,000	1,000	44	S	2DFT	M	256 × 256	
		100						
Bone	1,500	500	44	S	2DFT	PC	256 × 256	
	1,500	100	44	S	2DFT	M	256 × 256	

Abbreviations: CSF, cerebrospinal fluid; DIR, double inversion recovery; PR, projection reconstruction; ROPE, respiratory ordered phase encoding; TE, echo time; TI, inversion time; TR, repetition time; 2DFT, two-dimensional Fourier transformation.

19). Lobar atrophy is seen associated with a hemangioma in Fig. 20.

In Fig. 21 contrast enhanced CT, IR_{1,500/100/44}, SE_{544/44}, and SE_{1,500/80} scans are compared. The abscess, thickened abnormal abdominal wall, fluid tracking posteriorly, and paraaortic lymph node are best displayed with the IR sequence.

The margin between tumour and normal bone marrow is better shown with the IR scan than with the SE scan in Fig. 22. Separation of tumour and fatty marrow (both of which have a long T2) by use of STIR sequences (exploiting the short T1 of fat) may be useful although care is necessary to distinguish red marrow from tumour.

DISCUSSION

With the range of options and apparent advan-

tages outlined above, why is the IR sequence used so little in clinical practice? There is probably no straightforward answer to this question but a number of possible explanations are listed below.

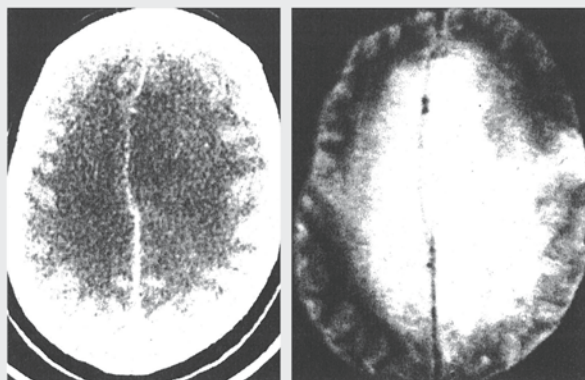
1. *The IR sequence is generally thought of only as the medium TI variant.* Very little attention has been paid to the short TI and long TI variants of the IR sequence although they were described early in the development of MR (2) and offer many useful options at both high and low fields.

2. *The significance of the T2 dependence of the medium TI IR sequence has not been fully appreciated.* Since many lesions produce an increase in both T1 and T2, the T2 dependence of the IR sequence produces a net reduction in the T1 dependent contrast. To obtain useful disease detection with a medium TI IR sequence, TE should be kept as short as possible. This was done in earlier studies

666

G. M. BYDDER AND I. R. YOUNG

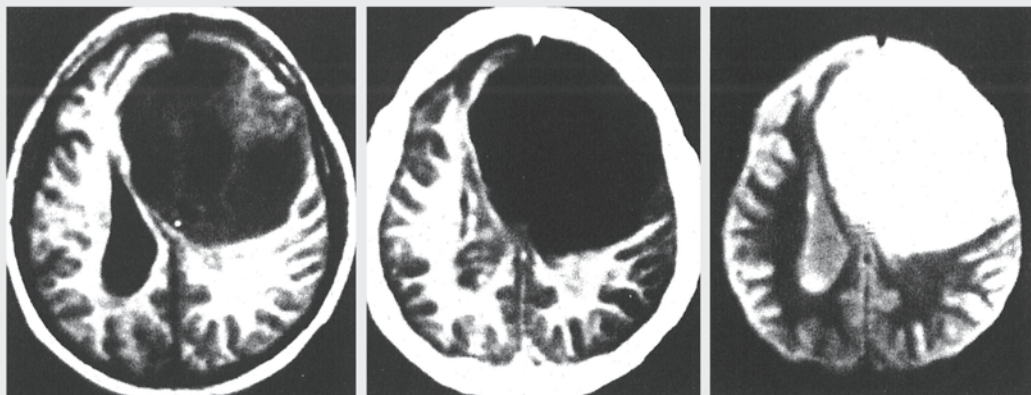
FIG. 9. Frontoparietal astrocytoma grade II: contrast enhanced CT (a) and inversion recovery (IR)_{1,000/100/44} (b) scans. The tumour is seen to be bilateral in (b). (A central artefact is noted on this and some subsequent scans.)



with projection-reconstruction and field echo data collection (2,3). The more recent use of 2DFT and SE data collection has resulted in longer values of TE being used with more T2 dependence. In addition, since body tissue T2 values are half those of

the brain (excepting fat), the relative T2 dependence of the IR sequences is increased in body examinations producing even further net loss of lesion contrast and decreasing the apparent usefulness of the medium TI IR sequence.

10a-c



10d

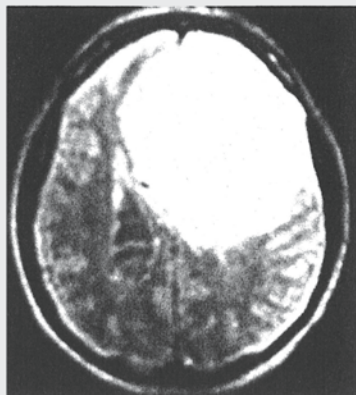


FIG. 10. Frontal astrocytoma grade III: inversion recovery (IR)_{1,500/100/44} (a), phase corrected IR_{1,500/100/44} (b), magnitude processed IR_{1,500/100/44} (c), and spin echo (SE)_{1,500/80} (d) scans. The tumour is well seen on all four scans. Note in (c) the grey-white matter reversal and the lesions at the periventricular margin (left).

MR IMAGING: THE IR SEQUENCE

667

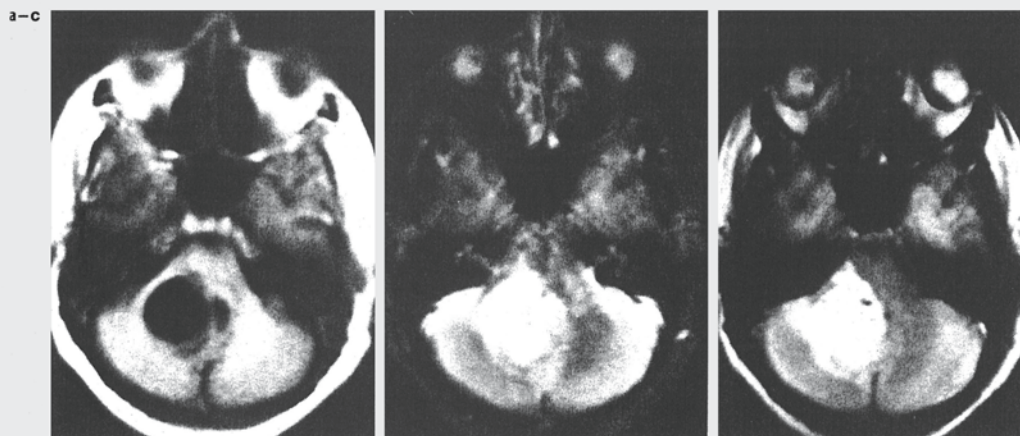


FIG. 11. Cerebellar astrocytoma grade II: inversion recovery (IR)_{1,500/500/44} (a), IR_{2,000/100/44} (b), and spin echo (SE)_{1,500/80} (c) scans. Separation of tumour from oedema is better with the IR scans. The cerebrospinal fluid signal is greater than brain in (b).

3. *The IR sequence has been thought of as "noisy."* Medium T1 sequences of the brain provide a quick visual assessment of three machine parameters: tissue contrast, spatial resolution, and noise level. Grey-white matter contrast provides an assessment of tissue contrast; resolution can be assessed by looking at fine anatomical detail (e.g., the cerebellar vermis); and noise level can be assessed by looking at the background, as well as tissues or structures with a very low proton density or those with a moderately long T1, since with a phase corrected IR scan random noise appears in the middle of the grey scale. If the sequence is modified to improve any one of these factors, one or both of the others will suffer to some degree and this is relatively easy to assess on an image. The same type of analysis is not so straightforward on an SE image, as assessment of tissue contrast is not so

easy since grey-white matter contrast is less (and a function of proton density in any case), and noise, although present in the image, is at one end of the grey scale and can be "windowed" out. Hence, in comparison with high resolution low noise SE sequences with short values of TE and TR, medium T1 sequences appear noisy. However, it is being increasingly accepted that the most useful SE sequences in clinical practice are those with a long TE (1,12), and this type of sequence is more "noisy" than the short TE short TR SE sequence so that the noise levels for comparable disease sensitivity of SE sequences is similar to that of the equivalent IR sequence. Thus, IR_{1,500/80/44} and SE_{1,500/80} sequences show similar disease sensitivity and similar noise levels.

Both with the SE (long TE and long TR) and IR sequences improvements in machine signal/noise

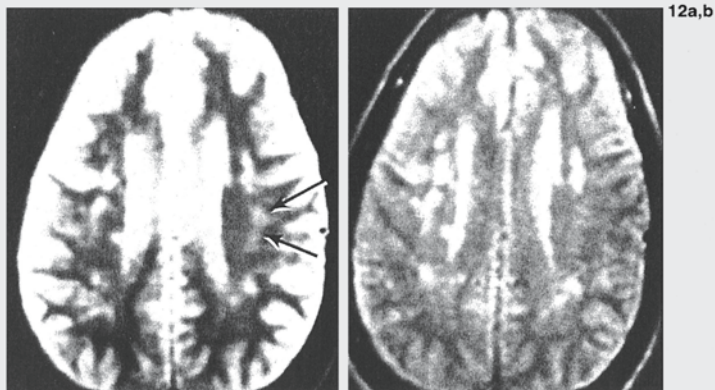
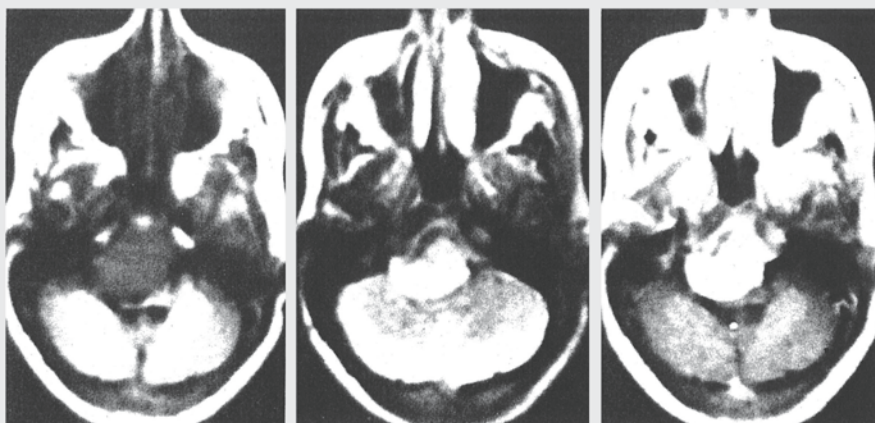


FIG. 12. Cerebrovascular disease: inversion recovery (IR)_{1,500/100/44} (a) and spin echo (SE)_{1,500/80} (b) scans. Note that some lesions in the left centrum semiovale are better seen in (a) (arrows).

668

G. M. BYDDER AND I. R. YOUNG

13a-c



13d



FIG. 13. Clivus meningioma: inversion recovery (IR)_{1,500/500/44} (a) and spin echo (SE)_{1,500/80} (b) scans before intravenous Gd-DTPA compared with IR_{1,500/500/44} (c) and SE_{1,500/80} (d) scans after enhancement. Marked enhancement is seen in (c) but little change is evident in (d).

14a,b

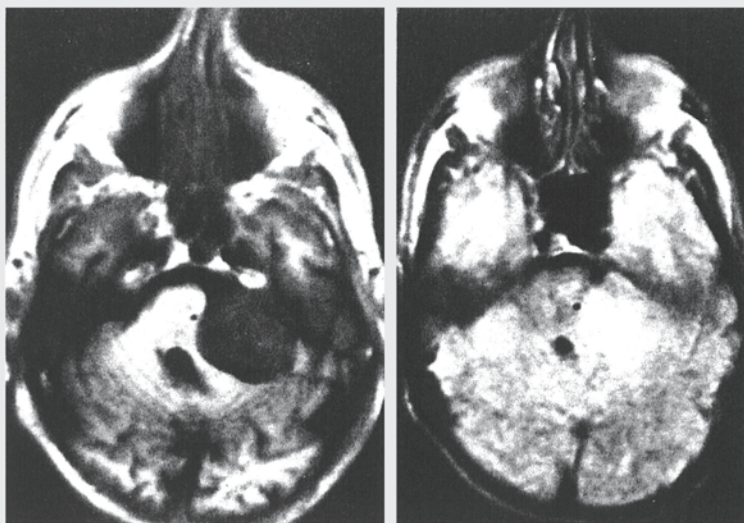


FIG. 14. Acoustic neuroma: inversion recovery (IR)_{1,500/500/44} (a) and spin echo (SE)_{1,500/80} (b) scans. The tumour is better defined in (a).

MR IMAGING: THE IR SEQUENCE

669

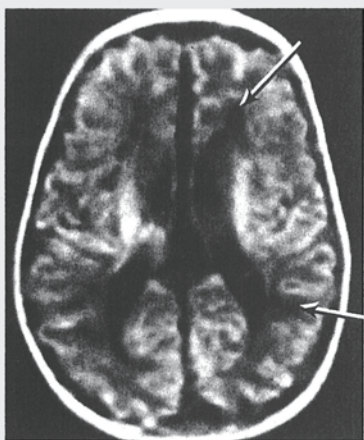


FIG. 15. Cystic leucomalacia in a 3-week-old neonate: inversion recovery (IR)_{3,000/1,000/44} scan. The cysts are well shown (arrows).

ratio result in improved image quality. Methods of improving signal/noise ratio with surface and closely coupled coils have recently been or are soon to be published in this journal (13–15).

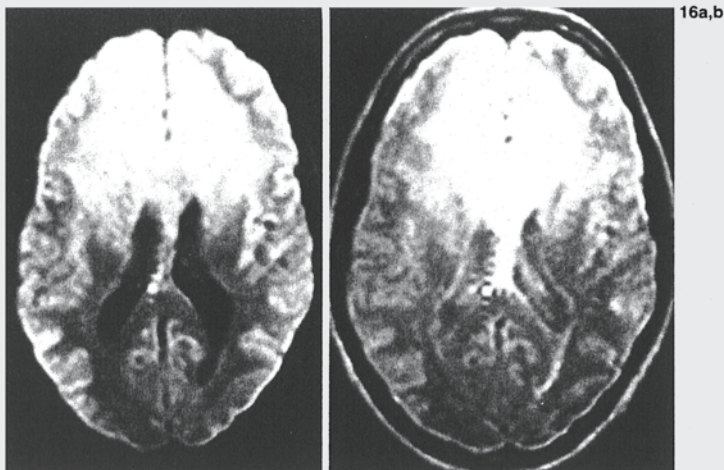
4. *The IR sequence is said to be "slow."* This is regarded as less of a problem since the clinical limitations of SE sequences with short TE and short TR have been more widely recognized and SE sequences with long TE and long TR have come into more general use. The use of interleaved slices also provides time to do additional slices during the relatively long TR of the IR sequence. A genuine disadvantage of IR is the fact that with medium and

long TI IR sequences it is more difficult to construct an interleaved multislice set because of the relatively isolated 180° inverting pulses, than it is for a comparable SE multislice set. This limitation does not apply to short TI IR sequences to the same extent. The DIR sequence is slow but its use is generally confined to specialised applications.

5. *"It is not possible to obtain useful additional echoes with the IR sequence."* Additional echoes can be obtained with all three groups of IR sequences. They increase T2 dependent contrast with the STIR sequence in a straightforward manner analogous to multiple echo SE sequences, but, with medium TI IR sequences, T1 and T2 contrast are moving in opposite directions and confusing images may result. Additional echoes with these sequences are generally of little value but may be of use in providing a range of T1 and T2 dependent weightings that can be useful in separating tumour from oedema or in its calculation of tissue parameters. With long TI IR sequences (e.g., the DIR sequence) additional SE can be used effectively.

6. *Practical problems.* There are some more specific problems with particular variants of the IR sequence that are worth listing: (a) Partial volume effects with medium TI IR sequences between grey and white matter of the brain may simulate brain lesions. This can be reduced or avoided by using short TI variants. (b) The phase corrected version of the medium TI scan displays zero signal intensity in the midgrey region. This signal may simulate tissue in the sinuses, etc. This is not a problem with STIR sequence. (c) Increased time may be needed for a low resolution phase calibrating scan for the phase corrected version of the IR sequence. We use a 64 × 64 matrix SE_{544/44} scan, which adds approx-

FIG. 16. Glioma of the corpus callosum: double inversion recovery (DIR)_{3,000/1,200/100/44} (a) and spin echo (SE)_{1,500/80} (b) scans. The tumour is well demonstrated on both scans. Both fat and cerebrospinal fluid are suppressed in (a). The ventricular margin is better defined in (a).



670

G. M. BYDDER AND I. R. YOUNG

17a,b

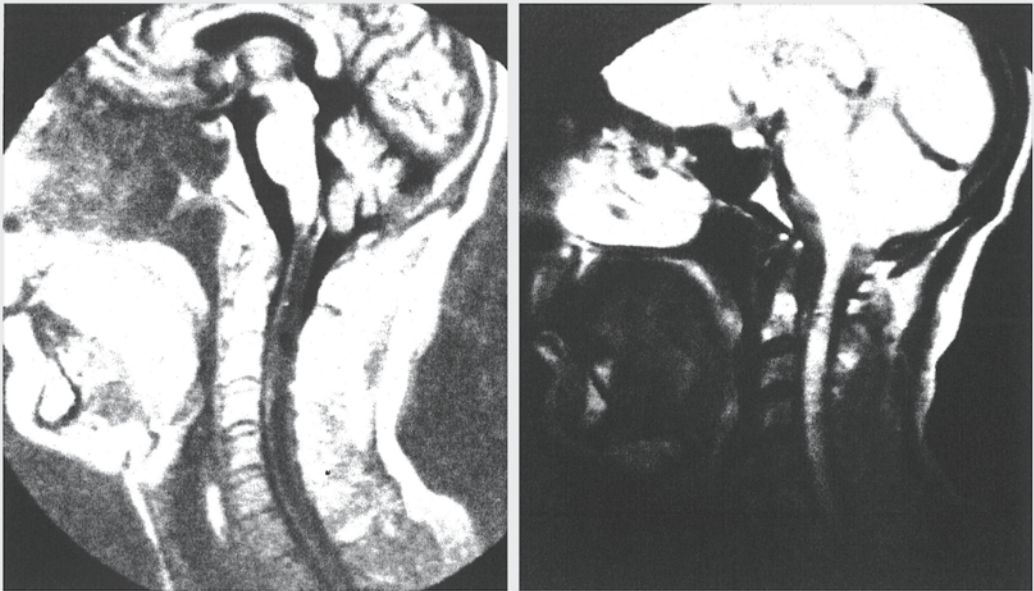


FIG. 17. Lymphoma of the cervical cord: inversion recovery (IR)_{1,500/500/44} (a) and spin echo (SE)_{1,500/80} (b) scans. Changes within the cord are better seen in (a).

imately 30 s to the imaging time. (d) Radiofrequency pulse calibration needs to be precise for the IR sequence since errors in the angle of rotation of the magnetisation produce a greater loss of tissue contrast than is the case with SE scans (16). This is a greater problem at high field where the loading of the transmitter coil is greater than that at low field. (e) The field echo data acquisition method is more susceptible to magnetic field inhomogeneity than the SE one. Again this problem is greater at high

field and limits the value of the short TE field echo data collection.

Advantages of the IR Sequence

As outlined in the introduction the range of possibilities with the IR sequence includes all the options available with both SE and PS scans. It is sensible to use these latter simpler scans in circum-

18a,b

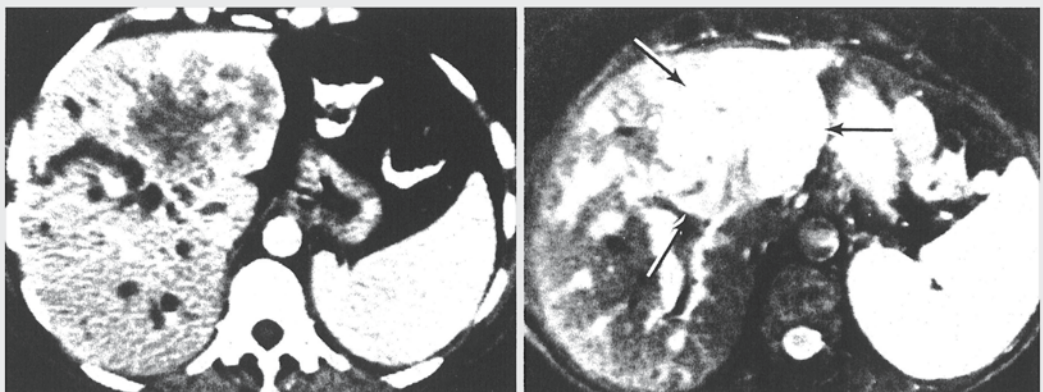


FIG. 18. Cholangiocarcinoma: contrast enhanced CT (a) and inversion recovery (IR)_{1,500/100/44} (b) scans. The extent of the tumour is well seen in (b) (arrows).

MR IMAGING: THE IR SEQUENCE

671

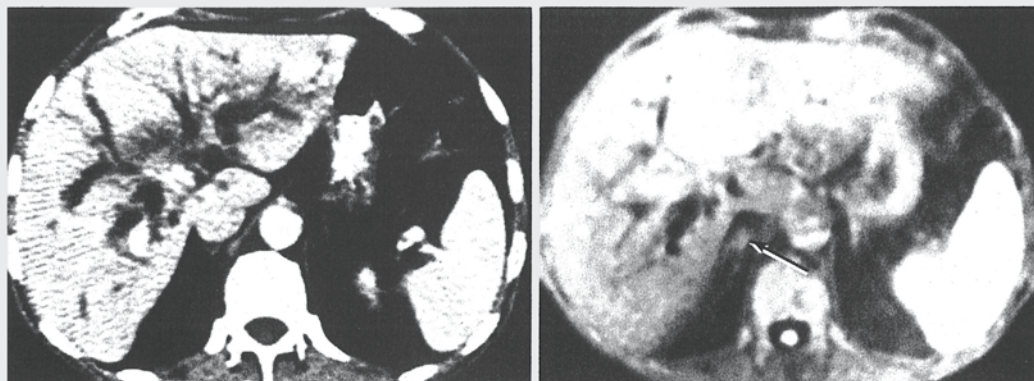


FIG. 19. Metastases from carcinoma of the colon: contrast enhanced CT (a) and double inversion recovery (DIR)_{3,000/1,200/100/44} (b) scans. Note the adrenal metastasis in (b) (arrow).

stances where there is no particular advantage in using the equivalent more complicated IR scan (e.g., for TI values in the region of 0–30 ms). However, there are many situations in which SE sequences may not provide the best imaging option.

Several particular applications of the IR sequence are worthy of emphasis, as detailed below.

Disease Detection in the Brain

The STIR sequences have a similar sensitivity to the corresponding SE sequences with IR_{1,500/80/44} approximately equivalent to SE_{1,500/80}. Although the IR sequences show greater grey-white matter contrast than the SE ones, the signal from CSF can be kept lower than that from brain by reducing TR or TI. Where the lesion is not periventricular and there is no problem with having the CSF signal greater than brain (or a benefit in having it greater), longer

values of TE, TR, and TI can be used. The advantage of the DIR sequence is that it allows longer values of these parameters to be used but keeps the CSF signal below that of brain to avoid confusion with partial volume effects in the periventricular region, which is a frequent site of relatively subtle pathology. This may be of particular value at higher fields where it is more difficult to obtain an SE sequence with a high level of lesion contrast and keep the CSF signal less than brain, because the TI of brain is closer to that of CSF.

Localisation of Lesions and Mass Effects

Although the T2 dependence of most medium TI IR sequences reduces their sensitivity in disease detection, the high level of grey-white matter contrast provides a series of interfaces of value in the localisation of lesions and assessment of mass effects.

20a,b

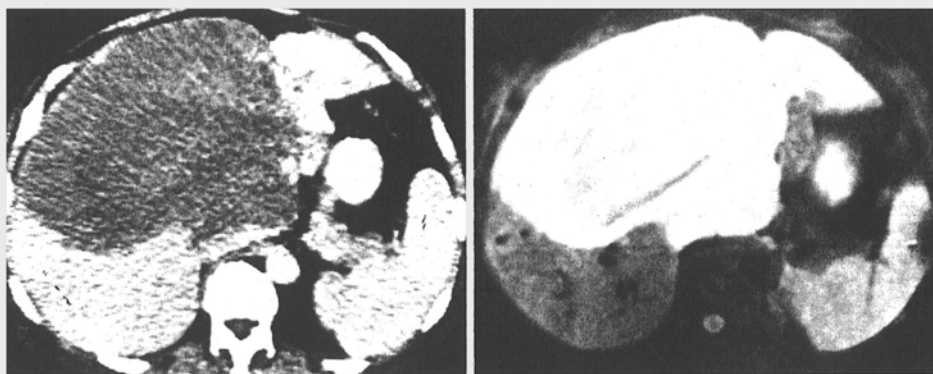
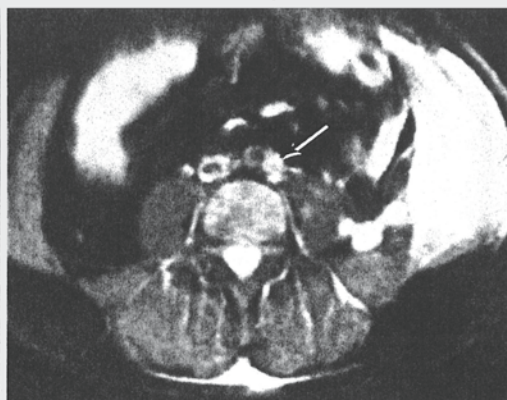


FIG. 20. Hemangioma with left lobe atrophy: contrast enhanced CT (a) and inversion recovery (IR)_{1,500/100/44} (b) scans. The atrophic left lobe is highlighted in (b).

672

G. M. BYDDER AND I. R. YOUNG

21a,b



21c,d

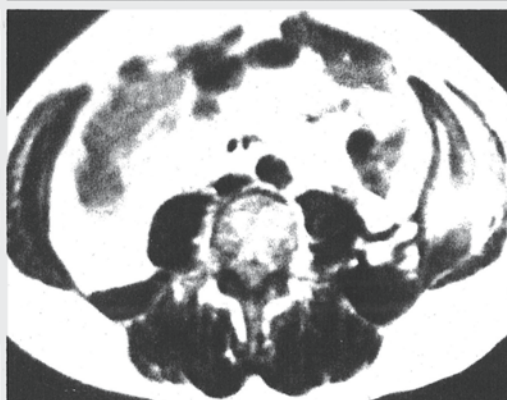
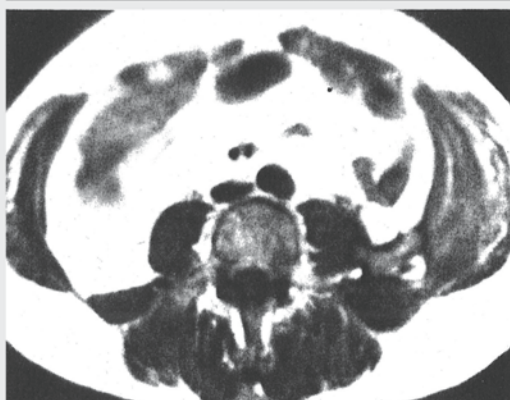


FIG. 21. Psoas abscess: contrast enhanced CT (a), inversion recovery (IR)_{1,000 100 44} (b), spin echo (SE)_{544 44} (c), and spin echo (SE)_{1,500 80} (d) scans. Changes to the abdominal wall and the fluid tracking posteriorly are best shown in (b) as is the paraaortic lymph node (arrow).

Pediatrics

The medium or long T1 IR sequences provide excellent demonstration of normal myelination as well as delays or deficits in this process. In addition, the fact that the T2 of the neonatal and infant brain is longer than that of adults means that IR sequences are less T2 dependent and therefore of more value in disease detection. The high water content of infantile brain (85–95%) means that oedema is often not so obvious and that oedema detection alone with an SE sequence is a less rewarding strategy in infants than adults. Age adjusted IR sequences are listed in Table 3, although in follow-up studies there is a dilemma in knowing whether to keep the sequence constant or adjust it for age.

Contrast Enhancement

Paramagnetic contrast agents produce the opposite effect to most disease processes; they decrease

both T1 and T2. The most sensitive sequence for detecting contrast enhancement is the medium T1 IR sequence (with T1 intermediate between the lesion T1 before and after contrast enhancement), with the short TE and short TR SE next best, and the long TE and long TR SE least sensitive (6,11,17). This may create a problem when long TE and long TR SE sequences are used for screening purposes since contrast agents (for example, gadolinium-diethylenetriamine pentaacetic acid) may not produce enhancement with this type of sequence. It is therefore necessary to perform an additional preenhancement scan of a different type if a contrast agent is used, so increasing the total time of examination.

Note that, with sequences such as the medium T1 IR and the SE with a short TE and short TR, there is usually an increase in signal intensity as the concentration of paramagnetic contrast is increased and this is followed by a decrease as the concentration is increased further (11).

MR IMAGING: THE IR SEQUENCE

673

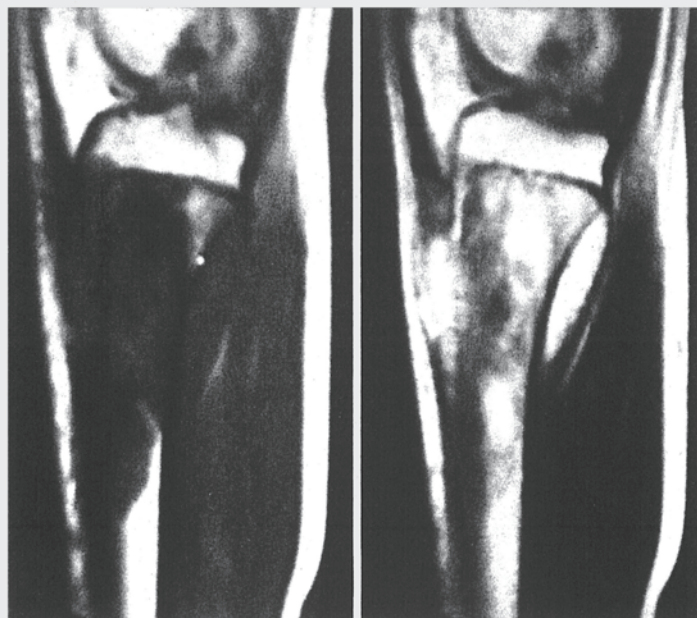


FIG. 22. Osteosarcoma: inversion recovery (IR)_{1,500/500/44} (a) and spin echo (SE)_{1,500/80} (b) scans. The extent of the tumour is better defined in (a).

Meningiomas and Other "Short T1 Short T2" Tumours

There are a number of tumours including meningiomas that may have a normal or only slightly increased T2 and a normal or low proton density. They usually have a T1 increased over white matter (17–20). With SE sequences there is very little T2 contrast to be exploited, but with medium TI IR sequences the low to normal proton density and slightly increased T1 both tend to reduce signal intensity producing lesion contrast with normal brain and providing better visualisation than with SE sequences (21,22). In addition this group of tumours may show a high level of contrast enhancement and this is best shown with medium TI IR sequences. Since meningiomas have a ubiquitous presentation and are important to exclude, this result has considerable significance in designing a routine screening strategy for MR imaging. The T2 dependence of the medium TI IR sequence, which is usually a significant disadvantage with malignant tumours, is not such a disadvantage with the type of tumour described above, since its T2 is normal or only slightly increased. The same general considerations apply to other tumours of this type (23).

Body Imaging

Although these are "noisy," there are a number of important advantages in using STIR sequences in imaging the body. (a) The T1 and T2 dependent

contrast after the 90° is *additive* so that loss of contrast with medium TI IR sequences is not a problem. (b) The STIR sequence provides a high level of tissue contrast using a relatively short TE. This is an advantage because the echo period (TE) in the SE component of the sequence is particularly vulnerable to degradation by motion. (c) The fat signal can be partially or completely suppressed. With long TE long TR SE sequences, the signal intensity of soft tissue lesions is usually increased but this unfortunately brings them into the normal range for fat and thus the margins of the lesion may be lost. This problem can be eliminated by suppressing the fat signal. (d) Much of the respiratory artefact arises from the fat of the anterior abdominal wall producing "ghosts" in the phase encoded direction of the image. Suppression of the fat signal produces a marked reduction in this problem although other techniques are also effective (24,25). We have found the technique of respiratory ordered phase encoding (26) useful in supplementing fat suppression techniques as the signal from spleen or ascites may still act as a source of artefact with STIR sequences. (e) At high fields, chemical shift artefact at the interfaces between fat and water can be a problem. Suppression of the fat signal controls this artefact. (f) Bowel labelling can be achieved with water although the option of using an oral paramagnetic contrast agent is useful to avoid ambiguity with tissues with a long T1 long T2. (g) With surface coils the fat layer adjacent to the coil is normally highlighted as a result of its close prox-

imity, producing difficulties in displaying the image. This is not a problem with fat suppression sequences. (h) In the body, IR sequences can be used to suppress both fluid and fat (DIR sequence) in situations where it is necessary to identify tumour in the presence of dilated bile ducts, to separate urine or cyst from renal tumour, and to control the signal from bowel contents. (i) The difference between the T1 of fat and that of other tissues increases with field, so that the signal intensity from tissues other than fat is relatively higher at higher fields when STIR sequences are used. The images therefore appear less noisy. The T1 of liver is close to that of fat so that it is difficult to obtain a high signal from liver with STIR sequences even at high fields.

The STIR sequence resolves many of the technical problems in MR imaging of the body although the images are noisy. These sequences appear similar to CT scans that have been windowed to show soft tissue except that with MR the level of soft tissue contrast is greater and calcified tissues are not seen. This resemblance corresponds closely to the pattern seen in the brain where MR images resemble CT but show better soft tissue contrast and little calcified tissue.

The theoretical analysis of the IR sequence has received excellent treatment in the literature (7,8,27–30) but little attention has been paid to the clinical application of this sequence, although favourable results have been reported in some specific clinical situations such as intracranial hemorrhage (31,32), brain stem MS (33), and liver disease (34). A notable exception to this general pattern has been the work of the Aberdeen group (35), which has used a medium T1 IR sequence with a good quality computed T1 map (the quality of a T1 map computed from IR images is usually better than that computed from two SE sequences of different TR). In many respects the T1 map functions like a STIR sequence giving a low signal intensity for fat and a high signal intensity for lesions with an increased T1. Clinically the Aberdeen group has formed a more favourable impression of body imaging with MR (36,37) than most other groups that have put the emphasis strongly on the nervous system. This may be because the Aberdeen sequence pattern is more suited to body imaging than the equivalent SE approach. The IR sequence has also been used more than usual by Droege et al. (28,29), who have also designed a pattern for screening in the brain using a long TE long TR SE sequence coupled with a short T1 IR sequence. This may prove a very worthwhile approach.

Acknowledgment: We are grateful to Dr. H. P. Niendorf of Schering A.G. for supply of Gd-DTPA and advice on its use. We are also grateful to the Medical Research Council and the Department of Health and Social Security for their continued support.

REFERENCES

1. Bailes DR, Young IR, Thomas DJ, Straughan K, Bydder GM, Steiner RE. NMR imaging of the brain using spin-echo sequences. *Clin Radiol* 1982;33:395–414.
2. Bydder GM, Steiner RE, Young IR, et al. Clinical NMR imaging of the brain: 140 cases. *AJR* 1982;139:215–36.
3. Doyle FH, Pennock JM, Banks LM, et al. Nuclear magnetic resonance (NMR) imaging of the liver: initial experience. *AJR* 1982;138:193–200.
4. Young IR, Bailes DR, Burl M, et al. Initial clinical evaluation of a whole body nuclear magnetic resonance (NMR) tomograph. *J Comput Assist Tomogr* 1982;6:1–18.
5. Johnson MA, Pennock JM, Bydder GM, et al. Clinical NMR imaging of the brain in children: normal and neurological disease. *AJNR* 1983;4:1013–26; *AJR* 1983;141:1005–18.
6. Carr DH, Brown J, Bydder GM, et al. Gadolinium-DTPA as a contrast agent in MRI: initial clinical experience in 20 patients. *AJR* 1984;143:215–24.
7. Kurtz D, Dwyer A. Isosignal contours and signal gradients as an aid to choosing MR imaging techniques. *J Comput Assist Tomogr* 1984;8:819–28.
8. Wehrli FW, MacFall JR, Shuttles D, Breger R, Herfkens RJ. Mechanisms of contrast in NMR imaging. *J Comput Assist Tomogr* 1984;8:369–80.
9. Bottomley PA, Foster TH, Argersinger RE, Pfeifer LM. A review of normal tissue hydrogen NMR relaxation time and relaxation mechanisms from 1–100 MHz: dependence on tissue type, NMR frequency, temperature, species, exercise and age. *Med Phys* 1984;11:425–48.
10. Young IR, Bailes DR, Bydder GM. Apparent changes of appearance of inversion-recovery images. *Magn Res in Med* 1985;2:81–5.
11. Gadian DG, Payne JA, Bryant DJ, Young IR, Carr DH, Bydder GM. Gadolinium-DTPA as a contrast agent in NMR imaging—theoretical projections and practical observations. *J Comput Assist Tomogr* 1985;9:242–51.
12. Meaney TF. Pulse timing for contrast in clinical imaging. In: *Scientific program and book of abstracts, Society of Magnetic Resonance in Medicine, third annual meeting, August 13–17, 1984, New York, NY*. Berkeley, CA: Society of Magnetic Resonance in Medicine, 1984:522.
13. Axel L. Surface coil magnetic resonance imaging. *J Comput Assist Tomogr* 1984;8:381–4.
14. Bydder GM, Butsen PC, Harman RR, Gilderdale DJ, Young IR. Technical note. Use of spherical receiver coils in magnetic resonance imaging of the brain. *J Comput Assist Tomogr* 1985;9:413–4.
15. Bydder GM, Curati WL, Gadian DG, et al. Use of closely coupled receiver coils in MRI: practical aspects. *J Comput Assist Tomogr* (in press).
16. Young IR. Considerations affecting signal and contrast in NMR imaging. *Br Med Bull* 1984;40:139–47.
17. Bydder GM, Kingsley DPE, Brown J, Niendorf HP, Young IR. Magnetic resonance imaging of meningiomas. *J Comput Assist Tomogr* 1985;9:690–7.
18. Araki T, Inouye T, Suzuki H, et al. Magnetic resonance imaging of brain tumors: measurement of T1. *Radiology* 1984;150:95–8.
19. Györfy-Wagner Z, England E, Larsson E-M, et al. T1 and T2 measurements in cerebral tumours and normal brain tissue. Presented at the European Society of Nuclear Magnetic Resonance in Medicine, Geneva, Switzerland, October 5, 1984.
20. Baierl P, Bauer M, Obermüller H. Measurements of relaxation times in intracranial tumours—an approach to tissue discrimination. Presented at the “MR 85” meeting Garmisch Partenkirchen, West Germany, January 24–27, 1985.
21. Li DKB, Robertson WD, Foche JS, et al. MR imaging in CNS tumors. *Radiology* 1984;153(P):85.
22. Zimmerman RD. MRI in intracranial meningiomas. In: *Scientific program and book of abstracts, Society of Magnetic*

MR IMAGING: THE IR SEQUENCE

675

- Resonance in Medicine, third annual meeting, August 13–17, 1984, New York, NY. Berkeley, CA: Society of Magnetic Resonance in Medicine, 1984:779.*
23. McKay IM, Bydder GM, Young IR. Magnetic resonance imaging of central nervous system tumors which do not display evidence of an increased T1 and T2. *J Comput Assist Tomogr* (in press).
 24. Ehman RL, McNamara MT, Pollack M, Higgins CB. Respiratory gated MRI: evaluation of technical approaches. In: *Scientific program and book of abstracts, Society of Magnetic Resonance in Medicine, third annual meeting, August 13–17, 1984, New York, NY. Berkeley, CA: Society of Magnetic Resonance in Medicine, 1984:210–1.*
 25. Runge VM, Clanton JA, Partain CL, James AE. Respiratory gating in magnetic resonance imaging at 0.5 tesla. *Radiology* 1984;151:521–3.
 26. Bailes DR, Gilderdale DJ, Bydder GM, Collins AG, Firmin DN. Respiratory ordered phase encoding (ROPE): a method for reducing respiratory motion artefact in magnetic resonance imaging. *J Comput Assist Tomogr* 1985;9:835–8.
 27. Bradley WG, Newton TH, Crooks L. Physical principles of nuclear magnetic resonance. In: TH Newton, DG Potts, eds. *Advanced imaging techniques*. San Anselmo, CA: Clavadel Press, 1983:15–61.
 28. Droege RT, Weiner SN, Rzeszutarski MS. A strategy for magnetic resonance imaging of the head; results of a semi-empirical model, part I. *Radiology* 1984;153:419–24.
 29. Droege RT, Weiner SN, Rzeszutarski MS. A strategy for magnetic resonance imaging of the head; results of a semi-empirical model, part II. *Radiology* 1984;153:425–33.
 30. Hendrick RE, Nelson TR, Hendee WR. Optimising tissue differentiation in magnetic resonance imaging. *Mag Res Imaging* 1984;2:193–204.
 31. Sipponen JT, Sepponen RE, Sivula A. Nuclear magnetic resonance (NMR) imaging of intracerebral hemorrhage in the acute and resolving phases. *J Comput Assist Tomogr* 1983;7:954–9.
 32. Sipponen JT, Sepponen RE, Sivula A. Chronic subdural hematoma: demonstration by magnetic resonance. *Radiology* 1984;150:79–85.
 33. Runge VM, Price AE, Kirshner HS, et al. Magnetic resonance imaging of multiple sclerosis: a study of pulse technique efficiency. *AJR* 1984;143:1015–26.
 34. Borkowski GP, Buonocore E, George CR, Go RT, O'Donovan PB, Meaney TF. Nuclear magnetic resonance (NMR) imaging in the evaluation of the liver: a preliminary experience. *J Comput Assist Tomogr* 1983;7:768–74.
 35. Mallard JR. The noes have it! Do they? *Br J Radiol* 1982;54:831–49.
 36. Smith FW, Mallard JR, Reid A, Hutchison JMS. Nuclear magnetic resonance imaging of liver disease. *Lancet* 1981;1:963–6.
 37. Smith FW, Reid A, Hutchison JMS, Mallard JR. Nuclear magnetic resonance imaging of the pancreas. *Radiology* 1982;142:677–80.

3 Ultrasound

- 3.1** Über die Möglichkeit, hochfrequente mechanische Schwingungen als diagnostische Mittel zu verwerten. *Zeitschrift gesamte Neurologie und Psychiatrie* 174 (1942): 153–168
K.T. Dussik 144
- 3.2** Application of echo-ranging techniques to the determination of structure of biological tissues. *Science* 115 (1952): 226–230
J.J. Wild, J.M. Reid 162
- 3.3** The use of ultrasonic Reflectoscope for the continuous recording of the movements of heart walls. *Kungl. Fysiografiska Sällskapets I Lund Förhandlingar* 24 (1954): 1–19
I. Edler, C.H. Hertz 170
- 3.4** The ultrasonic visualization of soft tissue structures in the human body. *Trans. Am. Clin. Climatol. Assoc.* 66 (1954): 208–223
J.H. Holmes, D.H. Howry, G.J. Posakony, C.R. Cushman, 193
- 3.5** Investigation of abdominal masses by pulsed ultrasound. *Lancet i* (1958): 1188–1195
I. Donald, J. MacVicar, T.G. Brown 213
- 3.6** Ultrasonic Doppler method for the inspection of cardiac functions. *J. Acoust Soc. Amer* 29 (1957): 1181–1185
S. Satomura 224
- 3.7** Neue Möglichkeiten der Ultraschalldiagnostik in der Gynäkologie und Geburtshilfe. *Fortschritte der Medizin* 84, 18 (1966): 689–693
D. Hofmann, H.-J. Holländer, P. Weiser 230
- 3.8** The prediction of fetal maturity by ultra-sonic measurement of the biparietal diameter. *J Obstet Gynecol Br Gwith* 76 (1969): 603–609
S. Campbell 236
- 3.9** Development of an ultrasonic system for three-dimensional reconstruction of the fetus. *J Perinat. Med.* 17 (1989): 19–24
K. Baba, K. Satoh, S. Sakamoto, T. Okai, S. Ishii 245

Introduction

The evolution of diagnostic ultrasonography has been the combined efforts of physicists, mechanical, electrical and bio-medical engineers, computer technologists, clinicians, sonographers, researchers, university and government administrators as well as adventurous and perceptive commercial enterprises. Diagnostic medical ultrasound had exclusively evolved from military technology used in mapping waves through liquid (Sonar by Richardson and Langévin, 1915-18), through air (Radar by Appleton and Watson-Watt, 1938) and through solids (pulse-echo method for non-destructive testing of metallic structures with the metal-flaw detector by Sokolov, 1940).

The association of ultrasonic with medicine dates from the late 1920s. Several investigation showed the biological effects of ultrasound on animal (Loomis, Wood 1927) and red blood cells (Johnson 1929). So it was obviously to start initially with its applications in therapy rather than diagnosis. Ultrasonic physiotherapy became popular in the 1930s and was used in the treatment of arthritic pains, gastric ulcers, eczema, asthma, thyrotoxicosis, hemorrhoids, urinary incontinence, elephantiasis and even angina pectoris.

The problems in detecting soft tissues with X-rays, particularly the brain, led the Austrian neurologist/psychiatrist Karl Theodore Dussik from the University of Vienna to develop an idea to locate brain tumors and the cerebral ventricles by measuring the transmission of ultrasound beam through the skull. He can be regarded as the first physician to have employed ultrasound in medical diagnosis. He and his brother Friedrich, a physicist, used a through-transmission technique with two transducers placed on either side of the head, and producing what they called "ventriculograms", or echo images of the ventricles of the brain. Later it could be shown that the images that Dussik produced were artifactual. In further experiments researchers at Siemens, Erlangen and the M.I.T. were able to show that the reflections within the skull and attenuation patterns produced by the skull were contributing to the attenuation pattern which Dussik had originally thought represented changes in acoustic transmissions through the cerebral ventricles in the brain. In conclusion, at this time ultrasound had no role to play in the diagnosis of brain pathologies.

Nevertheless, systematic investigation into using ultrasound as a diagnostic tool continued. In the late 1940s George Ludwig from Naval Research Institute in Bethesda, Maryland began experiments, exclusively for the Navy, on animal tissues using A-mode presentations of reflected echoes. Together with his collaborator F.W. Struthers he was able to detect gallstones and foreign bodies embedded in tissues.

The pulse-echo A-mode devices developed from the reflectoscope/ metal flaw detectors were soon employed in experiments on several medical diagnosis. Using an industrial Siemens "Reflectroscope," Inge Edler and Carl Hellmuth Hertz started in Lund, Sweden in 1953, their important cardiac investigations, which were followed on by Sven Effert in Germany in 1956. As head of the Department of Cardiology at the University Hospital, Lund, Inge Edler was responsible for evaluating the cardiac patients prior to the surgical repair of mitral stenosis. Edler finally established the characteristic motion pattern for the anterior leaflet of the mitral valve. He compared the shape of the fast-moving echoes in patients with enlarged hearts due to mitral stenosis during cardiac operations, and found empirically the shape correlated well with the severity of the stenosis. By early 1955, Edler had so much evidence of this relationship that he relied on ultrasound alone for the diagnosis of mitral stenosis. The typical time-motion patterns (M-mode) of other heart valves, pericarditis, tumors, and thrombosis in the left atrium showed up in the recordings and were identified by close cooperation with Dr. Olle Dahlback's heart surgery group. The advent of a barium titanate transducer

produced by Siemens in Germany in 1958 was an important advance for the group and enabled them to study not only the normal mitral valve but also many other heart structures. Sven Effert in Germany, who had been collaborating with Hertz in some of his work, further demonstrated the usefulness of M-mode echocardiography, which subsequently caught on as a mainstay investigation in cardiology.

In conclusion, the A-scan did not provide sufficiently accurate, reproducible and interpretable information to allow a firm diagnosis to be made. It would not have a lasting impact on clinical medicine without evolving into the B-scan, which had its origin in military radar.

In 1951 J.J. Wild and his collaborator J.M. Reid constructed the first B-mode echoscope that was ultimately used to visualize tumors by sweeping from side to side through breast lumps in patient scheduled for surgery. This first clinical B-mode instrument incorporated a water column that bathed the transducers and was sealed at the tip with condom rubber, providing the water-delay. Thus, this was indeed the very first hand-held contact scanner for clinical use. In May 1953 they produced real-time images at 15 MHz of a 7-mm cancerous growth of the breast.

In 1948 the radiologist Douglas Houwry started his pioneering ultrasonic investigations at the University of Colorado in Denver. His goal was to develop a new technique to display anatomical structures similar to the use of X-rays, and "in a manner comparable to the actual gross sectioning of structures in the pathology laboratory". He was able to demonstrate an ultrasonic echo interface between tissues, such as that between fat and muscle. Together with Joseph Holmes, the acting director of the hospital's Medical Research Laboratories, and the two engineers William Rodderic Bliss and Gerald J. Posakony, Howry constructed the first two-dimensional B-mode (or PPI, plan- position indication mode) linear compound scanner, and later on the motorized "Somascope", a compound circumferential scanner, in 1954. The transducer of the somascope was mounted on the rotating ring gear from a B-29 gun turret, which in turn was mounted around the rim of a large metal immersion tank and was filled with water. The machine was able to make compound scans of an intra-abdominal organ from different angles to produce a more readable picture. The PAN-Scanner, where the transducer rotated in a semicircular arc around the patient, was developed in 1957. The patient sat on a modified dental chair strapped against a plastic window of a semicircular pan filled with saline solution, while the transducer rotated through the solution in a semicircular arc. All of these systems, although capable of producing 2-D, accurate, reproducible images of the body organs, required the patient to be totally or partially immersed in water and remain motionless for a length of time. Lighter and more mobile versions of these systems, particularly with smaller water-bag devices or transducers directly in contact and movable on the body surface of patients, were urgently required.

Although much of the earliest interest in diagnostic ultrasound was directed towards the detection of foreign bodies, tumors or echocardiography, some of the most successful clinical applications were found in the field of gynecology and obstetrics. Ian Donald from the University of Glasgow's department of midwifery, Scotland, was the first physician in these fields. Like many other colleagues, Donald was introduced to military applications of ultrasound during wartime. Together with Tom Brown and John MacVicar and with support from the Kelvin & Hughes Scientific Instrument Company, he plunged into an intensive investigation into the value of ultrasound in differentiating between cysts, fibroids and any other intra-abdominal tumors that came their way. In 1957 Brown invented and constructed with Ian Donald the prototype of the world's first compound B-mode (PPI) contact scanner. The transducer operated at 2.5 MHz. The first contact B-scanner was designed and built by Tom Brown on the frame of a hospital bed-table. The 'bed-table' scanner was manually operated. A compound sector tech-

nique was used to build up a two-dimensional image with gray scaling. This was the world's first and only fully automatic scanner in order to give a consistent scanning pattern. Much of the early research was carried out with this machine.

Early results were disappointing and the enterprise was first greeted with a mixture of scepticism and ridicule. However, a dramatic case where ultrasound saved a patient's life by diagnosing a huge, easily removable ovarian cyst in a woman who had been diagnosed as having inoperable cancer of the stomach made people take the technique seriously. 'From this point', Ian Donald wrote, 'there could be no turning back'. Results eventually appeared in print in *The Lancet* of 7 June 1958 under the arid title "Investigation of Abdominal Masses by Pulsed Ultrasound". This was probably the most important paper on medical diagnostic ultrasound ever published.

The first application in medicine of the Doppler effect to the study of movement involved the measurement of the difference in the transit time between two transducers of ultrasound travelling upstream and downstream through flowing blood were demonstrated by Baldes et al in 1957. The Japanese physicists Shigeo Satomura and Yasuhara Nimura were the first to demonstrate the Doppler shift in the frequency of ultrasound backscattered by cardiac valvular motion and pulsations of peripheral blood vessels. In December 1955, Satomura published his first paper on the subject entitled "A new method of the mechanical vibration measurement and its application". In this paper he demonstrated that Doppler signals can be retrieved from heart movements when insonated with 3 MHz ultrasonic waves. In 1966, K. Kato and T. Izumi developed a directional flow meter using the local oscillation method. In 1967, the Rushmer group outlined the use of Doppler ultrasound in obstetrics in an article in *JAMA*, "Clinical Applications of a Transcutaneous Ultrasonic Flow Detector", which was confined basically to the detection of fetal life, placental location, blood flow through the uterine vasculature and fetal movements.

These early successes triggered a boom of new research and application of ultrasound especially in gynecology and obstetrics. A- and B-mode equipment were both in use. The A-mode scan had been used for early pregnancy assessment (detection of fetal heart beat), cephalography and placental localization. B-Mode placetography was successfully reported in 1966, in 1969 to measure the gestational sac diameters in the assessment of fetal maturity and in 1971 in relation to early pregnancy complications. Stuart Campbell described in 1968 the use of both the A- and B-mode scan to measure the fetal biparietal diameter. His method, described in his landmark publication "An improved method of fetal cephalometry by ultrasound," became standard for the next 10 years.

Using of the B-scan made an important technical improvement necessary. The storage or bi-stable cathode ray tubes that were used had a low dynamic range of about 16 decibels. Although there was good representation of size, shape and position, the images did not depict differences in echo amplitude. Gray-scaling was urgently necessary to expand the diagnostic capability and accuracy of a B-scan.

The most important innovation in ultrasound imaging subsequent to the invention of the compound contact scanner was the advent of the scan converter. In the mid-1950s machines such as that developed in Glasgow were actually gray-scale ready from the outset. Images could then be scaled, calipers moved and applied on-screen (something that had changed entirely the way measurements are made), gray-scaling applied to the images and the resultant image recorded on a variety of media including videotape, emulsion films and thermal printer devices. In 1964 the concept of the multi-element linear electronic arrays was first described by Werner Buschmann. Concepts of the real-time array (Bom 1971) and the phased-array scanning mechanism (Somer, 1968) paved the way for the concept of a linear-array system (Macovski, 1974)

The real revolution in diagnostic ultrasound started with the development of the real-time scanner at Siemens, Erlangen, Germany, by Walter Krause and

Richard Soldner together with Johannes Pätzold and Otto Kresse. This innovation soon completely changed the practice of ultrasound scanning. The manufactured "Vidoson" used three rotating transducers housed in front of a parabolic mirror in a water coupling system and produced 15 images per second. The image was made up of 120 lines and basic gray-scaling was present. The use of fixed-focus large-face transducers produced a narrow beam to ensure good resolution and image.

Fetal life and motions could clearly be demonstrated. D. Hofmann, H. Holländer and P. Weiser published its first use in obstetrics and gynecology in 1966 in the German language. Hofmann and Holländer's paper in 1968 on "Intrauterine diagnosis of hydrops fetus universalis using ultrasound" also in German, is probably the first paper in the medical literature describing formally the diagnosis of a fetal malformation using ultrasound. Hans Holländer, in another paper in 1968, demonstrated the usefulness of a 'real-time' scanner in the diagnosis of ovarian tumors which were not spotted on pelvic examination. Malte Hinselmann, using the Vidoson, demonstrated in 1969 the universal visualization of fetal cardiac action from 12 weeks onwards. The Vidoson was popular in the ensuing 10 years or so and was used in much scientific work published from centers in Germany, Switzerland, Austria, Belgium, Italy and other European countries.

Visualization of the fetus in 3-D has always been on the minds of many investigators. Kazunori Baba, at the Institute of Medical Electronics, University of Tokyo, Japan, first reported on a 3-D ultrasound system in 1984 and succeeded in obtaining 3-D fetal images by processing the raw 2-D images on a mini-computer in 1986. The images obtained were processed on elaborate computer systems. This approach successfully produced 3-D images of the fetus which were nevertheless inferior to those produced on conventional 2-D scanners. At the same time, to generate each 3-D image it took on an average some 10 min for data input and reconstruction, making the setup impractical for routine clinical use.

A 'technology push' situation further evolved when enhancement in diagnostic capabilities of scanners was propelled by the almost explosive advancements in electronic and microprocessor technology, most significantly in the 1980s and 1990s.

Part of this text was adapted from the website www.ob-ultrasound.net, with permission of Joseph Woo, MD, Hong Kong.

References

- Strutt JW, Third Baron Rayleigh: The Theory of sound, Volume 1+2 London Macmillan 1877
- Curie J, Curie P (1880) Développement par pression de l'électricité polaire dans les cristaux hémihédres à faces inclinées. C.R. Acad. Sci. Paris 91: 294
- Lippmann G (1981) Principe de la conversion de l'électricité. Ann. Phys. Chim. 24: 145.
- Curie J, Curie P (1881) Contractions et dilatations produites par des tensions électriques dans les cristaux hémihédres à faces inclinées. C.R. Acad. Sci., Paris 93: 1137
- Chilowsky CM, Langévin MP (1916) Procédés et appareil pour production de signaux sous-marins dirigés et pour la localisation à distances d'obstacles sous-marins. French patent no. 502913.
- Wood RW, Loomis AL (1927) The physical and biological effects of high-frequency sound waves of great intensity. Phys. Rev. 29: 373
- Langévin MP (1928) Les ondes ultrasonores. Rev Gen Elect 23:626.
- Sokolov SY (1929) On the problem of the propagation of ultrasonic oscillations in various bodies. Elek. Nachr. Tech. 6:454-460.
- Bergmann L (1937) Der Ultraschall. Stuttgart
- Pohlman R, Richter R, Parow E (1939) Über die Ausbreitung und Absorption von Ultraschall im menschlichen Gewebe und seine therapeutische Wirkung an Ischias und Plexus neuralgie. Deutsche Medizinische Wochenschrift 65: 251

- Pohlman R, Richter R, Parow E (1939) Über die Ausbreitung und Absorption von Ultraschall im menschlichen Gewebe und seine therapeutische Wirkung an Ischias und Plexus neuralgie. *Deutsche Medizinische Wochenschrift* 65: 251
- Dussik KT (1942) Über die Möglichkeit hochfrequente mechanische Schwingungen als diagnostisches Hilfsmittel zu verwerten. *Z Neurol Psychiat* 174: 153.
- Firestone FA (1945) The supersonic reflectoscope for interior inspection. *Met. Progr*, 48: 505-512.
- Ludwig GD, Struthers FW (1949) Considerations underlying the use of ultrasound to detect gall stones and foreign bodies in soft tissue. Naval Medical research Institute, Project MN 004-001, Report No. 4
- Dussik KT, Dussik F, Wyt L (1947) Auf dem Wege Zur Hyperphonographie des Gehirnes. *Wien. Med. Wochenschr.* 97: 425-429
- Ludwig GD, Struthers FW (1950) Detecting gall-stones with ultrasonic. *Electronics* 23 (2): 172
- Keidel W (1950) Über eine neue Methode zur Registrierung der Volumenänderungen des Herzens am Menschen. Sonderdruck aus der Zeitschrift für Kreislaufforschung, Heidelberg 39 Heft 9/10: 381
- Ludwig GD, Struthers FW (1950) Detecting gallstones with ultrasonic echoes. *Electronics* 23: 172-178
- Wild JJ, French LA, Neal D (1950) Detection of cerebral tumours by ultrasonic pulses. *Cancer* 4: 705
- Wild JJ (1950) The use of ultrasonic pulses for the measurement of biological tissues and the detection of tissue density changes. *Surgery* 27: 183-188
- Wild JJ, Neal D (1951) Use of high frequency ultrasonic waves for detecting changes in texture in living tissue. *Lancet* 1: 655
- Wild JJ, Reid JM (1952) Application of echo-ranging techniques to the determination of structure of biological tissues. *Science* 115: 226-230
- Howry DH, Bliss WR (1952) Ultrasonic visualization of soft tissue structures of the body. *J. Lab. Clin. Med.* 40: 579-592
- Howry DH (1952) The ultrasonic visualization of soft tissue structures and disease processes. *J. Lab. Clin. Med.* 40: 812-813
- Howry DH, Bliss WR (1952) Ultrasonic visualization of soft tissue structures of the body. *J. Lab. Clin. Med.* 40: 579-592
- Wild JJ, Reid JM (1952) Echographic studies on tumors of the breast. *American Journal Pathology* 28: 839-861
- Güttner W, Fiedler, G, Pätzold J (1952) Ultraschallabbildungen am menschlichen Schädel, *Acoustica Zürich Vol II*: 148-156
- Holmes JH, Howry DH, Posakony GJ, Cushman CR (1954) The ultrasonic visualization of soft tissue structures in the human body. *Trans. Am. Clin. Climatol. Assoc.* 66: 208-223
- Edler I, Hertz CH (1954) The use of ultrasonic Reflectroscope for the continuous recording of movements of the heart walls, *Kungl. Fysiografiska Sällskapets I Lund Förhandlingar* 24: 1-19
- Leksell L (1956) Echo-encephalography: Detection of intracranial complications following head injury. *Acta Chir. Scand.* 110: 301-315
- Mundt GH, Hughes WF (1956) Ultrasonics in ocular diagnosis *Amer. J. Ophthalmology* 41: 488-498
- Satumura S (1957) Ultrasonic Doppler method for the inspection of cardiac functions. *J. Acoust Soc. Amer.* 29: 1181
- Effert S, Erkens H, Große-Brockhoff F (1957) Über die Anwendung des Ultraschall-Echoverfahrens in der Herzdiagnostik. *Deutsche Medizinische Wochenschrift* 82: 1253-1257
- Wild JJ, Reid JM (1957) Current developments in ultrasonic equipments of medical diagnosis. *IRE Trans. Ultrason. Engng.* 5: 44-56
- Howry DH (1958) Development of an ultrasonic diagnostic instrument. *Am. J. Phys. Med.* 37: 234
- Donald I, MacVicar J, Brown TG (1958) Investigation of abdominal masses by pulsed ultrasound. *Lancet* 1: 1188-1195
- Donald I, Brown TG (1961) Demonstration of tissue interfaces within the body by ultrasonic echo sounding. *Br. J. Radiol.* 34: 539-546.
- Edler I (1961) Ultrasound -cardiography. *Acta Med. Scand. Suppl.* 370
- Donald I (1961) Ultrasonic radiations: Diagnostic applications. *Tools of Biological Research 3rd Series.* Blackwell Scientific Publications, Oxford. pp. 148-155.

- Franklin DL, Schlegel W, Rushmer RF (1961) Blood flow measured by Doppler frequency shift of back-scattered ultrasound. *Science* 134: 564-565
- MacVicar J, Donald I (1963) Sonar in the diagnosis of early pregnancy and its complications. *Br. J. Obstet. Gynaecol.* 70: 387-395
- Hofmann D, Höllander HJ, Weiser P (1966) Neue Möglichkeiten der Ultraschall Diagnostik in der Gynäkologie und Geburtshilfe. *Fortschr. Med.* 84: 689-693
- Hofman D, Mast H, Hollander HJ (1967) The importance of placenta localization by means of ultrasonics for amniocentesis. *Geburtsh Frauenheilk.* 27: 1199
- Krause W, Soldner R (1967) Ultrasonic imaging technique (B scan) with high image rate for medical diagnosis. *Electromedica* 4: 1-5
- Feigenbaum H, Zaky A, Nasser WK (1967) Use of ultrasound to measure left ventricular stroke volume. *Circulation* 35: 1092
- Rushmer R, Baker D, Johnson W, Strandness E (1967) Clinical Applications of a Transcutaneous Ultrasonic Flow Detector. *JAMA*, Jan 30, 199(5): 326-8
- Hofmann D, Hollander HJ (1968) Intrauterine diagnosis of hydrops fetus universalis using ultrasound. *Zbl. Gynaekol.* 90: 667-669
- Campbell S (1968) An improved method of fetal cephalometry by ultrasound. *Br. J. Obstet. Gynaecol.* 75: 568-576
- Ashitaka Y, Murachi K, Takemura H et al. (1968) Analysis of the fetal heart valve with the fetal electro-cardiogram, phonocardiogram and doppler signals. *Proceedings of the 14th Scientific Meeting of the Japan Society of Ultrasonics in Medicine.* 29-30. (in Japanese).
- Wells PNT (1969) A range-gated ultrasonic Doppler system. *Med. Biol. Eng.* 7: 641-652
- Campbell S (1969) The prediction of foetal maturity by ultra-sonic measurement of the biparietal diameter. *J Obstet Gynecol Br Cwlth* 76: 603
- Uchida R, Hagiwara Y, Irie T (1971) Electro-scanning ultrasonic diagnostic equipment. *Jap Med El.* 58: 1971. 141: 833
- Reid JM, Spencer MP (1972) Ultrasonic Doppler technique for imaging blood vessels. *Science.* 1972 16 176: 40 1235-6
- Hertz CH (1973) The interaction of physicians, physicists and industry in the development of echocardiography. *Ultrasound in Med. & Biol.*, Vol. 1: 3-11
- Kossoff G, Garrett WJ, Radovanovich G (1973) gray scale echography in Obstetrics and Gynaecology. Commonwealth Acoustic Laboratories, Report No. 59, Sydney, Australia.
- Watanabe H, Ingari D, Tanahashi Y et al. (1974) Development and application of a new equipment for transrectal ultrasonography. *J Clin Ultrasound* 2: 91-98
- Campbell S, Wilkin D (1975) Ultrasonic measurement of the fetal abdomen circumference in the estimation of fetal weight. *Br. J. Obstet. Gynaecol.* 82: 687-689.
- Hofmann D, Hollander HJ (1978) The application of the Vidoson Ultrasonic imaging unit in Gynaecology and Obstetrics. *Electromedica* 4: 103-105.
- de Vlieger M, Holmes JH, Kratochwill A, Kuzner E, Kraus R, Kossof G, Poujol J, Strandness DE (Hrsg.) (1978) *Handbook of clinical ultrasound*, John Wiley & Sons New York
- Feichtinger W, Kemeter P (1986) Transvaginal sector scan sonography for needle guided transvaginal follicle aspiration and other application in gynaec, routine and research. *Fertil. Steril.* 45: 722-725
- Baba K, Satoh K, Sakamoto S et al. (1989) Development of an ultrasonic system for three-dimensional reconstruction of the fetus. *J Perinat Med* 17: 1 19
- Cullen MT, Reece EA, Whetham J, Hobbins JC (1990) Embryoscopy: description and utility of a new technique. *Am J Obstet Gynecol* 162(1): 82
- King DL, King DL Jr, Shao MY (1990) Three-dimensional spatial registration and interactive display of position and orientation of real-time ultrasound images. *J Ultrasound Med* 9: 9 525
- Feichtinger W (1993) Transvaginal three-dimensional imaging. *Ultrasound Obstet Gynecol.* 3: 375
- Ritchie CJ, Edwards WS, Mack LA, Cyr DR, Kim Y (1996) Three-dimensional ultrasonic angiography using power-mode Doppler. *Ultrasound Med Biol* 22: 277-286
- Liang RI, Chang FM, Yao BL, et al. (1997) Predicting birth weight by upper-arm volume with use of three-dimensional ultrasonography. *Obstet Gynecol* 177(3): 632

3.1 Über die Möglichkeit, hochfrequente mechanische Schwingungen als diagnostisches Mittel zu verwenden

Karl Theodor Dussik (1908–1968)

Karl Theodor Dussik was born in Vienna, Austria, in January 1908. He graduated from the University of Vienna Medical School in 1931. From 1932 to 1938, he was psychiatrist and neurologist at the University of Vienna. He was later on made in charge of the clinic for diseases of the nervous system at the Allgemeine Poliklinik (General Polyclinic) in Vienna. Here, Dussik began his studies in ultrasonics during the late 1930s, working with his younger brother, the physicist Friedrich Dussik. It was a time when radar-technology was just in place and commercial metal flaw detectors had not even been invented. Ultrasound was just starting to be tested as a therapeutic tool in medicine, in European countries such as Germany and in the United States. Dussik was exploring the possibility of visualizing intracranial structures and making ventricular measurements with ultrasound waves. He soon became the first physician to apply ultrasound as a diagnostic method in human subjects.



At the beginning of the Second World War, when Austria was annexed by Germany in 1938, he left the country and moved to the United States, where he worked as attending psychiatrist from 1938 to 1941 at the now defunct Metropolitan State Hospital in Waltham, Massachusetts. On returning to Austria, Dussik set up experiments at the hospital at Bad Ischl, near Vienna, to image the human brain and ventricles with ultrasound, based on a two-dimensional representation of intensity attenuation of the ultrasound through human tissues. The Dussiks presented their experiments in 1942 and after the war in 1947, introducing the term “hyperphonography”.

They used a through-transmission technique with two transducers placed on either side of the head, producing what they called “ventriculograms”, or echo images of the ventricles of the brain. Coupling was obtained by immersing the upper part of the patient’s head and both transducers in a water bath, and the variations in the amount of ultrasonic power passing between the transducers were recorded photographically on photo paper as light spots. Their apparatus was quite elaborate with the transducers mounted on poles and railings (see below). Pulses of 1/10th second were produced at 1.2 MHz. The images produced were very rough two-dimensional images of rows of mosaic light intensity points. They had also reasoned that if imaging the ventricles was possible, then the technique was also feasible for detecting brain tumors and low-intensity ultrasonic waves could be used to visualize other internal organs of the human body.

In Dussik’s “ventriculograms” the image was thought to correspond to the shape of the lateral ventricles. These images were later thought to be artifactual by W. Güttner and others in Germany in 1952, as it was not quite possible to image the ventricles and intracranial tumors satisfactorily by such a through-transmission technique on account of the great absorption and reflection of ultrasonic waves by the skull bone. The images that Dussik obtained were found not to be true images of the cerebral ventricles.

Dussik’s work and images had led M. I. T. physician H. T. Ballantyne, physicist/engineer Richard Bolt, director of the newly established Acoustics Laboratory, and engineer Theodor Hueter from Siemens of Germany to investigate into similar techniques. Bolt, Ballantyne and Hueter obtained financial sup-

port from the Public Health Service and set up a project to evaluate the value of ultrasound as a diagnostic tool in neurology.

After some initial experiments which produced results similar to that of Dussik's, they put a skull in a water bath and showed that the ultrasonic patterns Dussik had been obtaining in vivo from the heads of selected subjects could be obtained from an empty skull.

It soon became apparent that the reflections within the skull and attenuation patterns produced by the skull were contributing to the attenuation pattern which Dussik had originally thought represented changes in acoustic transmissions through the cerebral ventricles. Further research in this area was subsequently terminated. The findings had prompted the United States Atomic Energy Commission to conclude that ultrasound had no role to play in the diagnosis of brain pathologies. Medical research in this area was apparently curtailed for the several years that followed.

After the mid-1950s, due to its ineffectiveness, the transmission technique in ultrasonic diagnosis was abandoned in medical ultrasound research throughout the world except for some centers in Japan, being replaced by the reflective technique which had received much attention in a number of pioneering centers throughout Europe, Japan and the United States. Karl Dussik, despite this, must be credited for being the first medical person to have applied ultrasound as a diagnostic tool, and in particular, in a planned and organized fashion. Douglas Gordon, a British ultrasound pioneer, in his book "Ultrasound as a diagnostic and surgical tool" published in 1964, expressly called Dussik the "Father of Ultrasonic Diagnosis".

After the war Dussik continued to work as director at the neurology department at the Salzkammergut Private Hospital at Bad Ischl, near Vienna. In 1949 he published the neurology treatise "Zentralnervensystem und Sauerstoffmangel-Belastung" (Central nervous system and hypoxic changes).

In 1952, Dussik hosted the International Medical Ultrasonic Congress at Bad Ischl and delivered John Wild's paper "15 Megacycle Pulsed Ultrasonic Reflection Studies on Biological Tissues" on behalf of Wild, who could not attend. Dussik moved to the United States again in 1953 and worked at the Boston Multiple Sclerosis Clinic of the Boston State Hospital and the Department of Physical Medicine and Rehabilitation of the Boston Dispensary (now the Tufts – New England Medical Center). He became involved with ultrasound used as a therapeutic tool in physical medicine. At the first American Institute of Ultrasound in Medicine (AIUM) scientific meeting in 1953 he presented a paper on the use of ultrasound in physical medicine and its diagnostic use in neurology. In his presentation he said about ultrasonic diagnosis: "*However complicated the problems may be the importance of these possibilities seems so great as to justify any and all efforts to overcome the technical difficulties.....*". His hope and vision seem to have reached fulfilment today.

In the following year, Dussik became a member of the executive committee of the AIUM. In 1958 he published his last paper on ultrasonic diagnosis: "Measurement of articular tissue with ultrasound" in the *American Journal of Physical Medicine*. He was re-elected to the Executive Board of the AIUM in 1963. Dussik continued to practise and collaborate in research in the field of psychiatry, in particular new drug treatments for schizophrenia. This included work in the late 1960s on thiothixene with renowned Boston neuro-chemist Samuel Bogoch.

Karl Dussik passed away in Lexington, Massachusetts, USA on 19 March 1968.

In part excerpted with permission from the website www.ob-ultrasound.net by Joseph Woo, MD, Hong Kong. Picture courtesy Joseph Woo, MD.

Über die Möglichkeit, hochfrequente mechanische Schwingungen als diagnostisches Hilfsmittel zu verwerten¹.

Von

Oberarzt (Kr.O.) Dr. Karl Theo Dussik,

dzt. Leiter einer Fliegeruntersuchungsstelle und Führer einer Lw.-San.-Staffel.

Mit 3 Textabbildungen.

(Eingegangen am 12. September 1941.)

Zu der Annahme, hochfrequente mechanische Schwingungen könnten auch medizinische Bedeutung erhalten, und zu dem Plane, ihre diagnostische Verwertung zu versuchen, wurde ich Ende 1937 durch einen kurzen Übersichtsartikel über Anwendung dieser Energieform in der Unterwasserschalltechnik zum Zwecke der Echolotung und bei der Prüfung von Werkstücken auf kleine Fehlerstellen angeregt. Der Durchführung meines Planes stellten sich erhebliche Schwierigkeiten entgegen, die in der Sache selbst, aber auch in äußeren Umständen lagen, weshalb sich eine Veröffentlichung bis heute verzögerte.

Vorliegende Untersuchung soll erstens die Frage zu klären versuchen, welche krankhaften Zustandsänderungen mit Hilfe der hochfrequenten mechanischen Schwingungen zu erkennen wären; zweitens ob eine Gefährdung eintreten kann und welche Bedingungen das praktisch zur Durchführung kommende Verfahren einhalten muß, um ohne Schädigung des Patienten genaue, verlässliche und doch einfach zu gewinnende Angaben am Menschen zu erhalten. Drittens erhebt sich die Frage der Indikation zu dieser Untersuchungsmethode, da aus physikalischen und anatomischen Gründen nur bestimmte Körpergegenden in Betracht kommen, zu denen der Hirnschädel und vielleicht auch die Wirbelsäule gehören dürfte. In diesen Gegenden könnten die durch das Verfahren erreichbaren Angaben praktischen Wert besitzen.

Einen physikalischen Überblick über dieses Gebiet zu geben, erübrigt sich. Heute liegen in den Monographien von *Bergmann* und *Hiedemann* sowie *Dognon* und *E. und H. Biancani* zusammenfassende Arbeiten vor, die jede Einzelheit leicht zugänglich machen. Eine Übersicht über das für den Arzt Wichtige gibt *Schliephake*. Ich kann mich daher darauf beschränken, die physikalischen Tatsachen nur soweit anzuführen, wie es zur Untersuchung der eben aufgestellten Fragen und zur Begründung der Ergebnisse nötig ist.

I.

Hochfrequente mechanische Schwingungen werden auch als *Ultraschall* bezeichnet. Die Frage nach der Art der durch sie erzielbaren diagnostischen Daten hängt zunächst von einer Reihe physikalischer

¹ Abgeschlossen am 1. Mai 1941.

Eigenschaften dieser Schwingungen ab, die in der Technik etwa seit der Jahrhundertwende (*Hiedemann*) eine Rolle spielen. Die Ultraschallwellen unterscheiden sich grundsätzlich von den elektromagnetischen Schwingungen, z. B. auch den Lichtwellen, dadurch, daß es sich beim Ultraschall um Schwingungen in einem elastischen Medium selbst handelt, daß es also zu periodischen Teilchenverschiebungen der durchschallten Substanz selbst kommt. Werden z. B. Schwingungen einer Saite erzeugt, so übernimmt die Luft diese Schwingungen und leitet sie zum menschlichen Ohr, wo sie den Eindruck eines um so höheren Tones hervorrufen, je rascher die Schwingungen erfolgen. Den höchsten hörbaren Ton vernehmen wir, wenn die Schwingungen etwa 20000mal in der Sekunde erfolgen, also bei einer Frequenz von rund 20000 Hz. Es können aber auch solche mechanische Schwingungen erzeugt werden, die eine weit höhere Frequenz haben und es ist nur in der Begrenztheit unseres Sinnesorganes gelegen, daß wir diese höherfrequenten Schwingungen nicht mehr hören, überhaupt nicht mehr unmittelbar wahrnehmen können. Die Wellenlänge λ dieser Schwingungen wird, wie aus der Beziehung $\lambda = c/f$ hervorgeht, mit steigender Frequenz f immer kürzer, sie ist ferner in Anbetracht der im Verhältnis zu den elektromagnetischen Schwingungen sehr geringen Geschwindigkeit c (nach *Bergmann* in Wasser Schallgeschwindigkeit etwa 1200 m/Sek.) wesentlich kürzer, als die gleichfrequenter elektromagnetischer Wellen, deren Geschwindigkeit bekanntlich rund 300000 km/Sek. beträgt. Bei der Frequenz, die wir bei unseren Versuchen meistens anwendeten (1500 kHz = 1500000 Schwingungen in der Sekunde), beträgt die Wellenlänge in Wasser

$$\lambda = c : f = 12 \cdot 10^2 \text{ m} : 15 \cdot 10^5 = 8 \cdot 10^{-4} \text{ m} = 0,8 \text{ mm.}$$

Diese Größenanordnung spielt bei dem Ausbau unserer Methodik eine Rolle; wir haben sie in einem entscheidenden Punkt zu berücksichtigen.

Die physikalischen Eigenschaften des Ultraschalls können in zwei Gruppen eingeteilt werden, und zwar in solche, die allen Schallwellen zukommen und in solche, die erst bei den höheren Frequenzen, also beim Ultraschall allein, auftreten. Die Eigenschaften der ersten Gruppe bedingen, daß die Gesetze der Akustik auch in den oberhalb des menschlichen Hörens gelegenen Frequenzen weitergelten, die auf allgemeine Gesetze des Hörschalls aufgebauten Erfahrungen — und solche spielen in der Medizin seit jeher eine Rolle — sind daher auch für die Anwendung des Ultraschalls von Bedeutung. Die Tatsache, daß seit *Auenbrugger* der Hörschall im Dienste der klinischen Untersuchung als diagnostische Hilfe nicht mehr wegzudenken ist, kann meines Erachtens nicht einfach als zufällig oder selbstverständlich genommen werden. Bei den Beziehungen zwischen krankhaften Veränderungen der Organe und Gewebe und ihren akustischen Eigenschaften, wie z. B. der Schalleitfähigkeit und der Resonanz, handelt es sich um einen Zusammenhang, der in bestimmtem Sinne tiefer bedingt ist, als z. B. der zwischen krankhaften Zustandsänderungen und dem für das Auge erfaßbarem Bilde.

mechanische Schwingungen als diagnostisches Hilfsmittel zu verwerten. 155

Wir schätzen nur deshalb im allgemeinen die optischen Daten wichtiger ein, weil wir als Menschen „Augentiere“ sind und gewöhnt sind, meistens optische Eindrücke für die Orientierung vorzuziehen. Wenn diese aber nicht mehr ausreichen, oder gar nicht mehr zur Verfügung stehen, greifen wir schon im gewöhnlichen Leben zu anderen Orientierungsmitteln und das gleiche tun wir bei der Perkussion und Auskultation. Wegen der souveränen alterprobten Geltung solcher alter Erfahrungen ist es gerade dann von Wert, sich ihrer zu erinnern, wenn wir komplizierte Apparate anwenden wollen. Fragen wir uns des Näheren, was für eine allgemeine Gesetzmäßigkeit in der Perkussion und Auskultation ausgenutzt wird, so ist die einfache Antwort, daß die krankhaften Vorgänge oft frühzeitig und verhältnismäßig stark gerade jene physikalischen Eigenschaften der Gewebe verändern, die die Schallphänomene beeinflussen, und daß zweitens der Schall in Tiefen dringt, die wir mit dem Auge nicht mehr erreichen können. Es handelt sich dabei offenbar um Veränderungen der Dichte des Gewebes, um seine Konsistenz, seinen relativen Wassergehalt und seine kolloidale Struktur. Über diese Eigenschaften der Gewebe und ihre Abweichung vom normalen Zustand könnte uns der Ultraschall Auskunft geben und damit würden nicht unwichtige Daten geliefert werden.

Ohne Zweifel hat der Hörschall für die Untersuchung auch eine Reihe objektiver Nachteile. Er ist weniger gut meßbar, folgt komplexeren Bedingungen und ist variabler als andere physikalische Daten. Akustische Erscheinungen sind auch im allgemeinen im physikalischen Sinne weniger gut reproduzierbar. Vor allem besteht kaum eine Möglichkeit, die Richtung zu bestimmen, die der Hörschall nehmen soll. Gerade in diesen Punkten kommen uns jene Eigenschaften des Ultraschalls zu gute, die erst bei höherer Frequenz auftreten. Bei den in der Medizin meist angewendeten Frequenzen bildet der größte Teil der hochfrequenten mechanischen Schwingungen einen *umgrenzten, gerichteten Ultraschallstrahl*, der sich geradlinig fortpflanzt. Durch Untersuchungen in verschiedenen Richtungen des Raumes können daher umschriebene Veränderungen der Schalleitfähigkeit gut lokalisiert werden. Die Reflexions- und Brechungserscheinungen stören dabei kaum. Die Möglichkeit der Verwertung der Echoerscheinungen analog der Verwendung als Echolot zur Bestimmung der Meerestiefen wird später noch besprochen.

Ultraschall kann zwar mit den Sinnen nicht unmittelbar wahrgenommen werden, sondern nur mittelbar an verschiedenen Wirkungen, z. B. an der auftretenden Wärme oder an mechanischen Folgen. Wie auf so vielen anderen Gebieten hat aber auch hier die moderne physikalische Forschung eine „Erweiterung unserer Sinne“ geschaffen, um mit dem von *Bernhard Bavink* in Ausführungen über den Erkenntnisprozeß in der Physik verwendeten Ausdruck zu sprechen. Dieser Aufgabe dienen verschiedene physikalische Verfahren, mit deren Hilfe sich Ultraschall verhältnismäßig einfach feststellen und messen läßt. Dadurch wird es

möglich, ein „Ultraschallfeld“ nach Frequenz, Geschwindigkeit, Wellenlänge und Amplitude, also Schallintensität, zu bestimmen. Diese physikalischen Größen sind untereinander mathematisch abhängig und werden außerdem durch das durchschallte Medium beeinflusst. Legen wir eine dieser physikalischen Größen, z. B. die Schallintensität, fest, nachdem sie ein gegebenes Medium, z. B. Wasser oder Öl eine bestimmte Strecke durchlaufen hat, und ändern nun das Schallmedium durch Einbringung eines Untersuchungsobjektes in das Wasser oder das Öl, und messen nunmehr wieder die Schallintensität in der gleichen Entfernung von der Schallquelle, so finden wir je nach dem Schallvermögen des Untersuchungsobjektes in dem durchschallten Bereich eine entsprechende Änderung der Schallintensität. Wir erhalten so ein relatives Maß für das Schalleitvermögen der durchschallten Objekte, ein Maß der bei dem bestimmten Objekt vorliegenden Schallabsorption. Man kann nun mit praktisch erlaubter Vernachlässigung einiger anderer Faktoren sagen, daß „die Absorption in einem bestimmten Medium mit der Schallfrequenz und der Viskosität des Mediums wächst und mit der Fortpflanzungsgeschwindigkeit und der Dichte des Mediums geringer wird“ (*Schliephake*). Bei gegebenen Größen des verwendeten Ultraschalls hängt also die Absorption von den Eigenschaften des durchschallten Objektes ab, wobei neben dem physikalischen Zustand auch bei verschiedenen untersuchten Stellen Dicke und Gestaltung der Schichten, aus denen das Gewebe sich aufbaut, sowie die Form des Objektes eine Rolle spielt. Prozesse, die die Dichte des Gewebes, also bestimmte Seiten des histologischen Aufbaues, den Wassergehalt und die kolloidale Struktur verändern, können sich daher in einer Veränderung der Schallabsorption anzeigen. Da die Perkussion und Auskultation seit alters her lehrt, daß der durch krankhafte Vorgänge erreichte Grad der Veränderungen der erwähnten physikalischen Eigenschaften ausreicht, sogar den Hörschall für das Ohr merkbar zu verändern, so ist die Annahme berechtigt, daß es durch Anwendung der viel empfindlicheren Ultraschallmethoden gelingen kann, praktisch verwendbare Angaben zu erzielen. Die Tatsache, daß die Kleinheit der Wellenlänge die Beugung gegenüber der strahlenförmigen, geradlinigen Ausbreitung der hochfrequenten mechanischen Schwingungen zurücktreten läßt, ermöglicht durch Untersuchungen in verschiedenen Richtungen des Raumes Abgrenzung und Lokalisation der Stellen umschriebener Veränderungen der Absorption.

II.

Wenden wir uns nun der Frage zu, welche Nebenwirkungen denkbar sind und ob und wie sich eine Gefährdung vermeiden läßt, so müssen wir einen Blick auf die biologischen Wirkungen des Ultraschalles werfen. Solche Wirkungen sind schon lange bekannt, als erster hat *Langevin* während des Weltkrieges beobachtet, wie kleine Fische getötet wurden, wenn sie in einen sehr intensiven Ultraschallstrahl gerieten, die er zu

mechanische Schwingungen als diagnostisches Hilfsmittel zu verwerten. 157

Unterwasserschallversuchen verwendete. Eine systematische Untersuchung der biologischen Einflüsse dieser Energieform setzte ein, als *Wood* und *Loomis* Beobachtungen an verschiedenen Einzellern und an roten Blutkörperchen veröffentlichten. *Dognon* und *Biancani* haben über dieses Gebiet eine Darstellung veröffentlicht, die über eigene Arbeiten und über solche von *Harvey* und *Loomis*, *Johnson*, *Schmitt* und *Uhlemayer* berichtet. Es wurde beobachtet, daß bei geringeren Energien trotz oft erstaunlich ausgesprochenen Veränderungen der mikroskopischen Struktur des Zellinneren die Wirkungen reversibel waren, während bei zunehmender Schallenergie eine Schwelle erreicht wird, von der ab irreversible Folgen eintreten. Sie fanden pathologisch-anatomisch nur am Muskelsystem Veränderungen («...dilacération et déchiquetage extraordinaire du tissu musculaire strié»), alle anderen Organe, auch das besonders genau an sehr lange bestrahlten Mäusen untersuchte Zentralnervensystem, erwies sich auch bei den durch Ultraschall getöteten Tieren autoptisch normal, auch Serienschnitte des Gehirnes. In diesem Zusammenhang ist ferner auf die Ergebnisse von *Gohr* und *Wederkind* hinzuweisen, die zeigten, daß durch Ultraschall sehr hoher Energien Fermente, Diastase, Pepsin und andere biologisch wichtige Stoffe, wie Insulin, Vitamin C, Ergosterin u. a. zerstört werden können. Die genannten Verfasser haben auch intra vitam und postmortal an Kaninchen durch sehr hohe Ultraschallenergie Schädigungen gesetzt.

Aus diesen Beobachtungen ergibt sich, daß Ultraschall keineswegs eine indifferente Energieform ist, sondern sehr wesentliche Wirkungen auf die lebende Substanz haben kann. Gerade die biologischen Versuche zeigen aber auch, worauf es ankommt, wenn Schädigungen vermieden werden sollen: wir müssen mit sehr kleiner Energie arbeiten, um jedenfalls unter der Schädigungsschwelle zu bleiben. Eine solche Schwelle ist ja schon deshalb von vornherein anzunehmen, da es sich bei den Kräften, die die Schwingungen bedingen, also Druck- und Temperaturverschiebungen sowohl in der Richtung der Erwärmung als auch der Unterkühlung sowie den daraus folgenden Wirkungen nicht um qualitativ neuartige Energien, sondern um solche Einflüsse handelt, denen die lebende Substanz allenthalben ausgesetzt ist und gegen die sie daher auch eine gewisse Widerstandsfähigkeit haben muß. Wegen der Trägheit der Protoplasmareaktion muß sich ferner der einzige neuartige Faktor, die hohe Frequenz, auch nicht ungünstig auswirken. Für die praktische Durchführung der Anwendung ergab sich allerdings die Frage, ob es ein Verfahren gibt, das so geringe Ultraschallenergien so genau nachzuweisen erlaubt, daß ohne Schädigung doch verwertbare Schlüsse ermöglicht werden. So wird die Frage, ob sich bei Vermeidung von Gefahren für den Patienten noch diagnostisch auszuwertende Daten ergeben, eine Frage des einzuschlagenden *speziellen Verfahrens*, dem wir uns daher nunmehr zuwenden.

Sowohl zur Erzeugung wie zum Nachweis von Ultraschall kennt die Physik eine ganze Reihe von Möglichkeiten. Wollen wir sehr hohe Frequenzen verwenden, was wegen der Gerichtetheit der höherfrequenten Ultraschallwellen gut begründet ist, so kommen von diesen verschiedenen Verfahren für die Erzeugung weder die mechanischen oder thermischen, auch weniger das magnetostriktive Verfahren in Betracht, sondern am ehesten das piezoelektrische Verfahren.

Der „piezoelektrische Effekt“ besteht darin, daß bei bestimmten Krystallen — vor allem kommen Quarz, Turmalin und Seignettesalz in Betracht — bei Druck oder Dehnung in krystallographisch ausgezeichneten Richtungen auf bestimmten Krystallflächen elektrische Ladungen auftreten. Dieser Effekt ist umkehrbar: wird ein solcher Krystall in der Weise in ein elektrisches Wechselfeld gebracht, daß die Feldrichtung mit der elektrischen Achse des Krystalls zusammenfällt, erfährt dieser in der einen Phase des Wechselstromes eine Dilatation und in der anderen Phase eine Kompression um den gleichen Betrag. Da Wechselströme in beliebiger Frequenz und Energie erzeugt werden können, ist es möglich, auf Grund dieses „reziproken piezoelektrischen Effektes“ auch Ultraschall beliebiger Frequenzen und auch beliebiger Energien — soweit dafür nicht durch die Festigkeit des Quarzes Grenzen gezogen sind — hervorzubringen.

Zur Untersuchung des Ultraschallfeldes nach Durchtritt durch das Untersuchungsobjekt kommen jene technische Prinzipien in Betracht, die mit kleinen Energien auskommen. Dieser Bedingung entsprechen wohl am besten das optische Verfahren sowie die Umkehrung der oben beschriebenen Ultraschallerzeugung, der piezoelektrische Nachweis.

Das optische Verfahren beruht darauf, daß Ultraschallwellen z. B. in einer durchsichtigen Flüssigkeit als optisches Gitter wirken und ein paralleles Lichtbündel, das senkrecht zum Ultraschallstrahl verläuft, beugen. An der Stärke der entstehenden Beugungsspektren läßt sich die Schallenergie ablesen. Das piezoelektrische Verfahren verwertet den direkten piezoelektrischen Effekt; ein piezoelektrischer Quarz, der diesmal als Indicator dient, formt die auf ihn auftreffenden Schallwellen in elektromagnetische Ladungen um, deren Stärke ein Maß für die Schallenergie darstellen.

Das optische Verfahren hat eine Reihe großer Vorteile; für eine rasche Orientierung ist aber doch das piezoelektrische Verfahren vorzuziehen, da es für unsere Zwecke in der Handhabung einfacher ist und vor allem rascher viele Werte verschiedener Stellen eines Objektes bestimmen läßt. Deshalb sind unsere Versuche viel öfters mit Hilfe des piezoelektrischen, als mittels des optischen Verfahrens ausgeführt worden, wobei sich zeigte, daß die Störungen, die aus der Rückwirkung des Indicatorquarzes auf das Schallfeld eintreten, offenbar nicht so groß sind, daß sie die Verwertbarkeit der Angaben entscheidend verringern. Es ist aber sehr gut möglich, daß in Zukunft das optische Verfahren mehr herangezogen wird.

So einfach an und für sich das Prinzip ist, sowohl für die Erzeugung als auch für den Nachweis des Ultraschalls den piezoelektrischen Quarz zu verwenden, so ist doch die Durchführung keineswegs ohne Schwierigkeiten möglich. Vor allem lassen sich die technischen Verfahren, die bisher auf diesem Prinzip aufgebaut sind, nicht ohne weiteres auf medizinische Angaben anwenden, besonders auch deshalb, weil sie besonders bei den medizinisch gegebenen Voraussetzungen nicht die Möglichkeit bieten, gut reproduzierbare Resultate zu erhalten. Wir waren daher

mechanische Schwingungen als diagnostisches Hilfsmittel zu verwerten. 159

gezwungen, für unsere Zwecke eine eigene Anordnung und ein spezielles Verfahren auszuarbeiten. An dieser Stelle ist es mir eine angenehme Pflicht, meinem Dank an Frau Dozent *Seidel* vom I. Physikalischen Institut der Universität Wien dafür Ausdruck zu geben, daß sie mir auf Grund ihrer besonderen Erfahrung auf dem Gebiete der Ultraschallforschung mit Rat und Kritik bei den ersten Schritten in dieses für den Arzt fremde Gebiet weitergeholfen hat. Ebenso danke ich dem Hochfrequenztechniker *C. Reisinger*, der mir bei der konstruktiven Ausgestaltung der Apparatur behilflich war. Ich konnte auch einen kleinen Kunstgriff finden, der durch Berücksichtigung der Wellenlänge eine ausreichende Reproduzierbarkeit der Meßergebnisse ermöglicht. Da eine genaue Beschreibung der Apparatur an anderer Stelle erfolgt, kann ich mich hier auf das Grundsätzliche beschränken.

Die durch das spezielle Verfahren technisch zu lösende Aufgabe war, die in einem Objekt bestehenden Absorptionsverhältnisse mit sehr kleinen Schallenergien für kleine Felder (z. B. 1 qcm) eines Untersuchungsobjektes zu bestimmen und die Ergebnisse mit Hilfe einer Registriermethode gut darzustellen, also ein anschauliches *Ultraschallbild* des Untersuchungsobjektes zustande zu bringen. Diese Aufgabe kann mit folgender Anordnung gelöst werden. Das Objekt befindet sich mit den zu untersuchenden Teilen in einem Wasserbad. In dem das Wasser fassenden Gefäß sind in zwei einander gegenüberliegenden Wänden Fenster angebracht, die nur mit einer dünnen Folie verschlossen sind. Je nach der Größe des Objektes kann entweder das ganze Wassergefäß in einem größeren Gefäß untergebracht werden oder es werden die den beiden Fenstern gegenüber angebrachten Quarze in einer Kapsel untergebracht. Jedenfalls müssen die beiden Quarze in isolierendem Öl untergebracht sein. Die gedachte Verbindungslinie zwischen den Quarzen

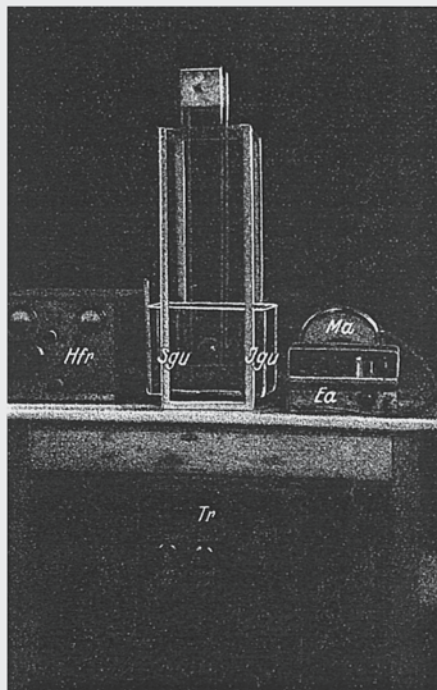


Abb. 1. Überblick über die Versuchsanordnung für kleine Objekte. [Die mit Lichtstrom betriebene Apparatur besteht aus einem Transformator *Tr*, einem Hochfrequenzgenerator *Hfr*, ferner aus dem Sendequarz *Squ* und dem Indicatorquarz *Iqu*, beide in entsprechenden Halterungen. Der am Indicatorquarz entstehende Wechselstrom wird in dem Empfängeraggregat *Ea* verstärkt, gleichgerichtet und der entstehende Gleichstrom mit dem Milliampèremeter *Ma* gemessen. Das zu untersuchende Objekt (hier ein Modell aus Wachs) wird zwischen Sender und Indicatorquarz gehalten und kann ebenso wie diese in allen drei Richtungen des Raumes verschoben werden.] Des besseren Überblicks halber ist auf der Abbildung ein Teil der Objekthalterung, der Registriereinrichtung sowie die Ölfüllung weggelassen.

geht durch die beiden Folien und durch die zu untersuchende Partie des Objektes. Objekt und beide Quarze können durch eine entsprechende Halterung in den drei Richtungen des Raumes verschoben und in jeder Stellung festgehalten werden. Auf der einen Seite befindet sich der Senderquarz, der durch das Wechselfeld eines Hochfrequenzgenerators zu den Schwingungen angeregt wird. Die dadurch entstehenden Ultraschallwellen bilden einen Strahl, der durch das Öl, die Folie der einen

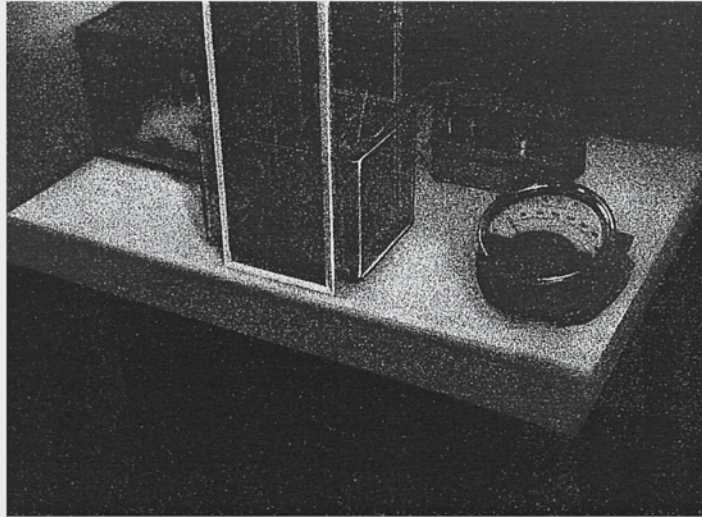


Abb. 2. Blick auf die Halterung der piezoelektrischen Quarze.

Seite in das Wasser und an das Objekt tritt, mit dem größten Teil der Schwingungen dieses geradlinig durchschallt und an der Gegenseite wieder austritt. Der Strahl geht wieder durch Wasser, Folie und Öl an den Indicator- oder Empfängerquarz, der die ankommenden Schwingungen übernimmt und sie in elektromagnetische Ladungen umformt. Der dadurch entstehende sehr schwache Wechselstrom wird einem Aggregat zugeführt, das nach Art eines Rundfunkempfängers arbeitet, den Strom durch geeignete Röhren verstärkt und gleichrichtet. Der gleichgerichtete Strom ist der Intensität des am Indicatorquarz ankommenden Ultraschalles direkt proportional, so daß wir in der an einem Milliampèremeter abzulesenden Teilstrichanzahl ein relatives Maß der Schallenergie, die am Empfängerquarz ankommt, haben. Wir stellen zuerst den „Leerwert“ der Apparatur fest, bringen dann zwischen Sender- und Empfängerquarz das zu untersuchende Objekt und untersuchen durch entsprechende Lageverschiebung Feld für Feld die durchgehende Ultraschallmenge, die von der Absorption im Objekt abhängt. Um reproduzierbare Werte zu erhalten, ist die Berücksichtigung der Wellenlänge erforderlich, wodurch dieses Ziel in ausreichender Weise erreichbar wird.

mechanische Schwingungen als diagnostisches Hilfsmittel zu verwerten. 161

Um die auf diese Weise erhaltenen Werte anschaulich zu registrieren, kann man entweder so vorgehen, daß man sie in eine Abbildung des Objektes feldweise einträgt oder daß man die Photographie zu Hilfe nimmt. Im ersten Falle wird das Maß der Absorption zweckmäßig dadurch sinnfällig gemacht, daß die betreffenden Felder durch eine Stufenleiter von Schwarz (vollständige Absorption, kein Schalldurchtritt) über Grautöne zunehmender Helligkeit (abnehmende Absorption, größer werdende Schallenergie am Empfängerquarz) bis zu Weiß (Durchtritt des gesamten zur Verfügung stehenden Schalles) gekennzeichnet werden. Zum Zwecke der automatischen Registrierung führt man den Gleichstrom nach der Messung einer Glühlampe zu, die um so mehr aufleuchten wird, je mehr Strom sie erhält. Bei gleicher Belichtungszeit in jedem Felde kommt es auf der photographischen Platte zu Schwärzungen, deren Kopie die gleiche relative Verteilung der Grautöne aufweist, wie eben beschrieben.

An Hand eines kleinen Beispiels mit leicht übersehbaren Formverhältnissen sei die praktische Ausführung im Prinzip demonstriert (Abb. 3 und Tabelle 1). Es handelt sich um ein Stück aus der rechten Hemisphäre eines normalen, in Formol gehärteten Gehirnes, in das von unten ein Ventrikelabschnitt reicht. Die Skizzen des Umrisses der basalen und vertikalen Schnittfläche mit dem eingezeichneten Umriss des Ventrikel-

abschnittes geben eine Vorstellung von den Formverhältnissen. Es wurde der unterste Streifen untersucht, der in sechs je ein Quadratzentimeter große Felder eingeteilt ist. Der Leerwert betrug 150 Teilstriche, die in den einzelnen Feldern gemessenen Werte sind aus der Tabelle zu entnehmen. Zum Zwecke der Kontrolle der Reproduzierbarkeit der Meßergebnisse wurden fünf Kontrollmessungen derart vorgenommen, daß nach Bestimmung der relativen Absorption in den sechs

basale Schnittfläche des Präparates

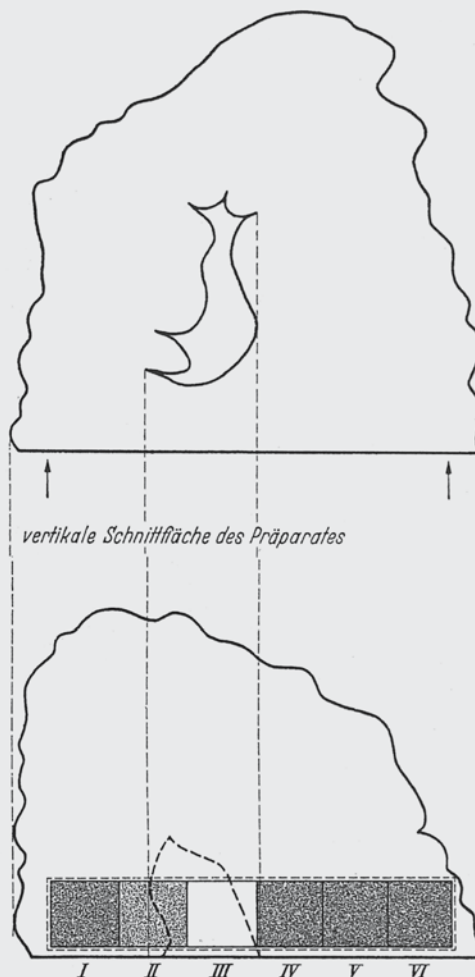


Abb. 3. Ultraschallbild, entsprechend dem Ergebnis der fünften Messung der Tabelle 1. Zur Übersicht eine Umrisskizze der basalen und vertikalen Schnittfläche des Präparates mit dem eingezeichneten Ventrikelschnitt. (Je heller das betreffende Feld im Ultraschallbild erscheint, desto mehr Schall wurde gemessen, desto geringer war also an dieser Stelle die Absorption.) Richtung des Ultraschallstrahles senkrecht auf die vertikale Schnittfläche (entsprechend den beiden kleinen Pfeilen).

Tabelle 1.

Meßergebnisse an einem 1 cm hohen Streifen eines in Formol gehärteten Stückes der rechten Hemisphäre eines normalen Großhirns bei fünf Kontrollmessungen.

Messung:	Feld:						
	I	II	III	IV	V	VI	
1.	50	50	90	50	30	60	Teilstriche
2.	55	70	80	55	35	55	„
3.	50	80	85	50	35	55	„
4.	60	85	85	55	35	55	„
5.	55	85	100	55	45	60	„

Feldern die Apparatur ganz ausgeschaltet wurde und nun die Messungen unter möglichst gleichen Bedingungen wiederholt wurden. Es zeigt sich, daß alle fünf Kontrollversuche die gleiche gut charakterisierte Verteilung der Werte zeigten. Im einzelnen differierten die Werte um Beträge unter 10 %, nur im zweiten Felde (zweite vertikale Reihe der Tabelle) ist die Streuung größer. Dies ist jedoch offenbar kein Meßfehler, sondern eine Folge der noch nicht exakt genug durchgeführten Halterung des Präparates. Im zweiten Felde wirkt sich der Umstand, daß nicht ganz genau das gleiche Feld wie bei dem vorhergehenden Versuch gemessen wird, wegen des Verlaufes der Ventrikelwand stärker aus. Die Werte der letzten Reihe von Kontrollmessungen sind relativ hoch, was mit der während der Versuche eingetretenen Temperaturerhöhung von 21,1 auf 22° zusammenhängt. Trotz dieser noch weit zu verringern den Fehler zeigt dieses kleine Beispiel doch, daß mit einem Blick ein guter Eindruck der Schallabsorptionsverhältnisse des vorliegenden Präparates aus dem Ultraschallbildchen zu gewinnen ist. (Soweit gemessen.)

Ultraschallbilder größerer Objekte setzen eine entsprechend gute Halterung voraus. Die Auffindung der gesetzmäßigen Beziehungen dieser Ultraschallbilder erfordert eine sehr große Reihe solcher Untersuchungen, die im Gange sind. Auch Vergleiche normaler und pathologischer Gewebe wurden bereits begonnen, worüber an anderer Stelle gemeinsam mit *I. Hofbauer* berichtet wird. Über die Absorption in normalem menschlichen Gewebe hat *Pohlmann* Untersuchungen mittels der Methode der Ultraschallwaage angestellt. Er bestimmte die „Halbwertschicht“ von Fett, Muskulatur und aus diesen zusammengesetzten Gewebepartien, mit der Fragestellung, für seine therapeutischen Versuche Anhaltspunkte über die Energie zu erhalten, die in der Tiefe liegenden Gebilde, wie z. B. der N. ischiadicus noch zugeführt bekommen. *Pohlmann* gibt an, eine überraschend geringe Absorption gefunden zu haben, die etwa den Werten einer stark absorbierenden Flüssigkeit entsprechen. Muskelschichten wiesen annähernd die doppelte Absorption auf, als Fettgewebe. Ferner hebt *Pohlmann* hervor, daß überraschenderweise die Absorption im Gewebe nicht frequenzunabhängig war, wie es eigentlich nach dem physikalischen Gesetz (a/v^2) erwartet werden müßte.

Es wurde weiters praktisch geprüft, ob sich mit diesem speziellen Verfahren auch tatsächlich Untersuchungen am Lebenden ohne Schädigungen durchführen lassen. Zu diesem Zwecke haben *I. Hofbauer*, *C. Reisinger* und Verfasser wiederholt Ultraschall von 1500 kHz und

mechanische Schwingungen als diagnostisches Hilfsmittel zu verwerten. 163

einer Energie, die gerade ausreichte, um ihn nach dem Wiederaustritt nachzuweisen, durch den eigenen Körper gehen lassen, solche mechanische Schwingungen schließlich auch quer durch den Schädel von Schläfe zu Schläfe geleitet, wobei wiederum gerade jene Energie verwendet wurde, die ausreichte, den Schall nach dem Wiederaustritt nachzuweisen. Bei dieser Energie war eigentlich überhaupt nichts zu spüren, es wurden auch keine schädlichen Folgen beobachtet. Der austretende Ultraschall war dabei nur in einem Felde nachweisbar, das dem Eintrittsfeld gegenüberlag, was durch die geradlinige Fortpflanzung des Ultraschallstrahles bedingt ist und diese auch für den Fall des Durchtritts durch den Schädel bestätigt. Diese Beobachtungen über die gute Verträglichkeit sehr kleiner Ultraschallenergien stimmt mit den Ergebnissen von Selbstversuchen *Pohlmanns* überein, von denen wir nachträglich Kenntnis erhielten. *Pohlmann* setzte seinen Daumenballen einem Ultraschallstrahl von 800 kHz unter Anwendung einer etwas größeren Energie als wir aus und hat ebenfalls keine schädlichen Folgen beobachtet, obwohl er wochenlang solche Bestrahlungen wiederholte.

In diesen Feststellungen liegt auch kein Widerspruch zu den Ergebnissen der biologischen Untersuchungen und zu denen von *Gohr* und *Wederkind*, die eine ganz wesentlich höhere (mindestens fünfzigfache) Energie anwendeten. Es handelt sich eben um eine Frage der Schallamplitude¹. Der Körper trägt bis zu einer bestimmten Schwelle die hochfrequenten mechanischen Schwingungen ebenso gut wie er z. B. auch hochfrequente Ströme trägt. Es ist trotzdem unbedingt notwendig, größte Vorsicht walten zu lassen und weitere Erfahrungen Schritt für Schritt zu sammeln. Es wäre aber ebenso verfehlt, wegen der bei den biologischen Versuchen beobachteten Schädigungen oder aus anderen Gründen vor Versuchen mit dieser Energieform zurückzuschrecken, wie es z. B. unrichtig wäre, wegen der Folgen eines Blitzschlages die elektrischen Untersuchungen der Nerven- und Muskel-erregbarkeit zu fürchten.

Zur Erläuterung einer anderen Möglichkeit, den Ultraschall zu diagnostischen Zwecken zu verwerten, soll zunächst die Frage besprochen werden, ob nicht auch die Echoerscheinungen einen brauchbaren Weg bieten könnten. Da dieser Weg in der Technik bei der Bestimmung der Meerestiefen die größte Rolle spielt, war es auch mein erster Gedanke, in Analogie dazu vorzugehen. Ich habe den Weg aber experimentell gar nicht beschritten, weil ich glaubte, daß bei den komplizierten Form- und Schichtverhältnissen im Körper so unübersichtliche Reflexionsverhältnisse herrschen dürften, daß bei der geringen Energie, die wir uns erlauben dürfen, klare Auskünfte nur sehr schwer erreichbar sein würden. Nun haben *Gohr* und *Wederkind* 1940 auf die Möglichkeit hingewiesen,

¹ Nach *Dognon* und *Biancani* ist noch ein guter Empfang möglich, wenn die am Empfängerquarz ankommende Vibration den Flüssigkeitsmolekülen Bewegungen erteilt, die 10^{-9} cm nicht überschreiten, also kleiner als die Molekülgröße sind.

die Ultraschallotung zu diagnostischen Zwecken, und zwar zur „Feststellung der Größe und Form innerer Organe und krankhafter Veränderungen (Tumoren, Exsudate, Abscesse usw.) zu verwenden“. *Gohr* und *Wederkind* meinen, dieser Weg zur Lagebestimmung sei durchaus beschreibbar und würde bei Anwendung geeigneter Wellenlängen sehr exakte Resultate ergeben, was eine wertvolle Ergänzung des Röntgenverfahrens bedeuten würde. Ergebnisse auf Grund dieser Annahme sind meines Wissens noch nicht bekanntgeworden. Auch *Schliephake* führt in der schon mehrfach zitierten Arbeit 1940 aus, daß sich „vielleicht auch diagnostische Möglichkeiten aus der Verwendung von Schall- und Ultraschallwellen ergeben könnten. Insbesondere käme eine Anpeilung von Verdichtungsherden, Tumoren usw. im Inneren des Körpers durch Erzeugung stehender Wellen in Frage, also eine Art verfeinerter Perkussion.“ Unser eigenes spezielles Verfahren ist von diesen beiden Vorschlägen grundsätzlich verschieden, da es mit dem Faktor der Absorption arbeitet, der bei diesen beiden Vorschlägen nicht herangezogen wird und vielleicht der einfachste ist.

Vorliegendes spezielles Verfahren stellt eine Modifikation jener Verfahren dar, die von der Technik bei der Werkstoffprüfung versuchsweise angewendet wurden, mußte jedoch für die medizinischen Aufgaben eigens adaptiert und in dem wichtigen Punkt der Reproduzierbarkeit der Meßergebnisse ausgestaltet werden. An Hand einer Erörterung dieser technischen Verfahren läßt sich dies noch näher erläutern, weshalb wir darauf kurz eingehen.

Bei den technischen Verfahren, die hier in Frage kommen, handelt es sich nach der Schilderung *Bergmanns* darum, mittels Ultraschall eine Prüfung größerer Werkstücke vorzunehmen, bei denen die Durchleuchtung mit Röntgenstrahlen nicht mehr möglich ist. Dadurch sollen Inhomogenitäten, wie Hohlräume, Risse usw. erkannt werden, da an solchen Fehlerstellen eine Reflexion oder Absorption der Ultraschallwellen stattfinden, demzufolge an der dem Schallgeber gegenüberliegenden Seite weniger Schallenergie austritt als an benachbarten Punkten. Als erster hat *Mühlhäuser* darauf aufmerksam gemacht, daß eine solche Möglichkeit gegeben wäre, die ersten praktischen Versuche hat *Sokoloff* an größeren Stahlstücken durchgeführt. Der Quarz wird an das Werkstück, dessen Flächen eben geschliffen werden müssen, angedrückt, die Schallwellen durchlaufen den Stahl und werden nach ihrem Austritt durch das optische Verfahren nachgewiesen. Zu diesem Zwecke werden die austretenden Schallwellen in eine Flüssigkeit geleitet, durch die im rechten Winkel zum Schallstrahl ein paralleles Lichtbündel geleitet wird. Die Schallwellen verursachen eine Beugung des Lichtes, die Intensität der Beugungsspektren läßt dann auf Inhomogenitäten im Innern des Werkstückes schließen. Für die praktische Durchführung ergeben sich aber große Schwierigkeiten (*Kruse, Bergmann*), insbesondere für eine serienweise Prüfung von Werkstücken. *Kruse* hebt drei Bedingungen hervor, die für einwandfreies Erkennen von Fehlerstellen nötig sind: erstens muß die verwendete Schallwelle im Inneren des Objektes kleiner sein als das kleinste zu erwartende Hindernis; zweitens muß die das Werkstück durchsetzende Schallenergie quantitativ und reproduzierbar einstellbar sein; drittens muß die hindurchgetretene Energie quantitativ und reproduzierbar meßbar sein. Die beiden letzteren Bedingungen seien schon sehr schwer und nur bei gut bearbeiteten Werkstücken erfüllbar, da schon kleine Inhomogenitäten ohne Bedeutung als Fehlerstellen Anlaß zu unerwünschten Beugungs- und Reflexionserscheinungen

mechanische Schwingungen als diagnostisches Hilfsmittel zu verwerten. 165

elektrischen Schallindikatoren gearbeitet, es zeigten sich jedoch auch hier praktisch wenig zufriedenstellende Resultate, da schon eine minimale Änderung der Frequenz oder eine etwas andere Anbringung des Schallgebers bewirken kann, daß die durch das Werkstück hindurchgetretene Energie von einem Maximum auf ein Minimum absinkt, ohne daß damit eine Verschiedenheit des Untersuchungsobjektes angezeigt würde. Ferner entstehen noch Schwierigkeiten durch das Auftreten stehender Wellen, durch die Mehrwelligkeit des Quarzes sowie durch die infolge gegenseitiger Beeinflussung einzelner Teilabschnitte hervorgerufenen Kopplungsschwingungen. — *Meyer* und *Buchmann* haben magnetostriktive Schallgeber verwendet, die an das Werkstück — eisenbewehrte Betonbalken — angekipst werden.

Eine Überlegung darüber, was diese bei der technischen Anwendung auftretenden Schwierigkeiten für unser Anwendungsgebiet bedeuten, muß davon ausgehen, daß unsere Aufgabenstellung wesentlich verschieden ist, vor allem der Größenordnung nach. Wir wollen nicht Fehler feststellen, die nach Zehntelmillimeter messen, da dies für unsere Aufgabe ohne Bedeutung wäre. Für uns handelt es sich um Gebiete, die mehrere Zentimeter messen und die außerdem nicht auf ein mehrere Meter großes Werkstück verteilt sind. Wir können ferner hoffen, auch bei weiter gezogenen Fehlergrenzen noch verwertbare Resultate zu erhalten, da es sich um Differenzen handelt, die schon den Hörschall beeinflussen und dann mit unserem Ohr unmittelbar zu erkennen sind. Auch besteht für uns nicht die Notwendigkeit, absolute Maße zu erhalten, wie sie den Physiker (bei anderen Untersuchungen) interessieren. Für uns genügen Vergleichsmessungen. Schließlich war es, wie oben erwähnt, möglich, eine Verbesserung der Reproduzierbarkeit der Meßergebnisse durch Anwendung eines kleinen Kunstgriffes zu erzielen.

Die zweite der unserer vorliegenden Untersuchung zugrunde gelegten Frage, wie sich eine Gefährdung vermeiden läßt und welche Bedingungen das zu wählende Verfahren einhalten muß, um ohne Schädigung genaue, reproduzierbare Angaben auf einfachem Wege zu liefern, ist somit grundsätzlich beantwortet. Die Prüfung der klinischen Anwendbarkeit ist Aufgabe weiterer, im Gange befindlicher Versuche.

III.

Eine erfolgreiche klinische Anwendung der hochfrequenten mechanischen Schwingungen setzt noch eine Abgrenzung der Indikation voraus, vor allem die Beantwortung der Frage, welche Körpergegenden sich für solche Untersuchungen eignen. Es muß nämlich noch auf eine Eigenschaft der Ultraschallschwingungen Bedacht genommen werden, die ihre Anwendung wesentlich einschränken dürfte. Ultraschall wird in gasförmigen Medien ganz wesentlich stärker absorbiert als in Flüssigkeiten und festen Körpern. Man erhält z. B. für Luft nach *Bergmann* bei gleicher Frequenz einen etwa 1700mal höheren Wert der Absorption als für Wasser. Infolgedessen muß dafür gesorgt sein, daß zwischen Senderquarz und Indicatorquarz die mechanischen Schwingungen auf ihrem Wege nirgends durch Luftschichten gehen. Da auch schon sehr kleine gasförmige Schichten wegen der an ihnen auftretenden Reflexion und

der hohen Dämpfung Ultraschall der verwendbaren Energiegröße praktisch vernichten, eine Steigerung der Energie sich aber wegen der Gefahr, an der Eintrittsstelle Schädigungen des Gewebes zu setzen, verbietet, kommen nur solche Körperteile und Organe für diese Untersuchung in Frage, bei denen keine lufthältigen Schichten passiert werden müssen. Damit fallen für unser spezielles Verfahren z. B. die großen Körperhöhlen weg. Ob die schon erwähnte, von *Gohr* und *Wederkind* vorgeschlagene Ultraschallotung oder die von *Schliephake* gedachte Ultraschallpeilung mit Hilfe stehender Wellen hier als Methoden einspringen können, kann von uns mangels Gelegenheit zu eigenen Untersuchungen nicht gesagt werden.

Es gibt jedoch ein Gebiet, das trotz dieser Einschränkung für Untersuchungen mit unserem Verfahren geeignete Bedingungen aufweist. Wir sehen dabei von den denkbaren Untersuchungen im Bereiche der parenchymatösen Organe (z. B. Leber, Nieren, Testes) sowie den Extremitäten und kleineren Fragestellungen ab, wenden uns vielmehr Untersuchungen im Bereiche des Hirnschädels und der Wirbelsäule zu. Hier liegen die anatomischen Verhältnisse günstiger, denn die lufthaltigen Nasennebenhöhlen und das Mittelohr mit den Mastoidzellen können durch entsprechende Wahl der Untersuchungsrichtungen umgangen werden. Außerdem ist es ohne weiteres klar, daß es eine Bedeutung für die neurologische Untersuchung hätte, wenn dadurch neue Möglichkeiten zu gewinnen wären, Aufschlüsse über Veränderungen der Konsistenz, der Elastizitätsverhältnisse und des kolloidalen Zustandes im Zentralnervensystem ohne chirurgischen Eingriff zu erhalten, die genau zu lokalisieren wären. Bei den bekannten Schwierigkeiten, röntgenologisch z. B. Tumoren im Schädelinneren nachzuweisen, die uns meist zu komplizierten Hilfsmethoden chirurgischer Art vor einer Operation zwingen, wobei wir dadurch außerdem meist nur annähernde Angaben über Art- und Ort diagnose erhalten, müßte hier ein Feld für die Anwendung unseres Verfahrens gegeben sein. Aber nicht nur Diagnose und Lokalisation der Tumoren und Abscesse, sondern auch andere Fragestellungen z. B. über Hirnödem und Hirnschwellung, sowie über beginnende und ausgesprochene Folgen von Gefäßerkrankungen und Kreislaufstörungen, sowie vielleicht auch über passagere Zustände bei Migräne und epileptischen Anfällen, sowie Reizversuche würden z. B. möglicherweise durch solche Versuche gefördert werden können, wobei es uns fernliegt, die Fülle von Schwierigkeiten zu übersehen oder auch übermäßige Erwartungen zu hegen oder auszusprechen. Es liegt in der Natur der Sache, daß die Versuche, die im Gange sind, langwierig und schwierig sind. Trotz der gerade bei diesen Untersuchungen bestehenden Unterschiede zwischen lebender und toter Substanz sind doch auch Aufschlüsse von der Untersuchung pathologisch-anatomischer Präparate zu erwarten, worüber an anderer Stelle gemeinsam mit *I. Hofbauer* berichtet wird, die diese Versuche teilweise selbständig weiterführte,

mechanische Schwingungen als diagnostisches Hilfsmittel zu verwerten. 167

Zum Schlusse sei noch kurz auf die Frage der therapeutischen Anwendung des Ultraschalls eingegangen. Schon *Langevin*, der den ersten Ultraschallgenerator für große Energien baute, hat an diese Möglichkeit gedacht und in den letzten Jahren sind auch eine Reihe von Arbeiten über dieses Problem erschienen. Dabei wurden teilweise auch Beobachtungen veröffentlicht, die ich bereits zitiert habe, obwohl sie mir bei Ausarbeitung unseres Verfahrens noch nicht bekannt sein konnten, jedoch — wie sich nachträglich für mich herausstellte — die Grundannahme gut stützten. Deshalb wurden sie auch im Zusammenhange der Darstellung geschildert und nicht etwa der Entwicklung entsprechend, die unsere eigenen Arbeiten genommen haben, nur von den eigenen Versuchen ausgegangen. In therapeutischer Hinsicht haben wir keine eigenen Beobachtungen gemacht. Für diese ergeben sich auf Grund der bisherigen Veröffentlichungen drei bisher bearbeitete Anwendungsgebiete. Erstens wurde versucht, Schwerhörigkeit mit Ultraschallwellen zu behandeln (*Hamm, Diesbacher, Frenzel* u. a., *Perwitzschki, Voß*). Das zweite Gebiet betrifft die Behandlung rheumatischer Erkrankungen, wie Neuralgien und Neuritiden (*Pohlmann, Freundlich, Söllner* und *Rogowski* und später andere). Drittens wurde versucht, verschiedene Substanzen durch Ultraschall in die Haut einzubringen (*Florstedt* und *Pohlmann*). Es war nämlich festgestellt worden, daß die Diffusionsvorgänge durch Ultraschall gesteigert werden (*Frenzel, Hinsberg* und *Schultes*), was auch in anderem Zusammenhange bemerkenswert ist. Es werden Erfolge berichtet, die auch dazu geführt haben, daß z. B. die Firma Siemens & Reiniger Ultraschallapparate zwecks therapeutischer Verwendung des Ultraschalls in den Handel gebracht hat.

Wir können nicht entscheiden, ob durch diese Anwendungsarten des Ultraschalls die Verfahren, an die sich die beiden letzten Anwendungsgebiete anschließen, also die Diathermie und Kurzwellendiathermie einerseits und die Jontophorese andererseits durch die Anwendung hochfrequenter mechanischer Wellen übertroffen oder ergänzt werden. Unseres Erachtens ist die Anwendung des Ultraschalls besonders insofern aussichtsreich als seine speziellen physikalischen Eigenarten ausgenützt werden können. Ebenso wie wir an die Anwendung im Bereiche der großen Körperhöhlen, wo überdies das Röntgen Lokalisation und Diagnose so gut ermöglicht, keine besonderen diagnostischen Hoffnungen auf den Ultraschall setzen, sondern mehr auf solche Gebiete, wo wie beim Zentralnervensystem der Röntgendiagnostik gewisse Schwierigkeiten entgetreten, in ähnlicher Weise halten wir es auf therapeutischem Gebiete für aussichtsreicher, speziellere Indikationen festzulegen und zu befolgen. Dafür geben bereits die experimentellen Ergebnisse über die Beeinflussung verschiedener Bakterien- und Virusarten (so der Lyssa-Poliomyelitis- und Fleckfiebererreger sowie der Vaccine), worüber eine Reihe von Arbeiten von *Kasahara, Takahashi, Blinkin* u. a., *Hirohashi, Williams* und *Gaines* sowie *Hopwood* u. a. be-

168 K. Th. Dussik: Über die Möglichkeit, mechanische Schwingungen zu verwerten.

Beeinflussung der kolloidalen Struktur der Zellen und Gewebe oder an die gefäßerweiternde Wirkung des Ultraschalls anschließen. Dasselbe gilt für die Beobachtungen über die Beeinflussung des Hühnersarkoms (*Namikawa*) und des Rattensarkoms (*Hirohashi* und *Hayashi*). Wir glauben jedenfalls, daß bei aller berechtigten Skepsis das Urteil verfrüht wäre, zu dem *Gohr* und *Wederkind* kommen, es seien therapeutische Anwendungen des Ultraschalls wahrscheinlich nicht möglich. Die Antwort auf alle diese Fragen kann nur das Experiment geben, zu dem für mich derzeit leider nur eine beschränkte Möglichkeit besteht.

Zusammenfassung.

1. Angeregt durch einen Bericht über die Anwendung des Ultraschalles in der Technik wurde untersucht, ob die hochfrequenten mechanischen Schwingungen als diagnostisches Hilfsmittel verwertbar wären. Es wurde gefolgert, daß diese Energieform Angaben über Zustandsänderungen der Gewebe und deren Lokalisation ermöglichen könnten.

2. Weiters wurden die Bedingungen erörtert, die ein Verfahren einhalten muß, um ohne Schädigung genaue, verlässliche Angaben bei einfacher Handhabung zu liefern. Es konnte ein Verfahren für die speziellen Aufgaben der diagnostischen Untersuchungen ausgearbeitet werden, das diese Bedingungen erfüllt.

3. Für die Untersuchung kommen nur bestimmte Körperteile in Frage, zu denen der Hirnschädel und die Wirbelsäule gehören dürften. Die hier zu gewinnenden Angaben könnten praktischen Wert haben.

Verzeichnis des Schrifttums.

Bergmann, L.: Der Ultraschall. 2. Aufl. Berlin: VDI-Verlag 1939. — *Blinkin, Polotzki u. Inosemzeva*: Z. Mikrobiol. **1940**, 132. — *Diesbacher*: Mschr. Ohrenheilk. **1932**, H. 11, 66. — *Dognon, E. et H. Biancani*: Ultrasons et biologie. Paris: Gauthiers-Villard 1937. — *Florstedt u. Pohlmann*: Z. exper. Med. **107**, 212 (1940). — *Frenzel, Hinsberg u. Schultes*: Z. Hals- usw. Heilk. **31**, **34** (1934). — Z. exper. Med. **89**, 24 (1933); **96**, 811 (1935). — *Freundlich, Söllner u. Rogowski*: Klin. Wschr. **1932 II**, 1512. — *Gohr u. Wederkind*: Klin. Wschr. **1940 I**, 25. — *Hamm*: Klin. Wschr. **1931 II**, 2262. — Mschr. Ohrenheilk. **1932**, H. 11, 66. — *Hayashi*: Jap. J. med. Sci. Trans. III, Biophysics **5**, 162 (1938). — *Hiedemann*: Grundlagen und Ergebnisse der Ultraschallforschung. Berlin: W. de Gruyter & Co. 1939. — *Hopwood, Salaman and McFarlane*: Nature (Lond.) **144**, 377 (1939). — *Kasahara u. a.*: Mschr. Kinderheilk. **72**, 8 (1938); **73**, 11 (1939). — Klin. Wschr. **1939 II**, 971; **1940 I**, 817. — *Kruse*: Akust. Z. **4**, 153 (1939). — *Langevin*: Zit. nach *Bergmann u. Dognon u. Biancani*. — *Meyer u. Buchmann*: Akust. Z. **3**, 132 (1938). — *Mühlhäuser*: DRP. Nr 56958 (1931). — *Namikawa*: Jap. J. med. Sci. Trans. III, Biophysics **5**, 162 (1938). — *Perwitschki*: Arch. Ohrenheilk. **136** (1933). — *Pohlmann*: Umsch. (1939) **43**, 725; (1940) **44**, 225. — Physik. **2**, **40** (1939) 159. — *Pohlmann, Richter u. Parow*: Dtsch. med. Wschr. **1939 I** 251. — *Rogowski u. Söllner*: Z. physik. Chemie A **166**, 428 (1933). — *Schliephake*: Med. Welt **1940**. — *Sokoloff*: Zit. nach *Bergmann*. Techn. Phys. USSR **2**, 522 (1935). — *Takahashi*: Science (N. Y.) **79**, 415 (1935). — *Voß*: Arch. Ohr- usw. Heilk. **135**, 258 (1932). — *Williams and Gaines*: J. inf. Dis. **47**, 458 (1930). — *Wood and Loomis*: Physiologic. Rev. **II 29**, 373 (1927).

3.2 Application of echo-ranging techniques to the determination of structure of biological tissues

John Julian Wild (born 1914)

John Julian Wild was born on 11 August 1914 in Kent, England and received his early education in London. He received a BA degree from Cambridge University in 1936 and an MA degree in 1940. In 1942, he received his MD degree from Cambridge University. In 1971 Wild got his PhD from Cambridge University Faculty of Investigative Medicine.

From 1942 to 1944, Wild was a staff surgeon at Miller General, St. Charles, and North Middlesex hospitals in London. In 1944, he joined the Royal Army Medical Corps and attained the rank of major; he served in the corps until 1945. He was elected a member of the Royal Society of Medicine in 1944.

After World War II (1939–1945), Wild emigrated to the United States. Until 1951, he was a fellow in the Department of Surgery at the University of Minnesota, Minneapolis. In the spring of 1949, Wild, supported by a U.S. Public Health Service surgical fellowship, started working on bowel failure. He had previously become interested in treating bowel distension or bloating at the Miller General Hospital, Greenwich, during World War II when the condition became common, and often fatal, following bomb blast from buzz-bombs. Working with similar surgical bloating conditions in Minneapolis he needed to measure the changes in thickness of the bowel wall in living, distended patients in order to select the best treatment. For this purpose, pulse-reflective ultrasound was considered a possibility. Furthermore he discovered differential ultrasonic properties of stomach cancer (1949).

Available commercial non-destructive testing equipment, developed by Donald Sproule in England and Firestone in the United States for detecting cracks in tank armour plate, operated at too low a frequency to achieve the theoretical resolution required for bowel wall measurement. Between 1950 and 1951, Wild's collaboration with Lyle French at the department of neurosurgery in making diagnosis of brain tumors using ultrasound also showed that method was not very useful.

A much more sophisticated piece of ultrasonic equipment developed during wartime to train flyers to read radar maps of enemy territory lay almost idle at the World-Chamberlain Naval Air Base in Minneapolis, Minnesota. This equipment operated at 15 m/c. Wild gained access to this equipment and with the help of Donald Neal, in technical charge, quickly confirmed the possibility of measurement of living bowel wall thickness at 15 m/c frequency. Further experimenting with a surgical specimen of cancer of the stomach wall brought forth the then completely novel concept, by Wild, of using pulse-echo ultrasound for tumor diagnosis and detection. This concept of the possibility of applying pulse-echo ultrasound usefully to medicine was skeptically received by the exact disciplines.

In February 1950 Wild's landmark paper "The use of ultrasonic pulses for the measurement of biologic tissues and the detection of tissue density changes" was published in "*Surgery*". This paper was received for publication 14 November 1949 and it was the first in the literature for the discovery of ultrasonic detection of cancer growth.

More and more proof of differential sonic energy reflection by tumor-disorganized soft tissues was gained by subjective comparison of the graphical time-amplitude (A-mode) trace pairs obtained from control and diseased tissues. Work



at the naval air base was concluded early in 1951 with examination of a clinically non-malignant nodule and a clinically malignant nodule of the living, intact human breast.

These further results were published in the "*Lancet*" in March 1951. Wild now envisioned the exciting possibility of non-invasive ultrasonic diagnosis and even detection of early cancer at accessible sites. He had two common sites in mind, the breast and the colon. Donald Neal was soon deployed to regular naval services at the naval air base after the Korean war. In mid-1950, financed by the National Cancer Institute of the U. S. Public Health Service, Wild and John Reid, a recent graduate electrical engineer, had begun working together as an interdisciplinary team. By early 1951 they had built the first hospital "echograph" on wheels and used it at 15 m/c to gain increasing subjective clinical evidence of differential sonic energy reflection by neoplastic tissues. Analysis of a series of clinical A-mode records of breast tumors by Wild revealed a statistically valid, objective index of sonic energy return from neoplastic tissue as compared to that of control tissue.

Real-time gross anatomical cross sectional images of Wild's arm were obtained by application of this first self-contained small parts scanner. He produced the first two-dimensional ultrasonic (B-mode) visual images in real time of the living arm and breast tumours. This work was published in a lead article in "*Science*" in February 1952 (115:226-230), and preceded Howry's first publication of laboratory images by 7 months.

Wild and Reid then built a linear B-mode instrument, a formidable technical task in those days, in order fully to visualize tumors by sweeping from side to side through breast lumps. In May 1953 this instrument produced a real-time image at 15 m/c of a 7-mm cancer of the nipple in situ, providing direct visual proof of the claimed differential sonic reflection. In 1954 Wild presented his work in a lecture at Middlesex Hospital in London, and to such notables as Prof. Mayneord at the Royal Marsden Hospital and Prof. Chassar Moir at Oxford, catalyzing work already in progress. Among the audience was also Dr. Ian Donald, who later was to become one of the most important pioneers in diagnostic ultrasonography. Wild's findings were independently confirmed in Japan in 1956 by Toshio Wagai.

By 1956, Wild and Reid had examined 117 cases of breast pathology with their linear real-time B-mode instrument and had started work on colon tumor diagnosis and detection. Analysis of the breast series showed very promising results for pre-operative diagnosis. Most importantly, tumors at the desirable maximum size for a good prognosis (1 cm) were visualized and tumors as small as 1 mm were seen in the nipple.

In 1956 Wild also developed a rectal scanner. The transducer was inserted rectally, rotated, and then withdrawn in a planned scanning pattern, thus visualizing tumor of the large bowel. He also constructed a double transducer scanner for the study of the heart. A yoke holding both transducers fit over the shoulder, thus the sending and receiving transducers were placed on different sides of the chest. Wild continued his research at the Medico-Technological Research Institute of Minneapolis, St. Louis Park, Minnesota under private funding as governmental grants were withdrawn subsequent to legal disputes.

Wild received many honors and much recognition from learned societies and universities throughout the world, including awards from the American Institute of Ultrasound in Medicine (AIUM) and the World Federation of Ultrasound in Medicine and Biology (WFUMB). Wild continued to serve as the Director of the Medico-Technological Research Institute in Minneapolis until it closed in 1999.

He was also presented the prestigious "Japan Prize" by the Science and Technology Foundation of Japan in 1991 for his pioneering work in ultrasonography. In that same year he was elected an honorary member of the Japan Society for Ultrasound in Medicine, becoming only the second foreigner to be so honored.

In 1994, Britain issued a set of stamps to commemorate Wild's pioneer work in ultrasonography. In 1998 he was presented with the Frank Annunzio Award by the Christopher Columbus Fellowship Foundation.

In part excerpted with permission from the website www.ob-ultrasound.net by Joseph Woo, MD, Hong Kong. Picture courtesy John Wild, MD, PhD.

John M. Reid (born 1926)

John M. Reid was born in Minneapolis, Minnesota June 26, 1926. He received his BS (1950) and MS (1957) degrees in electrical engineering from the University of Minnesota, and the PhD in Electrical Engineering from the University of Pennsylvania (1965). From 1950–1957, Reid worked on medical diagnosis with ultrasound at the Department of Electrical Engineering and Surgery, University of Minnesota and St. Barnabas Hospital, Minneapolis, where he worked on tissue characterization with ultrasound and developed the first clinical ultrasonic scanner with John J. Wild.

Reid was engaged through a grant from the National Cancer Institute as the sole engineer to build and operate Wild's ultrasonic apparatus. Wild and Reid built, amongst other ultrasonic devices, a linear B-mode instrument, a formidable technical task. In those days, in order fully to visualize tumors by sweeping from side to side through breast lumps. In May 1953 this instrument produced a real-time image at 15 m/c of a 7-mm cancer of the nipple in situ along with A-mode differential sonic reflections. Based on technology from the World War II radar, Reid devised important circuitry to compensate for the attenuation of ultrasound in tissues by setting the receiver gain as a function of the tissue depth. Similar mechanisms were deployed in most medical ultrasound systems that followed.

In 1957 Reid completed his MS thesis, which compared the theory for focusing radiators to experimental findings. In addition he had importantly verified that dynamic focusing was practical. He subsequently left Wild's laboratory and pursued his doctoral degree at the Department of Biomedical Electronic Engineering, Moore School of Electrical Engineering, University of Pennsylvania, Philadelphia.

From 1957–1965 he worked on echocardiography, producing and using the first such system in the United States, with cardiologist Dr. Claude Joyner. This required developing design and construction methods for making ceramic pulse-echo transducers and measuring their performance. Reid was responsible for constructing Joyner's equipment, which could display both the EKG and echocardiogram simultaneously. He also worked out methods for measuring the ultrasonic power levels used by diagnostic machines using a radiation force balance, and developed methods for making ultrasonic scattering measurements in tissues.

Reid became a Research Assistant Professor at the Department of Physiology and Biophysics (1966–1968) and the Center for Bioengineering (1968–1977) at the University of Washington, Seattle. Here he continued the tissue research, which culminated in measurement of the scattering cross section of red blood cells, with Professor Rubens Sigelman and Dr. K. Shung. In addition, he worked on the continuous wave and pulse Doppler and duplex imaging devices with the Donald Baker team. He participated in forming the Institute of Applied Physiology and Medicine in Seattle with Dr. Merrill Spencer, and also was affiliated with the Providence Hospital from 1971–1981, while working on measurements, gas bubble detection, Doppler imaging and other ultrasonic developments.

He also participated in the standards writing work of the International Electrotechnical Commission, as a United States delegate to their ultrasonics sub-



committees and working groups since 1981, funded by the National Electrical Manufacturers Association and the American Institute of Ultrasound in Medicine.

In 1981 Reid held the Calhoun Chair of Biomedical Engineering at Drexel University and became an Adjunct Professor of Radiology at Thomas Jefferson University, both in Philadelphia, where the work on ultrasonic diagnosis of tissue has continued to date. This is a Program Project funded by an NIH grant and involves nine projects with other professors at Drexel and Thomas Jefferson. He was Acting Director of the Biomedical Engineering and Science Institute at Drexel University for two years, and although retired from the Calhoun Chair in 1994, is currently an Emeritus and Research Professor at Drexel, a Professor of Radiology at Thomas Jefferson University and an Affiliate Professor of Bioengineering at the University of Washington. His current activities include directing an N.I.H. Program Project grant with other faculty members at Drexel and Thomas Jefferson Hospital on diagnosis of human breast cancer using ultrasound, consulting and writing on medical ultrasound systems and transducers. He is also involved in the investigation of the propagation and scattering of ultrasound waves in biological tissues (tissue characterization), and the study of cardiovascular system structure and function through the ultrasound Doppler effect.

Professor Reid is a Life Fellow of the IEEE, a Fellow of the Acoustical Society of America and of the American Institute of Ultrasound in Medicine, whose Pioneer Award he received in 1979, and of the American Institute for Medical and Biological Engineering. He received the Career Achievement Award of the IEEE Engineering in Medicine and Biology Society in 1993 and the Pioneer Award of the Society of Vascular Technologists in 1994. A special issue of the journal "*Ultrasound in Medicine and Biology*" dedicated to him and containing papers by his students and collaborators was published in 1994. In 2000, Professor Reid was elected Honorary Member of the World Federation for Ultrasound in Medicine and Biology.

In part excerpted with permission from the webside www.ob-ultrasound.net by Joseph Woo, MD, Hong Kong. Picture courtesy John Reid, PhD.

Reprinted from SCIENCE, February 29, 1952, Vol. 115, No. 2983, pages 226-230.

Application of Echo-Ranging Techniques to the Determination of Structure of Biological Tissues¹

John J. Wild and John M. Reid^{2,3}

Department of Electrical Engineering, University of Minnesota, Minneapolis

THE RESULTS OF PRELIMINARY STUDIES on the use of a narrow beam of 15 megacycle pulsed ultrasonic energy for the examination of the histological structure of tissues have been sufficiently encouraging to warrant the development of the apparatus that is the subject of this report.

Whereas the initial method of examination of tissues gave records of histological structure in one dimension analogous to a needle biopsy, the method to be described was designed to give a two-dimensional picture such as would be obtained by adding up the information from a series of needle biopsies taken in one plane across a given piece of tissue. Such differentiation of soft tissue structure is without precedent in the biological field. Theoretically it was thought possible to record soft tissue structure by tracing the information obtained from a sound beam sweeping through the tissues onto a fluorescent television screen. Thus, a tumor could be detected in soft tissues, provided the echoes returning from the tumor differed from the echoes returning from the tissue of origin of the tumor. Differences of sufficient magnitude obtained from the needle biopsy method of examination have already been demonstrated in the pilot studies reported elsewhere (1-4). The initial studies covered a variety of common tumors arising in the human stomach, brain, and breast. Work subsequent to these studies has confirmed the findings on a larger and wider scale.

Definition of terms. It is necessary to introduce some new words in order to make it possible to describe the

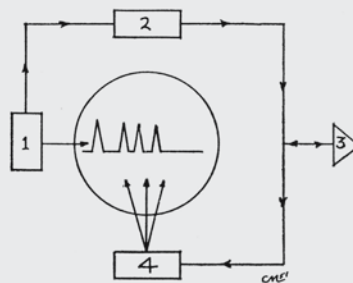


FIG. 1. Arrangement of the basic echographic system.

following material. Accordingly, the whole subject of examination of biological tissues by means of ultrasonic echo returns will be referred to as "Echography," corresponding with the term "electrocardiography." Similarly, the apparatus associated with production of the records will be referred to as an "Echograph." It is the basic machine used for both unidimensional and two-dimensional echography. The applicator units will be referred to as unidimensional "Echoscopes" and two-dimensional echoscopes. The records obtained will be referred to as unidimensional "Echograms" and two-dimensional echograms.

Unidimensional echography. To understand two-dimensional echography, or the moving sound beam method of tracing out the histological structure of biological tissues, it is necessary to review briefly unidimensional echography, or the stationary beam method of examination.

The basic principle of the echograph is the driving of bursts of sound energy into tissues. Sound travels through tissues as pressure waves, so that the effects are entirely mechanical. If the power of the pressure waves and the period of application are kept low, no damage results (5). In between the bursts of sound energy, which are generated by a piezoelectric crystal, or transducer, echoes returning from the tissues strike the same crystal, and electric charges are generated. These charges are amplified greatly and are made to

¹ This investigation was supported by a research grant from the National Cancer Institute of the National Institutes of Health, USPHS.

² We wish to thank Maurice B. Visscher, head of the Department of Physiology, and Henry E. Hartig, head of the Department of Electrical Engineering, University of Minnesota, for their help and suggestions in the preparation of this communication, particularly in regard to the section on terminology.

³ Formerly of the Department of Surgery, University of Minnesota Medical School, Minneapolis.

modify a beam of electrons sweeping back and forth on the face of a television screen at such a rate as to take advantage of persistence of vision. A static trace is thus produced that can be observed with the naked eye and photographed for permanent recording.

The echograph. The arrangement of the components of the electronic system is shown in Fig. 1. An electronic clock (1) times the bursts of sound energy and starts the trace on the face of the television screen (cathode-ray tube). The transmitter (2), upon receipt of the pulse from (1), creates the electrical impulses necessary to cause the piezoelectric crystal (3) to vibrate. The sound leaves the crystal in a narrow beam and penetrates the tissues. Echoes returning from the tissues are received by the same crystal (3), now quiescent, and are amplified by unit (4) to deflect the trace as shown. The process is repeated often enough to give a stable trace that can be observed and photographed.

In practice it has been found possible to use a self-contained instrument, called a unidimensional echoscope (Fig. 2, top), which provides hydraulic coup-

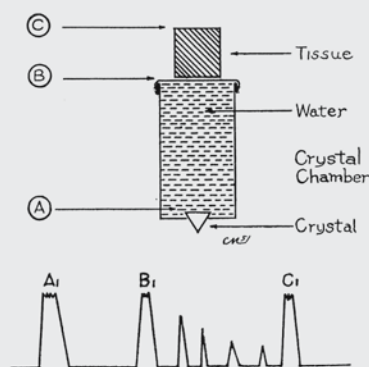


FIG. 2. Cross section of crystal chamber and tissue under examination (top) and a typical unidimensional echogram obtained from the arrangement (bottom).

ling between the crystal, or transducer, and the pieces of tissue under examination. A column of water is placed between the transducer and a wetted rubber membrane, which seals the unit. The sound energy passes in a narrow beam through the water, the wetted rubber membrane, and the tissue, and the echoes are returned. The unidimensional echogram obtained is also shown in Fig. 2 (bottom). A_1 is the transmitted pulse sent out by unit (2) in Fig. 1, which is amplified by unit (4) in the same manner as an echo. B_1 is the echo returned from the rubber-membrane-tissue interface. C_1 is the corresponding echo returned from the tissue-air interface. In between B_1 and C_1 can be seen echoes arising from within the tissue. It should be noted that the strength (loudness) of the echoes is recorded vertically, and the time of occurrence, or depth, of propagation of the echoes in the tissue is recorded horizontally. The part of the trace between A_1 and B_1 is constant and is deleted from the actual presentations in order to use the available

space on the television screen to the fullest advantage. (Reference to D in Fig. 7 will show a photographic record of the trace obtained from a piece of normal beef kidney cortex in the manner described here. X and Y correspond to B_1 and C_1 in Fig. 2.)

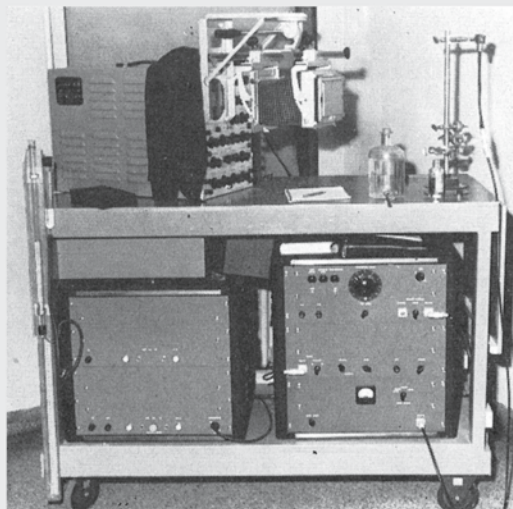


FIG. 3. The complete echographic apparatus as used in hospital. The unidimensional echoscope can be seen clamped to a stand on the right, connected to the transmitter-receiver unit. The cathode-ray screen with the camera in the recording position is to the left on the table.

A photograph of the echograph as used in hospital for cancer detection studies is shown in Fig. 3. The unidimensional echoscope shown in Fig. 2 can be held in the hand and applied to the tissues under examination.

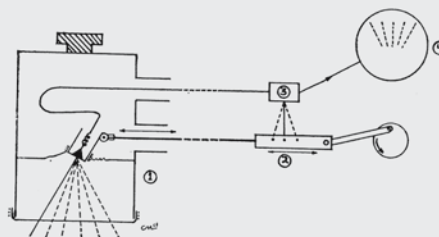


FIG. 4. Diagram illustrating the principle of operation of the two-dimensional echographic modification. The pivoted crystal mounted in the two-dimensional echoscope (1) is driven by the oscillating ram (2), which is connected mechanically to the electronic unit (3), which synchronizes the position of the sweep on the cathode-ray screen (4) with the path of the sound beam in the tissues.

Clinical studies on the living, intact subject indicated that a two-dimensional method of presentation would give additional information, greatly facilitating the interpretation of the unidimensional echograms. The type of record described in Fig. 2 is, in effect, the equivalent of a needle biopsy in that the path of the narrow beam of sound penetrating the tissues does not move for a given record. If a series of such unidimensional echograms could be taken in one plane

over an area of skin, a graph could theoretically be made from the echograms, and a structure such as a tumor could be delineated and located in depth, or detected in two dimensions. Practically, such a procedure would be extremely difficult. Fortunately, the same result can be obtained automatically by applying the principles of echo-ranging. A pilot model was fabricated for attachment to the basic echograph so that a rapid change-over could be effected when necessary.

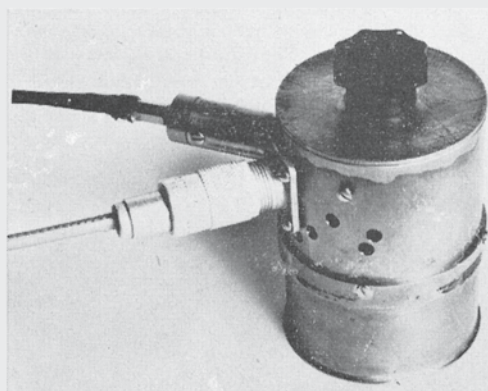


FIG. 5. The two-dimensional echoscope as used in the experiments. The flexible mechanical and electrical connections can be seen.

Two-dimensional echography. A functional diagram of the mechanism is shown in Fig. 4. The two-dimensional echoscope (1) containing the crystal mounted on pivots can be seen. (The actual instrument is shown in Fig. 5.) The pivoted crystal is mounted in a water chamber closed by a rubber membrane. As the crystal is moved through an angle of 45 degrees, an area of skin together with the underlying tissue is swept by the sound beam in one plane. The movement of the crystal is synchronized by means of an oscillating ram (2) connected flexibly and mechanically to the crystal

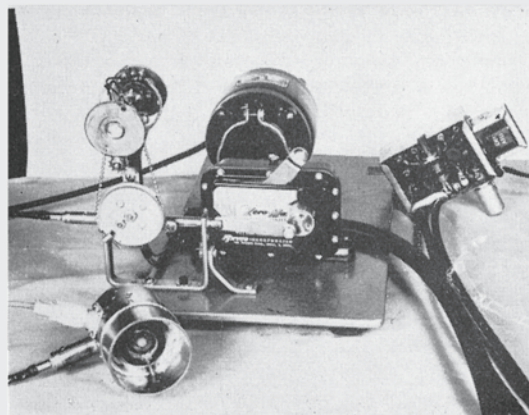


FIG. 6. The units for two-dimensional echographic conversion. Grouped about the oscillating ram, which is driven by a variable speed drive, are the echoscope (left foreground) and the plug-in electronic conversion box (right).

and electronically through unit (3) to the television or cathode-ray screen (4). The complete two-dimensional echographic conversion unit is shown in Fig. 6.⁴

Experiments. To orientate two-dimensional echography with unidimensional echography, a piece of beef kidney cortex approximately 1 cm thick was cut. This specimen was laid upon the wetted rubber membrane of the two-dimensional echoscope at *C* (Fig. 7), in the same manner as in Fig. 2. It will be noted that the specimen was thinner in the center than at the end of the range of travel of the sound beam, indicated by the broken lines. It will also be noted that the specimen was placed upon the membrane in such a manner that at one extreme of travel of the crystal the sound beam would pass into air. The crystal was

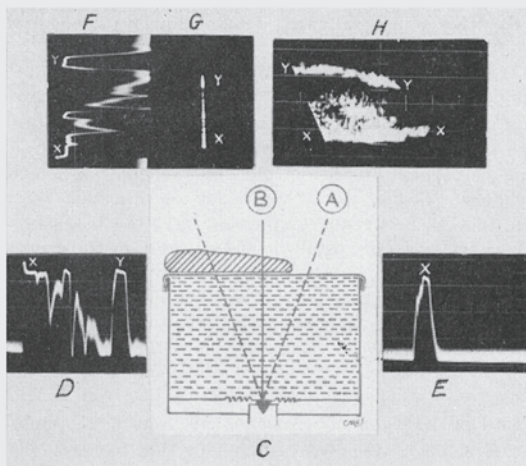


FIG. 7. At *C*, a cross section of two-dimensional echoscope set up for kidney cortex experiment. (Cf. Fig. 2, top.) At *E*, the unidimensional echogram of the membrane-air interface *X*; at *D*, echoes returned from the kidney cortex tissue between the rubber membrane signal *X* and the tissue-air leaving interface *Y*; at *F*, the echogram *D* oriented vertically; at *G*, an alternative method of presentation of echogram *D* obtained by variation of intensity. The time axis is vertical in both traces. Variations in the strength of echoes can be seen between *X* and *Y* as deflections of the baseline in trace *F* and as areas of differing intensity in the trace *G*. At *H*, the two-dimensional echogram obtained by sweeping the unidimensional echogram *G*. The outline of the tissue can be seen "painted out" by the tissue-air leaving interface *Y*. The membrane signal *X* can be discerned at the bottom of the record. It can be seen from *H* that the kidney did not extend completely across the applicator.

locked in position pointing in the direction *A* so that the sound beam passed into air after leaving the rubber membrane. The unidimensional echogram *E* was obtained. It will be observed that the rubber-membrane-air interface returned a strong echo *X* and that no echoes returned from the air beyond the rubber membrane in the path of the sound beam.

Next the crystal was rotated so that the sound beam traveled in the direction *B* through the tissue, in a manner analogous to the arrangement shown in Fig. 2. The crystal was locked in this position, and the

⁴ We wish to thank Revco, Incorporated, 405 Thorpe Building, Minneapolis, for supplying the widely variable gearbox shown in Fig. 6.

4

unidimensional echogram shown at *D* was obtained. Again the rubber-membrane-tissue interface returned a strong echo *X*, as did the tissue-air interface *Y*. In between *X* and *Y* can be seen echoes arising from within the kidney substance. In the echogram *D* the time base for the returning echoes runs from left to right horizontally. This means that the echoes returning from the rubber-membrane-tissue interface *X* appear sooner on the record than the echoes returning from beyond the rubber-membrane-air interface, because of the delay of sound in the tissue as greater depth of tissue is penetrated. The strength of the returning echoes is shown by the vertical deflections from the base line.

To facilitate understanding the next step, the unidimensional echogram *D* is turned 90 degrees, and the time base is now oriented from below up, as shown at *F*.

The next step is to present the echoes shown on the unidimensional echogram *F* (and *D*) as spots of varying intensity on the face of the television screen. Thus, the strong rubber-membrane-tissue interface echo *X* can be seen at the lower part of the unidimensional echogram *G*, and the strong tissue-air interface *Y*, at the top. In between are spots of light the brightness of which varies according to the strength of the echoes returning from the kidney tissue with the crystal locked in position *B* of Fig. 7, at *C*.

The echogram shown at *G* was then caused to move in synchronism with the pivoted crystal, as shown in Fig. 4 (1 and 4). As the unidimensional echogram *G* moved in its sector, lines were traced out by the spots of light on the cathode-ray screen. A photographic plate was exposed during this process. The internal structure of the kidney based on echoes from within the kidney substance was traced out as the sound beam swept in and out of the tissue.

The record shown at *H* is believed to be the first two-dimensional echogram of biological tissue to be recorded. The varying thickness of the specimen can be seen as the tissue-air interface *Y-Y* was traced out on the photographic film. The rubber-membrane-tissue and the rubber-membrane-air interfaces *X-X* were also traced out. The absence of signals beyond the rubber membrane when the sound beam swept out of the tissue into air (position *A*) was clearly recorded. Theoretically such a picture could be observed with the naked eye by moving the echogram *G* rapidly enough to obtain visual persistence on the face of the cathode-ray tube, but the apparatus was not sufficiently well developed at the time.

A limited clinical trial of two-dimensional echography was decided upon. A patient (Case No. 782,109)

was hospitalized for a recurrence of a tumor on the inside of the left thigh above the knee. The tumor, which had been previously diagnosed as a myoblastoma by biopsy, could be palpated in the adductor muscles, but no swelling of the skin was observed over it. Two two-dimensional echograms obtained from this patient are shown collectively in Fig. 8. The echogram of the normal right thigh is shown to the right. The two-dimensional echoscope (Fig. 5) was positioned in a comparable site on the left thigh in such a way that the sound beam swept from normal into tumor tissue. The two-dimensional echogram shown to the left in Fig. 8 was obtained. The signals *X-X* were believed to arise from the growth as the sound beam swept into it. These signals were almost continuous in the nega-

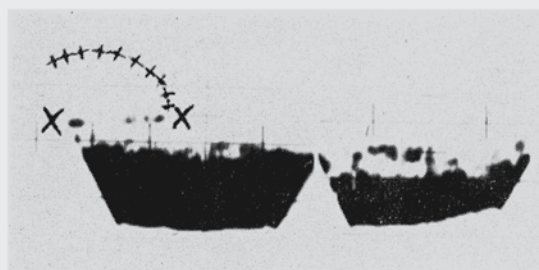


FIG. 8. The two-dimensional echogram obtained from a patient with a tumor of the adductor muscles of the left thigh above the knee. The right-hand picture was taken from the normal right thigh. The left-hand picture was taken with the sound beam sweeping from normal into tumor tissue. The deep signals *X* were believed to arise from the tumor. (The line *X-X* was almost continuous in the negative.) Had the machine been more powerful the tumor would probably have been outlined by an echo pattern within the area enclosed by the crosses, which were added to the record as shown.

tive. Had the apparatus reached a greater state of perfection, the tumor might have been revealed by echo patterns within the area enclosed by the cross-lines inserted on the record.

Further development of the methods described for examination of living, intact, biological tissue in such a manner as to reveal structure in depth should be of great value in many branches of biology. The immediate application of echography to the detection of tumors in accessible sites in the living intact human organism is envisaged.

References

1. WILD, J. J. *Surgery*, **27**, 183 (1950).
2. FRENCH, L. A., WILD, J. J., and NEAL, D. *Cancer*, **3**, 705 (1950).
3. ———. *J. Neurosurgery*, **8**, 198 (1951).
4. WILD, J. J., and NEAL, D. *Lancet*, **1**, 655 (1951).
5. FRENCH, L. A., WILD, J. J., and NEAL, D. *Cancer*, **4**, 342 (1951).

3.3 The use of ultrasonic Reflectoscope for the continuous recording of the movements of heart walls

Inge Edler (1911–2001)

Inge Edler was born on 17 March 1911, in Burlöv, Malmöhus County, Sweden. His parents were Carl and Sophia, who were teachers in the primary school in that vicinity. He graduated from the local high school, Högre Allmänna Läroverket, in 1930. Young Edler wanted to continue with university studies in physics, particularly micronics, but he was convinced by his sister to go for dentistry instead. As it was too late to enroll in the faculty of dentistry, he was able to be accepted by the faculty of medicine at Lund University. This was supposed to be a stopgap measure. However, medicine intrigued him so that he continued his studies at the university, receiving his medical degree in 1943.

Dr. Edler's professional career was initiated in the field of general medical practice, but was soon restricted to his employment in the Department of Internal Medicine at the University Hospital of Lund, and in the space of several years revolved primarily around cardiology. He was appointed director of the Laboratory for Heart Catheterization at the University Hospital in 1948 and functioned in this capacity until 1950. At that time, he was appointed director of the Department of Internal Medicine and the Cardiovascular Laboratory at the University Hospital, Lund. He remained in this capacity until 1960, assuming additional administrative duties in 1953 as Head of the Department of Cardiology until his retirement in 1977. In this position he was responsible for the preoperative diagnosis of heart disease. At that time, cardiac catheterization and contrast X-rays of the heart failed to give enough data for a correct appraisal of the status of the mitral valve. Since a correct diagnosis is of great importance before an operation, Edler felt strongly the inadequacy of the existing methods. This concern caused him to look for a new non-invasive alternative, which he thought might resemble some kind of radar.

At the same time in the early 1950s Carl Hellmuth Hertz, the son of the famed Nobel Laureate Gustav Hertz, was working as a graduate student at the nuclear physics department of the University of Lund. Because of this interest, he also studied ultrasound. He was acquainted with the ultrasonic reflectoscope developed for non-destructive materials testing. An ultrasonic reflectoscope was borrowed from the Tekniska Röntgen-Centralen, a company in the nearby town of Malmö, which specialized in non-destructive testing. With the equipment, they were able to obtain well-defined echoes on the CRT screen moving synchronously with his heart beat. Since Hertz's father had been the director of the Siemens Research Laboratory before the end of the war, they were able to contact director Wolfgang Gellinek of the Siemens Medical Branch in Erlangen, Germany, to borrow one of their Siemens reflectoscopes. Edler and Hertz received the reflectoscope in October 1953 and set to work on it immediately.

In 1953, the first ultrasound heart examination in the world was performed in Lund. Edler finally established the characteristic motion pattern for the anterior leaflet of the mitral valve. He compared the shape of the fast-moving echoes in patients with enlarged hearts due to mitral stenosis during cardiac operations, and found empirically the shape correlated well with the severity of the stenosis.

By early 1955, Edler had so much evidence of this relationship that he relied on ultrasound alone for the diagnosis of mitral stenosis. The typical motion patterns



of other heart valves, pericarditis, tumors, and thrombosis in the left atrium showed up in their recordings and were identified by close cooperation with Dr. Olle Dahlback's heart surgery group. The advent of a barium titanate transducer produced by Siemens in Germany in 1958 was an important advance for the group and enabled them to study not only the normal mitral valve but also many other heart structures.

Edler was active as a member of many societies devoted, in whole or in part, to the advancement of ultrasound. Among them were the American Institute of Ultrasound in Medicine, Deutsche Gesellschaft für Ultraschall Diagnostik in der Medizin, the Swedish Society of Medical Ultrasound, the Yugoslav Association of Societies for Ultrasound in Medicine and Biology, the Swedish Society of Cardiology, and the American College of Cardiology.

Throughout his professional career, Dr. Edler was awarded many honors. The Albert and Mary Lasker Foundation awarded him and Hellmuth Hertz the Clinical Medicine Research Prize in 1977 for pioneering the clinical application of ultrasound in the medical diagnosis of abnormalities of the heart. This was followed in 1983 by the Rotterdam Echocardiography Award for his outstanding and pioneering work applying ultrasound as a diagnostic tool in cardiology. In December 1984, he received the Lund Award for "scientific work of extraordinary significance" from the Royal Physiologic Society. In 1987, Lund University bestowed upon him the title of Professor H.C. One year later he was again honoured with the Münchener and Aachener Preis für Technik und angewandte Naturwissenschaft, and finally, in 1991, he was awarded the Eric K. Fernströms Stora Nordiska Pris

Inge Edler died on 7 March 2001, just 10 days short of his 90th birthday.

Information and picture courtesy Lars Edler, MD.

Carl Hellmuth Hertz (1920–1990)

Carl Hellmuth Hertz was born in 1920 as the son of a very prominent father, and Nobel Prize laureate Gustav Hertz. Early in 1950 Hellmuth Hertz began research on ultrasound in medical examinations, thereby becoming known throughout the world. A Swedish physician, Inge Edler, told Hertz that he wanted to devise a non-invasive method for examining the heart. Echocardiography has revolutionized cardiovascular diagnostics.

Since Hertz's father had been the director of the Siemens Research Laboratory before the end of the war, they were able to contact director Wolfgang Gellinek of the Siemens Medical Branch in Erlangen, Germany, to borrow one of their Siemens reflectoscopes. Edler and Hertz received the reflectoscope in October 1953 and set to work on it immediately.

In 1977 Hertz and Edler received the American equivalent of the Nobel Prize in medicine, the Lasker Prize. The use of ultrasound in medical diagnostics is increasing sharply in a number of different fields.

Carl Hellmuth Hertz became founding professor of the Department of Electrical Measurements, Lund Institute of Technology at Lund University. Hellmuth Hertz received several prizes, from the Westrupska Prize in 1963 for his work in biophysics of plants to the Lasker Prize for medical ultrasound in 1977 together with Inge Edler. Many other prizes and accolades followed.

The activities in the field of ultrasound created a demand for some kind of printer suitable for the printing of color pictures. This brought the beginning of a new activity. Hertz invented ink-jet printing, a method for the electrical control of tiny droplets, which enabled him to put a dot of ink on a piece of paper in about



one-millionth of a second. The pixel size was 0.1 x 0.1 mm with continuously variable color saturation in each pixel. The first steps in ink-jet printing were taken during the sixties. The common mingograph – a multi-channel ink-jet printer – designed by Elmquist and in common use at hospitals for registration of ECG came to serve as the basic instrument on which the first experiments were made. The original goal was that the ink-jet plotter would replace the conventional film for printout of medical images, such as X-rays, CT and ultrasound images, for use in the future “digital” hospital!

KUNGL. FYSIOGRAFISKA SÄLLSKAPETS
I LUND
FÖRHANDLINGAR

PROCEEDINGS OF THE ROYAL PHYSIOGRAPHIC SOCIETY
AT LUND

BAND 24

1954



KUNGL. FYSIOGRAFISKA SÄLLSKAPETS I LUND FÖRHANDLINGAR

Bd 24. Nr 5. 1954.

The Use of Ultrasonic Reflectoscope for the Continuous Recording of the Movements of Heart Walls.

By

I. Edler¹ and C. H. Hertz².

Communicated by Prof. B. EDLÉN, March 10, 1954.

Introduction.

The effectivity of the pumping action of the heart is essentially dependent on cyclic variations in the volume of the heart chambers and the function of the valves. Increased difference between the diastolic and systolic volume in a heart chamber implies greater amplitude in the movements of the walls. In patients with valvular stenosis or insufficiency the curve for the variation in the volume of heart chambers will deviate from normal (1). Therefore, methods showing the variation in the volume of the heart chambers or the movements of the walls of the heart during the cardiac cycle should be useful in the investigation of cardiac function. Roentgenkymography and electrokymography are methods applied in the investigation of changes in the outline of the heart during the cardiac cycle. RUSHMER *et al.* (2) made continuous measurements of left ventricular dimensions in intact, unanesthetized dogs. The method they used is based on the introduction of a variable inductance gauge in the ventricle, but their method can only be used in animal experiments. In recent years serial angiocardiology with several exposures per second has become an important method for the study of the variation in the volume of the heart chambers during systole and diastole. This method has been used in the clinic, among other things, for the investigation of mitral valvular disease, but it must be performed under anesthesia, it is time-consuming and by no means free of risks.

Many other methods for registering periodic movements caused by the

¹ Medical Clinic, University of Lund.

² Dept. of Physics, University of Lund.

heart are under investigation, but only one of these uses ultrasonic sound (3). But that method differs fundamentally from that presented here, since it uses continuous sound waves of 60 kc that pass through the body from the praecordium to the posterior of thorax. On its way, the sound passes the heart and other parts of the body, whereby the sound intensity is decreased by absorption, reflection and refraction. By measuring the sound intensity at the back of thorax it was found that it varied in phase with the heart frequency, but no relation between these intensity variations and the heart volume could be shown.

None of the methods mentioned above give the actual movements of the inner walls of the heart, the knowledge of which would be of importance both for studying the movements of the heart in the body and for clinical diagnosis of heart diseases. It was therefore thought that a technique already well known for some years in industry for the non-destructive testing of materials with respect to flaws might be used (4, 5).

Experimental Method.

The method, known as supersonic reflectoscope, uses short supersonic sound pulses, which are generated by an electrically excited quartz crystal and delivered to the material under investigation. This is done by pressing the disk-shaped quartz crystal directly against the surface of the material under investigation. A good acoustical contact should be secured by using a thin oil film between the quartz and the surface of the material.

If there are any boundaries in the material which are impinged by the sound pulse and which reflect part of the sound back in a direction opposite to its original direction, this reflected sound pulse (echo) will reach the quartz crystal, which then acts as a microphone. If the velocity of the sound in the material under examination is known and constant, the time elapsed between the emission of the sound pulse and the reception of the echo is a measure of the distance between the quartz crystal and the reflecting boundary. This time difference (or distance) can be read directly on a cathode-ray-tube (CRT). This CRT forms part of an apparatus which also contains the electrical equipment for the generation of the electrical signal for the excitation of the quartz crystal, etc. The quartz crystal is connected with this apparatus by a coaxial cable about 3 m. long.

On the left side of the CRT screen, the outgoing sound pulse is represented by a vertical signal 0 (see Fig. 2), while each returning echo pulse shows up as a vertical signal to the right of this outgoing sound pulse. The distance between the outgoing signal and the echo signal along the

x-axis on the CRT screen is directly proportional to the distance between the crystal and the reflecting boundary. Further, the height of the echo signal shown on the CRT screen is a measure of the echo intensity.

The apparatus used in the investigations described here was the Ultraschall-Impulsgerät manufactured by the Siemens Reiniger Werke (Erlangen, Germany). In this apparatus the pulse length and intensity could be varied, the pulse length used was usually about $2-5 \times 10^{-6}$ sec., the maximum pulse intensity about 2 W/cm^2 . The pulse repetition rate was 200 per second. Sound frequencies of 0.5, 1, 2.5 and 5 Mc could be chosen at will.

In nearly all of the experiments described below a frequency of 2.5 Mc was used. When selecting the frequency, different factors have to be observed, the most important of which are the sound absorption in the material under examination and the divergence of the sound beam due to diffraction. Since the absorption of the sound waves increases with increasing sound frequency in both tissue (6, 7, 8) and blood (9), it would be advantageous to use as low a frequency as possible. On the other hand, the necessity of sharp echoes requires both short pulse length and, to reduce diffraction, small wave length of the sound in tissue or blood. With a crystal shaped like a disk, 12 mm. in diameter, as used in these experiments, a frequency of 2.5 Mc was usually found to be the best compromise, except for children below 12 years, when better results were often obtained with 5 Mc.

The apparatus used in these experiments was equipped further with an electronically controlled "lens" device to enlarge and thereby facilitate observation of echo signals on the CRT screen along the x-axis. This device proved to be valuable in the investigations. Finally, a time scale was incorporated in the apparatus, which appeared as a broken line along the x-axis on the CRT screen. This scale could be adjusted so that the breaks in the line between the outgoing and the echo pulse on the CRT screen give the distance directly in centimeters between the quartz crystal and the reflecting boundary for a certain homogeneous medium. In this work the scale was adjusted in such a way that the distances between the quartz crystal and the reflecting boundary could be read directly in centimeters on the CRT screen if the medium between was blood or muscle tissue, the velocity of sound in both being nearly the same.

Preliminary Experiments on Isolated Hearts.

It has been pointed out above that only sound reflecting boundaries can be detected by this method. Thus for the present purpose it was ne-

4]

The Use of Ultrasonic Reflectoscope

43

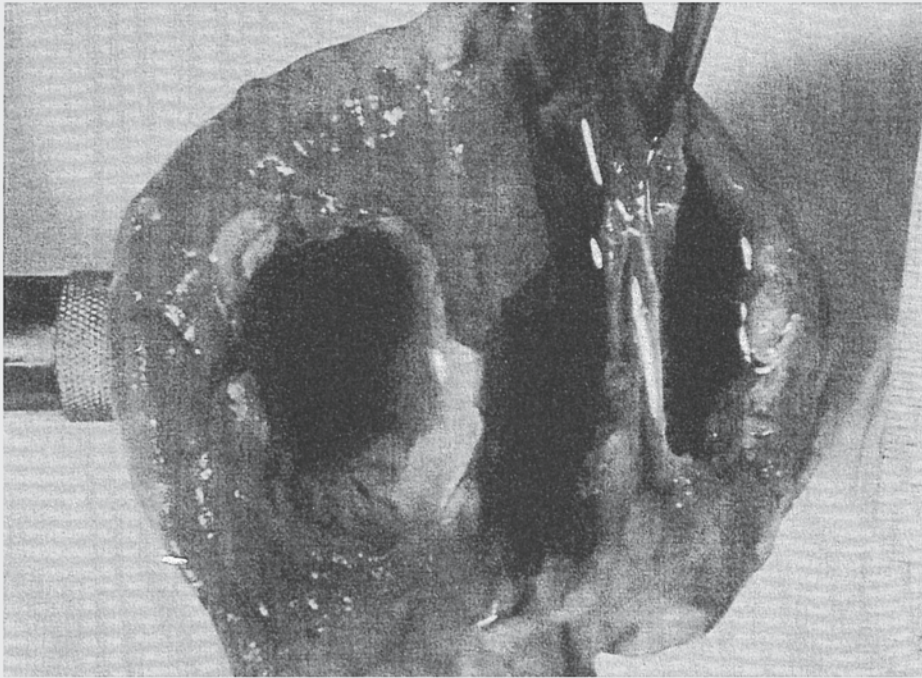


Fig. 1. Quartz — crystal applied to isolated human heart. Crystal frequency 2,5 Mc.

cessary to check that the boundary blood-heart wall fills this condition. This was not to be expected for certain, since the acoustic impedances (10, 11) for blood and muscle tissue are nearly the same. Therefore experiments with isolated hearts were made before starting the investigations on human hearts *in vivo*. The most informative of these experiments is shown by Fig. 1. It shows a human heart from above, which is cut transversely. From left to right we see the left ventricle, the right ventricle and the right atrium. All the chambers are filled with water, and the quartz crystal of the supersonic reflectoscope is applied to the outer heart wall in such a way that the sound beam traverses the heart just under the water surface. The echogram seen on the CRT screen is shown in Fig. 2. According to the figure, many echoes arise, but the co-ordination of the echoes to the different heart walls cannot be seen at a glance. But this is evident at once if both pictures are cut in halves and put together at the line along which the ultrasonic beam is traversing the heart, as is shown by Fig. 3. Each boundary of the type water-heart tissue that is traversed by the sound shows up as an echo signal on the CRT screen, even the thin wall between the right atrium and the right ventricle. The

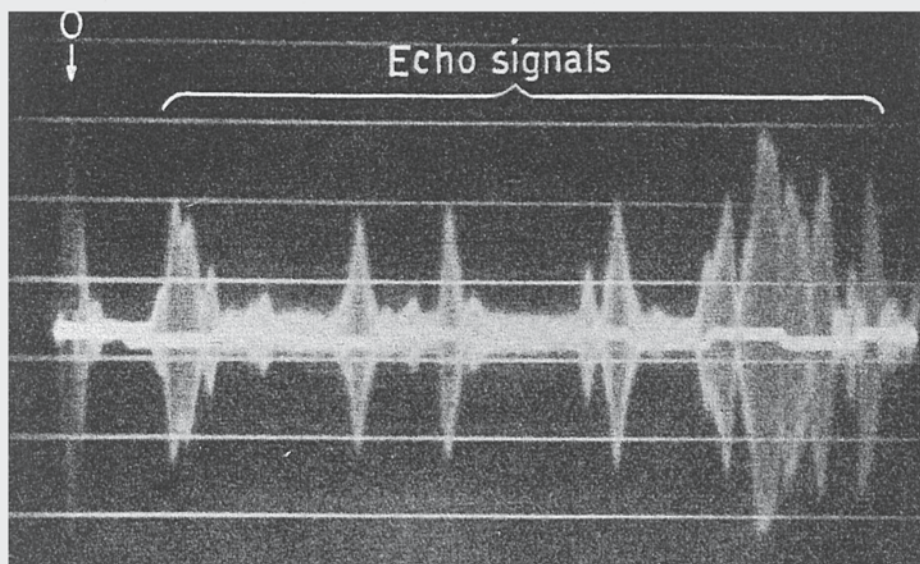


Fig. 2. Echogram obtained on the CRT screen by the arrangement shown in Fig. 1.
O = outgoing pulse signal.

places at which the heart wall is curved or irregular give rise to diffuse echo signals, since the distance quartz crystal — reflecting boundary at these spots is not constant for different parts of the 12 mm. wide ultrasonic beam. On the other hand, the wall between the right atrium and right ventricle, which has been artificially stretched so as to lie precisely perpendicular to the ultrasonic beam, gives rise to sharp echo signals. The complex echo signal seen at the place where the sound beam, after traversing the heart, strikes the outer heart wall is probably due to the highly convex form of the heart at this place. Naturally, the height and the width of the echo signals vary very much if the direction of the sound beam is changed. The experiments described here were done with water so that the shape of the heart chambers under the water surface can be seen on the photographs. In later experiments the heart chambers were filled with blood instead of water but the results obtained were exactly the same as those found with water.

To check that the co-ordination between the heart walls and the echo signals on the CRT screen given above was correct, the following experiment was performed. An injection needle ca. 0.5 mm. thick was dipped from above into one of the heart chambers shown in Fig. 1 in such a way that it crossed the axis of the ultrasonic beam. This resulted in an additional echo signal on the CRT screen from reflection at the needle.

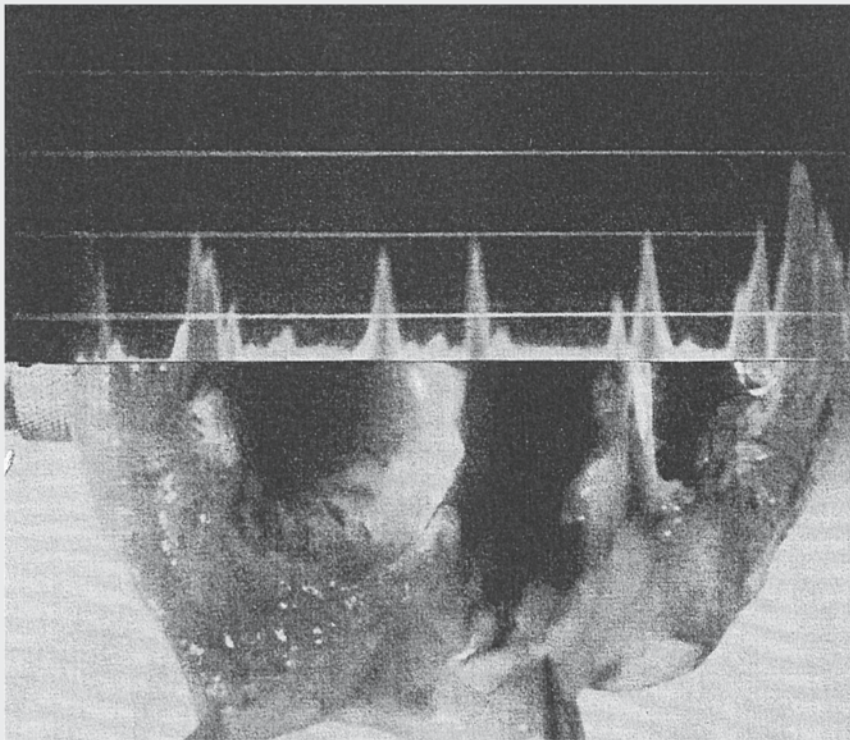


Fig. 3. (For explanation, see text).

The lower half of the Figs. 4 a—c shows the echogram without the needle in one of the heart chambers, as already shown by Fig. 2. In Fig. 4 a the needle was placed in the right atrium and in Fig. 4 b it was placed in the right ventricle and in Fig. 4 c it was placed in the left ventricle. As can be seen from the echograms, the echo signal due to the needle always shows up between the echo signals from the walls of the heart chamber into which the needle was dipped in each case. By moving the needle along the axis of the ultrasonic beam from one wall to the other in the heart chamber, the needle echo signal could be seen moving between the echo signals of the respective walls.

In other experiments, the authors examined echograms from the right atrium of the isolated calf heart. With the aid of a heart catheter passed into the atrium, the volume of the latter was varied, with a resultant corresponding shift of the echo signal from the medial wall of the atrium.

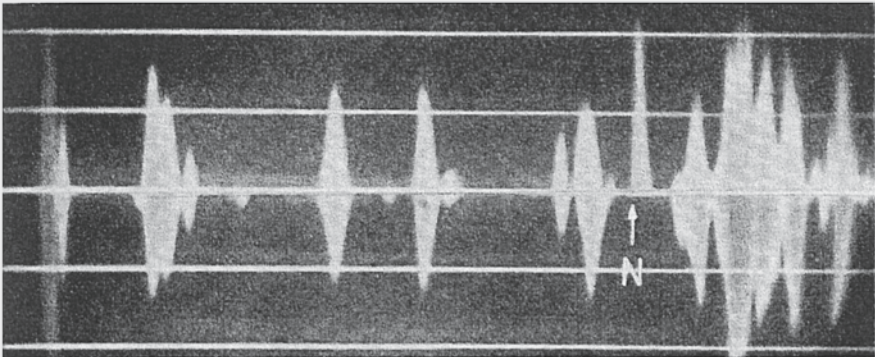
Fig. 4. Needle echo signal (N) appeared on the echogram when the needle was dipped into the right atrium (4 a), right ventricle (4 b) and left ventricle (4 c).

46

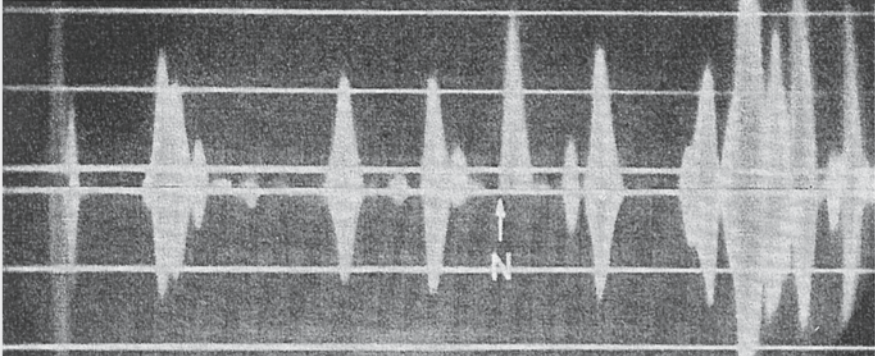
I. Edler and C. H. Hertz

[7

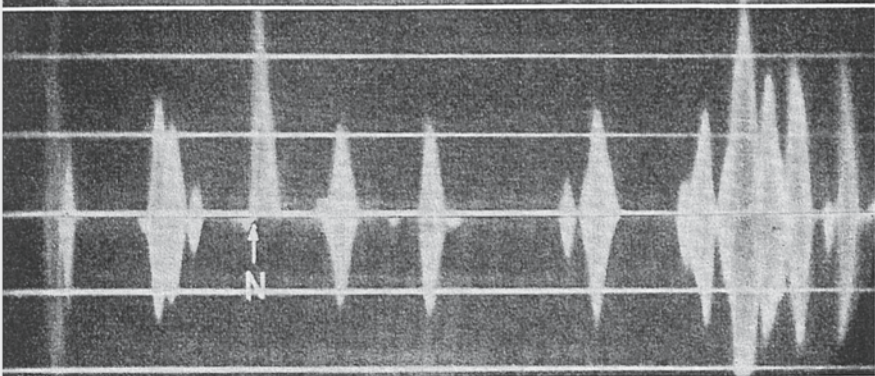
4a



4b



4c



During the experiments it was felt that the reason for the unexpected large reflection coefficient encountered at the inner heart walls were due to the endocardium, since the removal of the latter seemed to diminish the reflection coefficient appreciably. This would be in agreement with the results obtained by J. J. Wild & J. M. Reid (12) with the supersonic reflectoscope on muscle tissue. As yet, no convincing evidence has been produced in support of this assumption.

Short experiments showed, further, that auricular thrombosis may also be located by this method. This should be of interest in the diagnosis of such cases. Even here, more detailed experiments are required.

Experiments on Human Beings.

After the preliminary experiments stated above, an investigation as to the applicability of the supersonic reflectoscope method for the study of the movements of human heart walls *in vivo* was started. In all cases described below a 12 mm. disk shaped quartz crystal was directly applied to the praecordium. Paraffin oil was used to ensure good acoustic contact. The quartz crystal was brought into such a position that the sound beam could pass through an intercostal space and was directed into the heart regions under investigation. A typical echogram obtained on the CRT screen is shown in Fig. 5. It was taken on a patient with enlarged heart. The distance between the outgoing signal 0 and the echo signals along the x-axis on the screen is directly proportional to the distance between the quartz crystal and the reflecting boundaries in the heart. This is true with a fair degree of accuracy, even if the sound passes muscle tissue and blood alternately, since the sound velocities in muscle tissue and blood are nearly the same. Thus, the time scale incorporated in the apparatus was adjusted in such a way that the distance between the outgoing pulse signal and the echo signals could be read directly in centimetres. Each part of the broken line of the time scale seen in Fig. 5 represents 1 cm. sound path in muscle tissue or blood.

There are two reasons for interpreting the echo signals found in this way as echoes resulting from reflections on inner or outer heart walls. The most important is that the echo signals on the CRT screen oscillate both along the x-axis and in their magnitude with the frequency of the heart under investigation. This is very convenient for the correct interpretation of echo signals arising on the CRT screen. Since the experiments on the isolated heart shown above prove that reflections can occur at the

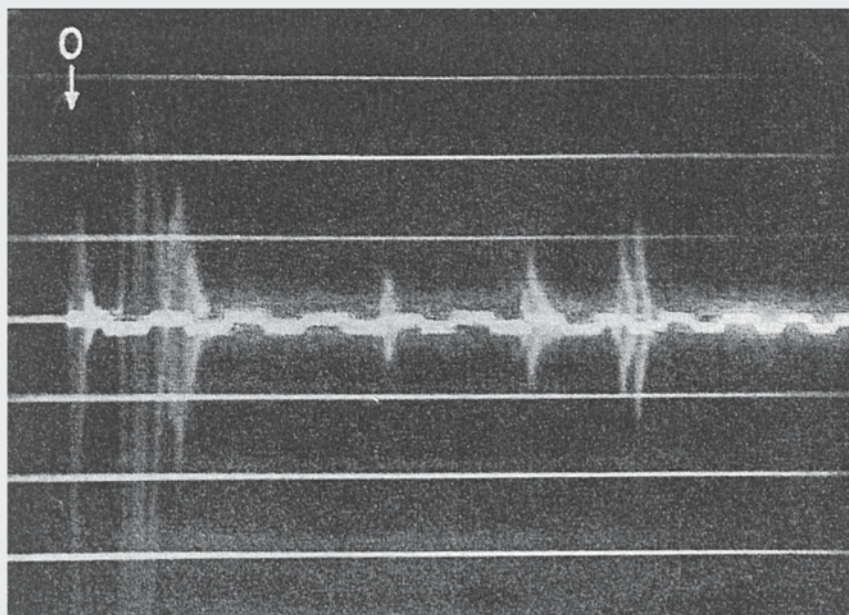


Fig. 5. Echogram obtained on the CRT-screen when quartz crystal was applied to the praecordium of a patient with cardiac enlargement.

boundary blood – heart tissue, this assumption is not contradicted. Further, no such echo signals can be found when the crystal is placed elsewhere on the thorax of a person except on the praecordium. This is due to the large absorption coefficient of the aerated lung tissue for high frequency sound.

On account of this large absorption of high frequency sound in lung tissue and pronounced reflection in skeletal parts (13), the sound beam should be delivered in such a manner as to avoid these media as far as possible. It was found that, when the quartz crystal was placed against the skin of the praecordium and in the intercostal space and when the ultrasonic beam was directed against the heart, one or more echoes ranging from 4 cm. to 11 cm. were recorded in persons with a heart of normal size. The echo signals were best obtained when the crystal was placed in the left I: 4 and I: 3. In the investigation of apparently normal adults, the ultrasonic beam is directed in sagittal direction from the left I: 4 adjacent the sternal border, whereby the posterior echo signal was recorded at a distance of 9–11 cm. from the outgoing pulse signal. If the heart is enlarged, this posterior reflecting surface will lie at greater distance from the anterior wall of the chest. Table 1 shows the relationship between

Table 1.

	Distance in centimeters of the echo signals from the outgoing signal.	Distance in centimeters from the anterior thoracic wall to the posterior of the heart, as measured on the roentgen film.	Total heart volume in millilitres.
E. L.	16	17	2440
A. L.	9,7	10,5	
B. N.	8,8	9,5	510
M. L.	12	13	
E. B.	11,3	13	1185
G. M.	12,2	13,5	1090

the distance to the posterior wall, as measured by the echo signal, and the distance from the anterior thoracic wall to the posterior part of the heart shadow, as measured by the roentgen film at the same level, in persons with varying heart volume. It is in this plane which passes through the left sternal border that the sagittal diameter of the heart is greatest, for which reason the distance measured on the roentgen film corresponds to the plane passed by the ultrasonic beam. It is apparent from the table that the posterior echo signal lies within the structure of the heart and thus represents a partition in the heart. The difference between the distance to this partition and the distance to the posterior part of the heart shadow corresponds to the thickness of the posterior wall of the heart and therefore the echo signal may correspond to the inner surface of this wall.

If the sound passes a rib, the results obtained are less accurate, and sometimes no reflection is obtained from the heart walls. If the crystal is placed against the chest outside the praecordium and where the sound waves will meet lung tissue as soon as the thoracic wall has been passed, no echo from the heart walls will be obtained. As mentioned above, this was expected.

In patients with cardiac enlargement, reflections are obtained over the major part of the praecordium which is explained by the fact that the lung tissue between the wall of the chest and the heart has been pushed aside. On the other hand, patients with emphysema and those of pyknic body build have more lung tissue between the anterior wall of the chest and the heart, which explains that it is much more difficult to obtain satisfactory echo signals in such persons.

Continuous Recording of the Echo Signals.

Since mere visual observation of the motion of the echo signals seen on the CRT screen does not yield much more information than the

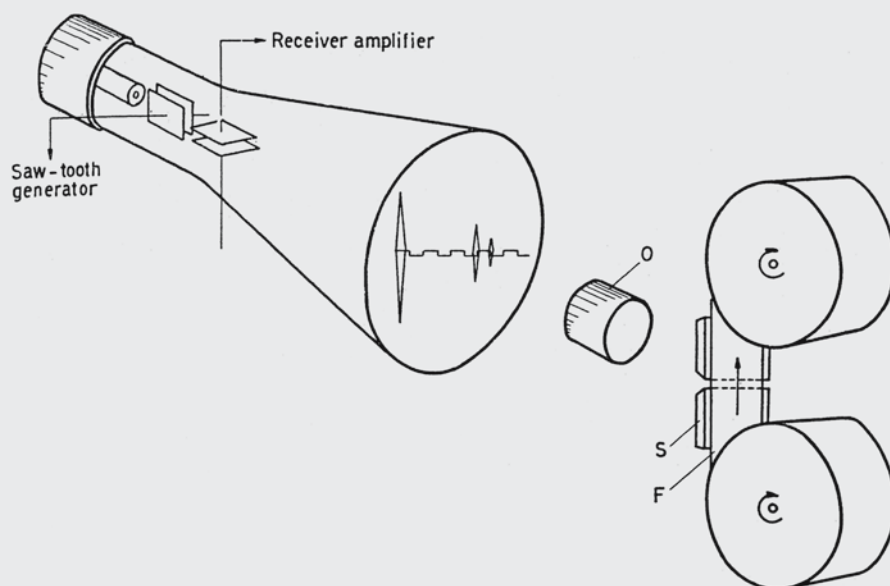


Fig. 6. Apparatus for recording UCG-curves.

distance of the reflecting heart walls from the crystal surface, a continuous photographic recording of this motion was required. To this end a horizontal slit *S* (see Fig. 6) was mounted in the image plane of the camera objective *O*, otherwise used for photographing the CRT screen, the slit width being 0.5 mm. Directly behind this slit, a 24 mm. Ilford HP3 film *F* was continuously moved at right angles to the slit at a rate of 1 cm/sec. The slit should be placed parallel to, but a little above, the image of the *x*-axis of the CRT, so that no light coming from the *x*-axis and the time scale visible on the CRT screen reaches the film. If no echo signal appears on the CRT screen, nothing will be marked on the film except the outgoing pulse signal which will be recorded as a straight line parallel to the direction in which the film is moved. If a constant, non-pulsating echo signal appears on the screen, even this will produce a straight line on the film parallel to the outgoing pulse line. The distance between these two lines is then proportional to the distance crystal-reflecting boundary. If the echo signal pulsates along the *x*-axis (which is the case in these investigations) a curve will be recorded on the film. The distance of this curve to the outgoing pulse line will correspond at any moment to the distance crystal-reflecting boundary. In this way, the variations of the distance crystal-reflecting boundary can be recorded with respect to time.

Because of the relatively large slit width relative to the film velocity, the resolving power of the present apparatus is not too good. Using higher

12]

The Use of Ultrasonic Reflectoscope

51

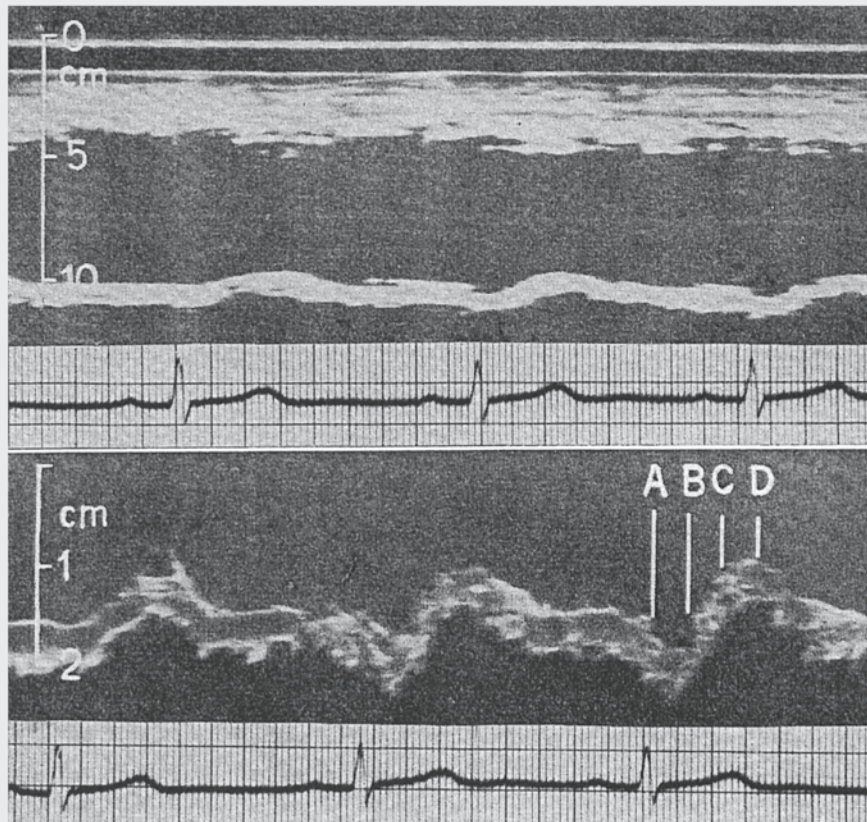


Fig. 7. Top: General view. Bottom: Enlargement of the movements of the posterior wall of the heart. A-B indicates the isometric contraction when the wall moves 2–3 mm. in dorsal direction. B-C denotes the first part of the emptying phase, maximum ejection, when the wall rapidly moves in ventral direction. C-D denotes the final phase of emptying, reduced ejection, when the wall moves slowly in ventral direction.

light intensities on the CRT screen, it will be possible without much difficulty to increase the resolving power to the same degree as is achieved in commercial ECG apparatus.

Typical curves obtained in this way from heart walls are shown in Fig. 7 to Fig. 11. Since the method uses supersonic sound to gain information about the function of the heart, in the following these curves will be referred to as UCG (Ultrasonic Cardiogram). In the lower figures the electronically controlled "lens" device mentioned above has been used. In these cases the movements of the echo signals are magnified about 4 times, whereby a more detailed study of these movements is possible. Using the scale given on the side of each figure, the actual size of the movements

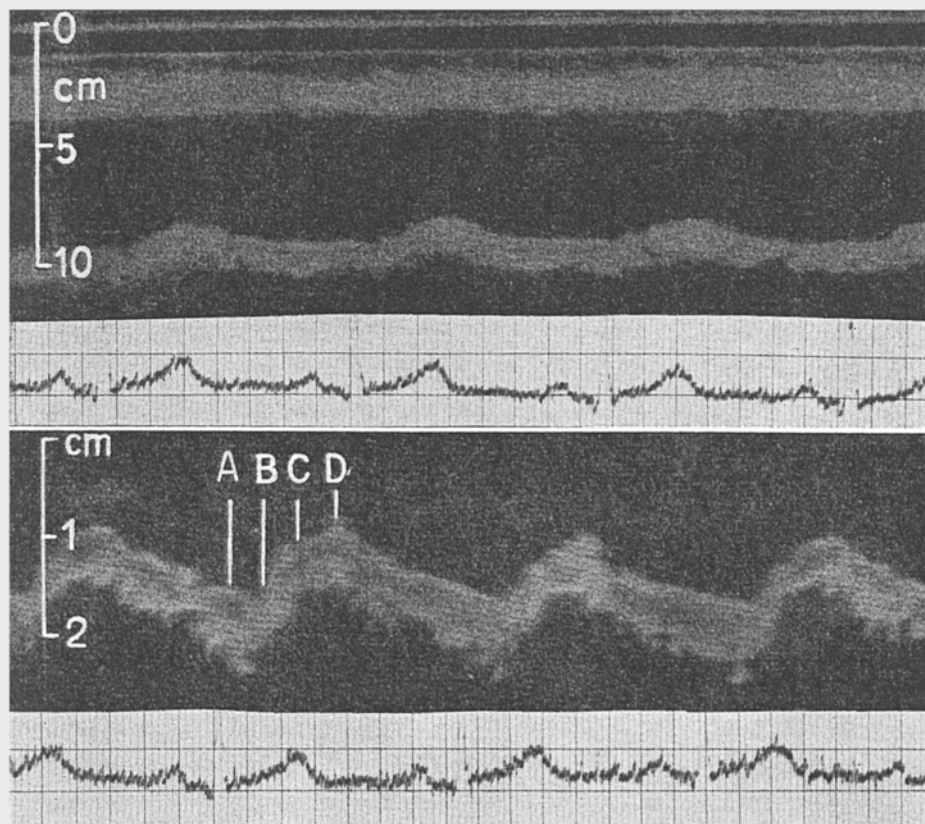


Fig. 8. UCG from a normal case. Top: General view. Bottom: Enlargement of the movements of the posterior wall of the heart.

of the heart wall under observation can be measured directly. The film velocity is the same both for the normal and for the enlarged recordings.

As can be seen from the figures, the echo signal width on the CRT screen also varies periodically. There are two reasons for this behaviour. If the reflecting boundary is not a plane or is not placed exactly at right angles to the sound beam, the echo signal will broaden, since the distance crystal-reflecting boundary is different at different places on the crystal surface. Further, in the apparatus used in these experiments, not even an echo signal reflected from an ideal plane placed at right angles to the beam direction will show up as a thin vertical line on the CRT screen, but more like an isosceles triangle with a very narrow base along the x-axis. This base width increases with the strength of the returning echo signal. Thus the base width of the echo signal pulse on the CRT screen increases with the height of the pulse, thereby making both the base width and the

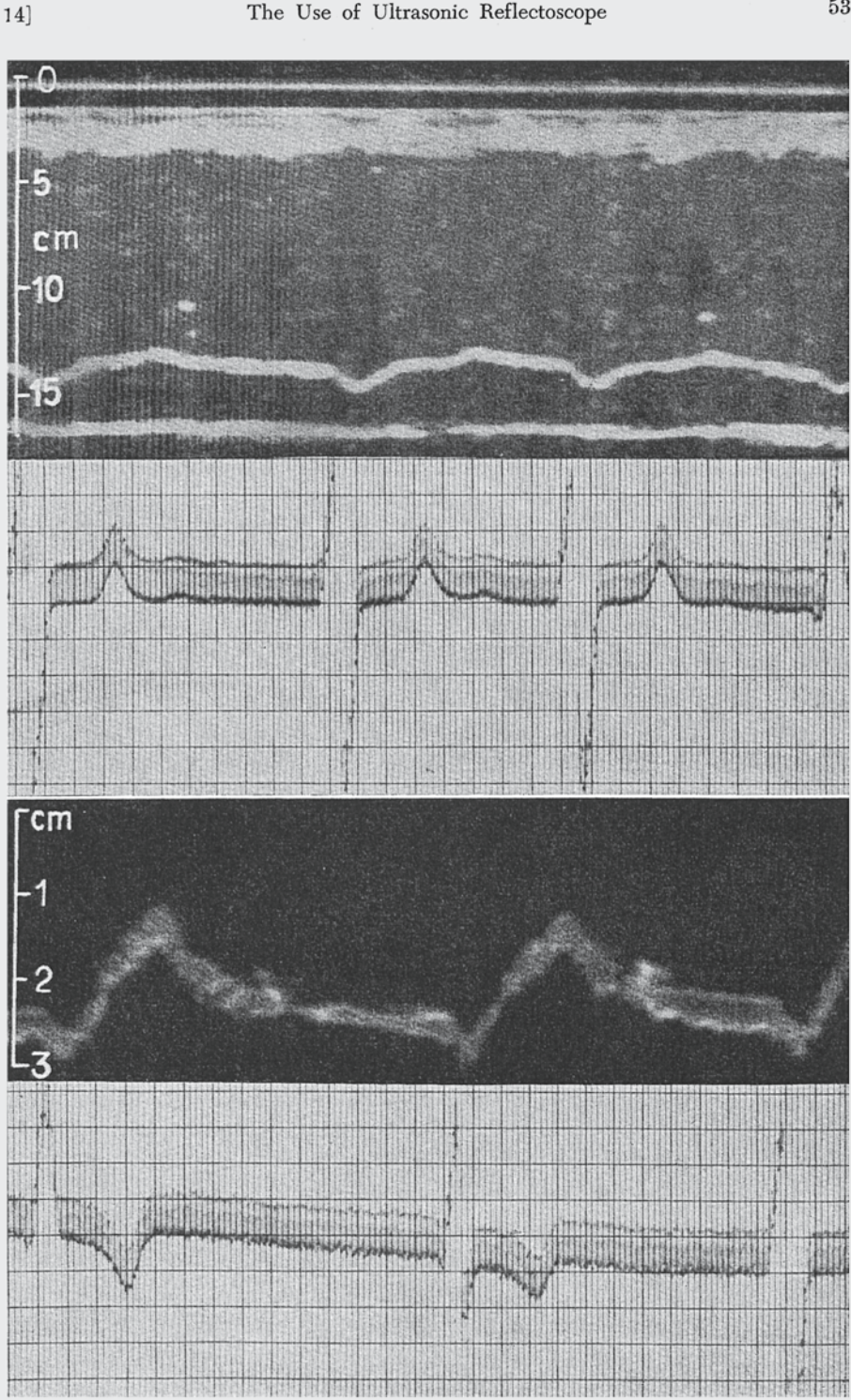


Fig. 9. UCG from a patient with aortic regurgitation. Top: General view. Bottom: Enlargement of the movements of the posterior wall of the heart.

height of the echo signal a measure of the strength of the reflected sound pulse. Thus the cause of a broad track in the UCG's may have been that the reflecting boundary was curved or not situated at right angles to the sound beam or that the echo signal was very strong. A thin track indicates a sharp but faint echo.

Since it was felt that the information about the movements of different parts of the heart gained by this method would be much easier to interpret if a simultaneous recorded and synchronized ECG were available, a synchronization device was applied to the UCG and ECG apparatus. After developing the 24 mm. UCG-film, the negative was enlarged just so much that the synchronization marks on the UCG film and ECG paper coincided. In this way a synchronization of UCG and ECG was achieved.

Preliminary Results.

The factors influencing the distance crystal-reflecting boundary are respiratory excursions of the chest and the movements of the heart. The influence of respiratory movements in the experiments hitherto performed appear to be of minor importance, so that it was not necessary for the patient to hold his breath during the examination. The movements of the heart during the cardiac cycle are complex. They are determined partly by the movements of the individual walls in association with the variation in the volume of the respective heart chambers and, second, by movements of the heart as a whole. The latter movements are due to changes in the shape of the heart during isometric contraction and relaxation.

Figs. 7 and 8 show curves for two normal persons. The crystal was placed in the left I:4 immediately lateral to the sternal border and the ultrasonic waves were delivered in sagittal direction. The maximum distance to the reflecting wall of the heart was 10.0 respectively 9.3 cm. The curves thus represent the dorsal part of the heart. In the enlargement of Fig. 7 the various phases of the movements occurring during the cardiac cycle are marked.

Fig. 9 shows the curve for the posterior wall of the left ventricle in a patient with aortic regurgitation and hypertrophy of the left ventricle. The curve deviates from normal by showing much greater amplitude during ejection systole and a much more abrupt return in dorsal direction during the beginning of diastole. This latter movement coincides in time with the rapid regurgitation in the beginning of diastole in advanced aortic insufficiency (1).

UCG's taken from the left I:3 about 3–5 cm. lateral to the sternal border over the region of the left atrium showed very rapid movements

16]

The Use of Ultrasonic Reflectoscope

55

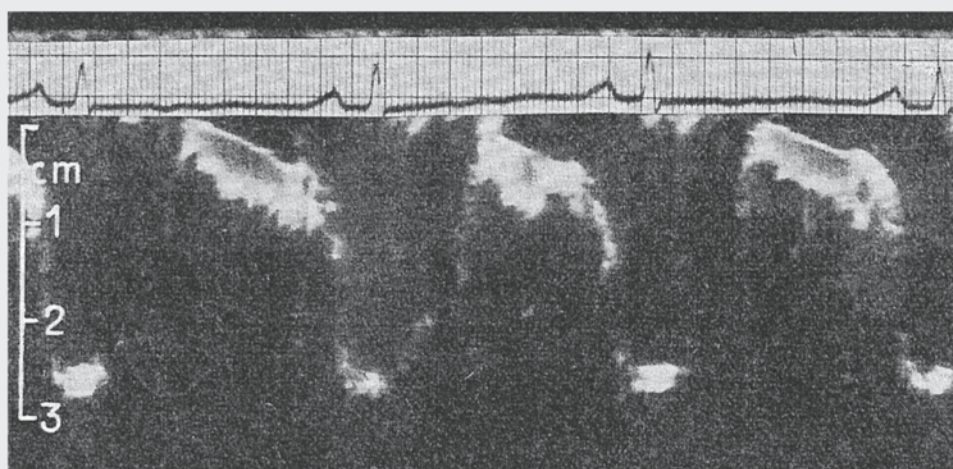
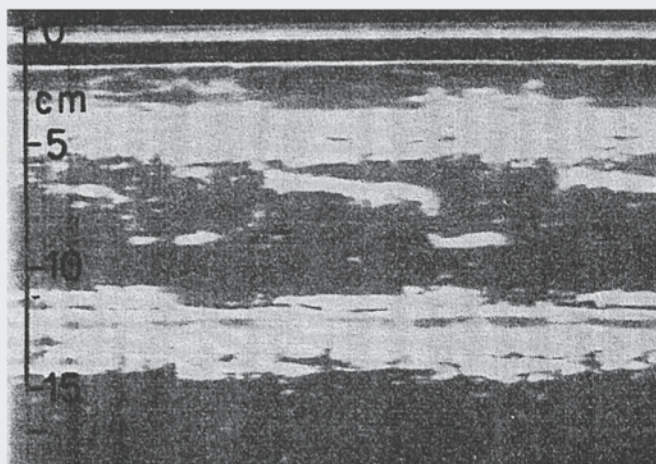


Fig. 10. UCG-curve showing the movements of left auricular wall in a case of mitral stenosis. Top: The curve shows a reflecting surface about almost 6 cm. from the anterior thoracic wall in the beginning of diastole. Bottom: Enlargement of the reflecting surface. From the beginning of ventricular diastole, when the atrio-ventricular valves open, the reflecting surface moves 6–7 mm. in dorsal direction. Immediately after the beginning of the P-wave in the electrocardiogram the sound reflecting surface makes a rapid movement in dorsal direction. This movement has an amplitude of about 2 cm.

During ventricular systole the wall returns to its original position.

at a depth of 5–7 cm. in some cases. In normals such movements were recorded only as fragmentary curves. All of them, however, showed a rapid movement of about 1 cm. in dorsal direction at the time of atrial systole, for which reason the relationship with atrial activity is obvious. For this reason, these sequences were studied in some patients with mitral

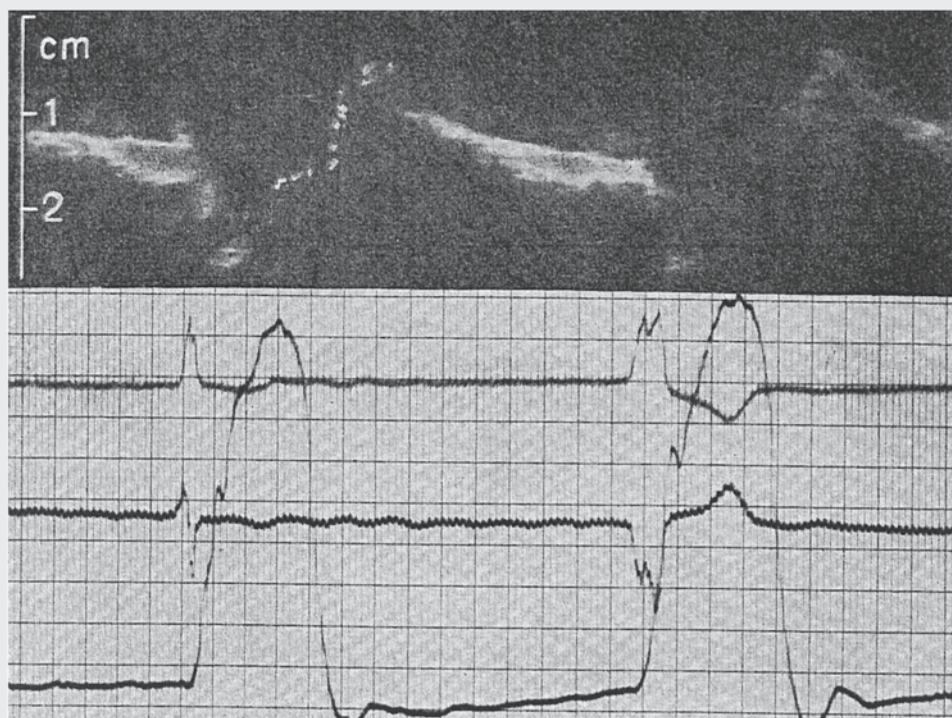


Fig. 11. UCG-curve showing the movements of left auricular wall in a case of mitral stenosis with auricular fibrillation. As in fig. 10, there is a gradual movement in dorsal direction after opening of the atrio-ventricular valves. A rapid movement is recorded at the time of the isometric contraction of the ventricle. At the time of the isometric relaxation of the ventricle, the reflecting surface returned in ventral direction.

valvular disease and enlarged left atrium. Better curves then were obtained from the left I:3. Fig. 10 shows a curve for a patient with pure mitral stenosis. Valvulotomy had been done before and post-operatively there were no signs of mitral regurgitation. The curve lies at a depth corresponding to the position of the anterior wall of the left atrium, and shows at the time of the atrial systole a rapid movement in dorsal direction. In cases of mitral stenosis with auricular fibrillation, in which effective mechanical contraction of the atrium is absent, this movement is missing (Fig. 11). In both cases, the wall during the first part of ventricular diastole is gradually displaced in dorsal direction. Fig. 11 shows a retraction of the wall during ventricular systole, which corresponds to the systolic collapse seen in pressure curves from the left atrium and which is due to the pull exerted by ventricular contraction.

The echosignals obtained from left I:3 over the region of the auricle correspond thus in position to the anterior wall of the left atrium. The movements of the echosignals correspond to the variation in the volume of the left atrium and to the contractions and displacements caused by the ventricular activity.

Summary.

- 1) It has been shown that it is possible to locate blood-heart wall boundaries by the supersonic reflectoscope method using frequencies of about 2.5 Mc.
- 2) The method was applied for the locating of heart walls on living human beings and continuous registration of movements of the heart walls was found possible.
- 3) Recordings are shown of the movements of the left ventricle wall in the normal and in the diseased heart. Further, movements of the left atrial wall in mitral stenosis were recorded.

The authors wish to express their sincere gratitude to Professor H. Malmros and Professor S. v. Friesen for invaluable support and interest in the study. Further thanks are due to Siemens Reiniger Werke, Germany, for placing the apparatus at our disposition.

References.

1. C. J. WIGGERS, *Circulatory Dynamics*, New York, Grune and Stratton, 1952. Pp. 53 ff.
2. R. F. RUSHMER *et al.* Continuous Measurements of Left Ventricular Dimensions in Intact, Unanesthetized Dogs. *Circulation Research* 2: 14 (1954).
3. W. D. KEIDEL, Über eine neue Methode zur Registrierung der Volumänderungen des Herzens am Menschen. *Zeitschr. f. Kreislaufforschung* 39, 257 (1949).
4. F. A. FIRESTONE, Supersonic reflectoscope, an instrument for inspecting the interior of solid parts by means of sound waves. *J. Acoust. Soc. Am.* 17, 287, (1945).
5. L. BERGMANN, *Der Ultraschall*, p. 530 (1949).
6. R. ESCHÉ, Untersuchung zur Ultraschallabsorption in tierischen Geweben und Kunststoffen. *Akustische Beihefte* 2, AB 71 (1952).
7. L. BERGMANN, *Der Ultraschall* p. 649 (1949).
8. T. HÜTER, Messung der Ultraschallabsorption in tierischen Geweben und ihre Abhängigkeit von der Frequenz *Naturwiss.* 35, 285 (1948).
9. E. L. CARSTENSEN, K. Li and H. P. Schwan. Determination of the acoustic properties of blood and its components. *J. Acoust. Soc. Am.* 25, 286 (1953).

10. G. D. LUDWIG, The Velocity of Sound through Tissues and the Acoustic Impedance of Tissues. *J. Acoust. Soc. Am.*, 22, 862 (1950).
11. A. H. FRUCHT, Die Geschwindigkeit des Ultraschalles in menschlichen und tierischen Geweben. *Naturwiss.* 39, 491 (1952).
12. J. J. WILD and J. M. REID. The Effects of Biological Tissue on 15 Mc pulsed Ultrasound. *J. Acoust. Soc. Am.* 25, 270 (1953).
13. W. GÜTTNER, G. FIEDLER and J. PÄTZOLD, Über Ultraschallabbildungen am menschlichen Schädel. *Acustica* 2, 148, (1952).

3.4 The ultrasonic visualization of soft tissue structures in the human body

Joseph H. Holmes (1902–1982)

Joseph Holmes was born in Champaign, Illinois in 1902. After graduating from Amherst College with an BA in 1930, Holmes completed his MD degree at the Case Western Reserve University in Cleveland, Ohio, in 1934. He finished his internship at Emory University in 1934–1935. From Emory, Holmes went to the University of Maryland School of Medicine for his residency in internal medicine, which he completed in 1937. Holmes did graduate work at Columbia University in the Department of Physiology from 1937–1941. In 1941 he received his Doctorate of Medical Science degree. Holmes served in the army from 1943–1947, and worked as an instructor in the School of Aviation Medicine. He continued as an assistant professor in physiology at Columbia and from 1947 he began his long career at the University of Colorado.

Being a nephrologist, his initial interest in ultrasound was its ability to detect bubbles in hemodialysis tubings and improve solute transfer across the cellophane dialyzing membrane. Holmes began work in ultrasound at the University of Colorado Medical Center in 1950, in collaboration with the group headed by Douglass Howry. Holmes served as a liaison between Howry and the institutional backing that was needed badly if the project was to gain financial support and proceed further. Holmes functioned as a general administrator and financial planner during those early years. Through Holmes' help, laboratory space for the ultrasound project was found at the Denver Veterans Administration Hospital and a grant was obtained from the Veterans Administration. Under these somewhat more secure conditions the Howry team constructed the most successful to date of their "home-built" scanners, which incorporated the best of their transducer, amplification, and display systems.

The pan scanner fabricated by the Holmes, Howry, Posakony and Cushman team in 1957 was a real breakthrough and landmark invention in the history of B-mode ultrasonography. The team's achievement in visualising body tissues by ultrasound was commended by the American Medical Association in 1958 at their Scientific Meeting at San Francisco, and the team's exhibit was awarded a Certificate of Merit by the Association.

Holmes was also involved with the building of the first artificial kidney machine in the Rocky Mountain region in 1953, and he made hemodialysis treatment available to patients on an out-patient basis. He also studied the health hazards of anticholinesterase chemicals of the United States army at the Rocky Mountain Arsenal and made such information available to the medical community at large and the public. Holmes together with Howry and Wright and Claude Joyner and John Reid from the University of Pennsylvania constructed the first echocardiograph in the United States in 1960. The first commercial m-mode echocardiograph was manufactured by SmithKline in 1964.

In 1951 Holmes was named Professor of Medicine at the University of Colorado, and received a joint appointment as Professor of Radiology in 1970. Holmes served as President of the American Institute of Ultrasound in Medicine (AIUM) from 1968–1970. During Holmes' presidency, the AIUM expanded membership and increased meeting attendance. The William J. Fry Memorial Lectureship began at the Winnipeg meeting (1969). He was also founding editor of the *Journal of*



Clinical Ultrasound in 1973. Joseph Holmes and Ian Donald became good friends across the Atlantic, and Ian Donald and John Flemming were invited to speak on their experiences at the International congress at Pittsburg hosted by Holmes in 1963. Donald spoke about Holmes in a speech he gave in 1967 to the World Federation for Ultrasound in Medicine and Biology (WFUMB): *'I think Joe Holmes has done more than anyone to pull us all together from our several pathways'*. At his death in 1982, the AIUM renamed the Pioneer Award in his honor, the Joseph H. Holmes Pioneer Award.

Joseph Holmes retired in 1977 but continued as Professor Emeritus of Medicine and Radiology at the University of Colorado. He spend his last years writing and editing publications in the field of ultrasound. He passed away on 5 April 1982.

In part excerpted with permission from the webside www.ob-ultrasound.net by Joseph Woo, MD, Hong Kong. Picture courtesy Joseph Woo, MD.

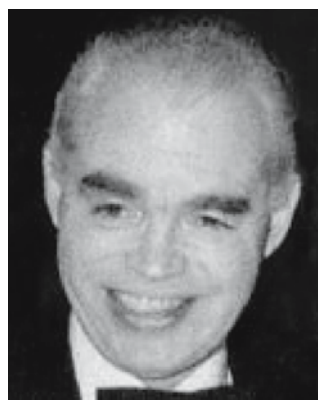
Douglass H. Howry (1920–1969)

Dr. Douglass Howry was born in 1920. He received his medical degree from the University of Colorado Medical School in 1947. In 1948 he looked into the possibility of applying ultrasound in the production of diagnostically valuable images. Working at first in his own basement, Howry began investigating the notion that ultrasound beams directed into the body would be reflected from tissue interfaces.

Howry employed frequencies of around 2.5 MHz, characteristic of industrial flaw detection equipment. He was chiefly interested in achieving accurate anatomical pictures of soft-tissue structures, rather than the A-mode spikes reported by John Wild at the University of Minnesota, Minneapolis, and was committed to improving the imaging quality at these frequencies. Working in collaboration with his wife, Dr. Dorothy Howry and two engineers, Roderick Bliss and Gerald Posakony, Howry produced in his basement in 1949 a pulsed-echo ultrasonic scanner. The equipment was constructed from spare parts that were then adapted and integrated to produce a functioning imaging system: electronic parts from radio-surplus stores, a Heathkit oscilloscope, and surplus Air Force radar equipment. A second incarnation successfully recorded echoes from tissue interfaces, and in 1950, using a 35-mm camera, Howry recorded his first cross-sectional pictures obtained with ultrasound.

During 1951, Dr. Joseph Holmes became associated with Howry's project. Holmes served as a liaison between Howry and the institutional support needed so badly if the project was to gain financial support and proceed further. Holmes functioned as a general administrator and financial planner during those early years. Through Holmes' help, laboratory space for the ultrasound project was found at the Denver Veterans Administration Hospital and a grant was obtained from the Veterans Administration. Under these somewhat more secure conditions the Howry team constructed the most successful to date of their "home-built" scanners, which incorporated the best of their transducer, amplification, and display systems.

By 1951 Howry, Posakony and Bliss had introduced multiposition, or compound, scanning to eliminate "false" echoes and produce better images. This incarnation incorporated an immersion tank system using a cattle-watering tank with the ultrasonic transducer mounted on a wooden rail. The transducer, immersed in the tank with the object under study, moved horizontally along the rail. When this equipment produced improved pictures, the Howry team published for the first time in 1952. A later version, introduced in 1954, included a transducer



mounted on the rotating ring gear from a B-29 gun turret, which in turn was mounted around the rim of a large metal cup that served as the immersion tank. This permitted complete horizontal circling of the periphery of the tank, while a second motor produced back-and-forth motion as the transducer moved around the tank, resulting in compound scanning of the immersed subject. The resulting image was called a “somagram”. The innovative apparatus was reported in the medicine section of LIFE Magazine in 1954.

A final incarnation, the pan scanner, was developed at the University of Colorado Medical Center in the late 1950s under a Public Health Service Grant. This scanner, in which a transducer carriage rotated on a semi-circular water-filled pan that was strapped to the patient’s body, was developed specifically to eliminate the need for total immersion of ill patients. The achievement was commended by the American Medical Association in 1958 at their Scientific Meeting at San Francisco, and the team’s exhibit was awarded a Certificate of Merit by the Association.

Howry’s team recognized the problems inherent in the water-bath coupling system; furthermore, by this time several other investigators, including Wild and Reid and Ian Donald’s group in Glasgow, had published on their work with direct contact scanners. Howry met Donald for the first time in 1960 at an exhibition in London of Donald and Brown’s new contact scanners. After he returned to the United States, Howry’s group produced a device similar to that of Donald’s, but which had quickly evolved into the multi-joint articulated arm (elephant-trunk) scanner.

Douglass Howry subsequently moved to Boston in 1962 where he worked at the Massachusetts General Hospital. He passed away in 1969. The work of Howry and his team is considered to be the most important pioneering work in B-mode ultrasound imaging and contact scanning in the United States, the direct precursor of the kind of ultrasound imaging we have today.

Excerpted with permission from the website www.ob-ultrasound.net by Joseph Woo, MD, Hong Kong. Picture courtesy Joseph Woo, MD.

Gerald J. Posakony

Gerald J. Posakony received a BSEE degree in electrical engineering from Iowa State University in Ames, Iowa. After working several years as an engineer for Decimeter, Inc., which was a small electronics firm in Denver, CO, and as a field engineer for Motorola, Inc., he joined the faculty of the University of Colorado Medical Center as a research engineer. There he conducted pioneering research in medical diagnostic ultrasound with Douglas Howry, William Roderick Bliss and Richard Cushman at the University of Colorado, and produced the first B-mode scanner in the United States.

Posakony left the university to join Automation Industries, Inc., advancing to Vice President and General Manager of the Research Division in Boulder, Colorado. In this capacity, he was responsible for the developmental research, instrument design, technical procedures and manufacture of systems for nondestructive evaluation (NDE) technology in ultrasonic, eddy current, infrared and magnetic methods.

Posakony acted in the capacity of consultant in later developments of the Denver group. In 1973, he joined the Pacific Northwest National Laboratory (PNNL), one of nine U.S. Department of Energy multiprogram national laboratories, as manager of the NDE Section. This section was responsible for the design, development and deployment of advanced NDE technology. He became manager



of the Automation and Measurement Sciences Department in 1986. The department staff included physicists, computer scientists, electrical and mechanical engineers, and technicians engaged in design, development and deployment of “first of a kind” inspection and measurement systems. In 1989, he became Deputy Manager of the Applied Physics Center with managerial responsibility for staff in the Automation and Measurement Science, Computational Science and Energy Science Departments of the Center.

While officially retired from PNNL, he remains on staff as an hourly professional to continue research, development and deployment of NDE Technology. Posakony has spent more than 35 years in the design, development and deployment of first-of-a-kind NDE inspection and measurement systems. He has continued personal research in ultrasonic transducers, inspection technology and ultrasonic wave propagation as well as other activities in the field of NDE.

Posakony personally holds more than 12 important patents in the field of ultrasonics and is author of more than 60 technical articles and publications. He is Associate Editor of *Research in Non-destructive Evaluation* (Springer), and *Journal for Non-destructive Evaluation* (Plenum).

During his career he has received the following honours, awards and professional affiliations: Fellow, American Institute for Ultrasonics in Medicine 1980; William Fry Memorial Lecture Award, AIUM 1981; AIUM, Pioneer Award 1988; Fellow, American Society for Nondestructive Testing (ASNT) 1974; ASNT Lester Honor Lecture Award 1976; ASNT Gold Medal Award 1985; Fellow, American Society for Testing Materials (ASTM) 1990; ASTM, Award of Merit 1990; ASTM, 25 Year Recognition 1998; Member, American Society of Metals (ASM); Registered Professional Engineer (PE) (Quality Engineering); ASNT Level III Certification – ULTRASONICS – (MB-703); and National Research Council, NMAB Committees, 1969, 1977, 1983.

In part excerpted with permission from the webside www.ob-ultrasound.net by Joseph Woo, MD, Hong Kong. Picture courtesy Joseph Woo, MD.

C.R. Cushman

THE ULTRASONIC VISUALIZATION OF SOFT TISSUE STRUCTURES IN THE HUMAN BODY

By JOSEPH H. HOLMES, M.D.,
and (*by invitation*) DOUGLASS H. HOWRY, M.D.,
GERALD J. POSAKONY and C. RICHARD CUSHMAN

DENVER, COLORADO

I think most of you are aware of the fact that ultrasonic techniques are currently being used in three principal areas in medicine; namely, for its destructive action in the central nervous system and in therapy of tumors,¹ in physical medicine especially for the treatment of arthritis,¹ and in diagnostic visualization of body structures, particularly those soft tissue structures where current diagnostic techniques are not of optimum value. This paper will be limited to a discussion of the diagnostic use of ultrasonic techniques. Our particular equipment works with power, only a fraction of that used for therapy and much less than that used in the field of physical medicine. For this reason the problem of damage to tissues has not been encountered in our work. The observers working with this equipment and the test animals used in this work have shown no evidence of any tissue damage. Usually intense pain precedes induction of tissue damage with ultrasonic waves. There has been no pain or other evidence of tissue damage in the use of our techniques.

Several other groups have worked on this general problem^{1, 2, 3, 4, 5,} but we will limit the present discussion to our own experience.^{6, 7} Perhaps a series of questions and their answers will best explain what we are trying to accomplish with this method.

Supported in part by a grant from the Veterans Administration and in part by a Grant No. C-2423 NSS from the U. S. Public Health Service.

ULTRASONIC VISUALIZATION

209

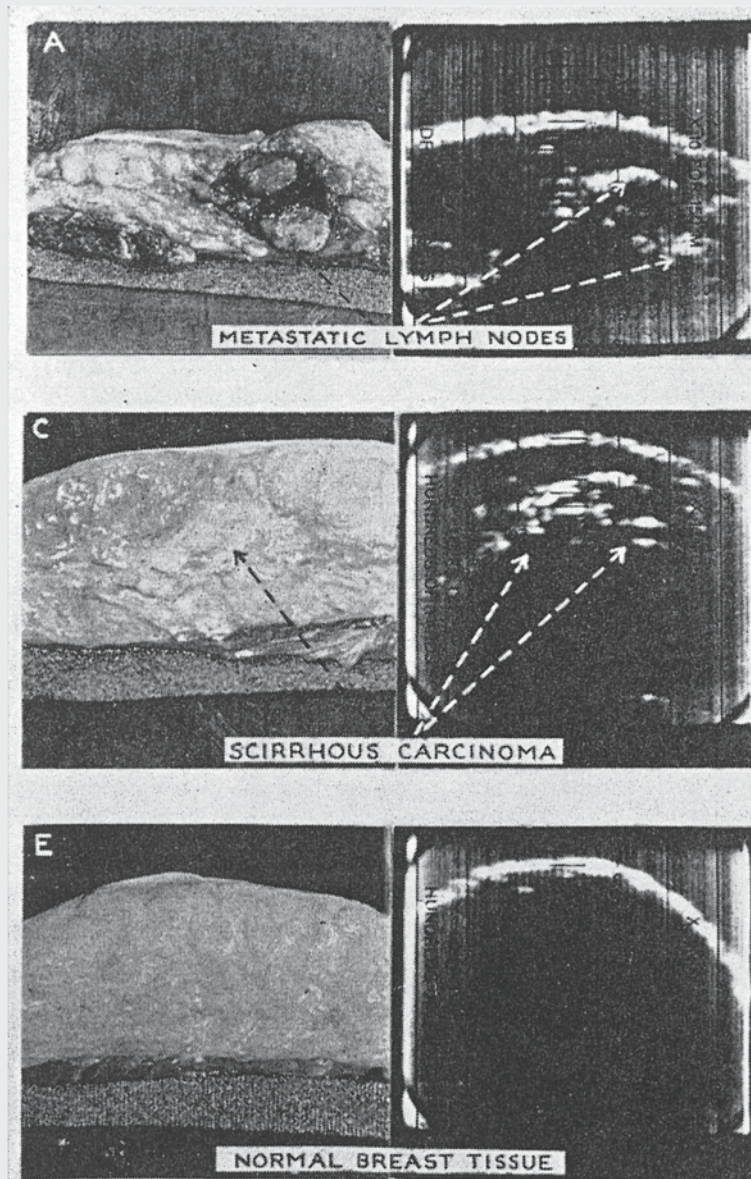


FIG. 1. The middle picture shows a pathological specimen of a breast with scirrhous carcinoma.

The upper picture shows metastatic lymph nodes from the same specimen.

The lower picture shows a non-carcinomatous area of the same breast. The corresponding somagrams for each specimen are shown. It will be noted that the areas of carcinoma show up as white patches inside the general outline of the breast.

What does ultrasonics technique offer that cannot be obtained with current diagnostic methods? Figure 1 (middle picture) shows a pathological specimen of a breast with scirrhous carcinoma which was not palpable prior to surgery. The somagram, or picture, taken with our equipment is shown beside it. There is the outline of the skin surface of the specimen, and then a series of contrasting areas are shown at the level where the carcinoma was identified by the pathological sections. The remainder of the breast tissue casts no particular shadow. In an area where there is no carcinoma, as shown in the lower picture (Figure 1), no shadows are noted on the somagram. In the upper specimen containing the metastatic lymph nodes, definite shadows appear in an area corresponding to the site of the lymph nodes containing the carcinomatous lesion. Thus, it can be seen that areas of different tissue density such as carcinoma will show up on the somagram.

How is this visualization accomplished? Figure 2, in the lower part, shows a pathological specimen of a kidney cyst. The upper part of this figure shows how the somagram of this kidney cyst appeared on the somascope screen. There is the large outline of the cyst wall and then the homogenous area inside the cyst wall which corresponds to the clear cyst fluid found when the specimen was sectioned. The outline of the kidney is seen adjacent to the cyst, and some of the structures inside the kidney, especially the central portion are visualized.

The general method by which visualization is accomplished closely parallels the echo ranging techniques which are used in sonar and radar. In essence, we are using the electronic techniques of radar as applied to the field of ultrasonics.

A trigger generator (timing mechanism) causes the pulse generator to develop a simple square wave pulse of approximately 0.25 microseconds duration, which is controllable from zero to 3000 volts amplitude. This pulse is passed to an ultrasonic crystal which is mounted in a waterproof housing and which under the influence of the pulse voltage, is caused to expand and contract violently for a short period of time, thus producing a mechanical wave. By using ultrasonic

ULTRASONIC VISUALIZATION

211

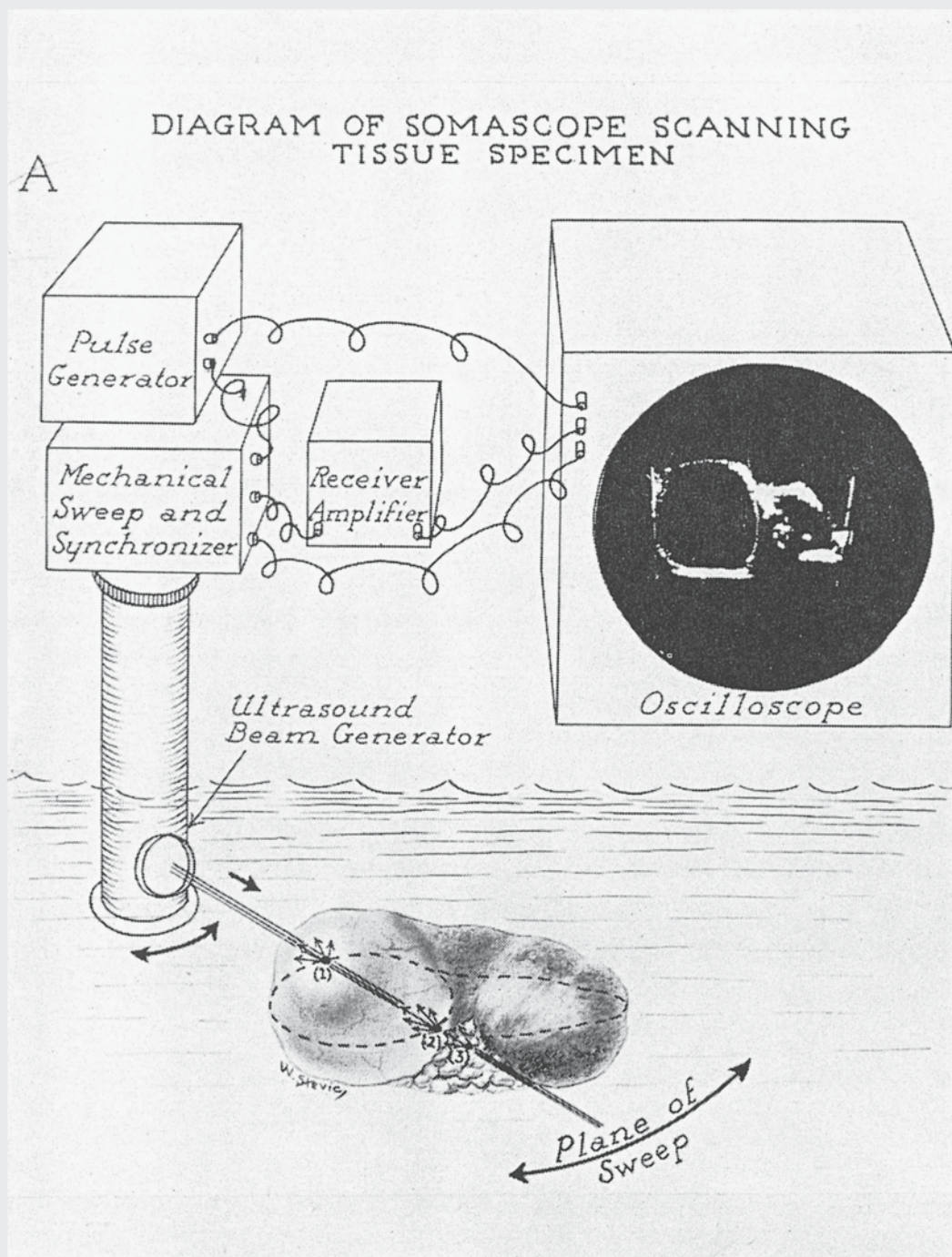


FIG. 2. Shows the major units of the somascope and the manner in which the kidney cyst depicted in the lower part of the diagram appears on the somascope screen.

lenses, the mechanical wave is confined to a beam of narrow dimensions, which has a cross section considerably less than that of the driver crystal. The ultrasonic beam or burst of energy travels through liquid until it strikes some discontinuity, such as the object to be examined. At the surface of this object a small portion of the sound pulse is reflected back through the liquid until it again strikes the crystal. The crystal driver is so designed that after transmitting the pulse it reaches a quiescent state before the echoes return to it, thus allowing the crystal to become a receiver. The mechanical echo is transformed into an electrical signal by the crystal. This signal is then amplified by the receiver amplifier, and presented as a single spot on the cathod ray oscilloscope. Each discontinuity of structural change within the object similarly produces an echo which becomes a single spot on the oscilloscope. Thus, as the beam of energy penetrates the object, a line of spots representing reflective surfaces is formed on the oscilloscope, the distance between these spots corresponding to the distance between sound reflecting surfaces in the object studied. As soon as the echoes have all returned from the initial ultrasonic pulse, a new pulse is generated which travels in a slightly different path, because of a mechanical shift in position of the sound generator. The new pulse thus passes adjacent to the path of the previous pulse. Accordingly, a new line of spots is produced on the cathode ray oscilloscope adjacent to the old line. Thousands of pulses or bursts of energy are formed in this same manner every second, each passing in a slightly different direction through the object being studied. Thus the beam is swept mechanically back and forth across the object by the mechanical sweep and synchronizer while single pulses draw lines of spots on the screen. Due to the rapidity of this operation it is possible to form a visually continuous picture on the oscilloscope screen in a manner which is very similar to that employed in television. It should be noted that by this operation the somascope produces only a cross sectional picture, much as would be produced if the specimen were sectioned with a knife and the resultant slice seen from above.

ULTRASONIC VISUALIZATION

213

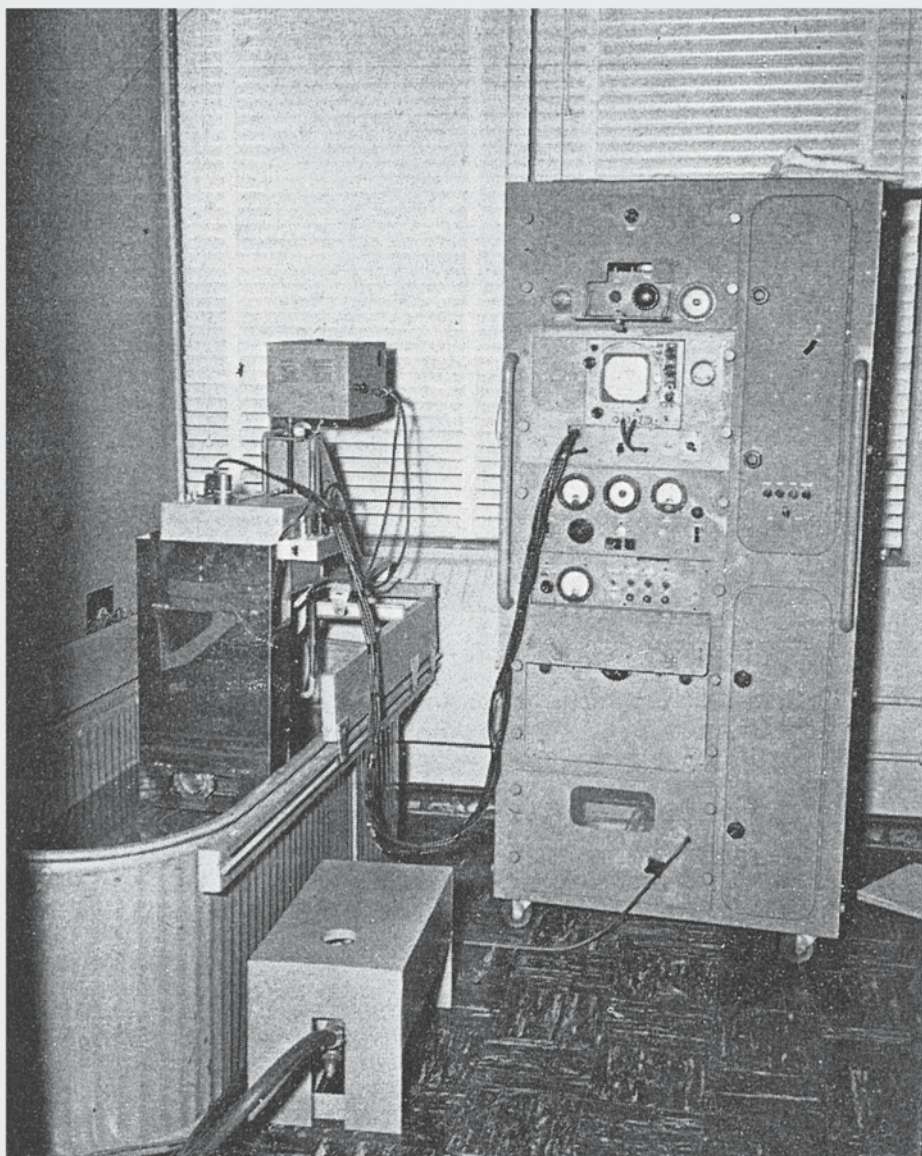


FIG. 3. A picture of the somascope in its present form.

Ultrasonic mechanical waves in the megacycle region will not pass through air without prohibitive losses; therefore, the subject or specimen to be examined must be either submerged in a liquid media or be in direct contact with some solid material through which the sound can travel. In our work, the

anatomical structure being studied is submerged in a water-filled tank.

The somascope is in the physical form shown in Figure 3. The power supplies, pulse generator, amplifiers, synchronizing systems, and oscilloscope are housed in the large steel cabinet. The mechanical scanning system and sound generator are mounted on the large tub. The patient is placed in the tub which is filled with warm water and the sound head is moved into position for study. The somagrams or sound pictures appear on the white square (face of the oscilloscope) seen in the upper portion of the steel cabinet. The picture formed may be interpreted directly by the observer as in the case of a fluoroscopic examination, or for permanent recording photographed with a standard camera. All somagrams are studied carefully on the screen frequently from different angles before the final picture is taken, thus, it is possible for the observer to identify structures which might seem difficult to identify in the pictures being presented to you.

How well can this equipment differentiate between structures of different density which are closely approximated? Figure 4 shows a cross section of the neck of a normal person taken at the level of the fifth cervical vertebra. The general surface of the neck can be seen and within this one can locate the skin, trachea, carotid artery, jugular vein, and most of the muscles by their surrounding fascia. The neck represents one of the most difficult areas in the body to study since the structures are closely approximated and hence somewhat difficult to separate and identify. This identification is easier when the structure is moving as in the case of an artery. In the lower part of the figure can be seen the wave motion of an artery, and the A, C and V waves of one of the deep veins. The first pictures show the reflected wave motion to the skin over the carotid artery. If one were to adopt to our equipment the "moving target" technique of radar which has been well worked out for spotting of planes or determining the speed of a car on the highway, then one might study in greater detail the wave motion of the heart and great vessels. Thus, it might be possible in the future to determine the size of the

ULTRASONIC VISUALIZATION

215

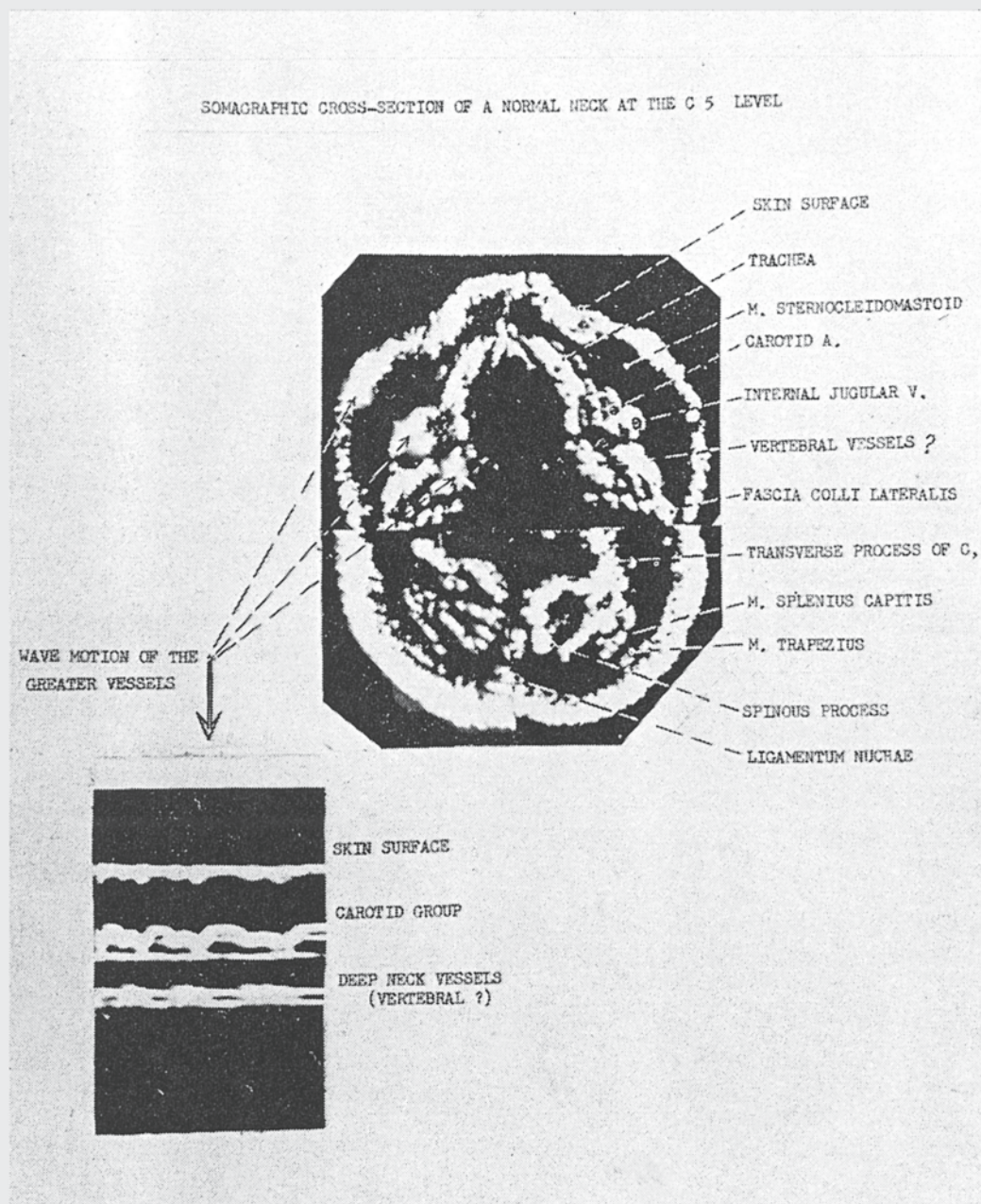


FIG. 4. Shows a cross section of the neck of a normal person taken at the level of the 5th cervical vertebra.

In the lower left hand corner can be seen the somagram of the wave motions of the skin over the carotid artery of the carotid artery, and of one of the deep cervical veins.

ventricle in various phases of contraction, size of the large vessels at different time phases of the cardiac cycle and any abnormalities in the contractile phase such as might be present with defects of the vessel walls.

What diagnostic use can be made of the displacement of anatomical structures? A tumor may be detected not only by the fact that it abnormally reflects sound waves, but also by the fact that it may displace adjacent structures. When a somagram was taken of the neck of a patient with benign colloid goiter, the gland was quite homogenous so echoes were produced principally at its surface, and only the outline of the enlarged gland could be seen. If there had been adenomas or cystic degeneration, then these areas might well have shown on the somagram.

How well does a non-metallic foreign body show with this technique? This instrument can readily detect the presence of foreign bodies, such as plastic or rubber. When small rods of metal, plastic, rubber and wood were embedded in a piece of liver, the somascope readily detected all four objects; whereas, the x-ray showed clearly only the metal rod.

What picture do fluids present on the somagram? From preliminary studies it would appear that the somascope could differentiate between clear and cloudy fluids in the body. When a thin walled rubber condom was filled with clear fluid the somagram showed only the outline of the condom. The fluid within was clear, or homogenous, and cast no shadow on the screen. When talc was introduced into the fluid, then the sound waves were reflected by the talc particles and the previous homogenous appearance of the fluid had changed to approximate the appearance of a "snow storm".

What other areas in the body can be visualized by this technique? The liver and spleen are good subjects for partial examination by our current equipment. Figure 5 (first picture) shows a somagram of the abdomen of a normal person. The outline of the right half of the rectus muscle and other layers of the abdominal wall are easily identified. The bowel peristalsis and the progress of food through segments

ULTRASONIC VISUALIZATION

217

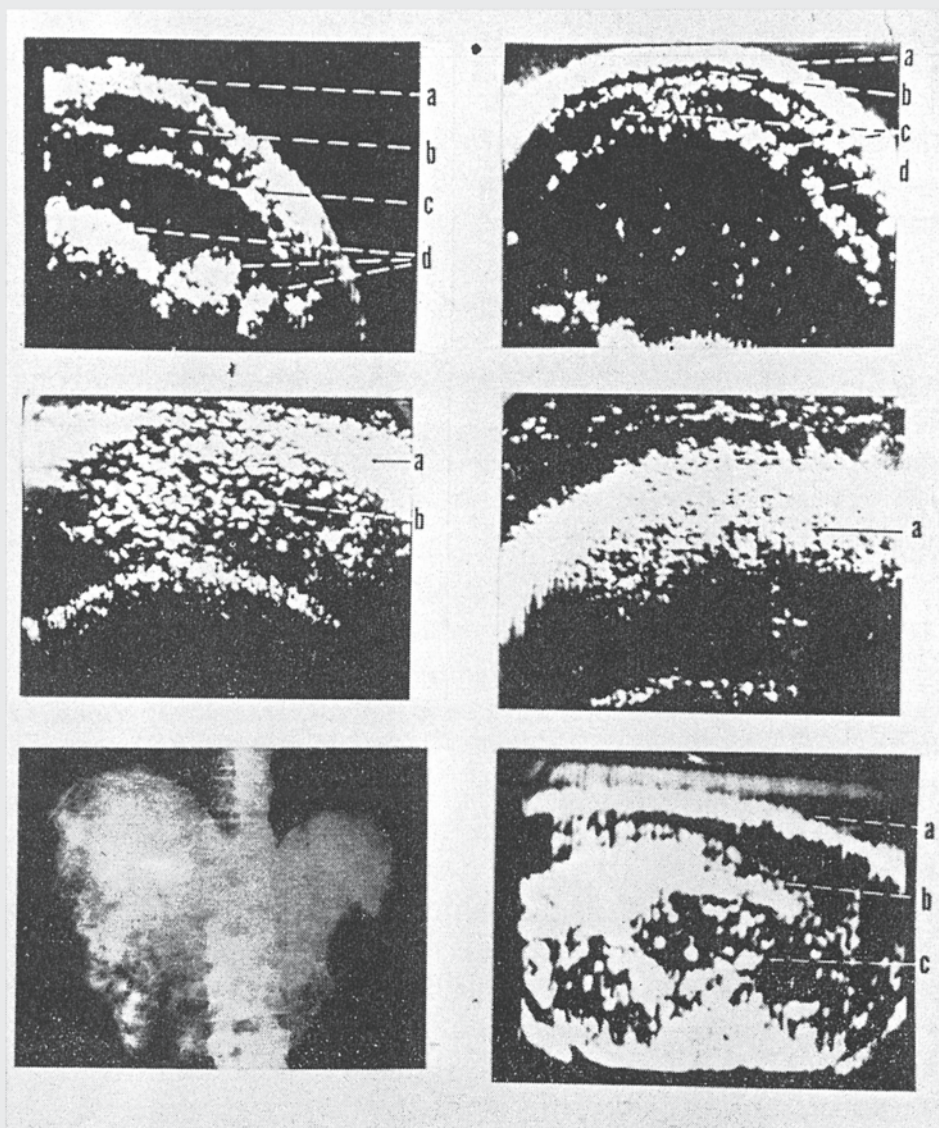


FIG. 5. Shows a series of somagrams taken over the liver area of the abdomen.

The first is of a normal individual as food is passing down the intestinal tract. The second is of a patient with moderately advanced cirrhosis with hepatomegaly. The third is of a patient with far advanced cirrhosis where one can note the "snow storm" like appearance of the liver. The fourth is of a patient with diffuse miliary melanoma of the liver. The fifth is a thorium dioxide radiograph of a patient with nodular metastases in the liver. The sixth picture is the corresponding somagram of the same patient.

of the small bowel could be followed on the somascope screen much as the barium is followed in the fluoroscopic examination by x-ray. The adjacent somagram in Figure 5 is that of a patient with moderately advanced cirrhosis and hepatomegaly. The patient had a marked accumulation of ascitic fluid at the time of examination. The somagram shows a thin anterior abdominal wall which correlated with the thin atrophic abdominal wall seen on physical examination. Immediately below this is seen a dark clear strip which probably represents an accumulation of ascitic fluid between the abdominal wall and the anterior liver surface. This dark strip was not present after the ascitic fluid had been removed. Both lobes of the liver are partially outlined and the anterior and posterior surfaces are seen. Few echo signals are returned from within the liver, thus suggesting that it is relatively homogenous at all levels.

The next somagram was taken from a patient with far advanced cirrhosis. The abdominal wall and both surfaces of the liver can be seen. Within the liver outline there is a "snowstorm like" appearance which was obtained at all the power levels considered to be reasonable. Autopsy examination of this patient was done three weeks after this study. Gross examination of the pathological specimen showed a typical "hobnail" liver, which on cross-sectioning showed miliary foci of dense fibrous tissue and areas of hepatic necrosis. Comparison of this with the previous figure suggests that this might be of diagnostic value in determining the degree of involvement of the cirrhotic process.

A somewhat similar picture to that of the above patient was obtained from a young man who had had a malignant melanoma removed from the back of the neck eighteen months prior to examination. At the time of examination he had cutaneous metastases and a marked hepatic enlargement which suggested liver metastases. The somagram in Figure 5 shows the same "snowstorm like" appearance which was seen in the previous case. No discrete areas of tumor metastases can be seen. One month later at autopsy, the cut liver surface presented a dense, black, stippled appearance due to diffuse miliary

ULTRASONIC VISUALIZATION

219

metastatic malignant melanoma. There were no discrete areas of metastatic nodules.

The next patient studied had a carcinoma of the thyroid which had been proved by surgery and radio-iodine uptake studies. In the thorium dioxide radiograph (5th picture, Figure 5) the liver was found to be markedly enlarged and showed definite nodular metastases. In the somagram powerful echoes were obtained of a more localized nature than was obtained in any of the previous liver examinations. On the somascope screen many of these areas had the appearance of being roughly circular in shape and seemed to correspond to the radiographic findings. This is shown in the 6th picture, Figure 5.

What are some of the problems which must be solved before this instrument will be clinically useful in the average physicians' hands? It should be remembered that all pictures presented represent cross-sections of the anatomical areas studied. Most physicians are accustomed to seeing anatomical structures in three dimensions and are not familiar with the cross-sectional presentation. In studying a tumor of moderate size, it may be necessary to make as many as 48 cross sectional pictures before the exact size and outline of the tumor can be shown. Recently we have developed a 3 dimensional technique which will also permit stereoscopic viewing of the tissues studied. This is accomplished electronically so that sequential cross sectional pictures are partially superimposed to achieve a three dimensional form. The projection of view can be changed electronically from 0 to 90°. In the upper pictures, Figure 6, we utilized as a test object, a small box made of wire which contains a small wire in the center running from one edge at the top to the opposite edge at the bottom of the box. When two views are separated by about 10 degrees then it is possible to view the object stereoscopically. The lower part of the figure shows the results of this technique as applied to visualization of the normal forearm. One can note the 3 dimensional projection of the skin surface and some of the fascial structures.

Another current problem is the inability to visualize structures immediately behind a strong reflecting surface, particular-

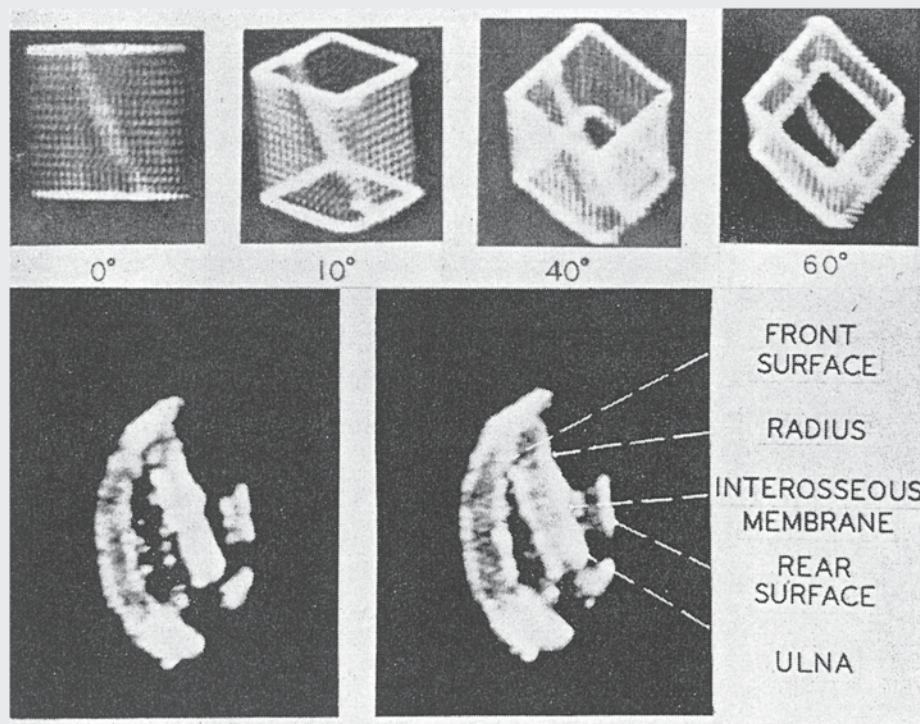


FIG. 6. Shows projection at several different angles of a small wire box. The lower picture represents a three dimensional view of a section of the forearm of a normal person.

ly dense tissues such as bone. This problem was solved in the somagram of the neck (Fig. 4) by obtaining a combination of four pictures with the scanning device placed in four different quadrants. Had the scanning head been placed only in one position, then the anatomical structures lying behind the vertebrae and trachea would not have been visualized. This problem is currently being solved by devising a scanning system which will move all the way around the test object, thus making it possible for example to visualize the entire neck in a single picture.

One of our most important problems at present is the improvement of definition. Currently, we have a definition of approximately 16 lines per inch. We would be able to obtain ideal definition if we could obtain definition up to

approximately 32 lines per inch. Various types of picture artifacts have proved troublesome in this work and have been partially eliminated. By constructing a gain compensator we have corrected for the absorption of sound in tissue in such a way that objects on the surface of the body appear on the screen as of the same size and density as those deep within the structures. Sound waves traveling circuitous pathways are eliminated by altering the time of pulsing of the crystal so that only those waves directly reflected by a structure are recorded on the screen continuously.

What areas cannot be studied by this equipment at the present time? Many body areas have not yet been explored. With the present equipment it is still not feasible to study an organ such as the pancreas because of the many structures overlying it. The skull presents a quite difficult problem since the ultrasonic wave cannot readily penetrate the bone without an extreme loss of amplitude. Dr. Ballentine and Dr. Hueter have been studying the ultrasonic visualization of the brain structures using a different approach, but have not yet found a solution to this particular aspect of the problem.⁸

What might such equipment promise to do for medicine in a diagnostic manner in the future? Certainly one can speculate about the use of this equipment in many different fields, and those of you with special interests will think of something which has not yet come to our mind. One might well be able to visualize the interior structures of the heart and to define such anatomical entities as the size of the ventricular wall, the valve structure, papillary muscles, the septum, etc. One can certainly locate non-metallic foreign bodies which are not readily apparent by external examination. One might well define the limits of an area of injury in the deep soft tissue structures which followed trauma. Certainly one would hope to define accurately such structures as the kidney, pancreas, liver and spleen. These represent structures where current diagnostic methods are limited. Fat is a good reflector of sound waves, and fortunately many of these organs are surrounded by a layer of fat which makes it much easier to define their general structure by the somascope. The ability to define

the extent of a metastatic lesion might prove of great value to the surgeon, especially if we could also define structures such as nerve and artery which enter the tumor tissue.

When will such an instrument be available for clinical use, and what will it look like? You may well have gathered from the previous discussion that we are devoting all our efforts to improve the equipment, especially its definition and ability to penetrate to deeper structures. Another essential improvement is some method which will obviate the use of a tub of water since this presents many problems in the examination of sick patients. It should be possible to pass the sound waves into the tissues by means of a probe consisting of a fluid-filled, thin walled rubber bag located between crystal and skin.^{4,5} It will be necessary by clinical experience to define the limitations and abilities of this particular instrument. For example, no attempt has been made at present to use contrast media, but one might well expect that an injection of .9 per cent saline would serve as a simple contrast medium, could readily be absorbed by the tissues after examination, and would not present the hazards of the present radio-opaque materials necessary for x-ray examination. The completed unit would probably be about the size of a large television set and its operation no more difficult than the usual x-ray equipment. The cost of such equipment would certainly be a guess at this time, but several manufacturers have suggested that it would run somewhere in the neighborhood of \$10,000.00 to \$15,000.00. A new unit which was recently constructed for our own work cost in the neighborhood of \$18,000.00.*

SUMMARY

We have described the operation of new diagnostic equipment which we have called the somascope and which utilizes the principals of sonar and radar to visualize soft tissue structures in the body. The pictures are presented on an oscil-

*Partially constructed by Denver Research Institute, University of Denver.

ULTRASONIC VISUALIZATION

223

loscope screen, and their presentation can be watched much as on a fluoroscopic examination, or photographs can be made with an ordinary camera for permanent preservation of records. Examples of the visualization of such pathological lesions as breast cancer, kidney cyst and cirrhosis or metastatic malignancy of the liver have been presented. The ability of this instrument to visualize small and closely approximated structures such as nerve, artery and vein have been shown in a somagram of the neck. The future of this instrument has been discussed, including the necessary developments before it becomes a clinically useful tool, what it may offer to medicine from a diagnostic standpoint, and what the final equipment may look like and cost.

REFERENCES

1. 3rd Annual Conference, American Institute of Ultrasonics in Medicine—Symposium to be published *J. Phys. Med.*
2. BALLANTINE, H. T., JR., BOLT, R. H., HUETER, T. F., and LUDWIG, G. D.: On the Detection of Intracranial Pathology by Ultrasound. *Science*. 112:525-528, 1950.
3. HUETER, T. F. and BOLT, R. H.: An Ultrasonic Method for Outlining the Cerebral Ventricles. *J. Acous. Soc. American*. 23:160-167, 1951.
4. WILD, J. J. and REID, JOHN M.: Further Pilot Echographic Studies on the Histologic Structure of Tumors of the Living Intact Human Breast. *Am. J. of Path.* 28:839-61, 1952.
5. WILD, J. J. and REID, JOHN M.: Application of Echo-ranging Techniques to the Determination of Structure of Biological Tissues. *Science*. 115:226, 1952.
6. HOWRY, D. H. and BLISS, W. R.: Ultrasonic Visualization of Soft Tissue Structures of the Body. *J. Lab. and Clin. Med.* 40:579-592, 1952.
7. HOWRY, D. H., STOTT, D. A. and BLISS, W. R.: The Ultrasonic Visualization of Carcinoma of the Breast and Other Soft Tissue Structures. *Cancer*. 7:354-58, March, 1954.
8. BALLANTINE, H. T., JR., HUETER, T. F., and BOLT, R. H.: On the Use of Ultrasound for Tumor Detection. *The Jour. Acous. Soc. American*, Vol. 26, 581, 1954.

3.5 Investigation of Abdominal Masses by Pulsed Ultrasound

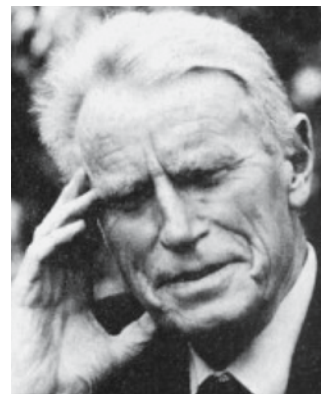
Ian Donald (1910–1987)

Ian Donald was born in Scotland in December 1910, the son and grandson of Scottish doctors. He was educated at Warriston School in Moffat, Fettes College in Edinburgh, and following the family move to South Africa he graduated BA from the Diocesan College in Cape Town. He returned to England in 1931 and graduated in medicine at St Thomas's Hospital Medical School in 1937. He was awarded MB BS at London University in 1937. During 1942–1946 he served as a medical officer in the RAFVR; he was mentioned in dispatches and awarded the MBE for rescuing airmen from a burning aircraft. Service in the RAF stimulated his interest in gadgetry of all kinds and he became familiar with radar and sonar.

On returning to London at the end of the war, he took up obstetrics and gynecology and held appointments at various London hospitals. His first research work was directed towards respiratory problems in the newborn, and he devised apparatus to help babies breathe when respiration did not get off to a flying start. Because of his interest in machines, Ian Donald was known as 'Mad Donald' by some of his London colleagues, who caricatured him as a crazy inventor, but his talent was spotted by that great university statesman, Sir Hector Hetherington, and he was appointed to the Regius Chair of Midwifery at the University of Glasgow in 1954.

His interest soon turned to the idea that sonar could be used for medical diagnosis, and the idea was first put into practice on 21 July 1955, when he visited the research department of the boilermakers Babcock & Wilcox at Renfrew on the invitation of one of the directors, who was the husband of a grateful patient. He took with him two cars, the trunks of which were loaded up with a collection of lumps such as fibroids and ovarian cysts which had recently been removed from patients in his Department. He carried out some experiments with an industrial ultrasonic metal flaw detector on these tumors, and on a large lump of steak which the company had kindly provided as control material. Later he formed a link with the Kelvin & Hughes Scientific Instrument Company, and particularly with a young technician called Tom Brown. Quite by accident, Brown had heard the strange tale of a professor who was attempting to use a metal flaw detector to detect flaws in women. He telephoned Professor Donald and suggested a meeting, and it was not long before Donald and Brown, together with Dr John MacVicar, later Professor of Obstetrics & Gynaecology at the University of Leicester, plunged into an intensive investigation into the value of ultrasound in differentiating between cysts, fibroids and any other intra-abdominal tumors that came their way.

Early results were disappointing and the enterprise was greeted with a mixture of skepticism and ridicule. However, a dramatic case where ultrasound saved a patient's life by diagnosing a huge, easily removable, ovarian cyst in a woman who had been diagnosed as having inoperable cancer of the stomach, made people take the technique seriously. 'From this point', Ian Donald wrote, 'there could be no turning back'. Results eventually appeared in print in the *Lancet* of 7 June 1958 under the arid title "Investigation of Abdominal Masses by Pulsed Ultrasound". This was probably the most important paper on medical diagnostic ultrasound ever published. Ten years later all doubt had been cast away and Ian Donald was able to review the early history of ultrasound in a characteristic forthright manner.



In 1959 Ian Donald noted that clear echoes could be obtained from the fetal head and began to apply this information. The group applied the method of fetal head measurement to assess the size and growth of the fetus. When the Queen Mother's Hospital opened in 1964 it became possible to refine the technique greatly and fetal cephalometry became the standard method for the study of fetal growth for many years.

Within the next few years it became possible to study pregnancy from beginning to end and diagnosis of complications like multiple pregnancy, fetal abnormality and placenta previa (which causes life threatening hemorrhage) became possible. Professor Donald had gathered around him a team of talented young doctors and technologists, including the research engineers John Flemming and Angus Hall, who were engaged by the university when the Kelvin Hughes company was closed in 1966.

In recognition he received many honours including the Eardley Holland Gold Medal (RCOG), Blair Bell Gold Medal (RSM), Victor Bonney Prize (RCS of England), honorary DSc from London and Glasgow Universities, CBE in 1973 and an honorary FRCR in 1983. In 1984 Ian Donald and Tom Brown were made the first honorary members of this Society. Only a fortnight before he died Ian made the journey to the Royal College of Physicians of London to receive an honorary fellowship. In honor of Professor Ian Donald, Professor Asim Kurjak founded the Ian Donald Inter-University School of Medical Ultrasound in Dubrovnik, Croatia in 1981. It is one of the world's largest schools of medical ultrasound and each year many celebrated students come through their advanced courses in medical ultrasonography. And in recognition of Donald's pioneering work in ultrasound, an Ian Donald Gold Medal was awarded each year by the International Society of Ultrasound in Obstetrics and Gynaecology (ISUOG) to the person whose pioneering work is considered to have the most profound influence in the development of Obstetrical and Gynecological ultrasonography.

Professor Ian Donald passed away on 19 June 1987 and was buried in the quiet country churchyard of St. Peters, Paglesham, Essex. He was survived by his wife Alix, whom he married in 1937, their four daughters and thirteen grandchildren.

In part excerpted from an article in the University of Glasgow publication 'Avenue' No. 19: January 1996 entitled 'Medical Ultrasound - A Glasgow Development which Swept the World', by Dr. James Willocks MD.

Thomas Graham Brown (born 1933)

Thomas Graham Brown was born in Glasgow in 1933. He attended Allan Glen's School in Glasgow, which in those days was a notable 'feeder' for the science faculties of the local universities. After leaving school he joined the local branch of the engineering firm Kelvin and Hughes Scientific Instruments Company as a "technical apprentice". All along Brown had a hobby interest in model-making, radios and valve-based electronics. Within Kelvin & Hughes he gained experience in many different facets of electronic and instrumentation engineering.

About two years into the apprenticeship Brown became involved in ultrasound used for non-destructive testing of materials, under Alex Rankin, who was a pioneer in the use of these techniques. He developed a system which would select for recording only echoes from particular regions of the test piece, by means of electronic time 'gating'. He also found a way of stabilizing the overall sensitivity of the system by selecting a reference echo from the test piece boundary, and using it indirectly to control the overall sensitivity. This was a difficult task in those days. Brown went to the University under a company sponsorship and studied applied



physics. However he did not finish his second year and went back to work at Kelvin and Hughes. In 1956, having learned that Ian Donald had much difficulty with the metal flaw detector that he was using (which had been passed on from Professor Mayneord at the Royal Marsden Hospital, who used it to investigate the brain), Brown called Donald personally and subsequently offered to lend him a brand-new M4 metal flaw detector together with photographic facilities from his company, through the generous foresight of his superior, Alex Rankin. Although Ian Donald was pleased with the results from this machine, both he and Brown had felt the need of a 2-D B-mode apparatus (not unlike the technique of the military radar) on top of the uni-dimensional A-scan that he was getting.

Together with Dr. John MacVicar, who joined the department as registrar in 1956, Brown and Donald came up with the world's first compound contact scanner, where the transducer can be moved manually over the patient's abdomen with a resultant 2-D image reproduced on an oscilloscope. The transducer was mounted on a frame with linear potentiometers to measure its mean X- and Y-positions and a sine/cosine resolving potentiometer to give a measure of the angle at which it was pointing into the patient.

Patents were applied for by Kelvin and Hughes prior to the publication of their early results in the 'Lancet' in June 1958. Tom Brown was named as inventor, though commercial rights were assigned to the company. The design was updated and improved at the several versions that followed. The design was taken up for commercial production as the Disonograph by the Smith Industrials of England which had bought Kelvin and Hughes. By 1963, Brown took over as department head of the Medical Ultrasonics operations in Glasgow, after the death of former head Alex Rankin. In 1964 the Glasgow operation became the subject of an internal "take-over" by Smith's Aviation Division. Brown left to become Chief Engineer at Honeywell's Medical Equipment Division in Hemel Hempstead. There he became involved with equipment for open-heart surgery, coronary care and prefabricated operating theatres.

In mid-1967, Smiths decided to close down the Glasgow factory, largely on account of the so-called "Firestone patents" on ultrasound, and sold the medical business to Nuclear Enterprises in Edinburgh. The NE 4102, later revamped and re-designed by Brown's successor Brian Fraser and Alan Cole, was an extremely successful machine and became the de facto standard in ultrasound scanners in Britain.

Brown's early scanner design set an important standard for other designs that followed. The Denver group (Howry, Wright and Meyers) fabricated a machine with a similar design after meeting up with Donald and Brown in London in 1959. A comparable design was also developed by Chinese investigators in Wuhan in the early 1960s.

Brown also invented and patented an elaborate and expensive automated compound B-scanner in 1958 which took care of a number of scanning variables of the operator. It was at the machine's exhibition in London in 1960 that Ian Donald met for the first time Douglass Howry from the United States, who had been using the much larger water-tank circumferential scanner for several years. The automated scanner was, however, considered too expensive for full commercial production and had never become popular.

Brown left the company in 1965 and returned after a lapse of 2 years when Nuclear Enterprises Ltd. acquired Kelvin and Hughes's medical ultrasound business. In 1970, Brown was research fellow at the University of Edinburgh studying three-dimensional imaging possibilities. He joined Sonicaid Ltd. in 1973 and led a team to develop an entirely new three-dimensional stereoscopic contact compound scanner. The machine, which was called the Multiplanar Scanner, was ex-

hibited at the AIUM meeting in 1976, followed by commercial production in the following year.

Commercial sales were nevertheless scant and production was discontinued in 1979. Although Brown's venture into the realm of 3-D ultrasonography was not met with success (at a time when computing technology was meager), his foresight was prudent and admirable. Brown did not find further employment in the medical instruments industry and moved to work in the offshore oil and gas business, where he remained until 1998. After his retirement, Brown worked part-time as Quality Manager for the Radiological Protection Centre at St George's Hospital at Tooting, London.

In 1984 Tom Brown and Professor Ian Donald were elected the first two honorary fellows of the British Medical Ultrasound Society. In 1988 Brown was presented the "History of Medical Ultrasound Pioneer Award" by the World Federation of Ultrasound in Medicine and Biology (WFUMB). In 1996 he received the Ian Donald Gold Medal for Technical Merit from the International Society of Obstetrics and Gynecology (ISUOG).

In part excerpted with permission from the webside www.ob-ultrasound.net by Joseph Woo, MD, Hong Kong. Picture courtesy Joseph Woo, MD.

J. MacVicar

Conclusion

Such is a very rough-and-ready sketch. I am profoundly aware that already a few courses organised on these lines exist and that much may be learned from them. I am also aware that the best results of such a course could be obtained only if it interlocked with the teaching in the clinical years far more closely than does the present preclinical course. Such interlocking is implicit in the structure of the new course's third year: much of the sociology, for example, would be taught by medical men from the fields of social medicine and of the psychology of industrial and group relations. Doubtless some crusading zeal could be lavished on the last years of our present curriculum too! But I am trying to be very strictly practical; everything I have suggested could actually be put into practice—as an experiment—without too much trouble with regulations, I believe, at any of a number of medical schools in the United Kingdom.

The General Medical Council in its 1957 *Recommendations as to the Medical Curriculum* has removed its previously rather detailed recommendations about the teaching of particular subjects. The present recommendations have been drawn up specifically to foster experimentation with the curriculum: they “refrain from specifying the period of time to be allotted to particular subjects or the sequence in which they should be taught . . . and from specifying subjects in which separate examinations should be held”. The Council make a particular point of asking schools not to regard their activities as “in any way limiting their own right, which may equally be described as a duty, to experiment with different courses and various methods of teaching”.

The present proposals should be viewed in the light of this recommendation. Summing them up one could say they imply a three-year preclinical course covering all the present ground of 1st M.B., 2nd M.B., and general pathology, but reorientated in consecutive courses entitled Cellular Biology, Organisation of Mammals, and Organisation of Man. Biochemical genetics enters the course at the start; ethology is part of it all along. The growth process is used to introduce anatomy and physiology and at the same time behavioural development. The concepts of maturation and learning introduce normal psychology, family studies, sociology, and finally a discussion of the role of the doctor—or various sorts of doctors—in our society.

I am sure much more thought and a great deal of experiment must go towards making a real course in human biology for doctors; but I think we ought to face squarely the implications of the modern nature of medical practice in our society. I believe we should seriously consider giving thought to the reorganisation of the curriculum from the point of view of the human biologist. We might further invite the views upon this of a variety of disciplines outside our own to see what their representatives conceive of as the doctor's role and his training for it. In this way we would gradually work towards the time when we could envisage setting up an experimental training in line with these emerging conceptions, and in which studies of human biology would exert their true usefulness in the training of medical men.

This essay has benefited much from the constructive criticism of a number of persons who have long thought about problems in medical education. In particular I would like to thank Dr. C. F. Harris, Prof. A. A. Moncrieff, Prof. J. Z. Young, Sir Geoffrey Vickers, and Dr. J. S. Weiner. Needless to say, however, the views above are not to be imputed in whole or part to anyone but myself.

INVESTIGATION OF ABDOMINAL MASSES BY PULSED ULTRASOUND

IAN DONALD

M.B.E., B.A. Cape Town, M.D. Lond., F.R.F.P.S., F.R.C.O.G.
REGIUS PROFESSOR OF MIDWIFERY IN THE UNIVERSITY OF GLASGOW

J. MACVICAR

M.B. Glasg., M.R.C.O.G.

GYNAECOLOGICAL REGISTRAR, WESTERN INFIRMARY, GLASGOW

T. G. BROWN

OF MESSRS. KELVIN HUGHES LTD.

VIBRATIONS whose frequency exceeds 20,000 per second are beyond the range of hearing and therefore termed “ultrasonic”. One of the properties of ultrasound is that it can be propagated as a beam. When such a beam crosses an interface between two substances of differing specific acoustic impedance (which is defined as the product of the density of the material and the velocity of the sound wave in it), five things happen:

(1) Some of the energy is reflected at the interface, the amplitude of the reflected waves being proportional to the difference of the two acoustic impedances divided by their sum (Rayleigh's law). Therefore the greater the difference in specific acoustic impedance between two adjacent materials the higher will be the percentage of energy reflected. This fact makes a liquid-gas interface almost impenetrable to ultrasound and is important in relation to gas-filled intestine within the abdominal cavity.

(2) Much of the energy which is not reflected is transmitted into the second medium but is somewhat attenuated.

(3) Some refraction may occur, particularly when the ultrasonic beam is not at right-angles to the plane of the interface.

(4) Some of the energy may be absorbed and produce heat. The ability to absorb ultrasound varies with different tissues—e.g., that of bone is considerable.

(5) Cavitation may be produced if considerable energies are present at the lower ultrasonic frequencies. This phenomenon, whose mechanism is not yet fully understood, can develop when the negative sound pressure exceeds the ambient hydrostatic pressure, giving rise to small temporary voids in the material. Cavitation becomes increasingly difficult to produce as the frequency of the ultrasound is raised, and usually develops only when the ultrasonic energy is applied continuously or in pulses of much greater duration than those we use. Nervous tissue is more susceptible than other tissues to cavitation (Fry et al. 1950).

For diagnostic purposes reflection and transmission are the important phenomena. Transmission is ruled out in our type of investigation because of the multiplicity of interfaces within the abdominal cavity and the impenetrability of tissue-gas boundaries. The recording and mapping of echoes from the reflecting interfaces is therefore the method of choice, which has been extensively used for many years in industry for detecting flaws in homogeneous materials, particularly metals, and the information so obtained may in some instances be superior to radiography, even with 2,000,000-V X-ray machines.

The use of ultrasonic echoes in studying human tissues promises to be much more complicated because of the great variety of tissues concerned and, it is believed, the not very large differences in specific acoustic impedance between them. It is therefore not surprising that results so far do not appear to have matched the technical ingenuity which has been shown in recent years.

A-scope Presentation

To confirm that echoes were obtainable within the body we started modestly with this method of presentation,

7 JUNE 1958

ORIGINAL ARTICLES

1189

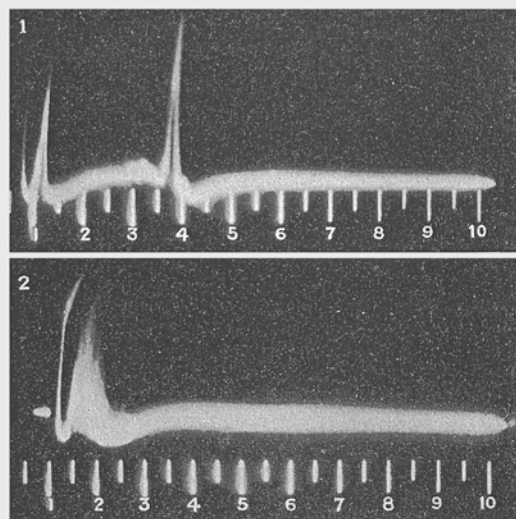


Fig. 1—A-scope presentation of acute retention of urine, showing bladder walls separated by gap representing urine.

Fig. 2—Same bladder as in fig. 1 after having been emptied by catheter, showing bladder walls no longer separated by gap.

which is standard practice in industry. By this method any echoes picked up are represented by vertical blips on a cathode-ray oscilloscope screen on a horizontal linear time-base sweep, the propagating source of ultrasound being represented by the left-hand end of the sweep. Since the velocity of propagation of ultrasound is very nearly the same in the various soft tissues encountered, the distance to the right along the base-line at which an echo blip is shown gives a measure of the distance of the reflecting interface from the propagating source. Figs 1 and 2 illustrate the principle of A-scope presentation. The patient from whom these figures were obtained had acute retention of urine following colporrhaphy, and the ultrasonic probe was placed over her distended bladder. The clear space in fig. 1 between the two blips represents the urine within the bladder. A catheter was then passed, and the blips closed up together as the bladder emptied (fig. 2). The apparatus used was the standard 'Mark IV' Kelvin Hughes flaw-detector, with which we had considerable experience, making 165 A-scope records of various solid and cystic swellings both in vivo and postoperatively in vitro.

It was not long before we discovered that the pattern of the blips is altered considerably by changing the angle of incidence of the ultrasonic beam, and it appeared that only the simplest reflecting interfaces could be diagnosed by conventional A-scope technique.

We were using at that time a standard frequency of $2\frac{1}{2}$ megacycles per second, and we compared the quality of echoes from the same subjects at $\frac{3}{8}$, $1\frac{1}{4}$, and 5 megacycles as well, but we appeared to obtain the best results at $2\frac{1}{2}$ megacycles. The higher the frequency and therefore the shorter the wavelength the greater can be the resolution; but attenuation within the transmitting medium also increases with the frequency, as does "scatter", which confuses the picture, and therefore range is restricted for a given power. Reid and Wild (1952), using a higher frequency of 15 megacycles, were restricted to a range of about 2 cm. only, but they suggested that this could be

extended by the principle of time-varied sensitivity, in which the receiver gain is increased as a function of the elapsed time between propagating signal and echo. A compromise has to be reached between frequency and resolution and depth of penetration.

The use of A-scope presentation has been applied in ingenious ways, especially by Effert et al. (1957), who studied the movements of the left atrial walls of the heart simultaneously with electrocardiography and phonocardiography in the relative assessment of mitral stenosis and incompetence. They also demonstrated pericardial effusion.

B-scope Presentation

In this arrangement the direction of the probe is kept constant, and the area is scanned by moving the probe sideways along a line at right-angles to the ultrasonic beam. The display on the cathode-ray tube is made to follow this sideways movement of the probe. If the size of the echo is represented by variations in brightness of a spot on the cathode-ray screen instead of as a blip, it is possible to build up a composite picture on a long-persistence screen or on a photographic plate.

A variant of this method was used by Wild and Reid (1951) using a hand-held instrument in which a propagating crystal scanned to and fro over a range of 6.5 cm. within an elliptical water-chamber. Another variant is to place the test object in a water-tank round the outside of which a probe travels directing a radial beam inwards. Similarly, in Japan, Kikuchi et al. (1957) graduated from A-scope presentation to a type of B-scope scan, which they call "ultrasono-tomography", for the exploration not only of the abdomen but also of the cranial cavity, as much of the head as possible being placed in a water-tank. The method appears to be still under development.

Our experience was like that of Howry (1955), who noted that even quite small angular displacements from the perpendicular in the incidence of the ultrasonic beam produced very great differences in the amplitude of the reflected echo. Howry calculated that an angle as small as 6° off the perpendicular reduced the amplitude of the detected echo to a tenth, and 12° reduced it to a hundredth. Howry and his colleagues have done a lot of fundamental work with simple geometrical test objects in water-tanks and have used ultrasonic lenses to narrow the beam and to improve penetration and resolution. They have also attempted three-dimensional and stereoscopic observations of body structure by building up two composite pictures taken from angles differing by 10° in respect of each other and studying them in a stereoviewer (Howry et al. 1956).

Radial Scan or Plan-position Indicator

A plan-position-indicator (P.P.I.) display is produced by rotating the probe about a fixed point in or near the area being scanned and causing the time-base sweep to follow the angular movement of the probe while originating from a fixed point on or off the face of the cathode-ray tube. If the origin of the display is off the face of the tube, the display is known as a "sector scan". None of the aforementioned methods is sufficient by itself to produce a satisfactory echo pattern of a deep-seated structure within the body, because echoes are only detected by the receiving crystal if the reflecting surfaces from which they originate are at right angles to the incident energy beam.

For these reasons it was decided to attempt to produce a scanning and plotting mechanism which, so far as possible, would enable each individual part of the surface of the structure under investigation to be scanned by the

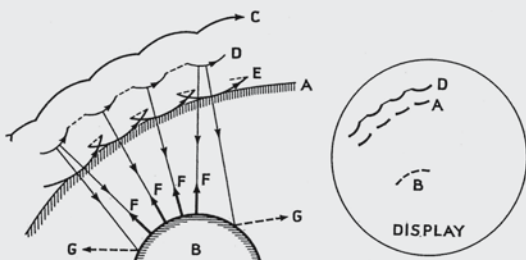


Fig. 3—Diagram of method combining B-scope and P.P.I. presentation: A, patient's skin; B, reflecting mass; C, D, E, paths traced by probe spindle, transducers, and probe face respectively; F, paths of echoes returning to receiving transducer (where reflecting surface is at right-angles to incident ultrasonic beam); G, paths of useless reflections (where beam strikes surface obliquely).

ultrasonic beam from a large number of different angles, all, however, lying in the plane of the cross-section to be represented. In this way we have sought to reproduce a composite cross-sectional view of the parts of the body examined, "collecting" echoes on the one picture from as many angles as possible, registering simultaneously not only the echoes and their strength but also the position of the probe and the angle of the incident beam. Our

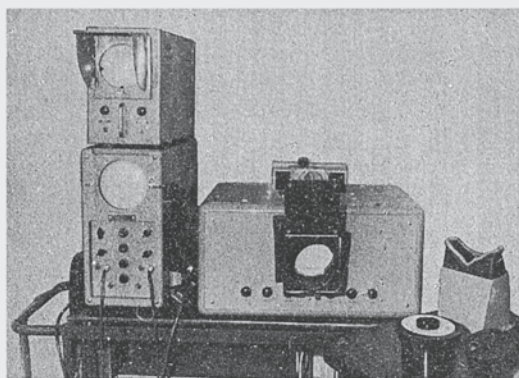


Fig. 4—Recording apparatus, showing three cathode-ray tubes with camera folded back over cathode-ray tube on the right.

apparatus thus combines B-scope and P.P.I. presentation (fig. 3).

Apparatus

A probe containing both transmitting and receiving transducers is mounted on a measuring jig, which is placed above the patient's bed. The probe is free to move vertically and horizontally and, as it does so, operates two linear potentiometers, which give voltage outputs proportional to its horizontal and vertical displacements from some reference point. The probe is also free to rotate in the plane of its horizontal and vertical freedom, and transmits this rotation via a linkage to a sine-cosine potentiometer. The voltage outputs from this system of potentiometers control an electrostatic cathode-ray tube, so that the direction of the linear time-base sweep corresponds to the inclination of the probe, and the point of origin of the sweep represents the instantaneous position of the probe.

The apparatus is so calibrated that the same reflecting point will repeat itself in exactly the same position on the cathode-ray tube screen from whatsoever angle it is

scanned, and likewise a planar interface comes to be represented as a consistent line.

The probe mounting and measuring jig have been built on to a standard hospital bed-table, which is placed over the patient's bed. The patient's abdomen is smeared with olive oil to establish acoustic coupling by excluding intervening air, and the probe is applied directly to the abdominal skin. We have been able to dispense with the water-tank or water-column transmission system of other workers; this enables us to scan far larger areas. The echoes picked up by the probe are displayed on three oscilloscope screens: an A-scope display; a combined

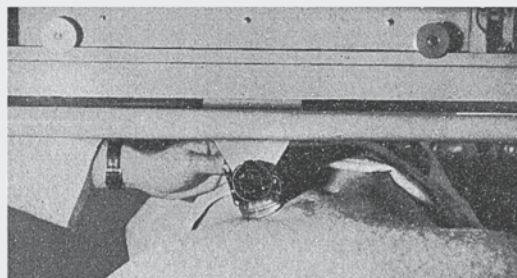


Fig. 5—Rotating probe applied to abdomen.

B-scope and P.P.I. display on a long-persistence screen for monitoring; and a similar screen and display of short persistence with a camera mounted in front of it (fig. 4).

The probe is moved slowly from one flank, across the abdomen, to the other flank, being rocked to and fro on its spindle the whole time to scan the deeper tissues from as many angles as possible. At present this is done by hand, but we have plans for mechanical scanning, which should produce far more consistent results. Thus the entire cross-sectional picture is composed of a large number of overlapping sector scans, and each potential reflecting surface within this cross-section is "seen" by the probe from a great number of angles (figs. 3 and 5). The process usually takes between 1½ and 2½ minutes, and the patient experiences no discomfort whatsoever. Several cross-sectional views are taken thus at different levels between the symphysis pubis and the xiphisternum.



Fig. 6—Transverse section of anterior half of thigh showing femur.

7 JUNE 1958

ORIGINAL ARTICLES

1191

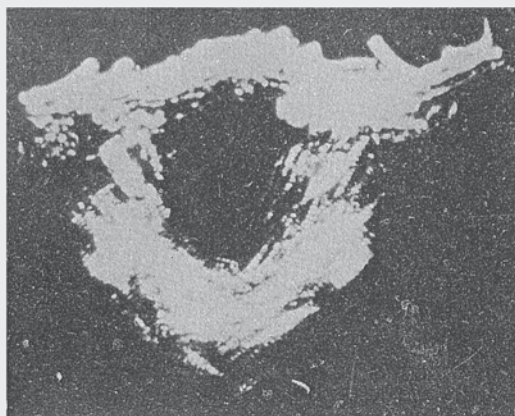


Fig. 7—Unilocular ovarian cyst of moderate size.

Probe System

We use separate piezo-electric transducer crystals, one for transmitting and one for receiving. Each is a barium-titanate rectangle 10 mm. \times 7 mm., and the two are placed with their 7 mm. sides adjacent. These dimensions were chosen empirically as likely to give the best compromise between beam divergence and beam diameter. The transducers lie on a conducting layer on a 'Perspex' block 1 in. thick, whose opposite side is in contact with the patient's skin. The transmitting transducer is "air-backed" and is electrically pulsed fifty times a second. At each pulse it vibrates mechanically for a very brief interval at a frequency determined by its elastic properties and its thickness. For a frequency of $2\frac{1}{2}$ megacycles, such as we use, the thickness is about one millimetre.

Transmitting System

A 100 pico-farad capacitor is charged to about 1400 V through a high resistance and is then discharged by a thyatron through the primary winding of a pulse transformer. The transmitting transducer is connected across the secondary of the pulse transformer in parallel with a damping resistance of 50 ohms. The amplitude of the transmitted acoustic pulse rises from zero to its maximum value in 0.3 microseconds and has decayed to 10% of

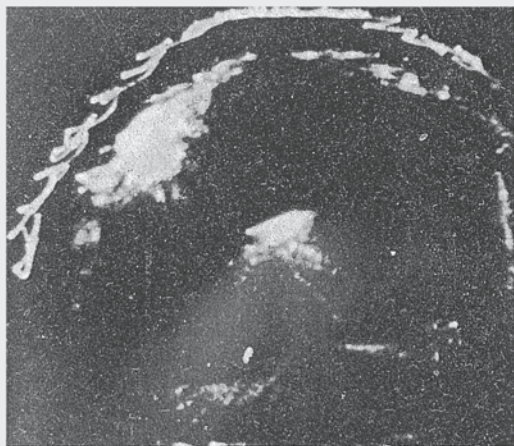


Fig. 9—Bilateral ovarian cysts. At operation left cyst's diameter was 26 in. and right cyst's $12\frac{1}{2}$ in.

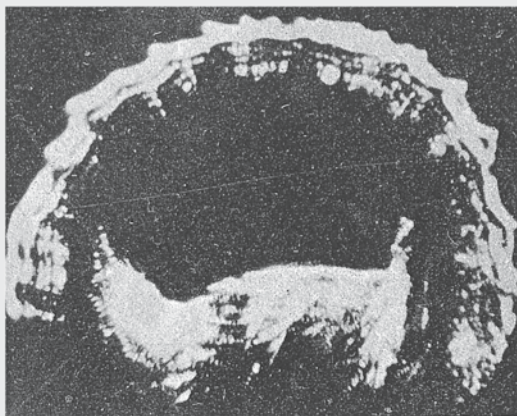


Fig. 8—Large simple ovarian cyst with posterior surface indented by vertebral column and posterior abdominal wall.

this value after a further 1.8 microseconds. Fifty such pulses are transmitted each second.

Results

We have now investigated 100 patients and made 275 records by this scanning technique, in addition to the previously mentioned A-scope work. Most of the cases were gynaecological or obstetrical because we mainly investigated the routine clinical material of our own department. Our work therefore deals chiefly with various conditions of pregnancy, ovarian cysts, fibroids, ascites, and abdominal carcinomatosis.

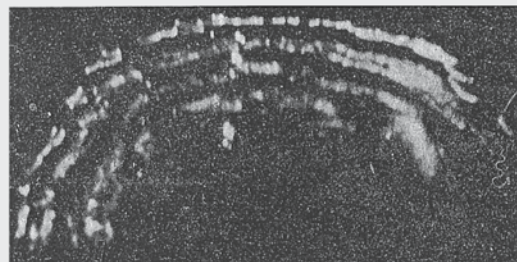


Fig. 10—Transverse section of healthy abdomen at level of umbilicus.

A transverse section of the thigh of one of us (T. G. B.) is shown in fig. 6. The outermost line represents the movement of the probe, and the wriggles in it represent the rotary movement applied to the probe. The femur appears crudely in cross-section.

A moderate-sized unilocular ovarian cyst is shown in fig. 7. The shadows below and behind it are believed to be due to displaced bowel, which gives very powerful echoes because of the tissue-gas interface which intestine provides.

A much larger cyst is shown in fig. 8, and the indentation of its posterior surface by the vertebral column is clear. The cyst was very tense and clinically diagnosed as a fibroid, but the ultrasonic characteristics of a fluid-filled cyst are here quite unmistakable.

Bilateral ovarian cysts are shown in fig. 9; only one cyst had been diagnosed clinically, but the outlines of both cysts can here be made out; two cysts were found at operation. The heavy collection of shadows in the centre of the picture and in the upper left part are believed to be due to coils of intestine.

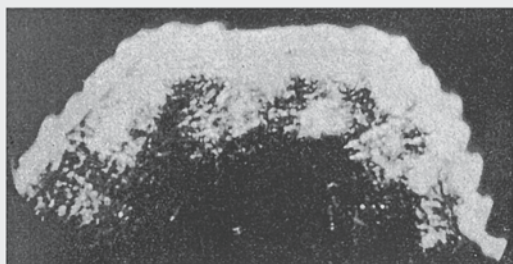


Fig. 11—Gross ascites due to cirrhosis of liver. Ultrasonic beam can penetrate more deeply in random fashion because of fluid between coils of intestine.

By contrast the *healthy abdomen* of one of us (J. M.), scanned at the level of the umbilicus, is shown in fig. 10. We are not yet certain of the identification of the various layers of the abdominal wall shown here, but the noteworthy feature is that deep penetration into the abdomen is prevented by normally situated coils of intestine.

In *ascites*, however, the fluid intervening between the coils of gut allows the ultrasound to penetrate to a much greater depth, yet without producing the clearcut margins of an ovarian cyst. This is shown in fig. 11, taken in a case of portal cirrhosis in which the patient's abdomen was scanned at umbilical level in the presence of gross ascites. This film is almost certainly overexposed and probably exaggerates the picture.



Fig. 12—Very large complex ovarian tumour, which proved at operation to be a multilocular pseudomucinous cystadenoma with almost solid plaques of minute loculi.

A huge and structurally very complicated ovarian tumour is shown in fig. 12. This was a large pseudomucinous cystadenoma of ovary with many areas of very small loculi clustered together so as almost to give the macroscopic impression of areas of solidity. Histology showed the tumour, however, to be benign.

Multiple fibroids are shown in fig. 13. Our findings so far indicate that fibroids tend to absorb and scatter ultrasound, with the result that only faint echoes can be recorded from the posterior surface of the mass (as in this figure) or none at all, in contrast to a fluid-containing cyst, in which the ultrasound is readily transmitted and reflected from its posterior wall. Here the outline of the fibroids can be roughly seen and the thickness of the tumour gauged. Our tentative conclusions at present are

that the ability of fibroids to transmit ultrasound depends on their vascularity.

The *pregnant uterus* offers considerable scope for this kind of work because it is a cystic cavity containing a solid foetus. In fig. 14 a suprapubic scan is shown of a patient at the 34th week of gestation in whom placenta praevia was suspected; we were trying to see the placenta in the lower segment. We are not yet sure about this, but the outline of the foetal head shows up very well.

Hydramnios is very vividly shown in fig. 15, in which the transverse section of the baby's body appears within the enormously distended amniotic sac. The period of

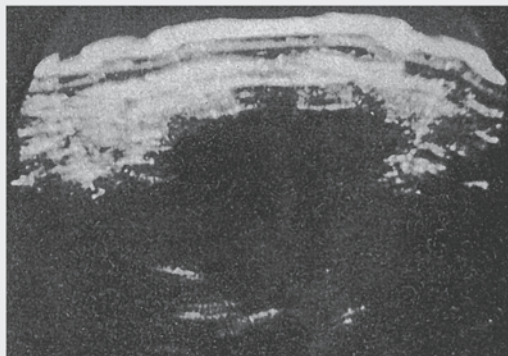


Fig. 13—Multiple fibroids, showing progressive attenuation of ultrasound, with only faint echoes from posterior surface of mass in contrast to ovarian cysts.

gestation in this case was 32 weeks, and the girth of the abdomen 44 inches.

Twins are shown in fig. 16. The scan was taken just above the level of the umbilicus at the 37th week of gestation. Both twins presented by the vertex, and what is visible here is the two breeches at the fundus.

Fig. 17 is very interesting. The patient had had three months' irregular vaginal bleeding and a very hard enlargement of the uterus corresponding in size to about 14 weeks' gestation. A year previously a fibroid had been found within her uterus, and she was now admitted to hospital for myomectomy. A scan taken one inch above the symphysis pubis showed, however, a very different picture: a cystic cavity containing in its left half a mass which is clearly a very early foetus. The result of the Aschheim-Zondek test ordered was awaited with considerable excitement since clinically the diagnosis was con-



Fig. 14—Outline of foetal skull in utero at 34 weeks' gestation (suprapubic scan).

7 JUNE 1958

ORIGINAL ARTICLES

1193



Fig. 15—Hydramnios, showing outline of transverse section of fetal body within enormously distended amniotic sac.

vincingly that of fibroid. The test was positive; and with rest in bed the patient's bleeding ceased, and she was discharged home with the pregnancy continuing. She has since been safely delivered.

In another instance, in which, unfortunately, we did not secure a permanent and satisfactory record, the usefulness of ultrasound in diagnosis was well shown. A woman, aged 64, was admitted to a medical ward with gross abdominal distension believed to be due to ascites. She had severe vomiting and had rapidly lost weight. Carcinoma ventriculi with secondaries at the portal fissure was provisionally diagnosed, and one of us (I. D.) was asked to see her to exclude malignant disease within the pelvis as an alternative source of her ascites. Her general condition was very bad, and the abdominal examination was very difficult owing to distension, but the diagnosis of ascites was agreed, and the pelvis was found to be clear of any palpable malignant deposit. The ultrasonic apparatus was applied and indicated unequivocally a very large cyst, which we were unwilling to believe. At laparotomy, however, a very large pseudomucinous cystadenoma was removed, and the patient continues well to this day.

Possibility of Harmful Effects of Diagnostic Ultrasound

Ultrasound, being a form of mechanical energy, can be expected to inflict and make apparent its injuries, if any,

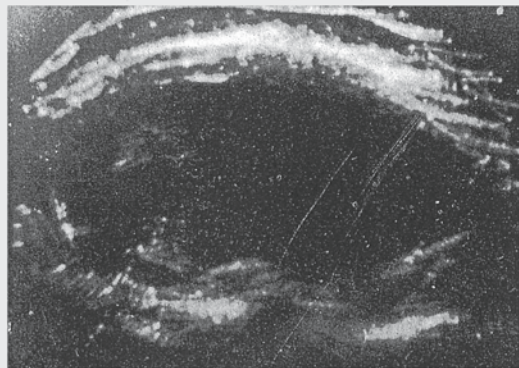


Fig. 17—Uterus at 14 weeks' gestation, showing echoes from fetus towards left half of uterus. Provisional clinical diagnosis had been that of fibroid.

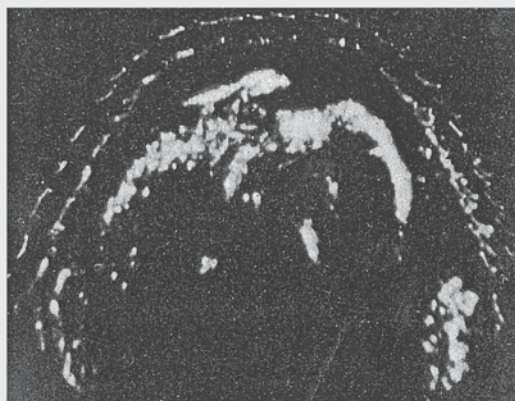


Fig. 16—Twins: both breeches shown on scanning across fundus uteri.

at once, like other forms of mechanical trauma. In this it differs from ionising radiations. There are two possible means whereby damage might be inflicted by the passage of a beam of ultrasound: (1) the production of heat associated with the absorption of the energy of the ultrasonic beam, and (2) cavitation. There can be no doubt that intense ultrasonic energy can produce damage, especially from powerful machines using the principle of magnetostriction at lower frequencies. In diagnostic work, however, very high frequencies in the megacycle ranges and low-power outputs are used. One of us (I. D.), using continuous 1-megacycle ultrasound—i.e., not pulsed—with an intensity of 7 watts per sq. cm., made experiments in haemolysing blood and observed that the rate of destruction of the red cells depended on the amount of heat generated within the sample of blood, because a similar degree of destruction could be achieved by heating the blood to the same temperature without ultrasound. Fry (1954), however, using intensities of 70 watts per sq. cm. and a 4-second exposure with multiple ultrasonic beams focused to a width of 2–3 mm. and working directly on animals' brains from which the overlying bone had been removed, produced immediate effects, particularly on the larger nerve-cells. He concluded that increased temperature was not the chief cause of damage, because the smaller nerve-cells would then have suffered as much as the larger.

Nerve-cells appear to be more susceptible to damage from ultrasonic energy than any other tissue, and Fry et al. (1950, 1951) showed that there was a linear relation, for a definite degree of paralysis in the frog, between the reciprocal of exposure time and the pressure amplitude of the sound-wave.

This structural damage was produced at intensities many thousand times higher than those used in diagnostic work. French et al. (1951), using Wild's 15-megacycle diagnostic apparatus, found no brain damage in four rabbits and a cat whose brains were directly exposed to diagnostic ultrasound. Wild and Reid (1952) calculated that the average intensity at the surface of their patients "was not more than 1.3 watts per square centimetre," a figure which strikes us as surprisingly high.

With our apparatus we have calculated that, even if we ignore the energy losses in the transmitting circuits, the greatest possible energy delivered to the transducer is 0.5×10^{-4} joules per pulse. If we take into account

the efficiency of the transducer and the attenuation of the energy in its passage through the perspex block, the greatest energy which can be radiated into the patient is 0.2×10^{-4} joules per pulse. This is equivalent to an average power at the body surface of less than 1.5 mW per sq. cm. The cross-sectional area irradiated at any one time is about 0.7 sq. cm. Thus the energy is truly very small. Nevertheless it was vital to establish beyond all shadow of doubt that susceptible tissues would not suffer even from these dosages, and we are indebted to Dr. P. Bacsich, of the department of anatomy of this University, for the following investigations which he made for us on newborn kittens. His report is quoted in full below:

2 day-old male sibling kittens were used, two of them being controls.

Under pentobarbitone-sodium anaesthesia two kittens were exposed to pulsed ultrasound from the standard flaw-detector for an hour, the crystals being placed on the left temporoparietal region after the scalp had been generously covered with olive oil; simultaneously the controls received "treatment" with a dummy crystal. All four kittens regained full consciousness within 9-10 hours and, after being put back to their mother, started to feed voraciously.

2 kittens (1 experimental and 1 control) were killed 24 hours after the start of the experiment. The other 2 were left under the mother's care for three weeks. During this period the experimental kitten showed no harmful manifestations of the treatment, in fact its development was considerably in advance of that of its sibling. It fed better and gained weight faster, its eyes opened a day earlier, and it left the mother's basket two days sooner.

At the end of this period the 2 kittens were killed with lighting-gas, and their brains were carefully removed and fixed in a 10% aqueous solution of formalin for three days. All 4 brains were embedded in celloidin-paraffin and sectioned serially in the coronal plane. The sections were mounted in four parallel "reduced" series as follows: after three consecutive 10- μ and one 20- μ sections had been mounted, the next 45 sections cut at 10 μ were discarded, and this procedure was repeated again and again. In every instance one series was stained with haemalum and eosin, one with toluidine-blue, one with a modified 'Protargol' method, and one with a modified Weigert method.

In the microscopical examination of the brain of the 24-hour experimental kitten signs of cavitation, coagulative necrosis, localised hyperaemia, haemorrhages, and chromatolysis were looked for; and the brain of the 3-week kitten was examined for any evidence of patchy cell destruction, neuroglial scarring, axonal degeneration, and localised lack of myelination.

All these tests were completely negative, and the brains of the experimental kittens and their respective controls were in every way comparable.

On the basis of these findings one must conclude that exposure of the kittens to more than thirty times the dose of ultrasound necessary in its diagnostic use produced no detectable neuropathological change, or at least any possible lesion could not exceed 450 μ in extent.

Discussion

To be of any use at all to the clinician, the echo patterns obtained by pulsed ultrasound must be not only intelligible but also consistently reproducible at the same level in the same case. That this is not always so we attribute to inadequate scanning methods and technique—hence the development of our combined B-scope and P.P.I. presentation and scanning. Even so we are very far from satisfied with the crude results so far obtained. Other workers have made claims which, in many instances, are more striking than substantial, judged by some of the

illustrations offered. The temptation to try to distinguish benign from malignant tissue by such simple, quick, and harmless means is well-nigh irresistible; but, being only too well aware of the difficulties which even the histologists on direct microscopy may have in assessing malignancy, we have not attempted this sort of assessment in the present state of crudity of an ultrasonic beam whose width is measurable in millimetres and whose wavelength is many times the diameter of any living cell, benign or malignant. Wild and Reid (1952) claim that it is possible to distinguish between a benign and a malignant tumour within the breast on the basis of positive differences observable on ultrasonic echography. The Japanese workers Kikuchi et al. (1957) have made the same claim; they also claim to have recorded echoes from human intracranial ventricles, as we have, in the newborn, and they make other claims which we have not explored. Howry and Bliss (1952) noted that fresh specimens *in vitro* differed in their sonic properties when compared with fixed specimens in formalin solutions. We also have noted differences between the tumour *in vivo* in a tank after removal from its host. We cannot explain this difference except by suggesting that blood circulating through a tumour alters its sonic properties.

Our experience of 78 cases in which diagnosis was quickly verified by laparotomy and subsequent histology indicates that ultrasonic diagnosis is still very crude, and that the preoperative diagnosis of histological structure is still far off, although such a possibility in the future is an exciting prospect. The fact that recordable echoes can be obtained at all has both surprised and encouraged us, but our findings are still of more academic interest than practical importance, and we do not feel that our clinical judgment should be influenced by our ultrasonic findings. Our most spectacular results have been obtained in dealing with fluid-filled cavities, which certainly show up well; but it is only fair to point out that the illustrations shown herewith are among the very best that we have so far been able to produce out of about 450. They do, however, encourage great efforts to refine our technique.

Summary

Large intra-abdominal masses, including the gravid uterus, pelvic tumours, and ascites, have been investigated by the echo patterns obtainable by pulsed ultrasound.

Masses containing fluid are easily but crudely demonstrated.

The possible identification of structures within the abdomen by their sonic properties is discussed.

A scanning mechanism is described whereby cross-sectional views of the abdomen are obtained, and illustrative examples are given.

The possible harmful effects of diagnostic ultrasound are discussed; they appear to be negligible.

The limitations of the technique so far developed in practical diagnosis are described, but further refinements in technique may provide a useful diagnostic weapon in cases in which radiological diagnosis with ionising radiations is either impracticable or undesirable.

Our apparatus was developed in the research department of the Hillington Factory, Glasgow, of Messrs. Kelvin Hughes Ltd., who cooperated in this research with generosity and enthusiasm, for which we are indeed grateful. One of us (T. G. B.) has been seconded by the directors of this firm for whole-time work in connection with this research. We also acknowledge, with thanks, the support received from the Scottish Hospital Endowments Research Trust.

References at foot of next column

3.6 Ultrasonic Doppler method for the inspection of cardiac functions

Shigeo Satomura (1919–1960)

Shigeo Satomura was born in 1919 in Osaka. He obtained his PhD from the Osaka University School of Physics in 1944 and thereafter worked at the Institute of Scientific and Industrial Research, Osaka University. Satomura was appointed Assistant Professor in 1952 and was conferred the degree of Doctor of Medical Sciences in 1960. He died from a sudden subarachnoid hemorrhage at the Osaka University Hospital in the same year, at the age of 41. He was posthumously promoted to Professor by the university.

In 1955, Satomura began using microwaves and ultrasound in industrial research, shortly following his initial efforts in measuring vibrations on wooden boards. Professor Kinjiro Okabe, his supervisor at that time, suggested that he apply his ultrasound techniques to medical diagnosis. In collaboration with T. Yoshida and Yasaharu Nimura, medical doctors (cardiac physicians) at the Osaka University Hospital, he tried to apply the techniques to the measurement of the heart and pulsations of peripheral and eye blood vessels. In December 1955, Satomura published his first paper on the subject entitled “A new method of the mechanical vibration measurement and its application”. In this paper he demonstrated that Doppler signals can be retrieved from heart movements when insonated with 3-MHz ultrasonic waves.

Together with Ziro Kaneko, he constructed the Doppler flowmeter to measure the Doppler noise from these blood vessels. These works were part of Satomura's Dr. Med. Sci. thesis which he presented in November 1959. Ziro Kaneko was Professor at the Department of Neuropsychiatry, Osaka University Medical School and he proposed to Satomura to study blood flow in the human brain in cases of dementia to differentiate the Alzheimer variety and those that were of cerebral vascular origin. From July 1958, they embarked on studies of the extracranial portions of the cerebral blood supply using Satomura's Doppler flowmeter. They were able to demonstrate in the same year that ultrasonic Doppler signals from arteries and veins could be found from the surface of the skin and pioneered early transcutaneous flow analysis in systole and diastole, in normal and in diseased blood vessels.

In October 1958, Satomura had presented a paper entitled “Study of blood flow in vessels by ultrasonics” at the meeting of the Japan Acoustics Society. This was in the Japanese language. A similar article “Study of the flow pattern in peripheral arteries by ultrasonics” was published in the *Journal of the Acoustic Society of Japan* in 1959. The paper was in Japanese with an English summary. On 4 December 1959, Satomura's apparatus was shown in the Japanese daily newspaper the *Mainichi News*.

In part excerpted with permission from the website www.ob-ultrasound.net by Joseph Woo, MD, Hong Kong. Picture courtesy Joseph Woo, MD.



ULTRASONIC ABSORPTION IN LIQUIDS

1181

excitation probability contains a factor $\exp(\epsilon/kT)$ where ϵ is the depth of the (attractive) potential well. In the liquids the neighbors are already near the bottom of the well, and therefore this factor should perhaps be omitted in liquids. Then, the ratio of collision times would be

$$(\tau_{gas}/\tau_{liq}) \exp(\epsilon/kT).$$

TABLE II. Factor $\exp(\epsilon/kT)$ at room temperature.

	CH ₂ Cl ₂	CHCl ₃	CCl ₄	C ₆ H ₁₄	C ₆ H ₆	CS ₂
$\exp(\epsilon/kT)$	3.9	3.0	3.0	4.0	4.3	5.1

The resulting factor is shown in Table II. This, however, increases the spread.

THE JOURNAL OF THE ACOUSTICAL SOCIETY OF AMERICA

VOLUME 29, NUMBER 11

NOVEMBER, 1957

Ultrasonic Doppler Method for the Inspection of Cardiac Functions

SHIGEO SATOMURA

Acoustics Laboratory, Institute of Scientific and Industrial Research, Osaka University, Hirakata, Osaka, Japan

(Received April 30, 1957)

When the continuous ultrasonic wave is sent forth towards the heart from the surface of the chest wall, the cardiac motion causes the Doppler effect upon the partial wave reflected from it. Therefore, an apparatus suitably constructed for sending and receiving ultrasounds is quite useful for the investigation of the movements of the atrium, ventricle, or valves, etc., through the analysis of the particular Doppler signals developed from the motion of the respective part.

The author developed a method for the inspection of cardiac functions by recording these Doppler signals simultaneously with the electro- and phonocardiographs on the oscillograph paper. This method made it possible not only to obtain direct informations for the valvular movement which could not have been ascertained up to present, but also to examine the transitional aspects of the myocardial excitation which is utterly undetectable by the electrocardiograph alone.

1. INTRODUCTION

A PRACTICAL application of the ultrasound to the field of the diagnosis has been developed in the technique employing ultrasonic pulses.¹ Since a slight change in the tissue density of the interior of the body is manifested in the deviation of the transmittivity or the reflectivity of the applied ultrasonic pulses, the pulse technique has been chiefly utilized for the detection of the cancer tissue. Meanwhile, the method under the main title is characterized by the use of the Doppler effect,²⁻⁴ caused by the mechanical motion of the heart, for the inspection of cardiac functions. By means of this method, it is possible to inspect the motion⁵ of the heart wall, the movement⁶ of the valves, and the heart noises produced in a diseased heart.

This paper proposes to describe the principle and the composition of the equipment in practical use, intro-

ducing another way for the clinical examination by discriminating the varieties of the Doppler signals recorded by this original apparatus.

2. PRINCIPLE

A sharp beam of an ultrasound being sent forth toward the heart from the surface of the chest wall on the movement of the heart wall or of the valvular structures induces the Doppler effect upon the wave reflected from them. Therefore, if an appropriate probe of sending and receiving the ultrasonic wave is available, it is possible to obtain the AF signals (the Doppler frequencies), frequencies of which are proportional to the motional velocity of the reflecting part of the heart by means of a composite demodulation of the reflected wave with the direct one.

It is obvious that the following relation⁷ is established between those quantities designated as $f_d(c/s)$, u_0 (cm/sec), and λ (cm):

$$f_d = 2u_0/\lambda,$$

where f_d is the Doppler frequency, u_0 the velocity component (parallel to the ultrasonic incidence) of the reflecting part, and λ the ultrasonic wavelength in the human body. Since the wavelength is determined by

⁷ The exact expression is as follows:

$$f_d = \frac{2u_0}{\lambda} \left(1 + \frac{u_0}{c} + \frac{u_0^2}{c^2} + \frac{u_0^3}{c^3} + \dots \right).$$

¹ J. J. Wild and J. M. Reid, *J. Acoust. Soc. Am.* **25**, 270 (1953); *Electronics* **28**, No. 3 (1955).

² E. J. Barlow, *Proc. Inst. Radio Engrs.* (1949).

³ S. Bagno, *I. R. E. Convention Record* (1954), Pt. 6.

⁴ Howry, the ultrasonic blood velocity transducer developed at the National Bureau Standards.

⁵ The Doppler signal obtained in a fixed position on the chest wall is a function of the distance of various portions of the heart depending upon the exact rotational and transitional motions that the heart goes through. It is similar to the Kinetocardiogram. E. E. Eddleman *et al.*, *Circulation* **8** (1953).

⁶ Moreover, the Doppler signals by the movement of the valves is the one which is produced by the component of the valvular velocity in the direction of the ultrasound sent forth from the fixed point on the chest wall.

1182

SHIGEO SATOMURA

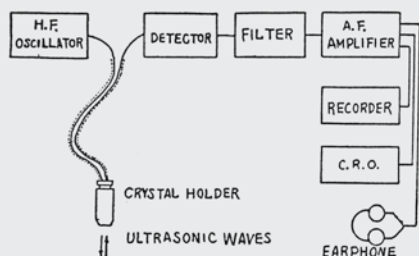


FIG. 1. Schematic block diagram of the apparatus.

the frequency of the ultrasound used, the measurement and the analysis of the frequency of the Doppler signal provides information about the reflecting part of the heart, namely, the ventricles or the valves, etc.

Moreover, the minute vibration⁸ of the reflecting part produces the corresponding small alteration in the phase⁹ of the reflected wave; a vibratory tone is detected, too.

Employing this method, it is possible to distinguish the Doppler signals produced by the movement of the

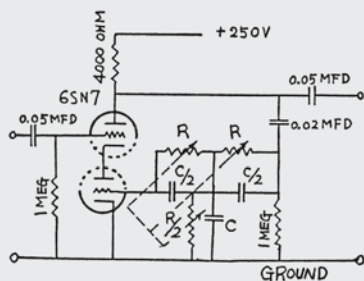


FIG. 2. Circuit and frequency characteristic of the band-pass filter.

⁸ S. Satomura, J. Inst. Elec. Commun. Engrs. Japan 38, No. 4 (1955).

⁹ Phase difference = $\frac{4\pi}{\lambda}(r+d) = \frac{4\pi}{\lambda}r + \frac{4\pi}{\lambda}d \approx \Delta\phi + \delta\phi$.

r = range of an object

d = displacement of minute vibration

λ = wavelength

$\Delta\phi$ = phase difference corresponding to

$\delta\phi$ = minute change of phase.

heart wall or valve, and, further, "the Doppler heart noises" originating at a diseased heart.

3. EQUIPMENT

The block diagram of the equipment is presented in Fig. 1. The high-frequency energy supplied by the HF oscillator is conducted to the barium titanate transducer through a flexible cable, and the ultrasound is sent forth into the body. The reflected wave is received by the same transducer, conducted to the demodulator together with a portion of the direct wave. The Doppler signals obtained by the detector are amplified by the AF amplifier, the output power of which drives the earphone or the recorder. The HF oscillator is a typical one of self-oscillation with the power of 1–2 w, and the operating frequency is 3 Mc. The power of the ultrasound is calculated to be about 20–50 mw/cm². The amplification of the AF amplifier is approximately 80 db.

A low-pass filter and a band-pass filter is added to the AF amplifier. The low-pass filter is of a simple π type,

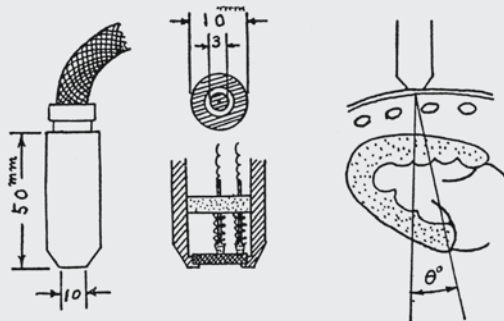


FIG. 3. The shape and the dimensions of the transducer and its holder.

the cutoff frequency of which is 500 cps, and the band-pass filter is a twin T circuit,¹⁰ the middle frequency of which is about 1000 cps and a little variable, and the Q is about 3–5. Figure 2 shows the circuit and the frequency characteristic¹¹ of the band-pass filter.

Figure 3 shows the shape and the dimensions of the barium titanate transducer and its holder. The positive electrode is separated in concentric circles, the circular part in the center being operated for the generation of the ultrasound, and the ring-shaped outer part for reception. The schema on the right of Fig. 3 indicates the shape of the ultrasonic beam. θ shows an angle of the sound intensity reduced to half ($\theta \div 8$ degrees).

4. CLINICAL EXPERIMENTS

Practical inspections of the heart are carried out according to the following procedure. The ultrasonic transducer is attached to the surface of the chest wall, searching for the Doppler signals arising from the

¹⁰ $f_0 = (1/2\pi CR)$, f_0 = middle frequency.

¹¹ Positive feedback amplifier by means of this filter.

various parts of the heart. The signals thus made audible through the earphone are recorded on the oscillograph paper parallel with the electro- and phonocardiographs.

The above described filters are chosen according to the object under inspection. That is, the low-pass filter is used in case of inspecting the heart wall motion and the band-pass filter is for valves with the middle frequency¹² set at about 1000 cps. In case of receiving the Doppler heart noises, no filter is employed.

Figure 4 shows the particular positions on the chest wall selected for the process of systematic inspections. The Doppler signals thus obtained have been classified into the following three distinct groups:

- (a) lower frequency Doppler signals (selected by means of the low-pass filter);
- (b) higher frequency Doppler signals (selected by means of the band-pass filter);
- (c) Doppler heart noises (no filter employed).

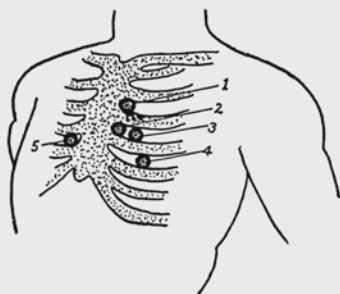


FIG. 4. The particular positions on the chest wall selected for the process of systematic inspections.

(a) Lower Frequency Doppler Signals

The Doppler signals in this group mainly consist of those arising from the motion¹³ of the heart wall, the frequencies being below 500 cps. They are further classified into two classes: those from the ventricular wall and those from the atrial wall according as the ultrasonic probe is placed on the respective position.

The positions for receiving the Doppler signals from the bottom part of the ventricular wall, the apex, and the right atrium are indicated in Fig. 4, (3), (4), and (5), respectively.

In Fig. 5 a representative curve of the Doppler signals is shown, indicating the motion of the bottom part of the ventricle. The curve of the Doppler signals is divided into three components; each one corresponds to the period of the atrial contraction, the ventricular contraction, and the ventricular relaxation, respectively.

A clinical significance is attributed to the investigation of the relations with the time interval between the

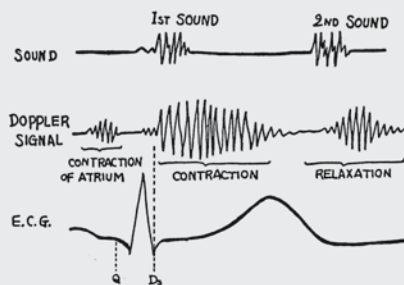


FIG. 5. Schematic graph of the oscillogram, indicating the motion of the bottom part of the ventricle.

electromotive excitement of the myocardium and the actual motion of the heart. An abnormal example such as the case with aortic insufficiency has demonstrated the fact that the mechanical motion lags behind the electric excitement of the myocardium at the period of contraction; i.e. as shown in Fig. 5, the time interval $Q-D_s$ between 0.05–0.10 sec for the normal case, whereas for this abnormal case it is about 0.12–0.15 sec.

(b) Higher Frequency Doppler Signals

Scanning along the left sternal border in the 3rd or the 4th intercostal space or along the parasternal line in the 4th intercostal space as well higher frequencies of approximately 1000 cps can be received coincidently with the lower ones. The higher frequency suggests that the reflecting objects possess the velocity about 5–10 times larger than that of the ventricle and their location makes it probable that they might be developed by the action of the semilunar or of the atrioventricular valves.

Figure 6 shows the ultrasonic probe directly applied to the exposed heart of an anesthetized dog indicating the positions where the higher frequency Doppler signals are supposed to be produced by the motion of the inner objects.

The position (1) indicates the bottom part of the right ventricle where the tricuspid valve is considered to exist within the position (2) the bottom part of the left ventricle covering the mitral valve and lastly the position (3) represents the bottom of the pulmonary artery the vicinity of the semilunar valve.

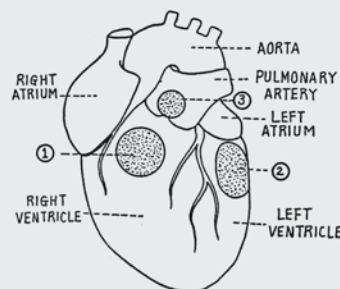


FIG. 6. The positions on the exposed heart of a dog, where the higher frequency Doppler signals are supposed to be produced.

¹² The middle frequency is so adjusted that the Doppler signal from valves is received with the best intensity.

¹³ C. H. Hertz and I. Edler, *Acustica* 6 (1956).

1184

SHIGEO SATOMURA

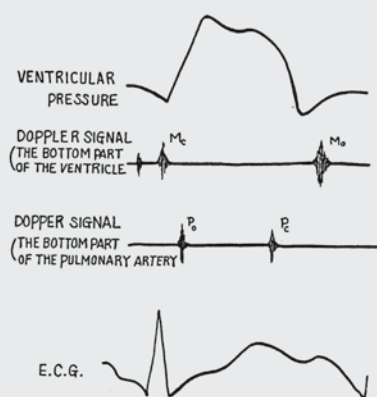


FIG. 7. Schematic graph of the oscillograph, for the experimental results on the heart of a dog.

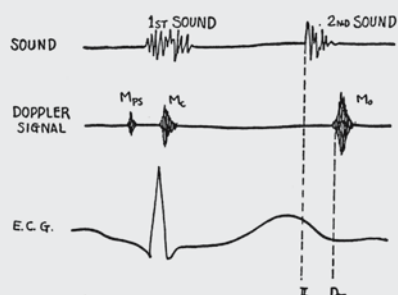


FIG. 8. Schematic graph of the oscillogram, indicating the motion of the mitral valve.

A typical curve of the higher frequency signals recorded on the oscillograph paper is exhibited in Fig. 7 for the experimental results on the heart of a dog. Those taken at the tricuspid position (M_c) develop coincidently with the onset of the increase in the pressure curve for the ventricle lagging as much as 0.04–0.05 sec behind the start of *QRS* of the electrocardiograph. M_o shows the signal corresponding to the closing of the mitral valve and M_o to its opening. Those at the position around the pulmonary artery (P_o) make appearance approximately in the midst of the increasing portion of the pressure curve lagging about 0.09 sec behind the beginning of *QRS*. P_c shows the signal corresponding to the closing of the pulmonary valve and P_o to its opening.

On the basis of the experimental results described above, these higher frequencies are considered to be produced by the movements of the semilunar or of the atrioventricular valve.

The higher frequencies for a human body recorded along the left sternal border in the 4th intercostal space on the chest wall are presented in Fig. 8, showing the movement of the mitral valve. These are produced both at the opening (M_o) and the closing of the valve (M_{PS} and M_c). The opening and the closing time of

this valve is closely related to the functions of the heart; i.e., the abnormal case with some myocardial change or with some defect at the kidney offers the universal result that the time interval between the 2nd sound and the mitral opening, ($II D_m$ in Fig. 8) is prolonged to be 0.19 sec for a most extraordinary case, whereas the normal value lies between 0.05 and 0.07 sec. Besides, the time of occurrence of the signal at the valvular closing, its amplitude, etc., are of high diag-

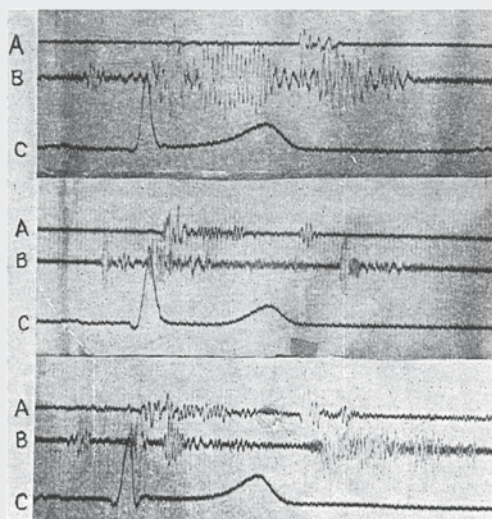


FIG. 9. Oscillograms; the lower frequency Doppler signal, the higher frequency Doppler signal, and the Doppler heart noise, respectively. (A—heart sound, B—Doppler signal, C—E. C. G.)

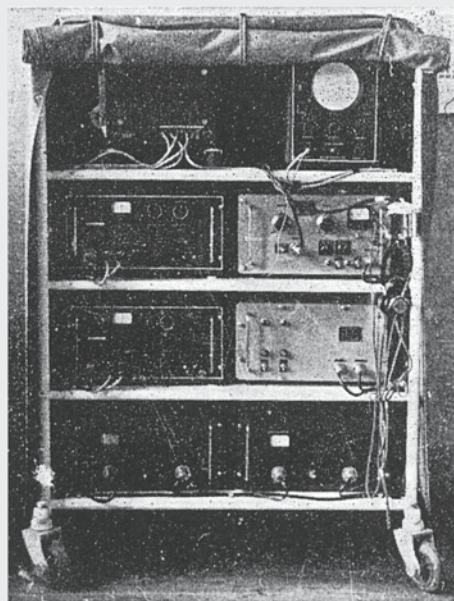


FIG. 10. Photograph of the apparatus.

METHOD FOR INSPECTION OF CARDIAC FUNCTIONS

1185

nostic significance, providing the possibility for inspecting the condition of the stiffness of the valvular structure. Moreover, the signals by the pulmonary artery itself is also detectable on the left sternal border in the 3rd intercostal space.

(c) Doppler Heart Noises

The Doppler heart noises are obviously audible only on a diseased heart. They are yielded when the reflecting object of the ultrasound, such as the ventricular wall, suffers an irregular vibration of small amplitude. A variety of tones are received according to the species of the objects or to the state of vibrations, etc. Since the amplitude of this cardiac vibration which causes the Doppler heart noises is supposed to be so small as to be less than a quarter-wavelength of the applied ultrasonic wave,⁹ the phase of the reflected wave is equivalent to be modulated by the vibration, the demodulation producing a vibratory tone. The important difference from the usual tone heard through a stethoscope is that the Doppler noises cannot be produced unless the ultrasound is applied to the source of the noises or to the vibratory portions. The stethoscope receives the sound considerably diffused from the source. These Doppler noises are also audible, though very weak, to a certain

degree from a normal human body, but an abnormal case provides a clearly distinguishable noise, characteristic of the particular defect in the heart. For example, when surplus liquid stays in the pericardium, the Doppler noises are sure to be audible, even if the stethoscope cannot detect the disorder (see Figs. 9 and 10).

5. CONCLUDING REMARKS

The usefulness of the ultrasonic Doppler method for the inspection of the cardiac functions has been described. Incorporating the principle, the equipment diagram, and the experimental examples, an original method for the cardiac diagnosis has been presented. Especially, the detection of the valvular movement is peculiar to this method and new information which other methods could not offer has been obtained. A variety of its application are in prospect for further investigations.

ACKNOWLEDGMENTS

The author wishes to thank the assistance of Dr. Yasuharu Nimura who presented cooperation in the medical field, and Mr. Shigeo Matsubara who carried out the construction of the apparatus.

THE JOURNAL OF THE ACOUSTICAL SOCIETY OF AMERICA

VOLUME 29, NUMBER 11

NOVEMBER, 1957

Ultrasonic Pulse Technique for Measuring Acoustic Losses and Velocities of Propagation in Liquids as a Function of Temperature and Hydrostatic Pressure

H. J. MCSKIMIN

Bell Telephone Laboratories, Inc., Murray Hill, New Jersey

(Received July 29, 1957)

A fixed path ultrasonic unit operating in the frequency range of 20–200 mcps is described which can be used for measuring acoustic wave velocities and losses in liquids as a function of temperature and hydrostatic pressure. A simple phase balance technique insures a high order of accuracy for velocity determinations.

Illustrative data for carbon tetrachloride, Dow Corning DC-703 and DC-200 silicone fluids, and water are shown. Determination of freezing points of liquids using ultrasonic waves for indication is also discussed briefly.

I. INTRODUCTION

OF the very great volume of work that has been done in studying the mechanical properties of liquids with ultrasound, only a relatively small amount has involved the use of hydrostatic pressure as a variable. This is partly due to the fact that means for providing and measuring high pressures are not as readily obtained as for, say, varying temperatures. Also, it is obvious that equipment suitable for use at atmospheric pressure may prove difficult to adapt to the closed system required for application of high pressures. Optical methods, for example, require specially constructed windows in the pressure vessel,¹ while variable path

interferometers add the complexity of a shaft which can be rotated from outside the pressure vessel.^{2,3}

Particularly for velocity measurements, methods involving fixed path lengths and high-frequency pulse techniques appear to have merit.^{4–6}

It is the purpose of this paper to discuss a method which is particularly good for determining velocities of propagation, but one which also yields attenuation. Operation at frequencies as high as 200 mcps appears

² J. C. Swanson, *J. Chem. Phys.* 2, 689 (1934).

³ T. A. Litovitz and E. H. Carnevale, *J. Appl. Phys.* 26, 816 (1955).

⁴ Gerald Holton, *J. Appl. Phys.* 22, 1407 (1951).

⁵ A. H. Smith and A. W. Lawson, *J. Chem. Phys.* 22, 351 (1954).

⁶ J. F. Mifsud and A. W. Nolle, *J. Acoust. Soc. Am.* 28, 469 (1956).

¹ P. Biquard, *Compt. rend.* 206, 897 (1938).

3.7 Neue Möglichkeiten der Ultraschalldiagnostik in der Gynäkologie und Geburtshilfe

Hans-J. Holländer (born 1936)

Hans Holländer was born August 2, 1936 in Coesfeld, Germany. He studied medicine at the Universities of Aachen, Muenster, Kiel and Goettingen. In 1962 Holländer attained his MD at the University of Muenster. In the same year he started his residency at medical clinics in Bamberg and Muenster. Between 1964 and 1971 he was research assistant under Professor Hermann Goecke at the gynecological clinic at the University of Muenster.

In 1965 Holländer started his research on medical ultrasonography. For the first time he tested the opportunities in using the prototype of the VIDOSON Real-Time-Ultrasound-Scanner that was developed by Soldner and Krause at Siemens Erlangen.

In 1971 he became lecturer and in 1975 he was appointed Professor at the University of Muenster. In 1973 he became director of the gynecological department of the St. Johannes Hospital in Duisburg until he retired in 1999.

Hans Holländer is a member of several scientific societies and a honorary member of the DEGUM (German Society for Ultrasonography in Medicine) In 1997 he was awarded the Hermann Goecke Medal of the University of Muenster.



D. Hofmann

P. Weiser

Sonderdruck aus der Zeitschrift „Fortschritte der Medizin“, 84. Jg., Nr. 18/1966, S. 689—693

Aus der Frauenklinik der Westfälischen Wilhelms-Universität Münster (Direktor: Prof. Dr. med. H. Goecke)

Neue Möglichkeiten der Ultraschalldiagnostik in der Gynäkologie und Geburtshilfe

Von Prof. Dr. med. D. Hofmann, Dr. med. H.-J. Holländer und Priv.-Doz. Dr. med. P. Weiser

Der Begriff „Ultraschall“ ist u. a. dadurch bekannt geworden, daß er seit Ende des ersten Weltkrieges bei der U-Boot-Ortung („Asdic-Verfahren“) Bedeutung erlangte. Ultraschall gelangt heute bei der Echolotung von Meerestiefen und bei der Materialprüfung weit verbreitet zur Anwendung. In den Jahren nach dem zweiten Weltkrieg schien es vorübergehend, als fände der Ultraschall auch in die Tumorthherapie Eingang. Einer kurzen Zeitspanne diesbezüglichen Optimismus¹ und leider auch allzu hoffnungsvoller Beurteilungen im Schrifttum folgte dann die Erkenntnis, daß der Ultraschall für die Tumorthherapie — auch in Kombination mit anderen Therapieverfahren — wertlos ist.

Es verblieben auf medizinischem Gebiet begrenzte Möglichkeiten der Diagnostik mit Ultraschall, vorwiegend im Bereich des Schädels. Immerhin hat sich die Echoenzephalographie ebenso wie die ophthalmologische Ultraschallanwendung einen festen Platz in der medizinischen Diagnostik erobert (Bannaski und Fischer, Kramer; Nover und

Glanschneider; Strik; Schiefer, Kazner und Brückner; dort ausgiebige weitere Literatur).

Bevor auf eigene Versuche, den diagnostischen Wert des Ultraschalls in Gynäkologie und Geburtshilfe zu überprüfen, eingegangen wird, seien in aller Kürze einige physikalische Gesichtspunkte erwähnt.

Die Bezeichnung „Ultraschall“ umfaßt Schallwellen, deren Frequenzen oberhalb des Hörbereiches liegen. Tab. 1 gibt einen Überblick über die heute gebräuchliche Frequenzeinteilung. Danach umfaßt der „Infraschall“ den Frequenzbereich 0 bis 16 Hz, der „Hörschall“ den Bereich zwischen 16 und 18 000 Hz; oberhalb dieser Frequenzen folgt der „Ultraschall“, wobei man noch einmal bei Frequenzen über 100 000 Hz von „Hyperschall“ spricht.

Je höher die Frequenz der Schallwellen ist, deren Ausbreitung im übrigen an Materie gebunden ist, desto mehr gleichen ihre Ausbreitungseigenschaften denjenigen freier elektromagnetischer Wellen. Im menschlichen Körper breitet sich der Ultraschall als Longitudinalwelle aus. Seine Ausbreitungsgeschwindigkeit hängt von Dichte und Elastizitätskonstanten der jeweiligen Medien ab. In Tab. 2 (nach Sundén) sind die Ausbreitungsgeschwindigkeiten für verschiedene Körpergewebe aufgeführt. Die Tabelle enthält auch die zugehörigen Werte der akustischen Impedanz, die für die medizinische Diagnostik wichtig ist.

Durchdringt eine Ultraschallwelle ein Medium und trifft auf ein zweites Medium, welches vom ersten durch eine Grenzfläche getrennt ist, so wird ein Teil der Schallenergie in das erste Medium zurückgeworfen, während der andere Teil in das zweite Medium eindringt. Für die Reflexion gelten die vom Licht her bekannten Winkelgesetze. Sie wird ferner bestimmt von dem erwähnten Begriff der akustischen Impedanz. Man versteht hierunter das Produkt $\rho \cdot v$ aus der Dichte des Mediums

Tab. 1: Frequenzeinteilung der Schallwellen

Frequenzbereich (Hz)	Bezeichnung
0—16	Infraschall
16—18 000	Hörschall
> 18 000	Ultraschall
> 100 000	Hyperschall

Tab. 2: Ausbreitungsgeschwindigkeiten der Schallwellen für verschiedene Körpergewebe (nach Sundén)

Substanz	Temperatur in °C	Frequenz (MHz)	Schallgeschwindigkeit (m/sec)	Dichte (g/cm ³)	Akustische Impedanz (g/cm ² sec)
Wasser ¹	25	—	1497	0,997	$1,49 \cdot 10^3$
Wasser ²	25	15	1495,6	0,997	$1,49 \cdot 10^3$
Kochsalzlösung ³	25	15	1504	1,005	$1,511 \cdot 10^3$
Menschl. Gewebe ⁴ (ohne Knochen)	37	2,5	1490—1610	1,06	$1,58—1,70 \cdot 10^3$
dasselbe, Mittelwert ⁵	37	2,5	1540	1,06	$1,63 \cdot 10^3$
Muskelgewebe (menschl.) ⁶	24	1,8	1568	1,058	$1,66 \cdot 10^3$
Lebergewebe (menschl.) ⁴	24	1,8	1570	1,055	$1,66 \cdot 10^3$
Fettgewebe (menschl.) ⁴	24	1,8	1476	0,928	$1,37 \cdot 10^3$
Gehirngewebe (menschl.) ⁶	24	2	1521	1,040	$1,58 \cdot 10^3$
Knochen (Rind) ⁷	—	2,5	3380	1,8	$6,1 \cdot 10^3$
Knochen (menschl. Schädel) ⁷	—	0,8	3360	1,85	$6,2 \cdot 10^3$
Luft ⁸	—	—	331	0,0012	41,3

¹ Bergmann, 1954. ² Barthel, 1954. ³ Ludwig, 1950. ⁴ Frucht, 1953. ⁵ Jeppsson, 1961. ⁶ Güttner et al., 1952. ⁷ Theismann und Pfander, 1949. ⁸ Carlin, 1949.

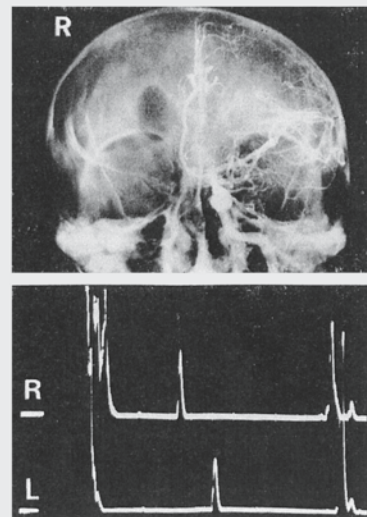
Vorgetragen vor der Med. Gesellschaft Münster am 10. November 1965.
Zur Veröffentlichung eingereicht: März 1966.

Abb. 1:

Echoenzephalogramm eines 51-jähr. Patienten mit Mittelechoverlagerung um 9,00 mm nach rechts.

Das Karotis-Angiogramm zeigt einen temporo-basalen Tumor links (Metastase). (Pat. M. W., Echo-Nr. 491/63.)

(aus: Schiefer, W. und Kazner, E.: Methodik und diagnostische Möglichkeiten der Echoenzephalographie. Fortschr. Med. 84, 4: 151, 1966).



und der Geschwindigkeit der Schallausbreitung in diesem Medium. Wenn eine Schallwelle in einem Medium 1 die akustische Impedanz $\varrho_1 \cdot v_1$ hat, und an einer Grenzfläche auf ein Medium 2 mit der akustischen Impedanz $\varrho_2 \cdot v_2$ trifft, und der Auftreffwinkel 90° beträgt, dann gilt für den Reflexionsfaktor R, das Verhältnis zwischen den Intensitäten des einfallenden und des reflektierten Strahls die folgende Gleichung:

$$R = \left(\frac{\varrho_1 v_1 - \varrho_2 v_2}{\varrho_1 v_1 + \varrho_2 v_2} \right)^2$$

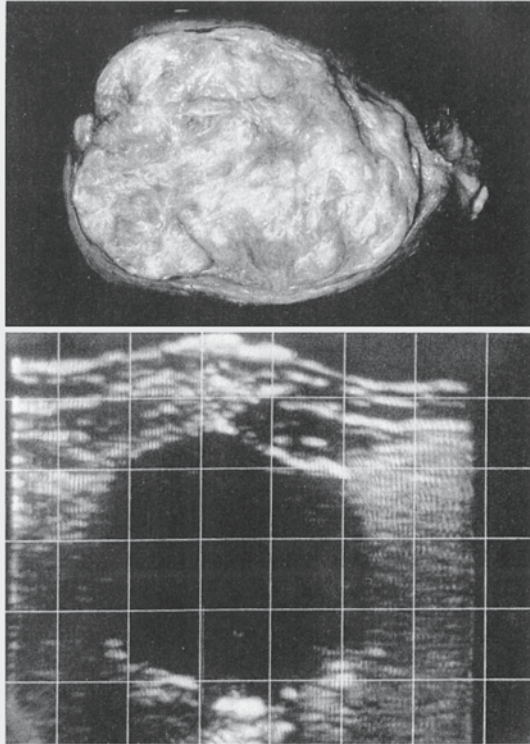


Abb. 2: Ultraschallechogramm und Operationspräparat eines Uterus myomatosus.

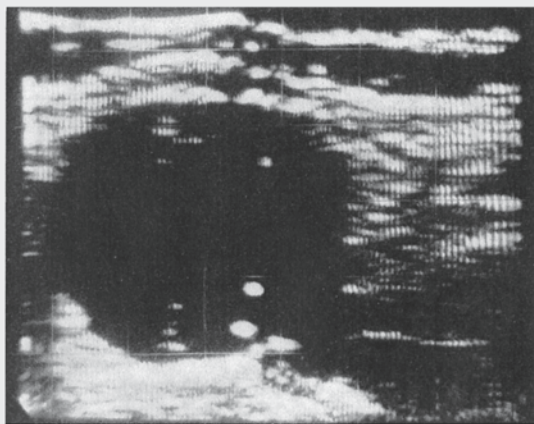


Abb. 3: Ultraschallechogramm einer Ovarialcyste.

Aus der Gleichung folgt, daß die Schallenergie an Grenzflächen zwischen Gasen einerseits und fester oder flüssiger Materie andererseits nahezu vollständig reflektiert wird. Rund 30% der Schallenergie werden an der Grenzfläche Muskel/Knochen reflektiert, wenn der Einfallswinkel 90° beträgt.

Die Schallabsorption in einem Medium folgt der bekannten e-Funktion

$$I = I_0 \cdot e^{-2\alpha x}$$

wobei α der sogenannte Amplituden-Absorptionskoeffizient ist.

Die medizinische Ultraschalldiagnostik basiert, wie bereits oben ausgeführt, auf der Reflexion von Schallwellen an Grenzflächen zwischen Geweben mit unterschiedlicher akustischer Impedanz. Das in der Praxis heute bevorzugte Prinzip besteht darin, daß Schallwellen, die in einem piezoelektrischen Kristall erzeugt werden, in den Körper hineingeschickt werden und nach Reflexion von dem gleichen Kristall wieder aufgenommen werden. Die hierbei wieder erzeugten elektrischen Potentiale werden verstärkt und oszillographisch dargestellt.

Die Forderung, die Schallwellen möglichst senkrecht in die zu untersuchenden Medien einfallen zu lassen, kann einfach erfüllt werden, wenn, wie etwa bei der Echoenzephalographie, die Lage eines „Mittlechos“ im Schädel festgestellt werden soll, um raumfordernde intrakranielle Prozesse zu diagnostizieren (Abb. 1). Ähnlich verhält es sich auf dem Gebiet der Augenheilkunde. Im Falle der geburtshilflich-gynäkologischen Diagnostik ist es jedoch erstrebenswert, komplette reelle Ultraschallechobilder zu bekommen, wobei genügende Eindringtiefe ebenso wie genügende Detailauflösbarkeit Voraussetzung ist.

Wir legten uns die Frage vor, ob und wie weit das Ultraschallechoverfahren auf unserem Fachgebiet eine diagnostische Bereicherung darstellt. An entsprechenden Untersuchungen liegen im wesentlichen eine schwedische (Sundén) und einige amerikanische Arbeiten vor, von denen sich letztere mit der intrauterinen Messung der Kindsgröße befassen (Taylor, Holmes, Thompson und Gottesfeld; Thompson, Holmes, Gottesfeld und Taylor). In neuester Zeit ist eine Arbeit von Donald erschienen, die etwas allgemeiner auf die gynäkologisch-geburtshilflichen Anwendungsmöglichkeiten der Ultraschalldiagnostik eingeht. Wie wir im weiteren noch darlegen werden, scheinen uns die Anwendungsmöglichkeiten des Ultraschalls in Gynäkologie und Geburtshilfe doch noch stärker begrenzt zu sein, als es von

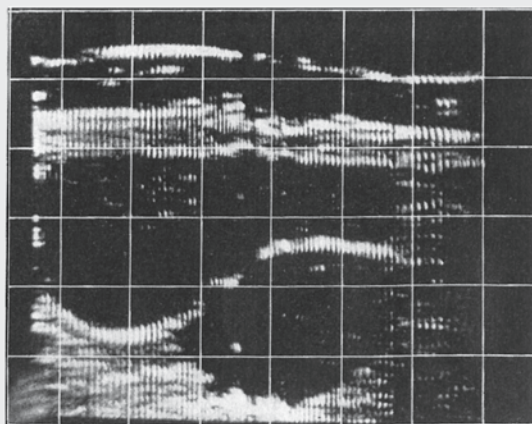


Abb. 4: Ultraschalldarstellung der Blase und ihre Abgrenzung gegen den Uterus.

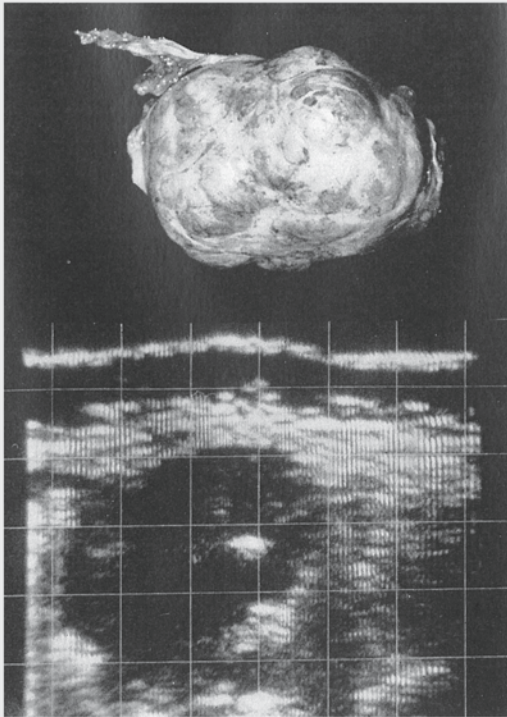


Abb. 5: Ultraschallechogramm und Operationspräparat eines durch Tastuntersuchung nicht eindeutig diagnostizierten Ovarialtumors. Einbettung des Tumors in Darm- und Netzhänsionen.

dem zuletzt zitierten Autor behauptet wird. Dies umso mehr, als uns die Qualität der betreffenden Bilder noch unbefriedigend erscheint.

Bei unseren eigenen Untersuchungen bedienten wir uns eines Ultraschallgerätes, bei dem ein stehender Schallkopf Ultraschallimpulse mit einer Frequenz von ca. 3000 sec^{-1} aussendet, die über ein größeres Körpersegment senkrecht einfallend verteilt und wieder aufgenommen werden. Das Auflösungsvermögen unserer Apparatur betrug in der Tiefe ca. 1,5 mm und in der Breite ca. 4 mm. Die Schallfrequenz belief sich auf 2,5 MHz.

Im folgenden seien einige Ultraschallechophotogramme demonstriert und ihr diagnostischer Wert erörtert. In den Abbildungen entsprechen die Zeilenabstände der Raster einem wirklichen Abstand von 2 cm. Es darf noch einmal hervorgehoben werden, daß die vorliegenden Ultraschallechogramme im Gegensatz zur Röntgenaufnahme, die bekanntlich ein Summationsbild darstellt, echte Querschnittsbilder sind, also Bilder, wie sie in der Röntgenologie vermittle der Schichtverfahren angestrebt werden.

Uterustumoren

Abb. 2 gibt das Beispiel eines Uterus myomatosus wieder, der im wesentlichen einen faustgroßen intramuralen Myomknoten aufwies. Völlig eindeutig lassen sich die Größenverhältnisse ablesen, indem die Durchmesser des Tumors 7 cm und 8 cm betragen. Die Abbildung läßt im übrigen die schalloptische Homogenität des Befundes erkennen, die im Gegensatz zu der recht deutlichen Strukturierung des Tumors selbst steht (vgl. Abb. 2 oben). Wie noch zu zeigen sein wird, ist die Unterscheidung von einem schwangeren Uterus in der Regel möglich. Auf die besonders scharfe Wiedergabe der Bauchwandgrenzflächen sei hingewiesen. Naturgemäß bestehen keinerlei histologische Aussagemöglichkeiten.

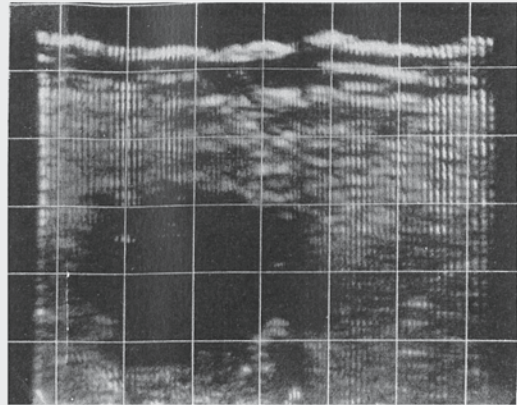


Abb. 6: Ultraschallechogramm eines tiefliegenden schwer tastbaren Ovarialtumors.

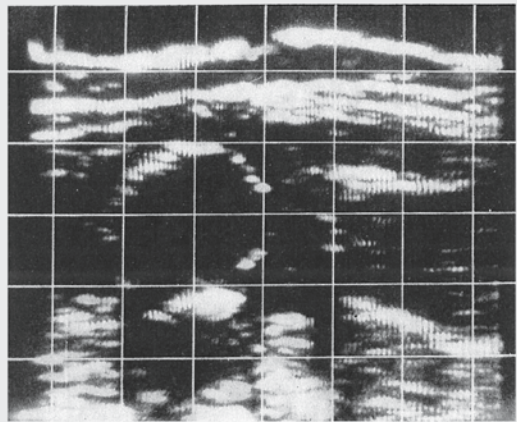


Abb. 7: Normaler 30 cm langer Foet in Längslage. Drohender Spätabort. Der Schädel (größter Durchmesser 4,5 cm) und die Grenzen des Thorax sind deutlich zu erkennen.

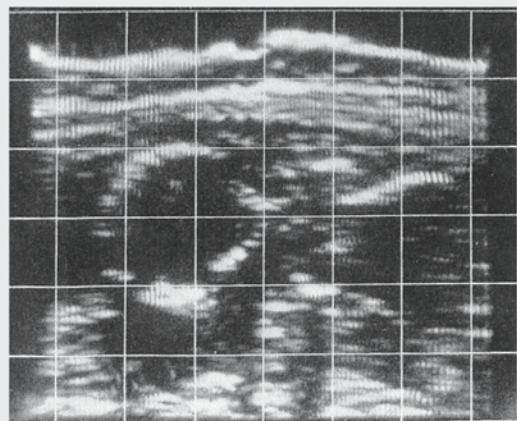


Abb. 7a: Der gleiche Foet wie oben. Bildebene jedoch etwa 2 mm parallel zur Längsachse verschoben.

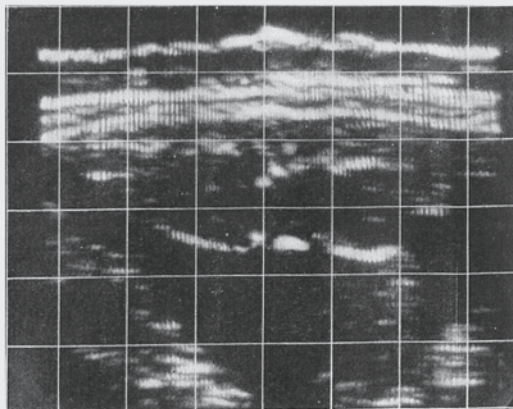


Abb. 8: Stark deformierter und mazerierter Foet bei partieller Blasenmole.

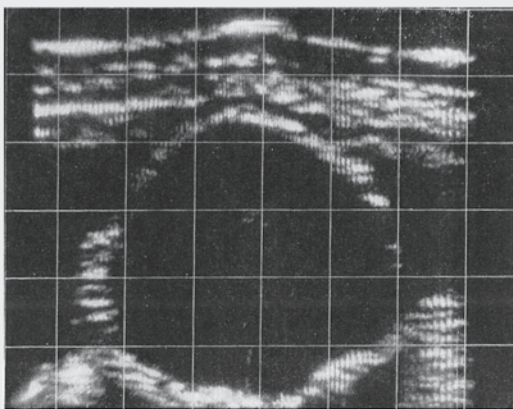


Abb. 9: Größter Umfang eines normalen kindlichen Schädels.

Ovarialtumoren

Erwartungsgemäß läßt das Ultraschallechogramm auch nicht immer einen sicheren Entscheid darüber zu, ob es sich um einen Uterustumor oder einen homogenen Ovarialtumor, z. B. ein Cystoma serosum, handelt. Reflexe, wie sie im Innern des Tumors von Abb. 3 zu erkennen sind, sprechen immerhin für das Vorliegen eines Ovarialtumors. Die Abb. 3 zeigt im übrigen, daß auch der Ovarialtumor gewissermaßen als Negativ, eingehüllt in inhomogene Strukturen, wie Darmschlingen, Netz usw., zur Darstellung gelangt. Eindeutige Grenzflächen, wie sie z. B. bei Mehrkammerigkeit oder teilweiser Solidität des Tumors zu erwarten sind, bilden sich vielfach ab. In Abb. 4 findet sich eine scharfe Grenze zwischen Uterus einerseits und Blase andererseits, deren Verschiebung bei sich änderndem Füllungszustand der Blase nachweisbar ist.

In den beiden Abb. 5 und 6 handelt es sich um die Ultraschalldarstellung zweier Ovarialtumoren, die ungünstigen Verhältnisse wegen durch die gynäkologische Untersuchung nicht eindeutig nachzuweisen waren. In beiden Fällen verhinderten ausgiebige Darm- und Netzhäsionen und im Falle der Abb. 6 die Tiefe des Tumors eine klare Diagnosestellung. Nach Anfertigung von Ultraschallechogrammen konnte die Diagnose einwandfrei gestellt werden.

Schwangerschaftsdiagnostik

Die Hoffnungen, die von vornherein auf eine geburtshilfliche Ultraschalldiagnostik gesetzt wurden, gründeten sich u. a. auf den Gesichtspunkt der Fruchtschädigung.

Bekanntlich vermeiden wir heute nach Möglichkeit röntgendiagnostische Maßnahmen in der Schwangerschaft, selbst dann, wenn die Gefahren der Fruchtschädigung und der Erbschädigung so gering zu veranschlagen sind, daß sie keine Kontraindikation gegen eine notwendige Röntgendiagnostik abgeben. Alle Überlegungen bezüglich einer Schädigung der Frucht würden aber entfallen, wenn die Schwangerschaftsdiagnostik mittels Ultraschall durchführbar wäre. Schon aus der Zeit einer versuchten, aber bald wieder aufgegebenen Ultraschalltumorthherapie wissen wir, daß selbst intensive Ultraschalleinwirkung nur geringe Gewebsschädigung herbeizuführen vermag. Ultraschalltherapiegeräte arbeiteten aber mit Flächenenergien um 3 Watt/cm^2 . Selbst bei Steigerung der Energiezufuhr auf 15 Watt/cm^2 im Tierversuch konnten nur relativ geringe Schädigungen erzielt werden. Die beim Echoimpulsverfahren zugeführte Energie liegt aber noch weit unter den genannten Werten: Sie liegt größenordnungsmäßig bei einigen Milliwatt/cm². Dies bedeutet, daß bei Anwendung in der Schwangerschaft keine Fruchtschädigung zu befürchten wäre.

Die Abb. 7 und 7a zeigen das Beispiel einer Schwangerschaftsdiagnostik bei 30 cm langem Föten, wobei die Bildebene — bei unserem Gerät automatisch — um 2 mm verschoben wurde. Es handelte sich hier um einen drohenden Spätabort. Deutlich sind der Schädel der Frucht mit einem größten Durchmesser von 4,5 cm und die Grenzen des Thorax zu erkennen. Einen abgestorbenen und stark mazerierten Föten bei partieller Blasenmole gibt die Abb. 8 wieder.

Nach unserer bisherigen Erfahrung verlieren die Ultraschallechogramme an Eindeutigkeit, wenn das Schwangerschaftsalter weniger als 4 Monate beträgt, ebenso, wie dies praktisch auch bei der Röntgenaufnahme der Fall ist. Völlig eindeutige Bilder erhält man demgegenüber in fortgeschrittenerem Schwangerschaftsalter. Abb. 9 gibt den größten Umfang eines kindlichen Schädels wieder, dessen Durchmesser ca. 8 cm beträgt, Abb. 10 zwei Schädel bei Zwillingsschwangerschaft.

Diskussion

Fassen wir unsere bisherigen Erfahrungen mit der Ultraschalldiagnostik in Gynäkologie und Geburtshilfe zusammen, so darf zunächst die im Vergleich mit anderen Untersuchungen gute Bildqualität unserer Echogramme hervorgehoben werden. Eine größere Eindringtiefe, wie sie nach unseren bisherigen Ergebnissen wünschenswert wäre, müßte allerdings auf Kosten der Detailauflösung gehen. Sie würde dennoch in der geburtshilflichen Diagnostik günstig sein.

Ungeachtet einer mehr oder weniger verfeinerten Technik dürften die gezeigten Beispiele aber deutlich gemacht haben, wo die Grenzen der Ultraschalldiagnostik in Geburtshilfe und Gynäkologie grundsätzlich liegen. Zweifellos läßt sich in der Gynäkologie die Tumordiagnostik vervollständigen. Dabei lassen sich Größe, Form und Tiefe eines Tumors bestimmen, wohingegen Art und Ausgangspunkt des Tumors nicht immer eindeutig diagnostiziert werden können.

Auf geburtshilflichem Gebiete ist es möglich, mittels Ultraschall fötale Teile von einer gewissen Mindestgröße an zu identifizieren, was gelegentlich zur Differentialdiagnose: Schwangerschaft/erweichtes Myom Bedeutung erlangen kann. Auch bei der Diagnostik einer Blasenmole kann das Ultraschallechogramm wertvoll sein, worauf in neuester Zeit Donald hingewiesen hat. Im Gegensatz zu

Abb. 10

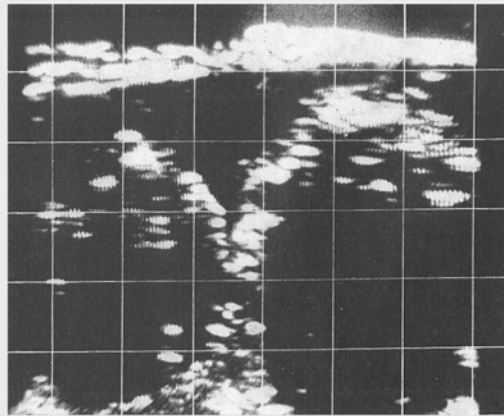
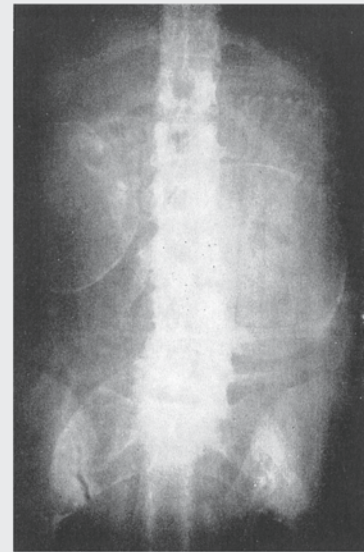


Abb. 10: Ultraschallechogramme zweier kindlicher Schädel bei Zwillingschwangerschaft.

Abb. 10a: Zu Abb. 10 gehörige Röntgenaufnahme.

Abb. 10a



diesem Autor scheint uns die Möglichkeit der Ultraschall-diagnostik einer Extrauterin gravidität nicht gegeben zu sein. Sicher gelingt die Größenbestimmung älterer Föten mit Ultraschall ebenso wie die Zwillingsdiagnostik. Desgleichen werden sich größere kindliche Mißbildungen in utero feststellen lassen. Ob ausgeprägtere Formen von Hydrops fetus genügend eindeutig zur Darstellung kommen, bleibt noch zu untersuchen.

Die Ultraschallechoimpulsdiagnostik hat somit im wesentlichen die Bedeutung einer diagnostischen Zusatz- bzw. Ergänzungsmethode, die keineswegs immer, wohl aber in vielen Einzelfällen eine Vervollständigung des geburtshilflichen oder gynäkologischen Untersuchungsbefundes gestattet.

Zusammenfassung

Die obigen Untersuchungen sollten Aufschluß über die Frage geben, welche Bedeutung der Ultraschalldiagnostik in Gynäkologie und Geburtshilfe beizumessen ist. Es konnten in beliebigen Ebenen Schnittbilder im Bereich des inneren Genitals angefertigt werden, deren Qualität in bezug auf Detailauflösung als gut bezeichnet werden darf.

Die Untersuchungen haben ergeben, daß die Ultraschalldiagnostik in der Gynäkologie zum Nachweis, zur Größenbestimmung und zur Lagediagnostik von Tumoren geeignet ist.

In der Geburtshilfe gestattet sie den Nachweis von gestörten Schwangerschaften, von Mißbildungen und von Mehrlingsschwangerschaften und eignet sich speziell zur Messung der Kindsgröße.

Literatur

- Bannaski, H., und Fischer, K. H.: Neue diagnostische Möglichkeiten des Ultraschall-Impulsechoverfahrens. *Med. Klin.* 53, 51 (1958).
 Donald, J.: Ultrasonic echo sounding in obstetrical and gynecological diagnosis. *Amer. J. Obstetr. Gynec.* 93, 7, 935 (1965).
 Kramer, G.: Zur Diagnostik raumfordernder intrakranieller Prozesse mit Hilfe des Echoimpulsverfahrens. *Chirurg* 34, 7, 290 (1963).
 Nover, A., und Glanschneider D.: Ultraschalldiagnostik intraokularer Tumoren. *Fortschr. Med.* 83, 11: 433 (1965).
 Schiefer, W., und Kazner, E.: Methodik und diagnostische Möglichkeiten der Echoencephalographie. *Fortschr. Med.* 84, 4: 151 (1966).
 —, —, und Brückner, H.: Die Echoencephalographie, ihre Anwendungsweise und klinischen Ergebnisse. *Fortschr. Neurol. Psychiatr.* 9: 457 (1963).
 Strik, W. O.: Die diagnostische Anwendung des Ultraschalls. *Med. Klin.* 56, 43: 1817 (1961).
 Sundén, B.: On the diagnostic value of ultrasound in obstetrics and gynaecology. *Acta obstetr. gynecol. Scand.* XL III, Suppl. 6 (1964).
 Taylor, E. S., Holmes, J. H., Thompson, H. E., und Gottesfeld, K. R.: Ultrasound diagnostic techniques in obstetrics and gynecology. *Amer. J. Obstetr. Gynec.* 90, 655 (1964).
 Thompson, H. E., Holmes, J. H., Gottesfeld, K. R., und Taylor, E. S.: Fetal development as determined by ultrasonic pulse echo techniques. *Amer. J. Obstetr. Gynec.* 92, 1: 44 (1965).

ÜBERREICHT DURCH:

SIEMENS AKTIENGESSELLSCHAFT
 Wernerwerk für Medizinische Technik · Erlangen

P 85-2/189 d
 Printed in Germany
 10663

3.8 The prediction of fetal maturity by ultra-sonic measurement of the biparietal diameter

Stuart Campbell (born 1936)

Stuart Campbell was born 1936 in an industrial part of Glasgow. He spent his childhood in Paisley, to the west of Glasgow. Here he went to grammar school and then later to Glasgow University. He graduated from the Faculty of Medicine, University of Glasgow in 1961. After qualifying for his Membership of the Royal College of Obstetricians and Gynaecologists in England in 1965, Professor Campbell started his life-long career in ultrasonography and prenatal diagnosis. Working as a research registrar under Professor Ian Donald at the Queen Mother's Hospital, University of Glasgow (opened in 1964 with a fully equipped ultrasound unit), Professor Campbell studied placentography and cephalometry with Dr. James Willocks, then senior lecturer in the department. Dr. Willocks published his studies on the A-scan measurement of the fetal biparietal diameter in 1962 and 1964. In 1968, with help in modifying the Disonograph scanning apparatus from Mr. John Flemming, then a research technologist engaged by the University of Glasgow, Professor Campbell described the use of both the A- and B-mode scans to measure the fetal biparietal diameter in his landmark publication "*An improved method of fetal cephalometry by ultrasound*". This elegant and practical 'maneuver' quickly became standard practice in an obstetric ultrasound examination for the next decade. In 1971, with improvements in the caliper system, he published normograms for the biparietal diameter from the 13th week of gestation and has made cephalometry a standard tool for the assessment of fetal growth and maturity.



After his brief tenure at the Queen Mother's Hospital, he took up in 1968 lecturership at the Institute of Obstetrics and Gynaecology at Queen Charlotte's Maternity Hospital in London, working under Professor Sir John Dewhurst, and soon became senior lecturer in 1973 and Professor of Clinical Obstetrics & Gynaecology in 1976. There he described varying patterns of intrauterine fetal growth, the 'late-flattening' growth associated with fetal hypoxemia and the 'low-profile' variety associated with constitutional reduced growth. He reported the diagnosis and management of a 17 weeks anencephaly in 1972 and the diagnosis of spina bifida by ultrasound in 1975. Both appeared as landmark papers in the *Lancet*. In collaboration with researchers at Guy's Hospital, London, he was active in the study of maternal serum AFP and amniotic AFP levels and their relationship with neural tube defects. His group also looked at the fetal hourly urine production rate in 1973 with Juiri Wladimiroff from Rotterdam. In 1975 he described another landmark fetal measurement, the abdominal circumference and subsequently its relationship with intrauterine fetal weight.

Professor Campbell moved on to become Professor of Obstetrics and Gynaecology at King's College Hospital Medical School, London in 1976. In the same year he followed on with the concept of head circumference to abdominal circumference ratio in the assessment of small-for-dates fetuses. In the following year, together with Dr. Charles Rodeck (now Professor) at King's College, he published experience with ultrasound-guided fetoscopy and diagnosis of neurotube defects with gray-scale ultrasound. In 1980, with the advent of real-time ultrasound scanners, his group described yet another landmark parameter, the fetal femur length in second trimester dating.

By about 1982, aside from looking at the various fetal malformations using real-time ultrasound, Professor Campbell had started systematic investigations in many other areas, including ovarian cancer screening with ultrasound, Doppler fetal and utero-placental blood flow in pathological conditions such as pre-eclampsia, ovarian follicular developments, routine ultrasound population screening, and umbilical and placental blood sampling. With the advent of transvaginal scanners and color flow mapping in the late 1980s, his group studied with renewed interest gynecological pathologies such as ovarian cancer, endometrial cancer, ectopic pregnancies and pelvic masses. In collaboration with his colleagues in reproductive medicine, Professor Campbell developed various ultrasound assessment criteria in enhancing the effectiveness of in-vitro fertilization programmes. Many of the large-scale studies were published as landmark papers in the *British Medical Journal*. Research in Doppler velocimetry, fetal interventional techniques and therapy were further expanded with the arrival of Dr. Kypros Nicolaides (now professor at King's College) in the department. Fetoscopic laser surgery was one of the incarnations and has been found to be useful in conditions such as the twin-to-twin transfusion syndrome by sealing off the communicating vessels. Professor Campbell moved on in 1996 to become Professor and Chair at the Department of Obstetrics and Gynecology and the Fetal Medicine Unit at St. George's Hospital in London.

Professor Campbell has served on the Council and committees of the Royal College of Obstetricians and Gynaecologists. He has been elected Honorary Fellow of the British Medical Ultrasound Society, the American College of Obstetricians and Gynecologists, the American Institute of Ultrasound in Medicine, the Italian Society of Echography in Obstetrics and Gynaecology and the Croatian Academy of Medicine. These are among the many honors and awards he has received throughout his career. He was made Doctor of Science by the University of London in 1996.

Professor Campbell is probably the most well-known figure in the field of obstetrical and gynecological ultrasound to date and his contributions to the specialty are truly legendary. His research in ultrasonography, prenatal diagnosis, fetal medicine and therapy span an incredible number of important areas and in his unfailing perseverance in breaking new ground in the last 30 years he has contributed to over 500 papers and articles and has been author or co-author of at least 100 books, monographs and book chapters. Professor Campbell has taught extensively as visiting professor in many major obstetrics and gynecology centers in the United States and Europe and has been invited keynote speaker at many important international meetings. He was the President of the Section of Obstetrics & Gynaecology, Royal Society of Medicine in 1995 and was the founding President of the International Society of Ultrasound in Obstetrics and Gynecology (ISUOG) in 1990 (up to 1998) and founding Editor-in-chief of its journal – the *Journal of Ultrasound in Obstetrics and Gynecology*. In 1992, Professor Campbell received the Ian Donald gold medal from the ISUOG. His current interest is in 3-D ultrasound.

In part excerpted with permission from the website www.ob-ultrasound.net by Joseph Woo, MD, Hong Kong. Picture courtesy Joseph Woo, MD.

J. Obstet. Gynaec. Brit. Cwlth.
July 1969, Vol. 76, pp. 603–609.

THE PREDICTION OF FETAL MATURITY BY ULTRASONIC MEASUREMENT OF THE BIPARIETAL DIAMETER

BY

STUART CAMPBELL, *Senior Registrar*

Institute of Obstetrics and Gynaecology, Queen Charlotte's Maternity Hospital, London, W.6

THE antenatal measurement of the fetal biparietal diameter by ultrasound has been used to predict fetal weight (Thompson *et al.*, 1965) and more successfully to assess intrauterine growth (Willocks *et al.*, 1967). By using both A and B scan display systems in combination Campbell (1968) obtained a high degree of accuracy and showed that the fetal head could be measured during the second trimester. This report indicated that from the 20th to the 30th week of pregnancy the biparietal diameter values were confined within narrow limits for a certain week of gestation, and that measurement during this period might be valuable in the prediction of fetal maturity. To test this hypothesis, a study was arranged in two parts. Firstly, patients in whom the duration of gestation was known and documented were studied to establish the normal growth pattern of the biparietal diameter during the second half of pregnancy; the information was then used to predict fetal maturity in patients in whom this was in doubt.

PATIENTS AND METHODS

In order to prepare a normal curve, it was considered that the duration of gestation was known if a patient was sure of the date of her last menstrual period, if clinical assessment of uterine size agreed throughout pregnancy with the period of amenorrhoea, and if delivery following the spontaneous onset of labour occurred within one week of the expected date. In addition it was required that the baby should weigh more than 2.63 kg. which is the tenth percentile (Lubchenco *et al.*, 1963) for 40 weeks gestation. There were 186 patients who fulfilled these criteria.

Patients in the second part of the study consisted of 170 women who were referred for

assessment because the fetal maturity was in doubt. In these cases there was either a discrepancy between the actual and expected uterine size in excess of two weeks, or there was absolute uncertainty about the date of the last menstrual period. A discrepancy was only accepted if it was found on more than one occasion by an experienced obstetrician (consultant or registrar grade). On the basis of information obtained in the first part of the study (*vide infra*), only cases in which the fetal biparietal diameter was less than the upper limit for 30 weeks gestation were included.

The method of cephalometry was as described by Campbell (1968) using the Diasonograph and Diasonoscope (Nuclear Enterprises, Limited). The position of the fetal head was first accurately determined by a two dimensional B scan display, and when the biparietal diameter was visualized a measurement by means of A scan was obtained. At the time of this study the electronic cursors on the A scan display, which are calibrated to convert time into distance, could not be fixed to echoes less than 4.9 cm. apart. For this reason, measurements before 20 weeks gestation were not obtained. All measurements were taken by one person.

RESULTS

Part I. From the first group of patients a total of 471 individual observations of the fetal biparietal diameter were made from the 20th week of pregnancy onwards (Fig. 1). This shows that up to and including the 30th week of gestation growth is more rapid (mean 2.8 mm./week) than in the last 10 weeks (mean 1.5 mm./week), and that in the later weeks of pregnancy the values show a wider scatter about the mean. It is probable, therefore, that for the purpose of predicting maturity, biparietal diameter values which fall into the 20 to 30 weeks range are more

604 CAMPBELL

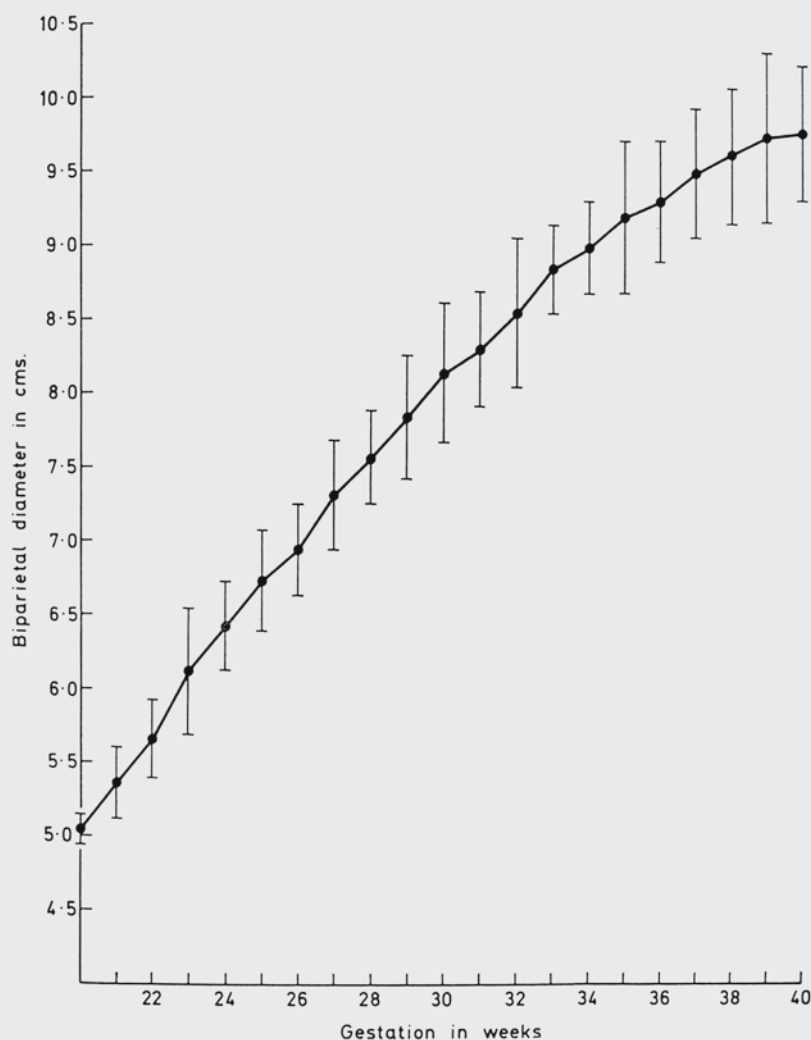


FIG. 1

Mean fetal biparietal diameter values ± 2 standard deviations for each week of gestation during the second half of normal pregnancy in 186 patients whose gestation was known (471 individual measurements).

useful. There were 173 measurements in this range and these are shown in relation to the duration of gestation in Figure 2. There is a high degree of positive correlation ($r = +0.9810$) and this is statistically highly significant ($t = 21.15$ $P < 0.001$). A regression line was fitted to the data and 5 per cent confidence limits drawn. This shows that for a given head measurement the regression line will predict the true week of gestation ± 8.4 days in 95 per cent of cases.

Part II. Table I shows the eventual outcome of the 170 pregnancies in which predictions of maturity were made; 106 patients went into labour spontaneously with the delivery of a mature baby and were considered to have been delivered at term; in 27 patients labour was induced for postmaturity and these will be considered further; in 37 patients labour was induced for reasons other than postmaturity, or they were delivered of babies which weighed less

ULTRASONIC MEASUREMENT OF THE BIPARIETAL DIAMETER 605

TABLE I
*Outcome of pregnancy in 170 antenatal patients
referred for measurement*

No. of cases	Eventual outcome	Included in study
106	Spontaneous labour and delivery	Yes
27	Induced for postmaturity	Yes
37	Induced for other reasons or baby <2.63 kg.	No
Total 170		

than 2.63 kg. and were excluded from the study.

All predictions in Part II patients were made by using the regression line (Fig. 2) and were taken to the nearest week of gestation. In each case a day of delivery was subsequently determined, counting forward from the day of

measurement. This was done so that the expected delivery date calculated from the ultrasonic measurement (Ultrasonic E.D.D.) and that calculated from the patient's last menstrual period (Calculated E.D.D.) could be compared in relation to the final outcome.

Figure 3 shows the distribution of discrepancies between all the ultrasonic estimates and the actual dates of delivery.

As the confidence graph indicated that the duration of gestation could be correctly predicted ± 8.4 days in 95 per cent of cases, it was decided that all predictions which fell within 9 days of the actual date of delivery would be regarded as correct. Conversely all predictions which fell outside this limit were considered incorrect. Table II shows that of the 106 patients who started labour spontaneously the ultrasonic E.D.D. was incorrect in 17 cases (16 per

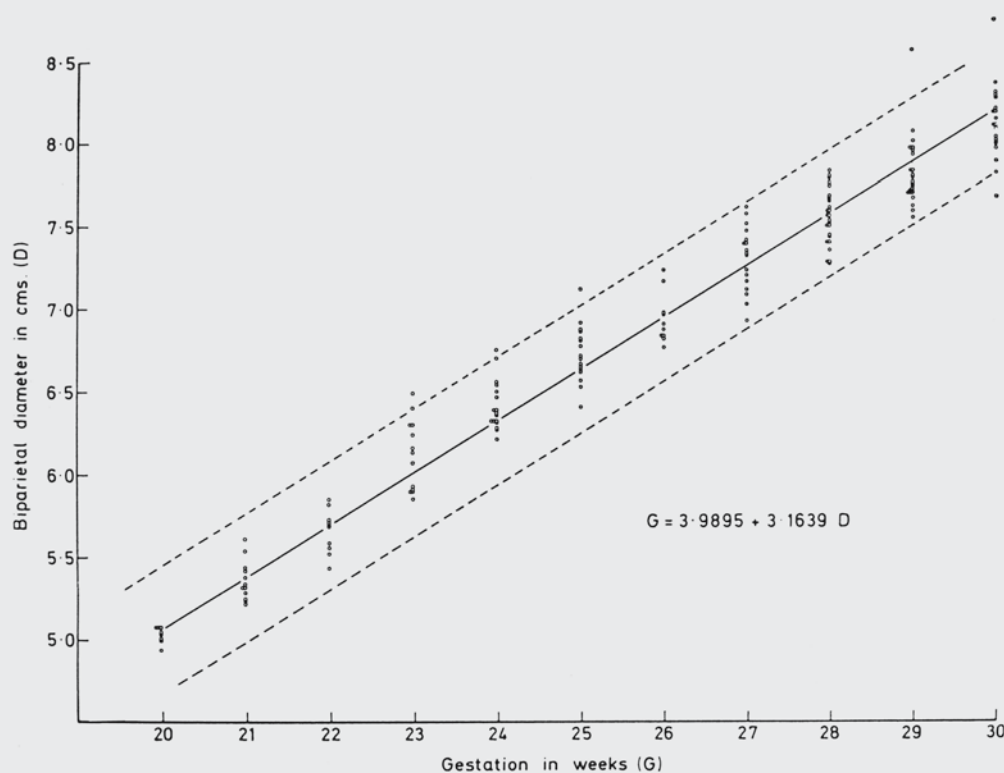


FIG. 2

Fetal biparietal diameter values plotted against each week of gestation from the 20th to the 30th week of normal pregnancy. A regression line and 5 per cent confidence limits have been drawn (173 individual measurements).

606 CAMPBELL

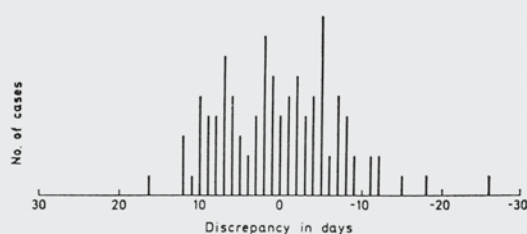


FIG. 3

Distribution of discrepancies in days between all the ultrasonic predictions and the actual date of delivery.

cent). In the 96 cases with a calculated E.D.D., 39 (40.6 per cent) of the predictions were incorrect. The overall prediction of the delivery

date was significantly better by ultrasound than by accepting the patients dates ($\chi^2 = 13.996$ $P < 0.001$).

The 96 cases who had both an ultrasonic and calculated E.D.D. were divided into two groups depending on whether these predictions agreed, i.e. fell within one week of each other, or disagreed, i.e. were one week or more apart. There were 57 cases in which there was agreement, and Table III shows that there were 9 errors (15.8 per cent) with the ultrasonic prediction and 7 errors (12.3 per cent) when the calculated E.D.D. was accepted. There is no statistically significant difference in this distribution ($\chi^2 = 0.07$ $P > 0.7$). In 39 cases the ultrasonic E.D.D. and calculated E.D.D. were not in

TABLE II
Prediction of the date of delivery in all patients having a spontaneous delivery

Method of assessment of maturity	Number of cases		
	Prediction correct	Prediction incorrect*	Total
Ultrasound	89 (84%)	17 (16%)	106
Calculated from date of last menstrual period	57 (59.4%)	39 (40.6%)	96†

$\chi^2 = 13.996$. $P < 0.001$. * An error is > 9 days from the date of delivery.

† 10 patients were uncertain of the date of their last menstrual period.

TABLE III
Prediction of the date of delivery in patients in whom ultrasonic E.D.D. and calculated E.D.D. agreed (i.e. fell within 1 week of each other)

Method of assessment of maturity	Number of cases		
	Prediction correct	Prediction incorrect	Total
Ultrasound	48 (84.2%)	9 (15.8%)	57
Calculated from date of last menstrual period	50 (87.7%)	7 (12.3%)	57

$\chi^2 = 0.07$. $P > 0.7$.

TABLE IV
Prediction of the date of delivery in patients in whom ultrasonic E.D.D. and calculated E.D.D. did not agree (i.e. were 1 week or more apart)

Method of assessment of maturity	Number of cases		
	Prediction correct	Prediction incorrect	Total
Ultrasound	34 (87.2%)	5 (12.8%)	39
Calculated from date of last menstrual period	7 (17.9%)	32 (82.1%)	39

$\chi^2 = 34.758$. $P < 0.001$.

ULTRASONIC MEASUREMENT OF THE BIPARIETAL DIAMETER 607

agreement (Table IV). The ultrasonic prediction was in error in 5 cases (12.8 per cent) and the prediction from the patient's dates was in error in 32 cases (82.1 per cent). This difference is statistically highly significant ($\chi^2 = 34.758$ $P < 0.001$).

Comparing the two groups, the errors in the ultrasonic predictions were not significantly different ($\chi^2 = 0.0012$ $P > 0.9$) while the difference between the calculated E.D.D. errors was highly significant ($\chi^2 = 43.884$ $P < 0.001$). This indicates that ultrasonic measurement can successfully separate those cases in which there is a mistake in the calculated maturity from those in which there is not.

The only accepted clinical sign indicating an error in the calculated maturity of the fetus was a discrepancy between the actual and the expected size of the uterus and this varied from 3 to 8 weeks. In order to determine if the size of this discrepancy might give an indication whether the calculated maturity was correct or in error the 96 cases were divided into two groups. In the first group the dates—uterine-size discrepancy was 3 or 4 weeks and in the second the discrepancy was more than 4 weeks (Table V). There were 68 cases in the first group of which 27

(39.7 per cent) of the predictions were incorrect. The second group of 28 cases had 12 errors (42.9 per cent). There was no statistically significant difference between the two groups ($\chi^2 = 0.0003$ $P > 0.9$), indicating that the degree of the discrepancy between the actual and expected uterine size did not help to distinguish those whose calculated maturity was in error from those who were normal.

Only in 10 cases was the patient totally unsure of the date of her last menstrual period. This is too small a group for statistical analysis, but the number of incorrect predictions was highest in this group (3 cases).

A total of 27 cases were induced solely because they were considered to be postmature. In 25 of these cases, the patient was between 12 and 14 days past her calculated E.D.D. These cases were combined with the 96 cases in which labour started spontaneously in order to determine the induction rates when the ultrasonic E.D.D. and calculated E.D.D. were in agreement and when they were not in agreement (Table VI). In the 65 cases where there was agreement, 8 were induced (12.3 per cent). In the 56 cases in which the ultrasonic E.D.D. and calculated E.D.D. disagreed, 18 patients were assessed by ultrasound

TABLE V
Prediction of the date of delivery calculated from the date of the last menstrual period

Degree of dates—Uterine size discrepancy								Number of cases		Total
								Prediction correct	Prediction incorrect	
3 or 4 weeks	41 (60.3%)	27 (39.7%)	68
>4 weeks	16 (57.1%)	12 (42.9%)	28

$$\chi^2 = 0.0003. \quad P > 0.9.$$

TABLE VI
Inductions of labour for postmaturity

Onset of labour	Number of cases			Total
	Ultrasonic E.D.D. and calculated E.D.D. agree	Ultrasonic E.D.D. and calculated E.D.D. disagree		
		Big by ultrasound	Small by ultrasound	
Spontaneous	57	16	23	96
Induced	8 (12·3%)	2 (11·1%)	15 (39·5%)	25 (20·7%)

608 CAMPBELL

to be "big for dates", of whom 2 were induced (11.1 per cent), and 38 to be "small for dates", of whom 15 were induced (39.5 per cent). A significantly greater number of patients were induced in this "small for dates" group than when the ultrasonic and calculated maturities agreed ($\chi^2 = 8.698$ $P < 0.005$). Two patients in whom labour was induced for postmaturity could not be classified with those described above. In the first the maturity was assessed by ultrasound to be 27 days greater than that calculated from the date of the last menstrual period. Labour was induced 18 days after the ultrasonic E.D.D. but 8 days before the calculated E.D.D.; this baby weighed 4.1 kg. In the second patient the assessment by ultrasound was 35 days less than that from the calculated maturity. Labour was induced 51 days after the calculated E.D.D. and 16 days after the ultrasonic E.D.D.; this baby weighed 3.4 kg. and was delivered by Caesarean section for inco-ordinate labour and fetal distress.

DISCUSSION

These results indicate that measurement of the fetal biparietal diameter from the 20th to the 30th week of gestation is clinically useful in the estimation of fetal maturity. The accuracy of this technique in predicting the day of delivery compares favourably with other methods of estimating maturity although these have not been subjected to assessment in the same way. It should be stressed that there is not necessarily disparity between the expected error incidence from the regression line and that obtained in the study. The regression line predicts correct gestation ± 9 days in 95 per cent of cases. A similar result would only be obtained in predicting a date of delivery if the duration of every pregnancy was 40 weeks ± 7 days, which is almost certainly not the case (Park, 1968).

The method depends on the fact that before 30 weeks gestation, fetal head growth is rapid and the biological variation in the biparietal diameter measurement for each week of gestation is small. This may be because the parietal eminences are less well developed during this period than in the later weeks. Figure 1 indicates that prediction of maturity from a biparietal diameter measurement after 30 weeks gestation

would be less reliable owing to the greater "overlap" of readings from week to week, though clinically useful results might be obtained up to 34 weeks.

The two clinical signs most used by obstetricians in the assessment of maturity are the date of the onset of quickening and the assessment of uterine size in the second trimester. The first sign is too subjective to be of more than marginal value and the second has been shown by this study to be frequently misleading. The most commonly used investigation to predict fetal maturity is an X-ray examination of the fetus during the last few weeks of pregnancy. Because of the biological variation in fetal size, ossification centres and subcutaneous fat during this period, there are limitations as to its accuracy (Dee *et al.*, 1966). More recently Brosens and Gordon (1966) described a method of estimating maturity by cytological examination of a specimen of liquor obtained by amniocentesis and stained with Nile Blue sulphate. This method is useful after 36 weeks maturity but is not specific for a particular week (Bishop and Corson, 1968).

Possibly because present ancillary investigations are only of help during the later weeks of pregnancy, most obstetricians feel that this is the most valuable time to obtain information as to the maturity of the fetus. There are occasions, however, when accurate estimation of maturity is of extreme value during the second trimester, especially when intrauterine transfusion of the fetus or premature delivery is contemplated. Furthermore, an early estimation of maturity would obviate repeated amniocentesis and X-ray examination later in pregnancy when the fetus was found to be "small for dates". As most patients in the United Kingdom attend for examination during the second trimester and most dates to uterine-size discrepancies become apparent at this time, an ultrasonic measurement of the biparietal diameter would be a useful investigation.

The significantly higher incidence of induction of labour in those cases that were diagnosed by ultrasound as being less than the calculated maturity, strengthens a well-known feeling among obstetricians that many inductions for postmaturity are performed unnecessarily before the fetus is truly postmature. It may be that a routine ultrasonic measurement of the biparietal

ULTRASONIC MEASUREMENT OF THE BIPARIETAL DIAMETER 609

diameter in the second trimester in all antenatal patients would reduce the number of inductions of labour and that more attention could be paid to cases of true postmaturity. Certainly in those maternity hospitals where ultrasonic equipment is available, routine assessment of the fetal biparietal diameter would be practically feasible as the method is safe, causes no discomfort to the patient and rarely takes more than ten minutes.

SUMMARY

Fetal biparietal diameter measurements were taken during the second half of pregnancy in 186 antenatal patients who were considered to be of known maturity in order to study the normal growth pattern. From this it was concluded that the correct duration of gestation could be predicted ± 9 days in 95 per cent of cases, providing the measurement was taken during the period from the 20th to the 30th week of pregnancy.

Clinical assessment of the method was also carried out in 170 antenatal patients in whom fetal maturity was in doubt. The maturity as calculated from the last menstrual period was incorrect in 41 per cent of patients who subsequently started labour spontaneously and were delivered of mature babies. Ultrasonic measurement of the biparietal diameter distinguished between those in whom the calculated maturity was correct and those in whom it was not. The degree of discrepancy between the expected and actual uterine size did not distinguish between these two groups. Delivery occurred within 9 days of the date predicted by ultrasonic assessment in 84 per cent of patients in whom labour began spontaneously and who were delivered of mature babies.

In those cases in which ultrasonic measurement indicated that the fetal maturity was less than that calculated from the last menstrual period, labour was induced in 39 per cent of patients for postmaturity, compared with only 12 per cent when the ultrasonic and calculated maturities agreed.

ACKNOWLEDGEMENTS

Most of this study was undertaken in the Queen Mother's Hospital, Glasgow, and I thank Professor Ian Donald for his encouragement. Later measurements were performed at University College Hospital; I thank Dr. Hodson for permission to use the ultrasonic equipment, Mr. Rowland Blackwell, B.Sc., for technical assistance, and the Consultants of Queen Charlotte's Maternity Hospital for allowing me to study their patients. Particular thanks are due to Mr. Anthony P. Roberts, B.Sc. for help in the preparation of the manuscript and for statistical advice.

REFERENCES

- Bishop, E. H., and Corson, S. (1968): *Amer. J. Obstet. Gynec.*, **102**, 654.
- Brösens, I., and Gordon, H. (1966): *J. Obstet. Gynaec. Brit. Cwlth*, **73**, 88.
- Campbell, S. (1968): *J. Obstet. Gynaec. Brit. Cwlth*, **75**, 568.
- Dee, P. M., Parkin, J. M., and Simpson, W. (1966): *Clin. Radiol.*, **47**, 125.
- Lubchenco, L. O., Hansman, C., Dressler, M., and Boyd, E. (1963): *Pediatrics*, **32**, 793.
- Park, G. L. (1968): *Lancet*, **2**, 1388.
- Thompson, H. E., Holmes, J. H., Gottesfeld, K. R., and Taylor, E. S. (1965): *Amer. J. Obstet. Gynec.*, **92**, 44.
- Willocks, J., Donald, I., Campbell, S., and Dunsmore, I. R. (1967): *J. Obstet. Gynaec. Brit. Cwlth*, **74**, 639.

3.9 Development of an ultrasonic system for three-dimensional reconstruction of the fetus

Kazunori Baba (born 1952)

Kazunori Baba was born in 1952. He graduated Bachelor of Engineering from the University of Electro-Communications in 1975. He entered medical school at Osaka University and graduated MD in 1979. In 1985 Baba became an Instructor at the Department of Obstetrics and Gynecology, University of Tokyo. He is presently Associate Professor at the Department of Biomedical Engineering, Graduate School of Medicine, University of Tokyo. Furthermore he holds the position as Obstetrician and Gynecologist at the Department of Obstetrics and Gynecology, Saitama Medical Center, Saitama Medical School and the Department of Obstetrics and Gynecology, Tokyo Women's Medical University.

Baba first reported on a 3-D ultrasound system in 1984 and succeeded in obtaining 3-D ultrasound fetal images by using a mini-computer in 1986. This was reported in *Acta Obstetrica et Gynaecologica Japonica*. He also applied this system to placental blood flow and breast disorders in 1990 to 1991. Baba wrote a comprehensive book on diagnostic ultrasound in obstetrics and gynaecology including 3-D ultrasound in 1992 and edited "Three-dimensional ultrasound in obstetrics and gynaecology" (Parthenon Publishing), the first book devoted entirely to 3-D ultrasound, in collaboration with Davor Jurkovic in London in 1996. In the mid-1990s, Baba collaborated with ALOKA on technology developed at the Biomedical Engineering Department of Tokyo University and was a driving force in the development of commercial 3-D ultrasound equipment in Japan, and indeed worldwide. In November 1996, with technical assistance from Takashi Okai and Shiro Kozuma from ALOKA, Baba published in the *Lancet* initial experience with real-time processible 3-D, which was a procedure simpler than conventional 3-D ultrasound rendering based on the method of 'acoustic impedance thresholding' to identify fetal surfaces in the amniotic fluid. Image quality was very high and required less expensive computers to make the calculations. Baba was invited to speak at the first World Congress on 3-D Ultrasound in Obstetrics and Gynaecology in Mainz in 1997 and the second congress in Las Vegas in 1999.

Baba has also been heavily involved with teaching of ultrasonography. He has been active in promoting conventional 2-D ultrasound and Doppler ultrasound in obstetrics and gynecology. He has given many educational lectures and made 11 videos and written many articles in books and magazines. In 1993 he published: A manual of diagnostic ultrasound in obstetrics and gynaecology which was a seven-part video series. He also developed a control system for an artificial uterus and succeeded in incubating a goat fetus in the artificial uterus for 3 weeks and is also involved in the development of an artificial heart.

Dr. Baba has been a member of the editorial board of "*Ultrasound in Obstetrics and Gynecology*" and "*The Ultrasound Review of Obstetrics and Gynecology*".

In part excerpted with permission from the website www.ob-ultrasound.net by Joseph Woo, MD, Hong Kong. Picture courtesy Joseph Woo, MD.



Original articles

J. Perinat. Med.
17 (1989) 19

Development of an ultrasonic system for three-dimensional reconstruction of the fetus

Kazunori Baba¹, Kazuo Satoh¹, Shoichi Sakamoto¹, Takashi Okai², and Shigeo Ishii²

¹Department of Obstetrics and Gynecology, Saitama Medical Center, Saitama Medical School, Japan

²Faculty of Medicine, University of Tokyo, Japan

1 Introduction

In recent years, diagnostic imaging using ultrasonic tomography has been commonly used in the field of obstetrics. But the ultrasonic diagnostic devices available at present can capture only one section of the fetus. We have developed a system for ultrasonic three-dimensional reconstructions of the fetus in order to facilitate the understanding of the three-dimensional structure of the fetus and also to make three-dimensional recording possible. Here we describe this system.

2 Principle

The procedure for 3-D reconstruction of the fetus from ultrasonic tomographic images is illustrated in figure 1. Successive parallel ultrasonic tomographic images are entered into a computer together with positional information. The computer extracts the part of the fetus from each tomographic image and builds up these images three-dimensionally according to the positional information.

The principle of three-dimensional (3-D) display is illustrated in figure 2. The direction of a viewing point relative to the three-dimensionally reconstructed fetal image is designated. The plane of projection vertical to this direction is assumed. The brightness of each element of the picture on the plane of projection is determined proportionally to the distance between the picture element and the fetal image. In other words, the shorter the distance, the brighter the pictorial element, and the longer, the darker that element. It is pos-

Curriculum vitae

KAZUNORI BABA M.D., was born in 1952. He received the B.E. degree from the University of Electro-Communications (Japan) in 1975. He then entered medical school at Osaka University (Japan) and graduated as an M.D. in 1979. He has worked in the Department of Obstetrics and Gynecology, University of Tokyo (Japan), and received M.D. of Science from the university in 1987. At present he is working in the field of perinatal medicine at Saitama Medical Center in Japan.



sible to visibly appreciate the fetus three-dimensionally by regenerating this projection plane on the monitor TV [1].

3 System and methods

3.1 Configuration

The configuration of the system that we have developed is shown in figure 3. The data from the position-sensor attached to an ultrasonic probe are entered into a microcomputer, where they are converted into a form that can be recorded on a video tape as an image. This new image is simultaneously superimposed on the ultrasonic tomographic image and recorded on the video tape [2].

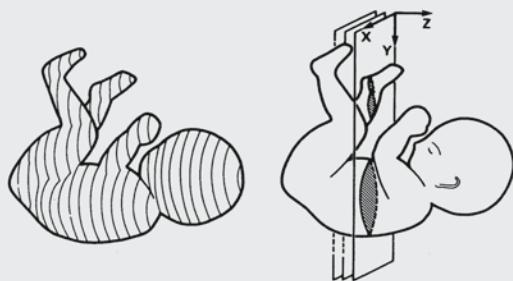


Figure 1. Procedure for 3-D reconstruction of the fetus from ultrasonic tomographic images.

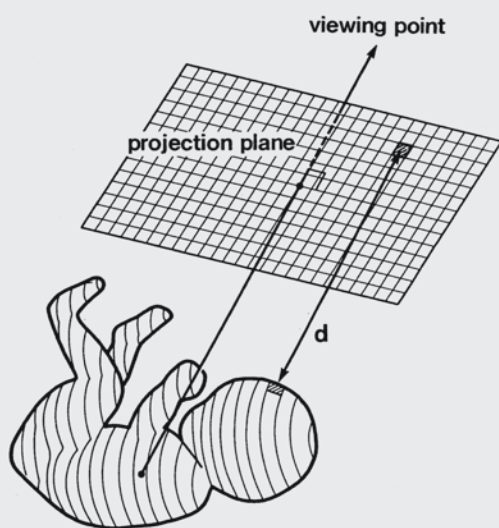


Figure 2. Principle of 3-D display.

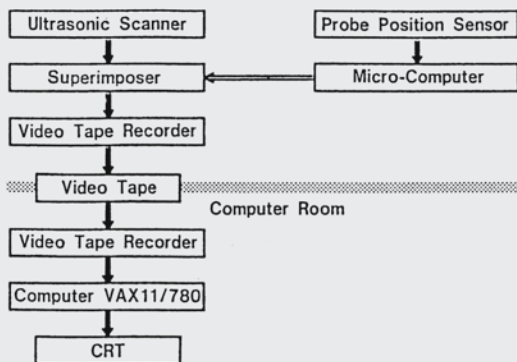


Figure 3. Configuration of our system.

Thereafter, these new data on the video tape are entered into the minicomputer. This minicomputer produces three dimensional reconstructions, and using computer-graphics displays the images which were generated on television monitor.

Separation of data acquisition from data entry was done in order to make the examination time for patients as short as possible, so that discomfort to the patients was reduced and the effect of fetal movement was minimised.

3.2 Position sensor

Either a real-time linear array probe of an ultrasonic scanner SONOVISTA-PX (Mochida Co., Ltd.) or a convex array probe of an ultrasonic scanner SSD-280 (Aloka Co., Ltd.) was mounted on the position-sensing arm of a manual compound scanner MSU-10c (Aloka Co., Ltd.) in order to detect the position of the probe (figure 4). The position detecting components are mounted on the bench in such a way as to have 5 degrees of freedom of movement as shown in figure 4 to enable the plane to be measured to be set easily.

3.3 Recording system

A microcomputer CZ-802C (Sharp Co., Ltd.) is used to convert the positional information to the recording of an image on a video tape. This image is superimposed onto the ultrasonic tomographic picture simultaneously using a superimposer CZ-8DT (Sharp Co., Ltd.) and recorded on the video tape. The ultrasonic tomographic image with its positional information is shown in figure 5. Each length of 3 lines on the right side represents the position (vertical and horizontal) and orientation of the probe when the tomographic image was recorded.

The speed of collection of the positional data and rewriting to the video RAM in the microcomputer is so fast that the positional display can follow rapid motion of the probe without any resulting flicker.

3.4 3-D Reconstruction and display

A minicomputer VAX11/780 (DEC) system was used for both the 3-D reconstruction and 3-D display. A repeating video tape through column feeding in the computer room, necessary images

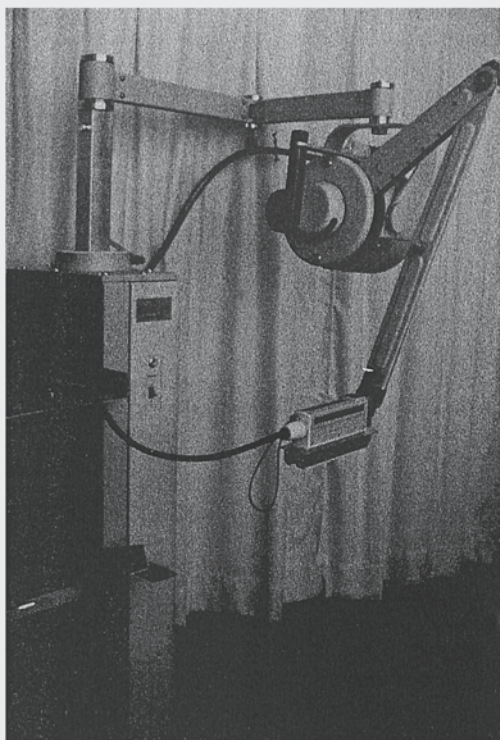


Figure 4. A real-time linear array probe mounted on a position sensing arm of manual compound scanner.

were input to this minicomputer on the basis of positional information of the probe displayed on the monitor TV. The image of the anterior uterine wall was excluded to define that of the fetus more clearly. Simultaneously, the data were compressed in the format of 128 by 128 picture elements which were then piled up in the memory of the minicomputer as 3-D data. The threshold level of brightness was designated in such a way that the fetus could be separated from the amniotic fluid. Thereafter, the 3-D images are displayed on a monitor TV using computer-graphics.

4 Results

Figure 6 shows the image generated by our system of a normal fetus of 19 weeks gestation in utero and is the composite image reconstructed three-dimensionally from 48 segments of ultrasonic tom-

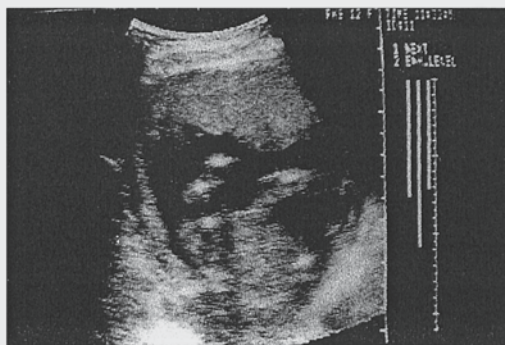


Figure 5. Ultrasonic tomographic image with its positional information superimposed.

ographic images taken at 2 mm intervals. This image shows the true shape of this 19 week gestation fetus in a flexed posture.

The probe was gently placed on the abdomen of the pregnant woman who was lying in a supine position and was then moved horizontally from the crown to the rump of the fetus to collect the data. The transverse images thus obtained were recorded on video tape. Since it takes only a few seconds for this data collection by ultrasonic inspection there is no effect of fetal movement.

Approximately 12 minutes are then required for further processing, that is, 10 minutes for the data input and 2 minutes for the 3-D reconstruction and display.

Figure 7 shows the three-dimensional image of twins at a gestation of 15 weeks, reconstructed from 54 pieces of ultrasonic tomographic images taken at 2 mm intervals.

5 Discussion

Comparison of the computer-generated image (figure 6) with a photograph of a fetus aborted at 18 weeks, (figure 8) provides us with good evidence of the usefulness and fidelity of our new system for visibly demonstrating the fetus in utero. A large head, an arm, a constricted wrist, a gripped hand, legs, heels and toes are easily identifiable. However, noise was a bar to the reproduction of an image with a surface as smooth as that of the actual fetus. Using the conventional tomographic image (figure 9) it is not easy to distinguish a twin from a singleton pregnancy unless an understand-

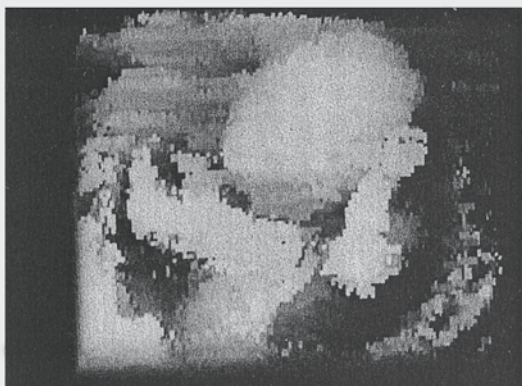


Figure 6. Computer-generated image of a normal fetus of 19 weeks gestation in utero.

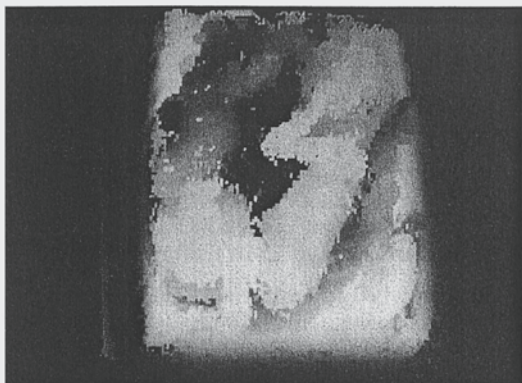


Figure 7. Computer-generated image of twins at 15 weeks gestation.

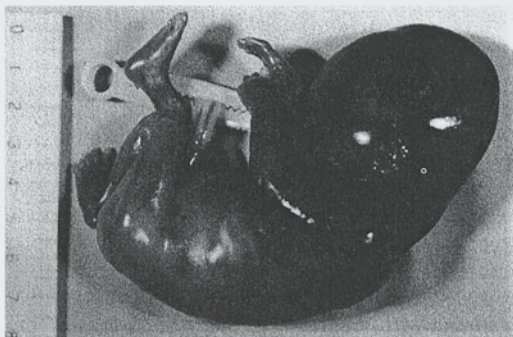


Figure 8. An aborted fetus at a gestational age of 18 weeks.



Figure 9. An ultrasonic tomographic image of twins at a gestational age of 15 weeks.

able explanation is given. Even if it is identified as a twin, it is not clear how the two fetuses are disposed. However, as shown in figure 7, the 3-D reconstructed image obtained with our system visibly demonstrates twins and shows that one is in the breech position while the other is a vertex presentation.

Amniography and fetoscopy may provide us with a more comprehensible shape of the fetus than the ultrasonic 3-D reconstructed image given by our system. However, these are invasive techniques and they cannot safely be repeatedly performed. On the other hand, ultrasonic 3-D reconstructed imaging is a non-invasive technique and can be performed repeatedly. Moreover by changing the position and direction of the viewing point, it allows easy appreciation of a solid object.

Use of this system is limited to cases in which the fetus is sufficiently separated from the anterior wall of the uterus. But if confined to a part of the body such as the face or hands, it is applicable even to the fetus at term.

The processing time of our computer system is too long for routine clinical application. But development of computer systems for industrial applications which use high speed 3-D displays, such as CAD (Computer Aided Design) are rapidly being developed present and if these are applicable, the clinical use of our system in a real-time mode is highly likely in future when it can be connected directly with the ultrasonic diagnosis device.

Future applications of this system to the screening for fetal anomalies and abnormalities of fetal growth are highly likely to be developed.

Summary

The ultrasonic diagnostic devices available at present can only represent one section of the fetus. We have developed a system for three-dimensional reconstruction of the ultrasonic fetal image in order to facilitate the understanding of the 3-D structure of the fetus and also to make 3-D recordings of this image.

Either a real-time linear array probe or a convex array probe of the ultrasonic scanner was mounted on a position sensing arm of a manual compound scanner in order to detect the position of the probe.

A microcomputer was used to convert the positional information to a recording of a visual image of videotape. This image was superimposed onto the ultrasonic tomographic image simultaneously using a superimposer and was recorded on the video tape, thereafter, being recalled by the image processing minicomputer.

The minicomputer VAX11/780 (DEC) system was used for 3-D reconstruction and 3-D display. In the memory system the image of the anterior uterine wall was identified and subsequently excluded in order to visualise the fetus more clearly. The threshold of brightness was set to a high level so that the fetus could be separated from the amniotic fluid. The fetus was displayed three-dimensionally using computer graphics.

Using this system, we have made it possible to observe the whole image of the fetus in utero non-invasively. This system offers a method for easier understanding of the 3-D structure of the fetus in utero and also makes 3-D recording possible.

In the future, we confidently expect that this system will be used for screening for fetal anomalies and abnormalities of fetal growth.

Keywords: Computer, fetus, image processing, three-dimension, ultrasonography.

Zusammenfassung

Entwicklung eines Systems zur sonografischen dreidimensionalen Darstellung des Feten

Mit der bisherigen ultrasonographischen Diagnostik läßt sich lediglich eine Schnittebene des Feten darstellen. Wir entwickelten ein System zur dreidimensionalen Rekonstruktion des Feten, um die räumlichen fetalen Strukturen und deren Aufzeichnungen zu erhalten.

Auf den Gelenkarm eines manuellen Compoundscanners wurden entweder eine Real-time-Sonde oder eine konvex angeordnete Sonde montiert, um die Position der Sonden zu bestimmen.

Diese Informationen wurden über einen Mikrocomputer so umgewandelt, daß eine bildliche Darstellung auf Videobändern möglich wurde. Dieses Bild wurde mit dem ultrasonographisch-tomographischen Bild überlagert und nach Zurückrufen durch den den Image-Processing-Minicomputer auf Cideo aufgenommen.

Zur dreidimensionalen Rekonstruktion und Darstellung wurde ein Minicomputer-System (VAX11/780; DEC) benutzt. Im Memory-System wurde das Bild der Uterusvorderwand eliminiert, um direkt das Bild des Feten zu erhalten. Der Schwellenwert für die Wiedergabedeutlichkeit lag dort, wo der Fet von der Amnionflüssigkeit zu unterscheiden war. Der Fet wurde über eine Computergraphik dreidimensional dargestellt.

Dieses System ermöglicht, ohne invasives Eingreifen ein ganzes Bild vom Feten in utero zu erhalten. Es liefert einen leicht zugänglichen Weg zum Verständnis der dreidimensionalen fetalen Strukturen und macht eine dreidimensionale Darstellung möglich.

Die zukünftige Anwendung dieses Systems ist vielversprechend im Hinblick auf die Mißbildungsdiagnostik sowie die Feststellung eines abnormen fetalen Wachstumsverhaltens.

Schlüsselwörter: Computer, dreidimensionale Darstellung, Fet, Image-processing, Ultraschall.

Résumé

Développement d'un système pour la reconstruction échographique à trois-dimensions du fœtus

Les appareils échographiques à visée diagnostique disponibles à l'heure actuelle ne peuvent saisir qu'une coupe du fœtus.

Nous venons de développer un système pour la reconstruction échographique tri-dimensionnelle afin de faciliter la compréhension de la structure tri-dimensionnelle du fœtus et aussi de rendre l'enregistrement tri-dimensionnel possible.

Une sonde linéaire en temps réel, ou sonde convexe de l'échographe a été montée sur le bras détecteur d'un lecteur manuel afin de détecter la position de la sonde.

On a utilisé un microordinateur afin de convertir l'information de position en ce qui pourrait être enregistré sur une bande vidéo comme une image. Cette image a été superposée sur l'image tomographique échographique simultanément par un appareil à surimpression et enregistrées sur la bande vidéo après rappel par le miniordinateur pour le traitement de l'image.

On a utilisé le système Miniordinateur VAX11/780 (DEC) pour la reconstruction et la visualisation tri-dimensionnelles. Sur le système de mémoire l'image du mur antérieur utérin a été séparée et éliminée pour recueillir l'image du fœtus. Le niveau de seuil de la clarté

a été désigné comme le plus élevé permettant la séparation du fœtus du liquide amniotique. Le fœtus a été visualisé en trois dimensions en utilisant un graphique d'ordinateur.

Ce système nous a permis d'observer l'image entière du fœtus in utero de façon non invasive. Ce système facilitait beaucoup la compréhension de la structure tridimensionnelle du fœtus in utero et aussi rendrait l'enregistrement tridimensionnel possible.

A l'avenir, on espère beaucoup que ce système sera très utile pour examiner les anomalies du fœtus et du développement fœtal.

A l'avenir, on espère beaucoup que ce système sera très utile pour examiner les anomalies du fœtus et du développement fœtal.

Mots-clés: Echographie, fœtus, ordinateur, traitement de l'image, trois-dimensions.

References

- [1] ISHII S, E WATANABE: Three-dimensional image reconstruction system using CT-tomograms and angiograms. *Iryou Jyohougaku* 5 (1985) 364
- [2] BAKA K, T OKAI, K SATOH: Development of scan head position indicator for ultrasonic fetal three-dimensional reconstruction. *Jpn J Med Ultrasonics* 13, Suppl 1 (1986) 121

Received July 10, 1988. Accepted August 10, 1988.

Kazunori Baba, M.D.
Department of Obstetrics and Gynecology
Saitama Medical Center
Saitama Medical School
1981, Kamoda, Kawagoe
Saitama 350, Japan

4 Digital Imaging

- | | | |
|------------|--|-----|
| 4.1 | Digital Processing of Videoangiocardigraphic Image Series.
Computers in Cardiology (1976): 255–260
<i>R. Brennecke, T.K. Brown, J.H. Bürsch, P.H. Heintzen</i> | 257 |
| 4.2 | Computerized fluoroscopy in real time for noninvasive visualization of the cardiovascular system.
Preliminary studies.
Radiology 130 (1979): 49–57
<i>R.A. Kruger, C.A. Mistretta, S.J. Riederer, C.G. Shaw et al.</i> | 266 |
| 4.3 | Intravenous angiography using digital video subtraction: X-ray imaging system.
Am J Roentgenol. 135 (1980): 379–386
<i>T.W. Ovitt, P.C. Christenson, H.D. 3rd Fisher, M.M. Frost, S. Nudelman, H. Roehrig</i> | 278 |
| 4.4 | Computed radiography utilizing scanning laser stimulated luminescence.
Radiology 148 (1983): 833–838
<i>M. Sonoda, M. Takano, J. Miyahara, H. Kato</i> | 289 |
| 4.5 | Digital radiography of the chest: clinical experience with a prototype unit.
Radiology 148 (1983): 1–5
<i>R.G. Fraser, E. Breatnach, G.T. Barnes</i> | 298 |
| 4.6 | A new digital detector for projection radiography.
Proc SPIE 2432 (1995): 237–247
<i>D.L. Lee, L.K. Cheung, L.S. Jeromin</i> | 304 |
| 4.7 | X-ray imaging using amorphous selenium: Feasibility of a flat panel self-scanned detector for digital radiology.
Medical Physics 22 (1995): 1595–1604
<i>W. Zhao, J.A. Rowlands</i> | 319 |

Introduction

The history of digital imaging goes back to the early 1930s. The country physician Helge Christensen developed an optical device with which images could be photographed from the fluorescent screen onto 25-mm roll film. He employed this device for 15 years in clinical routine. A. Bouwers from Oude Delft Enterprises, The Netherlands, continued these experiments in the 1940s using a 40-cm input screen and a 70-mm roll film. In Germany, Robert Janker used this ODELCA camera to take a large number of images in rapid succession because there was no longer a change of cassettes. Since 1937 there existed a patent from I. Langmuir for the electron-optical intensification of a fluoroscopy image. But it was only in 1948 that J.W. Coltman, from Westinghouse, was able to develop the first X-ray image intensifier in electron-optical design. Finally in 1953 this image intensifier was ready for clinical use. These image intensifier systems underwent further development and became an independent image receptor system. Several authors demonstrated that system theory applies to transmission systems for X-ray images. Introduction of the modulation-transfer-function (MTF) helped to evaluate complete X-ray-television system. In 1967 Fenner from Siemens, Erlangen reported on the characteristic values of image intensifiers and the use of electron-optical image intensifiers in radiological diagnostics. Another landmark was the using of a cesium iodide input screen instead of the usual zinc-cadmium sulfide input, which produced brighter, better defined and higher-contrast images. Melvin P. Judkins from Portland, Oregon and F. Mason Sones from Cleveland, Ohio were the first to use this new image intensifier technique successfully for coronary angiography.

Pioneer work in digital subtraction angiography (DSA) was done at the end of the 1970s by the groups of H.P. Heintzen (1976) at the Department of Cardiovascular Surgery, University of Kiel, Germany, Nudelman (1977), Department of Radiology at University of Arizona, and Mistretta (1978) at University of Wisconsin.

Digital imaging techniques were further developed in the 1980s when analogue to digital (A/D) converters and computers were also adapted to conventional fluoroscopic image intensifier/TV systems. In 1980 Philips introduced the first digital subtraction angiography system, DVI (digital vascular imaging), which ushered in the digital age of conventional radiology. It made use of the image intensifier and television technique and converted the analogue signal into digital format. A number of DSA systems appeared in the mid-1980s.

Another important technical improvement was developed in 1986. Siemens improved the image matrix standard from 512x512 to 1024x1024. First results in angiocardiology with the HICOM digital system in 1990 showed for the first time serious competition for cine film.

The conversion of the X-ray energy pattern into digital signals utilizing scanning laser-stimulated luminescence (SLSL) paved the way for a new technique in digital radiography. The basic principles were developed by the group of H. Kato at the Technology Development Center, Miyanodai, Fuji Film, Japan in 1983. An interesting prototype unit for digital chest radiography (DCU) was developed by GT Barnes and his group at the hospital of the University of Alabama in Birmingham in cooperation with the Advance Development Group, Picker International, Cleveland. In a first clinical field study over a six-month period 400 patients were examined during 1982–1983. The Philips Thoravision was the first digital chest radiography machine using a selenium detector for the market (Neitzel et al 1994).

Accompanying the advances being made at the start of the digital information age ideas were developed to build up a complete digital diagnostic system for radiography and fluoroscopy. In 1995 D.L. Lee, L.K. Cheung and L.S. Jeromin patented a new digital detector for projection radiography using a multi-layer structure

consisting of a thin-film detector array, selenium X-ray semiconductor, dielectric layer and top electrode. This prototype digital radiography technology electronically converts X-ray photons into digital image data.

In his article "Bringing the Missing Link to the All-Digital Department." (*Medical Imaging*, November 1996, p.102) Jeffery H. Bell predicted the achievement of the all-digital radiology department for the year 1998. This included conventional screen-film radiology which was the last remaining non-digital diagnostic imaging modality. Digital radiography provides a one-step, direct capture of images in a digital format, which can then be immediately sent to a variety of display devices. The new technology allows conventional radiographic imaging to switch from a film-based system to a quick, easy and effective digital system.

In 1997 John Rowlands and his group from the Imaging Research Program, Sunnybrook Health Science Centre, University of Toronto, Ontario, Canada, described the construction and evaluation of a projection real-time detector. For dynamic X-ray imaging ("fluoroscopy") they replaced conventional X-ray image intensifiers with an active matrix flat panel device modified to include one of three innovative approaches: avalanche multiplication in selenium, intelligent pixels, or a novel photoconductor – mercuric iodide.

During the next few years several authors described positive clinical results of full-size digital radiography detector arrays (Shaber et al 1997, Davros and Piraino 1998, Sakurai et al 1998, Colls et al 1999, Uhrmeister et al 1999) One other important aspect in using new digital systems was the possibility of the reduction of the radiation dose (Freund et al 1997).

Today, in several places digital radiography and fluoroscopy technology has taken the place of all conventional X-ray detector technologies. Hospitals are changing from handling analogue devices to digital systems. It seems that the FDP is now one key technology for the future of diagnostic radiology and the beginning of a new era of diagnostic X-ray systems.

References

- Brennecke R, Brown TK, Bürsch JH, Heintzen PH (1976) Digital Processing of Videoangiographic Image Series. *Computers in Cardiology*: 255-260
- Kruger RA, Mistretta CA, Houk TL, Riederer SJ, Shaw CG, Goodsit MM, Crummy AB, Zwiebel W, Lancaster JC, Rowe GG, Flemming D (1979) Computerized fluoroscopy in real time for noninvasive visualization of the cardiovascular system. Preliminary studies. *Radiology* 130: 49-57
- Ovitt TW, Christenson PC, Fisher HD 3rd, Frost MM, Nudelman S, Roehrig H, Seeley G (Dec 1980) Intravenous angiography using digital video subtraction: x-ray imaging system. *AJR Am J Roentgenol* 135 (6): 1141-4
- Heintzen PH, Brennecke R, Bürsch JH et al. (1982) Quantitative Analysis of Structure and Function on the Cardiovascular System by Roentgen-Video-Computer Techniques *Mayo Clin Proc.* 57: 78-91
- Sonoda M, Takano M, Miyahara J, Kato H (1983) Computed radiography utilizing scanning laser stimulated luminescence. *Radiology* 148: 833-838
- Fraser RG, Breatnach E, Barnes GT (1983) Digital radiography of the chest: clinical experiences with a prototype unit. *Radiology* 148: 1-5
- Tesic MM, Mattson RA, Barnes GT, Sones RA, Stickney JB (1983) Digital radiography of the chest: Design features and considerations for a prototype unit. *Radiology* 148: 259-264
- Lee DL, Cheung LK, Jeromin LS (1995) A new digital detector for projection radiography. *Proc SPIE* 2432: 237-249
- Jeromin, Lothar S, Denny LY, Lee, Eugene F, Palecki, Edward N, Lawrence (1996) A Direct Radiography System for the Future. *Computer Assisted Radiology*, by H. U. Lemke et al., editors. (Berlin: Springer-Verlag), 110-116
- Chabbal J, Chaussat T, Ducourant L, Fritsch J, Michailos V, Spinnler G, Vieux M, Arques M, Hahm, M, Hoeisel H, Schulz R, Spahn M (1996) Amorphous silicon x-ray image sensor. *Proc SPIE* 2708: 499-510

Bell, Jeffrey H (November 1996) Bringing the Missing Link to the All-Digital Department. Medical Imaging. 102-103

Shaber, Gary S (1996) Radiography Crosses the Final Boundary to Filmlessness. Diagnostic Imaging. 24-28

Zhao W, Belvis I, German S, Rowlands JA, Waechter D, Huang, Z (1997) Digital radiology using active matrix readout of amorphous selenium: Construction and evaluation of a projection real-time detector. Med Phys. 24: 1834-1843

Ning, Ruola, Denny Lee, Xiaohui Wang, Ying Zhang, David Conover, Dinghua Zhang, Cornell Williams (February 1998) Department of Radiology University of Rochester Medical Center. Selenium Flat Panel Detector-Based Volume Tomographic Angiography Imaging: Phantom Studies. SPIE Vol. 3336: 316-324

Yamada S (1999) Development of a Direct-conversion-type Flat-panel detector for Radiography and Fluoroscopy. Medical Imaging Technology 17.2: 110-116

Dalla, Palma L, Grisi G, Cuttin R, Rimondini A (1999) Digital vs. conventional radiography: cost and revenue analysis. European Radiology. 9: 8, 1682-1692

Frija, Guy (March 1999) Georges Pompidou Hospital, Paris. Flat Panel Sensors: Questions and Answers. Medical Imaging Technology. 17.2: 99-104

Rowlands JA, Winston G, Wei Zhao Wei, Denny L Lee (2000) Direct conversion flat panel X-ray imaging: reduction of noise by presampling filtration. SPIE (The International Society for Optical Engineering)

Zhao W, Rowlands JA (1995) X-ray imaging using amorphous selenium: Feasibility of a flat panel self-scanned detector for digital radiology, Medical Physics 22: 1595-1604

This paper gives the most complete description of the project and was awarded the Sylvia Fedoruk Prize for the best Canadian paper in medical physics in 1995.

The first presentation on the concept was given at the SPIE Conference in Medical Imaging held in Newport Beach in 1992; the published paper is:

Zhao W, Rowlands JA (1992) A large area solid-state detector for radiology using amorphous selenium. Medical Imaging VI: Instrumentation, Proc. SPIE 1651: 134-143.

Other important related papers are:

Zhao W, Rowlands JA (1997) Digital radiology using active matrix readout of amorphous selenium: Theoretical evaluation of detective quantum efficiency, Medical Physics 24: 1819-1833

which described the theoretical analysis of these detectors,

Zhao W, Blevis IM, Waechter DF, Huang Z, Rowlands JA (1997) Digital radiology using active matrix readout of amorphous selenium: Construction and evaluation of a prototype real-time detector, Medical Physics 24: 1834-1843

which described the first reduction to practice of the approach, and

Zhao W, Law J, Waechter DF, Huang Z, Rowlands JA (1998) Digital radiology using active matrix readout of amorphous selenium: Detectors with self-protection against high voltage damage. Medical Physics 25: 539-549

which described the most commonly used approach to high voltage protection of the active matrix necessary because of the high voltage that has to be applied to the amorphous selenium layer.

4.1 Digital Processing of Videoangiocardigraphic Image Series

Rüdiger Brennecke (born 1939)

Rüdiger Brennecke was born on 11 June 1939 in Arnsberg, Germany. In 1959 he started studying law but later changed to physics. He obtained the Diploma from the University of Göttingen in 1966. He became a research assistant in membrane biophysics at the Institute of Physiology of the University of Saarbrücken, Germany where he obtained the PhD in 1970.

In 1973 he went to Kiel, Germany, as a collaborator of Paul Heintzen in digital imaging projects. Here Dr. Brennecke was appointed lecturer in medical physics. In 1983 he became director of the Biophysical Computation Laboratory of the Second Medical Clinic at the University Hospital Mainz. He was involved in projects of X-ray and echocardiographic image analysis and wide area networks for interventional cardiology.

In 1992 he founded the initiative “Integrating Cardiology Information Systems” and he organized the corresponding ESC workshops 1992–1998 on DICOM standardization in cardiology. Dr. Brennecke retired in 2002 but is still active studying philosophy.

Picture courtesy Rüdiger Brennecke PhD, 2004.



Joachim H. Bürsch (born 1936)

Joachim Bürsch was born on 19 March 1936 in Kiel, Germany. He studied medicine at the universities of Kiel and Freiburg and obtained his MD in 1966. He took his postdoctoral training in pediatric medicine and pediatric cardiology at the Pediatric Department of the University Hospital Kiel (1966–1971). He was very interested in experimental cardiology and biomedicine and became a Research Fellow at the Department of Physiology of the Mayo Clinic, Rochester, USA (1971–1972).

He became lecturer in 1973, associated Professor in 1978 and full Professor and director of the Department of Pediatric Cardiology at the University of Göttingen in 1988.

Bürsch was appointed Director of the Centre of Pediatrics at the University of Göttingen (1993–1995). He was elected president of the German Society of Pediatric Cardiology and he was a delegate of the German Academy for Pediatric Medicine. In 1982 he was awarded the Harry Schaeffer Prize of the German Society for Cardiology.

Picture courtesy Joachim Bürsch, MD 2004.



Paul H. Heintzen (born 1925)

Paul Heintzen was born on 8 May 1925 in Essen, Germany. He attended primary school in Duesseldorf and in Hilden and obtained his high school degree (abitur) with excellent grades in 1943.

From 1943–1945 Heintzen undertook military service in Russia and Italy. After the war he started his medical studies at the universities of Bonn and Duesseldorf. Paul Heintzen received his MD from the University of Duesseldorf in 1952 with *summa cum laude*.

His clinical education was in Duesseldorf (internal medicine) and Muenster (physiology). In 1954 he started to build up the first cardiac catheter laboratory at the clinic for pediatric cardiology at the University of Kiel. In 1965 Paul Heintzen was appointed Professor of Internal Medicine at the University of Kiel and in the same year he started the Interdisciplinary Research Centre for Pediatric Cardiology and Biomedicine with support from the Volkswagen Foundation.

In 1964 Heintzen started his research on video densitometry, firstly analogue and later using a digital technique. His systematic research on the quantitative transfer properties of the new X-ray image intensifier TV systems formed a basis for quantitative X-ray image analysis. As a result of his research he developed the concept of a filmless cardiac catheter laboratory. In 1969 for the first time in Europe he was able to build up a complete automation heart catheter technique. The way was now clear for the catheter laboratory to become fully digital. Because of the lack of industrial resources Heintzen started to develop digital media for the digital storage of complete angio-cardiograms. In 1980 he and his group developed processes for the quantitative analysis of the structure and function of the cardiovascular system by using roentgen-video-computer techniques.

Paul Heintzen is honorary member of the German Society of Biomedicine Technique (1991), the European Association of Paediatric Cardiologists (1993), the German Society of Paediatric Cardiology (1996), and the German Society of Cardiology (1999). He was appointed Fellow of the American College of Cardiology (1968), Fellow of the European Society of Cardiology (1988). In 2003 he was awarded the highest order of the Federal Republic of Germany, the “Bundesverdienstkreuz”.

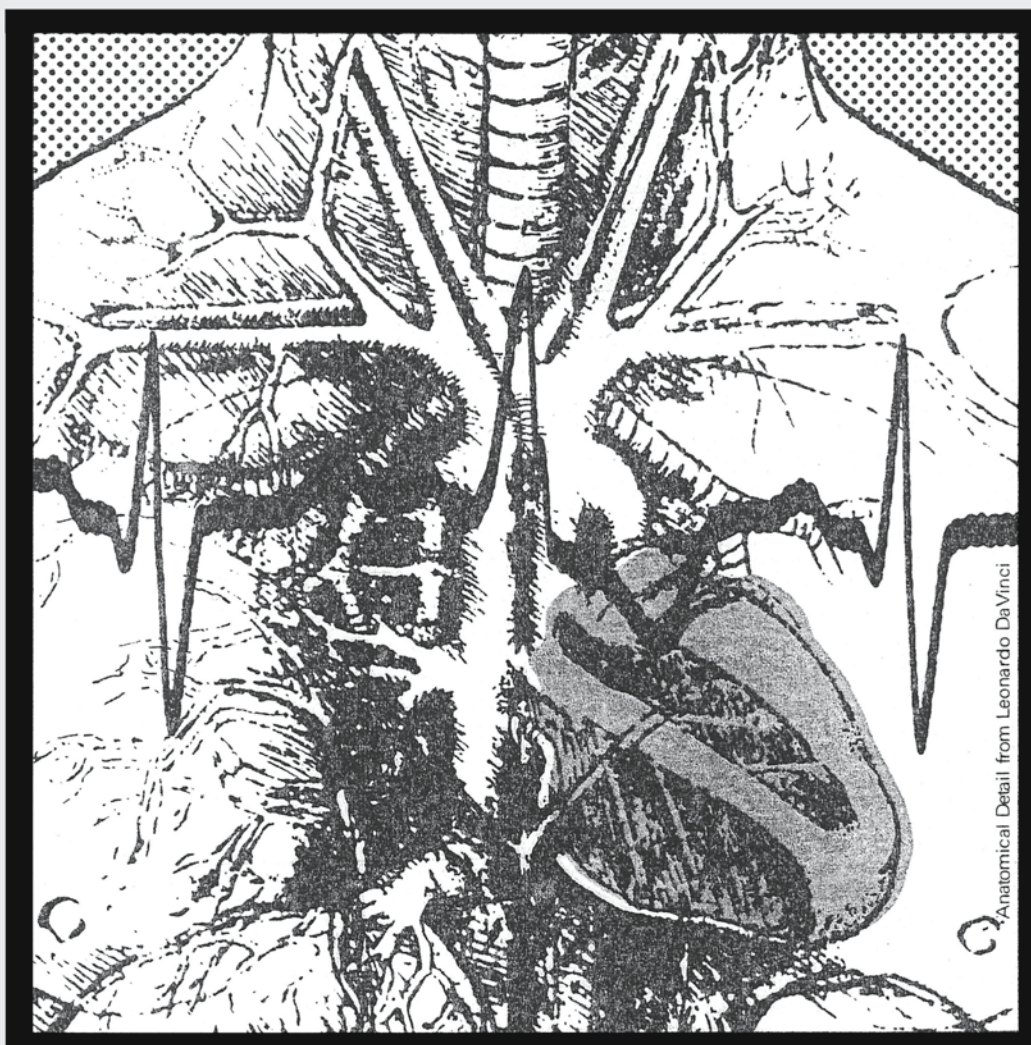
Picture courtesy Paul Heintzen, MD, 2004.



T.K. Brown

COMPUTERS IN CARDIOLOGY

October 7-9, 1976
Washington University
St. Louis, Missouri
USA



Anatomical Detail from Leonardo DaVinci

DIGITAL PROCESSING OF VIDEOANGIOCARDIOGRAPHIC IMAGE SERIES USING A MINICOMPUTER

R.Brennecke, T.K.Brown, J.Bürsch, P.H.Heintzen

Department of Pediatric Cardiology and Bioengineering
Christian-Albrechts-Universität, Fröbelstr., Kiel, W.Germany

Summary

We report on the enhancement of angiocardio-graphic image-series by digital preprocessing methods including digitized image subtraction, integration, and nonlinear representation techniques. Examples from animal experiments are presented. Image-series handling and storage is simplified by combining a new method of digitally formatted video-tape recording with conventional digital storage of selected image data in the computer periphery.

Introduction

Current developments in the processing of cardiovascular images such as automatic recognition of ventricular borders and computed tomography require the capability of computerized handling of large amounts of data for image acquisition, restoration, and analysis. We report on a new system which simplifies video-angiocardio-graphic image acquisition and preprocessing by a combination of analog and digital techniques. Primary applications of the system are digital image subtraction and integration. These techniques may help to attain adequate image quality with reduced amounts of injected dye. This is advantageous over conventional angiographic procedures where the rapid injection of relatively large amounts of high concentration dye can alter the parameters of heart action or blood flow under study. Animal experiments were performed to demonstrate the gain in the detectability of small x-ray density-changes provided by digitized image subtraction and integration.

Video-Computer-Interface

Although there is a general trend to digitized picture processing, application of these methods to complete angiocardio-graphic image series has been limited by the need to analyse from fifty to several hundred frames per angiogram. As an example requiring the processing of large parts of an angiographic image series (up to 300 TV-fields), we describe in this report a combined image subtraction and image integration routine developed for image enhancement. The problem of storing and handling these large amounts of data (up to 30 Megawords (16 bit) per angiogram) at high data rates has been solved by combining digitally formatted video-recording for computer-controllable mass storage with a fast digital disc for active storage.

In our system, conventional video-tape recordings are used for the low cost, real time mass storage required by angiocardio-graphs (50 TV-fields/sec, 5 MHz bandwidth, up to 500 fields per angiogram). To facilitate computer controlled digitization of recorded video image series and the generation of a file organization containing both image information and physiological data, digital parameters (TV-field number, patient code, etc.) as well as digitized physiological data (ECG, pressure) are stored on video tape in combination with

the video information. Fig.1 is a display of a TV-field with the bit pattern carrying these additional informations. Normally, this modulation is recorded in the invisible part at the begin of each TV-line.

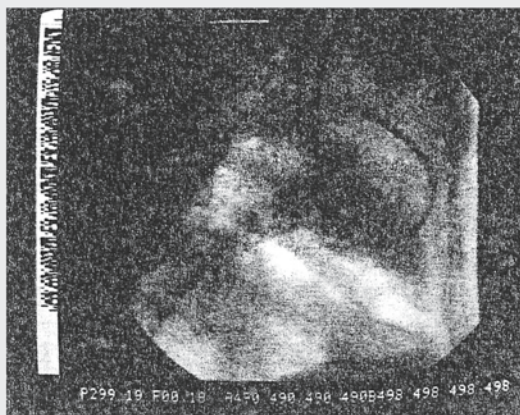


Fig.1: Digitized-data encoding used for combined video and physiological data storage on video tape. The bit pattern displayed at the left edge of the TV-screen represents six digitized analog channels (12 bit each, 200 Hz sampling-rate) and three digital channels (16 bit each, 100 Hz sampling rate), together with synchronizing and error detection information.

The components of the video-computer interface are shown in Fig.2. The video signal reproduced from video tape is read through a video-A/D-converter (43 Megabit/sec, 8 bit grey scale resolution) to a fast semiconductor buffer memory (matrix) capable of storing a whole TV-field (256 pixels x 256 lines x 8 bit) at this rate. Images selected by reference to the simultaneously recorded physiological data or field number are transferred at a slower rate (typically 4 Megabits/sec) from the matrix buffer to a digital disc. When this transfer is completed, a new TV-field is selected and read through the matrix buffer to the digital disc. Due to this discontinuous mode of transfer, complete digitization of an angiogram requires about 10 replays. The digitization scheme described avoids the use of an expensive video disc recorder as required for stroboscopic sampling of image information by systems with a smaller digital high-speed buffer memory^{1,2}. Additionally, the transfer of image data from a helical-scan video tape recorder to a video disc may introduce synchronization problems and it decreases the signal-to-noise ratio.

Pictures stored on digital disc can be transferred back to the digital matrix for conversion to a full grey scale (256 levels), single field display on a TV-monitor. This semiconductor TV-field store avoids problems of time-base jitter and tape wear, both critical in conventional stop action video reproductions from video tape recorders and thus also enhances the use of previously developed methods of video image processing such as border outlining by an operator for ventricular volume determination. Moreover, computer processed pictures can be recorded through the matrix on video tape making the large capacity of this medium available for the storage of computer enhanced images.

One of the disadvantages of video recording of angiocardigrams is that the signal-to-noise ratio of these recordings is markedly lower than that which can be provided by the x-ray TV-chain. Fig.3 shows a scheme now being evaluated in our laboratory for noise reduction in video angiographic image recording. One TV-field obtained before dye injection is digitized and stored in the matrix. This field is then digitally subtracted in real time from all succeeding images of this angiogram (43 Megabit/sec burst data-rate). The resulting differences are multiplied by factors between 2 and 8 and values exceeding the dynamic range of the D/A-converter are clipped. The output-signal of the D/A-converter, which represents amplified temporal grey-level changes, is recorded on a standard video tape recorder. Preliminary results indicate that for small signals a gain in the signal-to-noise ratio of about 6 dB can be obtained by recording amplified subtraction images instead of regular angiograms.

Image subtraction, integration, and subtraction-image enhancement.

Injection of contrast material into the circulation produces a local change in x-ray density. Taking one x-ray picture before dye injection and logarithmically subtracting it from an opacified picture on a pixel by pixel basis renders a value proportional to the density change in the respective projection of the dye-filled vessel. These density values can be used for dimensional or flow measurements^{3,4}. Image subtraction is also useful in suppressing background structures which can interfere with human or automated recognition of the shape of a dye-filled vessel when videometric analysis of heart volume or wall motion is performed⁵.

Although image subtraction is nearly a self-evident method of image enhancement⁹, its success in angiocardiology depends on the capability of handling the large amount of images involved at a reasonable expense while maintaining a high degree of spatial and temporal registration of background and opacified pictures. Photographic subtraction - as compared to electronic techniques - is complicated by the problems of correct film exposure, controlled development, and the requirement of a perfect inverse relation between the background picture negative and the original. The video techniques of image storage and A/D-conversion used in our system provide a high degree of linearity in image brightness recording and good spatial registration. The selection of pictures with

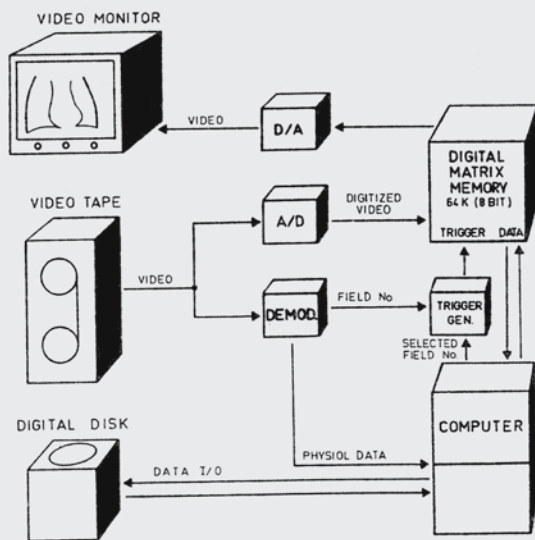


Fig.2: Video-computer interface. Transfer of digitized video data from the matrix memory to the computer is controlled by reference to digitized data which are modulated into the video signal as shown in Fig.1. These data are decoded by the demodulator.

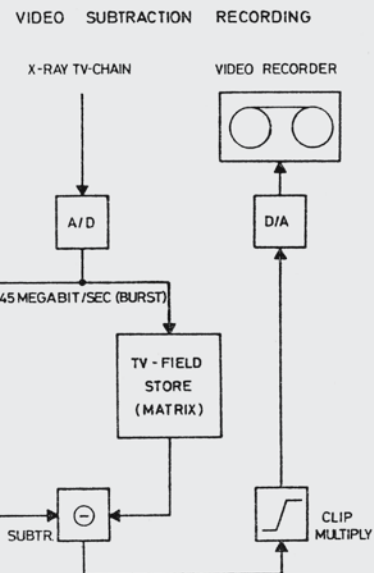


Fig.3: Real-time video image subtraction for recording small temporal signal-changes on video tape with an improved signal-to-noise ratio.

good temporal registration - the background image must be recorded at the same heart phase as the opacified picture - is greatly simplified due to the combined recording of video x-ray images and digitally encoded physiological data such as ECG and pressure signals on video tape as described above. Logarithmic subtraction of images selected by reference to the physiological data is performed by a digital computer.

Averaging a number of selected subtraction images may enhance image quality due to one or several of the following effects:

- 1.) Averaging a set of adequately opacified subtraction images taken at the same heart phase during succeeding heart cycles increases the signal-to-noise ratio proportional to the inverse square of the number of images averaged if noise is additive and its value is normally distributed with mean zero 6,7. Fig. 4 shows that one can expect these conditions to be approximated by x-ray video-image data recorded on magnetic tape.
- 2.) In some cases, non-ideal mixing of dye in the blood may be decreased by averaging subtraction-images.
- 3.) In studies of blood flow in vessels, the integration of series of succeeding subtraction-images makes visible all parts of the circulation transversed by the bolus during integration time. Anatomical and functional information otherwise obtained only subjectively by multiple replays of an angiogram is accumulated in one integration image.

Fig.5 shows schematically the process of heart phase synchronous image averaging and subtraction. In this example, two groups of four TV-fields each, one taken before dye injection and the other after opacification at the same heart phase are logarithmically averaged on a pixel by pixel basis and the two resulting averaged pictures are subtracted. Logarithmic conversion is performed before subtraction since the physical quantity of interest - the change in x-ray density due to contrast material - is logarithmically proportional to the change in grey level. The curvature of the logarithmic transfer characteristic may introduce a rectification effect and thus render unsymmetrical the distribution of noise amplitudes. This effect is, however, negligible as long as noise amplitudes are small compared to the grey levels in the relevant parts of the x-ray images analyzed 6.

The result of image integration and logarithmic subtraction is x-ray density data. For a display, these have to be rescaled to the dynamic range of the output device, i.e., to the 256 grey levels obtainable from an 8-bit video D/A-converter. The straight forward method of linear rescaling between the minimum and the maximum density values does usually not provide adequate results since a few large subtraction artifacts can limit the true density data to a small part of the usable grey scale. In videoangiocardigraphic subtraction-images, artifacts arise from videotape dropouts, catheter movement, and the time-base jitter of the signal reproduced from the tape recorder. Due to this jitter, the sharp brightness changes at the edge of the blanking circle of the video-camera give

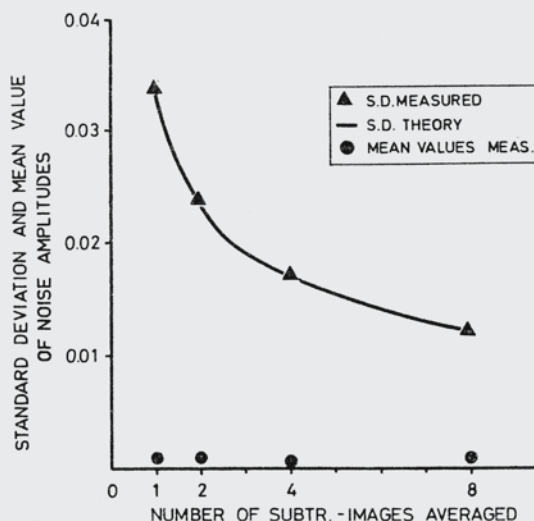


Fig.4: Decrease in RMS-noise amplitudes by averaging together increasing numbers of subtraction images according to the scheme of Fig.5. The pictures processed were recorded at constant x-ray intensity. The standard and the mean deviation from the expected zero density change was calculated for 4 K pixels in the center of each of the four averaged subtraction-images. Mean brightness in this image region was about 40 % of maximum brightness. The theoretical curve decreases inversely with the square root of images averaged.

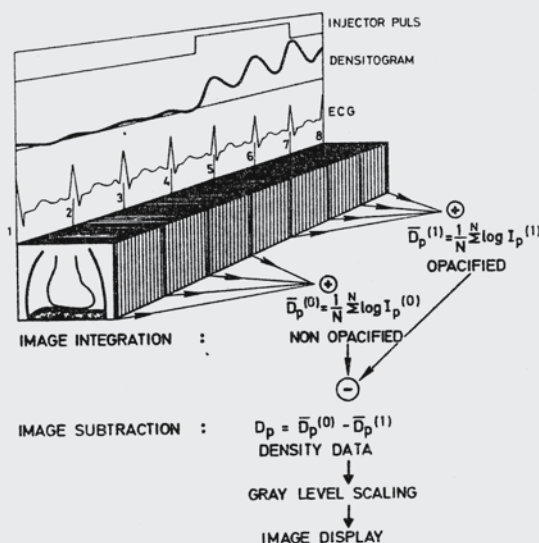


Fig.5: Schematic of the image integration and subtraction process.

rise to artifacts which are large compared to the minimum density changes to be observed.

The last-mentioned source of subtraction-noise can be eliminated if one confines the rescaling process to a window which excludes the critical blanking circle. Two other methods suited for rescaling the whole density picture without windowing are schematically displayed in Fig.6. The special technique of grey level mapping shown derives the range of displayed density values from noise measurements. The standard deviation of noise may be deduced from background pictures as described in Fig.4. Negative values of density must be artifacts or noise (if the temporal registration of the subtracted images is perfect and the x-ray radiation intensity is stable) and thus generally may be clipped. Positive density values are clipped at some multiple of the standard deviation (usually 5 S.D.).

However, useful information contained in the higher density values (e.g. the border between the left ventricle and the aorta) may also be eliminated in this process. Therefore we additionally tested a non-clipping method of rescaling also shown in Fig.6. Histogram equalization⁸ assigns an equal number of pixels to each grey level of the output image. Thus, ideally each of the n grey levels of a rescaled picture which consists of N pixels occurs N/n times. The few pixels containing large density artifacts are thus confined to a small part of the grey scale.

Applying this method to subtraction images which contain true density changes in only a small part of their total area (e.g. coronary arteriograms) may have the disadvantage that the large number of pixels with density values near zero force the information of the pixels containing true density changes to a small part of the grey-scale. Histogram linearization which is also shown in Fig.6 is a process which helps confine the noise to a smaller part of the grey-scale by assigning more pixels to a grey level in the noisy region of density data than at higher densities.

A qualitative assessment of the relative values of the described processing steps will be given in the next paragraph.

Results

A series of animal experiments was performed mainly in order to evaluate the improvement in the detectability of small amounts of dye by image subtraction, integration and subtraction-image enhancement. From these experiments, we selected the following angiograms:

LV: Experiment LV was performed by injecting 8 ml of 15 % Urografin into the left ventricle of an 18 kg pig (67mg Urografin per kg body weight) during three successive diastolies while respiration was suspended. Injection flow was 10 ml/sec. Conventionally, in order to obtain an angiogram of high contrast, about 18 ml of 76 % Urografin (760 mg Urografin per kg body weight) would have been injected during one heart cycle at a resulting flow rate of typically 20 ml/sec.

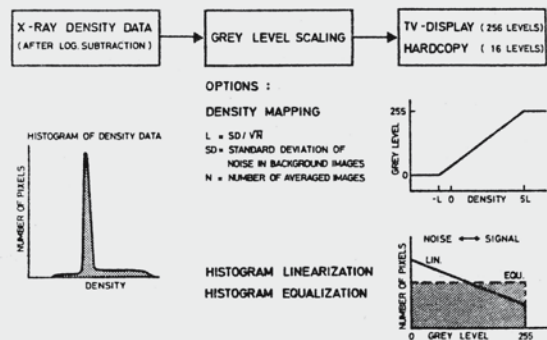


Fig.6: Techniques for enhancing subtraction-images by nonlinear rescaling.

PA: For experiment PA, 5 ml of 60 % Urografin (167 mg Urografin/kg) were injected into the pulmonary artery of the same pig. Usually 25 to 35 ml of 76 % dye (1050 to 1475 mg Urografin per kg) are necessary to obtain sufficient contrast for an angiogram of the left heart. Again, respiration was suspended during the experiments. While these experiments were to show the contrast enhancement and noise reduction provided by digital image subtraction and integration, the third experiment AA was to document primarily the additional advantage of image integration by rendering a coherent display of a vessel system transversely by a bolus of dye during integration time.

AA: 5 ml of 60 % Urografin were injected in this experiment at a flow rate of 40 ml/sec into the abdominal aorta of a pig.

Fig.7 shows in its upper part the best opacified end diastolic pictures taken from experiments LV and PA. Below them are shown the images resulting from the digital subtraction of one background picture taken in each experiment before dye injection from the displayed opacified pictures.

Fig.8 demonstrates the effect of image averaging performed on end diastolic pictures taken from experiment PA. Each of the four segments of this picture, which were assembled using the computer, carries the quantity of background pictures and the quantity of opacified pictures included into the averaging process.

An example of processing the angiogram obtained from experiment AA is shown in Fig.9. Every fourth TV-field was digitized. The four images of this series recorded immediately after dye injection and representing a time interval of 240 msec were subtracted from four background images and averaged to give a coherent image of all parts of the vessel system transversely by the bolus.

All of the preceeding images were obtained by rescaling the calculated x-ray density data to the grey scale range of the video monitor by determining the maximum and minimum

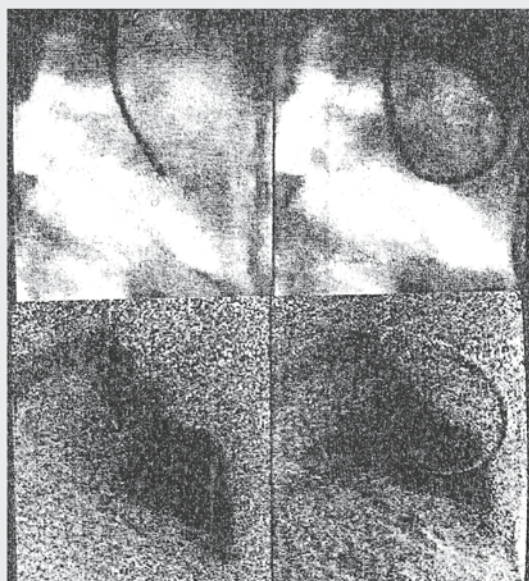


Fig.7: Effect of image subtraction (Experiment LV and PA). The slightly opacified pictures in the upper row were subtracted from background pictures to produce the subtraction images below.

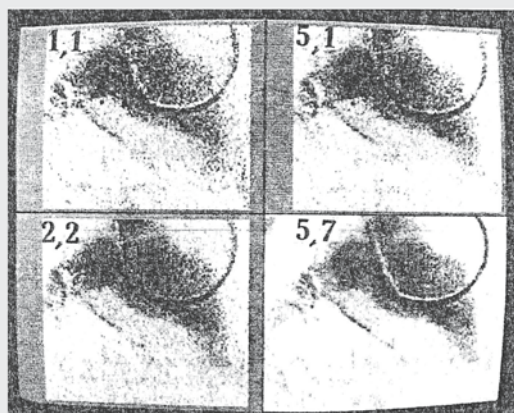


Fig.8: Effect of image averaging (Experiment PA). The figures given in the inserts indicate the number of background and opacified pictures, respectively, used in the integration and subtraction process.

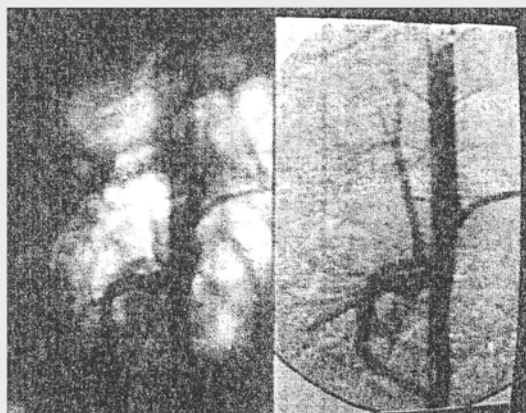


Fig.9: Effect of subtraction-image averaging (Experiment AA). The left part shows one TV-field recorded about 80 msec after dye injection while the right part shows the effect of averaging four subtraction-images (240 msec).

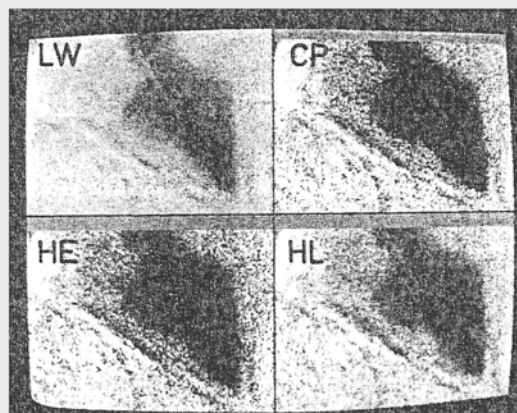


Fig.10: Effect of different rescaling methods (Experiment LV).
LW: Linear rescaling after windowing.
CP: Thresholding of linearly rescaled picture.
HE: Histogram equalization, HL: Histogram linearization.

density values from the density distribution in a window positioned over the region of interest and its immediate neighborhood. Fig.10 shows a comparison of this rescaling method with the other techniques described in the preceding paragraph. Here, the density-image obtained by averaging six end diastolic subtraction-images from experiment LV was linearly rescaled by the windowing technique (LW), and nonlinearly by the clipping (CP), histogram equalization (HE) and histogram linearization (HL) methods shown schematically in Fig.6.

Negative density values were forced to zero prior to rescaling. The resulting large number of pixels with zero density were excluded from the histogram modification processes. The parameter of histogram linearization was chosen to make the number of pixels per grey level greater by a factor of four at the low-density end of the grey scale than in the region of highest densities. This ratio helps to confine noise amplitudes near zero density to a smaller part of the grey scale as compared to the result of histogram equalization of the same image (HE). Thus, more grey levels are reserved for high-density values providing for a more detailed representation of the opacified ventricle. Normal linear rescaling between maximum and minimum density values of the full picture was omitted from this combination since the range of true density data occupied only less than ten percent of the difference between extremes.

Fig.11 compares the best opacified video image taken from experiment LV with a histogram equalized integration-image processed as described for Fig.10. The silhouette of the projection of the ventricle shown in the histogram equalized image compared well to the silhouette of the same ventricle as deduced from a regular higher contrast large dye-injection angiogram.

Presently, the quality of the processed image subtraction, integration, and subtraction-image enhancement is mainly limited by the signal-to-noise ratio of the videotape recording process. We hope to improve this ratio by subtraction-image video recording as described in the second paragraph and Fig.3. A further problem of the methods described which has to be studied especially in the case of clinical application is the influence of motion artifacts and their possible elimination by computerized image restoration.

An immediate application of these image series acquisition, preprocessing, and display options will be to interface them to our existing ventricular volume determination and contraction pattern analysis procedures (5) to increase their ease of handling, speed of operation, and, hopefully, accuracy of results. Another will be to reduce the amount of dye injected during videometric studies.

Acknowledgement

This work has been supported by the Deutsche Forschungsgemeinschaft.
The diagrams and picture prints were produced by Mrs.J.Bürsch.

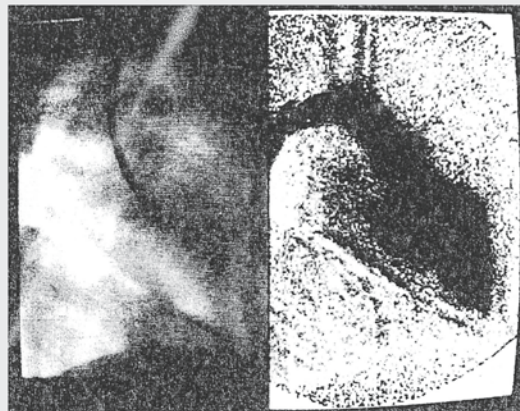


Fig.11: The information displayed at the right is extracted from a videoangiogram by image subtraction, integration, and subtraction-image histogram modification. The best opacified of the original pictures is shown at the left.

Literature:

1. Robb, R.A., Greenleaf, J.F., Ritman, E.L., Johnson, S.A., Sjostrand, J., Herman, G.T., Wood, E.H., *Comp.Biomed.Res.*, Vol.7, p.395-419, 1974.
2. McCaughern, R.W., Caughey, D.M., Rombeek, H., Davidson, W.S., *IEEE Trans.Comp.* Vol. C 21, p. 738-740, 1972.
3. Trenholm, B.G., Winter, D.A., Mymin, D., Landsdown, E.L., *Med.Biol.Engng.* Vol.10, p.163-173, 1972.
4. Robb, R., Ritman, E., Wood, E.H., *Cardio-vascular Imaging and Image Processing* (D.C.Harrison, Ed.), p.183-194, SPIE, Palos Verdes Estates, California, 1975.
5. Heintzen, P.H., Brennecke, R., Bürsch, J.H., Lange, P., Malerczyk, V., Moldenhauer, K., Onnasch, D., *Computer*, p.55-64, July 1975.
6. Chow, C.K., Kaneko, T., *Comp.Biomed.Res.* Vol.5, p.388-410, 1972.
7. Mistretta, C.A., Ort, M.G., Kelcz, F., Cameron, J.R., Siedband, M.P., Crummy, A.B., *Invest.Radiol.* Vol.8, p.402-412, 1973.
8. Hall, E.L., Kruger, R.P., Dwyer, S.J., Hall, D.L., Mc Larsen, R.W., Lodwick, G.S., *IEEE Trans.Comp.*, Vol. C 20, p.1032-1045, 1971.
9. Ziedses des Plantes, B.G.: *"Subtraktion"*, Thieme Verlag, Stuttgart 1961.

4.2 Computerized fluoroscopy in real time for noninvasive visualization of the cardiovascular system

Charles A. Mistretta (born 1941)

Charles A Mistretta was born on 5 January 1941 in Chicago, Illinois, USA. He was an undergraduate at the University of Illinois and obtained his BSc in engineering physics in 1962. In 1964 he was awarded his MSc in physics from Harvard University. His PhD thesis of 1968 also at Harvard University was on high energy physics and entitled “Pion Electroproduction Coincidence Experiments Near the First Pion-Nucleon Resonance”.

His undergraduate research at the University of Illinois was on betatron and Mossbauer effect experiments. In 1968 he started his postdoctoral positions as research associate (1968–1970) and lecturer (1970–1971) at the Department of Physics at the University of Wisconsin, Madison.

Charles Mistretta held faculty positions as Assistant Professor at the Departments of Physics & Radiology, U.W. Madison (1971–1972), Associate Professor at Department of Radiology, Medical Physics Section U.W. Madison (1974–1978), Professor Department of Radiology, Medical Physics Section U.W. Madison (1978–1982), and WARF Professor (1985–1986). In 1986 he became the John R. Cameron Professor of Medical Physics at the Departments of Medical Physics and Radiology, U.W. Madison. In 1999 he was appointed Vice Chairman Department of Medical Physics and in 2000 Faculty Affiliate at the Department of Biomedical Engineering.

In 1971 at the University of Wisconsin, John Cameron introduced Mistretta to the field of medical imaging. His early experiments in dual-energy X-ray imaging led to the development of a real-time digital imaging device that became the prototype for X-ray digital subtraction angiography (DSA). In 1972 he was the first physicist to become the James Picker Advanced Fellow in Academic Radiology. Mistretta received the Laufman-Greatbatch Prize in 1983 from the Association for the Advancement of Medical Instrumentation for developing DSA and in 1998 he shared the J. Allyn Taylor International Prize in Medicine for “distinguished lifetime achievement” and “outstanding contributions to the advances in the use of medical imaging in diagnosing and treating human diseases.” In 1999 he was elected Fellow of the American Association of Physicists in Medicine. He has served on numerous study sections for the National Institutes of Health (NIH), the Whitaker Foundation and various Canadian funding agencies.

Mistretta and his group developed DSA in the late 1970s. His recent work has related to the implementation of DSA-like methods using the angiographic applications of the less invasive magnetic resonance imaging with the goal of imaging and characterizing coronary artery lesions. These image-processing schemes will enable rapid reconstruction to be done so that 3-D MR DSA can be clinically implemented in a manner similar to X-ray DSA.

Picture courtesy Charles Mistretta, PhD 2004.



Stephen J. Riederer (born 1951)

Stephen J. Riederer was born on 22 July 1951 in Madison, Wisconsin, USA. He got his BA in Mathematics from the University of Wisconsin-Madison (1973), his MS in Nuclear Engineering from MIT-Cambridge, MA (1975) and his PhD in Radiological Physics from the University of Wisconsin-Madison (1979). He became Senior Physicist at General Electric Medical Systems (1980–83), Visiting Scientist, Department of Radiology, Stanford University Medical Center (1982), Assistant Professor of Radiology and Biomedical Engineering, Duke University Medical Center (1983–85), Associate Professor of Radiology and Biomedical Engineering, Duke University Medical Center (1985–88) and from 1988 on Professor of Radiology and Director, Magnetic Resonance Laboratory, Mayo Clinic.

Dr. Riederer has done research work in three diagnostic imaging modalities. In X-ray CT he developed with his masters' thesis advisor, Dr. David Chesler, one of the first mathematical filters which suppresses Gibbs' ringing in image reconstruction. His CT work also included fundamental statistical analysis of X-ray exposure requirements which dictate CT system design. In digital subtraction angiography (DSA) he worked in the laboratory of his PhD advisor Dr. Charles Mistretta in development of the prototype apparatus forming the basis for virtually all commercial DSA systems. In industry Dr. Riederer helped design a widely used commercial DSA system, and he coauthored one of the definitive books on DSA. Dr. Riederer has spent the bulk of his research career working in the area of magnetic resonance imaging (MRI). He has made numerous contributions to fast scan techniques, in particular various aspects of short (<10 ms) repetition time gradient echo methods, segmentation methods for breathhold vascular imaging, correction for view-to-view motion, MR fluoroscopy, centric phase encoding orders for 2-D and 3-D imaging, multi-shot echo-planar imaging techniques, breathhold feedback for reproducible breathholding, development of fast-spin-echo CSF-suppressed (FLAIR) pulse sequence for brain imaging, fluoroscopic triggering for contrast-enhanced MR angiography, and MR imaging using continuous table motion. Many of these methods have been commercialized by MRI vendors. For these achievements he was awarded the Gold Medal of the ISMRM in 2002.

Dr. Riederer has served as principal investigator for numerous NIH, foundation, and industrial grants. He has served as major advisor to 18 PhD students. In 1988 he established the Magnetic Resonance Research Laboratory at Mayo Clinic. He holds over 20 patents in medical imaging, has been a member of the editorial board of four international journals, and was a member in 1989–1993 of the NIH Diagnostic Radiology Study Section. He has been active in many societies and served as President of the Society for Magnetic Resonance Imaging (SMRI) in 1993. He was heavily involved in the merger between the SMRI and the Society of Magnetic Resonance in Medicine 1993 to form the International Society for Magnetic Resonance in Medicine (ISMRM) and served as the first President of the ISMRM. Dr. Riederer has been the principal advisor to six finalists for the ISMRM Young Investigator Award.

Picture courtesy Stephen Riederer, PhD, 2004.



Robert A. Kruger (born 1948)

Robert A. Kruger was born 13 August 1948 in Dublin, Ireland. He received his Bachelor of Science from University of North Carolina Chapel Hill, North Carolina, Department of Physics in 1970. From the University of Wisconsin Madison, Wisconsin, Department of Physics he received the Masters degree in 1972 and the PhD degree in 1978.

Robert Kruger became teaching assistant of introductory physics (1970–1971), and Research Assistant (1971–1978) at the Physics Department, University of Wisconsin, Madison, Wisconsin. In 1978 he became Research Associate in Department of Radiology/Medical Physics University of Wisconsin, Madison, Wisconsin. In 1980 he was appointed Research Assistant Professor of Radiology, and in 1984 Associate Professor of Radiology, University of Utah, Salt Lake City, Utah. In 1987 Dr Kruger became Director at the Medical Imaging Research Laboratory, Department of Radiology, University of Utah. In 1991 he was appointed Professor of Radiology at the Indiana University Radiology Department, Indianapolis, Indiana, a position he held until 2001. In 1994 Dr. Kruger became Director of Research, and in 2003 President, of OptoSonics, Inc., Indianapolis. Furthermore he is an Adjunct Professor of Bioengineering at the Purdue University and Adjunct Professor of Biophysics at the Indiana University.

Dr Kruger is a member of several scientific societies. He was awarded the Becton Dickinson Career Achievement Award for Development of “Dynamic Digitalized and Angiographic Tomography” by the AAMI, in 1984. He has published more than 128 scientific papers and has been issued 21 US Patents.

Picture courtesy Robert Kruger PhD, 2004

**Chris G. Shaw** (born 1949)

Chris C. Shaw was born on 18 July 1949 in Taiwan. He got his BS in Physics in 1971 from Tsinghua University, Hsinchu, Taiwan, his MS in Physics in 1976 from the University of Chicago, Chicago, IL and his PhD in Radiological Sciences in 1981 from the University of Wisconsin, Madison, WI.

He became Research Assistant, Radiological Sciences, University of Wisconsin, Madison, WI (1981–1983) and was appointed Assistant Professor, Radiology, U. of Rochester, School of Medicine, Rochester, NY (1983–1988). In 1981 he was awarded the Gold Medal for the scientific exhibit “Digital videoangiography” at the Annual Meeting of the American Roentgen Ray Society, San Francisco, CA. He was appointed Associate Professor, Diagnostic Radiology, University of Pittsburgh, School of Medicine, Pittsburgh, PA (1988–1998) and in 1998 Professor and Director of Digital Imaging, Imaging Physics, U. of Texas M. D. Anderson Cancer Center, Houston, TX.

Dr Shaw’s current areas of interest are the physics, instrumentation and applications of digital X-ray imaging and cone beam X-ray CT. The areas include digital chest, digital mammography, cone beam breast CT, and cone beam chest CT. He is also interested in the techniques and applications of parallel and distributed computing to image processing and reconstruction.

Dr. Shaw is a member of several scientific societies. He has published 36 original scientific papers and 23 invited articles.

Picture courtesy Chris Shaw, PhD 2004



Computerized Fluoroscopy in Real Time for Noninvasive Visualization of the Cardiovascular System

Preliminary Studies¹

Robert A. Kruger, Ph.D., Charles A. Mistretta, Ph.D., Theodore L. Houk, Ph.D., Stephen J. Riederer, S.M., Chris G. Shaw, M.S., M. M. Goodsitt, M.S., Andrew B. Crummy, M.D., William Zwiebel, M.D., Jerome C. Lancaster, George G. Rowe, M.D., and David Flemming, M.D.

A computerized fluoroscopic system with dedicated real-time hard-wired algorithms can be used for cardiovascular imaging with or without injection of iodine. Initial differentiated and integrated time subtraction displays are presented. Contrast studies appear adequate for visualization of cardiovascular dynamics. Cardiac images without contrast material suggest expected blood flow patterns but are difficult to interpret.

INDEX TERMS: Angiocardiology • Computers • Fluoroscopy (Heart and great vessels, fluoroscopy, 5[0].127) • Heart, flow dynamics • Subtraction

Radiology 130:49-57, January 1979

DIGITAL image processing has made possible a new class of images with high contrast sensitivity and moderate spatial resolution in computed tomography. Analogous techniques may be applied in fluoroscopy and radiography (1-5), with similar gains in contrast sensitivity but with as yet untested clinical importance. We wish to describe the types of images which can be obtained using standard fluoroscopic equipment and appropriate x-ray beam filtration assisted by digital image processing techniques. Our emphasis has been on noninvasive studies which involve insufficient contrast for standard film techniques and which require image subtraction processing at rates of up to 60 images/sec. Investigations have been carried out both with and without iodinated contrast material.

APPARATUS

A GE Maxiray 100 x-ray tube was typically operated at 100 kVp and 8-50 mA for studies not involving contrast material and at 60 kVp and 150-300 mA for most contrast studies. At 100 kVp, 2.5 mm Al filtration was used. Contrast studies were usually performed using a 60-kVp beam filtered by a cerous chloride water solution containing 100 mg/cm² of cerium, so that the x-ray spectrum peaked at 40 keV, just above the K-edge of iodine at 33 keV.

X rays were detected by a Philips 15-23-cm (6-9-in.) cesium iodide image intensifier/lead oxide vidicon system. Video information was collected at standard rates, amplified logarithmically, and digitized to 8 bits every 100 or 200 nanoseconds. After digitization, data were directed to one of three 256 × 256 × 13-bit memories for temporal integration of up to 32 video fields. Each memory was connected to identical hard-wired algorithms which per-

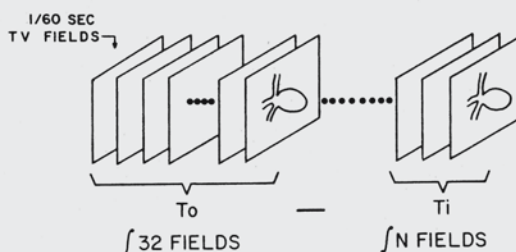


Fig. 1. Mask mode procedure. N field integrals at times T_i are sequentially subtracted from a mask image formed from 32 consecutive TV fields at time T_0 to form a live display of $60/N$ subtraction images per second.

mitted real-time conversion of data into linear combinations of images taken at different times, energies, angles, etc. After the data had been processed, they were reconverted to the analog format and displayed on a video monitor.

Procedure A: Mask Mode with Intravenous Contrast Injection

Technique: The mask mode procedure is illustrated in Figure 1. Prior to contrast injection, a *mask image* is digitally integrated in the memory. For studies involving dogs, 32 TV fields are integrated (1/60 sec. per field) to span one heart cycle. After injection, individual TV fields are integrated to N fields, appropriately normalized, and subtracted from the mask image, providing contrast-enhanced difference images at a rate of $60/N$ images per second. Increasing N improves the signal-to-noise ratio; however,

¹ From the Departments of Radiology (Diagnostic Division) (R.A.K., C.A.M., T.L.H., S.J.R., C.G.S., M.M.G., A.B.C., J.C.L., W.Z.), Medicine (Cardiology) (G.R.), and Anesthesiology (D.F.), University of Wisconsin, Madison, Wisc. Presented at the Work In Progress: Physics session of the Sixty-third Scientific Assembly and Annual Meeting of the Radiological Society of North America, Chicago, Ill., Nov. 27-Dec. 2, 1977. Received Feb. 27, 1978; accepted and revision requested June 16; revision received June 29.

This work was supported by grant APR 76-19076 from the National Science Foundation.

sjh

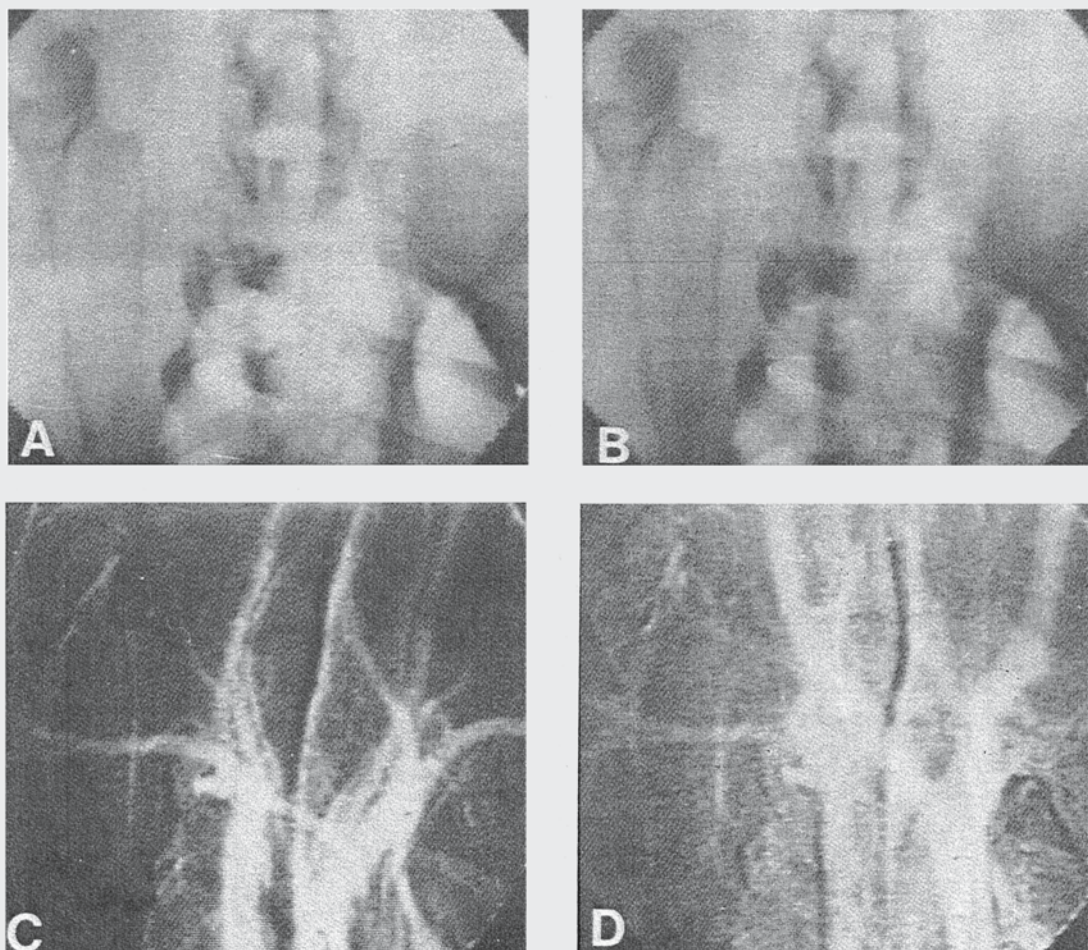


Fig. 2. Images taken just above the aortic arch of a 15-kg dog (AP projection).

A. Pre-injection mask.

B. Digitized fluoroscopic image (32 TV fields) initiated by an EKG trigger 12 seconds after intravenous injection of 15 ml of Renografin-60 (approximately 1 ml/kg) and generated by integrating 8 successive TV fields in each of 4 heart cycles.

C. The resulting 32-field image is subtracted from Figure 2, A, producing an image in which iodine appears white. The innominate, subclavian, carotid, and vertebral arteries can be seen. Except for some blurring of the lower innominate artery, similar results were obtained when 32 consecutive fields were added together within the same heartbeat.

D. Similar subtraction image corresponding to a later time after contrast injection, showing return via the jugular veins. This image was obtained without EKG gating, which was found to be unnecessary.

N must be kept small enough not to degrade perception of cardiac motion. We have found that N values of 1 to 4 give good images with useful dynamic information.

Contrast material was injected into a peripheral vein of the fore- or hind leg of a dog or the forearm of a human volunteer. In related studies, Ovitt *et al.* (4) injected 1 ml of Renografin-76 per kg into the jugular vein to demonstrate the heart and carotid arteries in dogs, while Brennecke *et al.* (5) have also used jugular vein injections for live digital subtraction displays of pig hearts.

There are four important features of the mask mode procedure:

1. For patient thicknesses up to about 25 cm, a samarium-filtered 60–65-kVp beam decreases the absorbed dose for a corresponding ratio of iodine contrast to quantum noise in the output beam approximately twofold compared to 2 mm Al filtration. Before realizing this, much of our work was performed with a cerium-filtered 60-kVp beam, which affords similar dose reduction but increased tube loading compared to samarium filtration.

2. Logarithmic processing ensures that attenuation changes of a fixed percentage will be of equal magnitude in the subtraction image, independent of the image brightness present in the unsubtracted fluoroscopic image.

It also ensures that there is sufficient digital gray-scale resolution for the dark as well as the bright portions of the image.

3. An integrated mask is preferred over one of shorter duration for several reasons. It reduces the overall noise component of the subtraction images. Moreover, it effectively removes the common-mode elements of the pre- and post-injection video images, thus allowing iodine increments to be displayed by the full dynamic range of the system. In heart studies, motion blurring ensures that the integrated mask contains few high-spatial-frequency (HSF) components and does not produce periodic HSF artifacts in the live subtraction display. It should be noted, however, that within the limitations of the system, all spatial frequencies of iodinated structures are seen.

4. Peripheral intravenous injection of contrast material is a noninvasive method which, in the case of cardiac imaging, permits visualization of all heart chambers with one injection.

Results: Figures 2–4 illustrate the use of mask mode procedures in imaging three different structures in a 15-kg dog. From 0.6 to 1 ml/kg of Renografin-60 (containing 0.2–0.3 g/kg of iodine) was injected *via* either a fore- or hind-leg vein. The total time from injection to display was less than 15 seconds, with the subtraction images being available for viewing during and immediately following the x-ray exposure. During these procedures the dog's respiration was suspended.

Figure 2 shows a series of anteroposterior images taken just above the aortic arch (75 kVp, 44 mA, 2 mm Al filtration). All images are shown in a 192×256 display (the first 64 horizontal addresses having been used for an EKG display) with each pixel corresponding to about 0.6 mm in the plane of the vascular structures. Such resolution is probably good enough to detect gross occlusive lesions and stenoses but not minor arterial wall disease. With present memory capacity and system architecture, 512-pixel horizontal resolution is possible, but not when subtraction images requiring temporal integration of more than 1 TV field are desired in real time.

Using the same entrance exposure (~ 200 mR per subtraction image), several attempts were made to obtain images with similar contrast using standard film–screen subtraction methods; however, they were unsuccessful using the opacification levels obtainable with intravenous injections.

The arterial and venous phases of the right pulmonary circulation in the left posterior oblique (LPO) (to the table) projection are shown in Figure 3, A and B, respectively. Images were obtained at a rate of 60 per second. The entrance exposure rate was 200 mR/sec., with individual fields representing only 3.3 mR apiece in addition to the 100-mR mask (32 TV fields). The use of a higher exposure for the mask ensures that its statistical variations (which are fixed in time and space) are small compared to the perceived noise of the live subtraction display, which is temporally averaged by the eye while viewing 60 images/sec.

Figure 4 shows the mask mode applied to the study of

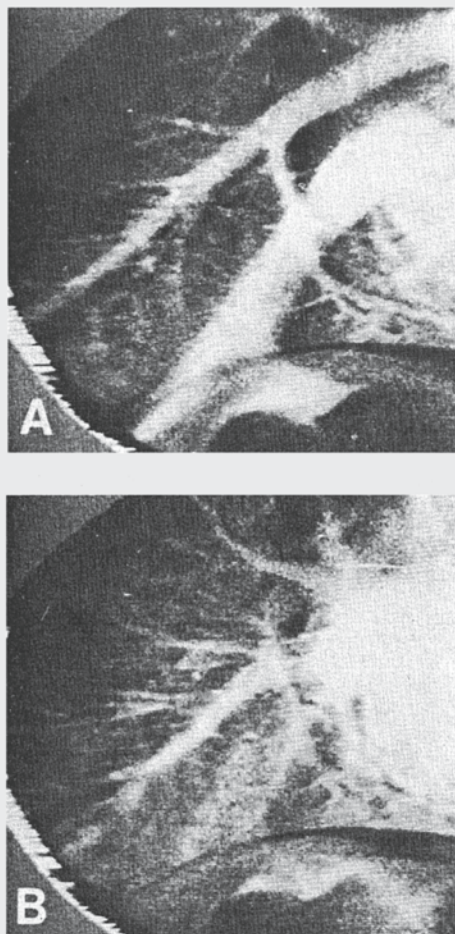


Fig. 3. A and B. Arterial (A) and venous phases (B) of the right pulmonary circulation of a 15-kg dog (LPO projection). 0.6 ml/kg of Renografin-60 was injected into a hind-leg vein and imaging was performed using a cerium-filtered 60-kVp beam. After the preinjection mask was made, no further field integrations were performed. After contrast injection, subtraction images were formed from individual fields at a rate of 60 per second, shown as a live display, and recorded on magnetic video tape.

cardiac chamber dynamics in dogs. These LPO projection images were formed by subtracting the sum of 4 fields from a mask at a rate of 15 per second. 1 ml/kg of Renografin-60 was administered into a hind-leg vein, and the 60-kVp cerium-filtered beam was used.

Several alternative procedures were attempted in the hope of improving spatial and temporal imaging resolution. Ciné pulsing for 4 msec. during the vertical retrace period of each video field was used in place of continuous fluoroscopy. 512×512 displays were presented with the TV camera both interlaced and noninterlaced. Ciné pulsing

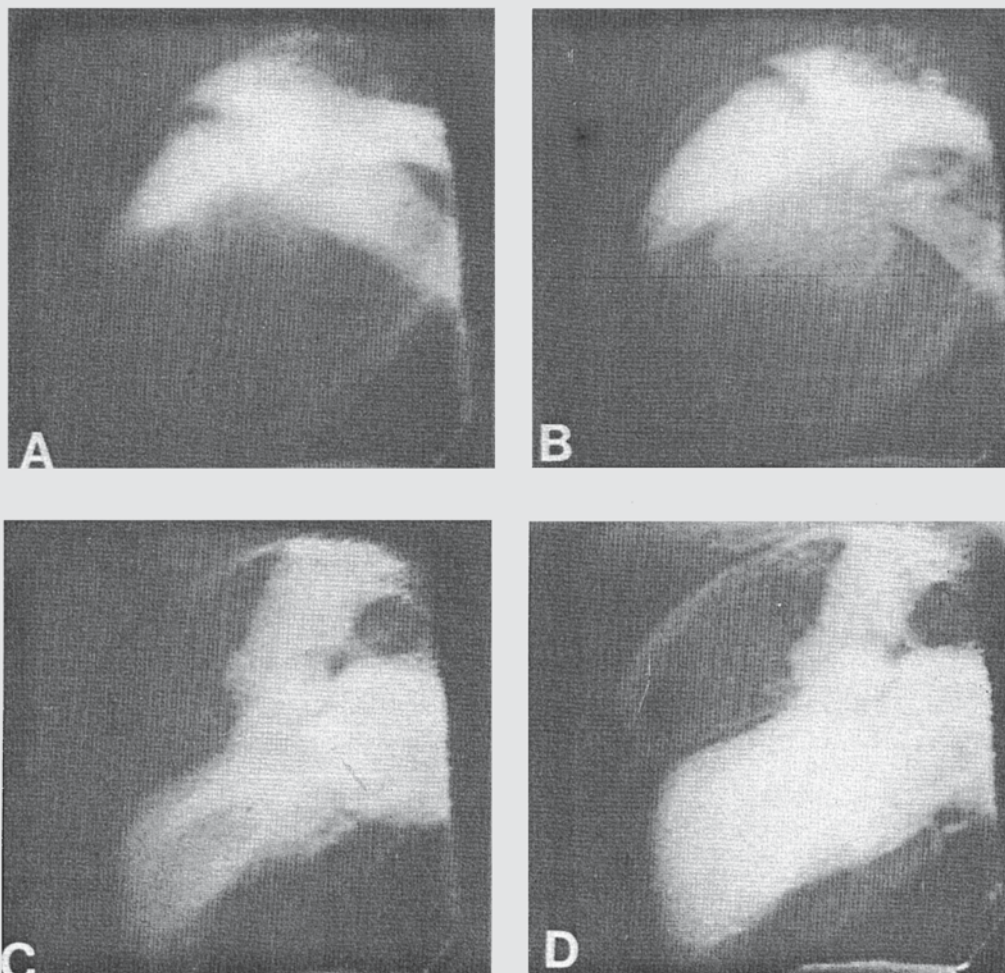


Fig. 4. Mask mode showing cardiac dynamics in a 16-kg dog (1 ml/kg Renografin-60 injected into a hind-leg vein). 15 subtraction images were formed per second. A. Right heart in ventricular diastole.
 B. Right heart in ventricular systole.
 C. Left heart in ventricular systole.
 D. Left heart in ventricular diastole.

and continuous fluoroscopy produced images of similar quality. No significant difference between interlaced and noninterlaced TV operation was observed. The 512×512 display was slightly better, but this was mainly attributed to its (less noticeable) higher pixel density rather than to any real improvement in spatial resolution. It was concluded that the limiting quantities for these images are (a) the intrinsically low contrast present in fine structures when opacified by the small concentration of contrast material we used and (b) the noise present in the TV system, which limits the dynamic range to ~ 40 dB per video field when scanned in the conventional fashion.

Figure 5 shows cardiac images of a human volunteer. For this study, bilateral 30-ml boluses of Renografin-60

were injected simultaneously. A 60-kVp beam was used with cerium filtration. The entrance exposure rate was 400 mR/sec. and produced a total exposure of 4 R during the 10-second examination. Using 4 field integrations, 15 subtraction images per second were formed, displayed continuously, and stored on magnetic tape. These images should be sufficient for densitometric determination of the left ventricular ejection fraction. A sampling rate of 15 per second has already been shown to be adequate for such determinations (6).

It is important that the patient stop breathing during the imaging procedure (approx. 15 sec.). Respiratory motion produces misregistration artifacts which obscure the signals associated with contrast flow. A second exami-

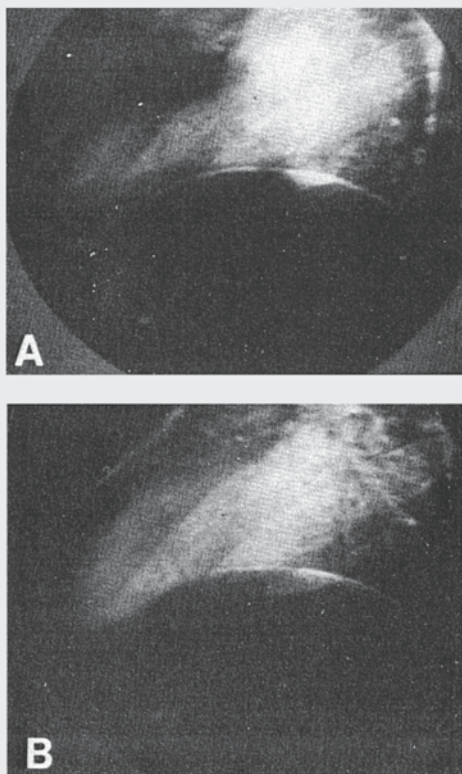


Fig. 5. Mask mode showing the left heart (LPO) of a human volunteer. Iodinated structures appear white. A. Left ventricular systole.

B. Left ventricular diastole.

nation on a human volunteer was unsuccessful primarily because of such artifacts. Excessive delay between the pre-injection mask and contrast injection made it impossible for the patient to stop breathing throughout the procedure. In addition, an insufficient amount of contrast material (20 ml of Renografin-76) was used. Future examinations will be conducted only after automation of the mode controls in the image processor so that excessive delays between the mask and the contrast injection can be avoided. Also, simultaneous bilateral forearm injections will be used when possible to improve image contrast without increasing the bolus duration. Use of low-pressure connective tubing should also increase the injection rate. We are hopeful that such a procedure will produce images approaching the quality of those obtained in dogs.

Using a mask mode technique similar to that employed for our initial human heart studies, 40 ml of Renografin-60 was injected into the forearm of a human volunteer in an attempt to show the bifurcations of the carotid artery (Fig. 6). Images were not obtained in real time because the volunteer moved after the preinjection mask had been

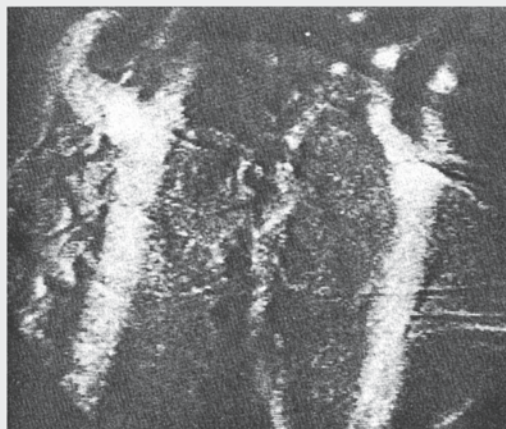


Fig. 6. Mask mode showing the carotid artery bifurcations of a human volunteer (0.6 ml/kg of Renografin-60 injected into a forearm vein).

taken. They were generated by reprocessing data which had been stored on analog video tape. The spine was cancelled out by using as a mask an image obtained after the contrast level had decreased in the carotids. Reprocessing from tape produces images with high noise and degraded spatial resolution associated with horizontal synchronization instability. Nevertheless, we feel that if motion misregistration can be overcome by using a head restraint, sufficient contrast can be obtained with the intravenous technique. Reprocessing of data stored in an additional digital memory is also feasible and will help in regeneration of images from examinations involving excessive motion.

Procedure B: Time Interval Difference Imaging with Contrast Injection

Technique: The primary limitation of mask mode procedures is the requirement that the patient stop breathing during passage of the contrast bolus through the heart. In many instances, *e.g.*, pediatric and critically ill patients, this would necessitate general anesthesia. A variation of the mask mode technique which is relatively insensitive to respiratory motion is time interval difference (TID) imaging (Fig. 7), in which a new subtraction mask is generated at each time interval cycle. With a short enough interval, respiration has little effect on the observed display. For short, contiguous intervals, the display becomes an approximation of the first time derivative of the logarithmic x-ray transmission. Since the time derivative of projected iodine concentration is a quantity fundamentally different from the concentration itself, the display requires modified interpretive skills. The display seems particularly useful for visualizing areas of turbulence, high blood flow velocity, and heart chamber boundaries.

At the other extreme, the TID mode can be implemented

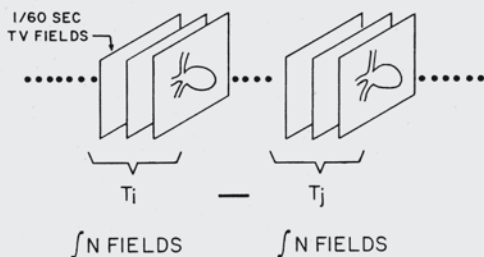


Fig. 7. In the time interval difference (TID) mode, data are integrated by one memory during N consecutive video fields starting at time T_i . A similarly integrated image initiated at a later time T_j is stored in a second memory and subtracted from the previous image. This difference is displayed while a third memory integrates a new image for later subtraction. By cycling the memories in this way, each image serves as a mask for the following image and a continuous sequence of images is displayed at a rate of $60/(j - i)$ images per second.

with arbitrarily long integration times and time interval separations. In this case it no longer represents an instantaneous time derivative display. An example of such use would include generation of EKG-triggered differences between systolic and diastolic images.

Results: Figure 8 shows two TID images taken after injection of 10 ml of Renografin-60 into a foreleg of a 15-kg dog (right posterior oblique or RPO projection, 60 kVp, cerium-filtered beam). Images were integrated over contiguous 1/15-sec. intervals and subtracted continuously as described above. Conceivably, dyskinesia in the borders of the cardiac chambers would show up as a black area in an otherwise white region or vice versa, depending on the heart phase. A thorough investigation of this possibility should proceed in a manner analogous to the ultrasound study of Gramiak *et al.* (7).

It is our impression that in cases where mask mode fluoroscopy can be employed, the information obtainable thereby is more easy to interpret than that provided by TID. However, the TID mode offers a display with comparable information density which may have great potential for evaluating cardiac function in patients incapable of holding their breath.

Procedure C: Mask Mode Without Contrast Material

Technique: The logarithm of the fractional transmission T of x-rays along a projection through the heart at time t can be described by the product of the effective attenuation coefficient μ and the patient thickness l projected to any point in the image plane x, y as:

$$-\ln T(x, y, t) = (\mu \cdot l)(x, y, t)$$

For cardiac imaging, $(\mu \cdot l)$ can be written conveniently as:

$$(\mu \cdot l)(x, y, t) = \overline{(\mu \cdot l)}(x, y) + f(x, y, t)$$

where $f(x, y, t)$ represents the temporal variation of $(\mu \cdot l)$

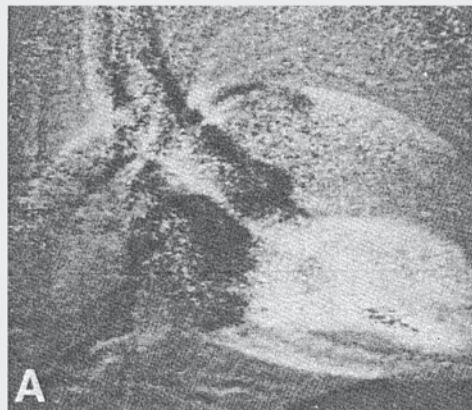


Fig. 8. Heart of a 15-kg dog. A. TID image shows iodine flowing from the left atrium into the left ventricle near end-diastole.

B. Opacified blood fills the left atrium while the left ventricle is pumping blood into the enlarging aorta just prior to end-systole. A white display implies increased opacification (expansion) over a period of 1/15 sec., while a black display implies a decrease in opacification (contraction). Gray indicates no change.

$f(x, y, t)$ about its time-averaged value $\overline{(\mu \cdot l)}(x, y)$. By the above definition, the time average of $f(x, y, t)$ over any integral number of heart cycles is zero. When mask mode subtraction is performed without contrast material, the image is

$$\overline{(\mu \cdot l)}(x, y) - (\mu \cdot l)(x, y, t) = f(x, y, t)$$

i.e., the image is time-dependent and displays the variation of the $(\mu \cdot l)$ product about its time-averaged value. Without contrast material, the subtraction image occupies only a small fraction of the dynamic range of the unsubtracted images. Because of this, the contrast of the subtraction image $f(x, y, t)$ may be enhanced by a large factor, typically on the order of 16 for our dog studies.

In the case of the heart, and in view of the limited sta-

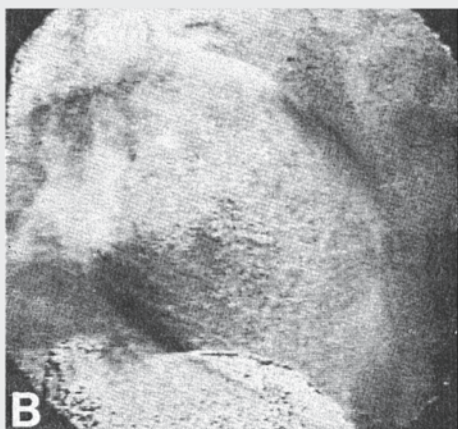
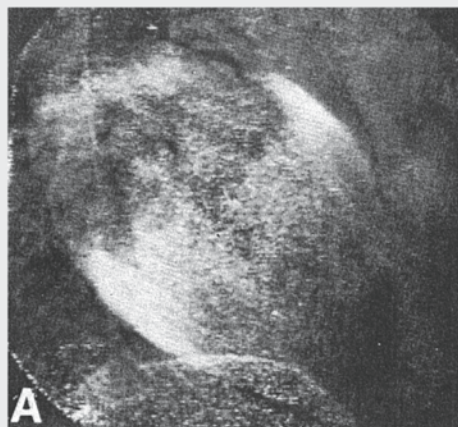


Fig. 9. Heart of a 15-kg dog imaged in the mask mode without contrast material. The imaging rate was 15/sec. A. In the ventricular diastolic image, the right and left atria appear dark, suggesting decreased atrial volume.

B. Image taken 180° out of phase with Figure 9, A. The atrial regions appear brighter than the average, the ventricular regions darker.

tistical precision of data acquired in individual television fields, displayed fluctuations in the product ($\mu \cdot I$) are almost entirely due to changes in the tissue thickness I along any x-ray path. These fluctuations are caused by changes due to blood flow in and out of the heart chambers as well as to changes in cardiac muscle orientation and muscle displacement. Similar changes in overlying fat and lung tissue can either contribute to or partially cancel changes in thickness due to blood flow. A study of our TV system indicates that the minimum attainable noise fluctuations per pixel per TV field simulate 1 mm of tissue variation for the x-ray beams and exposure rates we used. This implies that, including the effects of spatial integration, our system, when used at these exposure rates, should be able to

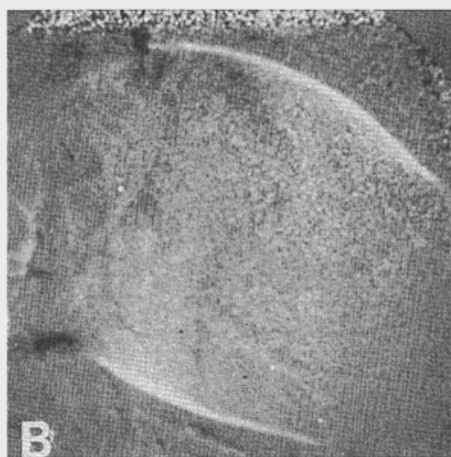
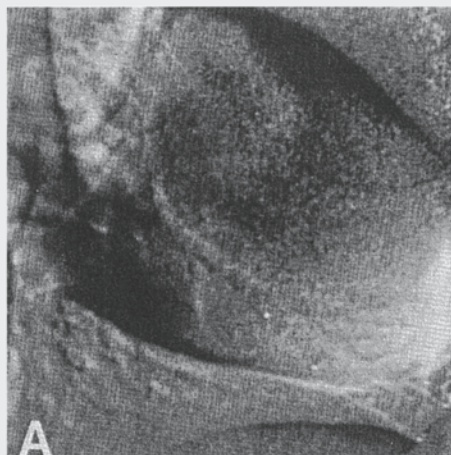


Fig. 10. TID without contrast material, showing images of a dog's heart taken 0.2 seconds apart (heart rate, approximately 120 beats/min.).

A. Start of systolic contraction, as indicated by the dark borders.

B. Detailed information is not present, but the image generally suggests a blood flow pattern tending toward ventricular diastole.

display thickness variations of ~ 1 mm for 9 mm^2 areas (25 pixels) in the plane of the heart with a signal-to-noise ratio of 5. Images integrated over N fields will increase this maximum contrast sensitivity in proportion to \sqrt{N} .

Results: Using the mask mode without contrast material, the heart of a 15-kg dog was imaged in the LAO projection (100-kVp beam, 8.5 mA, 2 mm Al filtration, entrance exposure rate 100 mR/sec.). In the absence of contrast material, the ratio of tissue contrast to integral exposure improves as the kVp is increased. After taking a mask image, 1/15-second time intervals were integrated over

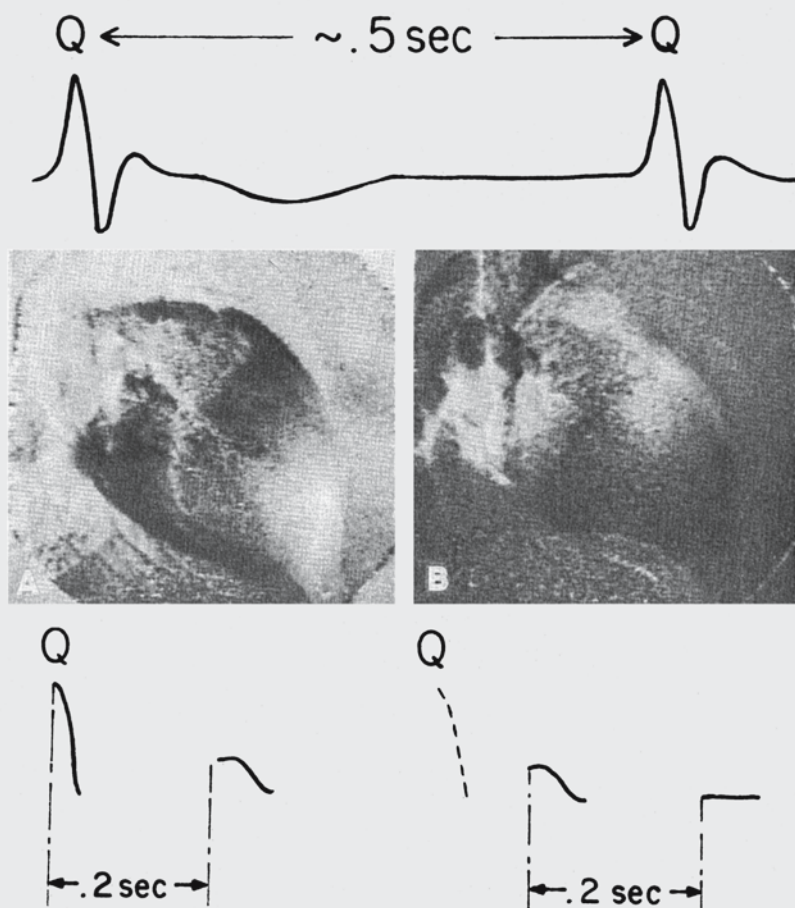


Fig. 11. TID of the heart (RPO) of a 16-kg dog. Two 1/15-sec. images taken 0.2 sec. apart were subtracted from each other to give the two images. A. Subtraction of two 1/15-sec. time intervals, one at end-diastole and the other near ventricular systole, again averaged over 8 heart cycles. Note the contraction of the myocardium and the overlying pulmonary vasculature. B. Subtraction of images at two time intervals, one near systole and another 0.2 sec. later. Increased brightness (decreased x-ray transmission) can be seen in the right ventricle and left atrium.

preselected phases of eight consecutive heart cycles to a total of 32 fields and subtracted from the mask. Two such phases are shown in Figure 9. Because a contrast bolus was not used, such images display equal-sized signals simultaneously in both the left and right heart. Such images also show the state of expansion (white border) or contraction (dark border) of the myocardial silhouette.

We are not yet in a position to say whether or not such studies will prove to be useful as diagnostic tools, especially in view of the superiority and simplicity of intravenous contrast studies. However, the noncontrast studies do merit further investigation. Some workers have reported successful correlations of disease with myocardial border information alone (8, 9). Such studies suggest that the greater quantity of information in a contrast agent-free

two-dimensional mask mode presentation might permit greater accuracy.

Procedure D: Time Interval Difference Imaging Without Contrast Material

Technique: TID can also be applied without contrast injection when suspension of respiratory motion is difficult or impossible. Using the notation of the previous sections, TID images obtained without contrast material display blood flow and solid tissue thickness variations which can be described by

$$(\mu f)(x, y, t + \Delta t) - (\mu f)(x, y, t) = f(x, y, t + \Delta t) - f(x, y, t) \propto \Delta f(x, y, t) / \Delta t$$

For a small enough Δt the displayed image depicts the time derivative of the function representing deviations from the time-averaged value of the product of attenuation coefficient times thickness. Such an image displays only those changes which have occurred over time Δt . Without using contrast material, canine heart images were obtained using such an approach.

Results: Two TID images taken with the same technique and in a similar though not identical projection to that of Figure 9 are presented in Figure 10. These images represent subtractions of contiguous 1/15-sec. integrations over eight consecutive heart cycles. The suggestion of a general blood flow pattern is as evident in contrast-free TID as in the contrast-free mask mode. In either procedure, static image presentations, even when averaged over several heart cycles, do not convey the blood flow information present in dynamic displays. Information degradation in the static displays is even more severe than in the contrast studies, where heart chamber structures are prominent.

TID can also be used to generate images associated with widely separated time intervals, as shown in Figure 11. Because of the questionable role of solid tissue in these images and because of the overlying great vessels in the atrial regions, it is not yet possible to interpret such images with certainty. However, we have observed in infused contrast injection experiments with the same dog that the right ventricle filled slightly ahead of the left, which is consistent with the brightness pattern seen in Figure 11.

CONCLUSIONS

We have reported on four preliminary investigations of computerized fluoroscopy, consisting of two general modes of data display, each with and without intravenous contrast material. Several conclusions can be made:

(a) In the mask mode, intravenous injection of 0.6–1.0 ml/kg of Renografin-60 provides excellent visualization of canine cardiac chamber dynamics at display rates of 15 to 60 subtraction images per second. Human left ventricular motion was adequately observed using 0.3 ml/kg of Renografin-60 but should be performed with larger contrast doses (0.6 ml/kg) injected into each forearm simultaneously. The patient must be able to hold his breath for about 15 seconds, which may not be possible with those who are unable to cooperate or in cases where respiratory suspension using drugs is dangerous. At present, the spatial resolution of mask mode contrast studies of the pulmonary system and carotid arteries is inferior to that of film subtraction techniques, but they do appear to have higher contrast sensitivity.

(b) Time interval difference imaging studies with contrast injection demonstrate the time derivative of the contrast concentration and are sensitive to rapid changes associated with chamber contraction, valve motion, and turbulent flow. The most important feature of the TID mode is that the patient does not have to stop breathing.

(c) When used without contrast material, the mask mode represents the deviation of the logarithmic transmission function from its time-averaged value. The TID mode without contrast represents the time derivative of this function. In both cases the display gives the same general impression of blood flow as observed in contrast studies but does not provide detailed visualization of cardiac structures. Moreover, the images are complicated by the simultaneous presence of dynamic contrast changes in the right and left sides of the heart, by overlying vasculature, and to an unknown extent by displacement of solid tissue.

(d) Intravenous contrast studies appear suitable for immediate study using human volunteers; contrast-free studies should be confined to experimental animals until they are understood more completely.

Department of Radiology
University of Wisconsin
Madison, Wisc. 53706

REFERENCES

1. Kruger RA, Mistretta CA, Riederer SJ, et al: Digital video processor for generalized subtraction imaging. [In] Digest of the Fourth International Conference on Medical Physics, Held in Ottawa, Canada, July 25–30, 1976. *Phys Canada* 32, section 7.9, Jul 1976
2. Kruger RA, Mistretta CA, Crummy AB, et al: Digital K-edge subtraction radiography. *Radiology* 125:243–245, Oct 1977
3. Kruger R, Lancaster J, Mistretta C, et al: Current results in real time computerized fluoroscopy and radiography. Presented at the Work In Progress: Physics session of the RSNA, Chicago, Ill., Nov. 27–Dec. 2, 1977
4. Ovitt TW, Nudelman SN, Fisher D, et al: Computer-assisted video subtraction for intravenous angiography. Presented at the Work In Progress: General Diagnosis session of the RSNA, Chicago, Ill., Nov. 27–Dec. 2, 1977
5. Brennecke R, Brown TK, Bursch J, et al: Computerized video-image preprocessing with application to cardio-angiographic roentgen image series. [In] Nagel HH, ed: *Digital Image Processing*. New York, Springer, 1977, p 244
6. Freeman E, Ziskin MC, Bove AA, et al: Cineradiographic frame rate selection for left ventricular volumetry. *Radiology* 96:587–591, Sep 1970
7. Gramiak R, Waag RC, Schenk E, et al: Ultrasonic characterization of myocardial ischemia and infarction in dogs. Presented at the RSNA, Chicago, Ill., Nov. 27–Dec. 2, 1977
8. Kazamias TM, Gander MP, Ross J Jr, et al: Detection of left-ventricular-wall motion disorders in coronary-artery disease by radarkymography. *N Engl J Med* 285:63–71, 8 Jul 1971
9. Rosen L, Silverman NR, Higgins CB: Differences in the velocity-displacement relationship of systolic contraction of normal and ischemic canine myocardium. *Radiology* 124:7–12, Jul 1977

4.3 Intravenous angiography using digital video subtraction: X-ray imaging system

Sol Nudelman (born 1922)

Sol Nudelman was born on 14 August 1922 in Brooklyn, New York in the USA. He obtained his BS in Physics from Union College in 1945, his MS in Physics from Indiana University in 1948 and his PhD in Physics from University of Maryland in 1955.

Dr. Nudelman became Instructor of Physics at Union College (1948–1949) and Knox College (1949–1951). Between 1951–1956 he became research physicist at the Naval Ordnance Laboratory and was appointed lecturer and head of the Semiconductor Group at the University of Michigan Institute of Science and Technology (1956–1961). In 1964 he was appointed Professor of Electrical Engineering at the University of Rhode Island. Here he became Acting Coordinator of Research (1967–1968) and Acting Chairman of the Electrical Engineering Department (1968–1969). Sol Nudelman was appointed Professor and Director of the University of Arizona Optical Science Center and Department of Radiology, Imaging Research Division (1973–1983) and the University of Connecticut Health Center, Department of Radiology, Imaging Research Division (1983–1995). Since 1995 he has been Visiting Professor at the University of Arizona, Department of Radiology, Imaging Research Division.

His major current interests are research and development of photo electronic imaging devices, the application of these imaging devices and techniques to diagnostic medicine and their evaluation.

Sol Nudelman is a Fellow of the American Association for the Advancement of Science, a Senior Member of the IEEE, and a Fellow and Governor of the SPIE.

Picture courtesy Sol Nudelman, PhD, 2004.



Theron W. Ovitt (born 1939)

Theron W Ovitt was born on 7 April 1939 in Milwaukee, Wisconsin, USA. He got his BA from Vanderbilt University, Nashville, Tennessee in 1961 and his MD from Marquette University, Milwaukee, Wisconsin in 1965. Dr. Ovitt started his internship at Santa Clara County Hospital, San Jose, California, rotating in 1966.

In 1966 he started his surgical residency at Marquette University Medical School and in 1968 his residency in radiology at University of Minnesota, Minneapolis, Minnesota. In 1971 he started his fellowship in cardiovascular radiology at the Variety Club Heart Hospital, Minneapolis. In 1972 he successfully passed his boards in radiology from the American Board of Radiology. He became a fellow of the American College of Radiology in 1985. His subspecialty is cardiovascular radiology. Dr. Ovitt became Assistant Professor at the Department of Radiology, University of Minnesota (1973–1974). In 1974 he went to the Department of Radiology at the University of Arizona Health Science Center and became Assistant Professor (1974–1977), Associate Professor (1977–1982) and Professor of Radiology (1982–present). He became Chief of the Diagnostic Division (1985–1992), Vice Chairman (1992–1993) and Chairman in 1993.



Theron Ovitt has published more than 126 refereed scientific articles and presented approximately 151 lectures, papers and scientific exhibits. He is a reviewer and associate editor of several radiological journals. He served on the board of directors of the American Heart Association in 1981. In 1992 he was appointed president of the Arizona Radiological Society.

Picture and information courtesy Sol Nudelman, PhD, Dep. Radiology University Arizona Tucson, 2004.

Henry Donald Fisher III

Continuing graduate level courses in the areas of digital signal and image processing, Henry D Fisher received his BS in Electrical Engineering in 1971 from the University of Rhode Island. He became electrical engineer at the Naval Electronics Laboratory Center, Infrared Division (1971–1975) and research associate professor at the Department of Radiology, University of Arizona (1975–1985). Here he conducted research in the area of digital subtraction angiography (DSA). He became senior engineer and group leader responsible for the development of the joint University of Arizona/Toshiba Medical Corporation PACS project. In 1985 Fisher was awarded a patent as a result of his research on design and construction on the first multimodality imaging workstation for PACS. After receiving his MS in Electrical Engineering from the University of Arizona in 1986, he became senior scientist at Science Applications International Corporation.

Picture courtesy Sol Nudelman, PhD, 2004.



Meryll M. Frost, Jr. (born 1949)

Meryll M Frost was born 8 September 1949 in Beverly, Massachusetts, USA. After receiving his BSEE from the University of Rhode Island, Kingston, RI in 1971 he started his professional career as instructor and research associate at the Department of Radiology, Arizona Health Science Center. Here he became a part of a four-member team responsible for the building of a state of the art medical imaging research laboratory. In 1981 Frost became research and development Manager of CGR Medical Corporation. From 1983–1987 he got an academic appointment at Cornell University Medical College as a research associate in conjunction with a consulting contract for the development of an ultra-high speed DSA system for cardiac acquisition and display. In 1992 he became refresher course faculty at RSNA and taught PACS basics. Since 1982 Frost has been President and Chief Executive Officer of Medical Imaging Consultants, Inc. This private consultancy provides expertise in all facts of medical imaging to individual hospitals and equipment manufacturers. Clients have included the University of Florida, where Frost became PACS consultant at the Department of Radiology.

Picture courtesy Sol Nudelman, PhD, 2004.



Hans Roehrig (born 1934)

Hans Roehrig was born on 29 November 1934 in Giessen, Germany.

He got his MS (1961) in experimental physics and his PhD (1964) from Justus Liebig University, Giessen, Germany. Dr. Roehrig started his professional career as a physicist at Farbenfabriken Bayer, Leverkusen, Germany (1965–1966). In 1967 he went to the United States to become physicist at the US Army Night Vision Lab, Fort Belvoir, Virginia. He then became Research Associate in physics at the University of Rhode Island (1972–1973) and the University of Arizona, Optical Science Center (1973–1976). Dr. Roehrig was appointed Research Associate Professor (1973–1976) and Research Professor (1990–present) at the University of Arizona, Department of Radiology and Optical Science. His major current interests are the development of the totally digital radiology department, physical evaluation of photoelectric and medical imaging devices, and the application of photoelectronic imaging devices to diagnostic radiology.

Hans Roehrig has published 7 book chapters, more than 130 refereed scientific articles and presented over 60 invited papers and scientific exhibits. He is a reviewer of several radiological journals and since 1988 a member of the editorial board of the *Journal of Digital Imaging*. In 1990 he became a fellow of the Society of Photo-electronic Instrumentation Engineers (SPIE).

Picture and information Courtesy Sol Nudelman, PhD, Dep. Radiology University Arizona Tucson.

**P.C. Christenson**

Intravenous Angiography Using Digital Video Subtraction: Intravenous Cervicocerebrovascular Angiography

Peter C. Christenson¹
Theron W. Ovitt
H. Donald Fisher III
Meryll M. Frost
Sol Nudelman
Hans Roehrig

The clinical application of intravenous angiography to study the cervicocerebrovascular system using the digital video subtraction system described in a companion article is reported. About 0.75 ml/kg of a standard 76% iodine contrast solution is injected into an antecubital vein using a power injector. Then 15–20 exposures of the head and neck region at a 1/sec rate are made on the image intensifier. The images are recorded by a high performance video system and the output signal is digitized for subsequent computer manipulation. The subtraction images of these vessels produced by the computer show the vessels clearly, even though they contain very low concentrations of contrast media. Standard exposure factors of 75–80 kVp, 9–10 msec at 800–1,000 mA are used. Clinically pertinent features of the data alteration and flow through the system and the step-by-step computer procedures used to achieve and analyze the various forms of subtracted images are described.

Five experimental and clinical cases demonstrate appropriate applications to cervicocerebrovascular disease: (1) evaluating the effects of surgical and medical therapy on atherosclerosis; (2) providing a screening angiographic test for patients with asymptomatic bruits and/or positive noninvasive studies; (3) evaluating patients who have significant generalized vascular disease either precluding or presenting hazardous contraindications to transarterial catheterization; (4) evaluating significantly aged patients in whom standard angiography has higher risk; and (5) evaluating currently asymptomatic patients who are medically at higher risk for developing atherosclerotic lesions. Numerous examples of the various types of image manipulations are presented: (1) linear subtraction; (2) logarithmic subtraction; (3) alterations of electronic contrast enhancement (map slope); (4) the usefulness of a series of angiographic images; and (5) the importance of multiple projections with this technique.

Intravenous angiography has added to the armamentarium of the neuroradiologist for evaluation of atherosclerotic disease [1–3]. Until development of a satisfactory intravenous angiographic technique, there was no safe method of visualizing and screening the entire cervicocerebrovascular system without intraarterial angiography. Although selective transarterial angiography will continue to play a major role in the detailed radiographic demonstration of cervical and intracranial lesions, it is not appropriately used as a screening test of these vessels. Because it has a small, but essentially irreducible morbidity even in skilled hands, it is a test with inappropriately high risk for use in neurologically asymptomatic patients. This morbidity increases significantly in elderly patients. Intravenous angiography provides an alternative method of visualizing vessels in patients in whom either a screening examination is desired or in whom catheter techniques are contraindicated or unachievable.

With the system described in our companion paper [4], we are achieving clinically diagnostic images of the cervical arteries and their proximal intracranial segments. We can use these images to make clinical decisions regarding operative versus nonoperative care in about 80% of cases. On several intravenous angiograms, questionably positive findings were confirmed with intraarterial angiography.

Received April 17, 1980; accepted May 13, 1980.

Presented in part at the annual meeting of the American Society of Neuroradiology, Toronto, Canada, May 1979.

This work was supported by National Heart, Lung, and Blood Institute grant NO1-HV-72931.

¹ All authors: Department of Radiology, University of Arizona, Tucson, AZ 85724. Address reprint requests to P. C. Christenson.

This article appears in September/October 1980 *AJNR* and December 1980 *AJR*.

AJNR 1:379–386, September/October 1980

0195–6108/80/0104–0379 \$00.00

© American Roentgen Ray Society

In this article, the techniques of the procedure and five representative clinical cases are described to illustrate the quality of images currently being produced. These also demonstrate some of the types of computer manipulations of the digitized images currently available.

We are currently using this intravenous angiographic technique primarily for the study of cervical arterial atherosclerosis. There are many additional cervical and intracranial vascular problems to which this technique can be applied as the resolution and capability of this system improve.

Electronic Computer System

Radiographic visualization of cervical and cerebral vessels has previously required direct, intraarterial injection of contrast material into or near the vessel being studied. This is because contrast material concentrations of less than 5%–6% are not radiographically visible even when subtraction techniques are used. Previous attempts at intravenous angiography of these vessels failed primarily because of the inability to achieve adequate intraarterial contrast concentrations.

Our digital, video subtraction system [4] allows visualization of cervical and proximal intracranial vessels containing an extraordinarily low concentration of contrast medium (down to 2%–3%). A 40%–50% intraarterial concentration is required in standard angiography to produce images of equal contrast.

Although each part of the system is vital to its overall performance, several parts have special significance. The television tube has a signal-to-noise ratio of 1,000:1, which is far superior to a conventional x-ray video system. This produces an output video signal with very low electronically induced noise to degrade the image. It also has a linear response that permits accurate density subtraction.

The digitization to 8 bits (2^8) of the TV signal means that the TV picture, at this point, is changed into 262,144 words of digital information (512 TV lines, each broken into 512 discrete digital units), each of which has an electronic contrast range of ± 256 units (2^8) of displayed density. Therefore, further degradation of the signal is impossible, since it is in discrete, digital form as it moves through the rest of the system.

This totally digitized image is then essentially rebuilt, line by line, into an image in the digital image store in 0.03 sec and transferred to the computer. There, a large number of very rapid manipulations can be performed on this digitized image. Image processing capabilities currently include: (1) linear (binary) subtraction; (2) log subtraction; (3) contrast slope and position manipulations; (4) edge enhancement; (5) image smoothing; (6) digital filtering; (7) signal averaging; (8) reference image movement; and (9) image addition.

When all digitized images are in the computer, any one can be requested for subtraction (or any processing) by a simple, single letter command on a standard computer address alphanumeric terminal. The requested image begins to be displayed virtually instantaneously and requires 2–5

sec to be completely displayed. Subsequent manipulations are also obtained by single letter command and are displayed at the same rate. Therefore, during the clinical studies, the subtraction images can be viewed immediately after each injection and decisions regarding the necessity of additional injections and projections can be made promptly.

Materials and Methods

Clinical Technique

Most of our current studies are performed on outpatients. They must be well hydrated and without food intake for 2 hr before the examination. No pain or sedative medication is given or has been required. The study is done with the patient in the supine position, usually using either a right or left posterior oblique projection for the cervical vessels. After about 0.1 ml of 1% intradermal lidocaine, a 6.4 cm 16 gauge "angio-cath"-type catheter is introduced into either a right or left antecubital vein. Dextrose solution (D5/W) is then slowly infused into this catheter before and between contrast injections. We prefer using the arm contralateral to the side of primary clinical interest, since there is rarely reflux of contrast material into the external or internal jugular venous systems, which interferes with obtaining a "clean" scout or reference image. However, this is not critical, as successful examinations have also been obtained ipsilateral to the side of injection even when reflux has occurred.

Numerous animal experiments (see fig. 1) demonstrated that about 0.75 ml/kg of contrast material provided very satisfactory visualization of cervical vessels with low background noise levels. For this reason, we currently use 0.70–0.75 ml of a standard 76% iodine contrast/kg of body weight. This is delivered using a standard power injector at a rate of 20 ml/sec for 2.0–3.5 sec (depending on patient's weight). The contrast material is injected with the patient's arm elevated to facilitate the central and intrathoracic flow. Two or three injections are usually required to obtain a complete and diagnostic set of studies.

Just before injection, the patient is hyperventilated and asked to hold his breath in midexpiration phase (if possible) for 15–20 sec. If the patient cannot do this, we find that quiet, shallow, respiration produces the least movement. Each patient has been questioned and has specifically denied the presence of any pain at or near the site of contrast injection using these volumes and rate of injection.

Using a 1.2 mm focal spot at a tube-intensifier distance of 78.7 cm and a neck-intensifier distance of 22.9 cm, a magnification of about 1.4 is achieved. Currently, we are using exposure factors of 75–80 kVp, 9–10 msec at 800–1,000 mA. Exposure rate is 1 frame/sec for 15–20 sec starting 2–4 sec after completion of the intravenous injection. Arrival time of the contrast material in the cervical vessels is 7–14 sec, depending on the patient's cardiac status; therefore, a rather long exposure sequence is required. We hope to diminish the length of this sequence as our experience increases. As stated above, after each set of exposures, the subtracted images are reviewed and the requirement for additional projections is determined.

At the completion of the study, the intravenous catheter is removed. The patient is either returned to the ward or sent home with instructions only to force fluids in the 24 hr after the procedure and to only report to us or to his physician if he notes inordinately diminished urine output. The average study currently takes about 45 min to 1 hr. We anticipate reducing this time by at least one-half with continuing refinements in equipment, setup procedures, programs, and system standardization.

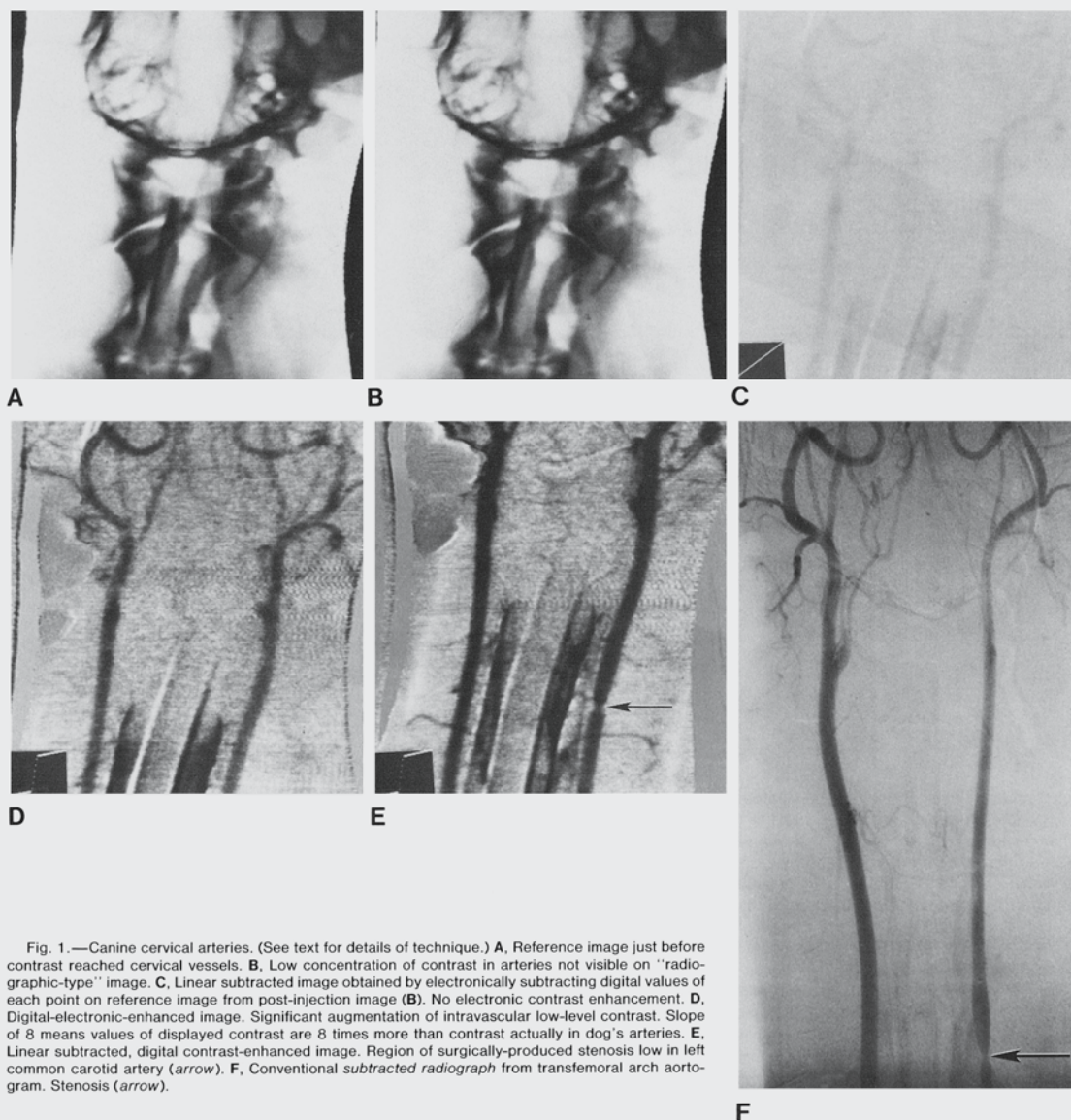


Fig. 1.—Canine cervical arteries. (See text for details of technique.) **A**, Reference image just before contrast reached cervical vessels. **B**, Low concentration of contrast in arteries not visible on "radiographic-type" image. **C**, Linear subtracted image obtained by electronically subtracting digital values of each point on reference image from post-injection image (**B**). No electronic contrast enhancement. **D**, Digital-electronic-enhanced image. Significant augmentation of intravascular low-level contrast. Slope of 8 means values of displayed contrast are 8 times more than contrast actually in dog's arteries. **E**, Linear subtracted, digital contrast-enhanced image. Region of surgically-produced stenosis low in left common carotid artery (arrow). **F**, Conventional subtracted radiograph from transfemoral arch aortogram. Stenosis (arrow).

Image Analysis

A number of clinical studies have been obtained using the technique described above. Analysis of the images of each series begins by selecting the best reference image obtained just before the appearance of contrast material in the cervical vessels. It is then subtracted from each of the remaining images of the study. The subtraction of each sequential image takes about 3 sec. By this method, the images with the best arterial visualization are selected. These images are then subjected to variations in electronic contrast

enhancement and may have some additional image manipulations performed on them (e.g., log subtractions, contrast slope and position manipulations, and, occasionally, edge enhancement). These manipulated images are then stored on the video disc recorder for subsequent display, review, and photography.

The data and graphic section on the lower left of each image (figs. 3–5) shows patient identification data, a description of the type of subtraction done (linear versus log), and a graphic display of the "map" or the slope and position of the electronic enhancement used on that individual image. The abscissa represents the

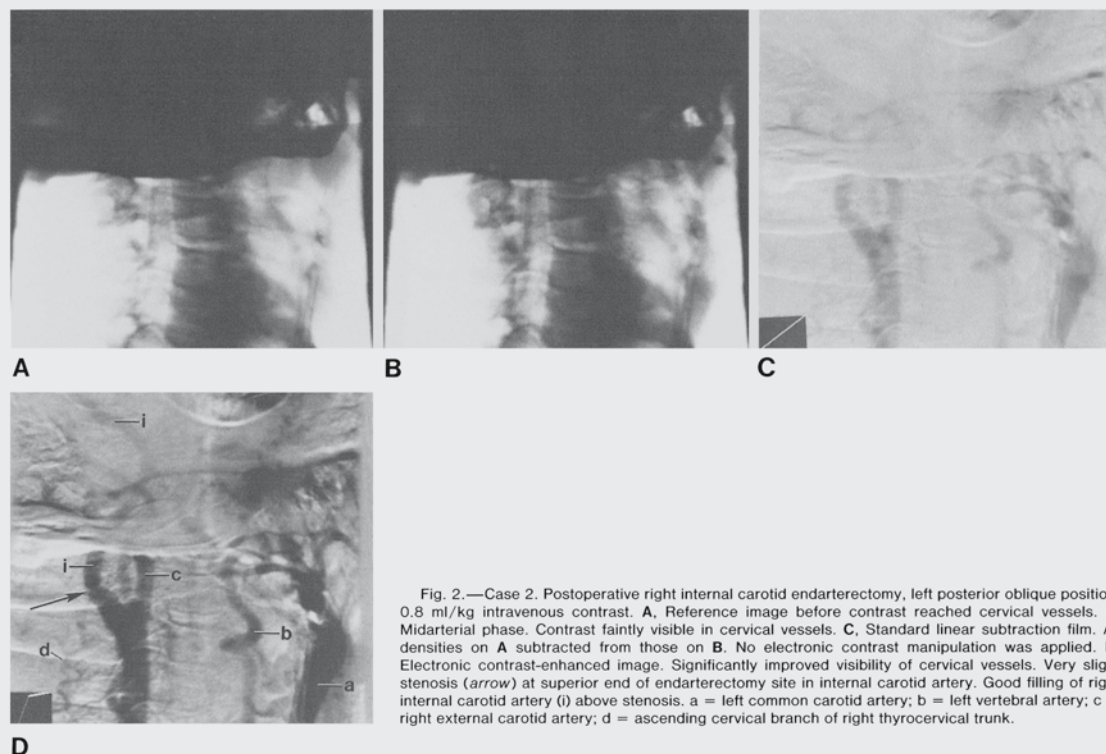


Fig. 2.—Case 2. Postoperative right internal carotid endarterectomy, left posterior oblique position, 0.8 ml/kg intravenous contrast. **A**, Reference image before contrast reached cervical vessels. **B**, Midarterial phase. Contrast faintly visible in cervical vessels. **C**, Standard linear subtraction film. All densities on **A** subtracted from those on **B**. No electronic contrast manipulation was applied. **D**, Electronic contrast-enhanced image. Significantly improved visibility of cervical vessels. Very slight stenosis (arrow) at superior end of endarterectomy site in internal carotid artery. Good filling of right internal carotid artery (i) above stenosis. a = left common carotid artery; b = left vertebral artery; c = right external carotid artery; d = ascending cervical branch of right thyrocervical trunk.

digital value of the electronic contrast material actually present and the ordinate represents the digital value of the electronic contrast enhancement that is displayed. The numerical value after slope refers to the ratio of electronic contrast enhancement displayed/electronic contrast material actually present. The numbers at the bottom of the "map" graph describe the range of numbers contained between the bottom and top parts of the steep part of the map. Varying the slope gradient (steepness) is analogous to changing the window width in CT. A steep slope is equivalent to a narrow CT window setting and produces a high contrast image. Changing the position of this steep part of the map (moving it to the left or to the right) is analogous to changing the position of the center of the CT window. In this system, the slope position and the slope steepness are independent manipulations.

Representative Case Reports

The following cases demonstrate some images achieved with the system and techniques described above and show the results of applying different methods of subtraction and digital image processing.

Case 1

A 32-kg greyhound had a 24 ml bolus of 76% contrast material hand-injected into a foreleg vein (volume equals about 0.75 ml/kg). (All images were photographed directly from the current 512-line

television video display.) The first image (fig. 1A) is the reference or scout image and was obtained before the arrival of contrast material in the cervical vessels. The arterial phase (fig. 1B) shows the contrast material in the arteries that is not seen on this standard radiographic-type image. To achieve a standard linear subtraction (fig. 1C), the digital densities of each point on the reference image are directly subtracted from those on the postcontrast image being studied (fig. 1B). As the densities being subtracted are perfectly numerically balanced, the resultant subtraction is the same as a "second order"-type subtraction done on standard radiographs. The only remaining density is that of the minimal contrast enhancement within the vessels. On the map, the slope is 1 (or 45°), indicating there has been no electronic contrast enhancement or manipulation. Figure 1D demonstrates the significant augmentation of the low-level contrast enhancement within the vessels when the images are displayed with digital-electronic enhancement, as evidenced by the steep slope shown in the map. A relatively steep slope of 8 means the digital value of the output electronic contrast is 8 times the input electronic contrast values.

Using a 1 ml/kg intravenous contrast injection in this same dog, the lower cervical region was studied. One of the linear subtracted, digital contrast-enhanced images (fig. 1E) clearly shows a region of stenosis in the left common carotid artery. This stenosis had been surgically produced in the laboratory. The accompanying image (fig. 1F) is a subtracted radiograph from a transfemoral aortogram using conventional radiography. This stenosis is as easily visualized on the intravenous angiographic study as it is on the standard radiographic intraarterial aortogram. However, the intravenous an-

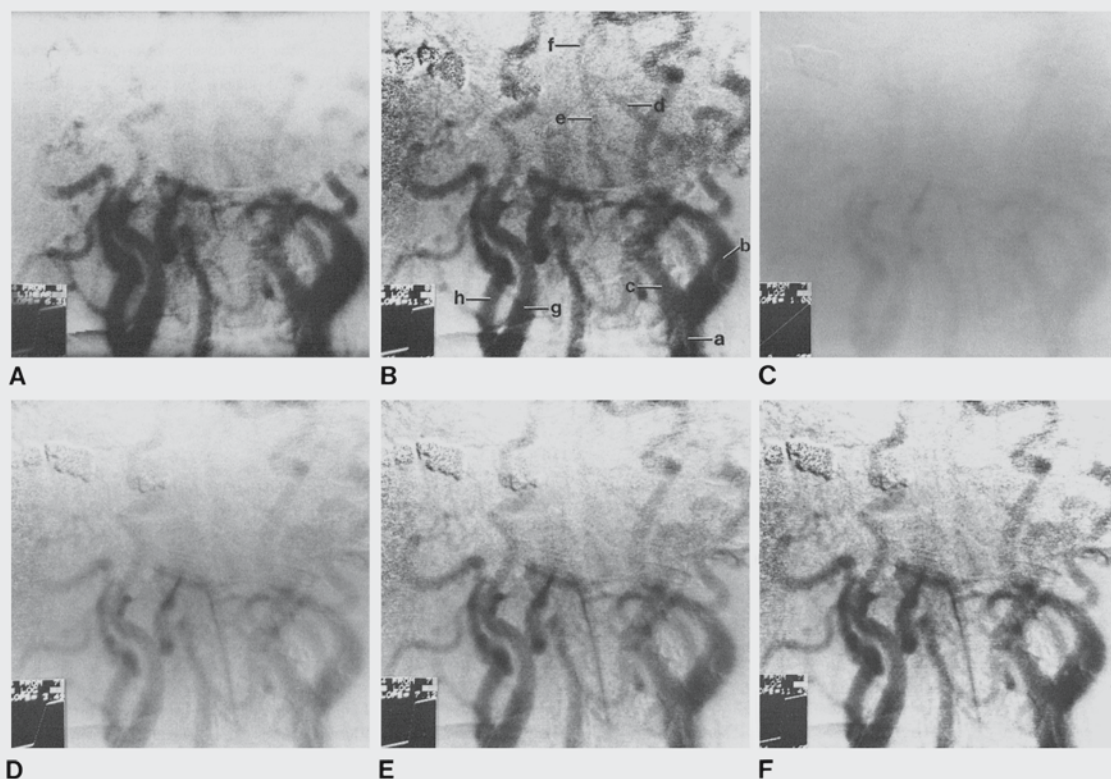


Fig. 3.—Case 3, 68-year-old presurgical patient with suspected stenosis or occlusion in left internal carotid system. Right posterior oblique position, standard amount of intravenous contrast. **A**, Linear, mapped subtraction of cervical vessels. Left and right internal and external carotid arteries well visualized and normal. Parts of vessels superimposed over bone not well seen. **B**, Log-type, mapped subtraction. Significantly improved visibility of vessels superimposed over bone. Left internal carotid artery entirely normal

up to cavernous segment with no stenosis or minor atheromatous irregularity. a = left common carotid artery; b = left internal carotid artery; c = left external carotid artery; d = left vertebral artery; e = right vertebral artery; f = basilar artery; g = right internal carotid artery; h = right external carotid artery. **C-F**, Progressively increased electronic contrast enhancement (slope). Slope of **C** = 1, **D** = 3.49, **E**, = 7.12, and **F** = 11.43. Single, computer manipulation produces substantially improved visibility of arteries.

giogram is much more sensitive to minor degrees of movement compared with standard angiography. There is minimal movement of the trachea in this anesthetized dog on the intravenous angiogram.

Case 2

A 71-year-old white man had recent right cerebral hemispheric transient ischemic attacks. Previous arch angiography demonstrated a 50% stenosis at the right carotid bifurcation. Selective right carotid angiography on this admission demonstrated a 75% stenosis at the origin of the right internal carotid artery with ulceration. The patient had a right proximal internal carotid endarterectomy. On postoperative day 4, the surgeons were interested in the patency of the right internal carotid endarterectomy site, but they did not believe the clinical status warranted a repeat transfemoral angiogram so intravenous angiography was performed.

While in the left posterior oblique position, the patient was injected with 0.8 ml/kg of 76% contrast medium. Figure 2A is the reference image. Intraarterial contrast enhancement is faintly visible in the midarterial phase (fig. 2B). The standard linear subtraction

image (fig. 2C) was obtained by digitally subtracting all the densities on figure 2A from those on figure 2B. Note the 45° slope of the map in the left lower corner of the image, indicating a numerical slope of 1. The results of applying electronic contrast enhancement at the cervical parts of the arteries are now well visualized (fig. 2D). There is a slight stenosis at the superior end of the endarterectomy site, probably of no clinical significance since the filling of the right internal carotid artery above this stenosis is satisfactory. A standard transarterial angiogram was not required and the patient was discharged several days later.

Case 3

A 68-year-old white man needed extensive oral-dental surgery with general anesthesia. Cardiac evaluation because of recent vague, nonspecific neurologic symptoms demonstrated moderate cardiac arrhythmias that were corrected by medical therapy. Doppler ocular sonography and ocular plethysmography (OSM/OPG), however, suggested a significant stenosis in the left internal carotid artery system. The patient and his physicians did not want to proceed with the surgery and general anesthesia without further

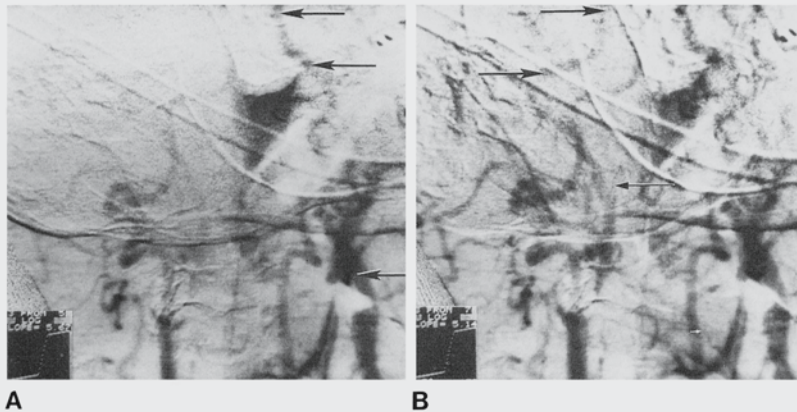


Fig. 4.—Case 4, older man with severe bilateral lower extremity claudication, total absence of all lower and upper extremity pulses, loud right carotid bruit and positive OSM/OPG tests on right. Left posterior oblique position. Logarithmic subtractions with electronic contrast enhancement. Large calcific plaque obscures visualization of proximal right internal carotid artery but good opacification of cervical, petrous, and cavernous left internal carotid artery (arrows). **A**, Minimal filling of right internal carotid artery but good opacification of cervical, petrous, and cavernous left internal carotid artery (arrows). **B**, 2 sec later. Delayed filling of right internal carotid artery (arrows). Probable high-grade stenosis of proximal right internal carotid artery in region obscured by calcific plaque.

evaluation of the internal carotid system. However, his neurologic symptoms had cleared with medical treatment for cardiac arrhythmias and formal transarterial angiography did not seem indicated. Intravenous angiography, however, seemed appropriate for this possible high-risk patient who had no current clinical neurologic symptoms or signs.

As the left carotid artery was of primary interest (positive left OSM/OPG studies), the intravenous angiogram was done with the patient in the right posterior oblique position using the standard amount of contrast medium delivered at a standard rate. The linear subtraction of the cervical vessels was mapped (i.e., the contrast was electronically enhanced) (fig. 3A). The cervical parts of the left and right internal and external carotid arteries are well visualized and entirely normal. However, those parts of the cervical and proximal intracranial vessels superimposed over bone are not well visualized.

To better demonstrate vascular structures that are partly superimposed over soft tissue and partly over bone, a logarithmic-type subtraction was done in which the computer program considered the logarithmic characteristics of the attenuation of x-ray by bone and soft tissue. This produces a more balanced image and improves the visibility of the vessels superimposed over bone. This is well demonstrated in figure 3B, which is a log-type subtraction film. Both carotid bifurcations and internal carotid arteries are excellently visualized up to and slightly above their petrous intracranial segments.

No abnormalities of the left internal carotid artery are evident on this study or on the several other projections. The patient went home for dinner after this outpatient procedure and the next week had general anesthesia and dental surgery without complication.

Figures 3C–3F are examples of the same logarithmic subtracted image (image 7 minus reference image 4) in which the electronic contrast enhancement (map slope) is progressively increased in steepness. They demonstrate the effect this single manipulation has on improving the visibility of arteries on the display TV image.

Case 4

A white man in his late 50's had severe, bilateral, lower extremity claudication. Examination demonstrated total absence of all lower and upper extremity pulses, severe, chronic obstructive pulmonary disease, and a loud right carotid bruit. He had no neurologic symptoms or findings. Noninvasive Doppler and ocular pulse studies

(OSM/OPG) were positive on the right. The surgeons were unwilling to consider major aortic and lower extremity vascular reparative surgery without a carotid study. As no arm or leg vessels were available for transarterial catheterization, intravenous angiography was indicated.

The study was done with the patient in the left posterior oblique position to best demonstrate the right carotid artery. The two logarithmic subtractions with electronic contrast enhancement (figs. 4A and 4B) are separated by 2 sec. A large amount of calcium obscures visualization of the right common carotid artery bifurcation. There is a minimal filling of the right internal carotid artery (fig. 4A) but good opacification of the cervical, petrous, and cavernous parts of the left internal carotid artery. Figure 4B shows definitely more contrast enhancement in the right internal carotid artery. This indicates that the cephalad flow of contrast medium in this artery is significantly slower than that on the left, probably secondary to a high-grade stenosis in the poorly seen, proximal, right internal carotid artery.

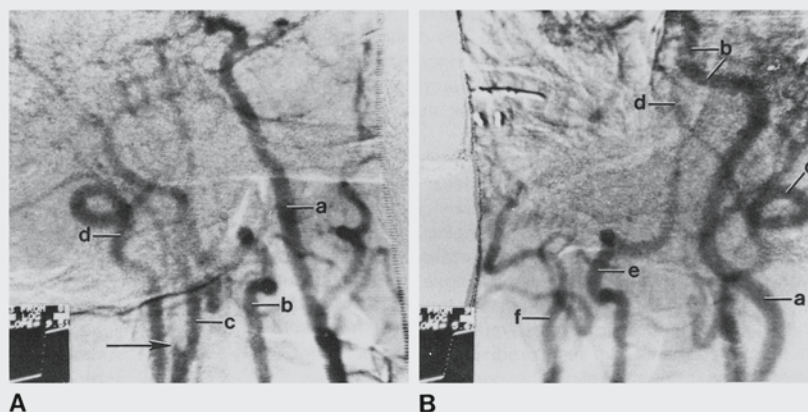
The images on this patient have significant superimposed motion artifacts in the neck and skull secondary to the prominent accessory respiratory muscular movements associated with his severe chronic obstructive pulmonary disease. Because of his compromised pulmonary status and asymptomatic neurologic status, surgery on the right internal carotid artery was deferred until lower extremity vascular reparative surgery is clinically imperative. Repeat intravenous angiography will be done at that time to determine if the right internal carotid artery really became occluded in the interim.

Case 5

A 78-year-old white man had vague "dizzy spells," but no other neurologic symptoms or positive neurologic findings. Later, however, positive right carotid OSM/OPG studies suggested either a high-grade stenosis or occlusion of the right internal carotid artery. In a patient this old with only minor neurologic symptoms and no neurologic deficit, standard transarterial angiography has an inordinately high risk unjustified by either symptoms or findings and intravenous angiography is appropriate.

This study was done first in a left posterior oblique position with standard technique and contrast material. A log-subtracted, mapped image of the cervical and proximal intracranial vessels (fig. 5A) shows complete occlusion of the right internal carotid artery. To confirm this finding, repeat angiography in a right posterior

Fig. 5.—Case 5, 78-year-old man with minor neurologic symptoms, but suspected high-grade stenosis or occlusion of right internal carotid artery. **A**, Left posterior oblique log-subtracted, mapped image of cervical vessels. Complete occlusion (arrow) of right internal carotid artery. a = left internal carotid artery; b = left vertebral artery; c = right external carotid artery; d = right vertebral artery. **B**, Right posterior oblique log-enhanced, mapped image immediately after first series. a = left internal carotid artery, cervical segment; b = left internal carotid artery, petrous and cavernous segments; c = left vertebral artery; d = basilar artery; e = right vertebral artery; f = right external carotid artery, cervical branches.



oblique projection (fig. 5B), also log-subtracted and mapped, demonstrates no visible right internal carotid artery. Right external carotid branches are seen, as are the left internal and external carotid arteries, both vertebral arteries, and the proximal basilar artery.

We concluded that this patient had asymptotically occluded his right internal carotid artery. Intravenous angiography obviated transarterial angiography and its risks in this elderly patient. It also answered the question raised by the positive right carotid OSM/OPG studies of whether this patient had an occlusion or a more dangerous, high-grade stenosis of his right internal carotid artery.

Discussion

Our goal has been to develop a noninvasive method of angiographically visualizing and screening the cervicocerebrovascular system. This was accomplished by using relatively small amounts of peripherally delivered intravenous contrast material. Development of a sophisticated, electronic, video subtraction system capable of displaying the resultant low levels of intravascular contrast agent was the first step. A low-noise video TV camera system for collecting the data is very important. Digitization of the TV image data allows diverse and high-speed manipulations of these images. After successful visualization of cervical and cerebral vessels in animals, we began to apply this technique to humans.

The test is usually done on outpatients and no hospitalization before or after the study is required unless indicated by the results. Patient acceptance has been very good. They have appreciated our attempt to avoid intraarterial catheterization and all have specifically denied any pain associated with the injection of contrast material into the antecubital veins. We have successfully attempted to keep patient manipulation and volumes of contrast medium to a minimum.

Several categories of clinical problems are specifically well addressed by intravenous angiography. Case 2 exemplifies how the effects of surgical or medical therapy for cervical atherosclerotic lesions can be evaluated by this

technique. This postoperative patient with only minimal symptomatology had his endarterectomy site evaluated without using transarterial angiography. Clinical questions about the patency and configuration of the postoperative artery were answered.

A second category of patients needing a screening-type angiographic test comprises those with asymptomatic bruits and positive noninvasive studies that may place them at higher anesthetic and surgical risk, as in case 3. This presurgical patient had a bruit and positive, noninvasive tests suggesting a significant carotid stenosis. The absence of clinical symptoms and neurologic findings were relative contraindications to transarterial angiography making him a good candidate for intravenous angiography. It demonstrated normal carotid arteries and he and his surgeons then confidently proceeded with his anticipated general anesthesia and surgery.

A third important group for which intravenous angiography is an important alternative includes those in whom significant, generalized vascular disease either precludes or presents significant and perhaps hazardous contraindications to transarterial catheterization, such as case 4, who had no palpable femoral or axillary pulses. This patient was also neurologically asymptomatic, another reason for avoiding a transarterial study. In addition, he had such severe pulmonary disease it was questionable whether he could remain supine long enough for a complete, transarterial study. Demonstration of a probable high-grade stenosis in one carotid artery gave the surgeons information pertinent to their preoperative plans for anticipated major aortic surgery.

A fourth group of candidates for intravenous angiography comprises aged patients in whom standard transarterial catheter angiography has a higher morbidity. This is because of increased vessel wall fragility, widespread atherosclerotic involvement with associated pelvic and cervical vessel tortuosity, and marked intimal surface irregularities. The latter predispose to higher possibilities of embolization during catheter manipulation. If these elderly patients have minor neurologic findings or have positive noninvasive tests,

angiographic evaluation is certainly desirable but selective catheterization carries a higher risk. The demonstration in case 5 of a complete occlusion of the right internal carotid artery and a normal left internal carotid artery precluded the necessity for any further angiographic evaluation in this older patient.

One other large and important group of patients that we have not begun to evaluate comprises those currently asymptomatic patients who are at high risk for development of atherosclerotic lesions. Some examples are: (1) patients with poorly controlled or chronic hypertension; (2) patients with insulin-dependent diabetes; (3) those with significant atherosclerotic disease in other parts of the vascular system (heart, kidneys, aortoiliac system); and (4) those with metabolic problems that may predispose to atheromatous disease (hypercholesterolemia, hyperlipidemias, ? obesity).

Our cases have demonstrated several features of current computer data manipulation. The striking increase in visibility of those vessels superimposed over bony structures when logarithmic subtraction is applied to the images is well demonstrated in case 3 (figs. 3A and 3B). This capability is necessary for studying extracranial vessels superimposed over bone and intracranial vessels within and adjacent to the base of the skull. The advantage of obtaining sequential images similar to a standard angiographic series is demonstrated in case 4, which shows delayed flow in the right internal carotid artery. This capability will soon be improved when this system is updated to accepting and digitizing up to 30 frames/sec. The study of cervical and intracranial arteriovenous malformations should be well served with this capability. The importance of high-speed digital computer processing and display of the data is emphasized in case 5, in which the initial intravenous angiogram was processed and displayed, immediately ascertaining the need for another projection. This capability is especially important with this technique because all the cervical and intracranial vessels are simultaneously opacified, and, therefore, are frequently superimposed.

In the clinical application of this technique, we have identified three problem areas not usually encountered with intraarterial angiography. The first, mentioned above, is that of the simultaneous opacification of all cervical and intracranial vessels. Currently, we are altering the patient's position to obtain different projections. In the first clinical unit now being installed, this study will be routinely done biplane, and stereoscopic capability is also planned. The latter will be especially important in intracranial studies. A second prob-

lem is that computer-generated subtraction techniques seem much more sensitive to skeletal and even minor soft tissue movement than standard radiographic subtraction techniques. Currently, software programs for reference image manipulation in two axes are being refined. A third problem related to the second is that any calcification in the arterial wall is in constant motion and the images presented in case 4 show how difficult this is to subtract. Other techniques, currently being developed, will be necessary to address this problem, which is a frequent associated finding in large atheromatous plaques.

Additional angiographic areas may become appropriately studied by intravenous angiography. These include post-operative evaluation of the patency and function of cervical-intracranial arterial bypasses, and follow-up studies of cervical, facial, and possibly intracranial arteriovenous malformations and tumors after surgery or transcatheter therapeutic embolization. With improved image resolution we also hope to follow intracranial aneurysms and the associated arterial spasm after subarachnoid hemorrhage, thereby avoiding repeated transarterial catheterizations.

ACKNOWLEDGMENTS

We thank Deena Neumaier for assistance in manuscript preparation and the Medical Photography and Medical Illustration Sections of the Biomedical Communications Department for assistance in preparation of the medical illustrations.

REFERENCES

1. Ovitt TW, Capp MP, Fisher HD, et al. The development of a digital video subtraction system for intravenous angiography. In: Miller HA, Schmidt EV, Harrison PC, eds. *Non-invasive cardiovascular measurements*, vol 167. Bellingham, WA: Society of Photo-Optical Instrumentation Engineers, 1978:61-65
2. Ovitt TW, Capp MP, Christenson PC, et al. Development of a digital video subtraction system for intravenous angiography. Recent and future developments. In: *Medical imaging II*, vol 206. Bellingham, WA: Society of Photo-Optical Instrumentation Engineers, 1979:73-76
3. Kruger RA, Mistretta C, Houk, T, et al. Computerized fluoroscopy in real time for noninvasive visualization of the cardiovascular system. *Radiology* 1979;130:49-57
4. Ovitt TW, Christenson PC, Fisher HD III, et al. Intravenous angiography using digital video subtraction: x-ray imaging. *AJNR* 1980;1:387-390

4.4 Computed radiography utilizing scanning laser stimulated luminescence

Minoru Sonoda (born 1932)

Minoru Sonoda was born with Japanese nationality on 9 January 1932, in Dalian, China. In 1954 he got his BTec in Industrial Chemistry (Physical Chemistry) from Kyoto University.

From 1954 to 1996 he worked at Fuji Photo Film Co. Ltd (Fujifilm). From 1954 to 1976, he worked in the field of R&D and commercialization of photographic emulsion in the Production Technology Division and Ashigara Research Laboratories of Fujifilm. In 1976 he moved to become a manager at the Fujinomiya factory of Fujifilm and then became the General Manager of the whole Fujinomiya factory during 1980–1983.

During the same period (1976–1983), he started and managed the R&D activities in the Ashigara Research Laboratories of the new diagnostic X-ray imaging system which resulted in the invention of computed radiography. From 1985 to 1989, he was the General Manager of the Ashigara Factory of Fujifilm. From 1989 to 1991 he directed R&D activities on digital imaging equipment for medical imaging, graphic arts and color photographic imaging, etc., as the General Manager of the Miyanodai Technology Development Center of Fujifilm. From 1991 he directed product planning and commercialization of imaging equipment as the General Manager of the Equipment Product Division in the Tokyo headquarters office while leading the company as a Managing Director, a member of the board of Fujifilm. In 1996 he retired from Fujifilm.

Minoru Sonoda was awarded the “Shin-Gijutsu Kaihatsu-sho” (New Technology Development Prize) by the Japanese Society for Medical and Bioengineering (JSMBE), for “the new technology development of computed radiography” in 1983 and the “Okochi Memorial Grand Technology Prize” by the Okochi Memorial Foundation, for “development of the new radiology imaging system” in 1992.



Masao Takano (born 1937)

Professor Masao Takano was born on 30 September 1937, in Kanagawa Prefecture, Japan. He got his B. Ed. in 1961 at the Department of Physics in the Faculty of Education of Yokohama National University.

From 1961 to 1990, he worked at Fuji Photo Film Co. Ltd. (Fujifilm). From 1961 to 1971 he worked as a Researcher at the Ashigara Laboratory of Fujifilm. During this period, his major work was on the physics of image quality evaluation methods for photographic imaging. From 1971 to 1980, he continued his work in this field as Research Manager. In 1975, he joined a basic research research on a new diagnostic X-ray system and later started a project for computed radiography (CR). From 1980 to 1987, he worked as Project Leader for development of CR. During this period, he conducted the first clinical evaluation of CR and headed the development of the first-generation CR product which debuted in Japan, the USA, and Europe in 1983. He headed continuing development of CR products at the Miyanodai Technology Development Center of Fujifilm. In 1987 he moved to the



Equipment Product Division of Fujifilm and headed business and product development of CR as Senior Manager until 1990. From 1991 to 2001, he was a Director, a member of the board of Fuji Medical Systems Co. Ltd. In 2001, he moved to Komazawa Junior College. Presently (2004), he is Professor in the Department of Radiology of Komazawa Junior College.

Masao Takano was awarded the “New Technology Development Prize” by the Japanese Society for Medical and Bioengineering (JSMBE), for “the new technology development of computed radiography” in 1983, the “Persons of health science merits: Commendation by the Minister of Health and Welfare”, for “New X-ray Imaging System” in 1987, the “Okochi Memorial Technology Grand Prize” by the Okochi Memorial Foundation, for “Development of a New Radiology Imaging System” in 1992, the “Special Development Prize” by the Japan Industries Association of Radiological Systems (JIRA), for the “Development of Computed Radiography” in 1997 and the “Persons of scientific and technological merits: Commendation by the Minister of Education, Culture, Sports, Science and Technology”, for “Image Processing System” in 2002.

Junji Miyahara (born 1942)

Professor Junji Miyahara was born on 9 April 1942 in the City of Shimizu, Shizuoka Prefecture, Japan. He got his BSc in Material Science in 1965 and his MSc in 1967 from Nagoya University.

From 1967 to 1970 Miyahara worked as a Researcher at NGK Insulators Ltd.

From 1970 to 1998 he worked as a Researcher at the Fuji Photo Film Co. Ltd. (Fujifilm). During this period, his major works were the development of medical X-ray film and basic researches on photo-stimulable phosphors and their product developments, which are used for computed radiography and digital biomedical imaging systems today. In 1975, he joined a basic research activity on the new diagnostic X-ray system and later a project for computed radiography, and played a major role in the development of the stimulable phosphor plate detector, which nowadays is known as the Imaging Plate. And he contributed to the introduction of CR in the 1980s. Through the 1980s and 1990s he was in charge of imaging material and new imaging device R&D as a Senior Manager at Fujifilm.

From 1998 to 2004, Miyahara worked as a professor at Hitotsubashi University and headed the Innovation Research Center.

Presently (2004), he is Professor in the Management of Science and Technology at the Postgraduate School of Tokyo University of Science.

Awards: 1983: “Shin-Gijutsu Kaihatsu-sho” (New Technology Development Prize) by the Japanese Society for Medical and Bioengineering (JSMBE), for the “new technology development of Computed Radiography”; 1988: “Invention Prize” by the Japan Institute of Invention and Innovation, for “Method and Apparatus for Manufacturing Silver-halide Particles”; 1992: “Okochi Memorial Grand Technology Prize” by the Okochi Memorial Foundation, for “Development of a New Radiology Imaging System”; 1992: “The Special Award of CrSJ” by the Crystallographic Society of Japan, for “Development of the Imaging Plate”; 2000: “The Prize of the Chairman of HATSUMEI KYOKAI (JIII)” by the Japan Institute of Invention and Innovation, for “Invention of the High-sensitivity Biomedical Imaging Method”.



Hisatoyo Kato (born 1944)

Hisatoyo Kato was born on 25 May 1944 in the city of Nagoya, Aichi Prefecture, Japan. He got his BSc in Applied physics in 1967 and his MSc 1969 from the University of Tokyo.

From 1969 to the present, he has been working at Fuji Photo Film Co., Ltd (Fujifilm). From 1969 to 1972, he worked in the Ashigara Factory of Fujifilm. From 1972 to 1974, he temporarily joined Stanford University, CA as a visiting researcher and conducted studies on the applying computer technology to photographic image processing. In 1974, he returned to Fujifilm and worked as a researcher in the Ashigara Research Laboratories. In 1975, he joined a basic research activity on the new diagnostic X-ray system and later a project for computed radiography, and played a major role in the development of the key technologies such as digital image processing and laser scanner. In 1981 he participated in the International Congress of Radiology (ICR) at Brussels, and contributed to the first announcement of the computed radiography technology. In 1981, he moved to Miyandai Technology Development Center of Fujifilm and managed development activities of computed radiography products as a Research Manager and later headed R&D activities of digital image processing as a Senior Manager until 1998. From 1998 to 2000, he directed product planning of imaging equipment as the General Manager of the Product Planning Division of Equipment Product Division in the Tokyo headquarters of Fujifilm. From 2000 to 2003, he directed R&D activities on digital imaging equipment for medical imaging, graphic arts and color photographic imaging, etc., as the General Manager of the Miyandai Technology Development Center.

Presently, he is Deputy General Manager and General Manager of Business Development Division, Research & Development Management Headquarters. From 2003 he has been leading the company as a Director, a member of the board of Fujifilm.

Hisatoyo Kato was awarded the “Shin-Gijutsu Kaihatsu-sho (New Technology Development Prize)” by the Japanese Society for Medical and Bioengineering (JSMBE) for the new technology development of “Computed Radiography” in 1983, the “Okochi Memorial Prize” by the Okochi Memorial Foundation for “Development of New Radiology Imaging System” in 1992, and “The Prize of the Chairman of Hatsume Kyokai” by the Japan Institute of Invention and Innovation for “Invention of High-sensitivity Biomedical Imaging Method” in 2000.



[Reprinted from RADIOLOGY, Vol. 148, No. 3, Pages 833-838, September, 1983.]
Copyright 1983 by the Radiological Society of North America, Incorporated

RADIATION PHYSICS

Minoru Sonoda, M.S.
Masao Takano, M.S.
Junji Miyahara, M.S.
Hisatoyo Kato, M.S.

Computed Radiography Utilizing Scanning Laser Stimulated Luminescence¹

A new system of computed radiography that is based on new concepts and the latest computer technologies has been developed. This system eliminates the drawbacks of conventional screen-film radiography. The basic principle of the system is the conversion of the x-ray energy pattern into digital signals utilizing scanning laser stimulated luminescence (SLSL).

Index terms: Lasers • Radiography, computer-assisted • Radiography, digital • Radiography, instrumentation

Radiology 148: 833-838, September 1983

CONVENTIONAL RADIOGRAPHS are usually produced by combining photographic film with an intensifying screen. The screen converts x-ray energy into light of corresponding intensity, and an image is formed on the exposed film. Thus, the film serves as the image sensor as well as the image display medium. The film must have high performance ability as both the image sensor, which requires high speed and wide latitude, and as the image display medium, which requires good contrast and low noise. Theoretically, however, these performance aspects are mutually conflicting in certain respects, and the film is necessarily designed with compromise, and performance is sacrificed to some degree in both capacities.

Inspired by the success of computed tomography (CT), new methods of radiographic imaging have come into vogue that utilize recent advances in electronics and computer technologies to realize better diagnostic efficacy, and to evolve new diagnostic modalities. These are generally known as digital radiography (1), where the x-ray sensor is mainly either the conventional image intensifier and television-camera combination or the linear array sensor as used in CT. The basic quality of the digital image is not limited by digital processing but in large measure by the performance of the sensor itself in regard to resolving power and signal to noise ratio. Unfortunately, existing sensors are incapable of yielding images with quality comparable to that of the screen-film method.

Other plate-transfer systems such as xeroradiography have been developed to overcome the limitation of the existing sensor technology (2, 3). We have developed a new type of computed radiography in which photostimulable phosphors are used as the memory material for temporarily storing the x-ray image.

MATERIALS AND METHODS

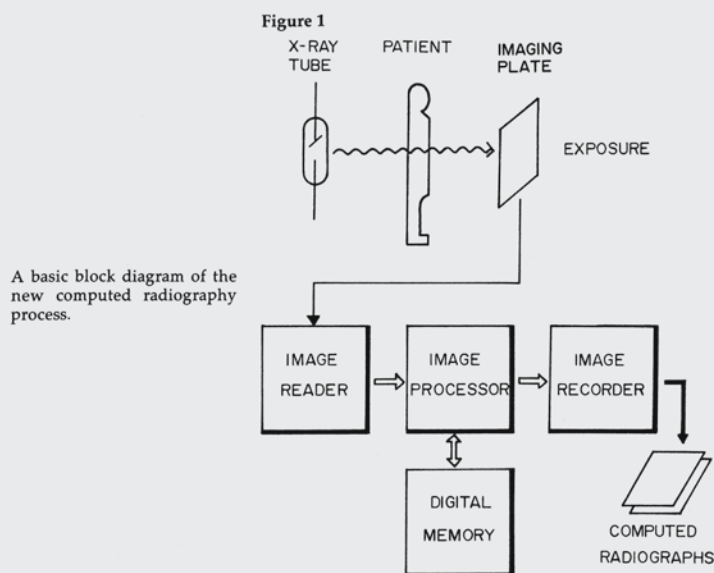
The basic constituents of the system are the image sensor, called the imaging plate in this specific system, which temporarily stores the x-ray energy pattern; the image reader, which converts the latent image on the imaging plate into analog and subsequently digital time-series signals; the image processor, which manipulates the image digitally; and the image recorder, which records the processed signals on a film (Fig. 1).

Imaging Plate

The imaging plate is a flexible plate less than 1-mm thick that is coated with minute crystals of photostimulable phosphor in an organic binder. It can be used to obtain radiographs in exactly the same way as the screen-film combination is used in conventional radiography.

Photostimulable phosphors (4) are capable of storing the energy absorbed in quasistable states when excited by x rays, electrons, ultraviolet rays, etc, and of emitting luminescence radiation corre-

¹ From the Technology Development Center, Miyanodai, Fuji Photo Film Co., Ltd., Kanagawa, Japan. Received Sep. 13, 1982; revision requested Nov. 10; revision received Feb. 15, 1983; accepted March 29. cp



sponding to the absorbed energy when stimulated by visible or infrared radiation. This phenomenon is generally called "photostimulable luminescence" (PSL).

After the x-ray image is stored on the imaging plate, it is scanned with a 633 nanometer (nm) helium-neon laser beam to produce PSL radiation corresponding to the absorbed x-ray energy, and this is then converted to time-series signals by a photodetector. The signal output from the detector is an analog signal as a function of time, and the output from the analog-to-digital converter is the time-series digital signal that is being processed. The most appropriate term to express the system

characteristics is "scanning laser stimulated luminescence" (SLSL).

The imaging plate can be used repeatedly to store x-ray images simply by flooding it with light to erase the residual energy it contains. The expected life of the plate is limited mainly by mechanical damage such as scratches; it is not limited by the physical fatigue of the PSL phenomenon.

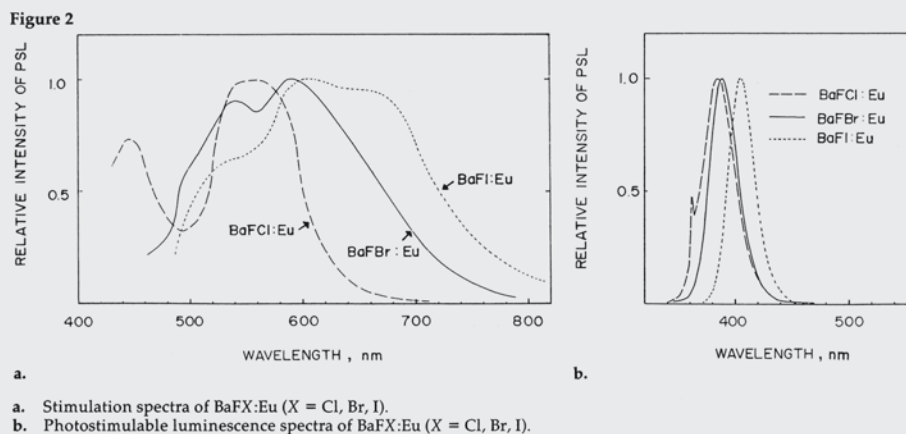
The requisite properties of the imaging plate are as follows: First, it must have high sensitivity in emitting PSL radiation when stimulated by 633 nm of visible light. The emission spectrum should be in the range of 300–500 nm where photomultiplier

tubes have high quantum efficiency. Second, the response time of the PSL must be less than 10 μsec to permit the high speed reading of the image for practical use. Finally, no substantial fading for eight hours (a typical working day) is necessary for practical use.

None of the photostimulable phosphors known can satisfy all of these requisites. We therefore made a search for the ideal photostimulable phosphors and discovered BaFX:Eu (X = Cl, Br, I), europium-activated barium-fluorohalide compounds. By controlling the composition and manufacturing process of these compounds, we were able to make them emit strong PSL radiation. The spectra of the light that stimulate the phosphor, called stimulation spectra, and the spectra of the light emitted as a result of the photostimulable luminescence process, called PSL spectra, are displayed in Figure 2. The stimulation spectrum in the case of X = Br is comparatively wide with its main peak at about 590 nm and a cluster of several peaks at about 530 nm. In the case of X = Cl, the peak shifts to the shorter wavelength, and in the case of X = I, it shifts to the longer wavelength (Fig. 2a). The PSL spectrum in the case of X = Br peaks at about 390 nm, which is interpreted as the luminescence of the Eu^{++} . Shifts similar to that of the stimulation spectrum occur by changing the halogen (Fig. 2b). The response times are 7.0 μsec (X = Cl), 0.8 μsec (X = Br), and 0.6 μsec (X = I). The dynamic range is extremely wide as shown in Figure 3, which means that it can accommodate a wide range of radiographic exposures when it is used as an image sensor.

Image Reader

The stored image must be read by



scanning to convert it into time-series signals. Scanning is performed with a laser beam that is deflected by a scanning mirror while the imaging plate is traversed so as to form an orthogonal scan as illustrated in Figure 4. The luminescence radiation stimulated by the laser scanning is collected through a light guide into a photomultiplier tube (PMT), which converts it into electric signals.

The contrast and energy detectivity of the SLSL system is basically determined by the number of available exposure quanta and its statistical changes in the following processes. The system is composed of cascade random processes (Fig. 5), and these processes are supposed to be ideal, with no loss of detectivity, in so far as each absorbed x-ray quantum is amplified to the sufficient amount of photons and electrons in these processes (5). We designed the system so that the average number of photoelectrons at the PMT cathode would be at least 10 times more than that of absorbed x-ray quanta, by adjusting design parameters such as the stimulation efficiency of the imaging plate, the stimulation energy of the laser, the light collection efficiency of the optics, and the quantum efficiency of the PMT cathode.

The contrast and energy detectivity is therefore determined only by the absorption quantum efficiency of the imaging plate, which is approximately 50% (80 kVp), although it should be more accurately estimated.

Image Processor

The image signals that are sent into the image processor are processed digitally (6,7). The main types of digital processing available are contrast enhancement; spatial frequency enhancement; and digital manipulation of images such as image subtraction, image addition, and functional imaging.

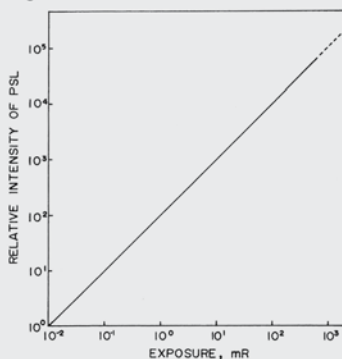
Image Recorder

The image recorder reconverts the processed digital signals back into analog signals that modulate the intensity of another helium-neon laser beam by means of an acousto-optical modulator. The modulated laser beam is then used to scan over a photographic film to imprint the processed image on it. The film is finally developed to produce the computed radiograph.

The specifications of the image reader and recorder (Fig. 6) were determined so that they are capable of producing images that are comparable or superior to those of the conventional screen-film system.

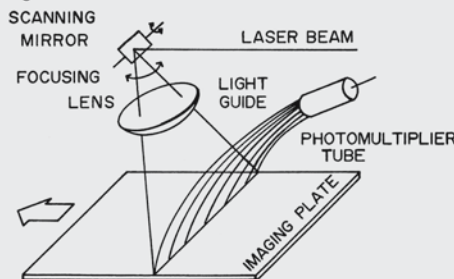
The operating characteristics of the SLSL system are shown in Figure 7. The first quadrant, which is essentially the same as Figure 3, shows the characteristics of the imaging plate. Notice again that the dynamic range is more than $1:10^4$, which means that the imaging plate can accommodate a wide range of radiographic exposures. The second quadrant shows the relationship between the input signals corresponding to the PSL radiation and the output electric signals for the film recording. The sensitivity and dynamic range of the radiation detector are automatically adjusted to the exposure level and exposure range of the stored image so that the digital signals are normalized for a wide range of radiographic exposure conditions. Examples I and II (in Fig. 7, quadrant II) represent higher exposure level/narrower exposure range, and lower exposure level/wider exposure range, respectively. These examples are processed in the computer using different processing conditions (such as Processings I and II, respectively), so that the output

Figure 3



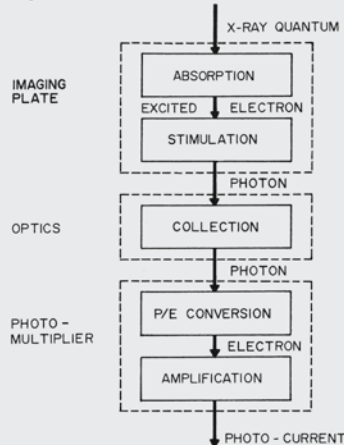
Dynamic range of the imaging plate.

Figure 4



Construction of the image reader.

Figure 5



Statistical analysis of the SLSL system.

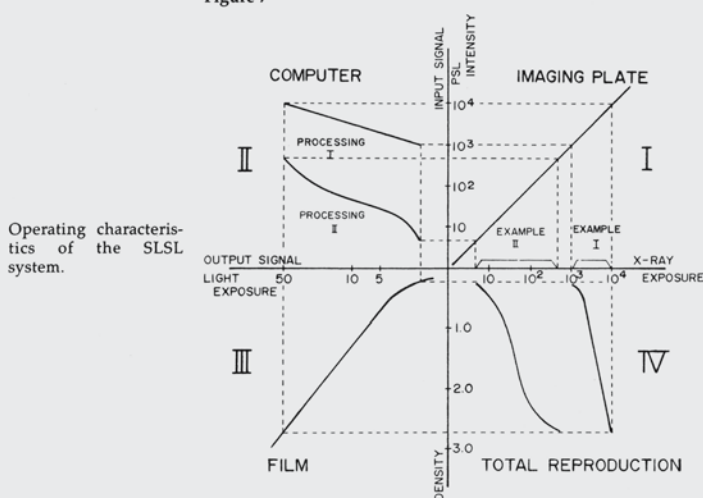
signals occupy the same range. Digital image processing such as contrast enhancement and spatial frequency enhancement can be done at this stage. For example, Processing II has an S-shape gradation as compared with the straight gradation in Processing I. The third quadrant shows the film characteristics. It features high sensitivity at the wavelength of 633 nm, fine grain, and wide exposure latitude for the faithful reproduction of the digital signals. Finally, the fourth quadrant shows a sum of the characteristics in the form of total reproduction curve, *i.e.*, film-density versus x-ray exposure curve. In the screen-film system, only one reproduction curve is available since the sensitivity and dynamic range of the screen-film combination is fixed. Suppose that a screen-film combination is designed for the exposure Example I. The right curve in the fourth quadrant may be the fixed reproduction curve, and it will not fit any

Figure 6

	READER	RECORDER
IMAGE FORMAT	43.2 x 35.6 cm	21.4 x 17.6 cm
	35.6 x 35.6 cm	17.6 x 17.6 cm
	30.5 x 25.4 cm	20.1 x 16.7 cm
	20.3 x 25.4 cm	20.0 x 25.1 cm
SAMPLING RASTER	10 ~ 5 pixels/mm	10 pixels/mm
LASER SPOT SIZE	100 microns	120 microns
GRAY LEVELS	8 bits (A/D)	10 bits (D/A)
SPEED	90 sec for 43.2 x 35.6 cm	90 sec for 21.4 x 17.6 cm
LASER POWER	15 mW	0.1 mW

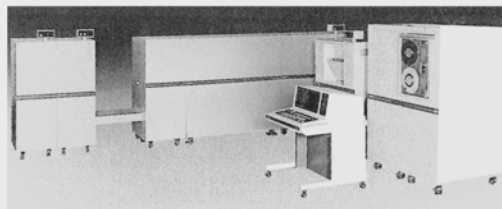
Specifications of the image reader and recorder.

Figure 7



Operating characteristics of the SLSL system.

Figure 8



Overall view of the prototype system.

other type of exposure conditions. In the SLSL system, however, innumerable reproduction curves are possible because of the sensitivity and dynamic range adjustment mechanism of the computer. The left curve in the fourth

quadrant may be one such example; it is adjusted to the exposure Example II. A clear conclusion is that compared with the conventional screen-film system the image reproduction range is much wider and more flexible.

RESULTS

Figure 8 shows an overall view of the prototype units developed for the SLSL system. All that is necessary is to insert the daylight type cassette or magazine containing the exposed imaging plate into the feeder. Image reading and processing conditions can be preset in the computer for full automatic operation. It takes about 90 seconds to read, process, and record the image simultaneously on film in the case of a 43.2 cm x 35.6 cm imaging plate, and another 90 seconds to develop the film; the total processing time is therefore about 180 seconds. Settings for image reading and processing can also be made manually through the console, in which case the digital signals are first recorded on a disc, and then manipulated to change digital processing parameters. The system is currently undergoing evaluation at several clinics.

Figure 9 compares the radiation dosage of conventional and computed radiography and demonstrates the possibility of dosage reduction. Figure 9a was obtained with a medium-speed screen-film combination. Figure 9b was obtained with the SLSL system but with one tenth the dosage used to obtain the conventional radiograph. The exposure can be reduced as much as the sensitivity of the PMT can be raised, but the excessive reduction will result in severe quantum mottle as compared in Figures 9c and 9d. How low the exposure should be would therefore depend on the diagnostic case.

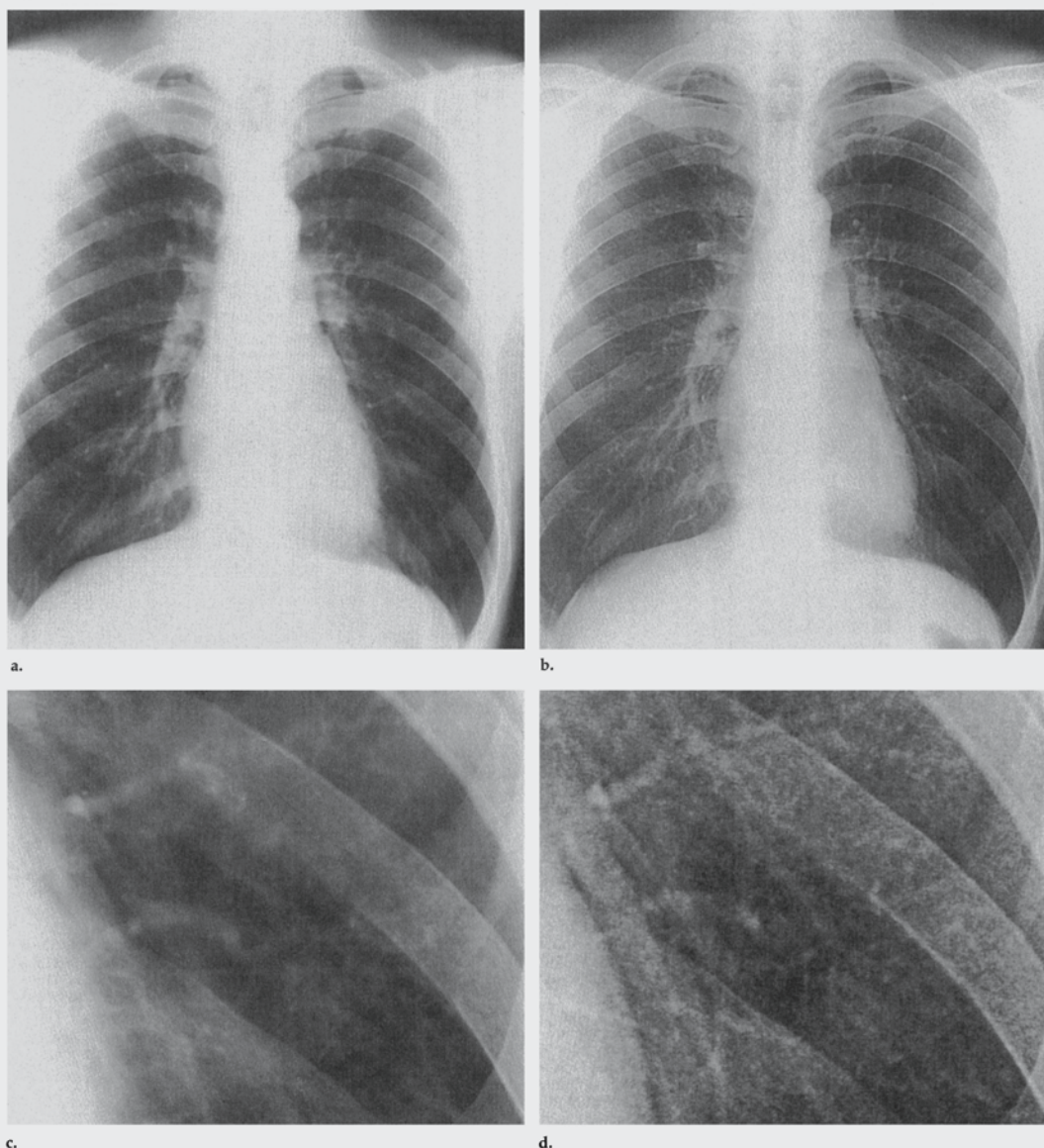
Figure 10 shows a lateral view of the abdomen. Because of the wide latitude and the proper image processing, both soft tissues and bones are clearly demonstrated in the SLSL system (Fig. 10a). The dynamic range of the image in this case is about 1:100, which is far beyond the acceptable range of the conventional screen-film radiograph (Fig. 10b). The spatial frequency enhancement in Figure 10a peaks in the vicinity of 0.5 cycles/mm.

Digital subtraction angiography can also be performed in the SLSL system. In this case, two images stored on separate imaging plates, one obtained before and another after injection of contrast material, are converted into digital signals and then subtracted from each other after the digital position-matching is carried out.

DISCUSSION

Computed radiography is a digital system and the first stage of development has just been completed. It is a possible replacement for some of the conventional screen-film methods, and

Figure 9



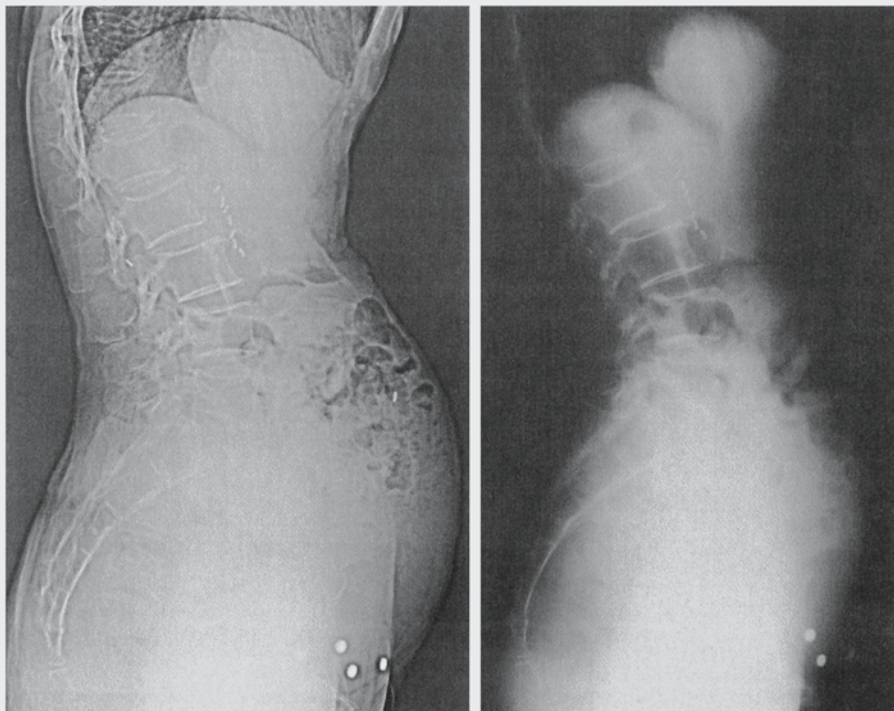
- a. A conventional screen-film radiograph. Exposure settings were 80 kVp, 7.7 mAs, 150 cm FFD, and grid 8:1.34 1/cm. The entrance exposure was 20 mR (5.16 μ C/kg). Fuji RX film and Fuji Hi-screen were used.
- b. A new computed radiograph. Exposure settings were 80 kVp, 0.64 mAs, 150 cm FFD, and grid 8:1.34 1/cm. The skin dosage was one-tenth of that used in obtaining the radiograph in Fig. 9a. The spatial frequency enhancement in the vicinity of 0.25 cycles/mm was performed.
- c. Enlarged portion of Fig. 9a.
- d. Enlarged portion of Fig. 9b.

it will open up new diagnostic modalities by taking advantage of the new technologies. For instance, the digitally processed image is presently reproduced on a photographic film, but de-

pending on the case, it could be projected on a CRT screen to meet various diagnostic requirements. The imaging plate and the image reader could be built into the x-ray stand or bed to re-

alize immediate conversion of the x-ray pattern into digital signals that would then be transmitted to a central reading room for image processing and reproduction. Radiographs could be per-

Figure 10



a.

a. A new computed radiograph.

b.

b. A conventional screen-film radiograph. Both radiographs were obtained under the same exposure settings of 95 kVp, 30 mAs, 120 cm FFD, and grid 10:1.40 1/cm. The entrance exposure was 350 mR (90.3 $\mu\text{C/kg}$).

manently stored on a digital memory disc so that radiographic film could be destroyed for silver recovery.

In the future, it has the potential of developing into a total radiographic filing system employing a large scale memory on optical discs to facilitate the exchange of medical images and information between hospitals.

Minoru Sonoda, M.S.
Fuji Photo Film Co., Ltd.
Technology Development Center, Miyanodai
Kaiseimachi, Ashigarakamigun
Kanagawa 258, Japan

References

1. Arnold BA, Eisenberg H, Borger D, Metherell A. Digital radiography: an overview. Application of Optical Instrumentation in Medicine IX. SPIE 1981; 273:215-226.
2. Boag JW. Xeroradiography. *Phys Med Biol* 1973; 18:3-37.
3. Lothar SJ, Klynn LM. Electronic recording of x-ray images. *J Applied Photographic Engineering* 1979; 5:183-189.
4. Leverenz HW. *An Introduction to Luminescence of Solids*. New York: Dover Publications, 1968:150.
5. Dainty JC, Shaw R. *Image Science*. London: Academic Press, 1974:172.
6. Ishida M, Kato H. Improvement of diagnostic quality of radiographic images by using image processing technique. Presented at the International Conference on Electronic Imaging (SPSE), Washington, DC, November 1980.
7. Ishida M, Kato H, Doi K, Frank PH. Development of a new digital radiographic image processing system. Application of Optical Instrumentation in Medicine X SPIE 1982; 347:42-48.

4.5 Digital radiography of the chest: clinical experience with a prototype unit

Robert Gordon Fraser (1921–2002)

Robert Gordon Fraser was born in Winnipeg, Manitoba, Canada on 30 June 1921. Dr. Fraser was educated at Upper Canada College (1929–1938), the University of Toronto (1939) and the University of Manitoba Medical School (1940–1945), where he got his MD. Much of his academic career was spent at McGill University in Montreal, where he became Chairman of Radiology (1971–1976); in 1976 he moved to Birmingham, where he was Professor of Diagnostic Radiology at the University of Alabama (1976–1988). He became Professor Emeritus in 1988.

Dr. Fraser was appointed Fellow of the American College of Radiology (1971) and the American College of Chest Physicians (1983). The Royal College of Radiology, UK awarded him their Honorary Fellowship in 1984. He was a gold medallist and a “living legend” of the Radiological Society of North America (1990) and the American Roentgen Ray Society (1989). He was appointed visiting Professor in Perpetuity at the University of Santiago de Compostela, Spain (1991) and was awarded Honorary Doctor of Science at McGill University (1992).

Dr. Fraser was also former president of the Canadian Association of Radiologists and a co-founder of the Fleischner Society, an International Interdisciplinary Society dedicated to studies of the chest.

He published 67 original papers, 7 books and 12 book chapters.

Dr. Robert Gordon Fraser died on 12 April 2002.

Picture courtesy Sheila M Wright, Department of Radiology, University of Alabama at Birmingham, 2004.



E. Breatnach

G.T. Barnes

Robert G. Fraser, M.D.
Eamann Breatnach, M.D.
Gary T. Barnes, Ph.D.

A prototype digital unit dedicated to chest radiography was used to examine 50 selected patients for a comparison study of the capability of digital images and conventional chest radiographs to reveal normal anatomic structures and a variety of pathologic states. The images in both modes were submitted for interpretation to seven experienced radiologists and a standardized questionnaire completed for each. Visibility of seven anatomic structures in the mediastinum was consistently better on the digital images than on the conventional radiographs. With minor exceptions, pathologic states were equally well seen in the two systems. Despite the less familiar viewing format of the digital images, the mean confidence levels achieved were higher than for those on the conventional radiographs; this difference was statistically significant both for normal anatomic structures ($p = 0.001$) and pathologic states ($p = 0.01$). The advantages and disadvantages of the digital technique are discussed.

Index terms: Radiography, digital • Thorax, radiography, 6(0).110

Radiology 148: 1-5, July 1983

¹ From the Department of Diagnostic Radiology, Hospitals of the University of Alabama in Birmingham, Birmingham, AL. Presented at the Sixty-eighth Scientific Assembly and Annual Meeting of the Radiological Society of North America, Chicago, IL, Nov. 28-Dec. 3, 1982. Received Nov. 26, 1982; accepted and revision requested Jan. 11, 1983; revision received Jan. 31, 1983.

See also the paper by Tesic *et al.* (pp. 259-264) in this issue.

ht

DIAGNOSTIC RADIOLOGY

Digital Radiography of the Chest: Clinical Experience with a Prototype Unit¹

SINCE February 1982, a prototype digital unit dedicated to chest radiography (designed and constructed by Picker International, Cleveland, OH) has been on clinical trial in the Department of Diagnostic Radiology of the Medical Center of the University of Alabama in Birmingham. Over a six-month period, approximately 400 patients have been examined; all examinations were governed by a strict investigational "human-use" protocol and patient acquiescence was almost universal. All patients underwent conventional chest radiography on a dedicated high-kV chest unit followed within minutes by identical projections obtained on the digital unit across the hall.

We report the results of a study designed to compare the capability of digital images and conventional chest radiographs to reveal normal anatomic structures and a variety of pathologic states.

METHODS AND MATERIALS

Apparatus

The operational principles and physical performance characteristics of the apparatus have been described in detail elsewhere (1-3). Briefly, the unit employs a vertical x-ray fan beam that scans transversely across the patient. The beam is defined by a 0.5-mm fore-slit collimator positioned between the x-ray tube and the patient, and a 1.0-mm aft-slit collimator positioned between the patient and detector array (Fig. 1). After traversing the patient and aft-slit collimator, the x-ray beam strikes a vertically oriented linear detector array that consists of 1,024 photodiodes coupled to a gadolinium oxysulfide screen. The diodes measure 0.5 mm and are contiguous, resulting in a total array length of 512 mm (1,024 pixels) or 20 inches. An equal number of horizontal values is obtained by sampling the pixels over a transverse scan of 20 inches. The photodiode signals are initially digitized with 12-bit precision by analog-to-digital converters and are later compressed to 8 bits. The x-ray tube, collimator slits, and detector array are mechanically linked together and scan across the patient in 4.5 seconds. The gantry that houses these elements offers convenience for erect patient positioning, the tube and detector assembly being raised or lowered to accommodate patients of different height.

The viewing console consists of four 525-line cathode ray tube (CRT) monitors, one for communication with the computer and three for displaying images: one in posteroanterior projection, one in lateral projection, and the third providing a two-times magnification zoom image of any selected region of either projection. Assuming the size of conventional radiographic images as 100%, the dimensions of the standard CRT images were 42% and of the 2 × magnification images 84%. Images appear on the monitors within four seconds of radiographic exposure and can be viewed in either the negative (traditional radiographic) or positive (reverse) phase (Fig. 2). Density and

Figure 1

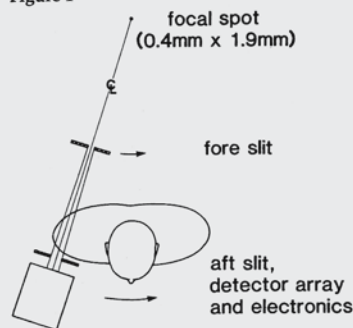


Diagram of the alignment of x-ray tube, fore-slit collimator, patient, aft-slit collimator, and detector array viewed from above. The line extending from the tube to the detectors represents the vertical x-ray fan beam.

brightness levels can be varied by window and level settings much the same as on computed tomographic apparatus (Fig. 3). Film copies of the CRT images in either the negative or positive phase can be made on an experimental multiformat camera.

Scatter is virtually nonexistent, in contrast to conventional screen-film systems. Entrance skin exposures of the digital system (approximately 25 mR [6.45×10^{-3} mC/kg]) are roughly double those of the conventional system.

Methods

From the approximately 400 patients examined, 50 were selected whose conventional radiographs displayed a variety of appearances, including no abnormality and a wide range of pathologic states. All patients were ambulant and the majority were hospitalized; there were 34 men and 16 women ranging in age from 20 to 58 years (the protocol excluded patients under 18 years of age).

The images in both modes were randomized, arranged in groups of seven, and submitted for interpretation to seven experienced, board-certified radiologists; only two of the seven observers (R.G.F. and E.B.) had any input into the selection of the 50 patients being studied or had any knowledge of the ratio of normal to abnormal cases. At each viewing session, 14 pairs of images, seven digital and seven conventional, were viewed and a standardized questionnaire completed for each. The questionnaire consisted of two parts, the first dealing with normal anatomic structures and the second with pathologic states. The visibility of seven normal anatomic structures was stated to be complete, partial, or none,

and each observation was given a confidence level ranging from one to three. Fourteen questions related to the presence of disease; specific pathologic states were identified on the questionnaire, and the reviewers were required to state presence or absence, again with confidence levels. Radiographic abnormalities included a number of readily identifiable high-contrast opacities (e.g., atelectasis, pleural effusion, large masses) and a range of more subtle abnormalities of finer definition (e.g., septal lines, oligemia, small nodules). All patient identity was obscured.

Viewing conditions were standardized and an unbiased observer was present at each reading session. Prior to the performance of the actual study, each observer took part in two pilot study sessions in which 14 digital and conventional radiographic examinations were reviewed to familiarize viewers with the operation of the digital apparatus, to standardize descriptive terminology, and to optimize the format of the questionnaire.

RESULTS

For each question asked on the questionnaire, there were 350 responses in each mode (50 patients \times seven viewers). The results are plotted in two bar diagrams, one for normal anatomic structures (Fig. 4) and the other for pathologic states (Fig. 5). The results can be summarized as follows.

Visibility of the seven anatomic structures in the mediastinum was consistently better on the digital images than on the conventional radiographs. In each case, the difference was statistically significant. The improvement was clearly attributable to the facility of digital image manipulation through the window/level capability and the resultant increase in exposure latitude and low-contrast detectability.

With minor exceptions, pathologic states were equally well seen in the two systems and in no case was the difference in detectability of abnormalities greater than would be anticipated from interobserver variability.

For each observation made on both the digital images and conventional radiographs a confidence level ranging from one (low) to three (high) was recorded. Despite the less familiar viewing format of the digital images, the mean confidence levels achieved were higher than for those on the conventional radiographs. This difference was statistically significant for both normal anatomic structures ($p = 0.001$) and pathologic states ($p = 0.01$).

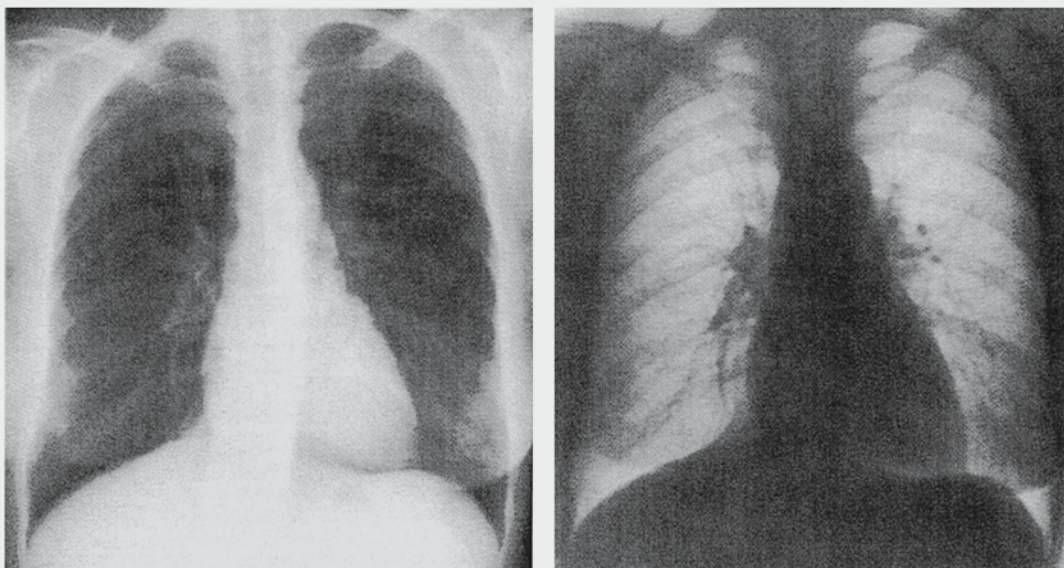
DISCUSSION

Certain aspects of the methodology of the study deserve comment. First, selection of patients was based on findings on conventional chest radiographs, a technique that introduced bias in favor of that mode of examination. However, this method was considered justified in order to include as wide a spectrum of radiographic appearances as possible within the sample of 50 patients; to have selected 50 patients at random would surely have introduced into the group an unreasonable number of normal subjects. Second, comparison between the two systems was not based on a specific truth-data requirement, as it was thought better to have questionable truth on a reasonable representative sample than to have highly accurate truth on the grossly distorted sample that would have been available were pathologic proof required (4). Third, a committee of excellence as a method for establishing truth was considered inappropriate because of the controversial nature of such strategy; rather, we considered that the reliability of results could be based on the comparative nature of the study itself and on the validity of response of seven certified and experienced radiologists who were seeing the same patients in the two systems. Differences in observer interpretation with regard to the completion of the questionnaire were minimized by initial discussion of exactly what was meant by each question and by the performance of two pilot studies, the results of which were discussed fully with each observer.

As might be expected, there was some variability in the technical quality of the conventional radiographs because of differences in patient weight and body habitus; three of the 50 patients in the study required repeat exposures for technical reasons. By contrast, none of the digital examinations had to be repeated, and, in fact, the digital images were of remarkably uniform technical quality; an image that initially appeared overexposed or underexposed could be rapidly brought to levels of ideal density and brightness by varying the window and level settings. Despite the 4.5-second scan time, heart motion was seldom if ever a problem, being minimized by the vertical beam geometry and a 9-msec regional beam transit time (beam width divided by scan velocity).

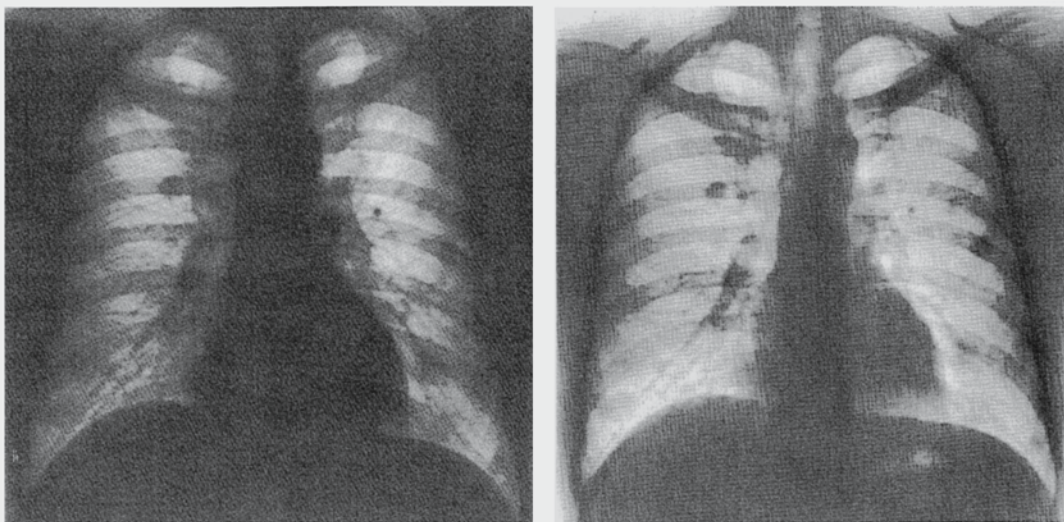
We were concerned about the facility with which the observers would adapt to the new format of viewing images on CRT monitors, although some of them had had considerable experience with computed tomography. In fact,

Figure 2



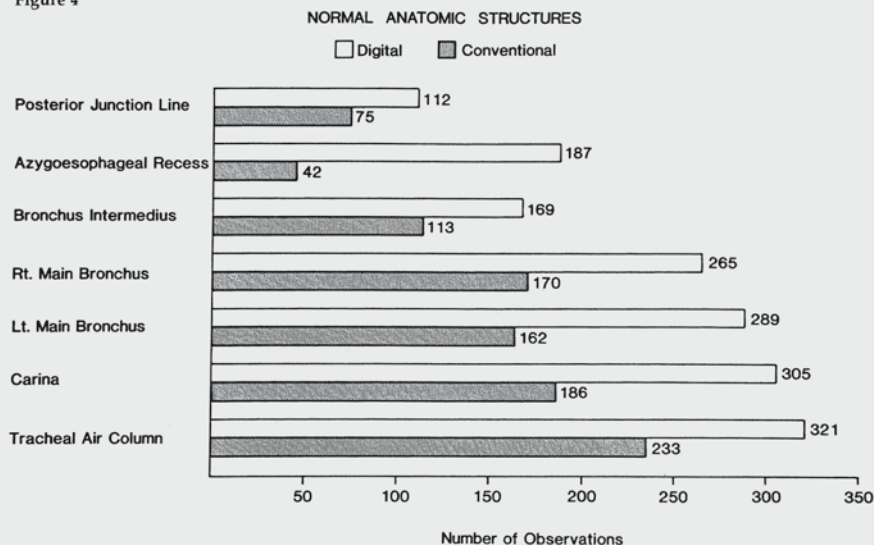
a. Digital images of the chest in posteroanterior projection reproduced in the negative (traditional) phase (a) and the positive (reverse) phase (b).

Figure 3



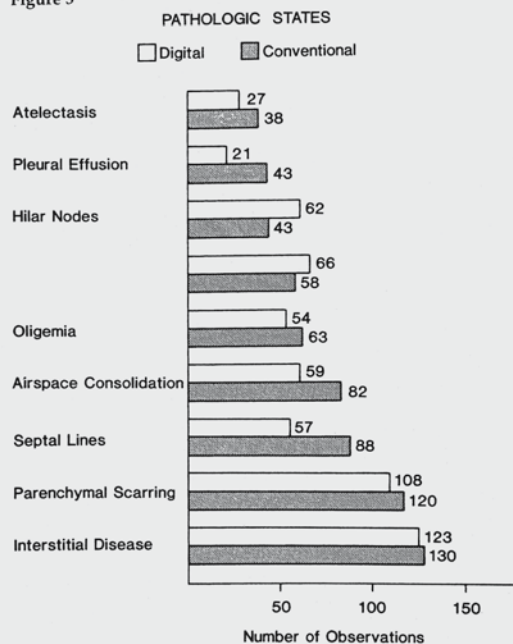
a. Digital images of the chest of a 25-year-old man with metastatic teratocarcinoma. The window and level settings in a were manipulated to depict the lungs to best advantage whereas those in b were modified to permit penetration of the mediastinum. In b, note the improved visibility of the trachea and main bronchi and of the large nodule behind the heart on the left.

Figure 4



Bar diagram comparing visibility of seven normal anatomic structures (listed along the ordinate) on digital images and conventional radiographs. A maximum of 350 observations was possible for each anatomic structure. See text for discussion.

Figure 5



Bar diagram comparing visibility of nine pathologic states (listed along the ordinate) on digital images and conventional radiographs. Although up to 350 observations were possible for each, in no case did the incidence of each pathologic state exceed 150 observations. See text for discussion.

this did not prove to be a major problem; all observers experienced relatively easy transition from the conventional mode of viewing radiographs to the CRT images. Throughout the study, records were kept of the duration of each phase of the study for each observer, and it was shown that the average viewing time for a group of seven pairs of digital images was 32 minutes (approximately 4 minutes/pair), compared with 22 minutes (approximately 3 minutes/pair) for the same number of conventional radiographs; it is important to note that these figures include the time consumed in completing the questionnaires for each pair of images. After an initial period of adaptation the time requirement for viewing digital images was substantially reduced; however, it is clear that despite improvements planned in the speed of image retrieval, viewing times for a pair of digital images will almost certainly remain greater than for conventional radiographs. This is due to the facility for manipulation available with the digital images, the use of which is inevitably time consuming.

Images on the CRT monitors could be viewed in either the negative (lungs black) or positive (lungs white) phase (Fig. 2), and it was rather surprising that the majority of observers favored the latter mode. The reasons for this

preference are not clear but appear to be entirely subjective; it was remarkable how much easier it was to appreciate minor changes in contrast on the positive than on the negative images, particularly shadows of low contrast.

In summary, advantages of the digital system include: improved exposure latitude and low-contrast detectability; scatter-free images; digital image format and prompt image reconstruction and manipulation; and reduced film consumption. Disadvantages include: decreased resolution (1 cy/mm); a long scan time (4.5 sec); increased tube loading; and a skin dose that is roughly double that of conventional radiographic techniques (although still within regulation limits).

Acknowledgments: In addition to two of the three authors, the participating radiologists included Doctors Sang Han, Rodrigo Luna, Charles Ochs, Eva Rubin, and Jack Tishler, whose display of devotion and good humor throughout their rather tedious assignments was much appreciated. We also acknowledge the support of the many physicians and surgeons of UAB who readily gave their permission to include their patients in the study. Throughout the investigation, Ms. Sarah Young exhibited patience and expertise in her capacity as radiographer and her devotion is sincerely appreciated. Ms. Shelley McCain typed the manuscript and helped in many other ways. We are indebted to Dr. Harold Kundell who gave invaluable advice on the design of the protocol and to Dr. Alfred Bartolucci and Mr. Robert Williams for patient guidance and assistance in the statistical analysis.

References

1. Mattson RA, Sones RA, Stickney JB, Tesic MM, Barnes GT. Design and physical characteristics of a digital chest unit. *Digital Radiography Proc. SPIE* 1981; 314:160-163.
2. Tesic MM, Mattson RA, Barnes GT, Sones RA, Stickney JB. Digital radiography of the chest: Design features and considerations for a prototype unit. *Radiology* 1983; 148:259-264.
3. Sones RA, Tesic MM, Barnes GT. Performance evaluation of a prototype digital chest unit. Submitted to *Radiology*.
4. Swets JA, Pickett RM. *Evaluation of diagnostic systems: methods from signal detection theory*. New York: Academic Press, 1982: 140.

Department of Diagnostic Radiology
Medical Center, University of Alabama in
Birmingham
619 19th Street South
Birmingham, AL 35233

4.6 A new digital detector for projection radiography

Denny L.Y. Lee (born 1945)

Denny Lee was born on 7 February 1945 in the Guang Tung province of China. He completed his undergraduate study in Physics at the Hong Kong Baptist College in 1967 and his PhD in Physics at the University of Houston in the USA in 1970.

Denny Lee continued his postdoctoral research at the University of Houston from 1970 to 1976 and also taught as a Visiting Assistant Professor. He also collaborated with the Physics Department of Rice University looking at the interactions between high-energy pions and matter. This research led to his first three US patents in the area of position-sensitive radiation detection instrumentation and methods.

From 1976 to 1979 Lee was employed at Hycel Inc. in Houston, first as a Research Scientist and later as Research Director. Hycel Inc. was in the business of manufacturing clinical analyzers for the life sciences and health care fields.

In 1979 he accepted the position of Research Coordinator at New England Nuclear (NEN), a Massachusetts company manufacturing radioisotopes for use in research and medical imaging. At NEN he received the NEN Prize for Exceptional Achievement for his work in cyclotron technology related to the increase of thallium-201 isotope production yield and for the reduction of radiation dose in cyclotron operation. In 1982 NEN was acquired by the E.I. DuPont de Nemours Company of Delaware. Dr. Lee continued his research in the imaging side of nuclear medicine and received several US patents during this period. In 1985 he joined the newly formed Electronic Imaging Research Group of DuPont in Delaware. He was appointed as a Research Associate and was promoted to Senior Research Associate and finally to Research Fellow in this DuPont organization.

In 1990 DuPont's Medical Product division started a project to develop a flat panel digital X-ray detector to replace the conventional film/screen combination. Together with Dr. Lothar Jeromin, who joined DuPont from Xerox Medical System, they Dr. Lee a research team to investigate these new digital X-ray-imaging technologies. They focused on the conversion of X-ray energy directly to electrical charge using selenium and capturing the image information with a thin-film-transistor (TFT) array, and they obtained their first 5 x 5 cm X-ray image in 1993. In 1995 they published a high-resolution image of a complete hand in this SPIE article.

In 1996 DuPont divested the Medical Product Division to Sterling Diagnostic Imaging, where Denny Lee became Vice President, Advanced Technology. At Sterling, he contributed to the development of X-ray imaging products based on the newly invented direct conversion technology of which he is a co-inventor. In 1999 Hologic Inc. of Massachusetts acquired this product line and technology and Dr. Lee continued in the role of V.P., Advanced Technology.

Today, Dr. Lee's research continues to focus on improvements to the direct conversion X-ray imaging process. With the distinct advantage of preserving high spatial resolution using direct conversion materials, Dr. Lee believes that the direct conversion technology could one day push the performance of digital X-ray imaging to the quantum limit allowed by physics.

Picture courtesy Denny Lee, PhD 2004.



Lawrence K. Cheung

Lawrence K. Cheung is a solid-state physicist who has been engaged in the research and development of imaging materials, devices, and systems for over 30 years. He received his BS degree from U.C. Berkeley, and his PhD degree from Harvard University in 1973.

From 1977 to 1985, he worked at the Xerox research laboratory and technology centre in Webster, New York. During that time, he performed experiments and modeling related to photoconductor materials and electro-photography systems.

From 1985 to 1991, he was engaged in applied research activities at the Electronic Imaging Department of Dupont in Wilmington, Delaware. His work was focused on color imaging mechanisms and digital color printing systems.

In 1991, he started working in the field of digital X-ray detectors and thin-film transistors at the Medical Products Department of Dupont. In 1999, this direct digital radiography effort became part of Hologic, Inc. Dr. Cheung was a co-inventor of the DirectRay digital radiography technology. He has co-authored many publications and patents in this field.

He is currently a Principal Scientist in the Advanced Technologies Department in Hologic, Newark, Delaware.

Picture courtesy Lawrence Cheung, PhD, 2004.

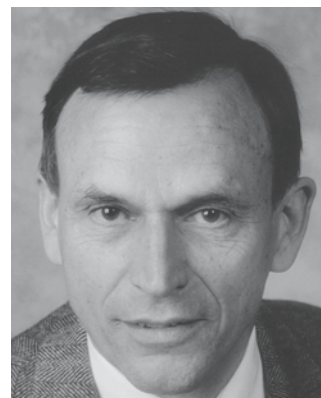


Lothar Siegfried Max Jeromin (born 1942)

Dr. Lothar Jeromin was born on 6 July 1942 in Neumalken, East Prussia in Germany. In 1966 he graduated from the Fach-Hochschule Wedel, Germany as a Diplom Ingenieur (FH) in Engineering Physics. In 1968, after a two-year employment with Phillips Research Laboratory in Hamburg, Germany as a Research Engineer in the field of electrostatic printing, Dr. Jeromin moved to the USA and received a Master of Science in Systems Engineering from West Coast University, Los Angeles, California in 1971. He obtained an Executive Master of Business Administration (EMBA) in 1982 and a Ph.D. in Executive Management in 1984, both from Claremont Graduate University, Claremont, California.

Dr. Jeromin began his career in the USA in 1968 as a Development Engineer at Xerox Medical Systems, Pasadena in California. At Xerox Medical he was instrumental in developing xeroradiographic products for mammography and intra-oral dental radiography based on selenium photoconductor plates. In 1973 he was given his first technical management position. His leadership and innovative style were recognized in 1980 with the Xerox President's Award. Dr. Jeromin's managerial responsibilities expanded until he became Manager of Development and Engineering in 1986. In this role he worked with numerous radiologists to improve the image quality of xeromammograms and to develop new products. This work led to the first prototype of a digital X-ray system in which the charge image on the surface of a selenium plate was read out with an electrometer scanner.

In 1990 Dr. Jeromin joined E.I. DuPont de Nemours' Diagnostic Imaging division in Wilmington, Delaware as a Senior Research Fellow to initiate and to lead their flat panel digital X-ray detector development project. The breakthrough for the research team occurred when the idea to deposit selenium directly on an amorphous silicon thin-film transistor array was translated into practice in 1993. The novel structure of selenium on an a-Si TFT array permitted the readout of the charge image in a self-scanning fashion such that an image reader like in computed radiography was no longer needed. Dr. Jeromin is a co-inventor of this first di-



rect conversion flat panel detector for digital projection radiography. In 1996 this detector technology, trade-named Direct Radiography, was acquired by Sterling Diagnostic Imaging, where Dr. Jeromin became Vice President, Development and Engineering. He continued in that role at Hologic, Inc. when the company became the new owner of Sterling's Direct Radiography Corp. in 1999. He remained involved in the production of digital products for general radiography, non-destructive testing, and mammography, all using the selenium detector until his retirement in 2003. Following retirement he continues to consult for Hologic, helping with technical problems and working on expanding the applications of Direct Radiography.

Picture courtesy Lothar Jeromin, PhD, 2004.

PROCEEDINGS REPRINT



SPIE—The International Society for Optical Engineering

Reprinted from

Medical Imaging 1995

Physics of Medical Imaging

26–27 February 1995
San Diego, California



Volume 2432

A New Digital Detector for Projection Radiography

Denny L. Lee, Lawrence K. Cheung, Lothar S. Jeromin

E. I. DuPont de Nemours & Co., Medical Products Department
Experimental Station, E357
Wilmington, DE 19880-0357

1. ABSTRACT

The operational principle of a new, patented digital radiographic system using a multi-layer structure consisting of a thin-film pixel array, selenium x-ray photoconductor, dielectric layer and top electrode will be described.¹ Under an applied electric field, a diagnostic x-ray signal is obtained by the direct conversion of x-ray energy to electron-hole pairs which are collected as electrical charges by individual storage capacitor associated with each pixel element. The electronic readout sequence is initiated immediately after the x-ray exposure, and in several seconds, the image data is available for display on a video monitor, for data storage, data transmission, and hard copy generation. Signal strength of this direct conversion method is estimated to be significantly higher than that of other indirect conversion methods where light is first generated using a scintillator or phosphor and then detected by charge-coupled devices (CCDs) or thin-film-transistor (TFT) arrays in conjunction with photodiodes. In addition, since charges generated by x-ray photons move mostly along the direction of the bias electric field, images of very high spatial resolution can be obtained. The resolution limits are principally defined by the smallest pixel that can be manufactured. Recent x-ray images obtained from experimental detector panels will be presented. X-ray sensitivity, dynamic range, signal-to-noise ratio, and spatial resolution will be discussed.

Keywords: digital radiography, x-ray imaging, selenium, thin-film-transistor array, x-ray detector panel, direct radiography, direct x-ray conversion

2. INTRODUCTION

There is an emerging consensus in the radiology community that the missing element for a filmless x-ray department is a suitable detector for projection radiography which can be used much like conventional film-screen cassettes. Key design and operating requirements for such a detector are 1.) its compatibility with existing x-ray equipment (x-ray sources, tables, etc.), 2.) image quality and patient dose comparable to that of film-screen combinations, and 3.) competitiveness in cost per image. Meeting or exceeding these requirements represents a formidable challenge as films have been technically perfected in their almost 100 year history to be the capture, display, and storage medium all in one.² Although this feature has made film-screens so successful, it also places some well recognized physical limitations on this diagnostic modality as is indicated by the marginal improvements which have been made in the past decade. Digital detectors, in contrast, are the subject of intense research because the steps of capture, display and storage are separated and therefore can be optimized individually. Benefits to be expected are improved diagnostic capability and enhanced productivity in the x-ray department.

While various digital detector technologies have been investigated, only a few research efforts have actually matured into commercial products. Fuji's CR system has been the earliest commercial introduction. Its wide dynamic range is recognized to be an advantage over conventional film-screen systems, especially in bedside examinations. Philips' Thoravision chest imaging system is a new entry. Initial evaluations have shown that this selenium-based technology may enable practical digital thoracic imaging in a clinical environment.³ The high capital cost for this dedicated chest system, however,

may prevent its broad customer acceptance. Two companies are marketing small field digital cameras for stereotactic localization in mammography.⁴ These x-ray intensifying screen/CCD detectors are presently constrained by the size of CCDs, but if scale-up technologies such as sensor tiling can be perfected, full-field digital mammography could become reality.⁵

Antonuk, Street and colleagues have approached the need for a digital detector by creating large area, non-tiled digital detectors using TFT and photodiode panels made from hydrogenated amorphous silicon (a-Si:H).^{6,7} These panels are sandwiched to an x-ray intensifying screen. In this indirect conversion method, the light generated by x-rays is detected by the photodiodes, and the resultant signals are scanned out by addressing the TFTs row after row. Zhao and Rowlands have chosen to convert x-ray photons directly to electrical signals using the photoconducting material selenium deposited on a TFT array.⁸ The advantages of direct conversion versus indirect conversion as in phosphor screens coupled to photosensors will be discussed in greater detail later. Detectors involving TFT arrays have been growing in size as a result of huge investments made in the active-matrix liquid crystal display (AMLCD) technology by the flat panel display industry.

Our detector introduced here has some elements which are common with the aforementioned technologies, but its performance is optimized and its design is configured for integration into a cassette to be used in projection radiography. A conceptual drawing of what we call a direct radiography cassette is depicted in Figure 1. The unique components are a multi-layer structure and associated readout electronics, which are both optimized for projection radiography. However, the detector described here cannot be developed with a commercial product in mind if it were not for recent technological advancements in other fields. These advancements are: large area TFT arrays; densely packaged charge amplifiers on a single silicon chip (VLSI circuits); high speed, low cost computers; and high density electronic interconnections and packaging.

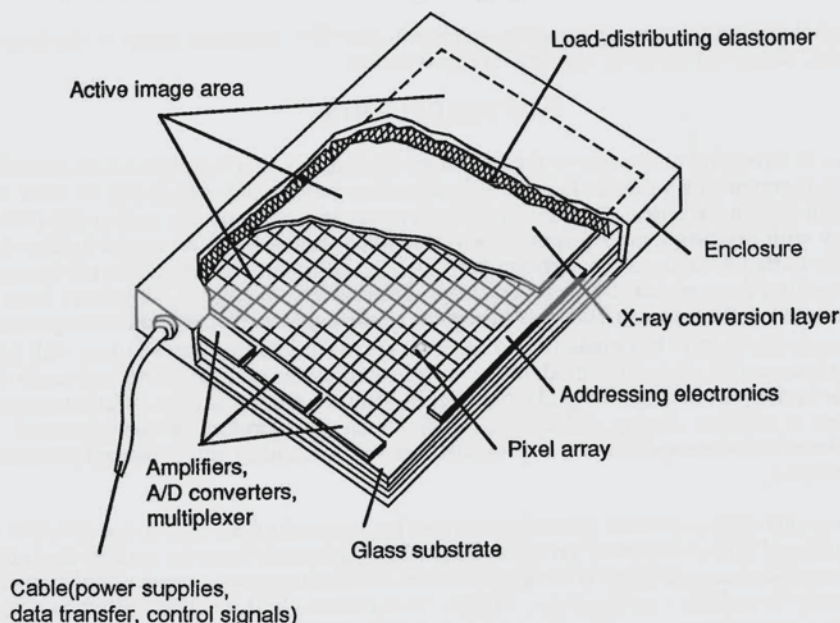


Fig. 1: Illustration of the DuPont Direct Radiography detector

3. DESCRIPTION OF THE DETECTOR

3.1 Layer Structure

A key to the operation and performance of our detector is its unique multi-layer structure. It is illustrated in Figure 2. The structural element is a rigid sheet of glass onto which is formed a pixel matrix by means of standard thin-film AMLCD manufacturing techniques. Each pixel consists of a storage capacitor, charge collection electrode, and an amorphous silicon field-effect transistor (FET). With one side connected to ground, the other pole of the storage capacitor is tied to the drain of the FET. The gate of each FET is connected to one of a set of gate lines, and the source of each FET is tied to one of a set of data lines. Figure 3 shows the pixel matrix, the orthogonally arranged gate and data lines, and the circuit of each pixel.

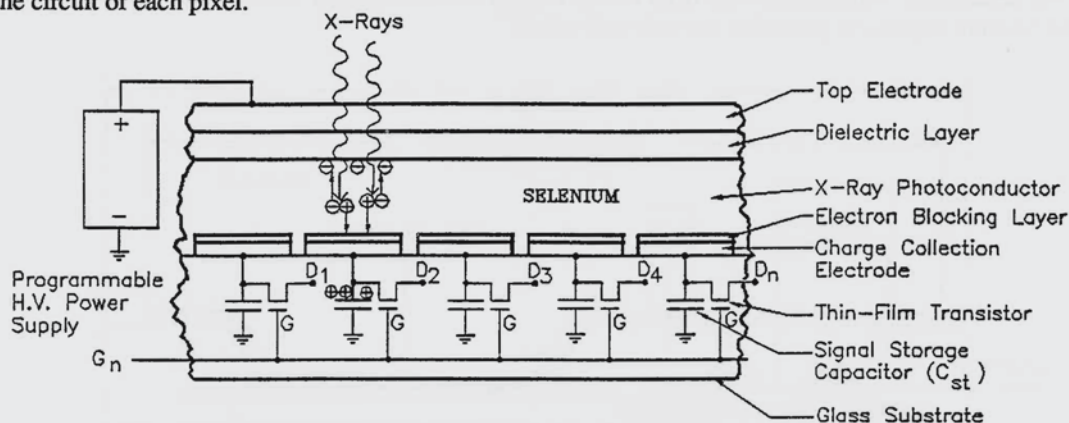


Fig. 2: Conceptual cross-sectional view of the multi-layer structure of the DuPont detector

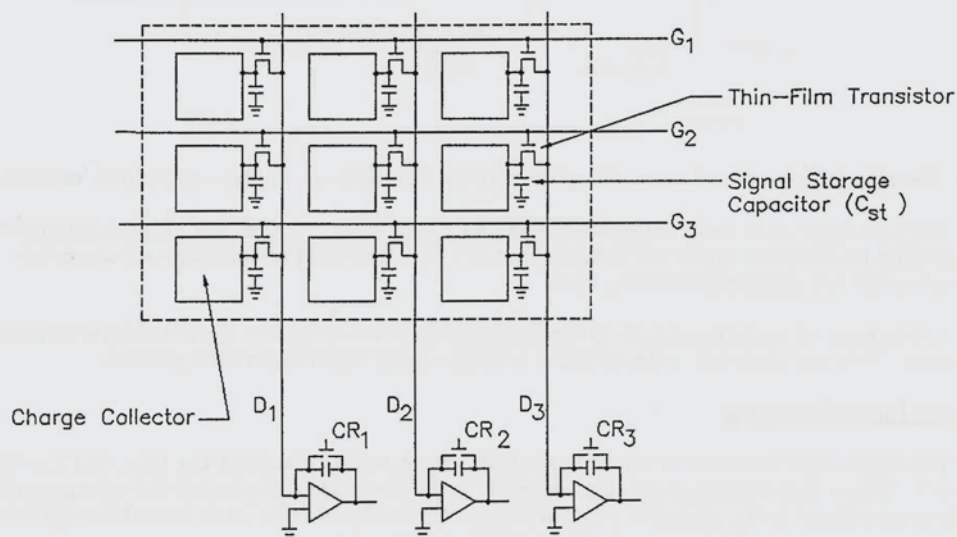


Fig. 3: Pixel matrix and readout electronics of the DuPont detector

The storage capacitor and charge collection electrode are configured in such a way that the electrode forms a "mushroom head" over much of the pixel area. This unique design is illustrated in Figure 4. The "mushroom" electrode serves three functions: 1) to shield the FET from the high electric field which is generated by the high voltage applied to the top electrode; 2) to shield the FET from signal charges which would collect on the insulation above the FET; and 3) to increase the charge collection efficiency of each pixel by maximizing its area. In the configuration shown in Figure 4, the mushroom electrode covers 86% of the total pixel area. The material of the mushroom electrode is chosen such that electrons are blocked from injecting into the x-ray photoconductor above.

The layer above the pixel array is the actual x-ray conversion material. We have chosen the photoconductive material amorphous selenium of 300 to 600 microns thickness to achieve sufficient x-ray absorption. This material has been widely used in xeroradiography so that its electrical properties and vacuum deposition processes are well understood.⁹

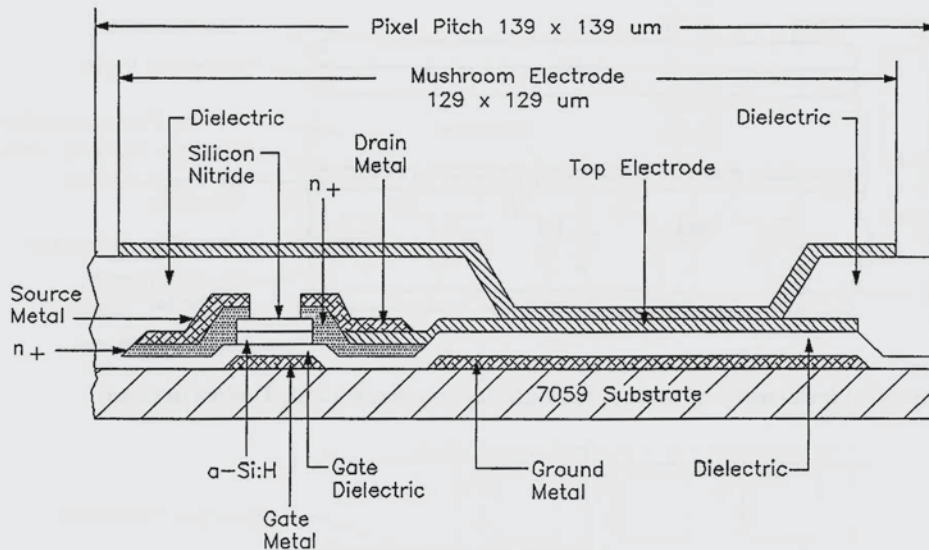


Fig. 4: Generic cross-sectional view of a pixel with the "mushroom" charge collection electrode design

The next layer is an insulating material having a high dielectric strength. Thickness uniformity, good adhesion to selenium, and a low defect count to avoid high field breakdowns are some key requirements for this dielectric blocking layer.

A thin layer of metal deposited on the dielectric material completes the multi-layer structure of our detector. This top electrode is deposited in a room temperature evaporation process.

3.2 Charge Image Formation

The multi-layer structure of our detector forms three series capacitors C_d , C_{Se} , and C_{st} depicted in Figure 5. When high voltage is applied between the top electrode and ground, the voltage is divided inversely proportional to the capacitor size. We have chosen C_d and C_{st} such that a bias applied to the top electrode results in a 10 V/micron field across the selenium layer.

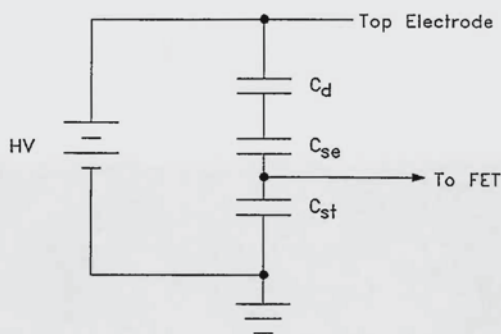


Fig. 5: Multi-layer structure represented as serial capacitors

intensities in areas where the x-ray beam is not attenuated by the patient's body. At the end of the exposure, the x-ray image resides in the pixel matrix in the form of charges whereby the charge in each storage capacitor is proportional to the absorbed radiation.

3.3 Electronic Readout

The readout of the charge image starts immediately at the end of the x-ray exposure. While all FETs, which are operated here as simple on-off switches, were not conducting during x-ray exposure, a positive gate pulse applied to the first gate line G1 simultaneously turns on all FETs connected to G1. This causes the image charge to flow to a bank of charge amplifier modules connected to the data lines. The net x-ray signal is multiplexed and shifted out to a 14-bit analog to digital converter (ADC) and subsequently stored in computer memory.

The readout of the charge image data continues row by row until the digital value of the charge in each storage capacitor has been transferred to memory. For our present 1,280 x 1,536 pixel matrix the readout time is about four seconds long. At the end of the readout cycle, a charge erase cycle will be initiated to restore the detector panel for the next exposure.

Once in computer memory, the image data can be processed and displayed on a video monitor or routed into a PACS system for further use. Figure 6 shows an x-ray image of a human hand phantom which was printed to a laser film. The image was captured with our 1,280 x 1,536 pixel matrix detector having a pixel pitch of 139 x 139 microns. The effective image area is 178mm x 213.5mm (7"x 8.5"). All crystalline silicon components of the readout electronics are shielded from x-radiation to avoid damage. The a-Si:H TFTs of the pixel array are resistant to very high x-radiation doses.¹⁰

4. X-RAY SENSITIVITY

The ability of the selenium x-ray photoconductor to convert incident x-rays into useful information depends on at least three important factors. First, the x-ray energy must be absorbed by the selenium layer. This absorption is a function of the photon energy and the thickness. The attenuation coefficient changes rapidly from about 700 cm⁻¹ at 12.6 Kev (the K-alpha edge) to about 8.5 cm⁻¹ at 70 Kev.¹¹ As a result, the percentage of absorption varies significantly through the useful diagnostic x-ray energy range, 40 KVp to 120 KVp, for the selenium thickness of interest, which is 500 microns. For example, the absorption is nearly 100% at 30 Kev, close to 80% at 40 Kev, and about 40% at 60 Kev. The typical mean x-ray energy for most examinations is between 55 and 65 Kev measured at the detector level. Figure 7 compares the absorption of selenium with two phosphor screens. Here it is

In actual operation, electron-hole pairs (e-h) are generated in the selenium layer by absorbed x-rays. In the bias field the charge pairs are separated whereby the holes are collected by the mushroom electrode and are stored in the storage capacitor. The electrons drift toward the selenium-dielectric interface and are collected there. The buildup of negative charge at the interface effectively reduces the positive bias and hence diminishes the charge generation and separation efficiencies. This phenomenon provides for an automatic safeguard against overcharging of the storage capacitor that could lead to damage to the FETs. This automatic protection mechanism is especially important when the detector is exposed to high x-ray



Fig. 6: X-ray image of a hand phantom captured with our 1,280 x 1,536 pixel matrix detector, printed to laser film. Exposure is higher than typical film-screen exposure due to sub-optimal operational conditions. (Se thickness 300 microns, electric field 4.2 V/micron)

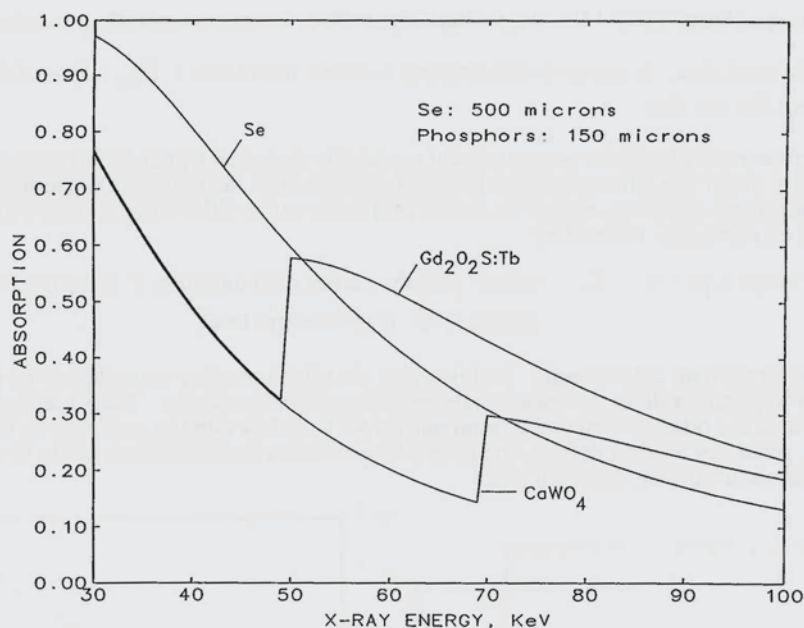


Fig. 7: Noise-equivalent x-ray absorption for selenium and two phosphors--calculated absorption corrected for scintillation statistics due to K-alpha loss

useful to remember that the average x-ray photon energy of the commonly used x-ray spectra is about one-half the maximum photon energy.¹² For example, a tungsten source operated at 80 KVP with filtration emits with an average photon energy of 42 KeV.

Second, a certain amount of the absorbed energy \mathcal{E}_{eh} is needed to generate one free electron-hole pair. The efficiency of electron-hole pair generation in selenium has been investigated by many researchers and the reported results differ by roughly a factor of two.¹³⁻¹⁹ Several techniques were employed in these studies including xeroradiographic discharge, photocurrent measurement, and pulse height spectroscopy. The value of \mathcal{E}_{eh} was found to be electric field dependent. At a field of

10 V/micron, the reported \mathcal{E}_{eh} ranges from 30 ev to 70 ev, with most reported values near 50 ev. The electric field dependence can be fitted to a power law relationship such that

$$\mathcal{E}_{eh} \sim E^{-n}, \quad \text{where}$$

\mathcal{E}_{eh} is the energy needed for electron-hole pair generation,

E is the electric field, and

n is the power.

In this case, n ranges from 0.6 to 1.0. We include Figure 8 to demonstrate the \mathcal{E}_{eh} values by replotting some of the published data. In our own experiments, we have found that a \mathcal{E}_{eh} value of 50 eV at 10 V/micron best fits our data.

Third, in order to obtain the maximum and repeatable electrical signal by collecting most of the generated charges under the influence of the imposed electric field, the transport properties of the carriers, both holes and electrons, should be maximized in the rather thick sample of 500 microns. More specifically the carrier range, defined by

$$\text{Carrier range} = \mu \cdot \tau \cdot E, \quad \text{where } \mu \text{ is the carrier drift mobility, } \tau \text{ is the deep trapping lifetime, } E \text{ is the electric field,}$$

should be much larger than 500 microns. In this sense, the selenium alloy material and its deposition process play an important role in the steady-state performance of the device. The situation is actually more complex because other related detector properties such as dark current, tendency to form crystallization, tendency to form defects, interface characteristics and adhesion have to be considered also as one develops a suitable selenium layer.

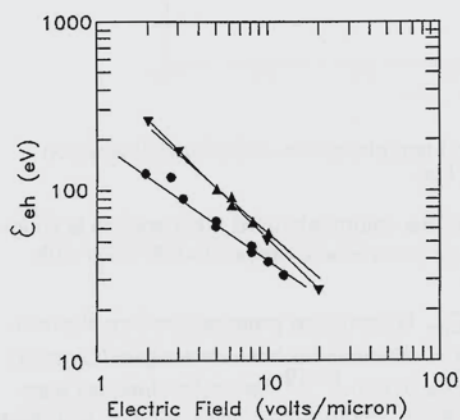


Fig. 8: The absorbed energy needed to create an electron-hole pair in amorphous selenium as a function of the electric field. ● data from ref. 19, ▲ data from ref. 18, ▼ data from ref. 15

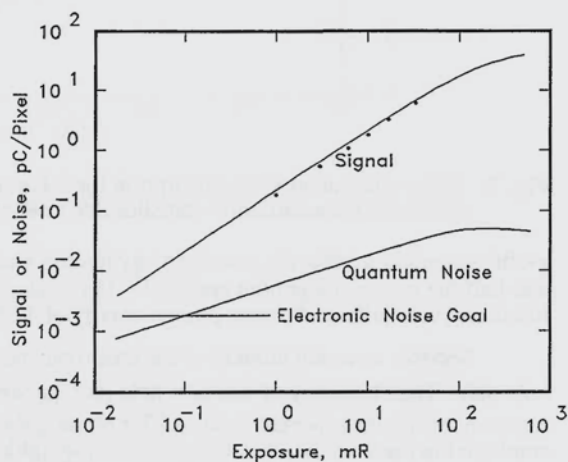


Fig. 9: Signal and noise as a function of exposure. Solid signal curve is calculated; dots are data measured for 10 V/micron field, 500 micron thick Se, 139 micron pixel pitch, 86% fill factor, 120 KVp W target

We have theoretically estimated the signal strength in pico-coulomb per pixel for our detector system by using the following parameter values: selenium thickness of 500 microns; dielectric layer thickness of 40 microns with a dielectric constant of 3.10; initial applied field across the selenium at 10 V/micron; power law dependence on electric field for electron-hole pair generation to be $2/3$ ($n=2/3$), 120 KVp tube voltage with 2mm aluminum filtration (tungsten target); pixel collection electrode fill factor at 86%; and assuming no loss of charge carriers due to deep trapping. The result is shown as the top curve in Figure 9 where the signal in pC/pixel is plotted as a function of the x-ray exposure in milliroentgen (mR). The signal is quite linear from a low exposure to about 60 mR. The signal strength begins to saturate when the exposure exceeds 200 mR.

We have also measured signal strength as a function of exposure by using experimental parameters closely resembling those mentioned earlier. The data points are plotted in Figure 9. One can see that there is reasonably good agreement between the theoretical estimate and the actual data.

It is interesting to compare our direct energy conversion technique using an amorphous selenium x-ray photoconductor with indirect energy conversion techniques using phosphors to first produce light. These two concepts are compared in Figure 10. We assume that the energy conversion efficiency of selenium is 50 ev per electron-hole pair at a field of 10 V/micron. In the case of phosphor screens, the conversion efficiency to light is reported to be approximately 20%.²⁰ Because the emission of light is isotropic, only a small portion of the generated light is emitting into the direction of the detector. Assuming the light is channeled to the sensor element, no more than 16% actually reach it. Using an effective sensor element fill factor of 50%, a photon energy of 2.5 to 3.0 ev, and a total absorption of light intercepted by the sensor element, we calculate the energy conversion efficiency to be 150 to 200 ev per electron-hole pair generation. The direct conversion technique using selenium is therefore 3 to 4 times more efficient than the indirect conversion techniques if x-ray absorption is the same for both materials. Depending on the x-ray energy, the thickness of the selenium, and the screen material, these absorption values can be quite comparable as is indicated in Figure 7.

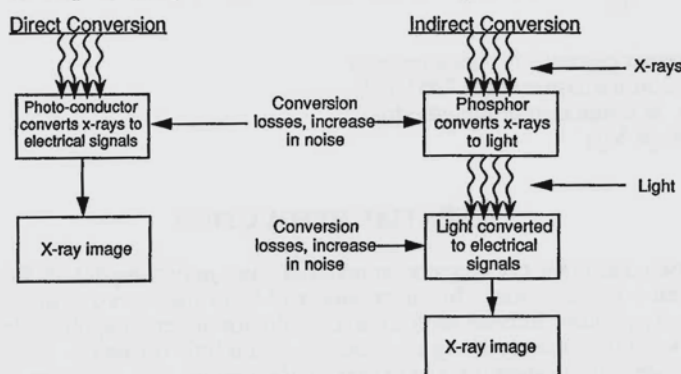


Fig. 10: Comparison of direct and indirect energy conversion steps to obtain an x-ray image

5. SIGNAL-TO-NOISE CONSIDERATIONS

For reading out the image information, we have chosen a charge integration amplifier instead of a voltage amplifier. In integration mode, with an integration time of more than 10 times the RC time constant of C_{st} and the "on" resistance of the FET, almost all the signal charge stored in C_{st} is transferred to the integration amplifier. The output signal of the amplifier thus is proportional to the charge accumulated during x-ray exposure, and is, to the first order, independent of C_{st} . This readout method therefore minimizes the noise due to variations in the value of the storage capacitor. Variations inevitably do occur in the manufacturing of the pixel array. The long integration time also helps minimize noise introduced by the FET's thermal noise and the random drain-to-source current differences between individual FETs.

Another noise reduction feature is built into the FETs. The FETs are designed to have low drain-to-source current in the "off" state. Typical drain-to-source currents in the "on" and "off" state are shown in Figure 11. An on-off current ratio of about 10^7 is illustrated here. The low "off" current is a necessity for our detector as the charge leakage through all the transistors in the "off"-state must be small compared to the charge measured from a single storage capacitor.

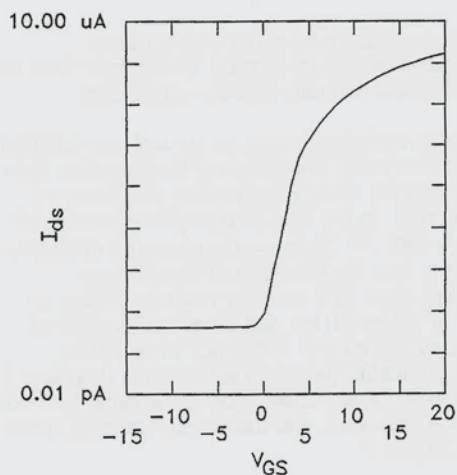


Fig. 11: Drain-to-source current I_{ds} characteristics of the thin-film transistor in the "on" and "off" states as a function of the gate-to-source voltage V_{GS}

Noise from charge injection into the selenium layer is dealt with through the use of blocking layers at both sides of the selenium. The material of the mushroom electrode and its surface treatment is chosen so that electron injection is minimized when the detector is operated below the electron injection threshold field. Selection of the proper material assures that there is no charge injection from the dielectric layer.

Referring back to Figure 9, the curves put the signal and the two major noise sources in perspective. The signal was calculated and verified by actual measurements. Assuming that the electronic noise is determined by the noise of 1,500 electrons at the charge integrator, the signal-to-noise-ratio (SNR) will be x-ray quantum noise-limited down to very low exposure levels.

6. SPATIAL RESOLUTION

It is well known that the x-ray conversion material has a major impact on the spatial resolution capability of any given x-ray detector. This discussion will be limited to x-ray photoconductors and phosphors. When x-ray photons interact with a photoconductor under an applied electric field, the resultant charge carriers move mostly along the field lines with little diffusion. Okamoto has demonstrated spatial resolution capabilities in excess of 100 cy/mm with selenium photoconductors by scanning the surface charge image with an electron microscope.²¹

The interaction of x-ray photons with phosphor screens produces a diffused signal due to internal light scattering. In Figure 12, the "footprint" of a highly collimated x-ray beam is illustrated for a typical photoconductor and film-screen conversion material.

Given the high intrinsic resolution capability of selenium, the resolution of our detector is principally determined by the pixel pitch. With the implementation of the mushroom electrode, pixel pitches of 50 microns can be manufactured presently with sufficient fill factor. As the pixel size decreases, one must trade off the benefits of higher spatial resolution against larger data sets, a smaller signal, and longer readout times. Our present pixel pitch of 139 x 139 microns was chosen to cover a broad range of radiographic applications. Because the presampled MTF of selenium is very high, we expect our detector to have a higher MTF up to the Nyquist frequency of 3.6 cy/mm than similar application film-screen combinations. The hand image of Figure 6 and an enlarged section of a resolution bar target in Figure 13 support our expectation.

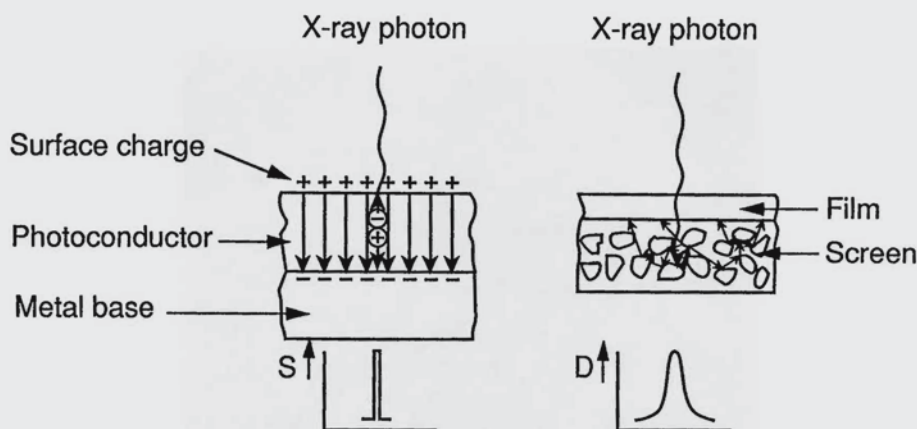


Fig. 12: Illustration of the interaction of x-ray photons with a photoconductor and a phosphor screen, and resultant signal "footprint"

7. SUMMARY AND OUTLOOK

We have described a new digital detector for projection radiography, and have presented the results which have been obtained just a short time ago with a research device.

Because this flat panel imager is fairly new, the analysis of its performance characteristics is necessarily incomplete. However, initial results indicate that our detector technology addresses many of the reported shortfalls of other digital systems. The direct conversion of x-rays to electrical signals, the high conversion efficiency of thick selenium layers, the prospect of an excellent MTF, and a self-scanning electronic readout scheme having manageable noise levels are all indicators that the detector described here has the potential to compete favorably with conventional film-screen combinations in terms of sensitivity and image quality. It has the advantage of delivering x-ray images almost instantly, and in digital form. These are attributes which would improve the productivity of x-ray departments.

Looking forward, we are encouraged by the fact that the physical behavior and performance of the detector have been very much predictable. Our theoretical modeling and calculations, so far, have been supported by our measurements. A key to success is the further reduction of electronic noise. Except for some defects in the TFT panels, structural noise sources have been virtually eliminated.

With respect to the detector panel dimensions, the research device described here is 7" x 8.5" in size, which is one-fourth the area of a 14" x 17" film. We are working on a method of tiling four pieces together without any dead space at the butt joints. By reading out the image information in the four independent tiles in parallel, any increase in readout time as compared to a single panel will be insignificant.

As we continue to make improvements, the imaging physics community will be kept abreast of our progress towards a commercially viable digital detector for projection radiography.

8. ACKNOWLEDGMENTS

The authors wish to thank Dr. William Bindloss of DuPont's Central Research & Development department for the generation of the x-ray absorption curves and the many helpful discussions related to the physical properties of the detector. We are grateful for Don Manley's preparation of the drawings, and Wilma Reilly's assembly of the manuscript.

4.7 X-ray imaging using amorphous selenium: Feasibility of a flat panel self-scanned detector for digital radiology

Wei Zhao (born 1966)

Wei Zhao was born in Beijing, China, on 12 January 1966.

She got her degree in Biomedical Engineering from Tsinghua University, Beijing, China in 1989, her MSc (1993) and PhD (1997) in Medical Biophysics from University of Toronto, Toronto, Canada.

Dr. Zhao started her professional career as an Engineer, Engineering Department, at Siemens Beijing (1989–1990). She became Research Associate, Imaging Research, at Sunnybrook Health Sciences Center, Toronto, Canada in 1997, Staff Scientist, R&D Department, at Trex Medical Corporation, Copiague, NY (1997–1999) and she was appointed Assistant Professor of Radiology and Biomedical Engineering State University of New York at Stony Brook, Stony Brook, NY (1999).

Dr. Zhao was awarded Honor Student, Tsinghua University (1985–89), the University of Toronto Open Fellowship (1990–91), the Sunnybrook Health Science Center Trust for Medical Research Graduate Studentship (1991–93), the Steve Fonyo Studentship, National Cancer Institute of Canada (1993–1997), the First Prize, Young Investigators Symposium, COMP Annual Meeting (1994), and the Sylvia Fedoruk Prize for “Best Scientific Paper in the Field of Medical Physics in Canada”. Between 2002–2004 she was awarded Whitaker Investigator, The Whitaker Foundation.

Dr. Zhao is a member of the American Association of Physicists in Medicine, the Society of Photo-optical Instrumentation Engineers, a Referee for IEEE MIC Conference in 2003, and External Reviewer, The Canadian Institutes of Health Research (CIHR).

Picture courtesy Wei Zhao, PhD, 2004.



John A. Rowlands (born 1945)

John Rowlands was born on the 4th May 1945 in Altrincham, Cheshire in England.

He obtained his BSc in Physics from Leeds University with 1st Class Honours in 1966, and his PhD in Solid State Physics also from Leeds University in 1971. He became a laboratory teaching assistant at the Department of Physics at the University of Khartoum in the Sudan (1966–1967) and at the University of Leeds, UK (1967–1970). From 1973–1976 he was Research Associate/Sessional Instructor at the Department of Physics, University of Alberta in Canada. He was appointed Visiting Assistant Professor, Department of Physics, University of Alberta (1976–1977) and the Department of Physics, Michigan State University, USA (1978–1979). In 1979 he was appointed Assistant Professor, Department of Radiology, University of Toronto where he became Associate Professor, Dept. of Medical Imaging (formerly Radiology) from 1990–1998. He was appointed Full Professor at the Department of Medical Imaging, University of Toronto in 1998. He became Senior Scientist, Imaging Research Group, Sunnybrook and Women's College Health Sciences Centre in 1990 and Head, Medical Physics Research, Toronto Sunnybrook Regional Cancer Centre in 2004.



John Rowlands became the European Fellowship of the Royal Society in 1970, the IW Killam Post doctoral Fellowship, University of Alberta, 1971–73. For best practice in research and development he was awarded the University Industry Synergy Award in 1995 from the NSERC and Conference Board of Canada. In 1995 he awarded the Sylvia Fedoruk Prize in Medical Physics for the best Canadian paper in the field of Medical Physics in 1995 (Canadian Organization for Medical Physics). John Rowlands is a Fellow of the Canadian College Diagnostic Radiology of Physicists in Medicine since 1987. He is a member the Canadian Association of Physicists (1971–), the Canadian Organization of Medical Physicists (1989–), the American Association of Physicists in Medicine (1979–), and the SPIE the International Society for Optical Engineering (1980–)

In 1984 he started working on digital videofluorography and he developed a real-time digital image processing for gastro-intestinal studies and cardiac angiography. In 1985 he became interested in digital mammography utilizing laser read-out of amorphous selenium. In 1988–98 he developed an x-ray video camera for fluoroscopy and flat panel sensors for digital radiography and fluoroscopy again using amorphous selenium. For dynamic x-ray imaging (“fluoroscopy”) he replaced the conventional X-ray image intensifiers either with an active matrix flat panel device modified to include one of three innovative approaches: avalanche multiplication in selenium, intelligent pixels or a novel photoconductor – mercuric iodide. The primary application area is in cardiac imaging where he is also looking at combining x-ray with MRI. For imaging during radiation therapy (portal imaging) the image quality needs to be improved significantly before it can be clinically relevant. He developed high quantum efficiency detectors for radiation therapy. Understanding the physical limits of systems will allow them to be optimally matched to clinical applications. His investigations are resulting in improved clinical devices and he continues to be interested in fundamentals of computed radiography.

Picture Courtesy John Rowlands PhD, 2004.

X-ray imaging using amorphous selenium: Feasibility of a flat panel self-scanned detector for digital radiology

Wei Zhao and J. A. Rowlands

Department of Medical Biophysics, University of Toronto, Reichmann Research Building, Sunnybrook Health Science Centre, 2075 Bayview Avenue, Toronto M4N 3M5, Canada

(Received 14 February 1994; resubmitted 30 December 1994; accepted for publication 13 July 1995)

We investigate a concept for making a large area, flat-panel detector for digital radiology. It employs an x-ray sensitive photoconductor to convert incident x-radiation to a charge image which is then electronically read out with a large area integrated circuit. The large area integrated circuit, also called an active matrix, consists of a two-dimensional array of thin film transistors (TFTs). The potential advantages of the flat-panel detector for digital radiography include: instantaneous digital radiographs without operator intervention; compact size approaching that of a screen-film cassette and thus compatibility with existing x-ray equipment; high quantum efficiency combined with high resolution. Its potential advantages over the x-ray image intensifier (XRII)/video systems for fluoroscopy include: compactness; geometric accuracy; high resolution, and absence of veiling glare. The feasibility of the detector for digital radiology was investigated using the properties of a particular photoconductor (amorphous selenium) and active matrix array (with cadmium selenide TFTs). The results showed that it can potentially satisfy the detector design requirements for radiography (e.g., chest radiography and mammography). For fluoroscopy, the images can be obtained in real-time but the detector is not quantum noise limited below the mean exposure rate typically used in fluoroscopy. Possible improvements in x-ray sensitivity and noise performance for the application in fluoroscopy are discussed.

Key words: Diagnostic x-ray imaging, digital radiology, amorphous selenium, solid-state imagers, flat-panel imagers

I. INTRODUCTION

X-ray imaging has been playing a very important role in diagnostics since the beginning of this century and it currently consists of two major imaging modalities: radiography (performed with screen-films) and fluoroscopy [performed with an x-ray image intensifier (XRII)/video system]. Since the 1970s, new digital imaging modalities have been developed which include computed tomography (CT), ultrasonic imaging, nuclear medicine, and magnetic resonance imaging (MRI). However, basic x-ray imaging has remained largely an analog technique. During recent years, with the rapid development of electronic and computer technology, digital radiological detectors have undergone considerable investigation and development. The advantages of digital radiology include: (i) The image receptor can be optimized independently from the image display and storage; (ii) digital image processing can improve the image visualization (e.g., contrast enhancement); (iii) computer-aided diagnosis can be implemented to assist radiologists in finding subtle abnormalities.¹

Recently, a new technology of large area integrated optical image sensors, e.g., hydrogenated amorphous silicon (*a*-Si:H) thin film transistor (TFT)-photodiode arrays, have been proposed for making a flat-panel detector for digital diagnostic and portal imaging by employing a phosphor screen to convert an incident x-ray distribution to optical images.² We are investigating the feasibility of another approach to making a flat-panel digital detector, which has been previously proposed by us^{3,4} and suggested by others.⁵ It also employs a two-dimensional array of TFTs, or "active

matrix," to electronically read out an x-ray generated charge image. However, instead of indirect conversion of x rays using a phosphor screen and an array of photodiodes, a uniform layer of x-ray sensitive photoconductor is used to directly convert the incident x-ray distribution to a charge image.

In Fig. 1(a) we show a diagram of the active matrix used for charge image readout. It consists of a two-dimensional array of TFTs, each of which acts as an electronic switch. Each TFT has three electrical connections: the gate (G) is for the control of the "on" or "off" state of the TFT; the drain (D) is connected to a pixel electrode and a pixel storage capacitor, which is made by overlapping the pixel electrode with either the adjacent gate line, or a separate ground line; the source (S) is connected to a common data line shared by all the TFTs of the same column, and subsequently to an external charge sensitive amplifier.

Radiation detection is accomplished with a uniform layer of x-ray sensitive photoconductor deposited on the active matrix. Shown in Fig. 1(b) is a cross section of a single pixel of the detector. The top surface is a continuous, high-voltage bias electrode, common to all the pixels of the detectors, which is used to apply an electric field (E_{ph}) across the photoconductor. X rays absorbed by the photoconductor release charge carriers (electron-hole pairs) which are separated and drawn to the photoconductor surfaces by E_{ph} . At the bottom surface this charge is collected by the pixel electrodes and stored on the pixel capacitors. During readout, the TFTs are turned on, one row at a time, to transfer the image charge from the pixel capacitors to the data lines and then to the external charge amplifiers. The signal outputs from the am-

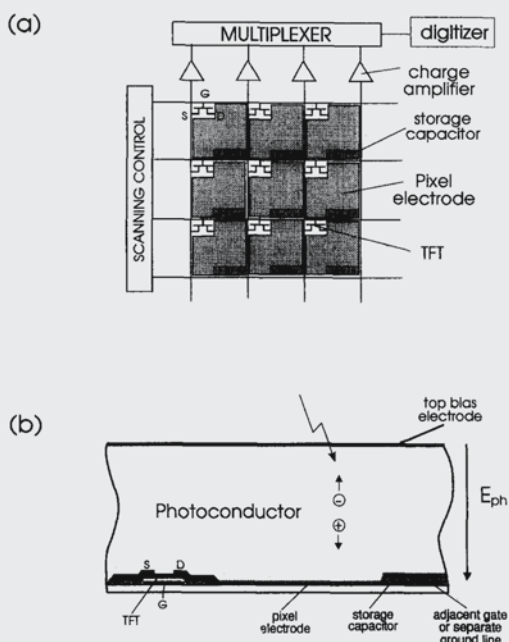


FIG. 1. Self-scanned readout of an x-ray photoconductor: (a) schematic of the active matrix and external electronic circuitry; (b) cross section of a single pixel showing detection of x rays by a photoconductor.

plifiers are transferred to the analog-to-digital (A/D) converter by a parallel-to-serial multiplexer.

In this paper the feasibility of this detector, also referred to as *self-scanned readout of x-ray photoconductor*, for x-ray imaging is analyzed based on the properties of a possible combination of x-ray photoconductor [amorphous selenium (*a*-Se)] and active matrix [using cadmium selenide (CdSe) as a semiconductor]. Although many different types of photoconductor have been proposed as x-ray detectors, such as *a*-Se,⁶ lead oxide (PbO),⁷ thallium bromide (TlBr),⁸ and cadmium telluride (CdTe),⁹ we are proposing the use of *a*-Se because it has low dark current and has already been demonstrated for use in medical imaging systems, such as xeroradiography¹⁰ and a digital chest radiography system¹¹ using *a*-Se thickness of up to 500 μm . Active matrices have been made with several types of semiconductor materials,¹² e.g., hydrogenated amorphous silicon (*a*-Si:H), polycrystalline silicon (*poly*-Si) and polycrystalline CdSe. We chose to use CdSe TFT because of its higher carrier mobility ($\sim 100 \text{ cm}^2/\text{Vs}$) than *a*-Si:H ($\sim 1 \text{ cm}^2/\text{Vs}$), while maintaining lower leakage current than *poly*-Si TFT. The high carrier mobility of CdSe permits great design flexibility, e.g., the TFTs can have a channel width to length ratio (*W/L*) of unity while maintaining low cross talk and desired properties for fast (real-time) image readout. A *W/L* of unity could minimize the space taken by each TFT, which is important for imaging applications requiring small pixel size.

TABLE I. Design requirements for digital radiological detectors.

	Chest radiography	Mammography	Fluoroscopy
Detector size (cm)	35×43	18×24	25×25
Pixel size (μm)	200×200	50×50	250×250
Number of pixels	1750×2150	3600×4800	1000×1000
Image readout time (second)	<5	<5	0.033
X-ray spectrum (kVp)	120	30	70
Mean exposure to image detector (mR)	0.3	12	0.001
Exposure range (mR)	0.03–3	0.6–240	0.0001–0.01

II. DESIGN REQUIREMENTS

A. Detector size and pixel size

Digital detectors have to cover the same field of view as conventional analog techniques: the screen-films are $\sim 43 \times 35 \text{ cm}$ ($17 \times 14 \text{ in.}$) for chest radiography and $\sim 24 \times 18 \text{ cm}$ for mammography, while the XRII for fluoroscopy is $\sim 25 \text{ cm}$ in diameter. The requirement for pixel size in digital radiography has been previously studied for each imaging task. The observer study performed by MacMahon *et al.*¹³ based on digitization of screen-film chest radiographs suggested that a pixel size of 200 μm square is satisfactory. It allows high-resolution tasks such as detection of pneumothorax and fine interstitial lung diseases.¹⁴ For digital mammography, Yaffe¹⁵ suggested, on the basis of providing equivalent spatial resolution performance as screen-film mammography, that a pixel size of 50 μm is necessary. In fluoroscopy, a $25 \times 25 \text{ cm}$ detector with 1000×1000 pixels should be comparable to the resolution provided by conventional analog XRII system using 1000 line video cameras with 20 MHz bandwidth.^{16,17} These requirements for detector and pixel size are summarized in Table I, and they are used as examples in subsequent calculations and discussions.

B. Readout rate and lag

Image readout rate is a critical requirement for fluoroscopy: it has to be real-time (30 frames per second)⁷ and with little image lag to blur moving objects. For radiography, there is no strict limit for the readout rate. However, an "instant readout" ($< 5 \text{ s}$) is desired for digital radiography systems, and there should be no significant loss of image charge from the pixels (due to the leakage current of the TFTs) prior to readout.

C. Quantum noise limited exposure range

For each imaging task, the detector is required to respond to a range of x-ray exposure due to the variation in transmission of the body for a given beam quality. Within this expo-

sure range the detector should be quantum noise limited, i.e., the noise added by the detector does not exceed the x-ray quantum noise.

We determine the x-ray spectrum and mean exposure to the detector as that currently used clinically (screen-films or XRII/video systems). The required x-ray exposure range is established from previous studies and we set the geometric mean of the x-ray exposure range to be the same as the mean exposure to detector. For chest radiography, we take Hi-Plus/XRP screen-films as an example where the mean exposure to the detector is ~ 0.3 mR using a 120 kVp spectrum.¹⁸ In order to obtain good image contrast for both the mediastinum and lung region, an exposure range from one-tenth to ten times the mean exposure is desirable (0.03–3 mR).¹⁹ In mammography, the mean exposure to the Min-R/Ortho-M screen-film is ~ 12 mR. With an x-ray spectrum generated by a molybdenum (Mo) target at 30 kVp with 30 μ m Mo filtration, the range of x-ray exposure between the raw beam and that attenuated by 8 cm of 50% glandular, 50% fat tissue is of the order of 400:1.²⁰ Thus the required quantum noise limited x-ray exposure range for digital mammography is 0.6–240 mR. For fluoroscopy, the detector should have at least the same range of x-ray response (100:1) as an XRII/video system.²¹ The mean fluoroscopic exposure rate to an XRII/video system is 30 μ R/s (for a field of view of 25 cm in diameter), thus the required quantum noise limited exposure range is 0.1–10 μ R/image (each image is taken in 1/30 of a second). These data for mean exposure and quantum noise limited exposure range are included in Table I.

D. Resistance to radiation damage

In order to apply the flat-panel detector to x-ray imaging, we have to make sure that its function will not be permanently damaged by the radiation it is expected to receive during its lifetime. In our study, the lifetime of the detector was taken as 5 yr. We then estimated 200 working per year with 100 images per day, and the dose to the detector to be 0.05 cGy/image. Thus the lifetime dose for the detector is 5000 cGy ($0.05 \times 100 \times 200 \times 5$).

III. THEORY AND METHODS

The feasibility of the self-scanned readout of an x-ray photoconductor is investigated based on the simplifying assumptions: (i) each pixel of the detector operates independently, i.e., without being affected by the surrounding structure; (ii) the active area for image charge collection on each pixel is equal to the pixel spacing squared, i.e., 100% fill factor. Then we can model the operation of the detector with an electronic circuit of a single pixel. The model thus consists of the *a*-Se x-ray sensor (represented by the capacitor C_{Se} , the current sources I_{dark} and I_{signal}), the pixel storage capacitor (C_{st}), the TFT switch, and the external charge sensitive amplifier, as shown in Fig. 2.

The parameters in the model are the pixel size, the x-ray response and dark current of *a*-Se, the value of C_{st} , the switching properties of the CdSe TFT, and the noise of the charge amplifier. The imaging performance of the detector is analyzed by incorporating previously published parameters

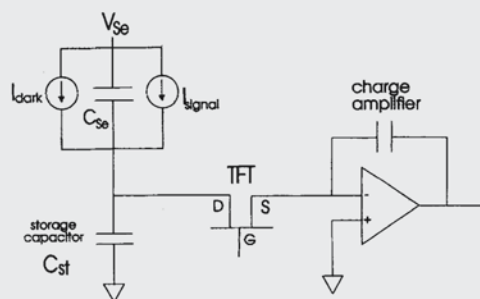


FIG. 2. Equivalent circuit diagram for each pixel of the detector, where V_{Se} is the bias potential applied on the top surface of the *a*-Se layer, I_{dark} and I_{signal} represent the current flow in *a*-Se at each pixel under dark and x-ray exposure, respectively, and C_{Se} is the capacitance of the *a*-Se layer for each pixel.

of the *a*-Se photoconductor (with similar doping and deposition procedure as for xeroradiographic plates²²) and measured characteristics of CdSe TFTs (manufactured by Litton Systems Canada) into the model. Then these imaging parameters are compared with the design requirements summarized in Table I.

A. Readout rate and lag

1. Readout rate

The function of a TFT as a switch can be represented by its resistance in the on and off states, R_{on} and R_{off} . During image readout, the image charge stored on each pixel will be discharged exponentially with a time constant τ_{on} given by the product of R_{on} and the pixel capacitance C_p , which is the sum of the storage capacitor C_{st} (~ 1 pF) and the capacitance of the photoconductor (~ 0.01 pF) for each pixel. For essentially complete discharge of each pixel it is necessary to wait several (M) time constants. The readout time for the entire detector T_{read} is the product of the number of rows, N_{row} , and the time to discharge each row, $M\tau_{on}$.²³

$$T_{read} = M\tau_{on}N_{row}. \quad (1)$$

In order for the detector to be applied for real-time x-ray imaging, T_{read} has to be smaller than the frame time $T_F = 33$ ms (at 30 frames per second readout speed).

When the TFT is off, charge accumulated during the x-ray exposure will leak through the TFT with the time constant τ_{off} which is the product of R_{off} and C_p . In order to prevent image information loss, τ_{off} should be much larger than T_{read} so that image charge leakage prior to readout is insignificant.

Individual TFTs were used for quantitative evaluation of R_{on} and R_{off} . These TFTs have the same design parameters as those on the active matrices, but were packaged such that all three electrical connections (gate, drain, and source) were accessible. The evaluation circuit is shown in Fig. 3. The source of the TFT was connected to an electrometer whose input is a virtual ground. First, the transfer characteristic (channel current I_D as a function of gate control potential V_G) was measured at a fixed drain bias potential V_D in order to determine the proper V_G for turning the TFTs on and off.

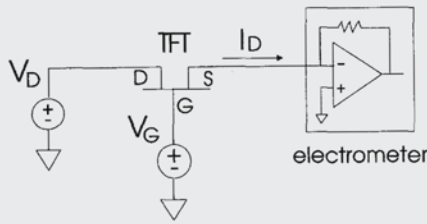


FIG. 3. Experimental arrangement for measuring characteristic curves of TFTs: I_D represents the TFT channel current, V_G and V_D represent the bias potential applied on the gate and drain of the TFT.

Then the output characteristic (I_D as a function of V_D) was measured in both the on and off states of the TFTs, and R_{on} and R_{off} were determined from the slope of the output characteristic curves.

2. Lag

Image lag arises from two sources: incomplete charge collection (photoconductive lag) and incomplete charge readout (image readout lag). Photoconductive lag is caused by the charge transit time across the a -Se layer. The maximum time delay, T_R , is for a charge carrier to traverse the whole thickness of a -Se, and is determined from²⁴

$$T_R = d_{Se} / \mu_c E_{Se}, \quad (2)$$

where d_{Se} is the thickness of the a -Se layer, μ_c is the mobility of the charge carrier (electron or hole), and E_{Se} is the electric field applied across the a -Se layer. For negligible photoconductive lag we require T_R much smaller than T_F . Image readout lag depends on how many time constants each TFT can be kept on during the image readout.

B. Quantum noise limited exposure range

In order to investigate whether the detector is quantum noise limited in the required x-ray exposure range, we first determine the signal and quantum noise level based on the x-ray sensitivity of a -Se and then determine the level of electronic noise based on the properties of the readout device. In the following, the signal, quantum noise, and electronic noise are given in number of electrons.

1. Signal

For a given pixel area A and incident x-ray fluence $\phi(E)$, the energy absorbed by one pixel of the detector E_{ab} (assuming no secondary interaction, e.g., K-fluorescence reabsorption) is given by²⁵

$$E_{ab} = \sum_E \phi(E) A \eta(E) \frac{\mu_{ab}(E)}{\mu(E)} E, \quad (3)$$

where E is the x-ray energy, $\mu(E)$ and $\mu_{ab}(E)$ are the x-ray attenuation and absorption coefficients of a -Se, and $\eta(E)$ is the x-ray quantum efficiency (QE) determined from

$$\eta(E) = 1 - e^{-\mu(E)d_{Se}}. \quad (4)$$

The x-ray fluence $\phi(E)$ is determined from the x-ray exposure and its spectrum. The tungsten²⁶ and molybdenum²⁷ x-ray spectra used in the calculation were obtained using a computer model. The charge signal created on each pixel q_s is determined by the ratio of absorbed energy per pixel E_{ab} and the energy W needed to create an electron-hole pair in a -Se:

$$q_s = E_{ab} / W. \quad (5)$$

2. Quantum noise

The ratio between signal and x-ray quantum noise is determined from the square root of the number of x rays attenuated by the a -Se layer, which is given by $\sum_E \phi(E) A \eta(E)$; thus, the charge representing the quantum noise q_{qn} at each pixel is given by²⁸

$$q_{qn} = \frac{E_{ab}}{\sqrt{\sum_E \phi(E) A \eta(E)}} \frac{1}{W}. \quad (6)$$

3. Electronic noise

There are four sources of electronic noise: photoconductor dark current shot noise, the two sources arising from the TFT (thermal and flicker noise), and the amplifier noise.

a. Dark current shot noise. The dark current in a -Se is due to thermal excitation in the bulk and charge injection from the bias electrodes. The dark current shot noise q_{nd} is determined by the dark current of a -Se at each pixel i_d and the time between successive readouts T_F , and is given by²⁹

$$q_{nd} = \sqrt{i_d T_F / e}, \quad (7)$$

where e is the charge of an electron.

b. TFT thermal noise. With the TFT turned on, the current thermal noise power spectrum (NPS) $W_{it}^2(f)$ due to the channel resistance R_{on} is given by³⁰

$$W_{it}^2(f) = 4kT/R_{on}, \quad (8)$$

where k is Boltzmann's constant and T is the absolute temperature. In our investigation, $W_{it}^2(f)$ was experimentally verified with the TFT turned on and channel current $I_D = 0$. $W_{it}^2(f)$ was obtained by measuring the TFT channel current noise power in a bandwidth of 1 Hz using a lock-in amplifier at a series of reference frequencies f_0 .

In order to estimate the final noise contribution of $W_{it}^2(f)$ in terms of noise charge q_{ni} referred to the input of the charge amplifier, we first determined the fraction of $W_{it}^2(f)$ that propagates to the input node of the charge amplifier. $W_{it}^2(f)$ is high pass filtered by³¹

$$H_1^2(f) = \frac{(2\pi\tau_{on}f)^2}{1 + (2\pi\tau_{on}f)^2}, \quad (9)$$

where τ_{on} is the image readout time constant given by the product of R_{on} and C_p . The filtered TFT noise is then integrated by the charge sensitive amplifier for a given charge integration time, $T_{on} = M\tau_{on}$ with a transfer function of³²

$$H_2(f) = T_{on} \text{sinc}(T_{on}f). \quad (10)$$

Thus the resulting thermal NPS of TFT, $W_{it}^2(f)$, is determined as the product of $W_{it}^2(f)$, $H_1^2(f)$, and $H_2^2(f)$:

$$W_{qi}^2(f) = \frac{4\tau_{on}^2 \sin^2(\pi T_{on} f)}{1 + (2\pi\tau_{on} f)^2} W_{it}^2(f). \quad (11)$$

Then q_{ni} can be calculated by integrating $W_{qi}^2(f)$ over f and the result is

$$q_{ni} = \frac{1}{e} \sqrt{2kTC_P(1 - e^{-T_{on}/\tau_{on}})}. \quad (12)$$

In order to read out the image charge completely, T_{on} should be greater than $5\tau_{on}$. Then $q_{ni} \approx 1/e(2kTC_P)^{1/2}$. Furthermore, the pixel capacitor C_P is reset to a reference potential through the resistance of the TFT which has thermal noise. Thus after the TFT is turned off, the pixel potential has an uncertainty due to this thermal fluctuation which results in a noise charge q_{nr} given by³⁰

$$q_{nr} = \frac{1}{e} \sqrt{kTC_P}. \quad (13)$$

This q_{nr} remains on the pixel after each readout, thus in a repetitively scanned system, q_{nr} will also contribute to the electronic noise. Therefore the total noise charge due to the thermal noise of the TFT, q_{ni} , can be estimated by adding q_{ni} and q_{nr} in quadrature:

$$q_{nt} = \frac{1}{e} \sqrt{3kTC_P}. \quad (14)$$

c. *TFT flicker noise.* The TFT flicker noise power is expected to depend on the channel current I_D .³³ For our experimental investigation of TFT flicker noise, the TFT was operated at a constant current I_D by applying fixed potentials on its gate and drain. The NPS of channel current I_D , $W_{if}^2(f)$, was measured using the same apparatus as in the $W_{it}^2(f)$ measurement. Then the NPS of the flicker noise, $W_{if}^2(f)$, was determined by subtracting the thermal noise power $W_{it}^2(f)$ [Eq. (8)] from $W_{if}^2(f)$. The total noise charge, q_{nf} , due to the TFT flicker noise can thus be estimated using Eq. (11) by substituting $W_{it}^2(f)$ with $W_{if}^2(f)$.

d. *Amplifier noise.* The amplifier noise q_{na} can be determined from³⁴

$$q_{na} = q_{na0} + \delta C_d, \quad (15)$$

where q_{na0} is the intrinsic noise of the charge amplifier, δ is a constant determined by the design properties of the charge amplifier, such as the noise voltage of the input FET and the feedback capacitor of the amplifier, and C_d is the external capacitance loading the input node of the amplifier.

e. *Total noise.* Each of the component sources of noise indicated in subsections a–d are independent. Hence we can estimate the total noise charge by adding them in quadrature.

C. Resistance to radiation damage

The long term effects of radiation on xeroradiographic *a*-Se plates have been studied by measuring the residual potential of a photodischarged plate after it has been subjected to radiation. It was found that the plates recover from the effects of radiation within hours.³⁵ Thus the focus of our investigation is to examine whether the active matrix is resistant to radiation damage.

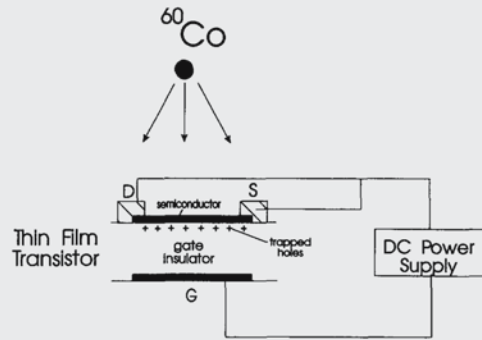


FIG. 4. Experimental arrangement for investigating the effect of radiation on thin film transistors.

The TFTs are the only components on the active matrix that are possibly subject to radiation damage. The effects of ionizing radiation on surface channel semiconductor devices such as a metal-oxide-semiconductor field effect transistor (MOSFET) have been widely studied.³⁶ The major effect is due to radiation absorbed in the gate insulator. Holes created in the insulator by radiation can be trapped practically indefinitely at the interface between the gate insulator and the semiconductor, and change the transfer characteristics of the MOSFETs. In particular it has been noted that the threshold voltage V_T changes as a function of irradiation level. Since TFTs have similar gate structure and principle of operation as MOSFETs,³⁷ ionizing radiation is expected to have a similar effect.

We measured the transfer characteristic curves of TFTs before and after they were irradiated with 5000 cGy. For practicality in applying very large doses a ^{60}Co radiation source was used, as shown in Fig. 4. Since it has previously³⁶ been noted that gate bias potential during irradiation of MOSFETs changes the effect of radiation, the gate bias potential, V_{GB} , was controlled in the irradiation experiment. Three V_{GB} conditions were studied: +20 V, –20 V (which are the highest operational gate bias potential for the “on” and “off” states, respectively), and 0 V.

IV. RESULTS AND DISCUSSION

A. Detector size and resolution

Electron–hole pairs created during x-ray interaction with *a*-Se are separated and drawn to the surfaces by the applied E_{se} without much spreading. The modulation transfer function (MTF) of an *a*-Se detector at mammographic energies ($d_{se}=200\text{ }\mu\text{m}$) has been estimated to be >80% up to 10 lp/mm³⁸ (corresponding to the 50 μm pixel size proposed for mammography). For higher x-ray energies used in fluoroscopy and chest imaging ($d_{se}=500\text{ }\mu\text{m}$), MTF is >90% up to 2.5 lp/mm,³⁸ corresponding to the pixel size requirements for fluoroscopy and chest radiography. Thus the resolution of the detector will be largely determined by the pixel size of the active matrix, and not the intrinsic resolution of *a*-Se.

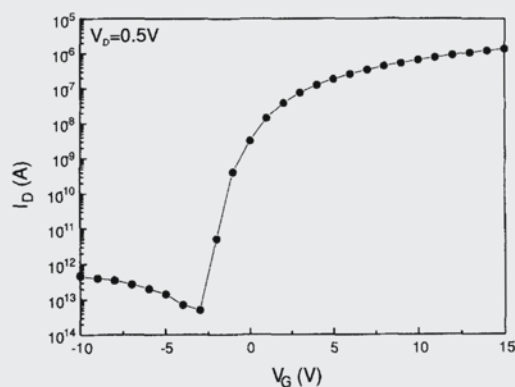


FIG. 5. Transfer characteristic curve of a typical CdSe thin film transistor: Channel current I_D as a function of gate bias potential V_G at drain bias potential $V_D=0.5$ V.

Currently, active matrices have been made 25×25 cm in area and with $90 \mu\text{m}$ pixel pitch.³⁹ Eventually, with the demand for larger area and higher resolution active matrices in the development of liquid crystal displays, an active matrix array as large as required by chest imaging and with a pixel size small enough ($50 \mu\text{m}$) to be suited for mammography will probably be feasible.

B. Readout rate and lag

1. Readout rate

A TFT with a channel $30 \mu\text{m}$ wide and $50 \mu\text{m}$ long, and the silicon dioxide (SiO_2) gate insulator $0.5 \mu\text{m}$ thick was investigated. Figure 5 shows the measured transfer characteristic curve at $V_D=0.5$ V. I_D covers a range of seven orders of magnitude, which provides a clear distinction between the "on" (e.g., at $V_G=10$ V) and "off" (e.g., at $V_G=-3$ V) states. When the TFT is turned on with $V_G=10$ V, shown in Fig. 6(a), I_D increases in an approximately linear fashion with V_D in the region of $V_D < 2.5$ V and the initial slope fits a R_{on} of $\sim 1.5 \text{ M}\Omega$. When the TFT is turned off at $V_G=-3$ V, as shown in Fig. 6(b), the initial slope of the curve indicates a $R_{\text{off}} > 10^{13} \Omega$.

The value of C_{st} , which is the dominant part of C_p , is ~ 1 pF for the active matrices used in our investigation, thus from the above values for R_{on} and R_{off} , τ_{on} is $\sim 1.5 \mu\text{s}$ and τ_{off} is ~ 10 s. If we allow five time constants to completely discharge each pixel, i.e., $M=5$ in Eq. (1), T_{read} for a 1000 line fluoroscopy detector is ~ 7.5 ms which is comfortably less than the T_F required for real-time x-ray imaging (33 ms). This result agrees with a similar analysis performed for the readout rate of flat-panel detectors using phosphor screen and α -Si TFT-photodiode arrays.^{40,41}

T_{read} is increased in proportion to the increased number of rows required for chest radiography and mammography to 13.5 and 36 ms, respectively, both of which satisfy the requirement of instant readout. With $\tau_{\text{off}}=10$ s, the image

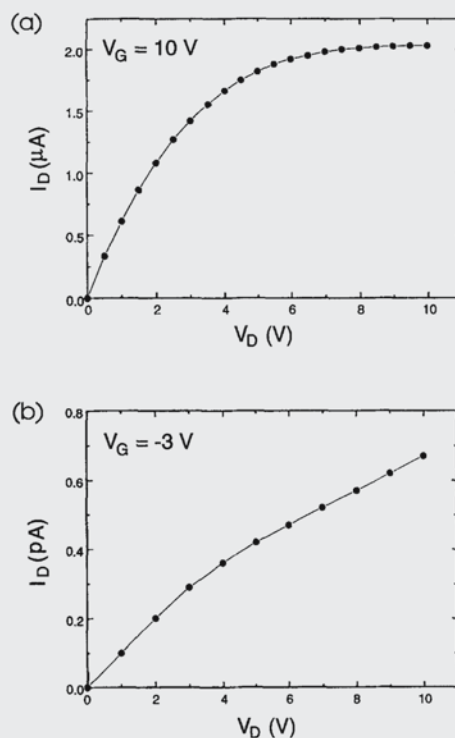


FIG. 6. Output characteristic curves: (a) Channel current I_D as a function of drain bias potential V_D with the TFT "on;" (b) I_D as a function of V_D with the TFT "off."

charge leakage is $<0.5\%$ even after the longest T_{read} (36 ms), thus the detector will not suffer from information loss due to leakage current of the TFTs.

2. Lag

The mobility of carriers for α -Se has been measured as $0.0063 \text{ cm}^2/\text{Vs}$ for electrons and $0.19 \text{ cm}^2/\text{Vs}$ for holes.⁴² From Eq. (2), when the thickness of α -Se $d_{\text{Se}}=500 \mu\text{m}$ and the applied $E_{\text{Se}}=10 \text{ V}/\mu\text{m}$, the maximum charge transit time T_R is $79 \mu\text{s}$ for electrons and $2.6 \mu\text{s}$ for holes. Thus the largest fraction of charge generated in one frame contributing to its following frame is 0.24% (the ratio between $T_R=79 \mu\text{s}$ and $T_F=33$ ms). Under the condition of $M=5$, as given in the previous discussion of T_{read} , 99.3% of the image charge at each pixel is read out. Therefore including both the above mechanisms, the maximum percentage of image charge that can contribute to the subsequent frames is $<1\%$, thus no significant image lag would be observed.

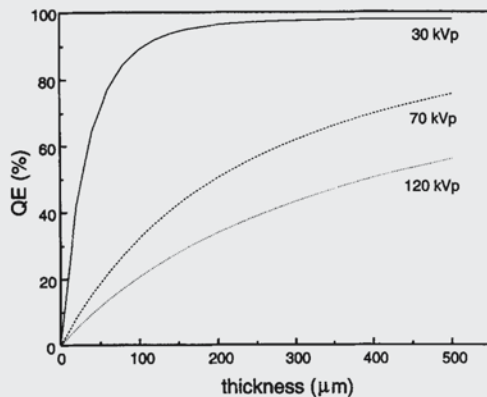


FIG. 7. Quantum efficiency (QE) of *a*-Se as a function of its thickness for x-ray spectra used in chest radiography (120 kVp), mammography (30 kVp) and fluoroscopy (70 kVp).

C. Quantum noise limited exposure range

1. Signal

The quantum efficiency, η , of *a*-Se is shown in Fig. 7, plotted as a function of d_{se} . For the 30 kVp mammographic spectrum, there is no significant increase of η for $d_{se} > 200 \mu\text{m}$, thus a value of $d_{se} = 200 \mu\text{m}$, where $\eta = 96.2\%$, should be suitable for digital mammography. The largest d_{se} reported is $500 \mu\text{m}$,¹¹ which provides $\eta = 55.9\%$ and 75.5% for the spectra required for chest radiography and fluoroscopy, respectively. The W for *a*-Se has been measured to be 50 eV at $E_{se} = 10 \text{ V}/\mu\text{m}$.⁴² Thus the image charge per pixel can be calculated using Eqs. (3) and (5) and is 4.91×10^6 , 3.45×10^6 , and $1.68 \times 10^5 \text{ electrons (pixel)}^{-1} \text{ mR}^{-1}$ for fluoroscopy, chest radiography, and mammography, respectively. The maximum image charge is obtained at the exposure of 240 mR , the raw beam exposure considered for mammography, and it is $4.02 \times 10^7 \text{ electrons/pixel}$ which results in a pixel potential of 6.43 V at $C_p = 1 \text{ pF}$. Since the pixel potential does not significantly reduce the E_{se} , the detector will have a linear x-ray response in the diagnostic radiation range.

The maximum x-ray exposure that the detector can respond to equals the product of the pixel capacitance C_p and the highest pixel potential, V_{DP} , at which the TFT can maintain its function. It has been shown that V_{DP} of CdSe TFTs can be as high as $\sim 200 \text{ V}$.⁴³ Thus the detector can respond up to an image charge level of 200 pC ($1.25 \times 10^9 \text{ electrons}$)/pixel.

2. X-ray quantum noise

The x-ray quantum noise as a function of x-ray exposure was calculated using Eq. (6) and the detector parameters defined in Table I. The result is plotted with solid lines in Fig. 8 for fluoroscopy, chest radiography, and mammography.

3. Electronic noise

a. Dark current shot noise. The *a*-Se plates used in xero-radiography are made by thermal evaporation of *a*-Se onto an aluminum substrate. The E_{se} is applied by coronotron charging the free top surface to a positive high potential. The dark current of such *a*-Se plates can be determined by measuring the dark decay of the surface potential as a function of time.⁴⁴ For a $300 \mu\text{m}$ thick *a*-Se plate at $E_{se} = 10 \text{ V}/\mu\text{m}$, the result showed that the dark current is $< 100 \text{ fA/mm}^2$. The dark current was unchanged when a thin indium electrode was evaporated onto the free top surface. Then from Eq. (7), the dark current shot noise q_{nd} is less than 36 electrons for a fluoroscopy detector, which has the largest pixel size ($250 \mu\text{m}$) thus highest q_{nd} among the three imaging applications. The dark current shot noise is therefore negligible.

b. TFT thermal noise. The thermal NPS of the TFT, $W_{it}^2(f)$, was measured with the TFT turned on at $V_G = 10 \text{ V}$ and $I_D = 0$, the result is shown in Fig. 9. The measured $W_{it}^2(f)$ is white and the noise power density is $(1.28 \pm 0.12) \times 10^{-26} \text{ A}^2/\text{Hz}$. This is in substantial agreement with the theoretical prediction of $1.10 \times 10^{-26} \text{ A}^2/\text{Hz}$ using Eq. (8) for the channel resistance $R_{on} = 1.5 \text{ M}\Omega$. The C_p for our active matrices is 1 pF ; thus, from Eq. (14), the TFT thermal noise q_{nt} is 700 electrons at room temperature. This is a dominant source of electronic noise, as shown in Fig. 10.

c. TFT flicker noise. The NPS of the TFT, $W_{if}^2(f)$, measured with $I_D \neq 0$ are also shown in Fig. 9, and they were found to increase with I_D . Then the relationship between $W_{if}^2(f)$ [obtained with $W_{if}^2(f) - W_{it}^2(f)$] and I_D was fitted to the empirical expression⁴⁵

$$W_{if}^2(f) = \alpha(I_D^\beta/f^\gamma) \quad (16)$$

where α , β , and γ are constants. From the measurement, the flicker NPS $W_{if}^2(f)$ has α of $(8.41 \pm 0.28) \times 10^{-10}$, β of 2.03 ± 0.06 , and γ of 0.82 ± 0.02 .

During image readout, I_D decays exponentially with time. Thus $W_{if}^2(f)$ at a given charge signal level q_s is estimated using a constant I_D which is the mean square average value of I_D during the readout period T_{on} . Then the noise charge q_{nf} due to the TFT flicker noise can be obtained by integrating $W_{if}^2(f)$ [Eq. (11), substituting $W_{it}^2(f)$ with $W_{if}^2(f)$] over the bandwidth of the charge amplifier (1 MHz). In Fig. 10, q_{nf} is plotted as a function of q_s , and it shows that q_{nf} is negligible compared to the TFT thermal noise q_{nt} at low q_s level.

d. Amplifier noise. As shown in Eq. (15), the amplifier noise q_{na} is linearly proportional to the input load capacitance C_d . An example of a suitable charge amplifier has q_{na0} of 250 electrons and a slope δ of 15.⁴⁰ The main contribution to C_d is the capacitance between each gate line and source (data) line C_{gs} . For our active matrices, C_{gs} is typically 0.05 pF . Thus for a detector with 1000 gate lines, as proposed for fluoroscopy, C_d is 50 pF . Then from Eq. (15), q_{na} is 1000 electrons. As shown in Fig. 10, q_{na} is the most dominant source of electronic noise.

e. Total noise. We obtain the total electronic noise q_n by adding all the noise components in quadrature, and the result is shown as a function of charge signal q_s in Fig. 10. In order

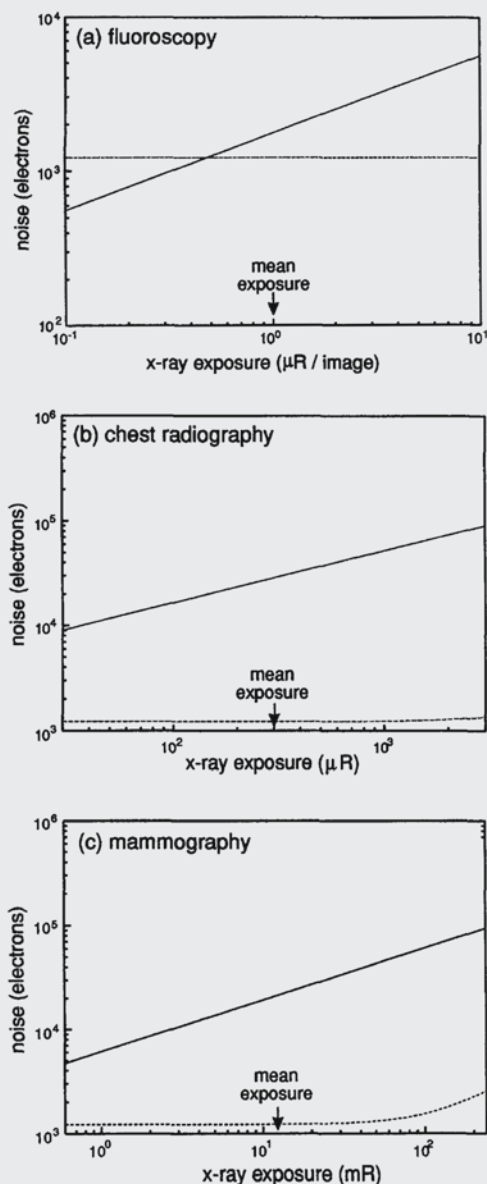


FIG. 8. Estimation of x-ray quantum noise and electronic noise of each pixel as a function of x-ray exposure for: fluoroscopy, chest radiography, and mammography. X-ray quantum noise is plotted using solid lines, and electronic noise with dashed lines.

to determine the quantum noise limited exposure range for each imaging application, q_n is replotted, as a function of x-ray exposure in Fig. 8.

As shown in Fig. 8 for chest radiography and mammography, the x-ray quantum noise is larger than the total electronic noise over the whole required exposure range, i.e., the

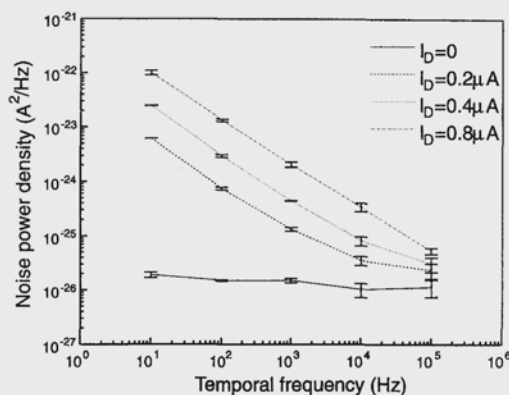


FIG. 9. The noise power spectra (NPS) of a CdSe thin film transistor measured with the TFT turned on ($V_G = 10$ V).

requirement for quantum noise limitation is satisfied. However, as also shown in Fig. 8 for fluoroscopy, the detector is not quantum noise limited below an exposure of $0.5 \mu\text{R}/\text{image}$ and thus does not cover the whole exposure range desired for fluoroscopy ($0.1\text{--}10 \mu\text{R}/\text{image}$). The dominant sources of electronic noise are the TFT (700 electrons) and the amplifier (1000 electrons). Thus the two possibilities for improvement are (i) to reduce the dominant sources of noise, e.g., by choosing amplifiers with lower noise or reducing the pixel capacitance C_p ; (ii) to increase the x-ray sensitivity of the detector by a factor of 2 so that the amount of charge associated with the x-ray quantum noise exceeds the electronic noise. This can be achieved by either decreasing the W of $a\text{-Se}$ or using other types of photoconductor with lower W , e.g., TlBr. The W for TlBr is ~ 7 eV (Ref. 8) which is seven times lower than that for $a\text{-Se}$.

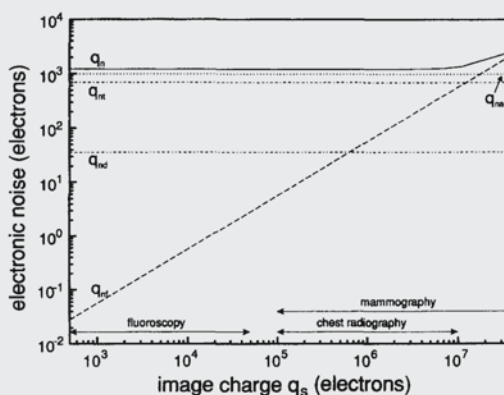


FIG. 10. Electronic noise from each pixel of the detector as a function of signal q_s . q_{nd} : dark current shot noise; q_{nf} : TFT thermal noise; q_{nf} : TFT flicker noise; q_{na} : amplifier noise; q_n : total electronic noise.

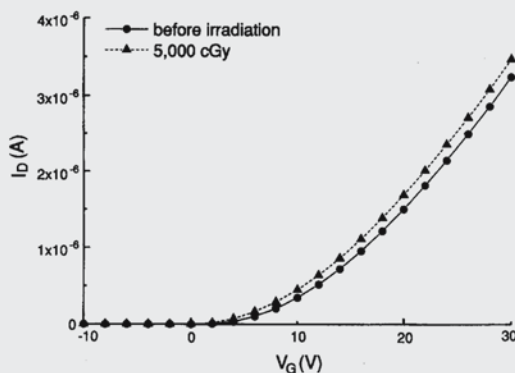


FIG. 11. The transfer characteristic curve of a thin film transistor before and after exposure to 5000 cGy of ^{60}Co radiation.

D. Resistance to radiation damage

Figure 11 shows the transfer characteristic I_D - V_G curves (with $V_D=0.5$ V) for a single TFT before and after irradiation at zero gate bias ($V_{GB}=0$). The dominant effect of radiation is the decrease of threshold voltage V_T by ~ 1 V, where V_T is determined as the intercept of the linear extrapolation of the I_D - V_G curve with the V_G axis minus $V_D/2$. The decrease of V_T suggests that TFTs need more negative gate operational voltage $V_{G(\text{off})}$ to be turned off. Table II shows the change of V_T , i.e., ΔV_T , at different V_{GB} . Since the TFTs are turned off (with $V_G \leq 0$ V) during most of the time under radiation, the amplitude of ΔV_T would be less than 2 V during the lifetime of the detector. Thus if we choose the operational $V_{G(\text{off})}$ to be -5 V for the TFT discussed in the section of readout rate, there will be sufficient safety margin so that the function of the TFTs will not be affected by radiation.

V. CONCLUSIONS

We have investigated a directly x-ray sensitive, solid-state, flat-panel detector for digital radiological imaging using self-scanned readout of an x-ray photoconductor. Our study is based on an idealized circuit model for the detector, known properties of α -Se, and measured properties of CdSe TFTs. The image readout rate is shown to be fast enough for both real-time x-ray imaging and instant radiography. The detector can be quantum noise limited for the exposure level used in radiography such as chest radiography and mammography. It can also be quantum noise limited above $0.5 \mu\text{R}$ /

image, i.e., half the mean exposure level typically used in fluoroscopy. Further improvement by either decreasing the electronic noise or increasing the x-ray sensitivity by a factor of 2 is needed for fluoroscopy. The detector components are shown to be radiation resistant to the lifetime dose expected for a diagnostic x-ray imaging system. This work suggested that a detector using self-scanned readout of an x-ray photoconductor can potentially satisfy all the design requirements for an x-ray imaging system and further investigation of practical aspects of its feasibility will be of interest.

ACKNOWLEDGMENTS

This work is financially supported by the National Cancer Institute of Canada through a Terry Fox Programme Project Grant "Imaging for Cancer" and a Steve Fonyo Studentship to W. Zhao. We thank Dr. D. Waechter, Dr. Z. Huang, J. Farrell, and J. Wright (Litton Systems Canada); A. Mouton and N. Araj (Noranda Advanced Materials); and our colleagues R. Luhta, D. Mah, and G. DeCrescenzo for helpful discussions.

TABLE II. Change of threshold voltage, ΔV_T , at different gate bias condition V_{GB} during irradiation of 5000 cGy.

Gate bias condition during irradiation V_{GB} (V)	Threshold voltage shift ΔV_T (V)
-20	-2.0 ± 0.1
0	-1.1 ± 0.1
+20	-6.2 ± 0.1

- ¹M. L. Giger, N. Ahn, K. Doi, H. MacMahon, and C. E. Metz, "Computerized detection of pulmonary nodules in digital chest images: Use of morphological filters in reducing false-positive detections," *Med. Phys.* **17**, 861-865 (1990).
- ²L. E. Antonuk, J. Boudry, W. Huang, D. L. McShan, E. J. Morton, J. Yorkston, M. J. Longo, and R. A. Street, "Demonstration of megavoltage and diagnostic x-ray imaging with hydrogenated amorphous silicon arrays," *Med. Phys.* **19**, 1455-1466 (1992).
- ³W. Zhao and J. A. Rowlands, "A large area solid-state detector for radiology using amorphous selenium," *Proc. SPIE* **1651**, 134-143 (1992).
- ⁴W. Zhao and J. A. Rowlands, "Digital radiology using self-scanned readout of amorphous selenium," *Proc. SPIE* **1896**, 114-120 (1993).
- ⁵L. E. Antonuk, J. Boudry, J. Yorkston, E. J. Morton, W. Huang, and R. A. Street, "Development of thin-film flat-panel arrays for diagnostic and radiotherapy imaging," *Proc. SPIE* **1651**, 94-105 (1992).
- ⁶L. A. DeWerd, "Electroradiography (xeroradiography)—Equipment and physical principles," *CRC Handbook of Medical Physics*, edited by R. G. Waggenger, J. G. Kereiakes, and R. J. Shalek (CRC Press, Boca Raton, FL, 1984), Vol. II, pp. 123-145.
- ⁷Y. Suzuki, K. Uchiyama, and M. Ito, "A large diameter x-ray sensitive vidicon with Beryllium window," *Adv. Electron. Electron Phys.* **28A**, 209-222 (1976).
- ⁸K. S. Shah, J. C. Lund, F. Olschner, L. Moy, and M. R. Squillante, "Thallium bromide radiation detectors," *IEEE Trans. Nucl. Sci.* **NS-36**, 199-202 (1989).
- ⁹Y. Tomita, Y. Hatanaka, T. Takabayashi, and T. Kawai, "X-ray imaging camera tube using sputter-deposited CdTe/CdS heterojunction," *IEEE Trans. Electron Phys.* **EP-40**, 315-319 (1993).
- ¹⁰J. W. Boag, "Xeroradiography," *Phys. Med. Biol.* **18**, 3-37 (1973).
- ¹¹U. Neitzel, I. Maack, and S. Gunther-Kohfahl, "Image quality of a digital chest radiography system based on a selenium detector," *Med. Phys.* **21**, 509-516 (1994).
- ¹²F. C. Luo, "Active matrix LC displays," in *Liquid Crystal Applications and Uses*, edited by B. Bahadur (World Scientific, Singapore, 1990), Vol. 1, pp. 397-436.
- ¹³H. MacMahon, C. J. Vyborny, C. E. Metz, K. Doi, V. Sabeti, and S. L. Solomon, "Digital radiography of subtle pulmonary abnormalities: An ROC study of the effect of pixel size on observer performance," *Radiology* **158**, 21-26 (1986).
- ¹⁴R. G. Fraser, C. Sanders, G. T. Barnes, H. MacMahon, M. L. Giger, K. Doi, A. W. Templeton, G. G. Cox, S. J. Dwyer, C. R. B. Merritt, and J. P. Jones, "Digital imaging of the chest," *Radiology* **171**, 297-307 (1989).
- ¹⁵M. J. Yaffe, "Digital mammography," in *Syllabus: A Categorical Course in Physics—Technical Aspects of Breast Imaging*, edited by A. G. Haus and M. J. Yaffe (RSNA, Oak Brook, IL, 1992), pp. 245-255.

- ¹⁶J. A. Rowlands, D. M. Hynes, and E. W. Edmonds, "System for digital acquisition of gastrointestinal images," *Med. Phys.* **16**, 553–560 (1989).
- ¹⁷W. F. Schreiber, *Fundamentals of Electronic Imaging Systems* (Springer-Verlag, Berlin, 1986), Chap. 1.
- ¹⁸M. M. Tesic, R. A. Mattson, G. B. Barnes, R. A. Sones, and J. B. Stickney, "Digital radiography of the chest: Design features and considerations for a prototype unit," *Radiology* **148**, 259–263 (1983).
- ¹⁹L. R. Goodman, C. R. Wilson, and W. D. Foley, "Digital imaging of the chest: Promises and problems," *Am. J. Roentgenol.* **150**, 1241–1251 (1988).
- ²⁰R. M. Nishikawa, G. E. Mawdsley, A. Fenster, and M. J. Yaffe, "Scanned-projection digital mammography," *Med. Phys.* **14**, 717–727 (1987).
- ²¹J. A. Rowlands, "Real-time image processing of video image sequences for videofluoroscopy," *Proc. SPIE* **1652**, 294–303 (1992).
- ²²A. G. Leiga, "Xerography in medical imaging applications," in *Proceedings of the 4th International Symposium on Uses of Selenium and Tellurium* (Selenium–Tellurium Development Association, Darien, CT, 1989), pp. 249–266.
- ²³L. E. Antonuk, J. Yorkston, W. Huang, J. Siewerdsen, and R. A. Street, "Considerations for high frame rate operation of two-dimensional a-Si:H imaging arrays," *Mat. Res. Soc. Symp. Proc.* **297**, 945–950 (1993).
- ²⁴A. Rose, *Concepts in Photoconductivity and Allied Problems* (Krieger, Melbourne, FL, 1978), Chap. 4.
- ²⁵H. P. Chan and K. Doi, "Energy and angular dependence of x-ray absorption and its effect on radiographic response in screen-film systems," *Phys. Med. Biol.* **28**, 565–579 (1983).
- ²⁶D. M. Tucker, G. T. Barnes, and D. P. Chakraborty, "Semiempirical model for generating tungsten target x-ray spectra," *Med. Phys.* **18**, 211–218 (1991).
- ²⁷D. M. Tucker, G. T. Barnes, and X. Wu, "Molybdenum target x-ray spectra: A semiempirical model," *Med. Phys.* **18**, 402–407 (1991).
- ²⁸W. Hillen, U. Schiebel, and T. Zaengel, "Imaging performance of a digital storage phosphor system," *Med. Phys.* **14**, 745–751 (1987).
- ²⁹T. H. Wilmshurst, *Signal Recovery From Noise in Electronic Instrumentation* (Hilger, Bristol, 1985), Chap. 4, p. 58.
- ³⁰A. Van der Ziel, *Noise in Measurements* (Wiley, Toronto, 1976), Chaps. 6 and 13.
- ³¹I. Fujieda, R. A. Street, R. L. Weisfield, S. Nelson, P. Nylen, V. Perez-Mendez, and G. Cho, "High sensitivity readout of 2D a-Si image sensors," *Jpn. J. Appl. Phys.* **32**, 198–204 (1993).
- ³²T. H. Wilmshurst, in Ref. 29, Chap. 6, pp. 69–85.
- ³³G. Cho, J. S. Drewery, I. Fujieda, T. Jing, S. N. Kaplan, V. Perez-Mendez, S. Qureshi, D. Wildermuth, and R. A. Street, "Measurements of 1/f noise in a-Si:H PIN diodes and thin-film-transistors," *Mat. Res. Soc. Symp. Proc.* **192**, 393–398 (1990).
- ³⁴P. W. Nicholson, *Nuclear Electronics* (Wiley, London, 1974), Chap. 5.
- ³⁵S. O. Kasap, V. Aiyah, A. Baillie, and A. G. Leiga, "X-ray induced hole trapping in electroradiographic plates," *J. Appl. Phys.* **69**, 7087–7096 (1991).
- ³⁶T. P. Ma and P. V. Dressendorfer, *Ionizing Radiation Effects in MOS Devices and Circuits* (Wiley, New York, 1989).
- ³⁷M. Powell, "The physics of amorphous-silicon thin-film transistors," *IEEE Trans. Electron Devices*, **ED-36**, 2753–2763 (1989).
- ³⁸W. Que and J. A. Rowlands, "X-ray imaging using amorphous selenium: Inherent resolution," *Med. Phys.* **22**, 365–374 (1995).
- ³⁹R. Martin, T. Chuang, H. Steemers, R. Allen, R. Fulks, S. Stuber, D. Lee, M. Young, J. Ho, M. Nguyen, W. Meull, T. Fiske, R. Bruce, M. Thompson, M. Tilton, and L. D. Silverstein, "A 6.3-Mpixel AMLCD," *SID Digest* **24**, 704–707 (1993).
- ⁴⁰L. E. Antonuk, J. Yorkston, W. Huang, J. Siewerdsen, and R. A. Street, "Considerations for high frame rate operation of two-dimensional a-Si:H imaging arrays," *Mat. Res. Soc. Symp. Proc.* **297**, 945–950 (1993).
- ⁴¹U. W. Schiebel, N. Conrads, N. Jung, M. Weilbrecht, T. T. Zaengel, M. J. Powell, I. D. French, and C. Glasse, "Fluoroscopic x-ray imaging with amorphous silicon thin-film arrays," *Proc. SPIE* **2163**, 129–140 (1994) (edited by R. Shaw).
- ⁴²J. A. Rowlands and G. DeCrescenzo, "X-ray imaging using amorphous selenium: Determination of activation energy by pulse height spectroscopy," *Med. Phys.* **19**, 1065–1070 (1992).
- ⁴³D. Waechter, T. Billard, and P. Gogna, "Properties of oxide-nitride-oxide stacked films for gate insulation in active matrix displays," *Mat. Res. Soc. Symp. Proc.* **284**, 443–448 (1993).
- ⁴⁴R. M. Schaffert, *Electrophotography* (Focal, London, 1975), Chaps. 10 and 11.
- ⁴⁵E. R. Chenette, "Noise in semiconductor devices," *Adv. Elec. Electron Phys.* **23**, 303–346 (1967).

5 PACS

- | | | |
|------------|--|-----|
| 5.1 | Applications of Picture Processing, Image Analysis and Computer Graphics Techniques to Cranial CT Scans.
Proceedings of the Sixth Conf. on Computer Applications in Radiology and Computer Aided Analysis of Radiological Images. IEEE Computer Society Press (1979): 341–354
<i>H.U. Lemke, H.S. Stiehl, H. Scharnweber, D. Jackél</i> | 334 |
| 5.2 | An All-digital Nuclear Medicine Department.
Radiology 147 (1983): 237–240
<i>J.A. Parker, H.D. Royal, R.F. Uren, D. Front, J.G. Bliss, M. Rabussi
D. Jansons, M.S. Kolodny, G.M. Kolodny</i> | 349 |
| 5.3 | Digital Radiology at the University of California, Los Angeles: A Feasibility Study.
Proc. SPIE 418 (1983): 259–265
<i>H.K. Huang, Z. Barbaric, N.J. Mankovich, C. Moler</i> | 358 |
| 5.4 | Assessment of the Integration of HIS/RIS with a PACS.
Proc. SPIE 1234 (1990): 391–397
<i>B.A. Levine, S.K. Mun, H.R. Benson, S.C. Horii</i> | 367 |
| 5.5 | Environmental Designs for Reading from Imaging Workstations: Ergonomic and Architectural Features.
Proc. SPIE 1091 (1989): 172–178
<i>S.C. Horii et al.</i> | 377 |

Introduction

The concept of digital image communication and digital radiology was introduced in the late 1970s and increasingly integrated into hospitals around the world. The vision of an all-digital department includes, besides all-digital diagnostic devices, a complete new digital communication structure and standard. With the support of the International Society of Optical Engineering (SPIE), the first conference and workshop on Picture Archiving and Communication Systems (PACS) for Medical Applications was held in January 1982. During that meeting, the term PACS was coined. Now PACS has become a routinely used clinical tool.

H.U. Lemke from the Technical University of Berlin published the earliest paper proposing the concept of PACS in 1979. This concept incorporated the multimedia electronic medical record, medical workstations, and local and global network communications. It provides the base of a PACS project specification and subsequent implementation as part of the Berlin Communication System (BERKOM), initiated by the Senate of Berlin in 1986. Within the BERKOM project, special attention was given to end-systems, particularly development of workstations with multimedia communication capabilities. Special emphasis was also given to medical applications. The medical image communication project RADCOM was one example of a special health care setting in radiological data communication. With varying degrees of success teleconferencing was held between the Rudolf Virchow University Hospital at Berlin-Charlottenburg and Berlin-Wedding. Cost considerations were probably the main reason why PACS realizations were not started before the mid-1980s in Germany.

The first clinical PACS paper was published by J.A. Parker et al from the Nuclear Medicine Department at Beth Israel Hospital, Harvard Medical School, Cambridge, MA, USA. A PACS concept was implemented for digital nuclear medicine images and integrated with a radiology reporting system and gamma cameras. Starting with nuclear medicine resulted from the relatively lower requirements for display, communication and storage compared with other radiology modalities. Furthermore, nuclear medicine was the first radiology modality to use computers for functional analysis. Certain design principles of the first PACS have remained constant and have proved useful through many changes through the years. The use of standard off-the-shelf hardware and software offered the opportunity to communicate with a wide range of nuclear medicine cameras from different manufacturers and to be able to display and analyze data from all of them. Insisting on three levels of backup and redundancy results in a concept of a mini PACS design, where each section of a radiology department has its own stand-alone PACS. Storing data over 17 years was possible with no meaningful downtime.

Another landmark paper was published in 1983 by HK Huang and his co-workers outlining the initial planning for the PACS efforts in the Radiology Department of the University of California (UCLA). It established the methodology on how to justify the costs of implementing a PACS system. Guidelines were established and subsequently the National Institute of Health and later the Department of Radiology Science funded the PACS in Radiology research and development project to provide a filmless radiology department.

At Georgetown University Hospital, Washington DC, USA, S. Horii and his group worked on development of all aspects of PACS. The design of a workstation with consideration of the environmental conditions for reading was described with a focus on ergonomic and architectural features. Outlining the problems of just putting a workstation in place of a film alternator, Horii made suggestions for some redesigns of the reading room at Georgetown.

Together with B. Levine, problems in sharing and exchanging information between a PACS and a hospital information system (HIS/RIS) were identified and outlined in a paper presented in 1990. The paper described the experience and the development of the interface and its impact on clinical operations.

References

- Early PACS Papers (2003) Laying the foundation for the future of Digital Medical Imaging. Journal of Digital Imaging. Special Issue 16: 1
- Computerized Medical Imaging and Graphics (2003) Special Issue: Picture Archiving and Communication System (PACS) – Twenty years later. Vol. 27: 2-3

5.1 Applications of Picture Processing, Image Analysis Computer Graphics Techniques to Cranial CT Scans

Heinz U. Lemke (born 1941)

Heinz Lemke was born on 25 March 1941 in Stettin, Germany. He started his education at University of London, Institute of Computer Science with extramural studies in computer science (1965–1966). He wrote a thesis: Interactive Graphics in an Integrated CAD System and got his PhD. from the University of Cambridge, Computer Laboratory. In 1981 he studied medical science and pathology at the Kings College, University of Cambridge. In 1975 Heinz Lemke was appointed Professor of Computer Science (Computer Graphics and Computer Assisted Medicine) at the Technical University Berlin, Germany. In 1976 he became director of the Institute of Technical Informatics and in 1979 Chairman and Speaker of the Faculty of Informatics, at the TU Berlin. He is a Visiting Professor at the University of California, Medical Center, Irvine, USA (1987), the University of Osaka, Japan (1992), the University of California, Department of Radiology and Informatics, San Francisco, USA (1994). In his original paper he introduced the concept of digital image communication and display in 1979.



Heinz Lemke is a founding member of Steering Committee for Euro PACS, Netherlands (1987-present), founder and Chairman of the working group “Radiology, Informatics and Communication” of the German Radiological Society (1992–1994), founding member and General Secretary of the International Society for Computer Aided Surgery (ISCAS), France (1996-present), founding member and member of the Executive Board of the World Academy of Biomedical Technology (UNESCO), Paris (1997-present), a member of the International Committee for Informatics of the Société Française de Radiologie, Paris (1997-present), member of the Information Technology Committee of the British Institute of Radiology, London (2000-present), founding member and General Secretary of the Deutsche Gesellschaft für Computer- und Roboter-Assistierte Chirurgie (2001-present).

He is a member of several national and international scientific and the societies editorial advisory boards of several scientific journals. He is a Honorary Member of Euro PACS (1996), the British Institute of Radiology (2003) and Österreichische Wissenschaftliche Gesellschaft für Telemedizin (2003).

Heinz U. Lemke is the organizer of the annual CARS meetings.

Picture courtesy Heinz Lemke, PhD, 2004.

R.S. Stiehl

H. Scharnweber

D. Jackél

APPLICATIONS OF PICTURE PROCESSING, IMAGE ANALYSIS AND COMPUTER GRAPHICS TECHNIQUES TO CRANIAL CT SCANS

H.U.Lemke, H.S.Stiehl, H.Scharnweber, D.Jackél

COMPACT Project Group, Institut für Technische Informatik,
Technische Universität Berlin

Summary - Systems for the processing and representation of cranial computed tomograms have become a significant addition to the use of computers in medicine, particularly radiology. This paper tries to outline a global view on some of the important technical capabilities such systems can provide using techniques from Picture Processing, Image Analysis and Computer Graphics. Experimental results of the COMPACT Project are presented wherever appropriate.

Further thought is also given to the framework in which CT processing may take place. To ensure clinical efficacy a concept of a Medical Work Station as part of a distributed computing network is discussed. Some consideration is then given to the physicians possible working modes within such a system.

1. Introduction

In the process of medical diagnosis and therapy, information is usually presented by means of the written word, pictures, graphics and the spoken word. For a particular patient the sum-total of this information may be labelled the medical record (MR). In the interest of a patient oriented health care system there are a number of important if not vital requirements on how the information in the MR should be organized and used, e.g. there should be

- a) access to the information in the MR at the right place in the right time by the right people,
- b) maximum utilisation of information for diagnostic and therapeutic purposes,
- c) reliable linkage of all patient specific information into one MR.

In addition, there are some desirable features of data representation and processing for the medical practitioner, e.g. there should be

- d) uniform, structured and easy to understand data representations of MR's,
- e) easily extendable MR's,
- f) safe, protected and easily accessible MR's,
- g) speedy statistical data gathering facilities on MR's,
- and most important of all
- h) flexible conferencing and consulting mode facilities

ities using MR's and all modes of communication (i.e. word, picture and voice communication).

It is suggested in this paper that each of the above requirements for information management and evaluation can be maximally satisfied by using medical work stations (MWS's) in a distributed computing network.

The development of such a system is currently being carried out at the Institut für Technische Informatik at the Technische Universität Berlin. The principal application of the MWS's is for the management of neurological disorders and includes a system for the Computerized Management, Processing and Analysis of Computed Tomograms (COMPACT).

Processing and analysis of Computed Tomograms (CT's) are mainly in support of requirement b). They are seen in the framework of picture processing and image analysis and are discussed respectively in chapter 2 and 3 of this paper.

Computerized management of CT's covers a wide spectrum of activities in support of all of the above mentioned requirements and features for MR processing. Computer Graphics is particularly suitable for feature d) and will be discussed in chapter 4.

Our approach to provide for feature h) will be outlined in chapter 5, that is transmission of CT's in a network for communication and filing purposes.

2. Picture Processing Techniques

Digital picture processing techniques, generally aimed at a transformation from one picture to a modified and improved picture have to meet when applied to computed tomography the following demands:

- a) improve the picture with respect to the human perceptual ability and/or
- b) reduce noise and scan and motion artifacts and/or
- c) obtain a more suitable representation of the picture for the segmentation process.

To achieve the most suitable representation of the computed tomograms for the physician the main requirement for improving the visualization of the

anatomic and pathologic picture content. This may require noise smoothing, edge and contrast enhancement and pseudo colour transformations. When automated analysis by an off- or on-line computer system is intended demand c) may be further divided into the categories i) improvement of the picture characteristics, e.g. edges and contrasts, and ii) data reduction to limit the size of the picture matrix.

Computed Tomogram Characteristics

In general, the two-dimensional representation of a picture contains a degradation which is dependent on the picture formation process. Degradations may be modeled by a convolution function over the picture and an additive component, the noise. For X-ray imaging in computed tomography, there may be several sources of degradations, e.g. as part of the modulation transfer function of the scanner, caused by scattering photons during traversal of the object and the nonlinearity of energy source and detectors, and the influence on picture quality of the algorithms for reconstruction from projections. Furthermore, picture quality is dependent on several parameters, in particular the scan energy, the number of projections and the spatial resolution.

It is obvious that all parameters are highly scanner dependent. Current work embedded in the COMPACT Project focus on cranial computed tomograms obtained from the EMI CT1010 scanner at the Department of Computed Tomography of The Free University Berlin. The computed tomograms are defined as a digital two-dimensional array with a total of 160×160 picture elements (pixels) each of which is associated with a numerical integer value in the range -1000 ... 1000 (HU-value) which corresponds to the average density of brain structures in a volume element (voxel) sized $1,5 \times 1,5 \times 10 \text{ mm}^3$. Notwithstanding the two-dimensional representation of the computed tomogram, the real information per pixel is of a three-dimensional nature.

Data Reduction

The task of data reduction may be defined as the suppression of irrelevant information within the entire picture domain. In cranial computed tomograms, the relevant structural content for diagnostic and therapeutic purpose is the distribution of HU-values describing the attenuation coefficients of the brain tissue. For computer processing purposes it is useful to reduce the great number of bits per tomogram so as to achieve only storage of the matrix line segments which refer to brain.

The preprocessing module for cranial computed tomograms includes smoothing, skull detection, detection of brain line segments and the computation of several statistics on the brain pixels. Cranial computed tomograms are stored on magnetic tapes by the processor of the EMI CT1010 scanner and read by an ITEL AS-5 of the Department of Computer Science at the Technical University Berlin. The complete set of picture matrices is transferred onto the disks of the graphics system Adage AGT 130 via a 4800 baud data line. The preprocessing algorithms were de-

signed for scan-mode processing via a software buffer holding 5 tomogram lines at a time. Subsequent processing has been adapted to the line-oriented tomogram storage structure on the tape and the limited main core size of 32K words of the ADAGE system which does not allow core resident storage of the complete tomogram matrix during processing.

Skull detection is performed simply by fixed thresholding of the smoothed pixels in the line buffer. Fixed thresholding is enabled by the fact that bone appears in a constant range of HU-values on the tomograms. After Skull detection each row lying within the skull is checked for brain candidates by a decision on the HU-value statistics of the pixels per line. By this simple and also fast method a distinction between brain and background is made. Once a brain line segment is detected several statistical computations are made on the line buffer:

mean HU-value and standard deviation of the HU-values of the brain,

the first order histogram of brain pixels,

the brain area,

the center of the entire brain region on the tomogram by moment analysis, and

the symmetry line, which may be rotated due to patient position in the gantry by the principal axis method (details are given in).

After preprocessing the reduced tomogram data are stored in a core resident list and can be referenced by a line descriptor block containing line and column indices followed by the pixels HU-values.

Preprocessing was tested on the whole CT data base including 120 cranial computed tomograms. The results for skull detection and background suppression were very exact. Preprocessing is done in approximately 60 seconds execution time including disk accesses and data transfer from disk to main core.

Image Enhancement

Noise degradation inherent in the tomogram is smoothed by a conventional average operator defined over a 3×3 neighbourhood. Since the averaging operator is in no sense adapted to the specific origin of the noise, edges are blurred within the brain pixels and image quality is overall degraded. Designing noise adapted smoothing operators needs careful analysis of the theoretical background of noise origin and properties in CT scanners.

However, not only smoothing techniques are important to improve CT images but also techniques for enhancement of CT images. These can either sharpen edges or make low contrast differences visible to the physician. Such a procedure may give substantial help to the physician in the diagnosis of low contrast mass lesions for which the border to surrounding tissue may not be clearly visible. Furthermore, the interior of low contrast lesions can be more clearly analyzed after contrast or edge enhancement.

In addition, pseudo colour transformations can improve visibility of neuroanatomic and -pathologic

structures. The selection of a gray-value to pseudo-colour mapping scheme must take into account that the range of colours does not overtax the perceptual ability of the physician.

The solutions to some of the sketched problems are part of the continuous development of the COMPACT system.

3. Image Analysis Techniques

In general, two distinct approaches to computerized analysis of the structural content of computed tomograms have been established:

- the interactive and
- the automated CT image analysis approach.

To achieve an optimal synergesis in an interactive environment between the physician and computer system careful design of the man-machine communication module is important. Numerous papers on interactive analysis of computed tomograms have been published within the last few years. An introduction to the above mentioned problems is given in⁶, a survey can be found in⁷.

Common to interactive and automated CT image analysis was the emphasis given to the diagnostic evaluation of the brain ventricles. Linear distance measures derived from pneumoencephalography were adapted to CT for descriptive analysis of atrophic diseases and infant hydrocephalus. To overcome their two-dimensional nature and also facing the three-dimensional nature of CT information, attempts have been made to estimate the ventricular volume on computed tomograms.

The development of techniques for automated analysis of CT images with respect to the brain ventricles are based on three demands:

- a) to overcome the tedious work of ventricle outlining over a range of up to 12 tomogram slices,
- b) to yield an exact parameterized description of the three-dimensional morphology of the ventricles, and
- c) to facilitate a realistic visualization of the complex ventricular structure.

It is easily seen that

- a) implies automated image segmentation and object recognition,
- b) means the automated determination of the ventricular volume, and
- c) requires a three-dimensional display with shading, hidden surfacing, and various picture transformations well known in Computer Graphics.

Segmentation

The selection of an appropriate segmentation scheme for cranial CT scans was influenced by the following design demands:

- a minimum on computational cost and storage requirements during processing time,

a fast and therefore quite "simple" approach, and

optimal adaptation to the line-oriented computed tomogram storage structure.

A dynamic thresholding approach was chosen (contrary to the approach with fixed threshold in⁸) and implemented in FORTRAN IV on the ADAGE AGT 130 graphic system.

The cerebrospinal fluid-filled cavities like ventricles, cisterns and the subarachnoid space are defined on the cranial computed tomogram by a characteristic range of HU-values and are well contrasted to the surrounding HU-values of brain tissue. The latter feature enables thresholding of the tomogram picture matrix with an automatically selected dynamic threshold range (it has been found that due to slice-, patient- and scan-energy-dependent CSF range variations, fixed thresholding yields unsatisfactory results).

Some considerations have also to be given to the CT generation process. The HU-values of the pixels in the two-dimensional tomogram matrix result from averaging the attenuation coefficients of the three dimensional density distribution of sometimes more than one material within one voxel sized 1,5x1,5x10 mm³. So, voxels defining the brain/ventricle edge may contain brain tissue as well as CSF and are therefore given a higher HU-value than the purely CSF containing voxels (usually referred to as "partial volume phenomena", the amount of, for example, CSF within one voxel is called "partial volume ratio" pvr). The upper CSF range bound is therefore defined by the maximal HU-value of the pixels representing the ventricular system.

For analysis of the ventricle/brain edges a sum-type gradient is computed over the entire brain on the tomogram and its magnitude is correlated with the HU-value at corresponding pixel indices by a modified two-dimensional (joint) histogram following the notion in⁹. A projection over all maximal gradients yields a one-dimensional histogram of HU-values of possible edge pixels⁷.

One problem, however, has to be discussed in more detail. In the ideal case, the resulting one-dimensional histogram is unimodal and its maximum gives the HU-value of the most frequently occurring pixels at the ventricle/brain edge associated with maximal gradients. However, the ventricle/brain edge has, in general, a non-constant edge profile due to a varying partial-volume ratio along the edge (analysis of brain anatomy makes it clear that the voxels at the periphery of the frontal horns must contain less CSF than those at the periphery of the third ventricle). In general, the histogram is bimodal referring to an edge part associated with minimum and one associated with maximum partial volume ratio. In cases where two strong peaks are present the valley of the histogram is chosen as threshold. It is clear that such a pure global analysis for threshold determination results in only an estimation for the upper threshold bound hence the influence of local contrast is ignored. This means that in respect to the distribution of partial volume

ratios within the slice only the ventricular system or the external liquor spaces are segmented well. If the external CSF containing regions are segmented exactly, the ventricles may well be in general too large and vice versa. An improved version of the segmentation scheme will combine both global statistics on the edges present within the tomogram and local contrast properties on a defined pixel neighbourhood.

The lower CSF range bound is chosen from the first non-zero entry of the overall brain histogram with minimum HU-value. Results of the segmentation scheme applied to computed tomograms in Figs. 1a-1f, are given in Figs. 2a-2f.

After automated threshold selection, a line sequential thresholding operation is performed on the core-resident brain line segments yielding CSF region line segments. The line segments are grouped together into regions via overlap checking between two abutting line segments in two consecutive lines (a method similar to [10]). The region growing approach was designed to save subregions which originate by merging and splitting occurrences on a line and to generate a hierarchic list-oriented picture.

Picture description is performed

- during region growing to compute area, mean etc. and
- after region growing on the generated data structure.

The basis for picture description is an assumed computed tomogram geometry defined by the brain center and the (possibly rotated) symmetry line. The brain is divided into four quadrants allowing for positional and relational orientation of the CSF regions within the entire brain on the computed tomogram. Each region is labeled and described by a set of descriptors: area, circumscribing rectangle, mean of HU-values, region center coordinates, distance to brain center, angle with symmetry line, index of quadrant and a ventricle candidate indicator with value either 1 or 0. The latter descriptor excludes all regions with minimal size and peripheral position from subsequent analysis as described in the next section (in Fig.3 results from picture description of the segmented computed tomogram in Fig.2d are shown).

The segmentation of CSF-filled brain cavities on cranial CT scans was tested on the CT picture data base of 120 computed tomograms with patients aged 20-75 years. A subset of 61 computed tomograms (tomograms with only third or fourth ventricle were not taken into account) with normal and diminished as well as dilated ventricles was processed and presented to three physicians with clinical experience in CT scan analysis. They were asked to rate the resemblance between the ventricles on the tomographic Polaroid photographs and those on the hardcopies of the computer processed tomograms. Given a range from 1 to 6 (1: good resemblance, 6: bad resemblance) the overall judgement for segmentation of the ventricles was: 1 (6%), 2 (35%), 3 (31%), 4 (21%), 5 (7%) and 6 (0%).

It is interesting to note that the judgements for range 4 to 6 are due to the binary representation of the segmentation results on the hardcopies. The physicians therefore felt that the ventricles were in general too large. Comparison by eye between hardcopy and tomographic Polaroid photographs requires the subjective extraction of the ventricle/brain edge from the photograph. This edge shows a strongly reduced gray-value range while the ventricle/brain edge on the hardcopy is defined by analysis of the original HU-value range. If the segmented region is too large within an accepted error range, the influence of the peripheral pixels (belonging to brain tissue but "classified" as CSF) on the volume determination is rather small (partial volume ratios of less than 6 %) and can therefore be ignored. Furthermore, the judgements of the physicians differ significantly, e.g. physician C: 4 (5 %), 5 (1 %), physician A: 4 (35 %), 5 (15 %). One fact was also clearly observed: the better the picture quality, the better the segmentation results.

The tomogram segmentation needs less than 15 seconds CPU time including automated selection of threshold range, thresholding, region growing, data structure generation and picture description

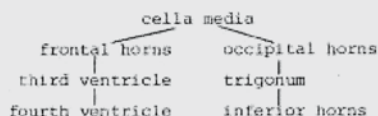
Recognition of the Ventricles

The task of automated recognition of the brain ventricle parts on contiguous computed tomograms was realized by a model-guided recognition strategy utilizing contextual information. Two types of context are available:

- the inter-region context per slice, given by the picture description and
- the inter-slice context, given by assumptions on the probable occurrence of specific parts of the ventricular system on the next processed computed tomogram, dependent on already recognized ventricle parts.

The inter-region context is revealed from the picture geometry and defines the positional relation between ventricle parts within one slice. Estimates of the positional range in which a ventricle part may be expected on a computed tomogram are obtained with the aid of anatomic a priori knowledge. The a priori knowledge for each ventricle part is represented by a production system with several highly problem- and object-dependent production rules.

The definition of inter-slice context is a much more complex problem and should aid the recognition strategy "to-look-where-for-what". Each tomogram is considered a frame within the complete tomogram sequence. The sequence is processed top-down starting with the tomogram with first occurring ventricle part. The structural top-down hierarchy of the ventricular system in man, namely from the "top" cella media "down" to the fourth ventricle, renders possible a forecast on the probable occurrence of ventricle parts on the next tomogram within the sequence and may be described by a tree (each vertex in the following simplified tree may be present n times on n contiguous tomograms).



Once the initial cella media regions are recognized, a context mask is defined by the circumscribing rectangle to minimize the search range for structural continuation on the tomogram to be processed next. All regions (objects) within the context mask range are treated as possible ventricle candidates and a decision has to be made on the selection of the abutting ventricle parts on contiguous tomograms.

The decision function may be executed on various criteria such as shape, size, location within the context mask, maximal overlap between context mask and region area, nearest neighbourhood of region centers or more general, on the best match with the ventricle model parameters. The main problem in providing sufficient inter-slice context is the high variability of the structure of the ventricular parts. Some parts may either be connected or isolated, shifted, dilated, diminished or even be absent due to the presence of a certain pathologic disorder, patient specific anatomical alterations, the position of the head in the scanner gantry (causing non-standard slices in respect to the orbito-meatal line as basis proposed for CT head scanning), the imperfect scanner resolution and the presence of specific noise and artifacts. The recognition strategy has to be invariant against these variabilities.

For achieving maximal flexibility, the recognition strategy must show independence from the number of processed tomographic slices. If the decision function fails, the recognition strategy will initialize the search for the next ventricle part on the current tomogram by a top-down traversal of the tree. If a part of the ventricular system, expected to be the next in the structural hierarchy, is not present, an unusual change in structural content is detected.

The overall recognition module is supervised and directed by a control structure.

The model-guided recognition of the ventricles results either in the description of the structural content of the complete tomogram sequence (see Fig. 4) allowing for further diagnostic evaluations or in the abortion of the processing if some conspicuous differences are present on the current tomogram (details of the proposed methods will be given in⁷).

Ventricle recognition was tested on the whole CT data base, 16 tomogram sequences were analysed. For 10 sequences, the detection of the ventricular parts (except the occipital horns, for which the algorithms are currently under implementation) was correct. From the remaining sequences, 3 were analysed incorrectly due to insufficient inter-slice context definition for the basal tomograms and for 3 sequences recognition was aborted due to significant structural changes. For ventricle recognition less than 3 seconds CPU time is spent.

Analysis of the Ventricles

The goal of the current program version is to achieve an exact estimation of the volume of the human brain ventricles. The partial volume phenomena does not allow simple multiplication of the overall ventricular area by the pixel size and slice thickness but needs a further processing step to retrieve the information of the three-dimensional brain tissue/CSF-distribution within the slice out of the two-dimensional computed tomogram picture matrix. The first attempt on automated partial volume corrected determination of the volume of fluid-filled brain cavities was made in¹¹ where a formula was given to compute the partial volume ratio of CSF within one voxel (however, the volume of all CSF-filled brain cavities was computed, not the ventricular volume). The summation of all partial volume ratios of the ventricle parts multiplied by the actual pixel size and slice thickness yields the most correct volume estimation of the ventricular system.

$$pvr = \frac{HU\text{-value} - z_{csf}}{z_{brain} - z_{csf}} \cdot 100 \% \quad /11/$$

The main problem in this procedure is the correct estimation of the typical HU-values for brain, z_{brain} , and cerebrospinal fluid, z_{csf} . The result of volume determination for the recognized ventricles in Fig. 2a is given in Fig. 5

The recognition of the ventricle parts per slice and per sequence allows for further analysis of the ventricular system. The characteristic descriptors of the ventricular system, e.g. occurrence/non-occurrence, symmetry, shape and position, are important indicators for the presence of some pathologic disorders on the slice and may give helpful information to the physician for diagnosis and therapy. Results from the ventricle recognition like statements on absence, size, positional shifting and structural asymmetry of the ventricle parts may serve as a priori knowledge to be input to an image analysis procedure for detection of pathologic processes. Such a procedure will be included in a future version of the COMPACT software system and will communicate with a data base describing pathologic processes in detail. Furthermore, global and local parameters on the hemispheric HU-value distribution can be computed (like textural features) for determining hemispheric asymmetries to aid in the search for probable pathologic processes.

Verification of the ventricular volume determination requires much effort and work in this direction is still in progress. The heads of 10 bodies were scanned (by Dr. med. S. Lange, formerly Department of Computed Tomography, Klinikum Charlottenburg, Free University of Berlin), the brains were then removed from the skull and sliced into 2 mm layers. A planimetric evaluation of the ventricles per layer yields a fairly exact estimate of the volume which has to be corrected because of some changes in the brain tissue (density, volume) due to death, freezing-in the whole body and fixation before slicing. Subsequently, the correlation between the volume computed by automated analysis of the

tomograms to the volume evaluated by manual planimetry can be determined (for details see⁷).

The time required for volume determination of the ventricular system depends on the number and the size of the ventricle parts per slice and is for one sequence with 6 tomograms less than 12 seconds CPU time.

4. Computer Graphics

Computer Graphics (CG) has established itself as a powerful tool for three-dimensional reconstruction and display of CT scans. Although 3-D reconstruction is not a traditional CG technique it can make extensive use of graphic oriented data structures and is therefore discussed conveniently as part of CG. 3-D display techniques, however, have a long tradition in CG and many of these techniques may therefore be applied to CT problems.

Perhaps the first system with CG capabilities was demonstrated by Maziotta and Huang in 1976¹². Contourlines in a CT-slice are defined manually using a light spot controlled by a joystick. Invisible parts of this contourline (when observed from a given viewpoint) are then masked out and followed by a definition of polygons between adjacent contourlines. This type of masking makes an expensive hidden surface algorithm unnecessary. Manual input of contourlines and the inability of the system to display concave objects (caused by restriction of one contourline per CT-slice) are, however, a definite disadvantage.

Semiautomatic extraction of contourlines in CT's employing manual error correction has been implemented by Sungenoff and Greenberg in 1978¹³. B-spline and Cardinal-spline techniques are used for smooth surface reconstruction. The quality of the picture appears to be excellent and is made even more attractive through transparent display of the skull. Not so advantageous is the strong dependence on interpolation between adjacent contourlines. The contourlines of the 5 CT-slices used, for example, for the reconstruction of the ventricular system may therefore well suppress important anatomical detail.

A system not based on "stacking" was introduced by Herman and Liu in 1977^{14,15}. Surfaces of three-dimensional objects are directly represented in a three-dimensional matrix by the exterior faces of the boundary voxels. Because voxel faces are of equal size and are normal to the axes of a three-dimensional Euclidean coordinate system, the hidden surface and stacking algorithms can be kept simple and fast¹⁶.

All methods so far considered, however, do not take account of the shape of objects within the 8-13 mm thickness of the CT-slice.

3-D Reconstruction

In the COMPACT system three-dimensional reconstruction of objects is also carried out within the CT-slice¹⁷. Input to the reconstruction process consists of the pvr-values and a suitable hierarchical data structure. Both are supplied by the ventricular

recognition module. Reconstruction is then based on the following three steps:

1. Search for object regions which show contiguity between adjacent CT-slices.
2. Determination of the probable spatial orientation of the pvr-part within a slice.
3. Definition of the contourlines of the object in n subslices for each CT-slice.

The first process is based on the assumption, that if two voxels of the same object but from adjacent slices share a common face, their content form a continuous column of tissue or CSF.

In the second step the pvr-value dependent alignment takes place, that is a shifting of the respective tissue or CSF to the superior or inferior boundary of the slice or centering it on the middle of the slice. Although satisfactory results are obtained using this method for alignment, usage of a priori information from anatomic models of the brain is currently being considered.

Finally, each CT-slice is partitioned into n subslices allowing the corresponding contour lines of the object to be defined (similar to the conventional "stacking" approach). Dependent on the size and orientation of the pvr-values some subvoxels of a voxel are positioned inside, others are outside of the object to be reconstructed. The centre points of the subvoxel faces belonging to the surface of the object serve as points for the object contour line (Figs. 6a-6h).

3-D Display

Basically, there are two types of display representations for 3-D objects, they are:

1. wire framed drawings,
2. shaded pictures.

To aid the human visual system in depth perception these display representations can be combined with one or several depth cues, e.g.

- 1) visibility (hidden line/surface removal)
- 2) intensity cues
- 3) perspective
- 4) stereoscopic views
- 5) kinetic depth effect (rotation, motion)
- 6) shadowing
- 7) transparency

Not all techniques for depth perception are, however, of use for 3-D display of objects reconstructed from CT-scans. For example, perspective and shadowing techniques are of little assistance in the representation of anatomical structures. Other methods, e.g. kinetic depth effects or stereoscopic views, require special technical backup and may therefore not always be easily implemented.

The algorithms for 3-D display implemented in the COMPACT project are wire frame plus hidden line removal and wire frame plus kinetic depth effect through real-time rotation. Both display facilities are implemented on a vector display (Fig. 7). Further algorithms for the generation of shaded

pictures on a raster display (GENISCO) are in the process of being implemented. One algorithm is based on the method of polygonal definition between adjacent contour lines followed by hidden surface removal and shading. Mapping and branching problems, however, may arise between adjacent contour lines and may defy a solution by automatic methods. A promising approach to this problem, although restricted to a certain class of contour lines, is the algorithm suggested by Christiansen and Sederberg¹⁸. This algorithm and the method which has been described by Herman and Liu are being investigated in the COMPACT project.

5. A Network of Medical Work Stations

The following is a brief summary of the processing facilities which a distributed MWS system should provide. It is assumed that all internal information in the system is represented in digital form.

Medical Work Station (MWS)

As shown in Fig.8 the main software components of a MWS are:

- a) Word processing
e.g. input and editing of constrained and free format text, searching, scrolling, and panning of text for patient history taking
- b) Signal and image processing
e.g. preprocessing, segmentation and pattern recognition of one- and two-dimensional data of ancillary investigations
- c) Graphics
e.g. graphic display of one-dimensional signals, two-dimensional images and reconstructed three-dimensional objects
- c) Communications
e.g. transmission of voice, text, picture and graphic data, filing of (voice), text, picture and graphic data, hardcopy, command language interpretation

For the system being developed at the Institut für Technische Informatik, facilities at the MWS are at first limited to the processing and representation of electro-encephalograms (EEG), magneto-encephalograms (MEG), and of computed tomograms.

Network

A ring communication facility of the type shown in Fig.9 is very attractive for interconnecting MWS on a restricted site allowing high bandwidth with very simple control. Communication of a MWS to resources outside the local ring network may be achieved through microprocessor controlled bridges or gateways to other rings or global network facilities. These possibilities, however, shall not be considered further in this paper, the interested reader is referred to 19,20,21.

Ring

- a) Local network facilities
e.g. graduated (incremental) work stations with resource sharing, process to process communication, concurrent transceiving, information security, conferencing mode
- b) Global network facilities
e.g. bridge and gateway controls

Central to this set of facilities is the interactive command language interpreter which controls the user interface with the system as shown in Fig. 8. Its main design features are:

1. Common syntax of driving commands for word, signal, image, graphics, and communication processing
2. Syntax and semantics as much as possible in line with "medical thinking"
3. Menu implementation
4. User oriented software (e.g. "sympathetic software")

Fig. 10 shows the data flow for the processing of computed tomograms between the main software modules of an idealized MWS. Not all facilities may be offered at every MWS, however, the command language interpreter for driving modules will always be present.

6. Conclusion and Aims

Although the technical capabilities so far discussed can be used for effectively demonstrating the potential of a MWS system, its real impact on the medical community will depend on its clinical efficacy.

Clinical efficacy addresses itself to the question of assessing the impact of a technique on diagnostic and therapeutic procedures. As regards signal and image processing for computed tomography and following a definition of diagnostic impact given by the Institute of Medicine²² it is safe to state that the extent to which CT scan information has come to replace other diagnostic procedures including diagnostic imaging, surgical exploration and biopsy, it has proved itself to be efficacious. For many disease patterns it has become the primary diagnostic tool.

Many other sources of information, however, apart from CT scans, must be considered for neurological disorders in the process of differential diagnosis and therapy. That is, information from the patient's history, examinations and other ancillary investigations must be integrated with CT images. A MWS for a particular clinical discipline such as neurology provides a physician with a means to vertically integrate this information into a MR.

In the patient-physician consulting mode a MWS system may promote a shift in the physician's way of working from patient data evaluation towards patient data gathering and structuring. In the physician-physician conferencing mode emphasis may then be given to patient data evaluation. Clinical efficacy

of a MWS system will be achieved when the potential of the two working modes are properly realized.

With this in mind a prototype system is being developed by the COMPACT group of the Technical University of Berlin. Some rather encouraging results in the area of automatic recognition of the ventricular system and other CSF containing cavities as well as ventricular volume determination and 3-D display have already been obtained.

For networking, initially only two workstations will be linked through a > 10 Mbit/sec communication medium organized as a ring network. It is expected that this minimum system will eventually be installed in a clinical environment so as to allow some experience to be gained on the impact of this technique on diagnostic and therapeutic procedures.

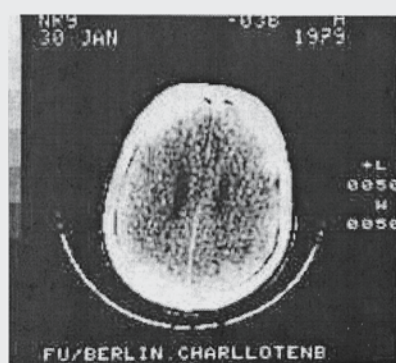
Acknowledgement

The authors gratefully acknowledge the advice given by S. Lange and H. Traupe (Free University, Berlin) on questions relating to the clinical efficacy of the system and by D. Graf von Keyserlingk (Dep. of Anatomy, RWTH Aachen) on problems concerning neuroanatomy.

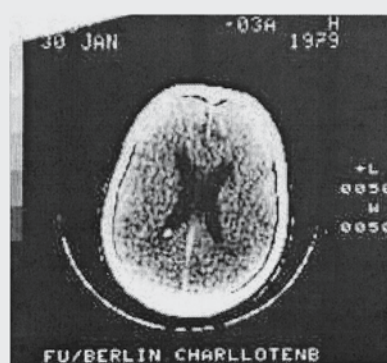
The completion of the 3-D display facility was very dependent on the work of M. Engelhorn whose participation in the project we greatly appreciate.

References

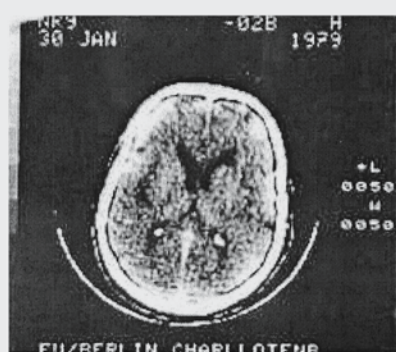
- 1 LEMKE H.U., STIEHL H.S. Processing and Representation of Computed Tomograms. Proc. Conf. on Medical Informatics, Berlin, Sept. 1979
- 2 ROSENFELD A., KAK A.C. Digital Picture Processing. Academic Press, New York, 1976
- 3 JOSEPH P.M. Image Noise and Smoothing in Computed Tomography (CT) Scanners. Proc. SPIE, Vol. 119, Application of Digital Image Processing, 1977, pp. 293-298
- 4 STONESTROM J.P., ALVAREZ E.E. 1977. Optimal Processing of Computed Tomography Images. Proc. SPIE, Vol. 119, Application of Digital Image Processing, pp. 293-298
- 5 HUTH G.C. et al. Image Enhancement Techniques in Computed Tomograms. Proc. Symposium on Computer-Aided Diagnosis of Medical Images, Coronado/CA, Nov. 11, 1976, pp. 67-83
- 6 LARSEN G.N. Interactive Image Processing for Computerized Tomography. University of Missouri at Columbia, Dept. of Electronics and Electrical Engineering, Ph.D. Thesis (August 1976)
- 7 STIEHL H.S. 1979. Automated Processing and Analysis of Cranial Computed Tomograms. Technische Universität Berlin, Inst. für Technische Informatik, COMPACT Techn. Report
- 8 BELANGER M.G., YASNOFF W.A. PENN R.D., BACUS J.W. 1978. Automated Scene Analysis of CT Scans. Rush-Presbyterian-St. Luke's Medical Center, Chicago, Medical Automation Research Unit, Techn. Rep.
- 9 PANDA D.P. 1977. Segmentation of FLIR Images by Pixel Classification. University of Maryland, Computer Science Center, Techn. Rep. TR-508
- 10 AGRAWALA A.K., KULKARNI A.V. A Sequential Approach to the Extraction of Shape Features. Computer Graphics and Image Processing, 1977, vol. 6, pp. 538-557
- 11 WALSER R.L. Automated Interpretation of Reconstructed Objects: Finding the Volume of Brain Ventricles. University of Illinois at Chicago Circle, Dept. of Information Engineering, Master Thesis (Nov. 1975)
- 12 MAZZIOTTA J.C., HUANG H.G. THREAD (Three-Dimensional Reconstruction and Display) with Biomedical Applications in Neuron Ultrastructure and Computerized Tomography. Proc. NCC, New York, June 1976, pp. 241-250
- 13 SUNGJUROFF A., GREENBERG D. Computed Generated Images for Medical Applications. Computer Graphics, vol. 12, no. 3, 1978, pp. 196-202
- 14 HERMANN G.T., LIU H.K. Display of Three-Dimensional Information in Computed Tomograms. Journal Computer Assisted Tomography 1 (1), pp. 155-160, 1977
- 15 HERMAN G.T., LIU H.K. Three-Dimensional Display of Human Organs from Computed Tomograms. Computer Graphics and Image Processing 8 (1979), pp. 1-21
- 16 ARTZY E. Display of Three-Dimensional Information in Computed Tomography. Computer Graphics and Image Processing 8 (1979), pp. 196-198
- 17 SCHARNWEBER H. Dreidimensionale Objektrekonstruktion aus sequentiellen Computer-Tomogrammen. Technische Universität Berlin, Institut f. Technische Informatik, Diplomarbeit, Juli 1979
- 18 CHRISTIANSEN H.N., SEDERBERG T.W. Conversion of Complex Contour Line Definition into Polygonal Element Mosaics. Computer Graphics, vol. 12, no. 3, pp. 187-192, 1978
- 19 WILKEN M.V. Communication Using a Digital Ring. PACNET Conf. Proc., Sendai, Japan, August 1975, pp. 47-55
- 20 HOPPER A. Local Area Computer Communication Networks. Computer Laboratory, University of Cambridge, Engl., Ph.D. Thesis
- 21 CLARK D.D., PROGRAM K.T., REED D.P. An Introduction to Local Area Networks. Proc. of IEEE, Vol. 66, no. 11, Nov. 1978, pp. 1497-1517
- 22 Computer Tomographic Scanning: A Policy Statement. Washington/DC, Institute of Medicine, National Academy of Science, April 1977



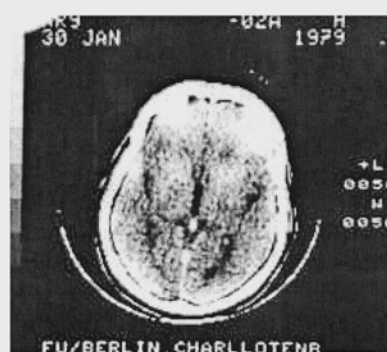
(a)



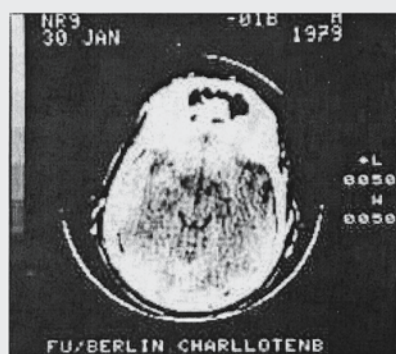
(b)



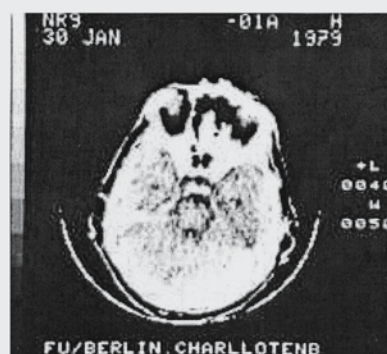
(c)



(d)



(e)



(f)

Figures 1a - 1f: Computed tomograms of one from 10 skulls
(specially prepared for this experiment
from dissections)

PAT.CODE: N89 -828 DATUM: 1 30 79 3:140



DIPYLOT MATRIX

SLICE STATISTICS

HU MEAN	54.4	GAUSSIAN HU RANGES BRAIN
SDMM	6.1	90 % : 44.4...64.3
BRAIN AREA	6043 PIXELS	95 % : 42.5...66.4
CENTER (X,Y)	70,77	99 % : 36.8...70.1
ROT ANGLE	11 DEGREE(S)	CORRANGE
BRAIN FOR SLICE	23.7 PERCENT	

(a)

PAT.CODE: N89 -838 DATUM: 1 30 79 3:140



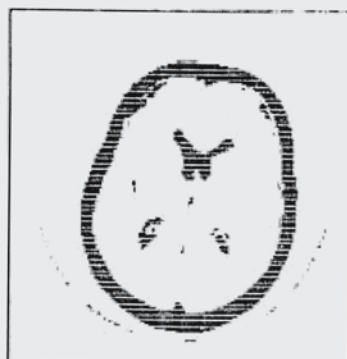
DIPYLOT MATRIX

SLICE STATISTICS

HU MEAN	51.9	GAUSSIAN HU RANGES BRAIN
SDMM	6.1	90 % : 36.4...65.2
BRAIN AREA	6043 PIXELS	95 % : 36.1...67.7
CENTER (X,Y)	70,77	99 % : 31.1...72.7
ROT ANGLE	13 DEGREE(S)	CORRANGE
BRAIN FOR SLICE	26.7 PERCENT	

(b)

PAT.CODE: N89 -828 DATUM: 1 30 79 0:160



DIPYLOT MATRIX

SLICE STATISTICS

HU MEAN	52.2	GAUSSIAN HU RANGES BRAIN
SDMM	7.3	90 % : 40.3...64.1
BRAIN AREA	7299 PIXELS	95 % : 38.1...66.4
CENTER (X,Y)	79,77	99 % : 33.6...79.8
ROT ANGLE	13 DEGREE(S)	CORRANGE
BRAIN FOR SLICE	26.9 PERCENT	

(c)

PAT.CODE: N89 -824 DATUM: 1 30 79 0:160



DIPYLOT MATRIX

SLICE STATISTICS

HU MEAN	53.2	GAUSSIAN HU RANGES BRAIN
SDMM	6.7	90 % : 42.1...64.2
BRAIN AREA	6043 PIXELS	95 % : 40.8...64.3
CENTER (X,Y)	77,81	99 % : 30.8...76.9
ROT ANGLE	13 DEGREE(S)	CORRANGE
BRAIN FOR SLICE	26.9 PERCENT	

(d)



Figures 2a - 2f: Results of the segmentation applied to the computed tomograms in Figs. 1a - 1f.

IMAGE ANALYSIS

11 REGIONS (TYPE : UNCLASSIFIED CSF) FOUND [7 REGIONS TYPE: VENTRICLE CANDIDATE]

LABEL	AREA	CIRCUMRECT	HU-MEAN	XC	YC	DIST	ANGLE	QUADR	CAND
1	2	81 82 24 24	35	81	24	53	3	1	0
2	267	70 98 47 69	31	81	58	19	8	1	1
4	2	120 120 56 57	38	120	56	46	63	1	0
8	9	51 52 70 75	37	51	72	27	79	2	1
9	9	77 79 77 81	36	78	79	2	0	3	1
10	74	54 65 87 101	33	58	93	25	51	3	1
11	5	120 120 87 91	31	120	89	43	74	4	0
15	6	88 91 92 94	37	89	92	18	36	4	1
16	7	94 96 94 97	35	95	95	24	43	4	1
17	1	34 34 97 97	37	34	97	48	65	3	0

Figure 3: Results from picture description of the segmented computed tomogram slice 2B (Fig. 2d)

VENTRICLE RECOGNITION PROTOCOL

SLICE: NR9 P3B
1 LEFT CELLA MEDIA DETECTED (LABEL: 1)
1 RIGHT CELLA MEDIA DETECTED (LABEL: 2)
* SLICE CONTEXT: ISOLATED CELLA MEDIA

SLICE: NR9 P3A
1 CELLA MEDIA DETECTED (LABEL: 2)
* SLICE CONTEXT: CONNECTED CELLA MEDIA

SLICE: NR9 P2F
7 NO CM CONTINUATION
1 FRONTAL HORNS DETECTED (LABEL: 2)
* SLICE CONTEXT: ISOLATED FRONTAL HORNS/3RD VENTRICLE
1 THIRD VENTRICLE DETECTED (LABEL: 9)
ON RECOGNITION

SLICE: NR9 P2A
1 FRONTAL HORNS DETECTED (LABEL: 4)
* SLICE CONTEXT: ISOLATED FRONTAL HORNS/3RD VENTRICLE
1 THIRD VENTRICLE DETECTED (LABEL: 6)
ON RECOGNITION

SLICE: NR9 B1D
7 NO FRONTAL HORNS CONTINUATION
1 THIRD VENTRICLE NOT IN EXPECTED RANGE
7 NO THIRD VENTRICLE CONTINUATION
7 FOURTH VENTRICLE MISSING
ON RECOGNITION

SLICE: NR9 B1A
1 FOURTH VENTRICLE DETECTED (LABEL: 35)
ON RECOGNITION

RECOGNITION DONE



Figure 7: 3-D reconstruction of the recognized ventricle system

Figure 4: Structural content of the CCT sequence derived from ventricle recognition model

VENTRICLE VOLUME ANALYSIS

ZBRAIN: 40 ZCSF: 26

SLICE: P3F
REGION LABEL: 1 VOLUME: 0.97 ML
REGION LABEL: 2 VOLUME: 0.18 ML

SLICE: P3A
REGION LABEL: 2 VOLUME: 9.88 ML

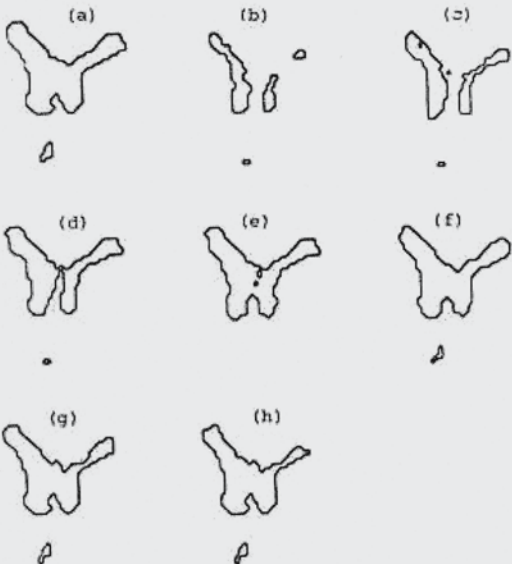
SLICE: P2F
REGION LABEL: 2 VOLUME: 4.12 ML
REGION LABEL: 9 VOLUME: 0.08 ML

SLICE: P2A
REGION LABEL: 4 VOLUME: 0.02 ML
REGION LABEL: 6 VOLUME: 1.01 ML

SLICE: B1B

SLICE: B1A
REGION LABEL: 35 VOLUME: 0.39 ML
OVERALL VENTRICULAR VOLUME: 16.65 ML

Figure 5: Volume determination of the recognized ventricle system



Figures 6a-6f: (a) Max. contourline of slice 28 (b-h) Contourlines of seven reconstructed sublices

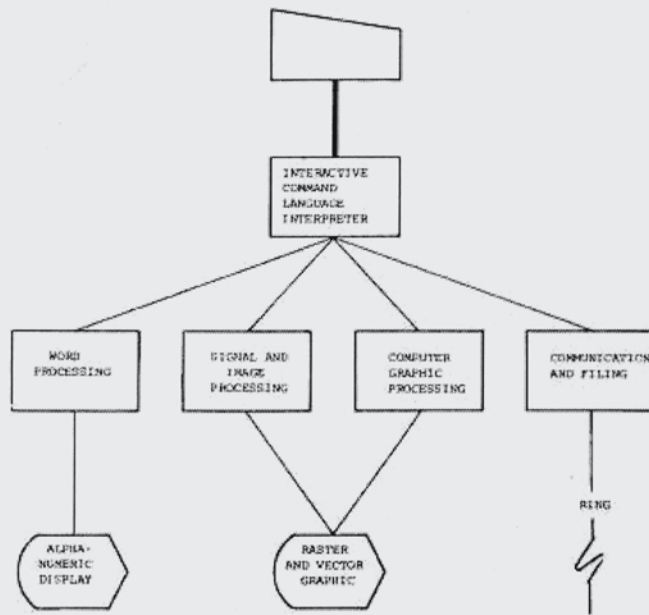


Figure 8: Software components of the MWS

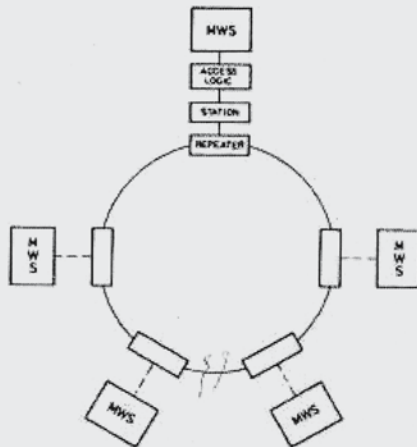


Figure 9: Ring communication for MWS

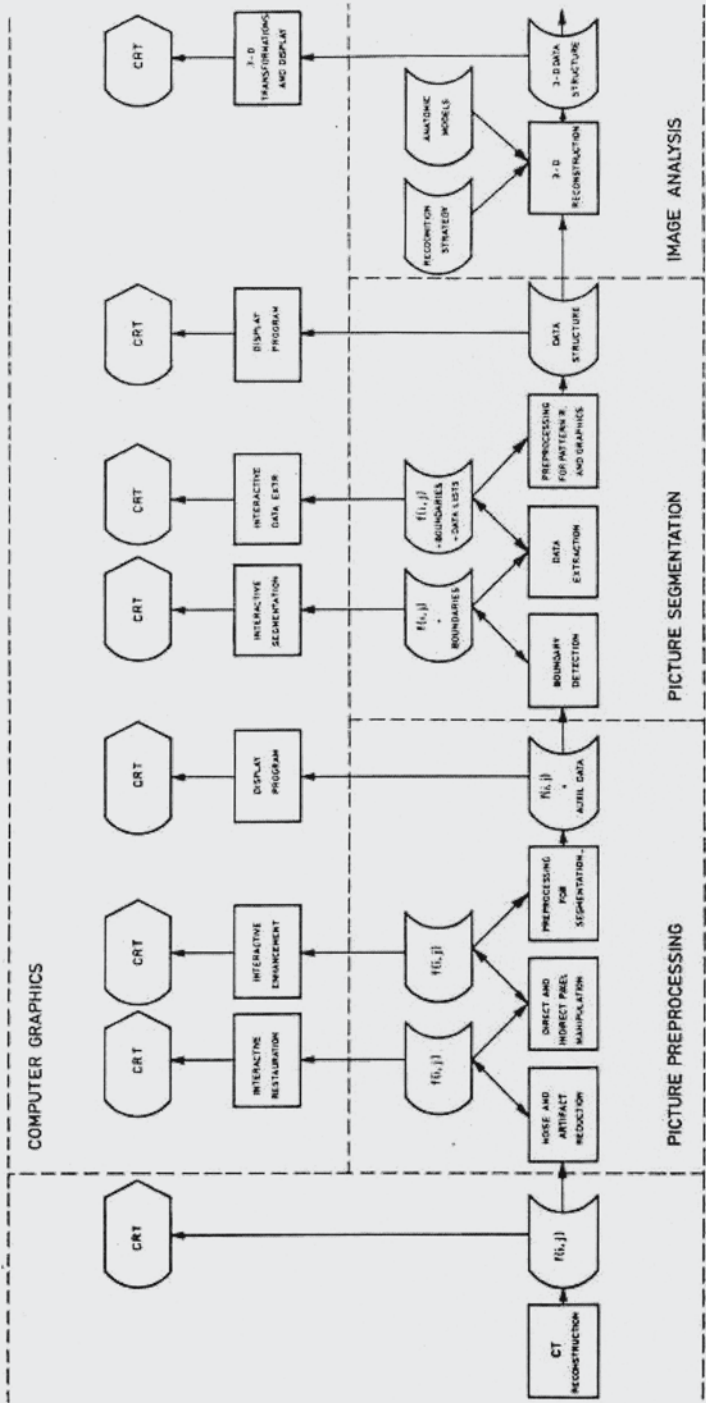


Figure 10: Data flow for the processing of computed tomograms

5.2 An All-digital Nuclear Medicine Department

Gerald M. Kolodny

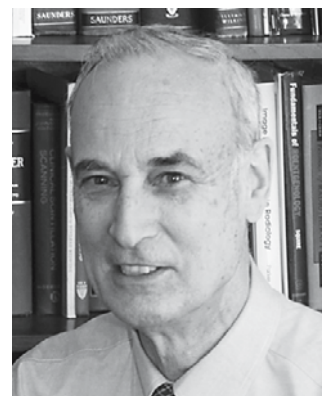
Gerald M. Kolodny was born in Boston, Massachusetts. In 1958 he got his BA at Harvard College and his MD from Northwestern University School of Medicine in 1962. He took his postdoctoral training as Intern in Medicine, Stanford University Hospital (1962–1963) and became resident in Radiology at the Massachusetts General Hospital (1963–1966). He started his Research Fellowships at Oak Ridge Institute of Nuclear Studies at the US Atomic Energy Commission, Oak Ridge, Tennessee (1964), became postdoctoral fellow at the Department of Biology, Massachusetts Institute of Technology (1966–1969) and Fulbright Senior Faculty Scholar, Department of Genetics, Hebrew University, Jerusalem (1991–1994). In 1969 Kolodny was appointed Instructor (1972–1975), later Assistant Professor in Radiology (1972–1975) and in 1975 Associate Professor of Radiology at Harvard Medical School. He had hospital appointments at Massachusetts General Hospital (1969–1979), the Beth Israel Hospital (1979–1996) and the Beth Israel Deaconess Medical Center from 1996.

His major research efforts have focused on the application of computers in radiology. After analyzing delays in radiology reporting, he described a solution to this serious problem based on rapid access to dictated radiology reports via telephone (RTAS). With the assistance of a USPHS grant and help from a local company, the first RTAS system was installed and evaluated.

In 1981, the Division of Nuclear Medicine became the first to implement teleraadiology on a routine basis for reading radiology studies when on call, and to send studies from remote sites for interpretation. From this early experience, he next proceeded to be the first to construct in the division of nuclear medicine, a completely all digital imaging department. By 1986, film was no longer used to display, interpret or archive studies. This involved new approaches to backup, security, display, archiving and transmission of images. In 1995, he and his colleagues were the first to use the internet and cable modems to routinely transmit radiological images, between hospitals and from hospital to home or cellular phone. Most recently he has been involved in the design and evaluation of a low-cost PC-based PACS applicable to an entire radiology department. In the use of RTAS and PACS, he was involved in the earliest efforts to evaluate and document cost effectiveness of our technology.

Kolodny's major research efforts have been dedicated to computer applications in radiology and nuclear medicine. Another area of research has been in the application of quantitative SPECT and the use of gallium to monitor treatment response in lymphoma. In 1980, the nuclear medicine department was the first to use SPECT in routine clinical practice. He published studies on its use for investigating cerebral blood flow using a gamma camera mounted on a tank turret. He has been involved for many years in collaborative research with the Department of Nuclear Medicine at Rambam Medical Center in Haifa, Israel, which began when the director of that department spent a sabbatical in his department.

He and his colleagues were among of the first to describe simple, clinically applicable methods to obtain in vivo quantitative tumor uptake of radiopharmaceuticals. They were also among the first to emphasize that clinically relevant doses of tumoricidal drugs depend ultimately on uptake in an individual tumor and in the



unique patient undergoing treatment, rather than blood levels, administered dose or extrapolation from genetically homogeneous tumors in genetically homogeneous animal models. Quantitation of labeled drug uptake by quantitative SPECT provides a better method to measure tumor uptake of drugs in individual tumors in individual patients. Using high-dose Ga-67 imaging and SPECT, they were the first to propose that Ga-67 could be used to monitor lymphoma treatment response. The use of gallium scanning to monitor lymphoma treatment is now universally accepted as superior to CT scanning for this purpose.

Other areas of clinical research that Kolodny has been engaged in include labeling of red cells and their use for localization of gastrointestinal bleeding, hemangiomas and angiodysplasia, and nuclear cardiology studies.

Since 1985, Kolodny has been invited on an annual basis as visiting Professor at the Department of Nuclear Medicine, Rambam Medical Center, Haifa, Israel. From 1993-1997 he was invited to chair sessions or to organize courses in PACS at the annual meetings of the society of Nuclear Medicine. His Division of Nuclear Medicine was honored in 1999 by the residents of the Department of Radiology for the first annual award in "Recognition of the Radiology Department section making an Exemplary commitment to Resident Education." As a result of their experience in Nuclear Medicine as radiology residents in our department, since 1996, one resident each year has decided to take a fellowship in nuclear medicine with the Harvard Medical School Joint Program in nuclear medicine, and another resident has been accepted for 2000.

Picture courtesy Gerald Kolodny, MD, 2004.

John Anthony Parker (born 1946)

Professor John Parker was born on 19 November 1946 in Rockford, Illinois, USA. He got his BA in physics from Yale College in 1968 and his MD in 1972 from Washington University School of Medicine. In 1983 Parker got his PhD in biomedical engineering from the Massachusetts Institute of Technology.

He started his postdoctoral training at the Jewish Hospital of St. Louis (1972-73) before he became resident at the Peter Bent Brigham Hospital and Children's Hospital Medical Center, Boston, Massachusetts from 1973-76, joining a program in Nuclear Medicine. During that time Professor Parker got his first academic appointment as a clinical fellow in radiology (Nuclear Medicine), at Harvard Medical School. In 1974 he became research fellow in radiology (Physics Research), at the Massachusetts General Hospital. Here he worked as a radiologist (Nuclear Medicine) between 1976-78.

From 1978-1996 Parker worked as a radiologist at the Nuclear Medicine Department at Beth Israel Hospital, Boston, Massachusetts. 1986 he was appointed Acting Director of the Department of Magnetic Resonance Imaging, Beth Israel Hospital. Since 1996 he is the Director of the Department for Nuclear Medicine at the Beth Israel Deaconess Medical Center. In the year 2000 he was appointed Associate Director of the Joint Program in Nuclear Medicine Training Program at Harvard Medical School.

1976-1980 he was Instructor in Radiology, at Harvard Medical School and from 1980-1983 he was appointed Assistant Professor in Radiology (Nuclear Medicine) at Beth Israel Hospital, Harvard Medical School. From 1983-89 he was visiting scientist at Francis Bitter National Magnet Laboratory, Massachusetts Institute of Technology. In 1983 Parker was appointed Associate Professor of Radiology (Nuclear Medicine), Harvard Medical School and Harvard-MIT, Division of Health Sciences and Technology. The same year Parker and his group published



the first clinical PACS paper from the Nuclear Medicine Department at Beth Israel Hospital. A PACS concept was implemented for digital nuclear medicine images and integrated with a radiology reporting system and gamma cameras.

Today Professor Parker's research is the application of engineering technology to Nuclear Medicine, particularly the development of new procedures and methods. He developed the count-based calculation of left ventricular ejection fraction from equilibrium-gated blood pool imaging, a method for regional fractional myocardial oxygen extraction using O-15, an image processing method for assessing ocular counter rotation, the use of intracoronary Tl-201 imaging for evaluation of thrombolytic therapy for myocardial infarction, a method for simultaneous respiratory and cardiac gated radionuclide ventriculography, a semiquantitative method for evaluation of thrombolytic therapy for pulmonary embolism, and the first Java program in the radiology literature. He was involved in the use of the slant-hole collimator for non-tomographic applications, the development of deconvolution analysis for shunt quantitation, development of an all-digital web-based nuclear medicine information and picture archiving system, and web-based nuclear medicine teaching file.

Picture courtesy John Parker, PhD, 2004.

R.F. Uren

H.D. Royal

D. Front

J.G. Bliss

M. Rabussi

D. Jansons

M.S. Kolodny

G.M. Kolodny

Journal of Digital Imaging

An All-digital Nuclear Medicine Department

J. A. Parker, M.D., H. D. Royal, M.D., R. F. Uren, M.D., D. Front, M.D., J. G. Bliss, B.S.,
M. Rabussi, D. Jansons, M.S., and G. M. Kolodny, M.D.

An all-digital nuclear medicine department is described. Nuclear medicine images are acquired by a separate computer interfaced to each camera. The digital images are viewed, manipulated, and interpreted from remote display stations in an interpretation area. The interpretation is dictated into a Rapid Telephone Access System (RTAS), where the voice is digitized and stored. By dialing the patient's identification number, the referring physician can hear the interpretation over any telephone. The images are filed on large storage discs. The digital scans can be rapidly and easily accessed for later review by the use of several directory programs. This system has brought not only efficiency and cost savings, but the ability for remote viewing elsewhere in the hospital and telephone transmission of nuclear cardiology studies from community hospitals for interpretation in the digital nuclear medicine department.

KEY WORDS: Radiology and radiologists, departmental management, Radiology and radiologists, design of radiological facilities, Radiology reporting systems, Radionuclide imaging, instrumentation

TYPICALLY, nuclear medicine scans are photographed from a cathode ray tube or video monitor. The films are developed in an automatic processor, and after scan interpretation they are filed for long-term storage. This system of processing scans has several important disadvantages. Filmed studies are easily misfiled or lost and require increasing space in file rooms for storage. A photographed study cannot be manipulated to change contrast, gray scale, or background, and this often results in physician requests to the technologist to repeat the images to obtain films of different quality. This is also a serious drawback when comparing previous studies with current studies. Studies acquired in a cine mode, e.g., gated cardiac studies, cannot be stored in this mode, and thus comparisons with prior studies are difficult and

incomplete. In addition, the cost of silver-based film continues to rise because silver is a precious metal, while digital storage media, such as magnetic media, have been falling in cost.

Digitally retained images have many advantages over photographically stored images. They can easily be manipulated by changing background, contrast, and gray scale. Such images can be superimposed for comparison purposes or displayed and stored in cine format. Digital studies can rapidly be accessed from storage on large random access discs and displayed on video monitors in various locations within a nuclear medicine department as well as at remote sites within the hospital. This easier access to studies can result in a significant savings of time for physicians who wish to review studies.

Because of the advantages inherent in digital storage of nuclear medicine images, proposals have been made for future systems that will use an all-digital storage framework.¹ We have developed an all-digital department of nuclear medicine, which is currently functioning with commercially available equipment and has re-

From the Charles A. Dana Research Institute and the Department of Radiology, Beth Israel Hospital, and the Joint Program in Nuclear Medicine, Harvard Medical School, Boston, MA.

Received: 29 April 1982/Accepted: 15 July 1982/Revised: 9 September 1982

Dr. Parker is the recipient of a research career development award from the National Heart Lung and Blood Institute (5 K04 HL00465).

Copyright © 1983 by the Radiological Society of North America. Radiology 147:237-240, 1983. Reprinted with permission.

Online publication 30 April 2003

doi: 10.1007/s10278-002-6028-3

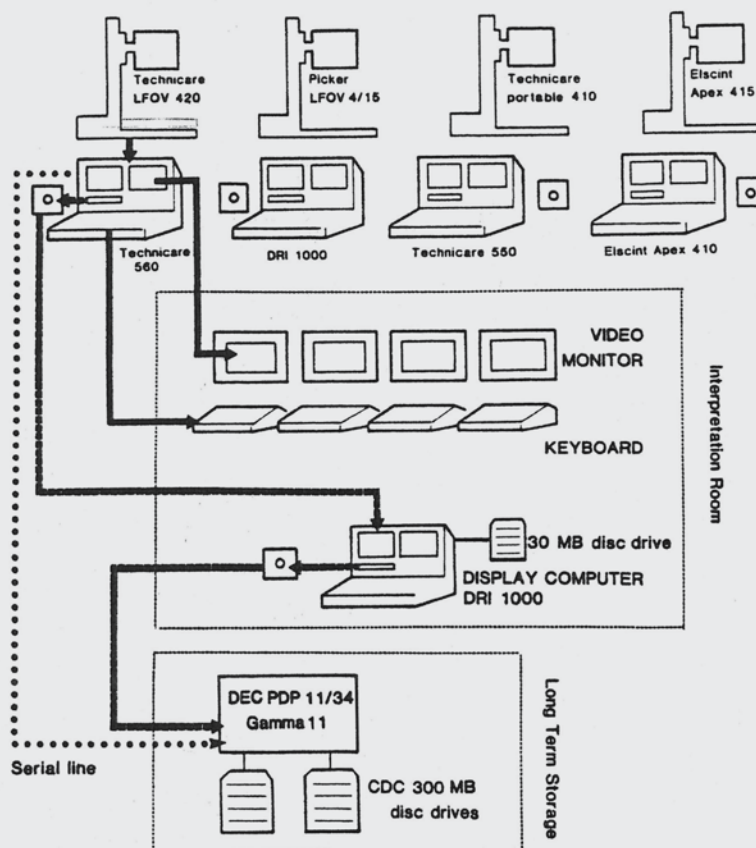


Fig 1. Equipment in all-digital department. Each of four gamma cameras is interfaced to a separate computer. Studies are examined in the interpretation room using remote video monitors and keyboards interfaced to each computer. Floppy discs are used to transfer studies to the display computer where the current week's studies can be displayed. Studies are then transferred via floppy disc to a PDP-11 computer and 300-megabyte discs for long-term storage. Alternatively, serial lines can be used to transfer studies from each camera computer directly to a PDP-11 computer.

sulted in efficiency in both cost and operation. Our all-digital department includes the interpretation and long-term storage of all studies in a digital format, the dictation and selective telephone retrieval of digitized voice interpretations, and the telephone transmission from local community hospitals of digital images for processing and interpretation by our staff.

HARDWARE

Figure 1 is a schematic representation of the hardware for acquisition, display, and storage of images in a digital format. We have four gamma cameras, each with a dedicated computer. Each computer is connected to a remote display within our interpretation room. The

remote display, which was the subject of a previous communication,² consists of a video monitor, keyboard, and controls (for cine rate, background subtract, and window) in parallel with the computer monitor, keyboard, and controls. When a study is ready for interpretation the technologist changes a switch, allowing manipulation of the images from the remote display station. After the images are manipulated and enhanced by the nuclear medicine physician at the remote display station to derive maximum information, an interpretation is dictated into our Rapid Telephone Access System (RTAS). Our referring physicians can then call RTAS from any telephone and dial the patient's identification number (I.D.) to hear our dictated report.³

Table 1. Equipment in All-Digital Department

1. Technicare 410 portable camera (a) Technicare 550 computer
2. Picker LFOV Dynacamera 4/15 (b) DRI 1000 computer (c)
3. Technicare LFOV 420 camera (a) Technicare 560 computer
4. Elscint Digital Apex 415 camera (d) with rotating gantry for ECAT Apex 410 computer
5. DEC PDP 11/34 computer (e)
 - Gamma 11 acquisition and color display
 - SMS floppy disc drive (f)
 - 2 CDC 300 megabyte disc drives (g)
 - MCT disc controller (h)
 - TS03 tape drive
 - 2 RK05 disc drives
6. DRI 1000 display computer with floppy disc drive and 30 MB Winchester disc (c)
7. RTAS Radiology Reporting System (i)

(a) Technicare Corp., Solon, OH; (b) Picker International Inc., Northford, CT; (c) Diagnostic Resources, Inc., North Boston, NY; (d) Elscint Corporation, Brookline, MA; (e) Digital Equipment Corp., Maynard, MA; (f) Scientific Micro Systems, Mountain View, CA; (g) Control Data Corp., Minneapolis, MN; (h) Minicomputer Technology, Palo Alto, CA; (i) Sudbury Systems Inc., Sudbury, MA.

Table 1 lists the equipment in our department. A central Digital Equipment Corporation (DEC) 11/34 computer provides access to central storage on two 300-megabyte¹ (MB) discs, and is used for more complicated analysis of cardiac, renal, or lung studies.

Each computer has a floppy disc drive and a serial line, each of which can be used to transfer images from that computer to the central mass storage or to the DRI computer used for display of recent studies. The serial line interprocessor communications and the floppy disc transfer have been the subject of prior reports.^{4,5}

The Diagnostic Resources, Inc. (DRI) computer holds about one week's worth of studies on its 30-megabyte Winchester disc. This display computer is used to show studies to referring physicians or for conferences. The central PDP 11/34 computer is used for long-term storage on 300-megabyte discs. The studies can be recalled by a directory on the system disc.

SOFTWARE

Our central PDP 11/34 computer uses the DEC Gamma-11 software under the DEC RT-11 operating system. Special programs were written to allow us to transfer studies *via* serial line or floppy disc between the Technicare VIP, the Elscint Apex, the DRI, and the DEC

Gamma-11 computers.^{4,5} Since RT-11 supports discs that are less than 32 megabytes, the device handler (supplied by Minicomputer Technology) has to divide each of the 300-megabyte CDC discs into 8 sections of 30 megabytes (the formatted capacity of the drives is 254 megabytes).

A directory program was written that records the locations of all of the studies on all of the disc packs. The directory is stored on the system's disc so that it is always available. The directory program performs three functions: (a) directory initialization, (b) directory updating, and (c) directory searching. At the time of initialization, the user selects the size of the directory and the data that are to be kept in the directory. Any combination of fields from the Gamma-11 administrative data block can be selected for inclusion in the directory. The fields that we have selected are patient name, patient number, study type, and study date. In addition, the name and section of the pack where the study is located are stored for each entry.

Directory updating is simple and reasonably error tolerant. Directory searching can be performed on any combination of the stored fields. In addition, matching can be performed on a combination of substrings within a field. Thus, a search could be performed on the last name and two digits of the hospital number if that was the only information available about the patient. The matching entries are displayed for the user, who can then select the entry (s)he wishes. The program then reports the location

¹One megabyte equals 2^{20} or about 10^6 bytes.

of the study and informs the user to mount a disc pack if the study is not currently on line. As the directory has grown over the last year, some operations have slowed. To solve this problem, a search algorithm based on B-tree data structures will be implemented.⁶

Each image of our static studies is acquired in a 128×128 pixel format, with each pixel containing 16 bits. The number of frames depends upon the study. Each view of our dynamic studies is acquired as frames of 64×64 16-bit elements. Our cardiac studies consist of four views: dynamic first pass, gated modified left anterior oblique (MLAO), anterior, and left posterior oblique views. Each view has 28 frames.

The 28 frames of each view are compressed to a 14-frame playback buffer combining the data from pairs of two consecutive frames into a playback buffer suitable for cine viewing. The original 16 bits per pixel is changed to 4 bits per pixel, preserving the 4 most significant bits. The playback buffers of the four views are then merged into a single 128×128 playback buffer for simultaneous multiviewing and interpretation. The original 28-frame data from the MLAO view are then used for computer analysis of ventricular function and wall motion. These data are then stored on a 300-megabyte disc.

Periodically, the contents of part of the disc, excluding the studies that have been merged into cardiac playback buffers, are compressed from the original 16 bits per pixel to 8 bits per pixel, preserving the 8 most significant bits. This compression represents a 2:1 compression for the static studies and an overall 4:1 compression for the gated cardiac studies. The studies are then transferred to a 300-megabyte long-term storage disc.

Backup is an important concept in the all-digital department, since disc crashes can occur on any of our discs and operator errors may occur. Disc crashes have so far been only a theoretical possibility, because we have not experienced a crash during the two years we have been using these 300-megabyte discs. Studies are transferred from each camera-computer to the display computer *via* floppy disc, where they remain for one week. After a week the study is transferred to a 300-megabyte disc and a second

300-megabyte disc as backup. When the oldest section of a disc is compressed and transferred to a long-term storage disc, a copy is made on a second backup disc.

REMOTE ACCESS

Our display computer is also being connected *via* coaxial cable to video monitors and remote keyboards in our division of cardiology and our department of radiology viewing rooms. Personnel in these departments will be able to call up studies from the past week for their own viewing. If they wish to access studies acquired more than one week previously, such studies will be transferred *via* floppy disc from a 300-megabyte disc on the PDP 11/34 central storage computer to the 30-megabyte disc on our display computer.

A telephone communications link *via* modems has been established with community hospitals, which allows them to transfer gated cardiac radionuclide ventriculograms to our DRI display computer. We analyze these studies on our computers and dictate our interpretations into our reporting system described below. Our transfer program is set to accept such studies whenever a telephone call is placed to a modem connected to our display computer. Further details on this function are found in another report.⁷

RTAS REPORTING SYSTEM

Reports dictated into our RTAS (Rapid Telephone Access System) radiology reporting system are available over the telephone either inside or outside the hospital simply by having the referring physician dial the system number followed by the patient I.D.³ The dictated voice is digitized, compressed, and stored on a 70-mega-byte Winchester disc. Standard or normal reports are printed automatically. All other reports are accessed by our transcriptionist for hard-copy typing. Physicians whose patients' gated cardiac studies are sent to us for interpretation *via* telephone can also use RTAS to hear the reports on their patients. A transcriptionist in the radiology department at the remote hospital also accesses RTAS *via* telephone to transcribe the dictated report.

COST EFFECTIVENESS

We have found significant cost savings associated with digital storage of studies. Photographed studies have the cost of technologist time associated with the taking, developing, mounting, and filing of films. There is also the cost of the film processor and its chemicals and maintenance, and the image formatter and camera. In addition, there is the cost of film, filing envelopes, and filing space.

If one analyzes these costs,⁸ photographic storage costs about \$3.46/study. The cost of digital storage of studies can also be derived. This includes the depreciation of the disc drive and controller, the cost of the disc packs, maintenance, and service. If we assume that the nuclear medicine department already has a computer necessary for routine clinical analysis, the cost of digital storage is \$1.19/study. This results in a savings of \$2.27/study using digital rather than photographic storage. If we were to include the depreciation of the DRI display computer, remote monitors, and keyboards as well, this would amount to about \$2.19/study, or a savings of \$1.27 per study. Since our department does about 6,000 studies per year, this results in a savings of up to \$13,620 per year.

DISCUSSION

We have been able to transform our department to all-digital data collection, analysis, and archival storage using commercially available equipment purchased over a number of years. Our referring clinicians have been particularly pleased with our all-digital format. Access to studies is instantaneous, without time wasted in searching through the file room. The ready manipulation of the images to contrast and highlight abnormalities they now consider essential to appreciate lesions properly on the scans. The ability to access an interpretation automatically over any telephone has been very helpful in making rapid diagnostic decisions. Analysis of the RTAS data indicates that over a one-month period 52% of all interpretations were accessed between 5:00 P.M. and 8:00 A.M.

Several individuals contributed software to this development, but the total effort was about

two man-years. The floppy disc communication and large archival store that were key to this transformation have been in operation for two years. We have experienced relatively few growing pains and find that our system not only provides us an excellent data base for research but also is easy to use on a day-to-day basis.

Putting together our system required us to write some special-purpose software to maintain a large data base and to communicate between the systems supplied by several vendors. Although one large computer could replace all of our microprocessor-based computers as well as our central minicomputer, there is the advantage of redundancy and backup inherent in having many stand-alone processors, each of which can operate independently in the event of a failure in another processor.

Currently, each of our 300-megabyte discs contains all of our studies for three months. If we wish to access older studies, we consult the directory on the system's disc to locate the disc that contains the desired study. It would be far more convenient if all studies for the past five years were accessible on the same disc. Such a disc would have to contain greater than 6 gigabytes, although further compression of our data would decrease the storage requirements.⁹ If nuclear medicine matrix displays become routinely 512×512 or 1024×1024 , the storage requirements could easily become 25 or 100 gigabytes. Technology for this may be provided by optical digital discs using laser light for recording and playback. Such discs currently cannot be erased; however, for archival storage, permanent recording is an advantage, not a disadvantage.

We hope that the nuclear medicine vendors will provide support for large data bases and for standard communications. The advantages of an all-digital department, in cost, data manipulation, and easy digital data retrieval, would then be provided without the need to write special-purpose software.

ACKNOWLEDGMENTS

Excellent technical support was provided by Sheila Flynn, Dana Cronan, Lisa Gwon, Pat Wright, Debbie Cohn, Paula Lenane, and Andrea Rousseau.

REFERENCES

1. Dwyer SJ, Templeton AW, Martin NL, et al. A distributed diagnostic imaging management system. Proceedings of the Computer/Instrumentation Council Meeting (in press)
2. Royal HD, Aker EM, Parker JA, Front D, Kolodny GM: An inexpensive auxiliary display station for a nuclear medicine computer system. *J Nucl Med* 22:1089-1090, 1981
3. Kolodny GM: A cost effective radiology reporting system. *Appl Radiol* 10:61-64, 1981
4. Parker JA, Beckmann RG, Smith K, Chung GH: Serial asynchronous communications between two different nuclear medicine computer systems. *IEEE Trans Nucl Sci* 145-27:541-542, 1980
5. Bliss JG, Parker JA, Royal HD, Uren RF, Kolodny GM: An all digital nuclear medicine department: interprocessor communications. Proceedings of the Computer/Instrumentation Council Meeting (in press)
6. Bayer R: Symmetric binary b-trees data structure and maintenance algorithms. *Acta Informatica* 1:290-306, 1972
7. Royal HD, Parker JA, Uren RF, Hyman R, Jansons GM, Kolodny GM: Telephone transfer of nuclear cardiology studies from community hospitals for interpretation at an academic center. *Radiology* (in press)
8. Royal HD, Parker JA, Uren RF, Kolodny GM: Cost effectiveness of the all digital nuclear medicine department (submitted for publication)
9. Parker JA, Zimmerman RE, Treves S: Potential for compression of dynamic scintigraphy using a modified Huffman code. Proceedings of 6th Annual Meeting on the Sharing of Computer Programs and Technology; 385-391, 1976

5.3 Digital Radiology at the University of California, Los Angeles: A Feasibility Study

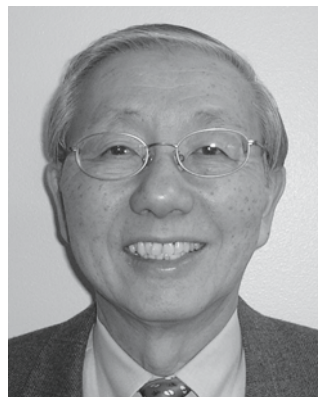
H.K. Huang (born 1939)

H.K. (Bernie) Huang, was born on 10 October 1939 in Canton, China. He got his BS in Meteorology in 1961 from National Taiwan University, his MS in Mathematics in 1962 from Kansas State University and his DSc in Applied Mechanics and Mathematics in 1972 from George Washington University. Dr. Huang took his postdoctoral fellowship in Anatomy and Physiology at Georgetown University in 1973 and was appointed lecturer at the Department of Physiology Biophysics at Georgetown University Medical School (1972–1975). He became Assistant Professorial Lecturer at the Department of Engineering Administration, the Department of Physiology and Biophysics (1976–1979) and the Department of Anatomy and Physiology Georgetown University (1978–1980). In 1982 he was appointed Professor and Acting Director Medical Physics Division (1982) and Chief of the Medical Imaging Division (1984) at the Department of Radiological Sciences at the University of California, Los Angeles. He became Member of the Jonsson Comprehensive Cancer Center at the University of California, Los Angeles.

In 1992 he was appointed Professor of Radiology and Director of the Laboratory for Radiological Informatics at the University of California, San Francisco, Visiting Professor, New York Hospital, Cornell Medical Center, N.Y. (1997), Guest Professor, Xi'an Jiaotong University, China (1998), Kan Tong Po Visiting Professor, Hong Kong Polytechnic University (1999). Since 2000 he has been a Professor of Radiology, Children's Hospital Los Angeles/University of Southern California, a Chair Professor of Medical Informatics, Hong Kong Polytechnic University (Honorary) and an Honorary Professor, Shanghai Institute of Technical Physics, Chinese Academy of Sciences. In 2003 he was appointed Professor of Radiology and Biomedical Engineering; Director, Division of Imaging Informatics, Department of Radiology, University of Southern California, USA; Chair Professor of Medical Informatics.

Dr. Huang pioneered in picture archiving and communication system (PACS) research. He developed the PACS at UCLA in 1991 and the hospital-integrated PACS at UCSF in 1995. Dr. Huang has taught at Georgetown University, U Iowa, UCLA, UC Berkeley and UC San Francisco, Hong Kong Polytechnic University, and the University of Southern California. His current research interest is in digital mammography, tele-imaging and telemedicine, imaging informatics, fault-tolerant PACS servers, PACS ASP models, Internet 2, PACS-based CAD and surgery. He has co-authored and authored seven books, published over 200 articles, and received several patents. His latest book: "PACS and Imaging Informatics" was recently published by John Wiley & Sons. During the past 15 years, Dr. Huang has received over 15 million US dollars in PACS, medical imaging informatics, tele-imaging, and image processing-related research grants and contracts from the US federal and state governments, and private industry. He has mentored 15 PhD students and trained over 30 postdoctoral fellows during the past 15 years. Dr. Huang has been a consultant for many hospitals in developing PAC systems around the world.

Dr. Huang was inducted into the Royal College of Radiologists, London as an Honorary Fellow for his contribution in PACS research and development in



November, 1992; the American Institute of Medical and Biological Engineering as a Founding Fellow, for his contribution in medical imaging in March 1993; and the Euro PACS Society as an Honorary Member for his contribution to PACS in October, 1996; and was elected as the Honorary President, 2003 International CARS Congress, London. Dr. Huang has been Visiting Professor in many leading universities around the world.

Picture courtesy Bernie Huang, PhD, 2004.

Z. Barbaric

N.J. Mankovich

C. Moler

Journal of Digital Imaging

Digital Radiology at the University of California, Los Angeles: A Feasibility Study

H. K. Huang, Zoran Barbaric, Nicholas J. Mankovich, and Charles Moler

This paper describes a set of feasibility studies on converting the Department of Radiological Sciences, UCLA from a film based operation to a digital based operation. The studies address the following topics: the departmental facility, the operating procedure and cost, a cost effective analysis and a proposed digital based operating system. In addition, we examine three prototype projects being carried out in our department. These include: a digital archiving and communication system, a hybrid archiving and communication system, and a multiple image viewing system.

INTRODUCTION

THE CONCEPT OF A DIGITAL OR ELECTRONIC RADIOLOGY DEPARTMENT was discussed as early as 1973. However the technology present at that time did not make its construction feasible. Now, with the increasing numbers of digital based diagnostic modalities, the maturity of the field of computer based hospital management, and the progress in digital electronics and communication systems, it is necessary to realize this concept.

The purpose of this paper is to summarize a study on the feasibility of converting our department into a digital department. A digital radiology department consists of two components; a radiology information management system and a digital image system. The radiology information management system represents a problem in data base management which has been addressed repeatedly in the past few years and will not be considered in this study. Development of a digital image system requires the technology of image acquisition from various diagnostic modalities, as well as the develop-

ment of systems of image archiving, communication, display, and manipulation. Moreover the economic aspect must also be considered. In the past some studies along this line have been performed and the indications favor a digital based approach.^{2,3} In this study we organize the analysis into four parts:

- a. *Facility study.* This part details an inventory of the existing major diagnostic equipment and the equipment to be added in the next two years as well as their distribution in the department.
- b. *Operating procedure and cost.* The daily and the monthly operating procedure in our department is reviewed. A post three-year cost breakdown is then given on staff FTE (full-time-equivalent), maintenance, operation, film, and storage.
- c. *Cost effective analysis.* A cost effective analysis on converting our department into digital is given.
- d. *A digital based operating system.* Several possible systems for converting our department into digital are considered. We also describe three ongoing prototype subsystems being investigated.

From the Department of Radiological Sciences, Center for the Health Sciences, University of California Los Angeles, Los Angeles, CA.

Copyright © 1983 by the International Society for Optical Engineering. Proc. SPIE 418:259-265, 1983. Reprinted with permission.

*Online publication 30 April 2003
doi: 10.1007/s10278-002-6015-8*

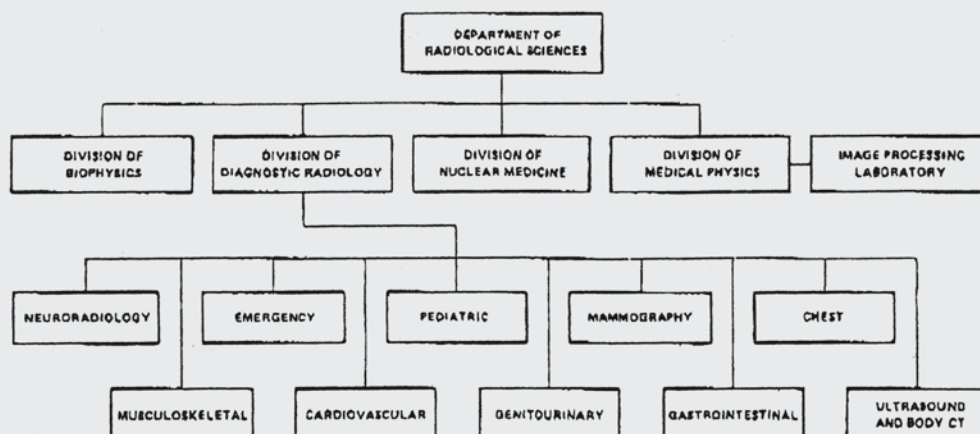


Fig 1. Organization chart for the Department of Radiological Sciences, UCLA.

FACILITY STUDY

1. The Department of Radiological Sciences

The UCLA Medical Center is a 685 licensed bed teaching hospital, and the Department of Radiological Sciences occupies about 80,000 square feet of space. The Department is composed of four divisions: Diagnostic, Nuclear Medicine, Biophysics, and Medical Physics. The Division of Diagnostic Radiology is patient-oriented and is decentralized into ten operationally independent sections: Neuroradiology, Emergency, Pediatric, Mammography, Chest, Musculoskeletal, Cardiovascular, Genitourinary, Ultrasound and Body CT, and Gastrointestinal. The Nuclear Medicine Division is also patient-oriented and together with the Division of Biophysics monitors one of the largest PET (Positron Emission Tomography) research programs in the nation. The Division of Medical Physics provides the scientific and technical resources for the Department and offers M.S. and Ph.D. degrees. This division also operates a dedicated image processing laboratory. Figure 1 depicts the structure of the department.

2. Major Diagnostic Equipment

An inventory on major diagnostic equipment in our department reveals the following:

2.1 Existing Equipment

- 1 Fonar QED 83000—3 kgauss permanent magnet whole body NMR scanner (being installed).
- 2 CT Scanners 1 GE 8800 (3rd generation) 1 Technicare 1440 (4th generation)
- 2 PET Scanners 1 Neuro ECAT—Positron Emission Tomographic brain scanner (Ortec) 1 Ecat III—Positron Emission Tomographic body scanner (Ortec)
- 7 Ultrasound units
- Digital fluoroscopic unit 1 Philips OVI connected to an angiographic unit 1 ISOCON connected to the GU fluoroscopic unit 1 ADAC DPS-4100S with two cameras and an imaging network processing station connected to a neuro fluoroscopic unit and an angiographic unit
- 1 ADAC-PDX-4800 Projection Digital X-ray System
- 1 Mammographic unit
- 6 Special procedures application x-ray systems

2.2 Equipment Being Ordered

- 1 Technicare 5-6 Superconducting magnet whole body NMR scanner
 - 1 Technicare Digital radiography system (DR 960-B) connected to an angiographic unit
 - 1 Prototype slit scanning digital chest system
- Figure 2 shows the relative location of this equipment in the department.

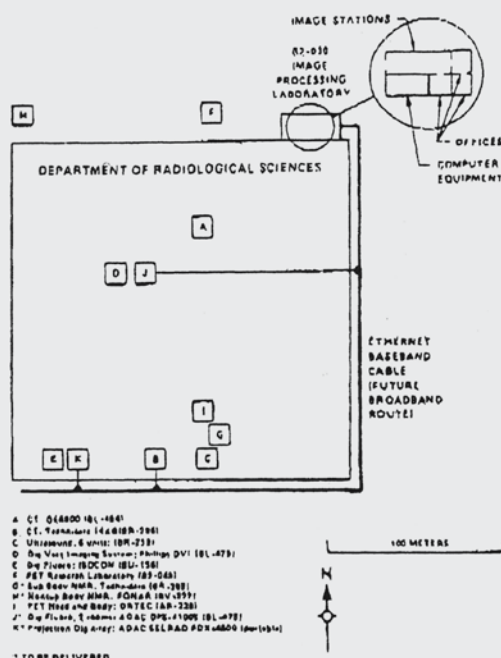


Fig 2. Location of diagnostic equipment, the Image Processing Laboratory, and the communication network.

OPERATING PROCEDURE AND COST

Conventional diagnostic images obtained from either x-ray or other energy sources are recorded on films. These films are viewed from illuminated viewboxes and later stored in the film library for future use. Diagnostic images

obtained from digital acquisition systems, for example, nuclear medicine, digital ultrasound, transmission and emission tomography, digital radiography, and nuclear magnetic resonance, are first displayed on TV monitors for immediate viewing and then recorded on magnetic tapes or disks for archiving. In addition, they are also recorded on films as a permanent record and for future viewing. Since films are convenient to use in a clinical setting, clinicians prefer to view these digital images as films even though this reduces image quality. As a result, our department still has to handle films from all diagnostic modalities without regard to their conventional or digital origin. Because of this, we investigate the costs for this film based operation. Table 1 is a three year estimate on the number of procedures and film usage in the ten diagnostic sections and the nuclear medicine division. Table 2 shows the three year estimate of the film and film related costs in our department.

In compiling these tables, we include negative preservers, x-ray film jackets, x-ray mailing envelopes, x-ray insert envelopes, rental on film storage, fleet services for film delivery, and miscellaneous supplies such as the film library coats, and film processor purchases, film solutions, replacement parts, facilities repairs and installations and other miscellaneous supplies as the film processor costs. As indicated in the tables, each year we perform about 113,000 procedures and use about 500,000 sheets of film. This film based operation costs about 1.5

Table 1. Three Year Estimate on Number of Procedures and Film Usage

Section	Number of Procedures			Film (Sheets)			Film (Cost)		
	79-80	80-81	81-82	79-80	80-81	81-82	79-80	80-81	81-82
Nuc Med				13,500	11,500	11,100	\$16,205	\$14,321	\$12,474
GU	4,382	3,849	4,007	34,500	31,875	31,075	41,656	48,269	47,158
Peds	8,873	8,447	8,041	41,850	33,650	38,250	52,198	54,003	65,431
GI	5,359	4,990	4,984	64,700	61,100	54,700	78,588	88,120	75,544
Neuro&CT-H	4,470	4,457	4,747	24,900	21,500	28,100	29,076	32,250	40,006
US&CT-B	7,227	8,222	8,293	25,100	35,400	34,300	28,972	31,271	32,818
Cardio	837	910	1,396	25,750	26,000	27,050	42,641	50,148	46,353
General OPD	19,637	18,269	21,890	124,725	96,950	96,950	155,841	173,267	164,568
General IP	39,810	41,432	35,573	106,215	99,330	95,800	143,650	182,770	154,985
Mammography	921	1,152	1,257	4,500	7,600	8,100	4,194	6,992	6,890
Emergency	26,296	23,911	22,884	74,000	80,100	78,900	94,287	128,579	120,042
TOTAL	117,812	115,639	113,072	539,740	505,005	504,325	\$687,308	\$809,990	\$766,269

Table 2. Three Year Estimate of Film and Film Related Costs

	1979/1980	1980/1981	1981/1982
Film Library	49,350	51,623	45,577
Indirect Expenses	25,823	30,251	25,204
Film Processor	60,674	58,518	86,809
Indirect Expenses	28,867	26,991	26,239
Personnel:			
Darkroom	135,012* (3.8)**	155,832 (9.1)	171,488 (9.8)
Film Library	371,199 (25.2)	388,608 (25)	432,524 (24.3)
Film-related Cost			
Total	670,925	711,823	787,841
Film	687,308	809,990	766,269
Total Costs	\$1,358,233	\$1,521,813	\$1,554,110

*Salary and fringe benefits.

**Full time equivalent (FTE).

million, about half of it is for films and the other half for film related costs. This operation requires about 34 FTE of which 70% is dedicated to the film library. The film operation requires approximately 2,600 square feet of space within the department and an additional 10,000 square feet for film storage in a satellite location. By performing this type analysis, we hope to be able to estimate the increased or decreased costs associated with a digital based operation.

COST EFFECTIVE ANALYSIS

Based on our study on operating procedure and cost we come up with a ten-year cost projections for a conventional film based and a digital based operation in our department. Table 3 shows these estimates.

It is seen from this comparison that we would be able to save about four million over a ten year span, of about 400,000/year. Two major factors contributing to the savings are the reduction in

Table 3. Ten Year Projection and Cost Comparison Between a Film Based Operation and a Digital Based Operation*

Film Based Operation	In Thousands	Digital Based Operation	In Thousands
Film	7,000	Replace conventional chest to digital chest	
H ₂ O for the processors (60 M gallon @ 10.0/1000 gallon)	600	Six units @ 500,000	3,000
FTE (34) [†]	7,000	Image memory	1,000
Processor	1,000	TV monitors 1000 unit	1,000
Film storage rental	500	Terminals 200 unit	2,000
Matrix camera purchase	500	Analog/Digital storage	1,000
Space (equivalent cost)	2,350	Communication network	1,000
Physicians time lost (\$10/hr)	1,500		
Equipment (x-ray)	2,000	Sub Total	9,000
		Maintenance 10%/year for ten years of equipment cost (9,000)	
		We take half of this value.	4,500
		FTE (15) [†]	3,000
		Sub Total	16,500
		10% of film based operation**	2,250
Total	22,450	Total	18,750

*Excluding digital based equipment purchase.

**We believe films are still necessary in a digital based operation.

[†]We anticipate the FTE qualifications will be the same in both operations.

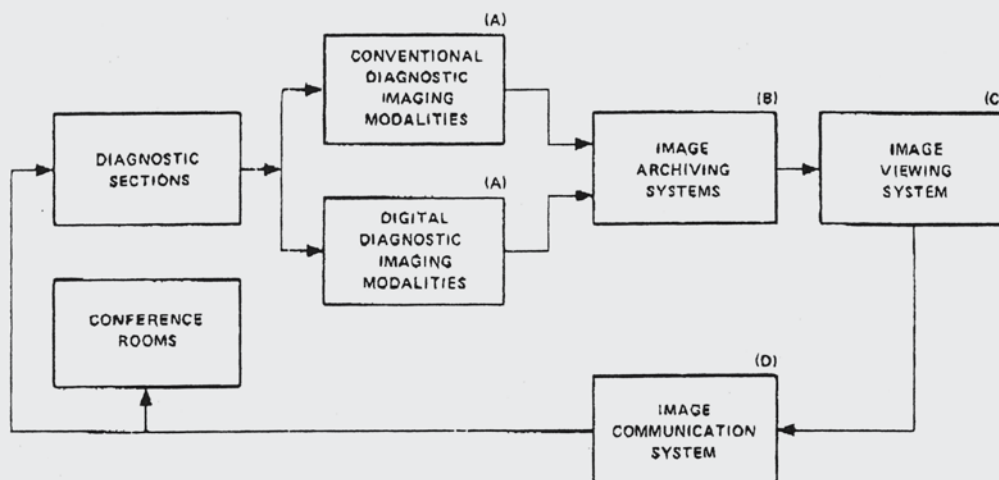


Fig 3. A general digital based radiology department operating system.

film cost and reduction in FTE positions. We agree that these cost estimates are not exhaustive and are certainly subject to challenge, especially when estimating the digital based operation. Nevertheless we believe the amount of saving is genuine. Moreover, there are benefits in a digital based operation which we cannot translate directly to the dollar amount. These include ease of record keeping, no loss of image information, and a savings in record retrieval time.

A DIGITAL BASED OPERATING SYSTEM

With all of these advantages in a digital based operation, we have decided to perform some preliminary studies on how to change our department from a film based operation to a digital based operation. At the present time we perceive that a digital based operation requires the components shown in Figure 3. We will not discuss the technical aspect of these components since they have been discussed elsewhere. Instead we will consider the possible combination of these components in such an operation.

A. Image Acquisition

Image acquisition is a component already in existence. It can arise from either a conventional or a digital diagnostic modality. We anticipate the former modality will contribute less and less as we move further towards digital.

B. Image Archiving System

An image archiving system has three components, an image storage device, a mechanism of transmitting images from diagnostic modalities to the storage device, and a means of image retrieval.

For digital based modalities, the storage device can be a very large magnetic disk system, an optical disk system, or a digital coded fiche. The mechanism of transmitting images could be through a digital communication line or a digital/video broadband communication system from the modality to the storage device.

For conventional x-ray films, the mechanism of transmitting images could be a digitizer converting the analog image to digital form and a communication system which transmits the digital information to the storage device. A less acceptable method is to reduce the x-ray films and store them on microfiche. In this case, the image storage device would be a hybrid system. The retrieval mechanism is necessary for sending the stored images to the proper viewing site. It is relatively straightforward in a digital storage device based system but not so simple for a hybrid system.

C. Image Viewing System

The image viewing system is for displaying multiple diagnostic images from the storage

device. This system requires a very large image memory, a video output control, a powerful image processor, and a bank of viewing monitors.

D. Image Communication System

The image communication system is for distributing the images from the viewing system to various locations within the department. The image viewing system, together with the communication system would replace the conventional x-ray film reading room.

PROTOTYPE SYSTEMS UNDER INVESTIGATION

Currently we are investigating three prototype subsystems: two for picture archiving and communication and one for image viewing.

A. A Digital Archiving and Communication System

A communication and archiving system based on the Ethernet communications protocol has been designed and is under installation. The preliminary communication network will connect our dedicated Image Processing Laboratory in the department to two digital fluoroscopic units, a projection digital x-ray unit, and a CT body unit. This communication system is relatively slow and will take from two to four seconds to transmit a $512 \times 512 \times 8$ diagnostic image. A parallel system using the broadband communication system which combines both digital and video communication is being designed. This system can communicate diagnostic images in real time.

B. A Hybrid Archiving and Communication System

We are collaborating with a manufacturer to design a hybrid archiving and communication system based on microfiche. Images are recorded on microfiche either in analog or in digital coded form. The microfiche is stored in a carousel for automatic retrieval. Analog images can be viewed through an optical reader and digital images can be transmitted to a proper

digital diagnostic console and viewed from the display monitor.

C. Multiple Image Viewing System

A four phase research project involving the installation of multiple digital image viewing stations in our department is being implemented. Each viewing station will be able to display and manipulate up to six 512×512 radiographic images simultaneously. The four phases of this project are: (1) simulation of a digital viewing station at the Image Processing Laboratory, (2) installation of a viewing station at a remote diagnostic section, (3) installation of a second mobile viewing station, and (4) an evaluation of the entire project. The first phase of this project has already been completed.

SUMMARY

We have described a feasibility study on converting our department from a film based operation to a digital based operation. In the next few years we perceive that all major diagnostic equipment in our department will be digital based with the exception of conventional chest units. It is therefore our goal to look into the possibility of changing our operation from film based to digital based. The two major cost factors in a film based operation are the films and FTE positions. A digital based operation can keep these two cost factors to a minimum. In addition, a digital based operation has the advantage of having better record keeping, better image information retention, and amount to a substantial savings in handling time. However, there is an unknown psychological factor which is difficult to assess at the moment. Namely, would a digital based operation be acceptable by physicians. In order to investigate this aspect we are in the process of studying three prototype subsystems. By developing these prototypes in a clinical environment we hope to assess the feasibility of fully implementing a digital based radiology department.

ACKNOWLEDGMENTS

We wish to thank Mrs. Lois Haas and Ms. Sandy Anglin for accumulating the data for Tables 1 and 2.

REFERENCES

1. Capp MP, et al: Photo electronic radiology department. Proc SPIE: Digital Radiography, Vol. 3A, 2-8, 1981
2. Dwyer SJ III, et al: Cost of managing digital diagnostic Images for a 614 bed hospital. Proc. SPIE: Picture Archiving and Communication Systems, Vol. 319, 3-8, 1982
3. Staab EV, et al: Medical image communication system: plan, management and initial experience in prototype at the University of North Carolina. Proc. SPIE: Picture Archiving and Communication Systems. Vol. 318, 19-22, 1982
4. Duerinckx AJ: Picture Archiving and Communication Systems (PACS) for Medical Applications, edited. Proc. SPIE: Picture Archiving and Communication systems, Vol. 318, 1982
5. Huang HK, et al: Design and implementation of multiple digital viewing stations. Proc. SPIE: Picture Archiving and Communications Systems II, May, 22-25, 1983

5.4 Assessment of the Integration of HIS/RIS with a PACS

Betty Ann Levine (born 1959)

Betty Levine was born November 9, 1959 in Glen Cove, New York, USA. She got her BS in applied mathematics and statistics from the State University of New York at Stony Brook in May 1981 and her MS in industrial engineering and operations research from the University of Massachusetts, Amherst in May 1983. She started her professional career in 1983 as a programmer analyst contracted to Pratt and Whitney Aircraft, East Hartford, Connecticut. Here she was responsible for design, coding, and documentation of data analysis systems for non-technical users and development of database libraries for easy user retrieval for subsequent data analysis.

In 1984 Ms. Levine went to Europe and became Assistant Professor at the Mathematics Department of the American College of Switzerland, Leysin, Switzerland. She returned to the US in 1985 to be employed as an applications programmer within the Research Department of Kaman Aerospace Corporation, Bloomfield Connecticut. Her main task was to design, code, and document technical applications software for large scale helicopter analysis system.

From 1986–1987 she became scientific programmer and instructor at the Department of Radiation Oncology, New England Medical Center, Boston, Massachusetts. She worked with physicists to design radiation therapy treatment planning and dosimetry calculation software.

From 1987–1998 she was a scientific programmer within the Department of Radiation Medicine, Georgetown University Hospital, Washington, D.C. In 1987 she also became a principal software engineer within the Department of Radiology, Georgetown University Hospital, Washington, DC where she is still employed. Her first responsibility was to develop, under an agreement with Philips Medical Systems NA, three interfaces between their Picture Archiving and Communication Systems and different Radiology Information Systems (DINS). She was also a member of a project team evaluating Digital Imaging Network Systems for the U.S. Army Medical Research and Development Command. Her other projects included: design and implementation of C language ACR-NEMA interfaces between hospital and radiology information systems and a DINS; network modeling and simulation of DINS using Q+ simulation software; development of C language programs to reconstruct CT and MRI images from manufacturers' data format specifications.

Ms. Levine's responsibilities included the management of digital imaging related projects for the department of radiology. These responsibilities included the design, installation, and implementation of digital imaging networks for the radiology department as well as other grant-funded operations. Primary responsibilities included network design for digital imaging systems, design of telemedicine projects, liaison with vendors regarding installation and implementation, working with hospital clinicians to integrate the systems into daily use.

Ms. Levine's current responsibilities as Head of the Division of Health and Telemedicine within the Imaging Science and Information Systems Center at Georgetown University include the design and integration of information systems requirements for the Mind-my-Heart home monitoring and case management project for congestive heart failure patients and the design, development, and



implementation of the My-Care-Team Internet-based diabetes management project. Some past telemedicine projects managed by Ms. Levine included telemedicine for hemodialysis patients, deployable radiology for the US troops in Bosnia and Kuwait, and the development of an Internet based Home Peritoneal Dialysis management system.

In 1998 Betty Levine was a finalist in the Global Information Infrastructure (GII) award competition, health category for Project DEPRAD.

Picture courtesy Betty Levine, PhD, 2004.

S.K. Mun

H.R. Benson

S.C. Horii

Journal of Digital Imaging

Assessment of the Integration of a HIS/RIS with a PACS

Betty A. Levine, Seong K. Mun, Harold R. Benson, and Steven C. Horii

The exchange of information between a Radiology Information System (RIS) and a PACS is essential to optimizing the utility of a PACS. Some of the benefits awarded by implementing an interface include a reduction or elimination of repetitious data entry, the availability of more accurate information on the PACS, a reduction in workload for the technologists, registration clerks, transcriptionists, etc, and the availability of more accurate data for automating the PACS. This paper discusses the Georgetown experience of interfacing an HIS/RIS and PACS, by describing the development of the interface and its impact on clinical operations.

INTRODUCTION

GEORGETOWN UNIVERSITY MEDICAL CENTER has an integrated patient information system solely supported by hospital staff. The departments within the hospital which are incorporated into the Hospital Information System (HIS) include: Clinical Laboratories, Continuing Medical Education, Emergency Room Admissions, Inpatient Admissions, Medical Records, Nursing, Pathology, Pharmacy, Poison Control Center, Private Outpatient and Inpatient Billing and Accounts Receivable, Radiology, and Transcription. The HIS software is written in MIIS, a dialect of MUMPS, and operates on five Data General mini-computers with eight 256M disk packs for archival storage and twelve 256M magnetic disk drives (3.072 gigabytes) of on-line storage.

The RIS is an integral part of the HIS and shares patient registration and order entry modules with other systems connected to the HIS. Also included in the RIS is a chronological index of patient activity, a film jacket tracking system, a report generating system, and an electronic physician sign-off. The HIS/RIS events which produce information required by a PACS include the registration of new patients

into the radiology department (including modification to patient demographics), the creation of new radiology orders, modifications to and cancellations of the orders, and the generation of radiology reports, from preliminary to approved status. The Georgetown PACS network is based on an AT&T CommView system using ACR-NEMA messages to transfer information from the HIS/RIS to the PACS. The PACS configuration at Georgetown currently supports 11 imaging devices and 10 workstations. The HIS/RIS interface has been in clinical operation since June 1989.

NECESSITY OF INTERFACE

The importance of an HIS/RIS-PACS interface is evident to any institution employing both systems. The overlap of functionality between the systems (that is, patient registration, exam or order entry, and transcription) requires that the systems be able to share information as a means for eliminating repetitious entry of data while maintaining consistent database information. At the beginning of the Georgetown digital imaging network (DINS) project, the information available in the HIS/RIS and required by the PACS was manually entered into the PACS by technologists, registration clerks, etc. As can be expected, this resulted in both numerous mistyped data being entered into the

From the Georgetown University Medical Center, Washington, DC.

Copyright © 1990 by the International Society for Optical Engineering. Proc SPIE 1234:391-397, 1990. Reprinted with permission.

Online publication 30 April 2003

doi: 10.1007/s10278-002-6022-9

PACS and missing data elements. Corrections on the HIS/RIS would have to be entered separately into the PACS and so were usually not made. The existence of a link between the HIS/RIS and the PACS virtually eliminates both of these problems, resulting in more compatible databases.

Besides the elimination of redundant data entry, the implementation of an interface between the HIS/RIS and the PACS has allowed for the development of a more automated, more intelligent PACS. Certain HIS/RIS data fields, (radiologist, modality, and referring physician) and PACS data fields (acquisition station, worklist category, and destination) are currently used by the CommView system for their auto-send feature to route exams to workstations as they are acquired. This works reasonably well within the Radiology Department where modalities or radiologists tend to use a single workstation. Outside of Radiology, it is not as easy for the PACS to determine where to send the exam. For example, auto-sending exams to the intensive care wards requires that the person capturing the images into the PACS first enter the destination of the images into the PACS. This is a workable solution although quite cumbersome. Information exists within most HIS/RIS (e.g., patient location or room number) and should be used by the PACS as an alternative key to determine to which workstations exams are to be routed. The auto-send feature available on CommView could be enhanced if this piece of information, currently available in an HIS/RIS, were used.

A thorough understanding of both systems' databases, of how information is stored, sent, and acquired, and of the functional overlap between the systems is crucial from the beginning of the interface design. In developing Georgetown's HIS/RIS-PACS interface, many conceptual, technical, and operational problems arose which were not evident at the start of the interface design. These issues, along with specifics about the Georgetown interface, will be discussed in the following sections.

TECHNICAL INTERFACE

Embarking on the development of an HIS/RIS-PACS interface requires a technical defi-

nition of the data format, communications protocols, and physical communications links, as well as an operational specification explaining what triggers the data transfer. All discussions in this section will assume an interface similar to the one existing at Georgetown, with data flowing uni-directionally from the HIS/RIS to the PACS.

Having a standard for transferring data, like ACR-NEMA, makes the interface design much simpler and more robust. The ACR-NEMA standard in its current form specifies a physical link as well as logical structure for connecting imaging equipment from different manufacturers for transferring image and text data. Working group VIII (WG VIII) of the ACR-NEMA Standards Committee is working on an extension to the original standard to define the transfer of information between an HIS/RIS and a PACS. This extension will define only the logical layers while maintaining the data formats of the current ACR-NEMA standard and expanding the already extensive data dictionary. The AT&T CommView system interface specification follows the ACR-NEMA format for receiving information from an HIS/RIS, however, it does contain extensions to the current standard. A Hexadecimal representation of an acceptable HIS/RIS-CommView message is shown in Fig. 1. Our HIS/RIS does not produce data for transmission in an ACR-NEMA format, thus requiring a gateway (an AT&T 6310 PC is used) between the two systems to generate ACR-NEMA formatted data from the HIS/RIS ASCII data. The HIS/RIS at Georgetown passes exam information to the PACS as shown in Fig. 2a, but passes report information as shown in Fig. 2b.

Similarly, the specified communications protocols for the PACS side of the interface are different from those defined by our HIS/RIS. The AT&T specification requires binary data sent over direct RS-232 lines using the KERMIT communications protocols, whereas our HIS/RIS sends ASCII data across a SYTEK network using the FTERM communications package which does not allow for KERMIT protocols. Again our converter box acts as a gateway for passing the data between the systems.

The use of a third computer system as a gateway between the HIS/RIS and PACS is a


```

0000 0000 0000 0004 0000 0064
0000 0001 0000 0004 0000 01ce
0000 0010 0000 000c 4143 525f 4e45 4d41 2031 2e30
0000 0100 0000 0002 0001
0000 0110 0000 0002 002f
0000 0200 0000 0004 5249 5320
0000 0300 0000 0008 436f 6d6d 5669 6577
0000 0700 0000 0002 0000
0000 0800 0000 0002 9001
0001 0000 0000 0004 0000 001e
0001 0001 0000 0002 9010
0001 0003 0000 0002 0000
0001 0005 0000 0002 0000
0008 0000 0000 0004 0000 008c
0008 0001 0000 0004 0000 0134
0008 0010 0000 000c 4143 525f 4e45 4d41 2031 2e30
0008 0020 0000 000a 3139 3839 2e30 362e 3037
0008 0030 0000 000a 3032 3a35 303a 3030 2e30
0008 0040 0000 0002 9001
0008 0060 0000 0002 5553
0008 0100 0000 000c 484f 592c 4445 424f 5241 4800
0008 1030 0000 000e 5553 2041 4244 2044 4f50 504c 4552
0008 1070 0000 0002 5646
0009 0000 0000 0004 0000 0042
0009 1001 0000 000c 2033 3733 3332 3533 2e32 3039
0009 100d 0000 001c 5345 5645 5245 2052 4553 5049 5241 544f 5259 2044 4953 5452 4553 5300
0009 1011 0000 0002 4920
0010 0000 0000 0004 0000 0040
0010 0010 0000 000c 4241 4b45 522c 4d41 5454 4845 5700
0010 0020 0000 0006 3735 3137 3731
0010 0030 0000 000a 3139 3839 2e30 352e 3139
0010 0040 0000 0002 4d20
4201 0000 0000 0004 0000 000e
4201 1010 0000 0006 4344 2c49 434e

```

Fig 1. Hexadecimal representation of acceptable HIS/RIS-PACS transaction.

satisfactory solution, but not without its problems. Mainly, the question remains as to which system, either HIS/RIS or PACS, maintains responsibility for the data after it leaves the HIS/RIS and before it enters the PACS. If data was passed directly to the PACS, then responsibility for the accuracy of the data would be more evident. The need for user intervention increases when the systems are not directly connected and only one-way communication is permitted. An operator must check log files and determine the appropriate action when transactions are not handled as expected on the PACS.

Defining the physical and technical parameters for passing information may require negotiations with both the HIS/RIS and PACS vendors. The goal of these negotiations is to develop one specification acceptable to both parties. However, in reality the two interface specifications are often quite different. The amount of work required to pass information between systems varies depending upon the similarity of their file formats, transmission parameters, and communications media.

APPLICATION

The logical relationship between transactions which occur on the HIS/RIS and their counterparts on the PACS is not so straightforward. Determining which actions will trigger data to be passed to the PACS is specific to the HIS/RIS. For a very robust HIS/RIS system, many actions may have a similar effect on the PACS. The HIS/RIS transactions for registering patients and updating their demographics, creating, modifying, and canceling radiology exams and orders, and creating, updating, and deleting radiology reports all produce information needed by the PACS.

The Georgetown integration effort began with the transfer of order entry information from the HIS/RIS to the PACS. The initial goal was to bring signed reports to the PACS as quickly as possible. In order to bring reports to the PACS directly from the HIS/RIS, the order data in the PACS must be exactly as it appears in the HIS/RIS. Therefore, initial efforts focused on sending all exam data to the PACS as it was entered into the HIS/RIS, including the

```
O;A;0;
D0;04;Doe,J;M;05/19/89;6;69119;;M8500H;777777;;694513;;01;26;;;;;;PED/NEO;;;8;01
D1;HOY,DEBORAH;SEVERE RESPIRATORY DISTRESS;00.0;39;;;;;;1
O0;9;3733253;;2688;423937293;;69129;;-261;HOY,D;CD,ICN;;;;69129;;;;69129;125
O2;
O6;;;CW,RAD;423957443;VF,RAD;423937260
O7;209;US ABD DOPPLER;;6377;;;;;;69129;;;;2:50 PM;VF;69129;3:50 PM
O7;217;US KIDNEY BIL;1;C7005;D;;
```

a

Fig 2a. Example of an HIS exam message.

```
T;A;0
2688;210
PATIENT: Doe, Jane          MRUN: 777777      AGE: 2M   PAGE: 7
ORDER #: 4241886  ACC#: 772343  DR: HOY,DEBORAH
ORDER DR: HOY,DEBORAH
SERVICE: 12/18/89          RAD #:
DICTATED BY: GARRA,BRIAN S
```

EXAM(S): 1) US BRAIN PEDS

HISTORY:
FOLLOW UP ON IVH PREMATURITY

U.S. BRAIN SCAN, NEONATAL CPT: 76506 ACR:
Scans of the head through the anterior fontanelle show no ventricular dilatation or hemorrhages. No definite parenchymal abnormalities. A wedge-shaped echogenic region near the inner hemispheric fissure probably represents an obliquely running sulcus.

IMPRESSION:
NO VENTRICULAR DILATATION OR HEMORRHAGES.

BG/laa

12/19/89 9:56 AM

SIGNED BY: BRIAN S GARRA, MD

12/20/89 3:22 PM

b

Fig 2b. Example of an HIS report message.

creation of new exam orders as well as the modifications to and cancellations of existing orders. Data from November and December 1989 was accumulated and analyzed to determine the average number of transactions coming across the interface daily. The results are presented in Table 1. Overall, an average of 156 exam transactions are transferred to the PACS per day, with 198 transactions per day on average during the week and 67 transactions per day on weekends or holidays. These numbers

are broken down by exam transaction type in Table 1.

One problem that has been avoided is the receipt of an add exam transaction for a patient not currently in the PACS database. The CommView system will first add the patient to the database before processing the add exam transaction. The obvious benefit of the CommView system handling this type of request is a reduction in the number of transactions sent across the interface. This is important

Table 1. Average Number of Exam Transactions

	Exam Transaction Type			Total
	Add	Cancel	Edit	
Weekdays	90	9	99	198
Weekends & holidays	37	4	26	67
Daily	73	8	76	157

for a system like that at Georgetown in which the RIS is a subset of a larger HIS and shares the same patient registration system with the rest of the hospital. The number of add patient requests which would come to the PACS each day, for patients not in the Radiology Department, would be prohibitive.

The most common problem seen at Georgetown with transferring exam transactions has been the mismatch of patient names between the systems thereby resulting in a PACS error. This is caused by errors in the initial entry of the patient name, or a newborn initially being recorded as Babyboy or Babygirl and named later. When the change is made in the HIS/RIS, that change is not captured in the PACS. In retrospect, the details for doing this should have been worked out as soon as exam transactions began coming across the interface. However, if every modification to patient demographics is sent to the PACS, since there is no easy method of determining from the registration system whether a patient has radiology exams on the PACS, this would result in a large number of unnecessary transactions. Any method for correctly limiting the transactions sent across the interface is desirable. To limit the passing of patient modification requests, the proposal is to have the PACS modify the patient demographics based on the exam or transcription requests received from the HIS/RIS. This may raise liability issues, but the specifics could be worked out, especially for hospitals with a single patient registration system used by both an HIS and a RIS. Compatibility between the two systems is the highest priority.

Limiting the number of transactions across the interface is important because of the expected volume. Filtering the information from the HIS/RIS is designed to capture only infor-

mation that is deemed necessary on the PACS. The two criteria used at Georgetown are based on the imaging modality referenced and the patient location. If a transaction from the HIS/RIS references either a modality known to be on the network, or a patient unit which has a workstation, that transaction is accepted. Otherwise, while not rejected, it is not processed further.

Another possibility for limiting transactions across an interface is to limit the transferring of transcription data to signed reports only. As long as a one-way interface exists between an HIS/RIS and a PACS, only approved reports need to appear on the PACS. This will increase the time lag between matching report data to exam information, but should drastically reduce the number of transactions sent across the network. This time lag, caused by sending only approved reports, may cause further problems depending on the amount of on-line storage of the system. If exams are archived before the reports are sent to the system, this will currently result in an error and the report not being matched to the exam. The exam must first be restored and the report transaction retransmitted to match the information. This problem can be solved by increasing local storage, rethinking archiving criteria, or modifying the CommView software to restore these exams automatically, to connect the reports with them, and archive the new information.

Operational issues surrounding the transmission of exam transactions cause integrity problems between the two databases since modifications to and cancellations of existing orders take place at many different places within our HIS/RIS and are usually done after the study is complete and the images are acquired into the PACS. This generates confusion on the PACS and results in an error causing the databases to become incompatible. This type of operational problem is common among the modalities connected to the PACS and may require some changes either in the operations of the department or modifications of allowable transactions on the PACS. This issue was discussed with technologists, radiology administrators, and radiologists in order to determine an acceptable solution. Due to the constraints of a one-way interface, confirmation of the ex-

ams cannot be done on the PACS and returned to the HIS/RIS.

Because of these operational issues, the initial goal was modified to be the transfer of exam information to the PACS to aid in acquisition and review while maintaining HIS/RIS and PACS compatibility. One way to obtain this goal is to insist that technologists confirm procedures or modify the information on the HIS/RIS prior to the start of the exam. This is not acceptable at Georgetown since HIS/RIS terminals are not always convenient to the scanning areas. Another solution would be to allow the technologist to easily modify the information on the PACS, select the appropriate study and change the information that arrived from the HIS/RIS. This may reduce some problems but could cause others. The modifications would need to be controlled by the PACS in a method that would maintain compatibility with the HIS/RIS, for example selection of appropriate exam names and descriptions from a predefined list as opposed to freehand editing.

Matching information on the RIS to similar information on the PACS is not always easy. The Georgetown RIS allows radiology orders to contain multiple exams for a single modality. This results in a unique order number on the HIS/RIS for all exams in the order and not for the individual exams. The CommView system, however, does not permit multiple exam orders and requires each exam be handled independently with an exam number unique to the PACS. The two ways of dealing with this are either to separate the HIS/RIS orders into individual exams when sending them to the PACS or to treat all the exams on an order as a single exam. Both of these solutions have their benefits and problems for acquisition, primary diagnosis, and general review.

Creating unique exam identifiers for each exam in an order creates more work for the technologists. It requires them to end acquisition on the PACS and start a new exam while scanning the patient or filming the images. However, it is not always apparent where one exam ends and the next begins. Also it is sometimes necessary to re-scan an area to take additional slices. It does not appear that this issue will be resolved with the installation of

digital interfaces to the imaging devices. With the current digital interface available to us in MR, images can be assigned different exam IDs but this requires that the technologist enter the image numbers and corresponding exam ID into a terminal before the images are acquired into the PACS.

This separation of the exams makes sense from the perspective of a radiologist or a referring physician. It will be easier to find the correct images if the exam procedures are specific to a type of study. For instance, if a physician is seeking an old chest exam on a patient, the exam should be clearly marked by procedure description, date, and time.

The other possibility for handling HIS/RIS orders is as a single exam. This solution is considered feasible only if one radiologist reads all the exams on the original order. This reduces the work load of the technologists since they would not be required to stop and start individual exams as they work. However, it would require anyone wanting to see one exam acquired from an order containing multiple exams to retrieve all the images and search through them until the desired ones are found. If the procedure descriptions could be generated to describe properly all the images in the study, this solution has its benefits. For primary reading, the radiologist only needs to pull up one exam, and the technologists would benefit as stated above. However, the referring physician or radiologist who requests only some of the images for comparison would receive superfluous information which could slow them down. Another potential obstacle is the CommView system's current 175 image limit per exam. With an MR study, it is highly likely this limit would be exceeded, especially if the HIS/RIS orders are not separated.

After discussions with technologists and administrators, it was realized that technical solutions are not always the best, and changes in the operations of the department may be necessary. It was decided to separate the HIS/RIS orders and monitor the results to determine the problem areas. The number of failed transactions from the HIS/RIS to the PACS, the types of transactions failing, and the areas in the department generating the problems will then be

reviewed further. We are prepared to initiate changes in the HIS/RIS in order to generate more compatible databases. It was decided, however, to allow certain exams to be combined into one exam on the PACS, in areas where the relationship between the studies is sensible and would therefore cause little confusion later on. The difficulty imposed by dealing with both an HIS/RIS which permits multiple exam orders and a PACS which does not, is not unique to the Georgetown system. Finding an acceptable solution requires input from many different users of both systems (radiologists, technologists, administrators) as well as the developers of both the HIS/RIS and the PACS.

Finally, matching HIS/RIS reports to PACS exams can be a problem because of the arguments considered above. At Georgetown, reports are generated on the RIS per order, not exam. Since we are splitting our orders into multiple exams, it was determined that instead of separating the report by exam, one report would be sent to the CommView system and automatically stored with each exam from the original order. This is possible since the exam number created for each exam in an order is a concatenation of the original order number and an exam identifier unique to the order. For the CommView system, the exam identifier is used to identify images, exam data, and reports as those belonging to a given patient. Therefore, the exam identifier is crucial to keeping all this information accurate as well as compatible with the RIS information.

ADDITIONAL CAPABILITIES

In general, HIS/RIS-PACS interfaces are still quite primitive and will need to evolve in order to approach the level of sophistication required to guarantee the compatibility of the databases, adapt to new transactions and operational issues, eliminate user intervention, and reduce failed transactions. The biggest change will be the inception of two-way interfaces and truly integrated workstations capable of accessing both the HIS/RIS and PACS databases. This would permit maximum access to all necessary information when reviewing a case and help maintain the integrity of the databases.

Until two-way communications or integrated workstations are realized, significant advances will need to be made to aid in the modification of information on the PACS in order to guarantee compatibility with the HIS/RIS. One way of doing this is to simplify the procedure for starting new exams on the same patient while acquiring images. A reduction in the number of steps required for this process would increase the technologists' use of this and would help the PACS and HIS/RIS databases be more compatible. Allowing the technologist to change procedure descriptions, and cancel and add exams easily from the acquisition screens would decrease the number of failed transactions on the PACS. This would require a confirmation on the PACS that the procedure descriptions and other exam related information was correct for the exam being performed, and thus in concert with what will change on the HIS/RIS. One acceptable method for doing this is for the system to prompt the technologist to on whether the exam information is accurate on the PACS, or if not correct, to display a menu of allowable procedure codes the technologist may choose. Then the technologist could enter the exam number for the exam being done, and a unique exam id comparable to what's produced on the HIS/RIS would be assigned.

As access to the information within an HIS/RIS increases, the "intelligence" of the PACS should improve. The information from an HIS/RIS scheduling module should prompt the PACS to restore related exams from the archive, compile a set of related exams for primary reading, and send the set to the workstation where the radiologist will read them. This should all take place during off-hours, when system usage is slow, but prior to the start of the Radiologist's review. Other functions which would increase the intelligence of the system based on HIS/RIS information, include a more robust auto-send feature (as described earlier) and automatic modifications to demographics.

ACKNOWLEDGMENTS

This work was supported in part by the U.S. Army Medical Research Acquisition Activity of the U.S. Army

Medical Research and Development Command. Contract Number DAMD 17-86-C-6145. The views and opinions contained in this document are those of the authors and should not be construed as official Department of Army position, policy, or decision unless so designated by other documents. The authors are grateful for the technical assistance supplied by Ben Zvi, Rajiv Kapur, Ann Lou, and Bruce Majors.

REFERENCES

1. Levine B, et al: Integration of a RIS with an IMACS. Proc. SPIE 1093:183-191, 1989
2. Lodder H, et al: HIS-PACS Coupling in practice. PROC. SPIE 1093:301-306, 1989
3. *ACR-NEMA Standards* (Publication No. 300), Washington, DC.

5.5 Environmental Designs for Reading from Imaging Workstations: Ergonomic and Architectural Features

Steven Chester Horii (born 1950)

Stephen Horii was born on 29 October 1950 in New York, NY, USA. He got his BA in Natural Sciences from The Johns Hopkins University (1968–72) and his MD from New York University School of Medicine (1972–76).

Dr. Horii started his Postgraduate Training in Diagnostic Radiology at New York University Medical Center and Bellevue Hospital Center (1976–79) and got his Fellowship Appointments in Abdominal Radiology (diagnostic) from New York University Medical Center, Bellevue Hospital Center, and Manhattan Veterans Administration Medical Center (1979–80)

He got his first Faculty Appointment as an Assistant Professor of Radiology at New York University Medical Center and Instructor, later Medical Director, in the Physics Ultrasound Technology Program, New York University School of Allied Health Professions (1980–86). He was appointed Associate Professor of Radiology at New York University Medical Center (1986–88) and Georgetown University Hospital (1988–92), where he was appointed Clinical Director of the Image Management and Communications Section at the Department of Radiology. He became Professor of Radiology at the University of Pennsylvania School of Medicine in 1992.

As the son of an architect Dr. Horii started to think early about necessary ergonomic and environment aspects when just putting a workstation in place of a film alternator. He consulted with his father about these conditions, and they developed some redesigns of a reading room at Georgetown Hospital where several of the PACS workstations were installed.

Dr. Horii was elected to fellowship of the American College of Radiology (1998) and the Society for Computer Applications in Radiology (2000). He got a Certificate of Appreciation at the National Institutes of Health, National Cancer Institute for serving as a member of Subcommittee H, Clinical Trials (2002).

Picture courtesy Steven Horii, PhD, 2004.



Journal of Digital Imaging

Environmental Designs for Reading from Imaging Workstations: Ergonomic and Architectural Features

Steven C. Horii, M.D., Howard N. Horii, R.A., F.A.I.A., Seong Ki Mun, Ph.D.,
Harold R. Benson, and Robert K. Zeman, M.D.

Despite the rapid progress made in the electronic design of imaging workstations for medicine, much less effort has gone into the design of environments in which such systems will be used. Based on studies of radiologist film reading sessions, considerable time will be spent working at such viewing systems. If the rooms in which the workstations are placed are not conducive to comfortable work, it will certainly not favor electronic viewing over film reading. In examining existing reading environments, it is also apparent that they are not optimum, even for film. Since some of the problems for film and electronic viewing overlap, such as heat generation (by the alternators, viewboxes, or workstation electronics) and glare from light sources, it should be possible to develop solutions which are applicable to both environments or to rooms which will feature both viewing systems. This paper will discuss some of the approaches to designing environments in which viewing of images is supported by the room architecture and engineering and not degraded by it. To illustrate these points, a design based on the constraint of a real room size and available architectural materials will be developed.

INTRODUCTION

AT THE SPIE MEDICAL IMAGING MEETING last year, we presented a paper which examined ergonomic features of radiology workstations and reading environments.¹ Both prior to and since that time, extensive work has been done on the design of such workstations to better suit the tasks which medical imaging specialists perform, and to make such performance more efficient from human factors and productivity viewpoints.²⁻¹⁰ In particular, analysis of the work patterns of radiologists⁷⁻⁹ have been combined with advances in person-computer interaction (user interfaces) resulting in viewing and reading systems which are far ahead of older approaches.^{6,8,10}

In addition to the workstation itself, we also examined the environment in which such equipment will be used. Unfortunately, aside from the paper by Bart ter Haar Romeny *et al.*,¹¹ little attention has been given in the medical imaging literature to such environmental design. The problem has both architectural and engineering concerns, and requires not inconsiderable use of human factors design principles. We have had the opportunity to work on design of a reading area within the Department. This area will support conventional film as well as PACS workstation reading, and will be used by the Abdominal Imaging Division. As such, a combination of plain film, CT, MRI, and ultrasound cases will be interpreted. This new reading room is a renovation of an existing space, and so is subject to the constraints of existing bearing walls, columns, and major ductwork.

We will examine the design for this space with discussion of the principles employed.

FACTORS IN WORKSPACE DESIGN

There are two excellent books on designing radiology departments,^{12,13} and both discuss some elements of reading room design. Both

From the Department of Radiology, Georgetown University Hospital, Washington, DC; and The Grad Partnership, Newark, NJ.

Copyright © 1989 by the International Society for Optical Engineering. Proc. SPIE 1091:172-178, 1989. Reprinted with permission.

*Online publication 8 April 2003
doi: 10.1007/s10278-002-6013-x*

facility easily accessible to all of these people. Rather, since the radiologists are most dependent on the space, some thought should be given to optimizing the location of the room for access to the areas they need to reach often. In the instance of our reading area, it is located proximate to the CT rooms, the ultrasound laboratory, and the Abdominal Division offices. In fact, it is relatively central to these, with CT across the north corridor, ultrasound to the west side, and the offices south. The MRI facility is located remotely, owing to the usual siting problems of such facilities, but is a short walk and elevator ride away.

In support of the uses of the reading room, we need to consider supporting **services**. Heating, ventilation, and air conditioning (HVAC), electrical power, communications, illumination, and acoustic control are typical factors which we will include with services. All of these will be discussed in more detail in subsequent sections of this paper. While all of these are part of the environment, electrical power requirements and communications systems have less of an immediate impact on bodily comfort than the other listed items. Providing these services for a workspace requires the coordination of several types of designers and contractors. A good architect will work with the client and the client's contractors so that the construction proceeds as smoothly as possible. In our design stage, we have evaluated the services necessary and will be proceeding with additional engineering detail needed for actual construction.

At the base of any workspace design, be it new or renovation, is the **budget** allotted for the project. This may determine what kinds of solutions to problems can be realistically implemented. Again, a good architect serves the client by being able to provide a number of possible solutions to any problem, so that an optimum design can be achieved for any budget level.

TASKS AND ENVIRONMENT

The major task to be supported in a reading room is the interpretation of medical images. However, this consists of a number of smaller tasks. A number of these were described in a very detailed fashion in the paper by Rogers

*et al.*¹⁴ and in a more general fashion by Mun *et al.*¹⁵ Aside from looking at images on alternators or workstations, a large amount of writing is done, results are dictated, and teaching is often incorporated into these processes. This means that facilities to support these activities must be provided, and features of the room should not hinder any task to a significant degree, or preferably not hinder any task at all. Some of these actions have requirements which are contrary to others. For example, image reading is best done with as little ambient light as possible, but some light is needed for writing and for searching through film folders.

The devices which need to be located in the room are also based on the work to be done. Film alternators and workstations are the equipment we have designed for. However, report generation requires some form of dictation system, and consultation requirements force heavy dependence on telephones. Because we have found that telephone use may be quite frequent, it would benefit users if the phones were located on the workstation or alternator tables, or were at least within reach without standing up.

The environment can be thought of as a combination of the physical space or structure, the services provided, and the equipment and people within. In addition to the size and layout of the room we are working with, there are ceiling constraints (fixed ducting) and flooring systems (raised flooring) to be considered. The fixed ducting to some extent affects placement of lighting fixtures. The raised flooring is an advantage in that it allows for very easy re-routing of cables, but does require more maintenance than plain flooring (the supports may get out of alignment, resulting in panels which rock a bit). The floor plan of our existing space with the equipment as located is shown in Figure 2. The changes made to the layout will be to move the existing neuroradiology reading area to a different location (which will probably not involve equipment relocation), moving GI/GU into the room, and relocating the two IMACS workstations for better user access. Figure 3 shows the changes to be made in the walls and alternator locations. Not shown are a number of storage shelves and cabinets to be used to house books, selected films, and other items

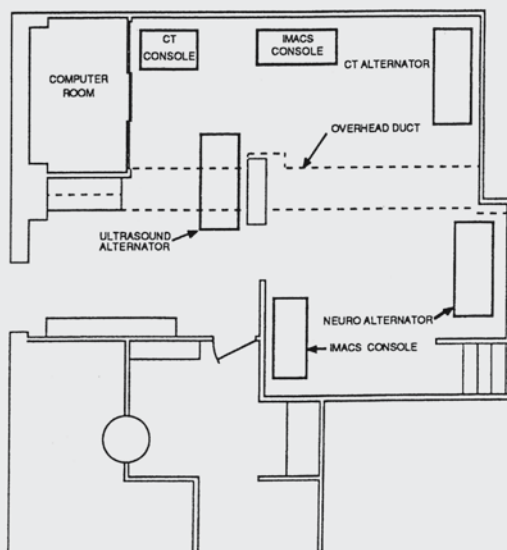


Fig 2. Existing reading room with major equipment.

used by the radiologists. This design is felt to be adequate given that approximately the same number of people will be using the room, and no new equipment is being added. This latter factor means that new electrical power and HVAC changes are not required for the larger reading area. The IMACS workstation (an A T & T CommView EDW4) for ultrasound is in a new location, and its heat load of 8500 BTU/hr (2144 Kcal/hr) will be considered.

Structural requirements may also have to include floor loading and vibration studies, and some local building codes will affect the impact of these issues on any design. Addition of heat sources or expanding a facility for a larger number of people will have to take these into account when considering HVAC requirements.

COMFORT FACTORS

Most important to the users of any given space is how comfortable they will be when

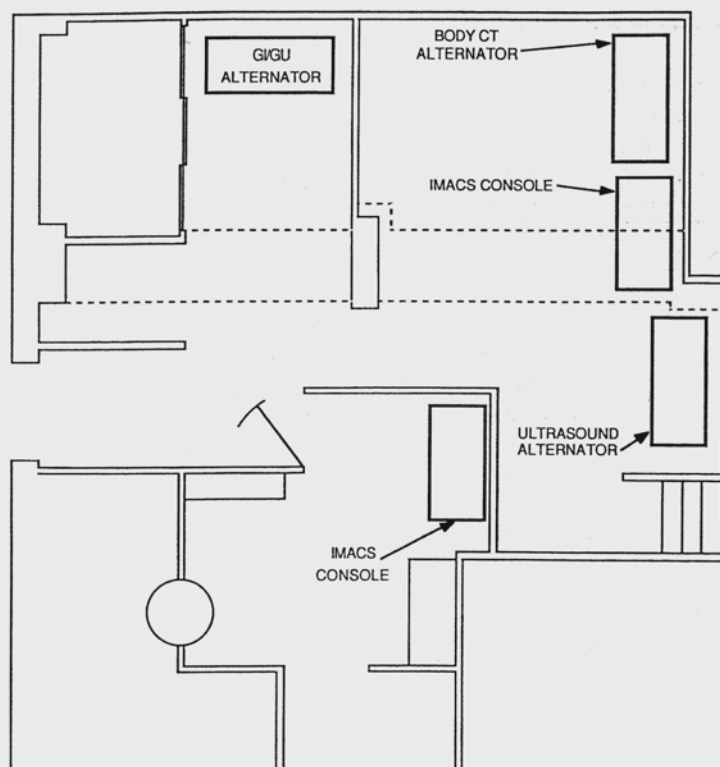


Fig 3. Reading room redesign with equipment placement.

using it. Quite separate from the user interface issues raised by electronic workstations are those things which directly affect comfort. These factors include seating, heat, noise, and light. Though people can operate within wide ranges of these variables, adverse values will impair function either temporarily or permanently (chronic exposure to high noise levels, for example, can do both). In some instances, the degree of impairment may not be noticed by the person working, but various measurements will show distinct performance losses.¹⁶

We have found that reading sessions may last from fractions of an hour to four hours,¹⁷ so that comfortable seating is a must. The "ergonomic" design chair has become quite popular in offices in which video display terminals (VDTs) are used. The major features of these chairs are adjustability, good low back (lumbar) support, arm rests (for keyboard users), and good padding. There are apparently a set of ANSI standards for such chairs, though the authors have not seen them. We have found this type of chair to be acceptable to the radiologists, and are presently in use in some reading rooms and offices.

The HVAC design should, having taken into account the equipment and personnel heat load, maintain the room temperature in a comfortable range. For most people, this range changes with seasons, but is approximately 63-71° F (17.2-21.7° C) in winter, and 65-75° F (18.3-23.9° C) in summer.¹⁸ The relative humidity of the air affects perceived temperature, and the most comfortable range is from about 20 to 60 per cent at 75° F.¹⁹ Electronic equipment is also constrained by temperature and humidity, but will generally operate well in the same ranges as those for which people are comfortable.

Sound is one of the environmental factors which is highly subjective. Most of us know that sounds may be irritating or not depending on the context. A newborn's first cry is probably music to most ears, but a child's cry which wakes one in the middle of the night is hardly so. It is sound quality as well as loudness and context which alter its perception. Noise is thought of as sound which is unwanted. Despite these problems defining noise, most designers think that an office-type workspace has a noise threshold of about 58dBA.²⁰ There are specific

OSHA limits for sound exposures, but these are for sound levels far above what should be encountered in any reading room environment. Standard methods for noise control are in a selection of materials for ceiling, floor, and walls. Acoustical ceiling and carpet are excellent sound absorbers, and matte wall finishes or even acoustic absorption panels on the walls are better than plain gloss or semi-gloss wall treatments.

Lighting is, we feel, one of the most critical issues to be faced in reading room design. This is particularly true for rooms in which CRT displays will be read as their brightness is usually less than that of film on a viewbox. As described previously, the tasks of reading images and writing notes will have opposite lighting requirements in a radiology reading room. Aside from general room illumination and task lights, the image displays themselves (whether CRT or alternator) are a source of additional light. The problem is that the lighting may result in glare from CRT screens or from film, and this may impair reading by reducing contrast sensitivity of the eye or by fatiguing the iris.²¹ The curved screens of CRTs are an additional complication in that they reflect light sources from a wider angle than a flat screen or film. In our reading room at present, most task lighting is stray light from the alternators. All the ceiling lights are usually turned off. This poses some problem for the IMACS workstation as some illumination is needed to see the keyboard and control panel.

Glare is a problem for at least two reasons. The first is that the glare light will cause the pupil to constrict more than it would if there were no glare. This results in less of the information illumination getting to the retina. Secondly, the glare source can result in veiling glare within the eye itself. This results from the scattering of light by the vitreous portion of the eye, and is increased with extraneous light entering the eye.

Lighting design is often aimed at achieving some brightness on the work surface and is adjusted for the task to be performed. This rarely takes into account the problems posed by glare, but with increasing use of VDTs, some lighting manufacturers are designing systems which control the output light beam. Figure 4 is

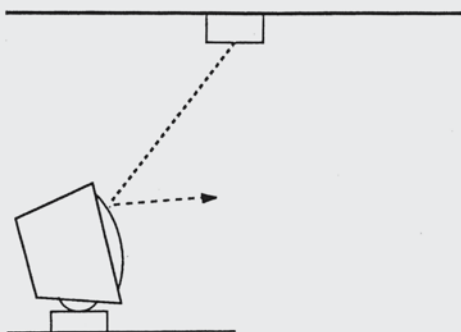


Fig 4. Screen glare from a diffuse luminaire.

a schematic illustration of the glare problem posed by a diffuse light source, and Figure 5 shows how this is reduced by using a directional luminaire (the term for a lamp plus fixture). Tilt and swivel monitors help relieve the glare problem to some degree, but may not be practical for all workstations.

Other methods of reducing the reflection from CRT screens include etching the envelope glass, coating the glass, and placing filters or screens over the tube. Etching the glass reduces specular reflection, but also blurs the image on the phosphor, reducing the apparent spatial resolution. Antireflection coatings work well, but suffer from sensitivity to fingerprints and smudges. Frequent cleaning of such screens is a must. Filters work by attenuating the light reflected off the tube more than the light coming from the tube, since the reflected light passes through the filter twice. Filters themselves are subject to reflection from their surfaces. Screens

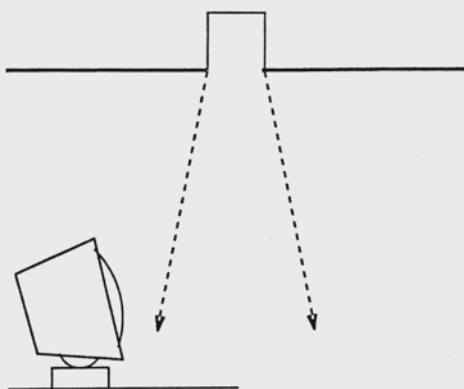


Fig 5. Reducing glare with a directional luminaire.

act as collimators, but are subject to collecting dirt. For high-resolution displays, the mesh of the screen may be visible. The monitors in our workstations all use antireflection coatings.

One consistent problem we have seen in reading room design is in the placement of viewboxes and alternators. Placement on opposing walls with the reading surfaces facing each other should be avoided if at all possible. Even placement on orthogonal walls can result in glare problems for anyone not viewing normal to the illuminator surface. Unfortunately, even some texts²² violate this principle in example designs. This is not a problem if the two sets of viewboxes or alternators are never used simultaneously, for the unused one is simply turned off.

We have given a great deal of attention to the lighting problem. The overhead ambient lighting plan uses a luminaire design (Lithonia Optimax) which has been widely used in VDT-intensive offices. A number of lighting manufacturers are now addressing this problem, so that architects have a choice of vendors. Overhead lighting on dimmers can further control brightness. Local fire codes may restrict very low illumination levels, and some consideration must be given to special lighting for exits in this regard. Also, good solutions for task lighting at a workstation are difficult to find. One problem is that some task lighting, when bright enough to read or write by, illuminates a user's face or clothing enough for them to become a glare source.

Figure 6 shows the existing reflected ceiling plan and light sources. Figure 7 puts this together with the equipment in the room. None of the ceiling lights is directional, and this is a major reason for turning them all off during reading sessions. Figure 8 shows the proposed reflected ceiling plan using the highly directional luminaires. We would provide separate switch/dimmer controls for the luminaires nearest the equipment so that their brightness could be individually adjusted.

CONCLUSION

We have tried to provide an outline of room design based on conventional architectural principles applied to the problems posed by

130

STEVEN C. HORII ET AL

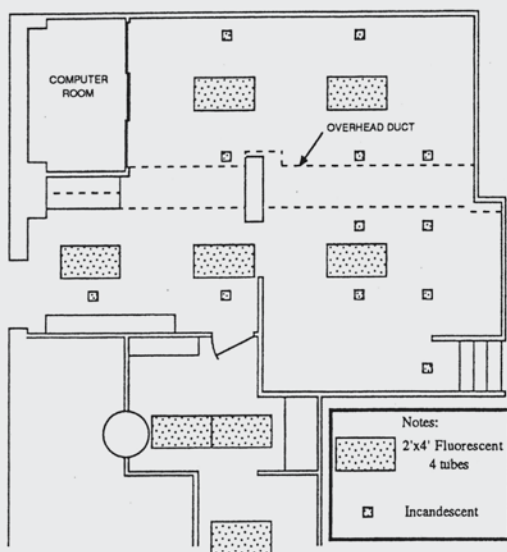


Fig 6. Existing reflected ceiling plan.

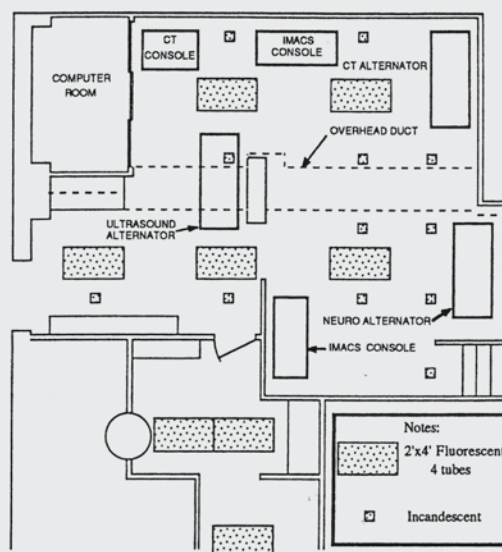


Fig 7. Existing reflected ceiling plan and major equipment.

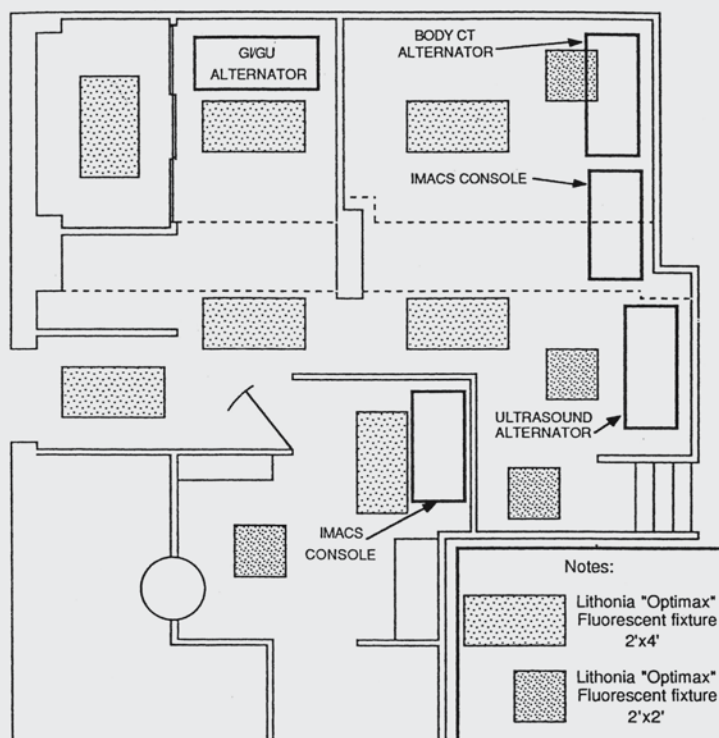


Fig 8. Proposed reading room design.

electronic image displays. In addition to the usual concerns about the equipment (powering it, cooling it, and paying for it) the most successful environments for the equipment will be those in which human factors have been given equal or more consideration than equipment requirements alone.

REFERENCES

1. Horii SC, Horii HN, Kowalski P: An eclectic look at viewing station design. Proc. SPIE v. 914, Medical Imaging II, pp 920-928, 1988
2. McNeill KM, Fisher III HD: A model for radiologic workstation user interface design. Proc. SPIE v. 767, Medical Imaging I, pp 713-716, 1987
3. Taira RK: Operational characteristics of pediatric radiology image display stations. Proc. SPIE v. 767, Medical Imaging I, pp 571-576, 1987
4. Schuttenbeld HHW, ter Haar Romeny BM: Design of a user interface for a PACS viewing station. Proc. SPIE v. 767, Medical Imaging I, pp 844-848, 1987
5. Beard D, Pizer SM, Rogers D, Cromartie R, Desirazu S, Ramanathan S, Rubin R: A prototype single-screen PACS console development using human computer interaction techniques. Proc. SPIE v. 767, Medical Imaging I, pp 646-653, 1987
6. Fuchs H, Pizer SM, Creasy JL, Renner JB, Rosenman JG: Interactive, richly cued shaded display of multiple 3D objects in medical images. Proc. SPIE v. 914, Medical Imaging II, pp 842-849, 1988
7. McNeill KM, Seeley GW, Maloney K, Fajardo L, Kozik M: Comparison of digital workstation and conventional reading for evaluation of user interfaces in radiology. Proc. SPIE v. 914, Medical Imaging II, pp 872-876, 1988
8. Beard D, Creasy JL, Symon J, Cromartie R: Experiment comparing film and the FilmPlane radiology workstation. Proc. SPIE v. 914, Medical Imaging II, pp 933-937, 1988
9. Good BC, Cooperstein LA, Gur D: Radiologists' perceptions of and preferences for a concise history form during radiologic interpretation. Proc. SPIE v. 914, Medical Imaging II, pp 970-975, 1988
10. Ratib O, Huang HK: Integration of a desktop image analysis work station based on a Macintosh II computer in a clinical PACS. Scientific Exhibit # 915, RSNA 74th Sci. Assy. and Ann. Meeting, Chicago, IL, 1988.
11. ter Haar Romeny BM, Raymakers J, van Waes JC, Helder JC, de Graaf CN, van Rijk PP, Schuttenbeld H, Zuiderveld KJ, Tiemann J, Scharnberg B: The Dutch PACS project: philosophy, design of a digital reading room and first observations in the Utrecht University Hospital in the Netherlands. Proc. SPIE v. 767, Medical Imaging, pp 787-792, 1987
12. Fischer HW: Radiology Departments: Planning, Operation, and Management. Edwards Brothers, Inc., Ann Arbor, MI, 1982
13. Scott WG (1966) Planning Guide for Radiologic Installations, Second Edition. Williams and Wilkins, Baltimore, MD
14. Rogers DC, Johnston RE, Brenton BC, Staab EV, Thompson BG, Perry JR: Predicting PACS console requirements from radiologists' reading habits. Proc. SPIE v. 536, Medicine XIII/PACS III, pp 88-96, 1985
15. Mun SK, Benson H, Welsh C, Elliott LP, Davros W: Baseline study of radiology services for the purpose of PACS evaluation. Proc. SPIE v. 914, Medical Imaging II, pp 978-987, 1988
16. Sanders MS, McCormick EJ: Human Factors in Engineering and Design, Sixth Edition. McGraw-Hill, Inc., New York, NY, 1987
17. Mun SK, et al.: *op. cit.*, p 985
18. Diffrient N, Tilley AR, Harman D: Humanscale 1/2/3, 4/5/6, and 7/8/9. M.I.T. Press, Cambridge, MA, 1981
19. Sanders MS, McCormick: *op. cit.*, p 432
20. Diffrient N, Tilley AR, Harman D: *op. cit.*, 4/5/6 p 13
21. Sanders MS, McCormick: *op. cit.*, pp 414-415
22. Tuddenham WJ: Rooms for Film Processing and Display, in: Scott WG, *op. cit.*, p 79

6 Contrast Agents

- | | | |
|-----|---|-----|
| 6.1 | Contrast agent design. Some aspects on the synthesis of water-soluble contrast agents of low osmolality.
<i>Journal of Theoretical Biology</i> 24 (1969): 216–226
<i>T. Almén</i> | 391 |
| 6.2 | Development of nonionic contrast media.
<i>Investigative Radiology</i> 20 (1985): S2–S9
<i>T. Almén</i> | 403 |
| 6.3 | Intravenous chelated gadolinium as a contrast agent in NMR imaging of cerebral tumours.
<i>Lancet i</i> (1984): 484–486
<i>D.H. Carr, J. Brown, G.M. Bydder, H.-J. Weinmann, U. Speck, D.J. Thomas, I.R. Young</i> | 412 |
| 6.4 | Characteristics of gadolinium-DTPA complex: a potential NMR contrast agent.
<i>Am J Roentgenology</i> 142 (1984): 619–624
<i>H.-J. Weinmann, R.C. Brasch, W.-R. Press, G.E. Wesbey</i> | 416 |
| 6.5 | Contrast-enhanced NMR imaging: animal studies using gadolinium-DTPA complex.
<i>Am J Roentgenology</i> 142 (1984): 625–630
<i>R.C. Brasch, H.-J. Weinmann, G.E. Wesbey</i> | 423 |

Introduction

From the earliest days after the discovery of X-rays, contrast media have been used to investigate the urinary tract [1, 2]. The initial use of bougies and catheters was followed by the injection of radio-opaque material to show the renal tract. For retrograde pyelography, a suspension of bismuth subnitrate was originally used.

The first major advance was made in 1918 when Douglas Cameron of Minnesota recommended the use of sodium and potassium iodide for retrograde pyelography [3]. Following the successful introduction of retrograde pyelography, Alexander von Lichtenberg (Professor of Urology at St. Hedwig's Hospital in Berlin) undertook extensive laboratory work in an attempt to develop intravenous urography, but without any result. In 1923 a team of workers at the Mayo Clinic described the use of intravenous and oral sodium iodide to visualize the urinary tract [4].

In 1925 and 1926, Arthur Binz and Curt Räth (Professors of Chemistry from the Agricultural College in Berlin) synthesized many organic iodine and arsenical preparations based on the pyridine ring in an attempt to produce an improved drug for the treatment of syphilis and other infections. The pyridine ring is a six-pointed ring made up of five carbon atoms and one nitrogen atom. Linkage to this ring greatly detoxified the arsenic and iodine atoms. Binz and Räth synthesized more than 700 of these compounds. One group of these iodinated pyridine compounds was found to be selectively excreted by the liver and kidneys and was therefore called the "Selectans". Some of these synthesized pyridine drugs were sent for clinical evaluation for the treatment of gall bladder and kidney infections.

In 1928, Moses Swick (1900-1985), who was working as a urology intern at Mount Sinai Hospital in New York, was awarded the Libman Scholarship encouraging medical research overseas. He went to work with Professor Leopold Lichtwitz at the Altona Krankenhaus in Hamburg, Germany, where he had some success in the treatment of infections with some of the iodinated Selectan drugs. Since these drugs contained iodine and it occurred to Swick that they might be of value in visualizing the renal tract by X-rays. Swick made radiological, chemical and toxicological studies in laboratory animals and in patients. The initial studies were encouraging and Swick transferred his work to gain access to the large number of patients at the urological department of Professor Alexander von Lichtenberg at St Hedwig's Hospital in Berlin. The first successful human intravenous urograms were produced with (non-ionic) *N*-methyl-5-iodo-2 pyridone (Selectan neutral) but Swick preferred the less toxic, more soluble salt 5-iodo-2-pyridone-*N*-acetate sodium (Uroselectan) which had been patented by Räth in May 1927. This new compound Uroselectan produced excellent quality intravenous urograms with relatively little toxicity. Swick and von Lichtenberg presented the work to the Ninth Congress of the German Urological Society in September 1929. Swick presented the first paper based on the animal work but with several excellent-quality human studies exhibiting various disease processes (e.g., hydronephrosis and horseshoe kidney) Von Lichtenberg and Swick together presented the second paper on the human clinical uses with the paper read by von Lichtenberg. The two papers were published in November 1929 in *Klinische Wochenschrift* [5,6].

Within two years of the introduction of Uroselectan in 1929, Binz and Räth developed two further modifications of the pyridine ring – diodrast (Diodone) and neo-ipax (Uroselectan B, Iodoxy), each molecule containing two iodine atoms. Schering Kahlbaum of Berlin supported Binz and Räth in developing these pyridine agents and they became the world's leading manufacturer of intravascular contrast agents. These compounds were successful and were the standard intravascular and urologic contrast media for 20 years.

A series of changes progressively reduced toxicity. Sodium acetizoate (Urokon, Diaginol) was introduced clinically in 1952 by Mallinckrodt and was the

first tri-iodinated contrast medium [7]. Hoppe and colleagues [8] in 1956 showed that a second acetyl amino- group could be added to the benzene ring at C5 to produce a fully substituted tri-iodinated acid radical and the toxicity was reduced even further. This compound, sodium diatrizoate, was introduced in the mid-1950s as Urografin (Schering AG, Germany), Renografin (Squibb, USA) and Hypaque (Sterling Drug). Sodium diatrizoate and its derivatives became the standard intravascular contrast agents until the development of the lower osmolar and non-ionic agents in the early 1970s.

In 1959 the Norwegian pharmaceutical company Nyegaard & Co. were accused by Schering of infringing their patent on diatrizoate which Nyegaard thought had not been patented in Norway. Following this, Nyegaard tried to synthesize diatrizoate by another route and developed a new fully substituted tri-iodinated benzene ring compound (metrizoate) which they marketed as Isopaque.

Torsten Almén was a Swedish radiologist working at Malmö and he studied the pharmacology of contrast agents [9]. He thought that the very high osmolality of the then conventional contrast media was responsibility for much of their toxicity. He taught himself chemistry and suggested reducing the osmolality of contrast media by substituting the non-radio-opaque cation by a non-ionizing radical such as an amide. His paper on this topic was prepared when he was a Research Fellow in Philadelphia in 1968-9. His thesis, which was theoretical and not supported by clinical research, was rejected by radiological journals, but was eventually published by the *Journal of Theoretical Biology* in 1969 [10], a journal of which most radiologists were not aware.

Almén's ideas were rejected by several leading pharmaceutical manufacturers but Hugo Holterman, the research director of Nyegaard, encouraged his team to attempt synthesis of some of Almén's theoretical molecules.

The research team at Nyegaard & Co. were not fully convinced that Almén's proposal could be implemented; however, they were willing to try the ideas. Almén also made known his ideas as to how these compounds might be constructed to facilitate water solubility, hydrophilicity and to reduce viscosity.

Less than six months were to elapse between the first meeting of Almén and the Nyegaard research group in June 1968 and the production of the first compound [11]. The team produced 80 different compounds. In November 1969, after biological and pharmacological testing, compound 16 (called "Sweet Sixteen") was shown to be the most promising and it was marketed as Amipaque (the first low-osmolar contrast medium, LOCM). Amipaque was based on the glucose amide of Isopaque (metrizoate), leading to its generic name, metrizamide. As it contained the glucose radical, metrizamide could not be autoclaved. It was also unstable in solution and therefore it could not be delivered as a pre-packed sterile solution. Because of the complexities of its production, it was expensive and inconvenient to use, being presented as a freeze-dried powder with a diluent. It was, however, a major toxicological improvement on all pre-existing water-soluble myelographic and vascular agents, and in the late 1970s it became the internationally recognized agent for myelography, enabling water-soluble myelography to replace oil (Myodil, Pantopaque) myelography. Although it had an advantageous intravascular profile, metrizamide was generally regarded as too expensive and too inconvenient for vascular studies.

A few years later, in the mid-1970s, metrizamide was replaced by the second-generation LOCM iohexol (Omnipaque) and iopamidol (Niopam), which are easier to synthesize and therefore much less expensive [12]. They do not contain the glucose radical and can therefore be autoclaved and they are stable in solution. These two second-generation LOCM were successful and became the agents of choice in spite of their high cost.

Metrizamide revolutionized contrast agents and marked the boundary between conventional ionic high-osmolar media (HOCM) and modern LOCM. As recorded above, iohexol and iopamidol were the first two second-generation non-ionic LOCM agents to be synthesized.

In order to further reduce the osmolality two molecules of non-ionic monomers have been linked to produce a large non-ionizing molecule containing six atoms of iodine. Such products include Visipaque (iodixanol) and iotrolan (isovist) which are of physiological osmolality at all concentrations [13]. These new agents have additional benefits and are significantly less nephrotoxic [14].

Torsten Almén has reviewed the development of non-ionic contrast media [15]. Development has resulted in agents isotonic with plasma and causing less pain and toxicity. It has been the development of these safe contrast agents that has greatly facilitated the development of modern radiology and interventional radiology in particular.

References

1. Swick, M (1978) Radiographic media in urology, the discovery of excretion urography. *Surgical Clinics of North America* 58: 977-994
2. Grainger RG, Thomas AMK (1999) History of the development of radiological contrast agents (1895-1996). In: Dawson P, Cosgrove DO, Grainger RG. *Textbook of Contrast Media*. Isis, Oxford. Pp3-14
3. Cameron D (1917) Aqueous solutions of potassium & sodium iodides as opaque media in roentgenography. *J American Medical Association* 70: 754-755
4. Osborne ED, Sutherland CG, Scholl AJ Jr, Rowntree LG (1923) Roentgenology of the urinary tract during excretion of sodium iodide. *American Medical Association* 80: 368-373
5. Swick M (1929) Darstellung der Niere und Harnwege in Roentgenbild durch intravenöse Einbringung eines neuen Kontraststoffes: des Uroselectans. *Klinische Wochenschrift* 8: 2087-2089
6. Von Lichtenberg A, Swick M (1929) Klinische Prüfung des Uroselectans. *Klinische Wochenschrift* 8: 2089-2091
7. Wallingford VH (1953) The development of organic iodide compounds as X-ray contrast media. *Journal of American Pharmacological Association (Scientific Edition)* 42: 721-728
8. Hoppe JO, Larsen HA, Coulston FJ (1956) Observations on the toxicity of a new urographic contrast medium, sodium 3,5-diacetamido-2, 4, 6 tri-iodobenzoate (Hypaque sodium) and related compounds. *Journal of Pharmacological and Experimental Therapeutics* 116: 394-403
9. Grainger RG (1982) Intravascular contrast media – the past, the present and the future. *British Journal of Radiology* 55: 1-18
10. Almén T (1969) Contrast agent design. Some aspects on the synthesis of water-soluble contrast agents of low osmolality. *Journal of Theoretical Biology* 24: 216-226
11. Amdam RP, Sogner K (1994) *Wealth of contrasts*. Oslo: Ad Notam Gyldendal
12. Dawson P, Grainger RG, Pitfield J (1983) The new low-osmolar contrast media: a simple guide. *Clinical Radiology* 34: 221-226
13. Dawson P, Saini S, Schild H, Niendorf HP, Schlieff R (1994) Continuing progress in contrast agents. *Imaging* 6: 273-284
14. Aspelin P, Aubry P, Fransson SG, Strasser R, Willenbrock R, Berg KJ (2003) Nephrotoxic effects in high-risk patients undergoing angiography. *New England Journal of Medicine* 348: 491-499
15. Almén T (1985) Development of non-ionic contrast media. *Investigative Radiology* 20: 2-9

MRI Contrast Media

The relaxation time of the protons (hydrogen nuclei) in water molecules is the physical principle that determines the signal intensity in magnetic resonance imaging (MRI) [1].

The possibility that manganese ions could be used for in vivo relaxation enhancement was first suggested in 1978 by Helena Mendonça-Dias, Paul C. Lauterbur and Andrew Rudin [2]. They used manganese and an experimental technique involving ligation of the coronary artery. They showed that the ischemic region was clearly delineated by the relaxation rates and manganese concentrations. However, all of the paramagnetic ions are inherently toxic for clinical use and can be administered only in a chelated form.

Schering AG in Berlin was looking at the topic of MRI contrast agents in 1980. The director of contrast agent research Ulrich Speck asked Hanns-Joachim Weinmann to study paramagnetic compounds in animals at Siemens AG in Erlangen, Germany [3]. The first studies were performed on 19 May 1981. The problem of toxicity was solved by Weinmann and his colleagues in 1981 and they were able to make well-tolerated paramagnetic contrast agents that were based on the metal chelates of manganese or gadolinium [4,5,6]. The first patent was applied for on 24 July 1981. The first commercially developed contrast agent was gadolinium diethylylene triamine penta-acetic acid (Gd-DTPA, gadopentetate) as the dimeglumine salt and was marketed by Schering as Magnevist. This process of chelation results in a rapid renal excretion after administration and removes the toxic effects of the free metal ions. Schering submitted a patent application for Gd-DTPA dimeglumine in July 1981. Weinmann and two associates presented the results of the phase I trials with images from the 0.35T super-conducting Magnetom (Siemens) at the Department of Radiology at the Free University of Berlin at the meeting of the Radiological Society of North America in November 1983. The first clinical trials were made in 1983 at the Free University of Berlin under Professor R. Felix and at the Hammersmith Hospital in London under Professor R. Steiner. In 1984, Dennis H. Carr from the Hammersmith Hospital and Wolfgang Schörner from Berlin published their results [4,7].

Since the late 1980s, Magnevist has been commercially available for clinical use, followed shortly afterwards by Dotarem from Guerbet and ProHance from Bracco. In general clinical practice about 20% of MRI scans require contrast enhancement.

The development of MRI contrast media continues [8]. These new agents may use new principles of contrast enhancement for organ-specific imaging or novel physico-chemical properties to allow the administration of gadolinium at a higher concentration. Blood pool agents are being developed for magnetic resonance angiography. Weinmann surmises that with new molecular biology techniques, tumor-specific agents may become a reality.

References:

1. Weinmann HJ (1999) Gadolinium chelates: physico-chemical properties, formulation and toxicology. In: Dawson P, Cosgrove DO, Grainger RG. *Textbook of Contrast Media*. Isis, Oxford. pp 297-318
2. Lauterbur PC, Mendonça-Dias H, Rudin AM (1978) Augmentation of tissue proton spin-lattice relaxation rates by in vivo addition of paramagnetic ions. in: Dutton PO, Leigh J, Scarpa A (eds). *Frontiers of Biological Energetics*. New York: Academic Press pp 752-759
3. Haën C (2001) Conception of the first magnetic resonance imaging contrast agents: a brief history. *Topics in Magnetic Resonance Imaging* 12: 221-230

4. Carr D, Brown I, Bydder G, Weinmann HJ, Speck U, Thomas DJ, Young IR (1984) Intravenous chelated gadolinium as a contrast agent in NMR imaging of cerebral tumours. *Lancet* i: 484-486
5. Weinmann HJ, Brasch RC, Press WR, Wesby GE (1984) Characteristics of gadolinium-DTPA complex: a potential NMR contrast agent. *AJR* 142: 619-624
6. Brasch RC, Weinmann HJ, Wesbey GE (1984) Contrast-enhanced NMR imaging: animal studies using gadolinium-DTPA complex. *Am J Roentgenology* 142: 625-630
7. Claussen C, Laniado M, Schörner W, et al. (1985) Gadolinium-DTPA in MR imaging of glioblastomas and intracranial metastases. *Am J Neuroradiol* 6: 669-674
8. Weinmann HJ (2003) History of MRI contrast media development, accompanied by Magnevist. 15 years of Magnevist, Satellite Symposium: ECR 2003

6.1 Contrast agent design. Some aspects on the synthesis of water-soluble contrast agents of low osmolality

Torsten Almén (born 1931)

Torsten Almén grew up in Ystad on the most southern coast of Sweden in Skåne. He trained in medicine at the University of Lund in the 1950s and moved to the Department of Diagnostic Imaging at Malmö General Hospital in 1959 and this is where he was to spend most of his working life. He very soon became interested in angiography and observed that patients often suffered short lasting pain when the contrast medium was injected by a pressure injector into the abdominal aorta. Almén wanted to reduce the pain of injection from contrast medium. He recalls being as a boy with his parents at the west coast of Sweden, in Bohuslän and finding swimming in the water not much fun because as soon as he opened his eyes they started to smart. He found that the salty water at Bohuslän drew the fluid out of the mucous membranes of my eyes and made them sore. The brackish water around Ystad did not cause his eyes to smart when he opened them. He reasoned that physiological saline solution in the femoral artery did not draw fluid from the endothelium of the vessel and so did not cause pain, whereas the hypertonic contrast medium in the femoral artery was drawing fluid from the endothelium of the vessel and this caused the pain. Therefore “a plasma-isotonic aqueous solution of contrast medium molecules might not cause pain, and should therefore be created!”

During 1965 and 1966 he made vain attempts to interest a Swedish pharmaceutical company in his idea, but without success. In December 1966 in Malmö he made a dissertation on “An instrument for guiding an angiography catheter” and a few weeks later traveled to the USA to Temple University in Philadelphia and worked closely with a Physiology Department on the effects of contrast medium on the microcirculation.

In 1968 Almén went to Oslo to work with Nyegaard & Co AS and developed the first non-ionic contrast medium Amipaque (metrizamide). He was named as the senior inventor on the patent for Amipaque and he has been co-inventor of several other contrast media patents.

Torsten Almén was awarded the Fernström Great Nordic Prize in 1987 and at the 1989 World Congress of Radiology he was presented with the Antoine Bécélère Prize.

Torsten Almén is currently Professor Emeritus of Diagnostic Radiology at Malmö, Sweden.



J. Theoret. Biol. (1969) **24**, 216–226

Contrast Agent Design

Some Aspects on the Synthesis of Water Soluble Contrast Agents of Low Osmolality

TORSTEN ALMÉN†

*Departments of Physiology and Radiology,
Temple University School of Medicine,
Philadelphia, Pennsylvania 19140, U.S.A.*

(Received 26 August 1968, and in revised form 29 April 1969)

All the modern radiographic contrast agents (diatrizoate, iodamide, iothalamate, metrizoate) for use in studies of the blood vessels (angiography) consist of a benzene ring, in which three hydrogen atoms have been replaced by three firmly-bound iodine atoms. In order to provide high water solubility and low toxicity one of the remaining three hydrogen atoms in the benzene ring has been replaced by a salt-forming carboxyl group while two of them have been replaced by other hydrophilic radicals, each containing a chain of one nitrogen and two to three carbon atoms. A high absorption of X-rays requires high iodine concentration and consequently the angiographic contrast agents are very concentrated solutions with osmolalities in the magnitude of 1500 to 2500 mOsm. For fast injection through narrow catheters, an angiographic contrast agent should have a low viscosity.

Several of the toxic effects of angiographic contrast agents are related to their high osmolality. There is thus a need for a water-soluble contrast agent for which the ratio osmolality/iodine content is lower than for the contrast agents available today. The ratio osmolality/iodine content could be decreased if oligomers or polymers of the modern contrast agents were synthesized. However, measurements of the viscosity of such agents showed that already oligomers had a high viscosity.

A discussion of physico-chemical laws gives the following conclusions. (1) The viscosity of polymeric contrast agents could be kept at a minimum if the axial ratio of the contrast medium molecule is kept as close to one as possible. (2) The synthesis of a non-electrolytic contrast agent, that does not contain any salt-forming radicals, raises the possibility of combining low osmolality with low viscosity in a water soluble contrast agent. A monomer of a non-electrolytic contrast agent could get a lower osmolality than a polymer of an electrolytic contrast agent.

† Associate Professor of Radiology, Temple University School of Medicine, Philadelphia, Pennsylvania 19140. Recent of Radiology, University of Lund, Sweden.

1A. Introduction

The contrast agents, in common use for angiography and intravenous pyelography, have a very low toxicity when this is evaluated as intravenous LD₅₀. The i.v. LD₅₀ for the modern contrast agents (diatrizoate, iothalamate and metrizoate) varies in different species between 10 and 20 g/kg body weight (Hoppe, Duprey, Borisenok & Bird, 1967).

The i.v. LD₅₀ values give no precise information on the local effects of contrast agents when they, in highly concentrated solutions, are selectively

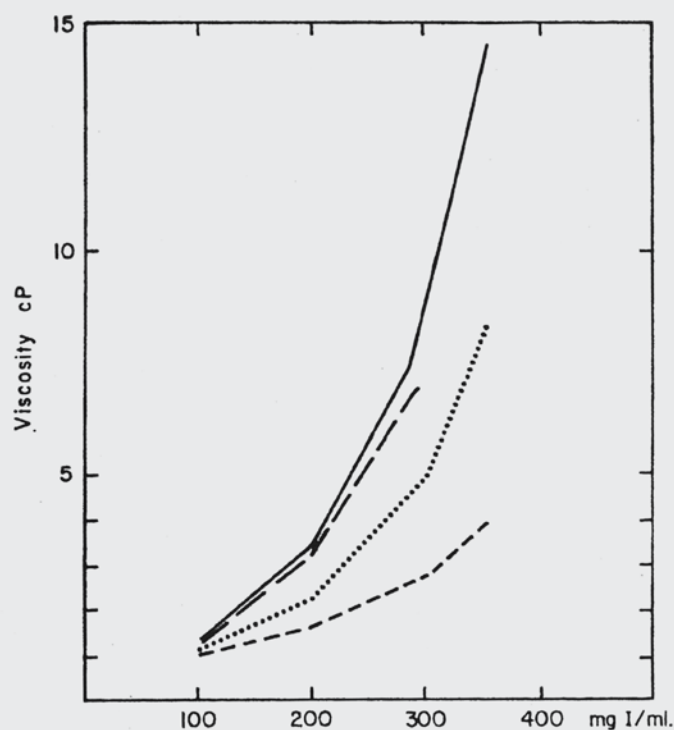


FIG. 1. The absolute viscosities at 37°C of the 2 dimers (MP 2032 and Cholografin) are higher than the absolute viscosities of the monomers (iothalamate and acetrizoate). —, MP 2032 (dimer of iothalamate); — —, adipiodone meglumine salt; ····, iothalamate meglumine salt; — — —, acetrizoate sodium salt.

injected into an artery to an organ during an angiographic examination. The toxic effects in such a target organ will be greater than in the rest of the body which the contrast medium reaches after dilution. Organs examined in arteriography are often damaged by a pathological process prior to the examination, which increases their susceptibility to toxic agents.

The water soluble contrast agents are *hypertonic*, relative to human plasma; and in the most commonly used concentrations for angiography, these contrast agents have an osmolality in the magnitude of 1500 to 2500 mOsm.

It has been shown that hypertonic solutions, among them contrast agents, can change the muscular activity in the small vessels (Margolis *et al.*, 1959; Read, Johnson, Vick & Meyer, 1960; Hilal, 1966; Lindgren, Saltzman & Törnell, 1967; Almén & Wiedeman, 1968*a,b*) and can also cause intravascular agglutination of red cells which results in temporary or permanent occlusion of these vessels (Margolis *et al.*, 1959; Read & Meyer, 1960; Read, Vick & Meyer, 1962; O'Connor, Sitzman & Dealy, 1967; Almén & Wiedeman, 1968*a,b*).

There are thus motives to synthesize water-soluble contrast agents of lower osmolality than those presently available.

Almén (1966) and Hilal (1966) have advocated the synthesis of polymers or dimers of contrast agents as a way of reducing their osmolality.

In angiography, there is often a need for fast injection of large amounts of contrast agents through narrow catheters. Therefore, the viscosity of angiographic contrast agents should not be too high. Accordingly, in an ideal angiographic contrast agent both osmolality and viscosity should be low.

With an Oswald viscometer the absolute viscosities at 37°C of some contrast agents† and their dimers‡ were measured and the high viscosity of the dimers was shown (Fig. 1).

It is the purpose of this presentation to explore theoretically what possibilities there are of making a water-soluble contrast agent of the triiodophenyl type which combines low viscosity with low osmolality and, to the extent it is now possible, to test the validity of the theoretical conclusions.

2A. Discussion

Viscosity is described as a resistance to flow. When a fluid starts to flow through a tube or a vessel, there is a shear stress. The opposing reaction is an internal friction; and the equilibrium, attained when the flow becomes steady, is brought about by the viscosity of the fluid opposing the shearing motion.

As one layer of fluid moves past an adjacent layer, the interaction of molecules at the boundary and the passage of molecules across this boundary in both directions result in the transmission of energy from the faster to the slower fluid layer and, hence, tend to check the relative motion between these layers.

Although a number of empirical and theoretical relationships have been developed between viscosity and other properties of liquids, the fundamental mechanism of transfer of momentum between molecules in a liquid under-

† Urokon (acetrizate) and Conray (iothalamate) from Mallinckrodt, U.S.A.

‡ MP 2032 is an experimental dimer of Conray (iothalamate) from Mallinckrodt, U.S.A. Cholografin (meglumine adipiodone) from Squibb, U.S.A., here regarded as a dimer of acetrizate.

going viscous shear is still unknown. In spite of this, one can discuss what factors at the molecular level of a solute determine the viscosity of the solution according to data available in the literature (Schmidt & Marlies, 1948; Flory, 1953; Jirgensons & Straumanis, 1962).

The viscosity of a solution at a certain temperature is a function of the viscosity of the solvent and the concentration, size, shape and charge of the molecules of the solute.

The angiographic contrast agents are highly concentrated solutions with water as the normal solvent. Their temperature should not exceed body temperature 37°C. Therefore, the problem of combining low osmolality with low viscosity in a macromolecular contrast agent has to be connected to the remaining factors that decide the viscosity of a solution, i.e. the size, shape and charge of the particles or molecules of the solute.

VISCOSITY OF A SOLUTION AND THE SHAPE OF THE SOLUTE

(a) *Linear colloids*

Most natural and artificial polymer molecules are not spherical but are rod-like or flexible chain-like molecules (linear colloids).

There is theoretical (Jirgensons & Straumanis, 1962) and experimental evidence that the viscosity of solutions of linear colloids depends on the axial ratio of the dissolved particles (longest diameter of particle/shortest diameter of particle). The more elongated the particles, the higher the viscosity becomes. The more spherical the particles, the lower the viscosity will be.

Eirich, Margaretha & Bunzl (1936) made uniform suspensions of glass fibers. At equal concentrations, suspensions of shorter fibers had lower viscosity than suspensions of longer fibers.

Doty, McGill & Rice (1958) exposed deoxyribonucleate to ultrasonic waves. The long chain molecules were degraded to shorter segments. A decrease in average molecular weight from 7,400,000 to 700,000 was followed by a decrease in intrinsic viscosity from 69 to 5.3.

Most polymer molecules are rod-like or flexible chain-like molecules and for such polymers, the intrinsic viscosity increases with increasing molecular weight. This relationship between the intrinsic viscosity (η) of a polymer of a given type and its molecular weight M is sometimes expressed by the following equation:

$$(\eta) = kM^a$$

where k is a proportionality constant characteristic of the dispersed phase and the dispersion medium and a depends on the shape of the particles. For rigid rod-like particles, a has a higher value than for flexible chain-like molecules (Flory, 1953; Jirgensons & Straumanis, 1962).

The viscosity of flexible linear polymers is more complex and varies in different solvents. In a 'good' solvent, the long molecules become solvated which prevents them from coiling and keeps them extended. The more extended they are, the higher is the viscosity. In a 'poor' solvent, there is little solvation and the linear polymers form coils, i.e. they become more like spherical particles and the viscosity of the system is lower (Flory, 1953; Jirgensons & Straumanis, 1962; Schmidt & Marlies, 1948).

However, contrast agent solutions must, for enough radiopacity, be highly concentrated solutions which excludes the use of a 'poor' solvent.

(b) *Spherocolloids*

Einstein, on the laws of hydrodynamics, made theoretical calculations on the viscosity of a colloid solution where the solute consisted of rigid spheres. He derived the equation:

$$\eta_{\text{rel}} = 1 + 2.5\phi$$

where η_{rel} means relative viscosity of the solution and ϕ represents the volume fraction occupied by the spheres (Jirgensons & Straumanis, 1962). The particle size does not appear in this equation. The relative viscosity for spherocolloids, according to this equation, is independent of particle size.

Gold sols have almost spherical particles and have low viscosities independent of their particle size (Jirgensons & Straumanis, 1962).

Glycogen molecules are spherical and the low molecular glycogens (mol. wt 20,000) have the same reduced viscosities as the high molecular ones (mol. wt 1,500,000) (Huseman, 1941).

3A. Conclusion

The data presented from colloid chemistry, comparing linear colloids and spherocolloids, give the conclusion that, for the purpose of a low viscosity, the molecules of a polymeric contrast agent should be spherical; if this is not possible, the axial ratio of the molecules should be as close to one as possible.

In order to test the validity of this conclusion the following investigation was designed.

1B. Introduction

It is the purpose of this investigation to compare the viscosities and micro-circulatory effects of a spherical and a linear polymer, both being polymers of the same monomer.

At present, both spherical and linear contrast agent polymers are not available for comparison. However, glucose polymers are available in two forms, as linear colloids (dextrans) and as spherical colloids (glycogens) (Huseman, 1941). The purpose of this investigation will be to compare equally

concentrated solutions of glucose and its two polymers, dextran and glycogen. Hopefully, this study on glucose polymers might give a hint on the properties of different contrast agent polymers, because in a previous study by Almén & Wiedeman (1968*b*) it was shown that hypertonic solutions of glucose and a contrast agent (metrizoate) had similar effects on the microcirculation following topical application. These effects on the microcirculation could be decreased following the polymerization of these substances.

2B. Materials and Methods

The effects on microcirculation of topical application of glucose, dextrans and glycogens were studied in the wing membrane of adult male bats (myotis). The technique used has previously been described in detail (Wiedeman, 1967; Almén & Wiedeman, 1968*a,b*). Solutions of glucose, dextrans† and glycogens‡ were prepared in concentrations of 10 and 15% with buffered saline as solvent. The effects of these solutions on the blood flow through the capillaries and on the spontaneous contractile activity of lymphatic vessels and veins were scored as earlier described (Almén & Wiedeman, 1968*a,b*) (see Table 1).

Water solutions of glucose, dextrans and glycogens were made in concentrations of 5, 10 and 15% (w/v) for the purpose of viscosity measurements at 37°C in an Oswald viscometer (see Fig. 2). Osmolalities were measured in a Fiske osmometer (freezing point depression).

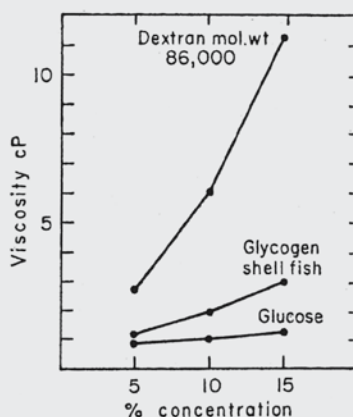


FIG. 2. Effects of shape of molecules on the absolute viscosity at 37°C. In equally concentrated solutions the absolute viscosity of the linear glucose polymer (dextran mol. wt 86,000) is higher than the absolute viscosity of the spherical glucose polymer (glycogen from shellfish). The different polymers have almost the same osmolalities. For 10% dextran, ml. wt 86,000, the osmolality is 13 mOsm., for 10% glycogen from shellfish it is 14 mOsm.

† Manufactured by Manns Research Laboratories (mol. wt average 17,000 and 86,000).

‡ Manufactured by Manns Research Laboratories (Shellfish Glycogen and Rabbit Liver Glycogen).

TABLE 1

Effect on micro-circulation of topical applications of 10 and 15% solutions of glucose and its polymers†

Concentration	Lymphatics	10% Veins	Capillaries	Lymphatics	15% Veins	Capillaries
		775 mOsm			1030 mOsm	
Glucose	++	+	—	++	++	+++
	++	++	+	++	++	+++
	++	++	+	++	++	+++
	++	++	++	++	++	+++
	++	++	++	++	++	+++
	++	++	++	++	++	+++
		440 mOsm			550 mOsm	
Dextran mol. wt 17,000	—	—	—	—	—	—
	—	—	—	+	—	—
	—	—	—	+	—	—
	—	—	—	+	+	—
	—	—	—	++	+	+
	+	+	+	++	++	++
		260 mOsm			270 mOsm	
Dextran mol. wt 86,000	—	—	—	—	—	—
	—	—	—	—	—	—
	—	—	—	—	—	—
	—	—	—	—	—	—
	—	—	—	+	—	+
	—	—	—	+	+	++
		280 mOsm			295 mOsm	
Glycogen Rabbit liver	—	—	—	—	—	—
	—	—	—	—	—	—
	—	—	—	—	—	—
	—	—	—	—	—	—
	—	—	—	—	—	—
	—	—	—	+	—	—
		260 mOsm			270 mOsm	
Glycogen Shellfish	—	—	—	—	—	—
	—	—	—	—	—	—
	—	—	—	—	—	—
	—	—	—	—	—	—
	—	—	—	—	—	—
	—	—	—	—	—	—

Each solution was tested in six different animals. A solution was considered to have produced a response if it affected either spontaneous contractile activity of veins and lymphatic vessels or altered blood flow in any of the vessels, especially capillary nets and adjacent arterioles and venules. The response was marked (+) if spontaneous contractions in some veins or lymphatic vessels were stopped and (++) if spontaneous contractile activity was inhibited in all of the observed veins or lymphatic vessels. The effects on blood flow in capillaries and adjacent small arterioles and venules were scored as follows:

- + Blood flow through the vessels *did not stop*, but the flow speed of red cells was subjectively evaluated to be less than half their original speed.
- ++ Blood flow *stopped in some* of the vessels under observation.
- +++ Blood flow *stopped in all* the observed vessels.

3B. Results

EFFECTS OF GLUCOSE AND ITS POLYMERS ON MICROCIRCULATION

The effects on the microcirculation following the topical application of 10 and 15% solutions of glucose and its polymers were in each experiment evaluated after an application time of five minutes. The results of each individual experiment are given in Table 1. The results show that following polymerization of glucose to linear colloids (dextrans) or spherical colloids (glycogens) there is a decrease in the osmolality of equally concentrated solutions of these substances. The decrease in osmolality is accompanied by reduced or eliminated effects both on blood flow through the capillaries and on spontaneous contractile activity of veins and lymphatic vessels (Table 1).

VISCOSITY

The viscosity measurements show that the glucose polymers (dextrans, glycogens) have higher absolute viscosities at 37°C than glucose when these substances are compared in equally concentrated solutions. At equal osmolality and concentration the absolute viscosity was higher for the linear colloid, dextran, than for the spherocolloid, glycogen. A 10% water solution of glycogen from shellfish had an osmolality of 14 mOsm and an absolute viscosity of 1.7 cP at 37°C. A 10% water solution of dextran mol. wt 86,000 had approximately the same osmolality (13 mOsm) as the shellfish glycogen but a much higher viscosity 6.0 cP. At 15% concentration the difference in absolute viscosity was still higher; shellfish glycogen then had an absolute viscosity of 2.8 cP and dextran mol. wt 86,000 had an absolute viscosity of 11.3 cP.

4B. Discussion

The present investigation has shown that: (1) several of the irritating effects on the microcirculation from topical application of concentrated solutions of glucose can be decreased by polymerizing the glucose; (2) these reduced effects on the microcirculation can be accomplished both by spherical polymers of glucose, glycogens and by linear polymers of glucose, dextrans. (3) The spherical polymers of glucose have lower absolute viscosity than the linear polymers of glucose when compared at equal concentration and osmolality (dextran mol. wt 86,000 and glycogen from shellfish). As an analogy to glucose and its spherical and linear polymers it is suggested that eventual polymers of contrast agents should be spherocolloids in order to get a low viscosity.

Efforts to synthesize spherical contrast agent oligomers or polymers will probably result in contrast agent molecules which have a shape that to some

extent deviates from an ideal sphere. This means that, depending on the axial ratio of such molecules, the viscosity of such contrast agents will to some extent increase with increasing molecular weight (increasing degree of polymerization) according to the equation ($[\eta] = kM^a$). To reduce viscosity the contrast agent molecules would have to be small; to decrease osmolality the contrast agent molecules should be large. Through the synthesis of non-electrolytic contrast agents there is a possibility to reduce the osmolality of contrast agents without increasing their molecular size.

All the modern angiographic contrast media (diatrizoate, iodamide, iothalamate, metrizoate) have three iodine atoms firmly bound to a benzene ring. In order to provide high water solubility and low toxicity these contrast agents possess per benzene ring one carboxyl group and two other hydrophilic radicals containing a chain of one nitrogen and two to three carbon atoms.

All these contrast agents are salts of sodium, calcium, magnesium and methylglucamine in different proportions. In water solutions these contrast agents are almost completely dissociated and each contrast medium molecule forms one anion and one cation. Only the anions contain the iodine atoms which are responsible for the radiologic information that is obtained from the use of contrast agents.

The cations carry no such information but are responsible for 50% of the osmolality of the contrast agents.

In view of the need for a reduction in the osmolality of the contrast agents (Margolis *et al.*, 1959; Read *et al.*, 1960; Read & Meyer, 1960; Hilal, 1966; Lindgren *et al.*, 1967; Almén & Wiedeman, 1968a,b), it is apparent that cations not carrying information should be eliminated. This could be achieved in two ways:

- (1) by the synthesis of non-electrolytic contrast agents, which eliminates the ions;
- (2) by the synthesis of contrast agents where both anions and cations contain iodinated benzene rings and carry information.

This would result in a 50% decrease in osmolality of the contrast agents without any polymerization. If a polymerization of three-iodinated benzene rings is chosen as a way of obtaining a contrast medium of low osmolality and the water solubility of the polymer is maintained through the use of one salt-forming carboxyl group per benzene ring, the polymerization of the anions cannot reduce the osmolality with more than 50% (Fig. 3). Furthermore, this 50% reduction in osmolality can only be reached at a high degree of polymerization (high molecular weight) with all the viscosity problems this implies.

CONTRAST AGENT DESIGN

225

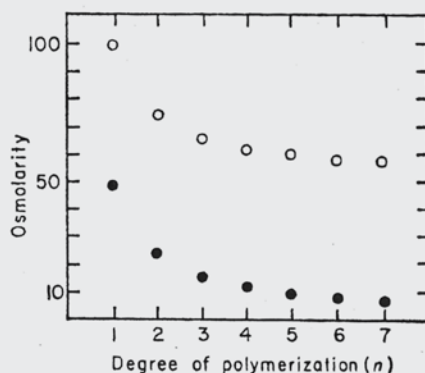


FIG. 3. The theoretical reduction in osmolarity following increased degree of polymerization (n) of electrolytic (○) and non-electrolytic (●) monomers. Each monomer contains a tri-iodinated benzene ring.

The osmolarity of a certain amount of a conventional contrast agent (metrizoate, diatrizoate, iothalamate) has been given the arbitrary number of 100. Increasing degree of polymerization (n) of an iodine equivalent amount of tri-iodinated electrolytic monomers will decrease the osmolarity towards an asymptote at value 50.

Increasing degree of polymerization (n) of an iodine equivalent amount of a non-electrolytic monomer (●) will decrease the osmolarity towards an asymptote at value zero.

The theoretical calculations were made as follows: A dimer ($n = 2$) of a conventional electrolytic contrast agent (MP 2032 a dimer of iothalamate) has two carboxyl groups per molecule. Such a molecule is in a water solution dissociated into two cations and one anion. Thus, each molecule forms three particles in a water solution.

Two molecules of a conventional contrast agent contain the same amount of iodine as the dimer described above. These two molecules form in water solution two anions and two cations. Thus, four particles are formed in a water solution. Thus, the relation between the osmolarities of iodine equivalent amounts of a salt-forming dimer and a conventional contrast agent becomes $3/4$ or $75/100$.

However, one molecule of a non-electrolytic dimer ($n = 2$) forms only one particle in a water solution but contains the same amount of iodine as two molecules of conventional contrast agents, which dissociate into four particles in a water solution. Thus, the relation between the osmolarities of a dimer of a non-electrolytic contrast agent and an iodine equivalent amount of a conventional contrast agent becomes $1/4$ or $25/100$.

Similar calculations are made for higher degrees of polymerization and result in the values given in Fig. 3.

○, Ionic solution (one ion-forming radical per monomer); ●, molecular solution.

However, a 50% decrease in osmolarity can be achieved without any polymerization; it can be achieved by the synthesis of non-electrolytic contrast agents, in which the carboxyl group has been exchanged to a non-electrolytic hydrophilic radical. By polymerization of such non-electrolytic contrast agents the osmolarity could be further reduced (Fig. 3). A dimer of a non-electrolytic contrast agent would be 75% lower in osmolarity than an iodine equivalent amount of a conventional contrast agent (Fig. 3).

5B. Conclusions

An ideal water soluble contrast agent for angiography should have low osmolarity and low viscosity. In order to combine these properties the following approach is suggested:

(1) The synthesis of non-electrolytic contrast agents gives a 50% reduction in osmolarity of the contrast agents.

(2) The synthesis of small polymers (oligomers) of such non-electrolytic contrast agents could further reduce the osmolarity.

(3) The axial ratio of these oligomers should be as close to one as possible, the goal being a spherical molecule.

This work was supported in part by U.S. Public Health Service Grants, NIH, HE 08886 and HE 02280-12.

REFERENCES

- ALMÉN, T. (1966). *Acta Radiol. (Suppl.)*, **260**, 141.
ALMÉN, T. & WIEDEMAN, M. P. (1968a). *J. Invest. Radiol.* **3**, 151.
ALMÉN, T. & WIEDEMAN, M. P. (1968b). *J. Invest. Radiol.* **3**, 408.
DOTY, P., MCGILL, B. B. & RICE, S. A. (1958). *Proc. natn. Acad. Sci. U.S.A.* **44**, 432.
EIRICH, F., MARGARETHA, H. & BUNZL, M. (1936). *Kolloidzeitschrift*, **75**, 20.
FLORY, P. J. (1953). "Principles of Polymer Chemistry". Ithaca: Cornell University Press.
HILAL, S. K. (1966). *Radiology*, **86**, 615.
HOPPE, J. O., DUPREY, L. P., BORISENOK, W. A. & BIRD, J. G. (1967). *Angiology*, **18**, 257.
HUSEMAN, E. (1941). *J. prakt. Chem.* **158**, 167.
JIRGENSONS, B. & STRAUMANIS, M. E. (1962). "A Short Textbook of Colloid Chemistry", 2nd ed. New York: The Macmillan Company.
LINDGREN, P., SALTZMAN, G. F. & TÖRNELL, G. (1967). *Acta Radiol. (Suppl.)*, **270**, 44.
MARGOLIS, G., GRIFFIN, A. T., KENAN, P. D., TINDALL, G. T., RIGGINS, R. & FORT, L. (1959). *J. Neurosurg.* **16**, 390.
O'CONNOR, J. F., SITZMAN, S. B. & DEALY, J. B. (1967). *Radiology*, **89**, 20.
READ, R. C. & MEYER, M. (1960). *Surg. Forum*, **10**, 472.
READ, R. C., JOHNSON, J. A., VICK, J. A. & MEYER, M. W. (1960). *Circulation Res.* **8**, 538.
READ, R. C., VICK, J. & MEYER, M. (1962). *Fedn Proc. Fedn Am. Socs. exp. Biol.* **21**, 104.
SCHMIDT, A. X. & MARLIES, C. A. (1948). "High Polymer Principles and Practice". New York: McGraw-Hill.
WIEDEMAN, M. P. (1967). In "In vivo Techniques in Histology" (G. H. Bourne, ed.). Baltimore: The Williams and Wilkins Company.

6.2 Development of nonionic contrast media

Torsten Almén (born 1931)

see Chapter 6.1 on page 391

Development of Nonionic Contrast Media

TORSTEN ALMÉN, MD

In this brief history, the author reviews the observations that led to his developing a nonionic contrast medium. Current knowledge suggested that if a water-soluble medium could be made isotonic to human plasma, it would cause less pain and toxicity than the ionic media then in use. The principles and design of such a medium are discussed, as well as the subsequent chemical development and testing in animal models of first generation (metrizamide) and second generation (iohexol) nonionic media. Iohexol, which is described as a nonionic, monomeric ratio 3 contrast medium, was selected for clinical testing from among competing substances due to its low toxicity in a number of animal models. The results from these experimental models predicted that iohexol would cause fewer and less severe adverse reactions in clinical use than ionic ratio 1.5 media.

Key words: iohexol, metrizamide, nonionic contrast media.

ABOUT 20 years ago, my colleague Göran Nylander, MD, taught me how to do angiographies in dogs. In those days, we could only perform angiographies in animals at night, when there were no patients in the angiography laboratories. When we injected contrast media into the hepatic arteries of dogs, we could not visualize the hepatic veins. The contrast media were hypertonic solutions of ionic ratio 1.5 media such as diatrizoate (Renografin®, E. R. Squibb and Sons, Princeton, NJ; Hypaque®, Winthrop-Breon Laboratories, New York, NY), iothalamate (Conray®, Mallinckrodt, Inc., St. Louis, MO), and metrizoate (Isopaque®, Winthrop-Breon Laboratories, New York, NY) (Figs. 1 and 2).

We began to speculate about the lack of visualization of the hepatic veins. These discussions were the beginning of the effort that, many years later, yielded the first nonionic medium. We asked each other: Did the small contrast medium molecules diffuse through the capillary walls so that they reached the hepatic veins at a concentration that was too low to provide visualization? Would it then be better to synthesize large contrast medium molecules? For example, would polymers of the ratio 1.5 media remain in the vessel lumen and, therefore, reach the hepatic veins at a concentration high enough for their visualization? Perhaps hypertonic contrast medium solution drew water into the vessel lumen, thereby diluting the contrast medium. Would

a contrast medium solution isotonic to plasma become less diluted and produce better venous visualization?

These speculations inspired my study of textbooks on colloid, polymer, and organic chemistry. I was doing daily angiographies in patients then and frequently observed how painful the injections of hypertonic contrast media could be for these patients. These contrast media had an osmolality about five times higher than that of human serum.

It was known, however, that the contrast medium, thorium dioxide, a suspension almost isotonic to serum, did not produce pain when used for arteriography. Upon reading a 1930 Japanese study by Saito et al,¹ I learned that these investigators had prepared an emulsion of iodized oil, which was isotonic to serum and did not produce pain when used for carotid arteriography. Since contrast media suspensions or emulsions that were almost isotonic to serum did not produce pain in arteriography, I believed that there was a fair chance that water-soluble contrast media would not produce pain in arteriography if they, too, could be made almost isotonic to serum.²

Early History of Nonionics

The main reason for trying to develop such a contrast medium was to eliminate pain due to the contrast medium used in arteriography. There was also reason to believe that such isotonic contrast media might produce fewer adverse effects than hypertonic solutions. First, it was known that hypertonic solutions produced vasodilatation,³ which meant that they might cause a decrease in arterial pressure. Second, hypertonic solutions were believed to produce red blood cell aggregates, which were thought to block the pulmonary capillaries.⁴ (This mechanism was believed to be involved in deaths due to angiocardiology in patients with pulmonary hypertension.^{5,6})

It thus appeared as if water-soluble contrast media in isotonic solutions would produce less pain in arteriography and also would be less toxic than the hypertonic contrast media (ratio 1.5 media) commonly used. With these goals in mind, I devoted some years to the study and design of such isotonic water-soluble media and worked to obtain support for their development through research grants or company investment.

From the Department of Diagnostic Radiology, Malmö General Hospital, Malmö, Sweden.

Reprint requests: Torsten Almén, MD, Department of Diagnostic Radiology, Malmö General Hospital, 21401 Malmö, Sweden.

No. 1

NONIONIC CONTRAST MEDIA DEVELOPMENT

Almén

S3

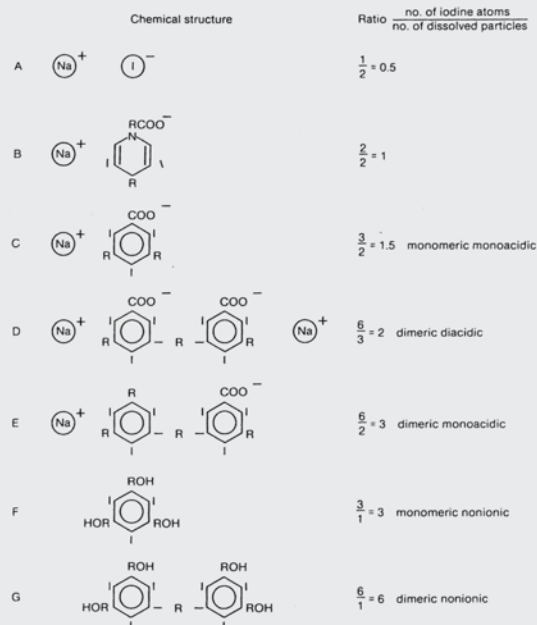


Fig. 1. Schematic illustration of the development of contrast media from ratio 0.5 to ratio 6.0. "R" means unspecified chemical structure.

In the 1960s, all the water-soluble contrast media commonly used for angiography were salts of iodinated benzoic acid derivatives. They were administered intravascularly as solutions highly hypertonic to human plasma. When these contrast media dissolved in water, each of their molecules dissociated into a cation and an accompanying anion that contained three iodine atoms bound to a benzene ring; thus, for every three iodine atoms in a water solution, there would be two particles in the solution—one cation and one anion (Figs. 1C and 2).

Examples of such media are diatrizoate, iodamide (Uromiro®, Bracco, Milan, Italy), ioxithalamate (Vasobrix®, Guerbet, Paris, France), iothalamate, and metrizoate. Today, they are still in common use for angiography. They are described as ionic, monomeric three-iodinated ratio 1.5 media, because the ratio between the number of iodine atoms and the number of particles in an ideal solution is 1.5 (Figs. 1C and 2).

The process of designing a water-soluble contrast medium isotonic to serum, or at least one with lower osmotic effects than those of the ratio 1.5 media, involved a number of speculations. To achieve these goals, I needed to design media with a ratio higher than 1.5; compared with the ratio 1.5 media, I needed to increase the number of iodine atoms per number of particles in water solution, or decrease the number of particles per number of iodine atoms. It would have been possible, for instance, to synthesize ionic media in

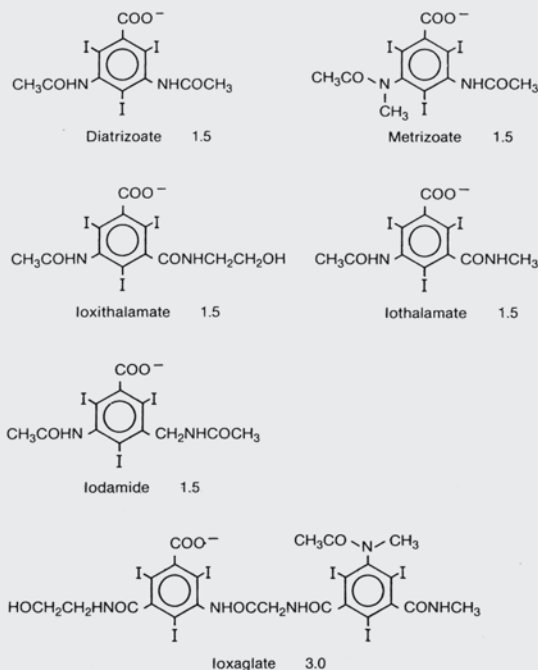


Fig. 2. Chemical structures of the anions of some urographic and angiographic ionic contrast media. Diatrizoate, metrizoate, ioxithalamate, iothalamate, and iodamide are described as monomeric monoacidic ratio 1.5 media, or as ionic ratio 1.5 media. Ioxaglate is described as dimeric monoacidic ratio 3.0 medium, or as ionic ratio 3.0 medium.

which both the anion and the cation each contained three iodine atoms. I intuitively thought that such media might be highly toxic, however. Another possibility was to synthesize media that contained dimers (Fig. 1D), trimers, or polymers of the anions of the three-iodinated media. With increasing degrees of polymerization, the ratio of such media approaches the value 3. This meant that the osmotic effects would have been reduced by 50%, but this also would have been a large molecule with viscosity too high for arteriography. This approach was therefore discarded.

The next approach I considered was to try to avoid using the cations of the ionic media, because these cations do not contain any iodine. They give no diagnostic information, but they are responsible for 50% of the osmotic effects of the media. The noniodinated cations could be avoided by synthesizing nonionic media, which might be made sufficiently water soluble by including a large number of hydrophilic hydroxyl groups in the contrast medium molecules (Fig. 1F). If dimers (Fig. 1G) or trimers of such media could be synthesized, it would be possible, theoretically, to get contrast media that were isotonic to human serum at concentrations used in angiography.

From 1965 until 1967, I tried unsuccessfully to interest

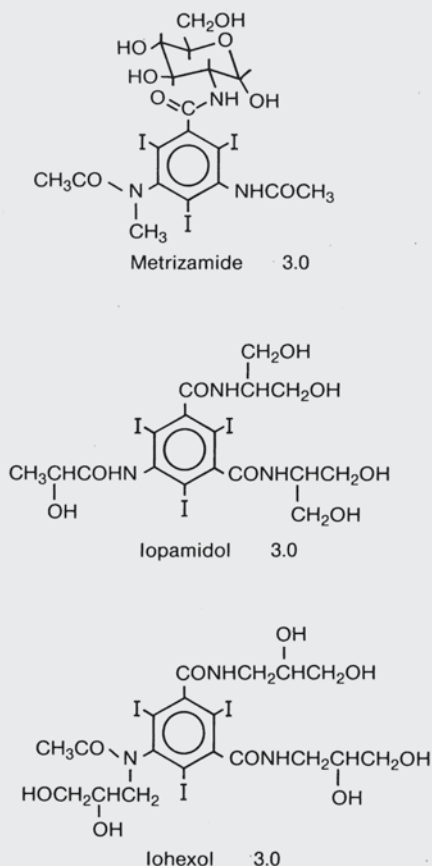


Fig. 3. Chemical structures of some urographic, angiographic and myelographic contrast media. Metrizamide, iopamidol and iohexol are described as monomeric nonionic ratio 3.0 media, or as nonionic ratio 3.0 media.

both Swedish and American companies in the synthesis of water-soluble contrast media isotonic to serum. In March 1968, I visited Miami, Florida, for a congress on lymphangiography and, on impulse, I quickly jotted down some chemical structures and had them notarized.

On returning to my work in the Department of Physiology at Temple University, Philadelphia, I found a letter from Dr. Hugo Holtermann, head of research at the pharmaceutical company Nyegaard & Co. in Oslo, Norway. Dr. Holtermann was going to visit the American pharmaceutical company, Winthrop Laboratories, in New York in April and asked if I would meet him. During our meeting in New York, he suggested that I fly to Norway to discuss my ideas on low-osmotic contrast media, and in June 1968 I met with the research staff of Nyegaard in Oslo.

There was general agreement about the need for a low-osmotic contrast medium, a medium with lower osmotic

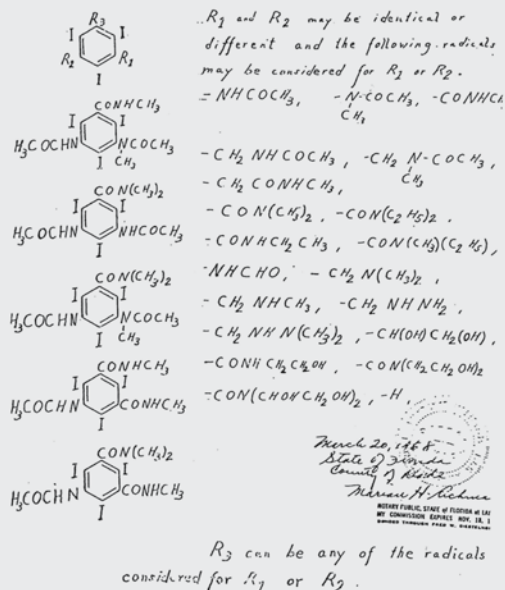


Fig. 4. Some chemical structures signed by the notary public. Use of hydroxyalkylamido groups are suggested as polar groups to confer water solubility to these nonionic contrast media. (Errors are due to hasty writing.)

effects than ionic ratio 1.5 media. Ideally, this medium needed to be isotonic to serum. Dr. Holtermann found the idea of nonionic contrast media very interesting. However, he believed that the chances of obtaining sufficient water solubility were small, because a very large number of hydroxyl groups per molecule probably would be required to reach the desired high water solubility. I then presented several examples of nonionic contrast media that were based on the structure I had notarized (Fig. 4). They contained eight hydroxyl groups per contrast medium molecule. The chemists at Nyegaard thought that an even higher number of hydroxyl groups might be required to obtain enough water solubility.

The chemical building blocks (moieties) that made up the media discussed were not readily available, but one of the company's dedicated chemists, Vegard Nordal, mentioned that the ionic ratio 1.5 medium, acetrizate (Urokon®, Mallinckrodt, Inc, St. Louis, MO) was a methylglucamine salt of acetrizic acid. He suggested that the first attempt to synthesize a nonionic medium should include the following steps: an acid chloride of acetrizic acid should be made. When this reacted with methylglucamine, the expected result would be the methylglucamide of acetrizic acid—a nonionic ratio 3.0 contrast medium. This substance was soon synthesized, and it had approximately the same toxicity as the common ionic ratio 1.5 media. Since the new substance had a very high water solubility, it was decided

that various nonionic compounds would be synthesized in the search for new low-osmotic and low-toxic clinical arteriographic media.

Development of First Generation Nonionics: Metrizamide

The hydroxyalkylamido groups in Fig. 4, as well as some other hydroxyalkylamido groups, were used as polar groups to confer water solubility to a number of experimental nonionic contrast media.^{7,8} As a result of that work, metrizamide (Amipaque®, Nyegaard & Co. AS, Oslo, Norway), the first nonionic water-soluble contrast medium for clinical use, was created under the leadership of Dr. Holtermann. When dissolved in water, metrizamide forms a molecular (nonionic) solution, and each dissolved molecule contains three iodine atoms. Thus, for every three iodine atoms there is only one particle in solution—one complete, nondissociated metrizamide molecule. The ratio of metrizamide in an ideal solution, therefore, becomes 3.0 (Figs. 1F and 3).

The low subarachnoid and acute intravascular toxicity of metrizamide⁹⁻¹¹ made it the first water-soluble contrast medium commonly used in myelography. Experience with metrizamide in angiography has demonstrated that general use of a ratio 3.0 contrast medium would almost eliminate pain in clinical angiography.¹² In spite of this advantageous property, metrizamide is not generally used in clinical angiography due to two of its disadvantages: the high cost of production results in a high price, and reduced stability upon autoclaving in aqueous solutions requires that metrizamide be dispensed as a lyophilized substance that must be dissolved in water before it can be used.

Development of Second Generation Nonionics: Iohexol, Iopamidol

In the years after the development of metrizamide, research of nonionic contrast media focused on developing substances that could be supplied in autoclaved solutions and priced to permit their general use as angiographic, urographic and myelographic contrast media. As a result of these efforts, iopamidol (Niopam®, Bracco, Milan Italy; Isovue®, E. R. Squibb and Sons, Princeton, NJ) and iohexol (Omnipaque®, Nyegaard & Co., AS, Oslo, Norway; Winthrop-Breon Laboratories, New York, NY) were dis-

covered (Felder, Pitre, and Tirone¹³; Holtermann). Like metrizamide, these new media are described as nonionic, monomeric ratio 3.0 contrast media (Figs. 1F and 3).

Iohexol and other similar media have a tendency to deteriorate due to a cyclizing reaction with release of inorganic iodide at the high temperature required for autoclaving (120° C).¹⁴ Below pH 5.5, iohexol tolerates autoclaving without deterioration. Contrast media for angiography should not be used in buffered solutions at pH 5.5, however, because at such low pH they cause greater decrease of aortic pressure¹⁵ than at pH 7.0 to pH 7.5. An elegant solution to this problem was found by Fritjof Rakli.¹⁴ Aliphatic amines are known to have pKa values that decreased about 0.025 units per degree centigrade upon heating. This means that an aqueous buffer of TRIS (2-amino-2[hydroxymethyl]-1,3-propanediol) with a pH of 7.3 at 20° C will decrease to about pH 5 at 120° C. At this pH and temperature, aqueous solutions of iohexol are stable for hours. After autoclaving and when the iohexol solution is cooled, the pH will return to its initial value. At room temperature and neutral pH, the stability of iohexol solution is acceptable.

Another ionic ratio 3.0 contrast medium, ioxaglate (Hexabrix®, Guerbet, Paris, France), was developed by Tilly, Hardouin, and Lautrou.¹⁶ It is intended for angiography and urography but not for myelography; it is described as monoacidic and dimeric (Figs. 1E and 2). The ionic ratio 3.0 medium ioxaglate has a lower acute intravenous toxicity than the ionic ratio 1.5 media (Fig. 2) but a higher acute intravenous toxicity than the nonionic ratio 3.0 media (Fig. 3) according to the data in Table 1.^{17,18}

Basic Characteristics of Iohexol

Like other nonionic media in clinical use, iohexol has both lower molecular toxicity (chemotoxicity) and lower osmototoxicity than the ionic ratio 1.5 media.

To investigate its toxicity, iohexol has been compared with various media in animal experiments. Studies of iohexol in different experimental models have been conducted to gain insight into its toxicity in animals so that clinical advantages and risks can be assessed.

Acute Intravenous Toxicity in Mice

The acute intravenous toxicity in mice of iohexol and some other contrast media is given in Table 1.^{17,18} The intravenous LD₅₀ values of the different ratio 3.0 media (nonionic and ionic) are at least twice as high as those of the ratio 1.5 medium, iothalamate, due to lower osmototoxicity and/or chemotoxicity of the ratio 3.0 media. The intravenous LD₅₀ of iohexol is about 80% higher than that of ioxaglate. This difference in intravenous toxicity must be due to the lower molecular toxicity of iohexol, because ioxaglate has the lower osmolality of the two media.

If arteriographic contrast media were chosen exclusively with regard to their acute intravenous toxicity, then iohexol

TABLE 1. Acute Intravenous LD₅₀ in Mice

Contrast Medium	g l/kg mouse
Iohexol, nonionic ratio 3.0	24.3
Iopamidol, nonionic ratio 3.0	22.1
Metrizamide, nonionic ratio 3.0	18.1
Ioxaglate, ionic ratio 3.0	13.5
Iothalamate, ionic ratio 1.5	7.0

TABLE 2. Median Pressure Increase in Pulmonary Artery After Injection of 3 ml/kg (370 mg I/ml) Into the Right Atrium

Ratio 3.0 medium iohexol	+14%
Ratio 3.0 medium ioxaglate	+21%
Ratio 1.5 medium metrizoate	+46%
Physiologic saline	+10%
Median Pressure Change in Aorta	
Ratio 3.0 medium iohexol	-1%
Ratio 3.0 medium ioxaglate	0%
Ratio 1.5 medium metrizoate	-43%
Physiologic saline	+8%

and iopamidol would be the safest media, according to the findings presented in Table 1.

Histamine Release

Histamine release has been investigated in vitro for several media.¹⁹ At a final concentration of 150 mg I/ml in the incubation mixture, iohexol released about 10% of the maximum amount of histamine available for release from the mast cells of rats. Metrizamide released about 25% and ioxaglate released 100%. Among the compounds compared, iohexol released the smallest amount of histamine.

Effects on Red Blood Cells

The effects of contrast media on red blood cells are an important consideration in angiography because red cells must be bent and deformed in order to pass through the capillaries of the lungs and other organs. These capillaries are smaller in diameter than the erythrocytes.²⁰ The hypertonicity of contrast medium solutions induces a loss of intracellular water from red cells, thereby making them rigid²¹ and reducing their ability to pass through capillaries. It has been shown that ratio 3.0 media (iohexol, metrizamide, and ioxaglate) produce less rigidification of red blood cells than ratio 1.5 media (diatrizoate, metrizoate).^{21,22} Iohexol has been found to have less influence on red blood cell morphology than metrizamide, ioxaglate, and metrizoate.^{19,23}

Effects on Pulmonary Arterial Pressure

Contrast media effects on pulmonary arterial pressure are of interest because several deaths in cardioangiography have occurred in patients with pulmonary hypertension, and an etiologic connection has been assumed.^{5,6} When injected intravenously or into the pulmonary artery, hypertonic solutions such as contrast media can produce increased pulmonary arterial pressure.^{24,25} It has been shown that the ratio 3.0 media (iohexol, metrizamide and ioxaglate), when injected into the right atrium of rabbits, produce less increase in pulmonary arterial pressure than the ratio 1.5 medium, metrizoate (Table 2).^{26,27} The same investigations also showed that the ratio 3.0 media produced less decrease in aortic pressure than the ratio 1.5 medium.

TABLE 3. Increase in Lung Weight of Rats (median values) Following IV Injection of Contrast Medium (6 g I/kg BW)

Nonionic ratio 3.0 medium	iohexol	12%
Nonionic ratio 3.0 medium	iopamidol	51%
Ionic ratio 3.0 medium	ioxaglate	112%
Ionic ratio 1.5 medium	diatrizoate	68%

In animal experiments, the advantages of iohexol over ratio 1.5 media, following intravenous bolus injection and in cardioangiography, are as follows: (1) smaller pressure increases in the pulmonary artery, and (2) smaller pressure decreases in the aorta. These advantages are especially important in patients with signs of obstruction of pulmonary circulation, such as pulmonary hypertension, pulmonary emphysema, pulmonary fibrosis, and cardiac disease.

Pulmonary Edema

Pulmonary edema occurred in 22 patients (16%) in a study of 140 urographic deaths.²⁸ An animal model has been designed in which changes in the wet weight of the lung have been used to measure the degree of edema produced by intravenous injections of various contrast media (Table 3).²⁹⁻³¹

In regard to production of pulmonary edema, the dominant role of the molecular toxicity of the contrast medium is demonstrated by the fact that the ionic ratio 3.0 medium, ioxaglate, produced significantly more pulmonary edema than the ionic ratio 1.5 medium, diatrizoate, in spite of ioxaglate's lower osmolality.

Due to its lower molecular toxicity, iohexol has less tendency to produce pulmonary edema than either the ratio 1.5 media or the ratio 3.0 media, ioxaglate and iopamidol. This should be considered before intravascular injections of contrast medium are given in patients with lung or heart disease.

Effects on Aortic Endothelium

Contrast medium effects on aortic endothelium are of interest because vasoactive substances may be released from damaged endothelial cells. Thrombus formation also may be initiated on damaged endothelial cells. Contrast medium damage to the endothelium of the rat aorta was evaluated by a silver staining method.³² Injury to the endothelium results in staining of subendothelial structures. More damage to the endothelium permits leakage of stain to subendothelial structures through a larger percentage of the endothelium surface (Table 4).

TABLE 4. Extent of Injury of Aortic Endothelium of Rats Following Exposure to Contrast Media (370 mg I/ml; median values)

Ratio 3.0 iohexol	less than 5%
Ratio 3.0 metrizamide	less than 5%
Ratio 3.0 ioxaglate	less than 5%
Ratio 1.5 diatrizoate	about 20%
Ratio 1.5 metrizoate	about 20%

All the ratio 3.0 media (iohexol, metrizamide, and ioxaglate) produced less endothelial damage than the ratio 1.5 media (diatrizoate and metrizoate). Sodium chloride solutions isotonic to the ratio 1.5 media produced the same extent of endothelial injury as the ratio 3.0 media. This indicates that the endothelial damage is more related to molecular toxicity of contrast media than to the osmolality of the contrast media solutions.

Vasodilatory Effects

The vasodilatory effects of contrast media have been investigated in experimental femoral arteriography of dogs.^{33,34} At the same dose (0.2 ml/kg BW, 280 mg/l/ml), the ratio 3.0 contrast media (iohexol, metrizamide, and ioxaglate) produced a 30% to 40% increase in femoral blood flow; the ionic ratio 1.5 medium metrizoate produced a 200% increase.

This means that there should be less risk of hypotension following intravascular injection of ratio 3.0 media than of ratio 1.5 media in clinical arteriography. This should be considered in elderly patients with reduced blood flow in some organs due to vascular obstruction; in such patients, a fall in aortic blood pressure may induce cerebral infarction, cardiac infarction, or renal failure, depending on the organs of vascular obstruction.

Since the ratio 3.0 media produced more vasodilation than an equiosmolal sodium chloride solution, it was concluded that the vasodilatory properties of the ratio 3.0 media are caused both by their molecular toxicity and their osmototoxicity.

Effects of Coronary Arteriography

Contrast media effects on coronary arteriography have been investigated in dogs.³⁵ When injected into the left coronary artery at a dose of 8 ml (370 mg/l/ml), the nonionic ratio 3.0 contrast media, iohexol and metrizamide, produced less decrease in left ventricular contractile force than the ionic ratio 1.5 medium, diatrizoate. At this dose, iohexol produced a mean decrease in contractile force of 15%; metrizamide caused a decrease of 10%; diatrizoate caused a decrease of 44%.

Renal Effects

Effects on renal function due to iohexol have been investigated following nephroangiography in dogs and aortic injection in rats.^{36,37} Ionic ratio 1.5 media produced a significantly higher albuminuria than iohexol. From these animal experiments, it is expected that clinical nephroangiography in man will be followed by less proteinuria if iohexol is used instead of ratio 1.5 media (diatrizoate, iothalamate, metrizoate).

It has been shown that iohexol, like other ratio 3.0 media, produces a smaller osmotic diuresis than the ratio 1.5 medium, diatrizoate.³⁸⁻⁴⁰ Two effects of this mechanism

have been demonstrated in animal experiments: (1) the urine iodine concentration becomes twice as high when iohexol and other ratio 3.0 media are used for urography compared with ratio 1.5 media (diatrizoate, iothalamate, metrizoate); and (2) when ureteric stasis is present, iohexol causes less increase in ureteric pressure than the ratio 1.5 medium, diatrizoate.⁴⁰ These animal experiments predict that when used in clinical urography, iohexol should produce films of high diagnostic quality due to the high iodine concentration in urine. They also suggest that the risk of contrast medium leakage from the renal pelvis to surrounding extrapelvic structures should be small, even when ureteric stasis is present, due to the smaller diuretic effect of iohexol compared with ratio 1.5 media.

It has been shown that iohexol can be used as a marker to determine renal function by glomerular filtration rate (GFR) because it is handled by the kidney like inulin or ⁵¹Cr-EDTA.⁴¹

Central Nervous System Effects

Effects on the central nervous system have been examined after subarachnoid injections of iohexol in nonanesthetized rabbits.⁴² Iohexol had the least effect on animal behavior among the nonionic media compared (iohexol, iopamidol, iogluclide, metrizamide). An investigation of the effects on the blood-brain barrier of iohexol and metrizamide showed significantly less injury by iohexol.⁴³

These animal investigations predict that in clinical use iohexol should be a safe medium both for myelography and for angiographic examination of the central nervous system.

Discussion

The following principles can be said to guide the search for a new contrast medium that causes fewer and/or less severe adverse clinical reactions than previous media: (1) Only one contrast medium effect is desired; to attenuate radiation; (2) All other contrast medium effects are unwanted and may or may not cause clinical symptoms; (3) Many different pathophysiologic mechanisms (toxicity mechanisms) are activated after injections of contrast media. It is therefore an important principle to examine many different toxicity mechanisms in animal experiments before a new contrast medium is selected for clinical trial.

Before a contrast medium is injected into a patient, it is not known which pathophysiologic mechanism, or which combination of mechanisms, happens to be the greatest risk for that patient on that particular occasion. Many contrast medium-induced pathophysiologic mechanisms may play a role. They include: (1) Vasodilation with possible arterial hypotension and cerebral, renal, or cardiac damage from hypotension; (2) Rigidification of red blood cells with possible pulmonary hypertension and cor pulmonale; (3) Endothelial damage with possible thrombosis on damaged

endothelium or release of vasoactive substances from damaged endothelium; (4) Cardiac effects with decreased contractile force, arrhythmias, ventricular fibrillation; (5) Pulmonary edema due to direct effects on pulmonary vessels or via reflexes on pulmonary vascular permeability; (6) Renal failure, sometimes with anuria, due to effects on glomerular membrane permeability, renal vessels, and/or tubular cells; (7) Penetration of blood-brain barrier by contrast medium molecules that reach nerve cells causing seizures or direct effects on the limbic system of the brain; (8) Interaction with various enzymes; (9) Direct cellular effects with release of histamine, serotonin, or other substances causing symptoms of anaphylactoid reaction; (10) Activation of complement system with signs of anaphylactoid reaction; (11) Interaction with antibodies with true anaphylactic shock.

The present review covers a comparison in many experimental models between several nonionic ratio 3.0 media (iohexol, various experimental nonionic media, and metrizamide) and several ionic ratio 1.5 media. The models have covered several toxicity mechanisms supposed to be involved when contrast media cause adverse reactions. No experimental model was found in which iohexol was more toxic than metrizamide or various ionic ratio 1.5 media. In some experimental models, iohexol was less toxic than metrizamide and, in many models, iohexol was less toxic than the ionic ratio 1.5 media. In the effort to identify a contrast medium that may cause fewer, less severe adverse reactions in clinical use, iohexol was not chosen for clinical study from among its competitors because of a single good parameter. It was selected because of its low toxicity in many different experimental models. The importance of using many experimental models that deal with many toxicity mechanisms must be emphasized.

Conclusion

It may be stated that iohexol was selected among other competing substances for clinical study because iohexol had lower toxicity than ionic ratio 1.5 media in many experimental models. From the results of those experiments, it was predicted that iohexol might cause fewer or less serious adverse reactions than ionic ratio 1.5 media when used clinically. Other articles in this symposium dealing with clinical trials of iohexol will show to what extent these predictions from animal experiments have been correct.

References

1. Saito M, Kamikawa K, Yanagizawa H. A new method for blood vessel visualization (arteriography, veinography, angiography) in vivo. *Am J Surg* 1930;10:225.
2. Björk L, Erikson U, Ingelman B. Clinical experience with a new type of contrast medium in peripheral arteriography. *Am J Roentgenol* 1969;106:418.
3. Hilal S. Hemodynamic changes associated with the intra-arterial injection of contrast media. *Radiology* 1966;86:615.
4. Read R, Johnson J, Vick L, Meyer M. Vascular effect of hypertonic solutions. *Circ Res* 1960;64:189.
5. Morgan R. Problems in angiocardiology. *Am J Roentgenol* 1950;64:189.
6. Snider G. Primary pulmonary hypertension. A fatality during pulmonary angiography. *Chest* 1973;64:628.
7. Almén T. Contrast agent design. Some aspects on the synthesis of water soluble contrast agents of low osmolality. *J Theor Biol* 1969;24:216.
8. Almén T, Nordal V, Haavaldsen J. Non-ionic iodinated ray contrast agents. British Patent Specification 1 321 591 (1969).
9. Salvesen S. Acute toxicity tests of metrizamide. *Acta Radiol (Suppl)* 1973;355:5.
10. Salvesen S. Suboccipital injection of metrizamide to anaesthetized and unanaesthetized rabbits. *Acta Radiol (Suppl)* 1973;355:93.
11. Salvesen S. Experimental investigations with metrizamide with relevance to the myelographic use. *Acta Radiol (Suppl)* 1977;355:9.
12. Almén T, Boijesen E, Lindell SE. Metrizamide in angiography. I. Femoral angiography. *Acta Radiol [Diagn]* 1977;18:33.
13. Felder E, Pitre D, Tirone P. Radiopaque contrast media. XLIV. Preclinical studies with a new non-ionic contrast agent. II *Farmacol Ed Sc* 1977;32:835.
14. Jacobsen T. The preclinical development of iohexol (Omnipaque). *Farmakoterapi* 1982;38:45.
15. Nyman U, Almén T, Landtman S. Effect of pH, buffer and osmolality of different contrast media on aortic blood pressure in the rabbit. *Acta Radiol [Diagn]* 1980;21:679.
16. Tilly G, Hardouin M, Lautrou J. Kontrastmittel für röntgenaufnahmen. Bundesrepublik Deutschland, Offenlegungsschrift 25 23 567. Priorität 1974.
17. Salvesen S. Acute intravenous toxicity of iohexol in the mouse and in the rat. *Acta Radiol (Suppl)* 1980;362:73.
18. Salvesen S. Kontrastmidler for angiografi og urografi. (In Norwegian). Paper read at the 39th Nordic Congress of Radiology. Abo, Finland 1981.
19. Mützel W, Siefert H-M, Speck U. Biochemical-pharmacological properties of iohexol. *Acta Radiol (Suppl)* 1980;362:111.
20. Branemark P, Lindström J. Shape of circulating blood corpuscles. *Biorheology* 1963;1:139.
21. Aspelin P. Effect of ionic and nonionic contrast media on red cell deformability in vitro. *Acta Radiol [Diagn]* 1979;20:1.
22. Aspelin P, Teitel P, Almén T. Effect of iohexol on red cell deformability in vitro. *Acta Radiol (Suppl)* 1980;362:127.
23. Aspelin P, Stöhr-Liessen M, Almén T. Effect of iohexol on human erythrocytes. I. Changes of red cell morphology in vitro. *Acta Radiol (Suppl)* 1980;362:117.
24. Binet L, Burstein M. Sur l'action vasoconstrictive du serum sale hypertonique au niveau de la petite circulation. *Compt Rend Soc Biol* 1951;145:1766.
25. Rowe G, Huston J, Tuchman H, Maxwell G, Weinstein A, Crumpton C. The physiologic effect of contrast media used for angiocardiology. *Circulation* 1956;13:896.
26. Almén T, Aspelin P, Levin B. Effect of ionic and non-ionic contrast medium on aortic and pulmonary arterial pressure. An angiocardiology study in rabbits. *Invest Radiol* 1975;10:519.
27. Almén T, Aspelin P, Nilsson P. Aortic and pulmonary pressure after injection of contrast media into the right atrium of rabbits. Comparison between metrizoate, ioxaglate and iohexol. *Acta Radiol (Suppl)* 1980;362:37.
28. Lalli AF. Contrast media reactions. Data analysis and hypothesis. *Radiology* 1980;134:1.
29. Mare K, Violante M. Pulmonary edema induced by high intravenous doses of diatrizoate in the rat. *Acta Radiol [Diagn]* 1983;24:419.
30. Mare K, Violante M, Fischer H. Pulmonary edema following high intravenous doses of ionic contrast media. Effect of the anion composition and concentration. *Invest Radiol* 1983;19:188.
31. Mare K, Violante M, Zak A. Contrast media induced pulmonary edema. Comparison of ionic and non-ionic agents in an animal model. *Radiology* 1983 (submitted for publication).

32. Nyman U, Almén T. Effects of contrast media on aortic endothelium. Experiments in the rat with non-ionic and ionic monomeric and monoacidic dimeric contrast media. *Acta Radiol (Suppl)* 1980;362:65.
33. Nyman U, Almén T. Arterial and venous blood pressure and blood flow following femoral angiography with a new non-ionic contrast medium. An experimental investigation in dogs. *Acta Radiol [Diagn]* 1978;19:1025.
34. Nyman U, Almén T, Landtman S. Effects of contrast media on femoral blood flow. Comparison between non-ionic and ionic monomeric and monoacidic dimeric contrast media in the dog. *Acta Radiol (Suppl)* 1980;362:43.
35. Trägardh B, Cederlund C-G. Coronary angiography with iohexol and other contrast media in the dog. III. Contractility of the left ventricle. *Acta Radiol (Suppl)* 1980;362:25.
36. Törnquist C, Almén T, Golman K, Holtas S. Proteinuria following nephroangiography. VII. Comparison between ionic monomeric, monoacidic dimeric and non-ionic contrast media in the dog. *Acta Radiol (Suppl)* 1980;362:49.
37. Holtas S, Golman K, Törnquist C. Proteinuria following nephroangiography. VIII. Comparison between diatrizoate and iohexol in the rat. *Acta Radiol (Suppl)* 1980;362:53.
38. Sjöberg S, Almén T, Golman K. Excretion of contrast media for urography. Urine volume and iodine concentration during free urine flow in rabbits. *J Belge Radiol* 1979;62:451.
39. Sjöberg S, Almén T, Golman K. Excretion of urographic contrast media. I. Iohexol and other media during free urine flow in the rabbit. *Acta Radiol (Suppl)* 1980;362:93.
40. Sjöberg S, Almén T, Golman K. Excretion of urographic contrast media. II. Iohexol and sodium diatrizoate during ureteric stasis in the rabbit. *Acta Radiol (Suppl)* 1980;362:99.
41. Olsson B, Aulie A, Sveen K, Andrew E. Human pharmacokinetics of iohexol, a new non-ionic contrast medium. *Invest Radiol* 1983;18:177.
42. Golman K, Olivecrona H, Gustafson C, Salvesen S, Almén T, Maly P. Excitation and depression of non-anesthetized rabbits following injection of contrast media into the subarachnoid space. *Acta Radiol (Suppl)* 1980;362:83.
43. Aulie A. Effect of iohexol, metrizamide and ioxaglate on the blood-brain barrier. *Acta Radiol (Suppl)* 1980;362:13.

6.3 Intravenous chelated gadolinium as a contrast agent in NMR imaging of cerebral tumours

Hanns-Joachim Weinmann

Hanns-Joachim Weinmann graduated in General Biology and Genetics at the Free University Hospital of Berlin in 1969. He then went on to attain his PhD in Biology in 1980.

He worked for Schering developing contrast media. Schering has been a key company in the development of radiological contrast media since the earliest days of the iodinated X-ray contrast media. Weinmann submitted a patent application for Gd-DTPA dimeglumine in July 1981 in a project which also involved Ulrich Speck.

Weinmann is currently the head of MRI and X-ray Research at Schering AG in Berlin, Germany and remains at the forefront of contrast media research.



D.H. Carr

J. Brown

G.M. Bydder

see Chapter 2.10 on page 219

U. Speck

D.J. Thomas

I.R. Young

see Chapter 2.9 on page 214

Preliminary Communication

INTRAVENOUS CHELATED GADOLINIUM AS A CONTRAST AGENT IN NMR IMAGING OF CEREBRAL TUMOURS

D. H. CARR J. BROWN

G. M. BYDDER

Departments of Diagnostic Radiology and Clinical Pharmacology,
Royal Postgraduate Medical School, Hammersmith Hospital, Du
Cane Road, London W12 0HS

H-J. WEINMANN U. SPECK

Schering, Berlin

D. J. THOMAS

Department of Neurology, St Mary's Hospital, Praed Street, London

I. R. YOUNG

Picker International, Wembley, Middlesex

Summary NMR imaging was performed on 12 patients with cerebral tumour before and after administration of intravenous gadolinium diethylene triamine penta-acetic acid (DTPA) (0.1 mmol/kg). Contrast enhancement was seen in all cases. Ring enhancement was most frequent (7 cases) but central, linear, patchy, and diffuse enhancement were also seen with both inversion-recovery and spin-echo sequences. The degree of enhancement was greater than that seen with X-ray computed tomography (CT) in 8 cases, equal to it in 3 cases, and less in 1 case. NMR distinguished between tumour and peritumoral oedema to the same extent as did CT. No side-effects were encountered and there was no significant change in urea, creatinine and electrolytes, liver function tests, blood coagulation, or urine testing after administration of gadolinium-DTPA. Gadolinium-DTPA is likely to be of considerable value in NMR imaging of the brain.

INTRODUCTION

CLINICAL NMR imaging of the brain has produced results comparable with X-ray computed tomography (CT) in many situations.^{1,2} In applications such as the diagnosis of multiple sclerosis, NMR is superior³ but in others, such as differentiation between tumour and peritumoral oedema, use of iodinated contrast agents gives CT an advantage.⁴ The development of contrast agents for NMR imaging equivalent to those used in CT has therefore attracted considerable interest. Paramagnetic ions of manganese, iron, and gadolinium (Gd) have been used in animal studies to increase NMR image contrast by decreasing the relaxation times T_1 and T_2 .⁵⁻⁸ The most promising ion so far investigated has been Gd^{3+} . Chelation of this ion reduces its toxicity and animal studies have suggested that gadolinium diethylene triamine penta-acetic acid (Gd-DTPA) may be a suitable agent for human use.⁹

We present the results of NMR imaging before and after administration of intravenous Gd-DTPA to 12 patients with cerebral tumours.

PATIENTS AND METHODS

12 patients (8 male, 4 female) aged 35 to 67 years were studied with the permission of the research ethics committee of the Royal

TABLE 1—PATIENTS' DIAGNOSES

Diagnosis	No
<i>Astrocytoma grade IV</i>	3
<i>Meningioma</i>	1
<i>Probable metastases*</i> :	
Carcinoma of the bronchus	2
Carcinoma of breast	3
Malignant melanoma	1
Cerebral tumour†	2

* Primary tumour but not cerebral tumour examined histologically.

† No histological examination.

TABLE 2—PULSE SEQUENCES

	TR (ms)	TI (ms)	TE (ms)
<i>Inversion-recovery:</i>			
1400/400	1400	400	..
1500/500/44	1500	500	44
<i>Spin-echo:</i>			
344/44	344	..	44
544/44	544	..	44
1580/80	1580	..	80

TR=duration of the scan cycle. TI=time between 180° and 90° pulse on inversion-recovery sequence. TE=time between previous 90° pulse and echo formation with inversion-recovery and spin-echo sequences.

Postgraduate Medical School and the Department of Health and Social Security Medicines Division. 4 of these patients had histological diagnoses of cerebral tumours (table 1). 6 had clinical, CT, and NMR diagnoses of cerebral metastases with histological examination of the primary lesion but not of the metastases. 2 had clinical, CT, and NMR diagnoses of a cerebral tumour without histological confirmation. In each case of cerebral tumour was diagnosed without histology, but the diagnosis was sufficiently certain for the patient to be treated with radiotherapy.

Urea, creatinine and electrolytes (Na^+ , K^+ , HCO_3^-), liver function tests (bilirubin, aspartate transaminase, alkaline phosphatase, total protein), blood screen (haemoglobin, red cell count, packed cell volume, white cell count, platelets) and coagulation studies (prothrombin time, partial thromboplastin time) were performed 24–48 h before the NMR scans. Urine microscopy was also performed; only if all these tests were normal was Gd-DTPA administered. NMR imaging was performed on an NMR scanner operating at 0.15 T which has been described previously.¹⁰ Inversion-recovery and spin-echo pulse sequences listed in table 2 were used. These are described by the American College of Radiology notation.¹¹ Image reconstruction was performed with projection-reconstruction and two-dimensional Fourier transformation. Scanning time was 4–2 to 12 min per image and a total of 8 to 12 images was obtained in each case. After baseline NMR scans had been obtained, intravenous Gd-DTPA (0.1 mmol/kg) was injected and further NMR scans were obtained for up to 65 min.

Contrast-enhanced X-ray CT scans were obtained in each case by means of a Siemens 'Somatom II' whole-body scanner (9 cases), or an EMI CT1010 scanner (3 cases). Intravenous meglumine diatrizoate (31 g of iodine) was used for contrast enhancement in these cases.

Patients were observed during the NMR scan and questioned about side-effects at the end of the NMR scan and 24–48 h later. Serum urea, creatinine, and electrolytes, liver function tests, blood screen, and coagulation studies as well as urine microscopy were repeated 24–48 h after injection of Gd-DTPA.

RESULTS

NMR Scans

Cerebral tumours were observed on the NMR images in every case. Contrast enhancement was also observed in each

THE LANCET, MARCH 3, 1984

485

of the 12 cases after injection of Gd-DTPA. Ring enhancement was seen in 7 cases, central enhancement was observed in 3 cases, and patchy enhancement was seen in 2 cases. Diffuse and linear enhancement were also observed in 1 case each. With inversion-recovery (1500/500/44) sequences, enhancement was apparent as an increase in signal intensity (light area) corresponding to a decrease in T_1 (fig 1). With spin-echo (544/44) sequences, enhancement also produced an increase in signal intensity (fig 2).

Comparison with CT

In all 12 cases tumours were identified on both NMR and CT. In 2 cases, additional lesions were seen with NMR but not with CT; in 1 of these cases, nine 0.3–0.5 cm central contrast-enhancing lesions were seen in both cerebral hemispheres and in the other a ring-enhancing lesion was seen in the right cerebellar hemisphere. Greater contrast enhancement was seen with NMR than with CT in 8 cases,

an equal degree of enhancement was seen in 3 cases, and less enhancement was seen in 1 case.

The extent of the tumour as defined by the margin of ring enhancement or that of the central enhancement was better seen with NMR in 5 cases, equally well seen in 3 cases, and better seen with CT in 1 case. In the 3 remaining cases, the boundary between tumour and oedema was poorly defined with both NMR and CT.

No untoward symptoms were noted by any of the patients during the NMR scans or in the subsequent 24–48 h. The flushing sensation and nausea experienced by many patients after injection of conventional iodinated contrast agents for the CT examinations were not experienced after Gd-DTPA injection.

No significant change was seen in urea, creatinine and electrolyte examinations, liver function tests, blood screen and coagulation studies after Gd-DTPA injection. No abnormality was seen on urine microscopy after Gd-DTPA administration.

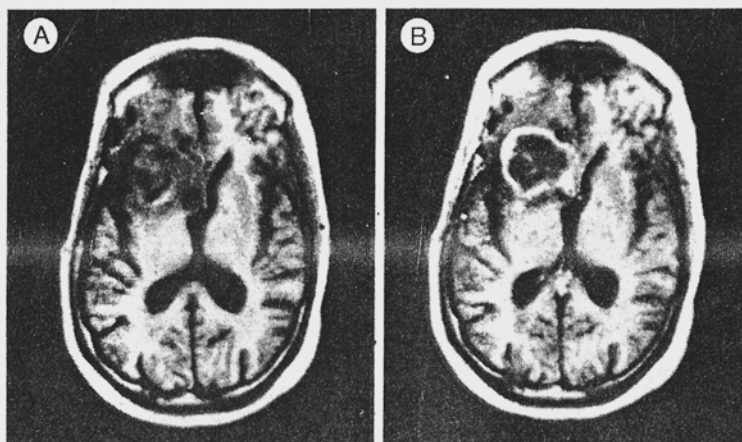


Fig 1—Astrocytoma grade IV: transverse inversion-recovery ($IR_{1500/500/44}$) scans before (A) and after (B) Gd-DTPA injection.

Tumour and oedema are seen in left frontal region (A). After Gd-DTPA administration a light ring of enhancement is seen around the bulk of the tumour.

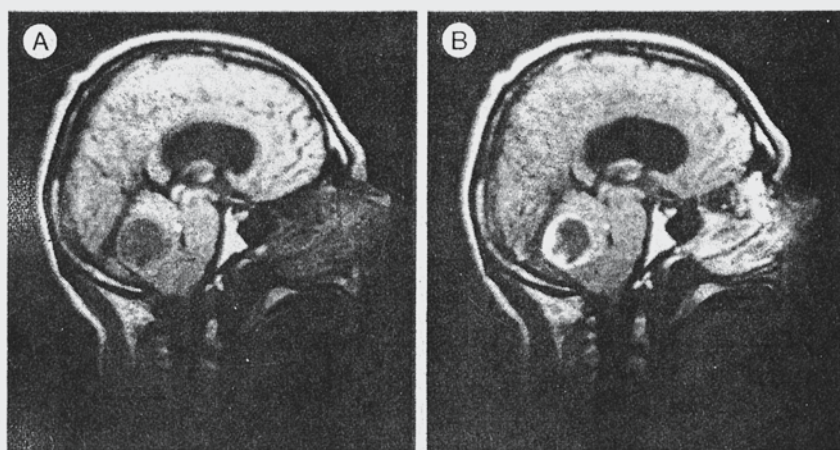


Fig 2—Metastasis from carcinoma of the bronchus: sagittal spin-echo ($SE_{544/44}$) scans before (A) and after (B) Gd-DTPA injection.

A dark lesion is seen in cerebellum (A). There is enhancement after Gd-DTPA (B).

DISCUSSION

Contrast enhancement with Gd-DTPA of NMR images of cerebral tumours resembles that seen with CT and in many cases is superior. The NMR demonstration of the margin between tumour and peritumoral oedema compared favourably with that seen with contrast-enhanced CT. Stereotactic biopsy studies have shown that tumour may extend outside the region of enhancement shown with X-ray CT, nevertheless contrast enhancement is a useful indication of the site of the bulk of the tumour and provides a guide for biopsy studies and radiotherapy planning in patients treated without biopsy.

Gadolinium-DTPA is a tightly bound chelate between the rare earth Gd and DTPA. After intravenous injection it is distributed within the vascular system and is excreted unchanged through the kidney. The unpaired electrons in Gd³⁺ give it a large magnetic moment and enable it to interact with protons, decreasing the time required for their return to equilibrium after they have been perturbed by radio-frequency pulses during NMR imaging. This is expressed as a decrease in the proton relaxation times T₁ and T₂.

The contrast seen between tumours and normal tissue on NMR images is usually a result of an increase in tumour T₁ and T₂. Gd-DTPA accumulates in tumours as a result of extravascular leakage and changes the appearance of tumours by decreasing their T₁ and T₂.

Disadvantages of Gd-DTPA include the need for intravenous injection and the increased time necessary for pre-contrast and post-contrast scans. There are also potential problems with spin-echo sequences if the concentration of the contrast agent is too high and produces marked shortening of T₂ with a reduction in signal intensity.

More work will be required to establish the optimum dose, time of examination, and pulse sequence for particular clinical situations and to study the incidence of side-effects, but Gd-DTPA is likely to be of considerable value in NMR imaging of the brain as well as the rest of the body.

We are grateful to the Department of Health and Social Security and in particular Mr John Williams and Mr Gordon Higson for their continued support and encouragement.

Correspondence should be addressed to G. M. B., Department of Diagnostic Radiology, Royal Postgraduate Medical School, Hammersmith Hospital, Du Cane Road, London W12 0HS.

REFERENCES

1. Bydder GM, Steiner RE, Young IR, et al. Clinical NMR imaging of the brain: 140 cases. *AJR* 1982; 139: 215-36.
2. Brant-Zawadzki M, Davis PL, Crooks LE, et al. NMR demonstration of cerebral abnormalities: comparison with CT. *AJR* 1983; 140: 847-54.
3. Young IR, Hall AS, Pallis CA, Legg NJ, Bydder GM, Steiner RE. Nuclear magnetic resonance imaging of the brain in multiple sclerosis. *Lancet* 1981; ii: 1063-66.
4. Bydder GM, Penneck JM, Steiner RE, Orr JS, Bailes DR, Young IR. The NMR diagnosis of cerebral tumours. *J Magnetic Resonance* 1984; 1: 1-23.
5. Doyle FH, Gore JC, Penneck JM. Relaxation rate enhancement observed in vivo by NMR imaging. *J Comput Assist Tomogr* 1981; 5: 295-96.
6. Brasch RC. Methods of contrast enhancement for NMR imaging and potential applications. *Radiology* 1983; 147: 781-88.
7. Runge VM, Stewart RG, Clanton JA, et al. Potential oral and intravenous paramagnetic NMR contrast agents. *Radiology* 1983; 147: 789-91.
8. Carr DH, Brown J, Leung A W-L, Penneck JM. The in vivo use of iron and gadolinium chelates as contrast in NMR imaging—preliminary studies. *J Comput Assist Tomogr* (in press).
9. Weinmann H-J, Brasch RC, Press W-R, Wesbey GW. Characterisation of gadolinium-DTPA complex used as an NMR contrast agent. *AJR* (in press).
10. Doyle FH, Gore JC, Penneck JM, et al. Imaging of the brain by nuclear magnetic resonance. *Lancet* 1981; ii: 53-57.
11. American College of Radiology. Glossary of NMR terms. Chicago: American College of Radiology, 1983.

Reviews of Books

An Introduction to Community Medicine

Charles du V. Florey, Peter Burney, Michael d'Souza, Ellie Scrivens, and Peter West, St Thomas' Hospital Medical School, London. Edinburgh: Churchill Livingstone. 1983. Pp 134. £3.95.

THIS short, readable, affordable, soft-backed text has an elder brother now in its third edition, Barker and Rose's *Epidemiology in Medical Practice* (Churchill Livingstone). The limited range of the latter justifies a broader text which in turn has led to five authors contributing not only on subjects inherent in everyday medicine but also on its interfaces with economics, planning, and government policy. The book starts by discussing the different perspectives on ill-health from the patient's self-perception of "illness", to his "complaint", "sickness" and the label of "disease" awarded by the doctor, and it plumps for "health-problem" as the best overall term for disease. It then reviews the information available on health-problems, starting with death certificates and going on to morbidity data. The story of the great smog of 1952 is used for a case-study on how initial epidemiological detective work led (eventually) to public realisation of the need for a change from an unhealthy way of living and thus to government legislation. Chapters follow on the options for treatment and prevention, on assessment of efficacy and effectiveness, on economic choices in medical care, and on the background to policy formation and health service management.

On the whole the book is successful, but the multiple authorship and need for brevity have made the text disjointed in places and have resulted in two different views on the value of exercise appearing on consecutive pages. The book is at its best in describing a broad range of community-medicine case-studies; it is less successful in woolly self-justificatory pleading for community medicine which should not now be necessary. The following quotation is an example—is it a compliment or criticism? "The position of the GP within the health-care system is unique and his approach to health problems provides the greatest argument for the value of a community perspective on the problem of ill-health."

Barker and Rose's book has greater cohesion over a much more limited range. The area of overlap between the two books is of course in epidemiology. Unfortunately the authors have used different definitions for terms such as attributable risk (Florey et al using the attributable risk fraction and Barker and Rose using the excess attributable risk). This difference may sorely vex students keen enough to study both books. Perhaps this can be reconsidered in any revisions.

Cardiovascular Epidemiology Unit,
Ninewells Hospital and Medical School,
Dundee

H. TUNSTALL-PEDOE

Autonomic Failure

A Textbook of Clinical Disorders of the Autonomic Nervous System. Edited by Sir Roger Bannister, National Hospital for Nervous Diseases, London. Oxford: Oxford University Press. 1983. Pp 666. £45.

DISORDERS of the autonomic nervous system impinge on different disciplines, and the present volume, which draws these threads together, is particularly welcome. Much is still unknown about the structure and function of the autonomic nervous system, and the intention, which is achieved, is to review recent advances in this area. The two common themes that run through the book are those of clinical description and measurement—to a large extent a reflection of the way that advances have occurred, with the tendency of the clinician to describe and categorise being complemented by that of the experimentalist to open up previously inaccessible areas to study.

The book begins with a short overview of autonomic failure and the control and integration of function. The rest of the book is divided fairly equally between a consideration of (primary)

6.4 Characteristics of gadolinium-DTPA complex: a potential NMR contrast agent

Hanns-Joachim Weinmann

see Chapter 6.3 on page 412

R.C. Brasch

see Chapter 6.5 on page 423

W.R. Press

G.E. Wesbey

Characteristics of Gadolinium-DTPA Complex: A Potential NMR Contrast Agent

Hanns-Joachim Weinmann¹
Robert C. Brasch²
Wolf-R. Press¹
George E. Wesbey²

Chelation of the rare-earth element gadolinium (Gd) with diethylenetriaminepenta-acetic acid (DTPA) results in a strongly paramagnetic, stable complex that is well tolerated in animals. The strongly paramagnetic gadolinium complex reduces hydrogen-proton relaxation times even in low concentrations (less than 0.01 mmol/L). The pharmacokinetic behavior of intravenously delivered Gd-DTPA is similar to the well known iodinated contrast agents used in urography and angiography; excretion is predominately through the kidneys with greater than 90% recovery in 24 hr. The intravenous LD₅₀ of the meglumine salt of Gd-DTPA is 10 mmol/kg for the rat; in vivo there is no evidence of dissociation of the gadolinium ion from the DTPA ligand. The combination of strong proton relaxation, in-vivo stability, rapid urinary excretion, and high tolerance favors the further development and the potential clinical application of gadolinium-DTPA as a contrast enhancer in magnetic resonance imaging.

Recent developments in nuclear magnetic resonance (NMR) technology have led to a new and extremely promising diagnostic technique, proton NMR tomography. Using a suitable radiofrequency pulse sequence (saturation-recovery, inversion-recovery, or spin-echo), it is possible to obtain images of high quality that often aid in the characterization of pathologic processes, especially within the brain [1-10]. Differentiation of tissue from normal is provided when a distinction exists between the spin-lattice and/or spin-spin relaxation times of a lesion and those of surrounding normal tissues. Other factors that influence signal intensity, such as hydrogen-proton concentration and proton motion, seem to play a lesser role than relaxation times in most cases.

If differences in relaxation times between contiguous healthy and pathologic tissues are only insignificant, or even identical, differentiation is impossible by NMR tomography [11]. Diagnosis is made more difficult by the fact that relaxation times of various malignant and benign lesions or normal tissue may overlap [12]. Another feature of NMR imaging that may be regarded as a disadvantage in comparison with conventional imaging techniques is that the NMR image does not provide a direct measurement of organ function [11].

Recent investigations indicate that paramagnetic compounds used as NMR contrast agents may augment the diagnostic yield from NMR tomography by enhancing the contrast between magnetically similar but histologically dissimilar tissues and by providing a direct measure of organ function [13-19]. Alternatively, continued development of NMR technology and the use of sophisticated computer-assisted analyses may render contrast agents unnecessary.

To date, experiments with NMR contrast agents have focused on three different types of paramagnetic substances. The first type belongs to the group of nitroxyl stable-free radicals; these compounds, containing one unpaired electron, have been shown to be relatively stable, to be well tolerated in experimental animals, and to decrease proton relaxation times [19]. Transition elements and rare-earth elements constitute the second major group of paramagnetic substances with

Received July 7, 1983; accepted after revision November 14, 1983.

¹ Schering AG, D. Kontrastmittelpharmakologie, P.O.B. 65 03 11, D-1000 Berlin 65, Germany. Address reprint requests to H.-J. Weinmann.

² Department of Radiology, University of California School of Medicine, San Francisco, CA 94143.

AJR 142:619-624, March 1984

0361-803X/84/1423-0619

© American Roentgen Ray Society

potential as NMR contrast agents. Considerable attention has focused on the bivalent manganese ion (Mn^{2+}), which owes its high degree of paramagnetism to five unpaired electrons [20]. Due to the potential of the Mn^{2+} ion to undergo spontaneous oxidation leading to a change or loss of paramagnetic properties and because of prolonged retention within the liver, the in-vivo possibilities may be limited. A third class of paramagnetic compounds is represented by molecular oxygen, which is paramagnetic by virtue of two unpaired electrons with parallel spins that do not cancel. Oxygen used as a NMR contrast agent has the disadvantage that within an organism, the molecule may rapidly lose its paramagnetic properties (e.g., in the formation of diamagnetic oxyhemoglobin) [21].

The general aim was to find a compound that remained stable in vivo, had a powerful influence on proton relaxation times, but was free of toxic effects in doses appropriate for contrast enhancement in vivo. Moreover, it was essential that the compound undergo tissue-specific or, at least, compartment-specific distribution in the living organism.

Gadolinium (Gd), a rare-earth element the ion of which (Gd^{3+}) has seven unpaired electrons, also has an unusually strong hydrogen-proton spin-lattice relaxation effect (fig. 1) [20]. The gadolinium ion has been used as a paramagnetic proton-relaxation probe in NMR biochemical studies [22]. Because of poor tolerance for unaltered gadolinium ions, a means of detoxification is necessary for in-vivo administration [23]. Since the atoms of the rare-earth elements do not form stable, covalent bonds with organic molecules, the paramagnetic Gd ion might be detoxified by complexation. Gadolinium is known to form stable chelates with ethylenediaminetetraacetic acid (EDTA) and diethylenetriaminepentaacetic acid (DTPA); the formation constants ($\log K$) for Gd-EDTA and Gd-DTPA are 17 and 22–23, respectively [24]. Our study examines the in-vivo stability, pharmacokinetics, and toxicity of Gd-DTPA and compares it with Gd-EDTA and gadolinium chloride.

Materials and Methods

Gadolinium chelates were synthesized by incubation of Gd_2O_3 (Auer-Remy, Hamburg, W. Germany) and the corresponding ligands. The synthesis of Gd-DTPA is an example. A suspension of 43.5 g of Gd_2O_3 and 94.5 g of DTPA in 1.2 L water was stirred, while being heated to 90°C to 100°C, for 48 hr. The undissolved material was then filtered off, and the filtrate was evaporated until dry.

The addition of N-methylglucamine yielded water-soluble salts of the gadolinium chelates, ethylenediaminetetraacetic acid (Gd-EDTA) and diethylenetriaminepentaacetic acid (Gd-DTPA) as described in the published patent application [25]. A 0.5 mol/L solution of dimeglumine-Gd-DTPA has an osmotic pressure of 49.8 atm (1.94 osmol/kg) and a viscosity of 2.9 mPa.s measured at 37°C by vapor-pressure osmometry and capillary viscosimetry, respectively. Free gadolinium ions were not detectable (below 0.01%) by use of xylenol orange as indicator [26]. Aqueous gadolinium chloride and diatrizoate (Angiografin [corresponds to Angiovisit]) were used as reference solutions.

Proton Relaxation Effects

The effects of the paramagnetic compounds on proton relaxation times were measured in aqueous solutions at 20 MHz (0.47 T) using

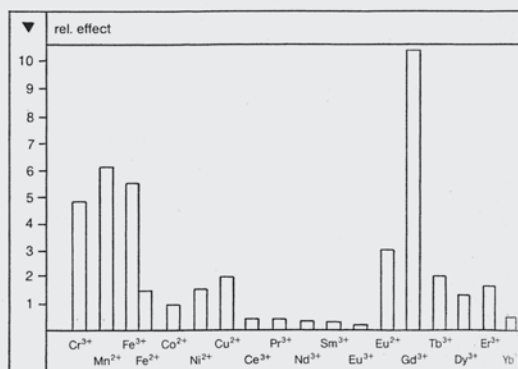


Fig. 1.—Influence of paramagnetic ions on proton spin-lattice relaxation time [20].

a pulse NMR spectrometer (Minispec pc 20, Bruker, Karlsruhe, W. Germany) for inversion-recovery and Carr-Purcell-Meiboom-Gill pulse sequences.

Tolerance

The acute intravenous tolerance (LD_{50}) of test solutions was evaluated by administration of different volumes of each agent directly into the tail veins of rats. Outbred male and female rats (strain: Wistar-Han-Schering) weighing 90–110 g were given a single intravenous injection at one of two to four dose levels; three to six animals were given each dose. The injection rate was 2 ml/min and the rats were observed for 7 days after the injection. The concentration of test solution was 0.5 mol/L Gd-DTPA, 0.1 mol/L $GdCl_3$ and Gd-EDTA, or 306 mg l/ml for diatrizoate. The amount of compound producing 50% mortality (LD_{50}) was determined by interpolation from the results of different dose levels. A 0.5 mol/L solution of Na_3Ca -DTPA (Heyl, W. Germany), a chelating drug used to treat heavy-metal poisoning, was also tested for LD_{50} as a comparison.

Neural tolerance was assessed by intracisternal injection in male and female rats. The amounts of each compound producing 50% morbidity (ED_{50}) (lack of motor coordination or epileptoid fit) and 50% mortality (LD_{50}) were determined by interpolation from the results of four to 10 dose levels, each administered to 10 animals [27].

Because the in-vivo tolerance of contrast media correlates with the hydrophilicity, the partition coefficients of Gd-DTPA and diatrizoate were determined in a n-butanol-buffer mixture at pH 7.6 [28]. In order to establish whether Gd-DTPA causes some of the side effects known from radiographic contrast media the potential influence of Gd-DTPA and diatrizoate on the complement system was measured using the method of activation described by Mützel et al. [29].

Pharmacokinetics

Pharmacokinetic studies were performed with ^{153}Gd -labeled compounds: $^{153}GdCl_3$ (382 MBq/mg Gd, Amersham, England) was added to a 0.25 mol/L solution of unlabeled $GdCl_3$; ^{153}Gd -labeled Gd-DTPA was prepared by incubation of $^{153}GdCl_3$ and DTPA. On the basis of molar concentrations, the amount of DTPA was 10% higher than the amount of the radioactive material; pH was adjusted to 7.2 by addition of N-methylglucamine. A small amount of this solution of high specific

JR-142, March 1984

CHARACTERISTICS OF Gd-DTPA COMPLEX

621

activity (high radioactivity but low Gd concentration) was mixed with 0.5 mol/L of unlabeled Gd-DTPA. The specific activity of the resulting solution, used for the study of excretion and organ distribution, was 2 MBq/mmol; for blood- and plasma-level studies, an activity of 0.15 MBq/mmol was used. Free gadolinium was not detectable (below 0.01%) by means of thin-layer chromatography or xylene orange as indicator [26]. The ^{153}Gd activity was measured with the aid of a gamma scintillation counter (Compu Gamma 1282, LKB/Wallac, Finland).

Renal and fecal excretions were analyzed for 7 days after intravenous administration of 0.5 mmol/kg radiolabeled Gd-DTPA or 0.25 mmol/kg radiolabeled GdCl_3 in five male rats (140–160 g). In another experiment using five rats, serial blood, urine, and plasma concentrations of Gd-DTPA were determined for 3 hr after intravenous injection of 0.5 mmol/kg. For each time point, blood was taken from three to five animals. Half-lives of Gd-DTPA disappearance were then calculated for blood, plasma, and urine from levels of radiolabel; values were based on computer calculation using an open one-compartment model [30]. Gadolinium concentrations in kidney, liver, and spleen and the amount of gadolinium remaining in the organism were determined 7 days after injection.

Results

Proton Relaxation Effects of Gadolinium Compounds

The free gadolinium ion (Gd^{3+}) and the two gadolinium chelates produced distinct effects on the T1 and T2 relaxation times of hydrogen protons in aqueous solutions (table 1); increases in the concentration of these paramagnetic agents resulted in a decrease in both T1 and T2 relaxation times. A straight-line relation was observed between concentration and the reciprocal value of relaxation times in the range of 0–1 mmol/L. Chelation with either EDTA or DTPA reduced the paramagnetic properties of nonchelated gadolinium. The proton relaxation times of demineralized water were reduced by half with about 50 $\mu\text{mol/L}$ gadolinium chloride and about the same amount of Gd-EDTA, but almost 80 $\mu\text{mol/L}$ was required to achieve the same proton relaxation effect with Gd-DTPA.

Tolerance

For gadolinium chloride and Gd-EDTA, half of the animals investigated died after a dose of less than 1 mmol/kg (table 2). Gd-DTPA demonstrated a considerably better tolerance; for this chelate, the LD_{50} was 10 mmol/kg. For comparison, the LD_{50} was 18 mmol/kg for the iodinated radiographic contrast agent, diatrizoate, corresponding to about 7 g/kg. For Gd-DTPA and diatrizoate administrations, the animals died within the first 3 hr. For Gd-EDTA and GdCl_3 , some animals died several days after administration, implying a different form of toxicity.

Animals receiving subarachnoidal administrations of GdCl_3 and Gd-EDTA displayed a poorer tolerance than that shown for Gd-DTPA and diatrizoate (table 3). Tolerance to free gadolinium ions was lowest of all gadolinium agents for the intracisternal route. In the case of GdCl_3 , the values of the ED_{50} and LD_{50} were virtually identical, meaning that minor neurotoxic effects were immediately followed by severe and

TABLE 1: Relation of Proton Relaxation Rates and Concentrations of Paramagnetic Agents

Agent	Relaxation Rate
GdCl_3 :	
T1	$\text{T1}^{-1} (\text{sec}^{-1}) = 0.49 + 9.09 \times \text{C}$
T2	$\text{T2}^{-1} (\text{sec}^{-1}) = 0.65 + 10.3 \times \text{C}$
Meglumine-Gd-EDTA:	
T1	$\text{T1}^{-1} (\text{sec}^{-1}) = 0.44 + 6.89 \times \text{C}$
T2	$\text{T2}^{-1} (\text{sec}^{-1}) = 0.55 + 8.19 \times \text{C}$
Dimeglumine-Gd-DTPA:	
T1	$\text{T1}^{-1} (\text{sec}^{-1}) = 0.39 + 4.52 \times \text{C}$
T2	$\text{T2}^{-1} (\text{sec}^{-1}) = 0.50 + 5.66 \times \text{C}$

Note.—Influence of concentration, C (mmol/L), of gadolinium compounds on the T1 and T2 relaxation times of hydrogen protons of water at 20 MHz. Values were calculated using regression analyses of the relation $1/T$ vs. C in concentration range 0–1 mmol/L.

TABLE 2: Acute Lethal Toxicity

Agent	Dose (mmol/kg)	No. Deaths/No. Rats	Interpolated LD_{50} (mmol/kg)*
Meglumine diatrizoate	12	0/4	18
	20	1/4	
	28	4/4	
GdCl_3	0.3	0/5	0.5
	0.45	2/5	
	0.6	5/5	
Meglumine-Gd-EDTA	0.3	2/3	0.3
	1.2	5/5	
Dimeglumine-Gd-DTPA	2.5	0/4	10
	7.5	0/4	
	12.5	4/4	
$\text{Na}_3\text{Ca-DTPA}$	1	0/6	5
	2	2/6	
	4	0/6	
	6	6/6	

* LD_{50} in male and female rats (90–110 g) after intravenous injection (2 ml/min).

lethal toxicity. The overall best neural tolerance was observed for gadolinium chelated with DTPA; for Gd-DTPA, the values of the LD_{50} were 10 times higher than ED_{50} values with both routes of neural administration.

Both Gd-DTPA and diatrizoate are very hydrophilic substances. Partition coefficients (log P) of -2.7 and -1.3 were measured for the gadolinium chelate and the iodinated contrast agent, respectively. However, the butanol-buffer partition coefficient of Gd-DTPA is about 25 times smaller than that of the iodinated compound.

The in-vitro investigation of complement activation showed that 50% of plasma complement remained at a diatrizoate concentration of 0.4 mol/L. In the case of Gd-DTPA, practically no influence on the complement system was detected; 50% activation required 2.5 mol/L.

Pharmacokinetics

At 5 min after intravenous injection of 0.5 mmol/kg Gd-DTPA into the rats, about 10% of the dose could be detected in the whole blood volume. The blood concentration subsequently decreased with a half-life of about 20 min (fig. 2). Gd-DTPA apparently did not penetrate the cell membrane of

TABLE 3: Tolerance after Intracisternal Administration in Rats

Agent	Dose* (mmol/kg)	No. Reactors	No. Deaths	ED ₅₀	LD ₅₀
Meglumine diatrizoate	4	1	NE	11 (8-15)	55 (44-67)
	8	2	NE		
	13	5	NE		
	17	7	NE		
	21	10	NE		
	32	NE	1		
	42	NE	3		
	63	NE	6		
	84	NE	8		
GdCl ₃	128	NE	10	6 (4-8)	8 (7-10)
	3	3	NE		
	4	3	0		
	6	5	2		
	8	7	6		
Meglumine-Gd-EDTA	17	10	10	12 (4-8)	23 (19-27)
	8	2	NE		
	16	7	1		
	27	NE	6		
Dimeglumine-Gd-DTPA	32	10	9	74 (49-112)	650 (544-800)
	17	0	NE		
	33	3	NE		
	67	4	NE		
	133	7	NE		
	198	9	NE		
	417	NE	1		
	617	NE	5		
	833	NE	8		
	1233	NE	9		

Note.—NE = Not evaluated; numbers in parentheses are 95% confidence intervals.
* $n = 10$ per dose.

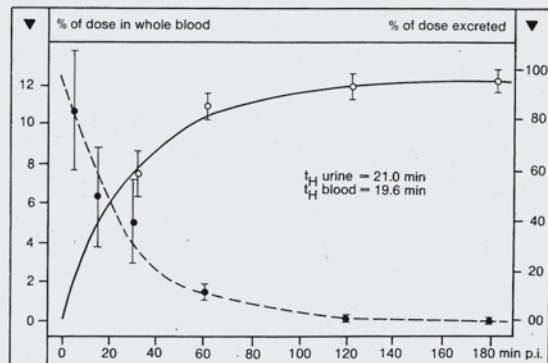


Fig. 2.—Blood level and urinary excretion of ¹⁵³Gd-DTPA after intravenous injection of 0.5 mmol/kg in five male rats (140–160 g body weight).

blood cells; the concentration in plasma remained 1.6 times higher than in blood over 2 hr of observation.

A half-life of about 20 min was observed for renal excretion up to 3 hr after injection. By 3 hr, more than 80% of the compound had been excreted from the organism in urine (table 4). By 7 days after intravenous injection, a total of 90% of the dose had been recovered in the urine and another 7%

TABLE 4: Excretion and Tissue Distribution after Intravenous Injection of ¹⁵³Gd-DTPA in Rats

Gd-DTPA	Time after Dose (days)*	% of Administered Dose
Excreted:		
Urine	0-3 hr	87.6 ± 1.9
	0-1	89.2 ± 2.6
	0-7	89.7 ± 2.7
Feces	0-1	5 ± 3.5
	0-7	7.4 ± 4.5
Residual:		
Liver	7	0.08 ± 0.01
Spleen	7	0.01
Kidney	7	0.1 ± 0.03
Remaining body	7	0.21 ± 0.05
Total recovery	7	97.5 ± 3.0

Note.—Data from injection of 0.5 mmol/kg ¹⁵³Gd-DTPA in five male rats weighing 140–160 g.

* Time given in days unless indicated otherwise.

was recovered in the feces. Less than 0.3% of the given dose was found in the organism, with 0.08% of the dose being detected in the liver and 0.1% in the kidneys.

By 7 days after intravenous injection of radiolabeled GdCl₃, only 2% of the dose had been excreted. The major portion was discovered in the liver and spleen, about 60% being in the liver and 25% in the spleen (table 5).

TABLE 5: Excretion and Tissue Distribution after Intravenous Injection of $^{153}\text{GdCl}_3$ in Rats

GdCl ₃	Time after Dose (days)*	% of Administered Dose
Excreted:		
Urine	0-3 hr	0.05
	0-1	0.07
	0-7	0.1 ± 0.0
Feces	0-1	0.6 ± 0.4
	0-7	2.1 ± 0.5
Residual:		
Liver	7	56.1 ± 8.9
Spleen	7	25.3 ± 3.7
Kidney	7	0.6 ± 0.1
Remaining body	7	16.3 ± 2.3
Total recovery	7	100.6 ± 8.9

Note.—Data from injection of 0.25 mmol/kg $^{153}\text{GdCl}_3$ in five male rats weighing 140–160

* Time given in days unless indicated otherwise.

Discussion

Of all elements, gadolinium has the strongest influence on T1 relaxation times of hydrogen protons (fig. 1) [20]. This powerful proton-relaxing effect of gadolinium can be attributed to a complex interplay of several factors including a strong magnetic moment, long electron-spin-relaxation time, isotropy of g-tensors, rotational tumbling time, configuration and mobility of molecules of hydration, and proximity of hydrogen nuclei to the paramagnetic center [31, 32]. Chelating gadolinium to EDTA or DTPA reduces, but far from eliminates, gadolinium's strong influence on proton T1 and T2 relaxation.

The coordination number of Gd^{3+} is estimated to be 9 or 10 [22, 33]. Thus, using DTPA with eight coordination sites as a chelation ligand, only eight of gadolinium's nine or 10 possible coordination sites could be filled. This leaves at least one or two sites open for fast-exchanging water protons to approach closely to the paramagnetic center of the complex. Proton relaxation enhancement is directly proportional to the number of available coordination proton ligands per paramagnetic ion. Thus gadolinium complexes (Gd-DTPA and Gd-EDTA), compared with the nonchelated gadolinium species, would be predicted to have reduced proton relaxation effects on water molecules. This prediction was supported by our experimental results. To obtain the same influence on proton relaxation as that achieved with the free gadolinium ion, the concentration of Gd-DTPA must be about twice as high.

The complexation of gadolinium with EDTA produced little or no improvement in tolerance compared with gadolinium chloride. Whether the chemotoxicity of the entire complex itself or a dissociation of the gadolinium ion from the EDTA ligand within the body caused the effect is not clear. It may be that the Gd-EDTA stability constant of about 10^{17} is insufficient to prevent the interaction of free gadolinium ions with high-affinity binding sites of enzymes. DTPA binds gadolinium several magnitudes more tightly ($\log k = 22$) than EDTA [24]. Gd chelation with DTPA does, in fact, produce a compound with much improved tolerance. The LD₅₀ is higher

than that of $\text{Na}_3\text{Ca-DTPA}$, which is a complexing agent used as an antidote for heavy-metal poisoning in man.

The acute intravenous tolerance (LD₅₀) of Gd-DTPA in rats is in the range of that of the most commonly used radiographic contrast agent, diatrizoate. The neural tolerance of Gd-DTPA is several times better than for diatrizoate. A high neural tolerance is particularly advantageous if a compound may pass the blood-brain barrier.

According to the hypothesis of Lasser (Lang et al. [34]), activation of the complement system by radiographic contrast media is correlated to certain of their untoward anaphylactoid reactions. Gd-DTPA, a very poor activator of the complement system, would not be expected to produce such adverse reactions.

The combination of gadolinium with DTPA reduces the toxicity of the two separate components, gadolinium and DTPA [35]. This is reflected in the pharmacokinetic behavior after intravenous administration of Gd-DTPA compared with gadolinium chloride. Whereas the gadolinium ion is largely retained by the organism, in particular in the liver and spleen, Gd-DTPA leaves the body within the first few hours after intravenous injection. Compared with GdCl_3 , there is no retention of gadolinium in liver and spleen. There seems to be no dissociation of gadolinium from the Gd-DTPA complex within the body.

The short (20 min) half-life of Gd-DTPA in blood and urine and the predominate renal elimination suggest that the compound has very little if any interaction within the body. The stable ratio of concentrations between plasma and blood and the fate of Gd-DTPA in the organism lead us to postulate that this complex is distributed exclusively extracellularly. The very high hydrophilicity, the charge, and the rather large molecular weight of Gd-DTPA (about 550) probably account for its exclusion by biologic barriers such as cell membranes. Gd-DTPA would be expected to remain within the extracellular space and not to penetrate the normal blood-brain barrier.

From the pharmacokinetic and in-vitro proton relaxation data for Gd-DTPA, we predict that an in-vivo dose of 0.1–0.5 mmol/kg would produce a significant tissue enhancement on NMR images. This predicted diagnostic dose is $1/100$ to $1/20$ of the observed LD₅₀ dose, a wide margin of safety. Independent from our study, Fobben and Wolf [36] have called attention to Gd-DTPA as a potential NMR myocardial contrast agent and noted an absence of cardiotoxicity.

In summary, our results indicate that Gd-DTPA is an agent capable of strong proton relaxation enhancement with relatively high in-vivo tolerance. This hydrophilic complex is rapidly excreted, predominately in the urine, and apparently does not dissociate in vivo. These characteristics favor the use of Gd-DTPA as an NMR contrast enhancer.

REFERENCES

- Partain CL, James AE, Watson JT, Price RR, Coulam CM, Rollo FD. Nuclear magnetic resonance and computed tomography. *Radiology* 1980;136:767–770
- Young IR, Burl M, Clarke GJ, et al. Magnetic resonance properties of hydrogen: imaging the posterior fossa. *AJR* 1981;

- 137:895-901
3. Pykett IL. NMR imaging in medicine. *Sci Am* **1982**;246:78-88
 4. Taveras JM. Nuclear magnetic resonance imaging. *AJR* **1982**;139:406-407
 5. Bydder GM, Steiner RE, Young IR, et al. Clinical NMR imaging of the brain: 140 cases. *AJR* **1982**;139:215-236
 6. James AE, Partain CL, Holland GN, et al. Nuclear magnetic resonance imaging: the current state. *AJR* **1982**;138:201-210
 7. Margulis AR. Nuclear magnetic resonance imaging: the present status. *J Can Assoc Radiol* **1983**;33:131-136
 8. Bydder GM, Steiner RE. NMR imaging of the brain. *Neuroradiology* **1982**;23:231-240
 9. Young IR, Randell CP, Kaplan PW, James A, Bydder GM, Steiner RE. Nuclear magnetic resonance (NMR) imaging in white matter disease of the brain using spin-echo sequences. *J Comput Assist Tomogr* **1983**;7:290-294
 10. El Yousef SJ, Alfidi RJ, Duchesneau RH, et al. Initial experience with nuclear magnetic resonance (NMR) imaging of the human breast. *J Comput Assist Tomogr* **1983**;7:215-218
 11. Brasch RC. Method of contrast enhancement for NMR imaging and potential application. *Radiology* **1983**;147:781-788
 12. Davis PL, Kaufman L, Crooks LE, Miller TR. Detectability of hepatomas in rat livers by nuclear magnetic resonance imaging. *Invest Radiol* **1981**;16:354-359
 13. Lauterbur PC, Mendonça-Dias MH, Rudin AM. Augmentation of tissue water proton spin-lattice relaxation rates by in vivo addition of paramagnetic ions. *Front Biol Energ* **1978**;1:752-759
 14. Young IR, Clarke GJ, Bailes DR, Pennock JM, Doyle FH, Bydder GM. Enhancement of relaxation rate with paramagnetic contrast agents in NMR imaging. *CT* **1981**;5:543-547
 15. Brady TJ, Goldman MR, Pykett IL, et al. Proton nuclear magnetic resonance imaging of regionally ischemic canine heart: effect of paramagnetic proton signal enhancement. *Radiology* **1982**;144:343-347
 16. Brasch RC, Nitecki ED, Brant-Zawadzki MN, Enzmann D, Tozer TN. "NSFR": NMR contrast agents for the CNS. Presented at the Symposium Neuroradiologicum, Washington, DC, October 1982
 17. Runge VM, Stewart RG, Clanton JA, James AE, Partain CL. Paramagnetic NMR contrast agents: potential oral and intravenous agents. *Radiology* **1983**;147:789-791
 18. Goldman MR, Brady TJ, Pykett IL, et al. Quantification of experimental myocardial infarction using nuclear magnetic resonance imaging and paramagnetic ion contrast enhancement in excised canine hearts. *Circulation* **1982**;66:1012-1016
 19. Brasch RC, London DA, Wesbey GE, et al. Nuclear magnetic resonance study of a paramagnetic nitroxide contrast agent for enhancement of renal structures in experimental animals. *Radiology* **1983**;147:773-779
 20. Pople JA, Schneider WG, Bernstein HJ. *High-resolution nuclear magnetic resonance*. New York: McGraw-Hill **1959**:209
 21. Pauling L, Coryell CD. The magnetic properties and structure of hemoglobin, oxyhemoglobin and carbonmonoxyhemoglobin. *Proc Natl Acad Sci* **1936**;22:210-216
 22. Reuben J. Gadolinium (III) as a paramagnetic probe for protons relaxation studies of biochemical molecules. *Biochemistry* **1971**;10:2834-2838
 23. Arvela P. Toxicity of rare-earth. *Progr Pharmacol* **1979**;2:71-114
 24. Moeller T. *Gmelin Handbuch der anorganischen Chemie: rare earth elements, part D1*. Berlin: Springer-Verlag, **1980**
 25. Gries H, Rosenberg D, Weinmann HJ. Patent application DE-OS 3129906 A 1; **1981**
 26. Schwarzenbach G, Flaschka H. *Die komplexometrische Titration*. Stuttgart: Ferdinand Enke, **1965**:161-163
 27. Siefert HM, Press WR, Speck U. Tolerance to iohexol after intracisternal, intracerebral and intraarterial injection in the rat. *Acta Radiol [Suppl]* (Stockh) **1980**;362:77-81
 28. Levitan H, Rapoport SI. Contrast media: quantitative criteria for designing compounds with low toxicity. *Acta Radiol [Diagn]* (Stockh) **1976**;17:81-92
 29. Mützel W, Siefert HM, Speck U. Biochemical-pharmacologic properties of iohexol. *Acta Radiol [Suppl]* (Stockh) **1980**;362:111-115
 30. Poland H, Woloszczak R. A program library for computing models in pharmacokinetics. *Int J Biomed Comput* **1980**;2:115-128
 31. LaMar GN, Horrocks WD, Holm RH. *NMR of paramagnetic molecules: principles and application*. New York: Academic, **1973**:1-85
 32. James TL. *Nuclear magnetic resonance in biochemistry*. New York: Academic, **1975**:179
 33. Dwek RA. *Nuclear magnetic resonance (N.M.R.) in biochemistry*. Oxford: Clarendon, **1973**:174-284
 34. Lang JH, Lasser EC, Kolb WP. Activation of the complement system by x-ray contrast media. *Invest Radiol* **1976**;11:303-308
 35. Catsch A. Zur Toxikologie der Diaethylentriamine Pentaessigsäure. *Naunyn Schmiedebergs Arch Pharmacol* **1964**;246:316-329
 36. Fobben E, Wolf G. Gadolinium DTPA—a potential NMR contrast agent: effects upon tissue proton relaxation and cardiovascular function in the rabbit. Presented at the annual meeting of the Association of University Radiologists, Mobile, March **1983**

6.5 Contrast-enhanced NMR imaging: animal studies using gadolinium-DTPA complex

Robert C. Brasch (born 1944)

Dr. Brasch was born in St. Louis, Missouri, US, in 1944. He received his bachelor's degree from Miami University in Oxford, Ohio, and his medical degree from Washington University at St. Louis, Missouri. After an internship at the University Hospital in San Diego, California, he completed a residency in radiology at the University of California, San Francisco, where he was also a fellow and clinical instructor in paediatric radiology. In 1977 he earned the position of assistant professor in residence in radiology and from 1982 to 1986 held the position of associate professor in residence in radiology and paediatrics.

In 1986 he accepted his present position as professor in residence in radiology and paediatrics with the University of California San Francisco. Since 1981 he has been director of the Center for Pharmaceutical and Molecular Imaging (CPMI) of the same university, where he also is associate chief of paediatric radiology. In addition, Dr. Brasch has worked as a consultant to the Children's Cancer Study Group since 1980.

Throughout his illustrious career, Dr. Brasch has served on the editorial boards of numerous journals, including Radiology, Magnetic Resonance Imaging, Pediatric Radiology, Clinical MRI, Advances in NMR Contrast, Academic Radiology, and the Journal of Magnetic Resonance Imaging.

An active researcher and prolific writer, Dr. Brasch has published over 250 scientific articles. He dedicates 25 hours or more to research each week and focuses on investigations of cancer microvascular characteristics as defined quantitatively by contrast-enhanced MRI, investigations of wound healing as reflected in contrast-enhanced MRI, and investigations of the immunologic basis of severe adverse reactivity to iodinated radiographic contrast media, as well as on the discovery of novel contrast agents for optical imaging. Currently, Dr. Brasch is principal investigator on two competitively reviewed research grants. He is a reviewer for the American Journal of Roentgenology, the American Journal of Cardiology, Pediatrics, and nine other journals. He has delivered over 475 presentations over the past 20 years on various topics in radiology at both national and international scientific events. For 25 years he has welcomed visiting research fellows from around the world and most notably from Europe to join his laboratory team for one or two years to learn the basics and the joy of radiology research.

Dr. Brasch is a member of a variety of international, state and local societies including the American Roentgen Ray Society, the Radiological Society of North America, the Society for Pediatric Radiology, the European Congress of Radiology, and the European Society for Pediatric Radiology. He was awarded the Memorial Award of the Association of University Radiologists (1976), the James Picker Foundation Fellow in Radiology Research (1977), and the Harry Fischer Award of RSNA for excellence in Contrast Media Research (1997). He became Baker Visiting Professor to Australasian Congress in 1984 and Fellow of the American College of Radiology (1989). He was a recipient of the Caffey Award for Research by Society for Pediatric Radiology (1992 and 1997). He served on the editorial boards of Academic Radiology, Magnetic Resonance Imaging, Pediatric Radiology and JMRI. He has served on the organizing committee of the International Contrast Medium Research Symposium since 1981 and held offices



in many renowned state and local professional organizations. In 2001, Dr. Brasch was awarded honorary membership of the European Society of Pediatric Radiology.

Dr Brasch's scientific accomplishments and contributions to radiology training in the United States and worldwide are outstanding. In 2004 he was invited as Honorary Lecturer of the European Congress of Radiology and the European Association of Radiology to present the Marie Curie Honorary Lecture.

In parts excerpted from www.ecr.org

H.-J. Weinmann

see Chapter 6.3 on page 412

G.E. Wesbey

Contrast-Enhanced NMR Imaging: Animal Studies Using Gadolinium-DTPA Complex

Robert C. Brasch¹
Hanns-Joachim Weinmann²
George E. Wesbey¹

Gadolinium (Gd)-DTPA complex was assessed as a nuclear magnetic resonance (NMR) contrast-enhancing agent by experimentally imaging normal and diseased animals. After intravenous injection, Gd-DTPA, a strongly paramagnetic complex by virtue of unpaired electrons, was rapidly excreted into the urine of rats, producing an easily observable contrast enhancement on NMR images in kidney parenchyma and urine. Spin-echo intensity of urine within the renal pelvis increased from 2263 to 4414 units; intensity of renal parenchyma increased from 2901 to 3893 after administration of 0.1 mmol/kg Gd-DTPA. Sterile soft-tissue abscesses demonstrated an obvious rim pattern of enhancement. A focus of radiation-induced brain damage in a canine model was only faintly detectable on spin-echo NMR images before contrast administration; after 0.5 mmol/kg Gd-DTPA administration, the lesion intensity increased from 3867 to 5590. In comparison, the normal brain with an intact blood-brain barrier remained unchanged in NMR characterization. Gd-DTPA is a promising new NMR contrast enhancer for the clinical assessment of renal function, of inflammatory lesions, and of focal disruption of the blood-brain barrier.

Ions and molecules containing unpaired electrons demonstrate a paramagnetic behavior when placed in an external magnetic field. Strongly paramagnetic substances are potentially useful as contrast-enhancing agents for nuclear magnetic resonance (NMR) imaging because they hasten relaxation rates of protons in their microchemical environment; T1 and T2 values are shortened [1-5].

Gadolinium ions (Gd³⁺) from the lanthanide series of rare-earth elements contain seven unpaired electrons in the 4-f electron orbitals, a position well protected from chemical interactions with other atoms. These electrons provide gadolinium with strong paramagnetic properties [6]. Gd³⁺ can be chelated with diethylenetriaminepentaacetic acid (DTPA) to form a stable complex (Gd-DTPA) with a formation constant of 10²²⁻²³ [7]. The meglumine salt of Gd-DTPA after intravenous administration is rapidly excreted into the urine with a small proportion appearing in feces. The pharmacologic properties of Gd-DTPA including stability, pharmacokinetics, and tolerance are described in the accompanying article [4]; all these factors favor the further investigation of Gd-DTPA as an NMR contrast agent.

We describe imaging experiments testing Gd-DTPA as an intravenous contrast agent for proton NMR imaging in animals. The ability of Gd-DTPA to contrast-enhance normally functioning kidneys was studied in rats. The potential to alter the signal intensity of edematous inflammatory lesions of the soft tissues was studied in rats and a dog. The utility of Gd-DTPA to identify focal disruption of the blood-brain barrier was investigated in a dog with focal radiation-induced damage. Our purpose was to estimate the potential clinical utility of Gd-DTPA-enhanced NMR imaging.

Received July 7, 1983; accepted after revision November 14, 1983.

This work was supported in part by a grant from the National Institute of Arthritis, Diabetes, Digestive and Kidney Diseases, R01 AM31937.

¹Department of Radiology, University of California School of Medicine, San Francisco, CA 94143. Address reprint requests to R. C. Brasch (M-397).

²Research Laboratories of Schering, D-1000 Berlin 65, Germany.

AJR 142:625-630, March 1984
0361-803X/84/1423-0625
© American Roentgen Ray Society

Materials and Methods

NMR Imaging

NMR spin-echo (SE)-intensity images were obtained on a 0.35-T resistive NMR unit previously described [8]. The useful aperture for imaging was 6.5 cm in diameter. Five contiguous axial sections were obtained during a 7.0-min data acquisition period. Each slice was 4.2 mm thick and spatial resolution was 1.0×1.0 mm. TR (pulse) interval was either 500 or 1000 msec; TE (echo delay) was either 28 or 56 msec after the 90° radiofrequency (RF) pulse. The same imaging factors were used throughout the in vitro and rat imaging protocols. For each of the five axial sections, four spin-echo images were obtained designated as SE 500/28, SE 500/56, SE 1000/28, and SE 1000/56 (the numbers indicating TR/TE).

Mean intensity values, in arbitrary units of intensity related to the voltage of the received RF pulse, were determined for operator-defined regions of interest. Each region of interest contained at least 50 pixels. Pixel-to-pixel standard deviation in each region of interest was also calculated. The receiver gain setting and RF output were not altered between pre- and postcontrast images.

Imaging of Gadolinium-DTPA Solutions in vitro

Gadolinium-DTPA (Gd-DTPA) as a meglumine salt was prepared as previously described [4] and the 0.5 mol/L stock solution was diluted with distilled water for in vitro imaging. Series of 7.0-ml test tubes filled with distilled water or gadolinium-DTPA in concentrations of 0.01, 0.1, 0.3, 0.75, 1.0, 1.5, 2.0, 5.0, and 20.00 mol/L were grouped together for NMR imaging.

Urographic Imaging

NMR spin-echo-intensity images were obtained in a series of five normal Sprague-Dawley rats weighing 300–400 g. Gd-DTPA was tested as an intravenous contrast-enhancing agent by injection into tail veins of rats anesthetized with pentobarbital (50 mg/kg intraperitoneal). SE images through the level of the kidneys were obtained before and at 5, 12, 30, 60, and 90 min after Gd-DTPA injection. The doses of Gd-DTPA ranged from 0.01 to 1.0 mmol/kg. Intensity region-of-interest measurements permitted the assessment of contrast enhancement within the renal parenchyma and within the urine.

Experimental Abscess Imaging

Sterile inflammatory lesions ("abscesses") were induced in the subcutaneous tissues of three Sprague-Dawley rats at the level of the kidneys by injecting 0.4 ml of carrageenan (0.1% wt/vol) by a modification of the method of Winter et al. [9]. Local reaction to this mucopolysaccharide was allowed to develop over 4 hr. Then rats were imaged by NMR before and up to 120 min after intravenous injection of 0.1 or 1.0 mmol/kg Gd-DTPA. Carrageenan previously has been shown to produce an edematous pathologic lesion within soft tissues, reaching a peak effect in 3–5 hr [9].

Radiation Cerebritis Imaging

A small focus of radiation-induced cerebritis was induced in a 7 kg beagle by surgical implantation of a ^{125}I seed directly into the right cerebral cortex for a 48-hr period [10]. The calculated radiation dose to brain tissue 1 cm from the center of the seed was 1500 rad (15 Gy). Seven days after extraction of the radioactive seed, the dog, anesthetized again by intravenous pentobarbital, was imaged using a 0.35 T superconducting NMR system previously described [11].

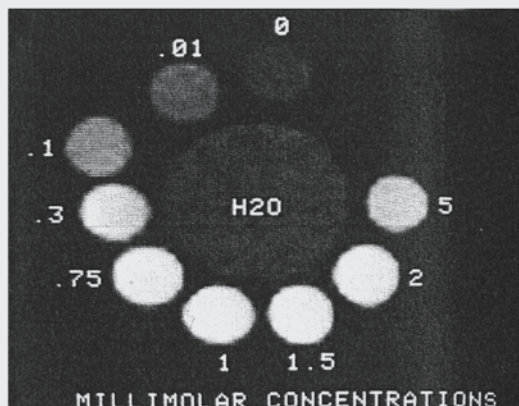


Fig. 1.—SE 500/28 NMR images of aqueous solutions of Gd-DTPA. Highest intensity was observed at concentration of 1.5 mmol/L. Not visible is 20 mmol/L sample, which gave no detectable signal due to very short T2 relaxation time, less than 28 msec.

From 500 and 1500 msec TR spin-echo images, we calculated T1 and T2 images of the dog brain [12]. The NMR imaging sequences were performed before and up to 40 min after administration of 0.5 mmol/kg Gd-DTPA. The injection was made slowly over 60 sec. Four data acquisitions at 500 msec TR were begun at 5, 10, 20, and 25 min after injection. A data acquisition at 1500 msec TR was begun 32 min after injection. An external reference solution, iron dextran, was placed in the imaging field to serve as a standard for consistency of pre- and postcontrast intensity and T1 and T2 values.

The pathology induced by the ^{125}I seed in this model has been described [10] and was reconfirmed in this animal. Briefly, a non-inflammatory area of necrosis was seen within the white matter with loss of nuclei and with axonal swelling. Adjacent vessels showed protein-rich fluid in the perivascular and interstitial spaces.

Results

Imaging of Gd-DTPA Solutions in vitro

The 1.5 mmol concentration of Gd-DTPA produced the highest NMR intensity signal ($12,123 \pm 463$) compared with the baseline intensity of distilled water (2172 ± 325) (fig. 1). Intensity was also enhanced for the 0.01 mmol solution (2428 ± 367) and the 0.1 mmol solution (5335 ± 384). The 20.0 mmol solution of Gd-DTPA had no observable signal and appeared black on SE images. This observation is compatible with a very short T2 relaxation time. A similar decrease in spin-echo intensity has been observed with other paramagnetic agents, ferric ions and nitroxide free radicals, in high concentrations [2, 13].

Renal Imaging

In the series of normal rats, the nonenhanced kidneys appeared as intermediate-intensity structures outlined by high-intensity perinephric fat. The central collecting structures

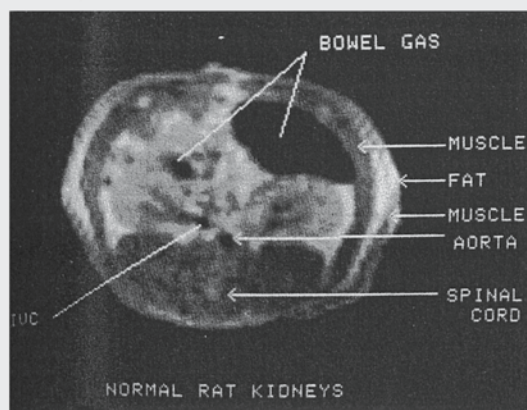


Fig. 2.—SE 500/28 NMR image of normal rat abdomen and retroperitoneum. Low intensity of nonenhanced urine in renal pelvis. Vascular structures with rapidly flowing blood, such as inferior vena cava (IVC), have even lower intensity than urine.

were seen to contain low-intensity urine (fig. 2). These observations agree with those previously reported [3, 14] (table 1).

At 5 min after administration of Gd-DTPA in a dose of 0.1 mmol/kg (the first image), there was an increase in renal parenchymal SE 500/28 intensity that reached a maximum of 3893 ± 562 after 10 min. By 90 min, the contrast agent was still evident within the kidney and renal intensity was 3517 ± 517 . Accompanying the increase in renal parenchymal intensity, the urine within the renal collecting structures became much higher in intensity, appearing white (fig. 3).

A lowest effective urographic dose of Gd-DTPA was not determined from this series of animals because the lowest tested dose (0.01 mmol/kg) produced marked contrast enhancement (fig. 4) within the urine. The parenchyma did not enhance significantly at this dose (<1 SD). Conversely, at the highest tested dose (1.0 mmol/kg), there was evidence of prompt renal excretion and diuretic effect; the renal calices became markedly distended (fig. 5). However, with this higher dose, the urine intensity decreased to lower than baseline intensity at 5 min. This observation, corresponding to the *in vitro* observations of concentrations approximating 20 mmol/L, indicates marked shortening of T2 relaxation times. Such marked T2 shortening is predictable from the spectrometric results noted for high concentrations of Gd-DTPA [4]. The same rat, by 85 min after administration, presumably when Gd-DTPA was more dilute within the urine, had increased SE intensity in the renal pelvis and parenchyma (table 1).

Experimental Inflammation Imaging

The NMR images of flank inflammatory lesions induced by carrageenan were strongly enhanced after intravenous administration of 0.1 mmol/kg Gd-DTPA (fig. 6). The 5-min image revealed a rim pattern of enhancement that filled in completely by 35 min. This change suggests a gradual accumulation of

TABLE 1: NMR Characterization of *in vivo* Rat Renal Compartments before and after Gd-DTPA Administration

Dose of Gd-DTPA (mmol/kg): Renal Compartment	SE 500/28 Intensity \pm SD		Time of Intensity Measurement (min)
	Before Contrast	After Contrast	
1.0:			
Parenchyma . . .	3509 ± 396	2355 ± 472	5
Urine	2703 ± 297	4089 ± 384	85
		1197 ± 416	5
		3819 ± 886	85
0.1:			
Parenchyma . . .	2901 ± 412	3893 ± 562	10
Urine	2264 ± 490	4414 ± 533	10
0.05:			
Parenchyma . . .	3261 ± 896	3783 ± 527	5
Urine	2902 ± 314	4670 ± 573	5
0.01:			
Parenchyma . . .	3890 ± 938	3934 ± 690	60
Urine	2943 ± 391	4281 ± 484	5

Gd-DTPA within the edematous inflammatory lesion; this effect may be due to the gradual diffusion of the paramagnetic complex from the plasma into the expanded interstitial space. Normal soft tissues in the contralateral flank and the ipsilateral muscles did not change significantly in intensity. The higher dose (1.0 mmol/kg) of Gd-DTPA similarly produced a marked increase in SE intensity within carrageenan-induced lesions for up to 120 min after injection.

Radiation-Induced Cerebritis

The focal area of radiation damage in the right cerebral hemisphere of a dog induced by a ^{125}I seed was barely perceptible as a low-intensity (3867 ± 316 , SE 500/28) zone on the nonenhanced NMR spin-echo images. A large soft-tissue swelling over the calvaria at the site of craniotomy was lower in intensity than cerebral tissues (fig. 7).

On all SE images at 5–32 min after intravenous injection of 0.5 mmol/kg Gd-DTPA, there was an obvious intensity increase at the site of radiation damage. The accumulation of contrast agent can be assumed to result from focal disruption of the blood-brain barrier. The maximum SE 500/28 intensity increase (5590 ± 628) was observed at 25 min. The external reference standard, iron dextran, gave internally consistent SE 500/28 intensity values (mean $12,495 \pm 35$) for the five acquisitions at 500 msec TR.

Similar to the carrageenan-induced flank abscesses, the surgical scalp lesion showed a rim pattern of enhancement after Gd-DTPA.

T1 images, calculated from SE 500/28 and SE 1500/28 data, demonstrated that the right cerebral lesion before contrast had a relatively long T1 value (747 ± 107 msec) as compared with the contralateral normal brain (650 ± 112 msec) (fig. 8). A corresponding T1 image 34 min after Gd-DTPA administration (fig. 8) showed shortening of T1 to 633 ± 132 msec in the core of the lesion, suggesting accumulation of the paramagnetic contrast agent. Yet, adjacent to the zone of T1 shortening, a rim of persistently long T1 tissue ($729 \pm$

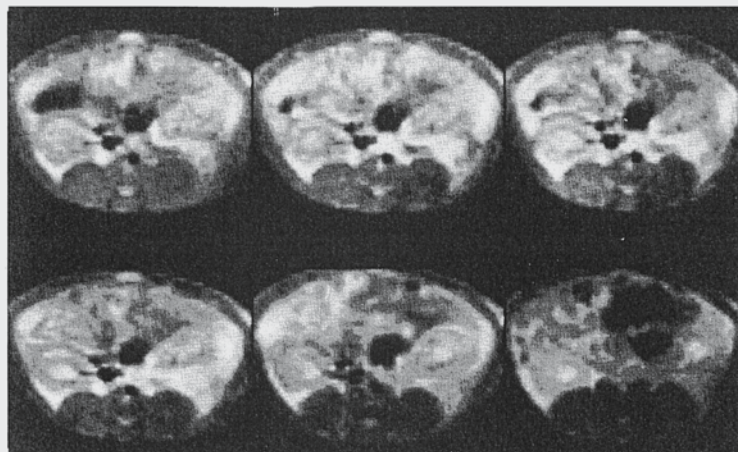
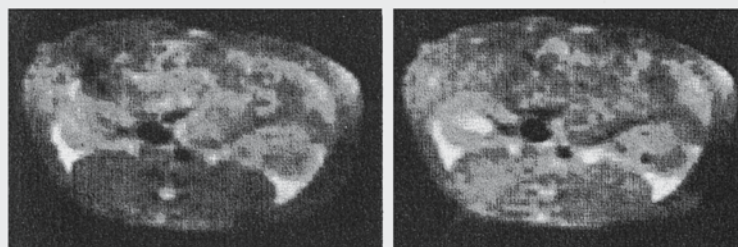


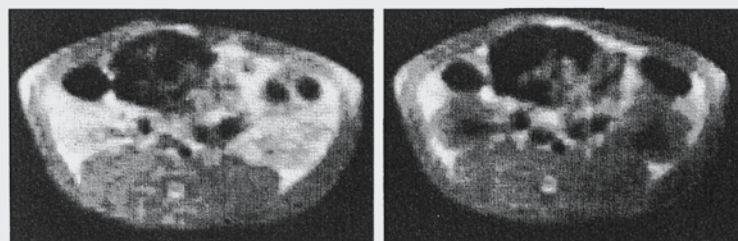
Fig. 3.—SE 500/28 NMR images of one rat arranged in temporal order (left to right, top to bottom) before intravenous administration of 0.1 mmol/kg Gd-DTPA and 5, 10, 30, 60, and 90 min after administration. Increased intensity of renal parenchyma and urine after Gd-DTPA administration (see table 1).



A

B

Fig. 4.—SE 1000/28 NMR images of rat before (A) and 5 min after (B) intravenous administration of Gd-DTPA (0.01 mmol/kg). High signal intensity in kidneys and urine after contrast.



A

B

Fig. 5.—SE 1000/28 NMR images of rat kidneys before (A) and 5 min after (B) administration of 1 mmol/kg Gd-DTPA. Urine in distended renal pelvis after injection is very low in intensity, attributable to marked shortening of T2 with high dose of contrast agent. Renal parenchyma is also lower in intensity (see table 1).

95 msec) was observed. This peripheral zone of tissue with long T1 is suggestive of an edematous zone without significant accumulation of paramagnetic contrast agent. The T1 time of the normal left cerebral hemisphere remained essentially unchanged 34 min after Gd-DTPA administration (625 ± 107 msec). The calculated T1 time of external standard solution was near constant, less than 0.5% difference between the two calculations.

Discussion

Results indicate that Gd-DTPA complex, administered intravenously to animals in experiments, accumulates in urine and certain diseased tissues to enhance intensity and increase contrast on spin-echo NMR images. Because of the rapid urinary clearance of Gd-DTPA, more than 85% of the injected dose appearing in the urine within 3 hr [4], the status

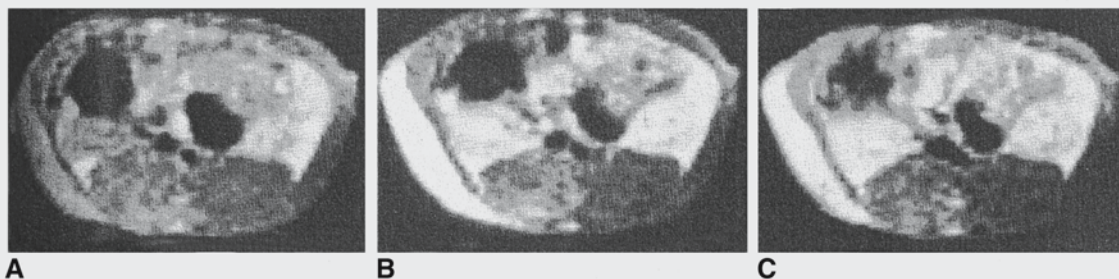


Fig. 6.—SE 500/28 NMR images of rat with chemically-induced right flank abscess. **A**, Before contrast administration. Soft-tissue thickening and relatively high signal intensity compared with contralateral flank. **B**, 5 min after intrave-

nous injection of 0.1 mmol/kg Gd-DTPA. Marked intensity increase within abscess, predominately in rim pattern. **C**, At 35 min. Gd-DTPA has reached core of abscess, producing more enhancement.

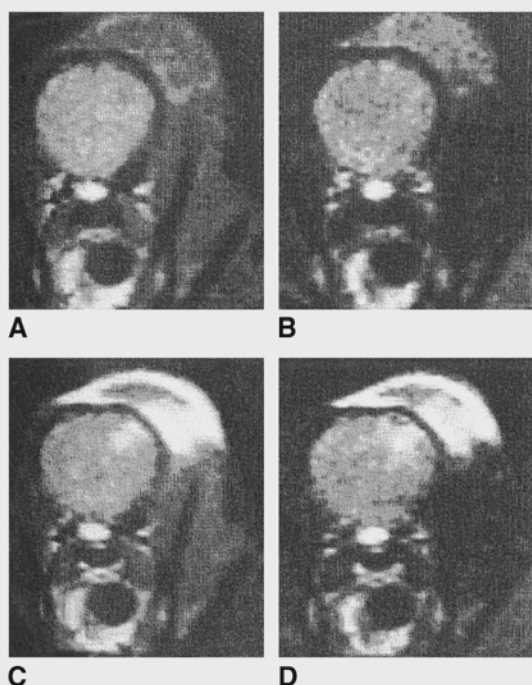


Fig. 7.—Precontrast SE 500/28 (**A**) and SE 1500/28 (**B**) NMR images of rat with focal radiation-induced cerebritis demonstrated as faintly lower-intensity region in **A**. Edematous surgical wound in soft tissues overlying brain lesion. **C**, SE 500/28 image 25 min after 0.5 mmol/kg Gd-DTPA given intravenously. **D**, SE 1500/28 image 7 min after **C**. Marked postcontrast signal-intensity enhancement at site of radiation-induced cerebritis and in scalp wound.

of renal functional integrity should be assessable by Gd-DTPA-enhanced NMR imaging. Additional studies in animals with renal functional abnormalities need to be performed to assess more completely the sensitivity of Gd-DTPA-enhanced NMR urography.

The ability to contrast-enhance sterile inflammatory lesions, induced either by a chemical irritant or by surgery, is another clinically important property of the Gd-DTPA complex. From our observations it seems likely that Gd-DTPA distributes primarily in the intravascular, extracellular space and quickly passes into the extravascular, interstitial space. A similar pattern of distribution is well established for diatrizoate, a commonly used radiographic contrast agent having a molecular weight of about 600. By comparison, the molecular weight of Gd-DTPA complex is 590. The composition of interstitial fluid within tissues is very similar to the plasma within the vascular compartment. Both fluids have rather long T1 relaxation times and yield low signal intensities on NMR images compared with the signal from highly cellular tissues. We postulate that after intravenous injection, Gd-DTPA in the plasma diffuses into the extravascular, interstitial space and thus will conspicuously enhance tissues with a high proportion of interstitial fluid (e.g., edematous tissue). Conversely, tissues with a relatively large cellular part and small interstitial part would be expected to contain a relatively smaller concentration of Gd-DTPA and thus to demonstrate little or no enhancement on NMR images.

The ability of Gd-DTPA to contrast-enhance selectively a pathologic focus within the brain is perhaps the most clinically significant of the potential applications demonstrated. The results of our study, limited to one animal with focal radiation cerebritis, suggest that Gd-DTPA contrast enhancement may aid in the differentiation of necrotic tissue from surrounding edema. Before clinical trials, a variety of central-nervous-system-disease animal models should be tested with Gd-DTPA NMR imaging.

The diagnostically effective intravenous doses of Gd-DTPA used in this study (0.01–0.5 mmol/kg) are far less than the LD₅₀ dose in rats (10 mmol/kg) [4]. In future imaging tests, using smaller Gd-DTPA doses, the ratio between LD₅₀ and lowest diagnostically useful doses may even be greater than the 1000:1 ratio suggested here.

In summary, testing of Gd-DTPA as an NMR contrast-enhancing agent indicates that this paramagnetic complex can be used effectively in animals for a variety of diagnostic

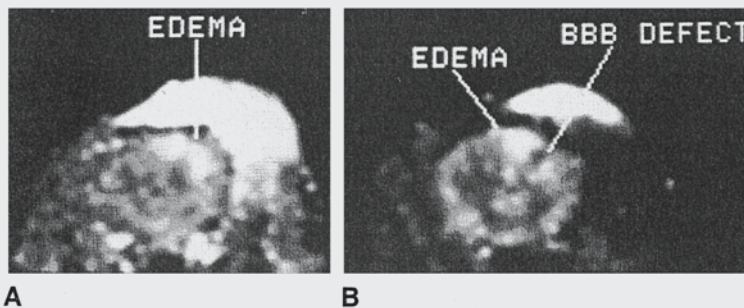


Fig. 8.—T1 images of same dog shown in fig. 7 calculated from SE intensity data. Long T1 values are depicted as white; short T1 values are relatively black on gray-scale assignments. A, Before contrast. Long T1 value of cerebral and soft-tissue lesions. B, 34 min after administration of 0.5 mmol/kg Gd-DTPA. Postcontrast T1 shortening in center of cerebral lesion (blood-brain barrier [BBB] defect) is shown as black area. Surrounding zone of white indicates region of persistently long T1, presumably zone of edema without significant accumulation of paramagnetic agent.

purposes. Gd-DTPA is strongly paramagnetic, is rapidly excreted, can be prepared from readily available materials, is not metabolized in the body, and was well tolerated in our small group of animals. Gd-DTPA, used clinically in patients after appropriate trials, may extend the diagnostic utility of NMR imaging examinations.

ACKNOWLEDGMENTS

We thank John R. Fike and Christopher E. Cann for assistance in preparing the model of cerebral radiation necrosis, and Frank Gorham for help in manuscript preparation.

REFERENCES

- Eisinger J, Shulman RC, Blumberg WF. Relaxation enhancement by paramagnetic ion binding in deoxyribonucleic acid solutions. *Nature* **1961**;192:963-966
- Brasch RC. Methods of contrast enhancement for NMR imaging and potential applications. *Radiology* **1983**;147:781-788
- Brasch RC, London DA, Wesbey GE, et al. Nuclear magnetic resonance study of a paramagnetic nitroxide contrast agent for enhancement of renal structures in experimental animals. *Radiology* **1983**;147:773-779
- Weinmann JH, Brasch RC, Press WR, Wesbey GE. Characteristics of gadolinium DTPA: a potential NMR contrast agent. *AJR* **1984**;142:619-624
- Mendonça-Dias MH, Gaggelli E, Lauterbur PC. Paramagnetic contrast agents in NMR medical imaging. *Semin Nucl Med* **1983**;13:364-376
- Pople JA, Schneider WG, Bernstein HJ. *High-resolution nuclear magnetic resonance*. New York: McGraw-Hill, **1959**:209
- Moeller T. *Gmelin Handbuch der anorganischen Chemie: rare earth elements, Part D1*. Berlin: Springer-Verlag, **1980**
- Crooks L, Hoenninger J, Arakawa M, et al. Tomography of hydrogen with nuclear magnetic resonance. *Radiology* **1980**;136:701-706
- Winter CA, Risley ED, Nuss GW. Carrageenin-induced edema in the hind paw of rats as an assay for antiinflammatory drugs. *Proc Soc Exp Biol Med* **1962**;111:544-547
- Fike JR, Cann CE, Bernstein M, et al. Radiation damage to the canine brain after ^{125}I implantation. *Radiat Res* **1982**;91:370-375
- Crooks L, Arakawa M, Hoenninger J, et al. Nuclear magnetic resonance whole-body imager operating at 3.5 KGauss. *Radiology* **1982**;143:169-174
- Herfkens R, Davis P, Crooks L, et al. Nuclear magnetic resonance imaging of the abnormal live rat and correlations with tissue characteristics. *Radiology* **1981**;141:211-218
- Wesbey GE, Brasch RC, Engeklstad BL, Moss AA, Crooks LE, Brito AC. Nuclear magnetic resonance contrast enhancement study of the gastrointestinal tract of rats and a human volunteer using nontoxic oral iron solutions. *Radiology* **1983**;149:175-180
- Hansen G, Crooks LE, Davis P, et al. In vivo imaging of the rat anatomy with nuclear magnetic resonance. *Radiology* **1980**;136:695-700

7 Angiography and Interventional Radiology

- 7.1** Catheter replacement of the needle in percutaneous arteriography: A new technique. 437
Acta radiol. 39 (1953): 368–376
S.I. Seldinger
- 7.2** Percutaneous trocar (needle) nephrostomy in hydronephrosis. 447
JAMA (1955) 157: 891–894
W.E. Goodwin, W.C. Casey, W. Woolf
- 7.3** Cine coronary arteriography. 452
Circulation 20 (1959): 773–774
F.M. Sones, E.K. Shirey, W.L. Proudfit, R. Westcott
- 7.4** Mesenteric Arteriography. 455
Am J Roentgenology 86 (1961): 103–113
A.R. Margulis, P. Heinbecker
- 7.5** Transluminal treatment of arteriosclerotic obstruction: description of a new technique and a preliminary report of its application. 467
Circulation 30 (1964): 654–670
C.T. Dotter, M.P. Judkins
- 7.6** Selective coronary arteriography. 485
Radiology 89 (1967): 815–824
M.P. Judkins
- 7.7** Non-operative retained biliary tract stone extraction. 496
A new roentgenologic technique.
Am J Roentgenology (1973) 117 (2): 388–399
H.J. Burhenne
- 7.8** Perkutane Rekanalisation chronischer arterieller Verschlüsse mit einem neuen Dilatationskatheter. 509
Dtsch. Med. Wschr. 99 (1974): 2502–2505
A.R. Grüntzig, H. Hopff
- 7.9** Transluminal dilatation of coronary-artery stenosis. 514
Lancet ii (1978): 263
A.R. Grüntzig
- 7.10** Percutaneous biliary drainage, technical and catheter related problems in 200 procedures. 516
Am J Roentgenology (1982) (Jan) 138 (1): 17–23
P.R. Mueller, E. van Sonnenberg, J.T. Ferrucci

-
- | | | |
|-------------|---|-----|
| 7.11 | Expandable intrahepatic portacaval shunt stents:
early experience in the dog.
Am J Roentgenology (1985) 145: 821–825
<i>J.C. Palmaz, R.R. Sibbitt, S.R. Reuter et al.</i> | 525 |
| | | |
| 7.12 | Intravascular stents to prevent occlusion
and restenosis after transluminal angioplasty.
NEJM 316 (1987): 701–706
<i>U. Sigwart, J. Puel et al.</i> | 531 |

Interventional Radiology

The subject of interventional radiology developed soon after the discovery of X-rays and continued unabated throughout the last century. The term interventional radiology itself was coined by Margulis in 1967 to describe the growing body of manipulative procedures performed by a physician skilful in radiological techniques and experienced in the clinical problems.

Interventional radiology really began in the 1920s and the first use was in the treatment of intussusception in children. In 1921 Burckhardt and Muller reported on the percutaneous puncture of the gallbladder both in cadavers and in vivo.

In 1929 the first documented human cardiac catheterization was performed by Dr Werner Forssman in Eberswalde, Germany. In 1941 Cournand and Richards employed the cardiac catheter as a diagnostic tool for the first time and used cardiac catheterization to measure cardiac output. These three pioneering researchers were awarded the Nobel Prize in 1956.

In 1953, Seldinger described a new method of angiography using catheters rather than the direct needle itself. This opened up the way for pioneering work in angiography throughout the latter half of the 20th century. Odman, Tillander and Edholm performed pioneering early studies on selective angiography soon after Seldinger's original description and these techniques were introduced around the world by the pioneers in their respective countries.

The diagnostic coronary angiogram was pioneered by the labors of Dr Mason Sones in 1958. This led to the concept of dilating the tubes and in 1964 transluminal angioplasty was introduced by Dr Charles T. Dotter. Meanwhile Dr Judkins introduced his catheters for the performance of coronary angiography in 1967. In 1974 Dr Andreas Gruentzig performed the first peripheral human balloon angioplasty. In 1976 Dr Gruentzig presented the results of his animal studies of coronary angioplasty at the American Heart Association meeting, where the delegates soon realized that this was a very important new technique. In 1977 Andreas Gruentzig performed the first percutaneous transluminal coronary angioplasty on an awake patient in Zurich. In 1978 Myler in San Francisco and Streutzer in New York performed the first cases in the United States. Intravascular coronary stents were reported in the 1980s, with an important contribution made by U. Sigwart. The use of stents in the peripheral vasculature had been pioneered by the studies of Palmaz and Strecker. The first stents developed by Dotter were made of nitinol. Gianturco introduced his self-expandable Z stent, Strecker a knitted tantalum stent and Palmaz a balloon expandable stent. Today insertion of stents in the peripheral vascular system is routinely performed after angioplasty in order to keep the vessels patent.

In the biliary system percutaneous transhepatic cholangiography was first described in 1937. Extraction of retained common duct stones was reported in 1962 by Mondet. Burhenne, however, built up a formidable experience with this particular technique with a success rate of 95% in 661 patients treated between 1972 and 1979. Stents were used in the biliary system as early as 1978. Today they are used in the peripheral vascular system through the shunts, in the tracheo-bronchial tree for stenosis from tumour, in the biliary tract for stenosis from tumours and in the urinary tract for urethral strictures and ureteric strictures.

Interventional radiological techniques for drainage of abscesses under ultrasound control were pioneered by Smith and Bartrum in 1974. CT-guided abscess drainage and image-guided biopsies were subsequently introduced by many workers, including Van Sonnenberg and his team, and have now become routine radiological practice.

Pioneering advances in interventional techniques continue unabated, and in a short introduction such as this it is not possible to do justice to all the innovators who have contributed to the development of image-guided therapeutic maneuvers.

References

- Burckhardt H, Muller W (1921) Versuche über die Punktion der Gallenblase und ihre Röntgendarstellung. *Deutsche Zeitschrift für Chirurgie* 162: 168-197
The first report of the percutaneous puncture of the gallbladder
- Huard P, Do-Xuan-Hope (1937) La ponction transhepatique des canaux biliares. *Bull Soc Med Chir de l'Indochine* 15: 1090-1100
First report of percutaneous transhepatic cholangiography
- Mondet A (1962) Tecnica de la extraccion incruenta de los calculos en la litiasis residual del coledoco. *Bol Soc Cir B Aires* 46: 278-290
Early report of retained common bile duct stone extraction through a t-tube
- Burhenne HJ (1980) Garland Lecture. Percutaneous extraction of retained biliary tract stones: 661 patients. *AJR* 134: 888-898
Large series of biliary stone extraction percutaneously
- Burhenne JH (1974) Nonoperative roentgenologic instrumentation techniques of the post-operative biliary tract: Treatment of biliary stricture and retained stones. *Am J Surg* 128: 111-117
- Burcharth F (1978) A new endoprosthesis for nonoperative intubation of the biliary tract in malignant obstructive jaundice. *Surg Gynecol Obstet* 146: 76
First report of endoprosthesis for biliary drainage
- Carrasco CH, Wallace S, Charnsangavej C, et al. (1985) Expandable biliary endoprosthesis: An experimental study. *AJR* 145: 1279
Early experimental study on biliary endoprosthesis
- Coons HG (1983) Carey PH Large bore long biliary endoprosthesis (biliary stents) for improved drainage. *Radiology* 148: 89-94
Early study of stent placements with 71 Teflon stents placed in 62 patients
- Coons HG (1989) Self-expanding stainless steel biliary stents. *Radiology* 173: 979-983
A series of 30 patients with Gianturco stents in the bile ducts showed good results, especially in benign strictures
- Lammer J, Neumayer K (1985) Biliary drainage endoprosthesis: experience with 201 placements. *Radiology* 159: 625
Series showing low complication rates
- Dick R, Gillams A, Dooley JS, et al. (1989) Stainless steel mesh stents for biliary strictures. *J Intervent Radiol* 4:95-98
- Irving JD, Adam A, Dick R, Dondelinger RF, Lunderquist A, Roche A (1989) Gianturco expandable metallic stents: results of a European clinical trial. *Radiology* 172: 321-326
One of the first trials of transhepatic biliary endoprosthesis insertion
- Goodwin WE, Casey WC, Wolf W (1955) Percutaneous trocar (needle) nephrostomy in hydronephrosis. *Jama* 157: 891-894
The first description of a series of percutaneous nephrostomies. Thomas Hillier from London in 1865 is credited with having done repeated nephrostomies in a four year old boy to drain abscesses although this was largely forgotten till the middle of the twentieth century
- Odman P (1956) Percutaneous selective angiography of the main branches of the aorta (preliminary report) *Acta Radiologica* 45: 1-14
- Edholm P, Seldinger SI (1956) Percutaneous catheterisation of the renal artery. *Acta Radiologica* 45: 15-20
- Tillander H (1956) Selective angiography of the abdominal aorta with a guided catheter. *Acta Radiologica* 45: 21-26
The above three papers were pioneering studies in selective angiography which followed on from Seldinger's original description

- Dotter CT (1969) Transluminally placed coilspring endoarterial tube grafts: long-term patency in canine popliteal artery. *Invest Radiol* 4: 329-332
One of the first animal experimental papers on the feasibility of intravascular procedures.
- Dotter CT, Buschmann RW, McKinney MR, Rosch J (1983) Transluminal expandible nitinol coil stent grafting: preliminary report. *Radiology* 147: 259-260
Early contribution to the subject of stenting by the father of interventional radiology.
- Palmaz JC, Sibbitt PR, Reuter SR et al. (1985) Expandable intraluminal graft: preliminary study. *Radiology* 156: 73-77
Important early study on vascular stents
- Sigwart U, Puel J, Mirkovitch V et al. (1987) Intravascular stents to prevent occlusion and restenosis after transluminal angioplasty. *NEJM* 316: 701-706
The first study on intracoronary stents
- Cragg AH, Lund G, Rysavy JA et al. (1984) Percutaneous arterial grafting. *Radiology* 150: 45-49
- Parodi JC, Palmaz JC, Barone HD (1991) Transfemoral intraluminal graft implantation for abdominal aortic aneurysms. *Ann Vasc Surg* 5: 491-499
Pioneering study on intraarterial stent repair of aortic aneurysm
- Wallace MJ, Charnsangavej C, Ogawa K et al. (1986) Tracheo-bronchial tree: expandable metallic stents used in experimental and clinical applications. Work in progress. *Radiology* 158: 309-312
Early report on tracheo-bronchial stents
- Fabian KM (1980) Der intraprostatiche "Partielle Katheter" (Urologische spirale). *Urologe A* 19: 236-238
Early paper on intraprostatic stenting
- Mobin-Uddin K, Smith PE, Martinez LO et al. (1967) A vena cava filter for the prevention of pulmonary embolus. *Surg Forum* 18: 209-211
Early paper on vena cava filters
- Gianturco C, Anderson JH, Wallace S (1975) Mechanical devices for arterial occlusion. *AJR* 124: 428-435
One of the first reports of embolization as a means of treating bleeding vessels
- Halasz NA, van Sonnenberg E (1987) Drainage of intra-abdominal abscesses. Tactics and choices. *Am J Surg* 146 (1): 112-5
Early studies of radiological techniques of abscess drainage
- Strecker EP, Liermann DD, Berth KH et al. (1989) Expandable tubular tantalum stents for treatment of arterial occlusive disease with specific reference to the iliac arteries. *Radiology* 173: 268
Early study on arterial stents in the peripheral vascular system.
- Gunther RW, Vorwerk D, Bohndorf K et al. (1989) Iliac and femoral artery stenosis and occlusion- treatment with intravascular stents. *Radiology* 172: 725-30
A pioneering study on peripheral vascular stents
- Nusbaum M, Baum S (1963) Radiographic demonstration of unknown sites of gastrointestinal bleeding. *Surgical Forum* 14: 374-375
Early description of selective arterial catheterisation to demonstrate bleeding.
- Viamonte JR (1964) Selective bronchial arteriography in man – a preliminary report. *Radiology* 830-839
First report of selective bronchial arteriography.
- Baum S, Nusbaum M (1971) The control of gastrointestinal haemorrhage by selective mesenteric arterial infusion of vasopressin. *Radiology* 98: 497-505
First report on pharmacoangiography
- Johnson AJ, McCarty WR (1959) The lysis of artificially induced intravascular clots in man by intravenous infusions of streptokinase. *J Clin Investigation* 38: 1627-1643
First description of intravenous thrombolysis
- Dotter CT, Buschmann RW, McKinney MR, Rosch J (1983) Transluminal expandible nitinol coil stent grafting: preliminary report. *Radiology* 147: 259-260
Early contribution to the subject of stenting by the father of interventional radiology.

Cragg AH, Lund G, Rysavy JA et al. (1983) Nonsurgical placement of arterial endoprosthesis: a new technique using nitinol wire. *Radiology* 147: 261-263

Early paper on vascular stenting

Cragg AH, Lund G, Rysavy JA et al. (1984) Percutaneous arterial grafting. *Radiology* 150: 45-49

Parodi JC, Palmaz JC, Barone HD (1991) Transfemoral intraluminal graft implantation for abdominal aortic aneurysms. *Ann Vasc Surg* 5: 491-499

Pioneering study on intraarterial stent repair of aortic aneurysms

Wallace MJ, Charnsangavej C, Ogawa K et al. (1986) Tracheo-bronchial tree: expandable metallic stents used in experimental and clinical applications. Work in progress. *Radiology* 158: 309-312

Early report on tracheo-bronchial stents

Fabian KM (1980) Der intraprostatische "Partielle Katheter" (Urologische spirale). *Urologe A* 19: 236-238

Early paper on intraprostatic stenting

Mobin-Uddin K, Smith PE, Martinez LO et al. (1967) A vena cava filter for the prevention of pulmonary embolus. *Surg Forum* 18: 209-211

Early paper on vena cava filters

Gianturco C, Anderson JH, Wallace S (1975) Mechanical devices for arterial occlusion. *AJR* 124: 428-435

One of the first reports of embolization as a means of treating bleeding vessels

Holm HH, Rasmussen SN, Kristensen JK (1973) Ultrasonically guided percutaneous puncture technique. *Clinical Ultrasound* 1: 27-31

Early paper on the use of ultrasound to guide interventional procedures

Smith EH, Bartrum RJ (1974) Ultrasonically guided percutaneous aspiration of abscesses. *AJR* 122: 308-312

Early report of use of ultrasound to guide abscess drainage

Halasz NA, van Sonnenberg E (1987) Drainage of intra-abdominal abscesses. Tactics and choices. *AM J Surg* 146 (1): 112-115

Early studies of radiological techniques of abscess drainage

Haaga JR, Alfidi RJ (1976) Precise biopsy localisation by CT. *Radiology* 118: 603-607

One of the earliest reports of CT-guided biopsy

7.1 Catheter replacement of the needle in percutaneous arteriography: A new technique

Sven Ivar Seldinger (1921–1998)

Sven-Ivar Seldinger was born in Mora, Sweden on 19 April 1921. He graduated in medicine from the Karolinska Institute in Sweden in 1948 and started his training in radiology in 1950. In 1953 he published his classic description of his percutaneous entry technique into arteries in the journal *Acta Radiologica*. The technique involved a thin-walled introducer needle and a wire and a plastic catheter. Using this particular technique it was possible to access any part of the body via the cardiovascular system. Dr Seldinger's technique was important in that it enabled angiography to develop with superspecialization and techniques such as selective angiography and embolization became a possibility. The simplicity of Seldinger's technique not only revolutionized cardiology but also enabled people to perform percutaneous transhepatic procedures and portal venography as well as using the technique to drain abscesses. It has found its use in urology and anesthesia and critical care medicine; central lines and pacemakers are all now put in using this particular technique. Seldinger's thesis was entitled 'Percutaneous transhepatic cholangiography' and was defended in 1966. He catheterized the biliary ducts using his techniques. In 1967 he returned to Mora to become chief of the radiology department of the local hospital. It is interesting that the pioneering technique was not initially thought of as important.

His chief of the department of radiology at the Karolinska Institute, however, did not think that his invention of the new technique was enough for the basis of a thesis and this why he had to start his second project on the development of percutaneous cholangiography.

Herbert Abrahams wrote the following about Seldinger's contributions:

"In the movement of angiography from the part of a bit-player to that of a protagonist in the scenario diagnostic medicine, probably no single contribution has weighed more heavily than the technique developed by Sven Seldinger. To a major degree its elegance and its usefulness lie in its very simplicity and although Seldinger has been modest about his contribution, it took both ingenuity and creativity to lead angiography into a new period and a new arena. All of us in radiology acknowledge our great debt to Seldinger for his vision. His contribution moved the field into a new and exciting direction and left a permanent imprint on medical imaging and diagnostic and therapeutic medicine." Sven-Ivar Seldinger died in his home in Mora on 21 February 1998.



FROM THE ROENTGEN DIAGNOSTIC DEPARTMENT (DIRECTOR: PROFESSOR KNUT LINDBLOM),
KAROLINSKA SJUKHUSET, STOCKHOLM, SWEDEN

CATHETER REPLACEMENT OF THE NEEDLE IN PERCUTANEOUS ARTERIOGRAPHY

A new technique

by

Sven Ivar Seldinger

The catheter method of angiography has become more popular in the past few years, as it provides the following advantages over the method of injecting the contrast medium by means of a simple needle:

- 1) The contrast medium may be injected into a vessel at any level desired.
- 2) Risk of extravascular injection of the contrast medium is minimised.
- 3) The patient may be placed in any position required.
- 4) The catheter may be left in situ without risk while the films are being developed, thus facilitating re-examination if necessary.

Until recently, however, the use of the catheter method was restricted because of the lack of a suitable flexible thin-walled catheter which could be used percutaneously. FARIÑAS, in 1941, described a method in which a urethral catheter was passed up into the aorta through a trocar inserted in the exposed femoral artery. In 1947, RADNER catheterized the exposed and ligated radial artery and performed vertebral angiography and later thoracic aortography. Since then, many authors have catheterized arteries for various purposes, by surgical exposure followed by ligation or resuturing of the artery. In 1949, JÖNSSON performed thoracic aortography after puncture of the common carotid artery by means of a blunt cannula provided with an inner sharp needle. The cannula, guided by a silver thread, was then directed downwards. Later

Briefly presented at the Congress of the Northern Association of Medical Radiology, Helsinki, June, 1952; submitted for publication, October 28, 1952.

the procedure was abandoned, partly because it was considered that the cannula might injure the aortic wall. This percutaneous method might have proved more useful if a technique for using a flexible catheter of adequate lumen had been available at the time.

The artery exposure technique of catheterization is time-consuming, troublesome and may present certain risks. The thin-walled polyethylene tube, however, makes percutaneous catheterization possible, as reported by PEIRCE in 1951, who passed in the tubing through a large bore needle. This method was suitable for aortography via the femoral artery. In the same year, DONALD, KESMODEL, ROLLINS and PADDISON, employing a similar technique, catheterized the common carotid artery in cerebral angiography. The method necessitates the use of a large bore needle which may make puncture difficult and limits its use to comparatively large arteries, hence PEIRCE's attempts to catheterize the brachial artery were disappointing. There is also extra damage to the artery and, as the hole in the artery is larger than the catheter, haemorrhage after removal of the needle may be troublesome. To prevent bleeding, the needle may be kept in situ during the investigation; this, however, increases the risk of injury to the patient during movement.

There is a simple method, however, of using a catheter the same size as the needle, and which has been used at Karolinska Sjukhuset since April 1952. The main principle consists in the catheter being introduced on a flexible leader through the puncture hole after withdrawal of the puncture needle. The details are as follows:

Equipment. (Supplied by A. B. Stille-Werner, Stockholm.)

- 1) A puncture needle with stylette.
- 2) A flexible rounded-end metal leader with increased flexibility of its distal 3 cm.
- 3) A polyethylene tube, of the same diameter as the needle, with an adapter for the attachment of a syringe.

26—530088. *Acta Radiologica*. Vol. 39.

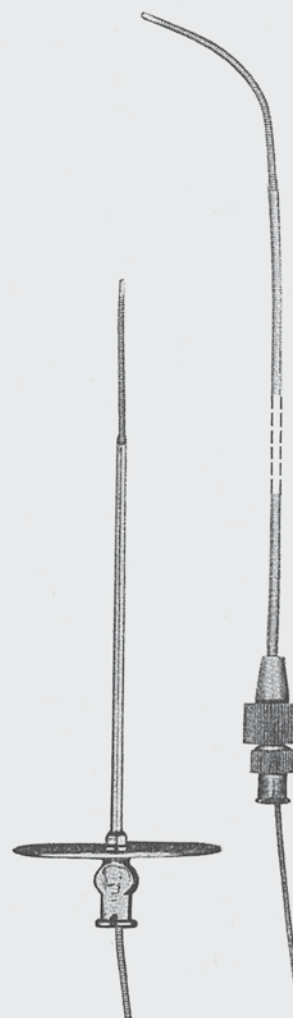


Fig. 1. The equipment. The stylette is removed and the leader inserted through the needle (left) and the catheter (right).

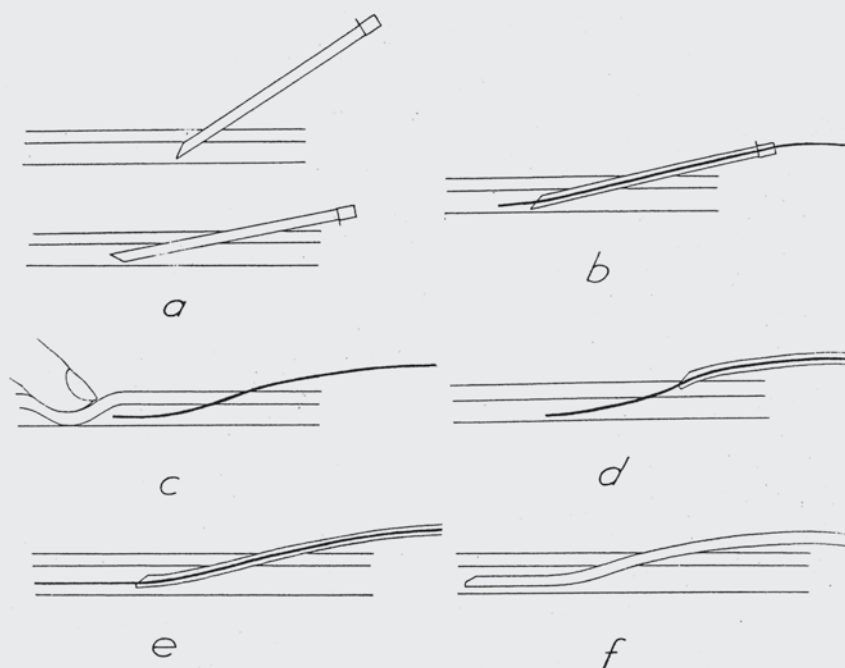


Fig. 2. Diagram of the technique used. a) The artery punctured. The needle pushed upwards. b) The leader inserted. c) The needle withdrawn and the artery compressed, d) The catheter threaded on to the leader. e) The catheter inserted into the artery. f) The leader withdrawn.

The leader should have a diameter slightly less than the bore of the needle and the catheter, so that it is capable of passing through both, and should be at least 8—9 cm longer than the latter; on the other hand it should just fit the lumen of the catheter (Fig. 1). The tip of the catheter may be cut before use as shown in Fig. 2.

Technique (see Fig. 2).

a) After local anaesthesia, the artery is punctured percutaneously at a relatively small angle.

After puncture it is best to rotate the needle 180° and push it a little into the artery using the bleeding as a guide to ensure that the needle remains in the artery. Puncture of arteries smaller than the femoral artery is facilitated by using an inner needle as a guide over which the outer needle is directed into the artery.

b) The supple tip of the leader is inserted a very short distance into the lumen of the artery through the needle.

c) The leader is held in place and the needle removed.

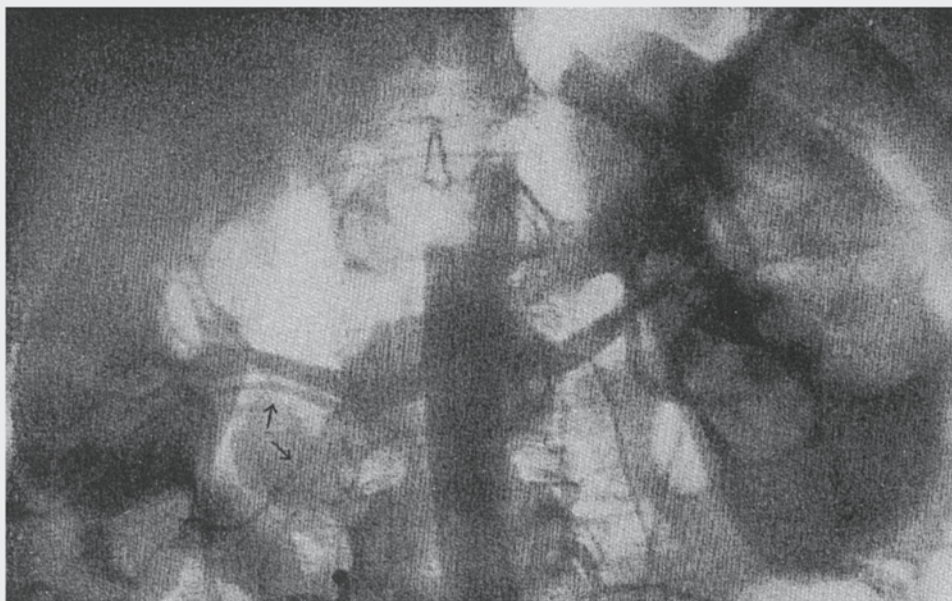


Fig. 3. Hypoplastic lower pole of the right kidney. Blood supply from two branches of a small aberrant artery. Catheter inserted through the right femoral artery with tip 2 cm below the renal arteries.

At this moment bleeding should be controlled by pressure on the artery proximal to the puncture site, because the diameter of the leader is smaller than the hole in the artery.

d) The catheter is threaded on to the leader; when the tip reaches the skin the free end of the leader must protrude from the catheter.

e) The catheter and leader are gripped near the skin through which they are inserted. The catheter enters the artery easily as an opening has already been made by the needle. The catheter and leader are pushed just far enough to ensure that the tip of the former is in the lumen of the vessel.

f) The leader is removed and the catheter directed to the level required, after good arterial bleeding through the catheter has been obtained. The unsupported catheter is usually pushed up the vessel without difficulty, but occasionally the leader must be re-introduced into the catheter in order to support it. The leader should not be passed beyond the tip of the catheter.

This technique is simpler than appears on paper and after a little practice should present no difficulties. It is important that the leader passes into the artery easily. When the tip of the catheter enters the artery, the same resistance is often felt as when puncturing is performed

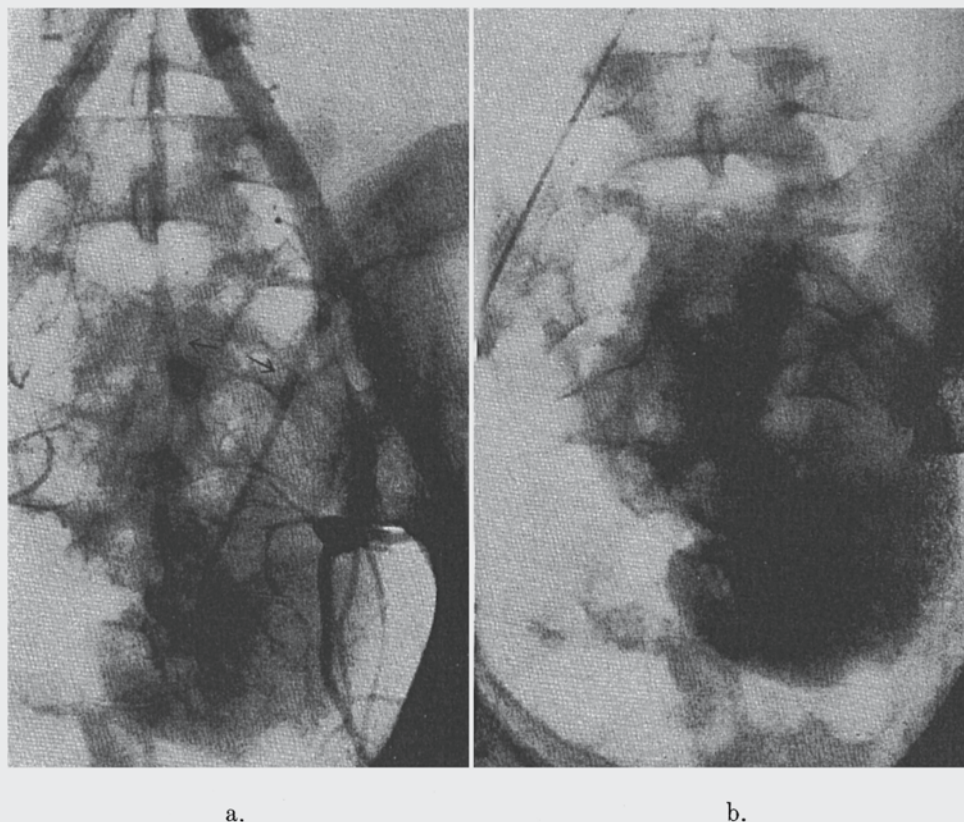


Fig. 4. Left-sided ectopic kidney in pelvis. (Right kidney absent.) Blood supply by one artery from the iliac bifurcation and one from the left internal iliac artery. Catheter inserted through the right femoral artery with tip at the bifurcation. a. Arterial phase. b. Capillary phase.

by means of a needle. However, the resistance is generally but slight or may be completely absent. If considerable resistance be encountered, it is probable that the tip of the leader is obstructed and force must therefore never be applied.

Polyethylene tubing is unfortunately not radio-opaque. For this reason, in aortography via the femoral artery, a small amount of contrast medium may be injected and followed by a test exposure. This will show the position of the catheter and also the exact situation of the renal arteries and of the iliac bifurcation. When the brachial artery is catheterized, the procedure is carried out in the fluoroscopy room and the leader used as an indicator of position; the catheter is then kept free from blood by the injection of saline solution.

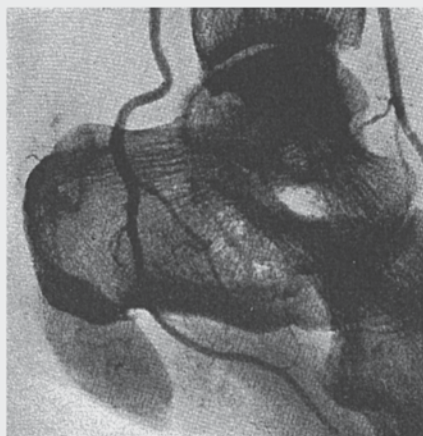


Fig. 5. Cavernous angiomas of the heel. Arterial phase. Catheter inserted through the femoral artery with tip in the popliteal artery. The difficult puncture of the popliteal artery was replaced by the easily performed catheterization from the inguinal region.

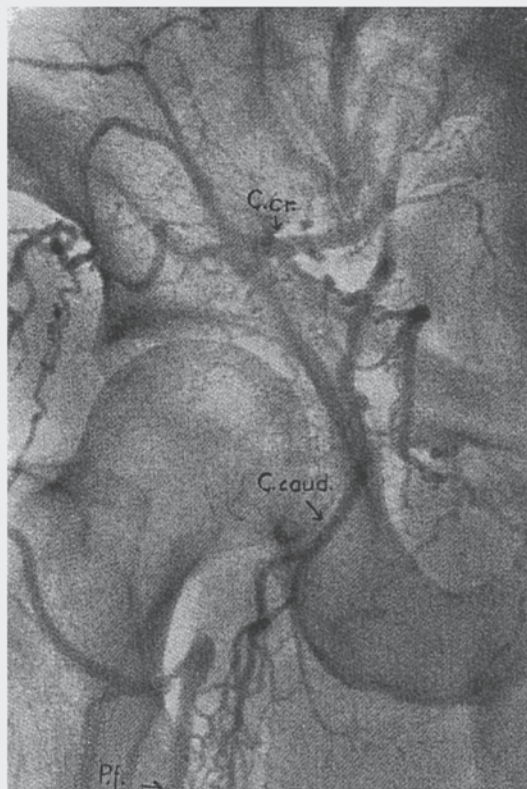


Fig. 6. Occlusion of the right external iliac artery. Collaterals from the superior gluteal to the deep femoral artery. Inner part of the thigh supplied from the inferior gluteal artery. Catheter inserted through the left femoral artery with tip at the bifurcation. G. cr. = superior gluteal artery. G. caud. = inferior gluteal artery. P. f. = deep femoral artery.

Summary of Investigations Performed

40 arterial catheterizations have been carried out; of these, 35 were aortographies via the femoral artery, 3 subclavian arteriographies by means of puncture of the brachial artery in the antecubital fossa, and 2 catheterizations of the femoral artery in a distal direction. In no case was general anaesthesia employed. Injection was made throughout by hand. The contrast medium used was 30 cc of Umbradil in each injection with a concentration of 35 % in peripheral arteriographies and 70 % in aortographies except in those cases in which compression of the femoral arteries was used, when a 50 % solution was employed. The tubing used was in all cases No. 200 (internal diameter 1.40 mm, external diameter 1.90 mm) or No. 205 (1.57 mm and 2.08 mm). The latter seemed to be the optimal one for aortography. As the thickness of the wall of the needles available is nearly

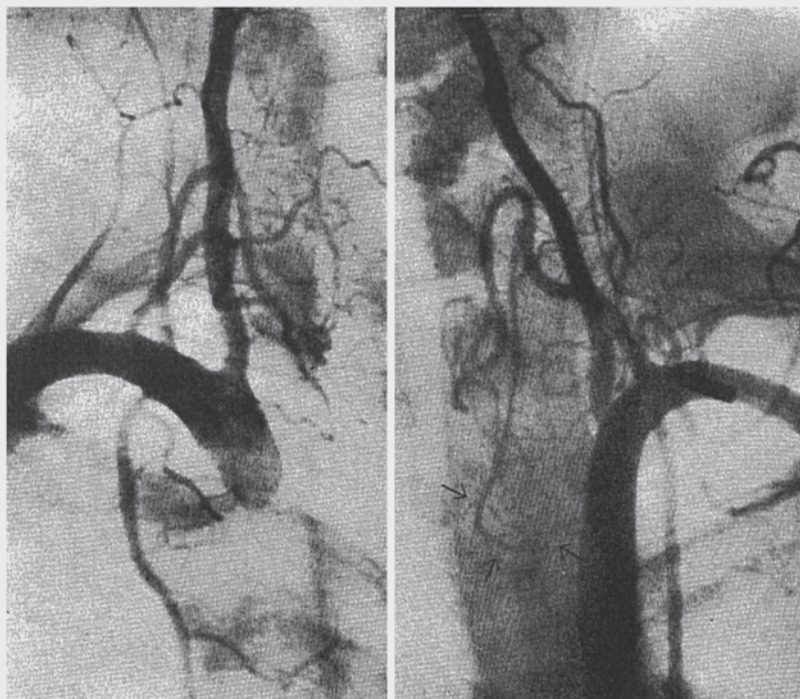


Fig. 7. Catheter inserted through the antecubital artery of both sides. The tip in the subclavian artery. (The metal tip is no longer in use.) The left inferior thyroid artery forks into two branches, the terminations of the longer and lower one of which run in a marked curve downwards and laterally as if around a tumour; examination of a resected part of the left lower lobe of the thyroid showed adenomatous parathyroid tissue in the parenchyma.

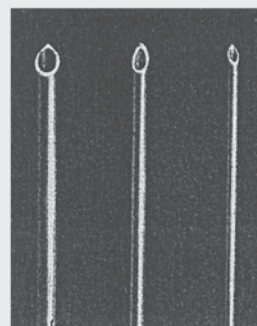
the same as that of the catheter, a needle of 2 mm outer diameter is required. If the catheter is 40–45 cm long it permits a faster injection of the contrast medium than the 12–15 mm needle of 1 mm lumen, used in this department for translumbar aortography.

25 catheterizations were performed by the author and 15 by four other workers in the department.

In one patient catheterization did not succeed, in spite of 3 attempts on the femoral arteries, as sufficient blood-flow through the catheter was not obtained. In one patient no attempt at catheterization was made as resistance to the leader was encountered. In one obese patient, introduction of the catheter into the right femoral artery failed, but was carried out without difficulty on the left side. In the other cases the catheter was inserted easily at the first puncture and the investigation resulted in good films excepting in two cases in which the tip of the catheter did not reach the level required. In one of the patients, 75 years old, resistance was encountered after 6–7 cm, and in another the deep femoral artery instead of the superficial one, was persistently catheterized.

In 6 of the aortographies and in the 3 subclavian arteriographies the catheter was fitted with a metal tip (Fig. 7), but this was abandoned because it was found easier to

Fig. 8. Natural size. The middle needle permits, with the technique described, the insertion of a catheter (in this case No. 205) which requires a needle of the size of that pictured on the left, were it to be passed through the lumen of the needle. The same relative advantage exists between the right and middle needles.



insert the catheter without it, and the artery wall sometimes contracted around it during its removal. Furthermore, it was realized that it might damage the arterial wall as happened in one of the subclavian arteriographies, so that part of contrast medium was injected extravascularly.

As regards complications any tendency to bleed at the site of puncture was unimportant and was mostly observed in elderly patients. No haematoma of clinical consequence ever formed. No thrombosis or any kind of circulatory disturbance in the region of the artery punctured was observed. There was no case of extravascular injection except the one previously mentioned. In the unsuccessful attempts at catheterization, the leader probably passed through the posterior wall of the artery or its intima via a hole made during puncture. In these cases the needle could not be pushed far enough up into the artery. In neither did the patient suffer any ill effects. No kinking or rupture of the catheter, or arterial spasm around it occurred. After local anaesthesia, the patients felt nothing during the manipulations and following the injection of the contrast medium there was, with individual variations, only the wellknown, rapidly passing discomfort.

In one case the patient was operated on two weeks after bilateral femoral catheterization and both arteries were exposed. Traces of blood under the fascia indicated the situation, but the exact site of puncture could not be discerned.

Figs. 3—7 form representative illustrations.

Discussion

The advantage of the author's method of percutaneous catheterization is the smaller size of needle required for a given catheter. As the catheter needs a certain clearance to enable it to glide through the bore of a needle, the difference is more marked than would appear from the thickness of the material (Fig. 8).

In other words, a larger catheter can be inserted by the same sized needle. POISEUILLE's law states that when pressure and viscosity are constant, the rate of flow through narrow tubes is:

inversely proportional to the length of the tube, and

directly proportional to the 4th power of the radius of the tube.

This shows the dominant influence of the cross section of the catheter. Catheter No. 205, used here for abdominal aortography, has an inner diameter, corresponding to a heart catheter No. 9—10. If a pressure

376

SVEN IVAR SELDINGER

apparatus were used, the gauge might doubtlessly be diminished considerably, *i. e.* to a size No. 160, corresponding to a heart catheter No. 8, and which may be inserted with the help of a needle, 1.5 mm in external diameter.

Though the extra manipulation with the leader is a disadvantage, it is very quickly performed. Furthermore, there is a little risk that the leader, when handled unskilfully, will pass through the posterior wall of the artery, although, no doubt, experience and improved equipment will eliminate this possible complication and avoid failure.

SUMMARY

The author describes a method by which it is possible, after percutaneous puncture, to insert a catheter of the same size as the needle used into an artery.

ZUSAMMENFASSUNG

Der Verf. beschreibt eine Methode, die es ermöglicht, nach perkutaner Punktion einen Katheter von derselben Grösse wie die benutzte Nadel in eine Arterie einzuführen.

RÉSUMÉ

L'auteur décrit une méthode qui permet, après ponction percutanée, d'introduire dans une artère un cathéter de même calibre que l'aiguille utilisée.

LITERATURE

- DONALD, D. C., KESMODEL, K. F., ROLLINS, S. L. and PADDISON, R. M.: An improved technic for percutaneous cerebral angiography. *Arch. Neurol. and Psych.* 65 (1951), 508.
- FARIÑAS, P. L.: A new technique for the arteriographic examination of the abdominal aorta and its branches. *Am. J. Roentgenol.* 46 (1941), 641.
- JÖNSSON, G.: Thoracic aortography by means of a cannula inserted percutaneously into the common carotid artery. *Acta radiol.* 31 (1949), 376.
- PEIRCE, E. C.: Percutaneous femoral artery catheterization in man with special reference to aortography. *Surg., Gynec. & Obst.* 93 (1951), 56.
- RADNER, S.: Intracranial angiography via the vertebral artery. Preliminary report of a new technique. *Acta radiol.* 28 (1947), 838.



7.2 Percutaneous trocar (needle) nephrostomy in hydronephrosis

Willard E. Goodwin (1916–1998)

Willard Goodwin was born on 22 July 1916. He graduated from the University of California at Berkeley and completed his medical studies at the Johns Hopkins Medical School. He trained in urology and joined the University of California at Los Angeles in 1951 and in 1953 became the founder and chief of urology. Here he built up an outstanding urology department and made numerous outstanding contributions to urology over the years, including his description of the technique of nephrostomy. He is credited with having made over 40 major innovations in urology and was one of the early pioneering renal transplant surgeons in the USA.

Willard Goodwin died in 1998.

Picture taken from <http://www.urology.medsch.ucla.edu/history.html> (12-03-04).



W.C. Casey

W. Woolf

PERCUTANEOUS TROCAR (NEEDLE) NEPHROSTOMY IN HYDRONEPHROSIS

Willard E. Goodwin, M.D., William C. Casey, M.D.

and

Wilford Woolf, M.D., Los Angeles

This paper describes indications for and the technique and results of trocar nephrostomy, performed by percutaneous lumbar tap of the renal pelvis with a large needle, followed by insertion of plastic tubing for temporary urinary drainage in selected cases of hydronephrosis. A previous paper¹ presented our experiences with antegrade pyelography, in which pyelograms were made by lumbar puncture of large hydronephroses followed by aspiration of urine and injection of a urographic contrast medium. The present study, trocar nephrostomy, was a natural outgrowth of antegrade pyelography.

TECHNIQUE

Lumbar tap of the hydronephrosis and insertion of plastic tubing is done with roentgenographic control with the patient under local anesthesia. The same precautions are observed as in performing spinal puncture. The patient lies prone. Preliminary x-ray films localize the approximate spot of puncture in relation to the landmarks of lumbar spine and vertebrae (fig. 1, inset). The skin is prepared with an antiseptic, and procaine infiltration anesthesia is used. The procedure should be limited to patients with large hydronephroses. The larger the hydronephrotic sac the easier it is to puncture. Ten, 12, or 14 gauge needles have been used. In most adults, a 12 gauge thin-walled needle, 6 in. (15 cm.) in length, seems to be optimum. Smaller needles have been used in children. On one occasion a bladder trocar was employed and a rubber catheter introduced; however, the smaller, 12 gauge needles cause less trauma, and drainage through the plastic tubing is usually satisfactory. After local infiltration anesthesia, the large needle is introduced through the lumbar area as indicated in figures 1 and 2. When the needle approaches the renal fossa, the obturator is withdrawn, and a long thin needle (such as that used in the Kreutzmann trocar for cystostomy) is introduced through the needle and into the hydronephrosis. When correct position is determined by appearance of a hydronephrotic drip of urine, the larger needle is advanced until it too enters the hydronephrosis. If at any time the operator is in doubt about position, x-ray control is indicated.

After the renal pelvis has been entered, the large needle is held in position by a needle stop. Polyethylene tubing,² is then introduced through it into the renal pelvis (fig. 2). Sizes of polyethylene tubing that will pass through needles of a given size are:

polyethylene 240.....	10 gauge
polyethylene 205.....	12 T gauge
polyethylene 190.....	14 T gauge

Before the tubing is inserted, additional lateral holes are made near the end by puncture with a hot needle. This makes several extra openings to increase urinary drainage. Approximately 2 to 4 in. (5 to 10 cm.) of

tubing is allowed to coil in the renal pelvis, depending on the size of the hydronephrosis. The passage of this tubing through the long needle is very much like that described in femoral aortography.³ Next the needle is removed and the tubing taped to the skin in such a way that it cannot be moved and will not kink. This may be done by supporting the tubing with a sponge at the skin level. It may be adapted to a collecting bottle by a Tuohy adaptor, or, if the patient is ambulatory, it may be connected to a rubber urinal on the leg.

RESULTS

This procedure was attempted 18 times in 16 patients as of June, 1954. In five of these patients the technique failed, either because of inability to enter the hydronephrosis or because of improper length of needles. In three cases there was a short period of drainage, from one to three days, without any benefit. In four further cases temporary nephrostomy drainage was later followed at intervals of from five days to two months by nephrectomy when it was determined that the kidney was not worth saving and that function would not improve with drainage. In four cases (two bilateral) it was used successfully for temporary diversion of urine in order to perform conservative surgery and preserve renal function. The procedure is most applicable in patients in whom it is desired to allow temporary drainage of a hydronephrosis to see if renal function will return sufficiently to allow conservative treatment (case 1) and in a second group of patients in whom temporary diversion is desired in order to perform some kind of restorative surgery of the lower urinary tract with the idea of later reestablishing normal drainage (case 3).

REPORT OF CASES

CASE 1.—A 1½-year-old child had bilateral hydronephrosis due to congenital ureteropelvic obstruction. When first seen by one of us (W. E. G.) on Dec. 21, 1953, he had an acute attack of abdominal pain and fever. An intravenous pyelogram (fig. 3A) showed right hydronephrosis and no evidence of function on the opposite side. An antegrade pyelogram (fig. 4A) demonstrated left hydronephrosis after an aortogram (fig. 3B) had shown that there was good blood supply to the left kidney. Bilateral pyeloplasties were indicated. It was decided to operate

From the Division of Urology, the University of California Medical Center; Harbor General Hospital; and Veterans Administration Center.

Read in the Symposium on Pediatric Urology before the Section on Urology at the 103rd Annual Meeting of the American Medical Association, San Francisco, June 24, 1954.

This study was supported in part by the Fund for the Advancement of Urology and by the Schering Corporation.

The needles used in this study were specially prepared and supplied by Becton Dickinson Company, Rutherford, N. J.

Case 2 is included with the permission of Dr. Robert C. Walter.

1. Casey, W. C., and Goodwin, W. E.: Percutaneous Antegrade Pyelography and Hydronephrosis, *J. Urol.*, to be published.

2. Ferris, D. O., and Grindlay, J. H.: Use of Polyethylene and Polyvinyl Tubing in Ureterostomy, Nephrostomy and Cystostomy, *Proc. Staff Meet.*, Mayo Clin. 23: 385-390 (Aug. 18) 1948.

3. Walter, R. C., and Goodwin, W. E.: Aortography and Retroperitoneal Oxygen in Urologic Diagnosis, *J. Urol.* 70: 526-537 (Sept.) 1953.

on the right side first, but it was desirable to have continuous drainage on the left side while working on the right. On Dec. 28, trocar nephrostomy was done on the left side (fig. 4B). This allowed good drainage, and it was possible two days later to perform Davis' intubated ureterotomy on the right side with the advantage of continued drainage from the left side during the postoperative period. A phenolsulfonphthalein test on Jan. 5 showed 26% excretion from the right and 20% excretion from the left kidney in two hours. The patient went home from Jan. 9 to March 7, 1954, with nephrostomy drainage from the left trocar nephrostomy and drainage from the splints of the Davis' intubated ureterotomy. He returned to the hospital March 7. A repeat phenolsulfonphthalein test on March 9 showed 26% excretion in two hours from each side, an improvement in function on the left. A retrograde pyelogram made at this time showed considerable improvement in the left hydronephrosis. The trocar nephrostomy fell out and could not be replaced on March 11. On March 12, a Culp-Scardino type of pyeloplasty was done on the left side. In this case trocar

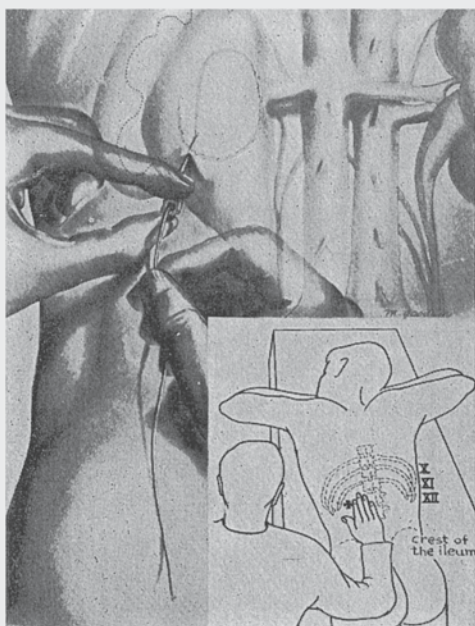


Fig. 1.—Method and landmarks of percutaneous trocar nephrostomy. Optimum site of puncture is usually about five fingerbreadths lateral to the midline and at a level where a 13th rib would be.

nephrostomy allowed continuous drainage for almost nine weeks in a child and obviated the necessity for another surgical operation to perform left nephrostomy during this period. Follow-up intravenous urograms and normal urinalyses showed a good end-result.

CASE 2.—A 12-year-old boy had had previous surgery elsewhere. There was a draining urinary sinus from the right flank, and intravenous pyelograms revealed a nonfunctioning right kidney. An antegrade pyelogram demonstrated right hydronephrosis with obstruction at the ureteropelvic junction. It was determined to divert the urine to see if renal function would improve. This was carried out by trocar nephrostomy with the patient under local anesthesia on Nov. 16, 1953. There was satisfactory drainage while he was at home for two weeks. His fever subsided, the sinus closed, and he gained weight. It was hoped to save the kidney; however, a phenolsulfonphthalein test showed only 4% excretion in two hours; therefore nephrec-

tomy was performed on Dec. 2. This illustrates the usefulness of the procedure to allow temporary drainage while waiting hopefully for return of function.

CASE 3.—A 54-year-old woman had a radical hysterectomy in September, 1953, because of squamous cell carcinoma of the uterus. She later developed a vesicovaginal fistula and a right ureterovaginal fistula. It was decided to close the vesicovaginal fistula and to deal with the right kidney at a later date. In order

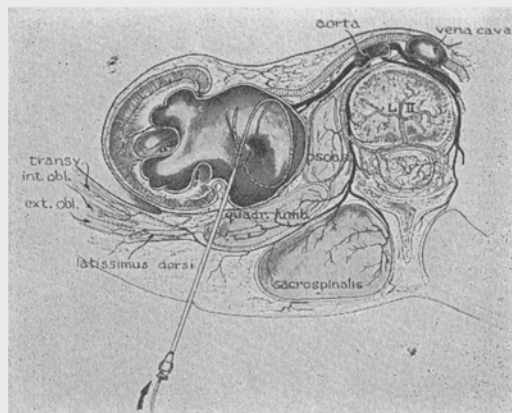


Fig. 2.—Cross sectional anatomy of left renal area (after Brödel). About 2 in. of tubing is allowed to coil in the hydronephrotic pelvis.

to divert the urine from the hydronephrotic, obstructed right kidney, translumbar needle nephrostomy was performed on Dec. 2, 1953. In the immediate period after this operation there was some bloody drainage and obstruction of the tubing by clots. A solution of streptokinase-streptodornase was introduced and allowed to remain in the renal pelvis. The clots apparently dissolved, and subsequent drainage was satisfactory. Reduction of the hydronephrosis followed. The vesicovaginal fistula was repaired with the use of the vaginal approach on Dec. 15. Drainage was continued from the polyethylene nephrostomy tube for five months. On March 23, 1954, when the right upper tract seemed nearly normal and the vesicovaginal fistula was well healed, an isolated loop of ileum was substituted for the destroyed lower third of the right ureter.⁴ The polyethylene nephrostomy tube was still in place and continued to divert

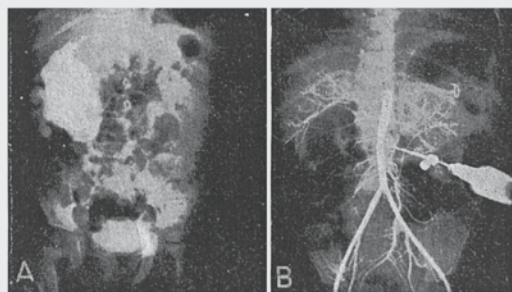


Fig. 3.—A, intravenous pyelogram of patient in case 1. B, aortogram.

urine during the postoperative period. Finally, on May 5, the tubing was removed from the right kidney, after five months, and the sinus promptly closed. It was of interest that there was no incrustation of the tubing with salts, and it acted very satisfactorily as a nephrostomy during this long period. On May 14 an intravenous pyelogram showed good function of both kidneys, with slight bilateral hydronephrosis. Blood chemistry studies were within normal limits. This case illustrates the ad-

Baum, W. C.: Use of Terminal Ileum as Substitute Bladder, *J. Urol.* 33 (July) 1954.

Vol. 157, No. 11

vantage of trocar nephrostomy as a temporary but effective diversion of the urinary stream while plastic surgery is performed lower in the urinary tract.

INDICATIONS

From the above examples it seems that the procedure is of greatest use in cases of large hydronephroses when a temporary diversion of the urinary stream, without open operation, is required before definitive surgery at a later date. The temporary diversion may be for the purpose of doing plastic work on the lower urinary tract (case 3), or

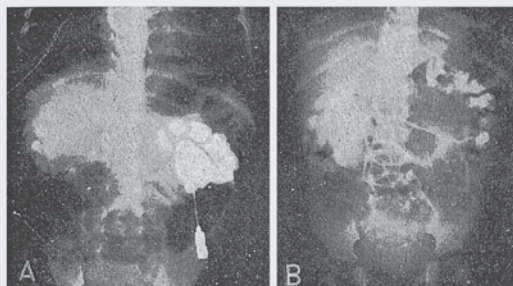


Fig. 4.—A, antegrade pyelogram of patient in case 1. B, polyethylene tubing coiled in left renal pelvis after trocar nephrostomy.

it may be to allow return of function while working on the opposite side (case 1). It may also be used as a test of function in cases of hydronephrosis when it is uncertain whether or not the kidney is worth saving. It may be employed to afford temporary drainage when the surgeon ordinarily would not subject the patient to an extra operation for this purpose.

Percutaneous trocar (needle) nephrostomy in cases of hydronephrosis may not appeal to some surgeons. Perhaps they will consider using it in conjunction with open surgery.⁵ After surgical exposure of a hydronephrotic kidney, nephrostomy or pyelostomy may easily be established by needle puncture of the renal pelvis with insertion of polyethylene tubing, possibly in several different areas to allow multiple drainage without actually mobilizing the kidney and subjecting it to the trauma often associated with manipulation for nephrostomy drainage.

COMPLICATIONS AND DANGERS

The following complications should be considered: infection, hemorrhage, obstruction of the tube, kinking of the tube, inadequate drainage, and intermittent obstruction. Contraindications are: uremia, bleeding tendency, tuberculosis, and neoplasm. When this paper was presented we had not seen severe or dangerous infection following the track of the tube even in cases in which the urine was known to be infected. Weyrauch⁶ called attention to this danger after trocar cystostomy and feels that potential infection without adequate drainage offers one of the most serious condemnations of trocar nephrostomy. This complication has happened in the experience of a colleague since this paper was presented. A polyethylene nephrostomy tube, which had been inserted via trocar, drained poorly and finally slipped out. Emergency surgical nephrostomy was then necessary, and the perinephric area contained a urinary abscess. This should be borne in mind by anyone who would attempt it.

HYDRONEPHROSIS—GOODWIN ET AL.

893

The possibility of severe hemorrhage certainly exists; however the fact that anatomically there are no vital structures between the skin of the back and the renal pelvis, except the kidney itself, makes this unlikely. It seems possible that large renal vessels have been punctured at one time or another. On one occasion arterial bleeding from the 12 gauge needle caused some alarm. It did not persist, however, after plastic tubing was inserted. This kidney drained intermittently, partly because the tubing was coiled and kinked upon itself. Nephrectomy was later performed because the chronically scarred and infected hydronephrotic kidney was not worth saving in the presence of normal renal function on the opposite side. This allowed an opportunity to examine the kidney after needle nephrostomy and to see how much damage had been done. Figure 5 is a photograph of the specimen. The polyethylene catheter was coiled in the upper calyx and was somewhat kinked upon itself. This probably explained the poor drainage. There were ecchymotic areas in the epithelium of the upper calyx but very little evidence of any severe bleeding within the kidney itself. There was no sign of gross infarction and no sign of subcapsular bleeding. This would tend to minimize the fear of hemorrhage, although it must always be borne in mind. In any nephrostomy, the possibility of hemorrhage exists, yet the skillful surgeon has no fear of placing a large catheter or clamp through the renal substance. The renal capsule itself seems to limit hemorrhage. The problems of intermittent obstruc-



Fig. 5.—Hydronephrotic kidney removed after five days of trocar nephrostomy drainage. Note tubing in upper calyx and kinking of tubing that interfered with drainage.

tion and poor drainage due to kinking of the tube, inherent in any nephrostomy, are exaggerated by trocar nephrostomy. This is due to the small caliber of the polyethylene tubing and its tendency to bend. It is also magnified by the worst defect of the procedure, its blindness. Even at best one must guess as to position and

5. Schinagel, G.: Trocar Nephrostomy, *J. Urol.* 62: 286-291 (Sept.) 1949.

6. Weyrauch, H.: Personal communication to the authors.

ability of the tube to drain during the first few hours after nephrostomy by this method. All these difficulties are less in large hydronephroses. When trocar nephrostomy works, it works very well indeed.

Admittedly the experience of this first study is so limited that it is impossible to tell how serious and how frequent complications may be. As noted in the Results, the procedure failed five times because of technical difficulties. Some moribund patients died within 24 to 72 hours after trocar nephrostomy and were examined at autopsy. It seemed that these persons died of uremia, which existed and was progressive before trocar nephrostomy was performed as a last effort without any real hope that it would change the prognosis. There was no indica-

tion from the pathologist's examination that trocar nephrostomy had contributed to death. Other patients died weeks or months later of other causes. There was no indication in these patients that nephrostomy had contributed to the patient's death; however, a large series would have to be collected to determine morbidity and mortality, if any, from this procedure.

CONCLUSIONS

Trocar nephrostomy may be a useful method of temporary urinary diversion in selected cases of large hydronephroses. Further evaluation of this technique is warranted.

University of California Medical Center (24) (Dr. Goodwin).

LATE SYSTEMIC COMPLICATIONS OF HYDRALAZINE (APRESOLINE) THERAPY

John C. Muller, M.D., Charles L. Rast Jr., M.D., William W. Pryor, M.D.

and

Edward S. Orgain, M.D., Durham, N. C.

During the administration of hydralazine (Apresoline) for the treatment of hypertension, a significant number of interesting and important but poorly understood reactions to the drug have been described. These reactions include significant fever occurring one to three weeks after the onset of therapy,¹ pancytopenia,² acute psychoses,³ gastrointestinal bleeding,⁴ and a collagen-like illness.⁵ In its milder form, the collagen-like illness resembles acute rheumatoid arthritis and subsides promptly in most instances when the drug is withdrawn. In severer form, the occurrence of fever, arthralgia, pleurisy, pericarditis, and L. E. cells suggests an illness that closely simulates acute systemic lupus erythematosus. The purpose of this paper concerns the report of seven patients with hypertensive vascular disease in whom this collagen-like illness developed while they were receiving hydralazine. Until the genesis of this syndrome becomes more clearly understood, the term "hydralazine reaction" will be used in preference to the ill-defined phrase, collagen-like illness.

From the Department of Medicine, Duke University School of Medicine, and the Cardiovascular Service, Duke Hospital.

Dr. Wayne Rundles of the Department of Hematology, Duke University School of Medicine, aided in the interpretation of the bone marrow aspirations and the paper electrophoresis for this study.

1. Morrow, J. D., Schroeder, H. A., and Perry, H. M., Jr.: Studies on Control of Hypertension by Hypex: II. Toxic Reactions and Side Effects, *Circulation* 8: 829-839 (Dec.) 1953.

2. Kaufman, M.: Pancytopenia Following Use of Hydralazine ("Apresoline"), *J. A. M. A.* 151: 1488-1490 (April 25) 1953.

3. Moser, M., Syner, J., Malitz, S., and Mattingly, T. W.: Acute Psychoses as a Complication of Hydralazine Therapy in Essential Hypertension, *J. A. M. A.* 152: 1329-1331 (Aug. 1) 1953.

4. Wilkins, R. W., and Judson, W. E.: Problems Arising from the Use of Hypertensive Drugs in Hypertensive Patients, *Tr. A. Am. Physicians* 66: 175-189, 1953. Mandelbaum, H.; Brook, J., and Mandelbaum, R. A.: Bleeding Peptic Ulcer Complicating Hydralazine and Hexamethonium Bromide Therapy, *J. A. M. A.* 155: 833-835 (June 26) 1954.

5. (a) Dustan, H. P.; Taylor, R. D.; Corcoran, A. C., and Page, I. H.: Rheumatic and Febrile Syndrome During Prolonged Hydralazine Treatment, *J. A. M. A.* 154: 23-29 (Jan. 2) 1954. (b) Perry, H. M., Jr., and Schroeder, H. A.: Syndrome Simulating Collagen Disease Caused by Hydralazine (Apresoline), *ibid.* 154: 670-673 (Feb. 20) 1954. (c) Sionium, N. B.: Arthralgia, Headache, Prostration, and Fever During Hydralazine Therapy, *ibid.* 154: 1419 (April 24) 1954. (d) Manter, W. B.: Late Reaction to Hydralazine (Apresoline) Therapy, *New England J. Med.* 250: 835-836 (May 13) 1954. (e) Footnote 1.

Fifty-three patients received hexamethonium chloride and hydralazine simultaneously for periods of 4 to 23 months. After initial regulation of these drugs during hospitalization, patients were subsequently followed by their private physicians at weekly to biweekly intervals and in the outpatient clinic by us under conventional laboratory control at intervals of one to three months. During ambulatory treatment, the hydralazine reaction developed in 7 (13%) of the 53 patients (see table). There were five women and two men. The average maximum daily dosage for these seven patients was 446 mg., with individual variations from 300 to 600 mg. For the remaining 46 patients free of this reaction, the average maximum daily dosage was 475 mg., with variations from 100 to 1,100 mg. The average time from the beginning of hydralazine therapy until the onset of this illness was 10.3 months, the shortest time being 6 months and the longest 12 months. At the time symptoms appeared, the blood pressure was normal in four of the seven patients and only moderately elevated in the other three. All seven patients complained of aching, stiffness, and soreness of the involved joints. In two patients the complaints were symptomatic, without objective physical findings. In four patients there was soreness and periarticular swelling of the proximal interphalangeal joints of the fingers; two patients of this group had increased temperature and pain, swelling, and redness of the knees and ankles, and one of these had joint effusion. In one patient (case 1) a severer illness appeared that closely simulated acute systemic lupus erythematosus, the details of which are summarized in the first case report. The most frequent associated symptoms were: fever, four patients; sore throat, three patients; chills or chilly sensations, two patients; pleuritic-like chest pain, two patients; and general malaise, two patients.

Laboratory studies were obtained in five of the seven patients. In four patients the hemoglobin level fell 2 gm. per 100 cc. or more. In two patients a leukopenia, with

7.3 Cine coronary arteriography

F. Mason Sones (1919–1985)

Dr Mason Sones was an early pioneering paediatric cardiologist who initially pioneered the use of image amplification in the fluoroscopic study of congenital heart defects. In 1959, however, he discovered that by using a catheter, contrast medium could be separately injected into the coronary arteries. Thus the first coronary angiogram was performed. Mason Sones used the brachial artery approach for coronary angiography and developed a vast expertise in this technique over his lifetime. He was awarded the Albert Lasker award in 1983 for his contributions to medical science. Mason Sones trained as a physician at the University of Maryland, qualifying in 1943. He spent most of his career in cardiology at the Cleveland clinic where his pioneering studies were carried out.



E.K. Shirey

W.L. Proudfit

R. Westcott

ABSTRACTS OF THE 32ND SCIENTIFIC SESSIONS

773

nary T waves or changing injury currents for from 1 to 10 years, and in 2 cases, the abnormalities appeared in the absence of significant cardiovascular symptoms. This illustrates the author's thesis that idiopathic pericarditis may be present with a striking paucity of characteristic stigmata.

Electrocardiographic Effects of Injecting Potassium and other Ions into a Coronary Artery of the Intact Dog

Louis A. Soloff, Guido Ascanio, and Morton J. Oppenheimer, Philadelphia, Pa.

The electrocardiographic changes of acute myocardial infarction may be related to regional chemical changes within the myocardium. West's technic of catheterizing a coronary artery was utilized to produce a variety of regional chemical changes within the otherwise healthy myocardium of the intact dog. This report is concerned with the electrocardiographic effects of potassium and other ions so used.

As little as 20-60 mg. KCl in a 10 Kg. dog immediately reverses the polarity of the T wave. Within a few seconds, a diastolic injury current appears. This current is characterized by a depression of the diastolic base line and elevation of S-T takeoff. As this injury current increases over the next few seconds, T slowly returns to its original direction, but with increased magnitude. As this injury current decreases over the next few seconds, the S-T segment becomes cove-shaped and the T wave again reverses its polarity. This pattern persists for a few seconds and then gradually returns to the pre-injection contour. With larger doses of potassium, the injury current is preceded by 1 or several premature beats. With still larger doses, ventricular tachycardia may follow the appearance of the injury current. At this time, necropsy sometimes discloses a small myocardial infarction. These electrocardiographic changes are reversible. With larger doses, irreversible ventricular fibrillation at a ventricular rate of about 1,200 per minute develops. The only consistent electrocardiographic depressant action of potassium in this sequence of events is (with larger doses) an early brief minimal slowing of sinus discharge. Potassium on occasion can, however, give results indistinguishable from acetylcholine when injected by the intracoronary route so as to reach selectively the A-V node. This reaction is characterized by transient complete ventricular standstill with sinoauricular action undisturbed.

Lithium chloride, CaCl_2 , MgSO_4 , NaOH and HCl require at least 200 times the minimal effective dose of KCl to produce electrocardio-

graphic changes. Only lithium chloride produced sequential changes comparable to those of KCl. However, in this case, the initial change in the polarity of the T was gradual rather than the abrupt one seen with KCl. Animal Ringer's solution produces no electrocardiographic changes. Sometimes, 0.9 per cent NaCl and CO_2 gas may produce a change in the voltage of the T wave when injected slowly into otherwise normal hearts.

Ions injected into a coronary artery of the intact dog produced sequential electrocardiographic changes different from those seen when the total heart is exposed to these ions. Of all substances tested, the electrocardiogram was most sensitive to potassium. The sequence of changes produced by potassium could not be duplicated by other ions. Potassium so injected, depending upon the dose, brought about reversible or irreversible myocardial infarction.

Cine-Coronary Arteriography

F. Mason Sones, Jr., Earl K. Shirey, William L. Proudfit, and Richard N. Westcott, Cleveland, Ohio

A safe and dependable method has been devised for contrast visualization of the coronary arteries to objectively demonstrate atherosclerotic lesions.

The ascending aorta is catheterized by an approach from the right brachial artery, in the antecubital fossa. Selective opacification of the right and left coronary arteries is performed serially by injecting 20 to 30 ml. of 90 per cent Hypaque into the right and left sinuses of Valsalva adjacent to the orifices of the vessels during x-ray motion picture photography of the area of distribution of each vessel. Adequate opacification has been obtained without resorting to mechanical aortic occlusion or cardiac arrest with acetylcholine.

In more than 50 patients studied by this technic, a broad spectrum of problems has been encountered, ranging from iatrogenic disease to multiple total occlusions in those with remote and recent myocardial infarction. Selective coronary artery opacification has not produced angina, ventricular arrhythmias, or myocardial injury, even in patients experiencing angina at rest.

The method has demonstrated: 1. The presence of normal coronary arteries in patients with chest pain or electrocardiographic changes which had been interpreted as indicating the presence of arteriosclerotic heart disease. 2. Complete or partial segmental occlusion of 1 or more major arteries. 3. The presence of collateral arterial channels from 1 major artery to the area of distribution of another totally occluded segment.

The ultimate usefulness of the method remains to be defined, but it should provide a more objective diagnostic standard than has previously been available for the evaluation of therapeutic measures which have been or may be applied in the treatment of arteriosclerotic heart disease.

Does Blood Pressure Normally Increase with Age?—Thirty Year Follow-Up Data on the Labor Force of a Chicago Utility Company

Jeremiah Stamler, Howard A. Lindberg, David M. Berkson, and Wilda A. Miller, Chicago, Ill.

A statistical analysis of serial blood pressure and weight data was made over a 30 year period, from young adulthood to middle-age, on several hundred men in the labor force of a Chicago utility company. An average of 11 blood pressures per person were available for this epidemiologic study.

For the group as a whole, a moderate increase occurred in mean blood pressure with age. However, a significant per cent with low normal pressures as young adults maintained these without any significant rise throughout middle age. Such persons had markedly lesser risk of developing coronary heart disease and other cardiovascular-renal diseases in middle age than men exhibiting a rise in blood pressure over the decades. It would appear that a rise in blood pressure is not an invariable concomitant of aging, and cannot be indiscriminately viewed as a normal phenomenon.

Histories of Over 200 Persons, Originally Healthy, Followed until Death or for 20 Years after Their First Ballistocardiograms

Isaac Starr and Francis C. Wood, Philadelphia, Pa.

Ballistocardiograms were first taken in 1936 and within the next few years many healthy persons were tested to provide normal standards. Over 200 of these have been followed up. Thirty-two are dead, 34 others have become ill and have entered a hospital. Eighty have returned for a follow-up study, 60 have replied to a questionnaire, and 23 others are well known to us. The men and women have been arranged in order of the amplitude of their original ballistocardiograms. The 174 males can be divided arbitrarily into 2 groups. In that with the larger ballistocardiograms, 3 per cent of 117 subjects developed undoubted heart disease, and an additional 3 per cent a doubtful cardiac status. Of the 57 with smaller ballistocardiograms, 51 per cent developed undoubted heart disease and 14 per cent a doubtful cardiac status. These are highly sig-

nificant differences. The data secured on women are confirmatory, but not so striking. In this series, unselected, as far as we can determine, persons with small ballistocardiograms showed a dramatically higher death rate in the next 20 years than those with larger complexes and a much higher incidence of, and death rate from, heart disease.

Safe and Practical Method of Intravenous Abdominal Aortography, Peripheral Arteriography and Cerebral Angiography

Israel Steinberg, Nathaniel Finby, and John A. Evans, New York, N.Y.

The Robb-Steinberg method of intravenous angiocardiology by the rapid injection of concentrated organic iodides and precisely timed roentgenography has been standard for over 20 years. Utilizing the same principles, and with rapid, simultaneous, intravenous injections into both arms, the abdominal aorta, peripheral arterial and cerebral circulations (almost total angiography of the circulatory system) is achieved.

The patient lies supine on an x-ray table that contains a Bucky grid and the special 12 gage needle-stopecock units are then inserted percutaneously or by cut-down. A circulation time via this needle with 3 ml. sodium dehydrochlorate and 15 cc. saline solution is obtained. A 2 second roentgen exposure of the abdomen is made $\frac{1}{2}$ second after the bitter taste. For peripheral arteriography, a portable apparatus exposes the legs immediately after the abdominal study. For cerebral angiography, serial films at 1 second intervals are secured, beginning 2 seconds before the systemic circulation time for a total of 10 seconds.

Forty-one patients have had only mild and transient heat after equally divided intravenous injections of a highly concentrated mixture of sodium and methylglucamine diatrizoates (average dose, 1 ml. per Kg.). The abdominal aorta and peripheral arteries were well visualized in all but 1 instance. In 6 patients, a second injection was needed for more complete opacification. Only 4 patients had studies of the cerebral circulation. Among the noteworthy findings were arteriosclerotic abdominal aortic and splenic artery aneurysms, a ruptured spleen, a postlaminectomy aorticoinferior vena cava fistula, and arteriosclerotic abdominal aortic and peripheral endarteritis.

Reduction of Serum Cholesterol Level in Patients with Coronary Atherosclerosis by Oral Neomycin

Alfred Steiner, Martin Finkel, and Jenes Bakke New York, N.Y.

7.4 Mesenteric Arteriography

Alexander R. Margulis (born 1921)

Margulis was born in the former Yugoslavia on 31 March 1921. After his secondary school education, he entered the University of Belgrade, Faculty of Medicine, in 1939, and finished his medical education at the Harvard Medical School in Boston, where he graduated in 1950. From 1950 to 1951, he was intern at the Henry Ford Hospital, and from 1951 to 1954 resident and clinical instructor at the University of Michigan Hospital. He has held a California Medical License since 1963 and a diploma from The American Board of Radiology since 1954.

Professor Margulis served as Captain in the U.S. Army Medical Corps from 1957 to 1959, was instructor and assistant professor at the University of Minnesota Hospitals from 1954 to 1957, associate professor and full professor at the Washington University in St. Louis from 1959 to 1963, and has since been professor and associate chancellor at the University of California in San Francisco. During this last permanent appointment, he has held ancillary positions as consultant, director or chairman at more than a dozen medical or scientific institutes and hospitals. It is worth mentioning his post as associate chancellor and founding director of the Magnetic Resonance Science Center at UCSF.

He has authored numerous books, chapters, papers and abstracts including the classic gastrointestinal radiology textbook.

Professor Margulis has been a permanent member of many radiological societies, an honorary member of a number of international radiological societies, including the European Congress of Radiology since 1993, and since 1966 has taken part as member, chairman, co-founder, president, etc. in more than forty professional organisations.

Professor Margulis has received several honorary degrees from prominent U.S. and European medical or scientific institutes and has won more than twelve awards and medals from U.S. and European radiological institutes.

Taken in part from www.ecr.org.



P. Heinbecker

Vol. 86, No. 1

MESENTERIC ARTERIOGRAPHY*

By ALEXANDER R. MARGULIS, M.D., and PETER HEINBECKER, M.D.
ST. LOUIS, MISSOURI

THERE has been little basic progress in the roentgenography of the gastrointestinal tract since Dr. Cannon introduced radiopaque contrast material into the gut of a cat. Although refinements of his basic methods have been made, all deductions as to the existence of an abnormality in the gastrointestinal tract roentgenographically still are dependent upon the detection of the lesion's effect on the lumen of the gut. Although dependable for demonstrating the shape and contour of the inner surface of the bowel, existing intestinal roentgenography fails to provide means of assessing the architecture and limits of the whole lesion. Consequently, roentgenologic inferences as to the specific cellular characteristics of a given lesion of the intestine can be little more than an intelligent guess based largely upon frequencies. This applies especially to the problem of differentiating benign from malignant ulcers of the stomach and benign polyps from polypoid carcinomas in the stomach and colon. In an attempt to learn more about the roentgenographic anatomic details of intestinal lesions, both neoplastic and inflammatory, we have been employing operative and isolated organ mesenteric arteriography.

Bierman *et al.*¹ succeeded in opacifying the celiac axis, the superior and inferior mesenteric arteries by transaortic intra-arterial catheterization of viscera. The procedure was unpredictable and dangerous. Ödman^{5,6} visualized the superior mesenteric artery by transfemoral arteriography. The results of this procedure are difficult to interpret because of superimposition of the opacified vessels of the intestinal mesentery.

Schobinger, Blackman and Lin⁷ and Schobinger⁸ demonstrated vascular patterns of benign and malignant neoplasms of the colon and of diverticulitis.

This study was undertaken to develop and to evaluate intestinal arteriography as a method for differentiating neoplastic from inflammatory lesions of the gastrointestinal tract and for distinguishing benign from malignant neoplasms.

METHOD

A limited trial of Schobinger and his co-workers⁷ method was disappointing because of the insufficient vascular detail obtained with it. In order to achieve the necessary detailed opacification of the intestinal vessels, we have used a film cassette wrapped in sterile plastic, placing it directly under the bowel. Then the roentgenograms were made before and during the terminal period of the injection of 8 to 10 ml. of contrast material into the proper artery through a plastic catheter or needle. The contrast material we first used was a solution of 37.5 per cent of diacetamido-triiodobenzoate (hypaque). However after Grayson *et al.*² showed that 40 per cent methylglucamine diacetylamino-triiodobenzoate (renografin) was less toxic to the bowel than hypaque, we used renografin exclusively. In order to facilitate subsequent arteriography of the removed piece of gastrointestinal tract, the plastic catheter was left in the proper artery after the *in vivo* examination was done.

CASE MATERIAL

Mesenteric arteriography was performed during an operation 35 times and upon 48

* From The Edward Mallinckrodt Institute of Radiology and the Department of Surgery, Washington University School of Medicine, St. Louis, Missouri.

Studies supported by a United States Public Health Grant, A4397.

Presented at the Sixty-first Annual Meeting of the American Roentgen Ray Society, Atlantic City, New Jersey, September 27-30, 1960.

TABLE I
LESIONS STUDIED BY MESENTERIC ARTERIOGRAPHY

Operative Arteriography	Colon	Lesion	No.
		Carcinoma	15
		Adenomatous polyps	6
		Villous adenoma	1
		Lipoma	1
		Mucocele of appendix	1
		Chronic ulcerative colitis	3
		Diverticulitis	1
	Multiple small arteriovenous malformations	1	
	Stomach	Carcinoma	3
Peptic ulcer	3		
	Total	35	

Arteriography on Specimens	Colon	Carcinoma	28
		Adenomatous polyps	2
		Lipoma	1
		Villous adenoma	1
		Chronic ulcerative colitis	6
	Stomach	Carcinoma	6
	Leiomyosarcoma	1	
Peptic ulcer	3*		
	Total	48	

* One also had antral gastritis.

stomachs or colons after their removal from the body during celiotomy (Table I).

RESULTS

The operative arteriograms of the intact bowel usually showed better arterial opacification than did the isolated organ arteriograms and therefore were easier to interpret. The vascular pattern outlined in an organ *in vivo* did not differ significantly from the pattern observed after the same organ was isolated.

CARCINOMA OF THE COLON

In all instances, operative and resected specimen arteriography of colonic carcinoma demonstrated destruction of the normal arcades of intestinal vessels. These were replaced by abnormal channels which were tortuous, angulated, had an irregular

lumen, and coursed through the lesion chaotically in many directions (Fig. 1, A-D; and 2, A and B). The irregularity of lumen consisted of sudden irregular widenings and narrowings. In many roentgenograms the vessels of the tumor were finer and narrower than those of the adjacent intestine. The arteriograms of all colonic carcinomas contained irregular, undelimited areas of opacification. These were either small patchy areas of radiodensity resembling lakes surrounding vessels or large uniform areas of laking in which discrete vessels could not be seen. The small perivascular lakes were seen on all the arteriograms of colonic cancer. The larger areas of laking were found in 8 of 15 carcinomas injected *in vivo* and in 8 of the 18 tumors studied following their removal. These areas of laking were not seen when

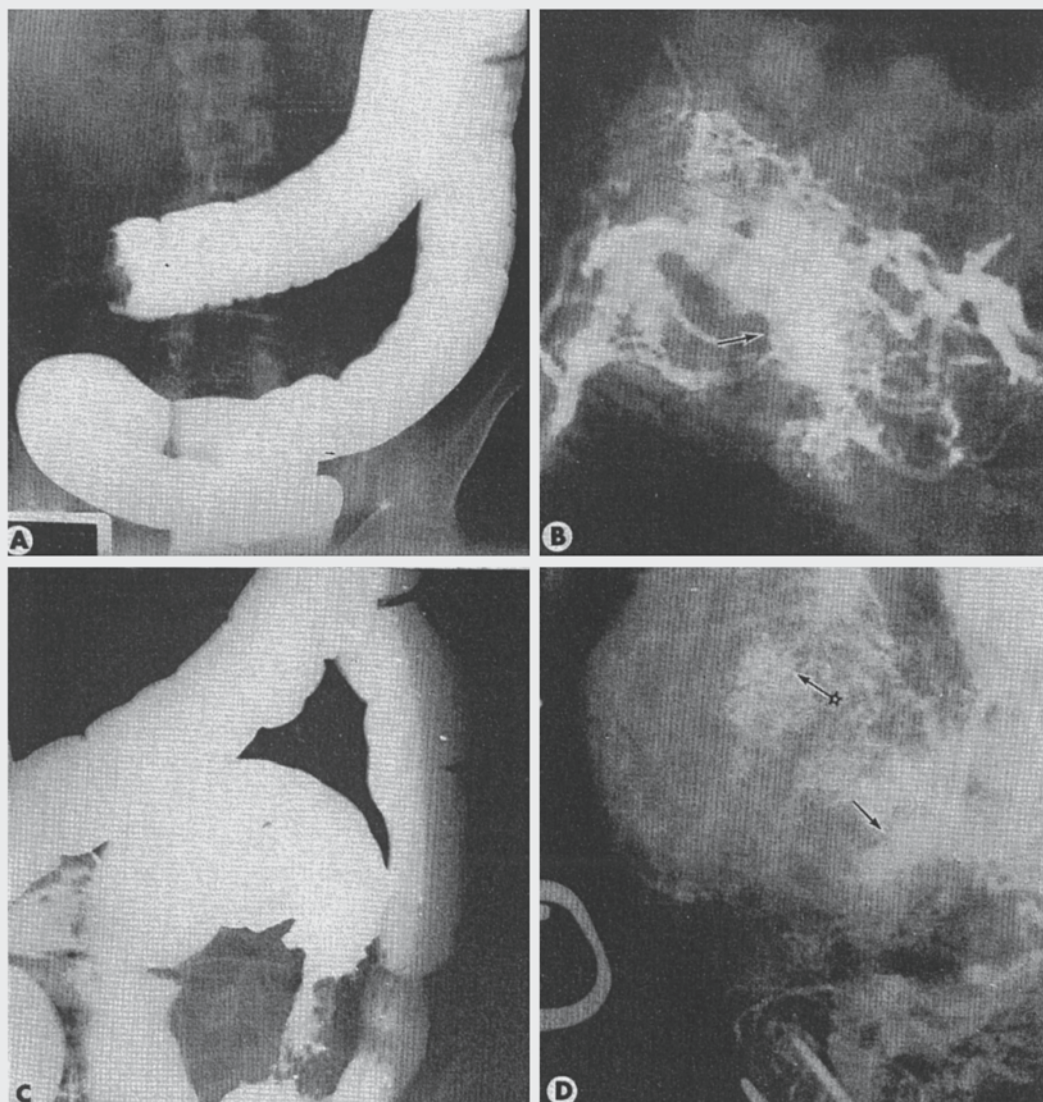


FIG. 1. (A and B) Annular carcinoma of the transverse colon. (A) A pre-evacuation barium enema roentgenogram showing the lesion. (B) An operative mesenteric arteriogram showing the lesion. The vessels are irregular and show sharp turnings. The blood vessels, in general, are more numerous than in the surrounding areas; however, close to the top of the lesion there are fewer vessels. Areas of dense opacification are seen in the tumor (arrow). (C and D) Carcinoma of the sigmoid colon. (C) Barium enema roentgenogram. (D) A mesenteric arteriogram, *in vivo*. Irregular, chaotically arranged vessels are seen throughout the tumor. There are areas of dense opacification (arrow) as well as smaller multiple perivascular areas of leaking (arrow with star).

barium sulfate (USP) was used as the arteriographic contrast material in specimens.

The mesenteric arteries to the tumor

always were prominent and numerous, often larger than adjacent mesenteric vessels. They originated from the marginal artery of the mesentery at irregular inter-

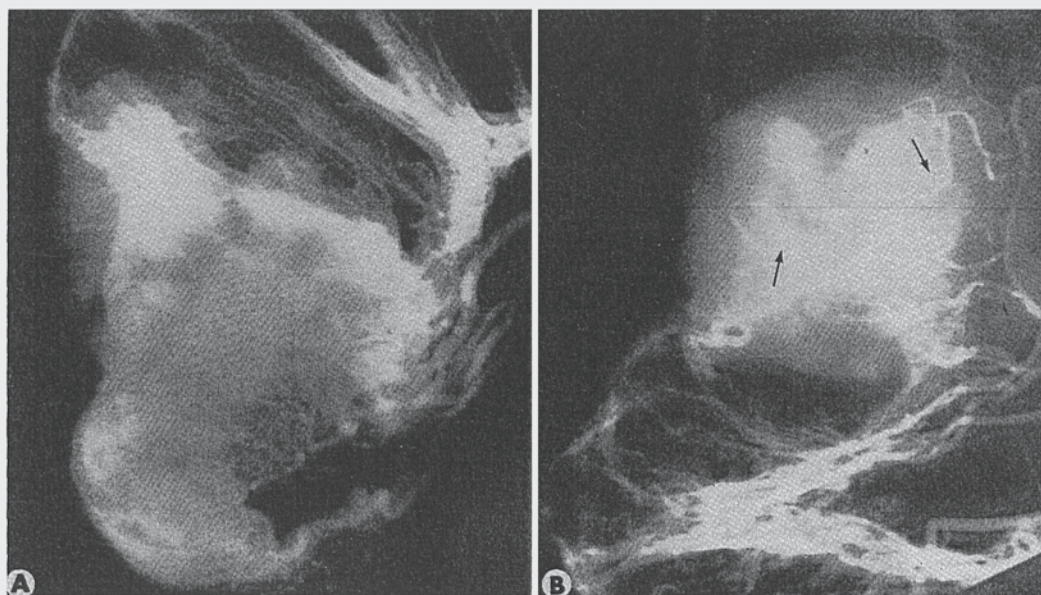


FIG. 2. (A) An operative mesenteric arteriogram showing a carcinoma of the cecum. Note that the mesenteric vessels to the tumor are quite large. The tumor shows large areas of laking along with multiple irregular vessels, sharply contrasting with the parallel normal vessels seen in the uninvolved bowel at the top of the figure. (B) Relatively avascular carcinoma of the sigmoid. The vessels in the tumor show an irregular lumen, sharp turnings and, in general, a chaotic direction. Arrows point to small areas of perivascular laking.

vals and often showed dilatations resembling aneurysms. The vascular channels visualized within the tumors were of smaller caliber and number than in the normal bowel wall in 3 of 15 cancers. Only 2 of the 15 carcinomas studied *in vivo* exhibited vessels uniformly more numerous than normal. The remaining 10 had areas in which only a few vessels were seen and other areas with numerous abnormal, opacified vessels.

BENIGN LESIONS OF THE COLON

Mesenteric arteriograms were performed in 6 patients being operated upon for adenomatous polyps. One had familial multiple polyposis. All others had one or more polypi that were larger than 2 cm. in diameter. One patient had a large villous adenoma (Fig. 3, C and D). The lesions in all 7 patients showed multi-directional vessels of larger caliber and number than

normal. Looking with a magnifying glass at individual vessels within polyps on the arteriogram, luminal irregularities and sharp turnings were absent, although the vessels often were tortuous. The polyps did not contain diffuse or perivascular laking seen in cancers. All polyps except for the very small had a greater vascularity than did the normal adjacent intestine (Fig. 3, A and B).

Operative arteriograms of a mucocoele of the appendix (Fig. 4, A and B) and of a colonic lipoma (Fig. 4, C and D) showed superficial vessels encircling the lesions but few if any within them. These arteriograms differed markedly from those of benign adenomatous polyps and of carcinoma.

The characteristics described serve as the basis for roentgenographic differentiation of benign from malignant colonic tumors (Fig. 1, A-D; 2, A and B; and 3, A-D) (Table II).

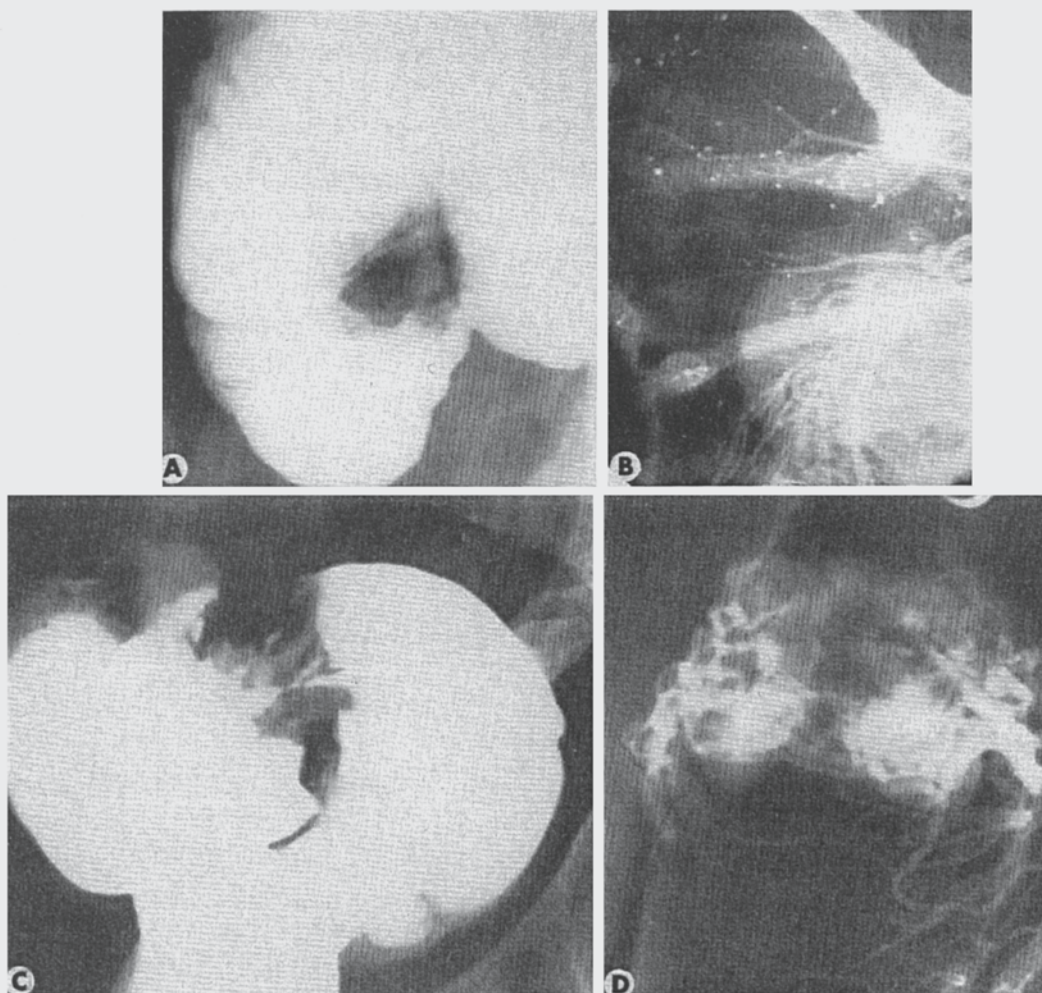


FIG. 3. (*A* and *B*) Adenomatous polyps of the cecum. (*A*) A spot roentgenogram during barium enema study showing the large filling defect in the cecum in the region of the ileocecal valve. (*B*) An operative mesenteric arteriogram showing one very large polyp and one smaller polyp. There are multiple winding vessels within the polyps but no areas of perivascular opacity or large areas of laking. The vessels fail to show irregular lumina and do not show sharp turnings. (*C* and *D*) Villous adenoma of the sigmoid. (*C*) A spot roentgenogram of the sigmoid obtained during a barium enema study. (*D*) An operative mesenteric arteriogram of the lesion showing numerous large tortuous vessels throughout the tumor, sharply contrasted with less numerous and smaller parallel vessels in the adjacent normal bowel. No areas of perivascular laking are seen.

Three patients with chronic ulcerative colitis had operative mesenteric arteriography. Six colons with the same disease were examined by arteriography after their removal. The colonic vessels were numerous, tortuous and gave off branches at close to a 90° angle. The normal parallel

vessels forming arcades were replaced by the vessels characteristic of this disease. The difference in appearance, orientation and distribution from vessels in the normal bowel is illustrated in Figure 5*A*. Figure 5*B* is an operative arteriogram of another patient, containing the same type of vessels

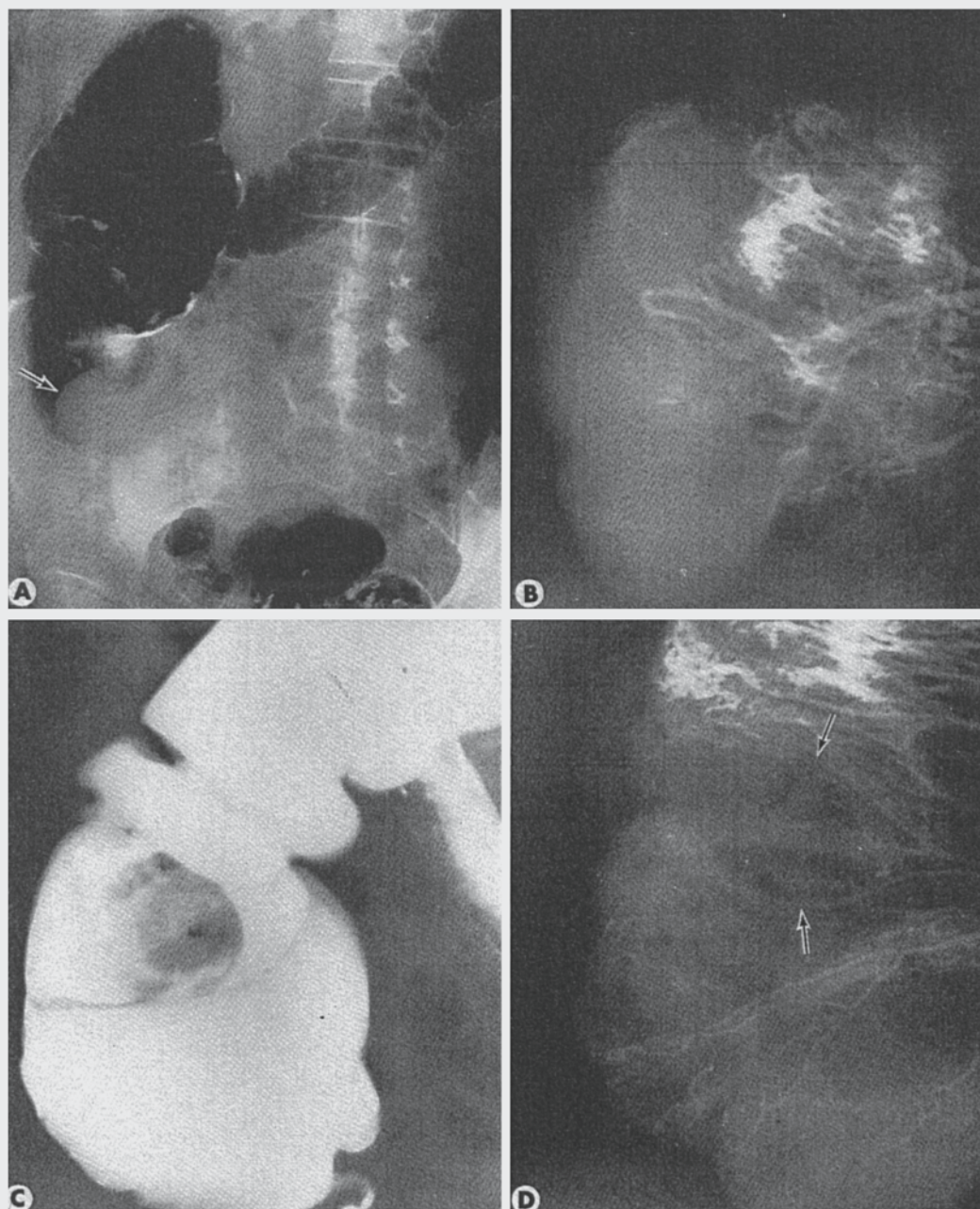


FIG. 4. (*A* and *B*) Mucocoele of the appendix. (*A*) A large rounded filling defect is seen on the medial aspect of the cecum (arrow). (*B*) An operative mesenteric arteriogram shows the lesion to be relatively avascular. Only a few vessels are seen coursing on the surface of the tumor, in sharp contrast to the numerous vessels in the mesentery. (*C* and *D*) Lipoma of the cecum. (*C*) A spot roentgenogram of the cecum obtained during barium enema study shows a smooth rounded defect. (*D*) An operative mesenteric arteriogram shows the lesion to be radiolucent and relatively avascular. Only a few vessels are seen coursing on the surface.

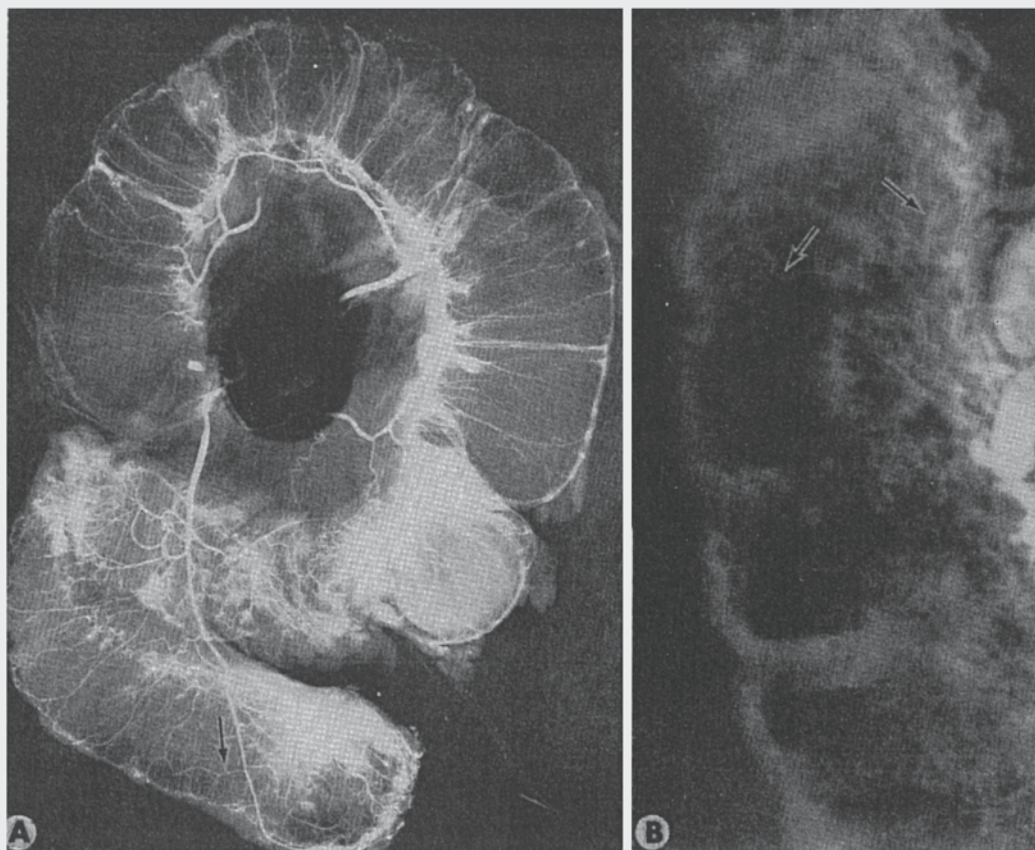


FIG. 5. (A) An arteriogram of the operative specimen following total colectomy. The distal colon is severely involved by chronic ulcerative colitis. The bowel wall is greatly thickened. The vessels are more numerous, tortuous and show branching at right angles (arrow). This is in sharp contrast to the normal arrangement of mesenteric vessels in the uninvolved bowel seen on the figure. (B) An operative mesenteric arteriogram in another case of chronic ulcerative colitis. Numerous tortuous vessels are seen. Many vessels show branching at right angles.

as seen in the specimen examination. The fecal stream had been diverted for a year in one case. This specimen showed only a few fine parallel blood vessels.

An operative arteriogram of a patient with diverticulitis of the transverse colon showed numerous dilated vessels in the area of inflammation just as seen by Schoinger.⁸

The vascular patterns of chronic ulcerative colitis and diverticulitis were different from that of malignant and benign neoplasms of the colon.

ARTERIOGRAPHY OF THE STOMACH

Operative arteriography of the stomach is not a formidable procedure. Anastomoses between arteries are abundant and injection of any vessels of the gastric arcades will visualize the area of abnormality. We have successfully studied lesions of the antrum, body and fundus of the stomach. Arteriograms of polypoid carcinoma of the stomach both *in vivo* and in the specimen showed the same type of vascular pattern described with the more vascular carcinomas of the colon. The normal paral-

TABLE II
FINDINGS IN MESENTERIC ARTERIOGRAPHY

Lesion		Increased No. of Vessels in Diseased Area	Decreased No. of Vessels in Diseased Area	Areas of Increased and Decreased Vessels Side by Side	Large Areas of Laking	Perivascular Small Areas of Laking	Irregular Vascular Pattern	Vascular Luminal Irregularities	Changes in Directional Coursing of Vessels	Right Angle Branching
Colon	Carcinoma	±	±	Most common	In about 50%*	+	+	+	+	o
	Adenomatous polyps	+	o	o	o	o	+	o	o	o
	Chronic ulcerative colitis	+	o	—	o	o	o	o	o	+
Stomach	Polypoid carcinoma	+	o	±	+	+	+	+	+	o
	Ulcerating carcinoma	o	+	o	o	o	o	+	o	o
	Peptic ulcer	+	o	±	o	o	o	o	o	o

* Except in specimen injected with USP barium sulfate.

lel arteries were absent. There were areas of diffuse and of small perivascular laking present (Fig. 6, *A-D*; and 7, *A* and *B*). The vessels in the tumor were irregular in lumen and showed sharp turnings in their course. Their direction was chaotic. Although certain areas of the tumor were relatively avascular, the vessels in general were more numerous. Arteries supplying the tumor were larger than those supplying normal areas.

Benign ulcers of the stomach showed numerous, wide, winding vessels surrounding the crater (Fig. 8, *C* and *D*). The immediate location of the crater and its margins may show few or no vessels. The vessels surrounding the ulcer crater were not irregular in either their lumen or distribution. Our series includes two malignant ulcers of the stomach. In both of them no evidence of cancer was detectable in the gross

specimen and the cancer cells grew in sheaths surrounded by fibrous tissue. The diagnosis of carcinoma could be made only histologically. The arteriograms of the stomach following removal of the organ showed only a few vessels in the region involved by cancer. No areas of diffuse or perivascular laking could be demonstrated. The vessels appeared finer and smaller than in the arteriograms of benign peptic ulcer. The lumen of some of the vessels showed irregularly spaced, asymmetric areas of narrowing and dilatation. The distribution of the vessels, however, followed the normal pattern (Fig. 8, *A* and *B*). The difference between benign peptic ulcers and ulcerating carcinomas will have to be evaluated by a larger series.

In one case having antral gastritis with a benign peptic ulcer, the arteriogram showed numerous vessels of normal ap-

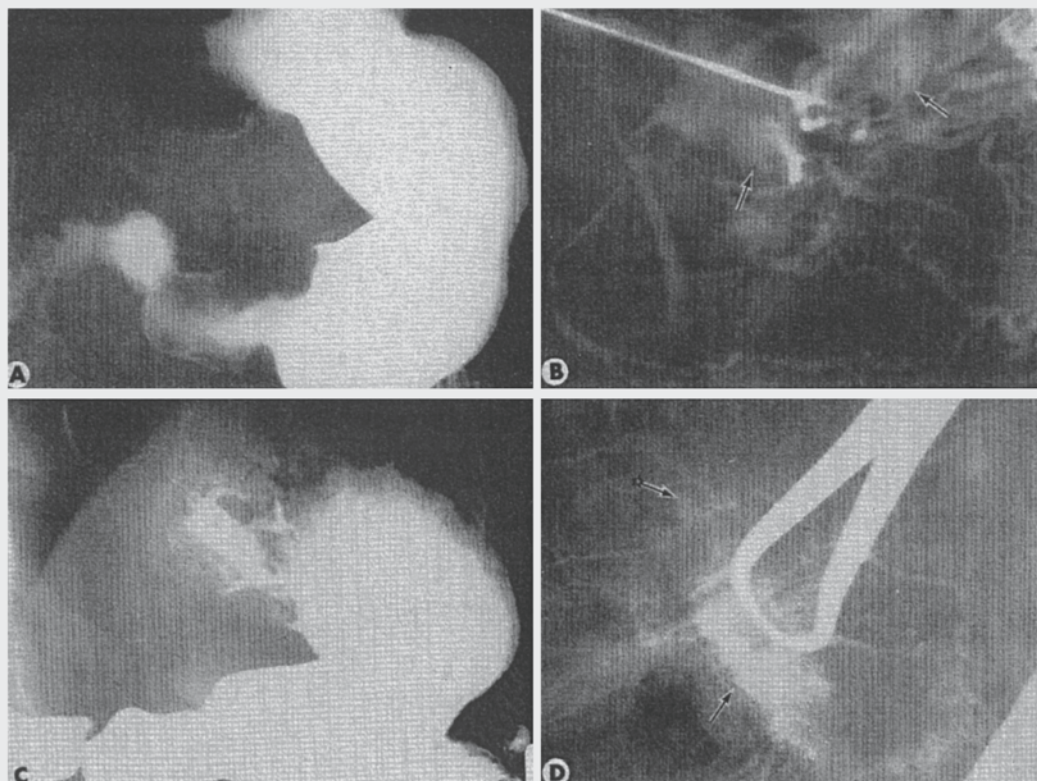


FIG. 6. (A and B) Polypoid carcinoma of the antrum of the stomach. (A) An upper gastrointestinal study with barium. (B) A mesenteric arteriogram with injection into the right gastric artery. Arrows point to areas of laking in the tumor. The vessels leading to the tumor are large and numerous. (C and D) Carcinoma of the fundus of the stomach. (C) An upper gastrointestinal study with barium. A large ulcer is seen within the mass in the fundus of the stomach. (D) An operative mesenteric arteriogram with injection into the left gastric artery shows areas of increased and decreased vascularity side by side. The vessels are irregular in distribution. Large areas of opacity in the tumor (arrow) are seen along with numerous small areas of perivascular laking (arrow with star).

pearance and distribution. An arteriogram of the specimen of a stomach containing a large leiomyosarcoma showed the same characteristics as seen in polypoid gastric carcinomas.

DISCUSSION

The definition of the location, extent and nature of internal lesions of the intestinal tract, without opening it, is surgically important. Operative arteriography promises to provide a fairly accurate way of doing this. The method, although seemingly simple and straightforward, is nonetheless

somewhat time consuming. It often requires mobilization of the bowel or stomach in order to place the film cassettes in proper contact. It would be easier to have the film under the patient in a Bucky device but with the present technique this gives much poorer detail. Differences in the vascular pattern of a benign adenoma of the colon and a polypoid carcinoma are very fine, and any sacrifice in detail may lead to the wrong diagnosis.

It is difficult to draw final conclusions on the basis of studies done to date. Undoubtedly, much more work will be needed

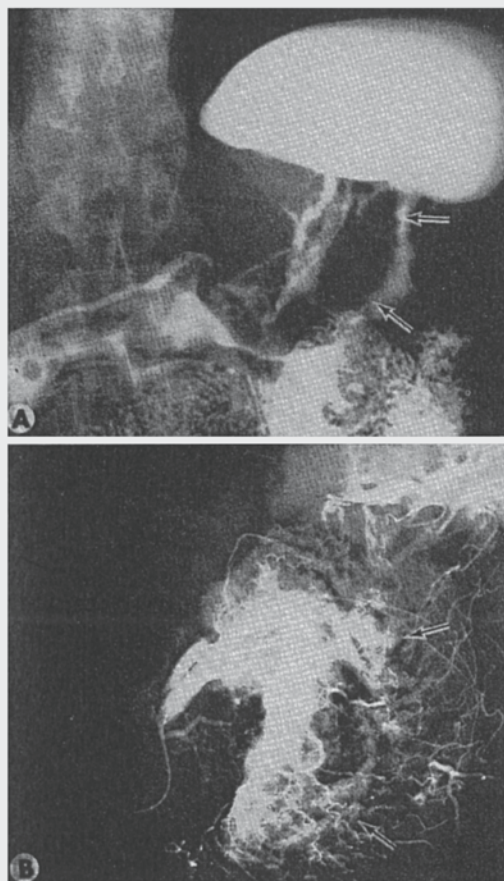


FIG. 7. Large polypoid carcinoma of the stomach. (A) A supine study with barium. The arrows point to the lateral margin of the mass. (B) An arteriogram of the dissected portion of the stomach. Within the tumor are numerous irregular vessels and large areas of opacification as well as those of perivascular density. The extent of the tumor is outlined by arrows.

before definite vascular patterns for various types of neoplasms of the stomach, small bowel and colon are established and before the validity of diagnostic criteria of this method survives repeated testing. The criteria arrived at from our material so far are given in Table II.

Besides the obvious utility of operative mesenteric arteriography for differentiation of various tumors and inflammations

of the intestinal tract, it is, at times, very useful for the location of the site of massive gastrointestinal hemorrhage. We have already reported its use in this regard.³ So far, we have used operative mesenteric arteriography only on the parts of the gastrointestinal tract that the surgeon has already decided to remove, having been worried about the toxic propensities of the contrast materials available. Evaluating the safety of this procedure in the dog, we² have found that methylglucamine diacetyl-amino-triiodobenzoate (renografin) is the safest contrast medium of those studied. Eight to ten milliliters of 40 per cent renografin in saline appear to be a safe amount to inject into a loop of bowel which is not to be resected.

SUMMARY

The method and findings of operative mesenteric arteriography are presented. Data obtained from injections of operative specimens of the colon and stomach are also referred to. Vascular patterns obtained by arteriography of malignant and benign tumors of the colon, chronic ulcerative colitis, carcinoma of the stomach and gastric ulcers are described.

Alexander R. Margulis, M.D.
Washington University School of Medicine
St. Louis, Missouri

REFERENCES

1. BIERMAN, H. R., MILLER, E. R., BYRON, R. L., JR., DOD, K. S., KELLY, K. H., and BLACK, D. H. Intra-arterial catheterization of viscera in man. *AM. J. ROENTGENOL., RAD. THERAPY & NUCLEAR MED.*, 1951, 66, 555-568.
2. GRAYSON, T., MARGULIS, A. R., HEINBECKER, P., and SALTZSTEIN, S. L. Safety of mesenteric arteriography; experimental study on dogs. To be published.
3. MARGULIS, A. R., HEINBECKER, P., and BERNARD, H. R. Operative mesenteric arteriography in search for site of bleeding in unexplained gastrointestinal hemorrhage; preliminary report. *Surgery*, 1960, 48, 534-539.
4. McAFEE, J. G. Survey of complications of abdominal aortography. *Radiology*, 1957, 68, 825-838.
5. ÖDMAN, P. Percutaneous selective angiography

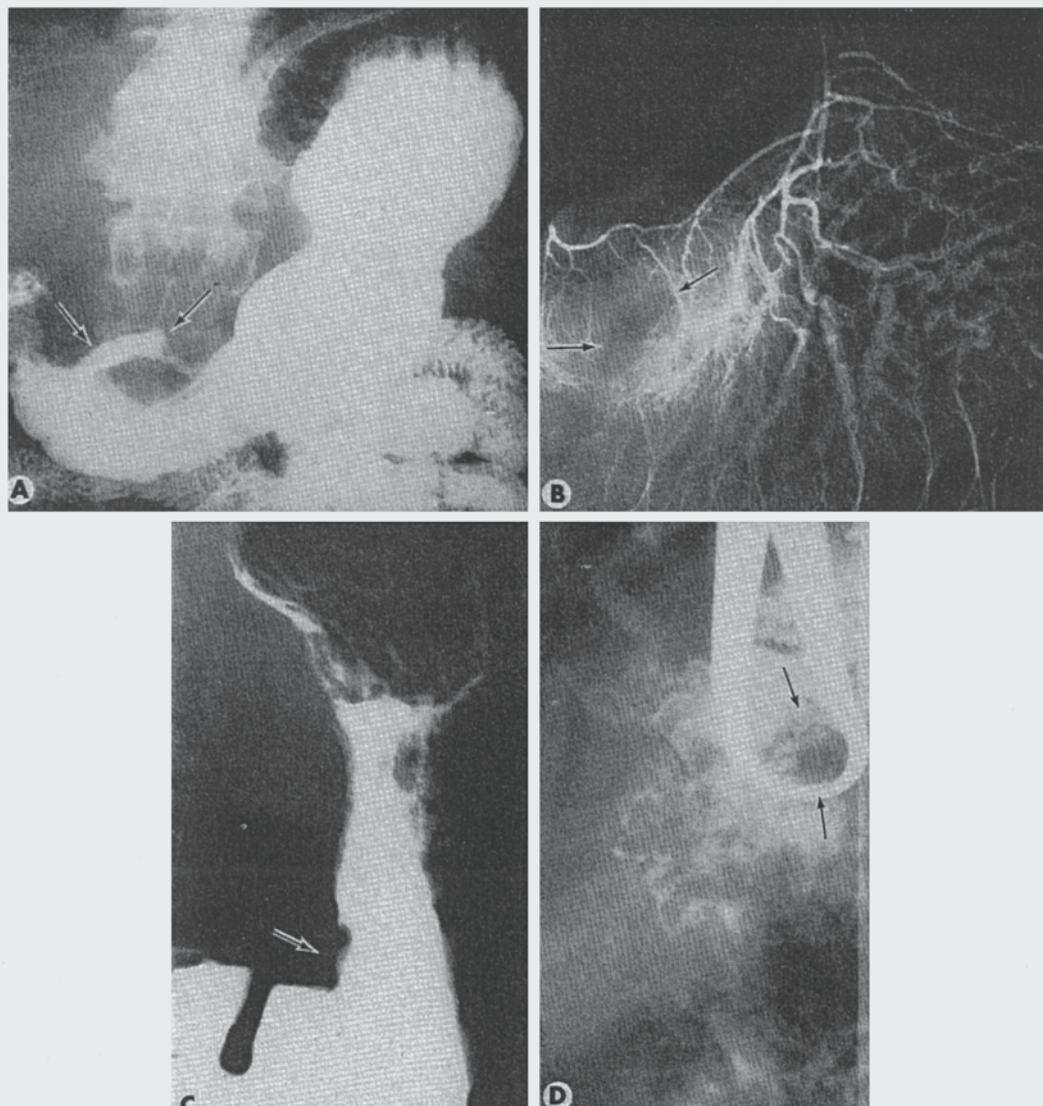


FIG. 8. (A and B) Large ulcerative carcinoma of the stomach. (A) A roentgenogram of the upper gastrointestinal tract with barium. (B) Only few vessels are seen in the area involved by the tumor. There is a strong suggestion of some irregularity in the lumen of the many attenuated vessels. (C and D) Benign peptic ulcer of the lesser curvature of the stomach. (C) An upright roentgenogram of the barium filled stomach with the ulcer shown in profile (arrow). (D) An operative arteriogram. Numerous tortuous vessels surround the ulcer which is the radiolucent area (arrows). There is no evidence of perivascular opacity. (A metallic instrument was left in the field of exposure by error.)

- of coeliac artery. *Acta radiol.*, 1958, Suppl. 159.
 6. ÖDMAN, P. Percutaneous selective angiography of superior mesenteric artery. *Acta radiol.*, 1959, 51, 25-32.
 7. SCHOBINGER, R., BLACKMAN, G., and LIN, R. K.

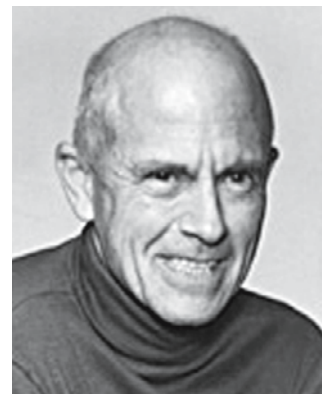
Operative intestinal arteriography. *Acta radiol.*, 1957, 48, 330-336.

8. SCHOBINGER, R. Operative intestinal arteriography in diagnosis of diverticulitis of colon. *Acta radiol.*, 1959, 52, 28-33.

7.5 Transluminal treatment of arteriosclerotic obstruction: description of a new technique and a preliminary report of its application

Charles T. Dotter (1920–1985)

Charles Dotter was born in Boston on 14 June 1920. He received a Bachelor of Arts degree in 1941 from Duke University. He then proceeded to study medicine at Cornell University. He completed his internship in the United States Naval Hospital in New York State and his residency at New York Hospital. At the age of 30 he became a full-time faculty member at Cornell Medical School. Two years later he became professor and Chairman of the Department of Radiology at the University of Oregon Medical School. He was only 32 years of age and was apparently the youngest person to have ever been made chairman of a radiology department in a major American medical school. He stayed at Oregon for 32 years. He is rightly considered the father of interventional radiology, publishing more than 300 papers, of which he was the first author on more than half. He is credited with performing the first transluminal angioplasty. His trainee for the first procedure was Melvin Judkins, who also went on to become a great angiography pioneer. The first patient to benefit from angioplasty was Laura Shaw, an 82-year-old woman who was admitted to the University of Oregon Hospital with a painful left foot. Her pain disappeared a week following the angioplasty and her ulcers soon healed. Dotter invented the balloon catheter and used it to study circulation. He also made contributions to forensic pathology, publishing a case report in 1961 entitled "Murder by Suffocation" in which dental radiography and photography was used to make a diagnosis. He even published an article on cardiac resuscitation in 1962 and was considerably ahead of his time. As a human being he was a polymath. He was a pilot, a flyer and a mountain climber. He was interested in classical music, painting, photography and outdoor living. He was nominated for the Nobel Prize in medicine in 1978 and his pioneering research into interventional radiology resulted in 4 gold medals. He passed away in 1985.



Melvin P. Judkins (1922–1985)

An associate of Dr. Charles Dotter at the University of Oregon in Portland, radiologist Dr. Melvin Judkins studied coronary angiography with Dr. Mason Sones. Judkins went on to create his own system of diagnostic imaging, introducing a series of specialized catheters and perfecting the transfemoral approach (introducing the catheter via a groin puncture rather than the more complex procedure used by Sones of introducing the catheter via surgical opening of the brachial artery in the arm).

A careful perfectionist, Judkins went to great lengths to educate his patients, train his colleagues and share his techniques, and continued his work at Loma Linda Medical Center. Judkins furthered the goal of an accessible, systematic approach to high-quality diagnostic radiology. The Judkins technique of coronary angiography remains the primary diagnostic tool used in catheterization laboratories around the world.



Transluminal Treatment of Arteriosclerotic Obstruction

Description of a New Technic and a Preliminary Report of Its Application

By CHARLES T. DOTTER, M.D., AND MELVIN P. JUDKINS, M.D.

DESPITE the frequency and importance of arteriosclerotic obstruction, current methods of therapy leave much to be desired. Nonsurgical measures, however helpful they may be, provide the patient little more than an opportunity to live with his disease. Consistent success in the use of surgical technics such as endarterectomy, angioplasty, and grafting has largely been confined to highly specialized vascular surgeons of whom there are far too few to cope realistically with literally millions of patients suffering the painful, disabling, or lethal consequences of the disease. Moreover, for practical purposes, surgical success is limited in the management of occlusions in smaller arteries.¹⁻³ Thus, while aorto-iliac thromboendarterectomy has been generally successful, gangrene due to femoropopliteal occlusion frequently results in amputation. Expert vascular surgeons are reluctant to intervene in low femoral lesions if tolerable intermittent claudication is the only resulting disability.⁴ With these facts in mind, pursuit of a previously proposed approach^{5,6} has led to the development of a safe, simple, and effective technic for directly overcoming arteriosclerotic narrowing and occlusion in the arteries of the leg. Impressive salvages already achieved in otherwise doomed legs amply justify this preliminary report even though long-term follow-up observations are not yet possible.

From the University of Oregon's Minthorn Memorial Laboratory for Cardiovascular Research through Radiology.

Aided by grants from the U. S. Public Health Service (H-3275 and H-6336), the Oregon Heart Association, and Mallinckrodt Pharmaceuticals.

Method

Procedure

Prior angiographic survey of the abdominal aorta, its iliac branches, and the leg arteries, including those beyond the suspected primary block, is best done by retrograde catheterization of the opposite femoral artery, thus insuring a hematoma-free femoral region on the side to be treated. If an attempt appears indicated, the procedure, including its present experimental status, is fully discussed with the patient and specific permission is obtained. Oral anticoagulant agents are discontinued and barbiturate sedation is given at an appropriate time. Local anesthesia was used in all but two patients who received low spinal block.

The actual procedure is begun with downstream or antegrade femoral catheterization and control arteriography. A preliminary injection of 2,000 units of heparin is given into the artery, and under fluoroscopic control an ordinary coil-spring catheter guide of about 0.05 inch OD is passed down the lumen until its tip has traversed the stenosis to reach the lumen beyond. A tapered, radiopaque, Teflon dilating catheter* of approximately 0.1 inch OD is then slipped over the guide and advanced until it, too, has traversed the block, thereby enlarging the pre-existing or newly opened lumen. The guide is passed across the atheromatous block without going through the wall more by the application of judgment than of force; both are often needed to effect the subsequent dilatation. Where desirable and possible, a second dilating catheter of nearly 0.2 inch OD is passed over the first. Although secondary thrombotic luminal obliterations can be traversed and dilated with surprising ease, it may be difficult or impossible to pass the larger dilating catheter across primary, chronic, lengthy atheromatous occlusions. Fortunately, in patients with severe, longstanding ischemia striking improvement is likely to result from modest dilatations.

*Cook Incorporated, 2305 East Second Street, Bloomington, Indiana.

TRANSLUMINAL TREATMENT OF OBSTRUCTION

655

During the course of dilatation, and especially with contrast injections, patients often experience increased pain in the foot, but there need be no other concern over the completely occluding catheter. Withdrawal of the guide permits confirmation that the desired lumen-to-lumen passage or dilatation has, in fact, been accomplished. To minimize the possibility of pain and arterial spasm associated with the periatheromatous and especially with the extramural injection of contrast agent, exploratory injections are delivered manually under direct fluoroscopic control with a minimum volume of dilute contrast agent. At present, we use Conray* diluted with an equal volume of heparin-saline irrigation solution; a suitable gaseous contrast medium may prove to have advantages in this application. In any case, pressure injection equipment and concentrated radiopaque agents have no place in this procedure.

After a successful transatheromatous dilatation,

considerable traction is usually needed to withdraw the impacted catheter to a point above the treated segment. Often at this juncture, the patient will happily announce the return of adequate blood flow to the troubled extremity. Concentrated heparin is again injected and a final angiogram is made prior to removal of the remaining catheter. Hemostasis is manually obtained, and a nonconstricting bandage is applied over the site of the femoral puncture. We now use low-dose heparin following recanalization (40 mg. intramuscularly every 6 hours for 3 to 5 days).

It is convenient and informative to monitor the procedure and follow its results with a Parks mercury strain-gage plethysmograph.* In addition to providing an objective, permanent record of pulsations, this simple, economical instrument permits the determination of blood pressure in legs not possible by ordinary sphygmomanometry.

* Conray, Mallinckrodt Pharmaceuticals, St. Louis, Missouri.

* Parks Electronics Laboratory, Route 2, Box 35, Beaverton, Oregon.

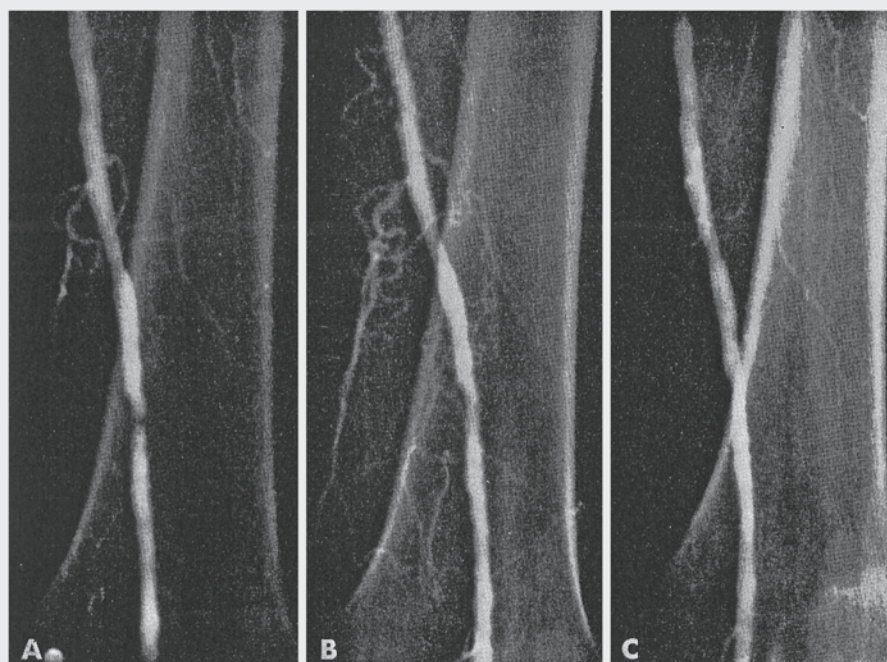


Figure 1

Case 1. Transluminal dilatation and segmental narrowing of the left superficial femoral artery. A. Control arteriogram showing threadlike lumen in region of adductor hiatus. B. Immediately after dilatation with catheter of 3.2 mm. OD. C. Three weeks after transluminal dilatation. Lumen remains open. Clinical and plethysmographic studies indicate continuing patency over 6 months later.

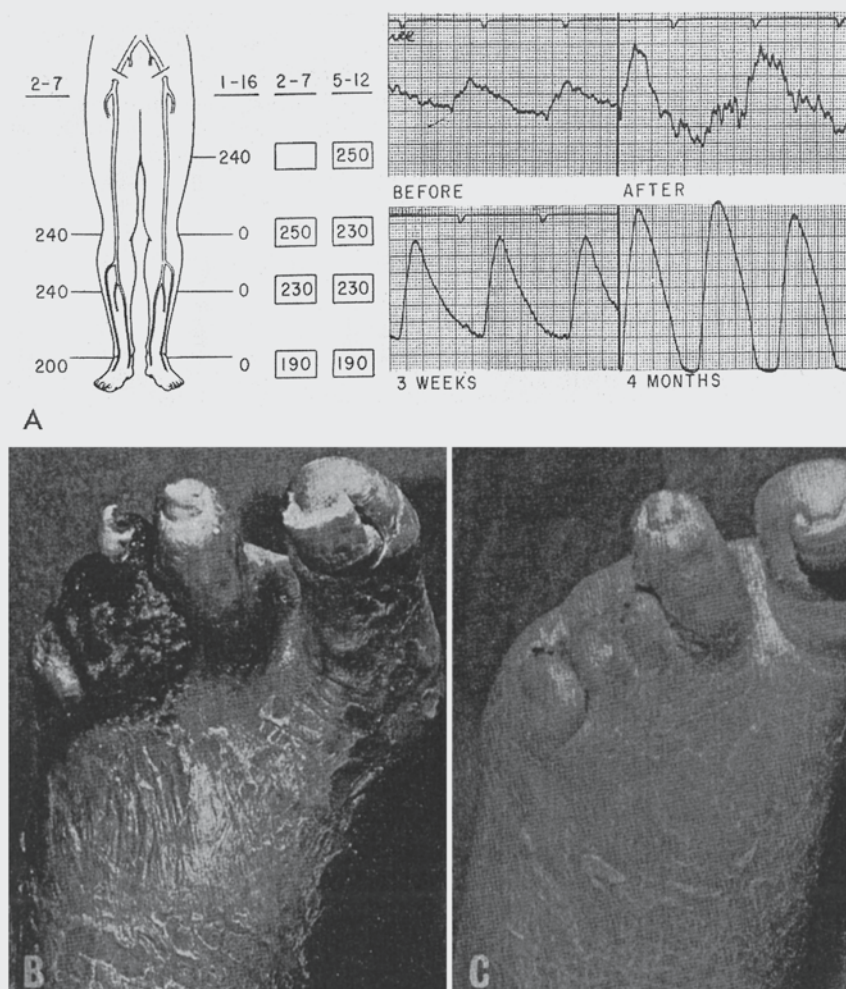


Figure 2

Case 1. Objective improvement after transluminal treatment of subtotal superficial femoral obstruction. A. Blood pressures at indicated sites and times, before and after treatment; plethysmographic pulse waveforms. B. and C. Photographs of left foot 1 week and 5 months after the procedure.

Technical Problems and Complications

While the entire procedure can at times be successfully completed in 10 or 15 minutes, technical problems may prolong matters and lead to impaired results or failure. Passage of the guide and dilating catheters through the periatheromatous cleavage plane is not a desirable method of approaching or traversing the primary site of atheromatous block. Basic to the success of this technic is the transluminal traverse and dilatation of the primary atheromatous block with the formation of an inelastic conduit out of the

patient's own previously obstructing tissues. Neither total luminal closure at the site of primary obstruction (usually at the femoropopliteal junction in the adductor hiatus), nor more proximal obliteration by secondary thrombotic material is a critical deterrent to success, since a properly directed guide will pass harmlessly through both obstructions. What is important, we believe, is that the site of sclerotic primary obstruction be bridged by a lumen-to-lumen transatheromatous rather than periatheromatous route. In the latter event, there may be

TRANSLUMINAL TREATMENT OF OBSTRUCTION

657

considerable improvement in the patient's ischemia, but the degree and permanence of benefit appears to be impaired.

Inadvertent entry into the periatheromatous cleavage plane is sometimes signaled by an increased sense of resistance and can be confirmed by the configuration and relative immobility of a small amount of contrast agent injected through the dilating catheter. Periatheromatous entry is somewhat more difficult to identify in the presence of pre-stenotic luminal thrombosis. Transmural passage, i.e., perforation of the artery, is usually easy to detect by the course of the guide. It does not require abandonment of the procedure, but rather indicates the need for withdrawal and redirection of the guide into the (patent or occluded) lumen. When avoidable, contrast agent should not be injected extraluminally, for pain and spasm of functioning regional arteries can ensue. A transluminal catheter path extending for several centimeters proximal to the site of occlusion aids the desired passage of the probe through the narrowed or obliterated lumen at the site of the primary atheromatous obstruction.

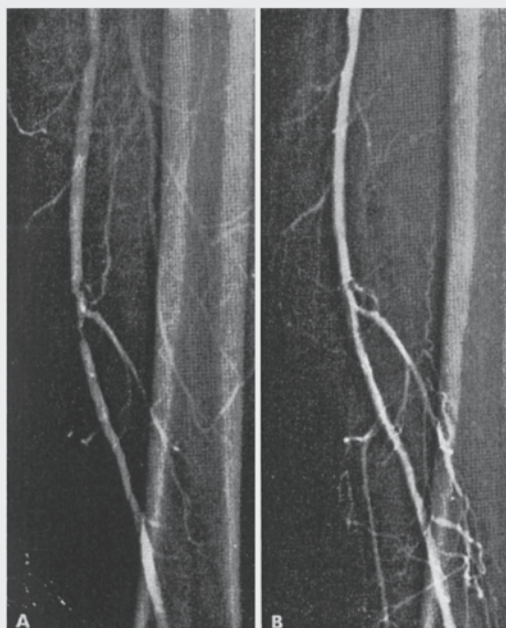


Figure 3

Case 2. Multiple short stenoses of superficial femoral artery before and after percutaneous transluminal dilatation. A. Control arteriogram showing two of the three segmental narrowings which were present. B. Improved luminal dimensions immediately after procedure.

Circulation, Volume XXX, November 1964

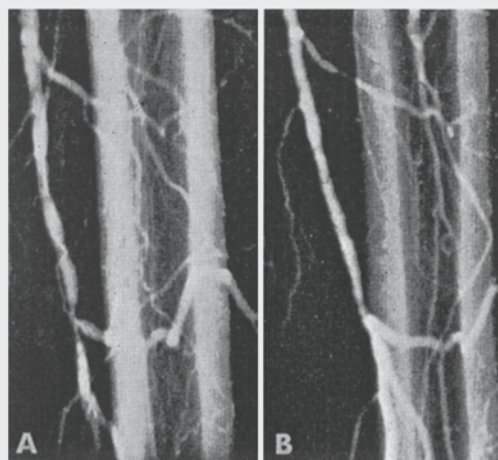


Figure 4

Case 3. Atherosclerotic narrowing of deep femoral artery. Before (A) and after (B) transluminal dilatation. The outer diameter of the treated artery is approximately 1 to 1.2 mm. The dilatation required only a few seconds.

While both are occasionally frustrating, neither entry into the periatheromatous cleavage plane nor transmural penetration of the artery constitutes an alarming complication of the procedure. Should an undesired pathway be so situated as to be subsequently unavoidable, the attempted recanalization is best postponed for a few days. Due to the small caliber of the guide and length of its tract, "inside-out" puncture occurring during probe-traverse of an occluded lumen is less likely to cause bleeding than ordinary needle puncture. To date, we have observed no clinical or radiologic evidence that this technique has caused embolization downstream. If this occurred, its consequences have apparently been overshadowed by the benefits of the procedure.

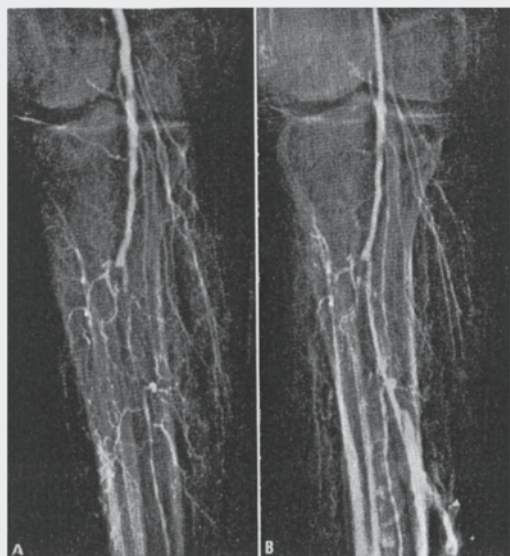
Results

Case Reports

Case 1 (figs. 1 and 2)

L.S., an 82-year-old woman, was admitted with a cold, pulseless, continuously painful left lower extremity with an associated 2 by 4 cm. ischemic ulcer and progressing gangrene of three toes. Femoral angiography on January 6, 1964, disclosed a 0.5 cm. long atherosclerotic obstruction of the left superficial femoral artery at the level of the adductor hiatus. The lumen of the artery, though patent, was hardly discernible. The popliteal and tibial arteries filled slowly and contained numerous areas of irregular narrowing.

Because of advancing gangrene, amputation

**Figure 5**

Case 4. Complete occlusion of popliteal artery at its trifurcation. A. A patent fibular artery is visible 5 cm. distal to site of primary obstruction. B. After attempted recanalization of fibular branch of popliteal artery. Radiographic confirmation of lumen-to-lumen patency with contrast agent visible in an adjacent vascular bundle (arrow). Pain was aggravated by procedure, presumably due to spasm. There was no opportunity to evaluate the result, since amputation was done 2 days later.

was strongly advised but the patient refused. On January 16, 1964, percutaneous transfemoral catheter dilatation of the segmental femoral obstruction was carried out in a matter of minutes and without difficulty. Coincident with the removal of the catheter from the site of the previous stenosis, good pulses were palpable for the first time in the lower leg and foot. Angiography showed that the stenosis was no longer present. Plethysmography demonstrated marked improvement in pulse and blood pressure, previously unobtainable on the left.

Pain, discoloration, and coldness of the foot, present on admission, diminished immediately following relief of the obstruction. During the following week, there was rapid healing of the ischemic skin changes, including ulceration of the lower leg.

Follow-up angiography on February 6, 1964, 3 weeks after dilatation, showed continuing patency of the lumen. At present, over 8 months after the procedure, the patient is ambulatory; the ulceration is gone; her gangrenous toes have separated and the sites are healed.

Case 2 (fig. 3)

J. R., a 58-year-old man, complained of increasing coldness and claudication in his left leg. Femoral arteriography revealed three short subtotal narrowings of the superficial femoral artery. On February 14, 1964, a transfemoral dilatation was produced as seen in the second angiogram (fig. 3B). During the procedure, the catheter entered the periatheromatous cleavage plane several times and one or more transmural perforations occurred. It was not then realized that the patient was taking an oral anticoagulant drug because of previous coronary occlusion. During the week following the procedure, a large hematoma developed in the left inguinal area. Surgical drainage and infection obscured any immediate benefit from the procedure. The patient has not permitted further angiograms.

Case 3 (fig. 4)

H. H., a 64-year-old man had been on anticoagulant therapy following a stroke in 1959. His present complaint related to claudication in a

**Figure 6**

Case 5. Complete midpopliteal occlusion; recanalization via periatheromatous route. A. Before procedure. The distal fibular artery is patent. B. Composite angiogram shows direct communication between popliteal and fibular arteries, catheter extending down an adjacent vascular bundle. The appearance of the contrast material in the popliteal artery is characteristic of a periatheromatous pathway.

TRANSLUMINAL TREATMENT OF OBSTRUCTION

659

cold, pulseless left foot and leg with gangrene in one of the toes. Angiography, with a distally directed catheter located in the profunda femoral artery, demonstrated by reflux a 3 to 4 cm. complete obstruction of the superficial femoral artery at the adductor hiatus. In addition, there was severe stenosis of the lower profunda femoral artery, clearly hampering flow through important collateral channels. A coaxial dilating catheter was passed downward until the inner catheter (OD 2 mm.) had traversed this stenosis. Subsequent angiography indicated that the luminal caliber had been increased several-fold with resultant improvement of collateral blood flow. An effort to relieve the complete obstruction was not desired by referring physicians, and this was subsequently treated by endarterectomy and vein patch angioplasty.

Case 4 (fig. 5)

M. D., a 78-year-old diabetic Negro woman gave a 2-year history of claudication with multiple ulcerations leading to gangrene of the right leg and foot. Right femoral arteriography showed a complete popliteal block at the level of the trifurcation. Neither the anterior nor posterior tibial arteries filled, and extensive small artery

disease was shown. A 5-cm. block of the fibular artery was noted, and it was decided to attempt to bridge it. This was accomplished with the extravasation of contrast material into distal vascular bundles. The procedure appeared to be of no immediate clinical benefit, presumably because of endarteritis. Continuing rest pain led the patient to demand amputation, which was done 2 days later.

Case 5 (fig. 6)

V. S., a 62-year-old diabetic woman, was admitted because of bilateral ischemic rest pain, right lower leg ulceration, and gangrene of the right first toe. Physical examination disclosed primary carcinoma of the epiglottis with involvement of the cervical lymph nodes. Her right leg exhibited reduced capillary filling, markedly reduced or absent distal pulses, and infected ischemic ulceration of the lower leg. Arteriography demonstrated subtotal obstruction of the right popliteal artery with obliterated anterior and posterior tibial arteries and a partially blocked fibular artery. There was extensive endarteritis. Despite these multiple obstructions, creation of an intravascular channel between the femoral and fibular arteries was thought to be possible and

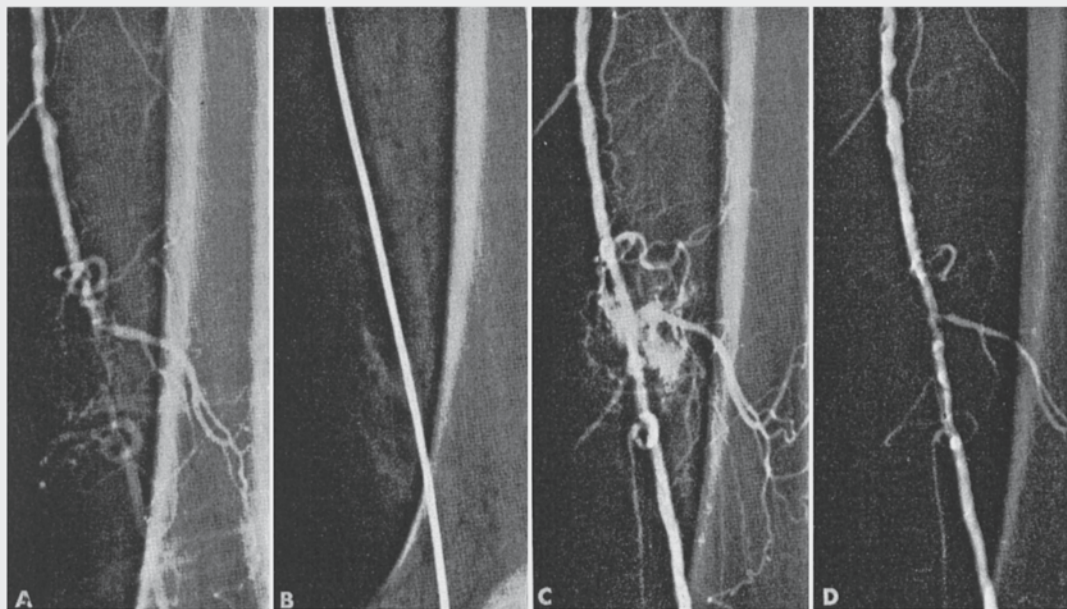


Figure 7

Case 6. Transluminal recanalization of complete obstructions of the superficial femoral artery. A. Before procedure. B. Tapered dilating catheter traversing the block. C. Luminal continuity and minor extravasation immediately after removal of catheter. D. One week later. Residual luminal narrowing did not prevent reversal of gangrenous changes and complete relief of symptoms. See also figure 8A.

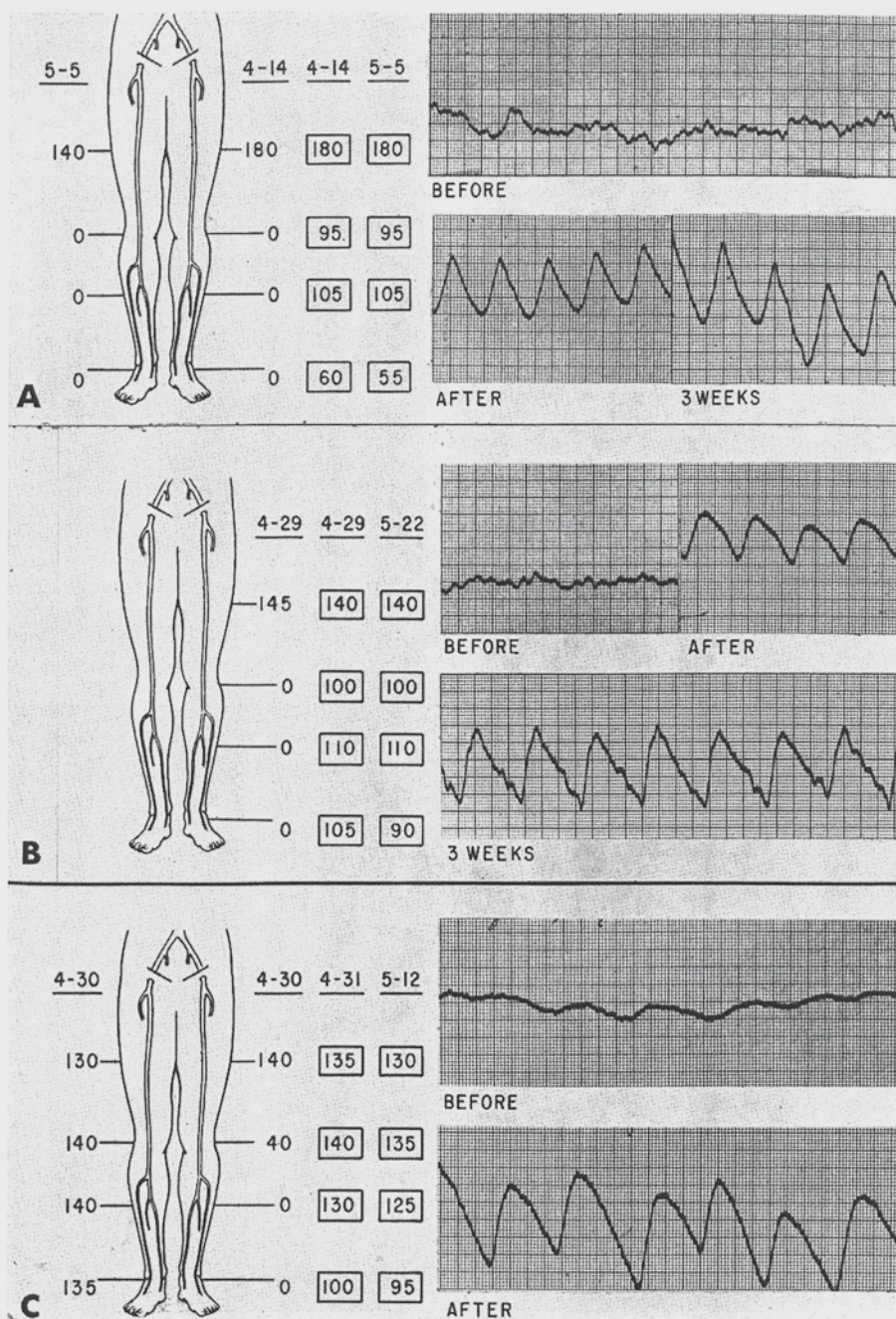


Figure 8

Plethysmographically determined blood pressures and pulse waveforms in three patients before and after percutaneous transluminal recanalization of complete obstructions of superficial femoral artery. A., B., and C: Cases 6, 7, and 8. Systolic pressures determined with Parks plethysmograph. Circled values are after the procedure.

TRANSLUMINAL TREATMENT OF OBSTRUCTION

661

worth while. On April 9, 1964, a guide and the smaller dilating catheter traversed the obstruction. Unfortunately, continuity was achieved via the periatheromatous route and, as was expected, her clinical improvement was limited to temporary progress in healing of the ulceration and diminution in rest pain on the treated side. Attention has centered on the treatment of the carcinoma and the appearance of severe ischemia has recently led to amputation.

Case 6 (figs. 7 and 8A)

F. S., a 65-year-old man, was hospitalized a year earlier because of increasing bilateral claudication, rest pain, and coldness of the feet and legs, most severe on the right. Distal pulses were

absent on the right and questionably present on the left. Right external iliac and common femoral endarterectomy and vein-patch angioplasty were done. His present admission on April 7, 1964, was occasioned by a cold, cyanotic, and atrophic right lower leg and foot; an ulceration 3 by 5 cm. in diameter was present on the lateral aspect of the lower leg. The left lower leg showed ischemic skin changes, markedly reduced popliteal pulsation, and no distal pulsations. Pulsation in the toes could not be detected by plethysmography.

On April 14, 1964, a percutaneously introduced antegrade guide spring and graduated dilating catheters quickly traversed the previously demonstrated 2-cm. area of completely ob-

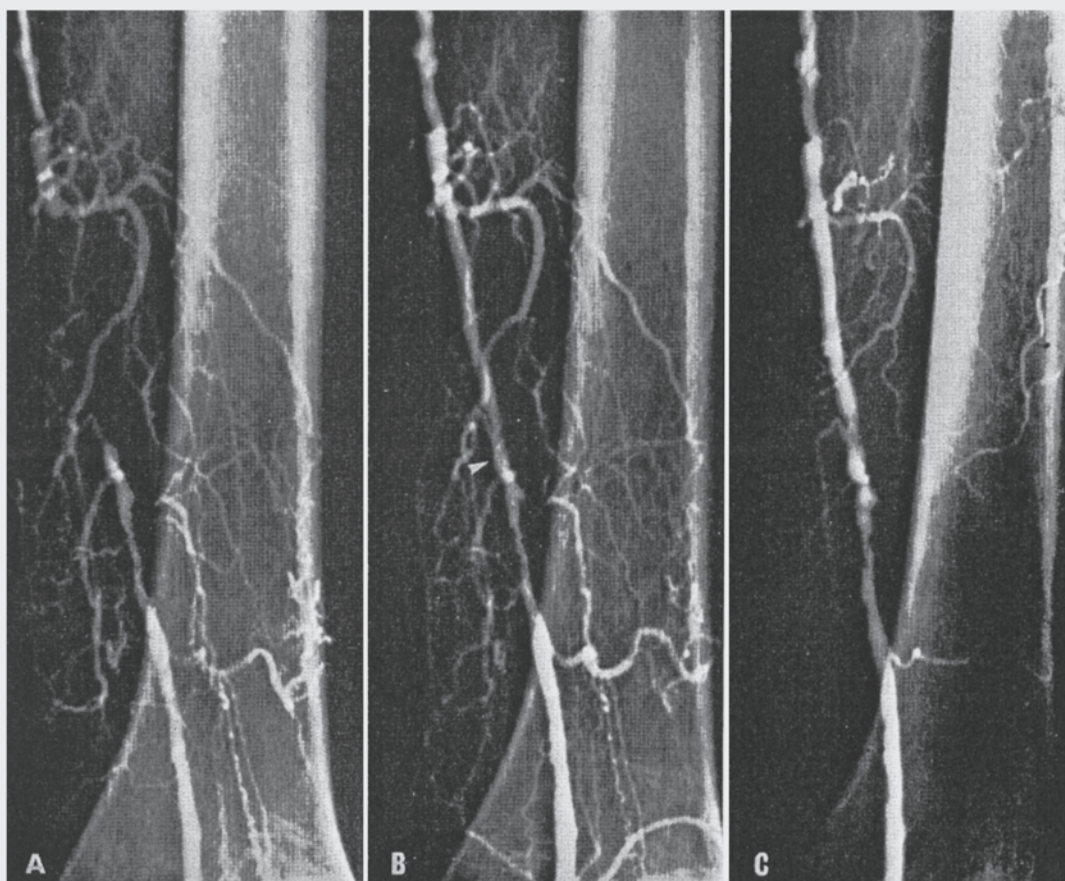


Figure 9

Case 7. Percutaneous transluminal recanalization of 6-cm. complete occlusion of superficial femoral artery in a diabetic man of 68. A. Control arteriogram. B. Immediately after recanalization (which was extended only to level of arrow). C. Six weeks later. Recanalized lumen appears even larger and now unnecessary collateral channels, though patent, are only faintly opacified. Excellent symptomatic result persists. See figure 8B.

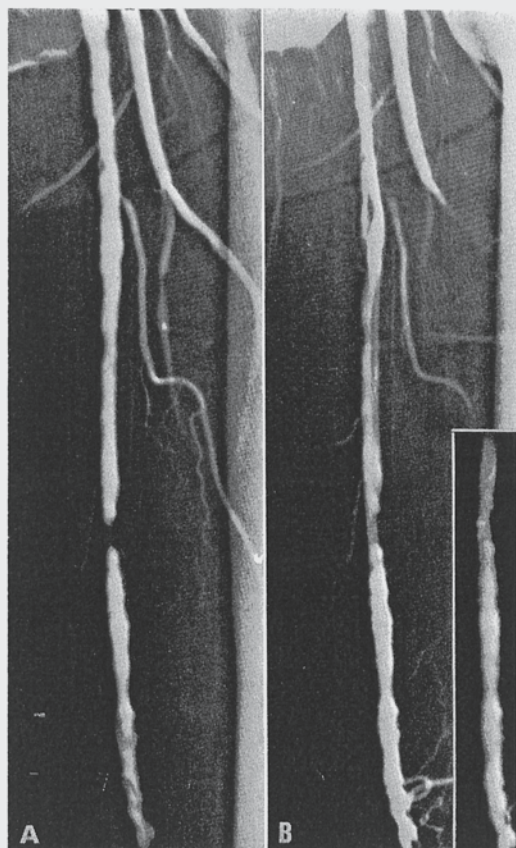


Figure 10

Case 8. Recanalization of segmental occlusion of superficial femoral artery. A. Spring guide only has passed through a complete 1-cm. occlusion. B. Immediately after full dilatation. (Inset: 8 weeks later. There appears to be a further increase in lumen size, especially distal to site of previous occlusion.) See figure 8C.

structed superficial left femoral artery near the adductor hiatus. After the procedure, blood pressure, previously unobtainable below the knee, was recorded at 105 mm. Hg and remains at that level at the present time. Plethysmography revealed vigorous arterial pulsation below the knee. The foot is now warm and ischemic skin changes have subsided.

Case 7 (figs. 8B and 9)

V. H., a 67-year-old diabetic man appeared because of rapidly progressive bilateral claudication, severe rest pain, numbness, and coldness in both lower extremities. Examination revealed good pulses in both common femoral arteries but no pulsation in the popliteal and distal

vessels. His legs were thin, atrophic, hairless, and cool below the knee.

Survey retrograde transfemoral aortography on February 27, 1964, revealed complete obstruction of the right superficial femoral artery 4 cm. distal to the femoral bifurcation. The partially stenosed profunda femoral provided meager collateral circulation to the popliteal artery. On the left, a 6 cm. complete segmental block of the superficial femoral artery was present within the adductor canal.

On April 29, 1964, a distally directed spring guide readily passed the obstruction in the left leg. Over the spring, a radiopaque Teflon catheter was passed to the popliteal area. A second dilating catheter of nonopaque polyethylene (P. E. 300) was passed through but not beyond this area of complete occlusion. Prior to the procedure, strain-gage plethysmography had failed to show a pulsation in the left first digit. When the dilating catheter was removed, the prompt appearance of the lower leg pulsations and an ankle blood pressure of 105 mm. Hg provided immediate objective evidence consistent with the patient's reported relief of ischemic pain. The improvement persists.

Case 8 (figs. 8C and 10)

O. W., a 55-year-old man, had experienced intermittent claudication for 2 years. He had, nevertheless, been able to walk one or two blocks without pain until 7 weeks before admission, when he rapidly developed numbness, tingling, coldness, and pain in his left lower leg and was admitted to the University Hospital. Physical examination showed that popliteal and distal pulses were absent in the left lower leg, which was cold and continuously painful. There were small ulcerations on the lateral aspect of the foot. A diagnosis of arterial occlusion with "impending gangrene" was made.

On April 30, 1964, a femoral arteriogram was performed with a distally directed catheter. This revealed a complete obstruction of the midsuperficial femoral artery. During its introduction into the femoral artery, the guide spring was inadvertently passed across the block admitting sufficient blood to the distal superficial femoral artery to elevate the popliteal blood pressure from a control level of 40 mm. Hg to 70 mm. Hg. Small inner and larger outer catheters were used to dilate the reopened lumen to an inner diameter of 3.2 mm. Distal femoral blood pressure immediately rose to 140 mm. Hg; all distal pulses became palpable and the patient said that his leg felt "normal for the first time in several years."

Follow-up arteriograms, although done, were unnecessary to demonstrate patency, since the

TRANSLUMINAL TREATMENT OF OBSTRUCTION

663

dorsalis pedis pulse is now clearly evident at a distance. Plethysmographic studies are shown in figure 8C.

Case 9 (fig. 11)

G. G., a man of 75 with diabetes, developed severe pain in his left foot and ankle while working on March 1, 1964. He was hospitalized elsewhere and left lumbar sympathectomy was carried out within 24 hours. He continued to have rest pain, which markedly increased with exercise. His leg below the knee was cold. On April 2, 1964, he was admitted to the hospital because of severe, unremitting pain and early gangrene of left toes. Pigmentation, patchy redness, and decreased skin temperature were present below the left knee. Right retrograde transfemoral aortoarteriography a week later showed patent iliac and common femoral arteries, but demonstrated complete obstruction of the distal left superficial femoral and popliteal arteries. After a 20-second delay, the junction of two patent tibial arteries filled faintly by way of devious collateral channels. Above-the-knee amputation was planned and accepted by the patient.

Told of the present technic, the patient gladly consented to experimental recanalization, which was undertaken on May 1, 1964. Qualified success resulted when a 35-cm.-long segment of completely occluded femoropopliteal artery was traversed by the spring guide and a 2-mm. dilating catheter of radiopaque Teflon. Extensive vascular calcification and the use of television fluoroscopy permitted several needed corrections of the course. These were achieved through appropriate bending of the tip of the removable central piano-wire stiffener of the spring guide. Resistance to the guide varied widely and unpredictably at various points within the occluded vessels. On two occasions, steady forward pressure on the guide led to transmural perforation of the artery. Redirection into a transatheromatous or periatheromatous route proved possible after the guide had been pulled back into the artery. When lumen-to-lumen passage had been accomplished, the small tapered Teflon catheter was advanced over the guide with considerable difficulty. Passage of a larger, outer polyethylene catheter appeared to be out of the question. After withdrawal of the Teflon catheter to the upper femoral artery, arteriography established beyond a doubt that lumen-to-lumen bridging had been achieved.

The patient noted a pronounced diminution in ischemic pain. This improvement led to cancellation of planned amputation and discharge of the patient. It was expected that the long (35 cm.), narrow (2.0 mm.) channel would soon thrombose. It was our plan to attempt a

more adequate dilatation as soon as an expandable guide could be devised. About 3 weeks later, at 7 p.m. on May 20, 1964, the patient suddenly developed recurrent rest pain. The following noon, emergency recanalization was performed. Again, there was immediate relief of his rest pain. Previously unobtainable plethysmographic pulses were recorded. The re-opened 2.0 mm. by 35 cm. channel has remained patent to the present (4 months). He anxiously awaits the development of a dilating catheter-probe.

Case 10

V. H. is the same patient reported as Case 7.

Right Leg: On May 5, 1964, an attempt to traverse a long segmental block of the superficial femoral artery failed presumably because of our inability to start the recanalization with the spring in a proximal, unoccluded segment of the superficial artery above the region of block. Repeated extravascular passage resulted. This effort is not regarded as a total failure, since dilatation of a stenosed profunda femoral artery at the level of the second perforating branch was easily accomplished and appeared to improve collateral flow. Digital plethysmographic pulsation was absent before and after this procedure.

On June 5, 1964, a second attempted recanalization resulted in a lumen-to-lumen channel, portions of which were subatheromatous. There was subjective improvement and plethysmographically measurable blood pressure.

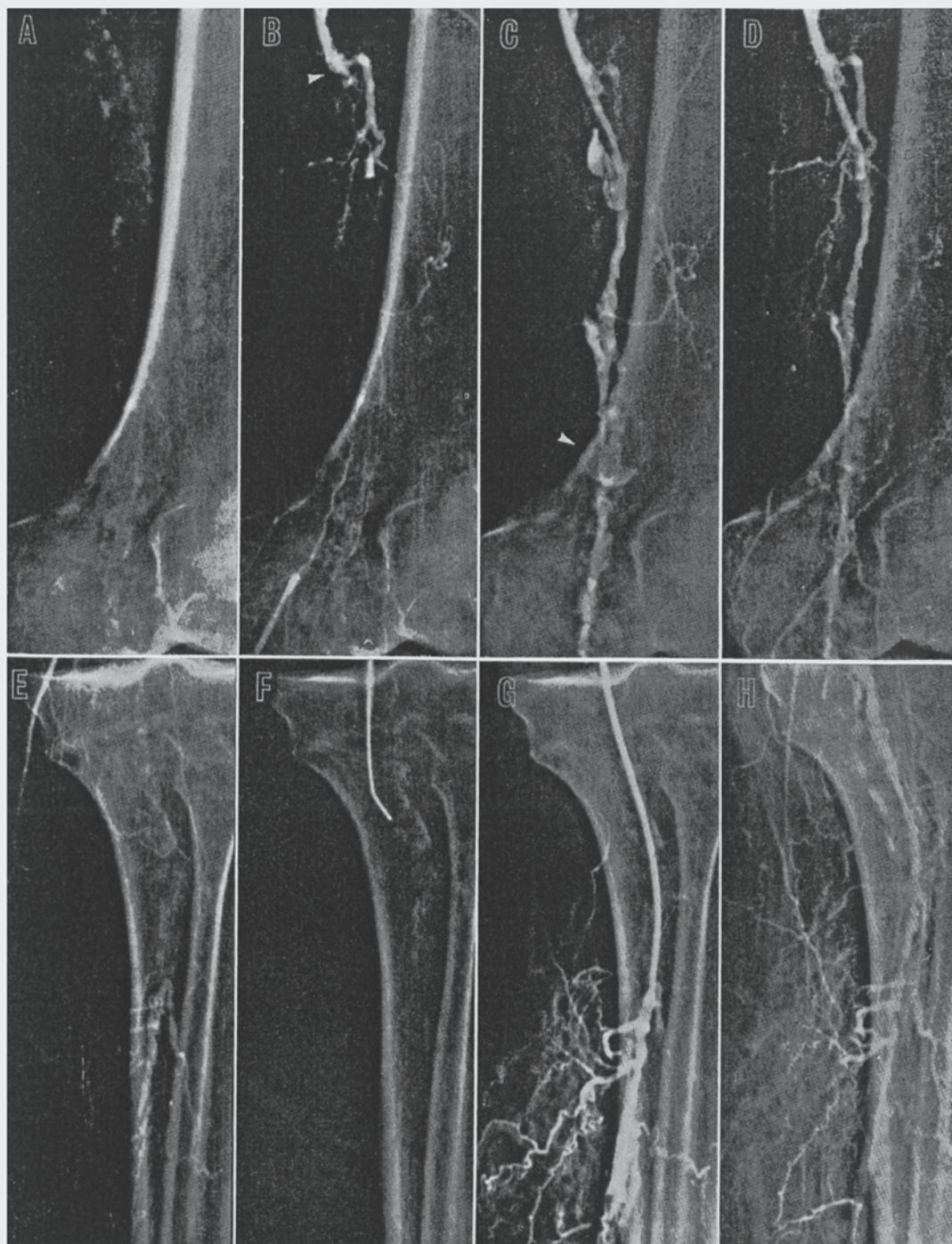
A third attempt 5 days later failed to develop a completely transatheromatous channel. In view of subsequent subjective improvement, a new approach has not been attempted.

Case 11

F. S. is the same patient reported as case 6.

Right Leg: On April 21, 1964, a spring guide was passed through a 30 cm., completely occluded segment of superficial femoral artery to connect with a patent distal popliteal artery. Continuity was observed fluoroscopically. A small dilating catheter traversed the obstruction to the knee joint space. Severe arterial spasm prevented further advance of this catheter or passage of a larger dilator. To this spasm and to insufficient irrigation during the procedure is attributed the prompt thrombosis which followed and then extended to include a short segment of stenosed, but previously patent lumen of the superficial femoral artery. There were no clinically evident untoward effects.

On May 5, 1964, this man was taken to surgery and the right popliteal artery was exposed. He was immediately transported to the Radiology Department where a catheter was passed through the exposed popliteal artery; the distal popliteal artery was likewise catheterized and a patent,

**Figure 11**

Case 9. Recanalization of 35-cm. continuous femoral and popliteal total obstruction. A. Calcification of walls but no filling of distal femoral artery with preliminary aortic injection. B. Upper

Circulation, Volume XXX, November 1964

TRANSLUMINAL TREATMENT OF OBSTRUCTION

665

but partly periatheromatous channel from the iliac to the distal popliteal artery was established. At the time of wound-closure, there was pulsatile flow in the popliteal artery and capillary flow in the previously cyanotic foot. Thrombosis occurred on the sixth day and the leg was amputated. This cold leg with gangrenous changes and ischemic ulcerations had been scheduled for amputation prior to the performance of these procedures.

Evaluation of Results

Fifteen procedures have been performed on 11 lower extremities in nine patients (table 1). Seven of the 11 extremities were those of diabetic subjects with moderate-to-severe microangiopathy. Most of these patients had been rejected for definitive surgery and were scheduled for amputation; of the 11 extremities treated, six were for gangrene, four for rest pain, and one for claudication. Six extremities improved markedly (four amputations averted). Clinical improvement quickly followed increases in blood pressure and circulation. Three are unchanged; two scheduled amputations were not averted; a third was delayed for 3 months. Results have been objectively gauged on the basis of healed ischemic or gangrenous changes and the return of measurable peripheral blood pressure. Symptoms were relieved in extremities that did not receive maximum benefit by these criteria.

Failures were unassociated with harm to the patient and did not appear to reflect on the method of approach as much as they did our early inexperience, the particular disease present in a given patient, and the inadequacy of our present instruments when used in long segment blocks.

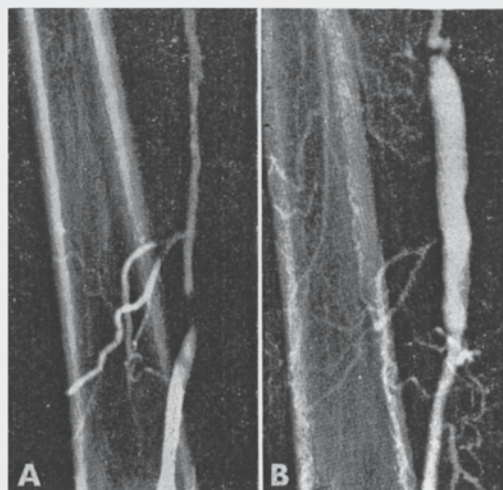


Figure 12

Endarterectomy, superficial femoral artery. A. Before surgery. B. Removal of atheroma leaves dilated segment of artery with abrupt change in lumen caliber. A good result but the inevitable disturbance in flow pattern could prejudice its durability. Compare to luminal caliber shown in figures 1 and 10. (Films through courtesy of Drs. Rogoff and DeWeese, Strong Memorial Hospital, Rochester, New York.)

Discussion

Rationale of Method

Surgery is the treatment of choice for obstructive lesions of the aorta and other large arteries, but its effectiveness bears a direct relation to arterial size. The failure of surgical measures applied to smaller arteries reflects an increase in the importance of limiting factors such as technical difficulty, operative trauma, postoperative perivascular swelling, mural fibrin deposition, and fibrocytic incisional repair. Particularly important

end of block (arrow) shown by Conray injected directly into blocked superficial femoral artery at outset of procedure. Collateral vessel near knee. C. Appearance of recanalized distal superficial femoral artery. Note partially visualized unsuspected aneurysmal cavity (arrow). D. Same, later phase to show branch filling. E. Tibial view corresponding to B., showing two patent tibial arteries at lower end of 35-cm. total block. F. During passage of spring guide. Tip of spring has been bent to follow lumen. Flexing-knee aided in establishing luminal continuity. G. Dilating catheter of Teflon, 2 mm. OD, is across the occlusion and injecting into the fibular artery. H. Corresponds to C and D. However irregular the lumen, it is filling two of the three popliteal branches. This stayed patent 3 weeks whereupon recurrence of leg pain indicated re-thrombosis. Opened a second time, it has now remained patent for 6 weeks. Scheduled amputation is not necessary at present.

666

DOTTER, JUDKINS

Table 1

Summary of Cases

Case no.	Pt.	Hosp. no.	Age, sex	Side	Before procedure, clinical	Diabetic	Before procedure, radiographic
<i>A. Partial Obstructions</i>							
1	L.S.	32-79-70	82 F	L	Cold, pulseless, painful foot with ulceration and gangrene of the toes	0	Near complete obstruction of superficial femoral artery at adductor hiatus. Moderate small artery disease
2	J.R.	32-91-34	58 M	L	Coldness, claudication, generalized atherosclerotic changes. Emotional instability	0	Narrowing of superficial femoral artery in adductor canal
3	H.B.	18-28-16	64 M	L	Cold foot and leg with claudication, markedly diminished peripheral pulses, and digital gangrene	0	Complete obstruction of superficial femoral in adductor canal. Narrowing of deep femoral collateral vessels
<i>B. Total Obstructions 6 cm. or less in length</i>							
4	M.D.	33-09-99	78 F	R	Cold, pulseless extremity with rest pain, ulceration, and extensive gangrene below the knee. Serious infection	+	Complete trifurcation block. Extensive small artery disease. Microangiopathy
6	F.S.	32-61-87	65 M	L	Pulseless, cold leg with ischemic skin changes and claudication. Rest pain	+	Complete obstruction superficial femoral at the adductor hiatus. Moderate small artery disease
7	V.H.	33-00-47	67 M	L	A cold leg with one block claudication and no distal pulses. Ischemic skin changes and some pain at rest	+	Complete obstruction superficial femoral artery within the adductor canal. Moderate small artery disease
8	O.W.	31-10-23	55 M	L	Numbness, coldness, and claudication progressing to rest pain and early gangrenous changes	0	Complete obstruction superficial femoral artery in the adductor canal
<i>C. Long-Segment Obstructions</i>							
5	V.S.	5-67-89	62 F	R	Cold, pulseless leg with ulceration and rest pain. Ischemic skin changes with ulceration	+	Complete obstruction of popliteal and the vessels of the trifurcation. Severe small artery disease
9	G.G.	33-22-45	75 M	L	(a) Sudden, severe claudication and rest pain. Cold leg. "Emergency" sympathectomy elsewhere. Gangrene (b) Sudden onset of rest pain 7 pm 5/19/64	+	(a) Complete obstruction distal femoral and popliteal arteries (b) Recurrent obstruction
10	V.H.	33-00-47	67 M	R	(a) Cold leg with ischemic skin changes and muscular atrophy. Rest pain (b) Same (c) Same	+	Complete obstruction of femoral and proximal popliteal. Moderate small-artery disease
11	F.S.	32-61-97	65 M	R	(a) Cold leg with no distal pulses. Rest pain + Gangrene (b) Same	+	Obstruction distal femoral and popliteal. Severe small-artery disease

TRANSLUMINAL TREATMENT OF OBSTRUCTION

667

Length of narrowing or obstruction, cm.	Procedure date	After procedures, radio- graphic findings	Follow-up
0.5	1/16/64	Lumen diameter increased to near normal	Healing of ulceration. Sharp demarkation and clean healing of sloughed gangrenous toes. Plethysmographic evidence of good pulse and B.P. Residual small-artery disease
2	2/14/64	Increased diameter of lu- men	Inguinal area hematoma secondary to anticoagulants. No subjective improvement. Plethysmography shows little change. Lesion may not have been a significant obstruction at time of dilatation
0.5	3/12/64	Increased diameter of the lumen of treated deep fem- oral branch. Superficial femoral was not treated percutaneously	The following week, patient had an endarterectomy and patch graft of superficial femoral artery lesion. Now doing well clinically. Slough of gangrenous toe healed well
5	3/25/64	Subatheromatous catheter travel from popliteal to fibular artery	No clinical improvement—probably secondary to severe small- artery disease. Amputation became necessary because of persistent severe rest pain
2	4/23/64	Patent lumen	Plethysmographic pulses and B.P. returned. Leg warmth increased. Skin changes decreased. Good B.P. levels to present. Excellent clinical results
6	4/29/64	Patent lumen	Increased warmth. Plethysmographic increase in B.P. and pulse. Distal pulses returned. Excellent clinical results
1	4/30/64	Patent lumen	Relief of pain, coldness, and numbness. Dorsalis pedis pulse now visible. Plethysmographic return of B.P. and pulse to good levels
10	4/ 9/64	Patent lumen, popliteal to fibular artery	Fair progress in ulcer healing. No distal pulses because of severe small artery disease. Amputation for pain 3 mo. later
35	5/ 1/64	(a) Patent lumen	(a) Relief of severe rest pain. Leg warmth increased. Addi- tional dilatation of vessel will be needed. Amputation canceled
	5/20/64	(b) Patent lumen to pres- ent	(b) Relief of rest pain. Amputation again averted. Pt. awaits development of "concentric dilating catheter"
30	5/ 5/64	(a) Unsuccessful pro- cedure; extravasation	(a) Unchanged
	6/ 5/64	(b) Partial extra-atheroma- tous course of the channel	(b) Improved warmth and B.P. for 5 days
	6/12/64	(c) Partial extra-atheroma- tous course of the channel	(c) Unchanged
30	4/23/64	(a) Partial extra-atheroma- tous course of the channel	(a) Unchanged
	5/ 5/64	(b) Small patent lumen- clotted after 3 days	(b) Return of popliteal pulse and capillary circulation. No distal pulse. Clotted after 3 days. Amputation not averted

are the irregularities likely to develop at the site of graft or endarterectomy (fig. 12). Abrupt variations in caliber and configuration of the postoperative lumen often cause turbulent blood flow and, thereby, undesired dilatation, mural trauma, platelet deposition, and thrombosis.

Several of the foregoing limitations can be avoided or minimized by use of a transluminal approach. Recanalization or luminal dilatation, the therapeutic objective, is brought about through relatively nontraumatic remodeling and lateral displacement of the encircling atheromatous material. Postmortem studies⁶ have shown that forceful intraluminal hydraulic injections can lead to surprising increases in perfusion rates. From this it appears that diffuse hydraulic, as well as local catheter dilatation, may have therapeutic value. Since in either case, surgical exposure, mural incision, and intra-arterial tissue dissection are eliminated, percutaneous arterial dilatation is, in comparison to surgery, remarkably free from trauma, especially at the site of the lesion.

The value of catheter recanalization in arteriosclerotic narrowing has been challenged by some of our colleagues on the hypothetical grounds that coexistent disease in distal branches defeats its purpose. (Similar faulty speculation retarded now-accepted corrective surgery for occlusive disease of the abdominal aorta, carotid, and renal arteries.) It is a simple, physical fact that removal of a proximal, gradient-producing stenosis causes an increase in the distal blood pressure and, therefore, a corresponding increase in flow through all patent run-off branches, narrowed or not. A further advantage presumably exists in the form of secondary pressure-induced dilatation of nonrigid elements of the run-off bed.⁷ (Even a rusty sprinkler may prove capable of doing a creditable job once the faucet is fully opened!)

It has been argued that attempted catheter dilatation will dislodge and make emboli of atheromatous plaques. The use of a gradually tapered recanalizing catheter (or a con-

centrically dilating catheter under development) was adopted to reduce the likelihood of this. Its rarity is evidenced by prior practical experience of a related nature. In connection with approximately a thousand arterial catheterizations done at the University of Oregon Medical School, we know of but one instance of embolization by dislodged atheromatous material.⁸ Minor, clinically undetected embolization probably occurs in the course of most arterial catheterizations done on patients with intimal atherosclerosis, a suspicion supported by reported funduscopic findings.⁹ In any event, if the dislodgment of a localized, proximal atheroma coincides with the relief of a proximal block, impingement of the embolic fragment in a distal branch would not necessarily prevent a decided improvement in over-all blood flow through most of the run-off vessels. (This might not always hold if a previously active collateral route were blocked as could occur in the coronary arteries.) Recognized clinical or radiographic evidence of embolization has not occurred in any of the patients in this series.

Atheromatous material has the characteristics of what an engineer would term a "cold-flow" substance; thus, it can be molded into a configuration that permits it to serve as an autogenous, in-situ graft. If intima existed before the remodeling, it presumably would remain afterwards, however stretched.

Transluminal recanalization is a simple technic. The hard-won skill of the vascular surgeon is not required, for the technic can be learned by any physician familiar with vascular catheterization. This is fortunate. A therapeutic approach to arteriosclerotic disease which requires the services of a highly trained vascular surgeon would hardly scratch the surface in the treatment needed for a disease responsible for the death of a million Americans every year!

Since the procedure is suitable for outpatient application, and at most requires brief hospitalization, the expense for the patient is kept to a minimum.

TRANSLUMINAL TREATMENT OF OBSTRUCTION

669

Present and Projected Clinical Applications of the Method

Transvascular recanalization is routinely considered in all patients who otherwise would require amputation because of arteriosclerotic ischemia. Such patients have little to lose and much to gain through trial of this experimental procedure. In any case, they can add to our knowledge and have always wished to do so when given the option.

To date, this method has been most successful in recanalization of relatively short segment blocks (up to 10 cm. in length) of the femoropopliteal system. Long-segment block failures have been primarily due to our mechanical inability to dilate an established 2-mm. lumen-to-lumen channel, a situation that could readily be reversed through the development and use of better instruments.

Transluminal recanalization appears quite applicable to other arterial systems, particularly those smaller than are usually considered suitable for conventional reconstructive arterial surgery. If its use in femoral disease can be taken as an indication, severe proximal narrowing of the coronary artery will be amenable to a manually guided dilator inserted via aortotomy or via the brachial artery by the Sones technic.¹⁰ Proximal stenosis of the renal, carotid, and vertebral arteries appears suitable for transvascular treatment. The technic is of potential usefulness in other than arteriosclerotic causes of narrowing, both anatomic and functional in character. Intense, gangrene-producing spasm has resulted from the prolonged use of vasoconstricting drugs and, here, catheter or hydraulic dilatation may prove useful.

In order to improve the technic, a major instrumental design effort is underway. It consists of the development of a device suitable for percutaneous insertion, which is a functional equivalent of the present spring guide but capable of externally controlled concentric expansion over a suitable portion of its length. Expansion from an initial OD of 0.05 to a final OD of 0.2 inch would be desirable. This, it is hoped, will minimize the possibility of inadvertent dislodgment of atheromatous fragments, since the dilator will be

positioned in the form of a thin, flexible guide, prior to providing forceful, local expansion as needed. In addition, our efforts are being directed toward the design and construction of a self-guiding, lumen-seaking guide to facilitate penetration as the first step in the recanalization of totally occluded arteries. Once a pathway has been created across an occluded segment, repeated dilatation or the temporary use of a Silastic endovascular (or, in some cases, paravascular) splint could maintain an adequate false lumen until the natural processes of fibrosis and re-intimalization had taken place. We believe re-intimalization is as likely to occur on the walls of a lumen formed by the patient's own tissues as on the fibers of a plastic prosthesis.

Conclusions

It seems reasonable to expect that the transluminal technic for recanalization will extend the scope of treatment beyond the limits of present-day surgery. The method offers early treatment for the ischemic leg. In view of its simplicity and low morbidity, it is now feasible to treat intermittent claudication without waiting for more serious symptoms to occur or collateral circulation to develop.

Although long-term results are not yet available, we are convinced that transluminal recanalization is the treatment of choice for patients suffering from arteriosclerotic ischemia of the lower extremities, especially two classes of patients, those generally regarded as the best candidates for surgical revascularization (i.e., those with short-segment obstructions of the adductor hiatus), and those beyond its aid and, therefore, candidates for amputation. Although most of our patients came from the latter category, all are now alive, only three of 11 extremities have been lost, subjective improvement resulted in seven of the remaining nine legs, and pulsating, near-normal blood flow has been restored to four. No patient was made worse by the procedure. While uncomplicated segmental blockage of the adductor hiatus of the superficial femoral artery is generally considered suitable for surgery, it is even more suitable for a nonsurgical procedure of equal potential benefit. The

transluminal approach can be applied when distal disease offers a significant contraindication to conventional surgery. In any case, it does not preclude or complicate future surgery and should be tried first. Since our first patient was treated on January 16, 1964, nine patients have had transluminal therapy for arteriosclerotic ischemia of the leg. Eight other comparable patients at this institution were subjected to amputation. All of those treated transluminally are alive and six have not required amputation. Of the eight others who were not available to us for attempted recanalization, all have lost a leg and two have lost their lives as well (one from gas gangrene of the stump; the other from postoperative myocardial infarction). Thus, however primitive its present state of development and though its application has largely been confined to surgical "cast-offs," transluminal recanalization has proved to be an effective alternative to surgical reconstruction and a safer and otherwise more attractive alternative to amputation. As such, it deserves a serious trial in the hands of competent physicians.

Summary

The rationale and technic of a new procedure—transluminal recanalization of arteriosclerotic obstructions—has been described.

Of the 11 extremities treated, six have shown marked improvement (four amputations averted). It is reasonable to assume that with a perfected technic and patients with less advanced disease, the percentage of successful recanalizations would increase.

Early treatment with this technic may well prevent otherwise serious disease, not just prevent amputation of extremities not suitable for definitive surgery. We are satisfied that percutaneous transluminal recanalization is the treatment of choice for many lesions of the femoral and popliteal arteries. We believe this method is ready for application to obstructions up to approximately 10 cm. by

those skilled in the use of vascular catheters. No doubt the interest and ingenuity of others will lead to refinements of technic as well as further clarification of the role of this attack on arteriosclerotic obstructions.

Addendum

Since this report was completed the number of treated patients has approximately doubled. There have been no further amputations and the success rate appears to have improved with experience in the selection of patients and the conduct of the procedure. Late thrombosis appears to be unlikely in the light of results to date.

References

1. EDWARD, W. S.: Autogenous vein patch reconstruction of small leg arteries after endarterectomy. *J. Cardiovas. Surg.* 3: 161, 1962.
2. DEWEESE, J. A., DALE, W. A., MAHONEY, E. B., AND ROB, C. G.: Thromboendarterectomy and autogenous vein grafts distal to the inguinal ligament. *Circulation* 28: 710, 1963; and *Cardiovascular Surgery* 1963, Supplement to *Circulation* 29: 171, 1964.
3. WILDER, J. R., AND MICHAELS, G. L.: Current status of vascular surgery. *Am. J. M. Sc.* 245: 582, 1963.
4. WARREN, R., JOHN, H. T., SHEPARD, R. C., AND VILLAVICENCIO, J. L.: Studies on patients with arteriosclerotic obliterative disease of the femoral artery. *Surgery* 49: 1, 1961.
5. DOTTER, C. T.: Catheter access and visualization of the cardiovascular system. (Chapter 3.) In VIAMONTE, M.: *Progress in Angiography*. Springfield, Illinois, Charles C Thomas, Publisher. In press.
6. NILES, N. R., AND DOTTER, C. T.: Coronary radiography and endarterectomy: Post-mortem study of feasibility of surgery. *Circulation* 28: 190, 1963.
7. MAY, A. G., VAN DE BERG, L., DE WEESE, J. A., AND ROB, C. G.: Critical arterial stenosis. *Surgery* 54: 25D, 1963.
8. JUDKINS, M. P., AND DOTTER, C. T.: An uncommon complication of thoracic aortography. A case report. *Radiology* 83: 433, 1964.
9. HALLENHARST, R. W.: Significance of bright plaques in retinal arterioles. *Tr. Am. Ophthalmol. Soc.* 59: 250, 1961.
10. SONES, F. M., AND SHIREY, E. K.: Cine coronary arteriography. *Mod. Concepts of Cardiovas. Dis.* 31: 735, 1962.

7.6 Selective coronary arteriography

Melvin P. Judkins (1922–1985)

see Chapter 7.5 on page 467

Selective Coronary Arteriography

Part I: A Percutaneous Transfemoral Technic¹

MELVIN P. JUDKINS, M.D.

UNTIL recently, there has been a reluctance to subject the coronary patient to the "added risk" of coronary arteriography. The recognition that coronary arteriography is no more hazardous than selective cardioangiography, that coronary visualization can depict precisely the presence and extent of disease, and that something can be done about coronary artery occlusive disease has extended the indications and increased the demand for detailed coronary delineation.

Numerous technics for coronary visualization have been proposed (2, 4, 5, 8-11). In general, the various forms of the aortic root flush have been favored in Europe, while more selective technics have gained acceptance in the American centers.

The new technic reported here facilitates

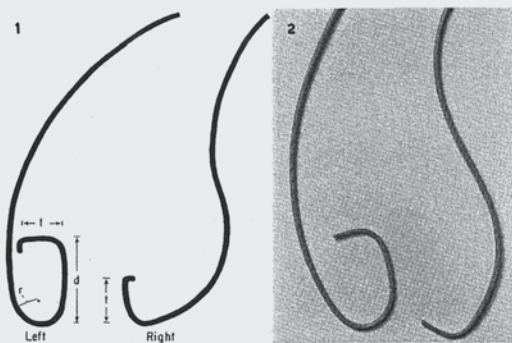


Fig. 1. *Catheter Bending Wires.* Bending wires are formed (from 0.038-in. stainless steel spring wire) into the above shapes. *Left:* $d = 4$ cm (medium size), 5.0 cm (large size), or 3.5 cm (small size); $t = 2$ cm; $r = 1.1$ cm. The primary angle is 90° , the secondary 180° , the radius of curvature of the tertiary curve about 10 cm. *Right:* $t = 1.5$ cm (medium size), 1.0 cm (small and large size); the secondary curve is 135° and has a radius of 5 to 6 cm (small and medium sizes) or 10-12 cm (large size).

Fig. 2. *Left and Right Coronary Catheters.* The tips are 5.5 F and have an I.D. of 0.041 in. The body is 8F with an I.D. of 0.056 in., and a 12-strand braid of stainless steel wire is incorporated into its wall. The braid insures good torque control.

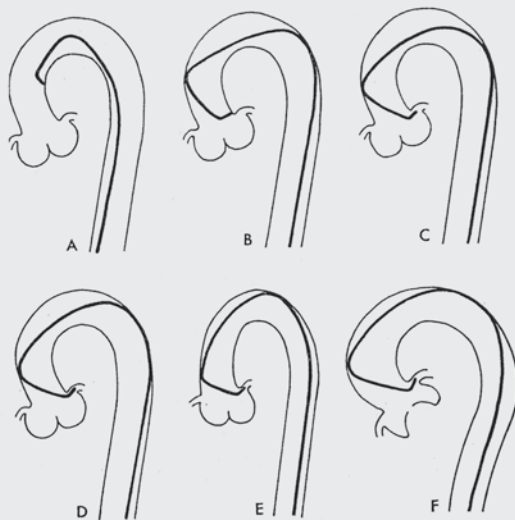


Fig. 3. *Left Coronary Catheter Technic.* The guide is removed as the catheter is advanced through the proximal descending thoracic aorta. A. The catheter is maneuvered to a "relaxed" position in the aortic arch, cleared, and the patient turned 20° RPO. B. Catheter is advanced slowly until (C) it drops into the coronary orifice. The spring afforded by the secondary bend holds the tip in the coronary orifice.

D, E, and F. Catheter position and the reason for "catheter arms" of varying lengths when used in (D) medium, (E) small, and (F) poststenotic (large) aorta.

consistent, rapid selective catheterization of both coronaries with a minimum of catheter manipulation; takes advantage of the ease, rapidity of performance, and low complication rate of percutaneous femoral catheterization; facilitates both direct serial and ciné filming; and is readily taught to residents, fellows, and practicing angiographers.

MATERIAL

One hundred consecutive patients between the ages of twenty-one and sixty-nine years were examined for suspected coronary disease. In each, both coronary arteries were selectively catheterized from

¹ From the Stella and Charles Guttman Institute for Vascular Research through Radiology (Director, Prof. Charles T. Dotter), University of Oregon Medical School, Portland, Ore. Accepted for publication in June 1967. Aided in part by USPHS Grants HE 03275 and 06336. RADIOLOGY 89: 815-824, November 1967.

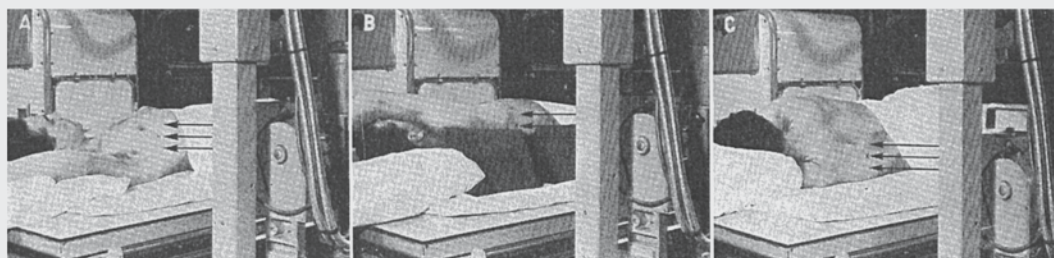


Fig. 4. *Radiographic Positioning.* (A) Lateral, (B) LAO 70°, (C) RAO 20°, to the lateral changer. All films are taken single plane, with a horizontal beam. Technical factors: 1,000 mA, 0.010 sec. (10 mAs); 80-95 kV; 38-in. distance; high-speed screens; Kodak Royal Blue film; 12:1 100 line grid; 1-mm spot—Dynamax 61 tube.

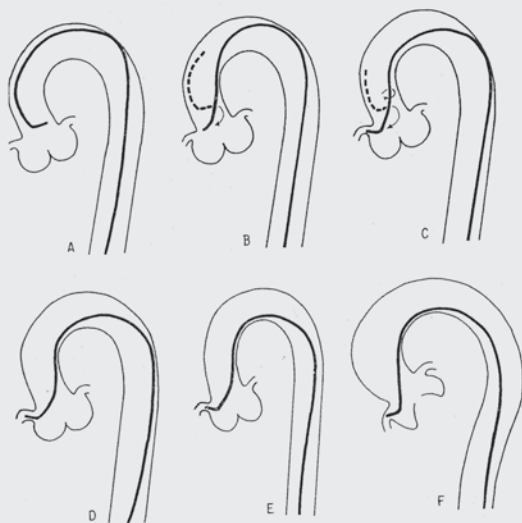


Fig. 5 (above). *Right Coronary Catheter Technic.* The catheter is advanced (A) to a point about 2-3 cm above the left coronary orifice, then rotated (B) slowly 180° until it drops (C) into the right coronary orifice. The curve of the aortic arch causes the catheter to descend in the ascending aorta as it is rotated. If the catheter does not enter the right coronary on the first try, the level of rotation should be adjusted up (if the catheter tip descends deep into the sinus of Valsalva) or down (if the tip rotates above the lip of the right coronary sinus) as indicated.

D, E, and F. Catheter position and configuration in (D) medium, (E) small, and (F) poststenotic (large) aortas. Note that the primary curve is decreased to about 70° and the secondary curve is flattened for the enlarged aorta.

the femoral artery, and contrast injections were filmed by direct serial radiography and cinephotofluorography. Over one-third of the patients were examined on an outpatient basis.

TECHNIC

Initially two 100-cm 8F Ducor catheters² (12) were shaped over preformed stainless steel bending wires (Fig. 1). The original configuration was removed, and a new one set by heating in boiling water for about two minutes.

This basic Ducor catheter (a polyurethane catheter with internal stainless

² Ducor is the trademark of Cordis Corp., 125 N. E. 40th St., Miami, Fla.

Fig. 6 (opposite page). *Serial Films of Selective Contrast Agent Injection in the Left and Then the Right Coronary Artery are Taken in 3 Projections:* RAO 20°, LAO 70°, and left lateral. Multiple projections are essential if all portions of the coronary system, splayed over an egg-shaped surface, are to be fully evaluated. The views selected give perspective and depth to the coronary anatomy.

A. Left coronary, RAO. The origin ↑, the proximal portion of the anterior descending †, and the distal circumflex system ‡ are well outlined.

B. Left coronary, LAO. In this view you are looking directly at the apex of the heart. The position of the 4 major left coronary vessels (the anterior descending ↑, its major branch, the diagonal †, and the circumflex ‡ with its obtuse marginal branch ‡) are best seen in relation to true apex. The septum is observed on end, and the left main coronary artery is foreshortened.

C. Left coronary, lateral. The proximal portion of the circumflex branch ‡ is in profile. Anteroposterior relationships of the peripheral part of both systems are clearly shown.

D. Right coronary, RAO. The mid portion of the right main coronary artery ↑, its acute marginal branch †, and the posterior descending branches ‡ are seen in profile.

E. Right coronary, LAO. The right main coronary artery ↑ is well seen. This view demonstrates the anatomy of the crux and the adjacent vessels, except for the posterior descending branch ‡, which is seen on end. This LAO view best visualizes the vascular ring that marks the atrioventricular groove. The right main coronary artery, its posterior branches, and the circumflex branch of the left coronary outline and complete the circle.

F. Right coronary, lateral. Proximal portions of the right ventricular vessels ↑ and the anteroposterior relationship of the right coronary system are shown. Note the small atheroma of the proximal right coronary not visible in the RAO view ‡.

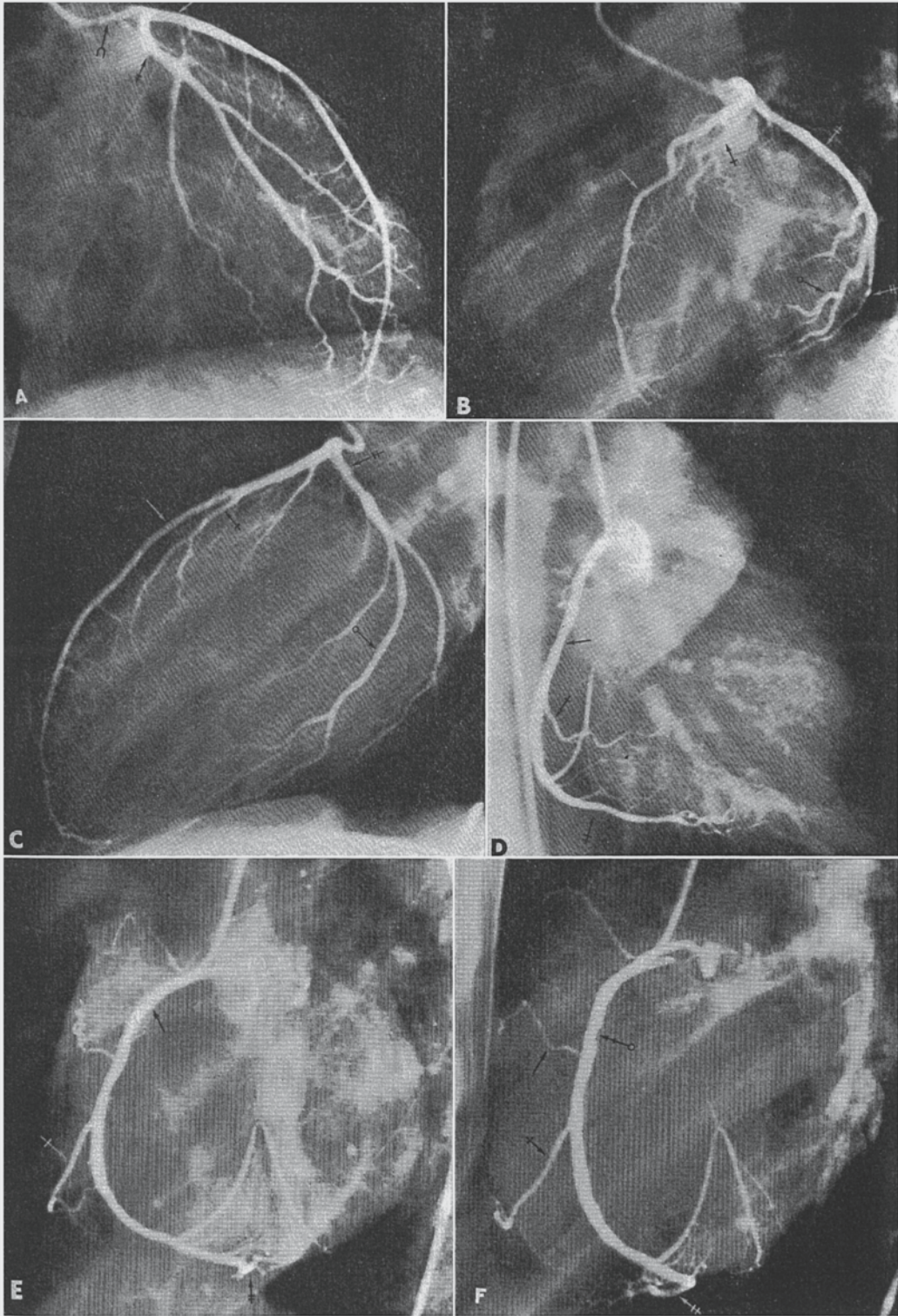


Fig. 6. For legend see opposite page.

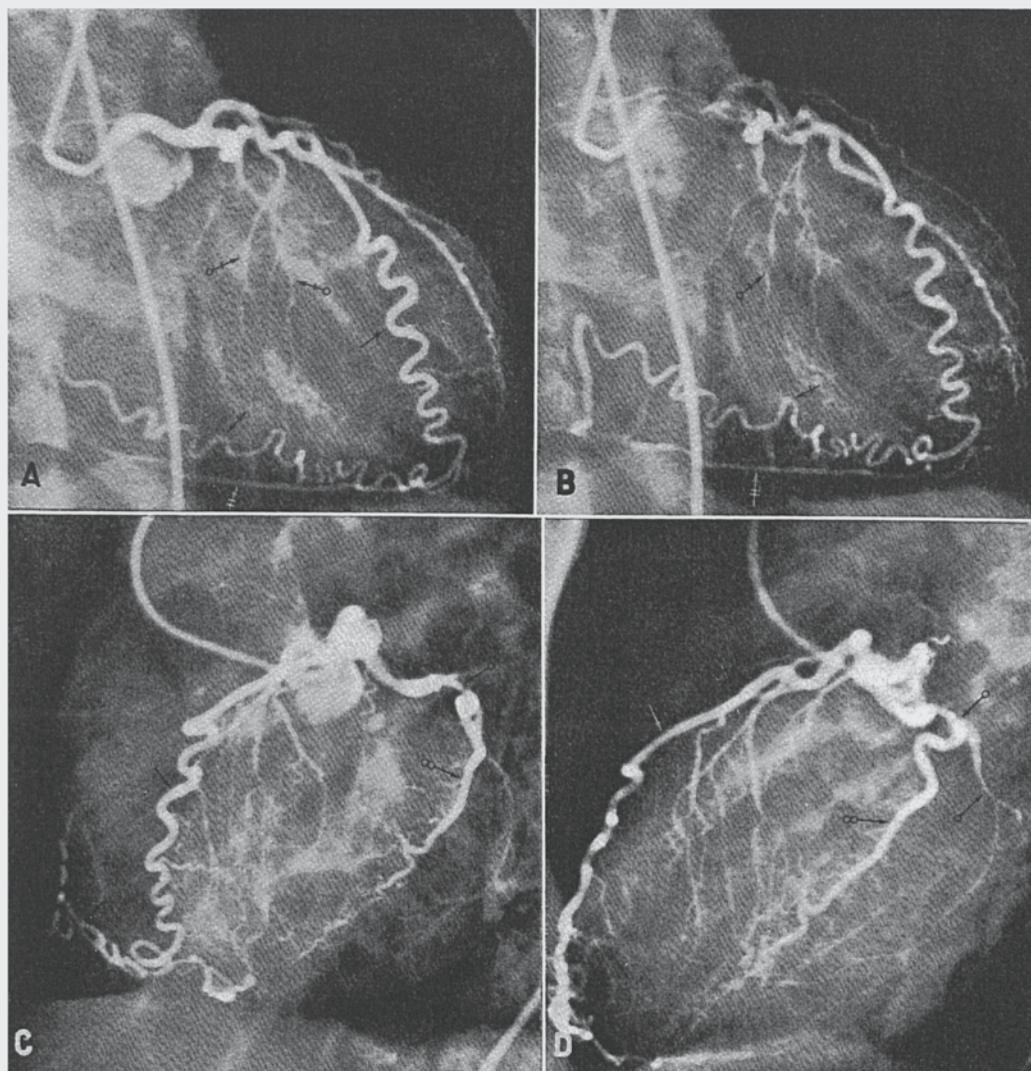


Fig. 7. *Selective Left Coronary Arteriogram*: A. RAO—early filling phase. Tortuous anterior descending branch ↑. Direct collateral filling of acute marginal ‡ and posterior descending branches ‡, right coronary artery. B. RAO—later views. Complete retrograde filling of entire distal right coronary. (Main right coronary is occluded from near its orifice to origin of acute marginal branch.)

C and D. LAO and lateral—large septal vessels contribute to the deficient distal right circulation. Marked narrowing of the circumflex ‡ proximal to its obtuse marginal branch ‡ can be seen on both views. The patient does not appear to have sufficient potential collateral circulation to the distal circumflex system to survive an occlusion of this narrowed vessel.

Septal branches ‡.

steel wire braid) has been modified. (a) The tip was changed from the usual “pencil tip” to a “bullet nose” configuration to minimize the chance of intimal injury. (b) The distal 2 cm was thinned to 5.5F (1.8 mm) to avoid coronary wedging. (c) The side-holes were eliminated to reduce possibility of clotting in the catheter tip

distal to the side-holes and to improve pressure monitoring. This modified catheter, developed with the aid of Robert Stevens,³ is preshaped into right and left configurations (Fig. 2) over the bending wires similar to those shown in Figure 1.

³ Research Consultant, Medical-Surgical Equipment, 4207 University Drive, Coral Gables, Fla.

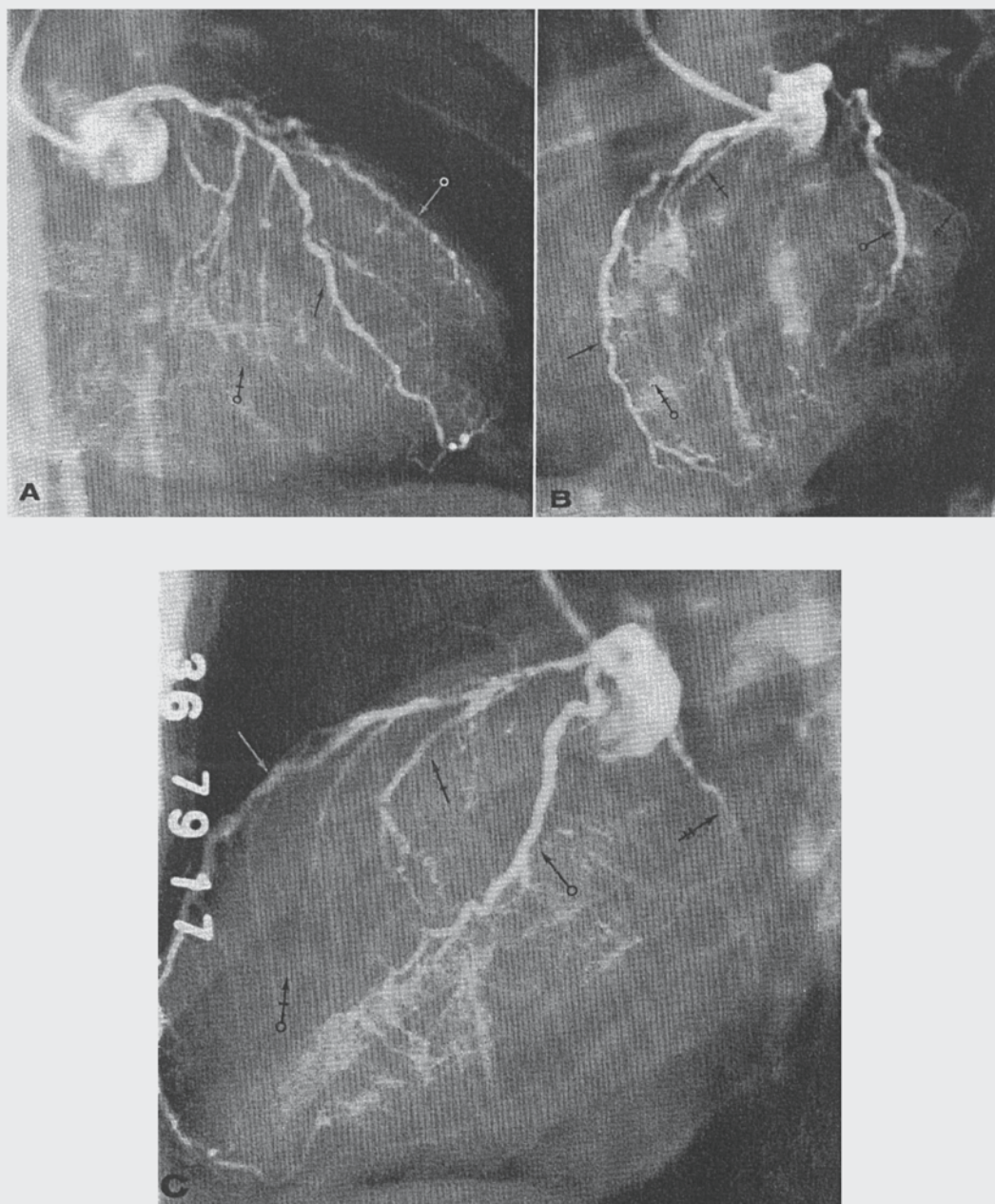


Fig. 8. *Selective Left Coronary Arteriogram:* Diffuse arteriosclerotic narrowing involves the entire left coronary system. Numerous fine vessels enter into local and cross system collateral networks. Anterior descending ↑, diagonal †, obtuse marginal ‡, circumflex ‡, septal branches ⊕. This patient's right coronary artery is occluded.

Left Coronary: The catheter is introduced percutaneously from the common femoral artery and advanced to the descending thoracic aorta; the leader is

then removed, and the catheter cleared and advanced to a relaxed position in the aortic arch (Fig. 3, A). With the patient in a 20° right posterior oblique position to

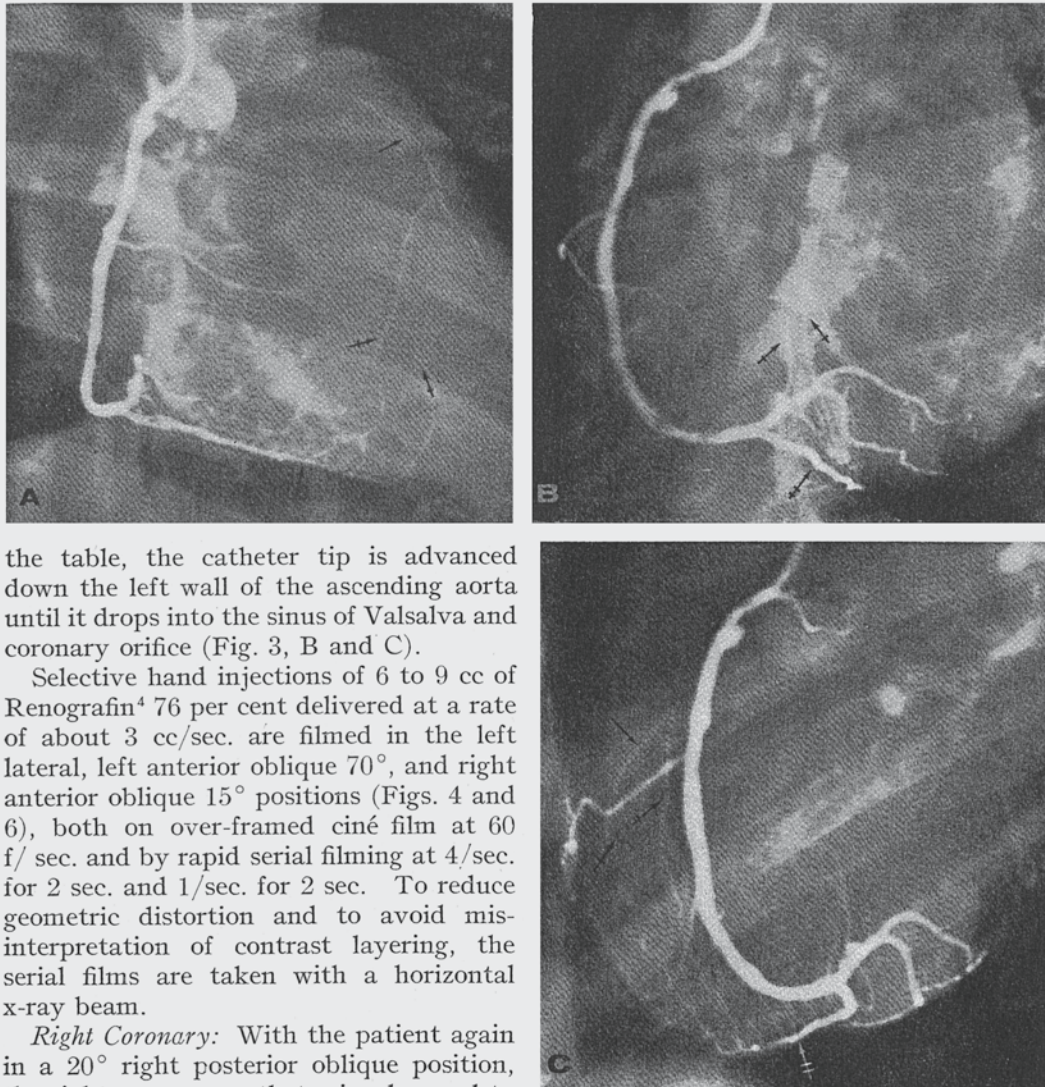


Fig. 9. *Selective Right Coronary Arteriogram: RAO, LAO, and lateral views. Distal segments of the anterior descending branch ↑ of the left coronary fill via septal collateral vessels † from the posterior descending branch ‡ of the right coronary. Small arteriosclerotic aneurysms of the proximal right main coronary are evident.*

TECHNICAL COMMENT

This technic is based on the use of catheters preshaped into optimal configurations for simple, rapid, selective coronary catheterization with a minimum of manipulation. Catheters are "over-bent" to obtain the necessary "spring" to hold them in position. To maintain their shape, unnecessary trauma to the catheter tips

the table, the catheter tip is advanced down the left wall of the ascending aorta until it drops into the sinus of Valsalva and coronary orifice (Fig. 3, B and C).

Selective hand injections of 6 to 9 cc of Renografin⁴ 76 per cent delivered at a rate of about 3 cc/sec. are filmed in the left lateral, left anterior oblique 70°, and right anterior oblique 15° positions (Figs. 4 and 6), both on over-framed ciné film at 60 f/sec. and by rapid serial filming at 4/sec. for 2 sec. and 1/sec. for 2 sec. To reduce geometric distortion and to avoid misinterpretation of contrast layering, the serial films are taken with a horizontal x-ray beam.

Right Coronary: With the patient again in a 20° right posterior oblique position, the right coronary catheter is advanced to a position a little above the left sinus of Valsalva. The catheter is then rotated *slowly* clockwise (about 180°) until its tip drops into the right coronary orifice (Fig. 5). Injections of 6 to 9 cc of contrast agent are filmed in the lateral, left anterior oblique 70°, and right anterior oblique 20° projections (Figs. 4 and 6).

Myocardial contractility and ventricular aneurysms are evaluated by fluoroscopy in multiple projections and by ventriculography, using a "hook-tail" catheter (1).

⁴ Brand of meglumine diatrizoate 76 per cent, from E. R. Squibb and Sons, New York, N. Y.

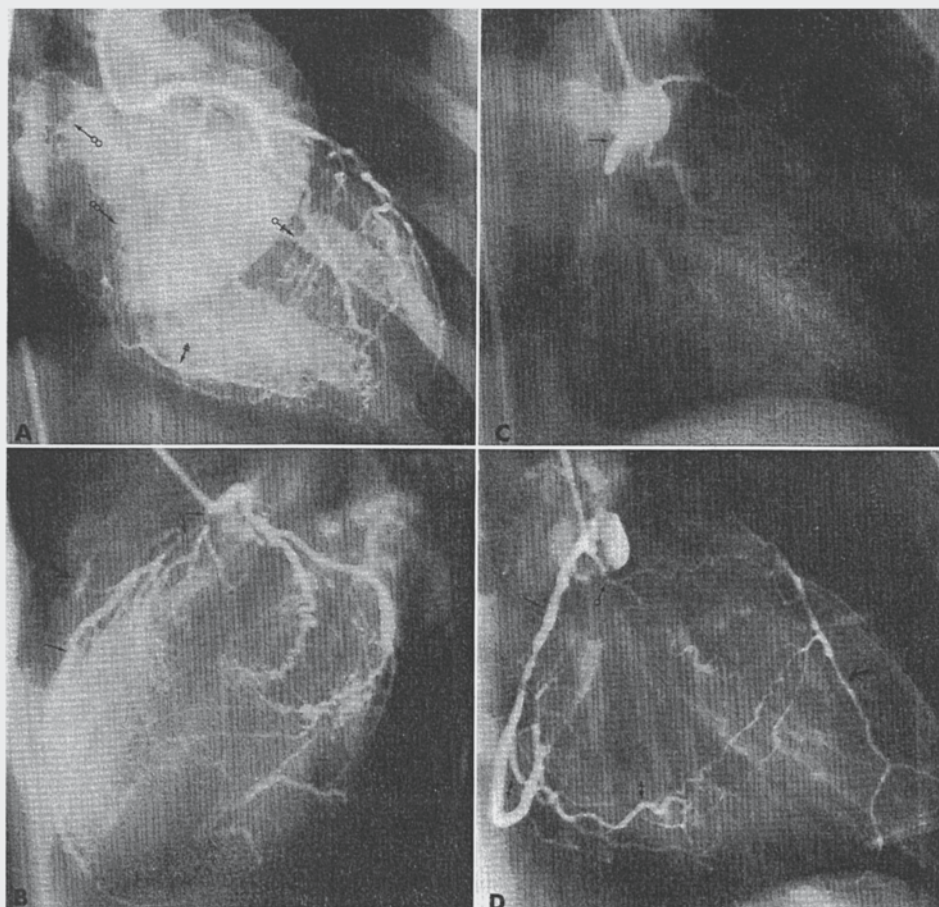


Fig. 10. Views of four different patients—each with collateral circulation to a proximally occluded coronary vessel. Note the anatomical detail in the collateral networks. A. RAO view, left coronary injection. There are numerous septal collateral pathways \rightarrow to the distal right system *via* its posterior descending branch \rightarrow . Atrial branches also enter into the collateral circulation \rightarrow .

B. Lateral view, left coronary. This film, for the most part, confirms the patient's undocumented history of two myocardial infarctions despite equivocal electrocardiographic changes. The anterior descending branch of the left coronary artery is all but occluded near its origin \uparrow . The right coronary artery is occluded proximally; a 1-cm fragment of its descending portion is patent \uparrow , fed *via* a conus branch from the left. It is occluded from this fragment to the crux where its posterior descending system \rightarrow fills from the circumflex coronary. Serial films show the anterior descending system \uparrow fills, in part, *via* numerous collateral channels.

C. Right coronary RAO. Right coronary \uparrow is occluded at the origin of a right ventricular branch \rightarrow . Collateral vessels cover the surface of the right ventricle to the area of the occluded anterior descending branch of the left coronary artery. This 38-year-old mother of 4 (youngest child is two years of age) has triple vessel disease (her circumflex is also markedly narrowed).

D. Right coronary RAO. The main right coronary artery \uparrow is narrowed at multiple points. The acute marginal branch \rightarrow and conus \rightarrow branches form a collateral net over the anterior surface of the right ventricle to the anterior descending coronary artery \uparrow .

must be avoided. The spring guide inserted through the needle is advanced to the aortic bifurcation before the puncture needle is withdrawn. If an obstruction is encountered, the spring is replaced with a safety J-guide⁵ (6). If the

⁵ Safety guides and safety J-guides are products of Cook, Inc., Bloomington, Ind.

J-guide will not negotiate the tortuous iliacs, forget it; the guide and needle may be removed with an arterial needle puncture the only penalty. The only reward for further effort to catheterize that side will be a high complication rate and/or an uncontrollable misshaped catheter.

Following guide passage to the aortic

bifurcation, a short length (6 in.) of 7F taper-tipped Teflon tubing is inserted into the artery over the guide. This maneuver dilates the soft-tissue tract and arterial puncture hole, making it unnecessary to push or twist the preshaped coronary catheter through the soft tissues and vessel wall. Once it has served its purpose, the Teflon tubing is replaced with the coronary catheter, and the latter is advanced into the aortic arch; prompt removal of the guide then allows the catheter to assume its preset configuration.

The relatively tight bends in the left coronary catheter make guide removal difficult; the pull necessary for removal tends to unravel most guides. The safety guide (3), which contains, in addition to the usual stiffening wire, a small diameter "safety" wire soldered to both ends, will not uncoil when used with these preshaped catheters. A nonstandard 0.038-in. guide is used to insure sufficient stiffness for ease of insertion and removal. A 0.035-in. guide is not satisfactory.

Selective catheterization of the coronary arteries or any other branch of the aorta requires a catheter of suitable configuration and a radius of curvature slightly greater than that required to span the aorta. The length of the left coronary catheter "arm" (the segment between the primary and secondary bend) is only moderately critical. If too short, however, the catheter will double back on itself. If too long, the arm will assume a relatively vertical position in the aorta and rest on the lip of the sinus of Valsalva, thus preventing the tip from reaching the orifice high and deep in the sinus. The relative size of the aorta is estimated on the basis of the patient's size, age, known valvular disease, and the appearance of the aorta in the preliminary films. Three sizes are illustrated in Fig. 3, D-F. The medium size coronary catheter will accommodate 85-90 per cent of the adult patients examined and almost 100 per cent of those without aortic valvular disease or aneurysm.

The shape of the right coronary catheter

varies with aortic dimensions. The tip may be shortened or the secondary curve flattened for the small vertical aorta (Fig. 5, E). A catheter with too long a tip or too great a secondary bend will tend to catch in the left sinus, "wind up" as it is rotated, then spin uncontrollably. The angle of the primary bend is reduced to about 70° and/or secondary bend flattened for a dilated aorta (Fig. 5, F). If a catheter becomes deformed as a result of manipulation or if an inappropriate size is selected, the catheter should be removed promptly and be replaced with a suitable new catheter.

Pressures are carefully monitored for signs of damping. If there is any evidence of damping or slowed wash-out on test injections, the catheter is removed and repositioned. An occasional patient will have a small or stenotic coronary orifice into which the catheter will repeatedly wedge. When this occurs, the catheter should be withdrawn, then briefly repositioned when everything is ready for filming; contrast injection must be done quickly, and the catheter removed during the filming.

The selection of contrast material is important to obviate arrhythmias. Meglumine diatrizoate 76 per cent⁶ is used exclusively in this laboratory for coronary arteriography, and there has been no instance of an arrhythmia other than transient bradycardia for over 3,000 contrast injections using this and a previous technic. Predictable electrocardiographic changes are noted with each injection (13).

When mitral and/or aortic valvular disease is suspected, the right coronary catheter can, in most cases, be manipulated through the aortic valve and, in many instances with the patient in the left posterior oblique position, advanced through the mitral valve. Pressure contrast agent injections into the left atrium or left ventricle, using the coronary catheter, are not advised, but pressure

⁶ Renografin 76 per cent, E. R. Squibb & Sons, New York, N. Y.

records may be obtained. A special percutaneous transfemoral retrograde left arterial catheter will be described in another paper.

Superb photography is essential to record the detail potentially available in any selective study. Special attention should be directed toward elimination of motion blurring, geometric unsharpness, and fogging due to scattered radiation (Fig. 7).

DISCUSSION

Until now, selective coronary catheterization *via* the femoral artery has been frustratingly uncertain and *time-consuming*. The curve of the aortic arch has foiled catheter control in the ascending aorta, making the coronary orifices elusive targets from the near 100-cm distance. Numerous tip-control gadgets and positive-control catheters have been developed, but all lose much of their control on the cardiac side of the aortic arch. The Ducor catheter is no exception, but, when coronary-seeking tip configurations are combined with its positive control feature, *the coronaries may be catheterized with startling consistency and ease*. High-quality selective coronary delineation is the rule (Figs. 8 and 9). Excuses have never been necessary, and there has been no need to resort to a sinus flush for the coronary that could not be entered. Any of the common moldable catheter materials can be used, but they lack the handling ease and control afforded by the positive control catheter.

This technic is an angiographer's approach to selective coronary artery study; the same principles traditional to selective visceral arteriography are employed. Catheters of soft, moldable material are pre-shaped to conform to the anticipated anatomy. The aortic valves are not used to deform the catheter during the procedure. Once positioned, the catheter will remain in the coronary orifice until it is removed. It may be left in place for multiple contrast injections in the various projections previously described so long as pressure

monitoring shows no evidence of damping and test injections quickly wash out. This feature of the technic facilitates direct serial filming.

Ciné photofluorography and direct serial radiography are complementary recording technics—*one never replaces the other*—each should be kept in perspective. Ciné studies vividly portray the dynamics of coronary flow; but anatomical detail is limited by the resolution of the intensifier system. Motion and flow, however, produce an image that fascinates and seems to mesmerize the novice viewer into believing he has seen all. Direct serial radiography depicts an unparalleled wealth of anatomical detail (Figs. 8–10) and portrays dynamic information to the experienced reader. This detail is essential for progress in definitive coronary surgery. *There are no more valid reasons for limiting study of the coronary anatomy to ciné photofluorography than there are for a similar limitation in the study of the cerebral, pancreatic, or renal anatomy.*

Even though selective coronary catheterization is technically simple, coronary arteriography should not be undertaken by the neophyte or without adequate laboratory facilities.

SUMMARY

A new percutaneous transfemoral selective coronary arteriography technic has been devised which can be quickly learned by the resident, fellow, or practicing angiographer. "Coronary-seeking" tip configurations set in a redesigned moldable positive control catheter implement rapid, consistent selective coronary catheterization. Special control equipment or special handles are unnecessary. When properly positioned, the catheters will remain in place for anatomical and dynamic filming in multiple positions. The inconvenience and possible complications of surgical cutdown on a brachial artery or those of percutaneous axillary approach are eliminated.

One hundred patients have been ex-

amed; in each case, both coronary arteries were selectively catheterized and contrast injection was filmed by conventional serial radiography and cinephotofluorography.

ADDENDUM: Since this article was prepared, an additional 200 patients have been studied with results similar to those described in this article. Experience has tended to standardize catheter "sizes." Left coronary catheters are now made up with a 4 cm, 5 cm, and 6 cm distance between the center of the tip and secondary bend (Fig. 1). These have been designated sizes 4, 5, and 6. The No. 4 size is standard. The No. 5 is most useful in the unfolded aortas of older patients and those dilated by long-standing hypertension or medial disease. The No. 6 size is usually needed when there is poststenotic dilatation of the aorta. The normal right, as shown in Figures 1 and 2 (tip length 1.2 cm), is used in all patients except those with severe deformity of the sinuses of Valsalva where the large is preferred. We are now using Teflon-coated safety wire guides. Their use will be described in a subsequent technical note.

3181 S. W. Sam Jackson Park Road
Portland, Ore. 97201

REFERENCES

1. BOIJSEN, E., AND JUDKINS, M. P.: A Hook-Tail "Closed-end" Catheter for Percutaneous Selective Cardioangiography. *Radiology* 87: 872-877, November 1966.
2. DOTTER, C. T., AND FRISCHE, L. H.: Visualization of the Coronary Circulation by Occlusion Aortography: A Practical Method. *Radiology* 71: 502-523, October 1958.
3. DOTTER, C. T., JUDKINS, M. P., AND FRISCHE, L. H.: Safety Guidespring for Percutaneous Cardiovascular Catheterization. *Am. J. Roentgenol.* 98: 957-960, December 1966.
4. GENSINI, G. G.: Coronary Angiography. *Progr. in Cardiovas. Dis.* 6: 155-188, September 1963.
5. HETTLER, M. G.: Die semiselektive, bilaterale Koronarographie: Eine neue klinische Untersuchungsmethode der Herzkranzarterien. *Fortschr. a. d. Geb. d. Röntgenstrahlen* 103: 249-261, September 1965.
6. JUDKINS, M. P., KIDD, H. J., FRISCHE, L. H., AND DOTTER, C. T.: Lumen-Following Safety J-Guide for Catheterization of Tortuous Vessels. *Radiology* 88: 1127-1130, June 1967.
7. LOWMAN, R. M., AND BLOOR, C. M.: Experimental Coronary Arteriography. III. Injuries Associated with Selective Coronary Arteriography. *Radiology* 85: 645-650, October 1965.
8. NORDENSTRÖM, B., OVENFORS, C.-O., AND TÖRNELL, G.: Coronary Angiography in 100 Cases of Ischemic Heart Disease. *Radiology* 78: 714-724, May 1962.
9. PAULIN, S.: Coronary Angiography: A Technical, Anatomic and Clinical Study. *Acta radiol., suppl.* 233, 1964.
10. RICKETTS, H. J., AND ABRAMS, H. L.: Percutaneous Selective Coronary Cine Arteriography. *J.A.M.A.* 181: 620-624, August 1962.
11. SONES, F. M., JR., AND SHIREY, E. K.: Cine Coronary Arteriography. *Mod. Concepts Cardiovas. Dis.* 31: 735-738, July 1962.
12. VIAMONTE, M., JR., AND STEVENS, R. C.: Guided Angiography. *Am. J. Roentgenol.* 94: 30-39, May 1965.
13. WEIDNER, W., MACALPIN, R., HANAFEE, W., AND KATTUS, A.: Percutaneous Transaxillary Selective Coronary Angiography. *Radiology* 85: 652-657, October 1965.



7.7 Non-operative retained biliary tract stone extraction. A new roentgenologic technique

H. Joachim Burhenne (1925–1996)

Dr Burhenne was born in Hannover in Germany in 1925. His medical qualification was from the University of Munich. He moved to the United States in 1959 and did his residency training in Radiology at the Peter Bent Brigham and other Boston hospitals. He was an instructor in Radiology at Harvard and conducted a research fellowship at the National Hospital for Nervous Diseases in Queen Square, London. He also worked at the University of California as a Professor until he moved to the University of British Columbia in Vancouver, Canada in 1978. He was the author of the definitive textbook “Abdominal Radiology”, which he co-authored with Dr Alex Margulis. Dr Burhenne’s contribution to gastro-intestinal radiology is well documented. He became President of the International Biliary Society as well as President of the San Francisco and California Radiological Society and the President of the Society of Gastro-intestinal Radiologists. He received many awards, including the gold medal of the American Roentgen Ray Society, and was an honorary member of 4 surgical organisations including an honorary degree from the Royal College of Surgeons of Ireland. Dr Burhenne was an award-winning photographer, an accomplished violinist and also published a book on ski touring. He passed away on 1 June 1996.

FEBRUARY, 1973

NONOPERATIVE RETAINED BILIARY TRACT STONE EXTRACTION*

A NEW ROENTGENOLOGIC TECHNIQUE

By H. JOACHIM BURHENNE, M.D.†
SAN FRANCISCO, CALIFORNIA

RETAINED, overlooked, or forgotten stones present a common problem in bile duct surgery. Of the one-third of one million cholecystectomies done each year in the United States,¹⁶ 20 to 40 per cent undergo common duct exploration. About 5 per cent or 5,000 patients require a second operation in order to remove retained biliary tract calculi (Table I), although this figure increases without the use of routine operative cholangiography. The morbidity and mortality of the second surgical procedure is higher when compared to the primary operative intervention.

A new roentgenologic technique of non-operative stone extraction in the ambulatory patient represents a significant improvement in postoperative medical management.

DEVELOPMENT OF TECHNIQUE

Trans-T-tube catheterization using standard vascular catheters and guidewires has been used to dislodge sediment and blood clots in order to re-establish drainage.^{24,36} Removal of the T-tube is indicated for the extraction of retained stones through the T-tube tract, with the tube left in place for 4 to 5 weeks after operation to establish a fibrous tract. Mondet²⁸ extracted stones through it as early as 1962 with a specially designed forceps. The same Mondet extraction forceps was successfully used by Mazzariello²⁵ even with larger stones after bouginage of the sinus tract. Magarey^{21,22} preferred, for instrumentation, the Desjardins forceps and the Dormia* ureteral basket and catheter.

* V. Mueller, Chicago, Ill.

† Presented at the Seventy-third Annual Meeting of the American Roentgen Ray Society, Washington, D. C., October 3-6, 1972.
From the Department of Radiology, Children's Hospital and Adult Medical Center, San Francisco; and from the University of California San Francisco Medical School.

TABLE I
PERCENTAGE OF RETAINED STONES

Author	General and Review	Improvement with Routine Operative Cholangiography
Hicken and McAllister ¹⁵	19	4.0
Shore ³⁵	17	3.0
Mixter <i>et al.</i> ²⁷	13	—
Parent and Peloquin ²⁹	10-20	3-5
Dowdy ⁹	10	—
Jolly <i>et al.</i> ¹⁷	8-28	6.6
Ferris and Sterling ¹³	8-27	—
Kourias ¹⁸	8-12	3.5
Bartlett and Dreyfuss ³	6-11	—
Colcock and McManus ⁶	5.0	—
Edmunds <i>et al.</i> ¹¹	3.5-27	3.5
Larson <i>et al.</i> ²⁰	3.1	—
Schulenburg ^{33,34}	—	1.4

We started to use the Dormia ureteral basket in 1971, passing it either through the T-tube or, as described by Magarey, through a small arterial catheter.⁵ Several case reports with this technique have appeared in the literature.^{2,7,23,26,37}

We found the technique with small pre-shaped arterial catheters for placement of the stone basket rather time consuming, and the small tip of the relatively stiff arterial catheter was sometimes difficult to place and tented the wall of the biliary ducts. Sufficient contrast medium for continuous cholangiography was difficult to inject for continuous visualization of the retained stones. A second small arterial catheter was used initially for this purpose. These problems were corrected, and the

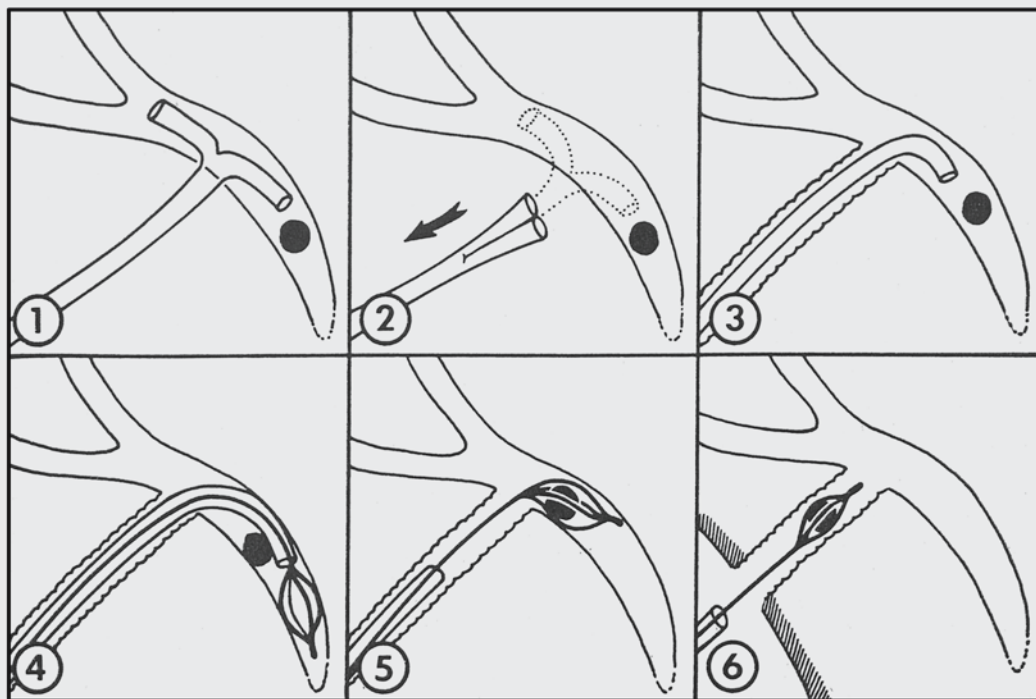


FIG. 1. *Technical steps for retained common duct stone extraction.*

1. Repeat T-tube cholangiogram is obtained on the day of stone extraction 4 to 5 weeks after choledochotomy
2. After the location of the retained stone has been ascertained, the T-tube is withdrawn
3. Using the sinus tract of the T-tube, the steerable catheter is guided into the bile duct, and its movable tip is advanced beyond the retained stone
4. The basket is inserted through the steerable catheter, the catheter is withdrawn and the basket is opened
5. The open basket is withdrawn in order to engage the stone. The basket is only retracted, never advanced, outside the enclosure of the steerable catheter
6. The stone is extracted through the drain tract.

procedure has been considerably shortened since we modified our instrumentation technique.

ROENTGENOLOGIC TECHNIQUE (Fig. 1, 1-6)

With the T-tube indwelling for at least 4 weeks after surgery, the ambulatory patient is returned to the x-ray department. T-tube cholangiograms are obtained for localization of retained stones. The patient is prepared and draped on the fluoroscopic table. Medication or anesthesia is not necessary. The T-tube is then extracted. This shows an average movement of the common duct by 1 or 2 cm.,³² with the duct

returning almost immediately to its previous position. This motion is absent in the presence of periductal adhesions.

A specially designed, polyethylene catheter† is then introduced through the T-tube tract. This steerable catheter permits remote control of the tip (Fig. 2, A and B) for easy passage through turns in the sinus tract and for direction of the tip into either the common hepatic or the common duct, depending on the position of the calculus. The catheter is 25 cm. in length. It has an external diameter of 4.3 mm. or No. 13 French and an internal diameter of 2.7 mm.

† Medi-Tech, Watertown, Mass.

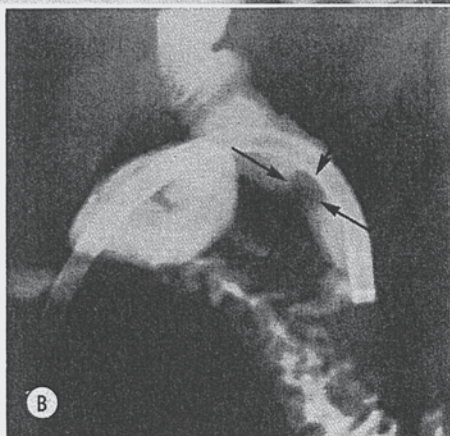
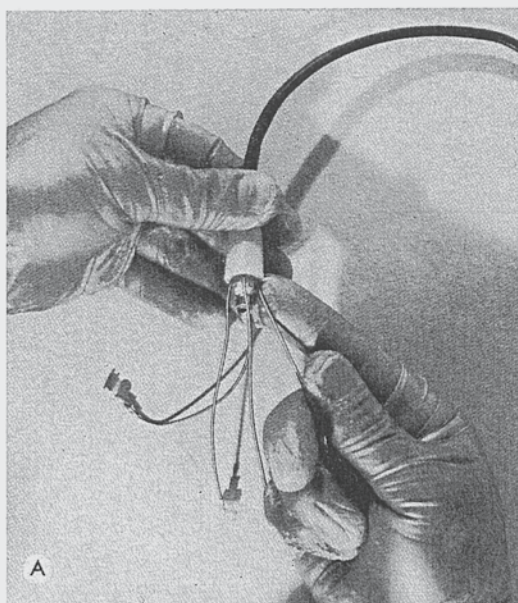


FIG. 2. Steerable catheter. (A) Traction from the outside on wires embedded in the wall of the catheter permits inside direction of the catheter. (B) The catheter is placed through the T-tube drain tract into the duct system, with its tip beyond the retained stone.

or No. 8 French, to permit passage of a variety of extraction instruments.

A side port is attached to the catheter for delivery of contrast material during the procedure. Intermittent contrast filling of the duct is obtained with a 300 cc. bottle of 30 per cent contrast medium, usually used for drip infusion pyelography.

After the large lumen steerable catheter

has been placed with its tip beyond the biliary calculus, the Dormia basket is advanced through it, the basket is opened distally to the stone and the catheter is withdrawn leaving the basket in position (Fig. 3). The small point of the basket is never advanced outside the enclosure of the catheter.

Stones up to 10 mm. fit readily into the basket (Fig. 4). The basket is then closed and the stone engaged by advancing the basket sheath (Fig. 5). If larger stones are present, we have had good success with the use of a single or double sling passed through the catheter (Fig. 6, A-C; and 7).

If stones are fragmented and small fragments remain, a straight rubber catheter is placed, left in the common duct for several days, and control cholangiography is obtained (Fig. 9, A and B; and 10).

MATERIAL AND RESULTS

Twenty patients with retained bile duct stones after cholecystectomy and choledochotomy underwent roentgenologic instrumentation for stone extraction through the T-tube tract. The material is summarized in Table II.



FIG. 3. The catheter has been withdrawn and the stone extraction basket has been opened.

Case 9 (Fig. 8) was a failure because catheterization of the tortuous sinus tract was impossible. The T-tube had been placed in a midline incision. This patient underwent re-operation for stone removal.

Case 2 with 2 stones had 1 stone extracted. The other small stone slipped into the cystic duct remnant during instrumentation. The patient is asymptomatic 9 months after instrumentation.

Case 1 (Fig. 6, A-C) with a 3 cm. stone had the calculus extracted from the common duct, but it could not be pulled through the sinus tract. It was deposited in the proximal portion of the tract. The patient is asymptomatic on 10 month follow-up without abscess and with the sinus tract closed.

Case 4 (Fig. 9, A and B) had a 5 mm. stone which was fractured and then expelled into the duodenum. The follow-up intravenous cholangiogram is normal.

Case 6 had a 3 mm. defect, difficult to visualize during the procedure, apparently expelled into the duodenum. A straight rubber catheter was left in place for 1 week and the control cholangiogram showed no remaining filling defects.

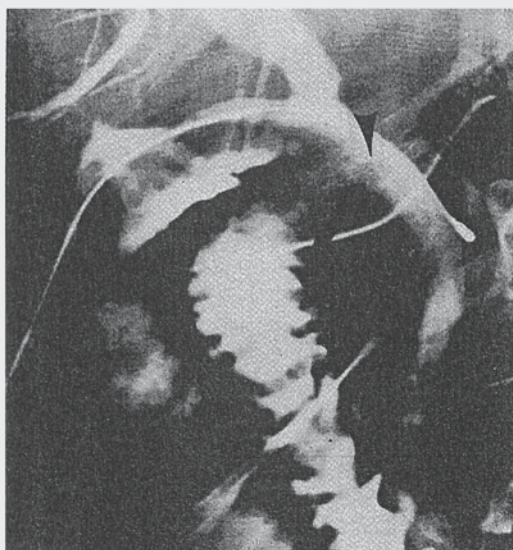


FIG. 4. The stone basket is withdrawn several times until the stone is caught in the open basket.

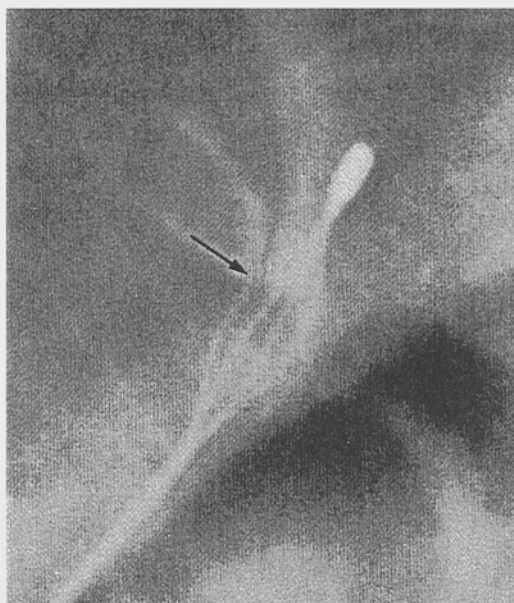


FIG. 5. The basket is closed around the stone by advancing the sheath.

Case 14 (Fig. 10) with an 18 mm. stone had a 14 mm. fragment extracted, the 4 mm. fragment passed into the duodenum. A straight French rubber catheter was introduced through the sinus tract into the common duct at the end of the procedure. The control cholangiogram 1 week later showed no remaining defects.

Fourteen patients with 20 stones had all of them completely extracted through the T-tube drain tract.

A second surgical intervention became unnecessary in all but 1 of the 20 patients. The sinus tracts healed and none of them have developed symptoms with follow-up ranging from 2 months to 12 months.

COMPLICATIONS

No complications occurred during instrumentation of 20 patients. No premedication and no local anesthetic was necessary. Some patients complained of pain during forceful contrast injection. Only dull pain sensation developed during instrumentation and only mild pain was experienced during extraction of a large stone through a small sinus tract.

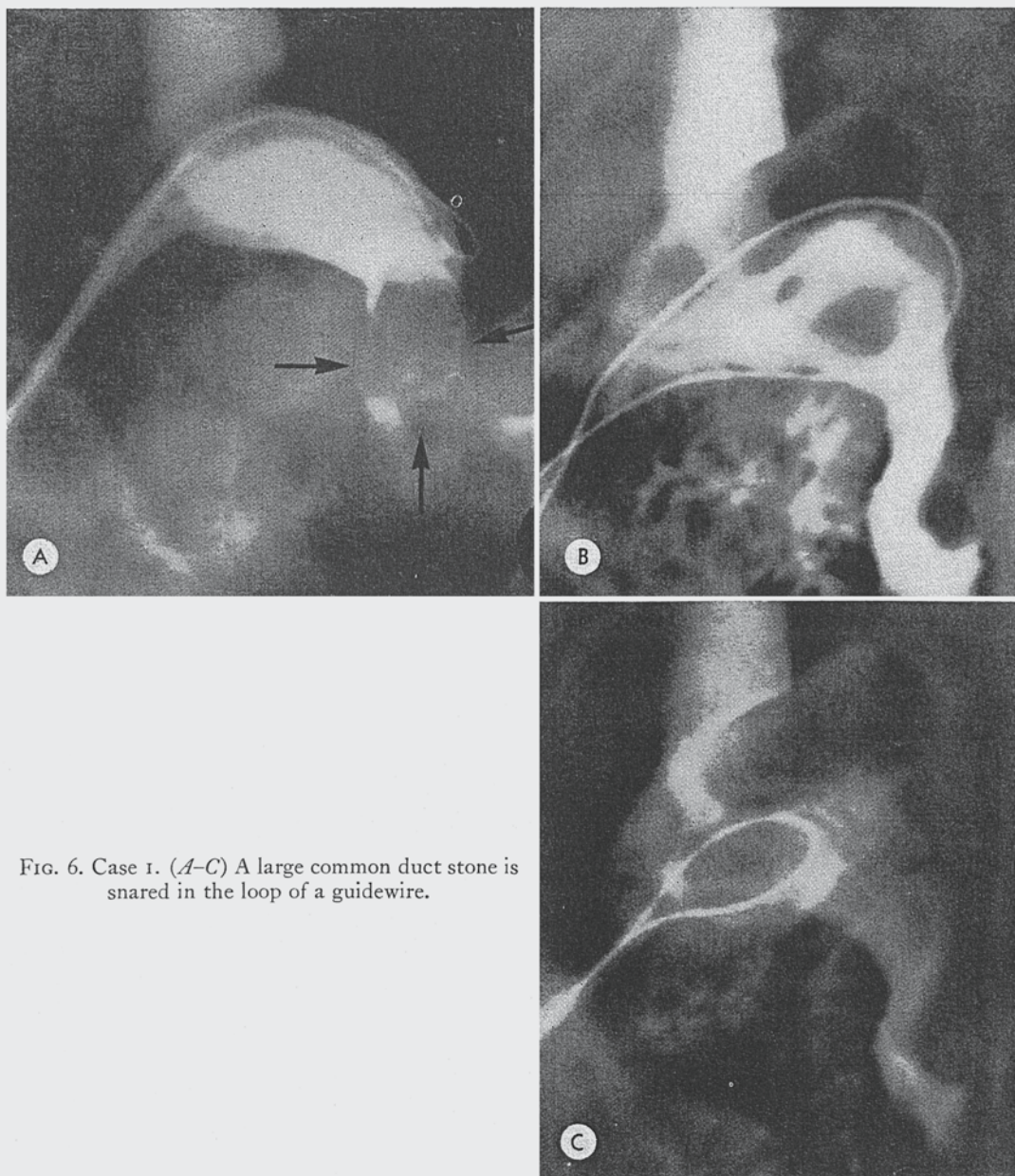


FIG. 6. Case 1. (A-C) A large common duct stone is snared in the loop of a guidewire.

Four of the 20 patients were placed on antibiotics by their referring surgeon, and a mild temperature increase occurred in 2 other patients on the first day after instrumentation.

The length of the procedure varied from 25 minutes for the patient in the room with $6\frac{1}{2}$ minutes of fluoroscopy time to $2\frac{1}{2}$ hours

in the room and 45 minutes fluoroscopy time. The length of the procedure shortened as we gained experience. None of the last 10 patients were longer in the room than 45 minutes.

Radiation exposure was monitored in 2 patients. One patient with a total fluoroscopy time of 21 minutes received 7.5 r at

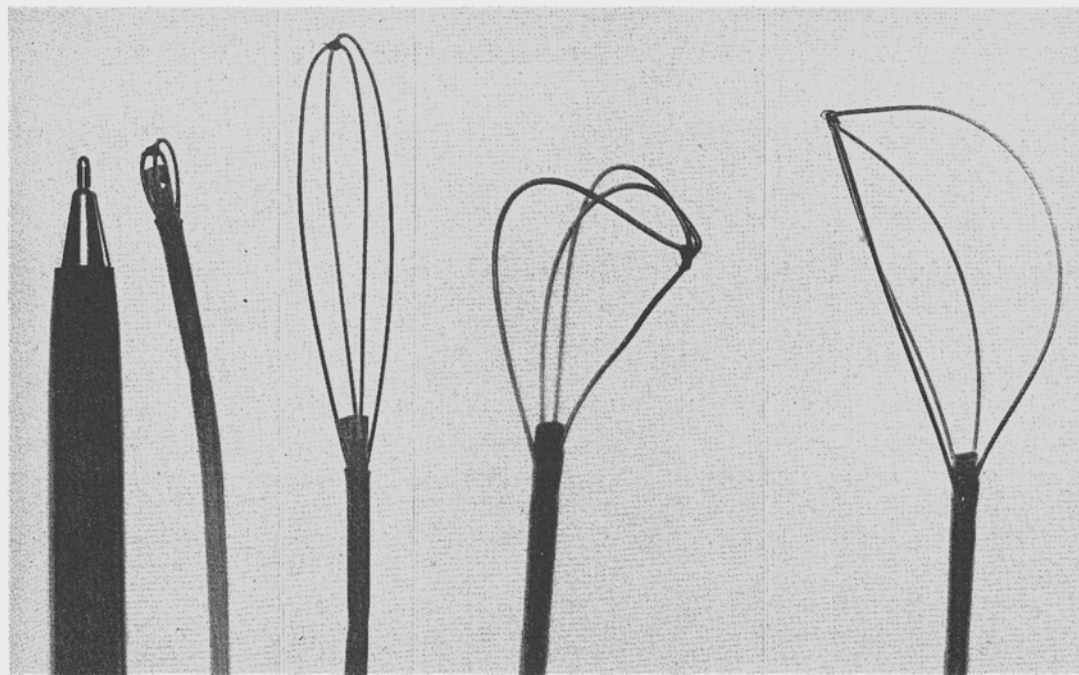


FIG. 7. A double snare forming a basket with 2 guidewires is placed through side holes in an arterial catheter. Traction on 1 of the 4 wire ends permits lateral manipulation distally to a retained stone.

the entry skin at the table top in the field and 120 mr on the anterior left chest wall outside the field. The roentgenologist received in the same case 40 mr at the dorsum of his right hand. A pocket dosimeter had been placed inside the rubber glove. A small shutter opening was used during the entire procedure with the roentgenologist's hands outside the field at all times. The roentgenologist received 27.0 mr during this procedure at the waist level outside his apron.

The radiation exposure dosimetry in the second case with $6\frac{1}{2}$ minutes of fluoroscopy and cinefluorography time showed 2.5 r at the skin entry port at the table top for the patient and 80 mr on his left chest anteriorly. The roentgenologist received 27 mr on the back of his right hand and 4 mr on the outside of his apron at waist level.

DISCUSSION

The first technique employed in the non-

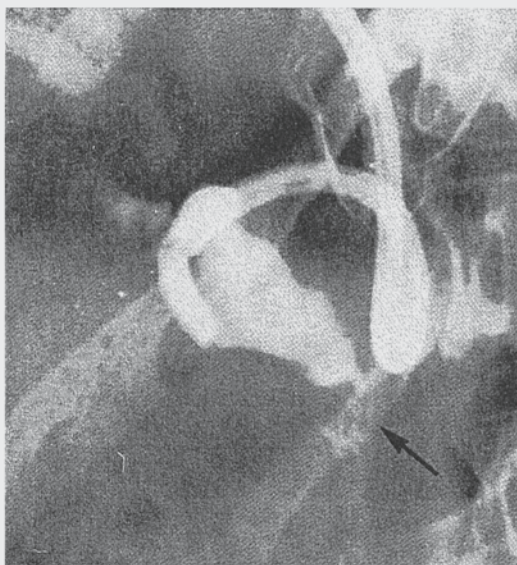


FIG. 8. Case 9. A second surgical procedure could not be prevented in this patient with retained common duct stone. The T-tube had been placed in the midline incision and the sinus tract was too tortuous for catheterization.

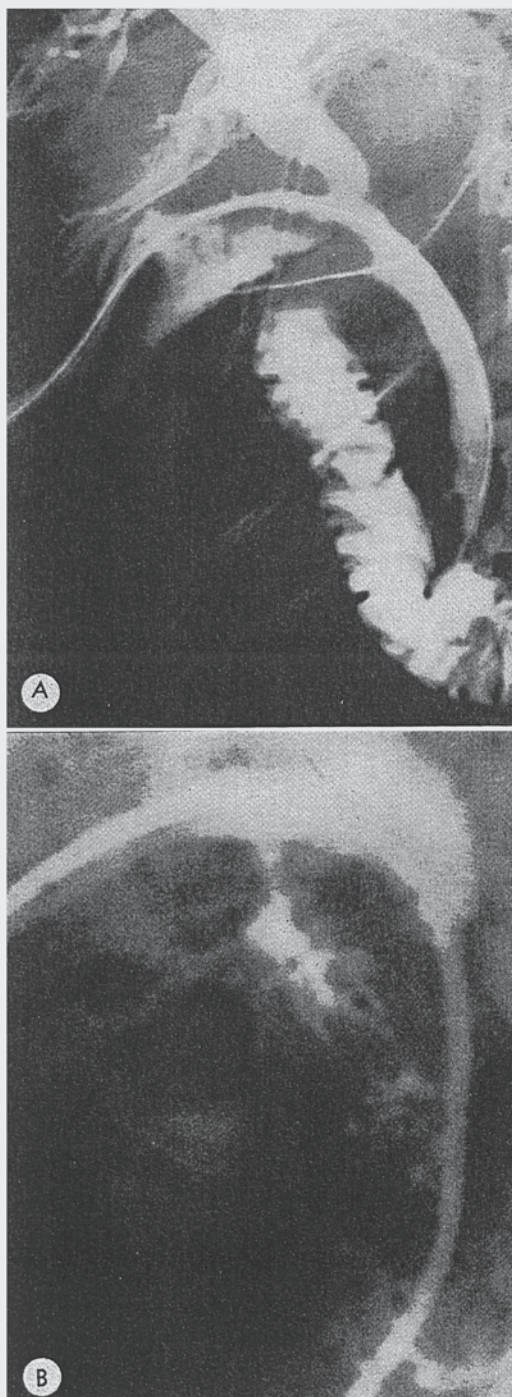


FIG. 9. Case 4. (A) The stone basket or (B) a small arterial catheter may be advanced through the distal common duct into the duodenum in order to expell small stones or stone fragments.

operative removal of retained biliary tract calculi was instillation of solvents such as ether or chloroform. Dissolution of stones was claimed by Pribram^{30,31} as early as 1939. Dissolution of cholesterol stones by chenodeoxycholic acid was reported recently.⁸ However, the vast majority of biliary tract stones contain little cholesterol. Eight of the 20 patients in our material underwent attempts of gallstone dissolution without success. Hospitalization for this procedure is costly and complications do occur.

Lamis *et al.*,¹⁹ and Fennessy and You¹² reported successful expulsion of retained calculi in 3 cases. They employed a soft rubber catheter inserted through the tract of the removed T-tube. Combined with irrigation, the catheter was advanced into the duodenum and the stones passed (Fig. 9, A and B). Irrigation with oil⁴ has also been reported.

The balloon-tipped Fogarty catheter has been used for stone extraction during cholecystectomy.¹ We have tried this method postoperatively. The balloon was filled



FIG. 10. Case 14. If small fragments remain in the common duct after extraction, a straight French rubber catheter may be positioned and left in place for control studies at a later date.

TABLE II
SUMMARY OF CLINICAL MATERIAL

No.	Case	Sex	Age	Size and No. of Stones	Location	Result
1	R.G.	M	84	30 mm.	Common duct	Deposited in sinus tract; 10 mo. follow-up: sinus tract closed, no abscess
2	L.S.	F	26	4 mm. 4 mm.	Right hepatic duct Left hepatic duct	Right hepatic stone extracted. Left hepatic stone deposited in cystic duct remnant; asymptomatic on 9 mo. follow-up
3	G.U.	M	50	5 mm. 4 mm.	Common duct	Extracted
4	E.H.	F	74	5 mm.	Common hepatic duct	Fragmented and expelled into duodenum; asymptomatic on 9 mo. follow-up, intravenous cholangiogram normal
5	D.L.	F	34	5 mm.	Common duct	Extracted
6	A.L.	F	68	3 mm.	Proximal branch of T-tube	Expelled; T-tube cholangiogram 1 week later normal
7	J.B.	F	72	5 mm.	Left hepatic duct	Extracted
8	S.A.	F	78	11 mm.	Right hepatic duct	Extracted
9	T.W.	F	40	7 mm.	Common duct	Unsuccessful, tortuous sinus tract, could not be catheterized
10	M.F.	F	71	4 mm.	Common duct	Extracted
11	H.P.	F	38	5 mm. 6 mm.	Common duct	Extracted
12	B.R.	M	48	7 mm.	Common hepatic duct	Extracted
13	W.S.	F	62	9 mm.	Common duct	Extracted
14	J.K.	M	76	18 mm.	Common hepatic duct	A 14 mm. fragment extracted, a 4 mm. fragment passed; normal tube cholangiogram 1 week later
15	S.C.	F	68	8 mm.	Common duct	Extracted
16	M.F.	F	48	10 mm. 8 mm.	Common duct	Extracted
17	N.S.	F	76	10 mm. 6 mm.	Common duct	Extracted
18	L.F.	M	62	9 mm.	Common hepatic duct	Extracted
19	E.F.	F	72	6 mm.	Common duct	Extracted
20	A.L.	M	63	11 mm. 11 mm. 11 mm.	Common duct	Extracted

with contrast medium and placed distally to the calculus. The direction of extraction force to the side of the stone resulted in angulation, and the stone was wedged against the wall of the bile duct. We do not recommend this procedure. Eaton *et al.*,¹⁰ and Henzel *et al.*¹⁴ reported 5 cases of injury resulting with the use of the balloon catheter.

The Dormia basket was designed for the extraction of ureteral stones, but is ideally suited for biliary tract stones up to about 10 mm. size. Differently sized baskets are now available.* We constructed single (Fig. 6, A-C) or double (Fig. 7) snares for the extraction of larger stones. An .021 guide-

* Medi-Tech, Watertown, Mass.

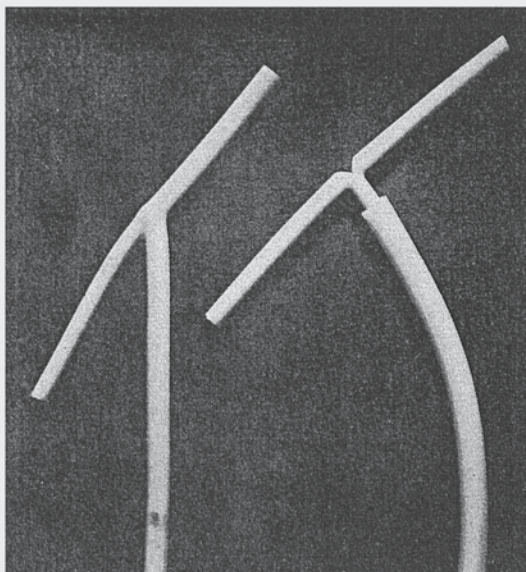


FIG. 11. A large caliber of the long arm of the T-tube is useful in stone extraction, because the diameter of the sinus tract limits the size of the calculus to be extracted. A larger catheter may be slipped over the T-tube in order to achieve this (*right*). T-tube catheters with an obtuse angle may be left in place after surgery if stones in hepatic radicals are known to remain. This will facilitate instrumentation postoperatively (*left*).

wire is well suited for this purpose. The 2 ends of the wire are maneuvered separately for positioning of the snare and in order to get behind the stone (Fig. 7). A single snare may slide off the stone during extraction, particularly if force is needed to pull a large stone through the sinus tract. If a stone is fragmented, we leave a soft, straight rubber catheter in place in the duct and repeat a control cholangiogram 1 week later to see if the small fragments were passed (Case 4, Fig. 9, *A* and *B*; and Case 14, Fig. 10).

If the stone is wedged distally in the common duct, the steerable tip of a smaller catheter is placed behind the stone and it is then moved to a more proximal position in the duct for extraction with the basket.

We have extracted stones up to 1.4 cm. in size through the sinus tract of a No. 16 French T-tube. We recommend that surgeons use T-tubes with a larger caliber of

the long arm routinely after biliary tract surgery in order to facilitate subsequent instrumentation. A catheter of this type can be constructed readily in the surgical suite by slipping a large Foley catheter over the long branch of the T-tube after the ends of the Foley catheter are cut off (Fig. 11). The long branch of the T-tube should be placed in a right angle to the common duct, then through a lateral stab wound using a straight and short line to the skin. If a stone is seen in the hepatic radicals at operation and if it cannot be extracted at that time, a T-tube with an obtuse angle (Fig. 11) may be placed for roentgenologic catheter instrumentation after operation. Blind instrumentation during surgery in an attempt to extract stones in biliary radicals should be avoided if fluoroscopic control is not available. It may result in traumatic extravasation (Fig. 12).

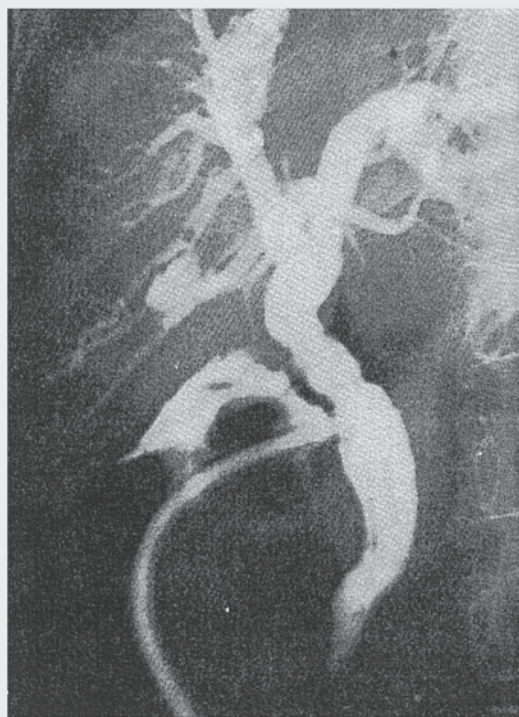


FIG. 12. Traumatic extravasation after attempt of operative instrumentation for small stone in hepatic radical. Extraction is best accomplished by nonoperative technique 4 weeks after surgery.

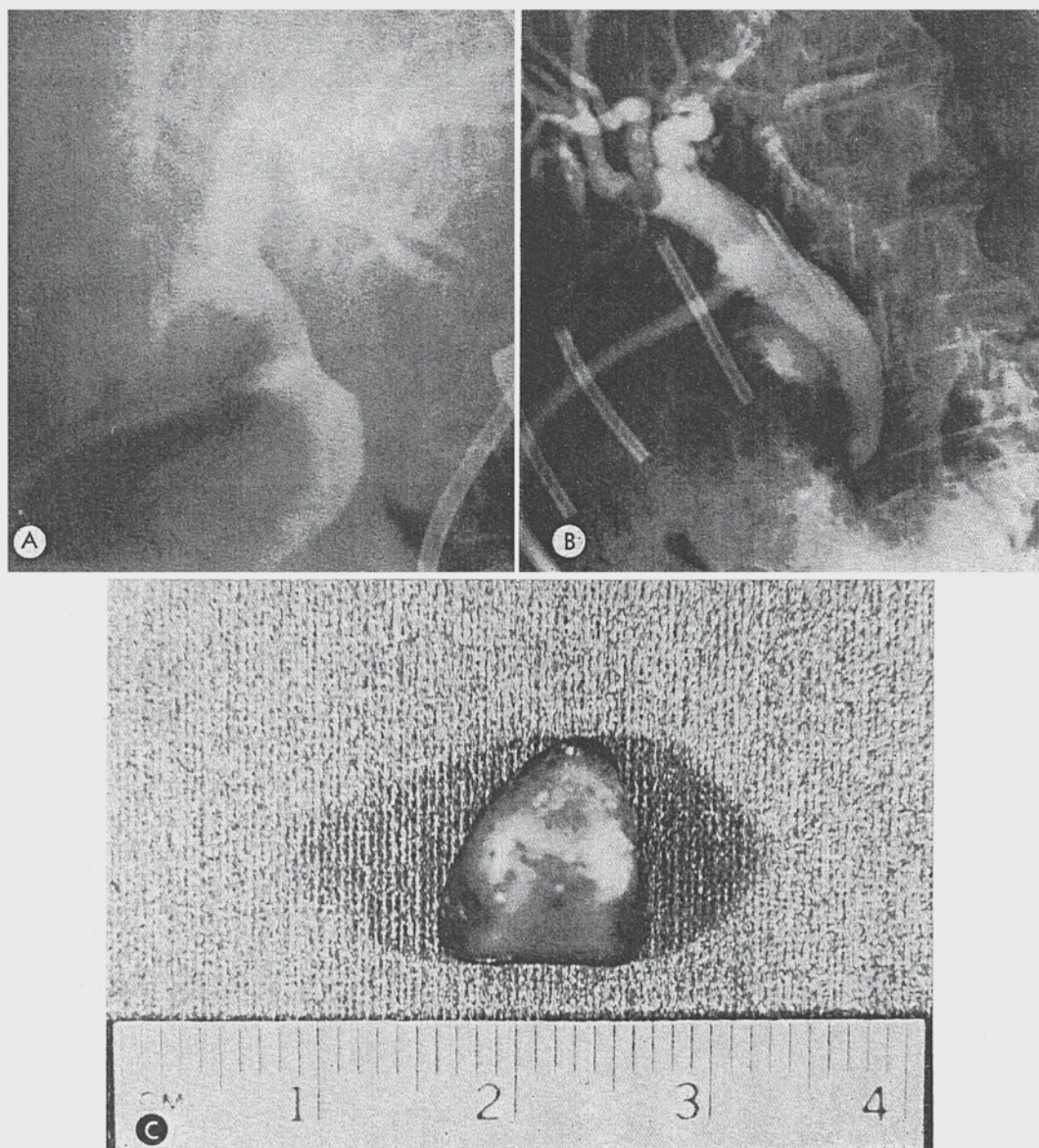


FIG. 13. Case 8. (A) This postcholedochotomy operative cholangiogram was called normal. The right main hepatic radical is amputated by a large remaining duct stone. (B) The postoperative T-tube cholangiogram shows the 11 mm. calculus clearly in the same patient. (C) The same stone was successfully extracted.

The stone is left in place and then extracted in the ambulatory patient by this roentgenographic method.

Small stones can present problems if they are smaller than 5 mm. They are difficult to visualize during the procedure (Case 6). Suction may be of use in these cases.

The entity of retained biliary duct stones will continue to be a common occurrence because of hepatic stones, silent stones, unreliability of duct palpation, 5 per cent falsely negative operative cholangiograms (Fig. 13, A-C), and because of the disuse of primary and secondary operative cholan-

giography.¹⁷ But the answer to this problem is now available with the technique of non-operative stone extraction. And even though some complications can be expected eventually, when compared to other therapeutic methods, the advantages of this roentgenologic technique are obvious.

SUMMARY

Our experience with 20 cases of nonoperative retained biliary tract stone extractions is presented.†

An improved instrumentation technique through a steerable catheter under roentgenologic control is described.

A second surgical intervention for stone removal became unnecessary in all but 1 of our 20 patients undergoing this new roentgenologic technique.

All 19 patients have remained asymptomatic after stone removal.

The technique was unsuccessful in 1 patient due to our inability to catheterize a tortuous T-tube drain tract.

Compared to re-operation or attempts of stone dissolution, extraction under roentgenologic control in the ambulatory patient is the method of choice for the treatment of retained biliary tract stones.

Department of Radiology
Children's Hospital and Adult Medical Center
San Francisco, California 94119

I am grateful to my surgical colleagues for their help and encouragement.

REFERENCES

1. ANDERSON, R. P., LEAND, P. M., and ZUIDEMAN, G. D. Uses of balloon-tipped catheter in biliary tract surgery. *Am. J. Surg.*, 1969, 117, 55-61.
2. BAKER, J. Q., CHISHOLM, D. P., and SCHALLER, R. T. Removal of retained biliary stone without reoperation. *A.M.A. Arch. Surg.*, 1972, 104, 702-703.
3. BARTLETT, M. F., and DREYFUSS, J. R. Residual common duct stones. *Surgery*, 1960, 47, 202-205.
4. BEST, R. R. Operative and nonoperative methods in management of common duct lesions. *Minnesota Med.*, 1948, 31, 192-196.
5. BURHENNE, H. J. Extraktion von Residualsteinen der Gallenwege ohne Reoperation. *Fortschr. a. d. Geb. d. Röntgenstrahlen u. d. Nuklearmedizin*, 1972, 117, 425-428.
6. COLCOCK, B. P., and McMANUS, J. E. Experiences with 1,356 cases of cholecystitis and cholelithiasis. *Surg., Gynec. & Obst.*, 1955, 101, 161-172.
7. COYLE, M. J., and THOMPSON, W. M. Non-surgical removal of retained common duct stones. *Alaska Med.*, 1971, 13, 89-90.
8. DANZINGER, R. G., HOFMANN, A. F., SCHOENFELD, L. J., and THISTLE, J. L. Dissolution of cholesterol gallstones by chenodeoxycholic acid. *New England J. Med.*, 1972, 286, 1-8.
9. DOWDY, G. S., JR. The Biliary Tract. Lea & Febiger, Philadelphia, 1969.
10. EATON, S. B., JR., WIRTZ, R. D., TEN EYCK, J. R., and RICHARDS, J. C. Iatrogenic liver injury resulting from ductal instrumentation with Fogarty biliary balloon catheter. *Radiology*, 1971, 100, 581-584.
11. EDMUNDS, M. C., JR., EMMETT, J. M., and CLARK, W. D. Ten-year experience with operative cholangiography. *Am. Surgeon*, 1960, 26, 613-621.
12. FENNESSY, J. J., and YOU, K. D. Method for expulsion of stones retained in common bile duct. *Am. J. Roentgenol., Rad. Therapy & Nuclear Med.*, 1970, 110, 256-259.
13. FERRIS, D. O., and STERLING, W. A. Surgery of biliary tract. *Surg. Clin. North America*, 1967, 47, 861-885.
14. HENZEL, J. H., BLESSING, W. D., and DEWEESE, M. D. Intrahepatic biliary disruption: report of two cases occurring during use of balloon-tipped biliary catheters. *A.M.A. Arch. Surg.*, 1971, 102, 218-220.
15. HICKEN, N. D., and McALLISTER, A. J. Operative cholangiography as aid in reducing incidence of "overlooked" common bile duct stones. *Surgery*, 1964, 55, 753-758.
16. INGELFINGER, F. J. Digestive disease as national problem. *Gastroenterology*, 1968, 55, 102-104.
17. JOLLY, P. C., BAKER, J. W., SCHMIDT, H. M., WALKER, J. H., and HOLM, J. C. Operative cholangiography. *Ann. Surg.*, 1968, 168, 551-565.
18. KOURIAS, B. Reintervention an den ableitenden Gallenwegen. *Chirurg*, 1968, 39, 283-289.
19. LAMIS, P. A., LETTON, A. H., and WILSON, J. P. Retained common duct stones: new nonoperative technique for treatment. *Surgery*, 1969, 66, 291-296.
20. LARSON, R. E., HODGSON, J. R., and PRIESTLEY, J. T. Early and long term results of 500 consecutive explorations of common duct. *Surg., Gynec. & Obst.*, 1966, 122, 744-750.

† Another 11 patients underwent successful stone extractions since the completion of this manuscript, bringing our total experience to 31 cases. As many as 4 retained stones were extracted in one patient. No complications occurred in any of the 31 cases.

21. MAGAREY, C. J. Non-surgical removal of retained biliary calculi. *Lancet*, 1971, 1, 1044-1046.
22. MAGAREY, C. J. Removal of retained bile-duct calculus without operation: case report. *Brit. J. Surg.*, 1969, 56, 312-314.
23. MAHORNER, H., and BEAN, W. J. Removal of residual stone from common bile duct without surgery. *Ann. Surg.*, 1971, 173, 857-863.
24. MARGULIS, A. R., NEWTON, T. H., and NAJARIAN, J. S. Removal of plug from T-tube by fluoroscopically controlled catheter: report of case. *Am. J. Roentgenol., Rad. Therapy & Nuclear Med.*, 1965, 23, 975-977.
25. MAZZARIELLO, R. Removal of residual biliary tract calculi without reoperation. *Surgery*, 1970, 67, 566-573.
26. McMURNEY, R. P., and GARDNER, H. C. Non-surgical removal of retained common duct stones: case report. *Ann. Surg.*, 1971, 173, 298-300.
27. MIXTER, C. G., HERMANSON, L., and SEGEL, A. L. Operative cholangiography: evaluation of 406 cases. *Ann. Surg.*, 1951, 134, 346-350.
28. MONDET, A. Técnica de la extracción incruenta de los cálculos en la litiasis residual del cólico. *Bol. Soc. Cir. B. Air.*, 1962, 46, 278-290.
29. PARENT, M., and PELOQUIN, A. Preoperative cholangiography. *Canad. J. Surg.*, 1963, 6, 129-135.
30. PRIBRAM, B. O. Ether treatment of gallstones impacted in common duct. *Lancet*, 1939, 1, 1311-1313.
31. PRIBRAM, B. O. Method for dissolution of common duct stones remaining after operation. *Surgery*, 1947, 22, 806-818.
32. SCATLIFF, J. H., MARK, J. B. D., and SIMARAK, S. Cinefluorography of T-tube extractions. *Surgery*, 1963, 53, 432-436.
33. SCHULENBURG, C. A. R. Operative Cholangiography. Butterworth & Co., Ltd., London, 1966.
34. SCHULENBURG, C. A. R. Operative cholangiography: 1,000 cases. *Surgery*, 1969, 65, 723-739.
35. SHORE, J. M. Prevention of residual biliary calculi. *California Med.*, 1971, 114, 1-6.
36. SHORT, W. F., HOWARD, J. M., and DIVEN, W. F. Trans T-tube catheterization. *A.M.A. Arch. Surg.*, 1971, 102, 136-138.
37. WENDTH, A. J., JR., LIEBERMAN, R. C., and ALPERT, M. Nonsurgical removal of retained common bile duct calculus. *Radiology*, 1972, 103, 207-208.



7.8 Perkutane Rekanalisation chronischer arterieller Verschlüsse mit einem neuen Dilatationskatheter

Andreas R. Grüntzig (1939–1985)

see Chapter 7.9 on page 514

H. Hopff

- schaften. Probl. u. Ergeb. Psychol. 31 (1969), 15.
- (6) Hackenberg, K., W. Grunewald, H. Gertz, D. Reinwein: Kritische Untersuchungen zur optimalen Substitutions-therapie der Hypothyreose mit synthetischen Schilddrüsenhormonen. Dtsch. med. Wschr. 96 (1971), 1375.
- (7) von Harnack, G. A., J. Farmer, R. Whitehouse, C. Rodriguez: Catch-up in height and skeletal maturity in children on long-term treatment for hypothyroidism. Z. Kinderheilk. 112 (1972), 1.
- (8) von Harnack, G. A.: Erkennung und Behandlung der Hypothyreose im Kindesalter. Mschr. Kinderheilk. 115 (1967), 9.
- (9) Horster, F., E. Klein: Die Anwendung von radioaktivem Trijodthyronin zur Diagnostik der Schilddrüsenfunktion in vitro. Dtsch. med. Wschr. 89 (1964), 983.
- (10) Lienert, E. A.: Testaufbau und Testanalyse (Beltz: Weinheim, 1969).
- (11) Klein, A., S. Meltzer, F. Kenny: Improved prognosis in congenital hypothyroidism treated before age three months. J. Pediatr. 81 (1972), 912.
- (12) Klink, K.: Behandlung der Hypothyreose im Kindesalter. Therapiewoche 24 (1964), 1198.
- (13) Lüders, D.: Kombination von ^{125}I -T₃- und T₄-Test zur Schilddrüsenfunktionsprüfung. Mschr. Kinderheilk. 118 (1970), 214.
- (14) Mittenecker, E.: Planung und statistische Auswertung von Experimenten (Deuticke: Wien, 1963).
- (15) Priester, H., J. Hardesty: Handbuch zum HAWIK (Huber: Bern-Stuttgart 1956).
- (16) Raiti, S., G. News: Cretinism: early diagnosis and its relation to mental prognosis. Arch. Dis. Childh. 46 (1971), 692.
- (17) Smith, D., R. Blizzard, L. Wilkins: The mental prognosis in hypothyroidism of infancy and childhood. A review of 128 cases. Pediatrics 19 (1957), 1011.
- (18) Spiess, H., D. Lüders, H. Schlage: Früherkennung und Entwicklung der angeborenen Hypothyreose. Mschr. Kinderheilk. 116 (1968), 317.
- (19) Struwe, F., H. Kempe: Radio-Jod-Diagnostik der Hypothyreose im Kindesalter. Mschr. Kinderheilk. 118 (1970), 217.
- (20) Stolecke, H., C. ter Huerne: Gesamthormonjod im Serum als Parameter für die Schilddrüsenfunktion. Z. Kinderheilk. 111 (1971), 175.
- (21) Wiebel, J., N. Stahnke, M. Menking, W. Blunck: Dosierung eines Kombinationspräparates aus synthetischem Trijodthyronin und Thyroxin im Kindesalter. Mschr. Kinderheilk. 118 (1970), 457.
- (22) Wiebel, J., N. Stahnke, M. Menking, W. Blunck: Untersuchung zur Dosierung eines Kombinationspräparates von synthetischem Thyroxin und Trijodthyronin im Kindesalter. Dtsch. med. Wschr. 95 (1970), 2336.
- (23) Winkelmann, W.: HAWIK (Beltz: Weinheim 1972).
- (24) Tanner, J.: Regulation of growth in size in mammals. Nature (Lond.) 199 (1963), 845.
- (25) Wool, M., H. Selenkow: Physiologic combinations of synthetic thyroid hormones in myxedema. Clin. Pharmacol. Ther. 6 (1965), 710.

Dr. K. Rager, Dr. M. Ranke, Prof. Dr. J. R. Bierich
Universitäts-Kinderklinik
74 Tübingen, Rümelinstr. 23

Dipl.-Psych. S. Blüthmann, Dipl.-Psych. W. Hoss
Psychologisches Institut der Universität
74 Tübingen, Friedrichstr. 21

Dtsch. med. Wschr. 99 (1974), 2502-2505
© Georg Thieme Verlag, Stuttgart

Perkutane Rekanalisation chronischer arterieller Verschlüsse mit einem neuen Dilatationskatheter

Modifikation der Dotter-Technik

A. Grüntzig und H. Hopff*

Departement für Innere Medizin (Prof. Dr. P. Frick, Prof. Dr. A. Labhart, Prof. Dr. W. Siegenthaler) und Röntgendiagnostisches Zentralinstitut (Prof. Dr. W. Wellauer) der Universität Zürich

Eine Modifikation der Dotter-Technik wurde bei 15 Patienten mit Stenosen und Verschlüssen der Oberschenkel- und Stenosen der Beckenarterien angewendet. Bei diesem neuen Verfahren wird das Verschlussmaterial nicht mehr durch die übereinandergeschobenen Dotter-Katheter komprimiert, sondern durch einen Grundkatheter mit dehnbarem (gerecktem) Überkatheter. Dieser Katheter hat den Vorteil, daß 1. während des Rekanalisationsvorganges keine längsgerichtete Bewegung im Gefäß stattfindet, was die Gefahr einer Embolisierung von Verschlussmaterial reduziert, 2. das dehnbare Segment des Katheters den individuellen Gegebenheiten und Dimensionen des Gefäßes (Becken-, Oberschenkelarterie) angepaßt ist, 3. der Außendurchmesser des Überkatheters im gedehnten Zustand größer als 4 mm sein kann und 4. das Punktionsloch in der Femoralarterie kleiner ist und jetzt den Dimensionen üblicher Katheteruntersuchungen entspricht. Das Verfahren ist einfach, und die Frühresultate sind günstig. Die Anwendung im Bereich der Beckenarterien wird erleichtert.

Die perkutane Rekanalisation chronischer kurzstreckiger Verschlüsse oder Stenosen der Femoralarterie wurde von Dotter und Judkins 1964 (1) eingeführt und von verschiedenen Arbeitsgruppen aufgegriffen (4, 8, 9).

Im deutschsprachigen Raum ist dieses Behandlungsverfahren insbesondere von der Arbeitsgruppe um

Zeitler (11-14) vertreten worden. Es hat inzwischen in Zürich seinen Platz im therapeutischen Konzept der interdisziplinären Gefäßsprechstunde¹ gefunden (5). Auf unsere bisherigen Erfahrungen möchten wir hier nur kurz eingehen, dafür ausführlicher über eine Modifikation

Percutaneous recanalization after chronic arterial occlusion with a new dilator-catheter (modification of the Dotter technique)

A modified Dotter technique was used in 15 patients with stenoses or occlusions in the upper leg and stenoses of the pelvic arteries. The occluding material is removed with a distensible catheter introduced over a guide catheter. The system has the advantage that (1) no longitudinal movement of the vessel occurs during recanalization and the danger of embolization of the occluding material is thus reduced; (2) the distensible segment of the catheter is adjusted to the individual circumstances and vessel dimensions; (3) the external diameter of the outer catheter in its distended state can be more than 4 mm; (4) the puncture hole in the femoral artery is smaller and corresponds to the size after the usual catheter studies. The procedure is simple and preliminary results are favourable. It is a relatively easy of achieving recanalization of the pelvic arteries.

* emeritierter Professor für organisch-chemische Technologie der Eidgenössischen Technischen Hochschule Zürich

¹ Leiter: Privatdozent Dr. A. Bollinger, Medizinische Poliklinik, Prof. Dr. U. Brunner, Chirurgische Klinik B, Privatdozent Dr. W. Meier, Chirurgische Klinik A der Universität Zürich

tion der Dotter-Technik berichten, die wir seit einem halben Jahr klinisch anwenden und die die bisherige Technik verbessert.

Vorgehen nach Dotter

Technik. In Lokalanästhesie wird vom Leistenband aus nach der Seldinger-Technik die A. femoralis superficialis sondiert und unter Röntgen-Fernseh-Durchleuchtung ein Führungsdraht (J-guide) durch den Verschuß oder die Stenose manövriert. Dieser dient für zwei nachfolgende Katheter als Leitschiene. Die beiden Katheter haben die Größen Charrière 8 und 12 (4 mm) und werden koaxial nacheinander durch den Verschuß gepreßt. Dadurch wird ein neues Lumen geformt und das Gefäß wieder für den Blutstrom durchgängig. In bezug auf technische Einzelheiten sei auf die Literatur verwiesen (1–3, 11–14).

Ergebnisse. Wir begannen mit dem Verfahren² Ende 1971. Die medikamentöse Zusatztherapie besteht zur Zeit in der Vor- und Nachbehandlung mit Acetylsalicylsäurepräparaten (12). Am Tage des Eingriffs beginnen wir zusätzlich mit Dauerantikoagulation (Cumarine) und setzen das Salicylat beim Erreichen von Quick-Werten zwischen 20 und 30% ab.

Bei 60 Behandlungsversuchen (mittleres Alter 67 Jahre, Bereich 45–81 Jahre) konnten 50 günstige Frühresultate erzielt werden. Infolge des Eingriffs besserten sich die systolischen Drücke in den Knöchelarterien, gemessen mit Doppler-Ultraschall, im Mittel von $97 (\pm 29)$ auf $122 (\pm 34)$ mm Hg. Die mittlere systolische Druckdifferenz zwischen Arm- und Knöchelarterien nahm von $64 (\pm 31)$ auf $24 (\pm 28)$ mm Hg ab. Das entsprach einer Reduktion auf 38% des Ausgangswertes und früheren Beobachtungen (5). Die vierteljährlichen Nachkontrollen ergaben, daß bei 27 Patienten, bei denen die gelungene Rekanalisation länger als ein Jahr zurücklag, sieben Rezidivverschlüsse bzw. -stenosen auftraten.

Zeitler und Mitarbeiter (13, 14) gaben bei einer größeren Zahl von Patienten folgende Ergebnisse an: 80% günstige Frühresultate und 34% Rezidive nach einem Jahr und 52% nach zwei Jahren.

Nachteile. 1. Die Dotter-Katheter werden in Längsrichtung des Gefäßes durch das Verschußmaterial geschoben, was zu einer Embolie führen kann. Diese Komplikation ist zwar relativ selten und wird am Unterschenkel zumeist in kurzer Zeit kompensiert (5, 12), sie verbietet aber die Anwendung des Verfahrens in Gefäßgebieten, in denen auch kurze Ischämiezeiten nicht toleriert werden (2).

2. Das Punktionsloch am Leistenband entspricht etwa dem Außendurchmesser des zuletzt verwendeten Katheters (4 mm). Dadurch werden die Risiken einer Nachblutung oder eines pulsierenden Hämatoms (Aneurysma spurium) größer als bei den üblichen Katheteruntersuchungen.

3. Für die Oberschenkelarterie ist das von den Kathetern geschaffene Lumen von etwa 4 mm Durchmesser hämodynamisch zumeist ausreichend. Für die Iliaca-Arterie genügt dieses Lumen jedoch nicht.

Zeitler und Mitarbeiter (12) empfahlen eine Dehnung der Stenosen mit einem Fogarty-Ballon-Katheter. Wir

konnten damit keine überzeugende hämodynamische Verbesserung erzielen. Der elastische Latex-Ballon folgt dem geringsten Widerstand und weicht einer Stenose sanduhrförmig aus. Eine Verbesserung wurde inzwischen von Porstmann (10) angegeben; es handelt sich um einen Korsett-Ballonkatheter, bei dem jedoch hinsichtlich Größe (Charrière 12), Oberflächengestaltung und Druckverteilung noch einige Probleme zu bestehen scheinen.

Modifikation der Technik mit einem Dilatationskatheter

Nachdem in Tierversuchen verschiedene andere Techniken studiert worden waren (6), fand sich mit der Herstellung des folgenden Katheters³ die bisher beste Lösung: Ein dünnwandiger Polyvinylchlorid-Schlauch wird in einem bestimmten Abschnitt durch Dehnung unter Parallelrichtung der langen Molekülketten (Reckung [7]) auf einen dem Gefäß entsprechenden Durchmesser und auf die dem Verschuß oder der Stenose entsprechende Länge vorgeformt. Dieses Schlauchstück wird über einen Grundkatheter (im allgemeinen Charrière 6) gezogen und wenige Zentimeter hinter der Spitze fest mit ihm verbunden. Unter dem aufgesetzten Schlauchstück hat der Grundkatheter Seitenlöcher. Der gereckte Teil des Überkatheters legt sich eng – etwa wie ein aufgerollter Regenschirm – um den Grundkatheter. Der Außendurchmesser des Gesamtkatheters vergrößert sich dadurch um 1–3 Charrière auf etwa 2,3 bis 3,0 mm. Zum Eingriff selbst wird das Gefäß wie üblich mit dem flexiblen Führungsdraht und einem Angiographiekatheter sondiert. Anschließend wird anstelle des üblichen Dotter-Katheters der neue Katheter eingeführt und mit seinem dehnbaren Segment, dem Führungsdraht folgend, im Verschuß oder in der Stenose in Position gebracht. Nach Rückzug des Führungsdrahtes verschließt man den Grundkatheter mit einem Tip-Occluder. Am Katheterende sind ein Y-Verschußstück und eine kleine Spritze (2 cm³) angeschlossen, so daß der Überkatheter über die Seitenlöcher mit Flüssigkeit (physiologischer NaCl-Lösung und Kontrastmittel) gefüllt werden kann. Übt man manuell mit der Spritze Druck (etwa 2–3 atü) auf die Flüssigkeit aus, so nimmt der Überkatheter die vorbestimmte Form an (Abbildung 1^ab und 2b), wobei das Verschußmaterial an die Wand gepreßt wird. Die Materialbeschaffenheit des Überkatheters verhindert, daß die Dimension des gereckten Schlauches überschritten werden kann. Dadurch ist es dem Überkatheter nicht möglich, einem geringen Widerstand zu folgen und etwa einer Stenose sanduhrförmig auszuweichen. Wird der Überkatheter zu stark unter Druck gesetzt, so reißt er in Reckrichtung längs ein, wobei sich der Innendruck augenblicklich reduziert, da Wasser nicht komprimierbar ist. Die Gefäßwand kann also durch das Platzen des Katheters nicht verletzt werden.

² Wir verdanken Prof. Dr. E. Zeitler die Einführung in die Dotter-Technik.

³ Der Katheter wird für uns von W. Schlumpf, Zürich, hergestellt.

⁴ Abbildungen 1 und 2 siehe Tafel Seite 2511

Nach erfolgter Dilatation wird der Überkatheter entleert und etwas Unterdruck erzeugt, wodurch das dehnbare Segment sich wieder eng um den Grundkatheter legt. Nun kann an anderer Stelle der Vorgang wiederholt oder der Katheter zurückgezogen werden. Für die Kontrolle des Befundes oder eine abschließende Angiographie wird jeweils der Tip-Occluder zurückgezogen.

Ergebnisse

Bisher konnten 15 Patienten⁴ behandelt werden (Tabelle 1). Für die *Oberschenkelarterien* verwendeten wir Katheter mit einem dehnbaren Segment in Längen von 2–10 cm und einem Außendurchmesser von 4–6 mm. Die Ergebnisse sind in der Tabelle 1 zusammengefaßt. Alle Patienten litten an Claudicatio intermittens und hatten zusätzlich Stenosen oder Verschlüsse in den Unterschenkelstammarterien. Die systolische Druckdifferenz zwischen Arm- und Knöchelarterien reduzierte sich auf 32% des Ausgangswertes. Die Patienten wurden beschwerdefrei. Die Ergebnisse der bisherigen Kontrollen nach 3 Monaten (Tabelle 1, Abbildung 1) sind günstig. Komplikationen traten nicht auf.

⁴ Inzwischen hat sich die Zahl der behandelten Patienten auf 25 erhöht. Die günstigen ersten Erfahrungen haben sich bestätigt.

Bei den kurzen *Iliaca-Stenosen* verwendeten wir dehnbare Segmente von 2–4 cm Länge und 7–10 mm Außendurchmesser. Bei fünf der sechs Patienten lag zusätzlich ein ausgeprägter arteriosklerotischer Befall anderer Gefäßareale vor. Die bisherigen Erfahrungen und Frühergebnisse sind günstig (Tabelle 1, Abbildung 2). Einmal trat nach der Behandlung eine Nachblutung auf, die eine Übernähung des Punktionslochs am Leistenband nötig machte⁵. Bei dieser Patientin (Fall 10) mit einer subtotalen Stenose der A. iliaca externa und einem gut kollateralisierten totalen Verschuß der A. femoralis superficialis wurde damals zur Dilatation der Iliaca-Stenose noch ein größerer Grundkatheter verwendet, so daß der Gesamtkatheter ebenfalls Charrière 12 erreichte, was die Nachblutung erklärte. In der Folgezeit konnte die Größe des Grundkatheters jedoch auf die oben beschriebenen Maße reduziert werden.

Diskussion

Die perkutane Rekanalisation chronischer arterieller Verschlüsse und Stenosen der Femoralarterie mit Hilfe des Dotter-Prinzips kann weder die Ursache noch die

⁵ Operateur: Prof. Dr. A. Senning, Chirurgische Klinik A der Universität Zürich

Tab. 1. Ergebnisse der systolischen Druckmessung mit Doppler-Ultraschall an den Knöchelarterien vor, am 3. Tag nach der Rekanalisation und nach 3 Monaten

Fall	Initialen, Geschlecht	Alter (Jahre)	Knöcheldrücke (mmHg)						Diagnose	
			vor		3. Tag nach		3 Monate			
			abs. P_{syst}^*	$P_{syst}^* -$ Diff. ^{**}	abs. P_{syst}	$P_{syst} -$ Diff.	abs. P_{syst}	$P_{syst} -$ Diff.		
Oberschenkelarterien (Verschlüsse oder Stenosen)										
1	H. G. ♀	73	72	118	108	65	106	39	Femoralis-Verschuß + periphere Stenosen	
2	O. F. ♂	67	170	20	189	6	190	10	Femoralis-Stenosen + periphere Stenosen	
3	Z. O. ♀	76	58	107	136	24	126	39	Femoralis-Verschuß + periphere Stenosen	
4	F. E. ♂	50	92	48	130	15	118	12	Femoralis-Stenosen + periphere Stenosen	
5	D. R. ♂	69	138	52	136	19	145	5	Femoralis-Stenosen + periphere Stenosen	
6	B. L. ♀	64	78	87	136	4	126	24	Femoralis-Verschuß + periphere Stenosen	
7	H. E. ♀	60	112	18	130	3	154	-14	Femoralis-Stenosen + periphere Stenosen	
8	A. C. ♀	74	115	15	126	9	144	- 4	Femoralis-Stenosen + periphere Stenosen	
9	W. F. ♂	50	57	73	112	28	150	0	Femoralis-Verschuß + periphere Stenosen	
	Gesamt	65±10	99±38	60±39	134±23	19±19	140±25	12±18		
Beckenarterien – Stenosen										
10	B. J. ♀	76	45	95	86	42	92	48	Iliaca-externa-Stenose + Femoralis-Verschuß	
11	H. H. ♂	73	162	43	163	- 8	170	0	Iliaca-communis-Stenose, 2 Herzinfarkte, Adipositas	
12	O. A. ♀	59	104	39	110	5	140	- 5	Iliaca-communis-Stenose	
13	N. H. ♂	47	150	-20	170	-37	165	-37	Iliaca-externa-Stenose, 2 Herzinfarkte	
14	C. H. ♂	54	80	50	88	27	108	22	Iliaca-externa- und -communis-Stenose + Femoralis-Verschuß	
15	V. R. ♂	52	160	30	124	26	135	25	Iliaca-communis-Stenose + Oberschenkelstenosen	
	Gesamt	62±12	117±48	40±36	124±36	9±29	135±31	9±29		

* abs. P_{syst} = absolute systolische Druckwerte

** $P_{syst} - \text{Diff.}$ = systolische Druckdifferenz Arm – Knöchel

Progredienz der arteriellen Verschlusskrankheit beeinflussen (13). Die zeitlich begrenzte Verbesserung der Hämodynamik stellt jedoch einen Erfolg dieser einfachen und unbelastenden Methode dar, die auch bei Patienten mit erhöhtem Operationsrisiko angewendet werden kann. Sie hat sich dadurch einen Platz in der Therapiewahl des angiologisch tätigen Internisten und Chirurgen sichern können (3, 5, 9, 13).

Mit der hier beschriebenen neuen Dilatationstechnik ist das Dotter-Verfahren modifiziert, nicht aber im Prinzip verändert worden. Das Verschlussmaterial wird ebenfalls in sich komprimiert und in die Wand gedrückt. Der Dilatationskatheter hat jedoch unseres Erachtens gegenüber den koaxial übereinander durch den Verschluss geschobenen Dotter-Katheter vier Vorteile:

1. Das Verschlussmaterial wird zusammengepreßt, ohne daß eine längsgerichtete Bewegung stattfindet.
2. Das gereckte Segment des Überkatheters kann den jeweiligen Dimensionen des befallenen Gefäßes (zum Beispiel Becken- oder Oberschenkelarterie) angepaßt werden.
3. Der Außendurchmesser, den der Katheter während des Dilatationsvorgangs erreichen soll, ist nicht auf 4 mm beschränkt.
4. Das Punktionsloch in der A. femoralis am Leistenband ist kleiner und entspricht jetzt den Dimensionen anderer Katheteruntersuchungen (zum Beispiel Linksherzkatheter).

Diese Vorteile sollten die Gefahr einer Embolie oder Nachblutung reduzieren können und die Anwendung im Bereich der Beckenarterien erleichtern. Die Technik ist einfach, und die Frühergebnisse sind gut. Eine Applikation des Verfahrens auf andere Gefäßareale ist denkbar. Wir möchten jedoch darauf hinweisen, daß es sich bei dem Dotter-Verfahren – auch in der beschriebenen modifizierten Technik – um einen Eingriff am arteriellen Gefäßsystem handelt, was wegen der Möglichkeit von Komplikationen eine haus eigene Gefäßchirurgie voraussetzt. Zudem sollte die Indikation zur Rekanalisation im Einzelfall gemeinsam von den Angiologen, Gefäßchirurgen und Röntgenologen besprochen und gestellt werden. Unter dieser Voraussetzung ist das Verfahren

unseres Erachtens eine wertvolle Ergänzung der bereits bewährten konservativen und operativen Behandlungsmethoden.

Dipl. chem. R. Bucher und Dipl.-Ing. W. Schmid, ETH Zürich, A. Asher, Zürich, E. Schaerer jun., Bandfabrik Niederlenz, und W. Schlumpf, Zürich, sind wir für ihre ständige Bereitschaft, uns bei technischen Problemen zu beraten und tatkräftig zu unterstützen, zu Dank verpflichtet.

Fräulein J. Mohacsi verdanken wir die Ausführung der Schreibebeit.

Literatur

- (1) Dotter, C. T., M. P. Judkins: Transluminal treatment of arteriosclerotic obstruction. Description of a new technique and a preliminary report of its application. *Circulation* 30 (1964), 634.
- (2) Dotter, C. T., M. P. Judkins, J. Roesch: Nonoperative treatment of arterial occlusive disease. A radiologically facilitated technique. *Radiol. Clin. N. Amer.* 5 (1967), 531.
- (3) Dotter, C. T., M. P. Judkins, J. Roesch: Nichtoperative, transluminale Behandlung der arteriosklerotischen Verschlussaffektionen. *Fortschr. Röntgenstr.* 109 (1968), 125.
- (4) Dow, J. D., C. Hardwick: Transluminal arterial recanalisation. *Lancet* 1966/I, 73.
- (5) Grüntzig, A., A. Bollinger, U. Brunner, M. Schlumpf, J. Wellauer: Perkutane Rekanalisation chronischer arterieller Verschlüsse nach Dotter – eine nicht-operative Kathetertechnik. *Schweiz. med. Wschr.* 103 (1973), 825.
- (6) Grüntzig, A., H. J. Leu, A. Asher: Mechanische Rekanalisation künstlicher Thromben der Arteria femoralis superficialis beim Hund. *Med. Welt (Stuttg.)*, eingereicht.
- (7) Hopff, H. S., A. Mueller, F. Wenger: Die Polyamide (Springer: Berlin-Göttingen-Heidelberg 1954).
- (8) Palayew, M. J., I. Sedlezky, H. H. Sigmann: Occlusive peripheral arteriosclerosis: treatment by percutaneous transluminal recanalization – »Dotter procedure.« *Canad. med. Ass. J.* 101 (1969), 66.
- (9) Porstmann, W., L. Wierny: Intravasale Rekanalisation inoperabler arterieller Obliterationen. *Zbl. Chir. (Suppl.)* 92 (1967), 1586.
- (10) Porstmann, W.: Ein neuer Korsett-Ballonkatheter zur transluminalen Rekanalisation nach Dotter unter besonderer Berücksichtigung von Obliterationen an den Beckenarterien. *Radiol. diagn. (Berl.)* 14 (1973), 239.
- (11) Zeitler, E., R. Mueller: Erste Ergebnisse mit der Katheter-Rekanalisation nach Dotter bei arterieller Verschlusskrankheit. *Fortschr. Röntgenstr.* 111 (1969), 345.
- (12) Zeitler, E., W. Schoop, W. Zahnnow: The treatment of occlusive arterial disease by transluminal catheter angioplasty. *Radiology* 99 (1971), 19.
- (13) Zeitler, E.: Die perkutane Rekanalisation arterieller Obliterationen mit Katheter nach Dotter (Dotter-Technik). *Dtsch. med. Wschr.* 97 (1972), 1392.
- (14) Zeitler, E., J. Reichold, W. Schoop, D. Loew: Einfluß von Acetylsalicylsäure auf das Frühergebnis nach perkutaner Rekanalisation nach Dotter. *Dtsch. med. Wschr.* 98 (1973), 1285.

Dr. A. Grüntzig
Departement für Innere Medizin
der Universität,
Medizinische Poliklinik
CH-8006 Zürich, Rämistr. 100

7.9 Transluminal dilatation of coronary-artery stenosis

Andreas R. Grüntzig (1939–1985)

Andreas Gruentzig was born in Dresden, Germany in 1939. He completed his formal education in Heidelberg. He graduated in medicine in 1964 from Heidelberg and completed the rotating internship by research in epidemiology. It was at that time that he developed his interest in coronary artery disease. He trained in the Ratchow clinic in Darmstadt, Germany. He moved to Zurich as a fellow of Dr Bolanger and in the angiology department he demonstrated his inventive techniques by developing a method to measure the one-half relaxation time of the Achilles' tendon reflex produced by electrical stimulation to evaluate ischemic limbs. He then moved to the department of radiology and visited Dr Zeitler in Frankfurt to observe the Dotter method. He introduced this method at the University of Zurich. An early demonstration of the technique of angioplasty resulted in the entire plaque embolizing into the popliteal artery. This resulted in radiologists becoming very sceptical of this new technique. He nevertheless persisted, like all great pioneers, and with the help of Dr Ake Senning, chief of cardiovascular surgery and Dr Walter Siegenthaler, chief of medicine he eventually managed to collect a small series of Dotter cases, working mostly during the lunch break while he was a full-time fellow in internal medicine. Gruentzig had heard of the ideas of Porstmann, who had placed a latex balloon in the slotted angiographic catheter. He worked evenings in his kitchen with his wife, Michaela, his assistant, Maria Schlumpf and her husband Walter. They designed many versions of the balloon catheter, which they built with bits of rubber thread in epoxy glue. A double-lumen catheter was first used in the iliac artery on 23 January 1975. The success of this method resulted in him wondering whether this technique could be used in the coronary arteries. His first attempts to dilate the coronary arteries were first performed in dogs on 24 September 1975. In 1976 Andreas Gruentzig visited the United States for the first time to present his experiments in the poster session of the 49th scientific session of the American Heart Association in Miami Beach. This exhibit was greeted with great interest. On 16 September the first procedure of coronary angioplasty was performed. The vessel remained patent without re-stenosis. Soon afterwards Dr Gruentzig had collected enough data to publish an important paper in the *New England Journal of Medicine* on this technique. Today the technique has become routine. Unfortunately Dr Gruentzig died in an air crash in 1985.



THE LANCET, FEBRUARY 4, 1978

263

Letters to the Editor

TRANSLUMINAL DILATATION OF CORONARY-ARTERY STENOSIS

SIR,—In September, 1977, we introduced a technique for percutaneous transluminal coronary angioplasty (P.T.A.). This technique consists of a catheter system introduced via the femoral artery under local anaesthesia. A preshaped guiding catheter is positioned into the orifice of the coronary artery and through this catheter a dilatation catheter is advanced into the branches of the artery. This dilatation catheter (outer diameter 0.5–1.25 mm) has a sausage-shaped distensible segment (balloon) at the tip.

After traversing the stenotic lesion the distensible segment is inflated with fluid (50% contrast material, 50% saline) to a maximum outer diameter of 3.0–3.8 mm by a pump-controlled pressure of 5 atmospheres (about 500 kPa). This pressure compresses the atherosclerotic material in a direction perpendicular to the wall of the vessel thereby dilating the lumen.

DETAILS OF FIVE CASES TREATED BY P.T.A.

Patient	Age	Sex	Date of dilatation	Stenosis	Primary success
1	38	M	Sept. 16, 1977	L.A.D. 85%	+
2*	44	M	Oct. 18, 1977	L.C.A. 70% (calcified)	—
			Jan. 10, 1978	R.C.A. 80%	+
3	43	M	Nov. 21, 1977	L.A.D. 75%	+
			Nov. 21, 1977	R.C.A. 95%	+
4*	43	M	Nov. 24, 1977	L.C.A. 80%	+
5	61	M	Dec. 20, 1977	L.A.D. 95%	+

L.C.A.=main left coronary artery; L.A.D.=left anterior descending; R.C.A.=right coronary artery.

*Dilatation done at University Hospital, Frankfurt.

Experience with over 250 peripheral-artery lesions treated by this technique has demonstrated, via morphological studies, that the atheroma can be compressed leaving a smooth luminal surface. The patency-rate, two years after dilatation of iliac and femoropopliteal atherosclerotic lesions, was greater than 70%.¹

After experimental² and intraoperative³ studies the first percutaneous coronary dilatation was done on Sept. 16, 1977. Five patients with severe stenotic lesions of the coronary arteries associated with refractory angina have so far been treated by coronary P.T.A. (table). Angiograms for one of these patients are shown in the figure. No complications were noted. Follow-up studies by serial stress-testing with myocardial imaging (thallium-201) and angiography suggest that P.T.A. may be an effective treatment in certain patients with severe discrete non-calcified lesions of the coronary arteries.

This technique, if it proves successful in long-term follow-up studies, may widen the indications for coronary angiography and provide another treatment for patients with angina pectoris.

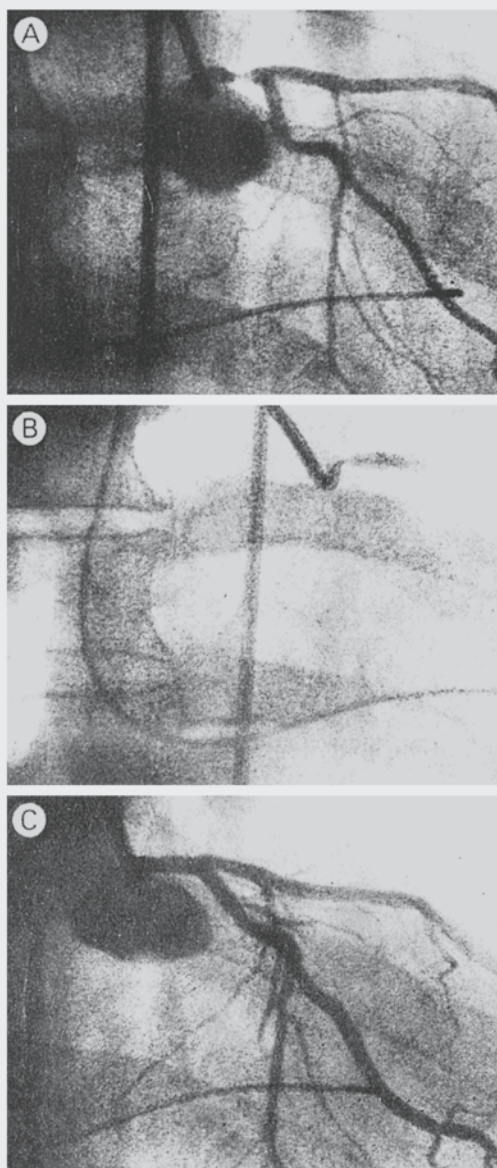
Department of Internal Medicine,
Medical Polyclinic,
University Hospital,
8091 Zürich, Switzerland

ANDREAS GRÜNTZIG

1. Grüntzig, A. Die perkutane transluminale Rekanalisation chronischer Arterienverschlüsse mit einer neuen Dilatationstechnik; p. 50. Baden-Baden, 1977.

2. Grüntzig, A., Riedhammer, H. H., Turina, M., Rutishauser, W. *Verh. Dt. ges. Kreislaufforsch.* 1976, **42**, 282.

3. Grüntzig, A., Myler, R., Hanna, E., Turina, M. *Circulation*, 1977, **56**, 84 (abstr.).



Details of patient 3.

43-year-old man with severe angina pectoris since September, 1977. First angiogram (Nov. 11) revealed severe stenosis of the main L.C.A. and only slight wall abnormalities in some of the branches of L.C.A. After informed consent P.T.A. was done on Nov. 21.

(A) The angiogram before P.T.A. (done under nitroglycerine cover), with the guiding catheter in the orifice showed 80% proximal stenosis of the L.C.A.

(B) After passage of the dilatation catheter the distensible balloon segment was inflated twice to a maximum outer diameter of 3.7 mm. During the dilatation the patient experienced a short period of angina pectoris which quickly disappeared after deflation of the balloon.

(C) The angiogram after the procedure showed a good result without complications. There was no enzyme rise or E.C.G. change after the treatment. A good clinical result has persisted in the following weeks, confirmed by stress tests.

7.10 Percutaneous biliary drainage, technical and catheter related problems in 200 procedures

Peter R. Mueller (born 1947)

Peter Mueller was born in Boston, Massachusetts on 20 June 1947. He received his BA from Harvard University, Cambridge, MA in 1969 and his MD, University of Cincinnati Medical School, Cincinnati, Ohio in 1973.

He started his Medical Internship in 1973 at Cincinnati General Hospital, Cincinnati and became Radiology Resident, Massachusetts General Hospital, Boston between 1974–1977. He became Instructor in Radiology (1977–1981), Assistant Professor of Radiology (1981–1984), Associate Professor of Radiology (1984–1999) and in 1999 he was appointed Professor of Radiology at Harvard Medical School, Boston and subsequently Division Head, Abdominal Imaging and Interventional Radiology, Massachusetts General Hospital, Boston.

Mueller is Fellow, American College of Radiology (1991), Honorary Fellow, The Royal College of Radiologists, London, England (1995), Honorary Fellow, Royal College of Surgeons in Ireland, Dublin, Ireland (1998). In 1993 he was appointed President of the Society for Minimally Invasive Therapy (SMIT). In 1994 he became Secretary of the Society of Hepato-biliary Radiology. In 1998–1999 he was President of the New England Roentgen Ray Society. He has published more than 300 scientific papers, 288 abstract presentations, 54 book chapters, and three textbooks.

Peter Mueller's early and main area of research was in the evaluation and development of non-vascular interventional techniques. Over the past 20 years his division has introduced or refined a number of interventional procedures. Early in his career most of the papers were analyses of interventional procedures in the biliary tree. These included a number of papers which described techniques for percutaneous treatment of benign and malignant biliary obstruction.

In addition, he and his colleagues, including Eric van Sonnenberg, introduced percutaneous drainage procedures of fluid collections and abscesses to the Massachusetts General Hospital. Techniques and procedures first developed at the MGH have been taught nationally and world wide through papers and lectures and are now standards of care. Although his first area of interest is abdominal radiology, he has introduced interventional techniques to other anatomic areas such as the pleural space. Drainage procedures of the pleural space are now used worldwide.

Throughout his career he has always tried to find innovative methods for dealing with interventional problems. Mueller helped develop a patented method for performing percutaneous gastrostomy as an alternative to either surgical or endoscopic placement of gastrostomy tubes. This method is essentially a percutaneous method for placing a tube that is analogous to that used by surgeons. He also was involved in the development of a metallic needle which can be used in magnetic resonance imaging.

More recently Mueller has been the point person for the use of alcohol and radiofrequency ablation of liver tumors and treatment of benign prostatic hypertrophy. Recent articles in his CV reflect both his laboratory work and clinical application of these methods. Both programs represent successful clinical methods of treatment of malignant tumors of the liver.

Picture courtesy Peter Mueller, MD, 2004.



Eric van Sonnenberg

Eric vanSonnenberg got his Bachelor of Science in Zoology in 1968 from George Washington University, Washington, D.C. and his medical degree from University of Cincinnati, School of Medicine, Cincinnati, Ohio in 1973. At the New York Medical College, Metropolitan Hospital he started his internship in surgery (rotating) in 1973 and became resident (1974) and chief resident (1976) in internal medicine. In 1976 van Sonnenberg started his residency in diagnostic radiology at Massachusetts General Hospital, Harvard Medical School, Boston, Massachusetts. Here he became fellow (1976–1979) in CT, Ultrasound, GI, and Interventional Radiology, Clinical Fellow (1979–1980) and Instructor in Radiology (1980–1981). He went to the University of California, San Diego and became Assistant Professor of Radiology (1981–1984), Associate Professor in Residence in Radiology and Medicine (1984–1989) and Professor in Residence, Radiology and Medicine (1989–1993). In 1993 van Sonnenberg was appointed Chairman and Professor of Radiology and Professor of Internal Medicine and Surgery at the University of Texas Medical Branch, Galveston, Texas. He was appointed Chief of Radiology at the Dana Farber Cancer Institute (2000) and Consultant Interventional Radiologist at the Children's Hospital of Boston (2002) at Harvard Medical School, Boston, Massachusetts. Since 1999 he has been Visiting Professor of Radiology at the Brigham and Women's Hospital, Harvard Medical School, Boston, Massachusetts.

Eric van Sonnenberg is a member of several national and international scientific societies. Among them the Radiological Society of North America (RSNA), American Roentgen Ray Society (ARR), Society of Gastrointestinal Radiology (SGR), American Institute of Ultrasound in Medicine (AUM), International Society of Hepato-Biliary Pancreatic Radiology (ISHBPR), American College of Radiology (ACR), International College of Surgeons, European Society of Interventional Radiology (2003). He is a reviewer and editor of several scientific journals. He has published 257 original papers, 96 books and chapters, 344 scientific abstracts, and presented 1194 lectures.

J.T. Ferrucci

Percutaneous Biliary Drainage: Technical and Catheter-Related Problems in 200 Procedures

Peter R. Mueller¹
Eric vanSonnenberg
Joseph T. Ferrucci, Jr.

Analysis of 200 consecutive percutaneous biliary drainages revealed critical technical and clinical components not previously emphasized. In this series, successful drainage was achieved in 188 (94%) of 200 instances, and 67 (36%) of the 188 patients were discharged from the hospital without formal surgical exploration. Severe acute periprocedural complications occurred in 16 (8%) of the 200 procedures (death, three cases; septicemia, seven; and bleeding, six). Minor periprocedural complications occurred in 39 (20%) of the 200 instances (postprocedural fever, 21; hemobilia, 18). Significant delayed in-hospital complications with catheter function occurred in 22% of procedures (postclamping cholangitis, 36; catheter leaking eight). In outpatients under chronic catheter care, complications including inadvertent catheter dislodgment, tube obstruction, and cholangitis occurred at least once in most patients. Details of the etiology, prevention, and management of these major and minor complications are outlined.

Previous reports from this and other institutions have documented the effectiveness of percutaneous biliary drainage for relief of biliary obstruction [1–5]. Until recently, however, limited case experience has not permitted critical analysis of the various technical and clinical problems that may occur during the procedure or during aftercare of the drainage catheter system as percutaneous biliary drainage becomes more widely applied and more difficult cases are attempted, the technical complexities encountered consistently exceed available descriptions in the literature. In an attempt to bridge this gap, we are supplementing our initial report of the first 62 cases undergoing percutaneous biliary drainage in this hospital [1] by reviewing procedural details and complications in our present total experience of 200 procedures through June 1981.

Materials and Methods

Percutaneous biliary drainage was performed on 200 occasions in 188 patients. Final diagnoses were: pancreatic cancer, 108 (54%) of 200 procedures; periportal metastasis (colon, breast, lung), 36 (18%); carcinoma of bile duct or gallbladder, (13%); failed biliary enteric bypass, 13 (7%); benign stricture, eight (4%); and common duct stone nine (4%).

The indications for biliary drainage were primary palliative drainage, 108; preoperative decompression (benign and or malignant), 68; sepsis, 25; failed biliary enteric bypass, 15; and stricture dilatation five. Some patients were drained for more than one indication (e.g., jaundice and sepsis).

Successful insertion of either an external or internally draining catheter was carried out in 108 (94%) of the 200 procedures. Internal drainage was achieved in 144 (72%) of 200 and external catheter drainage in 44 (22%).

Pancreatic cancer was the most common diagnosis (108 [54%] of 200). In 51 (50%) of the 108, biliary drainage was the primary palliative therapy; 42 of the 108 were drained preoperatively for 3–7 days. All patients undergoing preoperative decompression were allowed to drain externally even if the catheter had been negotiated through the obstructing lesion.

Received July 6, 1981; accepted after revision September 21, 1981.

¹All authors: Department of Radiology, Massachusetts General Hospital, Harvard Medical School, Boston, MA 02114. Address reprint requests to P. R. Mueller.

AJR 138:17–23, January 1982
0361–803X/82/1381–0017 \$00.00
© American Roentgen Ray Society

TABLE 1: Complications of Percutaneous Biliary Drainage

	No. Patients (n = 188)
Acute:	
Death	3
Bleeding	6
Sepsis	7
Fever	21
Hemobilia	18
Delayed (in-hospital):	
Postclamping cholangitis	21*
Cholangitis with multiple segmental obstructions	15
Leaking around catheter	8
	No. Patients/No. Episodes
Delayed (outside hospital):†	
Dislodgment	11/28
Cholangitis	13/20
Tube obstruction	7/14

* This is of the last 33 patients who underwent clamping.

† Follow-up data available on 40 of 67 patients discharged.

Of 108 patients who had an external or internal drainage procedure, 67 were discharged from the hospital. Accurate follow-up was obtained in 40 patients. Of the rest 66 were drained for preoperative decompression (malignant or benign disease), 37 died in the hospital for reasons not directly related to their drainage, three died as a result of the drainage, and 15 patients underwent insertion of a permanent biliary endoprosthesis. Of the 67 patients discharged, 51 had malignant disease; the average survival in this group was less than 7 months. Sixteen of the 51 patients survived 7 months or longer. Of these, two had a diagnosis of adenocarcinoma, presumably in the pancreas, and were alive and well 7 months after drainage. The rest had metastases to periportal nodes from a variety of sites, including lung (three), breast (two), colon (one), renal cell carcinoma (one), lymphoma (one), hepatoma (one), metastatic adenocarcinoma (two), and carcinoma unknown primary (three). All patients with periportal metastases were treated with a combination of chemotherapy and/or irradiation.

Results

Complications are listed in table 1 as either acute or delayed. Delayed complications are subdivided into in-hospital and postdischarge complications.

Acute Complications

Death. Three patients died from complications directly related to percutaneous biliary drainage. Of these, two died from bleeding believed to result from 10 or more punctures of the liver with an 18 gauge sheath needle. One patient with severe emphysema sustained a pneumothorax and bilious pleural effusion that led to his death.

Sepsis and fever. Seven patients had frank septic episodes (severe hypotension and positive blood cultures). All of these had infected bile or were febrile prior to the drainage. There was transient fever in 21 patients after catheter insertion, but it required no specific additional therapy.

Bleeding and hemobilia. There was clinically apparent internal bleeding (greater than 500 ml) in six patients, two of whom died. Only one of the other four required emergency surgery; the rest were treated with fluids and blood products. All were technically difficult procedures, requiring

10 or more punctures of the liver with an 18 gauge needle. One patient suddenly bled about 500 ml via the drainage catheter on the 3 days after the procedure [1]. This was caused by a side-hole positioned outside the bile duct lumen in the hepatic parenchyma, allowing communication with a major vascular channel. After repositioning, the catheter bleeding ceased.

Varying amounts of hemobilia were also demonstrated by injection of the biliary catheter in 18 other patients (fig. 1). In these cases, blood casts were often visible in the bile duct but no direct biliovenous communications were shown. Since blood casts may obstruct the bile ducts and/or the drainage catheter, one or two irrigations with 10 ml of normal saline are performed each hour in these patients for a 12–24 hr period. Within this interval, the clots are lysed and drainage of bile ensues.

Delayed Complications

In-hospital. An unsuccessful attempt at conversion to internal drainage by clamping a properly positioned catheter was the most common delayed in-hospital complication. This was manifested by cholangitis (fever, chills) and occurred in 21 (63%) of the last 33 patients who underwent clamping of a properly positioned internal drainage tube. The cholangitis was treated by unclamping the tube and again placing the catheter to external drainage. After the patient's condition stabilized, the original catheter was replaced with a larger (10–12 French) polyvinyl argyl tube (Brunswick Co., St. Louis, Mo.) with multiple side-holes and then reclamped. The incidence of cholangitis upon re-clamping after exchange for the larger catheter decreased to 11%.

In 15 patients who had undergone adequate right-sided drainage, cholangitis developed unrelated to tube clamping or tube manipulation. All of these patients had tumors involving the common hepatic duct as well as segmental obstruction of the left and right systems. Ten of these patients had a left-sided percutaneous biliary drainage to decompress a presumed infected system. Response to bilateral drainage is difficult to define. None of this group of 15 patients survived more than 12 weeks. Five of 10 with bilateral catheters became afebrile. The rest had periodic episodes of cholangitis. Two of the other five had only a single episode of cholangitis and responded to antibiotic treatment. The other three had recurrent episodes of cholangitis.

A less common complication, leakage of bile around the catheter insertion site, occurred in eight procedures (3%). In three cases, the cause was a malpositioned catheter (side-holes below the area of obstruction); three patients had ascites; in two, there was no discernible cause.

Outside hospital. Various degrees of catheter dysfunction will occur in any patient who maintains a drainage catheter for an extended period of time (over 2–3 months).

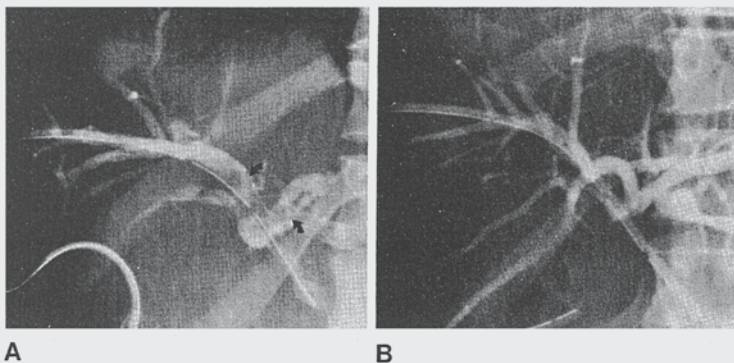
Of the 67 patients discharged from the hospital, follow-up data were difficult to obtain in 20 because they were discharged to other states or chronic care facilities. Complications in the other 40 are divided into the number of

AJR:138, January 1982

PERCUTANEOUS BILIARY DRAINAGE

19

Fig. 1.—Hemobilia complicating catheter insertion. **A**, Cholangiogram immediately after insertion of percutaneous drainage catheter. Elongated intraductal filling defects represent clotted blood (arrows). No direct venous communication evident. **B**, 48 hr later. Clear ducts indicate complete lysis of clot. Appearance of drainage changed from bloody to clear during interval.



patients and number of episodes because many patients were seen more than once for the same complication (table 1). Types of complications included catheter occlusion by bile encrustations, debris, or tumor (seven of 40), catheter dislodgment (11), and cholangitis (13). Perhaps more interesting is the fact that the actual number of significant complications was large if individual episodes are considered. A total of 62 complications was treated in the 40 individuals followed closely. However, the frequency of complications appeared to correlate with the degree of family and home nursing care received by individual patients.

In most cases, tube manipulations were performed on an outpatient basis in less than 1 hr and were followed by a 3 day course of broad-spectrum antibiotics. However, seven patients were readmitted for tube manipulations because of active cholangitis. In two cases, *de novo* catheter insertion was required when attempts to replace a dislodged tube were unsuccessful. One patient with an external drainage catheter who lived 7 months was seen on a biweekly basis for tube check and/or repositioning. Another external drainage patient eventually formed a well epithelialized biliary cutaneous fistula and the tube was removed completely to allow bile to drain directly into a colostomy-type bag.

Discussion

While many articles in the literature have commented on both the technique and complications of percutaneous biliary drainages, little has been written in the prevention and management of these problems [6–9].

Death and Bleeding

Death (three instances) or significant bleeding (six) occurred in nine (4.5%) of our 200 procedures. All were technically difficult procedures with six of nine requiring 10 or more punctures of the liver with an 18 gauge needle. This correlates with the known severe complication rate of about 3% that we reported earlier in a compilation of reports of complications from large needle punctures [10].

There are several methods that can be used to reduce the number of punctures performed. The most fruitful tech-

nique is to localize the anteroposterior orientation of the bile ducts by turning the patient into a lateral position. If the patient is thin and cooperative a straight lateral approach can be made. Hawkins [11] designed a long 22 gauge needle over which a 4 French sheath is placed for a single puncture method of percutaneous drainage. If an appropriate duct is entered during the fine needle cholangiogram, the needle acts as a guide wire and the sheath is advanced over the needle into the duct. We have used this method on occasion, but find the excessive length and flexibility of the 22 gauge needle to be cumbersome. Another method to reduce sheath needle punctures is to repeat the puncture of the opacified ducts with a 22 gauge needle directed at an appropriate duct for drainage. If the correct duct for drainage is then entered, the larger sheathed needle can be inserted adjacent to the 22 gauge needle.

In general, while there are several useful methods to minimize the number of sheathed needle punctures performed, most cases require no more than two or three. If the appropriate duct is not entered, reevaluation of the approach should be made and the methods described above should be applied. One must be aware, however, that some patients will require five to 10 punctures and the benefit of continuing the procedure in such cases should be weighed carefully against the increased risk of complications.

Acute Periprocedural Sepsis

Severe septicemia (positive blood cultures with hypertension) was relatively uncommon in our series (seven [3.5%] of 200). Most of these patients and those who had only a transient postprocedure fever (21 [10.5%]) were found to have infected bile.

While the latter was usually self-limited, severe septicemia can be life-threatening and prevention is important. We have found that two-stage delayed internal drainage not only prevents severe septicemia but also increases the chances of completing an internal drainage on patients who have a technically difficult obstruction.

The usual indications for a two-stage delayed approach included: (1) acute suppurative cholangitis, (2) marked duct dilatation with uncertain location of the exact position of the

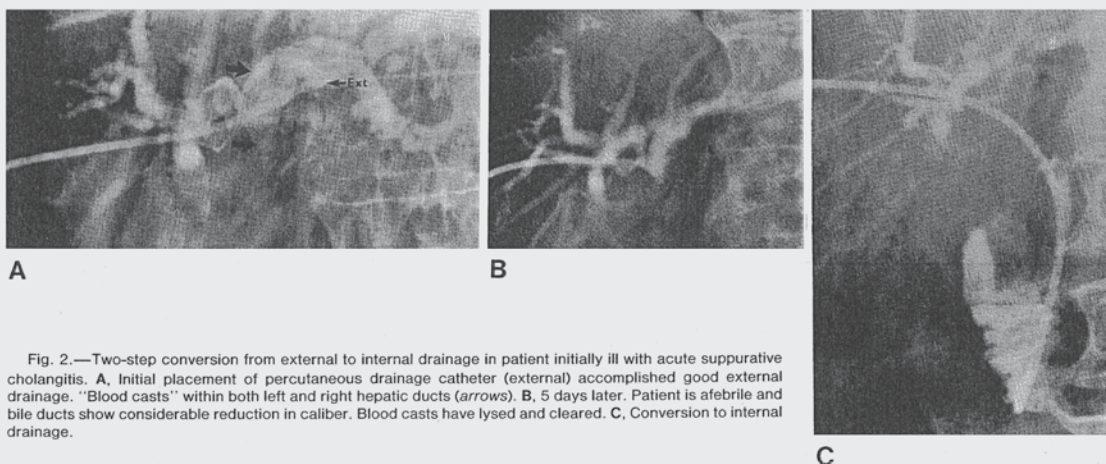


Fig. 2.—Two-step conversion from external to internal drainage in patient initially ill with acute suppurative cholangitis. A, Initial placement of percutaneous drainage catheter (external) accomplished good external drainage. "Blood casts" within both left and right hepatic ducts (arrows). B, 5 days later. Patient is afebrile and bile ducts show considerable reduction in caliber. Blood casts have lysed and cleared. C, Conversion to internal drainage.

residual lumen, and (3) exceptionally fragile or medically unstable patients (fig. 2). By limiting manipulations in gravely ill patients to those required to gain catheter access to the bile ducts and establish external decompression only, acute morbidity may be reduced without sacrificing subsequent options. About one-third of our recent cases initially drained externally were then successfully advanced to internal drainage at 3–5 days. However, the likelihood that successful catheterization of the stricture would be accomplished eventually could not be predicted on the basis of the initial cholangiographic appearance.

Several factors may account for easier catheterization of the stricture at a delayed second sitting: (1) decreased duct caliber above the obstruction straightens the course of the guide wire directing it into the strictured lumen; (2) reactive edema at the site of obstruction may resolve; and (3) development of a transparenchymal tract around the catheter may facilitate use of a larger caliber and a more varied assortment of catheter types. In difficult cases, a combination of a curved tip (Cobra visceral, C1, C2, C3, Cook, Bloomington, Ind.) catheter together with a memory torque guide wire (Ring, 0.089 or 0.097 cm, Cook) may allow circumferential searching by torque action until the guide wire finds the residual lumen. The guide wire is never forced through the obstruction but is allowed to fall along the path of least resistance.

Delayed In-Hospital Complications

Delayed in-hospital cholangitis occurred in 36 patients either after clamping a "well positioned" internal catheter (21 patients) in an attempt to convert a patient to antegrade flow or in patients who had a segmental obstruction of the left hepatic duct, which was undrained (15 patients) (table 1). Of the last 70 patients undergoing percutaneous biliary drainage, conversion from external to internal drainage by tube clamping was attempted in 33 and failed in 21 (63%) of cases as a result of cholangitis. Prompt unclamping

effectively corrected the sepsis initially in all cases but one.

However, the management of acute cholangitis following tube clamping has been a difficult problem. Contrast injection after unclamping does not usually reveal the cause. Initial low-pressure injection of the catheter may show "side-hole runoff" with contrast material visualized only above the strictured area (fig. 3). Injection with greater pressure (although more dangerous for sepsis) may be required to demonstrate contrast material within the duodenum. On the other hand, removal of the catheter will not necessarily reveal an obstructing sediment, plug, or debris.

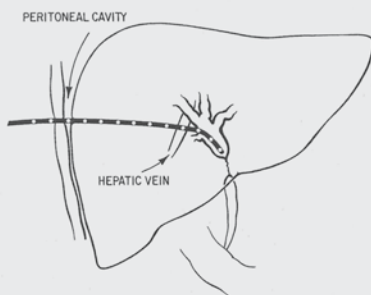
We believe the occurrence of cholangitis is actually related to several contributing factors: (1) Placement of a catheter with a protruding external segment will lead to colonization of the biliary tree with bacteria. Twenty-four hours after the initial drainage, all bile cultures will show growth of a combination of organisms. Nevertheless, this in itself is not necessarily the cause of cholangitis. (2) There is considerable epithelial damage to the biliary tree created by insertion of a catheter. A denuded epithelium contaminated by bacteria is susceptible to cholangitis [12–15]. (3) Most important is partial obstruction of the biliary duct, which may be due to one or more of the following causes: (a) the relatively small internal diameter of the commonly used 8.3 French Ring pigtail biliary catheter (Cook); (b) the inability of bile to gain entrance into the small side-holes of the 8.3 French Ring pigtail biliary catheter; or (c) an actual mechanical obstruction created by the tube itself.

The end result is partial obstruction superimposed on a damaged and contaminated biliary duct system. The potential of this combination has been clearly shown in animal studies in which bacteria placed in unobstructed biliary systems of dogs have no ill effects. However, when even partial obstruction is superimposed, cholangitis and death ensue [12–15].

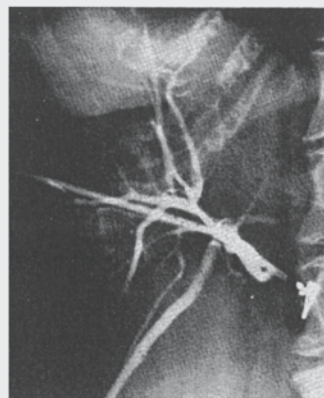
It is also apparent that patients who drain a large quantity of "duodenal contents" in the first few days may be more susceptible to postclamping cholangitis. Perhaps, retro-



Fig. 3.—Real or pseudoobstruction? Cholangiogram taken when acute cholangitis occurred after clamping appropriately positioned internal drainage catheter. Contrast visualized only above structure may be due to "side-hole runoff" rather than true catheter occlusion. Exchange of catheter for larger caliber is required to correct relative obstruction to bile egress.



A



B

Fig. 4.—External drainage due to complete periportal obstruction produces unstable or insecure catheter position due to "short purchase"; dislodgment is common. **A**, External drainage catheter with short purchase. Normal liver excursion during respiration may inadvertently retract catheter from intraductal position. **B**, Metastatic carcinoma to portahepatis with complete duct obstruction. Short purchase.

grade duodenal reflux is an indication of duodenal spasm and relative increase in intraluminal duodenal pressure and hence further obstructs the egress of bile.

The most effective solution to the postclamping cholangitis problem is to perform an exchange of catheters by inserting a 10 or 12 French polyvinyl (argyl catheter). These catheters have relatively thin walls and the internal diameter of the 10 French caliber is 1.6 times as large as the 8.3 French Ring pigtail catheter. Large side-holes may also be cut manually and positioned under fluoroscopy to contribute to better drainage. Placement of a polyvinyl argyl catheter is unfortunately not possible at the time of the initial drainage because the tube is too soft and flexible. However, after the initial drainage catheter has been in place for 5–7 days, a sufficient transparenchymal tract is formed to allow ready insertion. Introduction of the argyl system is also facilitated by use of a coaxial catheter technique (placement of the 10 or 12 French argyl catheter over a 6 or 7 French polyethylene catheter). The stiffening effect of the coaxial system aids placement of the soft argyl catheter.

Further benefits derive from catheter exchange to the argyl polyvinyl system. Patients find the softer tube more comfortable at the abdominal wall cutaneous opening. Because the argyl catheter is straight, it may be left in the distal common bile duct allowing the patient's physiologic sphincter at the choledochoduodenal junction to control egress of bile and obviate the potential problem of duodenal reflux. Also, catheters left in the distal common duct are less likely to cause duodenal irritations and are protected from the degradation of catheter wall material that results from chronic exposure to stomach and duodenal secretions.

Of the 21 patients who failed initial tube clamping, 19 were successfully treated by replacement with a 10–12

French argyl catheter and were discharged with successful internal drainage. Two patients who had repeated episodes of cholangitis were found to have diffuse tumor involvement of the liver and may also have had selective ductal obstruction that contributed to the cholangitis.

Delayed Posthospital Discharge Complications

The most common chronic complication seen in the 40 patients who were closely followed after hospital discharge was dislodgment of the biliary drainage tube (table 1). This is also one of the major reasons for cholangitis in this group of patients. It is interesting that this occurred in both patients with "internal" drainage catheters and "external." There appeared to be a correlation between the patients understanding the function of the catheter and need for proper catheter care and a lower incidence of dislodgment.

Recognition of the limitations of an external drainage catheter and the technical considerations in replacing a dislodged catheter are essential to preventing and managing these two complications.

When only external catheter drainage can be achieved because of complete obstruction in the mid-common duct or periportal region, catheter position is rarely secure and inadvertent dislodgment is not uncommon. In such cases, length of catheter "purchase" within the biliary ducts may be minimal (e.g., 2–3 cm) and predispose to dislodgment by simple body movements and respiratory excursions (fig. 4). One of our patients with an external drainage catheter and an extremely short purchase experienced spontaneous dislodgment on six different occasions. Often the small caliber of the intrahepatic duct radicle in which the catheter is situated in such cases requires a straight catheter (vs.

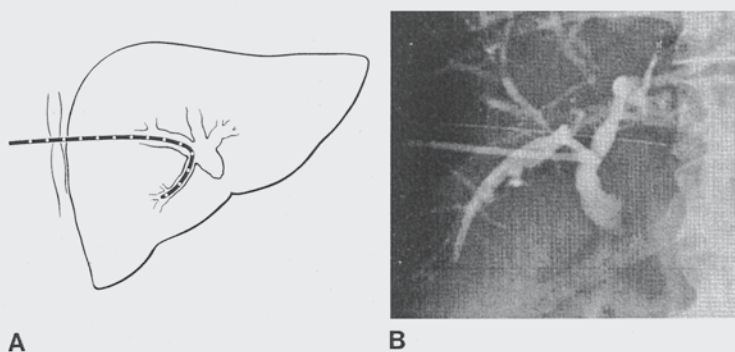


Fig. 5.—External drainage of obese patient with high common duct obstruction from pancreatic cancer. **A**, Potential position of external catheter may prevent easy withdrawal of catheter. **B**, 8.3 French catheter in posterior branch of right hepatic duct insures "longer" purchase.

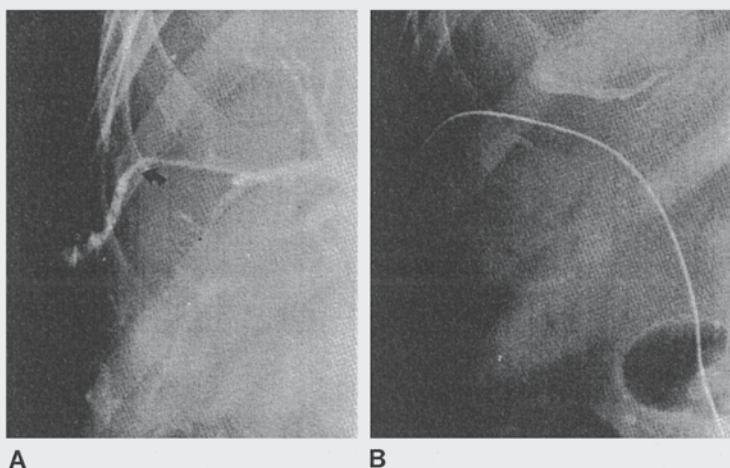


Fig. 6.—Direct replacement inadvertently dislodged catheter. **A**, Curved tip catheter in skin opening and torqued in cephalad (arrow) (skin opening and origin of hepatic tract do not align directly). Injection of contrast shows curved direction of tract. **B**, Guide wire inserted through catheter and advanced along hepatic parenchymal tract into duodenum.

pigtail) adding to the instability of catheter fixation.

An effective measure to improve catheter purchase in such situations is to divert the catheter tip from the immediate vicinity of the obstruction and direct it into a more peripheral radicle of either the left or right hepatic duct (fig. 5). This maneuver places a longer length of catheter within the lumen of the biliary tree, significantly lengthening "purchase."

Should the catheter be inadvertently dislodged, direct reinsertion through the original cutaneous puncture site is often feasible. After 7–10 days of catheter drainage, a granulating transparenchymal track forms, usually 2 French larger in caliber than the outer diameter of the catheter itself [1]. The tract will not seal over for 48–72 hr and can usually be reentered provided the cutaneous entry site can be lined up with the entry point through the liver capsule.

Gordon et al. [16] recommended a fluoroscopically guided contrast sinogram via a conical Christmas tree adapter placed in the cutaneous entry site to aid in locating and opacifying the transhepatic tract [16]. Guide wire/catheter systems are then inserted under direct vision. We prefer to insert a sheath from an 18 gauge needle directly through the skin entry and into the liver for easy insertion of a guide wire. If the skin and liver puncture sites are not in direct

continuity, a curved tapered tip catheter (Cobra C1, C2, C3) may be successfully negotiated into the liver and followed with a guide wire (fig. 6).

Nonoperative access to the biliary tree affords new options for the clinical and radiologic management of biliary tract obstruction. We believe the technical complexities of percutaneous biliary drainage have been generally understated in reports published to date. Despite the poor overall prognosis for many patients undergoing biliary catheter decompression procedures, complications of initial puncture and subsequent catheter function are not uncommon and require knowledge, evaluation, and management, as well as a commitment to long-term catheter aftercare by the radiologist.

ACKNOWLEDGMENT

We thank Ruth Brock for nursing care of these patients.

REFERENCES

1. Ferrucci JT Jr, Mueller PR, Harbin WP. Percutaneous transhepatic biliary drainage. Technique, results and applications. *Radiology* 1980;135:1–13

2. Nakayama T, Ikeda A, Okuda K. Percutaneous transhepatic drainage of the biliary tract. *Gastroenterology* **1978**;74:554-559
3. Pereiras R, Schiff E, Barbin J, Hutson D. Role of interventional radiology in disease of the hepatobiliary system and pancreas. *Radiol Clin North Am* **1979**;17:555-605
4. Ring EJ, Oleaga JA, Freiman DB, Husted JW, Lunderquist A. Therapeutic applications of catheter cholangiography. *Radiol* **1978**;128:333-338
5. Tylen U, Hoevels J, Vang J. Percutaneous transhepatic cholangiography with external drainage of obstructive biliary lesions. *Surg Gynecol Obstet* **1977**;144:13-18
6. Hellekant C, Jonsson K, Genell S. Percutaneous internal drainage in obstructive jaundice. *AJR* **1980**;134:661-664
7. Molnar W, Stockum AE. Relief of obstructive jaundice through percutaneous transhepatic catheter—a new therapeutic method. *AJR* **1974**;122:356-367
8. Mori K, Misumi A, Sugiyama M, et al. Percutaneous transhepatic bile drainage. *Ann Surg* **1977**;185:112-115
9. Hawkins IF. New fine needle for cholangiography with optimal sheath for decompression. *Radiology* **1979**;131:252-253
10. Harbin WP, Mueller PR, Ferrucci JT Jr. Complications and use patterns of fine needle transhepatic cholangiography: a multi-institutional study. *Radiology* **1980**;135:15-22
11. Wissmer B. Cholangitis. In: Bockus HL, ed. *Gastroenterology*, vol 2, 2d ed. Philadelphia: Saunders, **1973**:827-836
12. Dow RW, Lindenauer SM. Acute obstructive suppurative cholangitis. *Ann Surg* **1969**;169:272-276
13. Huang T, Bass JA, Williams RD. The significance of biliary pressure in cholangitis. *Arch Surg* **1969**;98:629-632
14. Williams RD, Fish JC, Williams DD. The significance of biliary pressure. *Arch Surg* **1967**;95:374-379
15. Hansson JA, Hoevels J, Simert G, Tylen U, Vang J. Clinical aspects of nonsurgical percutaneous transhepatic bile drainage in obstructive lesions of the extrahepatic bile ducts. *Ann Surg* **1979**;189:58-61
16. Gordon RL, Oleaga JA, Ring EJ, Freiman DB, Funaro AH. Replacing the "fallen out" catheter. *Radiology* **1980**;134:537-541

7.11 Expandable intrahepatic portacaval shunt stents: early experience in the dog

Julio C. Palmaz

Dr Palmaz is credited as being one of the early pioneers of intravascular stent therapy, which has revolutionized the way patients are treated for arterial blockages. He is currently a professor of interventional radiology at the University of Texas Health Science Centre at SanAntonio. He is the author of numerous papers and presentations on vascular radiology topics and has been the recipient of several awards and honors.



R.R. Sibbitt

S.R. Reuter et al.

Expandable Intrahepatic Portacaval Shunt Stents: Early Experience in the Dog

Julio C. Palmaz¹
Randy R. Sibbitt¹
Stewart R. Reuter¹
Francisco Garcia¹
Fermin O. Tio²

Intrahepatic portacaval shunts were established in dogs by the transjugular approach. The shunts extended from the anterior aspect of the inferior vena cava to the portal bifurcation through interposed liver parenchyma. The tissue track was created by a long transjugular needle and enlarged by balloon angioplasty catheter dilatation. The opening was then stented with a specially made, expandable, tubular, woven mesh of stainless steel wire. The stent was introduced mounted in a collapsed fashion around a folded angioplasty balloon. Inflation of the balloon expanded the stent and the tissue track simultaneously, leaving a large side-to-side portacaval shunt. Nine out of 12 animals survived the procedure and eight of them had functioning shunts as long as 9 months after placement. Pathologic examination showed complete endothelialization of the inner surface of the stents.

The percutaneous introduction of intrahepatic portacaval (IHPC) shunt in experimental animals was first described by Rösch et al. [1] in 1969. Connections were created between adjacent hepatic and portal veins through a track in the interposed liver parenchyma. The shunts were stented with a short segment of 12 or 14 French Teflon tubing. After this pioneering work, other investigators created intrahepatic shunts by various other means. Some involved resecting a cylindrical core of liver tissue by using a rotating drill [2] or a cryoprobe [3]. Burgener and Gutierrez [4] established temporary IHPC shunts by drawing an inflated latex balloon catheter through a parenchymal needle track. Colapinto et al. [5, 6] first reported the creation of IHPC shunts in humans using balloon angioplasty catheters.

Most investigators who have worked with IHPC shunts have not had difficulty correctly placing the shunt. Nevertheless, their efforts almost always were marred by early shunt closure. The use of some form of tubing to stent the shunt usually was accompanied by migration of the tube and early closure of the shunt [1, 7, 8].

Using a similar technique to that described by Rösch et al. [1, 7], we have created IHPC shunts in dogs stented by an expandable wire mesh tube [9]. Side-to-side portacaval shunts were made by inserting a transjugular needle to establish a tissue track extending through the anterior wall of the inferior vena cava, the portal vein bifurcation, and the interposed liver parenchyma. The track was enlarged with angioplasty balloons and stented with the balloon-mounted expandable mesh tube.

Materials and Methods

Twelve dogs of both genders weighing 15–25 kg were used. Under halothane anesthesia and after administration of 1000 U of intravenous heparin, a small bowel loop was exteriorized, and a valved 7 French Teflon sheath was introduced into a jejunal vein. The hub of the sheath was secured to the abdominal wall and the bowel loop returned to the abdomen. An 8 French Teflon catheter was then introduced percutaneously into the right jugular vein. After baseline right atrial, inferior vena cava, and portal pressure recordings, portal hypertension was

Received March 11, 1985; accepted June 18, 1985.

Presented at the annual meeting of the American Roentgen Ray Society, Boston, April 1985.

This work was supported in part by University of Texas Health Science Center grant OR5 and Audie Murphy Veterans Administration Hospital.

¹Department of Radiology, University of Texas Health Science Center at San Antonio, and Audie Murphy Veterans Administration Hospital, San Antonio, TX 78284. Address reprint requests to J. C. Palmaz, University of Texas Health Science Center, 7703 Floyd Curl Dr., San Antonio, TX 78284.

²Department of Pathology, University of Texas Health Science Center at San Antonio, and Audie Murphy Veterans Administration Hospital, San Antonio, TX 78284.

AJR 145:821–825, October 1985
0361–803X/85/1454–0821
© American Roentgen Ray Society

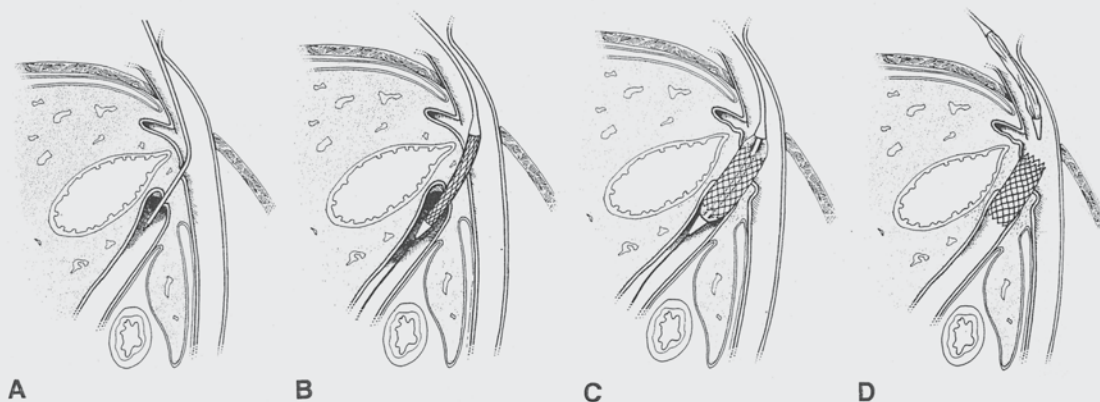


Fig. 1.—Sagittal cut of dog through inferior vena cava. A, Needle advanced through transjugular catheter perforates anterior wall of inferior vena cava, portal bifurcation, and interposed liver parenchyma. B, After balloon dilatation

of needle track, balloon-mounted stent is positioned within track. C, Inflation of balloon expands track and stent. D, Expanded stent keeps portacaval shunt lumen open.

created by injecting granular Ivalon (polyvinyl alcohol, Unipoint Industries, High Point, NC; particle size, 250–420 μ m) through the portal catheter in 0.1 g aliquots as described by Burgener et al. [10]. The Ivalon was made radiopaque by the addition of barium sulfate, 60% of dry weight. Creation of portal hypertension before shunt placement was necessary to promote a higher blood flow through the shunt. A 40-cm-long, 18 gauge metal cannula with a diamond-tip mandril, having a 20° distal bend, was used to penetrate the portal vein bifurcation through the jugular catheter (Cook, Bloomington, IN) (fig. 1). The ideal puncture site was determined by introducing a 15 mm occlusion-balloon catheter through the portal sheath and inflating it at the portal bifurcation to serve as a target. The distance between the balloon and the needle tip against the anterior wall of the inferior vena cava was less than 10 mm as measured on the lateral views. The caval wall was punctured cephalad to the portal balloon, under lateral fluoroscopy, to enter the portal vein along its longitudinal axis (fig. 1A). Injections of small amounts of contrast material and aspiration of blood through the cannula after withdrawal of the mandril indicated adequate position of the cannula tip. A 260-cm-long 0.035 inch (0.89 mm) guide wire was then advanced into the portal vein and grasped from the portal sheath with a snare loop. The wire tip was exteriorized through the portal sheath valve and tethered with a hemostatic clamp. This maneuver allowed good control as a tapered 8 French Teflon catheter was advanced with a rotary motion from the caval to the portal side. Track dilations with high-pressure balloon catheters (Cook, Bloomington, IN) with balloon diameters of 6, 8, and 10 mm were followed by the final positioning of the balloon-mounted expandable stent. The stent was fitted in a collapsed fashion around the folded balloon of an angioplasty catheter with a 10 mm balloon diameter. Oversized segments of tapered tubing were glued on both ends of the balloon to avoid dislodgment of the stent during manipulation. A 12 French sheath was inserted in the jugular vein before introduction of the stent-balloon assembly. Balloon inflation expanded the stent to the maximum diameter attained by the balloon. The graft stayed expanded after balloon deflation and withdrawal (figs. 1B–1D). For the graft to enter the portal bifurcation along the axis of the portal vein, it had to pierce the anterior wall of the inferior vena cava at a rather narrow angle so that, in most cases, part of the graft protruded into the caval lumen. Nevertheless, injected contrast material, pressure

readings, and direct inspection of the specimens did not show obstruction to the caval flow in any instance. Before stent expansion, hand-injected contrast material demonstrated adequate position of the stent in relation to the portal bifurcation. After stent expansion and withdrawal of the modified balloon catheter, pressure measurements and portography demonstrated hemodynamic and morphologic adequacy of the shunt (fig. 2A).

Follow-up was performed at variable intervals by percutaneous introduction of a 6.5 French Teflon catheter through either jugular vein. The catheter was advanced through the shunt into the portal vein, and pressure recordings were made before injection of contrast material. If the graft was found to be occluded and the clot still soft, it was reopened with a balloon angioplasty catheter. If residual stenosis persisted adjacent to the stent after dilatation, a second stent was expanded in a coaxial fashion, the new stent partially overlapping the previous one (fig. 2B). Patency was measured by comparing the diameter of the opaque column at its narrowest point with the diameter of the radiopaque wire mesh.

Construction of the Stent

We made the stents by hand by weaving 0.015 mm stainless steel wire under a low-power microscope. Specially made mandrils were used as templates to weave the interlaced crisscross pattern. The cross points of the mesh were soldered with low-temperature silver solder. The total wall thickness was 0.35–0.45 mm, and 80% of the stent itself was open surface. The weave density was equal for all stents used. In the expanded state, the spaces between wires were 2 \times 2 mm. The first seven stents were 20 mm long by 10 mm in diameter, except for one having a diameter of 15 mm. The three stents deployed coaxially to reduce residual areas of stenosis were also 20 mm long by 10 mm wide. The last four stents were 28 mm long by 10 mm in diameter.

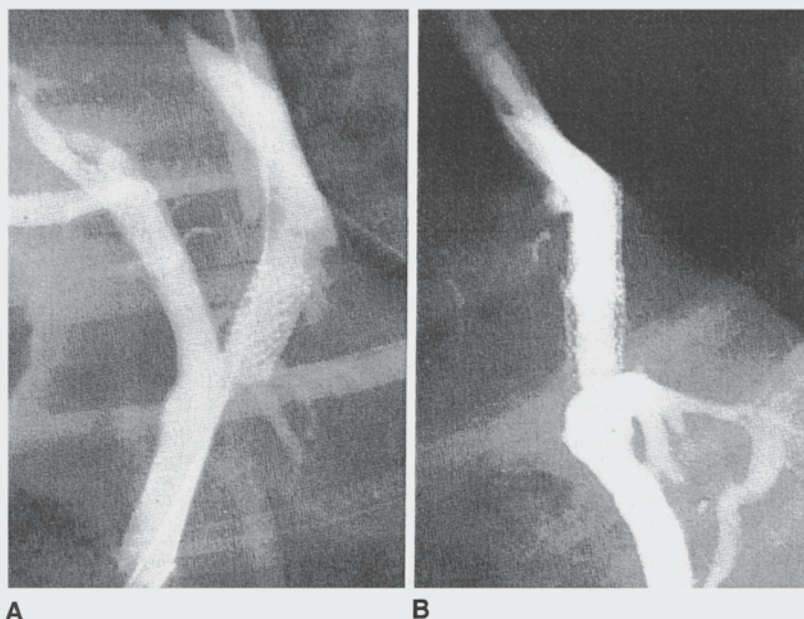
Great care was taken as the stent was collapsed to its smallest diameter over the balloon catheter to avoid overlapping of adjacent wires. This allowed the lowest possible diameter over the folded balloon. The collapsed-to-expanded stent diameter ratio was 1:3. Therefore, the collapsed, mounted stent could be introduced easily through a 12 French sheath. The ability of the stent to retain its shape

AJR, 145, October 1985

PORTACAVAL STENT

823

Fig. 2.—**A**, Dog 3. Lateral portogram. Good flow through shunt. Poor filling of portal radicles resulted from previous Ivalon embolization. **B**, Dog 8. Second stent placed in coaxial fashion to cover tissue track that caused shunt thrombosis. New stent partly overlaps old one.



after balloon expansion was based on the deformation of the wire segments between soldered points. Since there was no elastic recoil after maximal balloon inflation, there was no need to prolong balloon inflation after the stent reached adequate diameter.

Results

The various changes in experimental design during the study reflect its preliminary nature. Twelve dogs underwent IHP shunt placement. The first three animals died of peritoneal bleeding because the stent was expanded in tissue tracks that violated the peritoneal space. Better control of the puncture site was obtained in subsequent experiments by replacing the conventional beveled-tip, modified Ross needle with a diamond-shape-tipped mandril-cannula assembly. The new needle did not stray off the intended path as the beveled needles tended to do.

Of the nine animals that survived the procedure, five had shunt thrombosis within 3 weeks after placement (fig. 3). Shunt thrombosis was caused in all five dogs by luminal narrowing. Immediate postplacement portography demonstrated parts of tissue track not covered by the wire mesh in three dogs. In the other two, shunt flow was restricted by a blood clot in one and partial collapse of the stent in the other. Follow-up portography 1 week after placement showed that four of the thrombosed shunts had a thrombus soft enough to allow easy penetration with a catheter. In the other, recanalized 3 weeks after placement, the thrombus was too hard to allow piercing with the catheter, and an 18 gauge needle was needed to traverse the obstruction. Two of the thrombosed stents were reopened with simple balloon dilations

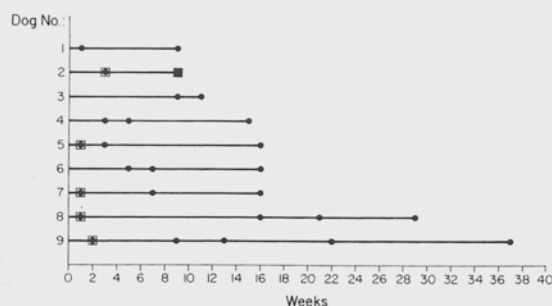


Fig. 3.—Shunt patent at follow-up portogram (circles); shunt thrombosed and recanalized (circles inside squares); shunt thrombosed and not recanalized (solid squares).

of the occluded stent lumen. The other three were extended either cephalad or caudad by placing a second graft in a coaxial fashion (fig. 2B). The shunt reopened 3 weeks after initial placement was again found occluded and impossible to recanalize 6 weeks later. Ultimately, eight shunts remained patent on follow-up periods of 9–37 weeks.

The amount of Ivalon embolized in the portal vein of each dog averaged 0.42 g. Allowing for the small number of animals, no relation was found between the dose of embolic material and the portal pressure elevation. The mean postembolization portal pressure was 22.5 ± 7.6 cm of saline and the mean portal pressure rise above baseline was 4.6 ± 2.9 cm of saline. After shunt placement the portal pressure drop averaged 8 ± 6.1 cm of saline (table 1). The pressure gradient

TABLE 1: Postshunt Hemodynamic and Angiographic Studies and Their Relations to Shunt Patency

	Dog No.								
	1	2	3	4	5	6	7	8	9
Portal pressure drop after shunt (cm saline)	11	9	9	6	14	20.5	8	0	6
Gradient across shunt (cm saline)	6.5	7.5	6	3	6	5	4.5	3.5	2
Partial shunt obstruction in postplacement portogram	+	+	...	+	+	+
Early shunt thrombosis	+	+	...	+	+	+
Shunt permanently reopened	No	Yes	...	Yes	Yes	Yes

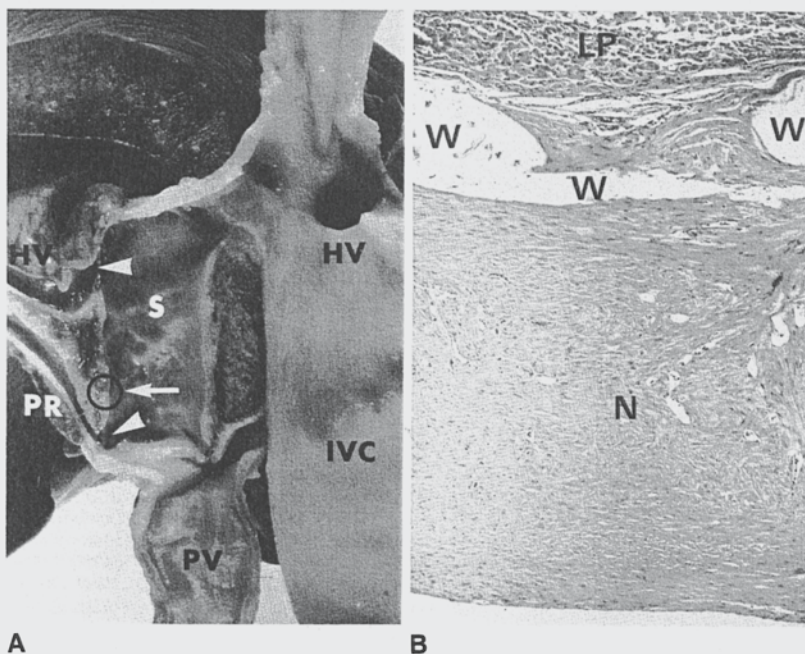


Fig. 4.—Dog 3. A, Sagittal section of portacaval shunt (S), inferior vena cava (IVC), and portal vein (PV). Circled area (arrow) corresponds to sample site for histology studies (B). Inner surface of graft is covered by neointima except at origins of hepatic veins (HP) and portal radicles (PR) (arrowheads). B, Longitudinal section of graft wall. Endothelialized 0.9-mm-thick neointimal layer (N) covers inner surface of graft wires (W). Liver parenchyma (LP) is adjacent to outer aspect of graft. (H and E $\times 120$.)

across the shunt immediately after placement averaged 4.9 ± 1.8 cm of saline. Neither measurement indicated whether or not the shunt was at high risk of thrombosis. Nevertheless, postplacement portography of all five shunts that thrombosed showed some degree of obstruction within or adjacent to the shunt. The lumen diameter of the stents averaged $69\% \pm 7.45\%$ among the eight dogs with open shunts in late studies. There was good correlation between the lumen diameter as measured on portograms and directly on the specimens of the animals that were sacrificed.

The eight surviving animals had normal or slightly altered liver function tests and steady weight. Their serum ammonia levels were markedly elevated on regular diet indicating patency of the shunt. The ammonia level was later lowered by feeding the dogs a low-protein diet. Except for dogs 5 and 9 which were undergoing prolonged observation, all animals were sacrificed 9–29 weeks after shunt placement. All shunts

were open, except the one in dog 2. The liver was soft with a few scattered, small infarctions in all six dogs. The inner surface of the stents was covered by a grayish layer, except at points where portal radicles or hepatic veins were in contact with the shunt. In those areas, blood flowed through the interstices of the mesh (fig. 4A). Direct inspection of the shunt in all six cases studied demonstrated that the shunt opened into the caval lumen at a point immediately below or between the main hepatic veins. Gross examination of the lungs with particular attention to those animals that had recanalization of obstructed shunts showed no evidence of infarction. Light microscopy studies of the shunt area showed viable hepatic parenchyma adjacent to the shunt. A neointimal smooth muscle layer averaging 1.5 mm in thickness covered the luminal side of the stent (fig. 4B). All the shunts studied showed complete endothelialization of the neointima as seen in transmission and scanning electron microscopy studies.

Discussion

The average dose of Ivalon embolized into the portal system to produce portal hypertension in our animals was considerably less than that used by Burgener et al. [10]. These authors performed repeated portal embolizations of Ivalon in dogs until a stable portal hypertension developed. They noticed that a single intraportal injection of embolic material caused transient portal hypertension that returned to normal within 1 week. Our goal was not to test the shunt in a situation of stabilized portal hypertension but rather was mainly focused on the anatomic aspects of the intrahepatic placement of the expandable graft. We have used intrahepatic injections of Ivalon before graft placement or recanalization to shift the flow to the shunt, thereby decreasing the chance of thrombosis. Whether the shunt flow decreased before a nonthrombogenic surface developed remains to be demonstrated.

An interesting observation arising from our study is the possibility of recanalizing occluded shunts and keeping them open. Burgener et al. [11] also noted that after periodic recanalizations of IHPC shunts created by balloon angioplasty catheters the shunts remained open. A definite advantage of the metal graft is its radiopacity, which allows easy catheterization from jugular approach in follow-up studies. A theoretic factor that may have had beneficial influence on our results is the favorable location of the shunt in relation to the portal vein and inferior vena cava. When the graft is placed at the portal bifurcation, the axis of the graft is continuous with that of the mesenteric and portal veins and almost parallel to the inferior vena cava.

The anchoring characteristics of the open crisscross mesh proved to be excellent since no graft migration was observed. Graft introduction and expansion was simpler in normal dog livers than it would have been in a liver cirrhosis model. Nevertheless, the possibility of enhancing the graft's ability to oppose recoil by increasing the wire size may overcome this problem. Further research in expandable IHPC shunts will include the substitution of the operative approach to place a target in the portal bifurcation by a transhepatic percutaneous access. The latter might be a reasonable alternative for human use.

Graft thrombosis correlated with an abnormal angiographic finding indicative of flow restriction at the time of placement. Therefore, an adequate portogram demonstrating unobstructed portacaval shunt and little or no flow to the hepatic radicles was the best indicator of success. On the contrary, hemodynamic factors such as a large portal pressure drop after shunt placement and a small portacaval gradient were not indicators of continued patency.

The human use of an expandable side-to-side IHPC shunt such as we have used in dogs would have the potential risk of peritoneal bleeding. Puncture of the inferior vena cava more caudally than is ideal may violate the peritoneal space and cause bleeding at the time of graft expansion. Nevertheless, precise localization of the caval puncture site and thorough understanding of the anatomy should minimize this risk. Further research in this area is currently underway.

ACKNOWLEDGMENTS

We thank Richard J. Haines, Beverly Combs, Cono Farias, and John Martini for assistance.

REFERENCES

1. Rösch J, Hanafée WN, Snow H. Transjugular portal venography and radiologic portacaval shunt: an experimental study. *Radiology* 1969;92:1112-1114.
2. Koch G, Rigler B, Tentzeris M, Schuy S, Sakulin M, Schmidt-Kloiber H. Der intrahepatische porto-cavale Shunt. *Langenbecks Arch Chir* 1973;333:237-244.
3. Reich M, Olumide F, Jorgensen E, Eiseman B. Experimental cryoprobe production of intrahepatic portacaval shunt. *J Surg Res* 1977;23:14-18.
4. Burgener FA, Gutierrez OH. Nonsurgical production of intrahepatic portosystemic venous shunts in portal hypertension with the double lumen balloon catheter. *ROFO* 1979;130:686-688.
5. Colapinto RF, Stronell RD, Birch SJ, et al. Creation of an intrahepatic portosystemic shunt with a Grüntzig balloon catheter. *Can Med Assoc J* 1982;126:267-268.
6. Colapinto RF, Stronell RD, Gildiner M, et al. Formation of intrahepatic portosystemic shunts using a balloon dilatation catheter: preliminary clinical experience. *AJR* 1983;140:709-714.
7. Rösch J, Hanafée W, Snow H, Barenfus M, Gray R. Transjugular intrahepatic portacaval shunt. An experimental work. *Am J Surg* 1971;121:588-592.
8. Gutierrez OH, Burgener FA. Production of nonsurgical portosystemic venous shunts in dogs by transjugular approach. *Radiology* 1979;130:507-509.
9. Palmaz JC, Sibbitt RR, Reuter SR, Tio FO, Rice WJ. Expandable intraluminal graft: an experimental study. Work in progress. *Radiology* 1985;156:73-77.
10. Burgener FA, Gutierrez OH, Logsdon GA. Angiographic hemodynamic and histologic evaluation of portal hypertension and periportal fibrosis induced in the dog by intraportal polyvinyl alcohol injections. *Radiology* 1982;143:379-395.
11. Burgener FA, Gutierrez OH. Produktion einer intrahepatischen portokavalen Fistel im Hund mit Leberzirrhose und Pfortaderhochdruck. *ROFO* 1984;141:327-332.

7.12 Intravascular stents to prevent occlusion and restenosis after transluminal angioplasty.

Ulrich Sigwart (born 1941)

Ulrich Sigwart has been credited with the concept and development of endoluminal stenting. Stents have fundamentally changed the treatment of cardiovascular diseases and have become the most important treatment of coronary and extra-coronary arterial disease. This work has resulted in a number of prizes including, the Medal of the European Society of Cardiology and an Honorary Doctorate of the University of Lausanne.

He also conceived and pioneered non-surgical myocardial reduction therapy, which has now become an accepted and widely used treatment of hypertrophic obstructive cardiomyopathy. Questions relating to this technique are now part of the written exams for the American Board of Cardiology.

Furthermore, his work on automation on cardiac catheterization carried out during the years 1974–1978 was the basis for the present day use of computers in hemodynamic evaluation. The sequence of events in myocardial ischemia (Sigwart curve) has found its way into numerous textbooks and is one of the most quoted illustrations. Ulrich Sigwart made fundamental observations on prosthetic heart valves that led to major modifications of the previously used designs.

Prof. Sigwart was born on 9 March 1941. He went to the medical schools of the universities of Freiburg (Germany), Basel (Switzerland) and Münster (Germany). In 1967 he gained his MD from the University of Freiburg (“magna cum laude”). In February 1985 he was appointed Professor of Medicine at the University of Düsseldorf. Since 1989 he has been an Associate Professor of Cardiology at the University of Lausanne and a Recognised Teacher at the Imperial College of Medicine, London. In 2001 he was appointed Professor of Cardiology at the University of Geneva (Switzerland).

Ulrich Sigwart is a Fellow, American College of Cardiology, American College of Angiology, Royal College of Physicians, The Bromptonian Society, and an Honorary Fellow of the Russian Society of Interventional Cardioangiography, Founding Fellow, European Society of Cardiology (Past Chairman, Working Group Myocardial Function). Furthermore, Prof. Sigwart is a member of several national and international scientific societies. Among other awards Sigwart was awarded the European Society of Cardiology Medal (1996), the ESC Grüntzig Award (1996), the Doctor honoris causa, University of Lausanne (1999), the Forssmann Prize (2001), the Sven Effert Prize (2003) and the King Faisal International Prize for Medicine (2004).

He is serving on the editorial board of several medical journals, e.g., the Journal of the American College of Cardiology, Clinical Cardiology, International Journal of Cardiovascular Interventions, Cardiology International, British Journal of Cardiology. He has published more than 500 separate publications and 7 books.

Ulrich Sigwart presently holds the Chair of Cardiology at Geneva University and directs the Centre of Cardiology. He keeps some activity at the Royal Brompton Hospital, where he headed the Department of Invasive Cardiology for more than twelve years.

Picture courtesy Ulrich Sigwart, MD, 2004.



J. Puel et al.

The New England Journal of Medicine

©Copyright, 1987, by the Massachusetts Medical Society

Volume 316

MARCH 19, 1987

Number 12

INTRAVASCULAR STENTS TO PREVENT OCCLUSION AND RESTENOSIS AFTER TRANSLUMINAL ANGIOPLASTY

ULRICH SIGWART, M.D., JACQUES PUEL, M.D., VELIMIR MIRKOVITCH, M.D., FRANCIS JOFFRE, M.D.,
AND LUKAS KAPPENBERGER, M.D.

Abstract Occlusion and restenosis are the most common reasons that transluminal balloon angioplasty may fail to provide long-term benefit. An intravascular mechanical support was therefore developed with the aim of preventing restenosis and sudden closure of diseased arteries after angioplasty. The endoprosthesis consists of a self-expandable stainless-steel mesh that can be implanted nonsurgically in the coronary or peripheral arteries. Experiments in animals showed complete intimal coverage within weeks and no late thrombosis during a follow-up period of up to one year.

We performed 10 implantations in 6 patients for iliac or femoral arterial disease; 24 coronary-artery stents were implanted in 19 patients who presented with coronary-artery restenoses ($n = 17$) or abrupt closure ($n = 4$) af-

ter transluminal angioplasty or deterioration of coronary-bypass grafts ($n = 3$). We observed three complications in the group with coronary disease. One thrombotic occlusion of a stent resulted in asymptomatic closure, a second acute thrombosis was managed successfully with thrombolysis, and one patient died after bypass surgery for a suspected but unfound occlusion. Follow-up in the patients has continued for nine months without evidence of any further restenoses within the stented segments.

Our preliminary experience suggests that this vascular endoprosthesis may offer a useful way to prevent occlusion and restenosis after transluminal angioplasty. Long-term follow-up will be required to validate the early success of this procedure. (*N Engl J Med* 1987; 316:701-6.)

ALTHOUGH most stenoses of coronary and peripheral arteries can now be traversed and dilated by balloon angioplasty, the unpredictable problems of abrupt closure and late restenosis of the dilated segment continue to compromise the overall results of this promising procedure. In addition to the pharmacologic,¹ mechanical,^{2,3} and thermal techniques⁴⁻⁶ under investigation to deal with these problems, intravascular stents may provide a useful approach to preventing both acute occlusion and late restenosis.⁷⁻¹³

None of the current designs of intravascular stents are ideal, however, especially with respect to homogeneous distribution of force, ease of placement, conformability, and stability. A new system has been developed, consisting of a stainless-steel multifilament, self-expanding, macroporous stent and an innovative instrument for placing it (Medinvent SA, Lausanne, Switzerland). We report our preliminary experience with the placement of stents in peripheral and coronary arteries after transluminal balloon angioplasty of a diseased arterial segment.

From the Division of Cardiology, Department of Medicine, Centre Hospitalier Universitaire Vaudois, Lausanne, Switzerland; and Centre Hospitalier Universitaire Rangueil, Toulouse, France. Address reprint requests to Dr. Sigwart at the Division of Cardiology, Centre Hospitalier Universitaire Vaudois, CH-1011 Lausanne, Switzerland.

Supported in part by a grant (3,835,083) from the Swiss National Fund.

METHODS

Description of the Stent

The stent is woven from a surgical-grade stainless-steel alloy formulated according to the specifications of the International Standards Organization. The prosthesis (Fig. 1) is geometrically stable, pliable, and self-expanding. Its elastic and pliable properties are such that its diameter can be substantially reduced by moderate elongation. It can be constrained on a small-diameter delivery catheter, and as the constraining membrane is progressively removed, the elastic device will return to its original (unconstrained) larger diameter (Fig. 1). When the prosthesis is implanted in a vessel whose caliber is less than that of its unconstrained diameter, the residual elastic radial force in the prosthesis will tend to dilate the artery. Dilation will continue until an equilibrium is attained between the circumferential elastic resistance of the arterial wall and the dilating force of the prosthesis. The constrained wire-mesh prosthesis is held at the distal end of the delivery catheter (Fig. 1A) by a doubled-over membrane, the outer layer of which can be progressively withdrawn. Two radiopaque metal markers on the delivery catheter facilitate identification of the end of the prosthesis at the time of its deployment. The outer diameter of the loaded catheter system is 1.57 mm, and prostheses up to 6.5 mm in expanded diameter can be mounted on this delivery device. Prostheses larger in diameter for use in peripheral arteries have correspondingly larger delivery systems.

Experiments in Animals

Prostheses up to 6.5 mm in diameter were mounted on the delivery catheter and were passed with conventional guiding catheters into the femoral, popliteal, and coronary arteries.

Peripheral Arterial Implants

In three mongrel dogs weighing 25 to 35 kg that were given heparin, eight transluminal implants were placed in branches of the femoral arteries at the level of the knee through the common femoral artery. The diameters of the prostheses ranged from 2 to 6.5 mm, and the lengths ranged from 20 to 70 mm. No anticoagulants were given after placement. All the dogs were evaluated weekly by Doppler-flow monitoring for four weeks and at three-month intervals by angiography.

Coronary Arterial Implants

In seven dogs, seven coronary prostheses were implanted through the femoral artery with use of 8 French coronary guiding catheters. Under fluoroscopy, one stent was placed in the right coronary artery, one was placed in the first marginal branch of the right coronary artery, and five were placed in the proximal left anterior descending coronary artery. One of the five last-mentioned prostheses extended into the left main coronary artery. The stents ranged from

2.5 to 3.5 mm in diameter and 15 to 20 mm in length. Again, no anticoagulants were given after implantation, but an intraoperative heparinized perfusion was given.

Implants in Humans

After the trials in animals, a protocol for implants in humans was approved by the hospital ethics committee, and informed consent according to the Helsinki Declaration was obtained from each patient before the intervention.

Peripheral Arterial Implants

For peripheral arterial implantation, highly symptomatic patients were selected who had (1) iliac or femoral arteries with long and complex stenoses in which balloon angioplasty had either failed or offered a poor prognosis, or (2) iliac or femoral restenosis after previous angioplasty.

Ten stents were implanted during seven procedures in six patients (four femoral and three iliac arteries). Stent diameters ranged from 6 to 12 mm, and lengths from 30 to 80 mm. Prostheses up to 6.5 mm in expanded diameter were delivered through an 8 French coronary guiding catheter; larger stents were deployed with use of an 8 French delivery system introduced directly through an ordinary 9 French arterial introducing sheath. Drug therapy consisted of acetylsalicylic acid (500 mg) the day before the intervention and a bolus injection of 10,000 IU of heparin during the implantation, followed by intravenous heparin (partial thromboplastin time at least twice the control value) until oral acenocoumarol had prolonged the prothrombin time to a therapeutic level ($2\frac{1}{2}$ times control). A fixed combination of aspirin (330 mg) plus dipyridamole (75 mg) once daily in addition to oral acenocoumarol was also given from the first postoperative day during the first three months of follow-up.

In two patients, totally occluded arteries were recanalized and stents were placed. One patient had a left superficial femoral-artery occlusion 30 cm in length, which failed to remain patent despite adequate balloon angioplasty followed by local infusion of urokinase. Two consecutive prostheses 6 mm in diameter and 8 cm in length were implanted. A longstanding 8-cm occlusion of the left external iliac artery was mechanically recanalized and dilated, and since no adequate flow was attained, a stent 8 cm in length and 12 mm in diameter was placed (Fig. 2). All the other prostheses were placed in stenotic arteries that had not responded satisfactorily to balloon angioplasty.

Coronary Arterial Implants

Three conditions were considered indications for the insertion of endoluminal stents in coronary vessels or coronary-bypass grafts: (1) restenosis of a major coronary artery after previous balloon angioplasty; (2) stenosis of aortocoronary-bypass grafts (in these patients the stents were placed in the bypass grafts themselves); and (3) acute coronary occlusion secondary to intimal dissection following balloon angioplasty (the placements of stents in these patients were categorized as emergency implantations).

Twenty-four coronary stents were implanted after transluminal balloon angioplasty in 19 patients during 20 operative procedures. In one patient the deployment of the stent in the left anterior descending coronary artery failed because of mechanical problems with the delivery catheter; since no reserve device was available, implantation was abandoned, without further complications.

After successful angioplasty, the balloon catheter was exchanged for the stent delivery system over a 0.014-inch (0.036-cm) exchange guide wire. The diameter of the stent was chosen to be about 15 percent larger than that of the native artery. Stents 15 or 20 mm in length, depending on the lesion, were placed to cover the entire diseased segment. Finally, the inner surface was smoothed by brief balloon dilatation.

The pharmacologic treatment involved inhibitors of platelet aggregation (1 g of aspirin the day before the procedure) and intraoperative heparin (15,000 units intravenously). During stent implantation, 50,000 to 100,000 units of urokinase were slowly in-

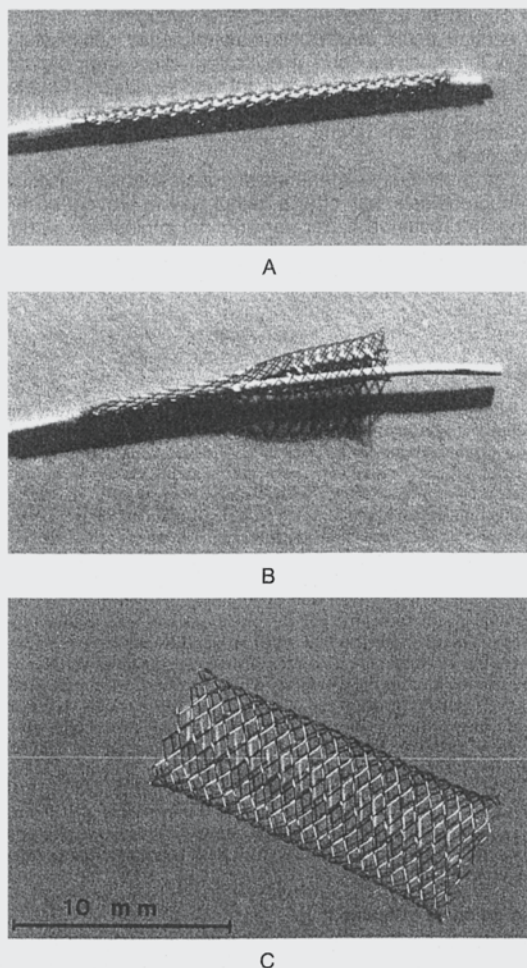


Figure 1. The Self-Expanding, Elastic, Macroporous Tubular Prosthesis, Which Is Woven from Stainless Steel, Is Shown (Panel A) Constrained on the Delivery Catheter, (B) Half Open during Deployment, and (C) Unconstrained and Fully Expanded.

fused through the coronary guiding catheter. Intravenous heparin was continued postoperatively until the oral anticoagulation with acenocoumarol became effective. All patients received calcium-channel-blocking agents, 330 mg of aspirin, and 75 mg of dipyridamole (Persantine) per day, starting four to eight hours after the operation.

Eleven stents were placed in the left anterior descending coronary arteries, eight stents in the right coronary arteries, two in the circumflex arteries, and three in venous coronary-artery bypass grafts. Two patients received a second stent at a later date, in each case for a new lesion, not adjacent to the original stent. There were four emergency implantations for acute occlusion following transluminal coronary angioplasty.

RESULTS

Experiments in Animals

Peripheral Arterial Implants

Two dogs were chosen to be killed after six months and one after nine months. Six stents were fully patent, one demonstrated a mural thrombus with a 50 percent reduction in luminal diameter, and one, which was perfused in a retrograde manner in an artery that had been ligated proximally, showed complete recanalization. The prostheses remained free from intimal

hyperplasia; moreover, all the side branches leaving the stented segments of the main vessel remained patent (Fig. 3). Figure 4 shows an example of a prosthesis firmly embedded in the arterial wall. This specimen was recovered from a branch of the femoral artery at the level of the left knee nine months after implantation. Scanning electron microscopy showed the neointima smoothly filling the pores between the stent filaments. The neointimal layer was about 450 μm thick, and no signs of necrosis due to the continuous mural pressure of the metal filaments were seen. The endothelial surface was very similar to the original arterial endothelium.

Coronary Arterial Implants

Angiography performed three and six months after implantation showed no signs of obstruction, either from thrombus or hyperplasia. However, after the dogs were killed at nine months, one unobstructive mural thrombus that was considerably larger than the coronary artery was seen in a stent (there had been a mismatching of diameters). In the single case in which the stent extended into the left main coronary artery, there was no interference with blood flow in the circumflex artery.

Clinical Experience

Peripheral Arterial Implants in Patients

There were no instances of restenosis as judged from a reappearance of symptoms, a decrease of peripheral blood flow by Doppler measurements, or digital subtraction angiography. No important side effects were reported, although one patient continued for two weeks to report an occasional sensation of a foreign body in the iliac area. Mean follow-up in this series is more than six months at this writing. Adequate blood flow and the disappearance of severe claudication were observed in each case. One patient's symptoms reappeared after three months because of high-grade stenoses of the nonstented femoral arterial segments proximal to and between the stents (Fig. 2). These stenoses were therefore dilated and reinforced with three additional stents — one overlapping the first two prostheses and two upstream of the first implants. Again, there was clinical improvement, reduction of the pressure gradient, and an increase in peripheral flow as demonstrated by Doppler evaluation. Although hemodynamically unimportant endothelial thickening within the stents was noted during follow-up angiography, the patient remained clinically well after nine months of follow-up.

Coronary Implants in Patients

Occlusion of the stent occurred twice when the myocardium perfused by the vessel was already hypokinetic from an old nontransmural infarction; however, the prosthesis was successfully recanalized in one patient after local infusion of 100,000 units of urokinase. Thrombolytic therapy was refused by the second

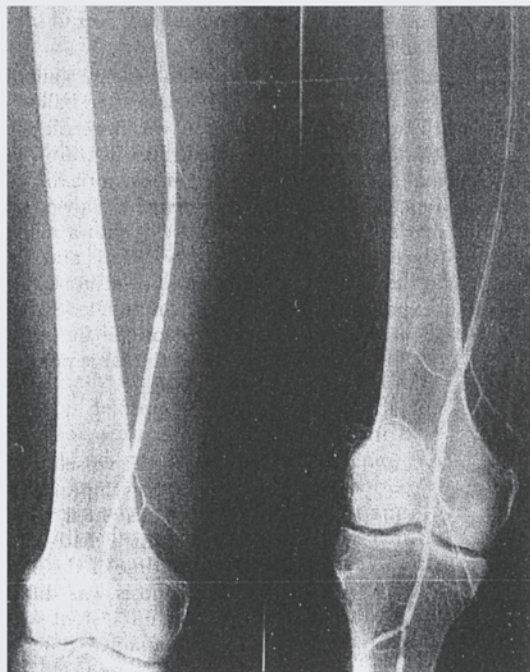


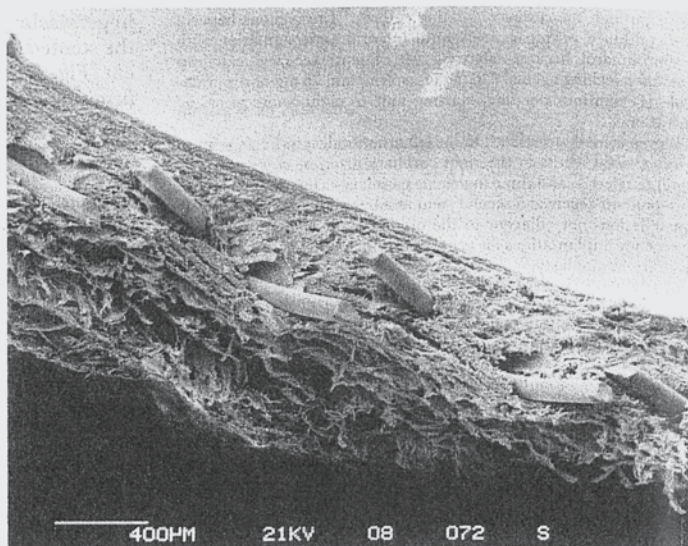
Figure 2. Superficial Femoral Artery after Mechanical Recanalization of a Total Occlusion 30 cm Long, Followed by Implantation of Two Endoprosthesis.

For better visualization of the stents, the right-hand panel shows contrast medium injected at a point distal to the two prostheses through a 4.5 French angiography catheter. Note the nonstented lesion 4 cm below the knee. Three more prostheses were implanted three months later to treat severe lesions within nonstented segments.

Figure 4. Scanning Electron Micrograph of a Prosthesis Firmly Embedded in the Femoral Artery of a Dog at the Level of the Left Knee Nine Months after Implantation.

patient, who now has mild angina with exertion, seven months after the procedure.

One patient presented a special problem. He was a 56-year-old man who had a 90 percent proximal stenosis of the left anterior descending coronary artery causing residual angina one week after an anteroapical infarction. After angioplasty, symptomatic restenosis occurred within two months. The lesion was redilated and a stent was placed. Two days later the patient underwent maximal stress testing with no evidence of ischemia. Fifteen minutes afterwards, electrocardiographic signs of anterolateral ischemia developed. In the absence of immediately available angiographic facilities, the patient was transferred for bypass surgery (internal mammary implant), at which time the signs of ischemia had disappeared and the prosthesis was found to be patent. The postoperative period was complicated by problems with hemostasis and signs of cardiac tamponade. The following day the patient had hypoxia and subsequently died. Postmortem examination revealed a patent bypass graft and some traces of a recent thrombus in the prosthesis, which was correctly situated without extension into the left-main bifurcation. No clear link could be established between death and the prosthesis, although the stent



may have contributed to coronary spasm soon after stress testing.

Emergency Implantation

In all four patients in whom a stent was implanted to relieve an acute coronary occlusion after balloon angioplasty, adequate coronary flow was immediately restored. Simultaneously, the electrocardiogram became normal and symptoms of angina pectoris disappeared. Myocardial enzyme measurements showed no signs of myocardial damage. Figure 5 shows a left anterior descending coronary artery before and six months after emergency implantation of a prosthesis 3.5 mm in expanded diameter and 20 mm in length. A

stent was later placed in the right coronary artery of the same patient because of restenosis.

Follow-up

The patient whose vessels are shown in Figure 5 had symptomatic restenosis of the nonstented right coronary artery, which had also been dilated at the time of the first procedure; this stenosis was dilated a second time and a stent was placed that has remained patent. A new stenosis proximal to the stent developed in one patient four

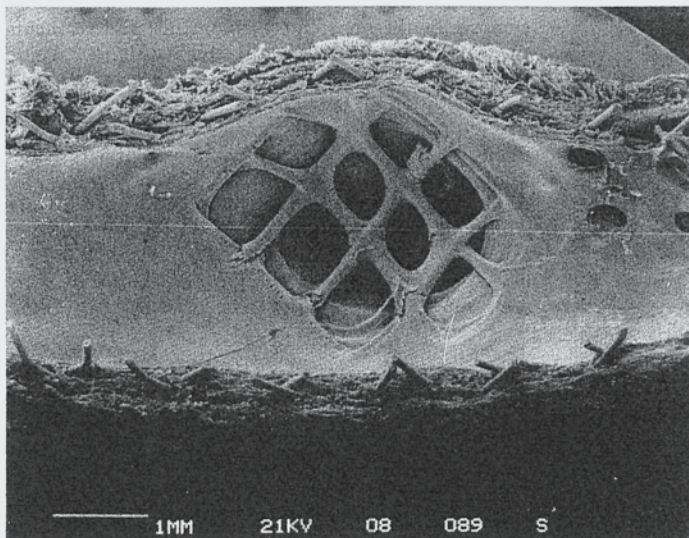


Figure 3. Scanning Electron Micrograph of a Stent Covering the Orifice of a Side Branch of a Canine Femoral Artery.

Nine months after implantation, the metal wires are completely coated with a smooth neointimal lining, which does not compromise blood flow to the branch artery.

months after the first procedure; this lesion was also dilated and reinforced with a separate stent.

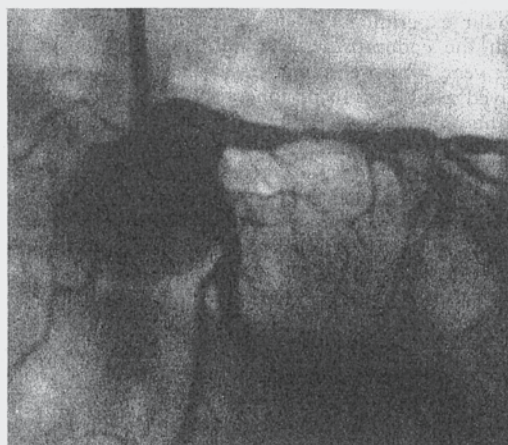
All the other patients recovered normally and left the hospital within four days of the procedure. Follow-up consisted of weekly and then monthly clinical examinations, stress tests at two-month intervals, and — up to now in 12 patients — coronary angiography within three to six months after the intervention. There were no clinical signs of restenosis (except in the patients in whom a second prosthesis was implanted because of new lesions) as judged by the clinical history and exercise testing. Coronary angiography showed the endoluminal stent smoothly embedded with no traces of serious luminal narrowing or suggestion of intimal hyperplasia within the stent.

DISCUSSION

Restenosis and acute occlusion following transluminal angioplasty of coronary and peripheral arteries restrict the usefulness of this procedure. With restenosis rates as high as 33 percent after coronary angioplasty and even higher (68 percent) in multivessel angioplasty, the overall value of balloon angioplasty is diminished even when one considers the low morbidity of this procedure, which is frequently repeated several times. The socioeconomic implications of repeated angioplasties for restenosis are important and compromise the comparatively low cost of the intervention.

The rates of early and late repeated occlusion after peripheral and coronary angioplasty are independent of the operator's skill and the quality of the equipment. Longer inflation times, high doses of calcium-channel blockers, steroids, and other drug regimens have so far failed to solve these problems. An alternative approach is to provide a suitable endoluminal support for the diseased vessel wall.

Several designs have been proposed, including elastically self-expanding spirals, memory-metal types (thermally expandable and relatively inelastic), and balloon deformable (quasi-rigid) models. Endothelialization with uniform and consistent intimal thickening and patency of side branches, such as we have described, has also been reported by others,⁹ but with some minor differences. It appears that the length of time it takes to cover the stent surface depends on the thickness of the metal element. Thus, Wright et al.⁹ reported only 30 percent covering after one month for wire 0.46 mm thick, whereas we found complete covering of 0.09-mm filaments within three weeks. As compared with inelastic devices, we think that the self-expanding stent, by virtue of its inherent pliability, provides a smooth transition between the stented segment and adjacent native artery; this has been corroborated by histologic studies of the junction between the stent and the non-stented artery. A longitudinal flexible stent, which is also flexible even when mounted on its delivery catheter, will permit easier access through tortuous vessels to the target site.



A



B



C

Figure 5. Left Coronary Artery (Panel A) before Angioplasty, (B) after the Development of Complete Occlusion after Angioplasty, and (C) Six Months after Emergency Recanalization of, and Stent Implantation in, the Left Anterior Descending Coronary Artery.

The stent is invisible (Panel C) because of the high density of the contrast material; its position is shown by the arrows (upper vessel), the distal end being just proximal to the septal branch (S).

Our experiments in healthy animals have shown that the endoprosthesis is well tolerated for up to one year. Our preliminary results in patients who received a total of 10 peripheral and 24 coronary implants revealed no cases of restenosis within the stented segment after follow-up ranging from nine weeks to nine months, whereas the statistical likelihood of such an event is approximately 30 percent or more. We also found it possible to reopen arteries that became occluded after a previous angioplasty, with favorable medium-term results. It is possible, of course, that many of the arteries that we studied might have remained patent after angioplasty even without the placement of a stent; randomized trials will be necessary to ascertain the long-term benefit.

As for the potential risks of this method, little is known about the possible longer-term complications. We have no long-term information (beyond 12 months in canine arteries) on the outcome of the patency of side branches, and although the prostheses are completely endothelialized, infection could conceivably be a future pitfall. We have specifically avoided traversing major branch vessels, not only because of uncertainty about long-term patency, but also because to do so would prevent later angioplasty should it be required. We have also specifically avoided placing stents in segments having sudden changes in vessel caliber, since we believe that these might pose a higher risk of thrombogenesis. Similarly, poor distal runoff or lesions leading to competitive flow might increase the risk of thrombosis and could have been responsible for the occlusion of the stent in two of our patients. It is also possible that stents may induce coronary spasm, since any foreign body (e.g., a guide wire) within the arterial lumen can enhance vasomotor tone; this could explain the ischemic reaction 15 minutes after

maximal stress testing in the patient in whom no signs of thrombus were seen at surgery.

Further studies will determine with greater precision the benefits and risks of this new approach. On the basis of our preliminary experience, we suggest that intravascular stents may represent a valuable adjunct to transluminal angioplasty.

REFERENCES

1. Leimgruber PP, Roubin GS, Hollman J, et al. Restenosis after successful coronary angioplasty in patients with single-vessel disease. *Circulation* 1986; 73:710-7.
2. Simpson JB, Zimmerman JJ, Selmon MR, et al. Transluminal atherectomy: initial clinical results in 27 patients. *Circulation* 1986; 74:Suppl 2:203. abstract.
3. Ritchie JL, Hansen DD, Vracko R, Auth D. In vivo rotational thrombectomy — evaluation by angioscopy. *Circulation* 1986; 74:Suppl 2:457. abstract.
4. Choy DSJ, Stertzer S, Rotterdam HZ, Sharrock N, Kaminow IP. Transluminal laser catheter angioplasty. *Am J Cardiol* 1982; 50:1206-8.
5. Abela GS, Normann SJ, Cohen DM, et al. Laser recanalization of occluded atherosclerotic arteries in vivo and in vitro. *Circulation* 1985; 71:403-11.
6. Isner JM, Clarke RH. Laser angioplasty: unraveling the Gordian knot. *J Am Coll Cardiol* 1986; 7:705-8.
7. Palmaz JC, Sibbett RR, Reuter SR, Tio FO, Rice WJ. Expandable intraluminal graft: a preliminary study: work in progress. *Radiology* 1985; 156:73-7.
8. Maass D, Kropf L, Egloff L, Demierre D, Turina M, Senning A. Transluminal implantations of intravascular "Double Helix" spiral prostheses: technical and biological considerations. *Proc Eur Soc Artif Organs* 1982; 9:252-6.
9. Wright KC, Wallace S, Chamsangavej C, Carrasco CH, Gianturco C. Percutaneous endovascular stents: an experimental evaluation. *Radiology* 1985; 156:69-72.
10. Dotter CT. Transluminally-placed coiled spring endarterial tube grafts: long-term patency in canine popliteal artery. *Invest Radiol* 1969; 4:329-32.
11. Cragg A, Lund G, Rysavy J, Castaneda F, Castaneda-Zuniga W, Amplatz K. Nonsurgical placement of arterial endoprotheses: a new technique using nitinol wire. *Radiology* 1983; 147:261-3.
12. Dotter CT, Buschmann RW, McKinney MK, Rösch J. Transluminal expandable nitinol coil stent grafting: preliminary report. *Radiology* 1983; 147:259-60.
13. Palmaz JC, Windeler SA, Garcia F, Tio FO, Sibbett RR, Reuter SR. Atherosclerotic rabbit aorta: expandable intraluminal grafting. *Radiology* 1986; 160:723-6.

Massachusetts Medical Society
Registry on Continuing Medical Education

To obtain information on continuing medical education courses in the New England area, write or call, indicating field(s) or specialty in which information is desired, the Committee on Medical Education, 1440 Main St., Waltham, MA 02254; telephone (617) 893-4610 (Metropolitan Boston) or WATS 1-800-322-2303 (Massachusetts).

8 Mammography

- | | | |
|------------|--|-----|
| 8.1 | Diagnóstico de los tumores de la mama por la radiografía simple.
Boletín de la Sociedad de Cirugía del Uruguay 20 (1949): 407–422
<i>R. Leborgne</i> | 545 |
| 8.2 | La radiographie de la glande mammaire
J Belge Radiologie 35 (1952): 226–268
<i>C.M. Gros, R. Sigrist</i> | 564 |
| 8.3 | Experience with mammography in tumor institution: evaluation of 1000 studies.
Radiology 75 (1960): 894–900
<i>R.L. Egan</i> | 608 |
| 8.4 | Evaluation of periodic breast cancer screening with mammography. Methodology and early observations.
JAMA 195 (9) (1966): 731–738
<i>S. Shapiro, P. Strax, L. Venet,</i> | 616 |
| 8.5 | Xerography of the breast.
Radiology 91 (1968): 231–240
<i>J.N. Wolfe</i> | 625 |
| 8.6 | Reduction in mortality from breast cancer after mass screening with mammography.
Lancet i (1985): 829–832
<i>L. Tabár, C.J.G. Fagerberg, A. Gad, L. Baldetorp, L.H. Holmberg, O. Gröntoft et al.</i> | 635 |
| 8.7 | Mammographic Microcalcifications: Detection with Xerography, Screen-Film, an Digitized Film Display.
Radiology 159 (1986): 673–677
<i>R.L. Smathers et al.</i> | 645 |
| 8.8 | Breast imaging: Dual-energy projection radiography with digital radiography.
Radiology 164 (1987): 869–870
<i>T. Asaga, S. Chiyasu, S. Matsuda, H. Mastuura, H. Kato, M. Ishida, T. Komaki</i> | 651 |
| 8.9 | Stereotactic breast biopsy with a biopsy gun.
Radiology 176 (1990): 741–747
<i>S.H. Parker, J.D. Lovin, W.E. Jobe, J.M. Luethke, K.D. Hopper, W.F. Yakes, B.J. Burke</i> | 656 |

Breast Imaging

Today mammography is one of the most frequent X-ray examinations. Particularly during the last two decades, mammography has experienced an enormous expansion. Since the mid 1990s there has been great interest in digital mammography. Due to the demand for high image quality there are still a lot of technical and financial challenges before changing completely from screen-film to digital mammography.

The main complementary imaging techniques to mammography are ultrasound and MRI, which both have the advantage of not using ionizing radiation. Ultrasound is relatively inexpensive and plays an important role as guidance for needle biopsy. MRI been performed as a Gd-DTPA contrast-enhanced dynamic study and it is a very sensitive and moderately specific technique. Certain indications such as the investigation of unclear findings on conventional examinations are already established. This includes multifocal malignant diseases and the investigation of the postoperative, postirradiated and augmented breast. Other indications for these complementary techniques such as screening of the high-risk patient are not yet established. X-ray mammography is still the golden standard for breast imaging. It is still largely the only technique that can detect breast cancer in a preinvasive stage.

At first there was hardly any interest in using X-rays for the diagnosis of soft-tissue diseases, because these usually superficial changes were accessible for inspection, palpation and clinical assessment. However, a special situation existed for the diagnoses of changes in the female breast. It took another 18 years before in 1913 the first paper on radiographs of breast diseases was published by Albert Salomon, a German surgeon of the Royal Surgical University Clinic in Berlin. Salomon's first mammographs already provided satisfactory information on tumor spread and the borders of the tumor. He was able to demonstrate the radiomorphological changes in various types of breast cancer. Because Salomon was unable to examine patients with breast diseases, *in vivo* mammography only won clinical recognition many years later.

Stafford L. Warren from Rochester, N.Y. noticed in 1926 that he could obtain a reasonable outline of the breast while performing thoracic aortic fluoroscopy. He published a report on 119 female patients of whom 48 had breast cancer. The first paper on radiographic diagnosis of the female breast in patients with problematic clinical findings was published by Otto Kleinschmidt from the University Hospital of Leipzig, Germany in 1927. Dominquez noted calcifications within breast cancers; Seabold studied breast changes associated with menses (1931); Vogel differentiated between cystic mastitis and cancer of the breast (1932) and Raoul Leborgne succeeded in to differentiating between micro-calcifications in mastopathic changes and those in malignant formations (1935). He especially outlined the need for vast technical improvement to allow study of those elusive calcifications in breast cancers. As early as 1951, Leborgne demanded the following main requirements for mammographic technique: Survey view in craniocaudal direction, entire breast with long cone (60 cm), slight compression of the breast, 30 kVp, 5 mA/6 s, film without intensifying screen further additional lateral views if the upper part of the breast is not clearly visible and a selective view with 20 kVp, 30 cm focus-film distance, cone opening as small as possible.

In 1937 Gershon-Cohen, Colcher and Sticker, in cooperation with the pathologist Helen Ingelby, correlated for the first time breast anatomy and pathology using breast radiography. In an extensive study from 1964 Gershon-Cohen was able to determine that the accuracy of clinical examination with palpation and inspection alone was only 48%, while the radiological examinations gave a diagnostic certainly of 90%.

Galactography was first performed by Ries (1930) and Hicken (1937) by filling contrast media for mammographic visualization of breast tumors.

In 1956 Robert L. Egan in collaboration with Gilbert F. Fletcher from the Tumor Institute, Department of Radiology of the University of Texas' MD Anderson Hospital in Houston reported on variations of technical factors that would be required for optimal mammographic examinations. Egan settled on a high-mA low-kV technique coupled with an unfiltered beam and a fine-grain industrial film. Egan also deserves credit as the first to use the term "mammography" for roentgenological examinations of the breast. Under the sponsorship of the Breast Cancer Detection Demonstration Project (BCDDP) and the results of mammographic study comprising 64,000 women, Egan emphatically proposed since 1973 mammographic screening for early detection of breast cancer.

A new method for soft tissue breast imaging was presented with xeroradiography in 1960, by Gould et al from St. Vincent's Hospital New York. This work was continued by Wolfe et al in 1968. A faithful delineation of microstructures could not be obtained, but this technique remains advantageous for large breasts and for visualizing breast structures that have substantially different absorption.

A real technical revolution in mammography goes back to the French physicist Charles M. Gros. By using a molybdenum-anode tube, which was originally applied for non-destructive testing procedures, he developed in 1966 the first X-ray unit dedicated to mammography. The Senograph (French for "picture of the breast"), with its incorporated compression device, lowered the entrance dose sufficiently to allow use of a molybdenum target and take advantage of the K radiation spectrum. In addition the Senograph used a molybdenum filter and a beryllium window. It produced an energy band that was nearly perfect for soft tissue radiography. The apparatus was flexible, allowing a full 360° arc of the tube. It opened the door to variable patient positioning. In 1969 CGR introduced this unit to the United States and dedicated mammography was brought into widespread commercial use. The Senograph and with the development of the rare earth intensifying screens paved the way for modern mammography and were fundamental for the enormous expansion of mammography during the last two decades.

Another considerable technical step forward was taken by Gajewski of Siemens Erlangen, Germany in 1967. To improve the standard low-radiation technique he developed a special X-ray tube with a rotating anode and thinner glass window. To obtain reproducible image quality an automatic exposure control for mammography was developed by Siemens and tested by Hoeffken, Heuss and Roedel in 1970.

In physical experiments Friedrich, from Berlin, was able to show that 44% of the total radiation in mammography was scattered radiation. To achieve a significant reduction in scattered radiation special grids are necessary to overcome this problem. Following his investigation grid mammography was introduced in 1978.

Innumerable improvements have been formulated in film sensitivity, optical film density and graduation, screen sensitivity and granulation as well as in the X-ray tube design. The introduction of the microfocus magnification technique and the clinical results of Georgi et al from 1978 have been verified and confirmed by several mammographic centers. Microfocus magnification is without any doubt an asset in recognizing fine structures and indispensable for the early diagnosis of breast cancer.

In the 1980s the design of the second generation of mammography units reduced exposure time significantly, giving patients more confidence during the procedure. The first motorized compression devices helped to simplify mammography procedures, opening the door for "mass screening" of women. In 1987 further design improvements, including add-on components for breast biopsies, were introduced. In 1992 a new and significant technical improvement was achieved

through the design of a bimetallic X-ray tube with a rotating molybdenum and rhodium focal track. This X-ray tube enables better penetration of the breast tissue with less radiation exposure to the patient.

One important and interesting study on mammography screening was introduced in Sweden in 1978. The long-term value of mammography screening has been the subject of considerable debate over the past few years. Laszlo Tabar from Falun Central Hospital, Sweden, and colleagues compared deaths from breast cancer in two Swedish counties 20 years before and after screening. Their analysis included 210,000 women diagnosed with breast cancer aged 20–69 years. Women aged 40–69 years who received screening had a 44% reduced risk of dying from breast cancer compared with women in the same age group who were diagnosed with breast cancer before screening was introduced. There was no evidence that improved treatment had a significant effect on breast cancer mortality for women younger than 40 years of age (an age group that has never been offered screening). Women aged 40–69 years who were not screened after screening had been introduced had a 16% reduction in death from breast cancer compared with women diagnosed with breast cancer before 1978.

For use with palpable masses fine-needle aspiration cytology was the first alternative to open biopsy. In 1977 Nordenström from Sweden introduced its application to nonpalpable lesions under stereotactic guidance. In 1982 Lindgren introduced core-needle biopsy using an automated large-core gun. This idea was adapted to stereotactic breast biopsies by Parker in 1990. Further improvements such as ultrasound-guided breast core-needle biopsy led to a revolution in breast-biopsy methods.

One of the most recent advances in X-ray mammography is digital mammography. First reports of digital mammography goes back to Smathers et al (1986) and Asage (1987). In 1996 digital spot view acquisition systems become available for mammography. Digital spot view mammography allows faster and more accurate stereotactic biopsy. This results in shorter examination times and significantly improved patient comfort and convenience since the time the patient must remain still is much shorter. Four years later GE introduced the first full-field digital mammography system. With continued improvements and more cost efficiencies, the “full-field” mammography systems may eventually replace the traditional screen-film technique.

A new approach to mammography was described first by Niklason et al., who introduced digital tomosynthesis mammography in 1997. This technique holds potential for greatly improving the detection of breast lesions and the ability to predict whether they are benign or malignant. By eliminating the overlapping breast structures it may be useful particularly in dense breasts where low-contrast objects are projected in the same image area.

Other modern techniques are in discussion. In contrast subtraction mammography, introduced by Watt et al. in 1986, the Gd-DTPA contrast agent is useful and enables the evaluation of net images as a function of time. Dual-energy mammography (Johns et al. 1985) recently has been improved by the development of special monochromatic X-ray sources. In 2002 first significant results were obtained with an experimental set-up. (Marziani et al. 2002)

References

- Barnes GT (1999) Mammography imaging physics: X-ray equipment considerations. In 1999 Syllabus, Categorical course in diagnostic radiology physics: Physical aspects of breast imaging – Current and future considerations. Edited by Haus A.G. and Yaffe M.J., RSNA, Oak Brook, IL, USA, 41-57
- Egan RL (1964) Mammography. Thomas, Springfield
- Friedrich M (1976) Der Einfluss der Streustrahlung auf die Abbildungsqualität bei der Mammographie. *Fortschr. Röntgenstr.* 125: 461-471
- First description of using special grids in mammography*
- Friedrich M (1978) Neue Entwicklungstendenzen in der Mammographietechnik: die Raster-Mammographie. *Fortschr. Röntgenstr.* 128: 2
- Gajewski H, Hoeffken W (1966) Verteilungsuntersuchung zur Mammographie mit Weichstrahltechnik und Isodenmethode. *Radiologe* 6: 407
- Gershon-Cohen JH, Colcher AE (1937) An evaluation of the Roentgen-Diagnosis of early Carcinoma of the Breast. *JAMA* 108: 867
- Gershon-Cohen JH, Ingleby H (1953) Carcinoma of the breast. Roentgenographic Techniques and Diagnostic Criteria. *Radiology* 60: 68-76
- Gershon Cohen J (1960) Technical improvements in breast roentgenology. *AJR* 84: 224-226
- Gould HR et al (1969) Xeroradiography of the breast. *AJR* 84: 220-223
- Gros CM (1963) Les maladies du sein. Masson, Paris
- Hicken NF (1937) Mammography: roentgenologic diagnosis of breast tumors by means of contrast media. *Surg. Gynec. & Obst.* 64: 593-603
- Johns PC, Drost DJ, Yaffe MJ, Fenster A (1985) Dual energy mammography: Initial experimental results. *Med Phys* 12: 297-304
- Kleinschmidt O (1927) Die Brustdrüse. Die Klinik der bösartigen Geschwülste. Zweifel, Payr Hirzel, Leipzig
- Lanyi M (1986) Diagnostik und Differentialdiagnostik der Mammaverkalkungen. Springer, Heidelberg, New York, Tokyo
- Leborgne R (1949) Diagnóstico de los tumores de la mamma por la radiografía simple. *Boletín de la Sociedad de Cirugía del Uruguay* 20: 407-422
- Leborgne R (1951) Diagnosis of tumors of the breast by simple roentgenography. *AJR* 65: 1-11
- Lindgren PG (1982) Percutaneous needle biopsy: a new technique. *Acta Radiol* 23: 653-656
- Löfgren M, Andersson I, Bonderson L, Lindholm K (1988) X-ray guided fine-needle aspiration for the cytologic diagnosis of nonpalpable breast lesions. *Cancer* 61: 1032-1037
- Löfgren M, Andersson I, Lindholm K (1990) Stereotactic fine-needle aspiration for cytologic diagnosis of nonpalpable breast lesions. *AJR* 154: 1191-1195
- Marziani M, Taibi A, Tuffanelli A, Gambaccini M (2002) Dual-energy tissue cancellation in mammography with quasi-monochromatic X-rays. *Phys Med Biol* 47: 305-313
- Norderström B (1977) Stereotactic screw needle biopsy of nonpalpable breast lesions. In: Logan W et al Breast carcinoma: the radiologist's expanded role. New York, Wiley: 313-318
- Niklason LT, Christian BT, Niklason LE, Kopans DB, Castleberry DE et al. (1997) Digital tomosynthesis in breast imaging. *Radiology* 205: 399-406
- Parker SH, Lovin JD, Jobe WE, et al. (1990) Stereotactic breast biopsy with a biopsy gun. *Radiology* 176: 741-747
- Parker SH, Lovin JD, Jobe WE et al. (1991) Non palpable breast lesions: Stereotaxic automated large core biopsies. *Radiology* 180: 403-407
- Parker SH, Klaus AJ (1997) Performing CNB with a directional, vacuum-assisted biopsy instrument. *Radiographics* 17: 1233-1252
- Important contributions to the modern management of breast lesions*
- Salomon A (1913) Beiträge zur Pathologie und Klinik der Mammakarzinome. *Arch clin Chir* 101: 573-668
- Shapiro S, Venet W, Venet L, Roeser R (1982) Ten to fourteen year effect of screening on breast cancer mortality. *J National Cancer Institute* 69: 349-355
- This is the report of the first randomized trial of breast screening carried out in New York (the health insurance plan – HIP study) which showed a mortality reduction in the screened patients.*

- Tabar L, Fagerburg CJG, Gad A et al. (1985) Reduction in mortality from breast cancer after mass screening with mammography. *Lancet* 1: 829-832
The Swedish two-county trial showing the benefit of breast screening
- Warren SL (1930) A Roentgenologic Study of the Breast. *AJR* 24: 113-124
- Wolfe JN (1968) Xeroradiography of the breast. *Radiology* 91: 234-240
- Yaffe MJ, Rowlands JA (1997) Review. X-ray detectors for digital radiography. *Phys Med Biol* 42: 1-39
- Yaffe MJ (2000) Digital mammography. In *Handbook of Medical Imaging, Volume 1*. Edited by Beutel J., Kundel H.L. and Van Metter R.L. pp 329-372. SPIE Press, Bellingham, USA
Describes special techniques such as dual-energy subtraction imaging and tomosynthesis

8.1 Diagnóstico de los tumores de la mama por la radiografía simple. Boletín de la Sociedad de Cirugía del Uruguay

Raúl A. Leborgne (1907–1986)

Raúl A. Leborgne was born in Montevideo, Uruguay, on 19 April 1907. In 1939 Leborgne received his MD from the Medical Faculty of the University of Montevideo. R. Raúl Leborgne was a student of Dr C. M. Domínguez. Domínguez and his associates were involved with the development of clinical mammography, and in 1929 and 1930 published several basic articles related to its clinical potential.

In co-operation with his brother Felix, Raúl Leborgne he worked since 1928 as a staff radiologist at the X-ray department of the Pereira Rosseel University Hospital. Leborgne specialised in radiological diagnosis of diseases of the breast and in the X-ray therapy of mammary cancer.

Based on the work of Domínguez, Leborgne subsequently demonstrated the diagnostic importance of the fine calcifications that may be detected radiographically in a high proportion of breast cancers. Leborgne stressed the need for high radiographic contrast and fine detail, a combination he obtained by the use of very low kilovoltage, a target-film distance of 60 cms, non-screen film, and optimal X-ray beam collimation. He also used the collimating cone to compress the breast, a technique that reduced both radiographic tissue scatter and patient motion. The combination of collimation and compression was later adopted by equipment manufacturers and is now a standard component of dedicated mammography machines. Of particular importance was Leborgne's observation that approximately 30% of breast cancers contained fine calcifications, particularly those of intra-ductal origin. These observations, made in 1949 and 1951, represented a significant step forward in the art and science of mammography.

Leborgne was appointed head of the Instituto de Radiología y Centro de Lucha Contra el Cáncer at the Hospital Pereira Rosseel and head of the Department of Cobalt Therapy of the Italian Hospital. Dr. Leborgne published numerous articles on radiological diagnosis of diseases of the breast. In 1949 he emphasizes breast compression for identification of calcifications. In 1953 he published his classic book on "The Breast in Roentgen Diagnosis".

Picture courtesy Alfredo Buzzi MD, Buenos Aires, Argentina 2004.



Malta MONTEVIDEANA



Es un alimento completo y de muy fácil asimilación

★ ★ ★

Todos los facultativos nacionales lo prescriben y recomiendan a sus convalescientes, por la persuasión adquirida en la práctica, y en el conocimiento de sus compuestos absolutamente naturales y de gran nutrición, y por la completa ausencia de alcohol.

★ ★ ★

Cervecerías del Uruguay



BOLETÍN DE LA SOCIEDAD DE CIRUGÍA DEL URUGUAY

Por eso a todo enfermo con un síndrome de oligo-anuria lo estudiamos del punto de vista humoral con hematocrito, proteinemia, volemia y estudio cuidadoso de su síndrome urinario (sedimento, densidad de orina). Se debe proceder frente a cada caso estudiando la fisio-patología del síndrome urinario para actuar sobre el factor pre-cámara renal; riñón o aparato excretor según la lesión predominante. Hemos visto en la Clínica casos de anuria en que teniéndose bien estudiado el déficit humoral benefician rápidamente con la transfusión en tanto que en otros casos esta medida terapéutica está contraindicada.

En otros ambientes se ha ido más allá en el estudio de la deshidratación; es así que por el volumen tiocianato se mide el espacio intersticial.

La importancia práctica de todo esto es que enfermos preagónicos con anurias de 48 horas de duración con uremias cerca de 4 grs., bien tratados, se restituyen.

Solo nos queda felicitar al Dr. Lockhart por su comunicación con la cual estamos enteramente de acuerdo.

Dr. Lockhart. — Yo quiero agradecer al doctor Fernández y al doctor Gordon el interés que se han tomado por mi comunicación, cuyo único valor es nada más que poner un poco al día un tema que me parece que es complejo, difícil, y en el que he tenido la suerte de tener experiencia y que me ha permitido sobre todo y en eso quiero insistir, ratificar dos cosas que son de importancia: 1º la existencia del síndrome de hepatonefritis traumática ratificado por la experiencia, ratificado por la clínica y por hechos necróticos inclusive; y en segundo término como cuestión terapéutica, la diálisis gástrica que ha sido tan eficaz, que hace que en el momento actual yo la haya adoptado casi sistemáticamente en los casos de oligo-anuria donde hay que esperar el período prudencial que implica la recuperación del nefrón.

BOLETÍN DE LA SOCIEDAD DE CIRUGÍA DEL URUGUAY

Instituto de Radiología y Centro de Lucha contra el Cáncer
del Ministerio de Salud Pública

Director: Dr. Félix E. Leborgne
Montevideo — Uruguay

*DIAGNOSTICO DE LOS TUMORES DE LA MAMA POR LA
RADIOGRAFIA SIMPLE*

Dr. Raúl Leborgne

Colaboración anátomo-patológica: Prof. Carlos M. Domínguez y
Dr. J. A. Mautone

A los clásicos elementos semiológicos que conducen al diagnóstico clínico en las afecciones mamarias, debe incorporarse actualmente el estudio radiológico de dicho órgano.

La patología mamaria es un tema de predilección en el Instituto de Radiología y Centro de lucha contra el Cáncer y tendremos el honor de someter a la consideración de la Sociedad de Cirugía, algunos capítulos y comentarios, sobre el diagnóstico radiológico de los tumores mamarios que ya han salido de la etapa de estudio y experimentación, para ser aplicados a la clínica diaria.

La exploración radiológica que fué tratada por primera vez en nuestro medio por los Profesores Carlos María Domínguez y Eduardo Blanco Acevedo no es lo suficientemente valorada y creemos que debe tener un sitio de preferencia en toda ficha mamaria.

El examen radiológico puede ser simple o mediante inyección de sustancias opacas en los galactóforos.

Nos ocuparemos en esta comunicación de la radiografía simple, debiendo destacar que su indicación es en las mamas con predominio de tejido adiposo donde el contraste radiológico es más notable y tal como suele verse en las mujeres más allá de los 40 años.

Con los perfeccionamientos técnicos radiológicos y de interpretación que en este campo hemos introducido, logramos actual-

* Esta comunicación fué presentada en la sesión del 4 de agosto de 1949.

BOLETÍN DE LA SOCIEDAD DE CIRUGÍA DEL URUGUAY

mente individualizar, con gran frecuencia, en medio del parenquima mamario, las distintas imágenes útiles para basar un diagnóstico preciso.

En estos casos, bien entendido que se requiere una amplia experiencia del tema, se obtienen tan brillantes resultados, que creemos que en un futuro próximo, la biopsia extemporánea verá limitadas sus indicaciones.

La compleja patología mamaria y la poca diferencia de opacidad entre los tejidos normales y patológicos hacen que el estudio radiográfico exija una técnica perfecta.

Técnica radiográfica

La proyección cráneo caudal es la indicada. Se realizará primeramente una placa topográfica utilizando un cono grande que abarque toda la mama y luego otra, localizando exactamente la región tumoral, con cono de diámetro lo más pequeño posible para evitar la radiación secundaria. — Fig. N° 1.

Esta última radiografía es la que tiene gran valor diagnóstico.

Como factores de técnica radiográfica empleamos los siguientes: 60 cm. de distancia foco placa, 30 K. V., 5 M. A. S. por centímetro de espesor de mama y películas "No Screen".

Creemos conveniente, además, para que se interponga la menor cantidad posible de tejido mamario, ejercer una ligera compresión con el cono, a través de una almohadilla de algodón interpuesta entre él y la mama.

Los tumores localizados en la proximidad del límite superior de la mama se aprecian con cierta dificultad en la proyección cráneo caudal, por cuya razón ésta debe ser complementada con una incidencia lateral.

Interpretación radiográfica

Vamos a considerar en esta comunicación las imágenes radiográficas más frecuentes, características y de real valor diagnóstico que hemos encontrado.

BOLETÍN DE LA SOCIEDAD DE CIRUGÍA DEL URUGUAY

Tumores benignos.

Los tumores benignos encapsulados, fibro-adenomas o quistes, dan una imagen redondeada o poli-lobulada, a límites nítidos, pudiendo presentarse a veces parcial o totalmente rodeada de un

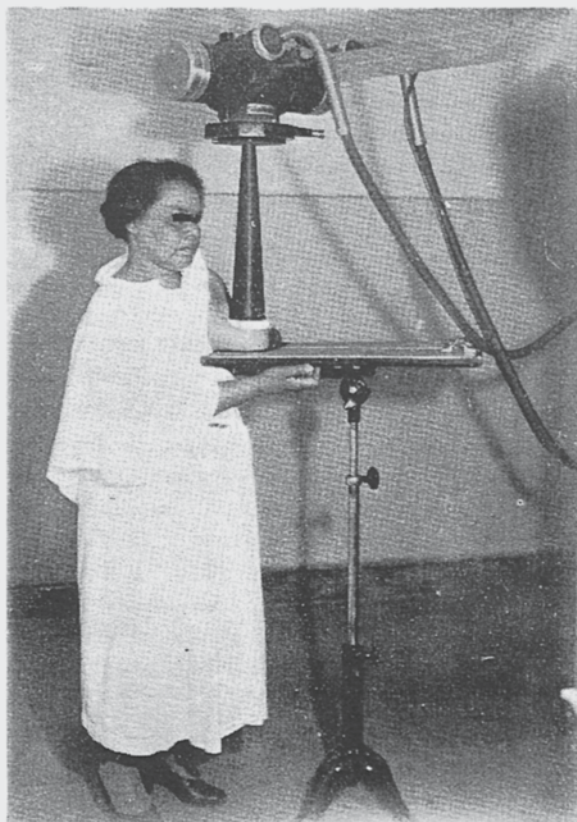


FIG. 1. — Posición de la enferma y enfoque radiográfico para la obtención de la placa cráneo caudal. Obsérvese las características del cono y la almohadilla compresora interpuesta entre él y la mama. La película está en contacto directo con la mama.

halo transparente que la separa del tejido mamario peri-tumoral (Fig. N° 5).

Son de tamaño sensiblemente semejante al que se aprecia clínicamente.

El estudio radiológico de los tumores encapsulados debe ser completado con la trans-iluminación en la cual el quiste a con-

BOLETÍN DE LA SOCIEDAD DE CIRUGÍA DEL URUGUAY

ESQUEMAS DE LOS PRINCIPALES ASPECTOS RADIOGRÁFICOS DE LOS TUMORES MAMARIOS

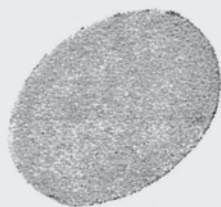


FIG. 2. — Tumcración encapsulada a límites nítidos.

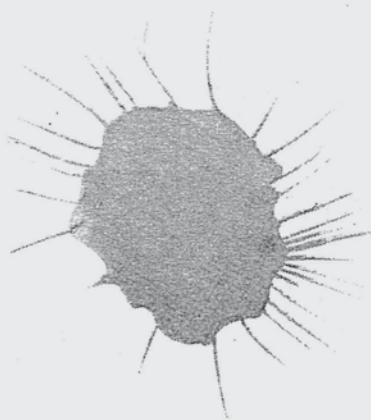


FIG. 3. — Contornos espiculados de un carcinoma esquirroso.

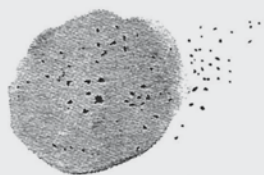


FIG. 4. — Pequeñas e incontables calcificaciones puntiformes, como granos de sal fina, en el nódulo tumoral y en su alrededores, propias de lesión maligna.

BOLETÍN DE LA SOCIEDAD DE CIRUGÍA DEL URUGUAY

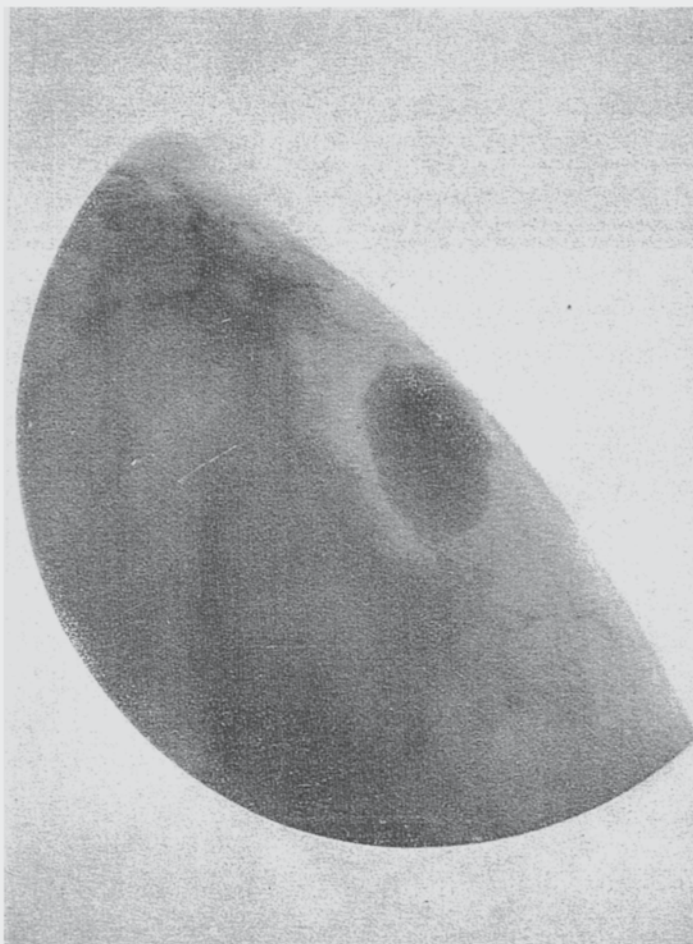


FIG. 5. — Nódulo a límites nítidos, discretamente polilobulados, con halo transparente en su límite externo. Fibroadenoma.

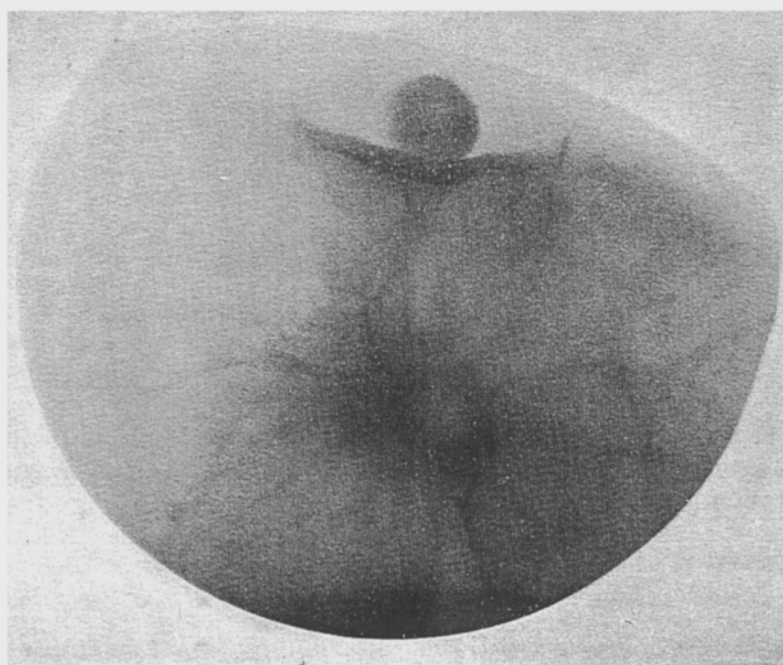
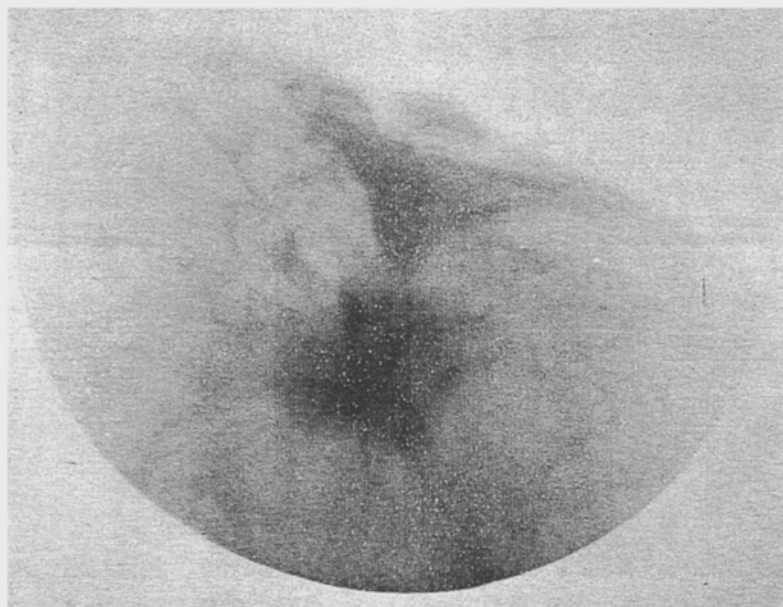
tenido citrino aparece transparente, el fibro-adenoma muestra mediana opacidad y el cisto-adenocarcinoma habitualmente por su contenido hemorrágico es de una notable opacidad.

Tumores malignos.

Las imágenes radiológicas más frecuentes de los adenocarcinomas de la mama tienen las siguientes características:

Forma: sensiblemente redondeada, pudiendo ser ocasionalmente polilobulada.

BOLETÍN DE LA SOCIEDAD DE CIRUGÍA DEL URUGUAY



FIGS. 6 y 7. — Nódulos de contornos espiculados típicos, propios del carcinoma esquirroso, con umbilicación del mamelón.

BOLETÍN DE LA SOCIEDAD DE CIRUGÍA DEL URUGUAY

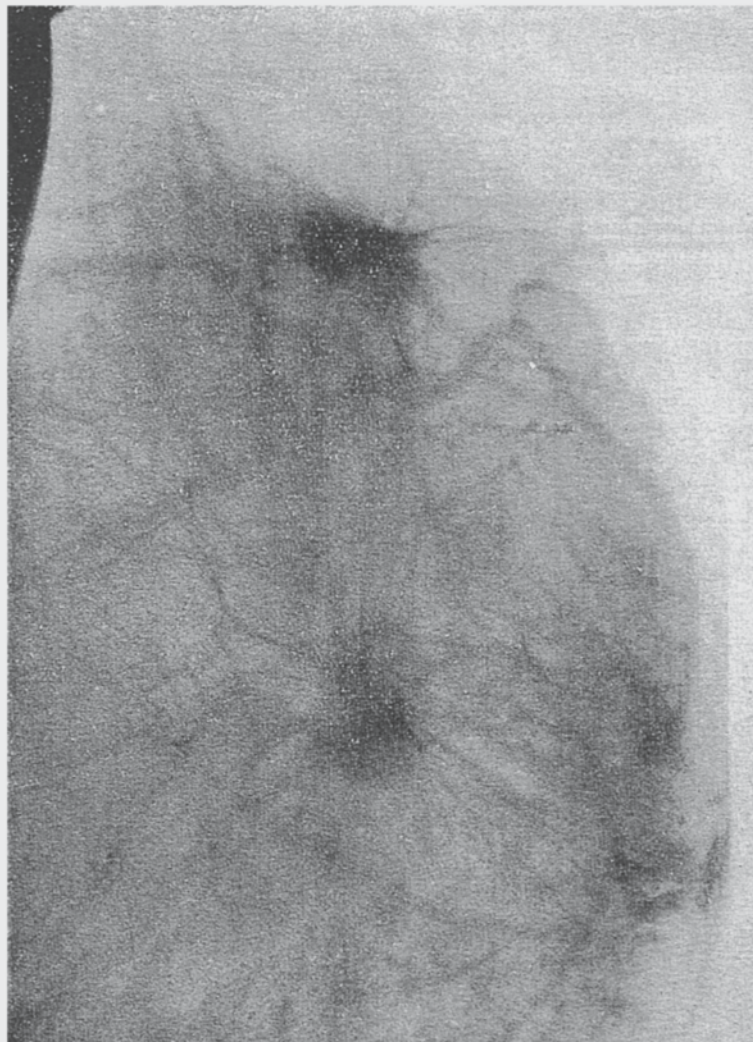


FIG. 8. — Se observan dos nódulos de contornos espiculados típicos, irradiados hacia el tejido mamario vecino y en forma de puente entre ellos. Corresponden a dos pequeños carcinomas esquirrosos, simultáneos en la misma mama, uno de ellos inapreciable a la palpación.

Tamaño: oscila generalmente entre 1 cm. y 4 cm., pero el elemento fundamental para el diagnóstico es que el tamaño que se aprecia en la radiografía es en general, menor que el que se determina clínicamente.

Contornos: habitualmente no muestran la nitidez de los tu-

BOLETÍN DE LA SOCIEDAD DE CIRUGÍA DEL URUGUAY



FIG. 9. — Forma espiculada típica, con incipiente propagación hacia la piel.

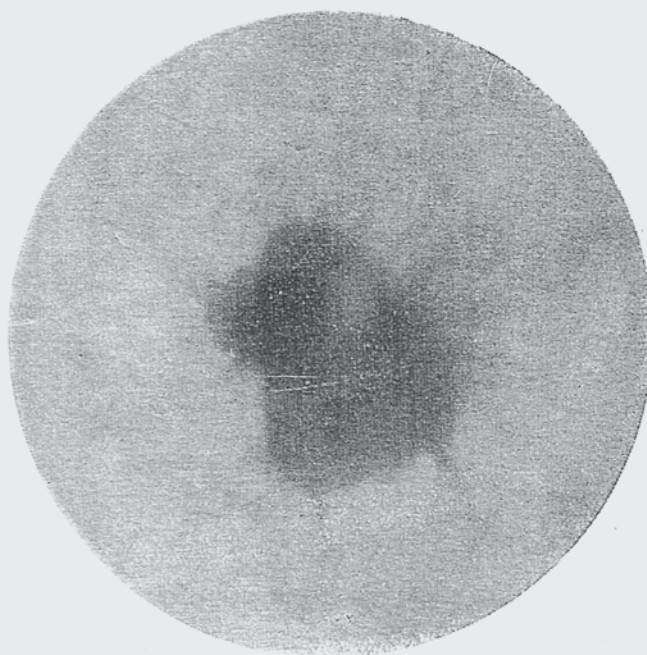


FIG. 10. — Forma poli-lobulada a límites netos, con escasas espículas.

mores benignos, presentando por el contrario numerosas espículas o dentelladuras, de longitud variable, que partiendo de su periferia se irradian hacia el tejido mamario vecino. Este aspecto espiculado les confiere un carácter típico de tumor maligno y tra-

BOLETÍN DE LA SOCIEDAD DE CIRUGÍA DEL URUGUAY

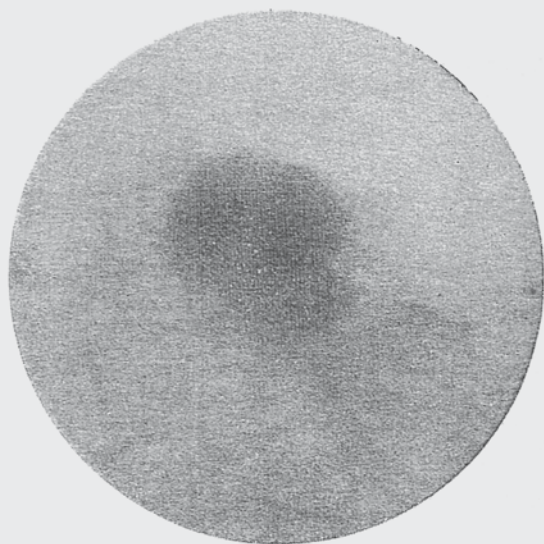


FIG. 11. Nódulo a límites precisos de contorno dentellado, epitelio-
ma.

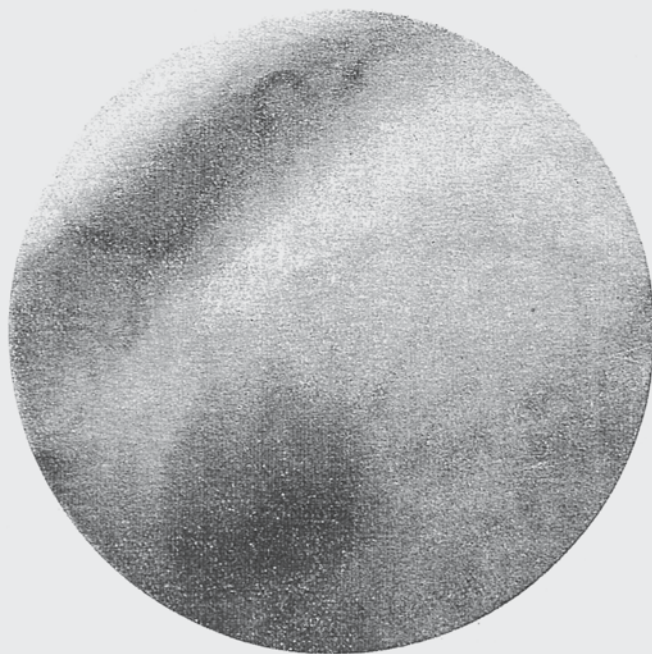


FIG. 12. - Nódulo a límites nítidos, con pequeñas espículas, epitelio-
ma esquirroso.

duce su naturaleza predominantemente esquirrosa. Fig Nº 3.

Ocasionalmente, presentan contornos nítidos bastante similares a los procesos encapsulados, y el diagnóstico radiológico

BOLETÍN DE LA SOCIEDAD DE CIRUGÍA DEL URUGUAY

diferencial en estos casos puede presentar dificultades, que se van allanando con la experiencia.

Densidad: sombra generalmente uniforme, pudiendo tener en

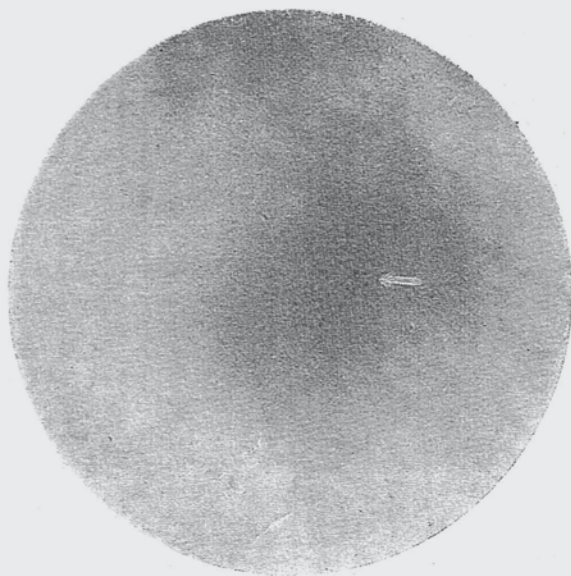


FIG. 13. — Numerosas e incontables pequeñas calcificaciones, como granos de arena, en el interior del nódulo tumoral.



FIG. 14. — Radiografía del corte anatómico de la pieza operatoria correspondiente a la radiografía de la figura anterior donde se aprecian las calcificaciones con más nitidez. El estudio histológico reveló un epiteloma canalicular del tipo comedo.

su interior una siembra de múltiples calcificaciones puntiformes. Estas calcificaciones que describimos, constituyen un signo radiográfico al cual le asignamos singular valor diagnóstico y pueden hallarse bajo estas tres formas: 1º — en el interior del nódulo,

BOLETÍN DE LA SOCIEDAD DE CIRUGÍA DEL URUGUAY

2º en el interior del nódulo y en su vecindad y 3º como único signo radiológico, es decir, sin imagen nodular tumoral.

Tanto los contornos espiculados como la siembra de calcificaciones puntiformes, cuando son bien características, constituyen

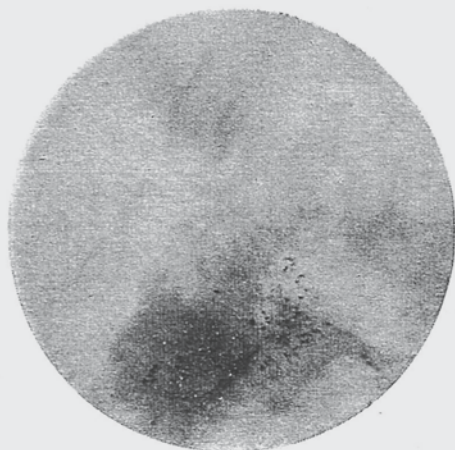


FIG. 15. — Se aprecian múltiples e incontables calcificaciones como granos de sal fina en el interior del nódulo y en su vecindad, características de lesión maligna

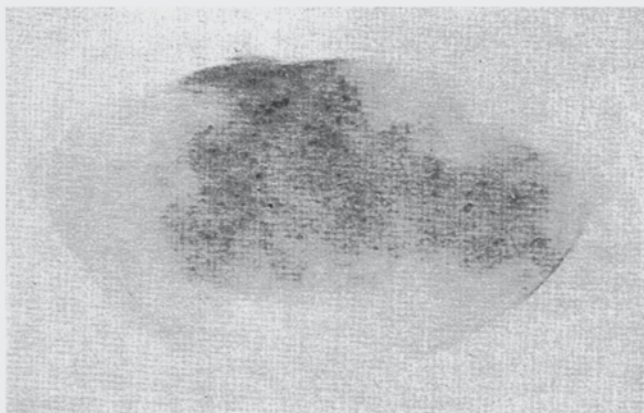


FIG. 16. — Siembra milliar de calcificaciones, sin imagen nodular en un carcinoma papilar.

yen imágenes radiológicas de tal jerarquía que permiten prescindir de la biopsia extemporánea.

Debemos recordar, que no todas las calcificaciones mamarias están asociadas a procesos malignos y que pueden encontrarse, también con mucho menor frecuencia, en procesos benignos, ya sea tumorales o como incrustaciones de los galactóforos o de los vasos sanguíneos.

BOLETÍN DE LA SOCIEDAD DE CIRUGÍA DEL URUGUAY



FIG. 17. En las paredes de los canales galactóforos se observan múltiples calcificaciones que no deben confundirse con las que describimos en este trabajo como propias de los tumores malignos.



FIG. 18. -- Imagen redondeada, encapsulada, transparente a los rayos X, correspondiendo a un galactoceles a contenido mantecoso.

Con cierta experiencia, el diagnóstico diferencial entre las calcificaciones de los procesos malignos, que hemos descripto y las calcificaciones de los benignos es en general fácil. Estas últimas, especialmente en el fibro-adenoma, se diferencian de las cal-

BOLETÍN DE LA SOCIEDAD DE CIRUGÍA DEL URUGUAY

cificaciones malignas en que son más grandes y por lo tanto más visibles, se presentan en menor número, tienen un carácter confluyente, o una disposición circular periférica en la cápsula del tumor.

Las calcificaciones de los galactóforos son también muy visibles, tienen límites paralelos o contornos circulares, según la proyección radiográfica y cierta tendencia a convergir hacia el mamelón cuando es un proceso generalizado.

El contraste de la sombra nodular, aunque no es muy grande, alcanza en general a distinguirse del tejido mamario, siempre que se reúnan las siguientes condiciones: el empleo de una técnica radiográfica apropiada, que la mama sea predominantemente grasosa y que el tumor no esté localizado en la periferia de los cuadrantes superiores.

El hecho de no visualizar un tumor no tiene valor diagnóstico, pues existen, especialmente algunas formas encefaloideas, sin traducción radiográfica, pudiéndose en este caso, emplear la tomografía como técnica auxiliar. Y en general diremos, que cuando no se encuentra imagen radiográfica que justifique el tumor palpable, debe practicarse la exploración bióptica sin pérdida de tiempo.

BIBLIOGRAFÍA

- ADAIR, (F. E.). — Sanguineous Discharge from the Nipple and its Significance in Relation to Cancer of the Breast. — "Ann. of Surg.", 91: 197 (Feb. 1930).
- BARALDI, (A.). — Roentgeno-neumo-mastia. — Bol. y Trab. de la Soc. de Cir. de Buenos Aires, 1934, 18, 1254-1267.
- BARALDI, (A.). — Roengeno-neumo-mastia, "Rev. Med. del Rosario", 1935, p. 1536.
- BARALDI, (A.). — Roentgeno-neumo- mastia. — "Rev. de Cir. de Buenos Aires", 1935, 14, 321-343.
- BLANCO ACEVEDO, EDUARDO y DOMINGUEZ, CARLOS MARIA. — La Radiografía de la mama dinámica. — "Anales del Departamento Científico de Salud Pública". Volumen II, Fascículo I, 1935.
- BOTTARO, (L. D.). — Pezón sangrante. — V Jornadas Rioplatenses de Obst. y Ginecolog., 1944, p. 539-554.
- BUTLER, (C.), CAPRIO, (G.) y DOMINGUEZ, (C. M.). — Cáncer de la mama, 1940. Edit. García Morales.

BOLETÍN DE LA SOCIEDAD DE CIRUGÍA DEL URUGUAY

- CONWAY, (J. H.). — Calcified Breast Tumors. — "Am. J of Surg.", 31: 72 (Jan. 1936).
- CHEATLE & CUTLER, (M.). — Tumors of the Breast. Ed Arnold, London 1931.
- DOMINGUEZ, (C. M.). — Estudio sistematizado del cáncer del seno. "Bol. de la Liga Urug. contra el Cáncer Genit. Femen.", N° 23, 1929.
- DOMINGUEZ, (C. M.). — Estudio radiológico de los descalcificadores. — "Bol. de la Soc. de Anatomía Patológica". Tomo I, Fascículos I y II. año 1930. Pág. 175.
- DOMINGUEZ, (C. M.) y LUCAS, (ANTONIO). — Investigación radiográfica y química sobre el calcio precipitado en tumores del aparato genital femenino. — "Bol. de la Soc. de Anatomía Patológica". Tomo I, Fascículos I y II, año 1930. Pág. 217.
- FRIEDMAN, (L.) and SLATER (C.). — Mammography-Soft Tissue Technique. — "Am. J. of Surg.". — 41:310 (Aug. 1938).
- GERSON-COHEN, (J.) and COLCHER, (A. E.). — An evaluation of the Roentgen Diagnosis of Early Carcinoma of the Breast. — J. A. M. A. — 108:867 (March. 13, 1937).
- GUNSETT et SICHEL. — Sur la Valeur Pratique de la Radiographie du Sein. — "Jour. de Radiol. et d'Electrolog.". — 18:611 (Dec. 1934).
- HICKEN, (N. F.). — Mammography; Roentgenographic Diagnosis of Breast Tumors by Means of Contrast Media. — "Surg. Gynec. & Obst.". — 1937, 64, 503-603.
- HICKEN, (N. F.). — Mammography. Preoperative Visualization and Diagnosis of Breast Tumors by Contrast Roentgenograms. Nebraska, M. 1937, 22, 211-213.
- HICKEN, (N. F.). — Radiographic demonstrations of Breast Lesions. — "Radiolog. & Clin. Photog., 1937, 13, 2-9.
- HIKKEN, (N. F.), BEST, (R. R.), MOON, (C. F.), & HARRIS, (T. T.). — Preoperative Visualization of Breast Tumors. — "J. Amer. Assoc., 1937, 108, 864-867.
- HICKEN, (N. F.), BEST, (R. R.) & TOLLMAN, (J. P.). — Mammographic Recognition of Intracystic Papillomas of the Breast. — "J. Surg.", 1937, 36, 611-617.
- HICKEN, (N. F.), BEST, (R. R.), & HUNT, (H. B.). — Discharges from the Nipple; their Clinical Significance & mammographic Interpretation, "Arch. Surg". 1937, 35, 1079-1094.
- HICKEN, (N. F.) & HUNT, (H. B.). — Evaluation of Various Diagnostic Procedures used in the Study of the Breast, with Particular Reference to Roentgenographic Examination. "Radiology", 1939, p. 71
- LINGLER, (J. R.) and ELLIOT, (W. J.). — The Roentgen Diagnosis of Lesions of the Breast. — in "Golden's Diagnosis Roentgenology",

BOLETÍN DE LA SOCIEDAD DE CIRUGÍA DEL URUGUAY

- New York, Tomas Nelson & Sons, 1941, Vol. II.
- LOCKWOOD, (I. H.). — The Roentgen-Ray Evaluation of Breast Simplex. — "Am. J. Roentgenol". 29:145, (Feb. 1933).
- LARGHERO, (P.) y COSTA, (S. S.). — Grandes Tumores Benignos del seno. — "Bol. de la Soc. de Ciruj. de Montevideo, Tomo III, N.º 11, 1932.
- LEBORGNE, (RAUL). — Monografía. Estudio radiológico del Sistema Canalicular de la glándula mamaria normal y patológica. Montevideo, 1943.
- LEBORGNE, (RAUL). — Diagnóstico de los procesos patológicos de la mama por la radiografía con la inyección de medios de contraste. — "Obst. y Ginec. Latino Americ." — Julio 1944, N.º 7, p. 551-561.
- LEBORGNE, (RAUL). — Biopsia por Vía endo-canalicular en los procesos patológicos de la glándula mamaria. — "Obst. y Ginec. Latino-Amer.", Agosto, 1944, N.º 8, pp. 605-614. — "Archiv. de Ginec. y Obst.", Diciembre 1944, T. III, p. 331-346. — Surgery, January, 1946.
- LEBORGNE, (F. y R.). — Endoscopia de los canales galactóforos. "V. Jorn. Rioplatense de Obst. y Ginecolog.". Junio 1945, T. IV, p. 107. 114. — "Archivos de Ginecología y Obstetricia", N.º 3, junio de 1945.
- LEBORGNE (RAUL). — Estudio radiológico de la glándula mamaria. — "Boletín de la Sociedad de Cirugía". — Tomo XVII, N.º 7 y 8, págs 336 a 364, 1946.
- LEBORGNE, (RAUL) y DOMÍNGUEZ, (C. M.). — Estudio Anátomo-Radiológico de los tumores intracanales de la mama. — Primer Congreso Uruguayo de Ginecología, 1949.
- LECENE, (P.), GALTIER, (M.). — Remarques sur le Traitement Chirurgical des Tumeurs Végétantes Intra Canaliculaires du Sein. — "Journ. de Chirurgie", T. 31, N.º 4 Avr. 1928, p. 481-496.
- LEDoux-LEBARD, (R.), GARCIA CALDERON, (J.) et ESPAILLAT, (G. A.). — Radiographie de Sein. — "Com. à la Soc. de Radiol. Medic. de France" (Seance 9 mai, 1933).
- ORWOOD, (J.), CAMPBELL, (D. M.). — The Bleeding Nipple, — "Surgery", January, 1946.
- RIESCO UNDURRAGA (A). — Estudio anátomo-radiológico de la glándula mamaria. — Monografía. — Santiago de Chile.
- REIS, (R. A.) and MESIROW, (S. D.). — Studies in the Evaluation of Mammography. — J. A. M. A. 110:1900, (June 4th), 1938.
- RIES, (E.). — Diagnostic Lipiodol Injection into the Milk Ducts Followed by Access Formation. — "Am. J. Obst. and Gynec.", 20:414 (Sept.) 1930.
- RITVO, (M.), BUTLER, (P. F.); O'NEIL, (E. E.). — Roentgen Diagnosis of Tumors of the Breast. — J. A. M. A. 105:343 (Aug. 3), 1935.

BOLETÍN DE LA SOCIEDAD DE CIRUGÍA DEL URUGUAY

- SALOMON. --- Beitrage sur Pathologie und Klinik der Mammatumoren, "Arch. f. Klins Chirurgie", 1913, 101, 573.
- SEABOLD, (P. S.). --- Diagnosis of Breast Diseases by X Ray., "Ann. Of. Surg.", 94:443 (Sept.) 1931.
- SEABOLD, (P. S.). --- Roentgenographic Diagnosis of Diseases of the Breast. --- "Surg. Gynec. and Obst.", 53:433 (Oct.), 1931.
- WARREN, (S. L.). --- A Rontgenologic Study of the Breast, "Am. Roentgenol", 24:113 (Aug.) 1930.

8.2 La radiographie de la glande mammaire

Charles Marie Gros (1910–1984)

Charles M. Gros was born on 12 August 1910 in Aigues. He studied mathematics and physics and received his diploma in 1928 and 1929. Under the direction of Professor Lamarque from Montpellier Gros started to study medicine and obtained his MD in 1943. He became chief of the radiotherapy service of the Centre Régional Anticancéreux de Strasbourg in 1947 and the department of radiology in 1949. In 1951 he became interested in investigations of breast pathology and published with his co-worker Sigrist his paper on “La radiographie de la glande mammaire” which initiated a new phase in mammography in Europe. In 1963 he described the interrelationship of pathology, clinical examination, histology and radiology. Gros also described the typical carcinomatous configurations of microcalcifications in intraductal comedo carcinoma and pointed out the irregularity of separate micro-particles. This work formed the basis for the future analysis of the differences between benign and malignant microcalcifications of the breast.

Gros’s revolutionary achievement was the technical improvement of mammography by using a molybdenum anode X-ray tube, which was originally developed for non-destructive testing. In co-operation with CGR he developed in 1965 the “Senograph”, which was the first X-ray unit dedicated to mammography.

He was appointed Professor of Radiology at the University of Strasbourg, a position he held until his retirement in 1979. Charles Gros died on 11 November 1984.

Picture courtesy Dr. René van Tiggelen, Belgian Museum for Radiology.



R. Sigrist



LA RADIOGRAPHIE DE LA GLANDE MAMMAIRE

par le Prof. agr. Ch. M. GROS et D^r R. SIGRIST (Strasbourg).
(Centre Anti-Cancéreux.)

La mammographie n'a pas encore la place qu'elle mérite dans le radiodiagnostic; née tardivement, son développement fut très lent. Malgré quelques discrètes apparitions dans différents pays à plusieurs époques, elle est restée pendant longtemps ou méconnue ou dédaignée. Cependant les différents travaux, surtout de ces dernières années, montrent qu'elle est en voie d'atteindre sa maturité et qu'elle peut prétendre compléter un examen détaillé de la mamelle et s'intégrer dans le radiodiagnostic.

Son histoire peut schématiquement se diviser en trois parties de 17 ans.

Première période : 1896-1913. — Nous n'avons pas trouvé de publications pendant cette période en dehors de celle faite par Salomon dans les archives de chirurgie de Berlin en 1913. Ce travail original, très détaillé, intéressant à plusieurs points de vue, étudia les rapports de la clinique, de la radiologie et de l'histologie des cancers du sein : ses conclusions si elles sont incomplètes, nous paraissent pleines d'actualité. Les clichés se rapportent aux pièces opératoires, mais sont démonstratifs.

Deuxième période : 1913-1930. — Ces radiographies restèrent sans écho.

Troisième période : 1930-1947. — C'est la période où vont apparaître régulièrement des travaux sur la radiographie du sein. Warren de Rochester étudie le premier sur le vivant, la grande pathologique. Ries injecte du lipiodol dans les galactophores. Pasqueta en France fait une communication à la Société de Radiologie Médicale sur l'intérêt de la mammographie dans le diagnostic de la grossesse. Romagnoni en Italie, Seabold à Philadelphie s'inté-

ressent aux modifications radiologiques au cours du développement de la glande. Vogel en Allemagne cherche les images qui distinguent la mastite chronique du cancer. En 1933, Espaillat dans sa thèse fait le point de la question en continuant les travaux de Ledoux-Lebard et Garcia-Calderon. Fray et Warren attirent l'attention sur la stéréoradiographie de la glande mammaire. Hicken publie en 1937 de nombreux documents et la Sémiologie Radiologique commence à se préciser. Cet auteur après Baraldi injecte comme moyen de contraste de l'air dans tout le tissu péri-glandulaire. Avec Raoul Leborgne de Montevideo, cette exploration prend à partir de 1947 un renouveau d'actualité. Ses nombreux clichés, ses confrontations anatomo-pathologiques, son étude des calcifications, démontrent l'intérêt de la radiographie simple.

Malgré ces quelques tentatives, ces publications faites dans divers pays, à différentes époques, ce radiodiagnostic surtout sans préparation, n'a pas encore connu une brillante carrière. Est-ce parce que les indications n'étaient pas impérieuses?

Les diagnostics des cancers avancés étaient les plus nombreux et les plus évidents; quant aux cas douteux, si les uns demandaient au microscope une ligne de conduite, d'autres se contentaient d'une impression clinique pour pratiquer une exérèse large et immédiate.

Ou bien, est-ce parce que la radiographie mammaire avait encore trop de servitudes : Technique délicate, clichés peu contrastés, perdant toute signification par projection ou publication, interprétation non codifiée.

Mais actuellement, les conditions se modifient.

D'une part : L'investigation de la glande mammaire devient plus précoce : que conclure après une palpation détaillée sur la nature d'un nodule avec ou sans signe d'accompagnement? La biopsie systématique n'est pas toujours la solution idéale; comment surveiller une mamelle tumorale sans comparaison de documents; la thérapeutique du cancer du sein est si variée que le moindre renseignement morphologique ne serait pas inutile.

D'autre part : La mammographie a fait des progrès suffisants dans la prise des clichés et l'interprétation pour être déjà une technique utile.

C'est à la suite de ces travaux, en nous aidant des recherches faites sur la radiographie des tissus mous par Zuppinger, Melot,

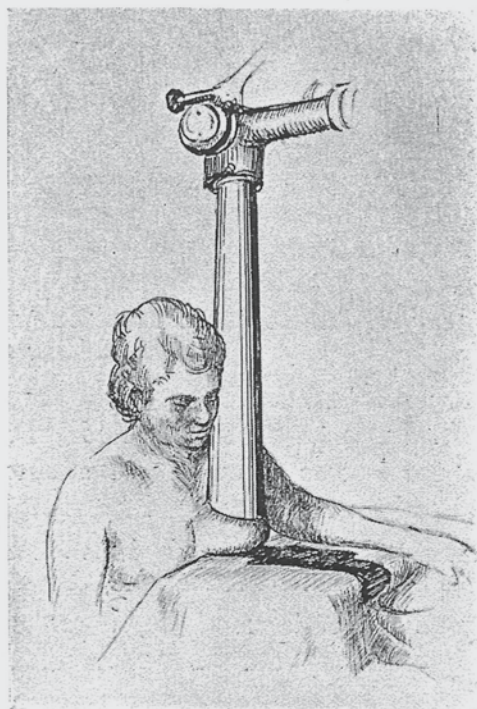


FIG. 1. — Incidence cranio-caudale.

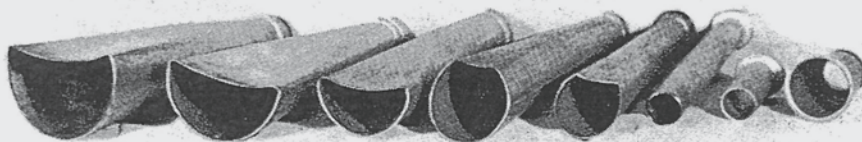


FIG. 2. — Les localisateurs utilisés pour la mammographie

Franz Arne, que devant les défaillances de la clinique, les servitudes de la biopsie, la nécessité d'avoir un document, nous avons depuis 20 mois abordé cette étude. Quatre cent cinquante seins normaux et pathologiques ont été radiographiés et plus de 2500 clichés ont été pris. Notre opinion sur cette investigation est faite : elle doit devenir un examen de routine. Sans doute, elle se perfectionne dans l'obtention et la signification des images, mais dès maintenant, son utilité, sa valeur sont suffisantes pour en généraliser l'emploi.

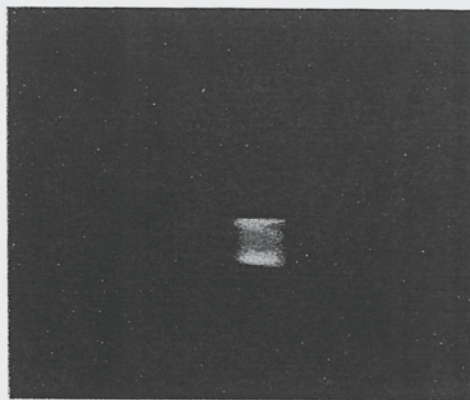


FIG. 3. — Image du foyer 3/3 mm. environ.

Technique.

L'analyse radiologique de la glande mammaire peut être faite sans préparation ou avec injection de produits de contraste.

I. — *Technique sans préparation :*

La radiographie simple.

C'est une radiographie des tissus mous, les clichés doivent être faits en séries dans le temps et dans l'espace; adoptés à la malade et à la maladie. C'est une technique facile, mais longue et méticuleuse, peu spectaculaire mais sans danger et sans douleur; demandant plus au radiologiste qu'à l'appareillage. Enfin l'étude des clichés eux-mêmes exige beaucoup de soins.

a) Radiographie adaptée aux tissus mous :

230

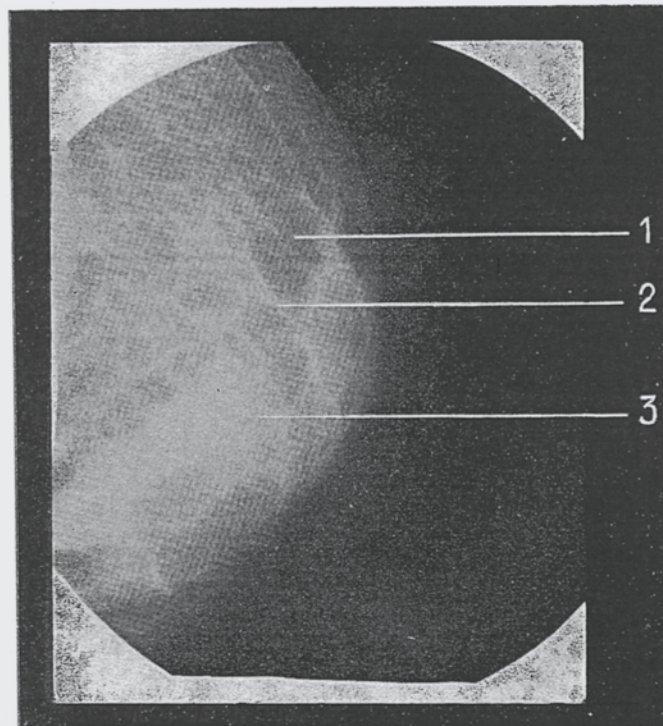
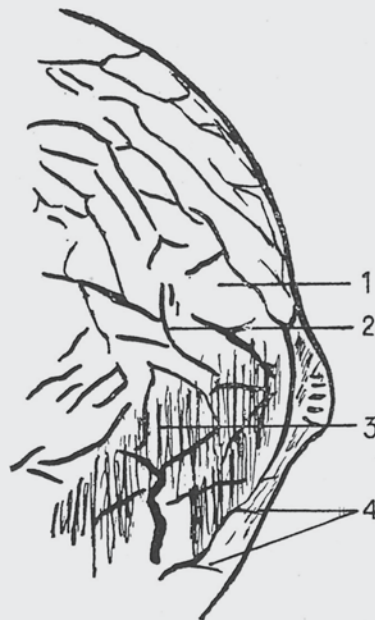
PROF. C. M. GROS & D^r R. SIGRIST

FIG. 4. — Sein normal chez une femme âgée de 35 ans normalement réglée.

- 1) Lobule adipeux.
- 2) Cloison fibreuse interlobulaire.
- 3) Tissu glandulaire.



Les constituants élémentaires de la glande mammaire normale ou pathologique, ont des poids atomiques faibles et très voisins en-dehors du calcium, élément rare ou peu abondant. Les images par conséquent sont peu contrastées et correspondent soit à des différences d'épaisseur traversées, toujours très faibles, soit à des légères différences de densité. Seules les images des calcifications seront très opaques. Les lobules de graisse sont les plus transparents tandis que la peau, surtout prise tangentiellement est l'élément le plus opaque.

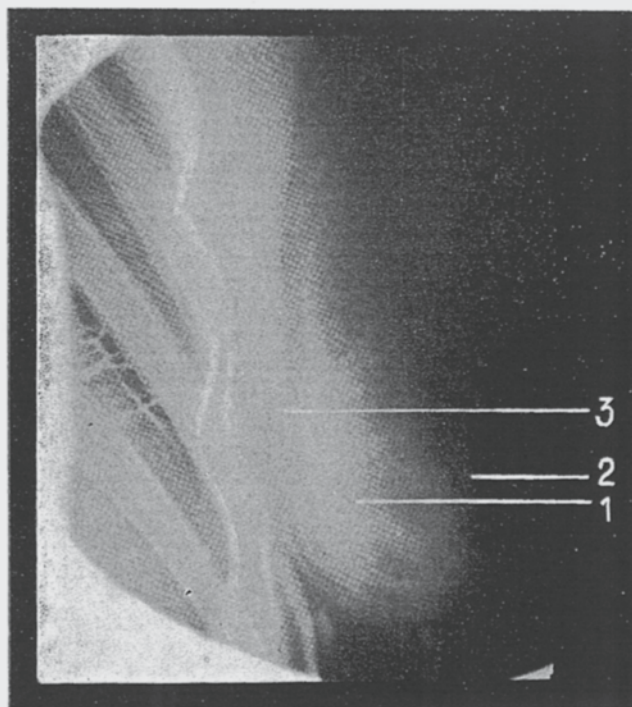


FIG. 5. — Sein normal, profil.

- 1) Glande mammaire.
- 2) Mamelon.
- 3) Ligne claire rétro-mammaire.

(Voici à titre d'exemple les densités prises dans une de nos pièces opératoires extirpée pour épithélioma du sein : Graisse 0,86; Mastite scléro-kystique 0,98; Tumeur 1,03, Mamelon 1,08; Peau 1,13).

Le contraste des images et la finesse du dessin ne sont obtenus qu'en tirant partie au maximum des différents facteurs géométriques, physiques et photographiques. Le foyer doit être fin (fig. 3) la distance est de l'ordre de 80 cm, mais quelques fois pour les

tumeurs superficielles nous pratiquons la radiographie de contact. Les meilleurs contrastes semblent obtenus avec des voltages variant de 30 à 40 kv selon l'épaisseur traversée. La diffusion est réduite le plus possible par la compression du sein, les localisateurs adaptés (fig. 2) exactement à la forme et au volume aussi bien du sein que de la tumeur. La grille antidiffusante n'est employée qu'exceptionnellement pour les seins trop épais; et les écrans renforçateurs sont supprimés. Le film est à grain très fin. L'examen des clichés doit être fait avec beaucoup d'attention, au

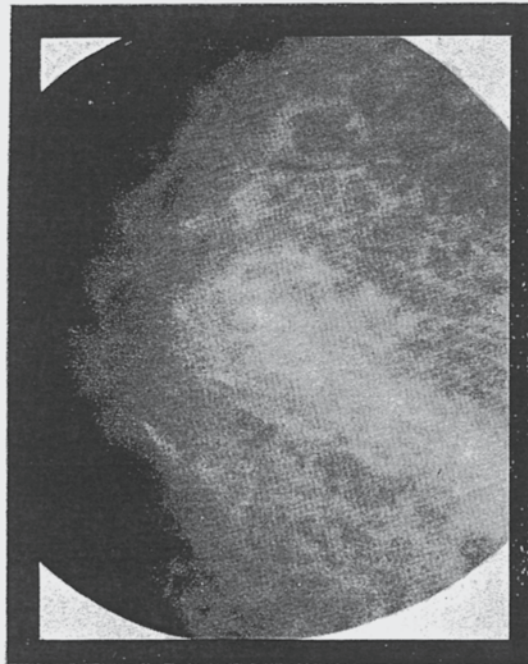


FIG. 6. (333/51.) — Rétraction du mamelon par sclérose banale.

Clinique : mamelon rétracté, ombiliqué chez une femme âgée de 57 ans, à la palpation des trainées dures et lisses rétractent le mamelon.

Radio : mamelon rétracté avec nombreuses trainées opaques filant vers les parties postérieures médianes de la glande mammaire sans image tumorale visible.

Histologie : après mastectomie totale sclérose sans signe histologique de malignité. (Prof. GÉRY.)

moyen d'un négatoscope dont la surface et l'éclaircissement variables s'adaptent aux images étudiées et permet ainsi de surprendre tous les détails du cliché, en particulier les calcifications miliaires.

Les constantes utilisées dépendent de trop de facteurs pour les préciser rigoureusement. Voici un exemple pour situer l'ordre de grandeur : 80 cms de foyer-peau, nous utilisons si la glande d'une

épaisseur de 8 cm. est normale, chez une femme jeune, 35 Kv et 100 mA-Sec. (Tableau I.)

Pour une même épaisseur, nous utilisons quelques kilovolts de plus si la mamelle présente une infiltration assez étendue avec le même nombre de mA-Sec; au contraire pour une glande adipeuse, chez une vieille femme nous diminuons de quelques K.V. Si la



FIG. 7. (997/51.) — Mastite chronique scléro-kystique avec gros kyste.

Clinique : Voussure de 4 cm. de diamètre avec rougeur des plans cutanés et circulation veineuse saillante dans la région tumorale; écoulement d'un liquide citrin de 3 canaux galactophores, à la compression on palpe une masse tumorale de 5 cm. de diamètre d'une dureté élastique, polycyclique, bien mobile, non adhérente, mais irrégulière.

Transillumination : transparence partielle avec léger flou.

Mammographie : opacité arrondie à contours nettement limités sur les bords externes, homogène. Tissus voisins glandulaires refoulés et parfaitement normaux dans le reste de la glande.

Histologie : mastite chronique scléro-kystique avec grand kyste sans signe de malignité. (Prof. GÉRY.)

mamelle est moins épaisse nous réduisons le kilovoltage. Lorsque le localisateur est très étroit le temps de pose est légèrement augmenté.

Enfin nous pratiquons systématiquement en incidence craniale sur le même film si le sein n'est pas trop volumineux.



FIG. 8. — Même malade, radiographie dite de contact reproduisant plus nettement tous les signes décrits sur l'image standard.

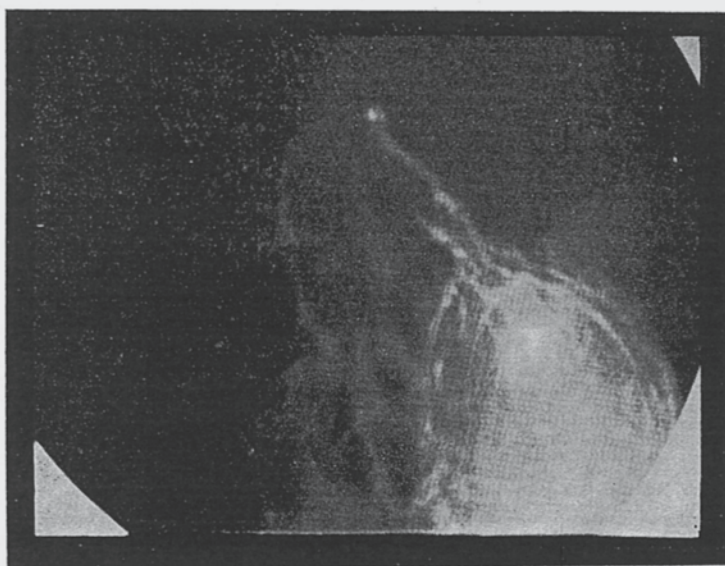


FIG. 9. — Même malade, injection du canal galactophorique qui met en évidence une formation kystique, dont le volume radiologique correspond exactement au volume tactile.

3 clichés de la mamelle suspecte en variant légèrement le temps de pose de façon à obtenir des radiographies de dureté différentes; 1 seul cliché pour le sein normal.

b) Nécessité des clichés en séries dans le temps et dans l'espace.

1° *Incidences* : La station debout avec incidence cranio-caudale nous paraît être fondamentale comme pour Leborgne (fig. 1). Le cliché peut aussi être pris dans d'autres conditions, mais pour

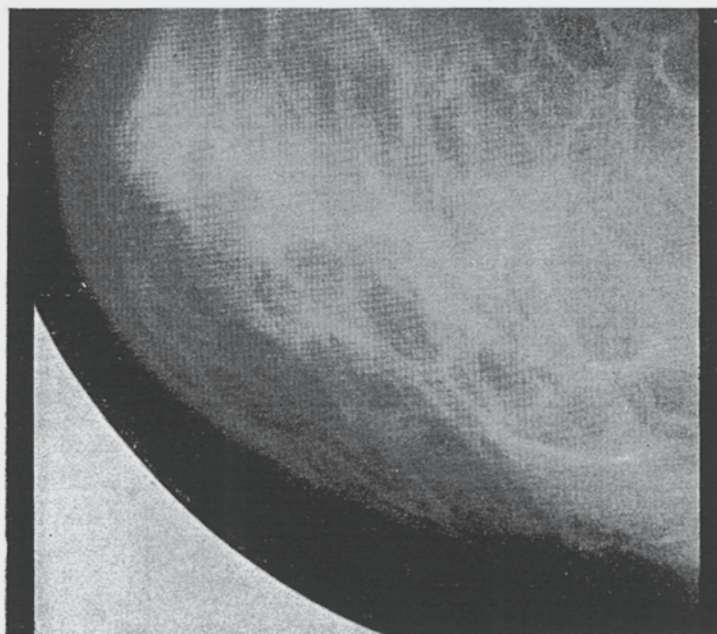


FIG. 10. (2175/51.) — Kyste suppuré.

Clinique : malade de 25 ans, peau d'orange rouge avec masse sous-jacente, dure, de 3 cm. de diamètre ayant rapidement augmenté de taille, ganglion dur et mobile au niveau du creux axillaire.

Radio : œdème très prononcé de la région cutanée sus-jacente à la tumeur, aspect feuilleté du derme, la formation tumorale est arrondie, son volume correspond au volume tactile, les contours sont nets, son opacité est homogène, il n'y a pas d'infiltration des tissus voisins.

Histologie : mastite subaiguë avec grand kyste, sans signe de dégénérescence maligne. (Prof. GÉRY.)

nous ce sont des incidences secondaires. Clichés en oblique ant. ou post. selon la situation de la tumeur ou de profil. Le décubitus est conseillé par Ledoux-Lebard; la malade est couchée sur la table radiologique, le bras relevé le long de la tête. Cette position permet de prendre outre l'image de la glande mammaire, la région axillaire. Le procubitus (—) sur une table spéciale creusée

236

PROF. C. M. GROS & D^r R. SIGRIST

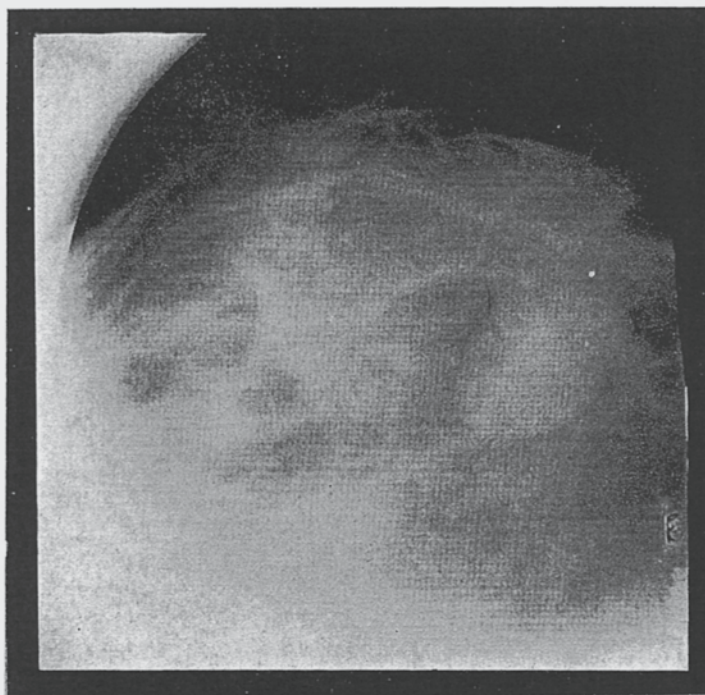


FIG. 11. — Même malade, radiographie dite de contact, tous les signes radiologiques sont plus accentués par rapport à l'image standard.

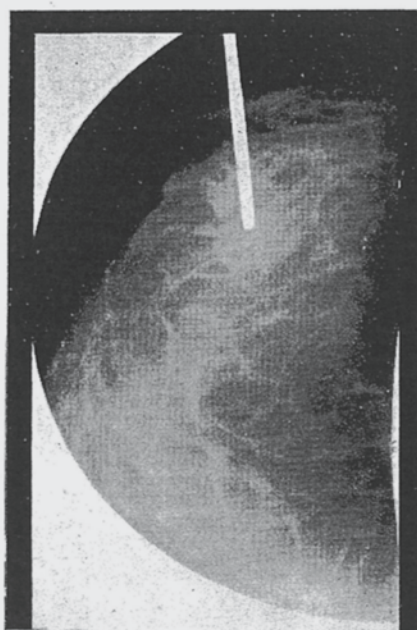


FIG. 12. — Même malade. ponction à la foreuse électrique

d'une ouverture à travers laquelle pend le sein, est utilisé par Gerson-Cohen. En dehors des 3 clichés en incidence fondamentale cranio-caudale qui sont faits systématiquement pour toutes les glandes mammaires, quelques radiographies sont prises dans des conditions qui varient avec la forme du sein et localisation tumorale.

Un cliché est pris toujours avec un localisateur étroit adapté aux dimensions de la tumeur.

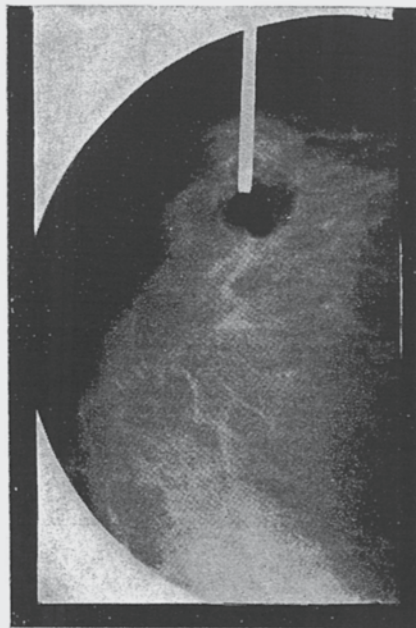


FIG. 13. — M:ême malade, injection d'air après évacuation au trocard.

2° Répétition des examens.

Quelques fois cet examen est repris loin des règles, le sein est alors moins congestionné, se laisse mieux analyser (Espaillat). Cet examen est aussi repris lorsque les premiers clichés paraissent douteux ou pour suivre l'évolution de la tumeur spontanément ou après une thérapeutique.

II. — Technique avec injection de produits de contraste : mammographie.

a) *Galactophorographie* : le corps utilisé est le diodone, substance qui n'a pas la viscosité du lipiodol auquel on a reproché

certaines complications inflammatoires par stagnation dans les canaux ou dans certaines cavités, ni la radio-activité du thorotrast. L'entrée des galactophores est légèrement dilatée avec des sondes

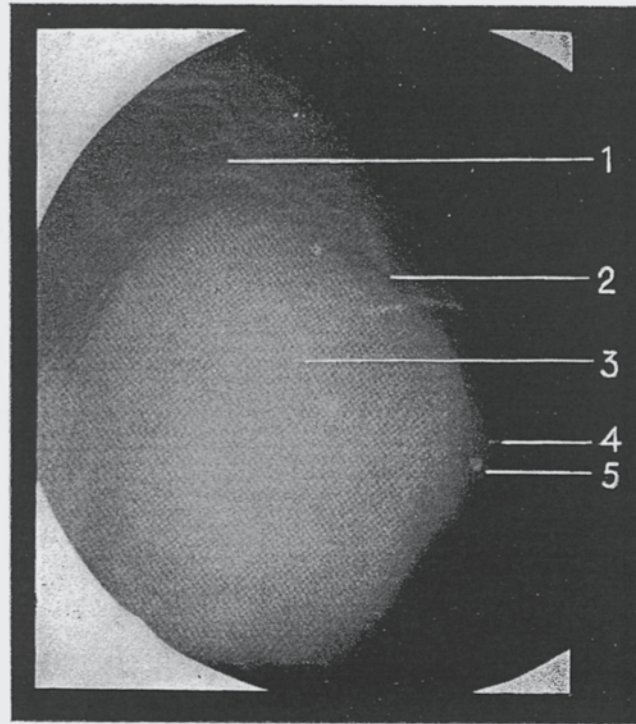


FIG. 14. (2077/50.) — Tumeur bénigne phyllode.

- 1) Tissu adipeux.
- 2) Liseré clair pérítumoral.
- 3) Masse tumorale.
- 4) Mamelon.
- 5) Calcification de type bénin.

Clinique : malade de 63 ans présentant une tumeur polycyclique à contours irréguliers de 7 cm. de diamètre avec légère peau d'orange au niveau des quadrants supérieurs, pas d'adénopathie, dureté ligneuse.

Transillumination : masse arrondie, très opaque à contours irréguliers.

Mammographie : opacité homogène relativement intense de volume égale au volume tactile, à contours nets, réguliers, avec liseré clair pérítumoral, sans infiltration du tissu glandulaire, qui est simplement refoulé, deux volumineuses calcifications se trouvent à la périphérie de la masse tumorale. Syndrome radiologique de tumeur bénigne.

Histologie : considérée cliniquement comme tumeur maligne, l'examen histologique est pratiqué après Halsted :

« Tumeur phyllode, hyperplasie épithéliale avec exubérance conjonctive sans aucun signe de malignité. » (Prof. GÉRY.)

métalliques comparables à celles utilisées pour le canal lacrymal. Le repérage des orifices est facilité par un léger massage et surtout par une goutte de sérosité. L'injection, faite à faible pression au

moyen d'une aiguille à glande lacrymale, n'est pas douloureuse. La radiographie doit être faite immédiatement car le diodone diffuse très vite dans la glande elle-même pour s'éliminer ensuite très rapidement. Une heure après l'injection, il n'y a plus trace de produit opaque dans les galactophores. L'injection des galactophores surtout s'il y a un écoulement est pratiquée successivement.

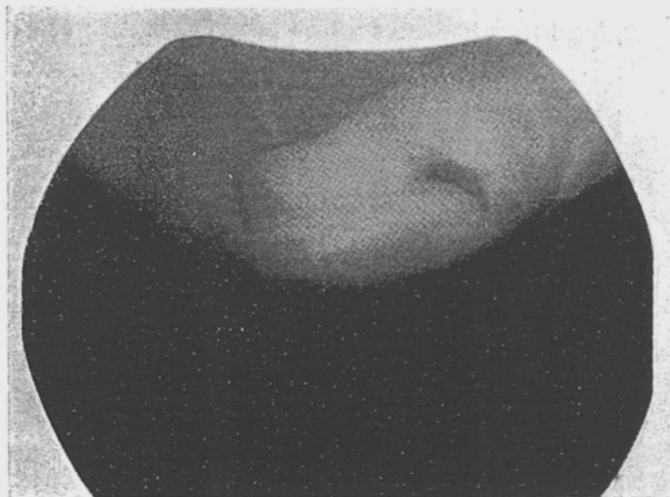


FIG. 15. (294851,) — Adénofibrome.

Incidence standard :

- 1) tissu mammaire,
- 2) liseré clair,
- 3) masse tumorale.

Jeune femme de 25 ans présentant depuis un an deux nodules rétro-mammaires soudés, réguliers, bien mobiles, de consistance élastique, indolores à la palpation.

Transillumination : opacité accentuée à la partie centrale et s'estompant sur les bords.

Mammographie : opacité biloculée, homogène, à contours nets et réguliers, avec liseré clair, complet, tissu glandulaire non infiltré, mais refoulé.

Histologie : groupe de plusieurs adénofibromes tubuleux, confluents régulièrement encapsulés, sans indice histologique de malignité.

b) *Pneumo-mammographie* : La technique de l'insufflation se fait avec des précautions après avoir repéré dans l'espace rétro-mammaire les points à injecter. Une injection de novocaïne peut être faite, mais pas nécessairement; le gaz contenu dans une vessie de football remplie de gaz carbonique est mis en relation avec une aiguille à injection et un système de robinet. Le gaz est envoyé dans les tissus par pression douce.

L'insuflation doit être arrêtée si une distension avec crépitation apparaît dans les régions sous-claviculaire ou thoracique latérale. Elle doit être alors recommencée dans une autre région à quelques centimètres en-dehors du mamelon. La dimension du sein peut atteindre un volume double ou triple du volume primitif, mais nous sommes toujours restés au-dessous de ces limites. La résorption du gaz étant très rapide, les clichés doivent être pris immédiatement après l'insuflation. La distension du sein régresse rapidement, quelques minutes après l'injection du gaz carbonique.



FIG. 16. — Même malade, radiographie de contact, le syndrome radiologique de tumeur bénigne se confirme nettement.

c) *Opacification des cavités kystiques.* — Lorsque l'examen clinique ou radiologique simple suspecte une formation kystique, qui ne s'est pas manifestée par un écoulement mamelonnaire, une ponction peut être pratiquée (précisée si c'est nécessaire par la radiographie), ensuite l'air ou tout autre produit de contraste est injecté.

III.. — *Stéréographies.*

Le déplacement de l'ampoule peut se faire si le malade est en position debout, horizontalement, et verticalement si le malade

est couché, parallèlement à l'axe du corps. Il faut disposer d'un tiroir spécial ou d'un pupitre utilisé par Ledoux-Lebard. Cette technique apporte évidemment des renseignements sur les nombreux entrecroisements et les nombreuses superpositions des traînées opaques.

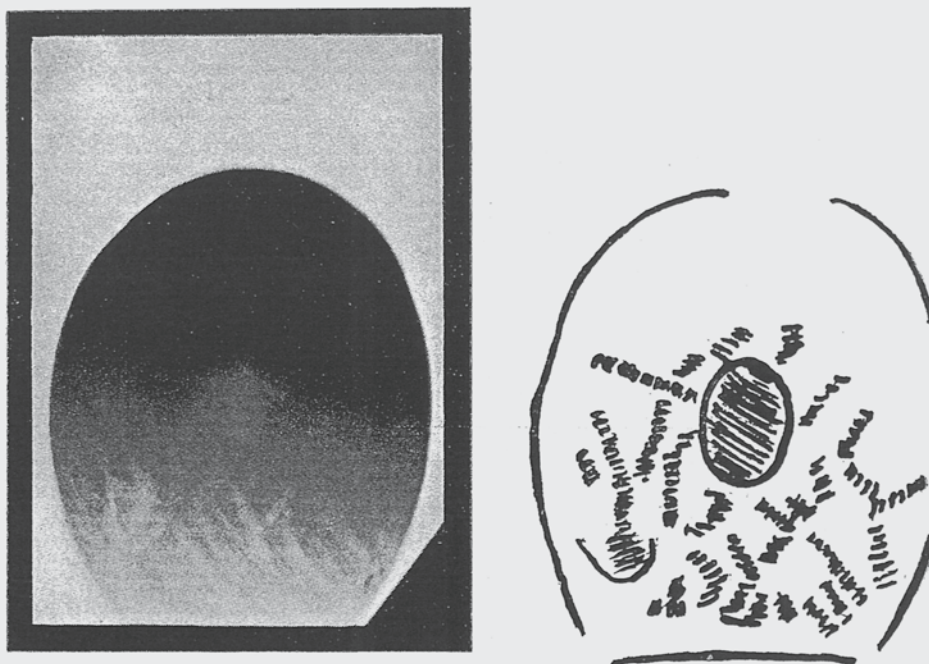


Fig. 17. (420/51.) — Petit ganglion banal de la gouttière pectorale du creux axillaire.

Clinique : malade de 48 ans, petit nodule dur, bien mobile, solidaire avec la masse glandulaire, sans adhérence au plan cutané, ni au plan profond au niveau du quadrant supéro-externe du sein droit.

Sur le bord externe du grand pectoral, petit ganglion de 1 cm. de diamètre, élastique et mobile.

Transillumination : glande mammaire parfaitement translucide avec petite ombre arrondie, assez bien limitée à la base du quadrant supéro-externe.

Mammographie : opacité arrondie de volume égale au volume tactile à contours nets et réguliers, sans infiltration des tissus voisins, donc syndrome radiologique de formation bénigne.

Histologie : après Halsted : « Mastose chronique scléro-kystique, très étendue et très scléreuse; les ganglions lymphatiques examinés, aucun ne montrait de néoplasme ».

Anatomie radiologique normale.

La mamelle au cours de la vie subit des transformations nombreuses et profondes : puberté, menstruation, grossesse, lactation, ménopause.

Sur le cliché le mamelon est quelquefois visible, selon la pénétration du rayonnement, de même la peau, surtout si une certaine épaisseur est prise tangentielle ou bien lorsque un œdème l'infiltré, s'individualise nettement. La glande se présente sous forme de traînées opaques d'aspect nuageux. La disposition



FIG. 18. (125/51.) — Cicatrice de furoncle.

Clinique : petite induration de la taille d'un grain de café au niveau du quadrant inféro-interne du sein gauche, qui est le reliquat d'un furoncle datant de deux mois.

Mammographie : image étoilée, cicatricielle de sclérose post-inflammatoire.

et la proportion des plages claires et opaques, l'aspect réticulaire, sont soumis aux multiples variations individuelles, il est cependant possible de distinguer avec Lockwood quatre zones à étudier, toujours discernables sur les radiogrammes :

1° la zone cutanée comprenant le mamelon, l'auréole et la peau;

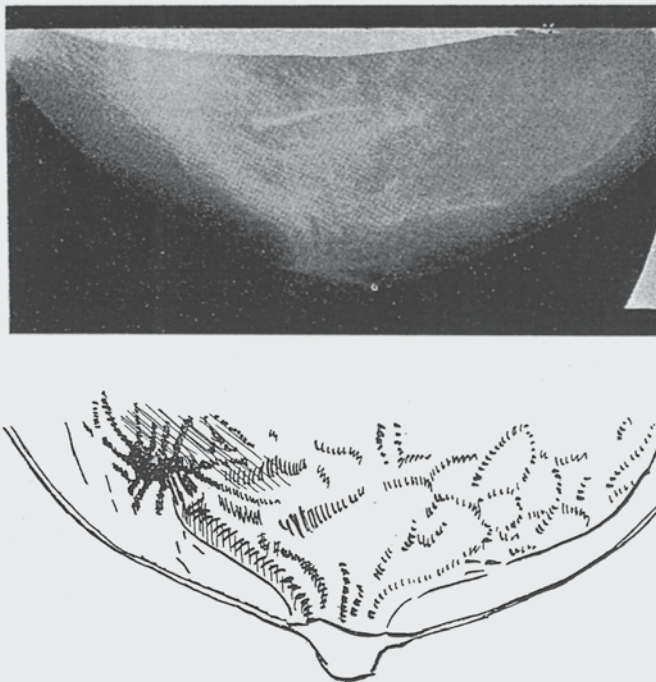


FIG. 19. (2341*51). — Epithélioma glandulaire.

Clinique : femme de 47 ans, sans enfant. Remarque en 1949 un empâtement du quadrant supéro-externe du sein droit de 2 cm. de diamètre, mobile et non douloureux. Malade normalement réglée : 28/3-4. En novembre 1950, augmentation de la taille de l'empâtement coïncidant avec des irrégularités menstruelles.

Inspection : les deux seins sont moyennement développés, d'aspect normal; sein droit : petite voussure discrète au niveau du quadrant supéro-externe, mamelon non rétracté, pas de peau d'orange, même aux manœuvres de contraction des pectoraux.

Palpation : sein droit : glande granuleuse au niveau du quadrant interne à la base du quadrant supéro-externe on palpe un empâtement de 3 cm. de diamètre et de 2 cm. d'épaisseur, lisse, polycyclique, faisant corps avec la glande mammaire, de consistance rénitente, pas d'infiltration des plans profonds ni des plans cutanés, cliniquement : d'un foyer de mastite chronique scléro-kystique.

Transillumination : ombre floue au niveau du quadrant supéro-externe du sein droit.

Mammographie : sein droit : trame normale, finement réticulée au niveau des quadrants internes, épaissie et irrégulière au niveau des quadrants externes, où l'on note l'existence d'une image étoilée avec spicules irradiantes et une rétraction localisée du tissu glandulaire à la périphérie externe.

Le volume radiologique est nettement inférieur au volume clinique.

2° la couche adipeuse péri-mammaire claire traversée par les ligaments de suspension opaques, dirigés vers la peau;

3° la zone glandulaire est projetée sous formes d'opacités floues, de forme généralement triangulaire, à sommet mamelonnaire, dont les côtés sont quelquefois bien limités et dont la base est toujours imprécise. Sur ces opacités étalées se projette le reticulum des cloisons fibreuses limitant les lobules ou les ligaments suspen-seurs (triangle strié de Seabold).

4° la zone rétro-mammaire très nette et régulière surtout sur le cliché de profil où elle se traduit par une limite claire située devant le muscle pectoral (Ledoux-Lebard) (fig. 5).

Dans la région aréolaire se distinguent quelquefois des opacités tubuliformes correspondant aux galactophores surtout si ceux-ci sont dilatés. Enfin quelques veines superficielles à direction et à contours multiples, variables s'individualisent sur le cliché.

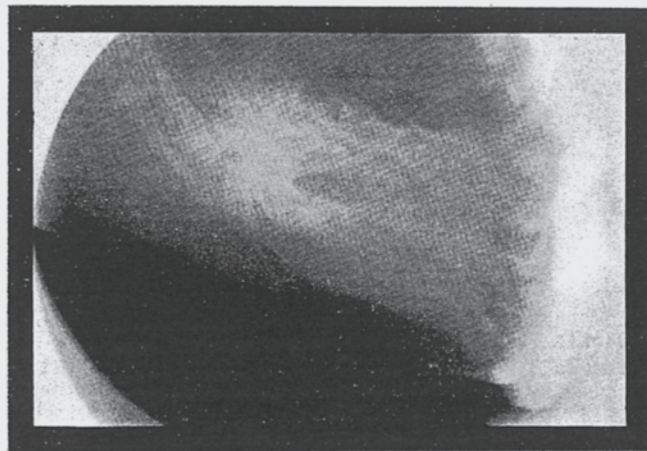


FIG. 20. — Même malade. La radiographie de contact confirme l'image de la radiographie standard et permet de faire le diagnostic de tumeur maligne.

Histologie : biopsie par ponction à la foreuse : « Petits fragments dont quelques-uns montrent la diffusion d'un épithélioma glandulaire parvi-alvéolaire, qui donne l'impression d'être voisin de la mastite carcinomateuse ». (Prof. GÉRY.)

Au cours du cycle menstruel la glande mammaire présente un maximum d'hyperplasie glandulaire autour des règles, ce qui se traduit à ce moment-là par une opacité plus marquée et surtout un aspect nuageux où se superpose l'image réticulaire. Au contraire à mi-chemin des règles au moment où le tissu glandulaire est le plus réduit, l'aspect strié est plus net; c'est donc à ce moment là que la radiographie peut présenter les détails les plus nombreux. Au cours de la grossesse l'élément glandulaire se développe, occupe toute la mamelle, celle-ci augmente de volume : l'aspect

brumeux, homogène des images augmente jusqu'à la lactation. Après le sevrage la régression se fait progressivement, lentement. Au cours de la ménopause le tissu fibro-adipeux envahi peu à peu les formations glandulaires : l'aspect strié est bien visible. Même si les seins sont volumineux la graisse est un excellent milieu de contraste pour la radiographie du sein. Les formations pathologiques se projettent toujours mieux sur les plages fibro-adipeuses

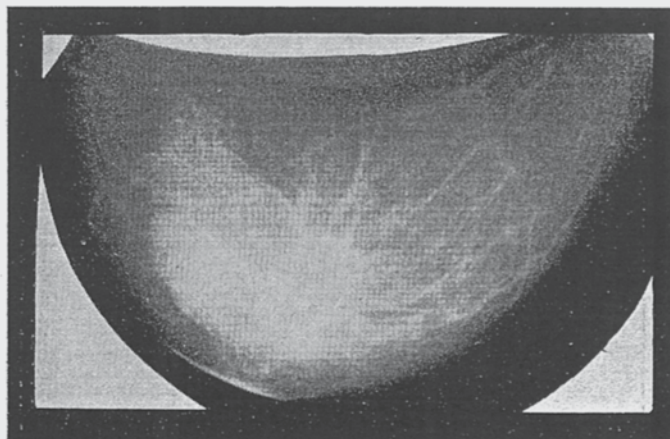


Fig. 21. (1805/51.) — Epithélioma glandulaire.

Clinique : Femme de 36 ans, ressent deux mois avant l'examen des douleurs au niveau du sein droit et constate l'existence d'un nodule intramammaire. Règles normales : 28/3.

Inspection : mamelon droit non rétracté, mais orienté vers le quadrant inféro-externe, il montre du doigt la zone tumorale, la contraction des muscles pectoraux accentue l'orientation du mamelon sans faire apparaître de peau d'orange. La circulation veineuse superficielle est augmentée à droite.

Palpation : le mamelon ne se déplisse pas complètement et l'on n'arrive pas à réduire l'orientation anormale. Dans le quadrant inféro-externe, on palpe une masse irrégulière, dure, rénitente de la taille d'une petite mandarine, elle est lisse et n'infiltré ni la peau ni les plans profonds. Par contre sur le bord interne de la tumeur, il existe de petites trainées infiltrantes dirigées vers le mamelon. Douleurs à la palpation. Cliniquement, diagnostic difficile de mastite chronique scléro-kystique avec suspicion de dégénérescence maligne. Pas de ganglions de type néoplasique.

Transillumination du sein droit : légère diminution de la transparence dans les quadrants externes.

Mammographie : Opacité arrondie centrale avec de nombreuses spicules infiltrantes au niveau des pôles postérieurs et antérieurs. Le tissu glandulaire est nettement rétracté. Le volume radiologique est inférieur au volume tactile.

En conclusion, on pose le diagnostic de tumeur maligne.

Histologie : « Epithélioma glandulaire typique à petites cellules glanduliformes ». (Prof. GÉRY.)

que sur les plages glandulaires. (Nous avons pratiqué quelques clichés de gynécomastie soit spontanée, soit après injection d'hormones femelles : les images n'ont rien de caractéristique.)

Quant aux galactophores normaux injectés, ils présentent l'image caractéristique d'arbre effeuillé dont les extrémités sont renflées (acini) (fig. 34).

Séméiologie radiologique.

Pour simplifier et pour éviter des redites, nous n'envisagerons pas les différents caractères que peuvent présenter les affections

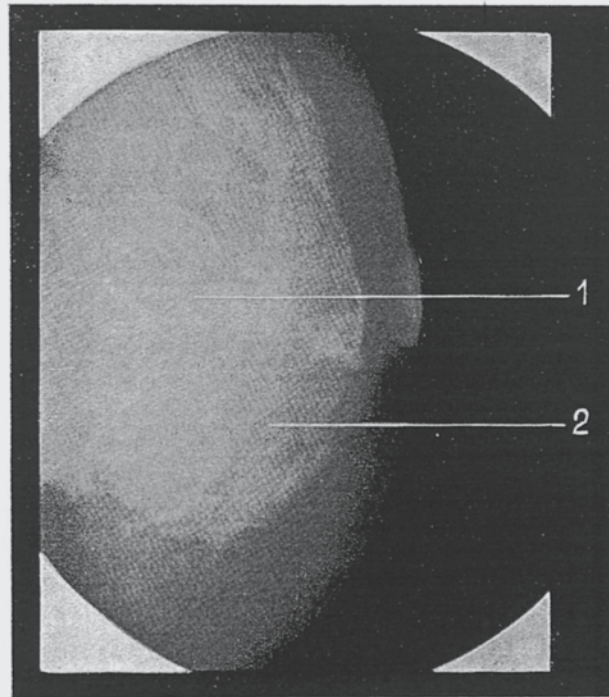


FIG. 22. (2200/50.) — Mastite chronique scléro-kystique dégénérée.

1) Noyau tumoral central avec petites calcifications ponctiformes.

2) Tissu glandulaire infiltré et rétracté.

Clinique : Femme de 52 ans, qui présente une masse plus ou moins molasse, irrégulière, prenant toute la glande mammaire. A la palpation, on individualise dans la masse, qui prend grossièrement toute la glande mammaire un noyau central, dur, irrégulier, de la taille d'une prune, bien mobile avec la glande mammaire. Pas de ganglions axillaire ni sus-claviculaire.

Transillumination : opacité centrale, irrégulière.

Mammographie : on n'individualise pas de tumeur proprement dite, mais toute la glande mammaire semble infiltrée et rétractée. Elle n'occupe plus qu'un tiers du volume par rapport à la glande normale de l'autre sein. A la partie centrale, il existe cependant une opacité plus importante, non homogène, avec trainées infiltrantes. De plus une dizaine de petites calcifications punctiformes se répartissent dans le noyau central. En conclusion, l'opacité centrale non homogène, la rétraction, les calcifications ponctiformes orientent vers une tumeur maligne.

Histologie : « Mastite chronique occupant toute la glande avec un gros noyau épithéliomateux central et une lymphangite cancéreuse responsable de la rétraction accentuée de la glande ». (Prof. GÉRY.)

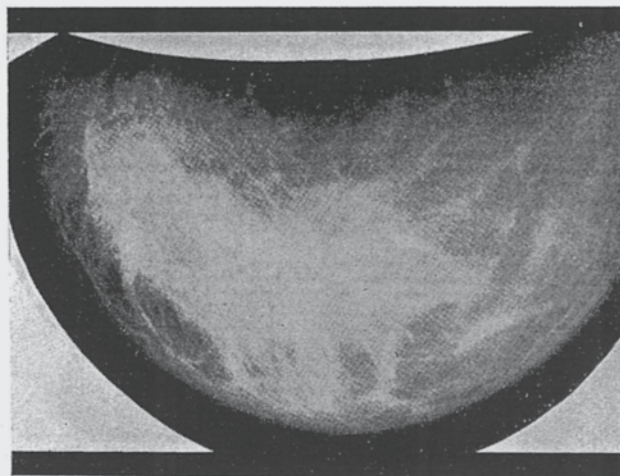


FIG. 23. (1858/51.) — Tumeur cancéreuse avec innombrables calcifications ponctiformes.

Clinique : Femme de 57 ans.

Inspection : le diagnostic clinique est évident avec ébauche de peau d'orange, tumeur partiellement fixée aux plans profonds. Mamelon fixé, mais non inversé.

Palpation : la tumeur prend les deux quadrants externes, déborde sur les deux quadrants internes, elle est dure, infiltre la peau, surtout dans la région aréolaire externe. Peau d'orange à la contraction des muscles pectoraux.

Transillumination : opacité des quadrants externes à bords flous et irréguliers.

Mammographie : masse tumorale irrégulière, infiltrante avec spicules se dirigeant vers les plans cutanés, mais dont le volume radiologique est nettement inférieur au volume tactile; rétraction des tissus glandulaires, d'innombrables calcifications ponctiformes sont visibles dans tout le noyau tumoral.

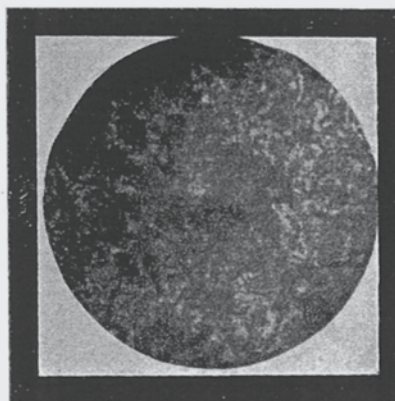


FIG. 24. — Même malade. Radiographie de contact avec cône rétréci mettant en évidence les innombrables calcifications en grain de sel de type malin dans le noyau tumoral.

de la mamelle. Mais nous chercherons à résoudre le problème qui se présente le plus fréquemment, le plus difficile à résoudre quelquefois et toujours le plus grave : celui de la nature maligne ou bénigne d'une induration de la glande mammaire.

Les critères suivants orientent vers l'une ou l'autre hypothèse.

Siège. — Les néoformations de la peau ou du mamelon ne sont pas envisagées, mais quelquefois une surface indurée, avec peau d'orange en rapport avec une affection inflammatoire cutanée peut égarer le diagnostic; la maladie de Paget ou l'épithélioma du mamelon ne sont pas étudiés.

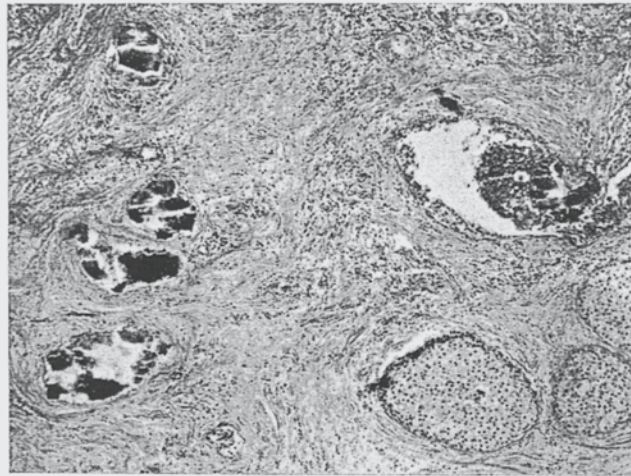


FIG. 25. — Même malade. Microphoto de la préparation histologique.

Epithélioma glandulaire généralement typique dont un certain nombre de grands alvéoles épithéliomateux devenant alors en général atypique montrent une calcification étendue du foyer nécrotique central. L'imprégnation de sels de chaux paraît être importante et le foyer nécrotique est fréquemment transformé en nappes calcaires denses et homogènes.

A côté des calcifications centrées par les alvéoles cancéreux, il est possible d'en trouver également qui sont localisées entièrement dans le tissu conjonctif. On a l'impression qu'il s'agit dans ces cas d'anciens noyaux épithéliomateux complètement nécrosés dont il ne subsiste plus que le foyer dégénératif momifié. (Prof. agrégé FRUHLING.)

Quant à la topographie de la tumeur à l'intérieur de la mamelle, son rôle n'intervient que dans la technique, pour bien individualiser les images. Par exemple le petit nodule situé contre le gril costal à la partie supérieure, ou dans le prolongement axillaire (fig. n° 17); les incidences, les localisateurs sont adaptés à cette topographie, mais celle-ci ne joue aucun rôle dans les caractères radiologiques de la malignité ou de la bénignité.

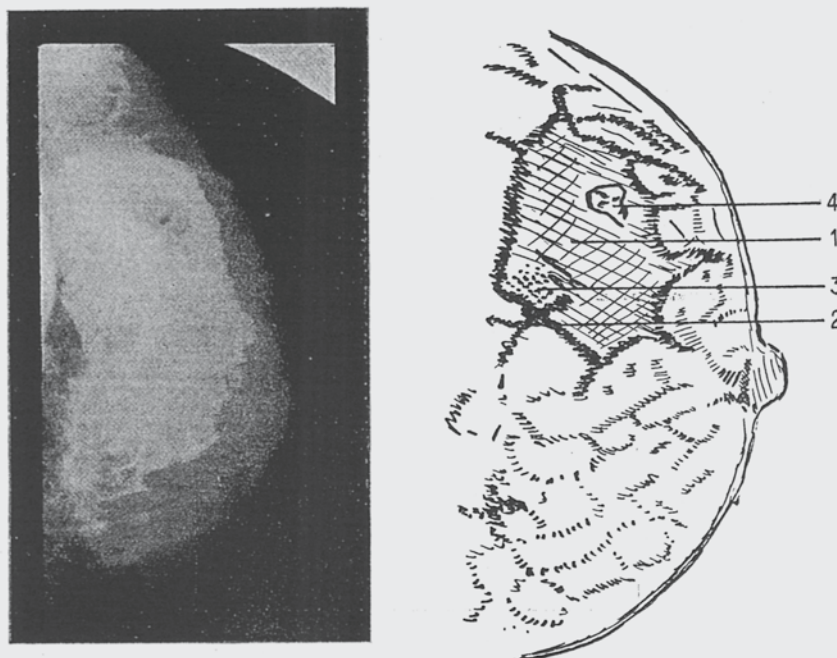


FIG. 26. (2381/51.) — Tumeur mammaire formée de deux noyaux, l'un squirrheux, l'autre encéphaloïde.

Clinique : Femme de 38 ans, sans enfant, qui ne remarque que 15 jours avant l'examen une induration suspecte du quadrant supéro-externe du sein gauche.

Règles prolongées : 28/6 avec douleurs et congestion prémenstruelle des glandes mammaires.

Inspection : les deux seins sont symétriques, cependant le sein gauche paraît plus lourd et le mamelon, non rétracté, est abaissé d'un cm. par rapport au mamelon droit. Nette prédominance de la circulation veineuse du sein gauche.

Palpation : empâtement diffus, dur, irrégulier, faisant corps avec la glande mammaire et prenant tout le quadrant supéro-externe du sein gauche; la contraction des pectoraux fait apparaître une voussure d'une dizaine de cm. de diamètre au niveau de ce quadrant, mais pas de peau d'orange et masse bien mobile sur les plans profonds. La masse est douloureuse à la palpation et d'une dureté ligneuse de 8 cm. de diamètre. Ganglion mou dans le creux axillaire gauche.

Diagnostic clinique : incertain.

Transillumination : transparence nettement diminuée au niveau du quadrant supéro-externe, ombre floue à limite imprécise.

Mammographie : masse opaque, non homogène de 4 cm. de diamètre et visible dans les quadrants externes du sein. Ses limites sont floues et irrégulières, surtout dans les parties postérieures, de plus à la périphérie, il existe quelques spicules se dirigeant vers la peau sans l'atteindre. Rétraction du reliquat glandulaire sur les bords internes, où l'on note l'existence d'un foyer squirrheux avec de nombreuses calcifications punctiformes. L'espace clair rétro-mammaire est partiellement interrompu. Une image claire arrondie est visible au milieu de l'opacité tumorale, elle est vraisemblablement en rapport avec ilôt graisseux englobé dans la masse tumorale en évolution.

Conclusion : tumeur maligne des quadrants externes du sein, se développant jusqu'au pectoral et infiltrant les deux tiers de la glande environ.

Schéma de la figure 26 :

- 1) Noyau tumoral encéphaloïde.
- 2) Noyau squirrheux.

- 3) Calcifications punctiformes.
- 4) Ilôt graisseux.

Forme. — L'anatomie macroscopique oriente, à priori, vers la différence d'aspect des formations bénignes et des processus malins. Les premiers auront une forme générale arrondie par exemple un ganglion : le fibroadénome (fig. 15) ou la tumeur

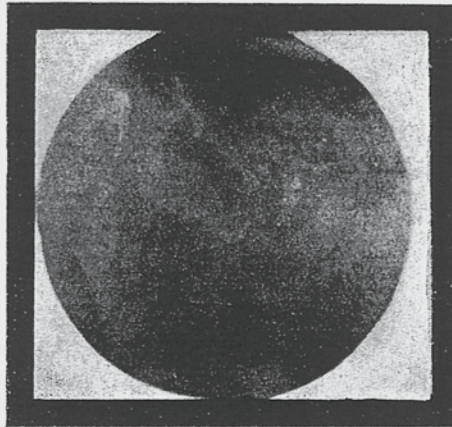


FIG. 27. — Même malade. Radiographie de contact à cône rétréci centrée sur les calcifications punctiformes.



FIG. 28. — Coupe de la pièce opératoire mettant en évidence les calcifications de type malin et l'îlot graisseux inclus dans la tumeur.

phyllode (fig. 14); forme ovale, (le grand axe étant dirigé suivant la plus grande épaisseur en ce point) pour le kyste solide (fig. 9); mais l'aspect lobulé peut se rencontrer.

La mastite scléro-kystique, si les kystes sont assez volumineux, se traduit par des images arrondies (fig. 7 et 8, fig. 10 et 11).

Au contraire les seconds, s'ils sont de type squirrheux, infiltrant, enverront des « pattes de crabe » ou de fins tractus dans toutes les directions (fig. 19 et 20, fig. 30 et 31), d'où une forme générale étoilée dont les prolongements sont plus ou moins grêles; la forme encéphaloïde souvent associée à la précédente a une forme quelconque, mais sans spicules.

Volume. — Le volume absolu apprécié sur le cliché n'a aucune signification, tandis que la comparaison de ce volume radiologique au volume clinique jugé par la palpation donne un renseignement facile à obtenir et précieux.

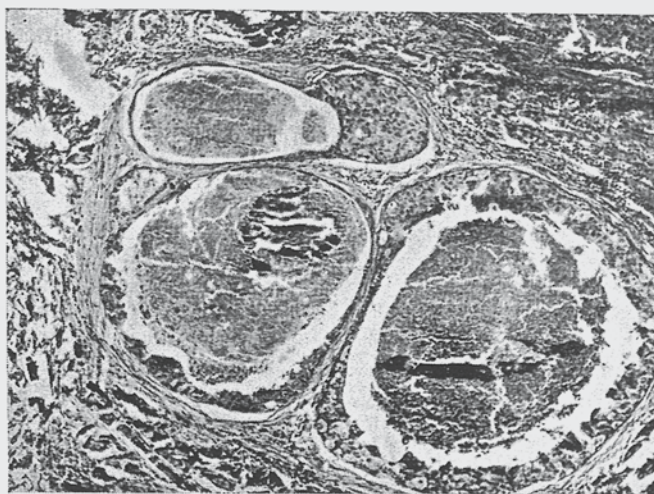


FIG. 29. — Microphoto de la préparation histologique.

Il s'agit d'un épithélioma glandulaire atypique encéphaloïde envahissant par petits alvéoles et par nombreuses lymphangites la glande mammaire. Dans certaines lymphangites les alvéoles mammaires se développent en massifs plus volumineux et la nécrose centrale très acidophile finit par s'imprégner de sels de chaux violacés. Les foyers de calcification paraissent constitués par la juxtaposition de grumeaux de sels de chaux. (Prof. agrégé FRUHLING.)

Les néoplasies (non inflammatoires) *benignes* donnent au toucher du sein et à la vue de la radiographie une impression de volume égal : le volume radiologique = volume clinique; les tissus péri-tumoraux refoulés glissent sur la masse tumorale (fig. 14, 15, 16). Au contraire le volume de l'image étoilée maligne est spectaculairement plus petite que celle à laquelle on s'attend après palpation : volume radiologique plus petit que le volume clinique; les tissus péri-tumoraux (glandulaire, fibro-adipeux, cutané) sont

infiltrés et forment bloc à la palpation avec le centre opaque de la tumeur (fig. 19, 20 et 22).

Contours. — Réguliers, nets dans les formations bénignes (tumeurs bénignes, kystes, abcès); ils sont irréguliers, imprécis dans les épithéliomas (fig. 7-8, 10-11, 14-15-16).

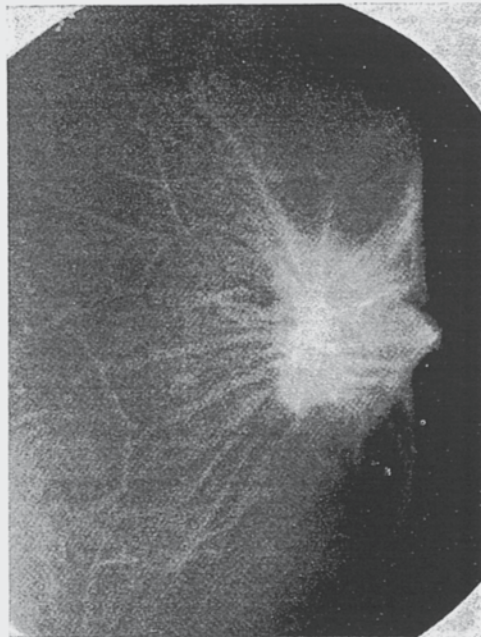


FIG. 30. (53/52.) — Squirrhe atrophique.

Clinique : Malade de 57 ans, remarque depuis 1950 une rétraction progressive du mamelon droit et une infiltration cutanée sous-mamelonnaire progressive; elle signale en 1927 un traumatisme important au niveau du sein droit (le sein est pris dans les rouages d'une sècheuse). Après un hématome et des douleurs passagères, le sein reprend un aspect normal et son développement est identique à l'autre sein.

Inspection : le sein droit est rétracté, mamelon complètement inversé et l'on note l'existence d'une peau d'orange creusant plusieurs sillons, dont la rétraction mamelonnaire forme la partie centrale en étoile. La contraction des pectoraux accentue tous les phénomènes.

Palpation : glande granuleuse et dans la région rétro-mamelonnaire, masse irrégulière, infiltrante, fixée au mamelon et à la peau, mais bien mobile sur les plans profonds de 4 × 4 cm. Pas de ganglion axillaire; deux petits ganglions plats, élastiques sus-claviculaires.

Cliniquement il faudrait faire le diagnostic différentiel entre une stéatonecrose et un squirrhe atrophique.

Transillumination : opacité irrégulière étoilée dans la région rétro-mamelonnaire.

Mammographie : opacité irrégulière, étoilée, non homogène, avec nombreuses spicules irradiant dans le reliquat glandulaire de 2 cm. de diamètre, volume radio plus petit.

Histologie : dans un tissu fibro-adipeux en grande partie scléreux, on voit une infiltration néoplasique étendue progressive en profondeur, en forme de petites trainées et en forme de petits boyaux situés dans les vaisseaux lymphatiques. Diagnostic : squirrhe étendu de la glande mammaire. (Prof. KELLER.)

De plus un liseré clair périphérique fin ou large, total ou partiel entoure l'opacité tumorale bénigne (adénofibrome, phyllode, kyste) alors que nous ne l'avons pas rencontré (il est difficile à concevoir) dans les carcinomes (fig. 19, 21, 22, 23, 30).

Opacité. — Variable suivant la nature et le volume des éléments tumoraux et la densité des tissus environnants. Un adénofibrome situé au centre du tissu glandulaire abondant, en activité chez une jeune femme, aura la même opacité que le reste de la glande, seul le contour l'individualisera (fig. 15 et 16); au contraire une même affection adénomateuse se projetant sur une plage claire, adipeuse formera une ombre opaque nette. De même pour toutes les autres formations bénignes ou malignes. Telle formation fibro-épithéliale volumineuse se traduira par une image pathognomonique de tumeur bénigne (fig. 14), alors que les petits kystes d'un bloc de mastite scléro-kystique seront mal individualisés; un

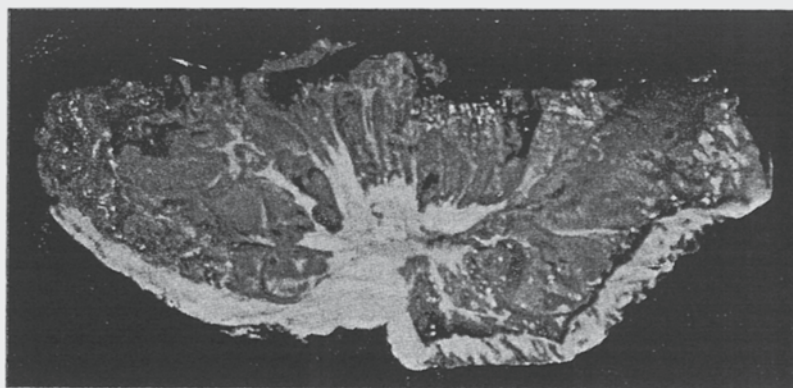


FIG. 31. — Photo d'une coupe complète de la pièce opératoire.

noyau épithéliomateux peu rétractile, chez une vieille femme, sera bien visible sur la plage claire d'involution fibro-adipeuse (fig. 21), tandis qu'un noyau de même volume, chez une personne âgée, attirant fortement l'atmosphère péri-tumorale sera à peine visible au centre d'une ombre, non homogène, assez opaque (fig. 22).

Rapport avec les tissus voisins. — La représentation radiologique va se superposer à l'anatomie pathologique. La formation bénigne, refoule simplement les éléments péri-tumoraux sans modifier leur structure, et ceux-ci se moulent sur la néoplasie, d'où la possibilité du liseré clair de sécurité : tumeurs bénignes (fig. 14, 15, 16), kystes (fig. 7, 8, 9). Cependant un abcès avec sa gangue inflammatoire périphérique n'a pas de liseré clair; il se

projetée dans un nuage homogène en rapport sans doute avec l'œdème qui infiltre le voisinage, même jusqu'à la peau (fig. 10-11-12).

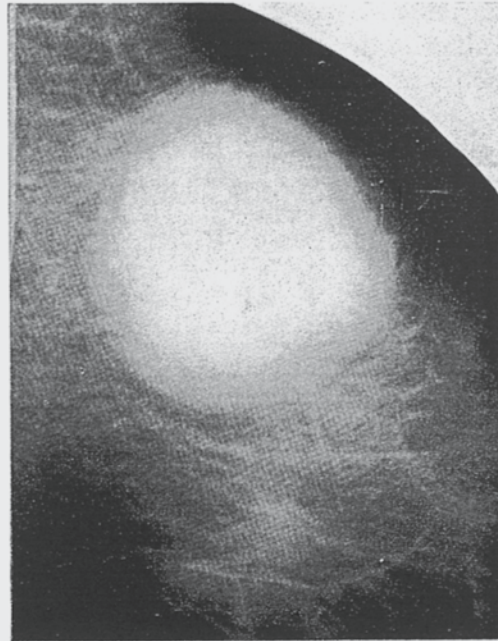


FIG. 32. (301/49.) — Clinique : Malade de 69 ans qui présente depuis 1948 un sarcome des parties molles de l'hypochondre gauche à point de départ des plans profonds sous-cutanés.

Exérèse chirurgicale en février 1949 et radiothérapie post-opératoire.

En cours des années 1949-50-51 des localisations cervicales droites, de l'hypochondre droit, de la fesse droite, des ganglions de l'aisselle gauche, de la région cervico-médiastinale supérieure, de la région inguinale droite : toutes ces localisations sont traitées par radiothérapie et la malade était apparemment guérie jusqu'en février 1952, où elle revient au service avec une masse tumorale de la taille d'une mandarine au niveau du quadrant supéro-externe du sein gauche. Elle est bien mobile sur les plans profonds, mais fixée à la peau qui a pris une teinte rouge violacée.

A la palpation, la masse est dure, à limite nette, paraissant refouler les tissus voisins, n'infiltrant pas la glande mammaire.

Transillumination : dans la clarté du champ glandulaire gauche se détache au niveau du prolongement axillaire du quadrant supéro-externe une opacité intense à limites floues de 5 cm. de diamètre.

Mammographie : sein gauche : opacité intense floue de 5 cm. de diamètre, nettement limitée avec halo clair complet de toute la tumeur, sauf dans sa partie externe, où elle est fixée à la peau, les tissus voisins sont refoulés, la trame glandulaire est par ailleurs finement réticulée d'aspect normal. A 4 cm. du bord interne de la tumeur, il existe deux petites opacités arrondies floues faisant penser à deux autres localisations sarcomateuses.

Histologie : sarcome réticulaire. (Prof. GÉRY.)

Les cancers se comportent différemment à ceux du type encéphaloïde, infiltrant d'une façon irrégulière les tissus voisins (fig.

19, 20) : peau (fig. 23), tissu mammaire (fig. 22) ou englobant par exemple un ilot de graisse (fig. 26). Les zones squirrheuses vont à la fois infiltrer et retracter plus ou moins : le mamelon (fig. 30, 31), peau (fig. 23), ce qui confirme l'inspection d'un mamelon dévié et retractoré vers la tumeur ou l'examen d'une peau

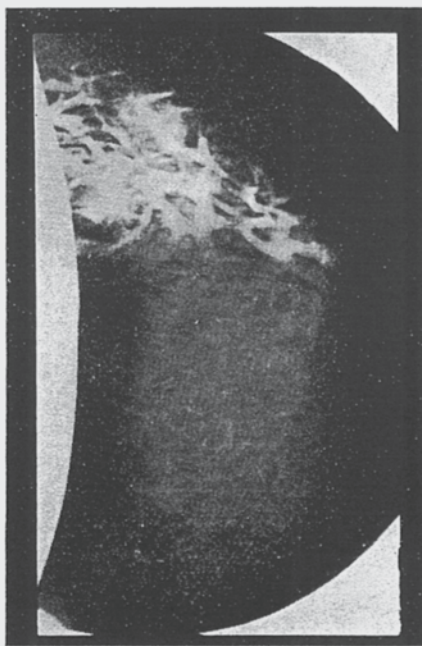


FIG. 33. (1784/51.) — Dilatation d'un système galactophorique.

Clinique : Malade de 51 ans, qui remarque depuis plusieurs semaines un écoulement brunâtre du mamelon du sein gauche. Sans douleurs, ni masse intra-mammaire.

Inspection : les deux seins sont normalement développés sans signe d'infiltration néoplasique.

Palpation : les deux glandes mammaires sont souples sans nodule suspect, non douloureuses, de consistance granuleuse; la compression du sein gauche provoque un important écoulement d'une sérosité brunâtre d'un seul canal galactophorique.

Transillumination : montre au niveau du sein gauche une ombre floue irrégulière, arborescente partant du mamelon à travers les deux quadrants externes.

Mammographie : simple du sein gauche : trame glandulaire fortement épaissie dans les quadrants externes.

Injection du canal suintant : énorme dilatation du système galactophorique injecté.

capitonée, peau d'orange; mais les rétractions importantes (fig. 22) ou discrètes (fig. 19, 20) de l'atmosphère fibro-adipeuse ou glandulaire, de l'atmosphère péri-tumorale, non soupçonnées cliniquement, doivent être recherchés attentivement et représentent

un élément précieux pour le diagnostic. Les fins tractus cancéreux opaques émanant du noyau tumoral et se dirigeant vers la périphérie cutanée ne doivent pas être confondus avec les crêtes conjonctives ou les cloisons interlobulaires; mais celles-ci peuvent être remaniées par le lit tumoral et leur individualisation peut devenir difficile.

Calcifications tumorales. — Elles peuvent être divisées en deux grandes variétés : les calcifications volumineuses exceptionnelles et les petites calcifications divisées en deux types : bénin et malin, assez fréquents :



FIG. 34. — Même malade; la malade revient pour contrôle deux mois après l'injection du canal suintant par du Diodone à 35 %, elle signale un arrêt de tout écoulement 15 jours après l'injection.

La transillumination montre une transparence complète et uniforme des deux glandes mammaires.

Mammographie simple : il n'existe plus d'opacité floue arborescente dans le quadrant externe du sein gauche.

L'injection du système galactophorique montre une restitution pratiquement ad integrum.

1° *Calcifications volumineuses* : Elles sont exceptionnelles puisque J.H. Conway n'a pu rassembler dans les publications au cours d'un siècle (1836-1936) que 31 observations. Ces importantes productions calcaires occupant en bloc une partie ou toute la

mamelle, voisinent souvent avec des formations osseuses ou cartilagineuses et sont classées en trois groupes : tumeurs teratoïdes mixtes du sein, les sarcomes ou carcino-sarcomes calcifiants, les dépôts calcaires dans les kystes. Cette variété n'est qu'une curiosité pour le radiologiste ou le chirurgien.

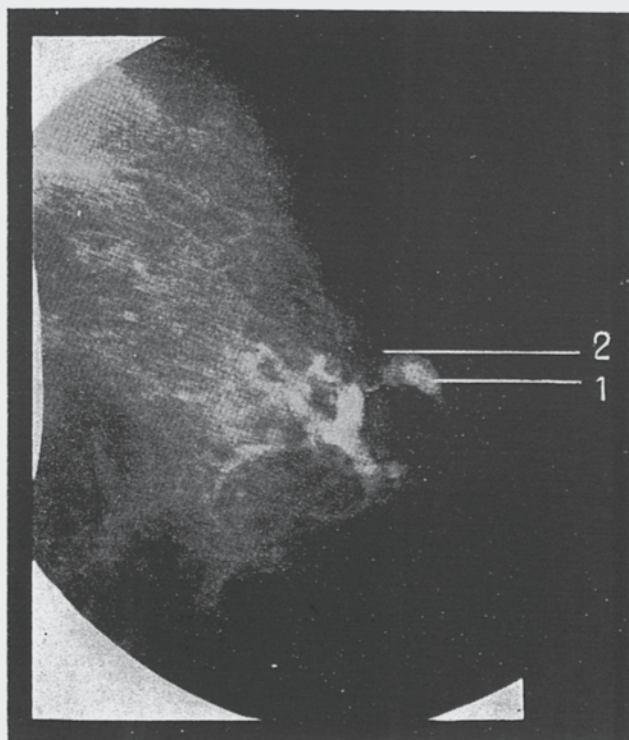


FIG. 35. (461/51.) — Image lacunaire dans un canal galactophorique dilaté.

1) Canal galactophorique dilaté.

2) Image lacunaire.

Clinique : malade de 39 ans qui présente depuis deux ans un écoulement citrin du mamelon du sein gauche; douleurs et congestions prémenstruelles des glandes mammaires.

Le sein gauche est souple à la palpation, granuleux, surtout dans les quadrants externes, les granulations sont de la taille d'un grain de riz à un grain de café, mais on n'individualise pas de masse tumorale. La compression de la glande mammaire au niveau du quadrant supéro-externe provoque un écoulement galactophorique, citrin, très abondant; l'écoulement se produit par un seul canal.

La *transillumination* montre une petite ombre floue dans la région juxta-aréolaire externe.

La *mammographie simple* ne montre pas d'opacité anormale de la glande mammaire.

L'*injection du canal* par contre révèle une énorme dilatation du système galactophorique opacifié avec une image lacunaire, régulière, arrondie, laissant passer sur son bord interne un mince filet de Diodone qui opacifie une partie du système galactophorique située en amont et également dilatée. Cette image lacunaire correspond vraisemblablement à un petit adénome ou papillome intra-canaliculaire.

2° *Petites calcifications*. — Elles sont caractérisées par leur nature calcaire pure sans productions osseuses, par leurs faibles dimensions; par leur multiplicité. Elles se divisent en deux groupes :

a) *Calcifications du type bénin* : Leur diamètre est de l'ordre du millimètre au moins, bien arrondie, facilement reconnaissables en nombre très limité. Nous les avons rencontrées dans quelques glandes d'apparence non pathologique et dans quelques tumeurs bénignes, siégeant à la périphérie, non groupées. Elles ne doivent pas être confondues avec des images micronodulaires, projections de nœud vasculaire ou conjonctif au calcifications systématisées à un vaisseau ou un galactophore (fig. n° 14).

b) *Calcifications du type malin* : Signe de Leborgne. Ce sont les plus intéressantes : observées en 1930 par C.M. Dominguez et A. Lucas, elles n'ont pas intéressées les histologistes, ni les radiologistes. C'est R. Leborgne qui a montré tout l'intérêt diagnostique de ces calcifications punctiformes dans le cancer du sein.

De dimensions ponctuelles (fig. 23, 24, 26, 27, 28), leur nombre est élevé, d'une dizaine à plus de mille. Elles sont groupées soit au sein de la tumeur visible ou palpable (fig. n° 23) soit en bordure (fig. 26), soit même en dehors de la masse clinique ou radiologique.

Ignorées en général des anatomo-pathologistes, passant inaperçues si la radiographie est faite avec un grand localisateur ou si le sein est volumineux ou ferme, ressemblant à des artefacts après examen rapide ou fait dans de mauvaises conditions, elles doivent être recherchées avec beaucoup de soins.

Après les avoir mis en doute les premiers mois de nos investigations, les avoir ensuite découverts par hasard et vérifiées; nous les trouvons assez souvent maintenant que nous les recherchons systématiquement et attentivement.

Nous explorons la glande mammaire par deux champs avec localisateurs étroits pour réduire la diffusion, et prenons chaque fois deux clichés avec des temps de pose légèrement différents pour obtenir le meilleur contraste. Avec une certaine expérience les calcifications punctiformes sont soupçonnées sur les clichés standards, de tout le sein, en incidence cranio-caudale et le petit localisateur est centré sur la région suspecte pour les confirmer ou non.

L'examen des images doit être minutieux, fait dans les conditions déjà indiquées; ces « grains de sel » sont alors bien recon-

naissables (fig. 24 et 27). Enfin la pièce opératoire est coupée en tranche de 1/2 centimètre. Celles-ci sont radiographiées; les images sont alors fort démonstratives (fig. 28) et la coupe histologique faite dans la région confirme la présence de ces points calcaires dans les foyers de nécrose (fig. microphotographiques 25 et 29).

L'examen microscopique de ces calcifications montre que leur forme est très variable.

Nous résumons dans le tableau les différents critères radiologiques de bénignité et de malignité qui semblent être les plus fréquemment observées (Tableau II).

Pour mettre en évidence les différentes images que nous signalons, il faut non seulement une technique rigoureuse, mais l'étude très attentive de tous les clichés.

Limites de la Mammographie.

Le cas le plus intéressant est celui de la consultante présentant un noyau intra-mammaire dont on doit préciser la nature bénigne ou maligne. Dans le tableau précédant nous avons donné un schéma du syndrome radiologique de la bénignité et de la malignité. Mais toute investigation radiologique a des limites; l'interprétation du cliché fait obligatoirement à la lumière de l'examen clinique n'apporte qu'une probabilité, plus ou moins grande sans doute, mais la certitude exige un examen microscopique.

1° *Limites dans l'obtention de la radiographie significative.* --- Quelquefois la prise du cliché est impossible, soit parce que le sein est aplasique, soit parce que les lésions collent le sein contre le grill costal, tel un squirrhe en cuirasse par exemple, mais en général l'examen clinique est facile dans ces cas là; alors que les seins volumineux au contraire, très adipeux, qui sont difficiles à palper, donnent d'excellents clichés, la graisse étant très transparente aux rayons X tout comme les lobules pulmonaires. Cependant, quelquefois même avec une technique rationnelle, les contrastes sont insuffisants, par exemple dans les mamelles volumineuses infiltrées au cours d'une mastite carcinomateuse, le dessin aura disparu si le sein est occupé en bloc par une masse homogène cancéreuse. Enfin, le silence pré-radiologique existe pour toutes les maladies dans tous les organes : les lésions ont un volume trop petit ou prennent d'emblée une forme diffuse sans signe d'accompagnement; très petit nodule, ou épithélioma au début s'étendant en patte d'araignée sans rétraction bien nette.

2°) *Limite dans l'interprétation du cliché.* — L'ampoule à rayons X ne voit pas les cellules cancéreuses, ne voit pas les bacilles de Koch, et par conséquent le diagnostic radiologique n'est qu'un diagnostic de probabilité, en particulier le tableau que nous avons donné est destiné à orienter ce diagnostic. Une même image peut être la traduction de maladies différentes, par exemple un nodule épithéliomateux squirrheux, un processus inflammatoire ancien, un processus stéato-nécrotique pourront donner des mêmes images en étoile comme quelquefois les mêmes signes cliniques. Inversement une même maladie peut avoir des traductions radiologiques diverses; par exemple certains cancers apparaîtront sur le cliché sous une image opaque étoilée, ou sous les seuls signes de rétractions de voisinage, ou se trahiront par de simples calcifications miliaires, ou même par un nodule arrondi (fig. 32). Donc sur un cliché mammaire présentant des anomalies, notre interprétation risque d'être incertaine ou erronée, comme pour tout radiodiagnostic; mais une technique parfaite, une lecture minutieuse des clichés, une meilleure connaissance des confrontations anatomiques ajoutées à un examen clinique attentif, une transillumination systématique, réduiront les hésitations et les erreurs.

Le radiologiste doit lui-même pratiquer un examen clinique attentif et complet, comme il doit lui-même prendre tous les clichés : son interprétation des images sera alors rationnelle. Les séquelles d'un traumatisme, l'évolution d'un abcès chronique banal, s'accompagnent quelquefois d'images cliniques et radiologiques simulant un nodule cancéreux rétractile, alors que l'interrogatoire lève l'hésitation.

L'inspection du mamelon en révélant des croûtelles, des traces d'écoulement, orientera vers la nécessité d'une galactophotographie; surtout si les autres examens sont négatifs, le massage du mamelon doit toujours être fait. La palpation est indispensable, aussi bien pour préciser les incidences et les conditions de la prise du cliché, que pour apprécier le volume tactile clinique permettant ensuite une comparaison avec le volume « radiologique ».

Enfin nous pratiquons systématiquement la transillumination. Si son renseignement est rarement utile, l'analyse moins fouillée, elle peut dans certains cas aider à la conclusion finale. L'absorption des rayons X et des radiations lumineuses est délicate. Pour les corps organiques à volume et épaisseur égale, l'absorption des rayons X dépend uniquement des atomes, tandis que l'absorption de la lumière dépend de la molécule, elle, responsable de la cou-

leur. Un kyste hématique est peu opaque aux rayons X, alors qu'il apparaîtra très noir à la transillumination sur toute la plage orangée du sein.

Nous avons pratiqué aussi à titre documentaire la photographie infra-rouge des veines superficielles du thorax comme l'a pratiqué Massopust. Mais les dessins veineux très variables ne nous paraissent pas apporter un complément d'investigation original et nous l'avons abandonné actuellement.

Lorsque le syndrome radio-clinique est douteux, nous pratiquons nous-même alors une biopsie. Cette biopsie est faite par ponction après introduction d'un trocart animé d'un mouvement rotatoire rapide, et d'aspiration à la seringue. Les boudins retirés dont les dimensions ont de 2 mm de diamètre et quelques centimètres de longueur, sont suffisants pour faire un examen microscopique. De plus la région biopsiée est précisée par radiographie, afin que le prélèvement porte sur la zone vraiment suspecte. Il arrive en effet qu'un très petit nodule de type squirrheux provoque une rétraction telle que la masse tumorale paraît volumineuse, alors que le nodule épithéliomateux est assez réduit; la palpation seule oriente mal la biopsie. Dans un cas la palpation ne révélait qu'une masse volumineuse arrondie, alors que le cliché mettait en évidence deux nodules étoilés, rétractiles, séparés par une zone d'apparence normale, non néoplasique qui aurait été biopsiée sans doute, car cette zone était cliniquement la partie centrale de la tumeur.

Les indications.

Elles découlent logiquement de ce qui vient d'être dit. Si la patiente se présente avec un sein volumineux, des bourgeons néoplasiques ulcérant la peau, des adénopathies le long de la chaîne axillaire ou sus-claviculaire, la radiographie n'a plus d'intérêt. Mais en dehors des cas où le diagnostic est vraiment évident, cancer très avancé, ou abcès simple au cours de la lactation, l'exploration rendra dans tous les autres cas, des services divers apportant toujours quelques renseignements complémentaires à l'investigation clinique seule.

1° *Dépister une lésion :*

La recherche d'un noyau tumoral dans un sein apparemment libre, à la palpation et l'inspection, de toute lésion, sera intéressante dans plusieurs cas.

- a) Exploration du sein restant : Nous savons en effet que celui-ci, assez souvent, 2 % environ des cas, est le siège d'un processus tumoral, lorsque l'autre sein a lui-même déjà été atteint de cancer;
- b) Une adénopathie axillaire d'un épithélioma glandulaire, est quelquefois d'apparence primitive, dans ce cas la radiographie peut dévoiler la tumeur restée muette à la palpation ou ne rien révéler. De même toute métastase exige une investigation mammaire;
- c) Les écoulements mamelonaires peuvent ne pas avoir de traduction clinique, seule l'injection des galactophores montre soit la dilatation (fig. 34) de ces canaux, soit la néoformation intracanaliculaire (fig. 36), de même toute anomalie acquise du mamelon, sans signe clinique de tumeur (fig. 6);
- d) Dans un centre de dépistage des tumeurs, un tel examen nous paraît indispensable. La radiographie a la faveur et la confiance du public, et rien ne doit être négligé dans le diagnostic précoce des cancers, en particulier du sein, condition nécessaire si non suffisante d'une thérapeutique efficace. Si des consultantes, inquiètes parce qu'elles ont « senti » quelque chose d'anormal dans leur sein, ou parce que dans leur famille il y a des cancéreuses, sont amenées par la voie de la radiologie, il faut s'en réjouir;
- e) Enfin chez certaines cancérophobes, l'analyse aux R.X. complétant un examen négatif, rassure la malade : notre tranquillité a souvent été assurée par ce moyen...

2° Préciser la nature des lésions.

Le cancer domine la pathologie de la mamelle, et c'est toujours en face d'un tel diagnostic, que se discutent toutes les autres hypothèses. Or si les cancers avancés ont un diagnostic clinique facile et sûr; le diagnostic précoce, la mise en évidence d'une tumeur maligne, au début, comme nous serons appelés à la voir de plus en plus, ne peut pas être faite par la clinique seule et l'exploration biopsique n'est pas toujours une technique systématique et parfaite.

Le diagnostic d'un cancer incipiens, le seul qui soit vraiment intéressant pour la thérapeutique, est souvent impossible à faire à la palpation ou l'inspection seule. L'expérience montre que l'examen clinique le plus minutieux engendre des erreurs dans les deux sens, tantôt un nodule est pris pour un cancer, alors qu'il est de nature bénigne, même si ce nodule paraît dur (fig. 14), même

s'il rétracte la peau (fig. 18) ou déforme le mamelon et même s'il est accompagné d'adénopathies axillaires. Inversement une tumeur intra-mammaire paraissant molle (fig. 22), bien limitée (fig. 26) sans peau d'orange (fig. 21), sans rétraction du mamelon (fig. 19, 21, 26), sans atteinte de l'état général, peut être de nature cancéreuse. Nous ne connaissons pas de signe clinique pathognomonique pour affirmer ou suspecter un cancer de la mamelle au début; surtout si cette mamelle est volumineuse ou assez ferme : les défaillances de la clinique à ce stade sont classiques. Inutile de dire que la conclusion doit toujours être une synthèse radio-clinique. Sans doute un prélèvement peut être fait, dont l'examen microscopique permettrait un diagnostic certain. Mais cette biopsie présente quelques servitudes : La malade, surtout lorsqu'elle est jeune et en parfaite santé ne se soumet pas toujours volontiers à une biopsie ouverte, chirurgicale; n'en comprenant pas la nécessité, redoutant une cicatrice inesthétique et certaines malades que nous avons jadis confiées à un chirurgien dans ce but, ne se sont pas présentées, immédiatement.

La maladie cancéreuse, si elle ne reçoit pas un coup de fouet ni une poussée d'essaimage, après un prélèvement suivi immédiatement d'une exérèse ou après une ponction-biopsie, peut exceptionnellement sans doute être aggravée si l'investigation chirurgicale est séparée de l'acte thérapeutique de quelques jours.

Le médecin peut prélever dans le voisinage du petit nodule cancéreux; l'anatomo-pathologiste peut n'avoir qu'un tissu insuffisant.

Les ponctions biopsies, guidées par la radiographie, échappent à ces critiques et nous ont donné jusqu'à maintenant des résultats microscopiques exacts.

3°) *Morphologie, Topographie des lésions.*

Si la présence de calcifications miliaires oriente vers une variété d'épithéliomas, les images n'ont pas de correspondance histopathologique. Mais les renseignements macroscopiques ne sont pas négligeables. L'étendue et le siège des lésions sont mieux appréciés; la ligne claire devant le pectoral pourra être légèrement envahie; les calcifications éloignées de la tumeur clinique, montrent que le processus est diffus; un noyau squirrheux retractant l'atmosphère glandulo-adipeuse fait croire à l'envahissement complet de la glande, alors que le cancer est de petite dimension. L'infiltration néoplasique vers certaines zones est mise en évidence. Certains épithéliomas sont squirrheux, infiltrant sur un

côté et encéphaloïde de l'autre côté (fig. 26). En résumé, le cliché est l'homologue de l'examen macroscopique de la pièce opératoire.

4° *Indication thérapeutique.*

Il semble que le polymorphisme du cancer du sein, polymorphisme clinique, radiologique, histologique doive entraîner des thérapeutiques nombreuses et variées, aussi bien dans l'indication que dans la conduite et le choix du traitement. Or les nuances anatomo-cliniques n'ont pas en général de répercussion sur la thérapeutique. Certains préconisent systématiquement le Halsted, associé ou non à la radiothérapie, pré- ou post-opératoire, d'autres envisagent systématiquement une mamectomie avec de la radiothérapie des ganglions, d'autres sont partisans de la curiepuncture ou de la roentgenthérapie et dans certains cas enfin un traitement médical peut s'imposer. Il est difficile de se faire une opinion exacte sur les avantages de ces différentes techniques, mais notre but est de les adapter à chaque cas plutôt que d'envisager un mode systématique de traitement quel que soit la maladie de la malade. Peut-être l'image radiologique par les renseignements sur la forme macroscopique, sur le siège exact, sur l'infiltration péri-tumorale, apportera dans certains cas, une information supplémentaire pour choisir la modalité de thérapeutique. Par exemple un aspect nodulaire cancéreux, petit et bien limité, apparaissant chez une jeune femme en voyage de noce relèvera plutôt d'une tumorectomie suivie de radiothérapie. Au contraire une forme bien limitée cliniquement, mais diffuse radiologiquement (fig. 26) relèvera d'autres thérapeutiques. La curiepuncture sera aidée par le cliché qui précisera les limites de la tumeur.

5° *Surveillance et contrôle.*

Toute masse dans la mamelle doit être surveillée, en particulier lorsque le médecin prend l'initiative et la responsabilité de traitements hormonaux plus ou moins intenses ou prolongés : adénofibrome, seins douloureux, mastite scléro-kystique ou pour d'autres affections intra-mammaires. De même la roentgenthérapie toute seule peut faire disparaître certains cancers des seins, or les seins volumineux ou même petits, qui ont été fortement irradiés, sont toujours, dans les premiers mois qui suivent le traitement, difficiles à explorer, par la palpation seule. Une infiltration fibro-œdémateuse rend impossible une exploration complète de ce sein post-radiothérapique. Alors que la radiographie donne des renseignements intéressants.

6° *Propagande.*

Le grand public a une grande confiance dans la radiologie qui sonde sans douleur les reins et les cœurs et se traduit par une image et non pas par une courbe ou un nombre; les femmes consulteront plus facilement un radiologiste à la moindre anomalie observée, qu'un chirurgien. Or, ce qui est fondamental dans la lutte anti-cancéreuse, c'est que les premières consultations se fassent au début de la maladie, quelque soit le spécialiste consulté. La radiographie nous paraît un bon moyen de propagande pour le cancer de la mamelle.

7° *Action curative des galactophographies au diodone.*

Un certain nombre de patientes présentaient un seul symptôme: écoulement non sanglant du mamelon et une seule anomalie radiologique : dilatation des galactophores. Quelques semaines après l'injection de diodone, l'écoulement diminuait et cessait, alors que le contrôle radiologique démontrait le retour des canaux dilatés à un calibre normal. La plus ancienne guérison remonte à un an (fig. 34-35).

Nous avons traité par cette méthode 9 malades dont 7 ont pu être contrôlées six mois après l'injection. 3 de ces malades ont présenté une restitution anatomo-radiologique et une guérison clinique. 4 de ces malades n'ont montré que des variations dans le sens de l'amélioration anatomique, mais toutes étaient guéries cliniquement.

CONCLUSION.

La radiographie du sein sans préparation est minutieuse, quelquefois longue; les images pourront être peu contrastées et difficiles à interpréter; mais cette exploration donne des renseignements objectifs, toujours utiles, souvent indispensables. La technique, comme la séméiologie iront en se perfectionnant : son intérêt s'étend, comme la radiographie pulmonaire, aux différents problèmes posés par le cancer du sein.

266

PROF. C. M. GROS & D^r R. SIGRIST

TABLEAU I. — TECHNIQUE UTILISÉE.
(Examen clinique préalable détaillé et très complet.)

Foyer (fig. 3).	Anode fixe 3 × 3 mm. (Picker).
Voltage :	25 à 40 KV suivant : \ épaisseur, / densité.
Milliampères-seconde :	100 m. A.S. pour 6 centimètres d'épaisseur à 30 KV.
Localisateurs : (fig. 2)	Longueurs : > 70 cm. — (télé) : systématique, < 10 cm. — (au contact) si tumeur périphérique. Formes adaptées : — au sein tout entier pathologique et normal; — à la région suspecte.
Incidences :	Cranio-caudale — systématique (fig. 1). Latérale { oblique { selon situation de la tumeur.
Temps de pose :	Sein normal : 1 cliché : temps de pose prévu (par ex. 4 secondes). Sein pathologique : 3 clichés, avec même long localisateur que pour le sein normal et sur le même film (24 × 30), différents entre eux d'une seconde, 3 sec., 4, 5. Temps de pose augmenté si étroitesse du localisateur, diminué si brièveté.
Nombre de clichés :	Sein normal (pour comparaison) 1 Dépistage, sans anomalie clinique 2 Sein pathologique 6 à 10
Moment de l'examen :	Indifférent : mais si images indécises le répéter une semaine après les règles de préférence; ou à un moment dicté par les données cliniques.
Compression systématique :	(Pas de grilles, ni d'écrans renforceurs, ni filtre.)
Injectons des galactophores :	Si écoulement mammaire : diodone à 35 %. (Film : Kodak sans écran : révélateur : fixateur.)
Examen du cliché :	— Long, minutieux, attentif (à la loupe). — Sur un négatoscope à surface et à éclaircissement variable.

TABLEAU 2.
Syndrome radiologique de la b nignit  et de la malignit 
d'une n oplasie de la mam lle.
 (Guide sch matique.)

	Formations b�nignes (tumorales ou non).	Tumeurs malignes (type squirrheux partiel ou total).
Forme.	— arrondie, — ovalaire, — polylob�e.	— �toil�e « en pattes de crabe », — radi�e : spicules, — quelconque.
Contours.	— r�guli�rs, — nets, — liser� clair, p�riph�rique.	— irr�guli�rs, — impr�cis, — sans liser� clair.
Volume radio- logique opaque.	— �gal au volume tactile.	— tr�s inf�rieur au volume tactile.
Opacit�.	— homog�ne.	— non homog�ne.
Rapports avec les tissus voisins.	— non modifi�s, — refoul�s, — ligne claire r�tromam- maire.	— infiltr�s, — r�tract�s, — ligne claire envahie.
Calcifications.	— peu nombreuses, — non punctiformes, — isol�es.	— tr�s nombreuses, — punctiformes, — group�es.

(G. M. GROS et R. SIGRIST.)

Bibliographie.

- BARALDI, A. — Roentgen-neumo-mastia. *Bol. y trab. de la Soc. de cir. de Buenos-Aires*, 1934, 18, 1254-1267; *Rev. med. del Rostario*, 1935, p. 1536; *Rev. de cir. de Buenos-Aires*, 1935, 14, 321-342.
- CHEATLE, G. L. and CUTIER, M. — *Tumors of the Breast*. J.-B. Lippincott Company, Philadelphia, 1931.
- CONWAY, J. H. — Calcified breast tumors. *Am. J. Surg.*, 1936, 31, 72-76.
- ESPAILLAT. — Contribution   l' tude radiographique du sein normal et pathologique. *Th se Alex. Espaillat*, 1933.
- FRANTZELL, A. — Soft tissues radiography. *Acta Radiologica*, supplement LXXXV.
- FRIEDMAN, J. L. and SLATER, C. — Mammography; soft tissue technique. *Am. J. Surg.*, 1938, 41, 310-314.
- GERSHON-COHEN, J. and COLCHER, A. E. — Evaluation of roentgen diagnosis of early carcinoma of breast. *J.A.M.A.*, 1937, 108, 867-871.
- GROS, Ch. M. et SIGRIST, R. — La radiographie et la transillumination de la mam lle. *Strasbourg M dical*, ao t 1951, pp. 1-15.
- GROS, Ch. M., SIGRIST, R. et SPEEG, P. — Radiographie de la mam lle tumorale. *Journ. de Radiol. et d'Electrol.*, 1951 (  l'impression).

- GUNSETT, A. and SICHEL, D. — Sur la valeur pratique de la radiographie du sein. *J. de Radiol. et d'Electrol.*, 1934, 18, 611-614.
- HICKEN, N. F. — Mammography : roentgenographic diagnosis of breast tumors by means of contrast media. *Surg. Gynec. & Obst.*, 1937, 64, 593-603.
- HICKEN, N. F., BEST, R. R. and HUNT, H. B. — Discharges from nipple; their clinical significance and mammographic interpretation. *Arch. Surg.*, 1937, 35, 1079-1094.
- LEBORGNE, R. — Diagnosis of tumors of the breast by simple roentgenography. Calcifications in carcinomas. *The Am. J. of Roentgenology and Radium Therapy*, vol. 65, n° 1, janv. 1951, pp. 1-11.
- LEBORGNE, R. — Diagnostico de los tumores de la mama por la radiografia simple. *Bol. Soc. cir. d. Uruguay*, 1949, 20, 407-422.
- LEDOUX-LEBARD, R., GARCIA-CALDERON, J. and ESPAILLAT, G. A. — Etude radiographique de la glande mammaire. *Bull. et Mém. Soc. de Radiol. Méd. de France*, 1933, 21, 418-423.
- LOCKWOOD, I. H. — Roentgen-ray evaluation of breast symptoms. *Am. J. Roentgenol. & Rad. Therapy*, 1933, 29, 145-155.
- MASSOPUST, L. C. — Etudes photographiques infra-rouges des veines superficielles du thorax en relation avec les tumeurs du sein. *Surgery, Gynecology and Obstetrics*, vol. 86, janv. 1948, n° 1, pp. 54-58.
- MELOT, G. — Contribution à l'étude radiographique des tissus de faible densité. (Thèse Bruxelles, 5-XII-45.) Edité par *Journal Belge de Radiologie*.
- RIES, E. — Diagnostic lipiodol injection into milkducts following by abscess formation. *Am. J. Obst. & Gynec.*, 1930, 20, 414-416.
- SALOMON, A. — Beiträge zur Pathologie und Klinik des Mammacarcinoms. *Arch. f. klin. Chir.*, 1913, 101, 573-668.
- SEABOLD, P. S. — Diagnosis of breast diseases by x-ray. *Ann. Surg.*, 1931, 94, 443-444.
- WARREN, S. L. — Roentgenologic study of breast. *Am. J. Roentgenol. & Therapy*, 1930, 24, 113-124.
-

8.3 Experience with mammography in tumor institution: evaluation of 1000 studies

Robert L. Egan (1920–2001)

Robert Lee Egan was born on 9 May 9 1920 in Morrilton, Arkansas in the USA, a cotton town with a population of less than 5,000. He took his undergraduate studies at the College of the Ozarks and majored in chemistry, mathematics and qualified as a metallurgical engineer. In 1941 he became a specialist in tools and steel. In 1946 Robert Egan entered medical school in the first post-war class at the University of Pittsburgh Medical School. His internship was served at the US Naval Hospital in Portsmouth, Virginia.

In the early 1950s he set up a general medical practice in Curtisville, Pennsylvania. He then started his residency in radiology at the Jefferson University Medical School in Pennsylvania and completed his residency at M.D. Anderson Hospital in Houston, Texas, where he became a fellow in diagnostic radiology. In 1956 he successfully passed his boards in radiology from the American Board of Radiology. He became a fellow of the American College of Radiology in 1967. After leaving M.D. Anderson Tumor Institute, he was in private practice in Indianapolis, Indiana. In 1965 he joined Emory University Medical School to work full time in research and development of mammography.

Robert Egan is recognized as the developer of modern mammography. His early residency training in Pennsylvania introduced him to the early work of Gershon-Cohen and Leborgne in breast imaging. In 1954, while at M.D. Anderson Hospital Tumor Institute in Houston, he started developing reliable mammograms. Following extensive experiments with various technical combinations he build up a non-filtered beam device using high current and low voltage suitable to the minor absorption differences of breast tissue. Multiple kinds of film material were also investigated. Egan used a polymer material to simulate breast tissue, embedding blocks of the substance with items of various density, from paper clips to talcum powder, and then X-raying the blocks and studying the film. M type industrial film was then chosen because of its high resolution and wide gray scale. By 1960, he had a usable system and tested it in clinical trials, showing it to be an acceptable and reproducible technique for early detection of breast cancer. The combination of different factors tested resulted in high-quality mammographic images.

Robert Egan received the James Ewing/Lucy Wortham clinical research award in 1977, the American Cancer Society's distinguished service award in 1975. He was a member of the Danish Radiological Society and the Scandinavian Association of Radiology and was awarded the Gold Medal of the American College of Radiology in 1992.

Robert Egan died on 4 February 2001.

Picture and information Courtesy RH Gold, MD, Dep. Radiology Science UCLA, 2004.



Experience with Mammography in a Tumor Institution

Evaluation of 1,000 Studies¹

ROBERT L. EGAN, M.D.

SOFT-TISSUE roentgenography of the breast is not new. In the American literature, Leborgne (4) of Uruguay described the technic of examination and the roentgenographic appearance of various mammary tumors. Warren (5) of the United States in 1929 reported on 119 cases, 58 of which were malignant. Interpretative errors were made in but 8 cases, 4 being in the malignant group. He stated: "In many of the cases, there was no unanimity of opinion in the preoperative clinical diagnosis. Several opinions were often held as to the presence of malignant or benign tumors in each case. The opinion from the roentgenogram, on the other hand, was often very definite and, most frequently, correct." Since Warren's publication an occasional enthusiastic proponent of this method of examination has appeared. However, as of the date of this study, no satisfactory statistical analysis of consecutive mammograms in patients with adequate follow-up has appeared in the American literature.

MATERIAL

One thousand consecutive x-ray examinations of the breast were performed at the M. D. Anderson Hospital and Tumor Institute in the period from May 1956 to May 1959. Adequate follow-up to date has been available on all except 2 patients. These were excluded from the series as both were examined in the terminal stage of malignant lymphoma, and neither biopsy nor autopsy was obtained. Six hundred and thirty-four patients were examined. For simplicity of presentation of results, each breast was considered a separate study. Frequently there was a lesion, benign or malignant, on each side, possibly with only 1 correctly diagnosed; or the

patient may have had a previous mastectomy, leaving only one breast for study.

Not all patients admitted to the Hospital's breast service were referred for mammography. During the three-year period 1,253 new patients with lesions subsequently proved by biopsy were seen at that clinic, and of these, 956 had malignant and 297 had benign lesions. Cases of a questionable or palpable nodule in the breast, an inverted nipple, or nipple discharge were referred for mammography. Occasionally breasts were normal to palpation even though there was undifferentiated carcinoma in the axillary nodes or osseous lesions resembling metastatic carcinoma of the breast. Breasts containing clinically obvious carcinoma or with a known diagnosis of carcinoma following recent biopsy were not studied. The opposite breast was examined when such a patient was referred for mammography, however. If the result of the previous biopsy was not stated on the request for roentgenography, both breasts were radiographed.

ROENTGENOGRAPHIC TECHNIC

Positioning of the patient is illustrated in Figures 1-3. One roentgenogram of the axilla is obtained and two of the breast, in 2 planes at right angles. These have resulted in good delineation of the quadrants, ease in positioning, and patient comfort with consequent cooperation. The entire breast is positioned on a pliable cardboard holder which may be placed to follow the contour of the chest wall in the oblique position, thus covering the smallest gland. "Kodak Industrial M" film is used. The range of technical factors is shown in Table I. Usually the only variable is the distance necessary to include the entire breast on the roentgenogram. In general, 26 kv

¹ From the Department of Radiology, The University of Texas, M. D. Anderson Hospital and Tumor Institute, Houston, Texas. Accepted for publication in May 1960.



Fig. 1. Positioning for the cranio-caudad view. Identification marker is kept on the axillary side of breast for localization of the mammary quadrant.

Fig. 2. Oblique or lateral position. The cardboard film-holder is supported on a small wood block.

Fig. 3. Axillary view. The central beam is centered to the apex of the axilla and also parallel to the retro-mammary space. This arm position provides maximum visualization of the axilla as it reduces the number of skin folds without superimposition of the scapula. Factors: 54 kv, 300 ma, 40 inches, three and a half seconds; in obese patients the distance is reduced to 30 in.

TABLE I: RANGE OF TECHNICAL FACTORS USED TO PRODUCE ROENTGENOGRAMS OF THE BREAST

Age Group, Breast Type	Technical Factors
I. Menopausal, average consistency	
Small	
Cranio-caudad projection	300 ma, 22 kv, 30 in., 6 sec.
Oblique projection	300 ma, 24 kv, 30 in., 6 sec.
Medium	
Cranio-caudad projection	300 ma, 26 kv, 36 in., 6 sec.
Oblique projection	300 ma, 28 kv, 36 in., 6 sec.
Large	
Cranio-caudad projection	300 ma, 26 kv, 40 in., 6 sec.
Oblique projection	300 ma, 28 kv, 40 in., 6 sec.
II. Postmenopausal	Average 2-4 kv less; if flabby and flat, 5 sec.
III. Premenopausal, 30- to 45-year age group	Same as menopausal if only residual glandular tissue; 2-4 kv added with firmer breasts
IV. Virginal type	Same as premenopausal firm breast, but because of usually smaller size, 26 to 30 in. covers breast; 32-34 kv occasionally required
V. Dense area	Distance reduced to 20 to 22 in.

for the cranio-caudad projection and 28 kv for the oblique view, with 300 ma and six seconds, will suffice. The decreased distance for the smaller breasts adds sufficient mas to penetrate the denser glands; the larger breasts containing more fat are less

dense, and require less mas. Only inherent tube filtration is used.

This technic has been productive of satisfactory roentgenograms in the hands of both student and staff technicians. Repeat examinations are rare. In practice the examination is no more difficult than routine chest studies and the time involved is comparable to that of a routine cervical spine study.

Neither the large focal spot nor the long exposure causes appreciable loss of detail. Use of a single fine-grain intensifying screen preserves most of the detail but with the addition of a second fine-grain screen soft-tissue detail is sacrificed. This is in contrast to the techniques of higher kilovoltage, fast intensifying screens, and coarse-grain film advocated in the American literature (1, 3).

At these kilovoltage ranges, true mas was not obtained due to electron fog at the tube filament. The usual diagnostic x-ray machine does not have compensatory filament voltage regulation below 40 kv. Kilovoltage settings below 30 kv actually produce film characteristics more in keeping with the changes in mas than with the quality of the x-rays reaching the film.

The amount of radiation to the eye, skin, or gonads could not be calculated; actual measurements had to be made. In the

cranio-caudad position the film-holder was placed over a lead shield to protect against possible gonadal radiation. Patient exposure was found to be negligible.

The aluminum wedge may be used to transfer technical factors from one x-ray unit to another. At a distance of 36 inches, and with employment of a cone, type "M" film in a cardboard holder, and 300 ma at six seconds, the kilovoltage is varied until 15 mm. of aluminum is just faintly penetrated. This kilovoltage setting may then be used as the average and changed accordingly.

STATISTICAL METHODS

When it was decided to set up a technic for soft-tissue roentgenography of the breast in our department we felt we should be as objective as possible in the interpretation of the examination and rely entirely upon the roentgenograms without benefit of history or physical findings. The report of each study would include the absence or presence of a lesion and an opinion as to its benignity or malignancy. The diagnosis would be designated by a specific code symbol so that in review no confusion would arise as to the original conclusion. In such a system, there would be no provision for indeterminate studies. The single most important diagnosis was used in tabulation of the results even though more than one pathologic entity was present in the same breast.

All patients having mammography were examined in the breast clinic and most of them have been followed by periodic examinations there. A few, referred for consultation only, had follow-up reports from the referring physicians in their charts, giving either the final pathologic diagnosis or the results of periodic examinations. The clinical diagnosis of fibrocystic disease has been substantiated by aspiration of a cyst in many instances. Papanicolaou studies were routinely made on all patients with nipple discharge.

The follow-up span on all patients varied from six months to three and a half years, including the 361 whose examinations were

read as negative. In none of these cases did breast carcinoma subsequently develop within the follow-up period.

The pathologist's most recent opinion on the breast biopsy tissue, the radical mastectomy specimen, or the postmortem findings was used as the diagnosis in each case. In the absence of a biopsy, those lesions diagnosed as benign have been considered verified by typical roentgenologic and physical findings which have remained constant on follow-up examinations.

ROENTGEN DIAGNOSIS

The important diagnostic signs in soft-tissue roentgenography of the breast have been lucidly described by Leborgne (4). He reported calcification in malignant mammary neoplasms and described "scattering . . . of innumerable punctate calcifications resembling fine grains of salt . . . in and surrounding the nodule."

These flecks, referred to as calcifications from their appearance on the roentgenograms, do not all take calcium stains, and may be partly due to detritus in the tumor. The percentage of cases in which they were demonstrated was, in part, proportional to the quality of the roentgenogram. Calcium or not, their presence is practically pathognomonic of carcinoma, and they were observed in 118 of the 245 cases of carcinoma in our series. Coarser and denser types of calcification were found only in benign conditions such as fibroadenoma, plasma-cell mastitis, calcifying cysts, or arteriosclerosis.

The benign breast masses were homogeneously dense, rounded or smoothly lobulated, and surrounded by a thin radiolucent layer of fat. They pushed normal tissue aside and produced only local changes. The malignant tumors were denser in the center, had irregular spiculated borders, invaded nearby tissue, and were usually associated with some secondary changes in the breast: localized or diffuse skin thickening, nipple retraction, venous engorgement, or involvement of axillary nodes. Diffuse thickening of the skin was a reliable sign of carcinoma.

TABLE II: DIAGNOSES IN 1,000 CONSECUTIVE MAMMOGRAPHIC STUDIES AS REPORTED AND CODED FROM MAY 1956 TO MAY 1959* ("Clinically negative" indicates breasts normal to palpation)

	Total	Coded as Benign	Coded as Negative	Coded as Malignant	Clinically Negative
Malignant lesion	245	0	7	238	19
Benign lesion; biopsy	182	162	0	20	0
No lesion; biopsy	4	0	4	0	0
Benign lesion; no biopsy	248	248	0	0	...
No lesion; no biopsy	321	0	321	0	321

* This is primarily a statistical review. Since preservation of adequate detail is difficult, no reproductions of roentgenograms are included.

RESULTS

The 1,000 studies were grouped as shown in Table II. The 7 cases of malignant disease coded as negative included 5 patients whose tumor was removed at the time of biopsy prior to admission, with no residual carcinoma being found in the postirradiated radical mastectomy specimen; 1 patient with a tumor in the tail of the breast not demonstrated on the roentgenograms as this was prior to the use of the axillary view; 1 patient with a small parasternal carcinoma that was not projected on the roentgenograms. Considering only the malignant lesions, the definite error in diagnosis by roentgenography was only 2 out of 240, or 0.83 per cent. Malignant tumors were found in 19 breasts clinically considered to be negative.

The benign lesions were diagnosed as indicated in Table III. Five small fibroadenomas in fibrocystic disease were overlooked; these were considered errors in diagnosis, with fibroadenoma used as the primary diagnosis.

DIFFICULTIES, SOURCES OF ERROR, OBSERVATIONS

Roentgenographic technics for soft-tissue study of most areas of the body are critical. This is not true of the breast where contrast of fat and surrounding structures ex-

TABLE III: FREQUENCY OF THE VARIOUS BENIGN CONDITIONS ENCOUNTERED IN 1,000 MAMMOGRAMS FROM MAY 1956 TO MAY 1959, TOGETHER WITH THEIR DIAGNOSIS BY MAMMOGRAPHY AND THE LESIONS MORE COMMONLY CONFUSED WITH CARCINOMA

	Total	Correct X-Ray Diagnosis	Coded as Malignant
Benign lesions with biopsy	102	99	3
Fibrocystic disease	36	30	1
Fibroadenoma*	16	8	8
Abscess	9	5	4
Sclerosing adenosis	4	4	0
Dilated ducts	4	2	2
Intraductal papilloma	2	1	1
Benign fibrosis	2	2	0
Sebaceous cyst	3	3	0
Cystosarcoma phylloides	1	1	0
Scleroderma morphea	1	1	0
Ectopic breast	1	0	1
Granulomatous tissue	1	1	0
Granular-cell myoblastoma	240	240	..
Benign lesions without biopsy	4	4	..
Fibrocystic disease	4	4	..
Plasma-cell mastitis	4	4	..
Fibroadenoma	430	405	20
TOTAL			

* Five fibroadenomas in fibrocystic disease were overlooked.

ists and the paramount aim is detail rather than contrast. There is, however, variability of contrast due to factors of age, size of breast, state of nutrition, pregnancy, lactation, time in menstrual cycle, and the wide range of other normal physiological cyclic changes as well as abnormal processes.

In late pregnancy or lactation, or in the larger and denser virginal type of breast, the roentgenograms tend to be of poorer quality due to the higher kilovoltage required for penetration. For a diagnosis of carcinoma in these dense breasts, the tumor must be large or secondary signs of malignant disease must be present. Although not encountered in this study, a small carcinoma may be overlooked under such circumstances.

The roentgenogram must be obtained with the nipple in profile, otherwise nipple retraction cannot be evaluated.

The false positives, benign processes called malignant, were the greatest source of error in this series. These lesions included abscesses, infected cysts, or fibrocystic disease associated with marked sclerosing adenosis and/or ductal hyperplasia. In a review of these cases, the presence of carcinoma could not be definitely excluded by roentgenography. These are the lesions that would comprise the indeterminate group and, unfortunately, they were also considered malignant clinically; in at least 2 cases biopsies were performed three times.

Another difficulty encountered with fibrocystic disease, as already indicated, was the presence of a small fibroadenoma that was overlooked or considered a part of the fibrocystic process. This was an incidental finding at biopsy. Dilated ducts and intraductal papillomas were frequently similar in appearance; however, the treatment was the same: local excision to control bleeding. The single case of scleroderma morphea was reported merely as benign localized skin thickening, and a granular-cell myoblastoma was also coded only as a benign lesion. Sebaceous or intradermal cysts were readily identified by their relationship to the skin; in accessible areas nevi were clearly shown without extension into the subcutaneous fat.

No comparison could be made with palpatory diagnosis as the clinicians frequently disagreed as to the diagnosis or withheld it with the simple remark "biopsy, frozen section, and, if positive, radical mastectomy." However, subsection of a patient to general anesthesia for diagnosis indicated a strong clinical impression of malignancy.

No attempt was made to record the incidence of primary lesions in both breasts since metastasis *versus* second primary is a difficult problem. The first case of metastatic melanoma to the breast was a single lesion and was coded as carcinoma; however, the second case with multiple lesions in both breasts was recognized and correctly diagnosed as metastatic disease in a patient known to have melanoma. Mucin-

ous adenocarcinoma, although not as aggressive-appearing as other malignant tumors, revealed sufficient changes for a diagnosis of carcinoma. Two cases of cystosarcoma phylloides were coded malignant purely on the basis of size, that being the only difference in appearance from the fibroadenoma or "giant fibroadenoma." Three other cases of cystosarcoma phylloides were coded as benign. The liberty was taken to leave these lesions as such in the tables since the pathologic diagnosis was on the basis of cell morphology rather than invasiveness of the tumor.

Postoperative changes following a biopsy for benign disease vaguely resembled localized carcinoma, without calcification or definite secondary signs of malignancy. In the absence of infectious complications, the mammogram reverted to a normal appearance in seven to ten days. Although many patients dated the onset of a breast nodule from trauma, no calcifying hematoma was encountered.

Usually in the breast with a previous biopsy for carcinoma, residual tumor or secondary signs of cancer were present and the diagnosis of carcinoma was readily made. The mammograms were obtained two to four weeks following the biopsy. The 5 cases with previous tumorectomy and normal mammograms were not considered unusual, however, as in these early lesions, following biopsy, the radical mastectomy specimen is often negative for residual carcinoma. These 5 patients did receive preoperative irradiation.

Of 4 cases of Paget's disease of the nipple, the underlying carcinoma was not detected clinically in 3, but was diagnosed by x-ray examination in all. Although the masses were not palpable, they could not be included with the unsuspected lesions, since the nipple changes reflected the presence of carcinoma clinically. In 1 of these cases, the nipple changes—slight elevation of 1 to 2 mm. and localized discoloration—were not roentgenographically apparent.

The smallest carcinoma demonstrated by roentgen rays was 8 mm. in diameter on sectioning. The presence of stippled cal-

cification led to the diagnosis. In the same breast the existence of a 4-mm. uncalcified nodule in a background of sclerosing adenosis was appreciated, although its malignant character was not. Small carcinomas in sclerosing adenosis were detected by the presence of calcifications; without such evidence, early malignant change cannot be recognized. With demonstrable calcification, the radiologist may be more definite than the surgeon in deciding which nodule should be biopsied or than the pathologist in deciding the question of malignancy *versus* benignity.

The demonstration of axillary nodes by roentgenography has some significance, but their finding is not a diagnostic criterion of malignancy. In 108 cases nonirradiated radical mastectomy specimens were available for pathologic study; axillary nodes were demonstrated by roentgen rays and found to be carcinomatous upon histopathologic study in 88. In 15 other cases microscopic carcinomas which had not been reported were present in axillary nodes, nearly all being less than 1 cm. in diameter. In 5 cases, however, noncarcinomatous nodes had been noted on the roentgenogram.

Despite these difficulties, the average study was simply obtained and readily interpreted. This is contrary to the views of the European authors who have stressed meticulous attention to technical details and special interpretative skills.

DISCUSSION

Soft-tissue roentgenography of the breast can be definitive in the diagnosis of malignant, benign, and normal conditions. Provision must be made for indeterminate studies and is just as necessary and valid for the radiologist as for the pathologist. Clinical judgment is mandatory but the typical carcinoma on a roentgenogram should not be ignored. The time-honored approach of palpation of a breast lesion followed by a decision to observe or prepare the patient for immediate radical mastectomy is necessary and well appreciated. While roentgenography has not established

the absolute preoperative diagnosis, its use and refinement should substantially reduce the preoperative diagnostic errors. At times the radiologist may express an opinion contrary to that of the surgeon and on occasion may find it necessary to challenge the pathologist's interpretation of a breast lesion.

In this group of patients, where mammography used as a guide to definitive treatment, no carcinoma would have been overlooked except the 2 not projected onto the films. (At the time of roentgenography, if the location of the palpable nodule in the breast is known, such errors should be preventable.) One hundred and sixty-six general anesthetics would have been avoided and only 20 patients with benign disease would have been prepared for radical mastectomy. It could not be determined in the review of numerous other benign lesions whether the radiologist's report influenced the clinical decision to omit biopsy. In no instance where a lesion was described on the x-ray report was the patient found to have a normal breast.

CONCLUSIONS

The palpatory method of detection and diagnosis of breast lesions is inaccurate even in an institution where a limited number of clinicians evaluate all patients attending the breast clinic, numbering 2,430 yearly. Soft-tissue roentgenography of the breast can reduce the error of preoperative diagnosis and reveal a number of unsuspected lesions. In addition, it can obviate a significant number of general anesthetics now administered for diagnostic purposes. Experience has shown mammography to be a simple method of demonstration of a breast lesion with a high accuracy in prediction of its type. Analysis of the value of soft-tissue roentgenography in our institution has indicated its reliability as a diagnostic tool.

SUMMARY

1. The roentgenographic interpretations, without benefit of history or clinical

findings, of 1,000 consecutive soft-tissue examinations of the breast are given.

2. A simple radiographic technic, based on changing the one variable of distance, is explained.

3. With roentgenograms of sufficient detail, any radiologist with the average physician's knowledge of the anatomy and pathological processes of the breast can diagnose breast lesions with a high degree of accuracy.

4. Experience with this simple examination in our institution has indicated its reliability as a diagnostic tool, with an error of less than 1 per cent in malignant disease.

REFERENCES

1. GERSHON-COHEN, J., AND INGLEBY, H.: Carcinoma of the Breast: Roentgenographic Technic and Diagnostic Criteria. *Radiology* 60: 68-76, January 1953.
2. GROS, C.-M., AND SIGRIST, R.: Radiography of the Breast. [In] *Gynecologic Radiography*, by J. Dalsace and J. Garcia-Caldéron. New York, Paul B. Hoeber, Inc., 1959, Chapter 22.
3. LAME, E. L., AND PENDERGRASS, E. R.: Addition to Technic of Simple Breast Roentgenography. *Radiology* 48: 266-268, March 1947.
4. LEBORGNE, R.: Diagnosis of Tumors of the Breast by Simple Roentgenography: Calcifications in Carcinomas. *Am. J. Roentgenol.* 65: 1-11, January 1951.
5. WARREN, S. L.: Roentgenologic Study of the Breast. *Am. J. Roentgenol.* 24: 113-124, August 1930.

Texas Medical Center
Houston 25, Texas

SUMMARIO IN INTERLINGUA

Experientias con Mammographia in un Institution pro Tumores

Mille consecutive roentgeno-examines del mamma esseva effectuate in 634 patientes inter maio 1956 e maio 1959. Le serie non include casos de obvie carcinoma o de carcinoma cognoscite per recente biopsias.

Un roentgenogramma esseva obtenite ab le axilla e 3 ab le mamma, in 2 planos a angulo recte. Un dispersion de innumerabile punctos de calcification, resimilante granos fin de sal, in e circum un nodule tumoric indica malignitate. Plus grossier e plus dense typos de calcification esseva trovate solmente in conditiones benigne: in fibroadenoma, mastitis plasmocytic, cystes calcificante, o arteriosclerosis. Benigne massas mammari esseva homogeneamente dense, ronde o lisiemente lobulate, e circumdate de un tenue strato de grassia radioluciente. Illos retroprimeva tissu normal e esseva responsabile solmente pro alterationes local. Maligne tumores esseva responsabile solmente pro alterationes local. Maligne tumores esseva plus dense in le centro; illos habeva spiculate margines irregular, invadeva le tissu adjacente,

e esseva usualmente associate con le un o le altere lesion secundari in le mamma.

Super le base de constatationes roentgenologic sol, 238 ex 245 canceres del mamma esseva registrate como maligne. In 5 del non assi registrate casos de cancer, le tumor esseva removite al tempore del biopsia ante le hospitalisation, e nulle residue carcinoma esseva trovate in le specimen del post-irradiatori mastectomia radical. In 2 casos le examinador non habeva essite informate del location probable del tumor, e isto non esseva projectate in le roentgenogramma. Omne le lesiones benigne, con solmente 20 exceptiones, esseva registrate como tales. Si nos considera solmente le neoplasmas maligne, le error definite in le diagnose per roentgenographia esseva 2 ex 240 o 0,83 pro cento. Maligne tumores esseva trovate in 19 mammas considerate, a base clinic, como negative. Nulle mamma esseva trovate normal pro le qual le reporto radiologic describeva un lesion.

Difficultates e fontes de error es discutite detaliatemente.

8.4 Evaluation of periodic breast cancer screening with mammography. Methodology and early observations.

Philip Strax (1909–1999)

Philip Strax was born in 1909 in New York, NY, and grew up in Brooklyn, NY. He graduated from New York University (NY) in 1931, where he received his BS and MD degrees. After initial experience as a general practitioner, he received additional training in radiology at New York Post-Graduate Medical School (NY) and, in 1942, became a diplomat of the American Board of Radiology. In 1962, he was named a fellow of the American College of Radiology. He practiced radiology in the New York City area for many years and had affiliations with many area hospitals, including City Hospital in New York, where he was director of radiology from 1950 to 1964.

In 1947, his first wife died of breast cancer, which ignited his passion to fight and cure the disease. At that time, mammography was not generally available. By the 1960s, early advocates of mammography, including Dr Robert Egan, were studying the value of the technique. Dr Strax heard about Dr Egan's work, learned to perform mammography and interpret its results, and began to offer mammography to his patients. In 1963, he and Samuel Shapiro, MD, initiated a study of the effectiveness of mammography for reducing mortality, the impressive results of which prompted routine use of mammography for breast cancer screening and led to other extensive studies. In 1988, they were honored for their work by the General Motors Cancer Research Foundation.

Dr Strax established the Guttman Institute in New York, NY, which made mammography available at little or no cost. In 1979, he moved to Ft. Lauderdale, Fla., and established the Strax Institute. Both institutes are in operation today. Dr Strax continued to perform clinical examinations until his retirement in 1989.

In addition to his accomplishments as a physician, he possessed qualities that set him apart as a humanitarian. He cared little about money and much about people. He was quick to lighten up a situation with his wonderful sense of humour. He was dignified and humble about his accomplishments and always praised others. Most of all, he was like a compassionate grandfather; he provoked the urge to hug him and thank him for his inspiration. Owing to his efforts in laying the foundations for breast cancer screening, his passion to combat the disease survives and flourishes.

Dr Philip Strax died in Bethesda, MD, on 9 March 1999, at the age of 90 years.

Reproduced with permission from Stuart S. Kaplan 2004.

Picture courtesy S.S. Kaplan.

Kaplan SS, Lemberg S (1999) In Memoriam, Radiology 213: 621

S. Shapiro

L. Venet

Evaluation of Periodic Breast Cancer Screening With Mammography

Methodology and Early Observations

Sam Shapiro, Philip Strax, MD, and Louis Venet, MD

Periodic breast cancer screening with mammography and clinical examination is being evaluated to determine its value in reducing breast cancer mortality among women. Representative samples of women aged 46 to 64 years enrolled in the Health Insurance Plan of Greater New York are randomly assigned to study and control groups, each of which will contain 30,000 women. Results of the study to date are consistent with the hypothesis that the screening leads to earlier detection of breast cancers than is ordinarily experienced and that mammography contributes significantly to detection. While these relationships are encouraging, they must be viewed with caution since the study is still in its early stages. Furthermore, the crucial question is whether mortality from breast cancer is lowered because of the screening, and definitive findings on this issue will require at least five years of follow-up.

This paper presents basic elements of the methodology and some of the early observations in a long-term study designed to evaluate periodic breast cancer screening. The project has been undertaken at a point in time when the outlook for significant reductions in mortality from breast cancer with current detection and treatment procedures is poor.¹ Breast cancer is the leading cause of death from malignancies among women in the United States. It develops in an estimated 6% of women during their lifetime.² About half of these women die within five years,³ and in succeeding years the mortality among women with the disease continues to be higher than among other women⁴⁻⁶ (Fig 1). Follow-up studies of long-term survivors of breast cancer in Connecticut indicate that breast cancer, regardless of the type involved, is the cause of death for a large proportion of these women.⁶ Fifteen to 20 years after initial diagnosis of the condition, a third of the deaths are attributed to breast cancer.

From the Division of Research and Statistics, Health Insurance Plan of Greater New York (Mr. Shapiro), the Department of Radiology, City Hospital Center at Elmhurst, Queens (Dr. Strax), and the Department of Surgery, New York Medical College and Beth Israel Medical Center (Dr. Venet), New York.

Reprint requests to 625 Madison Ave, New York 10022 (Mr. Shapiro).

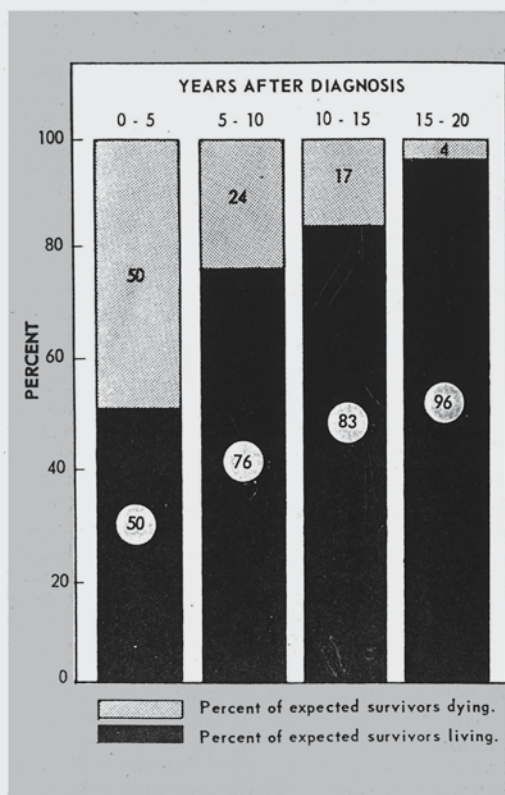
Cancer detection programs have for years emphasized the importance of early diagnosis in breast cancer. Proponents of periodic physical examinations have reported the detection of breast cancer in asymptomatic patients. Some have suggested an increase in the survival rate of patients with cancer of the breast so detected.⁷⁻⁹ However, in the United States there has been no rigorous study of the effect of such programs on the reduction of breast cancer mortality in a defined population.

The fact is that, despite increased attention given to measures to detect breast cancer early and technical progress in the medical armamentarium,¹ the breast cancer mortality in the female population has remained unchanged for about 30 years. Between 1935 and 1963 the age-adjusted mortality in the United States for women 25 years of age or older decreased by 39%, from 15.2 per

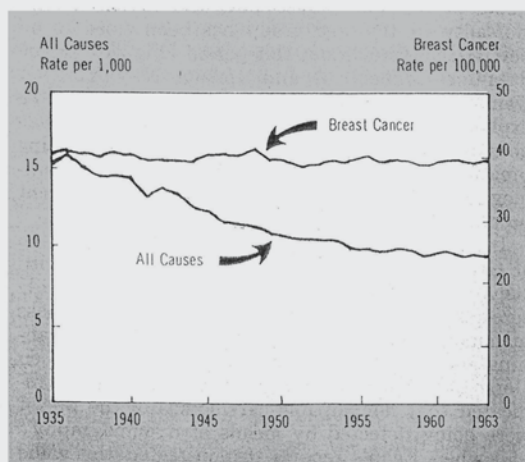
For editorial comment, see page 775.

1,000 to 9.3 per 1,000. But, the breast cancer mortality in this age group has been close to 40 per 100,000 throughout this period (Fig 2).¹⁰ (From data for Connecticut and upstate New York, it would appear that this lack of change could not be explained by increases in the incidence rate.) The possibility of changing this situation by detecting breast cancer in a preclinical stage through mammography has been advanced as holding sufficient promise to warrant an evaluation study.

In December 1963, the Health Insurance Plan of Greater New York (HIP) in cooperation with affiliated medical groups launched a large-scale screening program for breast cancer which uses mammography and a clinical examination. Planning for this study started early in 1962 when Gershon-Cohen's periodic reexamination survey indicated that nonpalpable carcinomas of the breast were being detected by means of mammography¹⁰ and when Egan's reports demonstrated the value of mammography for differential diagnostic purposes.¹¹ The significance of these events was brought to HIP's attention by one of us (P.S.), and



1. Relative survival rates for women with cancer of the breast diagnosed in Connecticut, 1935-1944, by time interval after diagnosis. (From Cutler et al¹)



2. Age-adjusted mortality from all causes and from breast cancer for women aged 25 years or more, United States, 1935-1963. Age-adjusted to 1940 population.

steps were taken under the direction of Edwin F. Daily, MD, medical vice-president of HIP, to evaluate mammography for breast cancer screening. Coincidentally, Michael Shimkin, MD, who was then with the National Cancer Institute, had begun to explore possible sites for a major study of this issue.

Several months later a pilot study was initiated by HIP under contract with the National Cancer Institute to test the feasibility of a full-scale screening program and to develop the procedures and research instruments that would be required. Successful culmination of the pilot study resulted in the decision to undertake the repetitive screening program being reported here. An important contributory factor was the evidence of a high degree of reproducibility of Egan's technic of mammography that was being accumulated in the Public Health Service—M. D. Anderson Hospital and Tumor Institute study.¹² This was encouraging although it was recognized that the HIP screening study would be conducted under different conditions. In this investigation, unlike the reproducibility study, a large majority of the patients would have no suspicious lesions, and a substantial proportion of the biopsy recommendations were expected to be made on radiologic evidence alone, involving small, nonpalpable lesions.

Objectives

The current study is concerned with breast cancer detection and mortality from this disease in a defined population of women who are placed under initial observation when they are 40 to 64 years of age and who are then followed up for a number of years. The "exposed to risk" population excludes only those women with a prior mastectomy or those who are pregnant at the time of the screening examination.

The primary objective of the project is to establish whether a breast cancer screening program using mammography and clinical examinations holds substantial promise for lowering mortality from breast cancer in the female population. Linked to this is the objective of determining the frequency with which breast cancer is detected through mammography alone, clinical examination alone, and both mammography and clinical examinations; also, the stage of the disease when diagnosed by each procedure and later the mortality experience in each category. This will provide a basis for assessing the contribution that mammography may be making toward the lowering of mortality from the disease.

The study also provides an unusual opportunity to investigate the relationship of a wide range of factors to the development of breast cancer. Of interest is the relationship of radiologic and clinical observations made at time of the screening examinations among women with no evidence of breast cancer and the later development of this disease. Also of interest are relationships involving

demographic variables such as age, race, marital status, country of birth, religion, occupation, educational attainment, and family income. Other variables are pregnancy, breast feeding, and menstrual history; past and present breast conditions; hormonal, surgical, and radiation therapy; and familial history of cancer.

Methodology

Study Setting.—Twenty-three of the 31 medical groups in HIP are participating in the study. These groups are located in four of the boroughs in New York city (Bronx, Brooklyn, Manhattan, and Queens) and in Nassau County. Their 490,000 members, 85,000 of whom are women 40 to 64 years of age, cover a broad spectrum of ethnic and socioeconomic groups. About two thirds are employees of local, state, and federal agencies and the employees' families. The next largest sources of enrollment are union groups outside of government service.

In return for a premium, HIP members are entitled to receive comprehensive medical care from physicians associated with the affiliated medical groups. Coverage is for preventive, diagnostic, and therapeutic services in the office, home, and hospital. All enrollees are required to carry hospital insurance.

Study Design.—Within each of the participating medical groups, two random samples of women aged 40 to 64 years with at least one year's membership in HIP have been selected. These samples are matched by age, size of insured family, and employment group through which the family joined HIP. One sample is designated as the "study" group; the other, the "control" group. The total number of women in each sample is 30,000, with each medical group contributing a share proportionate to its size, adjusted to the availability of physician and technician time in its facility. The sample of "study" women in a medical group is randomized, and women are drawn in sequence from the list as their turn is reached for screening examinations. The date they are scheduled for the examination becomes their entry date into the study and all observations start from this date. Women in the control group are also assigned entry dates to determine their future periods of exposure.

Study-group women are offered a screening examination in their medical group centers and 64% cooperate. If a woman who has had a mastectomy appears, she is examined but the findings are not included in the study. Two annual follow-up examinations are being obtained except for those women who on their initial examination are found to have conditions that require earlier follow-up. The response rate for the first annual follow-up is 83%.

Women in the control group follow their usual practices in receiving medical care. No special effort is made to encourage them to have general physical examinations. On the other hand, they

are not discouraged from having such examinations. Mammography is not routinely included in the general physical examination but it is increasingly being used in HIP for differential diagnostic purposes.

Preliminary analysis of personal characteristics and factors implicated in the epidemiology of breast cancer suggests that the 64% of the study population that appears for screening examinations is very similar to the total study population and to the total control population. The differences that exist in age composition, socioeconomic status, pregnancy and breast feeding history, and other characteristics appear too small to bias seriously the screened group of women with regard to breast cancer incidence. In the long run, the issue will be resolved through data on breast cancer incidence collected in the study.

Sources of Information on Biopsies.—Several overlapping sources of information help to identify women who undergo breast biopsy. They include the patient's medical record in HIP and records of hospital admissions. Surgical and pathological findings in breast cancer cases are obtained from hospital charts. The project's coordinating pathologist reviews slides and conducts special studies of tissue blocks, when available. Each case of pathologically confirmed carcinoma of the breast is investigated to establish whether a mastectomy had been performed prior to the woman's entry into the study (if so, she is excluded from the study), and to establish the type of surgery performed and histologic type, nodal involvement, and size of the lesion.

Follow-up for Mortality.—It is estimated that a minimum of five years of follow-up after the screening program has been completed will be needed to determine whether screening by mammography and clinical examinations holds substantial promise for improving survival rates among women with breast cancer and for lowering mortality from breast cancer in the female population. (Comparisons of survival rates will require allowances for the acceleration in the date of diagnosis of breast cancer among screened women. Estimates are to be derived for the amount of time in the natural history of the disease between when breast cancer is detected in a screening program and when it is ordinarily detected.)

Deaths will be identified through intensive follow-up of all confirmed breast cancer cases and by matching death records on file in New York city and upstate New York against the total files of study and control groups to locate deaths attributed to breast cancer. It should be noted that women in both the study and control groups are maintained under observation even if they discontinue their enrollment in HIP.

Examination Sessions

Location.—Examination sessions are conducted in the medical group centers. The organization of

the examination sessions on a decentralized basis has several strong advantages. Unquestionably, the most important is that it provides a clear link between the examination and the follow-up medical care. The patient appears for a screening examination in a familiar setting, the medical group center, and she knows that the group's surgeon and radiologist are participating directly in the program. Her responsiveness to the initial invitation to participate is increased, as is the likelihood that follow-up care will be obtained. The surgeon who functions as the examining physician is a member of the medical team in the group responsible for the patient's care, and the findings of examinations in which he has been a critical participant are more readily translated into action than might ordinarily be true in a screening program.

Content.—Each examination consists of a clinical and x-ray examination and interview with the patient to obtain relevant demographic information and a health history, with special emphasis on factors implicated in the epidemiology of breast cancer. The interview is carried out by a nonphysician on the study staff. Each participating medical group has assigned one or more of its clinicians to the project. In almost all cases, the clinician is a surgeon; in the remaining instances he is an internist. Examination sessions are scheduled outside of the physician's regular clinic hours, and he gives his total attention during the session to the screening program. The clinician conducts his examination without knowledge of the radiologic findings and records his observations and recommendations for follow-up medical care on specially designed study forms.

Cephalocaudad and lateral x-ray views of each breast are taken for each woman (technique discussed later) by technicians who have been specially trained. The radiologist of the medical group has the opportunity to read the films before they are sent to the central staff and to record his findings without reference to the clinical observations.

Assessment of Evidence.—Clinical, radiologic, and lay interview reports emanating from the examination session, together with the mammograms, are sent to a central location where a medical chart is established for the patient. The mammograms are separated from the rest of the chart for independent readings by two of the radiologists on the staff. The project's chief radiologist, Dr. Strax, reviews positive findings by the staff radiologists and the radiologists in the participating medical groups. In selected cases, Robert L. Egan, MD, serves as a consultant to the study. Final responsibility for resolving differences rests with the chief radiologist on the study team.

At a later stage, clinical information derived from the screening examination is reviewed in conjunction with the radiologic findings. Participating in this assessment of the total evidence are clinicians on the study staff. The chief clinician, Dr. Venet, has primary responsibility for estab-

lishing close liaison with the surgeons in all participating medical groups and discussing with them the basis for biopsy recommendation when this derives exclusively from mammographic findings. The follow-up system for biopsy cases and for early recall cases is under his direction.

Special measures have been introduced to increase the likelihood that when a biopsy is recommended the woman will accept hospitalization. This poses no significant problem when the recommendation is based on the finding of a palpable lesion which is suspected as being malignant. When mammography provides the only evidence for biopsy, the woman is often hesitant to accept hospitalization even if a malignancy is suspected. A team approach has been developed to minimize the likelihood of "losing" the patient. Responsibility for communicating with the patient is assumed by the medical group surgeon assisted by a registered nurse on the central staff who has wide experience in the fields of health education and research.

Mammography Technique and Radiation Exposure.—In consultation with Dr. Egan, his technique has been modified for use as a screening procedure in the HIP study. Favorable features in Egan's technique are retained. These include industrial fine-grain film (M type), low kilovoltages, long distance, and close coning. The changes that have been made are directed at reducing the radiation dose, the strain on radiographic equipment, and the amount of time required to screen a patient. These objectives are accomplished by restricting the films to a cephalocaudad and mediolateral view for each breast and by slightly increasing the kilovoltage.

The modified mammography technique has made it possible to screen women at the rate of 13 patients per three-hour session. Quality of films is regularly determined by the study staff, and periodically a sample of films is sent to Dr. Egan for his opinion concerning quality. Improvements in technique are introduced as suggested by these reviews. Assessment of films taken after September 1964 indicates that 98% of the cephalocaudad views were adequate; in 79% of the cases both lateral views were adequate.

Measurements taken by the consultant physicist in the project indicate that with the technique described the skin dose to the breast is about 5 rads, assuming overlapping fields; at a depth of 3 cm the dose from both fields is of the order of 2 rads.

Several safeguards have been taken in the study against undue radiation exposure which might result from technical failures or from human factors. Each x-ray machine being used is calibrated and measurements taken under the physicist's supervision before mammography screening begins. Repeat measurements are scheduled. A lead rubber shield is attached to the cone to attenuate scattered radiation to the neck and face. Also, lead rubber is placed under the film holder. Screen-

monitored closely to reduce to a minimum retakes due to equipment failures or faulty technique, and visits are made to medical groups while sessions are in progress to check on safety measures and technique.

Preliminary Observations

Results of Screening.—By the end of March 1965, about half (15,542) of the 30,000 women in the study group had been asked to appear for a screening examination. Of these, 9,883 were examined and recommendations for biopsy were made for 202 or about 2% of the women. Recommendations for "biopsy or aspiration" were made for an additional 0.3% (25 women), and 8% of the women were requested to have a reexamination within six months, primarily because of a clinical finding of fibrocystic mastopathy.

The basis for the biopsy recommendation, the number of biopsies performed, and the number of pathologically confirmed carcinomas of the breast are given in Table 1.

Almost half of the biopsy recommendations (97) were made as a result of mammographic findings only, 95 were made on clinical grounds alone, and 10 recommendations were based on both mammographic and clinical evidence. Of the 202 women with biopsy recommendations, 134 have had surgery; 11 of the 25 women with recommendations for "biopsy or aspiration" have also had surgery. Several more women are moving toward biopsy. The remainder will be followed up through reexaminations and available records to identify women who finally do undergo biopsy, in which case full information will be obtained about the outcome.

Twenty-three breast cancers have been confirmed pathologically, 15 within seven weeks after the patients were screened. Of the 23 women with confirmed carcinomas, 12 had biopsies on the basis of radiologic evidence only, 9 on clinical evidence only, and 2 on clinical and radiologic evidence.

Each of the above figures is subclassified in Table 1 to show the radiologic and clinical findings which resulted in the biopsy recommendation. Three categories are provided: "malignant," "suspicious or indeterminate," and "nonmalignant mass or benign." Eventually this type of information will be useful in assessing the procedures used in the current study for other screening programs that may be considered.

Table 2 gives, for each of the 23 confirmed cases of breast cancer, the age of the patient, radiologic and clinical findings and recommendations, approximate size of lesion when available, type of surgery, axillary nodal involvement, and histologic type. Several relevant observations can be made from this information. It is apparent that cancers are being detected through mammography alone in all age groups (Table 3). For 16 of the 23 confirmed cancers (about 70%), there was no histologic evidence that the axillary nodes were involved; no nodes were involved in 83% of the patients who

had biopsies on radiologic evidence only and in 67% of the "clinical only" cases (Table 4.)

Of the 12 cases in which the biopsy was recommended on radiologic evidence alone, six were cases of duct cell carcinoma and/or scirrhous carcinoma and six were cases of comedocarcinoma. The latter all showed intraductal calcification. Among the remaining 11 cases, there was only one case with a prominent intraductal component. With regard to size of lesion there is some uncertainty, since the measurements are those of the original examiner and procedures may vary from laboratory to laboratory. Also, measurements were not always available. Nevertheless, it would appear the mammography led to the detection of several very small lesions and that some lesions just over 1 cm in size were detected on clinical grounds alone.

Table 1.—Recommendations for Biopsy and Results Among 9,883 Women*

Evidence for Recommendation†	No. of Biopsy Recommendations	Biopsies Performed	
		Number	Pathologically Confirmed Cancer
Mammography only			
Total	97 (+14)‡	61 (+2)	12
Malignant	25	16	7
Suspicious of malignancy	49	30	5
Nonmalignant mass	23 (+14)	15 (+2)	0
Clinical only			
Total	95 (+8)	60 (+6)	8 (+1)
Malignant	8	7	4
Indeterminate	27 (+1)	17 (+1)	2
Benign	60 (+7)	36 (+5)	2 (+1)
Mammography and clinical			
Total	10 (+3)	6 (+3)	2
Both malignant	2	1	1
Clinical malignant, mammography suspicious	1	0	0
Both suspicious	2	0	0
Mammography suspicious, clinical benign	3	3	1
Clinical indeterminate, mammography benign	1	1	0
Both benign	1 (+3)	1 (+3)	0

*The women entered the study during the period December 1963 to March 1965 and were screened by April 30, 1965. Status as of May 31, 1965, is given.

†Radiologic and surgical recommendations made independently.
‡Figures in parentheses are additive to the other figures. They represent additional recommendations for biopsy or aspiration, biopsies performed following this recommendation, and pathologically confirmed carcinomas of the breast in these cases.

The patient's knowledge of the presence of a mass prior to the screening examination is determined at time of the examination. In only four of the 23 confirmed cases of carcinoma did the women state that they previously knew about the mass (one patient for 2½ years, two patients for six months, and one patient for two months). This is in sharp distinction to the general impression that the overwhelming majority of breast cancers become known because the women feel a lump.

A point of particular interest is the lack of correspondence between radiologic and clinical findings and recommendations in the screening program thus far, as indicated by the data in Tables 1 and 2. Further examination of this issue shows that, of the 74 patients with a biopsy recommenda-

Table 2.—Findings in the 23 Cases of Confirmed Carcinoma of the Breast*

Table 2. Findings in the 23 Cases of Confirmed Carcinoma of the Breast									
Case	Age (Yr)	Radiologic		Clinical		Size of Lesion (Cm)	Type of Surgery	Axillary Nodes Involved	Histologic Type
		Findings†	Recommendation‡	Findings§	Recommendation¶				
Biopsy Recommended on Radiologic Evidence Only									
1	49	Malignancy	Biopsy	No disease	1 yr	Unknown	Radical mastectomy	No	Scirrhous carcinoma
2	54	Malignancy	Biopsy	No disease	1 yr	1.8	Radical mastectomy	No	Comedocarcinoma
3	54	Malignancy	Biopsy	No disease	1 yr	4	Radical mastectomy	No	Comedocarcinoma
4	53	Malignancy	Biopsy	No disease	1 yr	1	Radical mastectomy	No	Mixed, scirrhous & duct cell
5	42	Malignancy	Biopsy	FCM	3 mo	Unknown	Radical mastectomy	No	Comedocarcinoma
6	56	Malignancy	Biopsy	No disease	1 yr	Unknown	Radical mastectomy	No	Comedocarcinoma
7	42	Malignancy	Biopsy	FCM	3 mo	Unknown	Radical mastectomy	Unknown	Comedocarcinoma
8	58	Suspicious	Biopsy	No disease	1 yr	1	Radical mastectomy	No	Comedocarcinoma
9	61	Suspicious	Biopsy	No disease	1 yr	1.2	Radical mastectomy	No	Mixed, scirrhous & duct cell
10	57	Suspicious	Biopsy	No disease	1 yr	1	Simple mastectomy & axillary node biopsy	No	Duct cell carcinoma
11	53	Suspicious	Biopsy	No disease	1 yr	2.5	Radical mastectomy	No	Scirrhous carcinoma
12	61	Suspicious	Biopsy	No disease	1 yr	3	Radical mastectomy	Yes	Duct cell carcinoma
Biopsy Recommended on Clinical Evidence Only									
13	64	Films inadequate		Malignancy	Biopsy	5	Radical mastectomy	No	Mixed, comedo & duct cell
14	55	NMNM	1 yr	Malignancy	Biopsy	1.2	Radical mastectomy	Yes	Duct cell carcinoma
15	50	Films inadequate		Malignancy	Biopsy	6×5×2	Radical mastectomy	Yes	Duct cell carcinoma
16	45	NMNM	1 yr	Malignancy	Biopsy	Unknown	Radical mastectomy	No	Mixed, comedo & duct cell
17	54	NMNM	1 yr	Indeterminate	Biopsy	1.5	Radical mastectomy	No	Mixed, scirrhous & duct cell
18	53	NMNM	1 yr	Indeterminate	Biopsy	4	Radical mastectomy	No	Scirrhous carcinoma
19	49	NMNM	1 yr	Benign	Biopsy	1.3	Radical mastectomy	No	Duct cell carcinoma
20	43	NMNM	1 yr	Benign	Biopsy	2.5+	Radical mastectomy	No	Colloid carcinoma
21	57	NMNM	1 yr	Benign	Biopsy or aspiration	5×4×2	Biopsy only	Unknown¶	Duct cell carcinoma
Biopsy Recommended on Radiologic and Clinical Evidence									
22	47	Malignancy	Biopsy	Malignancy	Biopsy	1.2	Biopsy only	Unknown¶	Mixed, scirrhous & duct cell
23	42	Suspicious	Biopsy	Benign	Biopsy	3+	Radical mastectomy	Yes	Mixed, scirrhous & duct cell

*Women recommended for biopsy on results of screening examination; study-group patients entered study December 1963 to March 1965.

†Findings before results of clinical examination became known. "NMNM" refers to "nonmalignant, no mass."

‡Time period refers to recommended interval for scheduling next examination.

§Findings before results of radiologic examination became known. "FCM" refers to "fibrocystic mastopathy."

¶Approximations based upon reports submitted by hospital pathologists. "Unknown" indicates that size of lesion was not reported by examining pathologist.

‡Clinical evidence of extensive metastases.

tion based entirely on radiologic evidence of malignancy or suspicion of malignancy (Table 1), two thirds or 53 had a recommendation from the screening clinician for a routine reexamination one year later. (The alternative recommendations open to the screening clinician are biopsy, aspiration, or early recall [less than one year].) Forty-six of the 74 women came to surgery and 12 cancers were confirmed; in two of the 12 confirmed cases the screening clinician had recommended an early recall (three months).

Similarly, among cases in which the clinical evidence in the screening examination started the chain of events culminating in a biopsy, a large majority of women had an initial radiologic recommendation for a reexamination one year later. Nine cancers were confirmed in this group of women. Mammograms in these cases were reviewed for possible reasons for the negative radiologic report. Several groups can be delineated:

1. In two cases, studies were judged to be inadequate. In one the difficulty lay in films too light for proper evaluation. Reexamination was advised and done at the hospital preoperatively. Positive diagnosis was obvious on improved films. In the other case, the cancer was very small and located in the axillary tail. Original lateral examination was inadequate and reexamination was advised. The patient was operated on before the new films could be reviewed. The cancer could be seen on the new films.

2. In two cases, films were judged to be adequate. These patients all had small dense breasts in which the cancer does not stand out in its milieu and could not be seen even after biopsy information had been obtained.

3. In two cases, films were judged to be adequate. These patients had average-sized breasts with average density. The cancers were of the same density as the glandular elements and did not be-

BREAST CANCER SCREENING—SHAPIRO ET AL

737

Table 3.—Confirmed Carcinomas of Breast Among Study and Control Groups of Women, by Age*

Population	Total	Age (Yr)		
		40-49	50-59	60-64
Study population, examined Results of screening†				
Total	23	8	12	3
Mammography only	12	3	7	2
Clinical only	9	3	5	1
Mammography and clinical	2	2
Between screening examinations‡	4	2	2
Study population, not examined	4	2	1	1
Control	14	4	5	5

*Patients entering study December 1963 through March 1965. See Table 5 for person-years of exposure corresponding to the above numbers of confirmed cancers.
†Biopsies performed on basis of findings in screening examinations.
‡Biopsies performed on basis of findings between screening examinations as patients appeared for regular medical care.

tray their presence by any signs we know at present. Positive radiologic diagnosis was not made even after biopsy information was available.

4. One case was judged negative on initial radiologic examination. The clinician diagnosed a benign lesion and advised excision. Reexamination of films led to a definite interpretation of malignancy.

Findings not Related to Results of Screening.—Follow-up procedures to identify new cases of breast cancer are applied to (1) women who have been screened and do not have a biopsy recommendation based on findings in the screening program; (2) women in the study group who do not appear for a screening examination; and (3) women in the control group. Data on pathologically confirmed carcinomas of the breast in each of these groups are given in Tables 3 and 4.

It will be noted that eight out of the 14 confirmed cancers (57%) in the control group involved no axillary nodes. As indicated previously, the corresponding figure (70%) for the 23 cancers detected through the screening program was higher, and in the subgroup "mammography only" the proportion (83%) was considerably higher. Although all of these percentages are subject to large sampling variability, it is encouraging to find that the direction of differences is towards higher

Table 4.—Confirmed Carcinomas of Breast Diagnosed by Histologic Evidence of Axillary Nodal Metastases*

Population	Total	Axillary Nodes		
		Not Involved	Involved	Unknown†
Study population, examined Result of screening‡				
Total	23	16	4	3
Mammography only	12	10	1	1
Clinical only	9	6	2	1§
Mammography and clinical	2	1	1§
Between screening examinations	4	3	1
Study population, not examined	4	1	2	1
Control	14	8	5	1

*Patients entering study December 1963 through March 1965.
†Cases in which there is no histologic evidence available to determine if there was axillary nodal metastases.
‡Biopsies performed on basis of findings in screening examinations.
§Clinical evidence of extensive metastases.
||Biopsies performed on basis of findings between screening examinations as patients appeared for regular medical care.

proportions among study women whose biopsies are attributable to the screening program than among control women. In general population studies, about 42% of the pathologically confirmed cancers of the breast are found to have no nodes involved.

The distribution of histologic types among the 14 confirmed cancers in the control group differ markedly from that of the 12 confirmed cases in which biopsies were done on radiologic evidence alone. Only in two of the 14 cases was the histologic type comedocarcinoma; ten were cases of duct cell and/or scirrhous carcinoma; the remaining two were cases of a mixed pattern of comedo and duct cell carcinoma.

Also of great interest are the breast cancers detected among screened women between screening examinations. (These cases were detected in the regular course of medical care.) Four such cases have occurred since the initial examination. In all of them, the initial clinical and radiologic findings were negative and a recommendation for a one-year reexamination had been made. Three out of the four cases had no axillary nodes involved. Reevaluation of the films taken in the screening examinations has been carried out with the following results:

1. Two patients (one with a seven-month interval [between screening time and biopsy], the other with a three-month interval) had the type of glandular breasts with cancers that do not stand out amidst the glandular elements. The cancers cannot be seen on review.

2. One patient (nine-month interval) had small breasts with cancer seen only on lateral view in the axillary tail. On review it can be seen on early film. It was obvious on the preoperative film.

3. One patient (three-month interval) had very

Table 5.—Exposure and Rates of Carcinoma of Breast Among Study and Control Groups of Women, by Age

Population	Total	Age (Yr)			
		40-49	50-64		
Study group, examined					
Total number of women*	9,883	4,887	4,996	3,970	1,026
Person-years following examination†	5,955	2,945	3,010	2,392	618
Study group, not examined‡	3,479	1,573	1,902	1,462	444
Control group§	9,889	4,759	5,130	4,011	1,119
Carcinoma Rate					
Study group					
Examined, carcinomas detected through screening (per 1,000 persons)	2.33	1.64	3.00	3.02	2.92
Examined, carcinomas detected between screening	0.67				
Not examined	1.15				
Control group	1.42	0.84	1.95	1.25	4.47

*Number of women entering study December 1963 to March 1965 and examined by April 30, 1965.

†Person-years of exposure among the 9,883 examined study women. Calculated from date of examination to April 30, 1965, with a maximum of 12 exposure-months included for all women whose actual exposure was 12 months or more.

‡Person-years of exposure among unexamined study women. Calculated from date of entry into study until March 31, 1965, and using actual months of exposure.

§Person-years of exposure based on a 20% sample of the control group. Calculated from date of entry into study until March 31, 1965 and using actual months of exposure.

||Rates per 1,000 person-years.

||Not calculated.

dense, small breasts. On review of early films no cancer can be seen. In later preoperative film, cancer can be seen in comparison with the early film. However, if the later film is seen alone, the cancer is not apparent.

Rates of Detection

Data from the Ten Cities Study of the US Public Health Service indicate that a breast cancer incidence of 1.4 per 1,000 women per year might be expected in the HIP study population aged 40 to 64 years.¹³ Experience in Connecticut and upstate New York suggests a rate of 1.2 per 1,000. Although more time is required to obtain a comparatively stable rate for the control group in the HIP study, this rate is now 1.4 per 1,000 person-years of exposure, a figure similar to the rate derived from the Ten Cities Study and not significantly different from the Connecticut and upstate New York rates^{2,3} (Table 5).

Prevalence of undiagnosed breast cancer in the study population at the start of the study consists of cases sufficiently advanced to be detected under the conditions of the current screening program. The 23 cases detected thus far through screening fall in this category (Table 5). Prevalence and incidence data will later be useful in estimating how much time is gained in the early diagnosis of breast cancer because of screening.

The 23 cases represent a rate of 2.3 per 1,000 women screened (9,883) and 1.5 per 1,000 women now in the study population of cooperating and noncooperating women (15,542). These are the cases whose detection can be attributed directly to screening. It will also be of interest to determine the overall amount of breast cancer detection in the study population without regard to whether it results from screening or routine medical care. Thus far among the screened women, the

rate of cancer detection not attributable to screening is 0.7 per 1,000 person-years; among noncooperating women, the rate is 1.2 per 1,000 person-years.

As the study progresses, the above rates will be recalculated and mortality data accumulated. The results will be examined for the total study population and separately for the cooperating study women. To the extent that the screened women are representative of the entire study population with respect to incidence of breast cancer, experience in this group will be particularly useful. It will represent the benefit of screening under ideal conditions of full cooperation in the program. Anticipated benefits of a screening program could then be estimated under various assumptions about completeness of population coverage in such programs.

This study is supported in part by Public Health Service contract PH43-63-49.

The following medical groups affiliated with HIP are participating in the study: Astoria Medical Group, Bay Ridge Medical Group, Bedford-Williamsburg Medical Group, Brooklyn Medical Group, Central Bronx Medical Group, Central Brooklyn Medical Group, Central Manhattan Medical Group, Central Nassau Medical Group, Circle Manhattan Medical Group, East Bronx Medical Group, East Nassau Medical Group, Empire Medical Group, Jamaica Medical Group, Kings Highway Medical Group, Lower Manhattan-Gramercy Medical Group, Metropolitan-Hudson Medical Group, Montefiore Medical Group, New York Medical Group, Queens Boulevard Medical Group, Upper Manhattan Medical Group, Upper Queens Medical Group, Washington Heights Medical Group, and Yorkville Medical Group.

Members of the central staff are Maurice Pomeranz, MD, F. Leon A. Lopez, MD, Mortimer J. Lacher, MD, Stanley Gross, MD, Raymond Fink, PhD, Herbert Levine, DSc, Wanda Venet, RN, and Norma Gelman. Robert L. Egan, MD, and J. Gershon-Cohen, MD, are consultant radiologists. Carl Braestrup and Richard T. Mooney assisted in standardization of radiologic equipment. George Hutchison, MD, is consultant epidemiologist.

The Administrative Advisory Committee consists of Theodore Barnett, MD, Hyman E. Bass, MD, Alan R. Bleich, MD, Edward E. Jemerin, MD, Sidney Lipton, MD, and Conrad Rosenberg, MD. Members of the Scientific Advisory Committee are John P. Lindsay, MD, Eugene P. Pendergrass, MD, I. S. Ravdin, MD, Michael B. Shimkin, MD, E. C. White, MD, and Warren Winkelstein, Jr., MD.

References

- Shimkin, M.B.: Cancer of the Breast, *JAMA* 183:358-361 (Feb 2) 1963.
- Ferber, B., et al: *Cancer in New York State, Exclusive of New York City, 1941-1960: A Review of Incidence, Mortality, Probability, and Survivorship*, Bureau of Cancer Control, New York State Department of Health, Albany, 1962, p 357.
- Cutler, S.J., et al: Survival of Breast-Cancer Patients in Connecticut, 1935-54, *J Nat Cancer Inst* 23:1137-1156 (Nov) 1959.
- Bragg, K.; Linden, G.; and Breslow, L.: The California Tumor Registry: A Summary Report on the Cancer Experience in 36 Hospitals, *Calif Med* 87:180-188 (Sept) 1957.
- Ederer, F., et al: Causes of Death Among Long-Term Survivors From Breast Cancer in Connecticut, *J Nat Cancer Inst* 30:933-947 (May) 1963.
- Day, E., and Venet, L.: "Periodic Cancer Detection Examinations as a Cancer Control Measure," in *Fourth National Cancer Conference Proceedings*, Philadelphia: J. B. Lippincott Co., 1961, pp 705-707.
- Shahon, D.B.; Santoro, B.T.; and Wagenstein, O.W.: "Periodic Examinations of the Breast," in *Fourth National Cancer Conference Proceedings*, Philadelphia: J. B. Lippincott Co., 1961, pp 225-227.
- Holleb, A.I., et al: Breast Cancer Detected by Routine Physical Examination, *New York J Med* 60:823-827 (March 15) 1960.
- Vital Statistics of the United States*, National Center for Health Statistics, Public Health Service, 1935-1963.
- Gershon-Cohen, J.; Hermel, M.B.; and Berger, S.M.: Detection of Breast Cancer by Periodic X-ray Examinations, *JAMA* 176:1114-1116 (July 1) 1961.
- Egan, R.L.: Mammography, An Aid to Diagnosis of Breast Carcinoma, *JAMA* 182:839-843 (Nov 24) 1962.
- Clark, R.L., et al: Reproducibility of the Technic of Mammography (Egan) for Cancer of the Breast, *Amer J Surg* 109:127-133 (Feb) 1965.
- Dorn, H.F., and Cutler, S.J.: *Morbidity From Cancer in the United States*, Public Health Monograph No. 56, publication 590, Public Health Service, 1959.

8.5 Xerography of the breast

John N. Wolfe

John N. Wolfe became a physician by accident and a radiologist by an even greater accident. After being drafted into the US Army in 1942, he was sent for basic training in the infantry. Towards the end of that period the Army gave a number of people a test, particularly those who had been drafted out of college. The US Army thought there were not enough engineers being trained. Wolfe was selected to be sent to college to study engineering and he spent one year at the University of Georgia at Athens, USA at the engineering school. At the end the Army made a new decision that there were not enough physicians and Wolfe passed this test too and started his career in medicine.

The army sent him to premed training at the University of Mississippi at Oxford, and then he started medical school at the University of Tennessee, Memphis. At the end of the war he was discharged and transferred to Western Reserve. In 1949 John N. Wolfe graduated from Western Reserve University Medical School. His internship was served at the Ohio State University (1949–1950). During his internship, he took advantage of a program whereby a salary of a second lieutenant was paid in exchange for joining the Air Force for two years. After his internship he was sent to the US Air Force Base in Great Falls, Montana. The day after his arrival he was informed that the radiologist has just left and he would be the radiologist and would be in charge of the outpatient service. Asndso began his career in radiology. Having no knowledge of radiology, and having slept through every X-ray conference during medical school and after qualification, he did his best to learn everything.

In 1952 Wolfe started his residency in radiology at the Wayne State University, Detroit. Wolfe became instructor in Radiology in 1955 at the University of Southern California, LA Country General Hospital. In 1957 he became radiologist at the Hutzel Hospital, Detroit, Michigan. Shortly after starting work he took a six-month leave of absence to learn radiation therapy. He attended the Karolinska Institute in Stockholm for three months studying pelvic tumors and then attended the Curie Foundation in Paris to learn more about pelvic malignancies and malignancies in general. In 1967 Wolfe became Chief of Radiology at the Hutzel Hospital. It was here where he developed his ideas of using xeroradiography in mammography.

Picture and information courtesy RH Gold, MD, Dep. Radiology Science UCLA, 2004.



Xerography of the Breast¹

JOHN N. WOLFE, M.D.

XEROGRAMS of the breast have the following advantages over film mammograms: (a) they are easier to interpret; (b) they require less radiation to produce than Eastman Kodak "M" film mammograms; (c) they afford greater detail; (d) they are probably more accurate; (e) xerography is a dry process; (f) the finished product is obtained more quickly and with greater ease.

The most important feature is that they are easier to interpret. Properly set-up xerograms could probably be read in a screening program at the rate of 4-5 cases per minute, whereas in a similar program film mammograms were read at a rate of 15-20 cases per hour (16).

An additional advantage of xerography is that all parts of the breast are clearly shown with one image. Some workers in mammography believe that two x-ray films of different densities are required to delineate all structures (17, 18). It is my opinion that xerograms are more accurate, although I have not conducted a carefully controlled study to prove this (10, 13).

The essential part of xerography is the "plate," which consists of a sheet of aluminum, 10 × 17 inches, coated with a thin layer of selenium and encased in a wooden "cassette," complete with a dark slide to protect it from light. The plate is used as one would an x-ray film insofar as performance of the examination is concerned.

REVIEW OF THE LITERATURE

Investigators at St. Vincents Hospital, New York City, have published three papers on xerography of the breast (4, 10, 13). The first was a description of the early experience with a small number of patients. The second paper was more complete and explained in detail the xero-

graphic principle and the equipment available. The technic was discussed, together with some shortcomings that had become apparent. The last paper from this group summarized the experience gained from 463 breast examinations. When results were compared, xerography and roentgenography were exactly the same in accuracy of diagnosis of malignant disease.

Other papers on xeroradiography, describing its use in aspects of radiology other than mammography, include two by Roach and Hilleboe. Their first article, which was of an introductory nature, explored the use of the procedure in the event of an emergency created by the explosion of an atomic bomb. They also discussed the physical aspects of the procedure and the results of early clinical testing (11). Their second article called attention to the relatively slow "speed" of xeroradiography in comparison with conventional roentgenography performed with "fast" film and intensifying screens (12).

Hills *et al.* (6) noted the slow speed and low contrast of xeroradiography but also cited the great detail possible with preservation of all structures of varying densities. Oliphant (9) described briefly the apparatus and method of use and noted the great detail attainable. Farmer *et al.* (3) utilized the process in radiation-treatment planning and cited its advantages in recording all tissue densities.

There are numerous articles on xerography and xeroradiography in nonradiological literature. McMaster (7) has written a very readable account on all technical aspects; included is a historical review of the basic principle, its discovery and patent by Charles F. Carlson in 1937, and its subsequent development by the Battelle Corporation.

¹ From the Department of Radiology, Hutzel Hospital, Detroit, Mich. Presented at the Fifty-third Scientific Assembly and Annual Meeting of the Radiological Society of North America, Chicago, Ill., Nov. 26-Dec. 1, 1967. Supported by grants from the USPHS Cancer Control, Michigan Cancer Foundation, and Hutzel Hospital Research Fund.

RADIOLOGY 91: 231-240, August 1968. (V.O.B.)

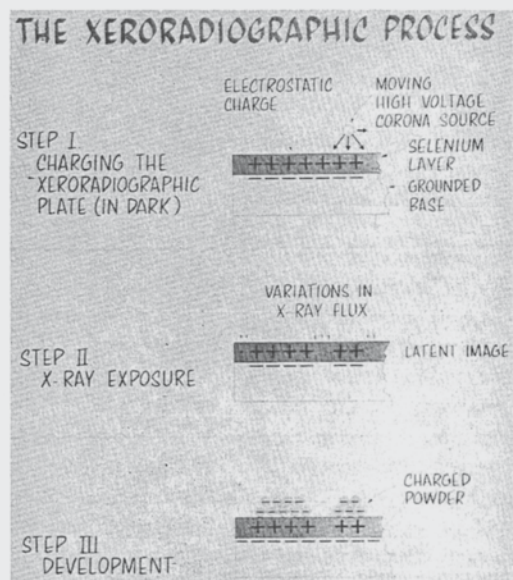


Fig. 1. Xerography is possible because selenium is a photoconductor. An electrostatic charge placed on its surface will remain in an absence of radiant energy. X rays make the selenium conductive perpendicularly. After exposure there is a residual charge pattern which may be made visible by "developing" with a negatively charged, pigment-containing powder.

TECHNICAL CONSIDERATIONS

Technical considerations that concern the radiologist are speed, contrast, and artefacts, which are interrelated, and dark decay.

The speed of the plate is a function of the number of carriers created within the selenium during exposure to x rays. This is proportional to the number of atoms of selenium present for interaction with the x rays (selenium thickness) and also to how close the radiant energy is to 12–13 kilovolts, which is the amount of force required to remove an electron from the k shell of the selenium. X rays significantly higher than 12–13 kilovolts are likely to pass through the plate without interaction. Very thin layers of selenium will be significantly slower than thick ones, as x rays will be more likely to escape through the photo-conductive layer without interaction.

We note an increase in speed and contrast in the following situations: (a) a thick selenium layer, as opposed to a thin one; (b) replacement of the aluminum dark slide of the cassettes (1/35 inch) with one made

of plastic (1/16 inch); (c) reduction to 30–32 kV with 900 mAs, as compared to 40–42 and 150 mAs. These factors affect contrast in that background color is diminished by more complete loss of the initial plate charge in the areas of exposure where there is no breast.

Contrast is also related to initial plate voltage and the amount of exposure. The higher the initial voltage, the greater the contrast. Too high plate voltage will result in 0.1 to 0.5-mm areas where no powder

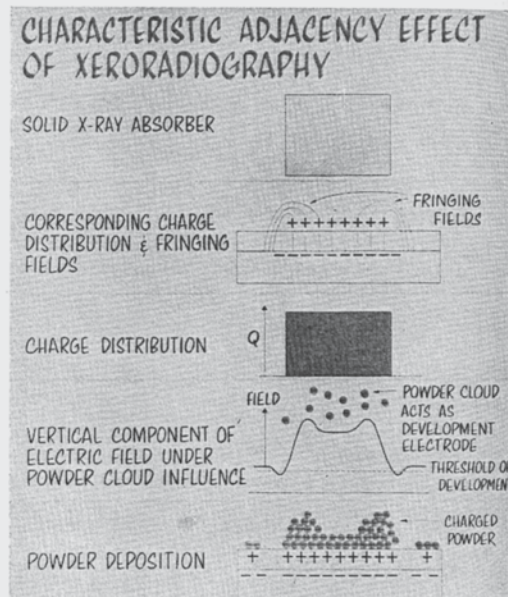


Fig. 2. Fringing electric fields around differences in potential effectively increase the charge. A heavier deposition of powder occurs at the edges of masses.

is deposited (powder deficient spots). These are unimportant outside the image area; their presence to a severe degree in it can destroy the xerogram's value.

Overdevelopment with the blue plastic powder will diminish contrast. The optimum is just enough developer to record all areas of interest with minimum background. There is competition between breast structures and background for the developing powder, and the stronger fields depicting dense structures are developed first, to a degree. Slow development—small amounts of powder over long periods of time (fifty seconds)—appears better than fast development with large

amounts of powder and ten to fifteen seconds.

DARK DECAY

Dark decay is an exponential loss of plate charge. This is due in part to cosmic radiations, free ions in the air, and the fact that selenium is not perfect in its resistivity. The decay is slight but is most marked immediately after plate charging. One cannot delay unnecessarily between plate charging, exposure, and development. These need not take more than three to four minutes at most.

EQUIPMENT

The equipment has been described by Ruzicka *et al.* (13). It was built in 1955 for field trial. The construction is such that there can be no large-scale use of this technic until more reliable and semiautomated machines are available. A design requiring only 2 or 3 manual steps and a finished product available in a minute or so is practicable.

TECHNIC

From the foregoing discussion, it is obvious that the best xerograms are obtained with low kilovoltage, high mAs, and slow developing. The beam should not be filtered any more than is unavoidable, either before or after striking the breast. A slice of breast tissue imbedded in plastic in which were placed small flakes of aluminum hydroxide (prepared by Dr. Robert Egan) was examined in studies with various factors. There is no significant loss in detail as one goes from 900 to 300 mAs (Fig. 3).

Twenty-four to thirty-two kilovolts and 600 mAs at 32 inches produce an image of good quality. These factors will vary according to the character of the selenium plates made available in the future.

TECHNICAL DIFFICULTIES

Damage to the xerographic plates during handling is likely to occur with present technics because the plates have to be manipulated a considerable number of times during processing. The surface of

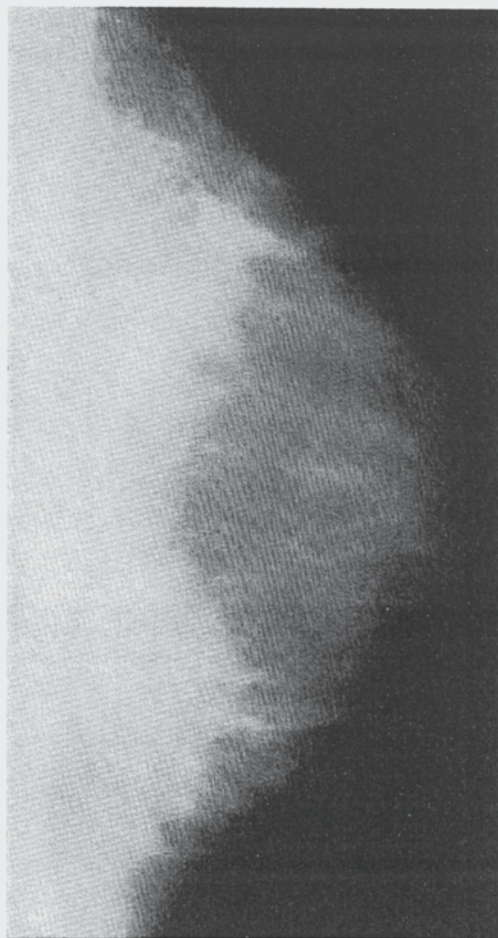


Fig. 4. Slight mammary dysplasia in 25-year-old woman.

the selenium is readily scratched, which will leave a permanent artefact. Semi-automated equipment would alleviate this problem by permitting the plate surface never to be exposed.

Humidity and subsequent clumping of the developing powder was a problem early in the investigation. This was solved by discontinuing the use of the air compressor furnished with the equipment for driving the powder and substituting a tank of dry nitrogen with a reducing valve and operating it at 50 p.s.i.

Leaks around the orifice of the developing unit in which the xerographic plate rests produced a deposition of clumps of powder around the periphery of the plate. These are troublesome but, because of their



Fig. 5. B. For legend please see Fig. 5, A, on opposite page.

distribution and large number, are not mistaken for calcifications.

A loss of contrast occurs if the developing unit accumulates a considerable amount of used developing powder, and it must be cleaned after about ten hours of operation. The powder is reusable.

Artefacts on the images occur if the cover used to protect the plate from light

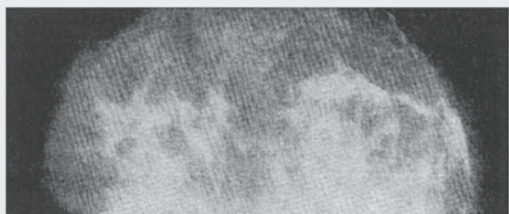


Fig. 6. B. For legend please see Fig. 6, A, on opposite page.

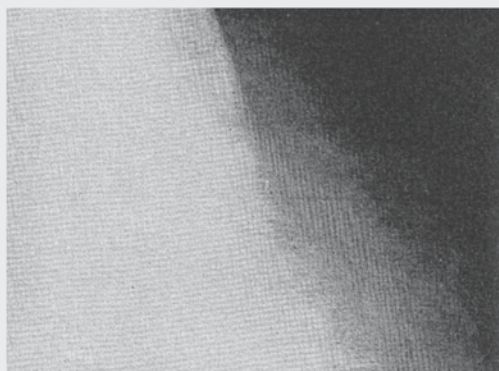


Fig. 5. D. For legend please see Fig. 5, C, on opposite page.

is sufficiently indented to touch the selenium surface after it is charged. This immediately discharges that area, and no powder will be attracted to it.

Difficulties have been encountered with the relaxing unit with the appearance of "ghosts" on the plates during subsequent examinations. Slight motion has occurred in the transfer unit during passage of the plate and paper through it, producing a blurring of the image. Wires have been broken by insertion of plates into the charging unit due to excessive canting of the plate. Uneven heat distribution in the fusing unit that is used to fix the powder image onto the plastic-coated paper has resulted in an uneven fusion. A change in plastic-coated paper at one time resulted in a supply that was too tacky, would not fuse properly, and gave poor images. It is apparent from the foregoing that major



Fig. 6. D. For legend please see Fig. 6, C, on page 237.

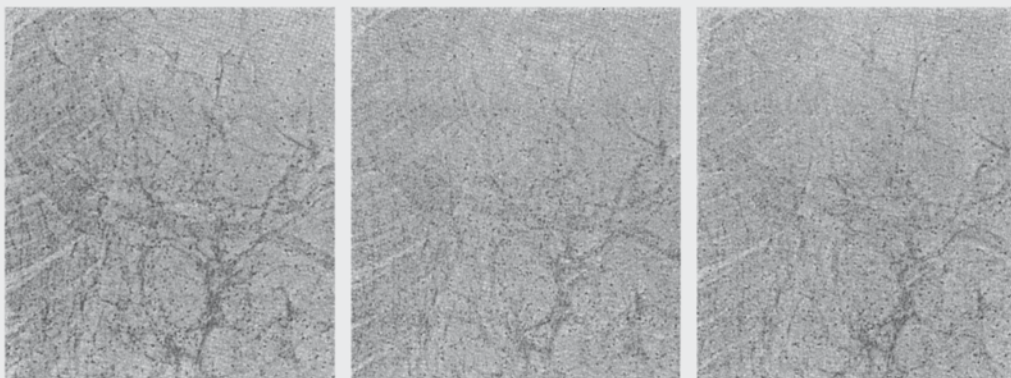


Fig. 3. Effect of mAs on contrast. A. 900 mAs. B. 600 mAs. C. 300 mAs.

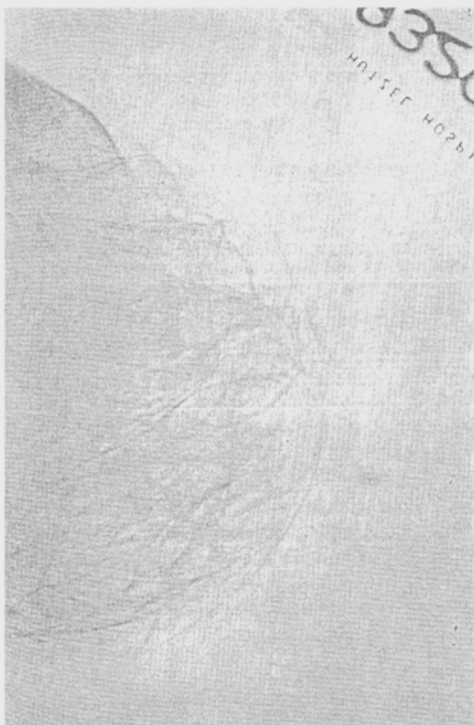
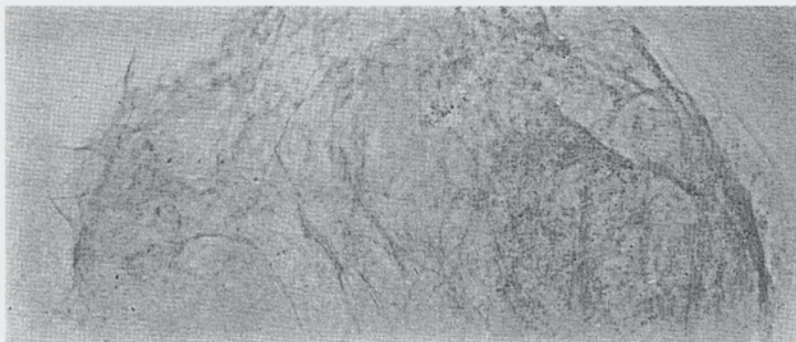


Fig. 5. A (*left*) and C (*above*). Scirrhous carcinoma. Note detail of retractions about the cancer obtainable by xerography over and above that recorded on the conventional film mammogram.

Fig. 6. A (*below*). Comedo carcinoma occupying about one half of the breast. The general architecture is depicted well on the xerogram.



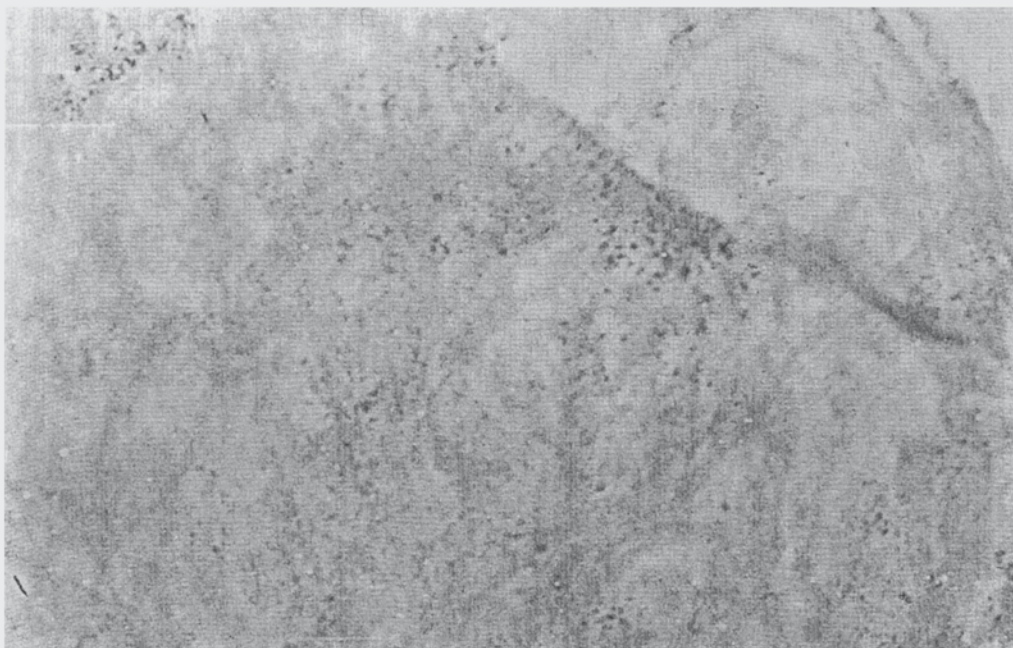


Fig. 6. C. Area of the cancer magnified ($2\times$), illustrating the superior ability of xeroradiography to demonstrate tumor calcifications.



Fig. 7. A. Circumscribed carcinoma, small mass more readily identified on xerogram.

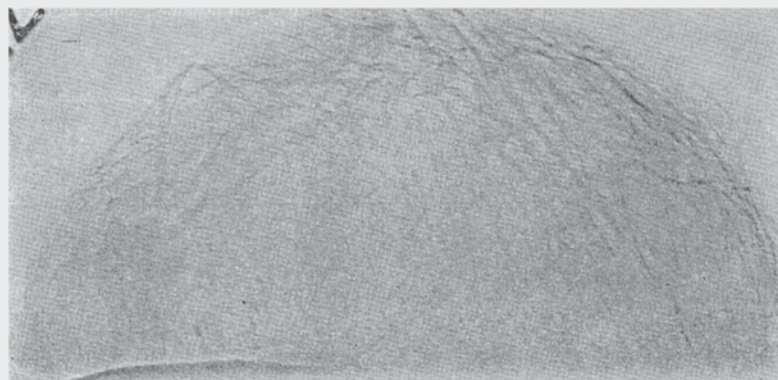


Fig. 8. A. Scirrhous carcinoma very evident on both examinations.

difficulties have been encountered with nearly every component of the equipment. Many were solved by experience. The main ones were overcome by the cooperation of the Xerox Corporation in refitting and bringing into good operating order the various components.

EXAMPLES

Examples are shown to illustrate all of the features of xeroradiography. The cases are selected to include both benign and malignant disease; the three commonly encountered forms of the latter—comedo, scirrhous, and circumscribed—are shown. Film mammograms for comparison were made *simultaneously* on Eastman Kodak "M" film by placing it on top of the xerographic cassette. The technic in the case presentations was 30–32 kV and 1200 mAs and 32 inches. The xerograms are not considered optimum, as all were made with an aluminum dark slide and many with thin selenium plates (Figs. 4–8).

DISCUSSION

A comparison between this evaluation and that of the workers at St. Vincent's Hospital is interesting to detail because of certain basic differences in approach (TABLE I). The changes were made because the physical properties of selenium make it more sensitive to low kilovoltages.

A comparison of xerograms and Eastman

TABLE I: COMPARISON OF TWO XEROGRAPHIC TECHNIQUES

	St. Vincent's Hospital	Hutzel Hospital
Kilovolts	Medium	Low
mAs	Low	Medium
Latitude of exposure	Wide	Narrow
Contrast	Low	Medium to high
Technical difficulties	Many, all aspects	Many, all aspects

TABLE II: COMPARISON OF XEROGRAMS TO EASTMAN KODAK "M" FILM MAMMOGRAMS

Speed	Faster than "M"
mAs required for good image	Less than "M"
Latitude of exposure	Narrow, but greater than "M"
Contrast	High, but less than "M"

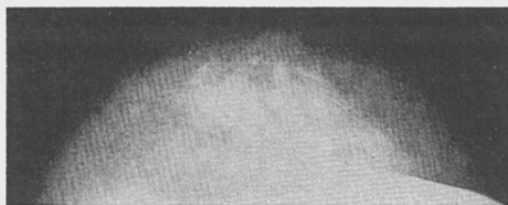


Fig. 7. B. For legend please see Fig. 7, A, on page 237.

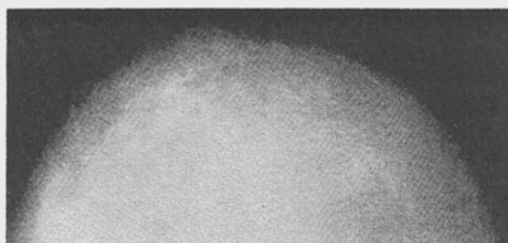


Fig. 8. B. For legend please see Fig. 8, A, on page 237.

Kodak "M" film mammograms, also of interest, is made in TABLE II.

CONCLUSION

Xerography is a simpler method of examination of the breast than that done with conventional x-ray film. It is my belief that more information can be obtained from a single xerogram than from any single film mammogram. With good technic, xerography will afford a more accurate examination, but, most importantly, it is more readily interpreted. The development awaits reliable equipment.

ACKNOWLEDGMENT: My greatest indebtedness is to radiologists closely associated with mammography who have encouraged and supported this work. Dr. John Martin, Houston, Texas, recognized before me some of the basic advantages of xerograms of the breast after only a brief encounter with it.

The cost of producing the xerograms in color was assumed by the Xerox Corporation. Figures 1 and 2 were furnished by Xerox Corporation.

Department of Radiology
Hutzel Hospital
432 Hancock Avenue, East
Detroit, Mich. 48201

REFERENCES

1. CAMPBELL, ET AL.: Xeroradiography: Evaluation of its Uses in Diseases of the Bones and Joints of the Extremities. *J. Bone & Joint Surg.* **41A**: 271–277, March 1959.
2. EGAN, R. L.: Experience with Mammography in a Tumor Institution: Evaluation of 1,000 Studies. *Radiology* **75**: 894–900, December 1960.
3. FARMER, F. T., FOWLER, J. F., AND HAGGITH,

- J. W.: Megavoltage Treatment Planning and the Use of Xeroradiography. *Brit. J. Radiol.* **36**: 426-435, June 1963.
4. GOULD, H. R., RUZICKA, F. F., JR., SANCHEZ-UBEDA, R., AND PEREZ, J.: Xeroradiography of the Breast. *Am. J. Roentgenol.* **84**: 220-223, August 1960.
5. HENNY, G. C.: Effect of Roentgen-Ray Quality on Response in Xeroradiography. *Am. J. Roentgenol.* **79**: 158, January 1958.
6. HILLS, T. H., STANFORD, R. W., AND MOORE, R. D.: Xeroradiography: II. The Present Medical Applications. *Brit. J. Radiol.* **28**: 545-551, October 1955.
7. McMASTER, R. C.: New Developments in Xeroradiography. *Non-Destr. Testing* **10**: 8-25, Summer 1951.
8. NAGAMI, H.: Discussion of the X-Ray Characteristic of Xeroradiographic Plates. *Electrophotography* **4**: 3-6, 1962.
9. OLIPHANT, W. D.: Xeroradiography: I. Apparatus and Method of Use. *Brit. J. Radiol.* **28**: 543-544, October 1955.
10. O'MARA, R. E., RUZICKA, F. F., JR., OSBORNE, A., AND CONNELL, J., JR.: Xeromammography and Film Mammography: Completion of a Comparative Study. *Radiology* **88**: 1121-1126, June 1967.
11. ROACH, J. F., AND HILLEBOE, H. E.: Xeroradiography. *Am. J. Roentgenol.* **73**: 5-9, January 1955.
12. ROACH, J. F., AND HILLEBOE, H. E.: Xeroradiography. *J.A.M.A.* **157**: 899-901, March 12, 1955.
13. RUZICKA, F. F., JR., KAUFMAN, L., SHAPIRO, G., PEREZ, J. V., AND GROSSI, C. E.: Xeromammography and Film Mammography: A Comparative Study. *Radiology* **85**: 260-269, August 1965.
14. TAYLOR, G. M., AND TENNEY, G. H.: Field Evaluation of Industrial Xeroradiography. *Non-Destr. Testing* **13**: 12-17, November-December 1955.
15. VYVERBERG, R. G., CLARK, H. E., AND DESSAUER, J. H.: Industrial Xeroradiography in 1955. *Non-Destr. Testing* **13**: 35-40, May-June 1955.
16. WOLFE, J. N.: Mammography as a Screening Examination in Breast Cancer. *Radiology* **84**: 703-708, April 1965.
17. WOLFE, J. N.: Mammography. Springfield, Ill., Charles C Thomas, 1967.
18. WOLFE, J. N.: A Study of Breast Parenchyma by Mammography in the Normal Woman and Those with Benign and Malignant Disease. *Radiology* **89**: 201-205, August 1967.



8.6 Reduction in mortality from breast cancer after mass screening with mammography

László K. Tabár (born 1943)

László Kornél Tabár was born on 21 October 1943 in Szikszó, Hungary. He graduated from high school in June 1961. He attended the Faculty of Medicine, University of Pécs, Hungary between 1961–1967. He became Resident in Radiology at the Radiologic Clinic, Medical University, Pécs, Hungary 1967–1971. He became staff radiologist and assistant professor at the Radiology Clinic, Medical University, Pécs, Hungary (1971–1977) and received his Doctor of Medical Sciences, PhD from the Hungarian Academy of Sciences in 1978. He took a course in pedagogy for teachers in the medical faculty at Uppsala University, Sweden, a British Council Course on Epidemiological Methods in Southampton, England, a course in statistics in Biomedical Research at Uppsala University, Sweden and an Advanced Course on Quantitative Methods in Cancer Epidemiology at the International Agency for Cancer in Lyon, France.

In 1977 he was invited from Hungary by the Kopparberg County Council, Sweden to chair the Department of Mammography, Central Hospital, Falun, Sweden. As the Director of the Mammography Department, he is responsible for a department consisting of two physicians, eight X-ray technologists and a clerical staff of four. He is also the Director of the Kopparberg County mammographic screening program, which began in 1977. The Department carries out breast cancer screening by mammography on about 300 women a day. In addition, 15–20 referred patients are examined by mammography daily.

During the past 23 years more than 1,000,000 mammographic examinations have been carried out by the Department of Mammography, Falun Central Hospital. The screening program started as a scientifically designed, controlled, randomized, population-based trial performed under the auspices of the Swedish National Board of Health and Welfare. Tabár is the project leader and Principal Investigator and has become an international authority on the benefits of screening mammography. He has published more than 130 articles in peer-reviewed medical journals, as well as books. In 1987 a political decision was made about “service screening” for all women living in Dalarna (Kopparberg) county in the age group 40–69.

The Department of Mammography also performs bone and soft tissue examinations on patients with rheumatic diseases. Tabár has been actively engaged in teaching mammography to radiologists in Scandinavia, The Netherlands, the United States, Australia, New Zealand, Ireland, Scotland and Canada.

Tabár is a Consultant Radiologist for numerous Comprehensive Breast Centers in the United States and the President of Mammography Education, Inc., Scottsdale, Arizona. He is the Author of a Teaching Atlas of Mammography, 1983 with Dr. Peter B. Dean, which has been translated into German, Italian, Portuguese and Spanish. The 3rd edition was published in 2001 and again translated into several languages. He has been the course director and principal lecturer of CME courses in mammography since 1980 in Europe and since 1985 in the USA, Canada, Australia, New Zealand and Asia. He has produced and directed two prize-winning teaching movies on mammography.



His most recent awards include the 1988 Terry Fox Award from the British Columbia Medical Association for his contributions to cancer research, the 2001 Gold Medal from the Society of Breast Imaging, the 2002 IMPACT award for lifetime achievement from the National Consortium of Breast Care Centers, Inc., and the American Cancer Society's Distinguished Services Award.

Picture courtesy Laslo Tabar MD, 2004.

C.J.G. Fagerberg

A. Gad

L. Baldeurop

L.H. Holmberg

O. Gröntoft et al.

Reprinted from THE LANCET, April 13, 1985, pp. 829–832

REDUCTION IN MORTALITY FROM BREAST CANCER AFTER MASS SCREENING WITH MAMMOGRAPHY

**Randomised Trial from the Breast Cancer
Screening Working Group of the Swedish National
Board of Health and Welfare**

L. TABÁR	C. J. G. FAGERBERG
A. GAD	L. BALDETORP
L. H. HOLMBERG	O. GRÖNTÖFT
U. LJUNGQUIST	B. LUNDSTRÖM
	J. C. MÅNSON
<i>Kopparberg County Project</i>	<i>Östergötland County Project</i>
<i>Group*</i>	<i>Group†</i>
G. EKLUND	N. E. DAY
F. PETTERSSON	

**Departments of Mammography, Pathology, and Surgery, Central Hospital, Falun; †Departments of Diagnostic Radiology, Oncology, Pathology, Surgery, and Laboratory of Clinical Cytology, University Hospital, Linköping, Sweden; National Board of Health and Welfare, Stockholm; International Agency for Research on Cancer, Lyon, France; and Department of Gynaecological Oncology, Karolinska Institute, Stockholm*

Summary A randomised controlled trial to investigate the efficacy of mass screening with single-view mammography in reducing mortality from breast cancer was started in Sweden in 1977. 162 981 women aged 40 years or more and living in the counties of Kopparberg and Östergötland were enrolled in the study and divided at random into 2 groups. Each woman in the study group was offered screening every 2 or 3 years depending on age. Women in the control group were not offered screening. This report is confined to the 134 867 women aged 40–74 years at date of entry. The results to the end of 1984 show a 31% reduction in mortality from breast cancer and a 25% reduction in the rate of stage II or more advanced breast cancers in the group invited to screening. 7 years after the start of the study the excess of stage I cancers in the study group largely outweighs the deficit of advanced cancers.

Introduction

IN 1977, the Swedish National Board of Health and Welfare started a randomised controlled trial in 2 counties to determine to what extent mass screening with single-view mammography could reduce mortality from breast cancer. It started in October, 1977, in Kopparberg and in May, 1978, in Östergötland. We present the first results of the study to the end of 1984.

2

Methods

A total of 162 981 women aged 40 years or more at randomisation, from Kopparberg and Östergötland counties, entered the study. The randomisation took place at the community level rather than at individual level.¹ For this purpose the combined population of the 2 counties was divided into 19 blocks selected to give relative socioeconomic homogeneity within each block. All women over 40 from a given block entered the study at the same time. The date of entry is taken as the date of randomisation. In Östergötland each block was divided into 2 units of roughly equal size; 1, chosen at random, was allocated to receive screening, and the other was allocated to the control group. In Kopparberg each block was divided into 3 units of roughly equal size, 2 of which were randomly allocated to receive screening and 1 to the control group (table I). In Kopparberg the control group is only half the size of the study group. Women over 74 years of age were invited to screening, but the compliance rate was less than 50%. This report is confined to the 134 867 women aged 40–74 at randomisation who had not received surgery for breast cancer before randomisation. Women in the study group aged 40–49 at date of entry were invited to screening on average every 24 months, and women aged 50 or more at entry were invited on average every 33 months. Individual letters of invitation were sent out at each screening round to all women in the original cohort still living in the county. The first 2 screening rounds have been completed for all age-groups in both counties. The compliance rate for the 2 counties combined is given in table II. The difference between the number of women invited at the first and second rounds

TABLE I—NUMBER OF WOMEN INCLUDED IN THE STUDY IN THE 2 COUNTIES BY AGE AT ENTRY

Age-group	Study group			Control group		
	Östergötland	Kopparberg	Total	Östergötland	Kopparberg	Total
40–49	10 312	9625	19 937	10 625	5053	15 678
50–59	11 918	11 863	23 781	11 416	5632	17 048
60–69	11 646	12 153	23 799	10 920	5674	16 594
70–74	5158	5410	10 568	4975	2487	7462
(≥75)	7967	8338	16 305	7997	3812	11 809*
Total						
40–74	39 034	39 051	78 085	37 936	18 846	56 782

*Not included in the present analysis because compliance was poor.

TABLE II—COMPLIANCE RATE WITH THE SCREENING PROGRAMME IN THE COUNTIES COMBINED

Age-group	1st screening			2nd screening		
	Invited	Participated	Attendance rate (%)	Invited	Participated	Attendance rate (%)
40–49	19 937	18 581	93·2	19 475	17 378	89·2
50–59	23 781	21 831	91·8	22 969	20 135	87·7
60–69	23 799	20 920	87·9	22 484	18 187	80·9
70–74	10 568	8313	78·7	9578	6400	66·8
Total	78 085	69 645	89·2	74 506	62 100	83·3

TABLE III—WOMAN-YEARS OF OBSERVATION* IN THE 2 COUNTIES
COMBINED BY YEAR OF FOLLOW-UP†

—	Time (mo) since date of entry								Total
	0–11	12–23	24–35	36–47	48–59	60–71	72–83	84–	
Control group	56 782	56 293	55 299	54 495	51 665	39 259	17 275	2948	334 016
Study group	78 085	77 348	76 004	75 075	71 359	54 760	27 960	5681	466 272

*The date of exit from the study is taken as the end of the year of last follow-up.

†Women aged 40–74 at entry.

gives the number of women from the original cohort who had died or left the county in the intervening period. All eligible women in the study group have received at least 2 invitations, and some women under 50 years of age have already received 4. The woman-years of observation in the study and control groups are given in table III, by year of follow-up. The average length of follow-up since date of randomisation is 6.0 years.

13% of women in the control group had a mammographic examination as part of routine medical care up to the end of 1984. Most of these examinations were in 1983–84.

The only screening modality used was mammography with the single medio-lateral oblique view.² Details of the technique and the organisation of the programme are given elsewhere.^{1,3,4} Nationwide cancer registration permits identification of breast-cancer cases even among women who have migrated out of the counties, and all deaths in the cohort were obtainable from the National Bureau of Statistics. The small number of subjects who have left Sweden were the only ones who could not be traced. A death was classified by members of the local project groups as being due to breast cancer only after a full review of the clinical and pathological records. When the cause of death was doubtful the records were reviewed by a combined committee from the 2 counties. The statistical analysis with Mantel-Haenszel techniques was based on individuals. The excess variation resulting from randomisation being at the community rather than the individual level was negligible. Analyses were stratified by county and age. Stratification by county was necessary because the dates on which screening started and the proportion of women allocated to screening were different in the 2 counties.

Results

Compliance at first screening was 89%. The numbers of women in the study and control groups with breast cancer diagnosed between randomisation and Dec 31, 1984, are given in table IV by stage of disease at diagnosis. In the study group there is a highly significant reduction (25%) in the absolute rate of stage II or more advanced cancers ($p < 0.001$, table V). This deficit is more than outweighed by the excess in the study group of stage I and in-situ cancers.

Fig 1 shows the evolving cumulative number of stage II or more advanced cancers in the study and control groups (the number of cases in the Kopparberg control group has been doubled to allow for the control-group size). Since the number of cases in the study population is a mixture of

TABLE IV—BREAST CANCER CASES DIAGNOSED BETWEEN THE DATE OF RANDOMISATION AND DEC 31, 1984, IN THE STUDY AND CONTROL GROUPS BY AGE AND STAGE OF DISEASE*

	Invasive cancer				Axillary nodes positive and/or disseminated disease	Ductal in situ
	Total invasive	Stage I	Stage II	Invasive ≤ 20 mm pNX§		
Study group:						
Ever screened†	951	589	324	38	223	93
Never screened‡	117	27	85	5	61	5
Total study group	1068 (13·7)¶	616 (7·9)	409 (5·2)	43 (0·6)	284 (3·6)	98 (1·3)
Control group	595 (10·5)	209 (3·7)	376 (6·6)	10 (0·3)	253 (4·5)	15 (0·4)

* Women aged 40–74 at entry.
† Includes screen-detected and interval cancers.
‡ Includes cancers among non-responders and cancers diagnosed between randomisation and invitation to screening.
§ pNX: invasive tumour, size ≤ 20 mm, axillary nodes not examined histologically.
¶ Figures within brackets denote no per 1000 women.

TABLE V—COMPARISON BETWEEN THE STUDY AND CONTROL GROUPS OF THE RATES OF STAGE II AND MORE ADVANCED CANCERS*

—	Kopparberg county		Östergötland county	
	Stage II+	Population	Stage II+	Population
Study group	228	39 051	181	39 034
Control group	151	18 846	225	37 936

$\chi^2 = 15.0$ ($p < 0.001$). Relative risk = 0.75.

95% confidence interval (0.65, 0.87).

*Women aged 40–74 at entry.

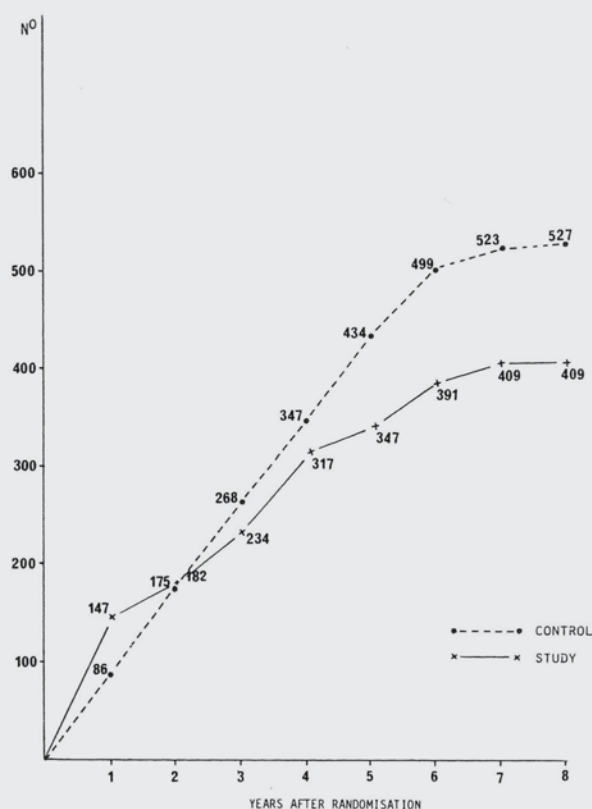


Fig 1—Cumulative number of women with stage II or more advanced breast cancer by time since randomisation, women aged 40–74 at entry.

The figures for the control group are adjusted for the different size of the control group in Kopparberg county.

prevalent and incident cases, rates related to woman-years at risk were not calculated. The concavity of the curves in the last 3 years of follow-up reflects the falling number of woman-years at risk. The number of deaths from breast cancer in the study and control groups is shown in table VI by county. Overall there is a 31% reduction in mortality in the study group ($p = 0.013$, 2-sided test). The cumulative mortality rate in the study and control groups is shown in fig 2. The

6

TABLE VI—DEATHS FROM BREAST CANCER IN STUDY AND CONTROL POPULATIONS*

—	Kopparberg county			Östergötland county		
	Deaths	Population	Relative risk	Deaths	Population	Relative risk
Study group	51	39 051	0.63	36	39 034	0.74
Control group	39	18 846		47	37 936	

Combined χ^2 on 1 d.f. = 6.17, $p = 0.013$ (2-sided).

Combined estimate of relative risk = 0.69, 95% confidence interval (0.51, 0.92).

*Women aged 40–74 at entry.

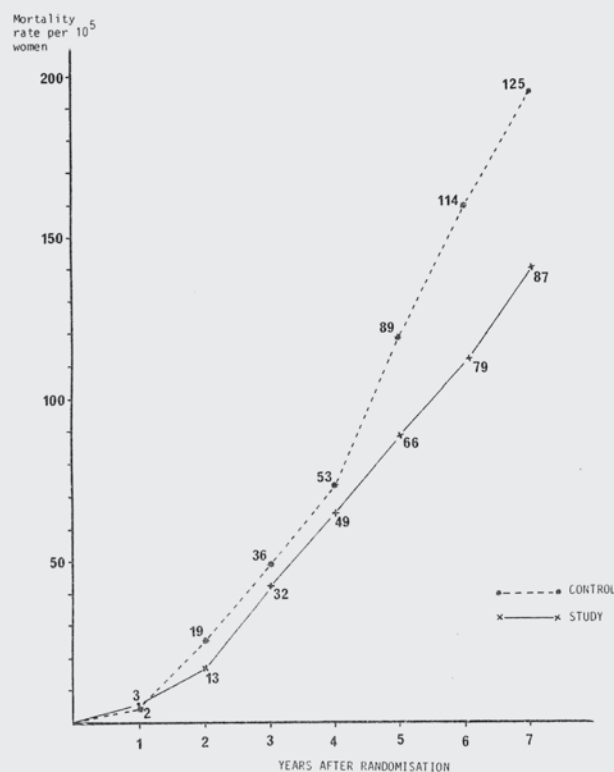


Fig 2—Cumulative mortality rates per 10^5 women by time since randomisation in the study and control groups, women aged 40–74 at entry.

The cumulative number of deaths is shown alongside the curves; the figures for the control group are adjusted for the different size in the control group in Kopparberg.

difference between both groups began to emerge 4 years after the date of randomisation and has steadily widened since. The numbers of deaths are also given in fig 2, with the Kopparberg control numbers doubled, as in fig 1.

Table VII gives the difference in mortality between the study and control groups for the 40–49 and 50–74 age-

TABLE VII—DEATHS FROM BREAST CANCER BY AGE AT ENTRY

—	Kopparberg county		Östergötland county		—
	Deaths	Population	Deaths	Population	
<i>Age-group 40–49:</i>					
Study	8	9625	8	10 312	Combined χ^2 = 0.31 Relative risk = 1.26, 95% confidence interval (0.56, 2.84)
Control	3	5053	7	10 625	
<i>Age-group 50–74:</i>					
Study	43	29 426	28	28 722	Combined χ^2 = 9.14 p = 0.003 (2-sided) Relative risk = 0.61 95% confidence interval (0.44, 0.84)
Control	36	13 793	40	27 311	

groups. In the 50–74 age-group, there is an overall reduction in mortality of 40% ($p=0.003$). In the 40–49 age-group no reduction has yet been observed, but the confidence interval is wide.

Discussion

This is the first randomised trial to show a reduction in mortality from breast cancer after mass screening since the Health Insurance Plan of New York (HIP) study.⁵ We used single-view mammography only, whereas complete mammography with physical examination was used in the HIP study. Also, we had a longer interval between consecutive screenings. Even with an interval of nearly 3 years the reduction in mortality in the 50–74 age-group is similar to that in the HIP study for the 50–64 age-group, in which annual screening was used.

2 non-randomised studies,^{6,7} one of which used mammography alone but with a shorter interval between screenings,⁶ support our results. The reduction in mortality closely parallels the reduction in the number of stage II or more advanced cancers diagnosed in the study population, compared with the control group. In over 90% of patients who have died breast cancer was diagnosed at an advanced stage. The fall in stage II or more advanced cancers has arisen even though a large number of such cases were diagnosed at the first screening round, most of which were in the 60–74 age-group.

The lack of effect on mortality, even with more frequent screening, in the 40–49 age-group may be explained by the small number of deaths seen so far in this group. In formal statistical terms the effect is not different from that in the

50–74 age-group, since the confidence interval for the effect includes the relative-risk estimate for the older age-group. It corresponds, however, with a similar absence of effect in this age-group in the HIP study after 7 years of follow-up. Further follow-up of this group in the HIP study eventually demonstrated a reduction in mortality.^{8,9} There is still a 30% excess of invasive cancers diagnosed in the study group, compared with the control group (13·7 per 1000 and 10·5 per 1000, respectively, table IV), whereas in the HIP study the number of these cancers in the 2 groups had equalised 5 years after entry to the study.⁸ This difference suggests that cancers are detected at a considerably earlier stage with modern mammography than they were with the detection methods used 15 to 20 years ago, and this may be of considerable importance for the mortality rates in the study group. It is possible that some of the excess cancers might never have surfaced clinically. Consideration of the incidence of interval cancers (ie, those occurring between screenings) should determine whether the deficit of cancers in the years after a negative screening examination corresponds to the numbers detected at screening and will be the subject of a future publication.

The present findings, together with the studies from New York and the Netherlands, show that early detection is effective in reducing breast cancer mortality.

Correspondence should be addressed to L. T., Mammography Department, Central Hospital, 79 182 Falun, Sweden; or G. F., Mammography Department, University Hospital, 38185 Linköping, Sweden.

REFERENCES

1. Tabár L, Gad A. Screening for breast cancer: the Swedish trial. *Radiology* 1981; **138**: 219–22.
2. Lundgren B, Jakobsson S. Single view mammography. A simple and efficient approach to breast cancer screening. *Cancer* 1976; **38**: 1124–29.
3. Tabár L, Gad A, Akerlund E, Holmberg L. Screening for breast cancer in Sweden. In: Feig S, McLelland R, eds. *Breast carcinoma. Current diagnosis and treatment*. New York: Masson Publishing Inc, 1983.
4. Fagerberg G, Baldetorp L, Gröntoft O, Lundström B, Månson JC, Nordenskjöld B. The effects of repeated mammographic screening on breast cancer stage distribution: Results from a randomised study of 92 934 women in a Swedish county. *Acta Radiol Oncol* (in press).
5. Shapiro S, Strax P, Venet L. Periodic breast cancer screening in reducing mortality from breast cancer. *JAMA* 1971; **215**: 1777–85.
6. Verbeek ALM, Hendriks JHCL, Holland R, Mravunac M, Sturmans F, Day NE. Reduction of breast cancer mortality through mass screening with modern mammography: first results of the Nijmegen project, 1975–1981. *Lancet* 1984; **i**: 1222–24.
7. Colette HJA, Day NE, Rombach JJ, de Waard F. Evaluation of screening for breast cancer in a non-randomised study (the DOM project) by means of a case-control study. *Lancet* 1984; **i**: 1224–26.
8. Shapiro S, Venet W, Strax P, Venet L, Roeser R. Ten-to-fourteen year effect of screening on breast cancer mortality. *JNCI* 1982; **69**: 349–55.
9. Moskowitz M. Minimal breast cancer redux. *Radiol Clin North Am* 1983; **21**: 93–113.

8.7 Mammographic Microcalcifications: Detection with Xerography, Screen-Film, an Digitized Film Display

Ralph L. Smathers (born 1953)

Dr. Ralph Smathers was born in Miami, Florida, USA in 1953. He graduated first in his class in 1974 from the University of Florida with special honors in Chemistry. He currently he is the owner and chief physician of Mammography Specialists Medical Group, Inc. in Los Gatos, California, USA.

Dr. Smathers is board certified in Diagnostic Radiology and has specialized in breast imaging since 1985. He is former Chief of the Mammography Section of the Department of Diagnostic Radiology and Nuclear Medicine at Stanford University Medical School. He has been a Medical Director for two large outpatient breast imaging centers in northern California. He has personally read over 500,000 breast imaging studies and participated in over 3,000 breast biopsies. He has authored many medical publications and created a comprehensive CD-ROM on breast imaging. He is a fellow in the Society of Breast Imaging and a member of the Radiological Society of North America. He has lectured internationally on breast imaging and has served as an expert witness in many medical legal cases related to breast imaging.

Dr. Smathers was the first to publish an electronic mammography teaching disc for personal use. It first came out on laser video disc in 1987 and then on CD ROM in 1989. It was the first medical CD published by Lippincott Raven. It allowed the student to interactively study hundreds of images with full teaching write-ups. Today this is a routine idea but at the time it was ground breaking. He was motivated to do this because he felt the knowledge, expertise, and teaching files of some of his professors were lost when they died. Dr. Smathers wanted a way to preserve teaching knowledge – a goal which historians and archivists can appreciate.

Picture courtesy Ralph Smathers MD, 2004.



E. Bush

J. Drace

M. Stevens et al.

Mammography

Ralph L. Smathers, MD • Ellyn Bush, MA • John Drace, MD • Melvin Stevens, MD
• F. Graham Sommer, MD • Byron William Brown, Jr., PhD • Bill Karras, MD

Mammographic Microcalcifications: Detection with Xerography, Screen-Film, and Digitized Film Display¹

Pulverized bone specks and aluminum oxide specks were measured by hand into sizes ranging from 0.2 mm to 1.0 mm and then arranged in clusters. These clusters were superimposed on a human breast tissue phantom, and xeromammograms and screen-film mammograms of the clusters were made. The screen-film mammograms were digitized using a high-resolution laser scanner and then displayed on cathode ray tube (CRT) monitors. Six radiologists independently counted the microcalcifications on the xeromammograms, the screen-film mammograms, and the digitized-film mammograms. The xeromammograms were examined with a magnifying glass; the screen-film images were examined with a magnifying glass and by hot light; and the digitized-film images were examined by electronic magnification and image processing. The bone speck size that corresponded to a mean 50% detectability level for each technique was as follows: xeromammography, 0.550 mm; digitized film, 0.573 mm; and screen-film, 0.661 mm. We postulate that electronic magnification and image processing with edge enhancement can improve the capability of screen-film mammography to enhance the detection of microcalcifications.

Index terms: Breast, calcification, 0.81 • Breast, radiography, 0.11 • Phantoms, 0.81 • Radiography, digital • Xeroradiography, 0.12

Radiology 1986; 159:673-677

Studies have reported that xeromammography can be used to detect smaller microcalcifications than can screen-film mammography (1, 2). We undertook this study to assess the capability of digital-image display and processing to enhance the detection of microcalcifications on screen-film mammograms. High-quality film digitizers have recently become available for use in clinical testing (3, 4). The laser scanner employed in this study (Digirad System One) produces a high-resolution, $2,048 \times 2,048$ data matrix from film radiographs, with 12 bits of pixel intensity. Because the detection of mammographic microcalcifications is one of the most technically demanding radiographic examinations (requiring both high spatial resolution and good contrast discrimination), such detection was considered to be a suitable test of the digital imaging system and its display monitor. Xeromammography was performed to compare the enhancement of microcalcification detectability using selenium plate technology with the detection capability of the digital imaging system.

MATERIALS AND METHODS

Speck Phantoms

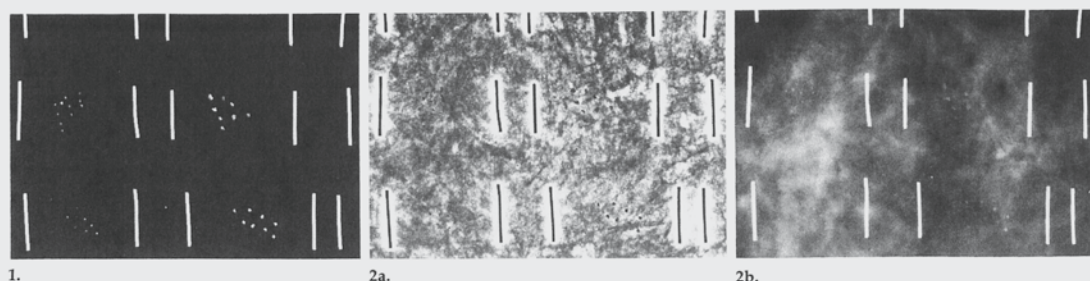
Dried human bone was pulverized and measured by hand (using an optical loupe with reticle) into specks ranging in size from 0.2 mm to 1.0 mm. Because alumi-

num oxide specks have been used in other phantom studies to evaluate microcalcification detectability (1, 5), we included aluminum oxide specks in our evaluation for purposes of comparison. A total of six speck phantoms were made: three phantom patterns of bone clusters and three phantom patterns of aluminum oxide clusters. The clusters were separated by vertically oriented, thin aluminum bars (Fig. 1). The clusters and bars were then sealed between two pieces of transparent tape to create a phantom similar to that described by Sickles (1). The number of specks in each cluster varied from five to 12. The total number of specks in all three phantom patterns (referred to as X, Y and Z) for each speck type for each speck size was always 25. Three phantom patterns of each speck type were considered the minimum necessary to avoid bias as a result of the location and number of microcalcifications on any one image. Actual speck sizes were as follows: 0.20 mm, 0.30 mm, 0.35 mm, 0.40 mm, 0.45 mm, 0.50 mm, 0.60 mm, 0.80 mm, and 1.00 mm. These nine different-sized specks were arranged in clusters on each phantom pattern in three rows of three columns, and the clusters were placed 0.6 cm apart.

Breast Tissue

A mastectomy specimen from a patient with breast carcinoma was obtained after the specimen was fixed and sectioned by a surgical pathologist (5). The skin of the breast tissue was largely intact; only two areas were defective due to biopsy study. The manner of pathologic sectioning allowed the breast to be reoriented into a near anatomically correct configuration. The breast tissue was then placed in a transparent plastic bag containing formaldehyde. Excess fluid and air bubbles were squeezed out of the bag by hand, and the bag was then sealed. The specimen was placed in a holder that compressed the tissue between two wooden frames and flattened the tissue. This simulated the compression applied by clinical mammographic units. The compressed tissue was 10 cm thick. A mammogram taken of this breast phantom confirmed that it was free of microcalcifications and had a moderate amount of glandular tissue.

¹ From the Division of Diagnostic Radiology, S 058D, Stanford University Medical Center, Stanford, CA 94305 (R.L.S., E.B., J.D., F.G.S., B.W.B.); the Palo Alto Medical Clinic, Palo Alto, Calif. (M.S.); and the El Camino Hospital, Mountain View, Calif. (B.K.). From the 1984 RSNA annual meeting. Received July 16, 1985; revision requested August 19; revision received December 19; accepted January 30, 1986. Address reprint requests to R.L.S.
© RSNA, 1986



Figures 1, 2. (1) Magnified area of speck phantom radiograph shows size range of several clusters of specks. Clusters are separated by vertically oriented, thin aluminum bars. (2) Speck phantom obscured by human breast tissue. (a) Xeromammogram. Note intense edge enhancement of metal bars and slight edge enhancement of specks. (b) Screen-film mammogram. Wide range of glandular densities (anatomic noise) makes speck detection more difficult.

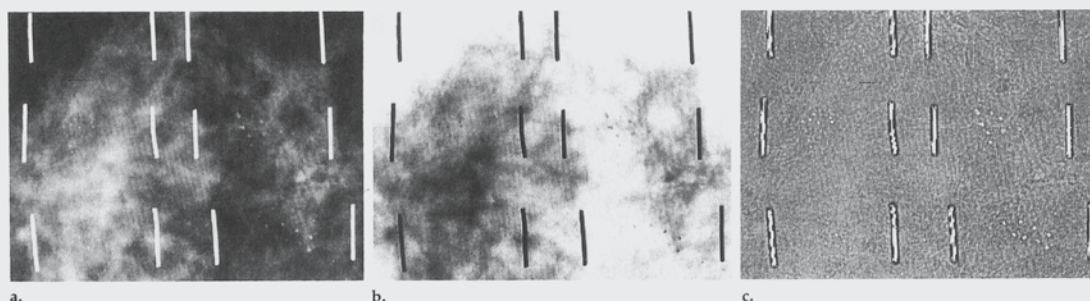


Figure 3. Photographs of CRT display of digitized film mammogram (X4 electronic magnification). (a) Conventional gray-scale display similar to original screen-film seen in Fig. 2b. (b) Reversed video display of a (preferred by some observers). (c) Digital image processing produces edge enhancement of specks and decreases anatomic noise of breast parenchyma.

Radiography

The speck phantoms were alternately placed both above and below the breast phantom when the xeromammograms and screen-film mammograms were made. Positive-mode xeromammograms (Fig. 2a) were made using a Picker (Cleveland) GX 600 with 40 kVp, 300 mAs, and a focal-spot-to-film distance of 91 cm. At 40 kVp, this unit had a nominal focal spot size of 1.4 mm and a measured focal spot size of 1.5 mm. Added filtration of 1.0 mm aluminum was used. The beam had a measured half-value layer (hvl) of 1.5 mm aluminum. A triple-phase generator was used. The exposure in air at 87 cm was 605 mR (0.156 mC/kg). The screen-film mammograms (Fig. 2b) were made using a Senographe CGR 500T triple-phase dedicated mammographic device with a molybdenum target. A 5:1 moving grid was used. Eastman OM-1 and Min-R screens were used. Exposure factors were 32 kVp, 63 mAs, and a focal-spot-to-film distance of 65 cm. At 32 kVp, this unit had a nominal focal spot size of 0.3 mm and a measured focal spot size of less than 0.5 mm. Molybdenum filtration of 0.03 mm thickness was used to produce a beam with a measured HVL of 0.8 mm Al equivalent. The measured skin entrance exposure in air at 65 cm was 700 mR. A 90-second X-Omatic film processor running at approximately 31° C was used. When a speck

phantom was placed below the breast phantom, the distance from the specks to the film in the cassette was 1 cm. When a speck phantom was placed above the breast phantom, the distance was 11 cm.

Film Digitizing

The screen-film mammograms were scanned by the Digirad System One laser. Scanning time was 35 seconds. The transmitted laser light through the film was recorded for each point on the film. The beam size was 180 μ m at full-width half-maximum. On each line sweep of the laser beam, 2,048 points were measured. The film was moved by a precision carriage between each line sweep, and a total of 2,048 lines were scanned. The field scan size used was 10 \times 10 inches (the screen-film mammograms were 8 \times 10 inches). This process yielded more than 4 million pixels per film and a density of 65 pixels per square millimeter of film. Including the 12 bits of intensity data per pixel, 6.3 megabytes of memory were used to store each full-resolution image. The computed image was displayed on three Electrohome 525 line monitors for viewing by the radiologists (Fig. 3). The viewing area was electronically magnified four times. The radiologists used all of the following options when they viewed the images: digital center level

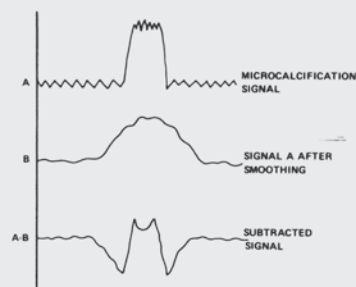


Figure 4. Schematic diagram of image processing used by digital filter algorithm to produce Fig. 3c. Laser scanner detects a "bright" signal A from a calcific density. Low-pass filter "smooths" signal A into signal B. Subtraction of signal B from signal A produces eye-catching edge enhancement effect (see metal bars in Fig. 3c). High-pass filtration of signal A may be performed before subtraction for further enhancement. (Reproduced, with permission, from [3].)

and window width variation (similar to computed tomography [CT] dials) and image processing (Fig. 4). The image processing option used a combined high- and low-bandpass filter algorithm, which is similar to blurred-image subtraction (6).

Table 1
Speck Size at 50% Detectability Level (D50) for Each Technique and Speck Phantom Location

Speck Type	Speck Phantom Location	Technique		
		Screen-Film (mm)	Xeromammography (mm)	Digitized Film (mm)
Bone	Under	0.602	0.518	0.508
	Over	0.721	0.582	0.638
	Mean	0.661	0.550	0.573
Aluminum	Under	0.466	0.466	0.451
	Over	0.467	0.467	0.458
	Mean	0.466	0.466	0.454

Table 2
Analysis of Variance

Source of Variance	P Value	Significance*
Technique (screen-film, xeromammography, digitized film)	< 0.01	Yes
Speck type (bone, aluminum)	< 0.0005	Yes
Position of phantom (over, under)	< 0.001	Yes
Technique and speck type	< 0.01	Yes
Technique and position of phantom	> 0.05	No
Speck type and position of phantom	< 0.01	Yes
Technique, speck type, and position of phantom	> 0.05	No
Interobserver	< 0.0005	Yes

* Significant if $P < .05$.

Table 3
Technique Comparisons

Source of Variance	P Value	Significance*
Xeromammography superior to screen-film	< 0.01	Yes
Digitized film superior to screen-film	< 0.01	Yes
Xeromammography superior to digitized film	> 0.05	No

* Significant if $P < .05$.

total of 324 speck clusters (nine clusters multiplied by 36 images). The six radiologists varied considerably in their experience with mammography. They included one chief resident, three assistant professors, and two senior radiologists with special clinical experience in mammography. The radiologists performed the speck counts on the xeromammograms, on the screen-film mammograms, and on the digitized film cathode ray tube (CRT) images on separate occasions within a period of 3 weeks. All identifying marks on the images were obscured.

Statistical Analysis

The data sheets collected from the radiologists were decoded and entered into a statistical program. The percentage of microcalcifications detected to those actually present were plotted against the size of the microcalcifications seen. A sample of the resulting sigmoidal detection curve (a logistic) is shown in Figure 5. Curve fitting was used to smooth each curve that resulted from the data, using a nonparametric procedure (7). The speck size that corresponded to a 50% detectability level (D50) was obtained for each smoothed curve by linear interpolation. The D50 speck sizes are reported in Table 1 for all techniques. To determine whether one technique was superior to another in the detection of microcalcifications at a statistically significant level, interobserver variation was taken into account using analysis of variance. The resulting P values are reported in Table 2, and compared according to technique in Table 3.

RESULTS

Speck Type

It was clearly demonstrated that for all techniques, all speck phantom positions, and all observers, aluminum oxide specks were significantly easier to detect than pulverized bone specks. Although the effective atomic number of aluminum oxide is close to that of calcium hydroxyapatite and tricalcium phosphate (5, 8, 9), there is an important difference in the empirical detectability between the two types of specks.

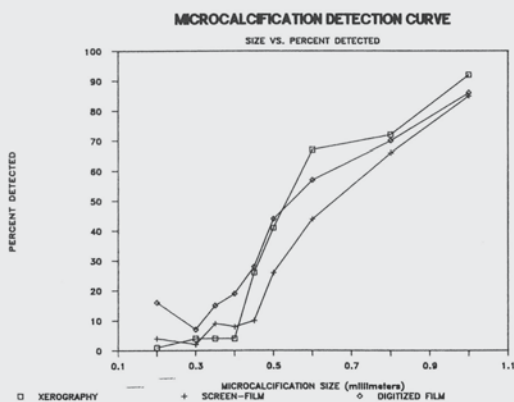


Figure 5. Percentage of microcalcifications detected plotted against their size in millimeters (for xerography, screen-film, and digitized film). Curve for digitized film shifts to the left away from the screen-film curve, resulting in a smaller D50 value. D50 can be approximated by interpolating from the curve at the 50% detection level to the abscissa corresponding to the size at which half of the specks are detected and half are missed (accurate determination requires nonparametric statistical analysis).

Data Collection

Six radiologists independently counted the microcalcifications contained in each cluster between the aluminum bars. For each image, nine numbers were counted, which represented the number of microcalcifications seen in each of the nine clusters. In the majority of images we expected that, for the smallest clusters, none of the specks would be seen, and for the

largest clusters, most of the specks would be seen. Each radiologist examined nine speck clusters on a total of 36 images (12 from each technique: xeromammography, screen-film, and digitized film). For each technique, the 12 images were obtained by alternately placing the three speck phantom patterns (X,Y,Z) of each type of speck (aluminum and bone) under and over the breast phantom.

Each radiologist therefore examined a

Positioning

The detection of specks was significantly enhanced when the speck phantoms were placed under the breast phantom rather than over it. Magnification of the images made under the breast phantom was 1.02. Magnification of the images made over the breast phantom was 1.14 for xeromammography and 1.22 for screen-film. The differences in magnification are due to the different focal-film distances used for xeromammography (91 cm) and screen-film mammography (65 cm) both in this study and in clinical practice. The magnification used (under vs over) at the 50% detectability level had considerably less effect on the aluminum oxide speck phantoms than on the pulverized bone speck phantoms. This raises a serious question concerning the use of breast phantoms that contain aluminum oxide specks to test equipment and compare techniques. Bone particles may be preferred to aluminum oxide specks for phantom testing, although the former are somewhat more difficult to quantify due to the porosity of bone. Ground cortical bone is preferable to trabecular bone as a means to minimize porosity.

Observer Variation

The Spearman rank correlation coefficient was used to assess the correlation between each observer's experience and the amount of variation each observer noted from the mean D50 value for each technique (10). There was a significant difference between the results reported by the observers that did not clearly correspond to the radiologist's years of experience ($P > .05$). In analysis of the data, it was apparent that an important observer variation resulted from the "threshold" factor of deciding whether to count any specks present or none present. The observers' most difficult "decision" was to discriminate true signals from background noise when the size of the speck was small enough to blend into the background noise of the image. The detection of microcalcifications dropped off rather abruptly below 0.600 mm (Fig. 5).

Technique

The mean 50% detectability values obtained for the aluminum speck phantoms by all three imaging techniques showed no statistically significant difference. For the bone speck

phantoms, the D50 values obtained with xeromammography and digitized film were significantly better than the D50 value obtained with screen-film (Table 1). The difference in the D50 values between the xeromammography and digitized film techniques was minimal and not statistically significant. The standard deviations of the D50 values were determined for each technique and averaged (for bone and aluminum specks combined) for all observers and for each speck phantom location (over, under) as follows: xeromammography, ± 0.072 ; screen-film, ± 0.115 ; and digitized film, ± 0.125 .

DISCUSSION

Since detection of microcalcifications is a critical factor in assessing the value of mammography in screening and diagnosing breast carcinoma (11, 12), improving detection should improve diagnostic accuracy. Sickles (1) has stated that xeromammography depicts smaller aluminum specks than screen-film mammography, which is probably due to the former's inherent edge enhancement properties. However, screen-film mammography is currently used by many radiologists because it projects a lower radiation dose to the breast tissue, provides greater equipment reliability, and also because it has a wider dynamic range, which improves soft-tissue contrast discrimination and facilitates detection of small noncalcified masses. Digitized screen-film mammography has the capability to combine the best features of both techniques (13). With the digitized image's high spatial and contrast resolution, the soft-tissue discrimination of screen-film mammography can be achieved and then surpassed by gray-scale variability. With the high-pass filter, the digitized image can produce edge enhancement of microcalcifications to an exact and reproducible amount that can be specified by the operator to be more or less than that inherently obtained by the xerographic selenium plate. Study has shown that specks can be detected at a much smaller size when they are not obscured by surrounding fibrous and glandular breast tissue (1). The capability of the combined high- and low-bandpass filter algorithm to produce edge enhancement of microcalcifications while simultaneously diminishing surrounding anatomic noise was found to be very useful in this study. This capability is similar

to blurred mask subtraction (6) but is exactly reproducible with the digitized image, and the filter parameters can be varied to adapt to the density of the breast tissue.

We advocate the use of the D50 for the quantification of speck detection. The D50 represents a well-defined statistical parameter similar to the LD50 (lethal dose for 50% survival of group) used for drug testing in animals (bioassay and quantal response). It permits an objective comparison of results among investigators and should replace less precise descriptions, such as "the smallest visible speck" and "the smallest speck easily seen." From a study of Figure 5, one might suppose that "the smallest visible speck" was located at the 10% detection level (D10) and was approximately 0.30 mm or 0.40 mm, and that "the smallest speck easily seen" was located at the 75% detection level (D75) and was approximately 0.80 mm. Obviously such wide variations in results would make comparisons meaningless, and standardization is therefore necessary.

Clinical mammographers may be surprised that half of the bone specks smaller than 0.55 mm were not detected in this study, since microcalcifications of 0.30 mm are frequently found on routine mammograms. Testing with commercial phantoms may lead to the conclusion that, by using standard equipment, one can routinely find 0.30-mm specks. In a study using silicon-carbide granules unobscured by tissue, Arnold et al. (14) found that the "smallest" granules depicted by four mammographic-screen-film systems were 0.29 mm in average diameter. Three important factors contributed to the apparently high D50 values in this study.

First, aluminum oxide is used in almost all commercially available phantoms. In this study, aluminum speck phantoms were found to have a D50 value of 0.46 mm, which was nearly 0.1 mm less than the D50 value of the xerographic bone speck phantoms and 0.2 mm less than the D50 value of the screen-film bone speck phantoms.

Second, specks are more easily detected when they are not obscured by breast tissue. The presence of 3–5 cm of compressed breast tissue will obscure many 0.30 mm specks that would otherwise be readily detected in a free-standing phantom. The anatomic noise of fibrous strands and glandular tissue is particularly effective in obscuring specks.

Third, the smaller specks (0.2 mm

and 0.3 mm) seen on clinical mammograms may be only a fraction of those actually present in that size range. Magnification-specimen radiography often demonstrates many more microcalcifications in breast tissue than are seen on preoperative mammograms.

Prior to routine use of digitized images for clinical applications, further studies must be done to gauge the suitability of digitized images for use in diagnostic interpretation. This study primarily evaluated the spatial resolution of the film digitizer and image-display capability of the Digirad System One for the detection of microcalcifications. Contrast discrimination was also evaluated because the full complement of digital information (12 bits of pixel intensity) is available on-screen for examination by the radiologist. The results support the conclusion that the detection of microcalcifications using screen-film mammography can be improved to equal that of xeromammography by image processing, gray-scale variation, and electronic magnification of the digitized film. Future

research should address not only the processes related to improving detection of microcalcifications but also the contribution of digital processing in characterizing microcalcifications as benign or malignant (15, 16). ■

Acknowledgment: We thank Joan Teo, Jerry Halperin, biostatistician, Irene Balcar, M.D., Solon Finkelstein, M.D., the Palo Alto Medical Clinic, the El Camino Hospital, and the Digirad Corporation for their valuable assistance on this project.

References

1. Sickles EA. Mammographic detectability of breast microcalcifications. *AJR* 1982; 139:913-918.
2. Stanton L, Villafana T, Day JL, Lightfoot DA, Stanton RE. A study of mammographic exposure and detail visibility using three systems: Xerox 125, Min-R, and Xonics XERG. *Radiology* 1979; 132:455-462.
3. Smathers RL, Brody WR. Digital radiography: current and future trends. *Br J Radiol* 1985; 58:285-307.
4. Sommer FG, Smathers RL, Wheat RL, Alvarez RE, Brody WR, Cassel DM. Digital processing of film radiographs. *AJR* 1984; 144:191-196.
5. Egan RL, Fenn JO. Phantoms for evaluating mammography techniques and roentgenographic detail. *AJR* 1968; 102:936-940.
6. McSweeney MB, Sprawls P, Egan RL. Enhanced image mammography. *AJR* 1983; 140:9-14.
7. Barlow RE, Bartholomew DJ, Bremner JM, Brunk HD. *Statistical inference under order restrictions*. New York: Wiley, 1972.
8. Burgess A. A mammographic quality assurance test program. *Radiology* 1979; 133:491-495.
9. Stanton L, Villafana T, Day JL, Lightfoot DA. A breast phantom method for evaluating mammographic technique. *Invest Radiol* 1978; 13:291-297.
10. Brown BW, Hollander M. *Statistics: a biomedical introduction*. New York: Wiley, 1977.
11. Moskowitz M, Gartside PS. Evidence of breast cancer mortality reduction: aggressive screening in women under age 50. *AJR* 1982; 138:911-916.
12. McLelland R. Mammography in the detection, diagnosis and management of carcinoma of the breast. *Surg Gynecol Obstet* 1978; 146:735-740.
13. Nishikawa RM, Yaffe MJ. An investigation of digital mammographic imaging. *Proc SPIE* 1983; 192-200.
14. Arnold BA, Webster EW, Kalisher L. Evaluation of mammographic screen-film systems. *Radiology* 1978; 129:179-185.
15. Millis RR, Davis R, Stacey AJ. The detection and significance of calcifications in the breast: a radiological and pathological study. *Br J Radiol* 1975; 49:12-26.
16. Colbassani HJ, Feller WF, Cigtay OS, Chun B. Mammographic and pathologic correlation of microcalcification in disease of the breast. *Surg Gynecol Obstet* 1982; 155:689-696.

8.8 Breast imaging: Dual-energy projection radiography with digital radiography

Tarou Asaga (born 1946)

Dr. Taro Asaga was born on 29 June 29 1946 in Tokyo, Japan. He graduated from Fukushima Medical University in 1971. He qualified as a doctor at Yokohama City University in 1983.

After graduating from Fukushima Medical University, he joined the resident course in Yokohama City University from 1971 to 1973. In 1973 he started his clinical work at the Department of Surgery in the Municipal Yokohama-Shimin Hospital. Since 1976 he has been working in the Kanagawa Cancer Center Hospital in the Kanagawa Prefecture in Japan. While performing clinical work in the Kanagawa Cancer Center, his major research field has been the diagnosis and treatment of breast cancer. This has involved the study of sentinel lymph node biopsy specimens in breast cancer, studies into determining the location breast cancer by dual-energy subtraction, and studies into prognostic factors for breast cancer. He is currently the Director of the Department of Surgery in the Kanagawa Cancer Center.



Shikibu Chiyasu (born 1945)

Mr. Shikibu Chiyasu, RT, was born on 16 January 16 1945 in Shizuoka Prefecture in Japan. In 1970 he obtained his National License as a Diagnostic Radiation Technologist.

From 1966 to 1988 he worked in the Kanagawa Cancer Center Hospital, which is a core facility for cancer diagnosis and treatment in Kanagawa Prefecture, Japan. During this period he conducted studies evaluating the efficacy of new imaging technology in clinical practice. More specifically, in the 1970s he conducted studies of the effects of the rare earth screen type and X-ray spectrum on the image characteristics of mammography. In the 1980s he conducted a series of studies into the clinical application of digital image processing using CR in the field of diagnostic chest X-ray, tomography and mammography, as well as evaluations of new imaging such as dual-energy subtraction mammography or chest one-shot energy subtraction. From 1988 to 1993 he worked in the Kanagawa Prefectural Ashigara-Kami Hospital as Chief Radiological Technologist. During this period, he conducted studies into image transmission over the public telephone line among multiple hospitals. In 1993, he was appointed Chief Radiological Technologist in the Kanagawa Cardio Vascular and Respiratory Center.

From 1993 to the present he has been working in the Yokohama Tsurugamine Hospital as Chief Radiological Technologist of the Department of Diagnostic Imaging, and presently is in charge of conducting mass surveys of stomach, lung, and breast cancers and also of MR imaging. His recent studies are evaluations of the efficacy of the CRT viewing system, mass survey of the gastrointestinal tract, and comparison of various digital radiography types applied to mass survey.

He is accredited by the Japanese Society of Gastroenterological Mass Survey as an expert technologist for stomach mass survey.



Syuuji Matsuda (born 1934)

Mr. Shuji Matsuda, RT was born on 7 January 1934 in Okayama Prefecture, Japan. In 1956 he graduated from Dai-Nihon Roentgen School and got his National License as a Diagnostic Radiation Technologist. From 1960 to 1962, he worked in the public health department which was located at the City of Odawara, and run by Kanagawa Prefecture.

In 1963 he moved to the Kanagawa Cancer Center Hospital, which is a core facility of cancer diagnosis and treatment in the Kanagawa Prefecture, Japan. He worked in this hospital as Chief Radiological Technologist until 1988. In the 1960s and the 1970s, he conducted studies evaluating and improving the characteristics of automatic exposure control equipment such as phototimer, under practical examination environments. In the 1980s, he headed series of studies on application of computed radiography systems to routine radiology practices, including evaluating and optimizing exposure conditions as well as digital image processing conditions.

From 1989 to 1993, he worked in the Kanagawa Prefectural Children Medical Center as Chief Radiological Technologist. During this period, he conducted studies on applications of computed radiography to pediatric studies. From 1993, he filled posts at several public health organizations successively until his retirement.

***Hirohumi Mastuura*** (born 1948)

Mr. Hirofumi Matsuura, RT, was born on 22 October 1948, in Tokushima City, Tokushima Prefecture, Japan. In 1969, he graduated from the School of X-ray Technologists of Tokushima University and got his National License as first-class technician handling radioactive materials. In 1970 he graduated from the School of Diagnostic Radiation Technologists of Tokushima University and got his National License as a Diagnostic Radiation Technologist.

From 1970 to 1996 he worked in the Kanagawa Cancer Center Hospital, which is a core facility for cancer diagnosis and treatment in Kanagawa Prefecture, Japan. In 1983, he was appointed a Senior Radiation Technologist. In the early 1980s he conducted studies regarding the optimization of X-ray filtering and its effect on the image quality and dose reduction. From 1986 to 1996 he conducted studies regarding clinical application of computed radiography, typically the optimization of digital image processing such as gradation and frequency enhancement for individual anatomies.

From 1996 to 1998 he worked in the Kanagawa Prefectural Ashigara-Kami Hospital and from 1998 to 2003 in the Prefectural Atsugi Hospital. In 2003 he moved to the Municipal Atsugi Hospital. Presently (2004) he is Head of the Radiation Technology Department of the Municipal Atsugi Hospital.



Masamitsu Ishida (born 1950)

Mr. Masamitsu Ishida was born on 23 March 1950, in the City of Hikari, Yamaguchi Prefecture, Japan. He got his BSc in Electrical Engineering in 1972 and his MSc in 1974 from Kyoto University.

From 1974 to the present he has been working as a researcher at the Fuji Photo Film Co. Ltd. (Fujifilm). He started his research career in the physics of electrophotographic imaging. In 1976, he joined a basic research activity on a new diagnostic X-ray system and later a project for development of computed radiography. During this period he played a major role in the development of the digital image processing of medical images. From 1981 to 1983 he temporarily joined the Kurt Rossman Laboratories at the University of Chicago as a research associate and conducted studies into the effect of image processing on perception by the human eye-brain system. Through the 1980s, he was in charge of research on medical image processing as Research Manager at Fujifilm. In the 1990s, he headed the laboratory for image designing and evaluation of photographic imaging and display systems. Presently, he is Divisional Manager of the Quality Design and Evaluation Center of Fujifilm.

**Takao Komaki** (born 1948)

Mr. Takao Komaki was born on 11 July 1948, in the City of Kawagoe, Saitama Prefecture, Japan. He got his BSc in Electrical Engineering in 1972 from Kogakuin University.

From 1967 to 1996 he worked at Fuji Photo Film Co. Ltd. (Fujifilm).

From 1967 to 1976 he worked as a researcher in the R&D laboratory. In 1976, he joined a basic research activity on a new diagnostic X-ray system and later a project for the development of computed radiography. During this period, he played a major role in evaluating image quality and conducting joint clinical evaluations with medical facilities on the CR system. From 1976 to 1988, he worked in the field of application of image processing to CR images. From 1988 to 1996, he worked as an Engineering Manager and was in charge of technical marketing in the medical group of the Equipment Products Division of Fujifilm.

In 1996 he moved to Fujifilm Medical Systems Co. Ltd., Tokyo (FMS). Presently, he is General Manager of the Technical Marketing Group of FMS.



Technical Developments and Instrumentation

Breast Imaging: Dual-Energy Projection Radiography with Digital Radiography¹

Tarou Asaga, MD
Shikibu Chiyasu, RT
Syuuji Mastuda, RT
Hirohumi Mastuura, RT
Hisatoyo Kato, MS
Masamitsu Ishida, MS
Takao Komaki, MS

Dual-energy projection radiography was applied to breast examinations. To perform the dual-energy subtraction radiography with use of a digital radiography unit, high- and low-energy projections were made at an appropriate time interval under differing x-ray exposure conditions. Dual-energy projection radiography appears to offer clear, detailed images and may be a useful supplement to standard mammography.

Index terms: Breast radiography, technology 00.121 • Radiography, digital • Subtraction, dual-energy

Radiology 1987; 164:869-870

ON conventional mammograms obtained with the compression method, normal soft tissue of the breast, tumor, calcium deposits, and other shadows may overlap one another in such a way as to mask a lesion. Therefore, tumors may not be clearly differentiated from adjacent mammary structures. With the use of mammography in dense breasts, it may be difficult to recognize the border of cancer infiltration.

Because of such drawbacks of conventional mammography, a clinical investigation was undertaken to establish a technique to identify tumors and recognize the border of cancer infiltration, thereby improving the accuracy of diagnosis. Breast dual-energy subtraction radiography was carried out clinically with use of computed radiography (CR) (1). In this way, an attempt was made to remove mammary structures with dual-energy subtraction in order to arrive at a more specific and accurate interpretation of the images.

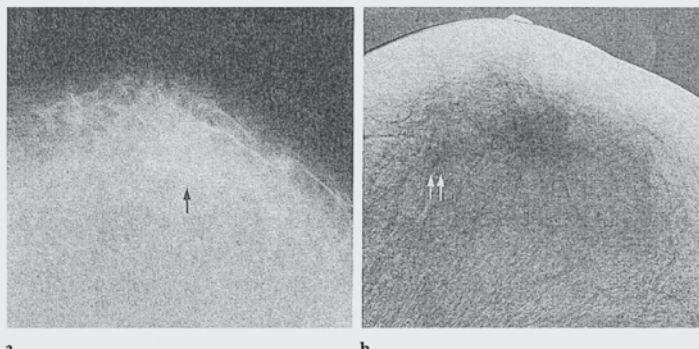


Figure 1. Infiltrating duct carcinoma. (a) Craniocaudal low-energy image. Arrow = tumor shadow. (b) Dual-energy subtraction image reveals the carcinoma was accompanied by a small daughter nodule (arrows).

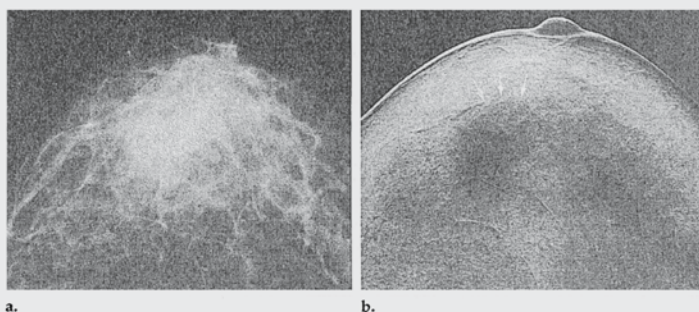


Figure 2. Scirrhous carcinoma. (a) Craniocaudal low-energy image. (b) The border of cancer infiltration (arrows) was revealed by dual-energy subtraction radiograph.

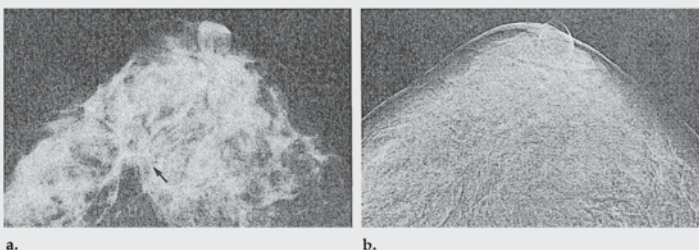


Figure 3. Sclerosing adenosis. (a) Craniocaudal low-energy image. Arrow = possible malignant tumor. (b) Dual-energy subtraction image.

Materials and Methods

The CR system (model 101; Fuji Photo Film, Kanagawa, Japan) was employed in compression mammography with both single-energy and dual-energy subtraction radiography (2-5). Dual-energy subtraction radiography was performed in 40 patients in whom (a)

the diagnosis of cancer was equivocal on the basis of results of ultrasonography or mammography or (b) the border of cancer infiltration was not clearly demonstrated by compression mammography with CR.

The CR system uses scanning, laser-stimulated luminescence (1). The image detector of the CR system—the imag-

¹ From the Department of Surgery (T.A.) and Department of Radiology, Division 1 (S.C., S.M., H.M.), Kanagawa Cancer Center, 54-2 Nakaocho, Asahi-ku, Yokohama, Japan; Fuji Photo Film, Kanagawa, Japan (H.K., M.I.); and Fuji Medical Systems, Tokyo (T.K.). Received November 19, 1986; revision requested January 6, 1987; revision received March 9; accepted April 29. Address reprint requests to S.C.

© RSNA, 1987

ing plate—is coated with minute crystals of photostimulable phosphor in an organic binder. A high-resolution imaging plate with a sampling rate of 10 pixels per millimeter was used in this study.

Mammography was performed with a Mammo Diagnost U-M system (Philips, Shelton, Conn.) (x-ray tube with molybdenum anode; focus size, 0.5×0.5 mm; grid ratio, 5:1; number of lines, 31/cm; drive, direct-current motor; protection, carbon-fiber covering). The exposure conditions of compression mammography were 30 kV and 45 mA (420 mR [0.108 mC/kg] skin dose). The exposure conditions of dual-energy subtraction radiography were 40 kV and 50 mA with add filter of 1.5 mm aluminum for high-energy images (150 mR [0.039 mC/kg] skin dose), and 28 kV and 42 mA with add filter of 0.025 mm molybdenum for low-energy images (600 mR [0.155 mC/kg] skin dose). The effective energies of high and low x-ray beams were 0.7 mm and 0.3 mm in aluminum half-value layer, respectively.

Two automatically controlled exposures were made in each case at an interval of about 10 seconds, and the breast was kept pressed against the tilt-table throughout the procedure. To remove soft-tissue structures and visualize calcifications and cancers, dual-energy subtraction radiographs were obtained with the CR system and the use of a photoelectric Compton effect algorithm.

Results

In 18 of 29 cases diagnosed as cancer on the basis of pathologic findings, dual-energy subtraction radiography

more clearly depicted the focus of tumor and the border of cancer infiltration. In nine of 11 cases of benign disease, such as fibrocystic disease, fibroadenoma, and cyst, the margins of the lesions were more clearly defined by dual-energy subtraction radiography.

Figure 1a is a compression mammogram obtained with CR. The tumor shadow can be recognized, but no other specific shadow can be pointed out. The dual-energy subtraction image (Fig. 1b) reveals that a daughter nodule was also present. Pathologic diagnosis in this case was a $1.5 \times 1.5 \times 1.2$ -cm infiltrating duct carcinoma with a small daughter nodule.

Figure 2a is a compression mammogram obtained with CR. A tumor shadow is apparent, but the border of the tumor cannot be clearly identified. The dual-energy subtraction image (Fig. 2b) delineates the tumor more clearly. Pathologic diagnosis in this case was a $2.5 \times 1.5 \times 1.5$ -cm scirrhous carcinoma.

The compression mammogram in Figure 3a indicates an irregularly concentrated breast, which suggests a malignant tumor. In the dual-energy subtraction image (Fig. 3b) the concentration in the mammary gland is removed, and there is no shadow of a malignant tumor, as seen in Figures 1b and 2b. Accordingly, a diagnosis of a benign tumor was made. Histopathologic examination of a specimen obtained at open biopsy yielded no findings suggestive of malignancy, and a diagnosis of sclerosing adenosis was established.

Discussion

Results of dual-energy subtraction radiography were satisfactory for several reasons: (a) because compression was used, there was little body motion (small motion artifacts were produced

at the border of the breast in only two cases); (b) the x-ray detector (imaging plate) with a linear response and a wide dynamic range helped improve image quality; and (c) a grid was used to produce images unaffected by scattered x rays.

This new technique has two definite advantages: (a) the diagnostic advantage of tumor identification and delineation of the area of infiltration and (b) easy production of diagnostically useful images with conventional mammographic equipment. The technique will be useful in clinical practice, especially in cases in which the possibility of cancer cannot be completely ruled out with any conventional method. ■

References

1. Sonoda M, Takano M, Miyahara J, Kato H. Computed radiography utilizing scanning laser stimulated luminescence. *Radiology* 1983; 148:833-838.
2. Brody WR, Cassel DM, Sommer FG, et al. Dual-energy projection radiography: initial clinical experience. *AJR* 1981; 137:201-205.
3. Kruger RA, Armstrong JD, Sorenson JA, Kiklasen LT. Dual energy film subtraction technique for detecting calcification in solitary pulmonary nodules. *Radiology* 1981; 140:213-219.
4. Lehmann LA, Alvarez RE, Macovski A, et al. Generalized image combinations in dual kVp digital radiography. *Med Phys* 1981; 8:353-357.
5. Sommer FG, Brody WR, Gross D, Macovski A, Hall H, Pele N. Excretory urography using dual-energy scanned projection radiography. *Radiology* 1981; 141:529-532.

8.9 Stereotactic breast biopsy with a biopsy gun

Steve H. Parker (born 1954)

Stephen Parker was born 28 January 1954 in Aberdeen, Maryland, USA. He got his BA cum laude in biological sciences from University of Missouri, Columbia, Missouri and his MD from St. Louis University School of Medicine, St. Louis, Missouri.

He started his flexible internship in 1979 and his residency in 1980 at Fitzsimmons Army Medical Center Aurora, Colorado. In 1983 Dr. Parker got his Board certification from American Board of Radiology. He then went to Germany and became Chief, Department of Radiology, 5th General Hospital, Stuttgart, West Germany. In 1985 he came back to the USA and became a fellow in body imaging (CT, MRI, US), University of Colorado Health Sciences Center, Denver, Colorado and in 1986 he was appointed Chief, Diagnostic Radiology Branch Department of Radiology Fitzsimmons Army Medical Center and Assistant Clinical Professor, Department of Radiology, University of Colorado Health Sciences Center. Here he was awarded "Teacher of the Year" (1986) and "Clinical Radiologist of the Year" (1987). In 1989 he became a staff radiologist, Radiology Imaging Associates, Englewood, Colorado. Since 1993 Dr. Parker has been Director, Sally Jobe Breast Centre Englewood.

In 1990 Stephen Parker adapted the ideas of alternatives to open biopsy introduced by Nordenström (1977) and Lindgren (1982) to develop stereotactic breast biopsies.

Stephen Parker is a member of several scientific societies. He has written 52 original articles, 36 abstracts, 6 book chapters, 15 exhibits and 138 presentations. His primary speciality is breast imaging and intervention.

Picture courtesy Dr. Parker, 2004.



Steve H. Parker, MD • Jeffrey D. Lovin, MD • William E. Jobe, MD • James M. Luethke, MD • Kenneth D. Hopper, MD • Wayne F. Yakes, MD • Brian J. Burke, MD

Stereotactic Breast Biopsy with a Biopsy Gun¹

One hundred three patients underwent stereotactic breast biopsy with an 18-, 16-, or 14-gauge cutting needle and a biopsy gun. After biopsy, a localization wire was placed and surgical biopsy performed. There was agreement of the histologic results in 89 cases (87%) including 14 of 16 cancers (87%) ($\kappa = 0.806$). The gun biopsy yielded the correct diagnosis in four cases involving a lesion (including one cancer) that was missed at the surgical biopsy. Nine cases in which the lesion was missed at gun biopsy can be related to insufficient needle size, the greater difficulty in using one of the two stereotactic devices, and early inexperience with the technique. A 14-gauge needle was used in the last 29 biopsies, the results of which agreed with the surgical pathologic findings in 28 cases (97%). With greater experience, stereotactic-guided large-gauge automated percutaneous biopsy may prove to be an acceptable alternative to surgical biopsy in women with breast masses suspected at mammography.

Index terms: Biopsies, technology • Breast, biopsy, 00.1299 • Breast neoplasms, diagnosis, 00.3 • Breast neoplasms, localization, 00.125

Radiology 1990; 176:741-747

GREATER utilization of breast screening in asymptomatic women is leading to the discovery of an ever-increasing number of nonpalpable lesions suggestive of cancer. Patients with more ominous-appearing lesions are referred for needle localization followed by surgical biopsy. While a relatively safe procedure, there is frequently some delay in arranging the biopsy, the cost is significant, and there is some potential for complications and disfigurement. Accurate, dependable needle biopsies would eliminate or considerably reduce these drawbacks.

Percutaneous biopsy of various sites other than the breast are routinely performed by radiologists (1,2), and we have enjoyed improved success in such biopsies with the use of an automated biopsy device (3). We were frustrated in our initial attempts to utilize the instrument for breast biopsies, however, because of our inability to sample breast lesions with pinpoint accuracy. The advent of commercially available stereotactic mammography provided us with the means to apply our experience with the biopsy gun to the breast and confidently target a mammographically suggestive lesion. Recent investigations conducted with use of stereotactic mammography in conjunction with fine-needle aspiration biopsy (FNAB) have been successful in enabling breast cancer diagnosis but have had significant numbers of

false-negative results and cases with insufficient tissue sampling (4-6). We therefore decided to compare results of stereotactic needle core gun biopsies to those of the corresponding, concomitant surgical biopsies in 103 consecutive patients referred for biopsy of mammographically suggestive nonpalpable lesions.

MATERIALS AND METHODS

During a 13-month period, under a protocol approved by the clinical investigation/human use committee and after informed consent was obtained, 103 stereotactic needle core breast biopsies were performed. After the needle core biopsy and localization wire placement, the patient underwent traditional surgical excisional biopsy. The surgical biopsies were performed by one of three surgical residents, all under direct staff supervision. All needle core biopsies were performed by one of four radiologists (two staff radiologists and two radiology residents) with the Biopsy gun (distributed by Bard Urological, Covington, Ga; manufactured by Radiplast, Uppsala, Sweden) in conjunction with 18-, 16-, or 14-gauge Biopsy-cut needles. Sixty-five patients underwent biopsy with use of 18-gauge needles, nine patients with 16-gauge needles, and 29 patients with 14-gauge needles. One hundred one patients underwent biopsy with the "long-throw" Biopsy gun, which has a 2.3-cm needle excursion. Two patients underwent biopsy with the "short-throw" Biopsy gun, which has a 1.15-cm needle excursion.

For the first 30 biopsies, stereotactic guidance was provided by the Senographe Mammographic System 600T (GE Medical Systems, Milwaukee) coupled with the Stereotix computerized stereotactic needle localization device (GE Medical Systems). The biopsy method used with this device is described elsewhere (7). Because of the logistical problems related to the use of the Biopsy gun with the Senographe unit, we switched to the Mammostest Stereotactic System (Fischer

¹ From the Radiology Imaging Associates, Englewood, Colo (S.H.P., W.E.J.); Department of Radiology, Fitzsimons Army Medical Center, Aurora, Colo (S.H.P., J.D.L., J.M.L., K.D.H., W.F.Y., B.J.B.); and the Department of Radiology, Pennsylvania State University, Milton S. Hershey Medical Center, Hershey, Penn (K.D.H.). From the 1989 RSNA scientific assembly. Received January 9, 1990; revision requested March 14; revision received and accepted May 8. Address reprint requests to S.H.P., Radiology Imaging Associates, 8200 E Bellevue, Suite 124, Englewood, CO 80011.

The opinions or assertions contained herein are the private views of the authors and are not to be construed as official or as reflecting the views of the Department of the Army or the Department of Defense.

© RSNA, 1990

See also the articles by Hopper et al (pp 671-676), Poster et al (pp 725-727), and Elvin et al (pp 677-679) and the editorial by Bernardino (pp 615-616) in this issue.

Abbreviation: FNAB = fine-needle aspiration biopsy.

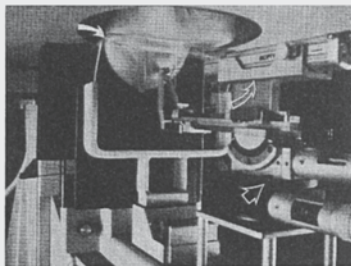


Figure 1. MammoTest stereotactic system. Patient lies comfortably on the table with her breast placed through an opening in the table. All hardware is located beneath the table, with the compression plate (solid arrow), stereotactic apparatus (open straight arrow), biopsy gun, and housing (open curved arrow) out of patient's sight. Biopsy gun is firmly locked into the housing mounted on depth slide, reducing the possibility of unwanted gun/needle displacement.

Imaging, Denver) after the first 30 patients. The remaining 73 patients underwent biopsy with this system.

The MammoTest unit allows the patient to lie prone on a table with her breast protruding through an opening at the front of the table. The compression plate, x-ray tube, stereotactic apparatus, and the biopsy device are all located underneath the table, out of sight of the patient and free from encumbrances (Fig 1). The manufacturer designed a dedicated housing for the Biopsy gun that attaches to the depth slide on the stereotactic apparatus. In addition, software was incorporated that provides an audible and visual warning on the digitizer if the 2.3-cm excursion of the needle would result in the needle striking the Bucky plate.

The first step in the MammoTest biopsy sequence is to obtain a mammographic localizing view that includes visualization of the whole breast to ensure that the lesion is indeed within the aperture of the compression plate. After confirmation, the breast within the aperture is cleansed with povidone-iodine (Betadine; Purdue Frederick, Norwalk, Conn). Stereo views are then obtained by swinging the x-ray tube 15° off center in each direction. The two stereo images are exposed adjacent to each other on the same film (Fig 2a).

Computer-generated coordinates derived from the stereo images are dialed into the stereotactic unit, and the Biopsy gun with needle already loaded is aligned automatically on the proper trajectory. The needle is then advanced (by moving the gun housing) through a small skin nick to the calculated depth, and stereo views are obtained again to confirm that the needle is poised over the lesion (Fig 2b). The needle is then backed up at least 2 mm to ensure proper postfire positioning of the sample notch within the lesion (3). The gun is fired, and a final set of stereo views ensures that the needle has tra-

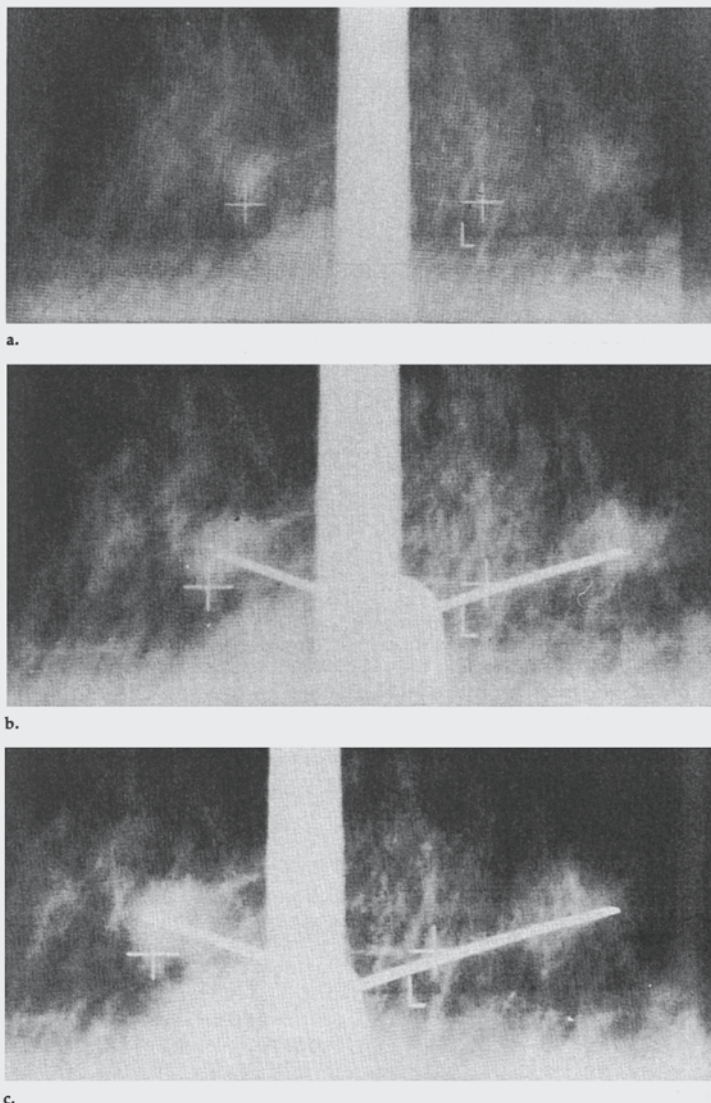


Figure 2. Aligning the gun and needle and confirming needle position. (a) Stereo views are obtained, and the coordinates generated from these views are dialed into the main unit aligning the gun and needle onto the proper trajectory. (b) The needle is advanced through the skin nick to the computed depth, and stereo views are obtained again to confirm that the needle tip is over the lesion. (c) Final set of stereo views is obtained after the gun is fired to document that the needle has traversed the lesion.

versed the lesion (Fig 2c). The needle is removed, and the core tissue obtained is placed in formalin. Three to four passes are made through the lesion to canvass it anteriorly to posteriorly in measured increments from the center of the lesion. All biopsy passes traverse the same skin nick.

After the stereotactic biopsy, a conventional needle localization hook-wire was placed by using the same coordinates as

used for the needle core biopsy. A conventional mammogram was obtained to ensure adequate wire placement. The patient then underwent outpatient surgical excisional biopsy under local anesthetic. The local anesthetic occasionally had to be supplemented by intravenously administered sedatives. The histopathologic specimens from each biopsy were then compared by the same pathologist to evaluate for agreement.

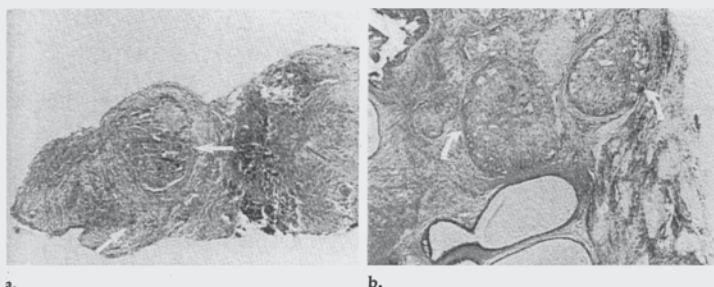


Figure 3. Comparison of gun needle core and surgical histopathologic specimens of breast cancer. (a) Intraductal carcinoma from the gun core specimen (arrows). (b) Same intraductal carcinoma from surgical excisional biopsy specimen (arrows).

Comparison between Histopathologic Results of Needle Core Biopsy and Surgical Excisional Biopsy

Needle Biopsy Results	Surgical Biopsy Results						Total
	Cancer*	FA	FCC	Normal	Other	Insufficient Tissue	
Cancer	14	0	1	0	0	0	15
FA	0	14	0	2	0	0	16
FCC	0	0	51†	0	0	0	51
Normal	1	3	4	6	0	0	14
Other	0	0	1‡	0	4	0	5
Insufficient tissue	0	1	0	0	0	0	1
Total	15	18	57	8	4	0	102

Note.— $\kappa = 0.806$ (values greater than 0.75 reflect strong agreement). FA = fibroadenoma, FCC = fibrocystic change.

* Does not include lobular carcinoma in situ found serendipitously.

† Includes partial agreement.

‡ Mammographic finding in this case corresponded to the needle core diagnosis (cicatrix).

RESULTS

The results from 102 of the 103 patients who underwent stereotactic gun biopsy were available for comparison with results from surgical excisional biopsy. (Needle biopsy specimens from one patient were lost.) Samples sufficient for histologic analysis were obtained by means of stereotactic needle core biopsy in 101 of the 102 patients (99%). The case in which insufficient tissue was obtained was one of the two biopsies performed with the "short-throw" Biopsy gun and an 18-gauge needle. In 12 other cases there was disagreement between the histopathologic diagnoses reached with the two biopsy methods. In eight of those cases, adequate tissue was obtained with the gun biopsy, but the diagnosis made was different from that made from the surgical specimen. In the other four cases, the results at gun biopsy corresponded to the mammographic findings, but these findings were not seen at surgery. For the 102 patients, $\kappa = 0.806$ reflecting strong agreement between the stereotactic needle core and surgical excisional

biopsy results (Table).

There were 16 cancers (13 infiltrating ductal, two intraductal, and one mucinous carcinoma) with agreement between findings from the needle and surgical biopsy specimens in 14 cases (Fig 3). The gun biopsy core specimen did not include a small focus of intraductal carcinoma found in a subsequent permanent surgical specimen. This was probably due to improper calibration of the stereotactic machine. In the other case of cancer without correlation, the stereotactic gun biopsy yielded a diagnosis of mucinous carcinoma that was missed at the ensuing surgical excisional biopsy. The presence of cancer was later substantiated by means of histologic examination of the surgical specimen after modified radical mastectomy. In another case, the gun biopsy core did not include a focus of lobular carcinoma in situ found in the surgical specimen that was obtained in a region remote from the area of fat necrosis that was causing the mammographic abnormality. The fat necrosis was successfully diagnosed from both the gun core and the frozen surgical material.

There were 20 fibroadenomas, with agreement between findings from the needle core and surgical specimens in 41 cases. Four fibroadenomas diagnosed at surgery were missed at stereotactic gun biopsy. One of the fibroadenomas was missed at gun biopsy because the stereotactic machine was out of calibration. Another fibroadenoma was missed because of patient movement. A third was most likely missed as a result of displacement of the lesion away from the advancing needle tip. The fourth fibroadenoma missed at gun biopsy was probably also due to lesion movement. Two fibroadenomas diagnosed at gun biopsy were missed at surgery (Fig 4).

In the 55 cases of fibrocystic change, the findings from the needle core and surgical specimens were in full agreement in 37 and partial agreement in 14 cases. Full agreements were tabulated when three or more of the elements of that particular area of fibrocystic change were correlated (Fig 5). If only one or two elements were correlated, then the case was tabulated as a partial agreement. There were four cases in which the gun biopsy specimen failed to contain any elements of fibrocystic change and contained only normal breast tissue. These may be a reflection of the random distribution of fibrocystic change within normal breast tissue.

There were 11 other diagnoses in the series including six cases in which only normal breast tissue was found in both the stereotactic and surgical specimens. There were two cases of intramammary lymph nodes with good correlation of results between biopsy techniques. In fact, in one of the two cases, results correlated so well that the pathologist believed he could identify the defect from the gun core on the surgical specimen (Fig 6). In one case with a radial scar and one with an area of fat necrosis, results also correlated well. Finally, a cicatrix diagnosed at stereotactic biopsy was missed at surgery.

Subjectively, it was noted that breast tissue (unlike prostate, liver, or kidney) was frequently fatty and friable and tended to fragment and disintegrate when placed in formalin. In consultation with our pathologists, it became clear that the histologic correlations were not perfect with the 18- or even 16-gauge needles, especially in cases of fibrocystic change. It was decided to use a still larger-gauge needle. Therefore, after 74 patients underwent biopsy with

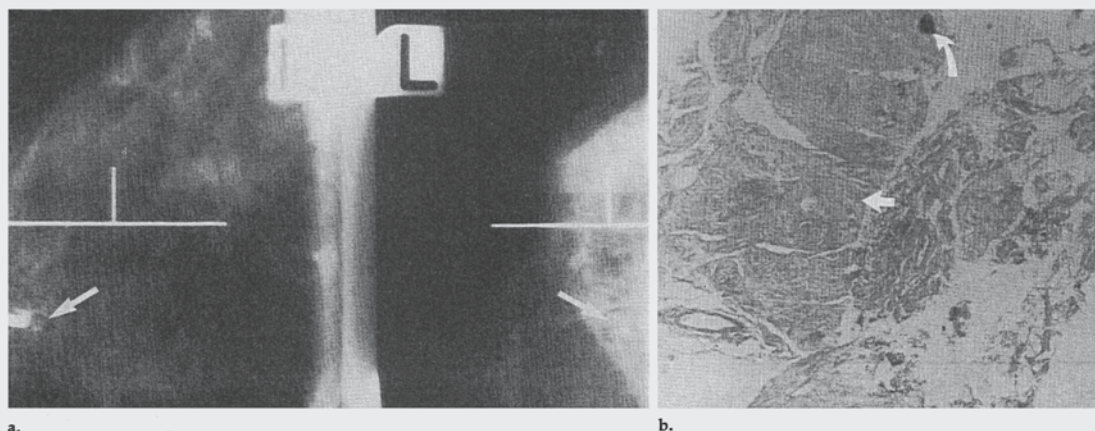


Figure 4. Fibroadenoma missed at surgical biopsy. (a) Stereo views demonstrating needle poised over cluster of microcalcifications (arrows). (b) Gun core sample showing the fibrous tissue (straight arrow) and microcalcification (curved arrow) of a sclerotic fibroadenoma. (c) Radiograph of surgical specimen showing end of localization hook-wire but no microcalcifications. At histopathologic examination, the specimen contained only normal breast tissue without evidence of the sclerotic fibroadenoma.

the 18- and 16-gauge needles, the remaining 29 underwent biopsy with 14-gauge needles. With the 14-gauge needle there was only one case of fibrocystic change without correlation of results. Evaluation of the 14-gauge needle cores by our pathologists revealed specimens that were much more consistent and uniform than those obtained with the smaller-gauge needles.

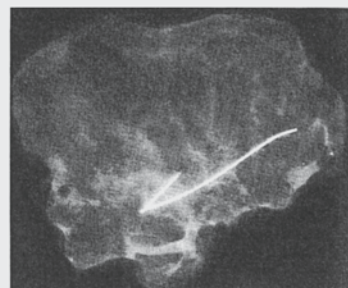
The one documented case of a fibroadenoma missed at gun biopsy resulted from breast movement with use of the Senographe Stereotix unit. No unwanted patient or gun/needle movement was observed with use of the Mammotest unit. In the two cases of documented lesions (one fibroadenoma and one cancer) that were missed at gun biopsy, calibration problems occurred with the Mammotest unit. These problems were solved by checking the calibration with a phantom prior to each biopsy. No calibration problems were encountered with the Senographe Stereotix unit. The time required for the procedure has decreased with experience such that the average time for the procedure (excluding placement of localizing hook-wire) is now approximately 20–30 minutes.

None of the 103 patients suffered immediate significant complications. Two vasovagal reactions occurred during use of the Senographe Stereotix; one caused patient and breast movement resulting in a gun biopsy miss. No reactions occurred with the Mammotest unit. No significant

bleeding occurred, even with use of the 14-gauge needle. Minor oozing was controlled easily with manual pressure. Three cases of local cellulitis occurred, and all were successfully treated with antibiotics. It is not possible to determine with certainty whether these three cases resulted from the needle core biopsy, needle localization, or surgical biopsy. However, cellulitis is a known complication of surgical excisional biopsy, and we have yet to log a single case of an infectious complication in nearly 1,000 gun biopsies of other anatomic sites.

DISCUSSION

As mammography screening becomes more commonplace and more suspicious lesions are detected, the need for an increasing number of breast biopsies will most likely result (8). In addition, some advocate lowering the threshold for breast biopsy to detect earlier cancers (9), and this would compound the increase in biopsy performance. Currently, the most common means of breast biopsy is surgical excision. This is an expensive, time-consuming, uncomfortable, and occasionally unreliable method of diagnosis (8,10). As radiologists whose role it is to make diagnoses and, more specifically, to perform image-guided percutaneous biopsies, it should be natural that we adapt our techniques to the diagnosis of breast disease. Most investigators have focused on FNAB in an attempt



c.

to accomplish this goal (4–6,11–13). Stereotactic mammographic guidance has improved the theoretical accuracy of skinny needle placement, but FNAB results in a substantial number of cases in which insufficient tissue is obtained (6%–47%) and in a significant number of false-negative findings (1%–31%) (14). In addition with FNAB, the occasional false-positive results (1% or less), the poor ability to make definitive benign diagnoses, and the inability to distinguish between in situ and invasive carcinoma have made surgeons and others reluctant to rely on percutaneous breast biopsy findings to make definitive treatment decisions (14–16). Compounding the above problems is the fact that cytopathology is a difficult art and science that is not available in its highest form in many institutions. Since many believe that aspiration biopsy will not achieve a high degree of success without the constant availability of a highly skilled and trained cytopathologist, attempts to perform breast FNAB at many institutions are likely to be unsuccessful (4,14,17).

Many pathologists and surgeons believe core tissue is superior to material obtained from needle aspira-

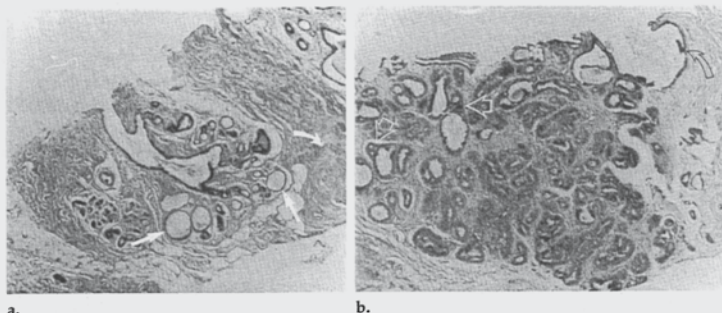


Figure 5. Histopathologic gun core specimen of fibrocystic changes showing several different elements. **(a)** Gun core specimen showing multiple ectatic ducts (straight arrows) and fibrosis (curved arrow). **(b)** Another portion of the same core shows ductal hyperplasia (open straight arrows) and papillomatosis (open curved arrow). These findings are difficult, if not impossible, to detect at aspiration biopsy.

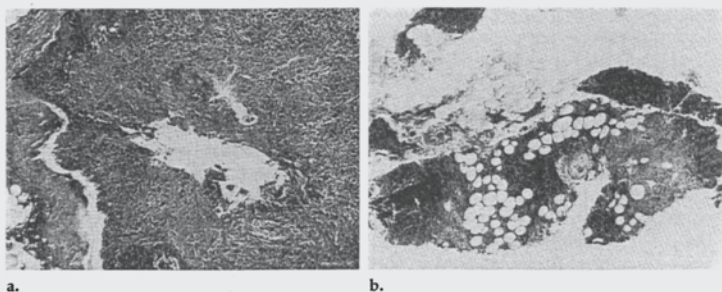


Figure 6. Comparison of histopathologic specimens of an intramammary lymph node. **(a)** Surgical specimen showing gun core defect in the center of the lymph node. **(b)** Portion of resultant gun core specimen.

tion biopsy, since it provides histologic information permitting definitive benign diagnoses and more complete characterization of malignant lesions (1,2,15,16). When a definitive benign diagnosis (eg, fibroadenoma) can be made, open biopsy can be confidently avoided. The reliable, complete, preoperative characterization of the type of malignant lesion present allows for the appropriate tailoring of the patient's treatment without repetition of biopsy when and if surgery is performed. One of the reasons that radiologists might not have routinely used large-gauge core needles in breast biopsy in the past is the theoretic increase in morbidity that is seen when large-gauge needles are used elsewhere in the body (1,2). In adapting FNAB techniques to breast biopsy, investigators naturally used the needles and the techniques that they had honed during their experience in biopsy of other areas of the body, apparently without considering the fact that the breast is quite forgiving and virtually devoid of structures that could result

in significant morbidity if transgressed by a core biopsy needle. Also, there have been conflicting reports regarding the relative efficacy of aspiration needles versus core biopsy needles in the breast (18–21). The studies purporting superior results with FNAB, however, compared multiple skinny needle passes to one core needle pass and were performed without an automated, rapid-fire core biopsy instrument or pinpoint imaging guidance (neither stereotactic nor ultrasound [US] guidance). They also failed to address the poor ability of FNAB results to enable a definitive benign diagnosis, an important consideration in breast biopsy as the majority of lesions sampled are indeed benign. Without definitive benign diagnoses, it is impossible to differentiate between a potential false-negative result due to a sampling error and a true-negative result such as fibroadenoma, sclerosing adenosis, or fibrocystic change.

Because the breast frequently consists of extraordinarily friable and fatty tissue, our pathologists found

that the 14-gauge needles most consistently provided the highest quality, intact cores. We also thought that the larger cores would further decrease the chances of sampling error. We continued to use the Biopsy gun rather than the conventional 14-gauge needle because of the ease of use of the gun, the decreased patient discomfort and increased specimen quality and integrity due to the split-second sampling, and the ability of the gun to pierce both hard and mobile breast lesions before they have a chance to move out of the path of the needle.

Despite the use of stereotactic guidance, with its theoretical accuracy of 1 mm in needle core gun biopsies, there were still nine cases in which the stereotactic gun biopsy failed to yield the diagnosis that was successfully made at surgical biopsy. However, we believe there were several possible explanations for these misses. First, our definite inexperience with two different stereotactic machines used during our study had to be overcome. In addition, our pathologists had to gain experience and confidence in handling and interpreting the cores. Second, because the 18-gauge needles used in the first 64 patients did not always obtain full intact cores, lesions may not have been as thoroughly canvassed as we believed from the stereo images. Also, the short-throw gun was used on two occasions until we realized, in conjunction with another study, that it did not reliably obtain high-quality tissue (22). Third, we experienced significant calibration problems on at least two separate occasions. Fourth, patient movement causing subsequent breast movement after the initial stereo calculations were made resulted in inaccurate coordinates in two cases. Fifth, we realized that at least one and possibly two fibroadenomas were missed because of lesion movement within the breast. This seems to be a frequent characteristic of fibroadenomas, confirmed under direct visualization during our US-guided biopsies, since they do not appear to be firmly anchored in the breast. Therefore, as a needle is manually advanced toward the lesion, it can rotate or slip out of the path of the needle. Presently, if we suspect that a lesion is moving away from our needle tip, we back the tip up as much as 1.5 cm from the lesion. Then, when the gun is fired, the split-second rapid-fire projection of the needle allows it to pierce the lesion before it can slip out of the way.

Finally, it is apparent that serendipity plays a role in breast diagnosis. In other words, there are occasions when the surgeons unwittingly make a diagnosis with their generous surgical sample that may have nothing whatsoever to do with the mammographic finding. We believe the surgical diagnosis of lobular carcinoma in situ in our series was just such an example; the mammographic finding in that case was fat necrosis. There is nothing that can be done about lesions missed at stereotactic gun biopsy that were serendipitously seen at surgical biopsy; however, the other causative factors in our misses can be addressed and if these factors are eliminated, the success rate should improve further.

In determining whether stereotactic gun biopsies might be performed as an alternative to surgical excisional biopsies, one should also take a close look at surgical biopsies, which have been referred to in some instances as "ritualistic rather than realistic" (15). Although surgery is considered a standard of reference, it should not be mistaken for perfection. On the contrary, needle localization breast biopsy is a semiblind operation with a technical difficulty that should not be underestimated even by the most experienced surgeons (23). The lesion miss rate is as high as one in five procedures with local anesthesia (10). Considerable bleeding can occur during a surgical biopsy that can obscure the operative field and preclude confident excision of deep lesions (23). Also, if the wire inadvertently dislodges, migrates, or is transected, the surgeon can become disoriented and excise the wrong tissue (24,25). Finally, lack of communication between the radiologist who has placed the localizing wire and the surgeon can result in a surgical miss (26). Surgical biopsies are also time-consuming, potentially nerve-racking, and require a great deal of resources (8). The delays frequently encountered impose a psychological stress on the patient awaiting the procedure. Combining the time in the radiology and surgery departments, the needle localization and surgical excisional biopsy may require up to 3 hours. Postoperative hematoma, cellulitis, and poor cosmesis can result.

By contrast, a stereotactic gun biopsy obtains surgical tissue with only a skin nick, leaving no scar. It can be performed quickly and easily after the original mammogram is obtained, even the same day. This technique

is actually a further extension of the "minimal volume excision" approach advocated by Gallagher et al (27); however, it is much more expeditious and eliminates surgery entirely for benign lesions. Thus, the potential for psychological stress and physical trauma is lessened considerably.

A beneficial by-product of needle core breast biopsy is the nearly immediate feedback the radiologist receives regarding the actual histopathologic makeup of the mammographic finding in question. This will naturally improve future mammographers' interpretation abilities, and a less experienced mammographer will become highly competent much more quickly. As noted by Hall, "no book or lecture can substitute for this type of teaching" (8). Also, the frequently puzzling and sometimes highly suggestive mammographic pseudolesions that can appear after surgical biopsy should no longer be a dilemma (19).

Previously, in patients with highly suggestive lesions or obvious mammographic cancers, the definitive surgery may have been performed in the process of the biopsy. Now such patients might still go straight to surgery; however, this sequence may change as the trend toward more conservative and nonsurgical treatment of primary breast cancer continues. Acquisition of a definitive histologic needle core biopsy specimen may be desirable prior to consideration of any type of treatment, surgical or otherwise.

Currently there is some debate about the advisability of short-interval follow-up of less suggestive or "probably benign" lesions versus recommendation of immediate surgical biopsy (28). The rationale for short-interval follow-up is the unfavorable cost-benefit analysis that occurs when benign to malignant ratios rise with the inclusion of such lesions for surgical biopsy. With the lower cost, discomfort, and psychological trauma associated with stereotactic gun biopsies, a more aggressive approach to the definitive histopathologic diagnosis of mammographic lesions could be forthcoming.

The cost of a surgical excisional biopsy in Denver varies between \$1,217 and \$2,673 depending on whether or not it is performed with administration of general anesthesia and whether it is performed on an in- or outpatient basis. The cost of a stereotactic gun biopsy is approxi-

mately \$675. With increasing utilization of mammographic screening and the resultant increase in performance of breast biopsy, the national cost of surgical biopsy could rise considerably. It is therefore important that cost-effective means of breast cancer diagnosis are identified and utilized. Stereotactic gun biopsy of the breast may help fill this need.

In conclusion, to justify a percutaneous breast biopsy triage system for suggestive nonpalpable mammographic lesions, the system must be extremely accurate, reduce or eliminate surgical biopsy with benign results, and reduce the amount of surgery required for therapy of the cancers diagnosed (29). Stereotactic mammography allows pinpoint needle placement, and the large cores obtained from 14-gauge needles further decrease the possibility of sampling error. The large cores also eliminate the need for an experienced cytopathologist and allow for histologic evaluation permitting definitive benign diagnoses and complete characterization of malignant lesions. Utilization of a mechanized biopsy device eliminates the need for mastery of difficult aspiration techniques with the push of a button. It is therefore our opinion that stereotactic breast gun biopsy overcomes many of the problems associated with FNAB and may prove to be a cost-effective, expeditious, and dependable alternative to surgical biopsy. ■

References

- Charboneau JW, Reading CC, Welch TJ. CT and sonographically guided needle biopsy: current techniques and new innovations. *AJR* 1990; 154:1-10.
- Gazelle GS, Haaga JR. Guided percutaneous biopsy of intraabdominal lesions. *AJR* 1989; 153:929-935.
- Parker SH, Hopper KD, Yakes WF, Gibson MD, Ownbey JL, Carter TE. Image-directed percutaneous biopsies with a biopsy gun. *Radiology* 1989; 171:663-669.
- Dowlathshahi K, Gent HJ, Schmidt R, Jochik PM, Bibbo M, Sprenger E. Nonpalpable breast tumors: diagnosis with stereotactic localization and fine-needle aspiration. *Radiology* 1989; 170:427-433.
- Ciatto S, Del Turco MR, Bravetti P. Nonpalpable breast lesion: stereotactic fine-needle aspiration cytology. *Radiology* 1989; 173:57-59.
- Azavedo E, Svane G, Auer G. Stereotactic fine-needle biopsy in 2,594 mammographically detected non-palpable lesions. *Lancet* 1989; 1:1033-1036.
- Lovin JD, Parker SH, Jobe WE, Luethke JM, Hopper KD. Stereotactic percutaneous breast core biopsy: technical adaptation and initial experience. *Breast Dis* 1990; 3:135-143.
- Hall F. Screening mammography: potential problems on the horizon. *N Engl J Med* 1986; 314:53-55.

9. Choucair RJ, Holcomb MB, Mathews R, Hughes TG. Biopsy of nonpalpable breast lesions. *Am J Surg* 1988; 156:453-456.
10. Norton LW, Pearlman NW. Needle localization breast biopsy: accuracy versus cost. *Am J Surg* 1988; 156(2):13B-15B.
11. Smith C, Butler J, Cobb C, State D. Fine-needle aspiration cytology in the diagnosis of primary breast cancer. *Surgery* 1987; 103:178-183.
12. Kahky MP, Rone R, Duncan DL, Cruz AB, Gaskill HV. Needle aspiration biopsy of palpable breast masses. *Am J Surg* 1988; 156:450-452.
13. Hann L, Ducatman BS, Wang HH, Fein V, McIntire JM. Nonpalpable breast lesions: evaluation by means of fine-needle aspiration cytology. *Radiology* 1989; 171:373-376.
14. Grant GS, Goellner JR, Welch JS, Martin JK. Fine-needle aspiration of the breast. *Mayo Clin Proc* 1986; 61:377-381.
15. Sheikh FA, Tinkoff GH, Kline TS, Neal HS. Final diagnosis by fine-needle aspiration biopsy for definitive operation in breast cancer. *Am J Surg* 1987; 154:470-475.
16. Abramson DJ. Outpatient breast biopsy. *Milit Med* 1987; 152:594-595.
17. Sundaram M, Wolverson MK, Heiberg E, Pilla T, Vas WG, Shields JB. Utility of CT-guided abdominal aspiration procedures. *AJR* 1982; 139:1111-1115.
18. Elston CW, Cotton RE, Davies CJ, Blamey RW. A comparison of the use of the "Tru-Cut" needle and fine needle aspiration cytology in the pre-operative diagnosis of carcinoma of the breast. *Histopathology* 1978; 2:239-254.
19. Vorherr H. Breast aspiration biopsy with multihole needles for histologic and cytologic examination. *Am J Obstet Gynecol* 1985; 151:70-76.
20. Pederson L, Guldhammer B, Kamby C, Aasted M, Rose C. Fine needle aspiration and Tru-Cut biopsy in the diagnosis of soft tissue metastases in breast cancer. *Eur J Cancer Clin Oncol* 1986; 22:1045-1052.
21. Shabot MM, Goldberg IM, Schick P, Nieberg R, Pilch YH. Aspiration cytology is superior to Tru-Cut needle biopsy in establishing the diagnosis of clinically suspicious breast masses. *Ann Surg* 1982; 196:122-126.
22. Hopper KD, Baird DE, Reddy W, et al. Efficacy of automated biopsy guns versus conventional biopsy needles in the pigmy pig. *Radiology* 1990; 176:671-676.
23. Norton LW, Zeligman BE, Pearlman NW. Accuracy and cost of needle localization breast biopsy. *Arch Surg* 1988; 123:947-950.
24. Davis PS, Wechsler RJ, Feig SA, March DE. Migration of breast biopsy localization wire. *AJR* 1988; 150:787-788.
25. Landercasper J, Gunderson SB, Gunderson AL, Cogbill TH, Travelli R, Strutt P. Needle localization and biopsy of nonpalpable lesions of the breast. *Surg Gynecol Obstet* 1987; 164:399-403.
26. Yankaskas BC, Knelson MH, Abernathy ML, Cuttino JT, Clark RL. Needle localization biopsy of occult lesions of the breast: experience in 199 cases. *Invest Radiol* 1988; 23:730-733.
27. Gallagher WJ, Cardenosa G, Rubens JR, McCarthy KA, Kopans DB. Minimal-volume excision of nonpalpable breast lesions. *AJR* 1989; 153:957-961.
28. Brenner RJ, Sickles EA. Acceptability of periodic follow-up as an alternative to biopsy for mammographically detected lesions interpreted as probably benign. *Radiology* 1989; 171:645-646.
29. Kopans DB. Fine-needle aspiration of clinically occult breast lesions. *Radiology* 1989; 170:313-314.

References

1 Computer Tomography

1.1

Radon J

Über die Bestimmung von Funktionen durch ihre Integralwerte längs gewisser Mannigfaltigkeiten.

Reprinted with permission. Ber. Sächs. Akad. Wiss 69: 262-277, 1917.

© 1917 Saxon Academy of Science

1.2

Cormack AM

Representation of a function by its line integrals, with some radiological applications.

Reprinted with permission. Journal Applied Physics 34: 2722-2727, 1964.

© 1964 American Institute of Physics

1.3

Hounsfield GN

Computerized transverse axial scanning (tomography). Part I. Description of system.

Reprinted with permission. British Journal of Radiology 46: 1016-1022, 1973.

© 1973 British Institute of Radiology

1.4

Ambrose J

Computerized transverse axial scanning (tomography). Part II.

Clinical application.

Reprinted with permission. British Journal of Radiology 46: 1023-1047: 1973.

© 1973 British Institute of Radiology

1.5

Kalender WA, Seifler W, Klotz E, Vock P

Spiral volumetric CT with single-breathhold technique, continuous transport, and continuous scanner rotation.

Reprinted with permission. Radiology 176: 181-183, 1990.

© 1990 Radiological Society of North America

2 MRI

2.1

Rabi II, Cohen VW

Measurement of nuclear spin by the method of molecular beams.

The nuclear spin of sodium.

Reprinted with permission. Physical Review 46: 707-712, 1934.

© 1934 American Physical Society

2.2

Bloch F, Hansen WW, Packard ME

Nuclear Induction.

Reprinted with permission. *Physical Review* 69: 127, 1946.

© 1946 American Physical Society

2.3

Purcell EM, Torrey HC, Pound RV

Resonance absorption by nuclear magnetic moments in a solid.

Reprinted with permission. *Physical Review* 69: 37-38, 1946.

© 1946 American Physical Society

2.4

Damadian RV

Tumor detection by nuclear magnetic resonance.

Reprinted with permission. *Science* 171: 1151-1153, 1971.

© 1971 AAAS

2.5

Lauterbur PC

Image Foundation by induced local interactions: Example employing nuclear magnetic resonance.

Reprinted with permission. *Nature* 242: 190-191, 1973.

© 1973 NPG

2.6

Mansfield P, Maudsley AA

Planar spin imaging by NMR.

Reprinted with permission.

J. Phys. C: Solid State Phys. 9 No 15: L409-L412, 1976.

© 1976 Institute of Physics and IOP Publishing Limited

2.7

Mansfield P, Maudsley AA

Medical imaging by NMR.

Reprinted with permission. *Brit Jour of Radiol* 50: 188-194, 1977.

© 1977 British Institute of Radiology

2.8

Mansfield P, Pykett IL, Morris PG, Coupland RE

Human whole body line scan imaging by NMR.

Reprinted with permission. *Brit Jour Radiol* 51: 921-922, 1978.

© 1978 British Institute of Radiology

2.9

Young IR, Hall AS, Pallis CA et al.

NMR imaging of the brain in multiple sclerosis.

Reprinted with permission. *The Lancet* ii: 1063-1066, 1981.

© 1981 Lancet Publishing Group (Elsevier)

2.10

Bydder GM, Young IR

MRI: Clinical use of the inversion recovery sequence.

Reprinted with permission. *J Computer Assisted Tomography* 9: 659-75, 1985.

© 1985 Lippincott Williams & Wilkins

3 Ultrasound

3.1

Dussik KT

Über die Möglichkeit, hochfrequente mechanische Schwingungen als diagnostisches Mittel zu verwerten.

Reprinted with permission. Zeitschrift gesamte Neurologie und Psychiatrie 174: 153-168, 1942.

© Springer-Verlag, Berlin Heidelberg

3.2

Wild JJ, Reid JM

Application of echo-ranging techniques to the determination of structure of biological tissues.

Reprinted with permission. Science 115: 226-230, 1952.

© 1952 AAAS

3.3

Edler I, Hertz CH

The use of ultrasonic Reflectoscope for the continuous recording of the movements of heart walls.

Reprinted with permission. Kungl. Fysiografiska Sällskapet I Lund Förhand-lingar 24: 1-19, 1954.

© 1954 Kungl. Fysiografiska Sällskapet I Lund

3.4

Holmes JH, Howry DH, Posakony GJ, Cushman CR

The ultrasonic visualization of soft tissue structures in the human body.

Reprinted with permission. Trans. Am. Clin. Climatol. Assoc. 66: 208-223, 1954.

© 1954 ACCA

3.5

Donald I, MacVicar J, Brown TG

Investigation of Abdominal Masses by Pulsed Ultrasound.

Reprinted with permission. The Lancet i: 1188-1195, 1958.

© 1958 Lancet Publishing Group (Elsevier)

3.6

Satomura S

Ultrasonic Doppler method for the inspection of cardiac functions.

Reprinted with permission. J. Acoust Soc. Amer. 29: 1181-1185, 1957.

© 1957 Acoustical Society Of America

3.7

Hofmann D, Holländer H-J, Weiser P

Neue Möglichkeiten der Ultraschalldiagnostik in der Gynäkologie und Geburtshilfe.

Reprinted with permission. Fortschritte der Medizin 84,18: 689-693, 1966.

© 1966 MMW

3.8

Campbell S

The prediction of fetal maturity by ultra-sonic measurement of the biparietal diameter.

Reprinted with permission. J Obstet Gynecol Br Cwlth 76: 603-609, 1969.

© 1969 BJOG The Royal College of Obstetricians and Gynaecologists

3.9

Baba K, Satoh K, Sakamoto S, Okai T, Ishii S
Development of an ultrasonic system for three-dimensional reconstruction of the fetus.
Reprinted with permission. *J Perinat. Med.* 17: 19-24, 1989.
© 1989 Walter De Gruyter

4 Digital Imaging**4.1**

Brennecke R, Brown TK, Bürsch JH, Heintzen PH
Digital Processing of Videoangiocardigraphic Image Series.
Reprinted with permission. *Computers in Cardiology*: 255-260, 1976.
© IEEE Computer Sciences

4.2

Kruger RA, Mistretta CA, Riederer SJ, Shaw CG et al.
Computerized fluoroscopy in real time for noninvasive visualization of the cardiovascular system. Preliminary studies.
Reprinted with permission. *Radiology* 130: 49-57, 1979.
© 1979 Radiological Society of North America

4.3

Ovitt TW, Christenson PC, Fisher HD 3rd, Frost MM, Nudelman S, Roehrig H
Intravenous angiography using digital video subtraction: x-ray imaging system.
Reprinted with permission. *Am J Roentgenol* 135(6): 379-386, 1980.
© 1980 American Roentgen Ray Society

4.4

Sonoda M, Takano M, Miyahara J, Kato H
Computed radiography utilizing scanning laser stimulated luminescence.
Reprinted with permission. *Radiology* 148: 833-838, 1983.
© 1983 Radiological Society of North America

4.5

Fraser RG, Breatnach E, Barnes GT
Digital radiography of the chest: clinical experiences with a prototype unit.
Reprinted with permission. *Radiology* 148: 1-5, 1983.
© 1983 Radiological Society of North America

4.6

Lee DL, Cheung LK, Jeromin LS
A new digital detector for projection radiography.
Reprinted with permission. *Proc SPIE* 2432: 237-247, 1995.
© 1995 The International Society for Optical Engineering

4.7

Zhao W, Rowlands JA
X-ray imaging using amorphous selenium: Feasibility of a flat panel self-scanned detector for digital radiology.
Reprinted with permission. *Medical Physics* 22: 1595-1604, 1995.
© 1995 American Association of Physicists in Medicine

5 PACS

5.1

Lemke HU, Stiehl HS, Scharnweber H, Jackél D
Applications of Picture Processing, Image Analysis Computer Graphics
Techniques to Cranial CT Scans. Proceedings of the Sixth Conf.
on Computer Applications in Radiology and Computer Aided Analysis
of Radiological Images.
Reprinted with permission. IEEE Computer Society Press 341-354, 1979.
© 1979 Institute of Electrical and Electronics Engineers

5.2

Parker JA, Royal HD, Uren RF, Front D, Bliss JG, Rabussi M, Jansons D,
Kolodny MS, Kolodny GM
An All-digital Nuclear Medicine Department.
Reprinted with permission. Radiology 147: 237-240, 1983.
© 1983 Radiological Society of North America

5.3

Huang HK, Barbaric Z, Mankovich NJ, Moler C
Digital Radiology at the University of California, Los Angeles:
A Feasibility Study.
Reprinted with permission. Proc. SPIE 418: 259-265, 1983.
© The International Society for Optical Engineering

5.4

Levine BA, Mun SK, Benson HR, Horii SC
Assessment of the Integration of HIS/RIS with a PACS.
Reprinted with permission. Proc SPIE 1234: 391-397, 1990.
© 1990 The International Society for Optical Engineering

5.5

Horii SC et al.
Environmental Designs for Reading. Imaging Workstations:
Ergonomic and Architectural Features.
Reprinted with permission Proc. SPIE 1091: 172-178, 1989.
© 1989 The International Society for Optical Engineering

6 Contrast Agents

6.1

Almén T
Contrast agent design. Some aspects on the synthesis of water-soluble contrast
agents of low osmolality.
Reprinted with permission. Journal of Theoretical Biology 24: 216-226, 1969.
© 1969 Elsevier

6.2

Almén T
Development of nonionic contrast media.
Reprinted with permission. Investigative Radiology 20: S2-S9, 1985.
© 1985 Lippincott Williams & Wilkins

6.3

Carr DH, Brown J, Bydder GM, Weinmann H-J, Speck U, Thomas DJ, Young IR
Intravenous chelated gadolinium as a contrast agent in NMR imaging
of cerebral tumours.

Reprinted with permission. *The Lancet* i: 484-486, 1984.

© 1984 Lancet Publishing Group (Elsevier)

6.4

Weinmann HJ, Brasch RC, Press WR, Wesbey GE
Characteristics of gadolinium-DTPA complex: a potential NMR
contrast agent.

Reprinted with permission. *AJR* 142: 619-624, 1984.

© 1984 American Roentgen Ray Society

6.5

Brasch RC, Weinmann HJ, Wesbey GE
Contrast-enhanced NMR imaging: animal studies using gadolinium-DTPA
complex.

Reprinted with permission. *AJR* 142: 625-630, 1984.

© 1984 American Roentgen Ray Society

7 Interventional Radiology

7.1

Seldinger SI

Catheter replacement of the needle in percutaneous arteriography:

A new technique.

Reprinted with permission. *Acta radiol.* 39: 368-376, 1953.

© 1953 Taylor & Francis Group

7.2

Goodwin WE, Casey WC, Woolf W

Percutaneous trocar (needle) nephrostomy in hydronephrosis.

Reprinted with permission. *JAMA* 157: 891-894, 1955.

© 1955 American Medical Association

7.3

Sones FM, Shirey EK, Proudfit WL, Westcott R

Cine coronary arteriography.

Reprinted with permission. *Circulation* 20: 773-774, 1959.

© 1959 American Heart Association

7.4

Margulis AR, Heinbecker P

Mesenteric Arteriography.

Reprinted with permission. *AJR* 86: 103-113, 1961.

© 1961 American Roentgen Ray Society

7.5

Dotter CT, Judkins MP

Transluminal treatment of arteriosclerotic obstruction:

description of a new technique and a preliminary report of its application.

Reprinted with permission. *Circulation* 30: 654-670, 1964.

© 1964 American Heart Association

7.6

Judkins MP

Selective coronary arteriography.

Reprinted with permission. Radiology 89: 815-824, 1967.

© 1967 Radiological Society of North America

7.7

Burhenne HJ

Non-operative retained biliary tract stone extraction.

A new roentgenologic technique.

Reprinted with permission. AJR 117 (2): 388-399, 1973.

© 1973 American Roentgen Ray Society

7.8

Grüntzig AR, Hopff H

Perkutane Rekanalisation chronischer arterieller Verschlüsse mit einem neuen Dilatationskatheter.

Reprinted with permission. Dtsch. Med. Wschr. 99: 2502-2505, 1974.

© 1974 Georg Thieme Verlag

7.9

Grüntzig AR

Transluminal dilatation of coronary-artery stenosis.

Reprinted with permission. The Lancet ii: 263, 1978.

© 1978 Lancet Publishing Group (Elsevier)

7.10

Müller PR, van Sonnenberg E, Ferrucci JT

Percutaneous biliary drainage, technical and catheter - related problems in 200 procedures.

Reprinted with permission. AJR 138 (1): 17-23, 1982.

© 1982 American Roentgen Ray Society

7.11

Palmaz JC, Sibbitt RR, Reuter SR et al.

Expandable intrahepatic portacaval shunt stents: early experience in the dog.

Reprinted with permission. AJR 145: 821-825, 1985.

© 1985 American Roentgen Ray Society

7.12

Sigwart U, Puel J et al.

Intra vascular stents to prevent occlusions and restenosis after transluminal angioplasty

Reprinted with permission. NEJM 316: 701-706, 1987.

© 1987 Massachusetts Medical Society

8 Mammography

8.1

Leborgne R

Diagnóstico de los tumores de la mama por la radiografía simple.

Reprinted with permission. Boletín de la Sociedad de Cirugía del Uruguay 20: 407-422, 1949.

© 1949 Sociedad de Cirugía del Uruguay

8.2

Gros CM, Sigrist R
La radiographie de la glande mammaire.
Reprinted with permission. J Belge Radiologie 35: 226-268, 1952.
© 1952 M Pacquet

8.3

Egan RL
Experience with mammography in tumor institution:
evaluation of 1000 studies.
Reprinted with permission. Radiology 75: 894-900, 1960.
© 1960 Radiological Society of North America

8.4

Shapiro S, Strax P, Venet L
Evaluation of periodic breast cancer screening with mammography.
Methodology and early observations.
Reprinted with permission. JAMA 195 (9) (1966): 731-738
© 1966 JAMA

8.5

Wolfe JN
Xerography of the breast.
Reprinted with permission. Radiology 91: 231-240, 1968.
© 1968 Radiological Society of North America

8.6

Tabár L, Fagerberg CJG, Gad A, Baldetorp L, Holmberg LH, Grøntoft O et al.
Reduction in mortality. breast cancer after mass screening
with mammography.
Reprinted with permission. The Lancet i: 829-832, 1985.
© 1985 Lancet Publishing Group (Elsevier)

8.7

Smathers RL et al.
Mammographic Microcalcifications: Detection with Xerography, Screen-Film,
and Digitized Film Display.
Reprinted with permission. Radiology 159: 673-677, 1986.
© 1986 Radiological Society of North America

8.8

Asaga T, Chiyasu S, Matsuda S, Mastuura H, Kato H, Ishida M, Komaki T
Breast imaging: Dual-energy projection radiography with digital radiography.
Reprinted with permission. Radiology 164: 869-870, 1987.
© 1987 Radiological Society of North America

8.9

Parker SH, Lovin JD, Jobe WE, Luethke JM, Hopper KD, Yakes WF, Burke BJ
Stereotactic breast biopsy with a biopsy gun.
Reprinted with permission. Radiology 176: 741-747, 1990.
© 1990 Radiological Society of North America